Synthetic evolution of azobenzene and arylazopyrazole photoswitches and translation into photoresponsive DNA nanosystems

Dissertation

zur

Erlangung des Doktorgrades (Dr. rer. nat.)

der

Mathematisch-Naturwissenschaftlichen Fakultät

der

Rheinischen Friedrich-Wilhelms-Universität Bonn

Vorgelegt von

Volker Adam

aus

Troisdorf

Bonn 2019

Angefertigt mit der Genehmigung der Mathematisch-Naturwissenschaftlichen Fakultät der Rheinischen Friedrich-Wilhelms-Universität Bonn.

1. Gutachter: Prof. Dr. Michael Famulok
2. Gutachter: Prof. Dr. Arne Lützen

Tag der Promotion: 25.09.2019
Erscheinungsjahr: 2019

„Und Gott sprach: Es werde Licht!
Und es ward Licht.
Und Gott sah, dass das Licht gut war.“

(Gen 1, 3-4)

Danke…

…Gott, dem Allmächtigen und Vater aller Dinge, für seine Führung, Eingebungen und Hilfen in der Not. Er ist der, der mich groß gemacht hat. Mein Licht, meine Erleuchtung und mein Heiland zu allen Zeiten und für alle Zeiten.

…meiner Frau Iman für die unendliche Liebe und Geduld, die sie mir in all den Jahren entgegenge-bracht hat.

…meiner Familie für all die Hilfe und Unterstützung, bedingungslos und zu jeder Zeit.

…Prof. Dr. Michael Famulok für ein großartiges Doktorthema, an dem ich mich austoben konnte, und die Hilfe und Unterstützung, um meinen Doktorgrad zu erreichen.

…den Mitgliedern der Prüfungskommission für die Begutachtung meiner Dissertation.

…Dr. Deepak Prusty für seine Hilfe und Unterstützung und all das Wissen und die Fähigkeiten, die er mir während meiner Doktorzeit beigebracht hat.

…Johannes Weigandt und Mathias Centola für all die Hilfe und Unterstützung in den Bereichen DNA-Nanotechnologie und in allen biologischen Aspekten der Arbeit.

…Dr. Jeffrey Hannam, Dr. Gerd Brändle und Jörg Ewers für die Unterstützung in allen synthetischen Bereichen meiner Doktorarbeit.

…Dr. Damian Ackermann von der Microsynth AG und Dr. Tim Gehrke von der Ella Biotech GmbH für die langjährige Unterstützung im Bereich der Synthese modifizierter Oligonukleotide.

…Justina Stark für tägliche Motivation mit guter Laune und ganz vielen Süßigkeiten.

…allen Mitarbeitern der Arbeitskreise Prof. Dr. Famulok und Prof. Dr. Mayer für Hilfe, Unterstützung und Diskussionen aller Art und zu jeder Zeit.

Parts of this thesis have previously been published in:

[A] V. Adam, D. K. Prusty, M. Centola, J. Hannam, M. Škugor, B. Klöckner, J. Valéro, M. Famulok, **Expanding the toolbox of photoswitches for DNA nanotechnology using arylazopyrazoles**, *Chem. Eur. J.* **2018**, *24* (5), 1062-1066.

[B] D. K. Prusty, V. Adam, R. Zadegan, S. Irsen, M. Famulok, **Supramolecular aptamer nano-constructs for receptor-mediated targeting and light triggered release of chemotherapeutics into cancer cells**, *Nat. Comm.* **2018**, *9* (535), 1-14.

Further scientific contributions:

[C] M. W. Haydell, M. Centola, V. Adam, J. Valero, M. Famulok, **Temporal and Reversible Control of a DNAzyme by Orthogonal Photoswitching**, *J. Am. Chem. Soc.* **2018**, *140* (49), 16868-16872.

[D] F. Lohmann, J. Weigandt, J. Valero, M. Famulok, **Logic Gating by Macrocycle Displacement Using a Double-Stranded DNA [3]Rotaxane Shuttle**, *Angew. Chem. Int. Ed.* **2014**, *53*, 10372-10376.

Patents:

[E] EP 16 202 754.4 "**Nucleic acid-based assembly and use of the assembly in cancer therapy**".

Table of contents

1. Abstract

Light as an external stimulus provides a powerful and versatile tool to control chemical reactions and biological systems. Light is easily available and permits a high spatial and temporal control while minimizing systemic contamination as often associated with invasive methods. Efficient photocontrol of a system of interest can be achieved by introduction of photochromic molecules which can undergo reversible interconversion from one conformation into another upon exposure to distinct wavelengths of light. Azobenzene thereby represents one of the best studied and most commonly used photochromic molecules in this context. Azobenzene molecules can be reversibly transformed from a planar *trans* conformation into a non-planar, sterically more challenging *cis* conformation by exposure to UV or visible light. Introduction of azobenzene into complex systems led to a series of applications ranging from light-controlled smart materials and nanodevices to light control over biological processes and cellular functions *in vitro*.

Introduction of azobenzene into desoxyribonucleic acid (DNA) afforded reversible photoinduced hybridization and dissociation of DNA double strands by means of UV or visible light irradiation. Coupling azobenzene to D-threoninol as a nucleobase surrogate led to the successful implementation into DNA backbones, thus paving the way for a series of photocontrolled applications. Photoresponsive DNA nanotechnology brought up structure-changing DNA nanoconstructs and devices as well as functional dynamic DNA nanotechnology, the *in vitro* control of biological and cellular processes up to the emerging field of photopharmacology. Despite the successful establishment of photocontrol *in vitro*, a translation towards *in vivo* systems in hampered by the mandatory use of UV light for *cis* isomerization, disrupting DNA and cellular tissue upon UV exposure. Furthermore, efficient azobenzene *cis* isomerization requires elevated irradiation temperatures and a high synthetic load inside DNA duplexes to achieve efficient duplex dissociation. Many efforts have been performed to circumvent these prerequisites by substituting D-threoninol for other diol linkers or adding substituents and functional groups to azobenzene moieties in different patterns to optimize photophysical properties. Yet, only few of these drawbacks could be overcome by the performed optimization studies.

Recent advances brought up a series of modified azobenzene molecules containing hetero atoms and functional moieties in all four *ortho* positions on both benzene rings. This substitution pattern results in a significant red-shift of isomerization wavelengths accompanied by an increased thermal stability of the *cis* state. Also replacement of benzene rings by heterocycles as in arylazopyrazoles led to near-quantitative conversion efficiencies accompanied by high thermal stabilities of the *cis* state up to three years. The recently reported molecules provide

tools for a possible improvement of photocontrolled DNA duplex hybridization, bearing potential for improved response wavelengths, thermal stabilities of the *cis* state and conversion efficiencies between both isomers. Studies towards translation into DNA strands and DNA-based applications have not been reported to date.

The following dissertation catches up the potential improvement of photocontrolled DNA duplex hybridization. Based on the reported azobenzene and arylazopyrazole small molecules, a systematic feasibility study of azobenzene and arylazopyrazole photoswitches attached to D-threoninol was performed to optimize the photophysical properties and translate these into modified oligonucleotide strands. A pre-selection of synthetically accessible D-threoninol bound small molecule candidates was investigated empirically by UV/Vis spectroscopy in combination with an irradiation device providing high output LEDs to determine maximum response wavelengths. Reversed-phase HPLC and UV/Vis spectroscopy were utilized to quantify the maximum switching efficiencies and thermal stabilities of the *cis* states. Consecutive DMT-protection and phosphitylation of the D-threoninol bound photochromes enabled the implementation of selected photoswitches into DNA strands *via* solid phase DNA synthesis. A translation of optimized photophysical properties into DNA strands was investigated *via* reversed-phase HPLC quantification and UV/Vis spectroscopy involving systematically modified DNA strands and duplexes in direct comparison to the newly designed small molecules. Melting curve analysis of modified duplexes revealed improved duplex dissociation efficiencies even with a lower synthetic load as compared to the reported azobenzenes.

Translation of improved photophysical properties was further demonstrated by introduction of arylazopyrazoles into higher order DNA systems. A double-stranded DNA catenane was designed and assembled to further investigate coherent and independent switching properties using a combination of release oligomers each containing different types of photochromes. Not only the catenane system was designed to determine coherent photophysical properties, but also the catenane building blocks were used to qualitatively demonstrate individual switching properties.

Besides the development of new photochromes, further nanotechnological applications have been developed. Lipid-mediated self-assembling micellar nano-constructs were designed as carrier moieties for targeted transport of doxorubicin into cancer cells. The system consists of an aptamer-based cell receptor targeting unit combined with a photo-triggered doxorubicin release mechanism. Successful cell internalization and photo-triggered release of doxorubicin inside the cells was applied *in vitro* in H1838 non-small cell lung cancer cells.

1. Abstract (deutsch)

Licht als äußerer Impuls stellt ein wirkungsvolles und vielseitiges Werkzeug zur Kontrolle chemischer Reaktionen und biologischer Prozesse dar. Licht ist leicht zugänglich und erlaubt eine hohe räumliche und zeitliche Kontrolle während systemische Kontaminationen vermieden werden, die häufig beim Einsatz invasiver Methoden auftreten. Effiziente Photokontrolle eines spezifischen Systems kann durch den Einbau photochromer Moleküle erreicht werden, die durch Bestrahlung mit unterschiedlichen Lichtwellenlängen eine reversible Umwandlung von einer Konformation in eine andere eingehen. Azobenzol stellt eines der am meisten verwendeten und am besten untersuchten photochromen Moleküle dar. Azobenzol kann durch den Einsatz von UV- und sichtbarem Licht reversibel von einer planaren *trans*-Konformation in eine nicht-planare, sterisch anspruchsvollere *cis*-Konformation umgewandelt werden. Der Einbau von Azobenzol in komplexe Systeme brachte eine Reihe von Anwendungen hervor, die von lichtschaltbaren Materialien und Nanomaschinen bis hin zur Lichtkontrolle von biologischen und zellulären Funktionen *in vitro* reichen.

Durch den Einbau von Azobenzol in Desoxyribonukleinsäre (DNA) konnte mit Hilfe von UV- und sichtbarem Licht eine reversible Photokontrolle über die Hybridisierung und Dissoziation von DNA-Doppelsträngen erreicht werden. Der Einbau von Azobenzol konnte mittels eines D-Threoninol-Linkers als Nukleobasenersatz erreicht werden und bahnte den Weg für eine Reihe an photoinduzierten Anwendungen. Azobenzol-modifizierte DNA wurde in einer Reihe von lichtgesteuerten Anwendungen etabliert, die von strukturändernden Nanokonstrukten and Maschinen über die funktionale lichtgesteuerte DNA-Nanotechnologie und die Photokontrolle von biologischen Prozessen und zellulären Funktionen *in vitro* bis hin zum neu aufkommenden Forschungsfeld der Photopharmakologie reichen. Trotz der erfolgreichen Anwendung *in vitro* ist eine Anwendung *in vivo* durch den notwendigen Einsatz von UV-Licht, das DNA und Zellgewebe schädigt, stark eingeschränkt. Darüber hinaus sind erhöhte Bestrahlungstemperaturen und eine Vielzahl von Modifikationen in DNA-Strängen notwendig um eine effiziente Duplex-Dissoziation zu erreichen. Zur Lösung dieser Probleme wurde D-Threoninol durch andere Diol-Linker ersetzt oder Azobenzol in unterschiedlichen Mustern zur Optimierung der photophysikalischen Eigenschaften substituiert. Bisher konnten nur wenige dieser Einschränkungen durch die Optimierung von Azobenzolen beseitigt werden.

Jüngste Fortschritte brachten eine Reihe substituierter Azobenzol-Moleküle mit Heteroatomen oder funktionellen Gruppen in allen vier *ortho*-Positionen an beiden Benzolringen hervor. Dieses Substitutionsmuster führt zu einer signifikanten Rotverschiebung der Absorptionswellenlängen und einer Erhöhung der thermischen Stabilität des *cis*-Zustands. Auch der Austausch eines Benzolrings durch einen heterozyklischen Ring wie bei Arylazopyra-

zolen führt zu nahezu quantitativen Schalteffizienzen und thermischen Stabilitäten des *cis*-Zustands von bis zu drei Jahren. Diese neu beschriebenen Moleküle könnten durch verbesserte Absorptionswellenlängen, thermischen Stabilitäten des *cis*-Zustands und Schalteffizienzen zu einer Verbesserung der Photokontrolle über die DNA-Duplex-Hybridisierung führen. Untersuchungen zum Einbau dieser neuen Moleküle in DNA-Stränge und -Duplexe sind bisher nicht bekannt.

Die folgende Dissertation greift das Thema der Verbesserung der photokontrollierten DNA Duplexhybridisierung auf. Basierend auf den publizierten Azobenzolen und Arylazopyrazolen wurde eine systematische Studie zur Optimierung der photophysikalischen Eigenschaften D-Threoninol-gekoppelter Photochrome und die Übertragung auf modifizierte DNA-Stränge angefertigt. Eine Vorauswahl synthetisch zugänglicher D-Threoninol-gebundener Photochrome wurde mittels UV/Vis-Spektroskopie nach Bestrahlung mit hochenergetischen LEDs untersucht, um empirisch die maximalen Absorptionswellenlängen zu ermitteln. Mittels reversed-phase HPLC und UV/Vis-Spektroskopie wurden die maximalen Schalteffizienzen und thermischen Stabilitäten der *cis*-Zustände ermittelt. Nachfolgende DMT-Schützung und Phosphitylierung der D-Threoninol-gebundenen Photochrome ermöglichte den Einbau in DNA-Stränge mittels DNA-Festphasen-Synthese. Die Übertragung der verbesserten photophysikalischen Eigenschaften auf DNA-Stränge und DNA-Duplexe wurde durch einen Vergleich von systematisch modifizierten DNA-Strängen mit den neu synthetisierten Molekülen durch weitere reversed-phase HPLC-Quantifizierungen und UV/Vis-Spektroskopie erreicht. Schmelzkurven modifizierter Duplexe zeigten eine Verbesserung der Schalteffizienz bei einem geringeren Verbrauch an Photoschaltern im Vergleich mit den bereits bekannten Molekülen.

Die Schalteffizienz und Praktikabilität der Moleküle wurde darüber hinaus durch den Einbau von Arylazopyzolen in komplexe DNA-Systeme gezeigt. Ein doppelsträngiges DNA-Catenan wurde für die Untersuchung kohärenter und unabhängiger Schalteigenschaften unterschiedlich modifizierter release-Oligomere mit verschiedenen Modifikationen entworfen und assembliert. Dabei wurde nicht nur das Catenan-System zur Bestimmung der Eigenschaften benutzt, sondern auch seine einzelnen Bauteile zur Analyse kohärenter Schalteigenschaften.

Neben der Entwicklung neuer Photochrome wurden zeitgleich Anwendungen in der Nanotechnologie entwickelt. Ein Lipid-basiertes selbst-assemblierendes Mizellen-Nanocarrier-System für den Transport und die Freisetzung von Doxorubicin in Krebszellen entwickelt. Das System besteht aus einer Aptamer-basierten Einheit, die an Zellrezeptoren bindet, und einem photoschaltbaren Doxorubicin-Freilassungs-Mechanismus. Die erfolgreiche Zellaufnahme und die Freisetzung von Doxorubicin wurde *in vitro* in H1838 Lungenkrebs-Zellen demonstriert.

2. Theoretical background

2.1 Radiation and matter

All matter exists in defined, discrete energetic ground and excited states. As a result from quantum theory, the energy difference between all energetic states is also quantised, i.e. the energetic differences between these states are quantised and a multiple of the Planck's constant h. For electronic transitions, Einstein described this relation by the equation:[19-20]

$$\Delta E = h \cdot \vartheta = \frac{h \cdot c}{\lambda} \quad \textbf{(1)}$$

Here, ΔE is the potential energy difference between two energetic states of an electron, h constitutes Planck's-constant h = 6,63·10^{-34} Js, ν the electron's frequency, λ the electron's wavelength and c the velocity of light in vacuum. The quantisation of all energetic states implies that every system can only absorb and emit radiation with distinct energy corresponding to the difference between the two states, or, as described by Einstein's equation, with light of distinct wavelengths.[19-20]

Radiation can be described as the migration of electromagnetic waves throug vacuum or light-transmissive media, while one can distinguish between ionizing and non-ionizing radiation.[21] When high energy radiation (λ < 100 nm) interacts with matter, the radiation is reflected by the electronic structure of an atom or molecule. If the energy conversion is sufficient enough to remove an electron completely from the nucleus, the atom is ionized and leaves the positively charged nucleus behind. In case of non-ionizing radiation, the molecular rotation, vibration or electronic structure are excited. Radiation in the range of ultraviolet light (100-380 nm), visible light (380-750 nm) or infrared light (> 750 nm) is absorbed by the electron shell and promotes electrons to higher energetic states without complete separation from the core where the absorbed wavelength has the same energy corresponding to the difference between the ground and excited state.[22-23]

Infrared radiation also excites the vibrational and rotational modes of molecules. The absorption of radiation by matter is best described by an exponential intensity decay, known as the Lambert-Beer-law (equation **2**), which correlates the attenuation of light when passing through matter of a distinct composition.[24-25] The measured light absorbance is given by the equation:

$$\frac{I}{I_0} = e^{-\varepsilon c d} \quad \textbf{(2)}$$

where I and I_0 are the intensities of the initial and detected radiation, c the concentration of the investigated liquid medium, d the thickness of the sample and ε the extinction coefficient of the medium. Absorbance measurements of molecules in solution require subtraction of the pure solvent, a blank sample, to achieve a precise absorbance measurement.

The extinction coefficient resembles a relative value and is a characteristic material constant. According to the Franck-Condon-Principle, electrons, when excited, always possess the highest migration probability into excited states that are most similar to the electronic ground state of the system (fig. 1).[26-29] During this transition, the movement of the much lighter electron is enormously faster than the movement of the nucleus. Approximately, the nuclear position can be considered fixed, which is also called the Born-Oppenheimer-Approximation.[31-32]

Excited electrons can undergo different relaxation processes. The direct radiative relaxation of an electron back into the ground state leads to emission of radiation.[33-34] Beyond the direct relaxation, an electron can undergo multiple depletion steps while falling back to the ground state. All multiple state relaxation processes are lower in energy than the direct relaxation thus leading to emission of radiation with lower energy, the so-called Stokes-shift. Also thermal relaxation processes and energy transfer reactions are possible in deactivation processes.

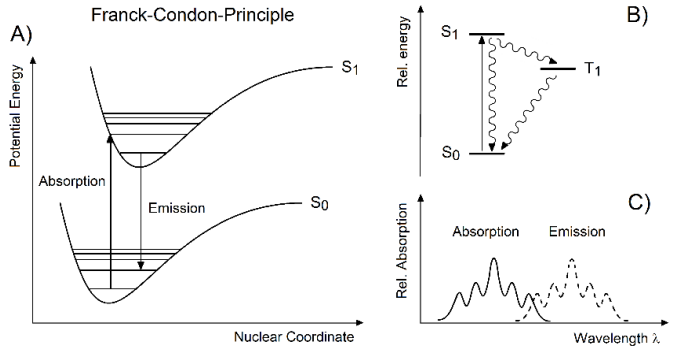

Fig. 1: A) Electronic excitation and relaxation processes according to the Franck-Condon-Principle for a diatomic molecule occur with the highest probability into states which are most similar to the groud state. B) One and two step electronic relaxation processes after excitation from state S_0 to state S_1. C) Absorption and emission wavelengths for electronic excitation and consecutive relaxation. The emission is lower in energy than the excitation, leading to higher emission wavelengths The figure shows an adapted version of the figures found in reference[30].

Resulting from a statistical energy content distribution for a large number of photons, not all absorbed photons contain sufficient energy higher than the activation energy of a process, thus not leading to the desired reaction. The fraction of absorbed photons inducing the reaction compared to all absorbed photons is defined as the quantum yield.[35-36] The quantum yield usually is a number between 0 and 1. In cases where absorbed photons induce chain reactions, the quantum yield can also reach values above 1. Disruption of the molecular structure upon absorption of light leads to photobleaching, thus preventing a molecule to further absorb or emit radiation with the initial intensity.[37]

2.2 Azobenzene chromophores

2.2.1 Photochromism and photochromic molecules

Photoinduced chemical isomerization of electronically excited states is well known for a variety of chemical species. Usually the excitation of electrons involving a C=C or an N=N double bond leads to formation of a single bond which permits a rotatory motion and leads to a change in stereo conformation. Photochromic molecules are capable of reversibly converting their structure from one conformation into another upon irradiation with two different wavelengths of light, wheras both states possess different characteristic absorption spectra.[38-39] Most photochromic reactions are of unimolecular nature, where only electromagnetic radiation and the molecule or system itself are involved. In bimolecular photochromic reactions, the reversible process depends on two chemical species, either the same or different molecules, forming an addition product or two new products. All photochromic processes are reversible, whereas the reversible back-transformation can occur either thermally (thermoreversible systems) or by radiation of a different wavelength (photoreversible systems). Some photochromic systems can undergo a back-transformation *via* both pathways.

The system's change in conformation can result from the E->Z-isomerization of a double bond as reported for stilbenes **(1)**,[40-41] azobenzenes **(2)**[42-45] or hemithioindigos **(3)**[46-48] or the electrocyclic ring-opening and ring-closure reaction of diarylethenes **(4)**,[49-51] fulgides **(5)**[52-54] and spiropyrans **(6)**[55-56] (fig. 2). Further conformational changes can result from the reversible ring-closure reaction of dienes and dienophiles as in Diels-Alder cycloadditions[57] or the reversible donor-acceptor adduct formation and dissociation as in case of Stenhouse adducts.[58-59] All these types of photochromic molecules can reversibly be transformed from one conformation into the other upon irradiation with two different wavelengths of light.

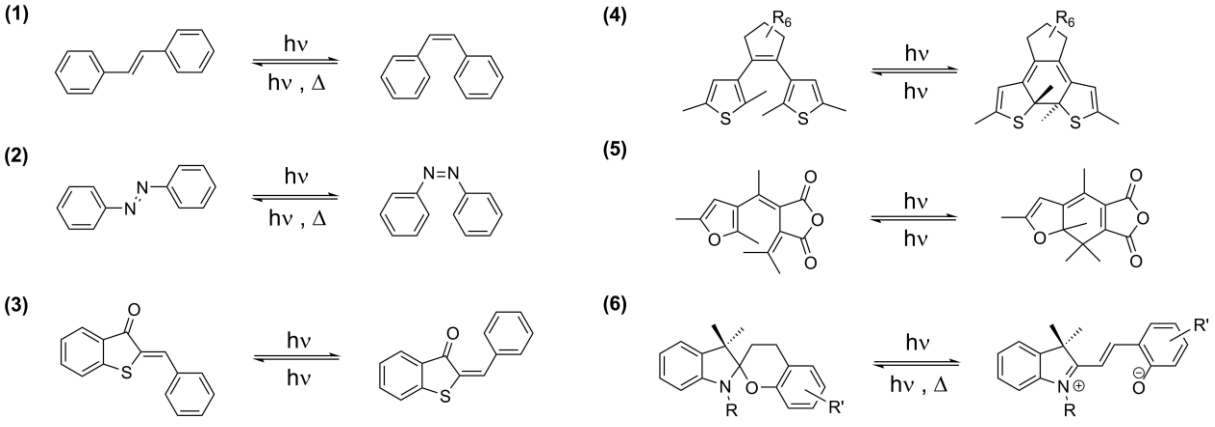

Fig. 2: Different classes of photochromic molecules. In stilbenes **(1)**, azobenzenes **(2)** and hemithioindigos **(3)** a reversible E->Z-isomerization can occur on a double bond, in diarylethenes **(4)**, fulgides **(5)** and spiropyrans **(6)** an isomerization can occur *via* electrocyclic ring opening and closing reactions.

2.2.2 The *cis* and *trans* state of azobenzene

Azobenzene is one of the best studied photochromic molecules and exists in two different conformations.[60-62] The molecular structure is composed of two phenyl rings separated by an N=N double bond. In *trans* conformation both phenyl rings are aligned in a coplanar arrangement and the dipole moment is nearly zero while in *cis* conformation the molecule has a nonplanar, sterically more challenging structure with one ring bent out of plane and a dipole moment of 3 Debye.[63-64] A reversible transformation between both states can be achieved by irradiation with UV or visible light as first reported by G. S. Hartley in 1937.[65-66] Regeneration of the *trans* isomer from the *cis* isomer is also obtained by heating while the *cis* isomer can only be formed *via* UV irradiation (fig. 3).

Fig. 3: Structural comparison of Azobenzene (A) and Stilbene (B): Azobenzene contains a central N=N double bond while stilbene contains a central ethylene bridge. Azobenzene isomerisation from *trans* to *cis* occurs upon irradiation with UV light and back relaxation by heating or visible light irradiation.

The planar *trans* conformation is 50 kJ/mol more stable than the sterically more challenging *cis* conformation.[67-68] In comparison to stilbene, the N=N double bond is less reactive to hydrolysis and cycloaddition reactions than the C=C double bond. The UV/Vis spectrum of *trans* azobenzene shows two different absorption maxima.[69-70] A high intensity signal at 350 nm is characteristic for the transition of a π-electron within the N=N double bond into an antibonding π-orbital (fig. 4). A broader absorption band with lower intensity at 430 nm shows

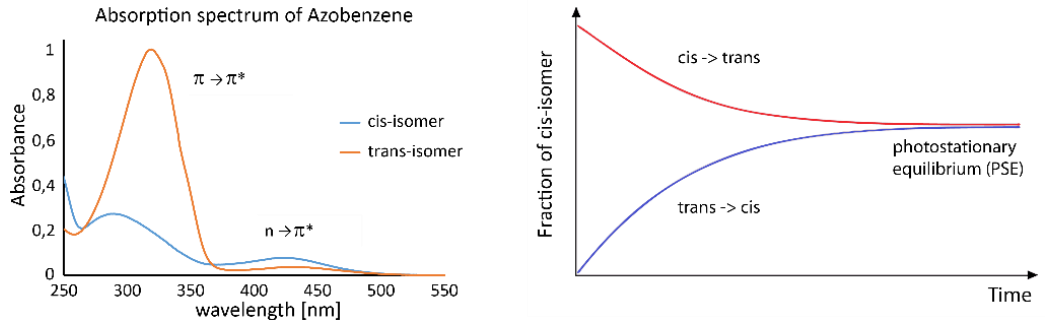

Fig. 4: Absorption spectra of *trans* and *cis* azobenzene (left). Azobenzene irradiation with light of a distinct wavelength results in the formation of a wavelength-dependent photostationary state (PSS), also called photostationary equilibrium (PSE), over time with a distinct composition of *cis* and *trans* isomer ratio (right). The figure shows an adapted version of the figure found in reference[70].

the n->π* transition which is symmetry forbidden but happens anyhow due to the loss of aromaticity and the increase in dipole-moment upon formation of the *cis* state. Experiments showed that the isomerization rate involving visible light irradiation is twice as high compared to an isomerization upon UV light irradiation. Overlay of the different absorption spectra of *trans* and *cis* azobenzene reveals a separation of both absorption maxima. Irradiation with light of a distinct wavelength induces the formation of a photostationary state (PSS).[70] The fractions of *cis* and *trans* isomer are characteristic for every irradiation wavelength and depend on the reaction rate of *trans* to *cis* isomerization compared to the *cis* to *trans* isomerization. The equilibrium formed upon irradiation directly depends on the extent of wavelength overlap of both overlaid absorption spectra. Only a complete separation of absorption maxima for both electronic transitions or the missing absorption at a distinct wavelength for one isomerization process permits the quantitative formation of a single isomer.

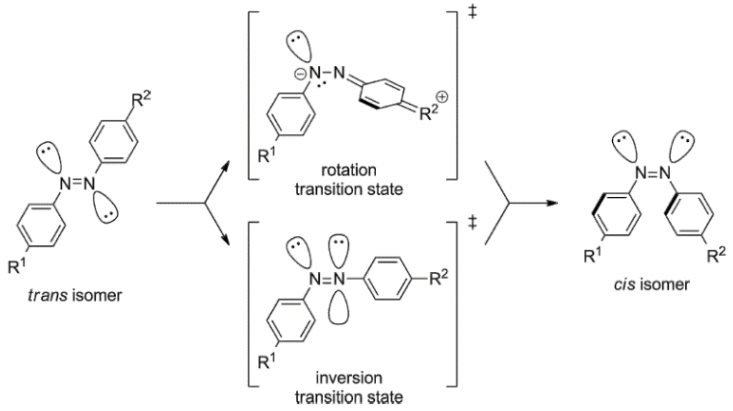

Fig. 5: Two different isomerization pathways have been reported for azobenzene's conformational change from *trans* to *cis* and vice versa: the rotation and inversion mechanism. While in the rotation mechanism the isomerization occurs *via* an N-N single bond (upper pathway), the inversion mechanism takes place around a planar transition state (lower pathway). The figure shows an adapted version of the figure found in reference**[71].**

Theoretical and spectroscopic studies revealed two different isomerization pathways when azobenzene is isomerized from *trans* to *cis* conformation and vice versa. These two mechanisms are the rotation and the inversion mechanism (fig. 5).**[71-72]** Following the rotation mechanism, a π-electron located in the N=N double bond is promoted into an antibonding π-orbital, thus allowing a rotation around the remaining N-N single bond. The inversion mechanism on the other hand involves the excitation of a non-binding lone pair electron located at one of the nitrogen atoms, leading to a formal rehybridization of the N=N sp^2 orbital to an sp^1 orbital without changing the double bond character between both nitrogens (fig. 5). The rotational mechanism follows a molecular phenyl ring motion out of plane while the inversion

mechanism occurs with both coplanar rings in plane. Several studies reported both isomerization mechanisms for both isomerization directions and revealed a strong dependency on the nature of substituents and substitution patterns on both phenyl rings.[71-72] While thermal relaxation from *cis* to *trans* mostly occurs *via* the inversion mechanism, photoinduced isomerization from *trans* to *cis* can undergo both mechanisms whereby the inversion mechanism is the dominating isomerization pathway.[72-76] Nevertheless, controversial discussions are still ongoing in literature, indicating evidence of both isomerization pathways in differently substituted azobenzenes.

2.2.3 Synthesis of azobenzene and azobenzene derivatives

Azobenzene and its derivatives can be obtained *via* six general synthesis pathways, all strongly depending on the chemical nature of the starting materials and the desired substitution pattern within the azobenzene product.[77-78] The main synthetic routes are depicted in fig. 6, which are:

1) Oxidative dimerization of anilines[79-82]

2) Reductive dimerization of nitroaromatics[83-85]

3) Azo coupling *via* aromatic diazonium salts[86-88]

4) Coupling of aromatic nitroso derivatives with anilines (Mills reaction)[89-91]

5) Oxidation of aromatic hydrazo compounds[92-93]

6) Reduction of azoxybenzenes[94-95]

Depending on the nature of the desired product, azo coupling reactions can be separated into two main groups: homo coupling reactions, leading to symmetrically substituted azobenzenes, and hetero coupling reactions, resulting in azobenzenes with two differently substituted phenyl rings. Oxidative dimerization of anilines **(1)** and reductive dimerization of nitroaromatics **(2)** result in symmetrically substituted azobenzenes.

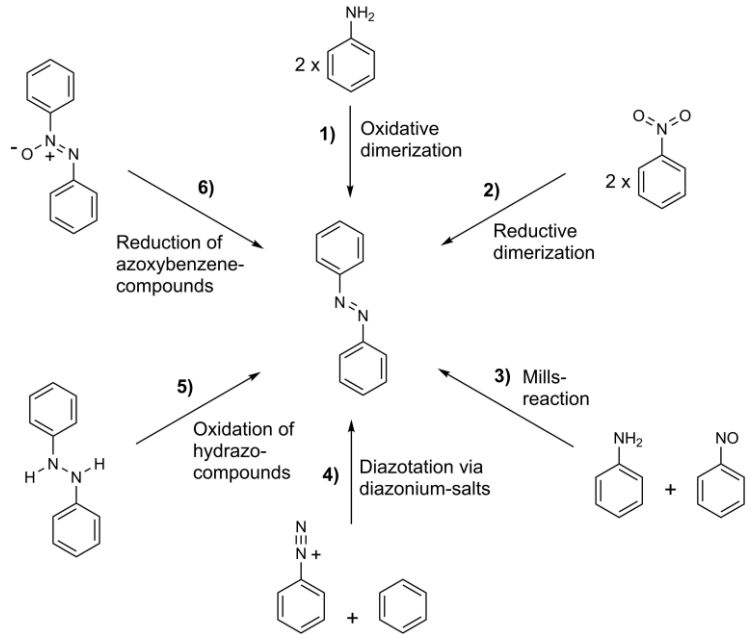

Fig. 6: The following main synthetic pathways have been reported for the formation of azobenzene molecules: 1) Oxidative dimerization using strong oxidation agents.[79-82] 2) Reductive dimerization of two nitro compounds with strong reduction agents.[83-85] 3) Mills reaction of anilines and nitroso compounds involving glacial acetic acid.[86-88] 4) Diazotation *via* formation of a diazonium salt and consecutive coupling to aromatic systems.[89-91] 5) Oxidation of hydrazo compounds using strong oxidation agents.[92-93] 6) Reduction of azoxybenzenes with strong reduction agents.[94-95] All reaction pathways lead to symmetrically or non-symmetrically substituted azobenzene products.

In case of oxidative dimerization of anilines **(1)**, a variety of strong oxidation agents like MnO_2[80], $KMnO_4$[81], H_3BO_3[82] as well as further organic and inorganic peroxides are available to form azobenzenes in high yields. Commonly, the oxidation agent and anilines are heated in organic solvents to achieve high yields. A recently published oxidation reaction involving two differently substituted anilines and highly reactive t-BuOCl at 0 °C and below achieved high reaction yields and selectivity for hetero coupling products.[98]

Reductive dimerization of nitroaromatics **(2)** involving zinc powder or hydrogen transfer reagents in catalytic amounts also lead to symmetrically substituted azobenzenes in yields similar to those of oxidative dimerizations.[94-95] The classic azo coupling *via* diazotation of aromatic amines[86-88] **(3)** and the Mills reaction[89-91] **(4)** represent two methods for the synthesis of azobenzenes containing differently substituted phenyl moieties. Both reactions require the preparation of synthetic precursors, an aromatic nitroso compound in case of Mills type reactions or a diazonium cation for a diazotation reaction. In both cases, azobenzenes with differently substituted phenyl residues are formed while minimizing the formation of undesired azobenzene side products.

Diazotation of aromatic amines by means of $NaNO_2$ or HNO_2 in combination with acids or bases leads to diazonium cations, which can be azo-coupled to form differently substituted aromatic or heteroaromatic residues **(3)**.[86-88] This classic azo coupling strongly depends on the electronic properties of the substituents and has to be performed at 0-5 °C to avoid a thermal decomposition of the unstable diazonium cation. Resulting from the weak electrophilic nature of the diazonium cation, the reaction only takes place in presence of strong +M-substituents. Despite all these limitations, most azo compounds are synthesized *via* this pathway since reaction yields and selective formation of the product is very high while the conversion time is rather low. Mills reactions **(4)** are carried out in glacial acetic acid at room temperature or elevated temperatures up to 60 °C.[91] These rather mild conditions foster the formation of azobenzenes with reactive or unstable substituents which are usually not accessible under harsh reaction conditions.

Two further synthetic pathways for the synthesis of azobenzenes have been reported, the oxidation of hydrazobenzenes[92-93] **(5)** and the reduction of azoxybenzenes[94-95] **(6).** In both cases, the pre-formed N-N single bond requires oxidation or reduction to form the N=N double bond (fig. 6). Hydrazobenzenes are oxidised under mild oxidation conditions involving agents like H_2O_2, O_2, MnO_2 or metal complexes to form the N=N azo bridge. Reduction of azoxybenzenes affords $LiAlH_4$, phosphines or reducing metals and metal complexes to yield azobenzenes. The use of H_2SO_4 or further strong acids leads to a transformation of azoxybenzenes into *para*-hydroxyazobenzenes by a Wallach rearrangement.[96]

A variety of further azobenzene syntheses are available in literature. More examples to be highlighted are the condensation of nitroaromatics with anilines under basic conditions,[97-99] triazene rearrangements,[100] metal-catalyzed reactions of arylhydrazines[101] and ring opening reactions.[102] Most of these pathways require the synthesis of complex precursors or harsh reaction conditions and are not suitable for synthesis of azobenzenes containing reactive functional groups.

2.2.4 Substituted azobezenes – optical tuning of photophysical properties

Hermann Rau first described differently substituted azobenzenes and classified these into three different categories: azobenzenes, aminoazobenzenes and pseudostilbenes.[103-104] All three classes of azobenzenes are determined by the nature and positions of substituents on both phenyl rings (fig. 7).

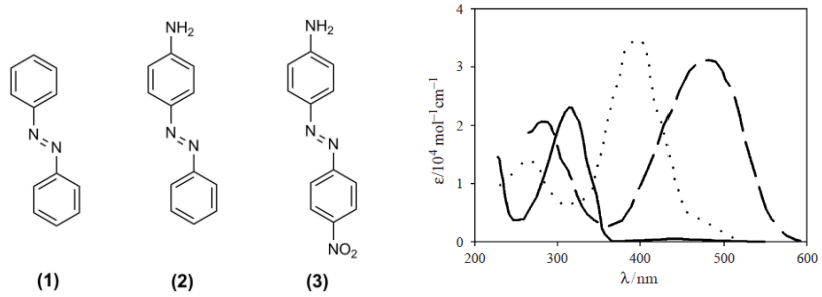

Fig. 7: UV/Vis absorption spectra of azobenzene **(1)**, aminoazobenzene **(2)** and pseudostilbenes**(3)** molecules. Azobenzenes of the azobenzene type (solid line) exhibit a high intensity π-π* transition band and a small n-π* transition band. Azobenzenes of the aminoazobenzene type (dotted line) and pseudostilbene type (dashed line) have highly red-shifted absorption maxima and strongly overlapping bands in visible light region. Each absorption intensity in visible light is more intense compared to unmodified azobenzene. The figure shows an adapted version of the figure found in reference[105].

Substitution of hydrogens on one or both phenyl rings alters the relative orbital energies of the highest occupied molecular orbital (HOMO) and the lowest unoccupied molecular orbital (LUMO) within the central N=N double bond, leading to red-shifted absorption bands in the corresponding UV/Vis spectra.[106-107] Electronic transitions during azobenzene isomerization

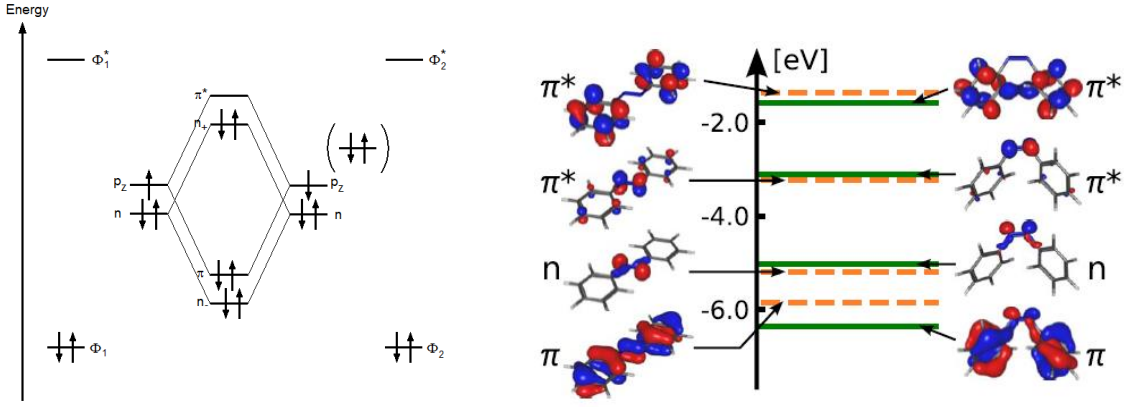

Fig. 8: Molecular orbital diagram of the N=N double bond in azobenzene (left).[108] The central binding π-orbital is located between both nitrogen atoms wheras the π*-orbitals are distributed over both rings (right).[109] Relative orbital energies of the N=N-HOMO and LUMO are given for azobenzene's *trans* and *cis* state. The figure shows an adapted version of the figures found in references[108] and [109].

always occur from the HOMO orbital into a LUMO orbital, hereby determining the energy of the absorbed photon as the energy difference between both orbitals (fig. 8).

Electron donating substituents increase the relative orbital energy of the HOMO orbital and electron withdrawing substituents decrease the relative energy of the LUMO orbital. In both cases, substitution results in a decrease in energy difference between both orbitals and consequentially a red-shift of absorption bands. Native azobenzene containing no substitutents on both phenyl moieties besides hydrogen is known as azobenzene type and serves as a reference when discussing other azobenzene types.[45] According to the classification reported by H. Rau, there are two further types of azobenzenes: aminoazobenzenes and pseudostilbenes. Varying substitution patterns in both azobenzene classes severely affect the native absorption maxima, isomerization rates and thermal half-life of the *cis* state.

Aminoazobenzenes contain strong electron donating residues in *para* position on either one or both phenyl rings.[110] The increased π-electron density in the π-system leads to an increased relative energy of the HOMO orbital as observed in a strong red-shift of both absorption maxima in UV/Vis spectra. Furthermore, the n->π* transition in the visible light region has an increased intensity accompanied by a higher overlap of both n->π*- and π->π*-transitions. The thermal half-life of the *cis* state is significantly decreased by +M *para* substituents, leading to a half-life within a range of minutes to seconds due to the decrease in relative energy difference between HOMO and LUMO.

Azobenzenes of the pseudostilbene type exhibit a strong electron donating and strong electron withdrawing moiety on both opposite phenyl *para* positions.[111] Pseudostilbenes are characterized by a strong red-shift of both n->π*- and π->π*-transitions in absorption spectra which can even change their relative positions towards each other. Isomerization and thermal back-relaxation in pseudostilbenes occur within seconds. Protonation of the N=N double bond through strong acids or complexation by Lewis acids further increases the relative energy of the n->π*-transition resulting in an improved thermal stability from a range of seconds to several muinutes.[112] Spectral emission of azobenzenes is generally very low for all three azobenzene types since the absorbed energy is converted into molecular motion, whereby pseudostilbenes retain light and fluorescence emission properties.

Taking the electronic properties for all substituents in different positions on both phenyl residues into account permits a prediction of relative orbital energies of HOMO and LUMO and consequentially permits a prediction of inherited photophysical properties.[113] Consecutively, the sophisticated introduction of specific substituents fosters the design of azobenzene photoswitches with predefined photophysical properties for versatile purposes. Three general properties characterize an efficient photoswitch is respect to biological and *in vivo* applications:

First, a significant separation of absorption bands must be achieved to facilitate individual addressing of both states and maintain high conversion efficiencies between the two states. Second, maintaining a high thermal stability of the *cis* state enhances the utility timespan for biological applications. Last but not least, a shift of absorption maxima further into the red range of visible light permits a higher penetration depth and decreased negative side effects when azobenzenes are introduced into biological systems. An ideal photoswitch exhibits quantitative switching efficiencies in both isomerization directions whereby both states can be addressed individually in visible light range while maintaining a high thermal stability of the *cis* state.

2.2.5 Recent advances in azobenzene photochemistry

The challenge of tuning azobenzene's photophysical properties emerged a variety of differently substituted azobenzene molecules. In 2009, the working group of F. Temps developed a bridged azobenzene which connects both opposite phenyl rings in *ortho* position by an additional ethylene bridge.[114-116] This bridged azobenzene exhibits strongly red-shifted absorption bands and allows efficient isomerization from *trans* to *cis* and vice versa both by use of visible light irradiation (fig. 9).

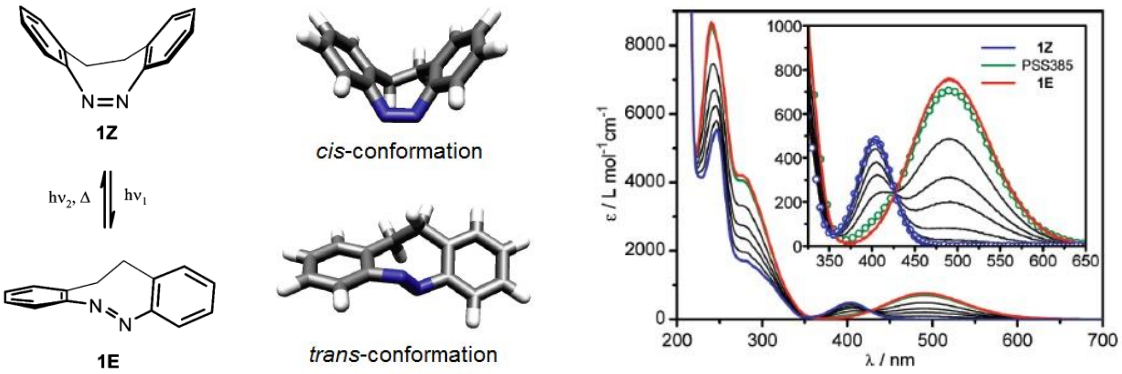

Fig. 9: An *ortho* ethylene bridged azobenzene has been reported to have high reversible isomerization efficiencies between the *trans* and *cis* state by use of visible light irradiation. The molecule is shown in *Z*- and *E*-conformation (left) and the predicted structural conformations (middle). UV/Vis spectra of the *trans* and *cis* conformation reveal highly separated n->π* absorption bands in visile light range (right). The figure shows an adapted version of the figures found in reference[114].

The *ortho* ethylene bridge leads to a decrease in relative orbital energy for both HOMO and LUMO, resulting in a strong separation of both n->π* absorption bands in visible light range. An efficient conversion between *trans* and *cis* could be achieved with 92 % *cis* at 385 nm irradiation and near-quantitative isomerization to *trans* at 530 nm irradiation with a thermal half-life of 4.5 hours at 28.5 °C.

A similar effect could be achieved by introduction of a Lewis-acidic BF_2 moieties in *ortho*

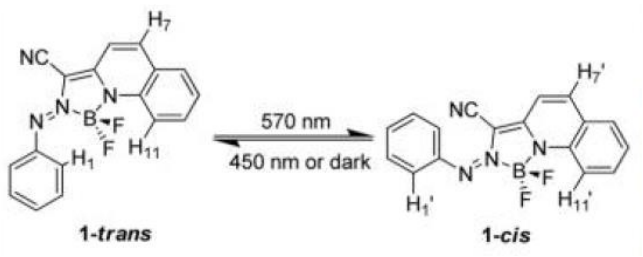

Fig. 10: *Trans* to *cis* isomerization of a BF_2-coordinated azobenzene leads to high switching efficiencies under visible light irradiation and represents one of the first *cis* convertable azobenzene molecules in visible light range. Coordination of the N=N double bond through the lewis-acidic BF_3 moiety strongly red-shifts the response wavelengths. The figure shows an adapted version of the figure found in reference[118].

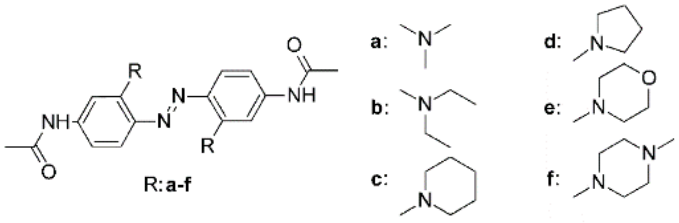

Fig. 11: Azobenzenes carrying amino substituents in *ortho* and *para* position at the same time have been reported as functional tools for biological applications *in vitro* and *in vivo*. This substitution oattern also leads to red-shifted response wavelengths, facilitating applications *in vivo*. The figure shows an adapted version of the figure found in reference[122].

position of azobenzene coordinating the central N=N double bond and thus lowering the relative n->π*-transition energy in both isomers (fig. 10).[117-118] The coordination permits electronic transitions of nonbonding π-electrons into π*-orbitals and fosters a reversible photocontrol in visible light range. Irradiation at 570 nm leads to 97% formation of the *cis* isomer and irradiation at 450 nm forms a PSS with 80% *trans* isomer. Thermal half-life of the *cis* state is reduced to 12.5 hours at room temperature.

Aminoazobenzenes containing two amino moieties in *para* position gained lots of attention since their large red-shift of absorption wavelengths was discovered, making these molecules ideal candidates for applications *in vitro* and *in vivo*.[119-121] As described before, the visible light switching properties are accompanied by the drawback of decreased thermal half-lifes of the *cis* state down to a millisecond range. To circumvent this issue, a series of azobenzenes with amino residues on both *ortho* and *para* positions has been published in order to utilize the red-shift of response wavelengths while maintaining a practicable half-life of the *cis* state by sterically challenging substituents in *ortho* position (fig. 11).

Introduction of two amino moieties with different alkyl substituents in *ortho* position on both opposite rings led to a significant red-shift of absorption wavelengths while increasing the thermal half-life from milliseconds to seconds.[122-125] Still, the decreased thermal stability is out of range for a variety of applications reqiring long half-lives. Another major drawback of *ortho* aminoazobenzenes is the occurrence of photobleaching over time upon exposure to ambient light.

As demonstrated by *ortho* aminoazobenzenes, substitution of azobenzene in *ortho* position leads to a red-shift of response wavelengths and an increased thermal stability. Further substitution with hetero atoms in all four *ortho* positions led to a series of azobenzenes with extraordinary photophysical properties.[126-127] The working group of G. A. Woolley reported red-shifted azobenzenes containing four hetero atoms or functional groups in all four *ortho* positions.[128] Introduction of methoxy moieties in all four *ortho* positions results in a distortion of the planar *trans* conformation and results in a blue-shift of the π->π*-transition as well as a

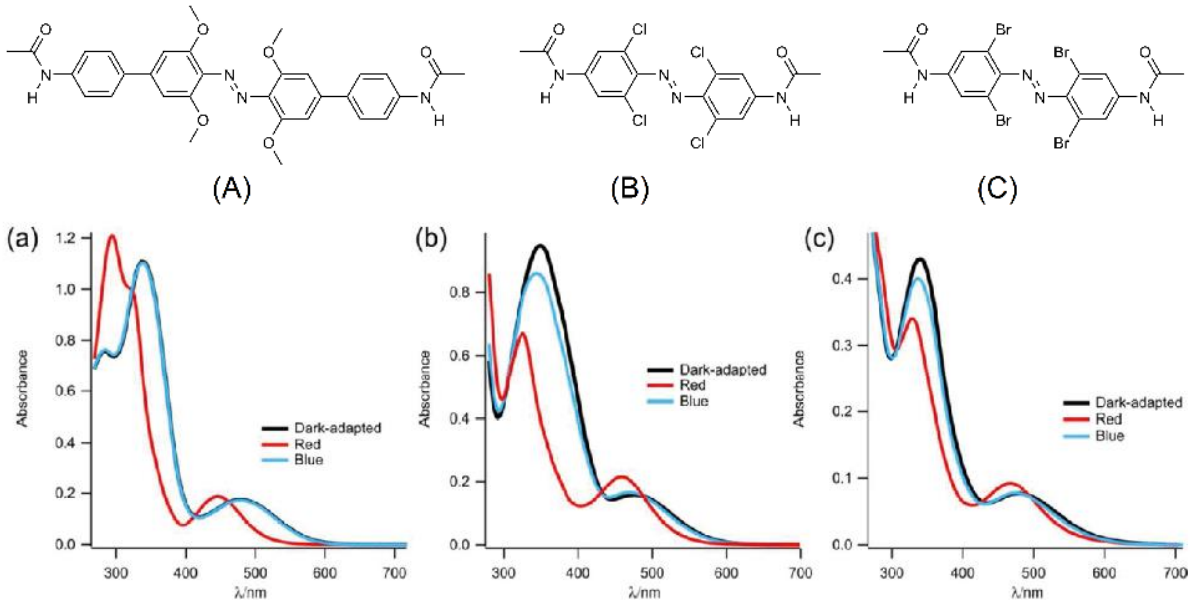

Fig. 12: Azobenzenes carrying four *ortho* methoxy (A), chloro (B), or bromo substituents (C) result in strongly red-shifted absorption bands and a separation of both n->π* transitions in visible light range. The substitution pattern results in near-quantitative isomerization efficiencies as well as highly stable *cis* states. The figure shows an adapted version of the figures found in reference[129].

red-shift of the n->π*-transition (fig. 12). *Trans* to *cis* isomerization could be achieved in near quantitative yields using red light and efficient back-switching was performed by heating or blue light. The *cis* state remains stable for more than two days at room temperature, lying in the range of unsubstituted azobenzene. Unfortunately, the molecule showed reduction in presence of glutathione, which therefore limits its applicability *in vivo*.

Besides *ortho* methoxy azobenzenes, a series of azobenzenes containing four chlorine or bromine atoms[129] as well as four methylthio residues in *ortho* position[130] were developed, all showing *cis* isomerization under red light irradiation.

The properties of the tetra *ortho* substitution patterns were generalized by the group of G. A. Woolley as reported by a series of red-shifted azobenzenes with high conversion efficiencies. The use of sterically challenging residues in all four *ortho* positions leads to a distortion of planarity in *trans* conformation, hindering these molecules from being applied in systems with a requirement for a planar *trans* conformation.

Protonation of tetra *ortho* methoxy azobenzenes yielded a protonated azonium ion which could be observed even at pH = 7.5, a neutral pH in which azonium ions usually don't form.[131] The reported azonium ions exhibit a strong *cis* absorption maximum at 600 nm with a thermal half-life of the *cis* state of about 10 seconds, magnitudes higher than previously reported azonium ions. Also, a planar geometry of the protonated *trans* conformation could be proven by DFT calculations.

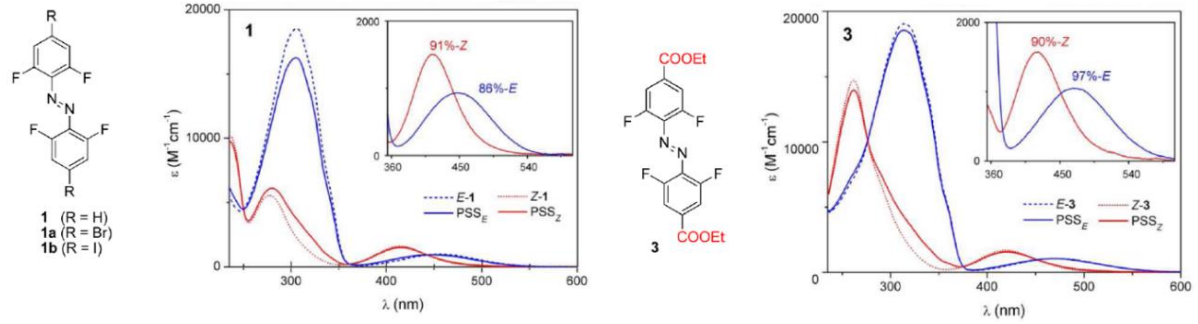

Fig. 13: Tetra *ortho* fluorinated azobenzenes exhibit high conversion efficiencies in visible light range while retaining thermal *cis* stabilities of 300 days at room temperature. Electron withdrawing substituents in all four *ortho* positions lead to a higher separation of n->π*-transitions in visible light range, resulting in almost quantitative isomerization yields upon irradiation with 420 nm and 530 nm light respectively. The figure shows an adapted version of the figure found in reference[132].

One key discovery was reported in 2012 by D. Bléger et al. with tetra *ortho* fluorinated azobenzenes.[132-134] Substituting all four *ortho* hydrogens by fluorine atoms highly red-shifts both the n->π*-transition bands including a significant separation of both absorption bands (fig. 13). The separation leads to an almost quantitative isomerization efficiency between both conformations by irradiation with blue and green light. Compared to methoxy or hetero atom substitution, the four fluorine atoms in *ortho* positions are relatively small and do not distort the planar *trans* conformation. An enormous thermal half-life of the *cis* state is retained with more than 300 days at room temperature. The high thermal stability and the intense shift of response wavelengths into visible light range for both isomers can be attributed to the change in polarity for the whole molecule when isomerizing the thermodynamically more stable *trans* isomer into *cis* conformation. In *trans* conformation all four fluorine atoms are oriented towards the center of the molecule resulting in a low total dipole momentum. In *cis* conformation, the dipole momentum of the molecule changes significantly and leads to the reported shift in absorption bands.

Perfluorinated and perhalogenated azobenzenes with a majority of fluorine atoms have been reported to bend whole crystals irreversibly when irradiated with green light.[135] These merely fluorinated azobenzenes retain a thermal half-life of the *cis* state of 60 days at room temperature in organic solvents. Thermal stability of these highly fluorinated azobenzenes afforded the formation of photoresponsive crystals and measurement of different crystal structures. Another example of interest was published in 2014 by C. E. Weston et al.[136-139] Arylazopyrazoles with five-membered heterocycles containing *ortho* methyl moieties showed high thermal stabilities of the *cis* isomer up to 1000 days at room temperature and a near-quantitative isomerization efficiencies in both directions (fig. 14). The response wavelength for *cis* to *trans* isomerization is strongly red-shifted wheras the reversed isomerization into *cis*

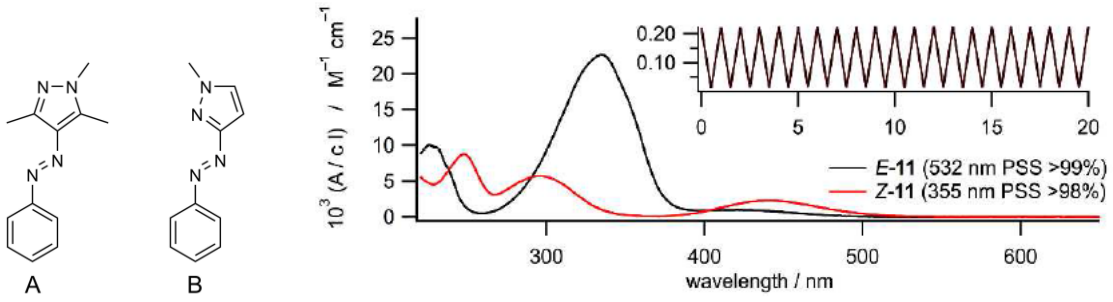

Fig. 14: Arylazopyrazoles carrying one (A) or three (B) methyl moieties on the pyrazole ring prove near-quantitative isomerization efficiencies in both isomerization directions (right). While the thermal stability of (A) exhibits a half-life of 10 hours at room temperature, the half-life of (B) is increased up to 72 days at room temperature throught the additional methyl substitution. The figure is an adapted version of the figure found in reference[136].

conformation requires irradiation with UV light. Interestingly, the reported near-quantitative conversion efficiencies are not caused by a high separation of absorption bands, but by the almost vanishing absorbance intensity of one isomerization direction compared to the response wavelength of the other isomerization direction. These high isomerization efficiencies combined with the retention of high thermal stabilities of the *cis* state makes arylazopyrazoles ideal candidates for long-term *in vitro* applications.

Further tuning of heteroaromatic azo molecules by the working group of M. Fuchter brought up a series of heterocyclic azo photoswitches with different photophysical properties.[140] The number and position of nitrogens in a five-membered ring, which is connected *via* an azo moiety to a phenyl moiety, strongly determines the thermal half-life of the *cis* state as well as the conversion efficiencies of both isomerization directions. Molecules with a T-shaped *cis* state revealed long-lasting half-life times while molecules with twisted moieties in the *cis* state exhibited excellent conversion efficiencies. Selective methyl substitution of the heterocyclic ring led to a molecule with near-quantitative isomerization efficiencies accompanied by a thermal stability of the *cis* state of 72 days at room temperature.

Theoretical studies in this context have shown that sophostocated design of substitution patterns concerning phenyl or heterocyclic moieties in azo compounds facilitates the design and synthesis of photrochromes with predefined photophysical properties for different applications.[141] Beyond all these newly developed photoswitches, a vast variety of more small molecules is available in literature which will not be discussed in this context.[142] For most of these recently developed azobenzenes, the basic constructs and functional groups in *para* position have been reported. Only few of these azobenzenes and arylazopyrazoles have yet been translated into *in vitro* or *in vivo* systems. The main applications encompass chemical reaction control and protein-based applications, but incorporation of photochromes with

improved photophysical properties into oligonucleotides and oligonucleotide applications is yet to be established. Current state of the art for azobenzene modified oligonucleotides and photocontrol of DNA duplexes is further discussed in chapter 2.4.

2.3 Structure, synthesis and functionalization of DNA and RNA

2.3.1 Primary, secondary and tertiary structures of DNA and RNA

The structure of deoxyribonucleic acid (DNA) as the cafrrier of the human genome was first resolved by James Watson and Francis Crick in 1953.[143-144] DNA consists of the four nucleobases adenine (A), guanine (G), cytosine (C) and thymine (T), each connected to the 1'-position of 2'-deoxy-D-ribose (fig. 15). These nucleotides form a one-dimensional macromolecular chain as the primary structure of DNA, where every 3'-end of the nucleotides is connected by a phosphate linkage to the 5'-end of each neighbouring nucleotide. The four nucleobases form two different complementary base pairs by hydrogen bonding following the Watson Crick terminology, where A pairs with T and G pairs with C. In case of ribonucleic aicd (RNA) the sugar-backbone consists of ribose instead of 2'-deoxyribose and uracil (U) replaces thymine (T) to form base pairs with adenine (A).

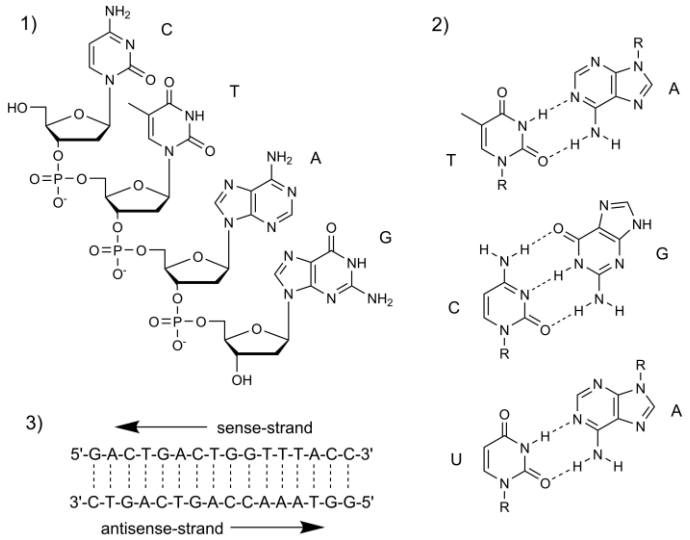

Fig. 15: Primary and secondary structures of DNA and RNA. 1) Formation of a one-dimensional DNA chain through a deoxyribose backbone connected *via* phosphate moieties. 2) Base pairing of DNA and RNA nucleobases adenine (A), guanine (G), cytosine (C), thymine (T) and uracil (U) in the double helix center. 3) Complementary sense and antisense strands following the Watson Crick terminology form the DNA double strand. The figure shows an adapted version of the figure found in reference[145].

Nucleotide base pairing within the one-dimensional primary structure leads to the formation of a stable double helical structure where all nucleobases are paired in the inner part and phosphate backbones point outwards of the helix.[145-147] Contrary to DNA, the nucleophilic 2'-hydroxy residue on D-ribose destabilizes RNA by a possible formation of cyclic intermediates with the phosphate group in presence of strong bases, which results in an intramolecular decomposition of RNA strands into single nucleotides. Formation of three hydrogen bonds in

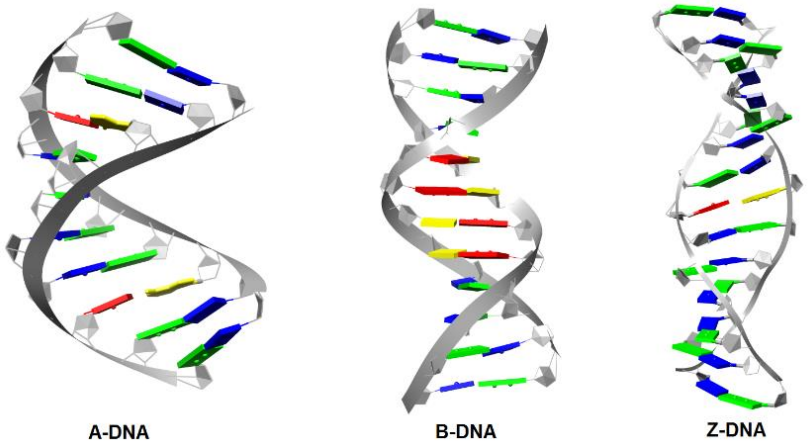

Fig. 16: Crystal structures of A-DNA, B-DNA and Z-DNA showing the three-dimensional structures. The four nucleobases are coloured red (A), yellow (T), green (G) and blue (C), the sugar phosphate backbone is depicted in grey. The structures were adapted from PDB IDs 213D, 1BNA and 3IRQ[144a].

G-C-base pairs leads to a higher stabilization of double-stranded DNA and RNA compared to A-T- and A-U-base pairs. Enhanced stability of G-C base pairs results in an enhanced duplex stability as observed by a higher dissociation temperature compared to A-T-rich sequences, thus determining the overall stability of oligonucleotide duplexes. The DNA double helix exists in three different conformations: A-DNA, B-DNA and Z-DNA (fig. 16). All three conformations are formed under different conditions and differ in the number of base pairs per helix turn, number of successive repeating base pairs and spatial dimensions.

B-DNA is the most stable and biologically most common type of DNA and is formed at low salt concentrations.[148-150] The helix axis is right-handed and all nucleobases are oriented in a vertical line along the helix axis, leading to a strong π-stacking of all base pairs. B-DNA exhibits 10.5 bases per helix turn with a total length of about 35 Å per turn and a helix diameter of 20 Å. In contrast to B-DNA, A-DNA and Z-DNA are formed in high salt concentrations, while all nucleobases are slightly displaced from the central helix axis. A-DNA has a right-handed helical structure similar to B-DNA and Z-DNA constitutes a left-handed helical structure with an opposed chain sense. Also strands with alternating G-C sequences favour the formation of Z-DNA.

Beyond these three main structural motifs, other secondary structural motifs are known for DNA and RNA, for example triple-helices,[151-153] G-quadruplex[154-155] and i-motif structures[156-157] all forming under different conditions. RNA mostly exists in a single-stranded form in biological systems, but is capable of forming two different double-stranded structures. A-RNA is formed at low salt concentrations and A'-RNA at high salt concentrations while both retain homologous structures. Both structures are similar to the A-DNA structure and consist of a right-handed double helix.

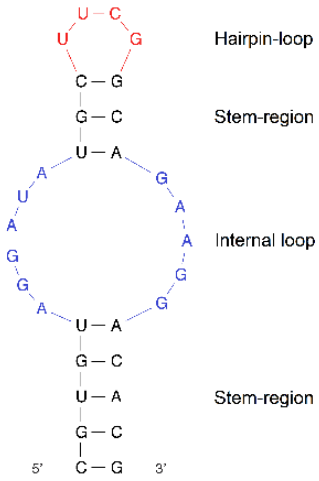

Fig. 17: Structural DNA and RNA motifs. All double-stranded regions (black) within the structure are called stem regions. An internal loop (blue) is a single-stranded region flanked by two double-stranded helices on both loop ends. A hairpin loop (red) is a terminal single-stranded loop which is only connected to one double-stranded region in the DNA strand. Tertiary structural motifs are three-dimensional structures built from secondary structural motifs. In RNA the general tendency for a formation of secondary and tertiary structural motifs is higher than in DNA. The figure shows an adapted version of the figure found in reference[160].

The extraordinary stability of the double helix makes it the most common structural motif in DNA and RNA. Nevertheless, both DNA and RNA show a high tendency of forming further secondary structural motifs. The hierarchy of structural formation highly depends on the local nucleotide sequence, whereby primary structure and nucleotide sequence of single strands determine the formation of secondary structures which further determine formation of tertiary and higher order structures. Important secondary structural motifs beyond the double helix are internal loops and stem loops, also called hairpin loops (fig. 17).[158-160] Internal loops are non-complementary non-hybridizing single-straded regions flanked by double helices, the so-called stem regions. Both single-stranded areas can have different amounts of nucleotides, separating them into symmetric or asymmetric internal loops. A hairpin loop is a terminal single-stranded loop with no self-complementarity, which is limited on 3'- and 5'-end by two strands of the same double helix. Stable loop sizes can vary between 1 and 20 nucleotides per single strand. Internal loops lead to a destabilization of the DNA duplex while hairpin structures have an overall stabilizing effect.

Formation of complex three-dimensional tertiary DNA and RNA structures strongly depends on the local base sequences and therefore the thermodynamic properties of oligonucleotide strands. RNA exhibits a higher tendency of forming complex three-dimensional shapes and structures compared to DNA. A precise prediction of secondary and tertiary DNA and RNA structural motifs was established by complex mathematical methods based on nearest neighbour parameters, i.e. the thermodynamic influence of flanking base pairs for all nucleotides in a specific sequence.[161-167] All mathematical models were improved by salt correction terms and take all possible influences of base stacking into account to approach melting temperature and structural motif prediction as precisely as possible. The complexity of further possible secondary and tertiary structural motifs exceeds a discussion in this context and is therefore not further described in detail.

2.3.2 Synthesis and functionalization of DNA and RNA

A variety of synthetic approaches to achieve artificial oligonucleotides has emerged throughout the last decades.[168-175] Solid supported phosphoramidite synthesis represents the most advanced and current standard method for providing synthetic oligonucleotides with high specificity and coupling yields. The approach utilizes 5'-DMT protected 3'-phosphoramidites in a repeating reaction cycle which consists of four consecutive steps: deprotection, coupling, capping and oxidation. Synthesis of artificial oligonucleotides with predefined sequences and chain lengths up to 100 nucleotides are accessible by this method. An overview over the single reaction steps is depicted below (fig. 18).

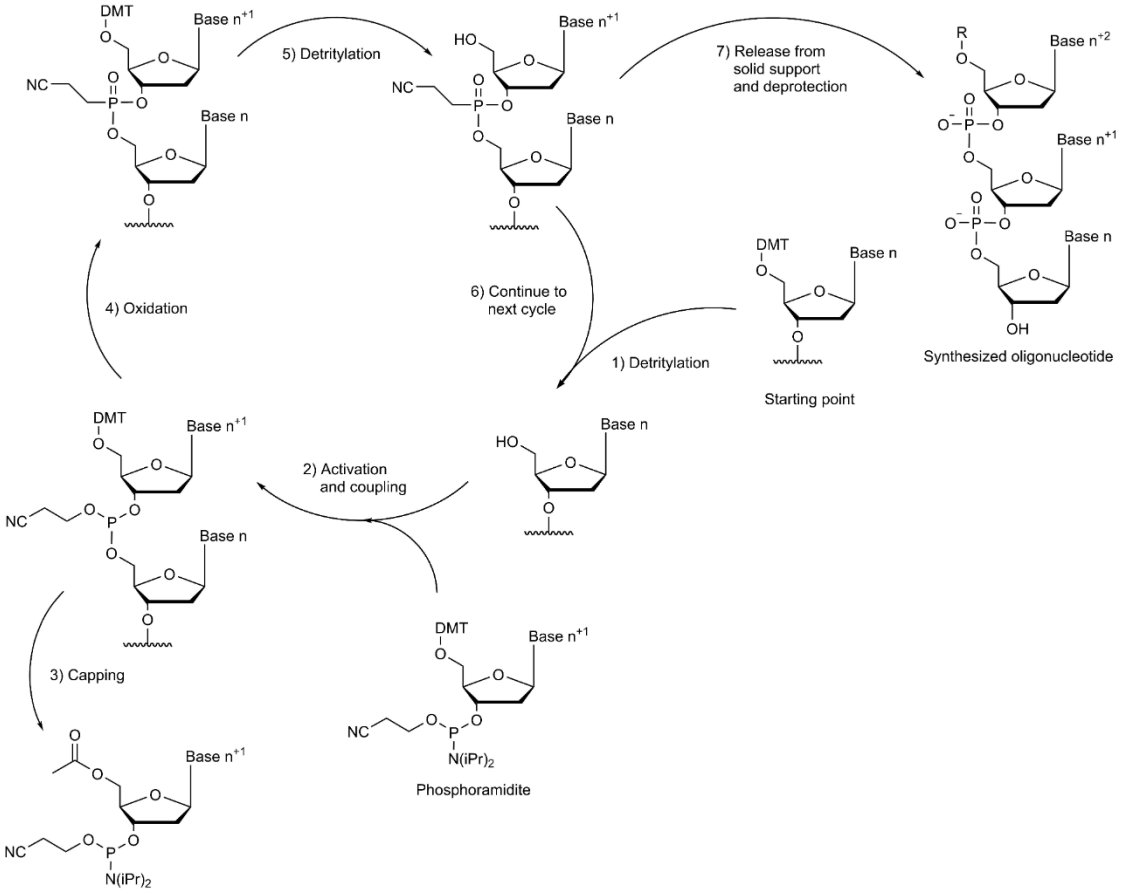

Fig. 18: Phosphoramidite method for the synthesis of oligonucleotides.[169-170] The single steps in each chain elongation cycle are: 1) detritylation of the DMT group, 2) activation and coupling of DMT-protected phosphoramidite, 3) capping of non-reacted fragments, 4) oxidation of phosphorous(III) to phosphorous(V) and 5) detritylation of the terminal 5'-end. After step (5) the cycle can be repeated (6) or the oligonucleotide can be deprotected and cleaved from the solid support (7) to deliberate the crude assembly product. The figure shows an adapted version of the figures found in reference[175].

The phosphoramidite synthesis cycle starts with a 5'-DMT protected nucleotide chemically bound on a controlled pore glass (CPG) support. The DMT group is deprotected in the first step by dichloroacetic or trichloroacetic acid in acetonitrile (deblock, 1). The resulting free 5'-hydroxy group reacts with the phosphorous of an introduced phosphoramidite, which is activated by 1*H*-tetrazole or substituted tetrazoles in acetonitrile before coupling in the second step (2). All unreacted free 5'-hydroxy groups are capped by acetic anhydride and N-methylimidazole in a THF/pyridine-mixture in the following capping step (3) to avoid undesired chain elongation of unreacted fragments. A mixture of iodine in THF, pyridine and water leads to an oxidation of the formed phosphorous(III) to phosphorous(V) in the elongated phosphate backbone (4). Consecutive DMT deprotection of the newly added nucleotide by trichloroacetic acid in dichloromethane activates the 5'-hydroxy moiety for the next coupling cycle (6), thus re-entering the synthesis cycle. The coupling cycle can be aborted after each coupling step and the synthetic oligonucleotide needs to be deprotect from the solid support. Cleavage of all remaining 2-cyanoethyl protecting groups and solid support cleavage are performed in a single step by means of 30 % aqueous ammonia 55 °C for 16 hours or a 1:1 mixture of aequous methylamine and 30% aqueous ammonia at lower temperatures (7). The resulting crude oligonucleotide requires purification by high performance liquid chromatography (HPLC) to yield the pure synthetic oligonucleotide.

Artificial design and synthesis of oligonucleotides emerged a series of artificially modified nucleotides for biological, biomedical and nanotechnological applications. Beyond synthesis of native DNA and RNA, a vast variety of chemical modifications have been introduced into oligonucleotide strands using solid support phosphoramiditie synthesis. Ranging from modifications on the sugar pucker over the synthetic modification of nucleobases up to the introduction of modifications *via* sugar analoga have been reported. A recent approach uses chemically modified diol linkers with high structural similarity to native D-deoxyribose for implementation of functional moieties into oligonucleotide backbones (fig. 19).[176] Among these diol linkers, D-threoninol shows the highest structural similarity to natural D-deoxyribose and could be successfully implemented into the backbones of DNA and RNA strands for implementation of functional moieties.[177] D-threoninol resembles a C_3-diol linker carrying a primary amino residue in the carbon chain. The primary amino group serves as a nucleophilic center for attachment of functional residues by formation of a peptide bond. Experiments showed that introduction of the diastereomer L-threoninol as sugar surrogate results in a destabilization of a modified ODN duplex since D-threoninol exhibits a higher structural similarity to the right-handed chirality of the DNA helix axis compared to L-threoninol.[178]

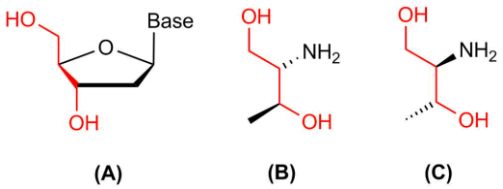

Fig. 19: Structural comparison of natural D-deoxyribose (A), D-threoninol (B) and L-threoninol (C). D-threoninol exhibits a high structural similarity to natural D-deoxyribose and is commonly used as a sugar surrogate in DNA backbones to introduce functional groups.

Even complete artificial basepairs and backbones have been reported in recent literature, mimicking natural DNA and RNA base pairs and backbones.[179-180] Besides the straight forward synthesis of nucleotide analoga, the introduction of functional moieties into oligonucleotide backbones *via* click chemistry by use of alkyne modified nucleobases became the center of interest for a post-synthetic functionalization of artificial oligonucleotide strands.[181]

2.4 Photocontrol of oligonucleotide duplex hybridization

Introduction of D-threoninol as a synthetic base surrogate into the backbone of DNA afforded an implementation of photoresponsive moieties into oligonucleotides. First established by the working group of H. Asanuma, the successful implementation of D-threoninol linked azobenzene residues into oligonucleotides could be achieved and led to the efficient photoinduced hybridization control of DNA duplexes.[182-191] Incorporation of D-threoninol moieties into the phosphate backbone of DNA leads to a distortion of the helical structure which is overcompensated by additional π-stacking interactions through intercalation of *trans* azobenzene between the stacked base pairs (fig. 20). The overall stabilizing effect on the DNA duplex can be observed by an increase in melting temperatures.

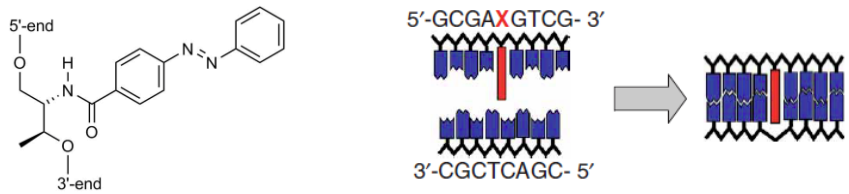

Fig. 20: Azobenzene attached to D-threoninol can be introduced into the backbone of DNA strands (left). Intercalation of azobenzene moieties between the base pairs of a DNA double strand (right). Additional π-stacking stabilization of intercalated *trans* azobenzene (red) stacked with the surrounding base pairs overcompensates a disruption of the DNA backbone caused by D-threoninol. The figure shows an adapted version of the figure found in reference[192].

Isomerization of azobenzene from *trans* to *cis* conformation upon irradiation with UV light removes the additional π-stacking interactions and induces a local or total duplex dissociation, depending on the number and positions of introduced moieties (fig. 21). As a general observation, introduction of multiple azobenzenes into a duplex leads to a more efficient decrease in melting temperature.[187] Depending on the number and positions of the moieties, a full duplex dissociation can only be achieved with a minimum number of one azobenzene moiety per two base pairs, but still an efficient duplex dissociation can only be achieved using elevated irradiation temperatures close to the melting temperature of the native duplex. Furthermore, a GC-content of 50 % or lower is required to achieve a full duplex dissociation.

Azobenzene can be introduced into a double strand in different motifs (fig. 22). The use of one azobenzene moiety per two base pairs is the so called wedged motif, where two nucleotides are separated by one azobenzene moiety in the same strand. This motif represents the optimal compromise between duplex stabilization through additional π-stacking interactions and disruption of the B-form helix through D-threoninol when hybridized with a non-

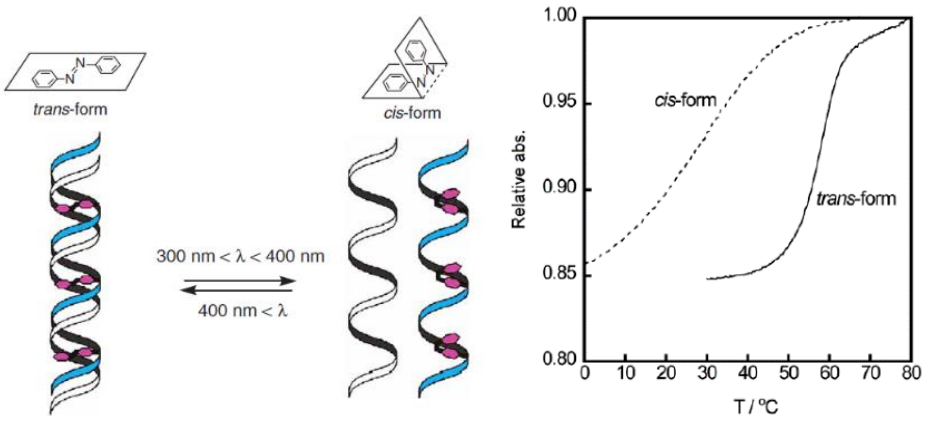

Fig. 21: Photocontrol of DNA hybridization upon irradiation with UV and visible light (left).[192] UV light irradiation leads to a destabilization and dissociation of the azobenzene-modified DNA duplex. Irradiation with visible light reverst the effect and leads to duplex formation by an additional π-stacking stabilization as proven by melting curves (right). The figure shows an adapted version of the figure found in reference[176]

modified complementary strand. The wedged motif achieves a duplex dissociation of 80 % when irradiated with UV light at 37 °C or higher temperatures.[193-194]

A maximum number of two azobenzenes per base pair can be introduced into DNA duplexes to remain photoswitchable. In this so-called dimer-motif, the two azobenzene moieties are located in opposite strands and are separated by one flanking base pair on each side. In both the interstrand wedged motif and the dimer motif complete dehybridization of the duplex is only possible at high irradiation temperatures of 60°C and above.[193]

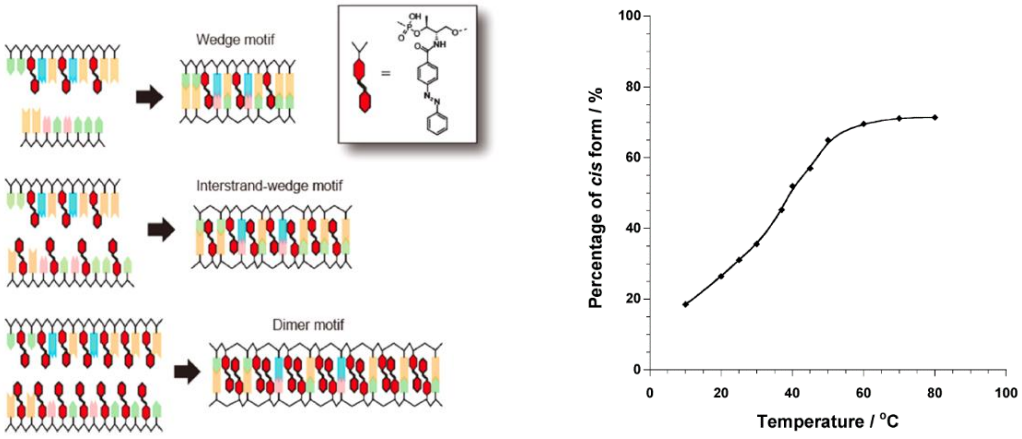

Fig. 22: Different azobenzene substitution motifs into DNA double strands (left): wedged motif (top), interstrand wedged motif (middle) and dimer motif (bottom) all contain different azobenzene numbers and positions, resulting in different duplex dissociation efficiencies.[194] Temperature dependency of DMAB isomerization to *cis* in ODN duplexes upon irradiation.[193] The figures show adapted versions of the figures found in references[193] and [194].

Overloading the duplex with azobenzene moieties increases the π-stacking stabilization to an extent that photoinduced dehybridization becomes impossible.As stated before, the wedged motif is the best compromise between the two stabilizing and destabilizing tendencies.Introduction of *ortho* methyl residues on azobenzene's peripheral phenyl moiety led to a drastic stabilization of the *cis* state, increasing the half-life of azobenzene from 50 hours up to 200 hours at room temperature.[195-197] Additional sterical hindrance through the methyl residues hampers a thermal back-isomerization from *cis* to *trans* conformation which leads to the increased thermal stability of the *cis* state. Unfortunately, the mandatory use of UV light to achieve formation of the *cis* state still persists. To circumvent this problem, the development of a 4'-methylthio substituted 2',6'-dimethylazobenzene was designed, further shifting the *cis* response wavelength into near-UV range.[198-199] A complete shift of response wavelengths into visible light range could not be achieved by methyl substitution. Further attempts of optimizing azobenzene's photophysical properties within DNA duplexes through additional substitutents have not been performed yet.

Despite the successful establishment of azobenzene and its derivatives as DNA photoswitches, the method is still to be improved. The main problems associated with azobenzenes is the incomplete conversion between the *cis* and *trans* state in both isomerization directions and the increased duplex stabilization, both causing mandatory high irradiation temperatures and high synthetic loads. This inherent problem was further tried to be obliterated by replacing the D-threoninol linkage for other diol linkers. An azobenzene C-nucleoside[200-201] and an R-glycerol linker[202] as base surrogates both led to a stronger destabilization of the oligonucleotide duplex (fig. 23). Introduction of azobenzene into oligonucleotides via a C-nucleoside surrogate was designed to avoid backbone disruption caused by D-threoninol and therefore avoid azobenzene possibly flipping out of the stack upon isomerization.

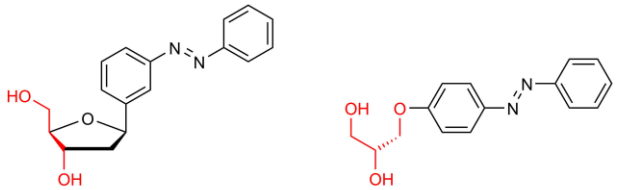

Fig. 23: An azobenzene C-nucleoside[200] (left) and azobenzene attached to an R-glycerol linker[202] (right) were developed as phosphoramidites and introduced into DNA backbones to facilitate room temperature photoconversion of modified DNA duplexes. Both modifications result in an efficient room temperature photocontrol of oligonucleotide duplexes.

Leading to 90 % *cis* isomer formation, room temperature switching could be achieved by attaching azobenzene to a C-nucleoside but only in RNA with high AU-content and a high synthetic load. An R-glycerol linker was designed to ensure more space in the base stack for isomerization which is limited when introducing azobenzene with D-threoninol. Only 80 % formation of the *cis* isomer could be achieved at room temperature irradiation but almost quantitative duplex dissociation at 37 °C.

Nevertheless, all attempts towards quantitative DNA duplex dissociation at room temperature still require low GC-contents and high synthetic loads. The inherent stabilizing effect of azobenzene on the DNA duplex and incomplete formation of both isomers in both isomerization directions could not be abolished by all previously described approaches. An efficient room temperature switching of DNA duplex hybridization with lower synthetic loads even in systems with high GC-content are yet to be established.

2.5 Application of azobenzene-functionalized DNA nanosystems *in vitro* and *in vivo*

2.5.1 From photoresponsive DNA nanoarchitectures to photon-fueled DNA nanomachines

Reversible photocontrol of oligonucleotide duplex formation brought up a multitude of innovations for applications *in vitro* and *in vivo*.[203-205] Complementary pattern recognition in DNA sequences facilitated the construction of complex three-dimensional nanostructures and nanotechnical devices which, including azobenzene moieties, can be reversibly converted between different states by light irradiation. DNA based nanoarchitectures have emerged ranging from three-dimensional tetra-hedra,[206] capsules[207-208] and even larger DNA origami structures[209] composed of double stranded DNA. Introduction of photoresponsive moieties permits dynamic reversible structural changes inside these constructs upon irradiation with UV and visible light. A photocontrolled double-stranded DNA nanotweezer can be reversibly opened and closed by irradiating an azobenzene modified closing strand (fig. 24).[210] In *trans* conformation, the closing strand hybridizes to both single stranded ends of the tweezer construct leading to a closed state. UV irradiation isomerizes azobenzene moieties to *cis*, leading to a dehybridization of the closing strand and results in tweezer opening. Both opening and closing states could be reversibly interconverted over several cycles without fatigue or disintegration of the system.

Sophisticated design of complementary patterns emerged even more complex three-dimensional DNA structures with a size up to several hundred nanometres. Introduction of azobenzenes into these structures permits a macromolecular dynamic photocontrol of shape, motion and functionality. A macromolecular DNA tetrahedron modified with azobenzene

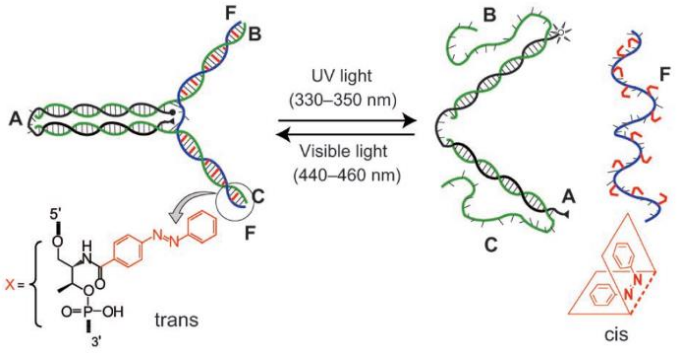

Fig. 24: A photocontrolled DNA nanotweezer containing azobenzene modified complementary sequences. Irradiation of the system with either UV or visible light leads to a hybridization or dissociation of the closing strand F to B and C, inducing an opening or closing mechanism of the whole nanotweezer. The figure shows an adapted version of the figure found in reference[210].

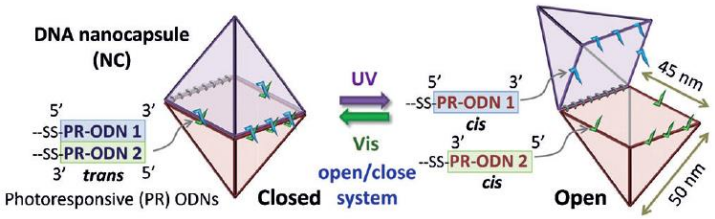

Fig. 25: Three-dimensional DNA capsules have been reported with an included photoresponsive opening and closing mechanism. The azobenzene-modified edges dissociate upon irradiation to *cis*, thus resulting in an opening of the nanocapsule. The figure shows an adapted version of the figure found in reference[207].

moieties in one flanking strand exhibited a structural change upon irradiation with UV and blue light as observed in AFM images.[206] A similar DNA nanocapsule was designed as a container with inbuilt photoresponsive open-close meachnism by means of azobenzene moieties (fig. 25).[207] The capsule top is thereby connected to the bottom part over one capsule edge and permits a flexibile rotatory motion around this axis in the open form with azobenzene moieties in *cis* conformation. The capsule could be opened and closed reversibly over several irradiation cycles.

Beyond photocontrol of structural motifs, generating functionality and controlled unidirectional motion are ongoing challenges in recent DNA nanotechnology. Most DNA nanoconstructs and devices create motion by interconversion between stalled states while permitting a diffusion of single strands or structural components between the states. A basic example for a reversible photocontrolled structural motion is an azobenzene modified DNA hairpin which exhibits a diffusion motion upon reversible opening and closing of the stem region. The stem region is hereby modified with several azobenzene moieties where alterna-

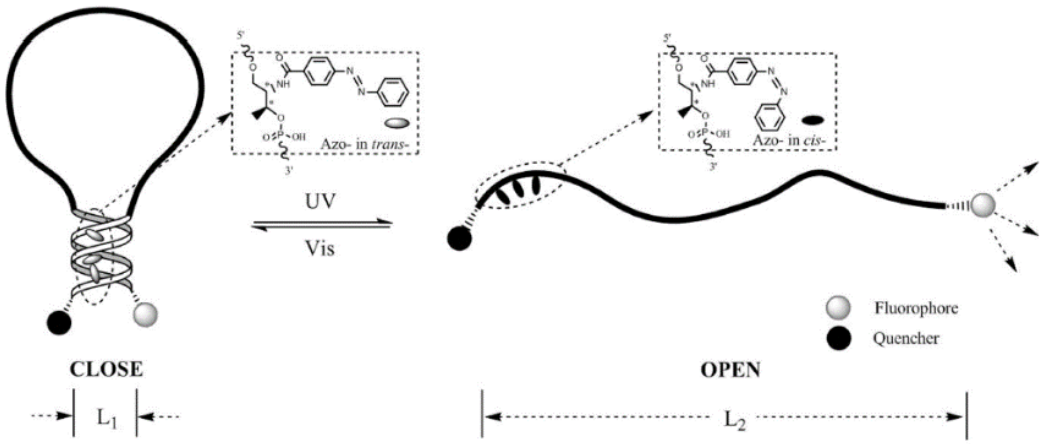

Fig. 26: A photoresponsive DNA hairpin carrying azobenzene modifications in the stem region can be reversibly opened and closed upon alternate irradiation with UV and visible light, resulting in the uncontrolled diffusion-like motion of the whole hairpin system. The figure shows an adapted version of the figure found in reference[211].

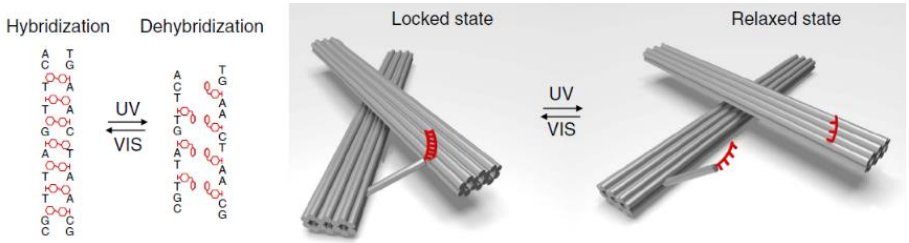

Fig. 27: A supramolecular dsDNA origami structure connected to an azobenzene modified linker facilitates the measurement of plasmonic resonance upon irradiation with UV or visible light. The structure can undergo free rotational motion around the central rotation axis through azobenzene isomerization from *trans* to *cis* ,resulting in reversible switching between a stalled (left) and a free rotational state (right). The figure shows an adapted version of the figure found in reference[212].

ting irradiation with UV or visible light leads to opening and closing of the hairpin resulting in an uncontrolled diffusion-like motion of the whole system (fig. 26).[211]An even larger DNA origami structure including azobenzenes was designed to provide detectable physical functionality in nanoscale.[212] Two origami tubes connected *via* a rotational dsDNA axis permit the direct measurement of plasmonic resonance of the system after irradiation with UV or visible light (fig. 27). The nanostructure translates photoisomerization of azobenzenes into reversible chiroptical motion depending on the hybridization state. In *trans* conformation, rotatory motion is suppressed by a hybridizing azobenzene modified connecting oligomer while in *cis* state the oligomer dehybridizes and permits a rotational degree of freedom around the connection axis.

Interlocked DNA nanosystems represent another approach to dynamic photon-fueled functional nanotechnology and permit higher degrees of freedom. Mechanically interlocked compartments of these systems can be stalled and liberated reversibly upon irradiation of azobenzene moieties to enable or disable a diffusive motion of the compartment. Photon fueled double-stranded DNA rotaxanes were the first examples to show DNA-based photocontrolled logic gating systems which can be reversibly forced from stalled states into interlocked states, wheras the structures facilitate free motion of single compartments within

Fig. 28: A two-state dsDNA rotaxane shuttle attached to a ring stopper construct on one end and a spherical stopper construct on the other end of the central double strand. Irradiation at 365 nm results in a ring release and blocking of the second gap through an azobenzene modified release oligomer at the same time, allowing the ring to move freely into the second gap. Irradiation with 450nm reverts this process to the initial state. The figure shows an adapted version of the figure found in reference[213].

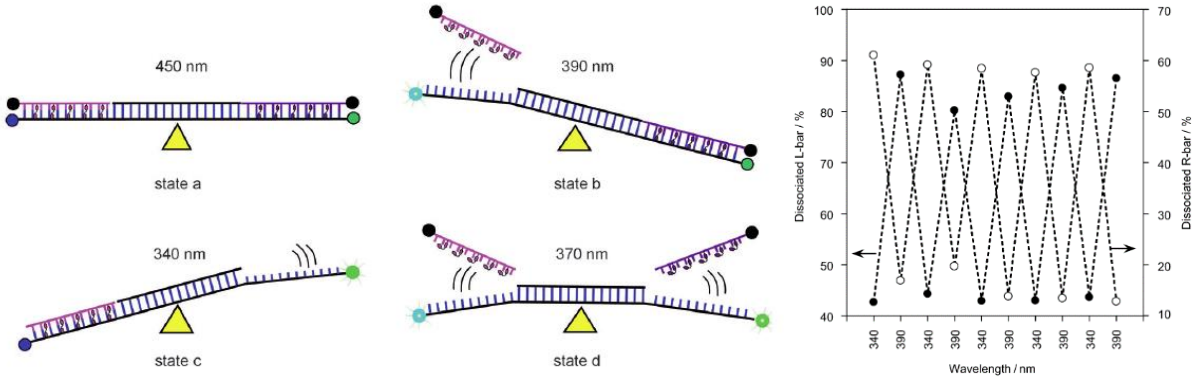

Fig. 29: A photocontrolled DNA seesaw system containing two different azobenzene photochromes azobenzene (AB) and 2',6'-dimethyl-4'-methylthioazobenzene (S-DMAB). While irradiation at 450 nm hybridizes both strands (state a), irradiation at 340 nm or 390 nm selectively dehybridizes one or the other strand (state b and state c) and irradiation at 370 nm results in dehybridization of both strands (state d). The system permits an orthogonal photocontrol of two different strands with 50 % efficiency upon alternate irradiation at 45 °C. Switching efficiencies were determined by fluorophore quencher measurements. The figure shows an adapted version of the figures found in reference[198].

an interlocked range (fig. 28).[213-214] A double-stranded DNA ring is threaded over a central rod while bulky stopper constructs on both ends prevent dethreading. The ring can move unhindered from one single-stranded position on the rod over an interlocked state to another single-stranded gap by relieving or blocking azobenzene-modified gaps or gaps with azobenzene-modified toehold oligomers. Irradiation of the system with UV or visible light permits reversible positional changes of the ring in different positions. This system provides a starting point for further functiona-lized DNA nanosystems which necessitate activation and inactivation of functions for larger logic gating devices. A DNA daisy chain as a further development step beyond DNA rotaxane systems mimics the contraction and relaxation motion of muscle cells.[215]

All these systems mark evolutionary steps to even more complex DNA systems with additional functionalities. An ambitious goal still is the development of artificial photon driven motor systems with autonomous propulsion for the development of nanomachines. Furthermore, origami-templated nanofactories and assembly lines based on multi-state DNA systems could enable light-induced control of chemical reactions or directed assembly of macromolecules. The more individual states a complex system requires, the higher is the mandatory amount of photoswitches which can be individually addressed. Expansion of the hitherto established two-way photocontrol of azobenzene based DNA systems, which only use the *cis* and *trans* isomerization of a single photoswitch, was developed by a series of substituted azobenzenes in DNA.

A combination of multiple photoswitches with coherent or independent isomerization properties facilitates addressing of multiple states by more than two wavelengths of light. Orthogonal photoswitching could be achieved using azobenzene and a 2',6'-dimethyl-4'-methylthioazobenzene derivative (S-DMAB) in a DNA seesaw system (fig. 29).[198] Fluorescence quenching experiments showed a 50 % orthogonal switching efficiency upon irradiation of both photochromes with different wavelengths of UV and visible light at 47.5 °C.

Unfortunately, orthogonal photoswitching is strongly decreased by a significant spectral overlap of response wavelengths within this system, thus leading to photostationary states with mixed compositions of all stereoisomers for both azobenzene derivatives. Further red-shifting and better separation of response wavelengths could drastically improve the photoswitching behaviour, but has not been established in DNA yet.

A further example for orthogonal and independent photoswitching outside DNA applications was developed by the interaction of azobenzene derivatives with donor-acceptor Stenhouse adducts as reported by the working group of B. Feringa.[216] Efficient orthogonal photoswitching could be achieved within this small molecule approach in cyclodextrins, but a translation of further efficient orthogonally photoswitchable systems into DNA has not been achieved yet.

Still, the potential range of applications in DNA nanotechnology and the development of more complex systems is strongly hampered by a lack of available photoswitches within DNA. An expansion of the photoswitch repertoire readily available in DNA strongly increases the usable wavelength range and fosters the development of new complex multi-state DNA nanodevices and DNA nanomachines.

2.5.2 Photopharmacology - photoactivated drug design for control of biological functions

DNA as a key regulator in metabolic functions controls key cellular processes. Introduction of visible light responsive azobenzene into DNA backbones possibly leads to a successful development of phototherapeutics. Azobenzene in DNA yet yielded a series of technical applications *in vitro*, but translation into living organisms to achieve photocontrol of biological and metabolic functions is still limited due to the mandatory use of UV light.[217-219]

Azobenzene modified oligonucleotides have recently only been established *in vitro* while further development of visible light responsive azobenzenes has not passed beyond the molecular level. Translation of these newly developed photoswitches towards *in vivo* systems still remains a highly ambitious goal to achieve phototherapeutics. One application of azobenzenes *in vivo* has been reported by A. A. Beharry et al. by introduction of azobenzene-modified coiled-coil fluorescence reporter proteins into zebrafish embryos (fig. 30).[220-221] Irradiation of these photoresponsive fluorescence reporters could be observed within two days of zebrafish growth without influencing the development of the embryo or showing any undesired systemic toxicity. However, electron withdrawing azobenzenes are accompanied by a high tendency to reduction by glutathione.

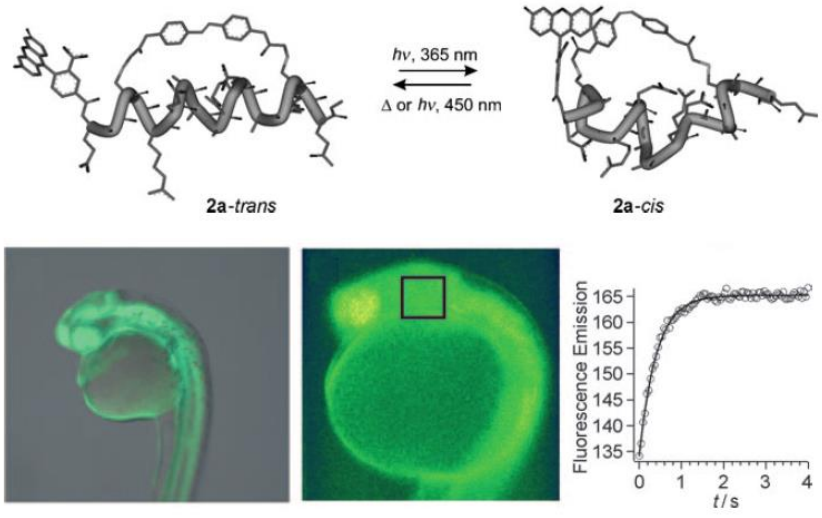

Fig. 30: Introduction of photoresponsive fluorescence reporter proteins into zebrafish embryos showed photoswitching properties and fluorescence response for more than two days without inherent side-effects. This experiment revealed the in vivo applicability of therapeutic oligonucleotides modified with azobenzene residues. The figure shows an adapted version of the figure found in reference[220].

A more convenient approach to photoresponsive therapeutics and theranostics has been postulated by D. Trauner[222] and B. L. Feringa.[223] Existing biologically active prodrugs and therapeutics including azobenzene or stilbene backbones exhibit photoresponsive

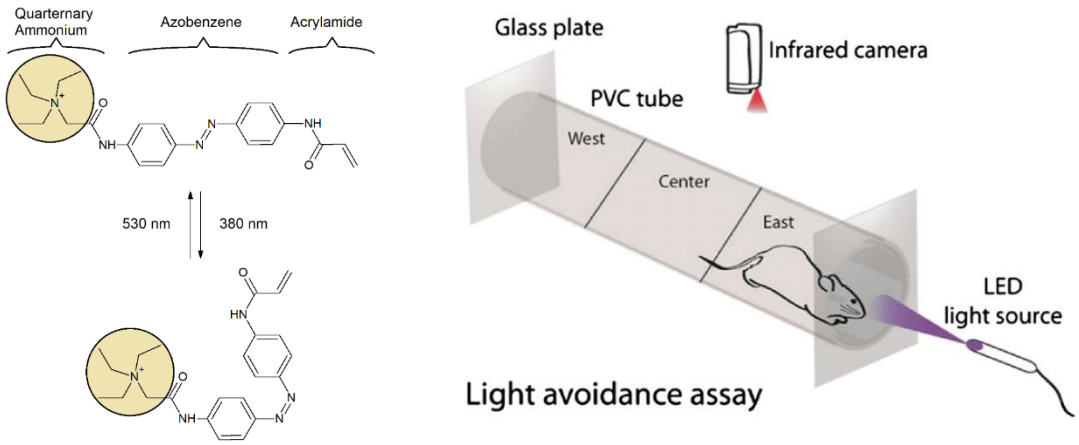

Fig. 31: The molecule acrylamide-azobenzene-quarternary ammonium (AAQ) leads to an activation of inactive retinal ganglion cells in *cis* conformation and restores vision when injected into blind mice. The figure shows an adapted version of the figure found in reference[228].

isomerization properties. In case of therapeutics with a stilbene backbione, these molecules can be chemically modified to result in photoresponsive therapeutics. Substitution of the central stilbene double bond by an azo linkage results in azobenzene prodrugs. If biological activity is retained within the newly designed azo-prodrugs, biological activity can be turned on and off reversibly by light irradiation. The potency of this approach was proven in a variety of *in vitro* applications to achieve photoreversiblebinding to insulin receptors,[224-225] sodium channels[226] and photoinduced proliferation of cancer cells.[227]

Translation of *in vitro* applications into living organisms was proven through injection of the molecule acrylamide-azobenzene-quarternary ammonium (AAQ) into mice (fig 31).[228] This photo-active prodrug was initially proven to block potassium channels in the nervous system in *trans* conformation and permits sodium exchange in *cis* conformation, whereby this effect could be turned on and off reversibly by irradiation with 380 nm or 500 nm light. Interestingly, the molecule showed another significant biological activity when injected into the eyes of blind mice. AAQ bears the potential of restoring light sensitivity of rods and cones in retinal ganglion cells in *cis* conformation after irradiation with 380 nm. The effect was suppressed after irradiation with 500 nm, converting the molecule back into the inactive *trans* conformation. The further optimized molecule DENAQ containing a reduced thermal stability of the *cis* state mimics the isomerization of opsins in photoreceptor cells of the human eye.[229-230] The molecule showed an increased visual restoration potential and a quick thermal back-relaxation in the dark, but was only tested in *in vitro* models.

Further potent photoresponsive receptor agonists[231] and bioactive prodrugs[232] showed high potentials as possible phototherapeutics, but yet did not overcome the barrier between *in vitro* and *in vivo* application. A highly promising photoactive anticancer drug has been deve-

loped as a photoactive combretastatin analogon,[227] which in *cis* conformation revealed reduction of negative systemic side effects as often associated with anticancer drugs. The agent could be activated by isomerization into *trans* conformation and still retained antiproliferate activity.

Photoactivation and deactivation of therapeutic drugs provides a powerful tool for a broad application range in targeted disease phototherapy. Unfortunately, the method is still limited to small molecules and has not been transferred towards DNA or RNA based therapeutic applications. The mandatory use of UV light, high synthetic loads and elevated irradiation temperatures thereby present the strongest limitations of the approach. Photoswitches with *trans* and *cis* converting wavelengths in visible light range accompanied with near-quantitative conversion efficiencies and high thermal *cis*-stabilities could provide ideal candidates to improve the applicability of new photoactive therapeutics.

2.6 Motivation and outline

Azobenzene and its derivatives have proven to be versatile tools for the reversible photocontrol over DNA duplex hybridization. The four reported D-threninol linked molecules azobenzene (AB), 2',6'-dimethylazobenzene (DMAB), 4'-methylthioazobenzene (S-AB) and 2',6'-dimethyl-4'-methylthio-azobenzene (S-DMAB) have successfully been introduced into oligonucleotide duplexes and permit a reversible duplex photocontrol as shown in diverse DNA nanosystems *in vitro*. The photoswitching potential of the described molecules has been demonstrated *in vitro* in functional DNA nanostructures and devices, photon-fueled DNA nanotechnology, photocontrol of cellular functions and photoactivated therapeutic molecules. Unfortunately, duplex hybridization control through the reported azobenzenes is highly limited to *in vitro* applications due to the mandatory use of UV and near-UV light and its associated negative side effects on biomolecules and living tissue, the mandatory use of elevated irradiation temperatures close to native duplex melting point and a high synthetic load associated with these molecules. Overcompensation of DNA backbone disruption by additional π-stacking of azobenzene with DNA base pairs as well as the incomplete conversion from *trans* to *cis* and vice versa are the main drawbacks which strongly limit feasibility *in vivo*.

The recently reported *ortho* substituted azobenzene and arylazopyrazole molecules state promising candidates for a potential improvement of photoinduced oligonucleotide duplex hybridization. Increased thermal *cis* stabilities and near-quantitative reversible conversion efficiencies between the *trans* and *cis* state accompanied by highly red-shifted response wavelengths match the three criteria for potent photoswitches and provide suitable properties for *in vivo* applications. An optimal photoswitch thereby matches three main criteria, which have to be fulfilled for improved DNA photoswitching: First, reversible interconversion between *trans* and *cis* in visible light range has to be established to minimize negative side effects on biological systems. Furthermore, near-quantitative conversion efficiencies in both isomerization directions are mandatory to reduce the synthetic load in oligonucleo-tides. Especially in DNA-nanotechnology, high switching efficiencies at low irradiation temperatures possibly minimize the synthetic load required for efficient photoswitching, thus decreasing structural disruptions. Last but not least, a high thermal stability of the *cis* state needs to be retained to ensure long-term applications in DNA nanotechnology and living systems.

The central goal of this project is the systematic synthetic development of substituted azobenzene and arylazopyrazole molecules for a general improvement of photophysical properties followed by the introduction of new photoswitches into oligonucleotide strands and duplexes *via* DMT-protected phosphoramidites. A series of newly designed molecules have to be investigated *via* spectroscopic methods towards their photophysical properties. Based on

the recently reported azobenzenes and arylazopyrazoles, a synthetic toolbox of D-threoninol linked photoswitches has to be synthesized and investigated by UV/Vis spectroscopy and reversed-phase HPLC quantifications. A selection of suitable candidates is further developed synthetically to achieve DMT-protected phosphoramidites. The synthetically accessible photoswitches with the most promising photophysical properties are further introduced into oligonucleotides *via* solid phase phosphoramidite synthesis.

Once successfully introduced into oligonucleotides, a systematic study of different synthetic loads, positional effects and irradiation conditions in DNA duplexes with different length and GC-content are performed to investigate a translation of photophysical properties from free molecules into oligonucleotide strands. The reported DNA photoswitches thereby serve as a reference under the same experimental conditions in a direct comparison. Duplex photocontrol efficiency is investigated by melting curve experiments as well as hybridization experiments in a double-stranded 168bp DNA ring system. Application of the newly developed photoswitches is established in competitive environments in DNA based hairpin systems as release oligomers to demonstrate photocontrol feasibility.

Successful development of multiple new photoswitches might bring up a whole toolbox of

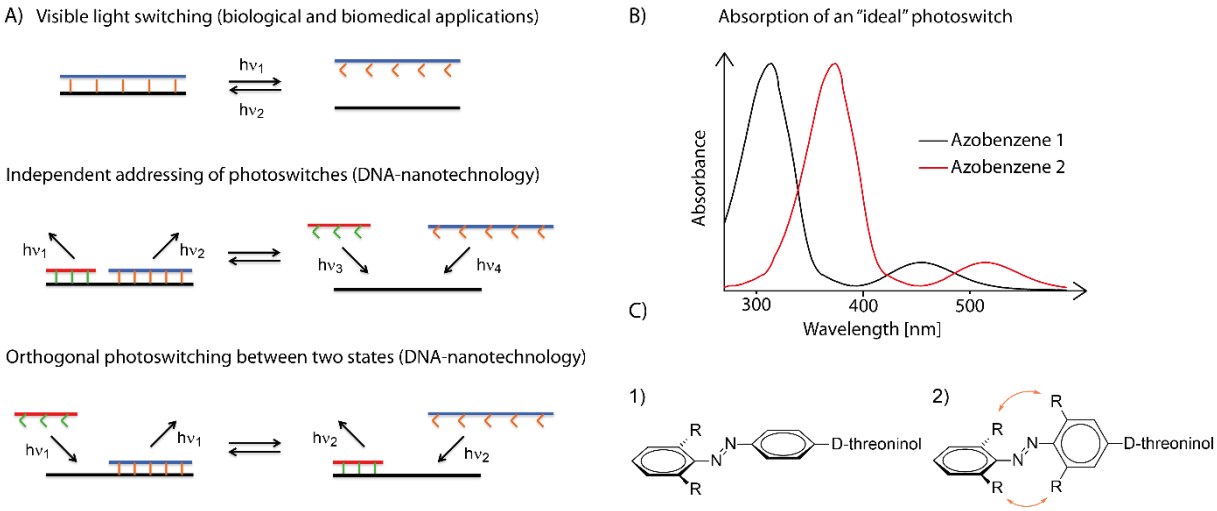

Fig. 32: A) Different potential applications of newly designed photoswitches ranging from visible light switching for biomedical applications over independent addressing of two different photochromes up to orthogonal photoswitching of two different azobenzenes for applications in DNA nanotechnology. B) Absorption spectra of two independently addressable photoswitches ideally do not show overlapping of absorption maxima, thus resulting in orthogonal controllability of modified DNA systems. C) Sterical hindrance of bulky *ortho* substituents possibly prevent the formation of a planar *trans* conformation which might distort the base pair stacking in DNA duplexes upon intercalation and consequently prevent duplex hybridization.

molecules with cooperative and independent photoswitching properties for introduction into multi-state DNA nanotechnology systems. Depending on the nature of the introduced photoswitches, systems with multiple photocontrolled states are thinkable which can be addressed independently (fig. 32). Yet, the number of possible different states for a combination of multiple photoswitches is strongly limited by the accessible irradiation wavelength range for the already available molecules established in DNA strands.

3. Development of new azobenzene and arylazopyrazole phosphoramidites for improved photocontrol of oligonucleotide duplex hybridization

3.1 Synthesis and spectroscopic investigation of substituted azo compounds

3.1 1 General spectroscopic investigation of *ortho* substituted azobenzenes

Since the first report of photocontrol over DNA hybridization through introduction of azobenzene residues into the backbone of DNA, a series of azobenzene derivatives have been developed and successfully implemented into oligonucleotide strands. Three of the four reported D-threoninol linked photoswitches azobenzene (AB), 2',6'-dimethylazobenzene (DMAB) and 4'-methylthio-2',6'-dimethylazobenzene (S-DMAB) were synthesized following pathways previously reported[192,198] (fig. 33) and serve as reference systems during the development of new photoswitches. D-threoninol as a base surrogate and linkage between the phosphate backbone and the photochromes is well studied and represents the most commonly used linkage for introduction of azobenzene into DNA. Photochromes bound to D-threoninol represent the switching moiety which is later introduced into oligonucleotides.

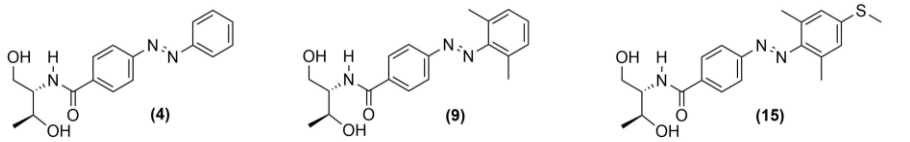

Fig. 33: Azobenzene (AB), 2',6'-dimethylazobenzene (DMAB) and 4'-methylthio-2',6'-dimethylazobenzene (S-DMAB) represent the three D-threoninol bound photochromes previously reported and established in DNA.[192,198].These molecules were synthesized and used as a reference for all newly synthesized and developed photoswitches.

The three azobenzene moieties AB, DMAB and S-DMAB were irradiated with a set of high power LEDs covering the main light-range between 320 nm (UV light) and 630 nm (red light), which were used in all further irradiation experiments (see chapter 7.1). The used LEDs permit irradiation within a low bandwidth range and, contraryt to commonly used white light in combination with cutoff filters, provide high irradiation intensities to foster the formation of photostationary states (PSS) within short irradiation times. The relative change in UV/Vis absorption intensity thereby correlates to the change in *trans* and *cis* composition. Empirical investigation of UV/Vis absorbance spectra after consecutive irradiation with all available LEDs

permits the profiling of wavelength-dependent photostationary states to determine absorption maxima and maximum response wavelengths. Every wavelength-dependent photostationary state is characteristic for each photochrome and strongly depends on the overlap of absorption bands for the pure *trans* and *cis* iomers. Empirical determination of a set of photostationary states further enables determination of wavelength-dependent fractions of *trans* and *cis* isomers within each PSS. The maximum *trans*- and *cis*-converting irradiation

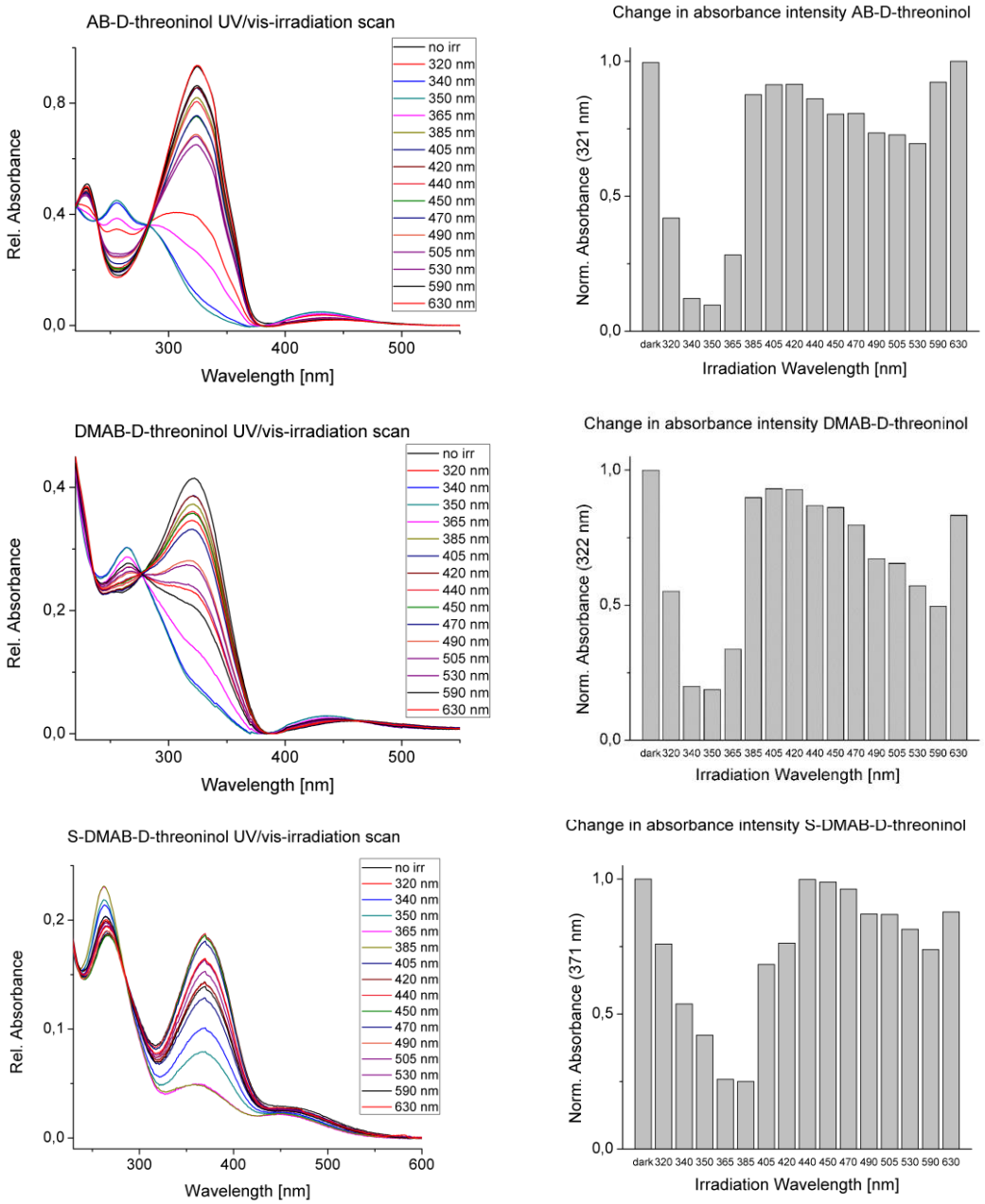

Fig. 34: UV/Vis absorption spectra of D-threoninol bound photochromes azobenzene (AB), 2‘,6‘-dimethylazobenzene (DMAB) and 2‘,6‘-dimethyl-4‘-methylthioazobenzene (S-DMAB). All spectra were recorded using a 50 µM photochrome solution in a 1:1 mixture of acetonitrile and water after 5 minutes irradiation with all available LEDs from the newly built LED irradiation source. The absorption values were normalized on the respective maximum absorption values at the absorption maxima.

Azobenzene	WL *trans*	WL *trans* ref.	WL *cis*	WL *cis* ref.
AB	405 nm	>400 nm	340 nm	340 nm
DMAB	420 nm	>400 nm	350 nm	340 nm
S-DMAB	450 nm	450 nm	385 nm	400 nm

Tab. 1: Comparison of empirically determined maximum excitation wavelengths for AB, DMAB and S-DMAB with the previously reported excitation wavelengths reveal a high similarity with the reported wavelengths when using the newly designed LED irradiation machine.[198,199] Comparable irradiation wavelengths are a main prerequisite for reproducibility of results when using the irradiation machine.

wavelengths as well as each wavelength-dependent PSS for a combination of multiple photoswitches allows a prediction of coherent switching properties for a combination of multiple photoswitches. The resulting empirical data set represents a spectroscopic “fingerprint” for each compound. Since azobenzenes do not emit radiation and only exhibit marginal photobleaching, the empirical excitation scan can be used for a qualitative investigation of the maximum *trans* and *cis* converting wavelengths and thus the separation of n->π* and π->π* transition bands for both stereo isomers. A high separation of absorption bands, especially in visible light range, is one of the main prerequisites for efficient and independent addressing of both states. Exact quantification of a UV/Vis spectrum is problematic due to the overlap of *cis* and *trans* absorption bands in the same spectrum and necessitates complex mathematical models to approach the composition of both isomers. The qualitative determination of absorbance intensity differences in UV/Vis spectra permits a qualitative characterization to determine the maximum *trans*- and *cis*-converting wavelengths and thus facilitates the pre-selection of suitable candidates for further implementation into oligonucleotides.The three molecules AB, DMAB and S-DMAB bound to D-threoninol were dissolved in a 1:1-mixture of acetonitrile and water and irradiated for 5 minutes at room temperature with all available LEDs immediately followed by recording UV/Vis absorption spectra (fig. 34). In agreement with literature,[198,199] all three compounds show a significant change in absorption intensity upon irradiation with the wavelengths given in table 1, but the maximum irradiation wavelengths reveal a slight hypsochromic shift compared to the reported ones, possibly caused by broader irradiation bandwidths by the used LEDs. Despite this observation, all maximum *trans*- and *cis*-converting irradiation wave-lengths are close to the reported ones.

Azobenzene (AB) exhibits the lowest absorption maximum when irradiated with 340 nm and the highest absorption maximum upon irradiation with 405 nm light. DMAB shows slightly red-shifted excitation wavelengths with 350 nm irradiation for the lowest and 420 nm for the highest measured absorbance while S-DMAB reveals 385 nm and 450 nm as the wavelengths with the maximum change in intensity. The previously reported wavelengths were determined after

irradiation with white light in combination with cutoff filters as stated before. High power LEDs possibly permit a lower irradiation bandwidth and a higher light output so the irradiation maxima are marginally shifted. The established method proved to be valid by confirming the maximum *trans* and *cis* switching irradiation wavelengths of the reported azobenzenes. This empirical method entails one major drawback: Determination of maximum response wavelengths is only possible for azobenzenes with thermal stabilities significantly higher than the irradiation and measurement times, usually within a magnitude of several hours. Azobenzenes with low thermal stabilities within seconds or minutes rapidly transform back thermally from *cis* to *trans* conformation, thus potentially changing the ratio of both isomers during the measurement. Since most of the investigated photochromes retain thermal stabilities of the *cis* state within a range of several hours to days, fast back-switching is not considered as a severe problem but has to be taken into account as a possible error source.

A distinct quantification of *trans* and *cis* composition for each photostationary state can be obtained by separating both stereo isomers *via* reversed-phase HPLC and integration of the corresponding peaks in the recordedcchromatograms. This method is later described in chapter 3.2.1.

3.1.2 Synthesis and spectroscopic investigation of an azobenzene toolbox

The first criterium for the development of new photoswitches with improved photophysical properties is a shift of response wavelengths into the red range of visible light. Substitution of azobenzenes in all four *ortho* positions has been reported to result in red-shifted response wavelengths and a separation of both a n->π* transition bands for the *trans* to *cis* isomerization and vice versa while maintaining high thermal stabilities of the *cis* state (see chapter 2.2.5). To confirm this observation and normalize all irradiation conditions to a newly developed high output LED irradiation machine, a series of differently *ortho* substituted azobenzenes was synthesized as a readily available “azobenzene toolbox” for pre-selection of possible molecules to be further implemented into oligonucleotides.

Azobenzenes with four equal substituents in all four *ortho* positions were synthesized by oxidative dimerization involving the corresponding anilines in dichloromethane utilizing a 1:1 mixture of potassium permanganate and copper(II)-sulfate (fig. 35).[81] The synthetic yields strongly depend on the electronic properties of substituted anilines and a possible sterical hindrance of the amine moiety throught the substituents. Asymmetric azobenzenes containing two differently *ortho* substituted rings carrying equal substituents on the same ring were synthesized by a Mills reaction, which involves an aniline and a nitroso compound in a glacial acetic acid mediated condensation. This type of reaction allows the selective synthesis of asymmetric azobenzenes while minimizing the formation of undesired by-products, a prerequisite for the successful introduction of a linker moiety (fig. 35).

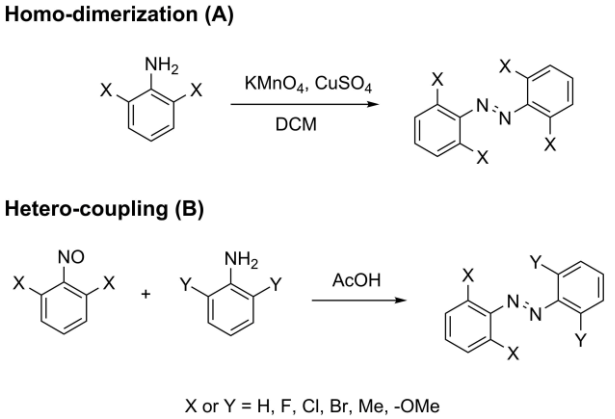

Fig. 35: Synthesis of symmetrically *ortho* substituted azobenzenes is performed by oxidative dimerization using strong oxidation agents (A) and asymmetrically *ortho* substituted azobenzenes are synthesized *via* Mills reaction from nitrosobenzenes and anilines involving glacial acetic acid (B).[91]

A pre-selection of suitable photochromes was performed using the molecules which were synthesized for the azobenzene-toolbox (fig. 36). Part of these molecules have previously been reported and serve as reference compounds for spectroscopic measurements and

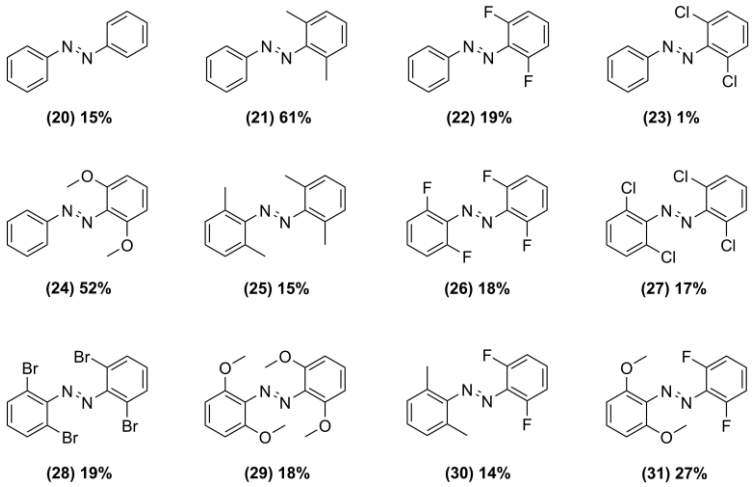

Fig. 36: Newly synthesized azobenzene toolbox containing azobenzenes with different *ortho* substituents. Aside unmodified azobenzene **(20)**, azobenzenes carrying either two substituents on the same ring in *ortho* position in molecules **(21)**-**(24)**, four equal substituents in all four *ortho* positons in molecules **(25)**-**(29)** or two different ortho substituent types on opposite rings in molecules **(30)** and **(31)** were synthesized.

irradiation conditions. Not only the response-wavelengths are of great interest, but also the synthetic accessibility of the molecules. Synthetic yields exhibit s strong variance between 1 % and 61 % while most reactions yielded azobenzenes below 20 %. A Mills reaction involving anilines with two activating *ortho* groups on the same ring shows the best yields among all reactions as observed for compounds **(21)** and **(24)**, possibly leading to an increase nucleophilicity of the amine residue.

A Mills reaction involving nitrosobenzene and 2,6-dichloroaniline yielded only 1 % of the target compound **(23)**, potentially due to sterical hindrance of the amine group through the bulky chlorine-substituents. All other Mills reactions exhibited yields between 14 % and 27 %. Symmetrically substituted *ortho* azobenzenes were accessible in moderate yields through oxidative dimerizations using the corresponding anilines and did not show a significant influence of the substituents on the reaction yields, which lie between 15 % and 19 %.

Spectroscopic investigation of the newly designed azobenzenes was performed after 5 minutes irradiation with all available LEDs and consecutive recording of UV/Vis spectra. The resulting set of absorption spectra yields irradiation wavelengths for the maximum decrease and increase in absorbance at the absorption maxima and permits a qualitative determination of the maximum *trans*- and *cis*-converting wavelengths as well as the relative n->π* and π->π* transitions.

Ortho substituents were reported to strongly red-shift response wavelengths while maintaining high thermal stabilities of the *cis* state. Azobenzenes with two *ortho* substituents on the same ring revealed a marginal shift in maximum response wavelengths compared to

Sample	Abs. max. t1	Abs. max. t2	Abs. max. c1	Abs. max. c2	max. *trans*-WL	max. *cis*-WL
(20)	319 nm	431 nm	288 nm	422 nm	405 nm	350 nm
(21)	312 nm	438 nm	278 nm	428 nm	405 nm	340 nm
(22)	315 nm	412 nm	300 nm	403 nm	385 nm	350 nm
(23)	299 nm	425 nm	282 nm	416 nm	405 nm	340 nm
(24)	325 nm	446 nm	280 nm	426 nm	405 nm	350 nm
(25)	305 nm	450 nm	290 nm	445 nm	405 nm	340 nm
(26)	306 nm	445 nm	284 nm	412 nm	385 nm	340 nm
(27)	290 nm	435 nm	N/A	N/A	N/A	N/A
(28)	304 nm	N/A	304 nm	N/A	320 nm	630 nm
(29)	310 nm	450 nm	301 nm	430 nm	405 nm	590 nm
(30)	313 nm	407 nm	282 nm	415 nm	405 nm	340 nm
(31)	321 nm	440 nm	289 nm	423 nm	405 nm	590 nm

Tab. 2: Absorption maxima and maximum irradiation wavelengths for all synthesized *ortho* substituted azobenzenes. Absorption maxima t1 and c1 correspond to both π->π*-transitions and absorption maxima t2 and c2 correspond to both n->π*-transitions.

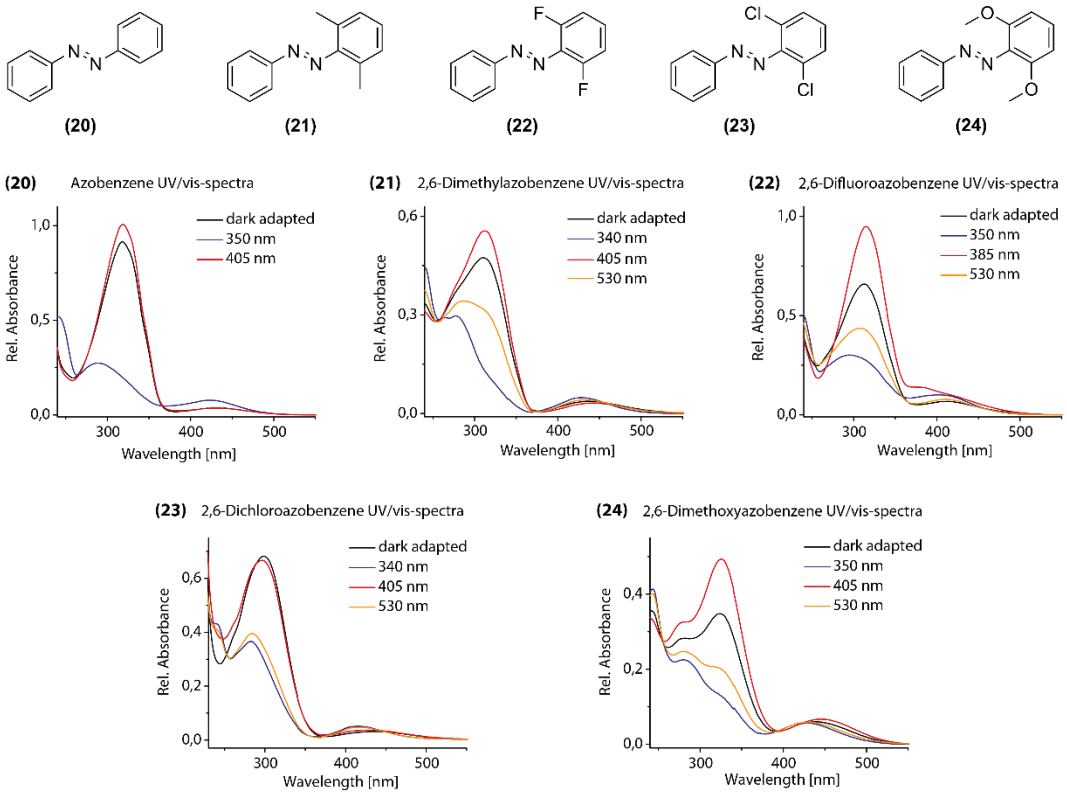

Fig. 37: Azobenzenes carrying two *ortho* substituents on the same ring were synthesized and investigated *via* UV/Vis spectroscopy after irradiation with different LED wavelengths. All *ortho* substituted azobenzenes exhibit a significant drop in absorption intensity after irradiation with UV light, indicating a successful *cis* isomerization. The same effect can be observed for irradiation with visible light wavelengths, where the intensity drop is slightly lower compared to UV irradiation.

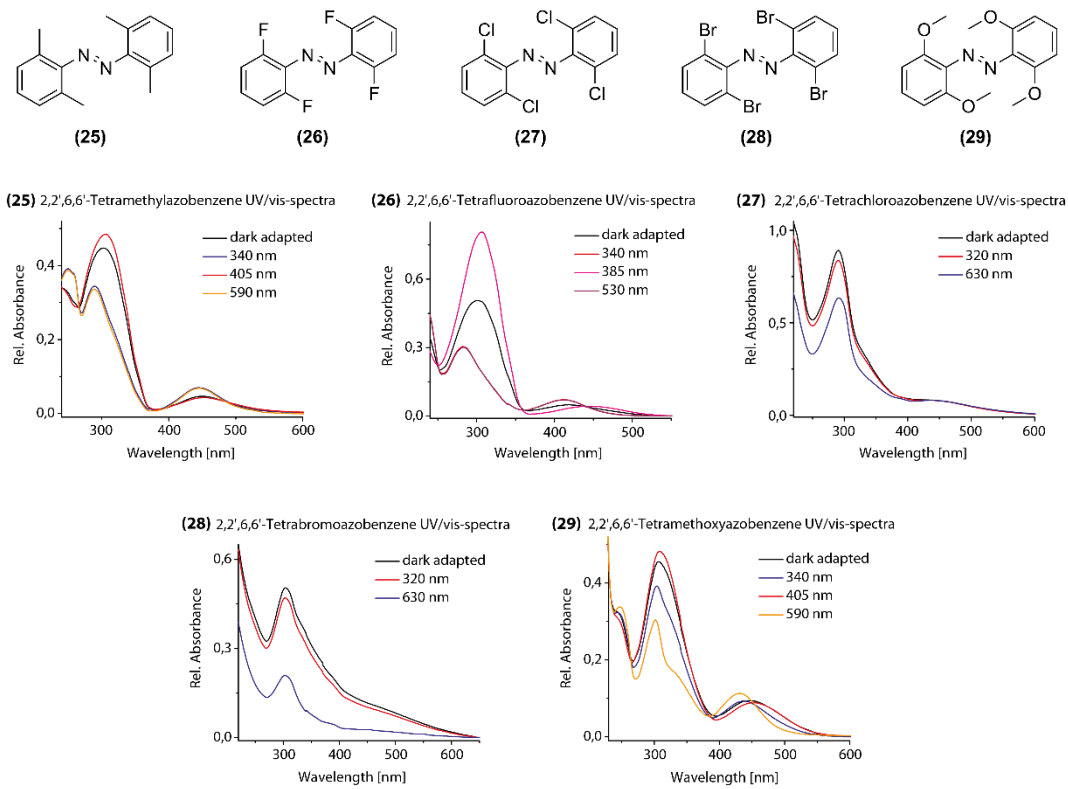

Fig. 38: Azobenzenes with substituents in all four *ortho* positions were investigated *via* UV/Vis spectroscopy, absorption spectra after irradiation with the maximum *trans* and *cis* converting wavelengths are depicted. All molecules **(25)**-**(29)** show a significant drop in absorption intensity when irradiated with visible light wavelengths beyond 500 nm.

unmodified azobenzene. 2,6-Dimethylazobenzene **(21)** and 2,6-difluoroazobenzene **(22)** exhibit a significant decrease in absorbance upon irradiation with λ = 530 nm, but no complete drop to the same absorbance intensity when irradiated with *λ* = 340 nm and *λ* = 350 nm (fig. 37). As stated before,[132,133] *ortho* fluorinated azobenzenes exhibit this effect for two and four *ortho* substituents. Two chloro **(23)** and two methoxy moieties in *ortho* position **(24)** on the same ring result in the same effect similar to *ortho* fluorinated azobenzenes as observed in a significant absorbance intensity drop at the absorption maximum when irradiated with *λ* = 530 nm. Both molecules exhibit a stronger decrease in intensity compared to *ortho* methylated and *ortho* fluorinated azobenzenes to an extent comparable to irradiation with *λ* = 340 nm and *λ* = 350 nm. Reversible switching in visible light range seems to be possible with high conversion efficiencies for both molecules, matching the first criterium for visible light responsive DNA photoswitches.The strongest separation of both n->π* transition bands are observed in 2,6-dimethoxyazobenzene **(24)** with both absorption maxima separated by 20 nm, while all other azobenzenes containing one substituted ring only show separated absorption maxima of 10 nm and lower (tab. 2).

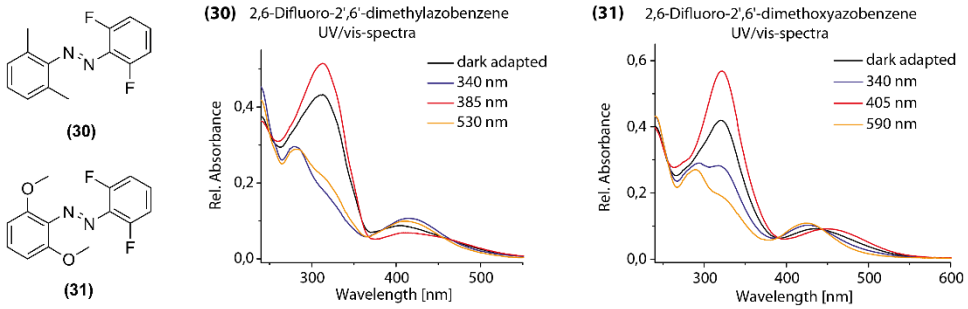

Fig. 39: Azobenzenes-with two differently *ortho* substituted opposite phenyl rings exhibit strongly red-shifted absorption bands and high conversion efficiencies in visible light range. While azobenzene **(30)** shows a similar drop in absorption intensity using UV and visible light irradiation, **(31)** reveals even a higher intensity drop when irradiating the molecule with 590 nm light compared to UV irradiation.

Azobenzenes with four *ortho* substituents result in stronger red-shifted absorption wavelengths compared to two *ortho* substituents (fig. 38). Four *ortho* methyl moieties **(25)** already decrease the intensity of the absorption maximum when irradiated with λ = 340 nm and λ = 590 nm although the separation of both n->π*-transitions are only separated by 5 nm. One isomerization direction seems to be strongly favored at this irradiation wavelength resulting in the observed effect. The same is observed in case of four *ortho* fluorine substituents **(26)** where both n->π*-transition maxima are separated by 33 nm. Irradiation with λ = 340 nm and λ = 530 nm light result in the same decrease in absorbance, indicating high conversion efficiencies between the *trans* and *cis* state in visible light range. In case of four chlorine **(27)** and bromine atoms **(28)** all electronic transitions significantly seem to overlap, resulting in a low decrease in absorbance. Four *ortho* bromine substituents indicate a decrease in absorbance, but as previously reported for these molecules,[129] long irradiation times of 30 mintes are mandatory to achieve a successful isomerization to *cis* using red light. The observed change in absorbance intensity could be enhanced by longer irradiation times, which is not intended in the workframe of this project. As stated before,[129] azobenzenes with bulky *ortho* substituents demand longer irradiation times up to 30 minutes for *cis* isomerization, excluding them as possible candidates for use in DNA applications. Furthermore, the four bulky *ortho* substituents possibly distort the planar *trans* conformation, thus possibly hampering successful intercalation between the nucleobases in double-stranded DNA. Tetra *ortho* methoxy azobenzene **(29)** reveals an even stronger decrease in absorbance when irradiated with λ = 590 nm compared to irradiation with UV light. As mentioned before, the four methoxy moieties potentially disrupt the mandatory planar *trans* conformation but might be useful for other non DNA-based applications.

Azobenzenes containing two different types of *ortho* substituents on both rings were also investigated in this study. Two electron withdrawing *ortho* fluorine atoms on one ring in

combination with two electron donating *ortho* methyl **(30)** or methoxy moieties **(31)** on the opposite ring both result in highly red-shifted absorption bands (fig. 39). **(30)** exhibits nearly the same decrease in absorbance when irradiated with λ = 340 nm or λ = 530 nm while in case of **(31)**, the decrease in absorbance becomes even stronger when irradiated with λ = 590 nm compared to UV irradiation. In direct comparison to azobenzenes with one modified ring, electronic influences of substituents seem to superimpose and lead to higher conversion efficiencies in near-infrared range of light. The formation of an *ortho* push-pull system possibly leads to a decrease in thermal stability of the *cis* state as previously reported for *para* push-pull systems.[111]

Based on the combined spectroscopic observations, a series of azobenzenes was selected to be further modified with a D-threoninol linkage for consecutive incorporation into oligonucleotide backbones. The most promising isomerization efficiencies even in visible light could be observed for azobenzenes carrying two or four *ortho* fluorine atoms and two *ortho* methoxy moieties on the same ring. Also an azobenzene carrying two chlorine atoms on the same phenyl ring could successfully be converted to *cis* with high efficiency in visible light range. Therefore compounds **(22)**, **(23)**, **(24)**, **(26)** and **(30)** were chosen to be further modified with D-threoninol for DNA implementation. Despite the very promising spectroscopic properties of **(30)** and **(31)**, using an *ortho* push-pull system possibly entails a decreased thermal stability as previously reported for *para* push-pull systems.[111] Thus, both molecules could be more suitable for short-time applications, but DNA-based applications rather demand a high thermal stability of the *cis* state.

When interpreting the relative change in absorption intensity after irradiation, it has to be kept in mind that different irradiation times might be mandatory to fully reach the photostationary state. This possibly error source can falsify the results for slowly isomerizing azobenzenes. Nevertheless, the spectroscopic investigations provide a good starting point for any further azobenzene development.

3.1.3 Synthesis and spectroscopic investigation of an arylazopyrazole toolbox

Beyond azobenzenes, arylazopyrazoles were reported showing near-quantitative conversion efficien-cies between the *trans* and *cis* state accompanied by red-shifted response wavelengths and thermal stabilities of the *cis* state of up to 1000 days at room temperature.[136] Unfortunately the molecules reported with the highest thermal stabilities do not achieve quantitative conversion efficiencies and vice versa,[136,140] but nevertheless arylazopyrazoles prove promising candidates for photocontrolled DNA applications *in vitro*. Furthermore, contrary to azobenzenes, arylazopyrazoles can be obtained synthetically in high total yields. Diazotation of anilines followed by addition to 2,4-pentadione and consecutive condensation with substituted hydrazines leads to arylazopyrazoles in near-quantitative yields (fig. 40).

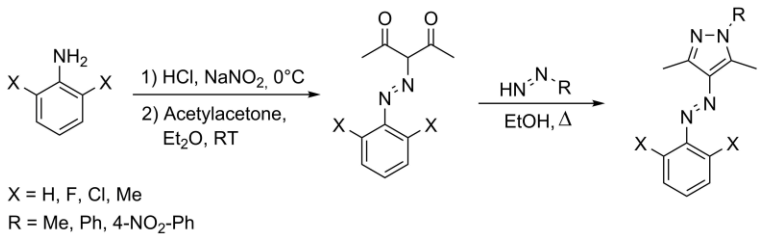

Fig. 40: General synthetic route for arylazopyrazole molecules carrying *ortho* substituents on the peripheral benzene ring for further spectroscopic investigation and optimization of response wavelengths. Diazotation of substituted anilines and consecutive addition of 2,4-pentadione followed by condensation with substituted hydrazines yields the *ortho* substituted arylazopyrazoles.

In analogy to *ortho* substituted azobenzenes, *ortho* substitution of arylazopyrazole's phenyl residue potentially results in a further red-shifted response wavelengths and further enhances thermal stability of the *cis* state. Therefore, a series of arylazopyrazoles has been synthesized carrying different substituents on the phenyl moiety as well as further functional modalities on the pyrazole ring. The resulting “arylazopyrazole toolbox” was examined towards the maximum response wavelengths and absorption maxima after irradiation through consecutive UV/Vis spectra as described before (fig. 41).

Arylazopyrazoles carrying three methyl moieties on the peripheral pyrazole ring were reported to achieve near-quantitative conversion efficiencies between the *trans* and *cis* state. The same effect could be observed under the irradiation conditions used in this study by means of high output LEDs. When irradiating **(79)** with UV and orange light respectively (fig. 42), the strong absorption maximum at λ = 341 nm corresponding to the π->π*-transition reaches its maximum upon irradiation with λ = 590 nm and almost drops to zero upon irradiation with λ = 365 nm. This implies a high conversion efficiency between both isomers as previously reported in literature. Further substitution of the phenyl residue in both *ortho* positions with

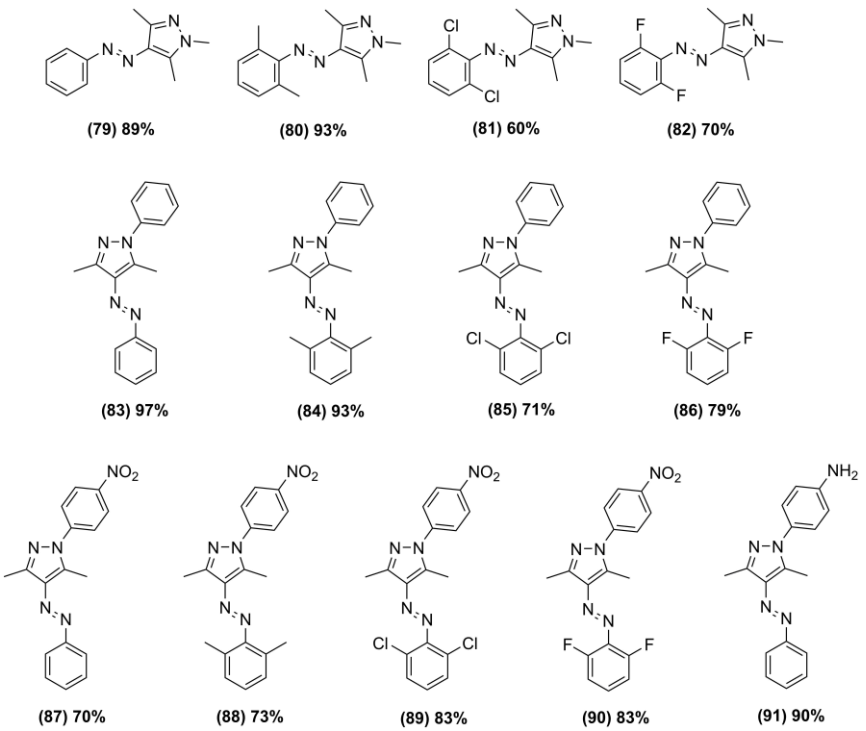

Fig. 41: Arylazopyrazole toolbox consisting of synthesized *ortho* substituted arylazopyrazole molecules **(79)**-**(91)** for optical tuning of response wavelengths into visible light range. All molecules carry two *ortho* substituents on the phenyl residue while molecules **(79)**-**(82)** contain an *N*-methyl moiety, molecules **(83)**-**(86)** contain an N-phenyl residue, molecules **(87)**-**(90)** containg a N-(4-nitrophenyl) residue and molecule **(91)** contains an N-(4-aminophenyl) residue.

Sample	Abs. max. t1	Abs. max. t2	Abs. max. c1	Abs. max. c2	max. *trans*-WL	max. *cis*-WL
(79)	341 nm	435 nm	299 nm	440 nm	590 nm	365 nm
(80)	315 nm	418 nm	294 nm	420 nm	405 nm	350 nm
(81)	313 nm	412 nm	298 nm	416 nm	405 nm	340 nm
(82)	323 nm	419 nm	295 nm	421 nm	420 nm	350 nm
(83)	335 nm	425 nm	296 nm	435 nm	530 nm	365 nm
(84)	320 nm	425 nm	293 nm	425 nm	420 nm	350 nm
(85)	315 nm	417 nm	299 nm	418 nm	420 nm	350 nm
(86)	326 nm	420 nm	297 nm	422 nm	590 nm	350 nm
(87)	343 nm	435 nm	332 nm	435 nm	590 nm	365 nm
(88)	331 nm	N/A	318 nm	N/A	590 nm	365 nm
(89)	340 nm	394 nm	320 nm	405 nm	530 nm	385 nm
(90)	337 nm	425 nm	325 nm	425 nm	590 nm	365 nm
(91)	343 nm	440 nm	292 nm	436 nm	530 nm	365 nm

Tab. 3: Absorption maxima and maximum irradiation wavelengths for all synthesized arylazopyrazole molecules given in fig. 41. Absorption maxima t1 (*trans*) and c1 (*cis*) correspond to π->π*-transitions in UV range and absorption maxima t2 (*trans*) and c2 (*cis*) correspond to n->π*-transitions in visible light range.

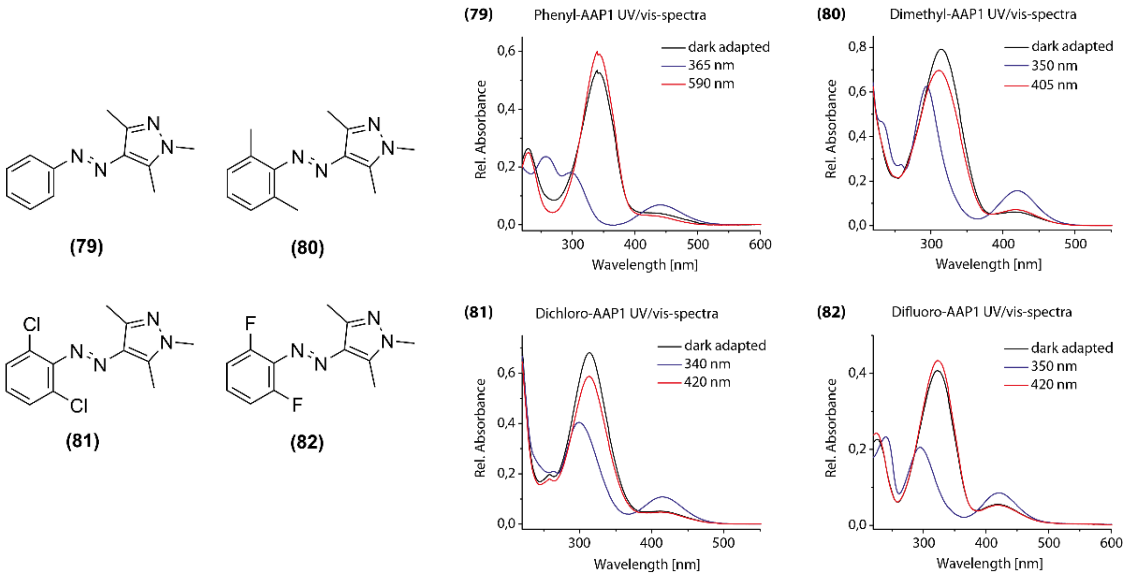

Fig. 42: UV/Vis absorption spectra of arylazopyrazole photochromes carrying an *N*-methyl group and different substituents in both phenyl *ortho* positions. UV/Vis absoption spectra after irradiation with the maximum *trans*- and *cis*-converting response wavelengths are shown. Substituents on both phenyl *ortho* positions appear to blue-shift the maximum *trans* converting excitation wavelengths.

methyl **(80)**, chloro **(81)** or fluoro substituents **(82)** results in significantly blue-shifted absorption bands and response wavelengths, shifting the maximum *trans* converting wavelengths into near-UV light range similar to the absorption properties of azobenzene. Also the maximum

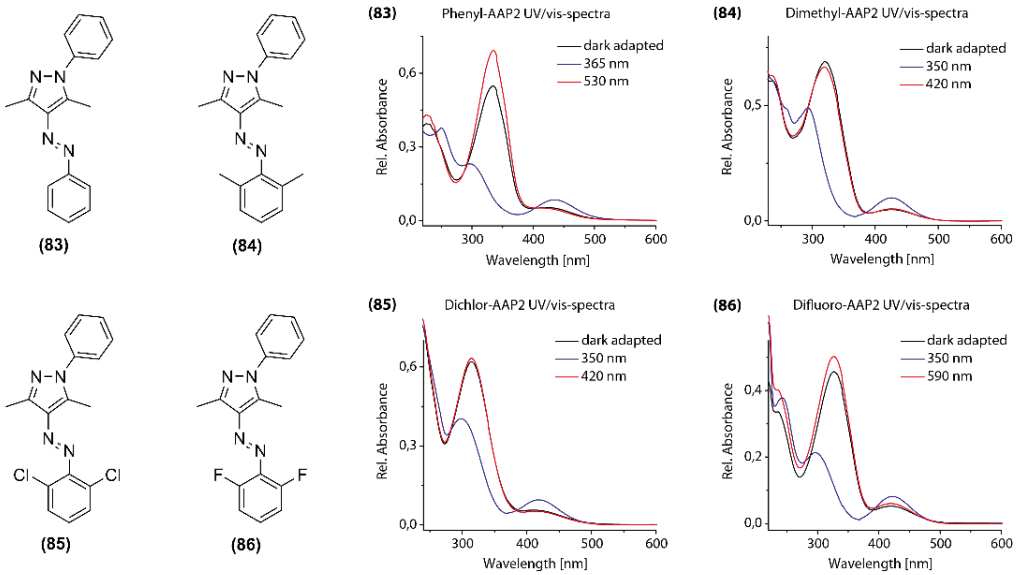

Fig. 43: UV/Vis absorption spectra of arylazopyrazole photochromes carrying an *N*-phenyl group and different substituents in both phenyl *ortho* positions. UV/Vis absoption spectra after irradiation with the maximum *trans*- and *cis*-converting response wavelengths exhibit a different photoswitching behaviour compared to *N*-methyl arylazopyrazoles as observed in UV/Vis spectra. Two methyl and chloro substituents in molecules **(84)** and **(85)** appear to blue-shift the maximum *trans* converting excitation wavelengths while two fluorine atoms in **(86)** apparently retain a near-IR photoswitching.

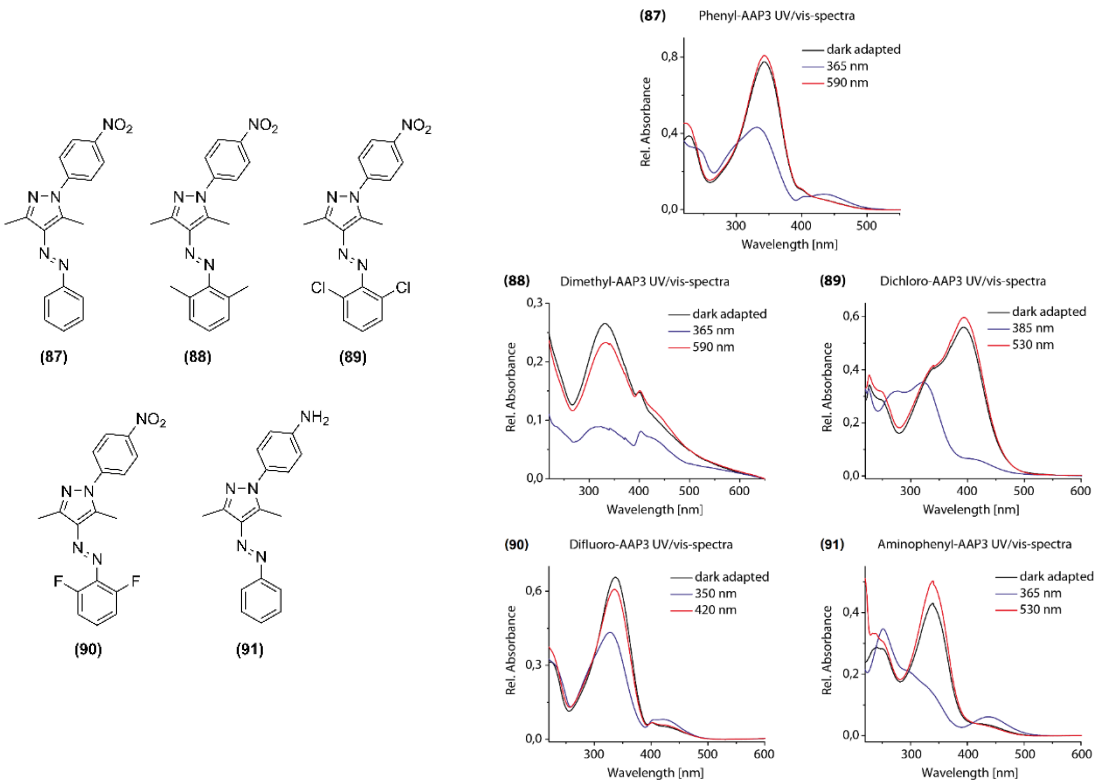

Fig. 44: UV/Vis spectra of arylazopyrazoles carrying an *N*-(4-nitrophenyl) residue in molecules **(87)**-**(90)** and an N-(4-aminophenyl) residue in **(91)** in combination with different substituents in both phenyl *ortho* positions. UV/Vis absorption spectra reveal a high overlap of absorption maxima after irradiation with different excitation wavelengths. The *cis* converting excitation wavelengths are slightly red-shifted while conversion to *trans* occurs at different visible light excitation wavelengths. **(90)** carrying two fluorine moieties shows a strong blue shift for the maximum *trans* converting excitation wavelength.

cis converting wavelengths are significantly blue-shifted, indicating an increased energy difference between the *trans* and *cis* state. Substituting the secondary pyrazole nitrogen atom with a phenyl residue **(83)** shows an absorption maximum at λ = 335 nm and also reaches its maximum under λ = 530 nm irradiation and its minimum upon irradiation with λ = 365 nm, similar to the *N*-methyl substituted arylazopyrazole **(79)** (fig. 42). Introduction of the phenyl residue leads to an expanded π-system, thus resulting in a possible influence the thermal half-life of the *cis* state. Also, it may have an influence on the base pair stacking when the moiety in intercalated into DNA duplexes.Further derivatization in both phenyl *ortho* positions reveals for the compounds **(83)** ,**(84)** ,**(85)** and **(86)** (fig. 43) the same tendency as observed for *ortho* substituted *N*-methyl arylazopyrazoles. All absorption maxima are blue-shifted and the maximum response-wavelengths for *cis* to *trans* conversion lie in the blue range of visible light. Only in case of *ortho* fluoro substituents the maximum *trans* switching response wavelength is red-shifted to λ = 590 nm. All maximum *trans* to *cis* converting response wavelengths are blue-shifted and lie in a range similar to the response wavelengths of unsubstituted azobenzene.

Introduction of a strong electron withdrawing nitro moiety in *para* position of the arylazopyrazole *N*-phenyl residue **(87)** leads to a strong overlap of absorption bands both in *trans* and *cis* conformation. Despite this, the maximum empirical response wavelengths could be determined as λ = 365 nm and λ = 590 nm, illustrating photoswitching in near-infrared range. Further derivatization by *ortho* methyl moieties **(88)** did not result in any significant effect, but led to blue-shifted response wavelenghts for fluorine residues **(90)** (fig. 44). In case of *ortho* chlorine atoms **(89)**, the π->π*-transition is strongly red-shifted above 400 nm resulting in a strong overlap of all absorption bands. Nevertheless, a maximum conversion efficiency could be observed when irradiated with λ = 385 nm and λ = 530 nm LEDs. Exchanging the nitro moiety for an electron donating amino residue **(91)** in the *N*-phenyl *para* position reveals a better separation of all absorption bands and a similar switching behaviour as observed for *N*-phenyl arylazopyrazole (fig. 44), but does not appear to achieve near-quantitative conversion efficiencies.

As a concluding remark, the spectroscopic determination of absorption maxima and maximum response wavelengths does not include the thermal stability of the *cis* state as an important factor. Fast back-relaxation as a possible error source might decrease the observed conversion efficiencies through back-switching during the measurement. This factor is further investigated using D-threoninol linked photoswitches (chapter 3.2.2). *Ortho* substitution of the azo phenyl moiety led to an undesired blue-shift of response wavelengths excluding these synthesized molecules from being introduced into oligo-nucleotides. Also the introduction of *para* substituents on the pyrazole *N*-phenyl residue did not significantly improve the absorption behaviour further into the desired red light range. The non *ortho* modified arylazopyrazoles **(79)**, **(83)** and **(87)** revealed the most promising spectroscopic properties and were therefore selected to be further derivatized with D-threoninol for further consecutive implementation into oligonucleotide strands.

3.1.4 Synthesis of D-threoninol linked azobenzenes for introduction into DNA strands

Based on the previous spectroscopic investigation of *ortho* substituted azobenzene and arylazo-pyrazole chromophores, a series of these molecules has been selected for further implementation into oligonucleotide strands. In analogy to the previously reported azobenzenes established in DNA, all molecules necessitate a D-threoninol linkage in *para* position through a peptide bond on one peripheral phenyl ring. Tetra *ortho* fluoroazobenzene **(26)** thereby revealed the highest conversion efficiencies in visible light range from *trans* to *cis* and vice versa (see chapter 3.1.2) and was therefore selected for implementation into oligonucleotide strands.

The synthetic pathway starts with the oxidation of 2,6-difluoroaniline to 2,6-difluoronitroso-benzene **(19)** using MCPBA in dichloromethane, which represents one part of the photochrome formed in a consecutive Mills reaction to yield the photochromic part of the asymmetrically substi-tuted tetrafluoroazobenzene backbone. The phenyl moiety containing the D-threoninol moiety was synthesized by *para* bromination of 2,6-difluoroaniline with *N*-bromosuccinimide in acetonitrile followed by catalytic substitution of bromine with copper(I)cyanide in DMF to form 4-cyano-2,6-difluoroaniline **(33)** (fig. 45). The following Mills reaction in glacial acetic acid involving 2,6-difluoro-nitrosobenzene **(19)** and 4-cyano-2,6-difluoroaniline **(33)** yielded a substituted tetrafluoroazobenzene carrying a cyano residue in *para* position on one peripheral phenyl ring **(34)**. The Mills reaction yield represents the bottleneck of the whole synthetic pathway, reaching a maximum yield of 10 %. The strongly electron withdrawing fluorines possibly hamper a nucleophilic attack of the nitrogen lone pair, resulting in the low reaction yield. Refluxing the resulting 4-cyano-2,2',6,6'-tetrafluoroazobenzene **(34)** in 1 M aqueous NaOH led to a 2,2',6,6'-tetrafluoroazobenzene carboxylic acid **(35)**. Consecutive D-threoninol coupling to the carboxylic acid as the required base surrogate part for DNA implement-tation could not be achieved. Using a series of peptide coupling reagents as HBTU, DCC in combination with OxymaPure, diethylcyanophosphonate and a direct formation of the carboxylic acid chloride followed by addition of D-threoninol did not show any formation of the desired product. Most reactions returned the unconverted starting material. The high electron deficiency involving all four fluorines appears to drastically stabilize the non-protonated form of the carboxylic acid which prevents a successful coupling to D-threoninol in these reactions. Using harsh reaction conditions possibly results in a favoured ipso-substitution of all fluorine residues instead of a peptide coupling.

A further attempt involved the attachment of D-threoninol to 4-carboxy-2,6-difluoroaniline **(36)** followed by D-threoninol protection using 2,2-dimethoxypropane in acetone **(38)** (fig. 46).

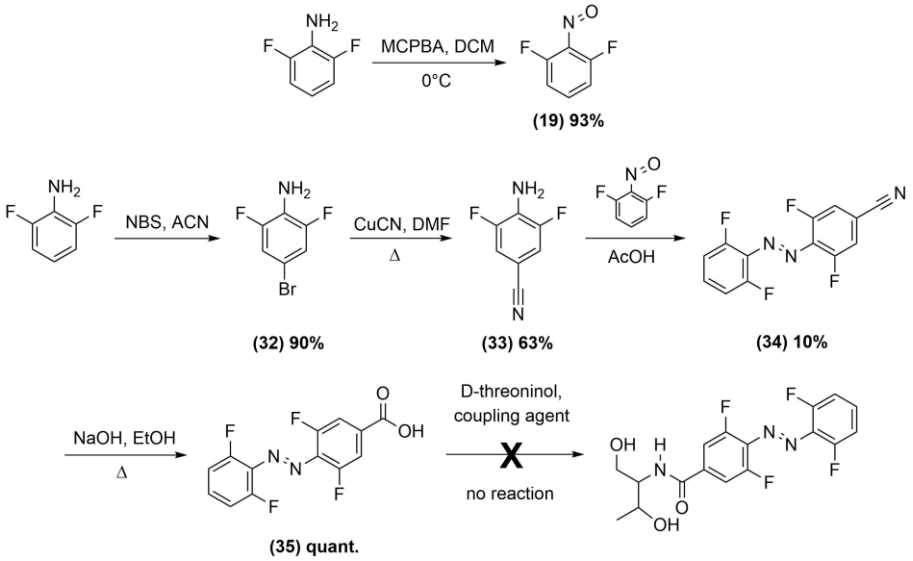

Fig. 45: Synthetic pathway for a 2,2',6,6'-tetrafluoroazobenzene phosphoramidite based on Mills reaction types. A successful coupling of D-threoninol to the 2,2',6,6'-tetrafluoroazobenzene carboxylic acid could not be achieved when using a series of different coupling conditions.

The consecutive Mills reaction involving **(38)** and 2,6-difluoronitrosobenzene **(19)** did not show any formation of the desired product but gave a series of non-identified by-products. This second pathway was therefore also considered to be not appropriate.

Beyond the two reaction pathways based on a Mills reaction to form the asymmetric tetrafluoroazobenzene, synthesis of the 2,2',6,6'-tetrafluoroazobenzene-D-threoninol molecule was attempted *via* a third pathway by coupling the protected 4-carboxy-2,6-difluoroaniline-D-threoninol **(38)** to 2,6-difluoroaniline in an asymmetric oxidative dimerization.

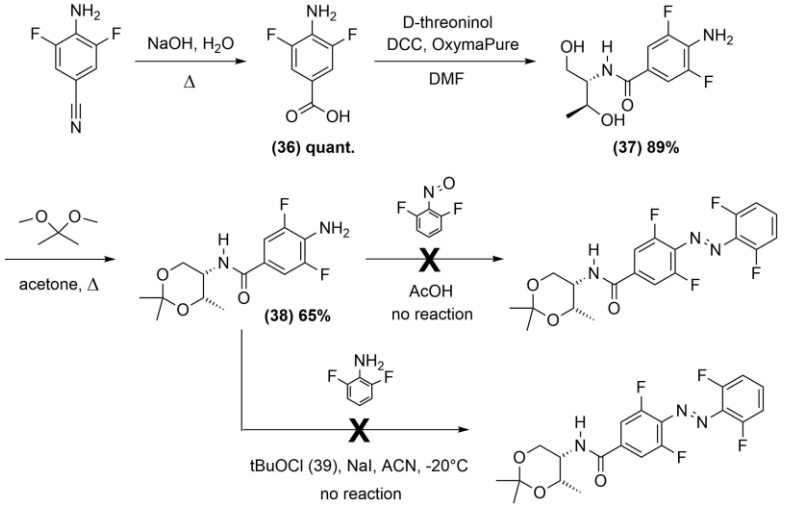

Fig. 46: Alternative synthetic pathway to achieve a 2,2',6,6'-tetrafluoroazobenzene phosphoramidite using either a Mills reaction with different starting materials (upper pathway) or an oxidative hetero dimerization pathway involving tBuOCl (lower pathway). Efficient coupling of a D-threoninol bound 2,6-difluoroaniline to 2,6-difluoroaniline could not be achieved by boh reaction pathways.

tert-Butylhypochlorite was reported to selectively favour hetero-substituted azobenzene products in oxidative dimerizations of two anilines at low temperatures, thereby minimizing formation of the undesired homo coupling by-products.[98] Successful oxidative dimerization could not be achieved using a series of oxidation agents, namely $KMnO_4$ in a 1:1 mixture with a copper(II)sulfate support in dichloromethane[81] as well as the mentioned oxidation involving *t*-BuOCl at low temperatures did not yield the desired product. Synthesis of 2,2',6,6'-tetrafluoroazobenzene-D-threoninol was stopped at this point and considered synthetically not accessible. Further attempts to achieve the target product have not been performed.Since a tetra *ortho* fluoroazobenzene could not be successfully obtained, the focus was put on further *ortho* fluorinated azobenzenes. 2,6-Difluoroazobenzene carrying two fluorine atoms in *ortho* position on the same phenyl ring as well as further *ortho* fluorinated derivatives were reported to exhibit strongly red-shifted response wavelengths while maintaining high conversion efficiencies between both conformations and high thermal stabilities of the *cis* state.[132,133] Also, the previous spectroscopic investigation of 2,6-difluoroazobenzene **(22)** revealed high conversion efficiencies between *trans* and *cis* in visible light range, although the conversion efficiencies were slightly lower than observed for 2,2',6,6'-tetrafluoroazobenzene **(26)**. A reduced number of two fluorine atoms attached to the aromatic system decreases the electron deficiency compared to four fluorines, thus possibly exhibiting a lower tendency of fluorine ipso substitution in reactions involving nucleophiles. Beyond the scope of synthesis, the tendency of fluorine to be prone to ipso-substitution by nucleophilic reactants possibly causes side reactions in DNA or cellular environments since a variety of nucleophilic moieties are present under these conditions.

2',6'-difluoroazobenzene-D-threoninol **(42)** was synthesized following the reported synthetic route for azobenzene and 2',6'-dimethylazobenzene phosphoramidites (fig, 47).[192] A Mills

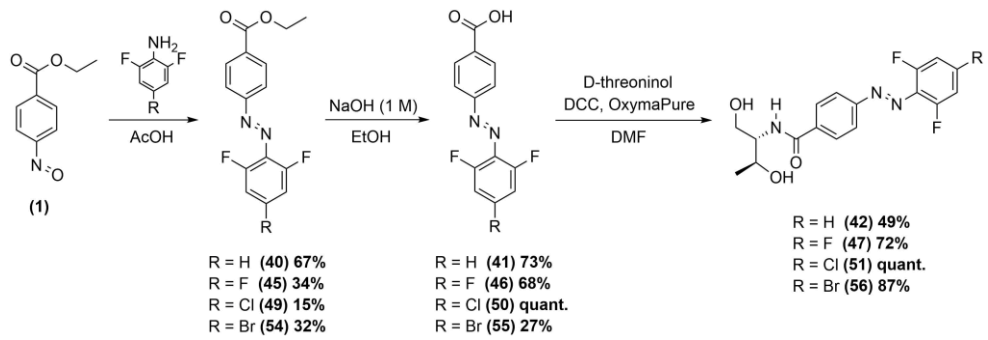

Fig. 47: Synthetic pathway for 2',6'-difluoroazobenzene coupled to D-threoninol (DFAB) and further derivatives carrying fluorine (DFAB-F), chlorine (DFAB-Cl) or bromine atoms (DFAB-Br) in *para* position. **(42)** could be obtained in moderate yields while the three other derivatives showed only low synthetic yields. The Mills azo formation still remains the bottleneck of the reaction pathways leading to highly decreased yields of intermediates.

reaction between 2,6-difluoroaniline and ethyl-4-carboxynitrosobenzoate **(1)** in glacial acetic acid yielded 67 % of the target compound **(42)**. Ester hydrolysis and consecutive coupling of D-threoninol to the carboxylic acid moiety using HBTU in DMF yielded the product in moderate yields.

Introduction of further electron donating or withdrawing moieties in *para* position of the peripheral fluorinated ring may have an improving effect on the photphysical properties and serves as a coupling site for further derivatization of the molecules. As previously reported, introduction of electron with-drawing substitutents in *para* position leads to a more efficient separation of both n->π* bands, thus facilitating reversible photoconversion in visible light range.[132,133] In respect to oligonucleotide strands, bulky substituents bear the potential of additionally disrupting base stacking of nucleobases, thereby decreasing the overall DNA duplex stability and relieving efficient photocontrol of duplex hybridi-zation. A series of *para* substituents were introduced on the peripheral 2',6'-difluoro-azobenzene ring to investigate synthetic feasibility and spectroscopic properties of further substituted derivatives. Following the same synthetic pathway, a 4'-fluoro **(47)** and a 4'-chloro derivative **(51)** were both accessible in low yields compared to 2',6'-difluoroazobenzene, possibly caused by additional electronic deactivation through the substituents. A derivative carrying bromine in *para* position **(56)** as well as a 4'-acetamido derivative **(59)** were synthetically accessible (fig. 48), but pure products could not be isolated. Furthermore, both molecules highly tended to *para* and *fluoro* substitution when trying to attach D-threoninol to the free carboxylic acid moiety. Fluorine substitution could be observed by shifted signals in ^{19}F-NMR towards lower ppm values (see appendix). Also, mass spectrometry revealed substituted by-products and decomposition of the target compounds.

Further derivatization of 2,6-difluoroazobenzene on the opposite ring carrying the carboxylic acid moiety by introduction of two methyl substituents in both *ortho* positions was performed

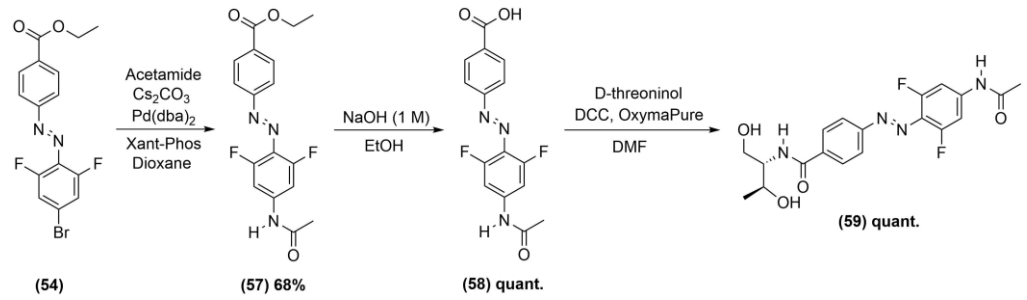

Fig. 48: Further derivatisation of DFAB by a *para* acetamide moiety was synthesized for optical tuning of response wavelengths. Using a 4'-bromo-2',6'-difluoroazobenzene derivative, the acetamide moiety is introduced by a Palladium catalysed reaction. Consecutive ester hydrolysis and coupling to D-threoninol yields the target product in high yields.

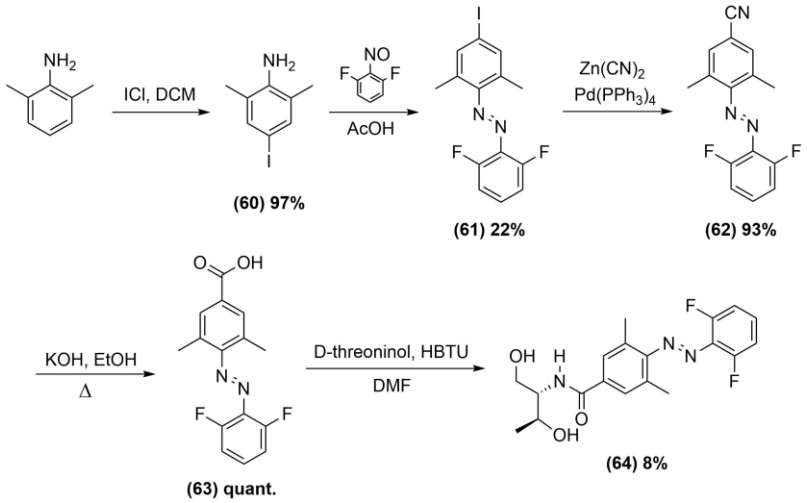

Fig. 49: Synthetic route to achieve a 2',6'-difluoro-2,6-dimethylazobenzene photoswitch coupled to D-threoninol in *para* position. Introduction of a cyano moiety by $Zn(CN)_2$ and consecutive transformation to form a carboxylic acid provides a coupling site for D-threoninol.

to investigate additional stabilization as observed for 2',6'-dimethylazobenzene (fig. 49). The target compound could be obtained by coupling 2,6-dimethyl-4-iodoaniline **(60)** to 2,6-difluoronitrosobenzene **(19)** in a Mills reaction. Catalytic introduction of a nitrile residue by zinc(II)cyanide mediated by $Pd(PPh_3)_4$ followed by nitrile hydrolysis yielded the photochrome including the carboxylic acid moiety **(63)**, which was consecutively linked to D-threoninol. The amount of additional necessary reaction steps to obtain the target 2',6'-difluoro-2,6-dimethylazobenzene-D-threoninol **(64)** lowered the overall yield significantly. Also, couling to D-threoninol could only be achieved in a very low yield.

Beyond the scope of *ortho* fluoroazobenzenes, further functional moieties in *ortho* position revealed promising spectroscopic properties in the UV/Vis irradiation scans performed before (see chapter 3.2.1). Azobenzenes carrying four chloro and methoxy substituents in all *ortho* positions have been reported to show highly red-shifted response wavelengths into visible light range.[128,129] Four sterically challenging substituents in *ortho* position possibly distort the planar aromatic system and consequently might prevent a successful intercalation between DNA base stacks, therefore azobenzenes with two substituents on the same ring in *ortho* position were selected.

2',6'-Dichloroazobenzene attached to D-threoninol **(67)** was synthesized following the same synthetic route as used before (fig. 50). The ethyl-4-carboxy-2',6'-dichloroazobenzene precursor **(65)** was synthesized in one step from 2,6-dichloroaniline and ethyl-4-carboxy nitrosobenzene **(1)** in a Mills reaction containing 1:1 glacial acetic acid and trifluoroacetic acid. Since **(65)** could not be obtained in a purified form, the synthetic pathway was continued with the non-purified crude product. Contrary to previous reactions, no product formation could be

observed in glacial acetic acid at room tempera-ture, possibly due to the strong sterical hindrance of the aromatic amine by both chlorine substituents, thus preventing a nucleophilic attack of the amine moiety. Reaction conditions had to be adjusted to a 1:1 mixture of glacial acetic acid and trifluoroacetic acid and elevated reaction temperatures (40 °C) to achieve the product. These harsh reaction conditions still yielded low impure amounts of the desired product. Ester hydrolysis and coupling to D-threoninol was performed analogous to the reactions before (fig. 50). Since a product mixture was used for consecutive reactions, the final product had to be purified by preparative HPLC to yield the pure product. Since synthesis and purification of the target compound and intermediate steps proved difficult, the molecule **(67)** was not further consi-dered for introduction into DNA, but was further used for spectroscopic investigations.

A 2',6'-dimethoxyazobenzene derivative coupled to D-threoninol **(72)** could be synthesized straight forward in high yields, although the 2,6-dimethoxyaniline precursor **(69)** had to be synthesized separately (fig. 51). Starting from 2-nitroresorcinol, methylation of both hydroxy moieties by dime-thylsulfate in acetone yielded 2,6-dimethoxynitrobenzene **(68)** in near-

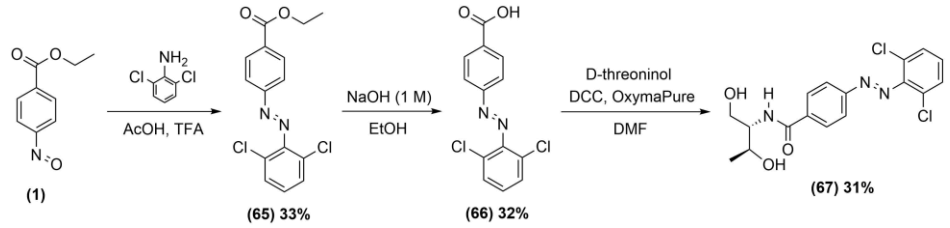

Fig. 50: Synthetic pathway for a 2',6'-dichloroazobenzene linked to D-threoninol in *para* position. The previously used Mills reaction conditions had to be adjusted to a 1:1 acetic acid:TFA mixture to achieve the target product **(67)**.

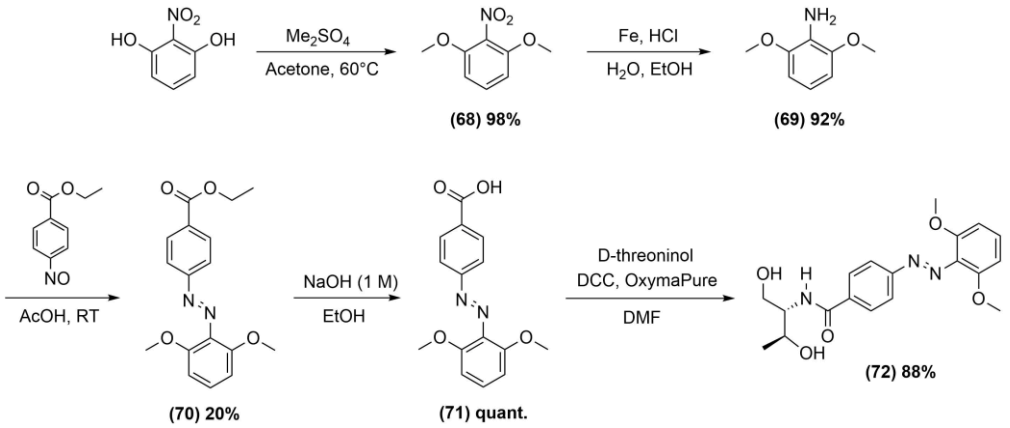

Fig. 51: Synthetic route for a 2',6'-dimethoxyazobenzene coupled to D-threoninol in *para* position. The required starting material 2,6-dimethoxyaniline **(69)** was prepared in two high-yielded steps. All following reactions were executed in analogy to the previously described reaction pathways to achieve successful formation of the product **(72)**.

quantitative yield, which was further reduced to the corresponding aniline using iron powder in combination with hydrochloric acid in a water ethanol mixture in high yield. A Mills reaction involving 2,6-dimethoxyaniline **(69)** and ethyl-4-nitrosobenzoate **(1)** led to the target molecule ethyl-4-carboxy-2',6'-dimethoxyazobenzene **(70)** in 20 % yield. Follow-up ester hydrolysis and coupling to D-threoninol using DCC and OxymaPure in DMF achieved the target D-threoninol coupled 2',6'-dimethoxyazobenzene **(72)** in high yield (fig. 51).

All synthetically accessible azobenzenes coupled to D-threoninol were selected for further intro-duction into oligonucleotide strands. The synthetically non accessible molecules 2,2',6,6'-tetrafluoro-azobenzene-D-threoninol and 2',6'-dichloroazobenzene-D-threoninol **(67)** were excluded from any other synthetic development since the synthesis of both target molecules failed or only yielded the desired product in very low amounts. All synthesized target molecules were further investigated towards their photophysical properties as described in chapter 3.2.1.

3.1.5 Synthesis of D-threoninol linked arylazopyrazoles for introduction into DNA strands

The pre-selection of suitable photochromes for DNA implementation from the previously synthe-sized arylazopyrazole toolbox (chapter 3.1.3) originated three main candidates with promising spectroscopic properties to be further synthetically developed for introduction into DNA. All three molecules contain an unmodified phenyl ring and a substituted secondary nitrogen on the pyrazole residue. The molecules *N*-methylarylazopyrazole (AAP1) **(95)**, *N*-phenylarylazopyrazole (AAP2) **(100)** and *N*-4-nitrophenylarylazopyrazole (AAP3) **(105)** could be synthesized successfully by attaching a carboxylic acid moiety in *para* position to the peripheral phenyl moieties to be further coupled to D-threoninol *via* a pathway similar to the reported synthesis routes (fig. 52).[192]

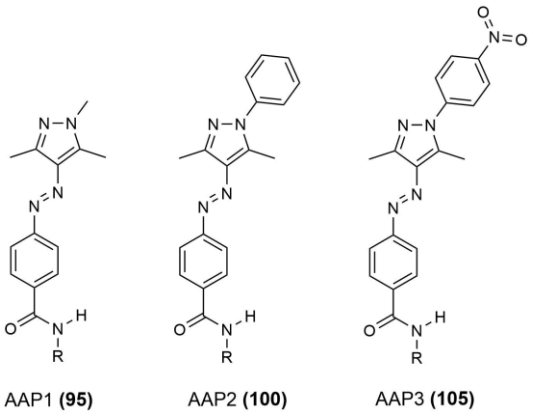

Fig. 52: Modified arylazopyrazoles for improved photocontrol of oligonucleotide duplex hybridization. AAP1 (left) was reported in literature without D-threoninol linkage,[136] AAP2 (middle) and AAP3 (right) represent newly synthesized modified derivatives of this reported arylazopyrazole.

The synthetic pathway started from diazotation of ethyl-4-aminobenzoate instead of aniline, followed by a diazotation involving 2,4-pentadione and condensation with the respective hydrazines carrying either a methyl, phenyl or 4-nitrophenyl residue to form the heterocyclic photochromes (fig. 53). Compared to azobenzenes, the total synthesis of all three arylazopyrazole carboxylic acids **(94)**, **(99)** and **(104)** reveals high-yielded steps, a major advantage concerning an economical use of materials. The previously discussed Mills reaction used for the synthesis of asymmetrically substituted azobenzenes represents the bottleneck in azobenzene synthesis and deteriorates the total synthetic yields of differently substituted azobenzenes. Since a Mills reaction is not required for accessing arylazopyrazoles, the total synthetic yield increases significantly.

Coupling to D-threoninol could be achieved successfully for AAP1 and AAP2 in moderate yields to form **(95)** and **(100)**, but coupling of D-threoninol to AAP3 proved difficult. A highly

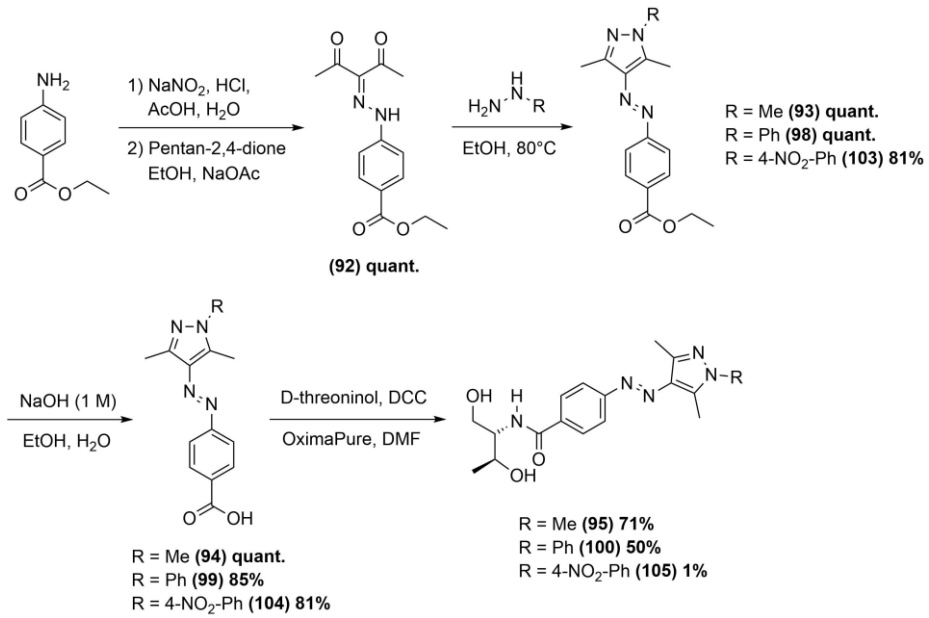

Fig. 53: Synthetic route for D-threoninol linked arylazopyrazoles AAP1, AAP2 and AAP3. All three molecules were synthesized following the same synthetic pathway. All single reactions are high-yielded, only an efficient coupling of D-threoninol to **(104)** could not be achieved.

decreased solubility of AAP3 carboxylic acid **(104)** as observed in a wide range of tested organic and inorganic solvents possibly prevents a successful reaction of AAP3 carboxylic acid to D-threoninol. The reduced solubility impedes further conversion of the compound and makes it synthetically not accessible as a DMT-protected phosphoramidite. AAP3 was consequentially not considered any further for a synthetic development and introduction into oligonucleotides.

High total synthetic yields of AAP1-D-threoninol **(95)** and AAP2-D-threoninol **(100)** provide two promising candidates for introduction into oligonucleotide strands and a possible improvement of photocontrol over DNA duplex hybridization. As stated before (chapter 3.1.3), the small molecules without D-threoninol linkage already exhibited high reversible conversion efficiencies between the *trans* and *cis* state upon irradiation with UV and orange light. If these properties sustain within DNA or RNA strands, both arylazopyrazoles possibly implicate an improvement of oligonucleotide duplex hybridization photocontrol.

3.2 Photophysical properties of D-threoninol linked photoswitches

3.2.1 UV/Vis investigation and conversion efficiencies of D-threoninol bound photochromes

The combination of synthetic accessibility and spectroscopic properties emerged a series of chromophores for an introduction into oligonucleotide strands. This final "photoswitch toolbox" consisting of D-threoninol bound photochromes constitutes a selection of molecules with promising photophysical properties for an improvement of photocontrol over oligonucleotide hybridization (fig. 54). All synthetically accessible D-threoninol linked azobenzenes and arylazopyrazoles described in chapter 3.1.4 and 3.1.5 represent potential candidates for introduction into oligonucleotides.

Since the introduction of D-threoninol bound to a carboxylic acid moiety in *para* position possibly influences the spectroscopic properties of each previously investigated photochrome. A further determination of maximum response wavelengths and switching efficiencies has to be performed. All molecules have to match the three criteria of a suitable photoswitch, wheras the first criterium, the synthetic accessibility is already fulfilled by the molecules selected.

The second criterium, high switching efficiencies of the photochromes and a shift of response wavelengths into visible light range, is investigated by quantifying the composition of *trans* and *cis* isomers after irradiation with each available LED *via* reversed-phase HPLC. In contrast to the previous investigations, UV/Vis spectroscopy after irradiation with every available wavelength is now used to determine the absorption maxima and isosbestic points of the

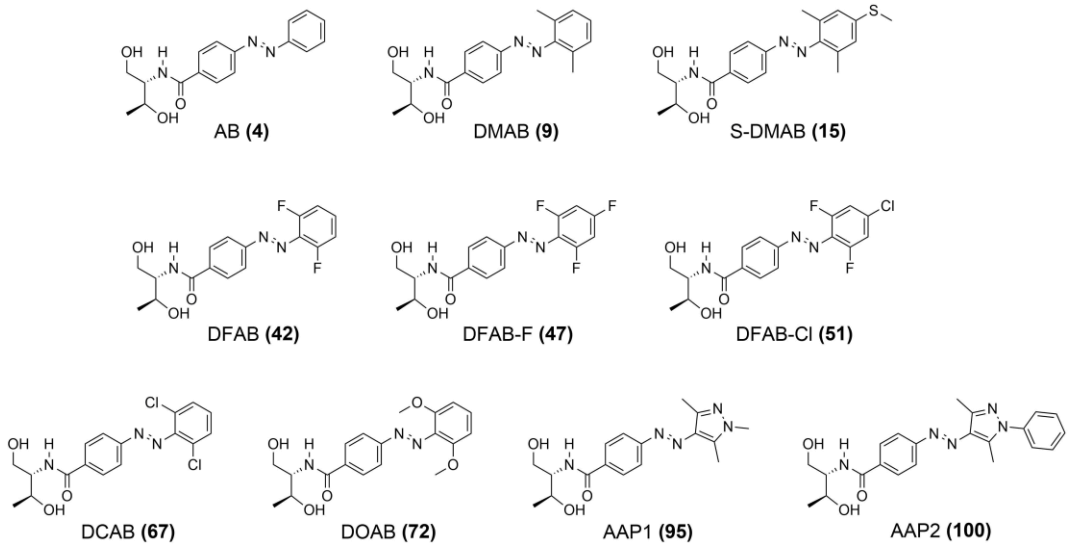

Fig. 54: Synthesis of a "photoswitch toolbox" containing a series of D-threoninol bound photochromes. The synthetically accessible photochromes described in chapters 3.1.4 and 3.1.5 were further investigated vie UV/Vis spectroscopy to select a series of potent photoswitches for further development of photochrome phosphoramidites and introduction into DNA strands.

molecules. The isosbestic point is a characteristic for all azobenzene and arylazopyrazole photochromes and constitutes the point in a set of absorption spectra where the total absorbance intensity does not change, independent from the present composition of *trans* and *cis* isomers. Detection of the isosbestic point is used for a distinct quantification of the *trans* and *cis* fraction within a photostationary state for each photochrome after irradiation with a specified LED wavelength. In analogy to all previous investigations, UV/Vis absorption spectra were recorded after irradiation with every available wavelength. The D-threoninol bound small molecules were dissolved in a 19:1 water:acetonitrile mixture to approximate the aqueous conditions used in DNA experiments. All UV/Vis irradiations and absorption scans bring out the isosbestic point by overlaying all recorded curves. Quantifying the *cis* to *trans* ratio of azobenzene mixtures implies the problem of a changing absorbance intensity after each irradiation step, significantly impeding an exact quantification. Detection of the absorption at the isosbestic point circumvents this problem since the total intensity does not change. All determined isosbestic points are used as detection wavelengths in consecutive reversed-phase HPLC quantifications using a Nucleodur pentafluorophenylpropyl (PFP) column. The column material facilitates separation of *trans* and *cis* isomers while detection at the isosbestic point minimizes absorption errors through different compositions of *trans* and *cis* isomers. Integration of all recorded signals permits the calculation of *trans* and *cis* isomer fractions for every applied irradiation wavelength (fig. 55).

UV/Vis spectroscopy of D-threoninol bound photochromes after irradiation with every available LED wavelength revealed a similar photoswitching behaviour as observed before. DFAB **(42)** exhibits a strong change in absorbance upon irradiation with 350 nm or 385 nm

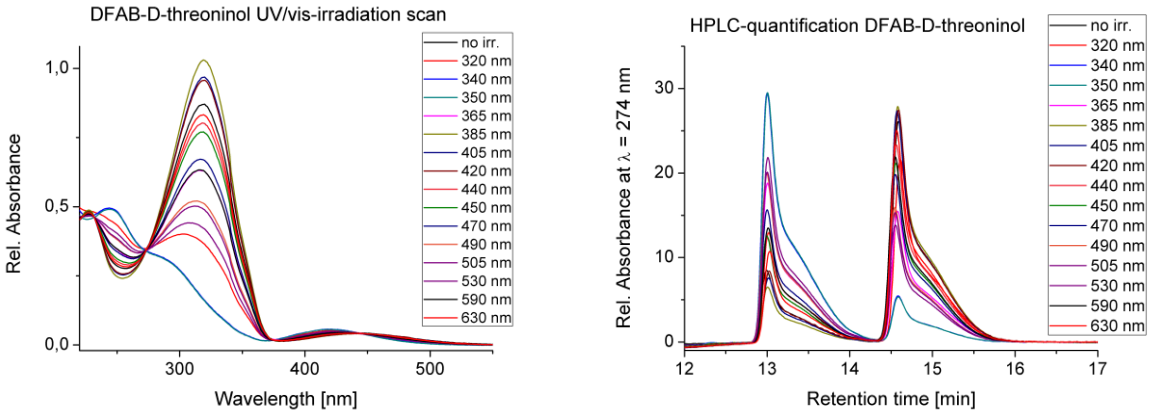

Fig. 55: UV/Vis spectra of all available photochromes after irradiation with every available LED wavelength permits a comprehensive determination of maximum *trans* and *cis* converting irradiation wavelengths and isosbestic points (left). Separation of both stereo isomers *via* reversed-phase HPLC while detecting the absorption at the isosbestic point permits a disctinct quantification of wavelength-dependent *trans* and *cis* fractions through integration of both peak areas (right).

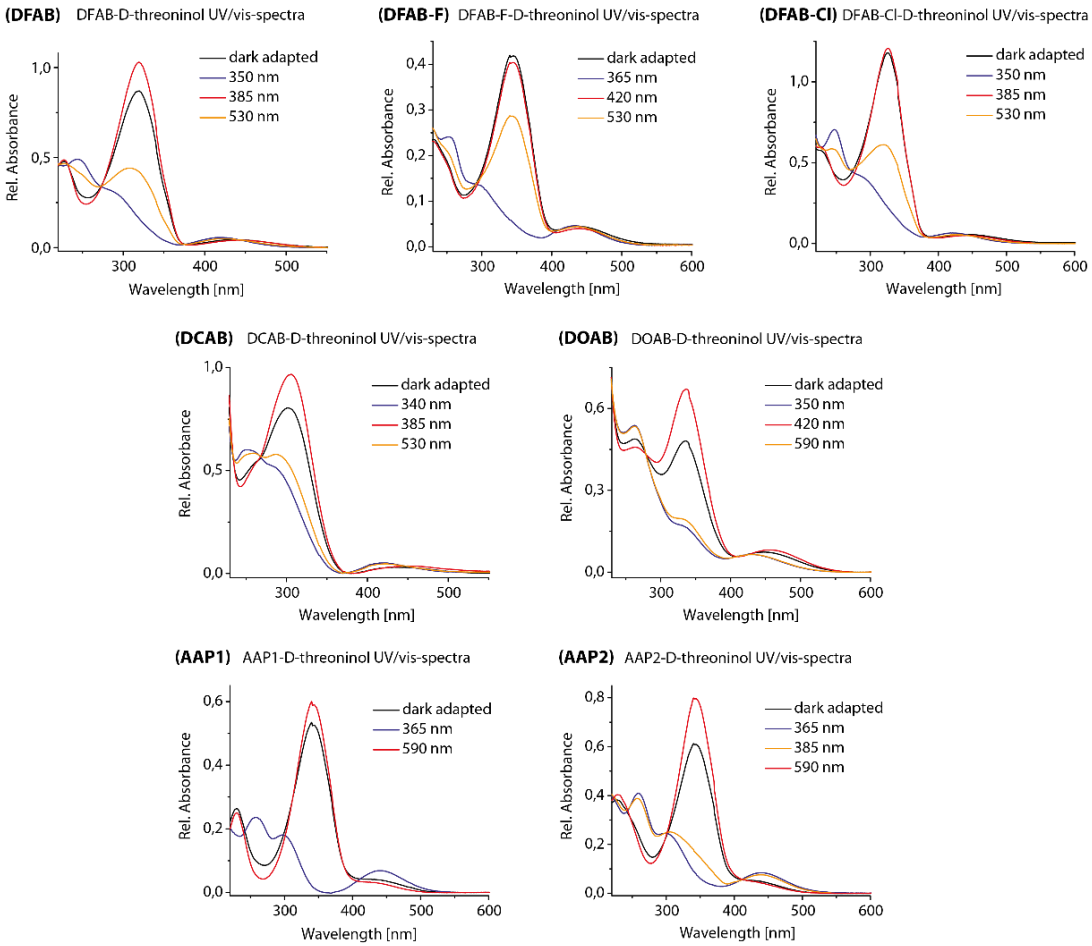

Fig. 56: Empirical UV/Vis spectra of D-threoninol bound azobenzenes and arylazopyrazoles after irradiation with all available LED wavelengths reveal the maximum change in absorbance at the absorption maxima, thus indicating the maximum *trans* and *cis* converting irradiation wavelengths in UV and visible light range.

light and a lower drop in absorbance upon irradiation with 530 nm (fig. 56, tab. 4). As observed before, DFAB shows a significant but incomplete *cis* photoswitching upon 530 nm irradiation. Introduction of a fluorine **(47)** or chlorine residue **(51)** in *para* position does not enhance visible light photoswitching. While chlorine in *para* position does not exhibit any change in absorption behaviour, the additional fluorine atom shifts the *trans* response wavelength from 385 nm to 420 nm, but visible light switching at 530 nm is significantly decreased as observed by a lower drop in absorbance after irradiation.

DCAB **(67)** and DOAB **(72)** both yield a stronger visible light switching compared to *ortho* fluoroazobenzenes (fig. 56, tab. 4). The maximum change in absorbance as observed for UV light irradiation could also be observed by a strong decrease in absorbance upon irradiation with 530 nm light in case of DCAB and 590 nm irradiation in case of DOAB. The same change in absorbance could be observed for both small molecules without D-threoninol linkage as well, but the maximum *cis* converting irradiation wavelength of DOAB is even stronger red-shifted

Sample	max. *trans* WL	max. *cis* WL	max. *cis* WL vis	Isosbestic point
AB	405 nm	350 nm	N/A	282 nm
DMAB	420 nm	350 nm	590 nm	277 nm
S-DMAB	440 nm	385 nm	N/A	288 nm
DFAB	385 nm	350 nm	530 nm	274 nm
DFAB-F	420 nm	365 nm	530 nm	292 nm
DFAB-Cl	385 nm	350 nm	530 nm	278 nm
DCAB	385 nm	340 nm	530 nm	268 nm
DOAB	420 nm	350 nm	590 nm	279 nm
AAP1	590 nm	365 nm	N/A	301 nm
AAP2	590 nm	365 nm	N/A	301 nm

Tab. 4: Maximum empirical *trans* and *cis* converting irradiation wavelengths in UV and visible light range as well as isosbestic points determined from UV/Vis absorption spectra after irradiation with different LED wavelengths for 5 minutes at room temperature. The full spectra for each irradiation and absorbance scan can be found in chapter 7.3.3.

than in non D-threoninol modified DOAB. Both arylazopyrazoles AAP1 **(95)** and AAP2 **(100)** on the other hand to not reveal any visible light *cis* switching, but a strong absorbance dropupon 365 nm irradiation indicates the same near-quantitative switching efficiency as observed for the molecules without D-threoninol. Absorption wavelengths of AAP2 are further red-shifted from 350 to 365 nm and even 385 nm irradiation reveals a decrease in absorbance almost as strong as observed for 365 nm irradiation. Both molecules exhibit the strongest increase in absorbance at 590 nm irradiation which is close to the infrared range.

To distinctly quantify the amount of *trans* and *cis* isomer in every PSS formed after irradiation with different wavelengths, a reversed-phase HPLC assay way performed. After irradiation, an aliquot of the sample solution was injected into HPLC and both stereo isomers were successfully separated for all photochromes. Detection at the respective isosbestic points (tab. 4) and consecutive integration of the corresponding signals in the resulting chromatograms permit a distinct determination of the *trans* and *cis* composition for every wavelength dependent PSS (tab. 5).

As a reference, the *cis* to *trans* ratios for all three reported azobenzenes AB **(4)**, DMAB **(9)** and S-DMAB **(15)** reveal isomerization efficiencies in good agreement with the efficiencies reported by Asanuma et al.[198] Azobenzene AB with a maximum *trans* conversion efficiency of 81 % at 405 or 420 nm irradiation can be isomerized to *cis* with a maximum efficiency of 86 % at 340 nm irradiation. DMAB shows a maximum *trans* conversion of 86 % at 405 or 420 nm irradiation and a maximum *cis* conversion of 77 % at 340 nm irradiation. The further red-shifted S-DMAB was reported to achieve formation of the *cis* isomer at 385 nm irradiation and shows

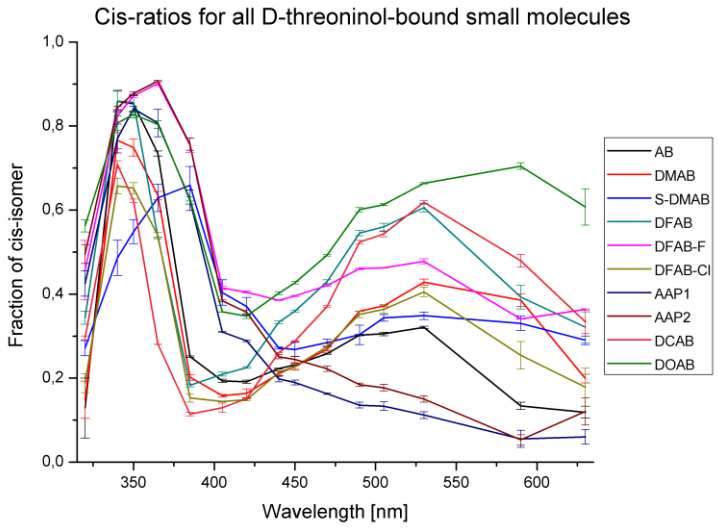

Fig. 57: Overlaid empirical *cis*-fraction results from multiple HPLC quantifications for all D-threoninol bound small molecules after irradiation with all available LED wavelengths facilitates a direct *cis-trans* ratio comparison across the whole visible light range. Details are given in table 5.

the highest *cis* conversion with 66 % at this wavelength. The maximum *trans* conversion efficiency can be achieved by means of a 450 nm LED irradiation with 73 % efficiency. The maximum irradiation wavelengths represent only one of many possible irradiation wavelengths, each forming an individual PSS. The excitation wavelength range often covers the whole spectral range in which the photochromes can be isomerized with different conversion efficiencies from one isomer to the other an vice versa. This plays a key role for the combination of two or more photochrome when used in the same system.

cis %	dark	320 nm	340 nm	350 nm	365 nm	385 nm	405 nm	420 nm	440 nm	450 nm	470 nm	490 nm	505 nm	530 nm	590 nm	630 nm
AB	3.6	12.9	85.9	85.3	73.4	25.1	19.3	19.1	22.3	23.1	25.8	30.2	30.5	32.1	13.4	11.9
DMAB	6.5	14.8	76.6	74.9	63.4	20.2	15.8	16.4	21.1	22.7	26.9	35.9	37.2	42.8	38.6	19.9
S-DMAB	15.4	27.1	48.6	54.8	62.9	65.9	40.4	37.1	27.1	26.8	28.4	30.3	34.3	34.8	33.1	29.0
DFAB	24.7	34.4	85.9	85.6	53.5	18.2	20.9	22.5	33.3	35.9	42.9	54.5	56.0	60.6	39.3	32.1
DFAB-F	25.8	45.7	82.4	87.2	90.1	75.5	41.5	40.5	38.5	39.5	42.1	46.1	46.3	47.8	34.1	36.3
DFAB-Cl	8.8	18.8	65.7	65.2	53.9	15.2	14.4	14.9	21.3	22.8	27.4	35.2	36.3	40.5	25.4	17.9
DCAB	23.6	29.6	70.9	62.2	28.1	11.4	13.0	15.1	26.1	28.8	37.1	52.4	54.3	61.8	48.0	33.4
DOAB	48.9	56.2	80.7	82.8	80.4	62.6	35.8	34.8	40.2	42.7	49.3	60.1	61.3	66.4	70.5	60.7
AAP1	6.8	42.5	77.0	84.1	80.7	62.3	30.9	28.8	19.8	18.9	16.3	13.6	13.3	11.2	5.5	6.0
AAP2	7.9	49.5	84.3	87.8	90.7	75.7	38.4	35.7	25.1	24.4	22.2	18.4	17.7	15.0	5.3	12.1

Tab. 5: Empirical *cis* percentage values determined for each photostationary state by integration of both *trans* and *cis* peak areas for all D-threoninol bound small molecules after irradiation with all available LED wavelengths.

The newly synthesized photochromic molecules can be directly compared to the reported ones by using the same irradiation method with the available LEDs (fig. 57, tab.5). DFAB can be isomerized into *cis* conformation upon irradiation with 340 or 350 nm light achieveing 86 % conversion efficiency, while the *trans* state is formed with 82 % at 385 nm irradiation. Isomerization upon 530 nm irradiation only achieves 60 % of the *cis* state. Introduction of *para* chlorine in case of DFAB-Cl **(51)** further reduces the conversion efficiencies of DFAB significantly. A *para* fluorine substituent slightly red-shifts the maximum response wavelengths and enhances formation of the *cis* state to 90 % upon 365 nm irradiation. Unfortunately, isomerization to *trans* is significantly reduced, yielding only 61 % of the *trans* isomer when irradiated with 440 nm light. Formation of photostationary states with a mixed composition of both *trans* and *cis* isomers possibly disturbs proper hybridization of oligonucleotide duplexes when introduced into DNA backbones. Therefore, DFAB-F and DFAB-Cl were not further taken into account for translation into oligonuleotides.

DCAB and DOAB on the other hand yield the highest *cis* fraction when irradiated in visible light range. *Trans* DCAB is formed in 89 % efficiency when irradiated with 385 nm light and the *cis* isomer with 71 % at 340 nm, compared to 62 % *cis* at 530 nm irradiation. *Cis* conversion efficiency under visible light irradiation of 62 % in combination with the sterically challenging chlorine substitutents possibly destabilize DNA duplexes to an extent that efficient dehybridization becomes possible upon irradiation in visible light range. Further introduction into DNA strands was, as stated before, not considered due to the low synthetic yield of DCAB. DOAB on the other hand provides the highest *cis* content upon visible light irradiation with 71 % using 590 nm LED. This high *cis* content might be able to efficiently break up DNA duplex hybridization. DOAB's *trans* isomer is formed with 65 % at 420 nm irradiation but heating the sample possibly yields a higher *trans* content.

Both arylazopyrazoles AAP1 **(95)** and AAP2 **(100)** reveal near-quantitative conversion efficiencies but unfortunately formation of the *cis* isomer can not be achieved with irradiation in visible light range. The *trans* isomer is formed with 95 % efficiency upon irradiation with 590 nm for AAP1 and AAP2 while the *cis* isomer is formed in 84 % yield using 350 nm for AAP1 and 91 % yield in case of AAP2 using 365 nm light. These high conversion efficiencies correlate well to the significant increase and decrease in absorbance upon alternate irradiation. Through their high conversion efficiencies, both arylazopyrazole molecules are of great interest for possible applications in DNA nanotechnology.

Introduction of the D-threoninol moiety as an electron withdrawing functionality only marginally influences the maximum response wavelengths. Not only the maximum *trans* and *cis* converting wavelengths are of great interest, but also the *trans* and *cis* fractions within the

photostationary states formed after irradiation with every available LED wavelength. The resulting values given in table 5 permit a direct comparison of each *cis* composition when combining two or more photochromes in a single DNA system. The wavelength-dependent scan permits a possible prediction for the combination of two or more photochromes to achieve coherent or independent photoswitching. By wisely selecting two or more photochromes from the designed photoswitch toolbox and directly comparing the empirical values, cooperative switching effects can possibly be predicted within limits.

For example, the previously reported combination of the two azobenzenes AB and S-DMAB used for orthogonally photoswitching a DNA seesaw system is based on the superposition of response wavelengths depending on the isomers of both photochromes. As reported before,

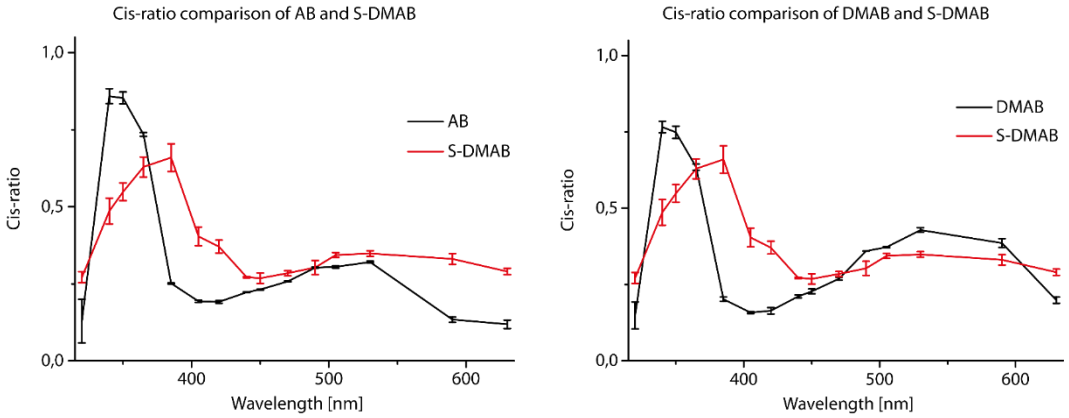

Fig. 58: Cooperative switching of AB, DMAB and S-DMAB as derived from multiple small molecule HPLC quantifications. Both photochrome combinations show a similar coherent photoswitching behaviour. At 340 nm irradiation, AB and DMAB are converted to *cis*, while S-DMAB forms a 50:50 *trans* to *cis* equilibrium. At 385 nm irradiation, S-DMAB converts to *cis* while AB and DMAB remain in *trans* conformation. Irradiation with wavelengths above 400 nm leads to formation of *trans* isomers for all three photochromes.

cis %	**dark**	**320 nm**	**340 nm**	**350 nm**	**365 nm**	**385 nm**	**405 nm**	**420 nm**	**440 nm**	**450 nm**	**470 nm**	**490 nm**	**505 nm**	**530 nm**	**590 nm**	**630 nm**
AB	3.6	12.9	85.9	85.3	73.4	25.1	19.3	19.1	22.3	23.1	25.8	30.2	30.5	32.1	13.4	11.9
S-DMAB	15.4	27.1	48.6	54.8	62.9	65.9	40.4	37.1	27.1	26.8	28.4	30.3	34.3	34.8	33.1	29.0

Tab. 6: Direct comparison of empirical *cis* percentage values between AB and S-DMAB photochromes for each photostationary state after irradiation with all LED irradiation wavelengths.

cis %	dark	320 nm	340 nm	350 nm	365 nm	385 nm	405 nm	420 nm	440 nm	450 nm	470 nm	490 nm	505 nm	530 nm	590 nm	630 nm
DMAB	6.5	14.8	76.6	74.9	63.4	20.2	15.8	16.4	21.1	22.7	26.9	35.9	37.2	42.8	38.6	19.9
S-DMAB	15.4	27.1	48.6	54.8	62.9	65.9	40.4	37.1	27.1	26.8	28.4	30.3	34.3	34.8	33.1	29.0

Tab. 7: Direct comparison of empirical *cis* percentage values between DMAB and S-DMAB photochromes for each photostationary state after irradiation with all LED irradiation wavelengths.

both photoswitches are converted to *trans* when irradiated with 450 nm light and to *cis* using 370 nm light, while AB switches to *cis* and S-DMAB to *trans* when using 340 nm light and vice versa upon irradiation with 390 nm light. Similar irradiation wavelengths can be deduced empirically from the photoswitch toolbox as well, giving the same results and similar conversion efficiencies. At 340 nm irradiation, AB forms 86 % *cis* isomer while S-DMAB remains in a 50:50 state between *trans* and *cis*. 385 nm irradiation turns S-DMAB into 66 % *cis* conformation while AB merely remains in the *trans* state (fig. 58, tab. 6). These two orthogonal irradiation wavelengths directly confirm the reported irradiation scheme. Also, the independently switching wavelengths are close to the reported values with 365 nm for *cis* conversion and 440 nm or 450 nm for turning boh photochromes to *trans*. A combination of DMAB and S-DMAB reveals the same tendency using the same irradiation wavelengths but since the conversion efficiency of DMAB into *cis* is significantly reduced, an orthogonal switching efficiency may be lowered within DNA (fig. 58, tab. 7). As reported by Asanuma et al., the combination of AB and S-DMAB proved most efficiently for an orthogonally photocontrolled DNA system. Validation of the photoswitch prediction can be assumed as observed in the proximity of empirical irradiation wavelengths and efficiencies compared to the reported ones. However, the difference in conversion efficiency for the reported system is decreased with a maximum conversion difference of 50 %, resulting from a maximum orthogonal switching efficiency of this photoswitch combination of 50 %. The incomplete conversion from *trans* to *cis* and vice versa possibly plays a key role in this context.

Translating the empirical results to all newly designed photochromes results in completely different options when bringing the new molecules into play. A combination of DFAB and S-DMAB reveals similar orthogonal switching properties when using 340 nm and 385 nm light irradiation with a conversion efficiency difference of about 50 % in both cases (fig. 59, tab. 8). Additionally, an orthogonal switching with 25 % conversion efficiency difference is observed at 530 nm irradiation. These conversion efficiencies might be used when translating the switching properties into DNA.

A combination of DOAB and AAP2 shows an example for a consecutive switching system (fig. 59, tab. 9). Both photochromes convert to *cis* when irradiated with 350 nm or 365 nm light and back to *trans* using 405 nm irradiation. At 590 nm irradiation DOAB converts to *cis* while AAP2 turns to *trans* conformation. This difference in switching efficiencies can be used to design consecutively switching logic gating systems. Starting from *trans*, DOAB can first be converted to *cis* while AAP2 remains in *trans* upon 590 nm irradiation and both photochromes can be switched to *cis* using 365 nm irradiation. In the opposite direction, both photochromes can be converted to *cis* using 365 nm light and AAP2 can be turned back to *trans* using 590 nm

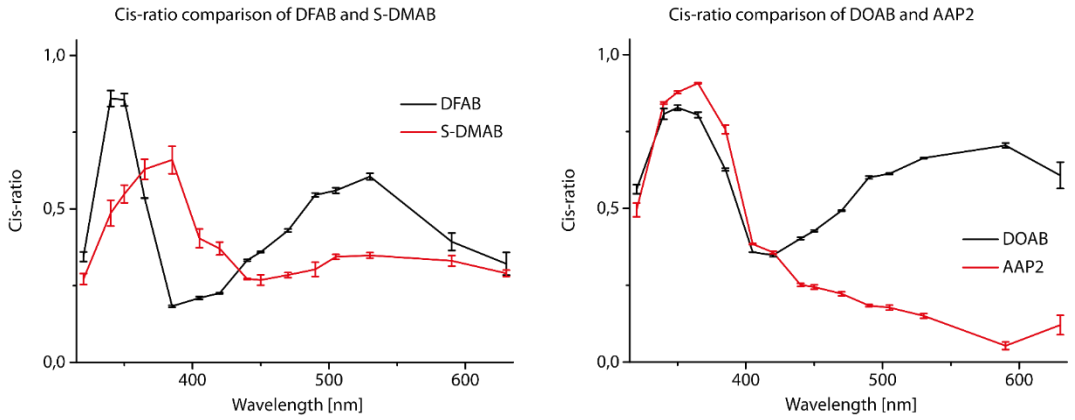

Fig. 59: Potential cooperative switching properties for a combination of DFAB and S-DMAB as well as DOAB and AAP2 photochromes derived from the complete small molecule HPLC quantification. While the combination of DFAB and S-DMAB shows a similar behaviour as the combination of AB and S-DMAB, the combination of DOAB and AAP2 shows a possible consecutive switching. While both photochromes can be converted to *cis* at 350 or 365 nm irradiation, DOAB can be selectively converted to *trans* upon 590 nm irradiation. At 420 nm irradiation, both photochromes are converted to the *trans* state.

cis %	dark	320 nm	340 nm	350 nm	365 nm	385 nm	405 nm	420 nm	440 nm	450 nm	470 nm	490 nm	505 nm	530 nm	590 nm	630 nm
S-DMAB	15.4	27.1	48.6	54.8	62.9	65.9	40.4	37.1	27.1	26.8	28.4	30.3	34.3	34.8	33.1	29.0
DFAB	24.7	34.4	85.9	85.6	53.5	18.2	20.9	22.5	33.3	35.9	42.9	54.5	56.0	60.6	39.3	32.1

Tab. 8: Direct comparison of empirical *cis* percentage values between S-DMAB and DFAB photochromes for each photostationary state after irradiation with all LED irradiation wavelengths.

cis %	dark	320 nm	340 nm	350 nm	365 nm	385 nm	405 nm	420 nm	440 nm	450 nm	470 nm	490 nm	505 nm	530 nm	590 nm	630 nm
DOAB	48.9	56.2	80.7	82.8	80.4	62.6	35.8	34.8	40.2	42.7	49.3	60.1	61.3	66.4	70.5	60.7
AAP2	7.9	49.5	84.3	87.8	90.7	75.7	38.4	35.7	25.1	24.4	22.2	18.4	17.7	15.0	5.3	12.1

Tab. 9: Direct comparison of empirical *cis* percentage values between DOAB and AAP2 photochromes for each photostationary state after irradiation with all LED irradiation wavelengths.

irradiation while DOAB remains in *cis* conformation.

Sophisticated design of more photochromes with different response wavelengths permits the prediction of more photoswitch combinations and facilitates the design of logic gating systems with three or more photoswitches. The development of such a toolbox facilitates the selection of photoswitch pairs for complex DNA or RNA applications. Selection of photoswitch pairs and system design can be used to construct complex photoswitchable DNA systems. However, it has to be considered that the theoretically unlimited toolbox of photochromes only considers free molecules. Interactions with nucleotides possibly further stabilize or destabilize DNA duplexes and have to be tested separately.

3.2.2 Determination of thermal stabilities and half-life times

The third criterium characterizing a potential photoswitch for improving DNA photoswitching is the thermal stability of the *cis* state which is usually given by half-life time. After converting a photo-switch into *cis* conformation, a thermal back-relaxation to *trans* occurs over time. The temperature dependent back-relaxation can be determined by monitoring the relative change in absorbance of the *cis* state at the absorption maximum over time. Half-life is defined as the time span during which half of the total number of photoswitches in *cis* conformation convert back into *trans* conformation.

Thermal stabilities of all D-threoninol bound photoswitches were determined in a 1:19 mixture of acetonitrile and water *via* UV/Vis spectroscopy. All photochromes were irradiated with the maximum *cis* converting LED wavelengths as determined before and an initial UV/Vis spectrum was recorded. The samples were kept in the dark at a given temperature and aliquots were taken after defined time intervals for measuring UV/Vis spectra. If the samples were kept at elevated temperatures, the aliquots were cooled down to room temperature before measurement to avoid a rapid back-relaxation of the photochromes during the measurements. Plotting the intensities at the absorption maxima against time results in an exponential curve converging towards an equilibrium absorbance A (fig. 60). All half-life times were calculated from the resulting curves using exponential fitting (fig. 60, tab. 10).

A comparison of all calculated half-life times facilitates a direct comparison of relative thermal stabilities of the *cis* state for all D-threoninol bound photochromes. Azobenzene's half-life time of 42.9 hours at room temperature serves as an empirical reference value which lies close to the reported value of around 50 hours at room temperature (tab. 10).[196-197] DMAB, which is reported to have a highly stable *cis* state, shows an empirical half-life of 87.5 hours at 60°C.

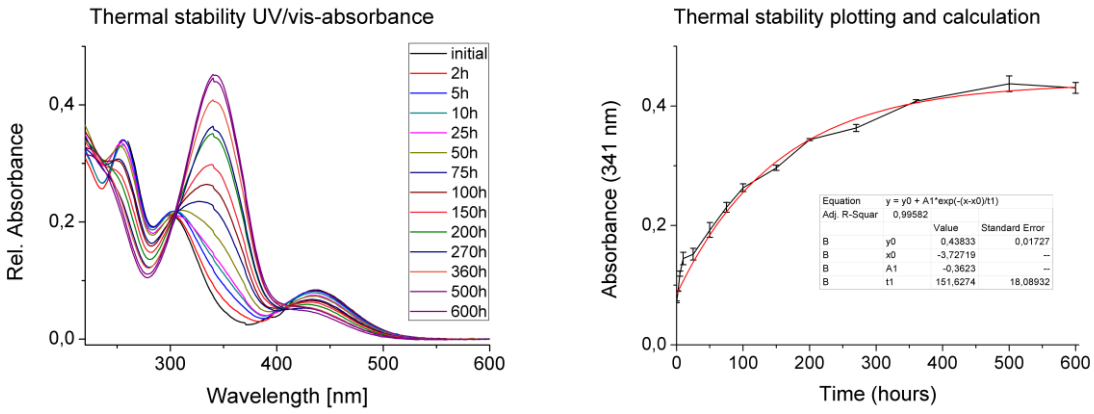

Fig. 60: Time-dependent UV/Vis absorption spectra for AB-D-threoninol (left). Plotting the change in absorption maximum against time shows an exponential decay of the *cis* state, which permits calculation of the half-life time (right).

Sample	Irr. wavelength	$t_{1/2}$ 20 °C	$t_{1/2}$ 40 °C	$t_{1/2}$ 60 °C
AB	340 nm	N/A	42.9 hours	N/A
DMAB	350 nm	N/A	N/A	87.5 hours
S-DMAB	385 nm	N/A	N/A	4.1 hours
DFAB	340 nm	N/A	N/A	36.7 hours
DFAB-F	365 nm	N/A	N/A	47.1 hours
DFAB-Cl	350 nm	N/A	85.0 hours	N/A
DCAB	340 nm	N/A	N/A	143.0 hours
DOAB	350 nm	N/A	96.1 hours	13.4 hours
AAP1	365 nm	14.0 hours	4.2 hours	N/A
AAP2	365 nm	108.8 hours	22.0 hours	N/A

Tab. 10: Measured and calculated half-life times for all D-threoninol bound photoswitches after irradiation with the maximum *cis* converting irradiation wavelengths. All thermal stabilities were measured at different temperatures in which the absorbance decay could be determined in an optimum time range.

Only the half-life of DCAB is even 1.5-fold higher which possibly results from the sterical hindrance of the bulky chlorine atoms in both *ortho* positions on the peripheral ring, thus sterically obstructing a back-switching from *cis* to *trans*.

Ortho fluorinated azobenzenes exhibit high thermal stabilities in agreement with the reported fluoroazobenzenes.[132,133] Introduction of a further fluorine substitutent in *para* position additionally enhances the thermal stability through a *para* pull-pull system in good agreement with literature.[133]

Para chlorination of DFAB reveals the opposite effect as observed by a decreased thermal half-life, although the stability remains 2-fold higher than azobenzene's half-life. Unexpectedly, DOAB exhibits a half-life of 96.1 hours at 40°C. Both electron donating *ortho* methoxy moieties do not seem to form a push-pull system with the opposite ring containing the peptide moiety. As reported for aminoazo-benzenes, both electronic effects seem to superimpose in a positive manner due to their different positions on the ring. S-DMAB on the other hand exhibits a 20-fold decreased thermal stability in direct comparison to DMAB, possibly due to formation of a *para* push-pull system between the elec-tron withdrawing carboxy moiety of D-threoninol and the electron donating methylthio residue.

Both arylazopyrazoles AAP1 and AAP2 exhibit the lowest thermal stabilities of all synthesized photochromes. AAP1 with a half-life of 14 hours at room temperature remains the least stable photochrome, while introduction of a phenyl residue in AAP2 significantly enhances the thermal stability of the *cis* state to 109 hours at room temperature and makes it

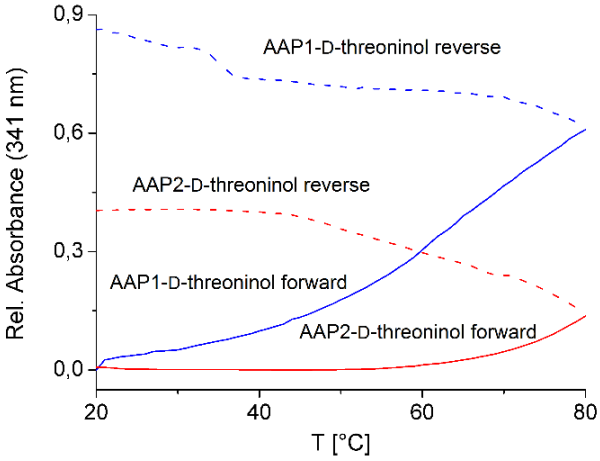

Fig. 61: Small molecule melting curves of AAP1 and AAP2 in a temperature range between 20 °C and 80 °C. While AAP1 shows a constant increase in absorbance under the applied thermal gradient, AAP2 does not indicate any thermal back-relaxation before reaching 50 °C. Thus the use of AAP2 appears to be more suitable for long-term applications.

at least stable four about one day at 40 °C. Compared to the reported stability of around 10 hours at room temperature for AAP1 without D-threoninol linkage,[136] the half-life times are increased 1.5-fold for AAP1 and more than 10-fold in case of AAP2. Seemingly a disadvantage, these results have to be considered in the context of possible applications. DNA applications do not necessitate a high thermal half-life of the cis state by default and the rapid thermal back-relaxation of AAP1 could even be an advantage, opening the door for thermally controlled nanosystems. Different back-switching velocities can be considered as one further degree of freedom for the control of DNA nanosystems. Nevertheless, the high conversion efficiencies of AAP1 and AAP2 provide promising tools for DNA-based *in vitro* applications.

To further investigate the thermal relaxation pertaining to the range of applicability for both arylazopyrazoles, melting curves of the D-threoninol bound small molecules were performed. Both molecules AAP1 and AAP2 were irradiated to *cis* conformation and directly submitted to melting curve measurements (fig. 61). Therefore, both molecules were dissolved in a 1:19 mixture of acetonitrile and water and irradiated at 365 nm for 5 minutes at room temperature to maximally convert both molecules into *cis* conformation. The samples were left in the dark and a thermal gradient of 1 °C per minute was applied in a range between 20 °C and 80 °C while detecting the absorption maximum at λ = 341 nm. Constantly increasing the temperature reveals the thermal back-switching rate and serves as a qualitative demonstration of applicability within a defined temperature range. While AAP1 shows a constant increase in absorbance even at lower temperatures and an increasing absorbance within a higher temperature range, AAP2 exhibits no significant change in absorbance below 60 °C. Above 60 °C absorbance of AAP2 increases, indicating a thermal back-relaxation to *trans*. In good agreement with the observed thermal stabilities for both molecules, the rather low thermal stability of *cis* AAP1 results in a rapid back-switching to *trans* when applying increased temperatures. This property prevents AAP1 from being used in long-term applications, while AAP2 on the other hand proves to be a benefitial candidate for long-term DNA applications

due to its near-quantitative conversion efficiencies while maintaining a 2-fold half-life compared to azobenzene. Also the very low back-switching rate below 60 °C constitutes an advantage for DNA nanotechnology applications.

As observed in this study, thermal half-lives as the third criterium play a key role when translating the new photochromes into oligonucleotides. Not only the absorption wavelengths and conversion efficiencies are of great interest, but also the thermal relaxation behaviour of the *cis* state. Yet, only photo-reversible systems have been developed within higher order DNA nanosystems. A photo- and thermoreversible system at the same time opens the door for more degrees of freedom as required in for example complex logic gating systems. For all synthesized azobenzenes the electronic properties of *para* substituents potentially stronger influence the thermal *cis* stability while sterical hindrance of *ortho* substituents appears to be subordinated. Sophisticated substitution of azobenzenes possibly further enhances thermal stabilities of the *cis* state.

3.3 Introduction of newly developed photoswitches into DNA strands

3.3.1 Synthesis of phosphoramidites and introduction of new photoswitches into DNA strands

Introduction of photochromic moieties into oligonucleotide strands *via* solid phase DNA synthesis requires a DMT protection of the primary D-threoninol hydroxy group in analogy to the 5'-hyroxy group in natural nucleotides, and a phosphoramidite moiety on the secondary hydroxy group which corresponds to the 3'-end of nucleotides. DMT protection of all selected D-threoninol bound photoswitches was performed in most cases by a slight excess of DMT-chloride in a 1:1 mixture of dichloromethane and pyridine including 4-DMAP in catalytic amounts. Using this procedure, the three reported azobenzenes AB, DMAB and S-DMAB as well as DFAB and its derivatives could be obtained in good yields (fig. 62, chapter 7.2). DMT protection of DOAB required the use of pure pyridine instead of a 1:1 dichloromethane pyridine mixture to obtain the DMT-protected product.

DMT protection of both arylazopyrazoles AAP1 and AAP2 required the use of different reaction conditions (fig. 63). Using DMT-chloride in a mixture of dichloromethane and pyridine as well as in pure pyridine strongly favoured the formation of double DMT-protected products. These reaction conditions only yielded small amounts of the desired single-protected product containing DMT on the primary D-threoninol hydroxy moiety. Consequentially, reaction conditions had to be adjusted by testing a series of organic amine bases in dichloromethane and acetonitrile. In both cases, DMT-chloride was first added dropwise to the solution at 0 °C, followed by slow addition of the amine base. In case of AAP1, *N*-methylmorpholine in dichloromethane proved best and exclusively yielded the single-DMT protected product in moderate yields when added in single portions. Contrary to AAP1, AAP2 yielded the single protected target product by means of *N*-methylpyrrolidine in dry acetonitrile when added very slowly dropwise to the reaction solution at 0 °C.

Synthesis of the respective phosphoramidites in the final reaction steps also necessitated different reaction conditions depending on the photochromic backbone.

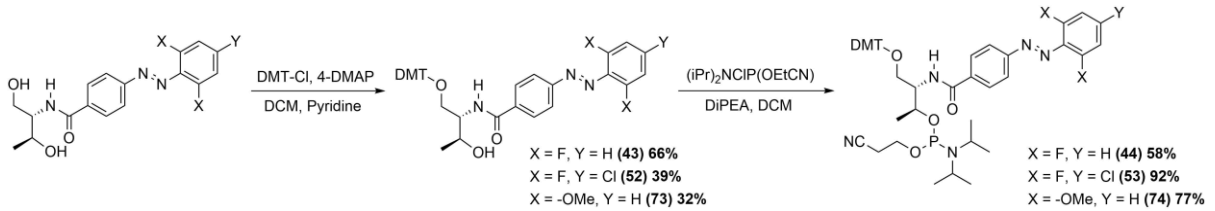

Fig. 62: General synthetic pathway to achieve a series of 2',6'-substituted azobenzene phosphoramidites coupled to D-threoninol. For all synthesized azobenzene phosphoramidites, similar experimental conditions were used.

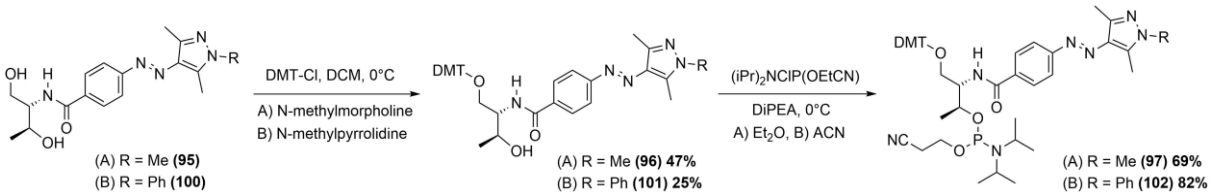

Fig. 63: Synthetic pathway used for the synthesis for arylazopyrazole phosphoramidites: *N*-methylarylazopyrazole phosphoramidite (AAP1) and *N*-phenylarylazopyrazole phosphoramidite (AAP2) could successfully be obtained under similar reaction conditions.

While phosphoramidites of AB, DMAB, S-DMAB, DFAB and DOAB could be obtained in high yields using DiPEA in dry dichloromethane followed by addition of 2-cyanoethyl-*N*,*N*-diisopropylchlorophosphoramidite at 0 °C under argon atmosphere, synthesis of AAP1 and AAP2 phosphoramidites proved more difficult.

Using the same reaction conditions as used in case of azobenzene phosphoramidite leads to an oxidation of the phosphorous for both arylazopyrazole phosphoramidites as observed on TLC and in ^{31}P-NMR. The reaction conditions were adjust to very short reaction times at 0 °C and immediate addition of the phosphitylation agent after adding the respective amine base. AAP1 phosphoramidite could be obtained using dry diethyl ether as solvent and AAP2 phosphoramidte using dry acetonitrile (fig. 63). Changing DiPEA for different amine bases did not result in any improvement. All synthesized phosphoramidtes were characterized by NMR and high resolution MS (see appendix).

Introduction of the newly designed photochrome phosphoramidites into DNA strands was perfor-med *via* solid phase phosphoramidite synthesis using an ABI 3400 DNA synthesizer and 200 nmol CPG solid supports. All phosphoramidites were irradiated into *trans* conformation and pre-dried in high vacuum for 24 hours prior to coupling. All compounds were diluted in DNA grade acetonitrile to yield 0.2 M solutions. In comparison to the standard DNA phosphoramidites dA, dG, dC and dT, higher concentrations of the custom phosphoramidites had to be used since the sterically more challenging *cis* states possibly prevent a successful phosphoramidite coupling to the deprotected 5'-end of the oligonucleotides. As observed empirically, photostationary states containing high amounts of the *cis* isomer thus decrease the coupling yield significantly.

As two different basic constructs the 8-mer DNA sequence 5'-GAATGGTG-3' and the 12-mer DNA-sequence 5'-CACCATTCCGGT-3' were designed and modified with photoresponsive residues in different amounts and positions (fig. 64). According to Asanuma et al., the number and position of azobenzene residues strongly determines an efficient photocontrol of DNA duplexes.[187] Therefore, different numbers and positions of modifications were investigated following the scheme below:

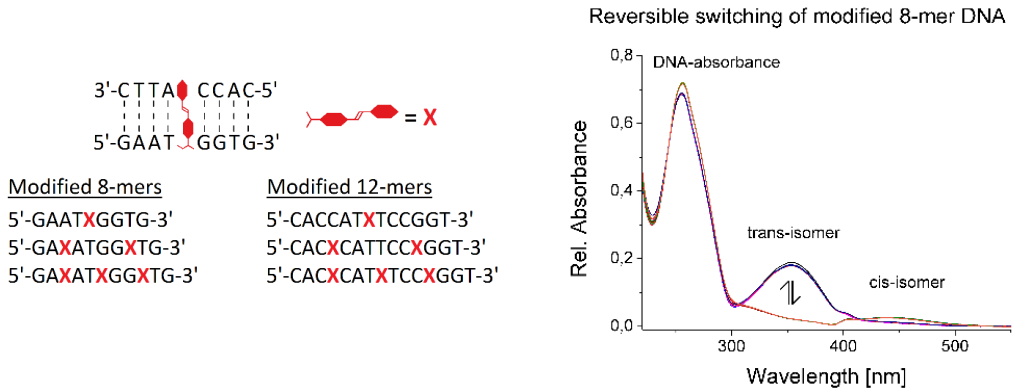

Fig. 64: A series of modified 8-mer and 12-mer DNA strands carrying modifications in their backbones were synthesized *via* solid phase phosphoramidite synthesis (left). Custom photochrome phosphoramidites were implemented *via* custom phosphoramidite synthesis cycles (X = modified azobenzene or arylazopyrazole). Reversible switching of all introduced modifications was proven by UV/Vis spectroscopy after alternating irradiation with the maximum *trans* and *cis* converting wavelengths prior to recording the UV/Vis spectra.

1) One central single photoswitch:

   5’-GAATXGGTG-3’ and 5’-CACCATXTCCGGT-3’.

2) Two independently incorporated photoswitches:

   5’-GAXATGGXTG-3’ and 5’-CACXCATTCCXGGT-3’.

3) Three consecutive photoswitches separated by two or three nucleobases:

   5’-GAXATXGGXTG-3’ and 5’-CACXCATXTCCXGGT-3’.

All DNA oligonucleotides were used in combination with their double stranded DNA using the complementary sequences 5'-CACCATTC-3‘ as 8-mer and 5'-ACCGGAATGGTG-3' as 12-mer antisense strands. Successful synthesis of all photochrome modified DNA strands was proven by ESI LCMS and reversible switching of the implemented modifications (fig. 64). All modified strands were dissolved in water and repeatedly irradiated with the maximum *trans* and *cis* response wavelengths followed by recording UV/Vis absorption spectra. The resulting spectra revealed two absorption maxima in near-UV und visible light range belonging to the modifications in proximity to the native DNA absorption at λ = 260 nm. Reversible change in absorbance could be observed for each modification in respect to the corresponding irradiation wavelengths (full spectra see chapter 7.4.3).

Unfortunately, not all synthesized phosphoramidites could be successfully introduced into DNA strands. Sequences containing DFAB or DOAB moieties could only be isolated with one single introduced modification. Two or more implementations per strand did not yield any target mass for the designed sequences. Possibly the phosphoramidite coupling conditions lead to a partial disass-embly of the modifications or overlapping of the stereo-isomers prevents a proper HPLC purification. Unfortunately, DFAB and DOAB are promising molecules for DNA

photoswitching with visible light. On the other hand, a variety of strands with single and multiple AAP1 and AAP2 introductions could be obtained using a standard phosphoramidite coupling protocol. The series of modified DNA strands described above could be successfully synthesized including AB, DMAB, S-DMAB, AAP1 and AAP2 modifications. DFAB and DOAB could only be introduced a single time per DNA strand. The available set of modified oligonucleotides was used as a starting point for all further investigations. A comprehensive overview of synthetic accessibility and DNA introduction is given in table 12.

Despite the unsuccessful introduction of multiple DFAB and DOAB moieties into single DNA sequences, DNA photoswitching properties of single modified strands as well as the influence of a single modification on the DNA duplex stability was investigated by reversed-phase HPLC and melting curve experiments (chapter 3.3.2 and 3.3.3).

The concentration of modified oligonucleotide strands had to be adjusted for custom modifications since all photochromes exhibit a strong absorption at λ = 260 nm. Since both isomers have a different absorbance at λ = 260 nm, the total absorbance at λ = 260 nm depends on the composition of the *cis* and *trans* state within a photostationary state. The absorbance of the dark adapted samples corresponds most accurately to the ratio of both isomers formed within a photostationary equilibrium. Every absorbance correction for each

Modification	Synthetic feasibility	Phosphoramidite synthesis	DNA introduction	Multiple DNA introductions
AB	√	√	√	√
DMAB	√	√	√	√
S-DMAB	√	√	√	√
TFAB	X	X	X	X
DFAB	√	√	√	X
DFAB-F	√	X	X	X
DFAB-Cl	√	X	X	X
DFAB-Br	X	X	X	X
DFAB-Pep	X	X	X	X
DMDFAB	X	X	X	X
DCAB	X	X	X	X
DOAB	√	√	√	X
AAP1	√	√	√	√
AAP2	√	√	√	√

Tab. 11: Complete and comprehensive overview of synthetic accessibility, possible DNA introduction and multiple DNA introductions for all newly synthesized photoswitches. While DFAB and DOAB could only be introduced into DNA once into a strand, only AAP1 and AAP2 phosphoramidites could reliably and successfully be introduced multiple times into DNA sequences.

dark adapted sample was determined by measuring the absorbance at 260 nm after leaving the sample in the dark in a 1:19 acetonitrile water mixture and calculating each extinction coefficient *via* the Lambert-Beer law (tab. 13). The concentrations were corrected according to the additional extinction coefficients for every modified DNA sample.

Sample	Concentration	Abs. (260 nm)	Extinction coeff.
AB	50 µM	0.182	3640
DMAB	50 µM	0.405	8100
S-DMAB	50 µM	0.181	3620
DFAB	50 µM	0.278	5560
DOAB	50 µM	0.487	9740
AAP1	25 µM	0.095	3800
AAP2	25 µM	0.234	9360

Tab. 12: Extinction coefficients determined for concentration measurements and calculations for solutions containing modified oligonucleotide strands.

3.3.2 Thermodynamic properties of modified single-stranded oligonucleotides

While double-stranded DNA preferably exists in a helical structure with all nucleobases stacked in the inner helix axis, single-stranded DNA can exist in a random coil state with no stacked nucleobases or a stacked conformation containing a distinct persistence length. Introduction of azobenzene stabilizes base stacking in single- and double-stranded DNA through an additional π-stacking along the stacking direction. Azobenzene photoisomerization in single-stranded DNA disrupts the stacked conformation upon conversion from *trans* to *cis* (fig. 65). Both DNA conformations carrying *trans* or *cis* azobenzene can be separated using reversed-phase HPLC while detecting the native DNA UV absorbance at λ = 260 nm. Separation and detection of both isomers of the single-modified 8-mer sequence 5'-GAATXGGTG-3' affords the distinct quantification of *cis* and *trans* conversion efficiencies of photochrome modified single-stranded DNA. Contrary to the quantification of *cis* and *trans* isomerization using the free molecules, a determination of an isos-bestic point is not required. The total absorbance of single-stranded DNA at λ = 260 nm is significantly higher compared to the absorbance of the photochrome, thus minimizing detection errors (fig. 65).

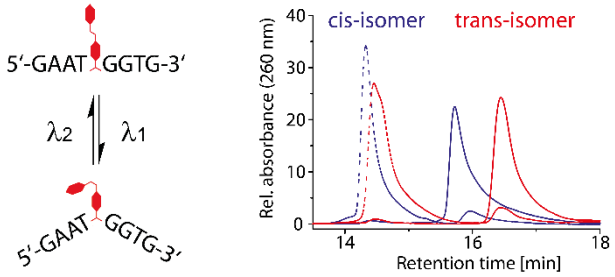

Fig. 65: Reversed-phase HPLC separation of *trans* and *cis* isomers using the modified 8-mer DNA strand 5'-GAATXGGTG-3' carrying a central photochrome permits a quantification of switching efficiencies in DNA through integration of the corresponding peak areas.

Additional or lacking π-stacking between the base pairs and the implemented photochromic modifications lead to a total gain or loss in additional stacking energy, thus facilitating or impeding photoswitching of inbuilt photochromes. A strong duplex stabilization decreases conversion efficiencies whereby weak or destabilizing effects support efficient photoswitching. Quantive values for all photochromes are achieved by integration of the corresponding *trans* and *cis* signals for all availablke irradiation wavelengths. The resulting wavelength-dependent excitation table analogous to the small molecules quantification (fig. 66, tab. 14) reveals slightly different quantification values compared to the small molecules conversion efficiencies.

The reported azobenzenes AB, DMAB and S-DMAB exhibit decreased switching efficiencies in DNA strands compared to the native molecules indicating an additional stabilizing effect on the base stack. Intercalation of azobenzene photochromes overcompensates disruption of the

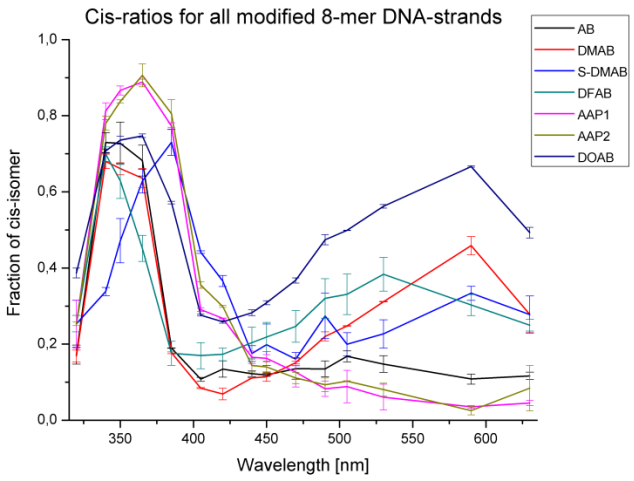

Fig. 66: Empirical *cis* percentage results from multiple HPLC quantifications for all single-modified DNA strands 5'-GAATXGGTG-3' after irradiation with every available LED wavelength.

cis %	dark	320 nm	340 nm	350 nm	365 nm	385 nm	405 nm	420 nm	440 nm	450 nm	470 nm	490 nm	505 nm	530 nm	590 nm	630 nm
AB	10.5	17.2	72.9	72.8	68.2	18.9	10.8	13.4	12.2	11.9	13.5	13.5	16.8	14.8	10.8	11.6
DMAB	10.5	16.9	68.0	66.1	63.6	17.7	8.4	6.9	11.1	11.4	15.2	22.0	24.7	31.2	45.9	27.8
S-DMAB	25.0	25.4	33.8	47.2	62.9	73.0	44.2	36.6	17.5	19.8	16.1	27.4	20.0	22.7	33.4	27.8
DFAB	23.2	25.4	69.9	62.9	45.1	17.6	17.0	17.3	20.4	21.8	24.6	32.0	33.1	38.3	30.3	25.0
DOAB	35.1	38.7	70.7	73.6	74.7	57.2	27.6	25.8	28.2	30.9	36.7	47.4	49.9	56.2	66.7	49.3
AAP1	4.5	25.2	81.2	86.7	88.9	77.3	29.1	26.8	16.5	16.3	12.6	8.3	8.8	6.1	3.5	4.6
AAP2	5.8	25.3	78.0	83.8	90.6	80.6	35.5	29.9	14.4	14.0	11.1	9.3	10.3	8.0	2.5	8.4

Tab. 13: Empirical *cis* percentage values for all photostationary states as determined by HPLC separation and integration of both *trans* and *cis* isomer peak areas. The 8-mer DNA strand 5'-GAATXGGTG-3' was used for calculation after irradiation with every available LED wavelength.

backbone caused by D-threoninol, thus leading to a total stabilization of the DNA stack.[176] In good agreement with literature, the resulting decreased isomerization rates require high synthetic loads and elevated irradiation temperatures to achieve efficient photocontrol over DNA duplex hybridization.

The newly introduced azobenzene chromophores reveal the same tendency. DFAB in DNA shows a 16 % reduced isomerization efficiency upon 340 nm irradiation and 530 nm irradiation yields an even 23 % reduced switching efficiency. DOAB introduced into DNA also yields reduced conversion efficiencies, but to a lower extent compared to DFAB, possibly due to the bulky methoxy moieties possibly distorting the DNA stacked bases. Nevertheless, visible light DNA photoswitching is possible with 67 % efficiency upon irradiation with 590 nm light. Using 420 nm irradiation results in the formation of 74 % *trans* isomer (fig. 67). Both isomerization

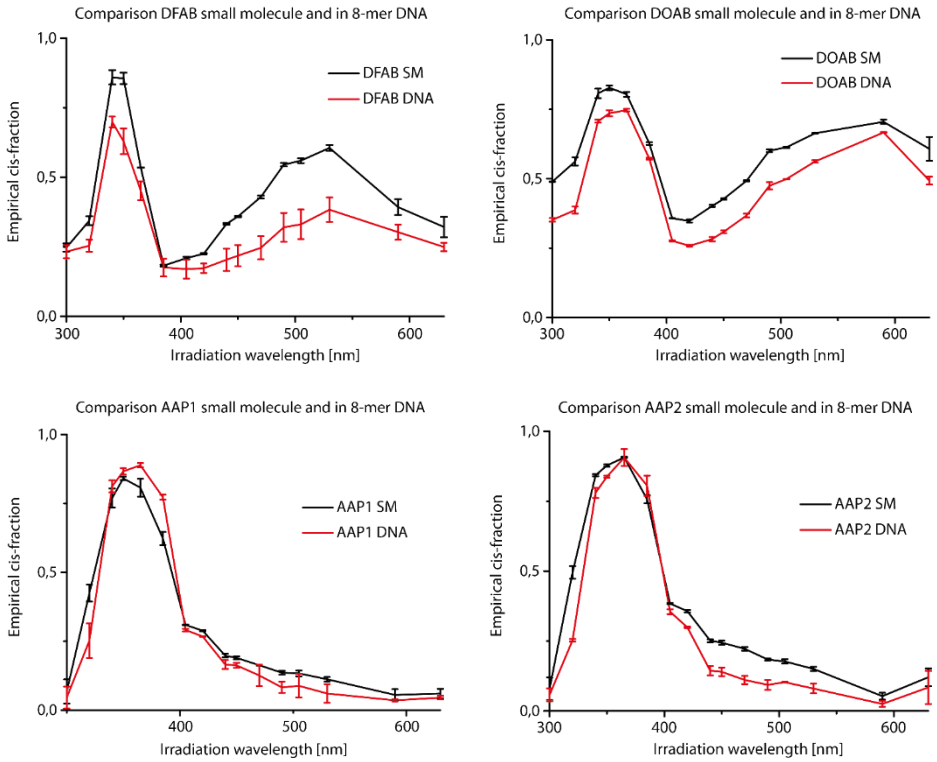

Fig. 67: Direct comparison of empirical *cis* percentage results from multiple HPLC quantifications for newly synthesized free D-threoninol bound photochrome molecules and modified 8-mer DNA strands. DFAB and DOAB (top left and top right) reveal reduced switching efficiencies in DNA while arylazopyrazoles AAP1 and AAP2 retain high switching efficiencies in DNA duplexes (bottom left and bottom right).

efficiencies lie in the same magnitude as azobenzene. Depending on the duplex stabilization or destabilization through intercalation of DOAB moieties, visible light DNA photoswitching can be achieved. Stabilization of the DNA stack seems to be significantly stronger in case of DFAB compared to DOAB.

In contrast to substituted azobenzenes, arylazopyrazoles exhibit even higher conversion efficiencies compared to the native molecules (fig. 67). Especially in visible light range, formation of the *trans* isomer appears to be favoured wheras the *trans* conformation can be achieved with 96 % efficiency.in case of AAP1 and 97 % efficiency in case of AAP2. The *cis* isomer is formed with about 2 % higher efficiency when irradiated with 365 nm light compared to the free molecule, 90 % for AAP1 and 91 % for AAP2, and irradiation with 385 nm light even leads to the formation of 77 % and 81 % *cis* isomer respectively. Retaining high conversion efficiencies upon translation into DNA is one main prerequisite for an improved duplex hybridization control. Near-quantitative isomerization efficien-cies in both isomerization directions proves arylazopyrazoles to be promising candidates for achieving an improved DNA duplex photocontrol efficiency.

In conclusion, a straight comparison of DNA single strands modified with a single reported and newly available photochrome with their D-threoninol bound native states results in reduced isomerizations for azobenzene based photoswitches while arylazopyrazoles appear to retain high conversion efficiencies when translated into the backbone of DNA. An additional stabilization is observed throughout all substituted azobenzene photochromes and possibly also hampers efficient photocontrol of DNA duplexes. Arylazopyrazoles on the other hand exhibit near-quantitative isomerization efficiencies in DNA in both isomerization directions without showing any fatigue during photoconversion. Further translation of the photoswitching properties into DNA duplexes has to be examined by additional melting curve experiments.

3.3.3 Duplex control efficiency of modified oligonucleotide duplexes

Introduction of newly designed photochromes into DNA strands proved successful for a series of molecules in different numbers and positions. Beyond conversion efficiencies between the *trans* and *cis* isomers in single-stranded DNA, the influence of the photochromes on DNA duplex stability plays a key role for the photoinduced dissociation and re-association of DNA duplexes. The influence of implemented modifications on the formation and dissociation of dsDNA upon photoisomerization was investigated by melting curve experiments. The sequences **ds8** 5'-GAATGGTG-3' and **ds12** 5'-CACCATTCCGGT-3' (see chapter 3.5.1) containing different numbers and positions of photo-chromes were used in combination with the unmodified complementary strands.

Melting curves present the method of choice for a determination of DNA duplex dissociation. As previously reported, introduction of azobenzenes into DNA duplexes leads to an overall dsDNA stabilization with azobenzenes in *trans* conformation due to additional π-stacking

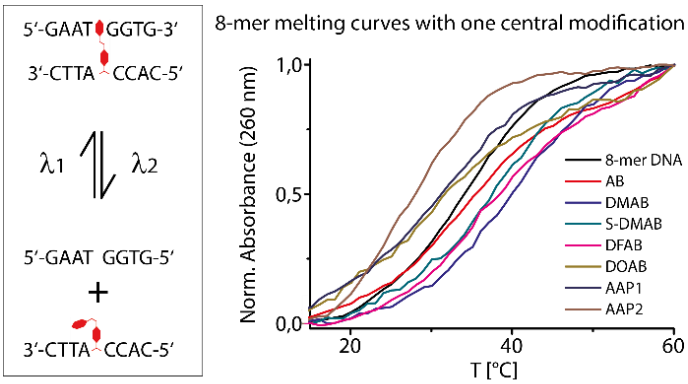

Fig. 68: Melting curves of the modified 8-mer duplexes 5'-GAATXGGTG-3' and their complementary sequence containing one central modification in *trans* conformation. Compared to the unmodified duplex, all azobenzene-based modifications exhibit higher melting temperatures while both arylazopyrazoles show a reduction in melting temperatures T_m.

Modification	T_m *trans*	T_m *cis* RT	ΔT_m *trans*	ΔT_m *cis* RT
AB	35.3 °C	28.0 °C	+1.4 °C	-5.9 °C
DMAB	40.3 °C	40.3 °C	+6.4 °C	+6.4 °C
S-DMAB	38.3 °C	38.5 °C	+4.4 °C	+4.6 °C
DFAB	36.8 °C	32.1 °C	+2.9 °C	-1.8 °C
DOAB	28.4 °C	16.4 °C	-5.5 °C	-17.5 °C
AAP1	30.3 °C	21.7 °C	-3.6 °C	-12.2 °C
AAP2	26.9 °C	22.1 °C	-7.0 °C	-11.8 °C

Tab. 14: Relative change in melting temperature T_m compared to the native DNA duplex melting temperature T_m = 33.9 °C using 3 µM single-modified ODN duplexes in *trans* and *cis* conformation.

stabilization between azobenzene and the stacked nucleobases. Compared to the native unmodified DNA duplex an increase or decrease in melting temperature permits a determination of duplex stabilization or destabilization or even a complete dissociation of the duplex. A single modification within the short DNA strand 5'-GAATXGGTG-3' with X as the modification in hybridized to the complementary strand 5'-CACCATTC-3' was used in 0.5 M NaCl to investigate a general influence of the introduced modifications on DNA duplex stability. Melting curves of the native 8-mer duplex exhibit a melting temperature of 33.92 °C for **ds8** under these conditions. Since irradiation temperatures are crucial for photoinduced duplex dissociation, all modified DNA duplexes were irradiatied to *cis* conformation at room temperature and 40 °C for 5 minutes before each measurement.

While a single azobenzene modification in *trans* conformation does not alter the melting temperature of the **ds8** duplex significantly, DMAB and S-DMAB in *trans* lead to an increased melting temperature by 6.4 °C and 4.4 °C using DNA with a single modification (fig. 68, tab. 15). A DNA duplex stabilization has previously been reported and requires high synthetic loads and elevated irradiation temperatures to achieve complete duplex dissociation.[176,198] Irradiation into *cis* conformation at room temperature does not show any melting temperature difference for DMAB and S-DMAB, while the azobenzene modified duplex reveals a reduction of 5.9 °C in *cis*. DMAB and S-DMAB in good agreement with literature stabilize the DNA duplex to an extent that only unstable duplexes with low GC-contents can be photodissociated efficiently.

The newly designed photochromes in DNA reveal a different behaviour compared to the reported azobenzenes. DFAB increases the native melting temperature in *trans* conformation by 2.9 °C and reduces the melting temperature by 1.8 °C in *cis* conformation (tab. 15). The temperature difference is not as significant as observed for a single DMAB or S-DMAB moiety. A single DOAB moiety in the **ds8** duplex shows a higher destabilizing effect even in *trans* conformation as observed by a decrease in melting temperature of 5.5 °C. The two methoxy moieties possibly destabilize the DNA duplex stacking significantly or the *trans* isomer is not completely intercalated. Also, DOAB exists as a *cis*-*trans* mixture within the DNA duplex, possibly leading to a statistical distribution of *trans* and *cis* isomers whereby the *cis* isomers locally disrupt the DNA duplex. Irradiation to *cis* shows a melting temperature reduction down to 16.4 °C, thus revealing the strongest destabilizing effect on the DNA duplex by a single modification among all tested photochromes.

Both arylazopyrazoles AAP1 and AAP2 significantly decrease the native melting temperature in *trans* conformation, where AAP1 shows a lower decrease in melting temperature with 3.6 °C compared to AAP2 with a reduction of 7.0 °C (tab. 15). The strong duplex destabilization may have a series of causes. As reported for azobenzene, DMAB and S-DMAB, disruption of the

phosphate backbone through D-threoninol is overcompensated by additional π-stacking stabilization through the intercalated photochromes. While DFAB shows an effect similar to azobenzene, the position and nature of substituents strongly affects π-stacking of the nucleobases. Sterically more challenging substituents like methoxy in DOAB possibly stretch the nucleobase stack leading to a total duplex destabilization. This effect also seems to facilitate isomerization of the moiety which, in case of the reported azobenzenes, is stabilized in a way that conversion to *cis* is hampered. As stated before, this effect was tried to be circumvented by use of different diol linkers.[200] Both arylazopyrazole molecules appear to disrupt the nucleobase stacking thus resulting in decreased melting temperatures even in *trans* conformation. Isomerization to *cis* at room temperature is also alleviated as observed in strongly reduced melting temperatures even with a single modification. The increased or decreased

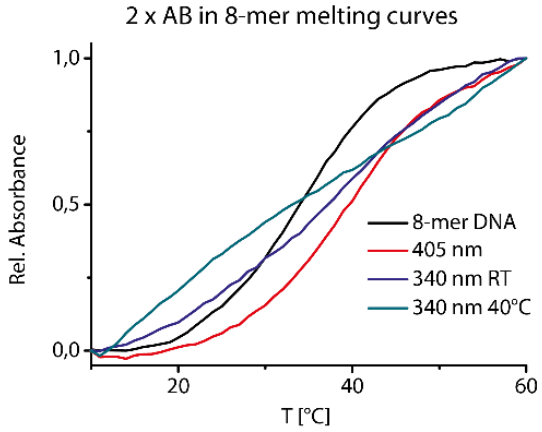

Fig. 69: Melting curves of 8-mer ODN-duplexes modified with two azobenzene moieties upon irradiation into *trans* and *cis* conformation at different irradiation temperatures. As previously stated, elevated irradiation temperatures are required to achieve an efficient reduction in melting temperature.[176,198]

Modifications	T_m *trans*	T_m *cis* RT	ΔT_m *cis* RT	T_m *cis* 40 °C	ΔT_m *cis* 40°C
1 x AB	35.3 °C	28.0 °C	-7.3 °C	22.9 °C	-12.4 °C
2 x AB	38.9 °C	32.7 °C	-6.2 °C	18.8 °C	-20.1 °C
3 x AB	32.7 °C	21.0 °C	-11.7 °C	18.3 °C	-14.4 °C
1 x DMAB	40.3 °C	40.3 °C	-0.0 °C	40.8 °C	+0.5 °C
2 x DMAB	47.1 °C	48.6 °C	+1.5 °C	47.8 °C	+0.7 °C
3 x DMAB	46.5 °C	44.9 °C	-1.6 °C	N/A	N/A
1 x S-DMAB	38.3 °C	38.5 °C	-0.2 °C	37.6 °C	-0.7 °C
2 x S-DMAB	39.1 °C	38.5 °C	-0.6 °C	36.1 °C	-3.0 °C
3 x S-DMAB	39.8 °C	16.9 °C	-22.7 °C	17.1 °C	-22.7 °C

Tab. 15: Melting temperatures T_m of AB, DMAB and S-DMAB modified 8-mer duplexes upon irradiation with the maximum *trans* and *cis* converting wavelengths at room temperature and 40 °C irradiation. The change in T_m becomes more significant with an increasing number of modifications.

stability of modified duplexes strongly depends on the local base sequence, GC-content, relative numbers and positions of photochromes and irradiation temperatures. In this study, the main focus is put on determination of the minimum amount of modifications required to achieve complete duplex dissociation. Unfortunately, DFAB and DOAB could only be introduced a single time into DNA sequences. Therefore, a systematic study involving arylazopyrazoles and reported azobenzenes was performed.

A systematic study with multiple modifications into the **ds8** duplex according to the sequences given in chapter 3.3.1 reveals a tendency of stabilizing and destabilizing effects. While multiple AB moieties in *trans* do not alter the native duplex melting point significantly, multiple DMAB and S-DMAB moie-ties in *trans* increase the duplex melting temperature significantly (fig. 69, tab. 16). Azobenzene reveals an increasing melting temperature reduction with an increasing synthetic load and elevated irradiation temperatures. Using three modifications at room temperature irradiation or two modifications at 40 °C irradiation result in

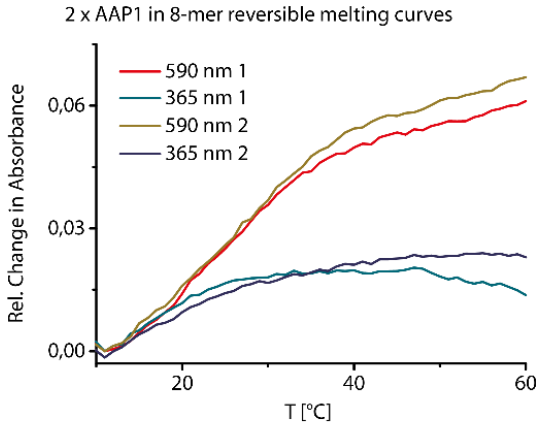

Fig. 70: Reversible melting curves of 2 x AAP1 in the 8-mer duplex sequence 5'-GAXATGGXTG-3' and its complement already reveals a reversible decrease and increase in melting temperature. Also the relative change in absorbance at λ = 260 nm is significantly reduced when AAP1 is isomerized into *cis* conformation.

Modifications	T_m *trans* 1st	T_m *cis* RT 1st	T_m *trans* 2nd	T_m *cis* RT 2nd
1 x AAP1	30.5 °C	22.0 °C	30.9 °C	22.5 °C
2 x AAP1	25.2 °C	18.3 °C	26.8 °C	16.2 °C
3 x AAP1	18.5 °C	N/A	20.7 °C	N/A
1 x AAP2	27.6 °C	20.8 °C	27.0 °C	19.5 °C
2 x AAP2	17.5 °C	17.7 °C	17.8 °C	16.8 °C
3 x AAP2	N/A	N/A	N/A	N/A

Tab. 16: Melting temperatures T_m for reversible melting curves of multiple AAP1- and AAP2-modifications in the 8-mer duplex **ds8** upon irradiation with the maximum *trans* and *cis* switching wavelengths at room temperature and 40 °C irradiation.

Modifications	T_m *trans*	T_m *cis* RT	T_m *cis* 40 °C
1 x AB	65.3 °C	65.0 °C	64.7 °C
2 x AB	65.3 °C	64.5 °C	63.1 °C
3 x AB	66.5 °C	64.7 °C	58.7 °C
1 x DMAB	66.5 °C	66.7 °C	67.1 °C
2 x DMAB	70.0 °C	68.0 °C	67.9 °C
3 x DMAB	72.1 °C	72.6 °C	64.6 °C
1 x S-DMAB	64.7 °C	66.3 °C	66.6 °C
2 x S-DMAB	64.7 °C	60.6 °C	59.6 °C
3 x S-DMAB	59.2 °C	59.8 °C	61.6 °C

Tab. 17: Melting temperatures T_m for multiple azobenzene modifications in the 12-mer duplex **ds12** upon irradiation with the maximum *trans* and *cis* converting irradiation wavelengths at room temperature and 40 °C. The native melting temperature of **ds12** was determined as 59.4 °C.

a full duplex dissociation since no melting point could be obswerved. Two and three AB modifications in *cis* upon 40 °C irradiation alter the melting temperature to room temperature and below, which leads to a partial or complete dissociation of the duplex. DMAB and S-DMAB only exhibit a compellingly decreased melting temperature using three modifications where S-DMAB exhibits a full duplex dissociation at room temperature irradiation and DMAB on the other hand necessitates 40°C irradiation to achieve complete duplex dissociation.

Multiple arylazopyrazole moieties in **ds8** continue the destabilizing effect in *trans* as observed for a single photochrome. While two and three AAP1 moieties in *trans* lower the melting temperature of the **ds8** duplex to 25.2 °C and 18.5 °C, incorporation of AAP2 already decreases the melting temperature below room temperature for two modifications in *trans* (tab. 17). **Ds8** containing three AAP2 moieties in *trans* does not show any clear melting point at all. Four consecutive melting curves were recorded after alternatingly irradiating the duplexes with 590 nm and 365 nm at room temperature. All melting temperatures could be reproduced and showed a significant decrease and increase in melting tempe-rature even with a low number of modifications (fig. 70, tab. 17). In comparison to azobenzenes, the reported NNX motif does not seem to be mandatory to achieve an efficient duplex dissociation.

The short 8-mer duplex **ds8** containing 50 % GC-content constitutes a rather unstable DNA duplex. Consequentially, melting curves using the 12-mer DNA duplex **ds12** with 58 % GC-content were investigated with modifications in different numbers and positions. All 12-mer duplexes were modified with one, two or three photochromes up to one modification per three base pairs (see chapter 3.3.1). As observed before, a full duplex dissociation of the modified **ds12** duplex should not be possible using reported azobenzenes at room temperature irradiation in an NNNX motif in strands with high GC-content. The observed melting tempera-

tures reveal a strong duplex stabilization for the reported azobenzenes. No significant decrease in melting temperature from 59.4 °C for the native duplex could be observed for a series of differently modified **ds12** duplexes containing either one, two or three AB, DMAB or S-DMAB moieties (tab. 18). Only azobenzene exhibits a slight decrease in melting temperature of 7.8 °C upon irradiation to *cis* at 40 °C. This stabilization prevents all three azobenzenes from achieving duplex dissociation in DNA systems with high GC-contents and low synthetic loads.

Introduction of AAP1 and AAP2 into the 12-mer duplex **ds12** on the other hand clearly indicates an increased duplex dissociation effiency even when irradiated at room temperature. While AAP1 does not significantly alter the native melting temperature of the **ds12** duplex in *trans* conformation, irradiation with 365 nm at room temperature already significantly decreases the melting temperature by 12.5 °C using two moieties (tab. 19). The two different 12-mer sequences 2xAAP1 (5'-CACXCAT TCCXGGT-3') and 2xAAP1sh (5'-CAC CXAT TCXC GGT-3') with different positions of the AAP1 modifications clearly indicate that careful design of modified oligonucleotides is mandatory to achieve a maximum switching efficiency. While the sequence 2xAAP1 exhibits a strong melting temperature reduction of 12.5 °C, the sequence 2xAAP1sh does not seem to decrease the melting temperature at all when converted to *cis* at room temperature. Introduction of AAP2 moieties into **ds12** results in a significant decrease in melting temperature even in *trans* conformation, while the destabilization significantly increases with an increasing number of modifications. A single modification already reduces the native melting temperature by 1.6 °C while two modifications lead to a reduction of 9.0 °C and three modifications to a reduction of 14.6 °C (tab. 19). Irradiation to *cis* at room temperature leads to a more significant decrease in melting temperature leading to a duplex dissociation using three modifications within **ds12**. Shifting both AAP2 moieties from 2xAAP2 with six base pairs in between the modifications to an NNNNX-motif where each photochrome is separated by four nucleobases in 2xAAP2sh significantly reduces the melting temperature of **ds12** even in *trans* conformation by 28.5 °C. This result is consistent with the effects observed for AAP1 modified **ds12** and underlines the necessity for a careful and sophisticated design of modified DNA sequences.

To further investigate the destabilizing effect of AAP1 and AAP2 on DNA duplexes, two more modified 12-mer DNA duplexes were investigated. The strands 12mer50 (5'-CACXCATXTCCXAGT-3') and 12mer50sh (5'-CAC CXATTCXCGGT-3') containing 50 % GC-content and different numbers and positions of AAP1 and AAP2 modifications compared to the strand **168ROo** (5'-TCCXCCAXGCAXTCG-3') containing 66 % GC-content and three modifications in an NNNX motif were investigated. In agreement with the previous obser-vations, two *trans* AAP1 moie-ties in 12mer50 do not significantly alter the native melting

Modifications	T_m *trans* 1st	T_m *cis* RT 1st	T_m *trans* 2nd	T_m *cis* RT 2nd
1 x AAP1	61.6 °C	60.4 °C	62.6 °C	58.9 °C
2 x AAP1	61.7 °C	49.2 °C	62.8 °C	48.2 °C
2 x AAP1sh	55.3 °C	59.1 °C	57.6 °C	60.6 °C
3 x AAP1	58.0 °C	25.9 °C	62.7 °C	31.7 °C
1 x AAP2	57.8 °C	53.1 °C	58.1 °C	52.6 °C
2 x AAP2	50.4 °C	44.7 °C	49.8 °C	44.2 °C
2 x AAP2sh	36.9 °C	31.1 °C	38.7 °C	34.4 °C
3 x AAP2	44.8 °C	24.5 °C	42.1 °C	N/A

Tab. 18: Melting temperatures T_m of AAP1- and AAP2-modified 12-mer duplexes upon irradiation with the maximum *trans* and *cis* converting wavelengths at room temperature and 40°C irradiation.

temperature of 54.6 °C but also do not result in a decreased melting temperature upon irradiation to *cis* even at 40 °C (tab. 20). Introduction of three AAP1 moieties decrease the native melting temperature in *trans* by 6.2 °C which is further lowered close to room temperature with a melting point of 26.8 °C upon irradiation to *cis* at room temperature. Two AAP2 moieties in *trans* already reduce the native melting temperature by 16.5°C but no significant change upon irradiation to *cis* could be observed. Three AAP2 moieties do not show any clear melting point, a duplex formation does not seem to take place. A GC-content of 50 % appears to be too unstable for AAP2 modifications which consequentially prevent a duplex formation.

Modifications	T_m *trans*	T_m *cis* RT
2 x AAP1sh	54.7 °C	58.2 °C
3 x AAP1	48.4 °C	26.8 °C
2 x AAP2sh	38.1 °C	35.5 °C
3 x AAP2	N/A	N/A

Tab. 19: Melting temperatures T_m observed for AAP1 and AAP2 modified 12-mer50 duplexes with the sequence 5'-CACXCATXTCCXAGT-3' and complement exhibiting 50 % GC-content upon irradiation with the maximum *trans* and *cis* converting wavelengths at room temperature.

Modifications	T_m *trans*	T_m *cis* RT	T_m *cis* 40 °C
3 x AB	74.3 °C	73.4 °C	64.3 °C
3 x DMAB	82.2 °C	79.2 °C	56.4 °C
3 x S-DMAB	71.1 °C	68.4 °C	67.9 °C

Tab. 20: Melting temperatures T_m of AB, DMAB and S-DMAB modified 168ROo DNA duplexes with the sequence 5'-TCCXCCAXGCAXTCG-3' and complement upon irradiation with the maximum *trans* and *cis* converting wavelengths after room temperature and 40 °C irradiation. The native melting temperature of the 168ROo duplex was determined as T_m = 63.8 °C.

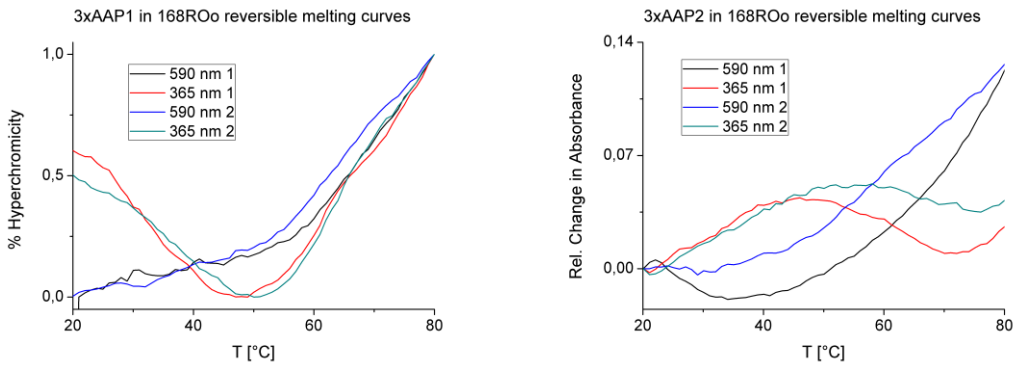

Fig. 71: Multiple repeating melting curve cycles for AAP1 and AAP2 modified **168ROo** duplexes upon alternating irradiation with 590 nm and 365 nm at room temperature. While AAP1 modified duplexes reveal an association behaviour in *cis* (left), AAP2 modified duplexes show a significant reduction in melting temperature when irradiated to *cis*.

Modifications	T_m *trans* 1st	T_m *cis* RT 1st	T_m *trans* 2nd	T_m *cis* RT 2nd
3 x AAP1	68.2 °C	62.6 °C	66.8 °C	66.7 °C
3 x AAP2	71.0 °C	30.6 °C	61.8 °C	33.2 °C

Tab. 21: Melting temperatures T_m determined for modified 168ROo duplexes upon irradiation with the maximum *trans* and *cis* switching wavelengths at room temperature and 40 °C irradiation.

The sequence **168ROo** 5'-CACXCATXTCCXGGT-3' containing 66 % GC-content and three modifications in an NNNX motif reveals a significant increase in melting temperature when modified with AB, DMAB or S-DMAB in *trans* conformation. Melting temperatures for duplexes with all three modifications are significantly increased for all moieties in *trans* conformation. Only irradiation at 40 °C results in a melting temperature reduction of 10.0 °C for AB, 24.8 °C for DMAB and 3.2 °C for S-DMAB, which still remains too low to achieve a full duplex dissociation (tab. 21).

Three AAP1 and AAP2 modifications slightly increase the native melting temperature of **168ROo** by 4.2 °C for AAP1 and 7.2 °C for AAP2 (tab. 22). AAP1 isomerization to *cis* does not significantly alter the *trans* melting temperature, but the shape of the recorded melting curves implies an association behaviour prior to the melting point in the dissociation part of the melting curve (fig. 71). The duplex seemingly dissociates upon irradiation and reassociates with increasing temperatures. Since a strong thermal back switching of AAP1-D-threoninol moieties could be observed when measuring small molecule melting curves, the result indicates a strong thermal hybridization of the duplex in three steps. Starting from the photoinduced duplex dissociation at room temperature, thermal AAP1 back-relaxation leads to an association of the duplex with elevated temperatures as observed in the shape of the melting curve. The duplex dissociates thermally when the temperature reaches beyond the melting point of 68.2 °C. In

sequences with high GC-content, *trans* AAP2 also does not show any significant decrease in melting temperature, but reduces the melting temperature down to 30.6 °C upon photoisomerization using 365 nm irradiation at room temperature. These results were reproducible even after four consecutive melting curve cycles when cooling down the samples back to room temperature after each measurement and starting the next irradiation and melting curve cycle. In addition to 12-mer melting curves, two further 10-mer sequences **126ROo** and **126ROp** were designed. The strands **126ROo** with the sequence 5'-CCXGATXGCTXGT-3' and 60 % GC-content and **126ROp** with the sequence 5'-GGXAATXGGTXGA-3' and 50 % GC-content contain three modifications per strand. AB- and DMAB-modified sequences exhibit a duplex stabilization of about 10 °C and above with all modifications in *trans* conformation (tab. 23). Converting AB-modified sequences to *cis* reduces the melting temperatures back close to the native melting temperatures while DMAB-modified sequences in *cis* do not reveal a change at all. *Trans* S-DMAB in the same sequences does not alter the native melting temperaturessignificantly but also shows no melting temperature reduction even when irradiated to *cis* at 40°C. A high synthetic load in combination with the duplex stabilizing properties of all three azobenzene derivatives apparently stabilize the two sequences to an extent that photoinduced duplex dissociation is not observed.

Since the duplex destabilization of AAP2 already shows no clear melting point in 12mer50 sequences and increasing numbers of AAP2 moieties additionally destabilize the DNA duplexes, only AAP1-modified strands were used for melting analysis of **126ROo** and **126ROp**. Both AAP1-modified strands **126ROo** and **126ROp** reveal complete duplex dissociation in *cis* conformation and interestingly the shape of all melting curves again indicates an associative behaviour followed by a thermal duplex dissociation (fig. 72). An association point of the *cis* irradiated duplexes can be observed in both cases, followed by a dissociation point at higher temperatures. Both association points lie in the same magnitude of about 35 °C,

Modifications	T_m *trans*	T_m *cis* RT	T_m *cis* 40 °C
3 x AB 126ROo	62.2 °C	56.5 °C	53.4 °C
3 x AB 126ROp	52.2 °C	45.5 °C	43.6 °C
3 x DMAB 126ROo	65.0 °C	66.9 °C	64.3 °C
3 x DMAB 126ROp	59.6 °C	63.1 °C	53.3 °C
3 x S-DMAB 126ROo	54.5 °C	47.3 °C	51.5 °C
3 x S-DMAB 126ROp	41.4 °C	41.5 °C	44.4 °C

Tab. 22: Melting temperatures T_m determined for modified 126ROo duplexes upon irradiation with the maximum *trans* and *cis* converting wavelengths upon room temperature and 40 °C irradiation. The melting temperatures of both native DNA duplexes are T_m = 53.9 °C for 126ROo and T_m = 44.3 °C for 126ROp.

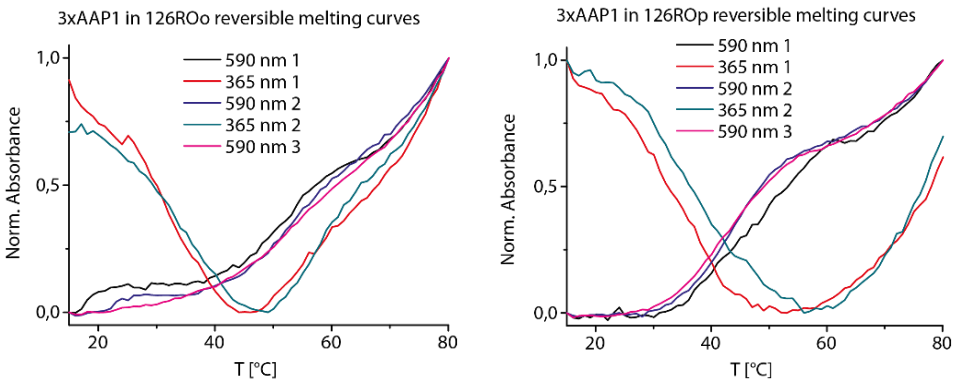

Fig. 72: Melting curve cycles of AAP1 modified 126ROo and 126ROp DNA duplexes upon alternating irradiation with 365 nm and 590 nm light at room temperature. All melting curves of modified strands show association curve behaviour after irradiation into *cis* conformation.

Modifications	T_m *trans* 1st	T_m *cis* RT 1st	T_m *trans* 2nd	T_m *cis* RT 2nd
3 x AAP1 126ROo	53.0 °C	56.7 °C	56.2 °C	58.7 °C
3 x AAP1 126ROp	47.0 °C	N/A	43.5 °C	N/A

Tab. 23: Melting temperatures T_m measured for AAP1 modified 126ROo and 126ROp duplexes upon alternate irradiation with the maximum *trans* and *cis* converting irradiation wavelengths at room temperature. Multiple repeated melting curve cycles indicate a reversible change in melting temperature as observed by reproducible melting temperatures.

only the thermal dissociation points are shifted relatively towards the melting points observed for modified **126ROo** and **126ROp** duplexes in *trans*. The appearance of association points in DNA melting curves is a novel observation and has not been reported for azobenzene modified DNA before. A repetition of melting curves with consecutively *trans* and *cis* irradiated AAP1 duplexes states the reproducibility of these results. A combination of AAP1 thermal back-relaxation with a complete duplex dissociation upon irradiation to *cis* possibly causes this effect.

In conclusion, both arylazopyrazoles AAP1 and AAP2 show a highly efficient duplex destabilization in *trans* and photoinduced dissociation upon irradiation into *cis* using UV light at room temperature. As a clear advantage in direct comparison to the reported azobenzenes, an efficient photoinduced duplex dissociation at room temperature as observed for both arylazopyrazoles could not be achieved with AB, DMAB or S-DMAB in the same DNA duplexes. The reported azobenzenes did not reveal any efficient decrease in melting temperature when using one modification per three base pairs and GC-contents of 50 % and above. While all of the investigated azobenzenes require elevated irradiation temperatures and high synthetic loads to achieve an efficient duplex dissociation, both arylazopyrazoles exhibit a significant decrease in melting temperature when irradiated with 365 nm light at room

temperature. Thereby, AAP1 does not affect the native DNA duplex melting point significantly in *trans* conformation. Unexpectedly, introduction of AAP2 on the other hand resulted in a significant duplex destabilization even in *trans* conformation which becomes less significant with increasing GC-contents of 66 % and above. When isomerizing AAP2 to *cis* conformation, the melting temperature reduces significantly in a DNA strand with 66 % GC-content. These highly stable DNA duplexes could not be photocontrolled efficiently using azobenzene moities due to their stabilizing effect on the double strand. A slight or significant destabilization of native DNA duplexes using arylazopyrazoles AAP1 and AAP2 in *trans* conformation implies a facilitated *cis* isomerization of the duplexes as observed by significantly decreased melting temperatures. To sum it up, not only a selection of the photochromic moiety is of vital importance to achieve an efficient photoinduced DNA duplex dissociation, but also the careful and sophisticated design of DNA sequences considering numbers and positions of modifications, GC-content and synthetic load at the same time. Stabilizing photoswitches like azobenzenes can enhance the stability of short DNA sequences with low GC-contents while destabilizing arylazopyrazole moieties are potentially capable of photoswitching highly stable long sequences with GC-contents above 50 %. Also a reduced synthetic load is a great advantage compared to the reported azobenzene derivatives, reducing the necessary NNX motif where each modification is separated by two base pairs to an NNNX motif with three base pairs separating each modification. The commonly used NNX-motif yet required for azobenzenes to achieve full duplex dissociation entails a disruption of DNA's B-form and possibly influences local sequences in higher order DNA applications. Using an NNNX motif with a reduced number of modifications possibly minimizes structural duplex disruptions leading to a reduced influence on the native melting temperature.

To further demonstrate the complexity of modification, position and sequence design, a series of DNA applications was designed to demonstrate a feasibility of the newly designed photochromes.

3.3.4 Investigation of duplex hybridization control efficiency in a 168 bp dsDNA ring system

To further confirm the previously monitored melting curve results in a qualitative manner, a circular 168 bp dsDNA construct containing a double-stranded 20 bp overhang and two asymmetric single-stranded gaps was designed and assembled. The ring design, which is based on a previously developed functional design for a 168 bp ring,[215] was redesigned and extended appropriately (fig. 73). Complementary strand hybridization to close the *ortho* and *para* single-stranded gaps revealed a significant difference in electrophoretic migration behaviour on a 6 % PAGE gel. This empirical observation, which possibly results from the relative position of both gaps in respect to the AT-track thus distorting the rings secondary structure if the complementary strands are hybridized or not, was used in combination with modified complementary release oligomers (ROs) to qualitatively confirm photoinduced hybridization and dehybridization of modified oligonucleotides to one or both gaps upon irradiation into *trans* or *cis*.

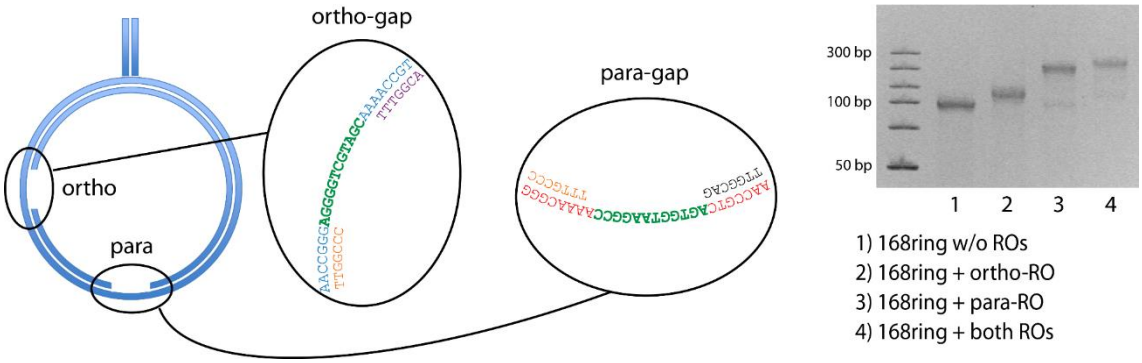

Fig. 73: Design of a circular 168 bp dsDNA system. The system contains two single-stranded gaps (*ortho* and *para*) and shows a difference in electrophoretic migration behaviour upon addition of release oligomers (ROs) complementary to both gaps. Both hybridization-sequences are highlighted in green.

While the single-stranded 12-mer *ortho* gap sequence exhibits 66 % GC-content, the 12-mer *para* gap sequence was designed with only 58 % GC-content. Both gaps were designed to hybridize to the previously synthesized strands **ds12** and **168ROo** as complementary ODNs. The previously designed sequences containing the same photoswitch modification patterns as described before (chapter 3.3.1) were used within this study, whereby each modification is separated by three consecutive base pairs (NNNX-motif). The ring system was incubated with two equivalents of the complementary *ortho* or *para* sequences for 30 minutes at room temperature to ensure complete hybridization of the oligomers. Subsequent irradiation with the corresponding *trans* or *cis* converting wavelengths for 5 minutes at the given temperature and

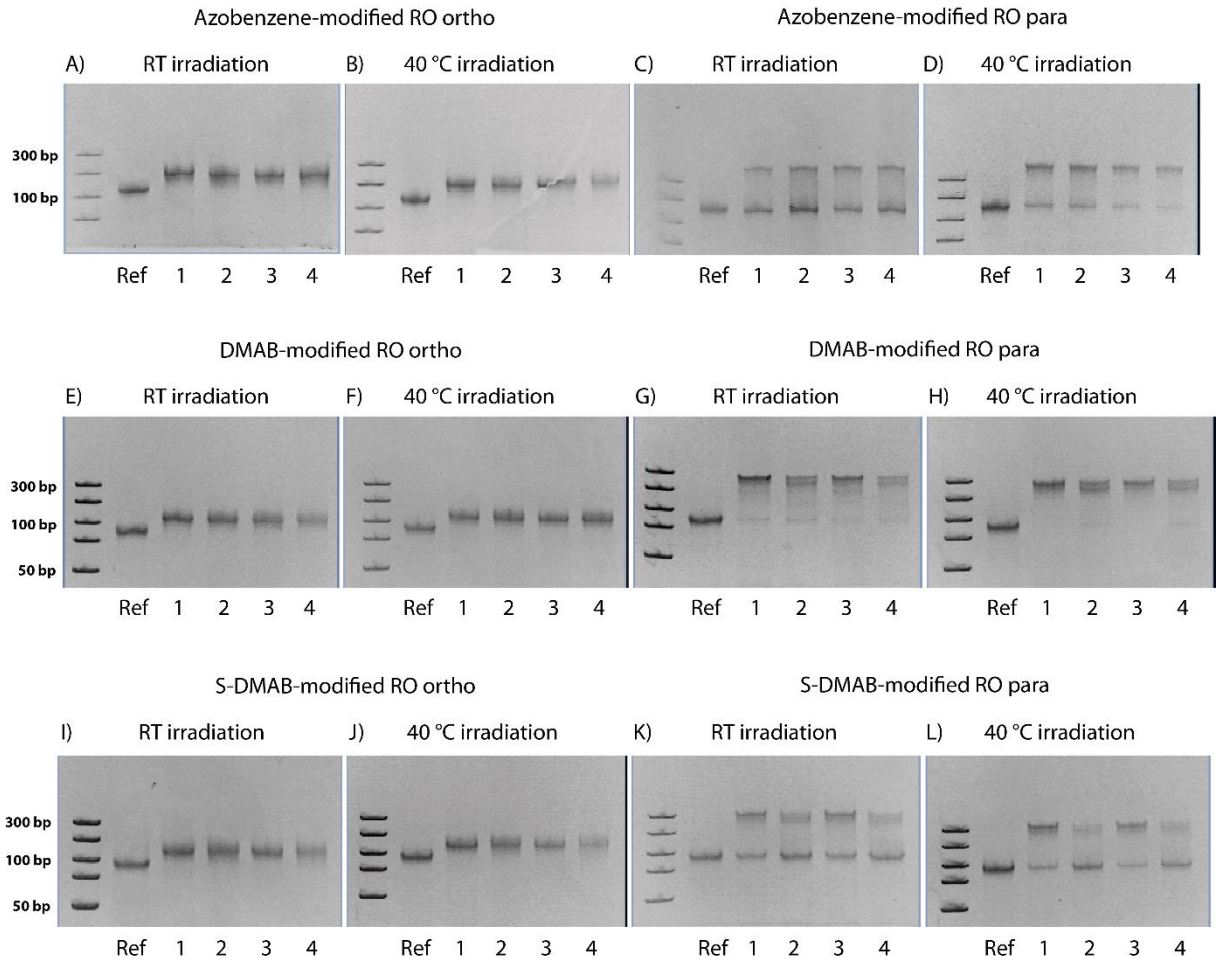

Fig. 74: Relative electrophoretic migration of the circular 168bp dsDNA system upon addition of AB, DMAB and S-DMAB modified *ortho* and *para* release oligomers complementary to the respective gaps. As a reference, the 168 bp dsDNA ring system without release oligomers was used. The ring system was incubated with the release oligomers and converted to *trans* (lanes 1 and 3) and to *cis* (lanes 2 and 4) consecutively (6 % PAGE, 200 V, 90 min, 4 °C). The used ladder (100 bp ladder) and corresponding gel bands are the same for all gel pictures.

subjection to PAGE gel chromatography results in qualitative bands, indicating hybridization or dehybridization to both single-stranded gaps.

An azobenzene modified *ortho* complementary oligomer shows an efficient hybridization as observed by an upper shift of the gel band but does not show any band shift upon irradiation at 40 °C (fig. 74). The azobenzene modified complementary sequence seems to hybridize strongly to the *ortho* gap but no photoinduced dehybridization could be observed. DMAB and S-DMAB modified complementary *ortho* sequences exhibit the same strong hybridization upon addition to the ring system but no photoinduced dehybridization was observed. Even elevated irradiation temperatures did not reveal any significantly shifted gel bands and thus did not indicate any dehybridization of the oligomers after irradiation (fig. 74). Furthermore, a DMAB modified complementary *para* oligomer shows the same stabilizing effect and no band shift

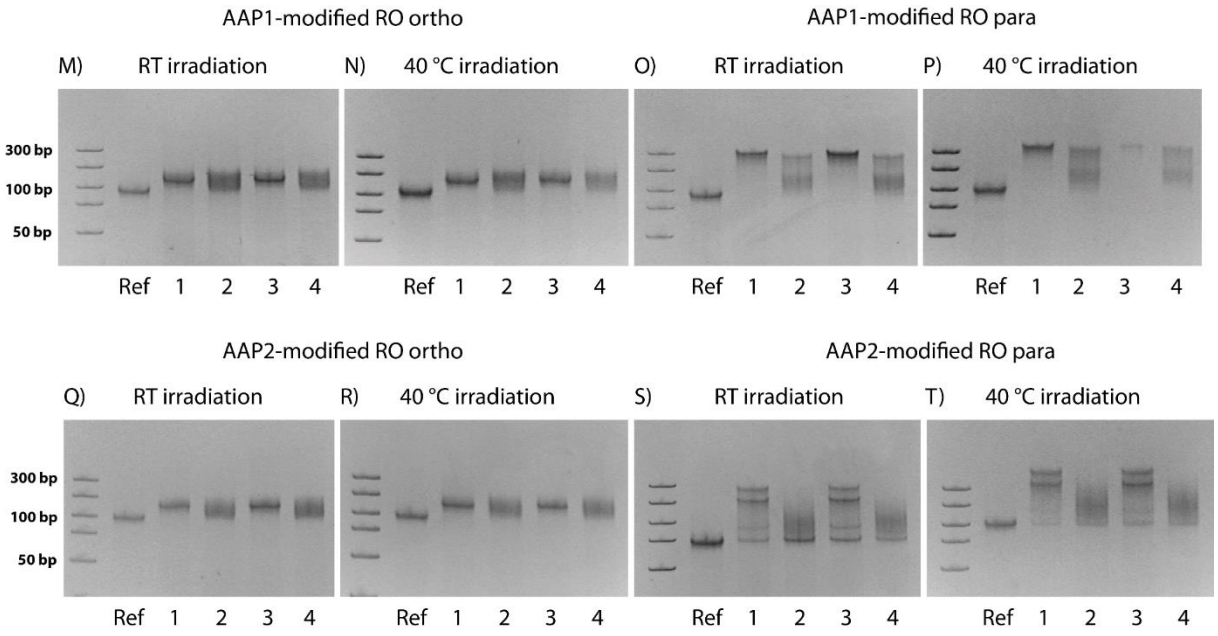

Fig. 75: Relative migration shift of the circular 168bp dsDNA system upon addition of AAP1 and AAP2 modified *ortho* and *para* release oligomers complementary to both gaps. As a reference, the 168 bp dsDNA ring system without release oligomers was used. The ring system was incubated with the release oligomers and converted to *trans* (lanes 1 and 3) and to *cis* (lanes 2 and 4) consecutively (6 % PAGE, 200 V, 90 min, 4 °C). The used ladder (100 bp ladder) and corresponding gel bands are the same for all gel pictures.

after photoirradiation, even when irradiated at 40 °C. In agreement with the previously performed melting curve experiments (chapter 3.3.3), DMAB does not indicate any duplex dehybridization even at 40 °C, possibly due to a strongly stabilizing intercalation between the duplex base pairs. AB and S-DMAB modified complementary *para* sequences exhibit an incomplete hybridization and dehybridization when irradiated to *trans* or *cis*. While an AB modified *para* release oligomer reveals a slightly improved hybridization at 40 °C in *trans*, only an incomplete reversible change in gel bands could be observed upon alternative photoswitching from *trans* to *cis* and vice versa. In agreement with the previously recorded melting curves, all gel shifts for the AB modified sequences indicate the same incomplete hybridization and dehybridization tendency. S-DMAB modified sequences on the other hand show an improved photoswitching behaviour as observed by alternatingly migrated gel bands upon alternate irradiation between the *trans* and *cis* isomers, whereby 40 °C irradiation further increases this effect. The different hybridization behaviour can be deduced from the chemical nature of the substitutents attached to each azobenzene derivative. Unsubstituted azobenzene slightly stabilizes the duplex hybridization to an extent that efficient photocontrol becomes possible at low GC-contents and elevated irradiation temperatures. DMAB shows a stronger duplex stabilization which consequentially prevents efficient photocontrol of hybridized

modified duplexes, independent from irradiation temperature and GC-content. The bulky methylthio residue in S-DMAB potentially counters this stabilizing effect from both *ortho* methyl residues and improves isomerization from *trans* to *cis* within the DNA duplex. An S-DMAB modified *para* oligomer is the only example in this study to show a significant but incomplete hybridization and dehybridization upon 40 °C irradiation. All observed gel shifts are in good agreement with the previously discussed melting curves and point out the necessity and limitations for a sophisticated sequence design for the use of photoswitches inside modified DNA duplexes.

In comparison to azobenzene based modified oligomers, both arylazopyrazoles AAP1 and AAP2 reveal improved photoswitching properties (fig. 75). An AAP1 modified *ortho* oligomer indicates a complete *ortho* gap hybridization in *trans* conformation and a significant but incomplete dehybridization upon irradiation with 365 nm at room temperature. The effect becomes more significant within a modified *para* oligomer which shows an even more efficient shift in gel bands when isomerized from *trans* to *cis* at room temperature, therefore indicating a better dehybridization in comparison to the *ortho* oligomer. Both AAP1 modified *ortho* and *para* complementary oligomers reveal a more incomplete dehybridization upon irradiation at 40 °C. A fact which is consistent with the low thermal stability and therefore rapid back-relaxation of the AAP1 *cis* isomer at elevated temperatures. Also the gel conditions may play a key role since all gels were run for 45 minutes at 4 °C, but local gel warming during the run can not be completely excluded.

AAP2 with a significantly higher thermal half-life shows stronger gel band shifts when incorporated into an *ortho* or *para* complementary oligomer (fig. 75). For the *ortho* release oligomer, a complete hybridization can be observed by an upper gel shift. Upon irradiation with 365 nm at room temperature, the reference band reveals a significant downward shift to a height comparable to the reference band. Gel band smearing possibly results from a dynamic equilibrium formed between the hybridized and non-hybridized complementary oligomers or an interaction between the *cis* modifications of the free oligomers with the construct. Different irradiation temperatures do not significantly alter hybridization and photoinduced dehybridization of the *ortho* complementary sequence. For the *para* oligomer with a decreased GC-content, AAP2 in *trans* reveals an incomplete hybridization as observed by the formation of two clearly distinguishable gel bands whereby the upper bands completely disappear upon irradiation using 365 nm at room temperature. This observation clearly indicates a complete dehybridization of the complementary oligomer even at room temperature irradiation. Using 40 °C irradiation, hybridization of the AAP2 modified *para* sequence in *trans* appears to be complete since no further bands are visible in the corresponding gel lanes. Irradiation to *cis* at

40 °C reveals the same down shift for the top gel bands as observed for room temperature irradiation.

Qualitative gel observations using the 168 bp dsDNA construct and its modified complementary sequences resemble similar results as observed for all previously measured melting curves. The intense duplex destabilizing effect observed for AAP2 modifications in all melting curve experiments apparently facilitates photoswitching within the hybridized duplexes and leads to a complete duplex dissociation even at room temperature irradiation. The highly decreased synthetic load necessary for photoinduced dehybridization of AAP1 and AAP2 modified complementary sequences could successfully be translated to the presented gel study. Incomplete dehybridization of AAP1 modified sequences appear to be decreased, possibly due to the low thermal stability of *cis* AAP1. Long lasting gel run times and potentially unavoidable gel warming during the run possibly lead to a thermal back-relaxation of *cis* AAP1 during the experiment.

3.3.5 Competitive photocontrol of modified oligonucleotides using a DNA hairpin

Strand displacement is a commonly used technique in DNA nanotechnology to replace functional DNA elements in nanosystems through controlled hybridization sites by further functional parts or elements to enable or disable functionalities. Opening a DNA hairpin structure by strand displacement provides an elementary functional system which can be utilized for investigating the photoinduced hybridization of modified strands in a competitive environment. The hybridization sequences are split into a short single-stranded four nucleotide toehold sequence, which facilitates hybridization of the modified opening oligomers to the hairpin stem region, and a hybridization sequence belonging to the hairpin stem (fig. 76). Opening oligomers containing photoresponsive moieties permit a reversible opening and closing of the hairpin structure upon repeated alternating isomerization into *trans* or *cis* conformation, thus opening or closing the hairpin through turning on and off hybridization.

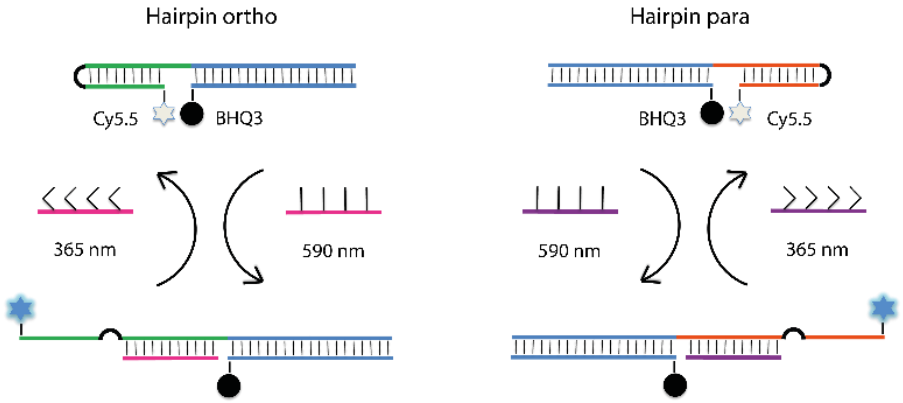

Fig. 76: Two DNA hairpins were designed for proof of competitive photoswitching. Both hairpins differ in their GC-contents in the hybridization sites. The hairpins were designed to use the same oligomers as opening sequences as used for *ortho* and *para* gaps in the 168 bp ring (168ROo and 168ROp).

Two different DNA hairpins were designed and assembled to be examines in combination with the previously synthesized modified sequences **ds12** and **168ROo** towards their reversible photocontrolled opening and closing efficiencies. In analogy to the previously performed dsDNA ring hybridization experiments, both hairpins were called *ortho* and *para* hairpin. Both hairpins differ in their relative GC-content inside the hybridizing sequences, antisense to the complementary *ortho* sequence 5'-TCCXCCAXGCAXTCG-3' (**168ROo**) with 66 % GC-content and the complementary *para* sequence 5'-CACXCATXTCCXGGT-3' (**ds12**) with 58 % GC-content. Reversible hairpin opening and closing was monitored by a Cy5.5 and BHQ3 fluorophore quencher pair. In the closed state, the Cy5.5 fluorescence is quenched by a BHQ3 quencher attached to one end of the hybridizing 7-mer stem region. A change in Cy5.5 fluorescence throughout the irradiation cycles could be monitored upon hybridization of **ds12**

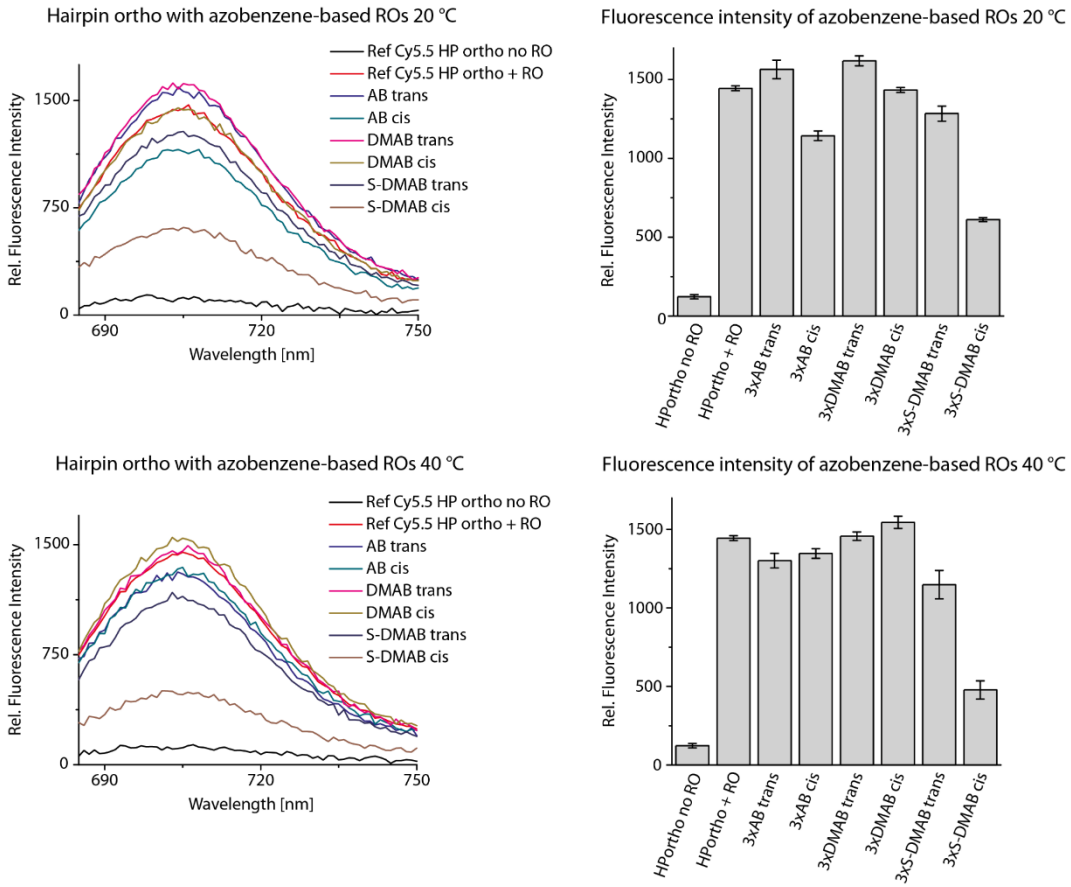

Fig. 77: Fluorescence intensity of DNA hairpin *ortho* was measured with 2 equivalents of modified opening oligomers containing AB, DMAB or S-DMAB in the 12-mer sequence 5'-TCC X CCA X GCA X TCG-3'. AB and DMAB modified oligo-mers exhibit an efficient hairpin opening but no closing upon irradiation to *cis*. The S-DMAB modified oligo-mer shows a complete hairpin opening in *trans* but only incomplete closing upon irradiation to *cis*.

and **168ROo** to their respective single-stranded gaps, consequentially opening the hairpins. A free single stranded Cy5.5 modified oligomer served as a reference in all measurements. Relative Cy5.5 fluorescence changes indicated the opening and closing efficiencies for both hairpins for each modified sequence under different irradiation conditions.

As a reference, both hairpins were incubated with two equivalents of the unmodified complementary sequences in 1x DA buffer and the resulting fluorescence intensity was recorded. Using two equivalents of AB, DMAB or S-DMAB modified opening oligomers with modifications irradiated to *trans* all lead to an efficient opening of hairpin *ortho* as observed in increased Cy5.5 fluorescence signals. Incubation at 40 °C results in even increased fluorescence intensities, indicating improved opening rates for hairpin *ortho* at elevated temperatures (fig. 77). Upon isomerization to *cis* using the respective irradiation wavelengths, only the S-DMAB modified **168ROo** exhibits a significant but incomplete drop in Cy5.5 fluorescence intensity, indicating a partial dehybridization and closing of hairpin *ortho*.

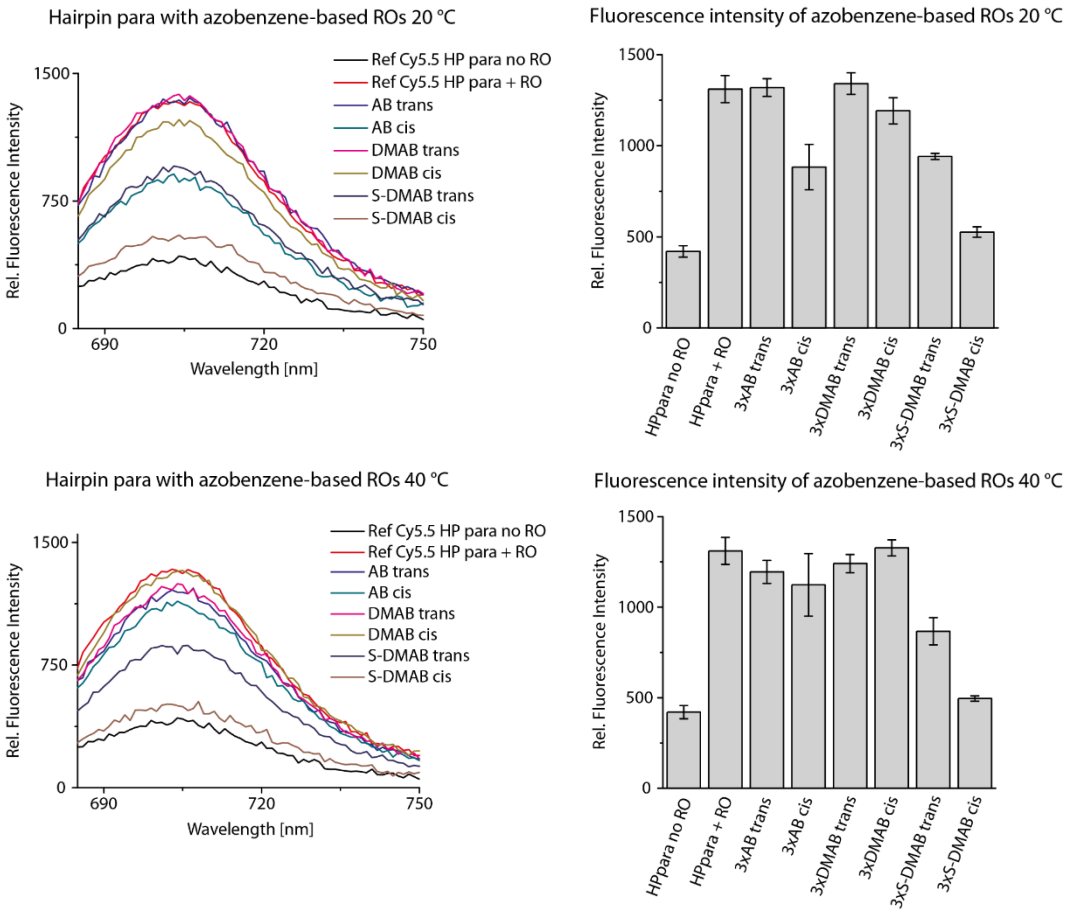

Fig. 78: Fluorescence intensity of DNA hairpin *para* was measured with 2 equivalents of modified opening oligomers containing AB, DMAB or S-DMAB in the sequence 5'-CAC X CAT X TCC X GGT-3'. AB and DMAB modified opening oligo-mers exhibit an efficient hairpin opening but no consecutive closing upon irradiation to *cis*. The S-DMAB modified oligomer indicates an incomplete hairpin opening in *trans* and a complete dehybridization in *cis*.

AB and DMAB modified **168ROo** oligomers did not show any significant decrease in Cy5.5 fluorescence in hairpin *ortho*, hereby indicating no photoinduced dehybridization of the modified sequences while the same behaviour was observed for room temperature and 40 °C irradiation. No efficient reversible opening and closing of hairpin *ortho* could be observed for all three azobenzene modifications upon irradiation at the two temperatures. The equilibrium between opened and closed hairpin state strongly seems to favour the opened hairpin where this observation is in good agreement with the previous melting curve experiments (chapter 3.3.3). All three azobenzene based modifications in hairpin *para* show the same tendency as observed for hairpin *ortho* (fig. 78). AB and DMAB modified opening oligomers exhibit an efficient opening of hairpin *para* upon addition of oligo-mers with modifications in *trans*, but an incomplete dehybridization upon irradiation to *cis* at room temperature for AB and no dehybridization at all could be observed for DMAB. At 40 °C irradiation both modified oligomers seemingly open the hairpin efficiently as observed by an increasing Cy5.5 fluorescence signal

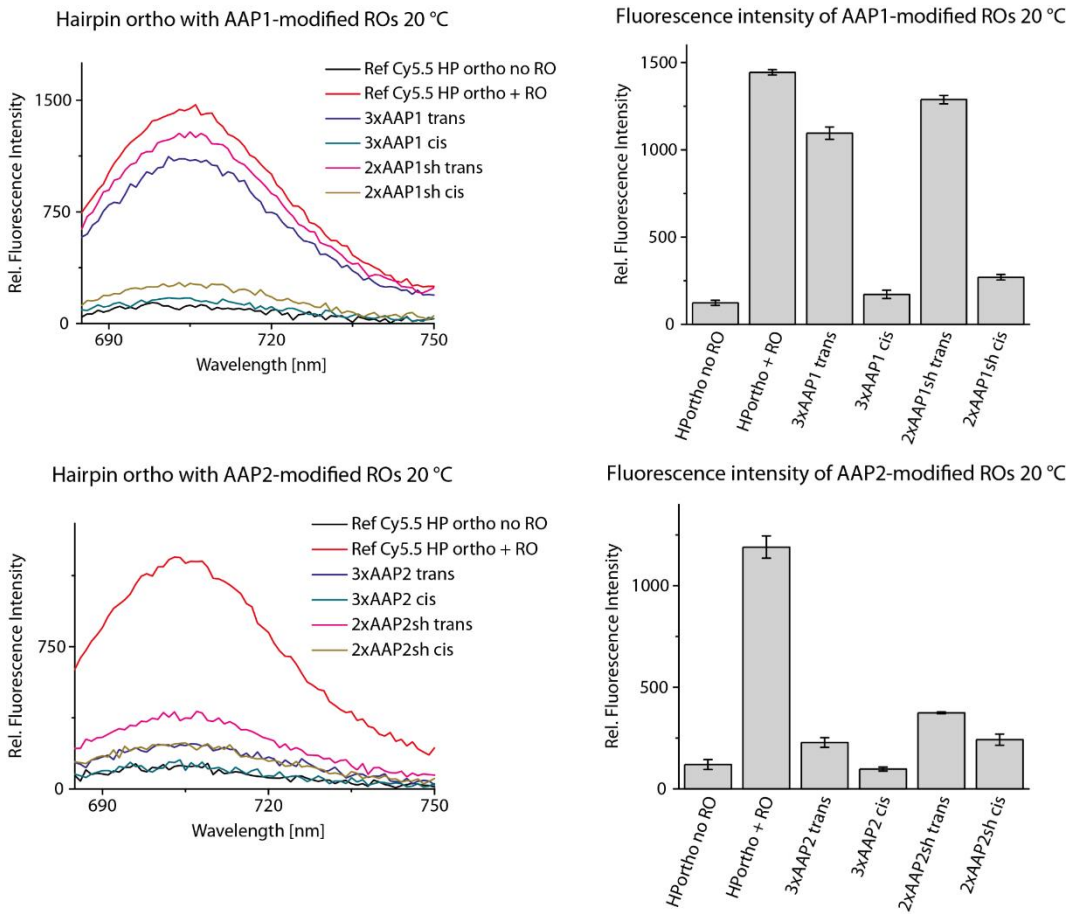

Fig. 79: Opening of hairpin *ortho* with AAP1 (top) and AAP2 modified opening oligomers (bottom) containing two and three modifications. Efficient hairpin opening and closing upon irradiation is observed for two and three AAP1 modifications in the modified opening oligomers. AAP2 modified oligomers do not show any hairpin opening at all.

but do not reveal any decrease in Cy5.5 fluorescence when irradiated into *cis* conformation. S-DMAB on the other hand reveals an incomplete hairpin opening in *trans* conformation but an efficient dehybridization upon irradiation into *cis* while room temperature and 40 °C irradiation do not show any significant difference. The stabilizing effect of AB and DMAB on DNA duplex stability apparently strongly shifts the equilibrium between open and closed state to the side of the open hairpin as observed by an increased Cy5.5 fluorescence. S-DMAB on the contrary favours a closed hairpin state in *cis* conformation but an incomplete hairpin opening in *trans* conformation. The observed stabilizing effect for AB and DMAB is consistent with the previously recorded melting curves and can be successfully transferred to the competitive hairpin environment.

Both arylazopyrazoles AAP1 and AAP2 on the other hand revealed a destabilizing effect on the duplex in the previous melting curve experiments (chapter 3.3.3). Therefore, not only strands with three AAP1 and AAP2 modifications were used, but also strands containing two modifications since the destabilizing properties of AAP1 and AAP2 possibly prevent a

successful hybridization of the opening oligomers. The strands 2xAAP1sh and 2xAAP2sh with the sequence 5'-TCC CXCA GCXA TCG-3' for hairpin *ortho* and 5'-CAC CXAT TCXC GGT-3' for hairpin *para* exhibit one modification per four nucleobases in an NNNX motif. The decreased number of modifications might be mandatory for an efficient hybridization to the hairpin stem regions. In a competitive environment, the stabilization of the hybridizing oligomers is of higher priority than an efficient duplex dissociation since closing of the hairpin is thermodynamically favoured.

Using two or three AAP1 modifications in an oligomer complementary to the *ortho* hairpin in both cases leads to an increase in Cy5.5 fluorescence with AAP1 in *trans* conformation and irradiation to *cis* at room temperature leads to a significant drop in Cy5.5 fluorescence (fig. 79). The difference in fluorescence intensity indicates efficient photoinduced opening and closing for two and three AAP1 modifications. Interestingly, an opening oligomer carrying only two modifications separated by four nucleobases was able to successfully open and close the

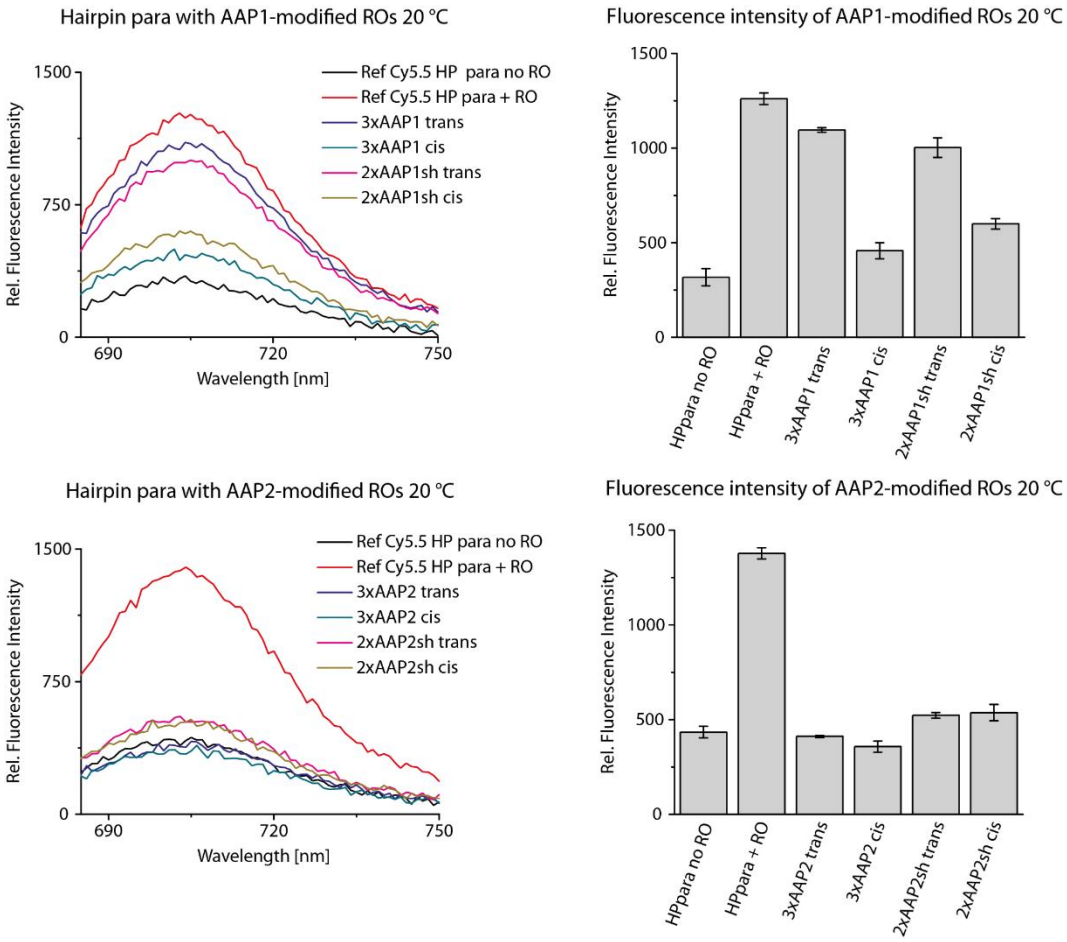

Fig. 80: Opening of hairpin *para* with AAP1 (top) and AAP2 modified opening oligomers (bottom) shows the same tendency as observed for hairpin *ortho*. Incomplete hairpin opening and closing is observed for two and three AAP1 modifications in the modified opening oligomer while AAP2-modified oligomers do not show any hairpin opening at all.

hairpin to the same extent as observed for three modifications. The additionally hybridizing stem region of hairpin *ortho* apparently facilitates hairpin closing when converting AAP1 to *cis*. Unexpectedly and even more important, hairpin switching seems to improve when using only two modifications instead of three.AAP2 modified opening oligomers on the other hand did not disclose any increase in fluorescence, neither in *trans* nor in *cis* conformation, indicating no hairpin *ortho* opening at all (fig. 79). Thereby the amount of AAP2 modifications within the opening oligomer does not show any significant effect. The strongly destabilizing properties of AAP2 on the DNA duplex possibly prevent the formation of a stable duplex, thus hampering an efficient hairpin opening. Since room temperature irradiation already succeeded in efficient hairpin opening and closing for AAP1, elevated irradiation temperatures were not further investigated in this respect.

Photoinduced opening and closing of hairpin *para* reveals the same tendency for AAP1 and AAP2 modified opening oligomers as observed for hairpin *ortho*. Interestingly, two AAP1 modifications led to a less efficient increase and decrease in Cy5.5 fluorescence, indicating a less efficient opening and closing of hairpin *para* (fig. 80). AAP2 modified opening oligomers did not show any increase in fluorescence in the same matter as observed for hairpin *ortho*. Multiple irradiation cycles with AAP1 modified oligomers in hairpin *ortho* and hairpin *para* were performed to demonstrate the reversible opening and closing efficiencies (fig. 81). Hairpin *ortho* and *para* in combination with two equivalents of the corresponding opening oligomers including two or three AAP1 modifications were used to reversibly open and close the hairpins upon alternating irradiation with 365 nm and 590 nm light at room temperature. In agreement with the previous hairpin opening experiments, efficient reversible opening and closing of hairpin *ortho* could be achieved with release oligomers containing two or three AAP1 modifications (fig. 81). Hereby, modified opening oligomers carrying two and three AAP1 modifications resulted in en efficient reversible fluorescence intensity drop and recovery upon alternate irradiation with 365 nm and 590 nm at room temperature. Reversible irradiation did not show any significant fatigue even after 5 alternate irradiation cycles. Using only two AAP1 modifications in an NNNNX-motif proves efficient reversible photocontrol of the hairpin. This proves a reduction of the mandatory synthetic load as commonly used for azobenzenes by half compared to the NNX-motif.

Hairpin *para* in combination with AAP1 modified opening oligomers carrying two or three modifications exhibited an increase and a decrease in Cy5.5 fluorescence upon alternating irradiation with 365 nm and 590 nm, but the fluorescence intensities did not reach the minimum or maximum reference values. An equilibrium between the open and closed hairpin form seems to prevent a complete opening and closing of the *para* hairpin when using AAP1 modi-

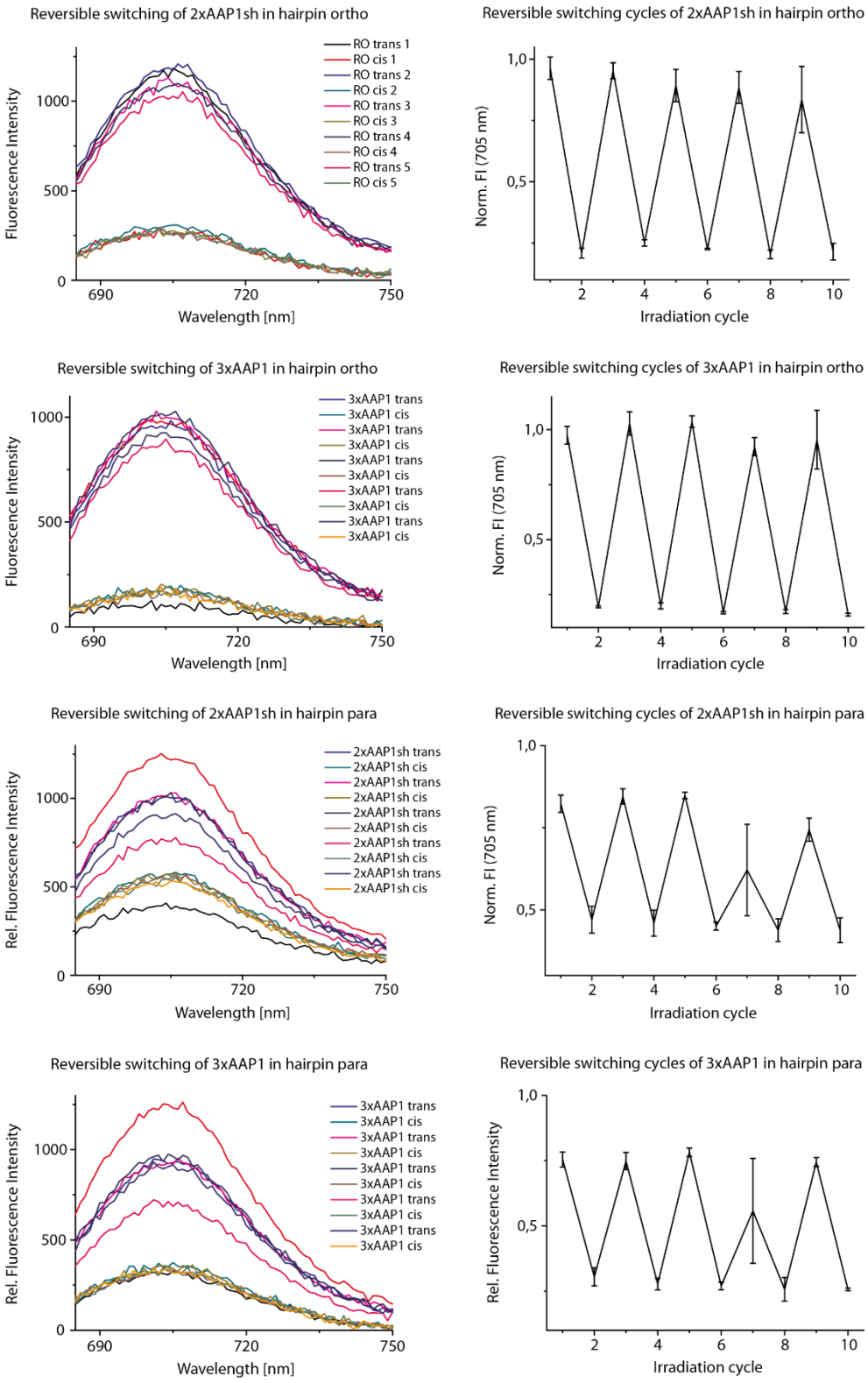

Fig. 81: Reversible hairpin *ortho* and hairpin *para* opening using AAP1 modified opening oligomers including either two or three modifications. While hairpin *ortho* can be reversibly opened and closed by UV and orange light irradiation, hairpin *para* only shows incomplete opening and closing upon alternate irradiation. Details of the modified sequences are given in the experimental section in chapter 7.10.3.

fied oligomers. Both hairpin conformations could be transformed from the open into the closed conformation and vice versa, but the steps were not converted quantitatively. The lower GC-content of the stem region in hairpin *para* probably favours the formation of the closed hairpin structure which prevents successful hybridization of the oligomer through the additionally introduced destabilizing AAP1 residues.

To sum it up, both hairpins in combination with opening oligomers modified with one of the three azobenzene derivatives showed strong Cy5.5 fluorescence signals but no decrease in fluorescence upon irradiation to *cis*. This clearly indicates a successful opening of both hairpins through hybridization of the modified sequences, but no efficient dehybridization from the stem regions to close both hairpin structures. The tremendously stabilized hybridization of AB and DMAB modified oligomers prohibited a photoinduced dehybridization from the stem region once the oligomers were hybridized to the hairpin. S-DMAB modified oligomers could not efficiently open both hairpins but indicated a partial dehybridization from the hairpin stem regions when transformed into *cis* as observed by a drop in Cy5.5 fluorescence.

Arylazopyrazole AAP1 proved to be a superior photochrome for photoregulation in competitive hairpin structures. Even a 12-mer opening oligomer containing AAP1 in an NNNNX motif exhibited efficient reversible opening and closing of hairpin *ortho* with minimal fatigue upon alternating irradiation at room temperature. Hairpin *para* could be opened and closed reversibly by AAP1 modified complementary oligomers, but only to an inefficient extent since no complete drop or recovery of the initial fluorescence signal could be obtained. AAP1 modified oligomers in competitive environments only appear to work in systems exhibiting high GC-contents. This apparent drawback opens the door for photocontrol in highly stable duplexes, a range of GC-content which was not accessible yet for azobenzene photoswitches. Using AAP2-modified release oligomers did not point out any hybridization to both hairpins, possibly due to its strongly destabilizing properties on the DNA duplexes. The strongly destabilizing effect of AAP2 prevents this photoswitch from being used in competitive environments since no efficient hybridization to any of the two hairpins could be observed for AAP2 modified complementary oligomers.

4 A photocontrolled two-state dsDNA [2]catenane system

The following project was designed and executed in cooperation with Johannes Weigandt. Part of this work is based on his results and observations.[237]

4.1 Design and assembly strategies for a two-state dsDNA [2]catenane system

DNA catenanes and rotaxanes provide versatile building blocks in DNA nanotechnology resulting from pioneering works in macromolecular chemistry[233,234] and DNA nanostructures.[235,236] DNA catenanes and rotaxanes both represent complex interlocked DNA nanostructures with the potential to serve as molecular transporters and logic gating devices. Upon introduction of photoresponsive moieties, such a system can be reversibly controlled by light. Hitherto, reversible photocontrol of [2] and [3]rotaxane shuttles has been reported by introduction of DMAB moieties into the structure and photoresponsive complementary release oligomers.[213,214]

Resulting from the empirical observations during the design and development of new photoswitches and their consecutive introduction into DNA strands, the idea of a reversibly photocontrolled two-state DNA [2]catenane emerged. A dsDNA [2]catenane construct was designed to prove coherent and independent photoswitching properties when combining multiple photochromes in a nanotechnology system. The [2]catenane construct consists of the double-stranded 168 bp dsDNA ring described in chapter 3.3.4, which was mechanically interlocked with a double-stranded 126 bp dsDNA ring (fig. 82). Both rings contain two complementary single stranded functional gaps with different sequences in *ortho* and *para* position in respect to a double-stranded overhang on the 168 bp ring. Hence, the two inter-

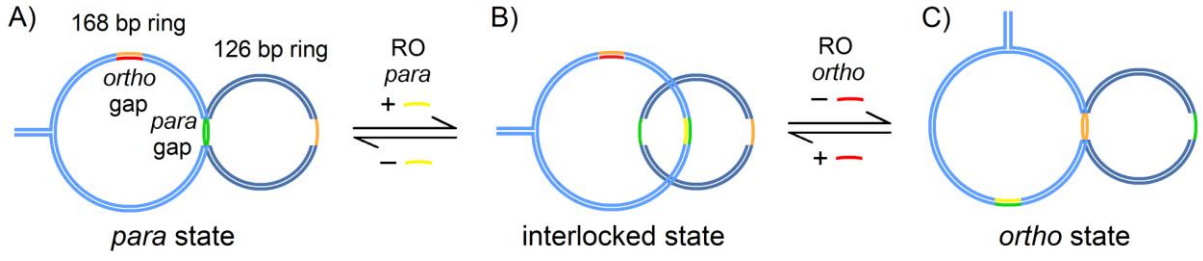

Fig. 82: Design of a functional two-state DNA [2]catenane system reversibly controlled by two different photoresponsive release oligomers. A) Hybridization of the *ortho* toehold oligomer (red) into the *ortho* gap forces the 168 bp ring to hybridize in *para* position. B) Addition of *ortho* (red) and *para* toehold oligomers (yellow) block both hybridization sites and force the ring into an interlocked state. C) Hybridization of the *para* toehold oligomer (yellow) blocks the *para* gap and forces both rings to hybridize in *ortho* position.

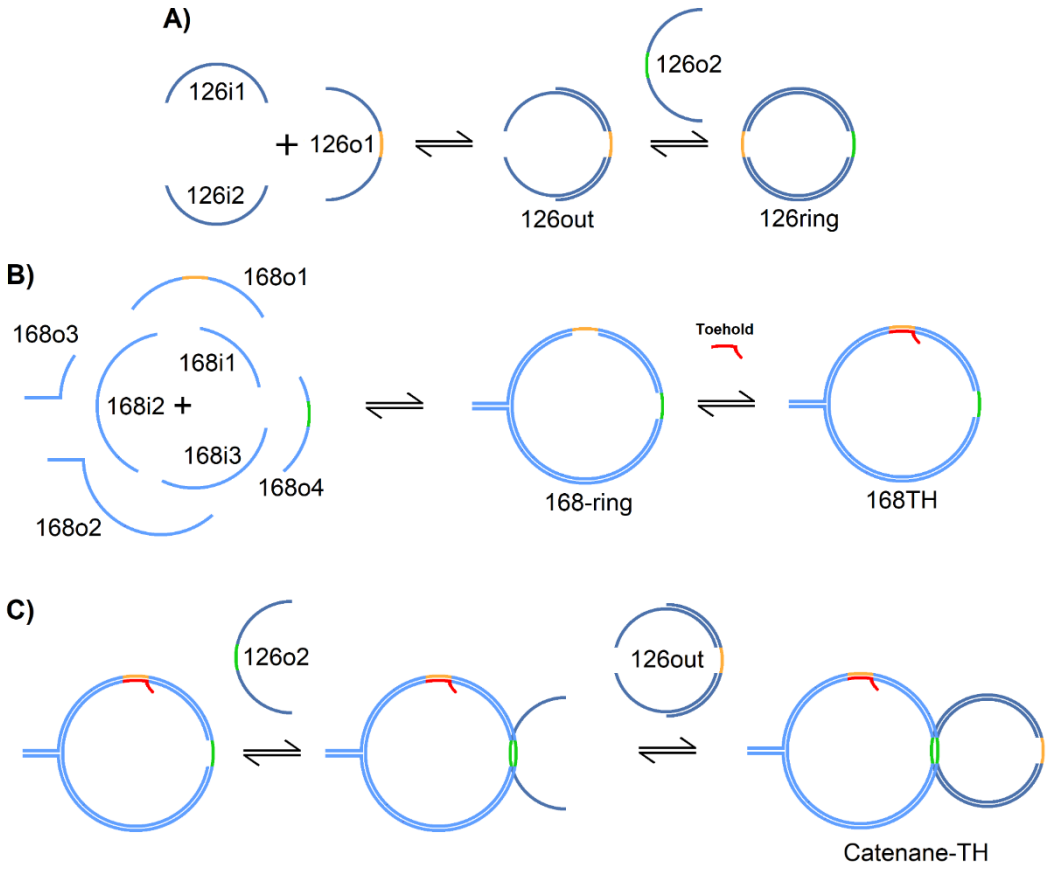

Fig. 83: Assembly strategy for the [2]catenane system. A) The outer construct 126out is assembled separately by combining the three strands 126i1, 126i2 and 126o1 in a 1:1 ratio. B) Starting from the assembly and ligation of the 168 bp ring, a toehold oligomer (red) is hybridized into the *ortho* gap to avoid formation of by-products through hybridization of strands into the *ortho* gap. C) The catenane system is assembled *via* hybridization of 126o2 into the free *para* gap and consecutive addition of the 126out construct. Ligation and liberation of the toehold oligomer by a complementary strand forms the [2]catenane system.

locked rings can be stalled in two different hybridization states upon addition of release oligomers hybridizing to one of the two single-stranded gaps.

Addition of either a modified *ortho* or *para* release oligomer blocks one of the hybridization sites and forces the system *via* an interlocked transition state to be stalled in the opposite conformation. This process can be reversibly photocontrolled by means of photoresponsive release oligomers which, upon alternate irradiation into *trans* or *cis* conformation, reversibly blocks or relieves one of the single-stranded gaps. Release oligomers containing two different photoswitches with orthogonal photoswitching properties possibly forces the system from one defined state into the other and vice versa. The difference in electrophoretic migration behaviour for both [2]catenane states permits the investigation of independent or coherent photoswitching properties through distinguishable gel bands when adding release oligomers modified with two different photochrome types. Two additional fluorophore quencher pairs

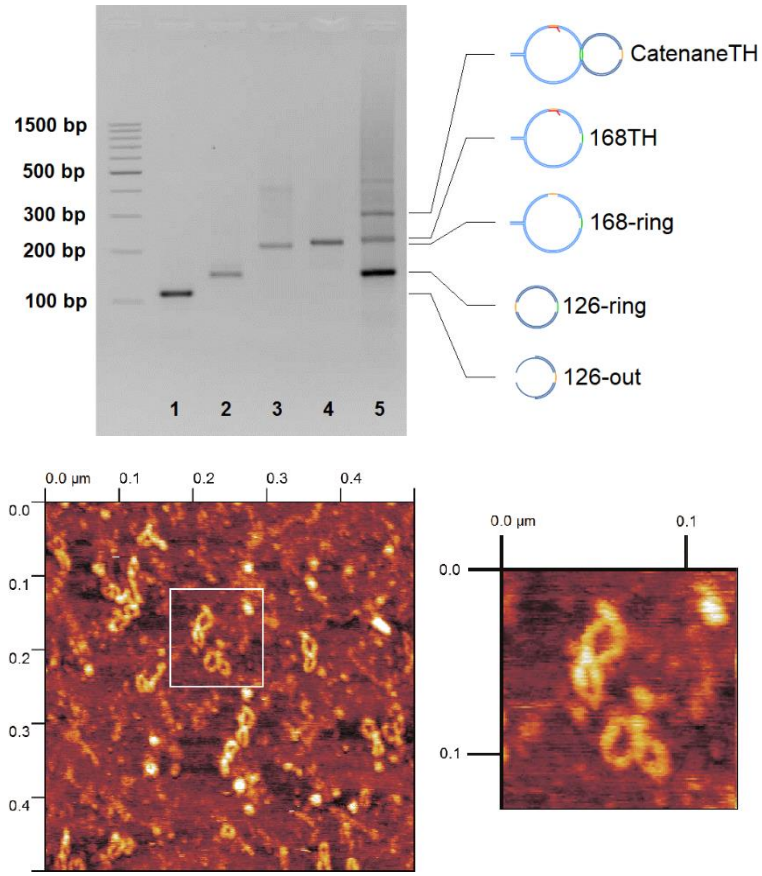

Fig. 84: Upper image: 2 % agarose gel (30 min., 200 V, 4 °C) of the [2]catenane assembly and all intermediate steps. 1) Outer construct of the 126 bp ring (126out) consisting of the three oligomers 126i1, 126i2 and 126o1. 2) Completely assembled and ligated 126 bp ring consisting of all four oligomers (126-ring). 3) Assembled and ligated 168 bp ring (168-ring). 4) Complete 168 bp ring including *ortho* toehold oligomer (168TH). 5) Assembled [2]catenane system containing the toehold oligomer (Catenane-TH). All intermediate steps were purified by weak anionic exchange HPLC. Lower image: Strcutrual proof of the [2]catenane system *via* AFM reveals the three-dimensional structure of the catenane. Both interlocked rings are visible as well as the double-stranded overhang. The image was recorded by Johannes Weigandt and reworked with Gwyddion image software.

attached to the terminal ends of each functional gap on both rings supports these measurements. The [2]catenane was designed to utilize modified release oligomers instead of modifying the functional gaps inside the catenane since the introduction of modifications into release oligomers is much more facile than assembling a whole modified [2]catenane for each photochrome pair.

[2]catenane assembly starts from the previously described 168 bp ring (chapter 3.3.4) followed by addition of a toehold oligomer to block undesired hybridization to the *ortho* gap. The use of a toehold oligomer for one gap forces the system into one conformation during the catenane assembly, thus avoiding the formation of side-products by default. Addition of the oligomer **126o2** hybridizing to the free *para* gap followed by the addition of the pre-formed

outer construct of the 126 bp ring consisting of the remaining three oligomers results in the formation of the crude [2]catenane which was obtained after purification by weak anionic exchange HPLC in about 5 % yield. Assembly progress and formation of all intermediates was monitored by agarose gel electrophoresis (fig. 84, left).

Two different assembly pathways are possible to achieve the [2]catenane, one pathway by blocking the *ortho* gap or the other pathway by blocking the *para* gap by a toehold oligomer and further assembly of the small ring around the free gap. The main focus was put on the *para* assembly pathway in order to guarantee a continuous hybridization of the short toehold oligomer in *ortho* position during the assembly since the *ortho* gap possesses a higher GC-content than the *para* gap.

Purification of the crude [2]catenane product was performed in two different manners. A workup by weak anionic exchange HPLC only yielded very low amounts of the target product, whereby a freeze and squeeze agarose gel purification and multiple consecutive freezing and centrifugation steps of the cut-out product bands brought up the catenane in up to 5 % yield. Also, the *ortho* toehold oligomer needs to be removed to permit free [2]catenane motion. During the freeze and squeeze workup the toehold oligomer gets removed while after weak anionic HPLC the toehold oligomer is still attached to the 168 bp ring. The [2]catenane structure containing random conformations was proven *via* AFM in hyperdrive mode (fig. 84, right). The double-stranded overhang is clearly visible on AFM as well as the interlocked structure with both rings stalled in both *ortho* and *para* position.

Addition of unmodified release oligomers complementary to two of the four free gaps blocks the corresponding hybridization sites and forces the ring to be stalled into one conformation. Extended toehold sequences permit a release of both unmodified release oligomers upon incubation with the complementary sequences to permit a conformational change without light irradiation. The change in conformation was proven by a relative gel band migration in a 2 % agarose gel and by an additional structural poof *via* AFM. In addition to both methods, the two complementary fluorophore and quencher pairs placed at one terminal end of each gap can be used to distinguish between both stalled states and the interlocked state. In both stalled states, one of the fluorophores is quenched while in the interlocked state no quenching of both fluorophores can be observed.

4.2 Proof of catenane switching by unmodified release oligomers

The purified [2]catenane system contains a total number of four gaps where two times two gaps are complementary to each other. Towards testing conformational switching of the [2]catenane, unmodified release oligomers with a length of 23 nucleotides containing 12-mer hybridization sequences and 11-mer overhangs were used to block one complementary gap in the 168 bp ring to force the system into the stalled *ortho* or *para* state. An interlocked state is achieved by blocking both single-stranded hybridization sites in the same ring. Addition of oligomers complementary to the unmodified toehold oligomers followed by addition of a second release oligomer complementary to the opposite gap results in a gel band shift. Consecutive blocking and relieving cycles for opposite gaps reversibly forces both rings from one conformation into the other and vice versa as observed by relatively shifted gel bands in a 2 % agarose gel. The up and down shift of the gel bands indicates a reversible transition from one conformation over the interlocked state into the second conformation and back (fig. 85).

The [2]catenane without any added release oligomer was used as a reference in the gel. Addition of two equivalents of both toehold release oligomers shows a smeary band indicating the interlocked catenane state in different dynamic conformations. Addition of two equivalents of either the unmodified *ortho* or the *para* toehold release oligomer leads to the formation of

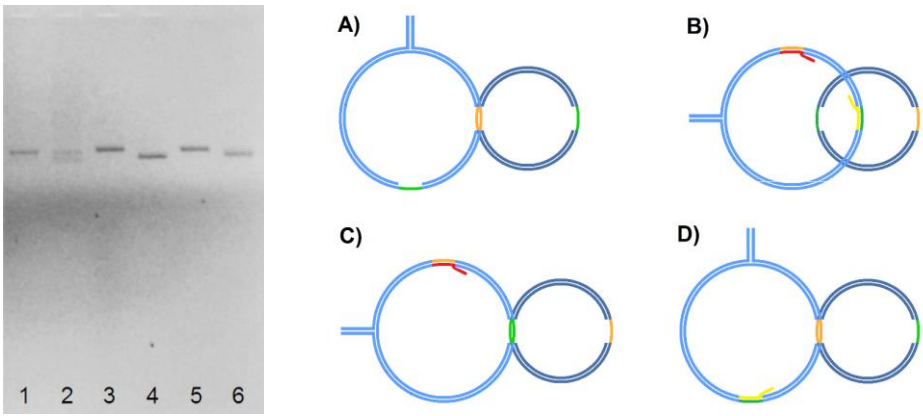

Fig. 85: Reversible [2]catenane switching from one stalled state into the other upon consecutive addition and release of *ortho* (red) and *para* release oligomers (yellow). A shift of gel bands on a 2 % agarose gel (200 V, 45 min, 4 °C) indicates the successful transformation between both states. Lanes: 1) [2]catenane reference without toehold oligomers (structure A). 2) [2]catenane with both unmodified toehold oligomers (structure B), 3) [2]catenane system containing the *ortho* toehold oligomer (C). 4) [2]catenane system containing the *para* toehold oligomer. (D) 5) [2]catenane system containing the *ortho* toehold oligomer. (C) 6) [2]catenane system containing the *para* toehold oligomer (D). Reversible switching was achieved through release of hybridized toehold oligomers by complementary sequences before addition of the opposite toehold oligomer.

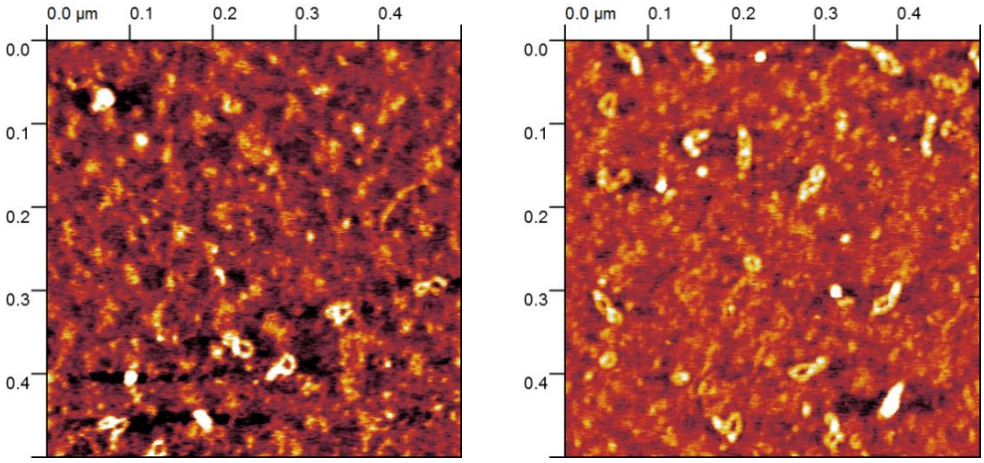

Fig. 86: Structural proof *via* AFM showing the [2]catenane in *ortho* (left) and *para* conformation (right). Both pictures were recorded after incubating the [2]catenane with the *para* toehold oligomer (left) or the *ortho* toehold oligomer (right). The images were recorded by Johannes Weigandt and reworked with Gwyddion image software.

clear bands, indicating the formation of the pseudo-interlocked [2]catenane in *ortho* or *para* conformation. An upper shift indicates the formation of the *ortho* pseudo [2]catenane and a lower shift the formation of the *para* pseudo [2]catenane. Further structural proof for both conformations was performed via AFM in hyperdrive mode (fig. 86).

The [2]catenane in *ortho* conformation merely reveals the double-stranded overhang in close proximity to the small ring (fig. 86, left) while the [2]catenane in the pseudo-interlocked *para* state carries the double-stranded overhang in a peripheral *para* position in respect to the 126 bp ring (fig. 86, right). Since an interaction of the [2]catenane with the MICA AFM surface possibly partially disintegrates the tertiary [2]catenane structure, a structural proof can only be seen as an indication and not as a definite proof. Also the adsorption conditions to the surface play an important role since polyornithine (PO) was used for the measurements instead of pure buffer. Nevertheless, both AFM images indicate a favoured conformation upon addition of the complementary release oligomers as observed by relative changes in gel bands.

Unfortunately, the total catenane yield was too low to perform additional fluorophore quencher expreiments and thus give an additional proof to further confirm the dynamic interconversion between a [2]catenane in *ortho* and *para* conformation. Furthermore, due to the missing orthogonal switching properties of possible photochromes and a combination thereof after introduction into DNA strands, further development and application of the [2]catenane project was stopped at this point and any further development was aborted. Nevertheless, reversible interconversion of the [2]catenane could be demonstrated and might be useful for future development of additional photochromes to provide a practical system for further investigation of photoswitch combinations in DNA nanotechnology.

4.3 Structural considerations of asymmetric dsDNA rings and the [2]catenane system

The designed double-stranded 168 bp ring containing two asymmetric single-stranded gaps revealed a difference in electrophoretic migration upon addition of the complementary release oligomers in *ortho* and *para* position. Since the difference in electrophoretic migration may have numerous causes, two further dsDNA ring systems were assembled to clarify this observation. The relative shift in electrophoretic migration observed for the 168 bp ring **(A)** as well as the assembled [2]catenane upon addition of one or both complementary release

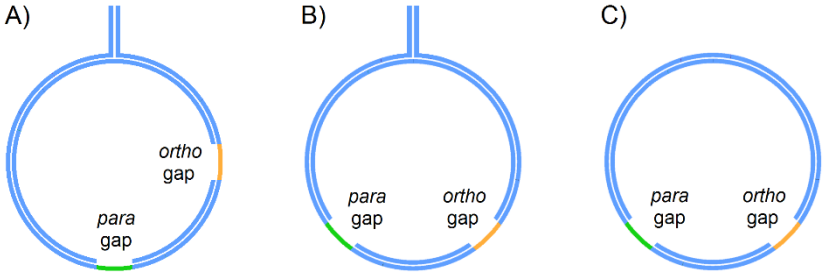

Fig. 87: Two further double-stranded circular 168 bp dsDNA rings were assembled as control systems to prove the asymmetry shift of all ring and catenane systems *via* gel electrophoresis: A) 168 bp dsDNA ring with overhang and two asymmetric gaps, B) 168 bp dsDNA ring with overhang and two symmetric gaps and C) 168 bp ring with two gaps and no overhang. All three rings exhibit a similar electrophoretic migration upon addition of the complementary gap sequences (fig. 88).

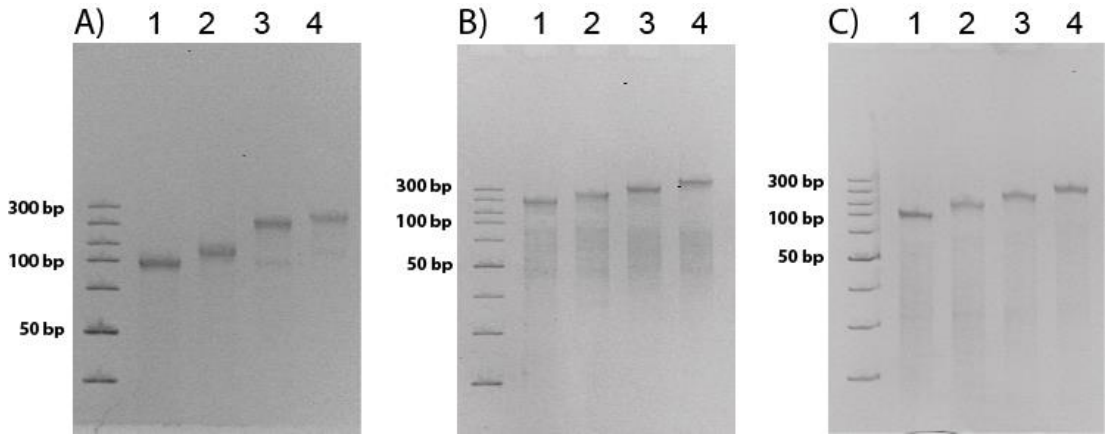

Fig. 88: Relative electrophoretic migration of all three 168 bp dsDNA rings described in fig. 87. A) 168 bp ring containing non-symmetric gaps and a dsDNA overhang. B) 168 bp ring containing symmetric gaps and a dsDNA overhang. C) 168 bp ring containing symmetric gaps and no overhang. The gel lanes show each ring system with addition of different release oligomers. 1) Ring systems without release oligomers. 2) Ring systems with hybridized *ortho* release oligomer. 3) Ring systems with hybridized *para* release oligomer. 4) Ring systems with hybridized *ortho* and *para* release oligomers. A change in relative electrophoretic migration for the rings B and C indicates a shift similar to the asymmetric 168 bp dsDNA ring system A on a 6 % PAGE gel (200 V, 30 min, 4 °C).

oligomers was assumed to be caused by the asymmetric nature of the 168 bp ring in respect to the double-stranded overhang. In addition to the 168 bp ring **(A)** containing two asymmetric gaps, a 168 bp dsDNA ring **(B)** with two symmetric gaps was assembled as well as a 168 bp ring **(C)** containing two single-stranded gaps but no double-stranded overhang (fig. 87). All three ring systems were investigated towards their relative electrophoretic shift upon addition of one or both release oligomers.

Using each of the three 168 bp rings without release oligomers as a reference, addition of the *ortho* and *para* release oligomers result in a significant upper shift, similar to the shifts observed for the non-symmetric 168 bp dsDNA ring system **(A)** containing the double-stranded overhang. Addition of both release oligomers at the same time increases the upper shift similar to the 168 bp ring **(A)**. Unexpectedly, this gel band migration behaviour can be observed for all three rings **(A)**, **(B)** and **(C)**. Even the 168 bp ring **(C)** without overhang exhibits a significant gel band difference upon addition of either the *ortho* or the *para* release oligomer (fig. 88). Initially, it was expected that addition of a release oligomer either in *ortho* or in *para* position changes the symmetry of the ring in respect to the double-stranded overhang, thus leading to the difference in electrophoretic migration. Observing the same effect for all three ring systems rather implies a secondary structural change occurring in each ring upon addition of the corresponding complementary release oligomers, thus leading to a change in the hydrodynamic radius . The possible change in secondary structure can be deduced from the respective hybridization sequences inside the 168 bp ring backbone. Both gaps differ in their relative extent of overlap concerning the AT-track which is covered by the hybridizing release oligomers. The consecutive AT-sequence causes DNA double strand bending and is one of the reasons why double-stranded DNA rings are formed. Existing in either a single-stranded or double-stranded AT-sequence possibly changes the system's secondary structure, thus leading to the significant difference in gel bands. To further investigate this effect, three different [2]catenane systems have to be assembled based on the three different 168 bp rings and have to be investigated towards their relative shift in electrophoretic migration. The assembly and switching proof for three different catenane systems might be mandatory to fully clarify the symmetry aspects and secondary structure influences concerning both gaps upon addition of *ortho* and *para* sequences.

As demonstrated in these control experiments, further investigation has to be performed to fully explain all empirical observations. Since adsorption of the [2]catenane samples on a MICA surface in atomic force microscopy possibly distorts the secondary and tertiary structures, cryo electron microscopy in solution might be a useful technique to clarifiy the structure of every [2]catenane systems in both stalled states. If a change in secondary structure causes the

relative shift in gel bands, the introduction of the double-stranded overhang is potentially not required for a gel proof and possibly improves the assembly and total yield of future [2]catenane systems designed for this purpose.

5. A photoresponsive aptamer nanoconstruct including a phototriggered release mechanism for active cell targeting and photoinduced drug release

The following project was planned and executed in cooperation with Dr. Deepak Prusty. Part of this work is based on his results and observations and has previously been published.[238]

5.1 Design and assembly of photoresponsive micellar hybrid aptameric nano-constructs

Targeted delivery of therapeutic agents into diseased cells and tissue has been an ambitious goal for the development of versatile drug delivery platforms,[239-242] emerging complex drug carrier systems including triggered drug release mechanisms with the aim to increase therapeutic efficacy while mini-mizing undesired side-effects. Especially in case of cancer, drug delivery systems against solid tumors are of high interest to decrease any inherent systemic toxicity.[241-242] Doxorubicin as one of the most commonly applied anticancer agents leads to an increased risk of heart failure during treatment, being responsible for 50 % of deaths during doxorubicin therapy.[243-244] Several drug delivery platforms have been developed to circumvent systemic side-effects by shielding agents until they reach their target.[239-242] The potency of these carrier systems strongly depent on stability in human serum, drug loading capacity, selective cell targeting and drug release efficiency. One possible way of selectively targeting tumor cells is the use of cell receptor targeting aiming for proteins which are highly overexpressed on the cell surface. cMet prevails a cell surface protein which is widely overexpressed in several tumor models and can be successfully targeted by a DNA aptamer cln0003.[245-246] The combination of a cMet binding aptamer combined with a doxorubicin carrying moiety facilitates selective cancer cell targeting combined with the targeted release of doxoru-bicin inside the cells. To selectively release doxorubicin inside the cells after uptake, a phototriggered release mechanism in the system allows a triggered liberation of intercalated doxorubicin molecules, thus minimizing systemic side-effects. cMet binding aptamers were mediated with doxorubicin carrying moieties *via* lipid-mediated self assembly to form supramolecular micelles.

These supramolecular hybrid aptamer nanocarriers (HyApNc) consist of a 5’-lipid modified cMet targeting aptamer and a GC-rich doxorubicin carrier sequence including 2’,6’-dimethylazobenzene (DMAB) moieties as phototriggers (fig. 89). Doxorubicin has been reported to intercalate between GC-rich DNA duplexes with alternating Guanine and Cytosine nucleotides.[247-249] A 5'-lipid modified GC-rich hairpin was designed to serve as a doxorubicin

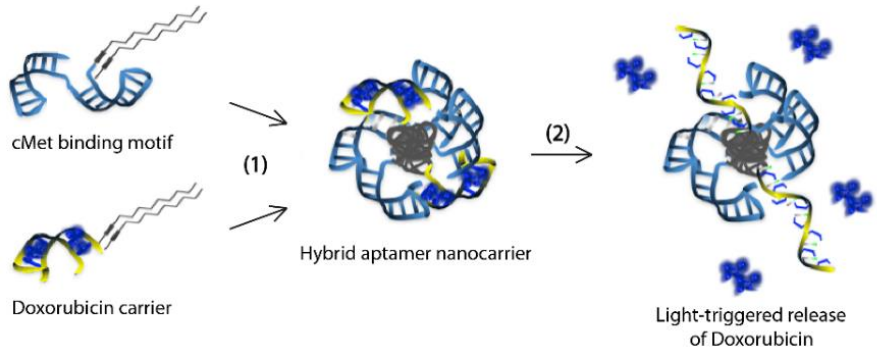

Fig. 89: Design of an aptamer based lipid mediated nanocarrier with an inbuilt phototriggered release mechanism for targeted delivery and release of doxorubicin into cMet overexpressing cancer cells. The figure shows an adapted version of the figure found in reference[238].

carrier, thus shielding the intercalated molecule between the duplex to reduce systemic toxicity. The combination of these two motifs leads to supramolecular mixed micelles with selective cell targeting properties and a triggered release mechanism for doxorubicin.

Lipid modifications were synthesized as DMT-protected 5-dodecynyl-2'-deoxyuridine phosphoramidites and DMT-protected 2',6'-dimethylazobenzene phosphoramdite (DMAB) were intro-duced into DNA sequences *via* solid phase phosphoramidite synthesis. Lipid-modified uridine residues were attached to the 5'-ends of both motifs and DMAB moieties were placed into the alternating GC-sequence of the doxorubicin carrier hairpin structure (fig 90). The cMet targeting moiety is based on the reported cMet targeting aptamer trcln0003, which contains two G-quadruplex structures,[246] wheras the truncated aptamer sequence was modified with 5'-lipid modifications. The newly designed doxorubicin carrier sequence consists of a hairpin structure with alternating GC base pairs and a central AT base pair. The sequence represents a structural compromise between possible doxorubicin intercalation sites and the intercalation of covalently bound DMAB moieties. Since doxorubicin and DMAB compete for intercalation sites, the design was optimized to provide a maximum doxorubicin loading capacity while maintaining a photoresponsive hairpin opening upon irradiation. Irradiation at 365 nm isomerizes DMAB into *cis* conformation and opens the hairpin, thus releasing the loaded doxorubicin molecules.

Doxorubicin loading efficiency was determined by titration using an aqueous solition with a fixed 10 µM doxorubicin concentration with multiple equivalents of the carrier sequence containing DMAB in *trans* conformation. Doxorubicin autofluorescence at λ = 480 nm is quenched upon intercalaton between the GC base pairs, which is used to calculate a maximum loading efficiency of eight doxorubicin molecules per carrier hairpin.[238] As discussed before, azobenzene has a stabilizing effect on a DNA duplex which is possibly countered by a secondary structure disruption through the additional intercalants. Taking all intercalating

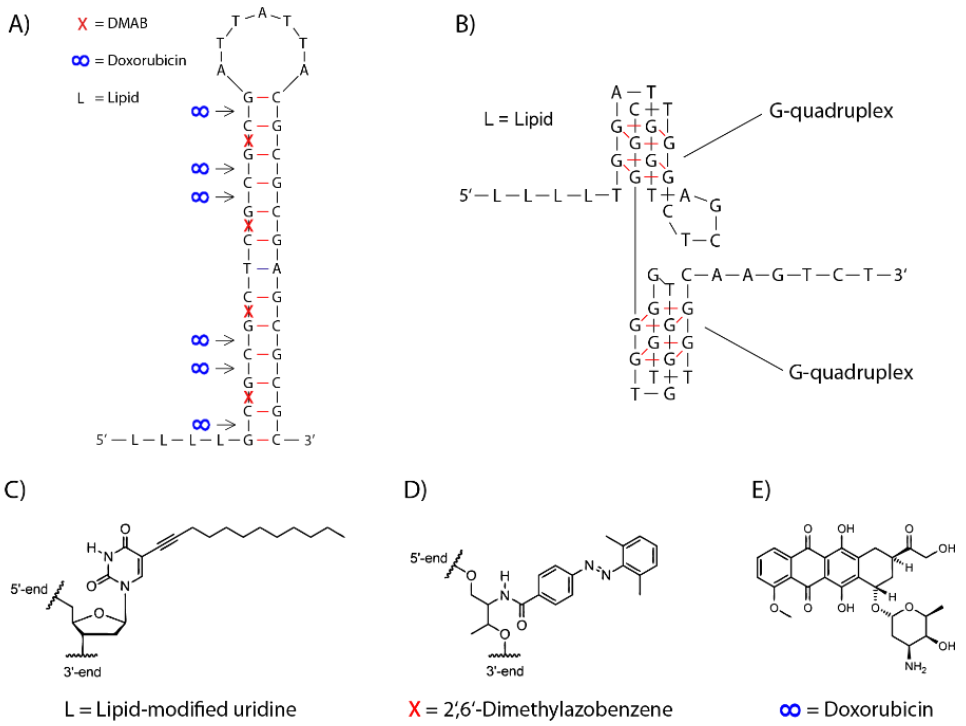

Fig. 90: A) Design of the doxorubicin carrier sequence carrying four lipid modifications (C) in the 5'-end presents a compromise between the duplex opening efficiency of DMAB moieties required for efficient dehybridization (D) and a maximum doxorubicin loading efficiency into the duplex (E). B) Design of a lipidated cMet targeting aptamer carrying four lipid moieties (C) on the 5'-end. The figure shows an adapted version of the figure found in reference[238].

moieties together, a disruption of the B-form duplex structure becomes apparent to an extent that 40 °C photoswitching of the GC-rich hairpin becomes possible. Contrary to the reported required elevated temperatures and the possibility of DMAB to switch only duplexes with low GC-contents, a photoswitching of the highly stable GC-rich hairpin only becomes possible through the multiple doxorubicin intercalations.

In addition to the doxorubicin quenching experiment, doxorubicin loading and light-triggered release efficiency was further determined by a reversed-phase HPLC assay. The doxorubicin carrier sequence was irradiated at 450 nm for 5 minutes to fully convert DMAB into trans conformation and was consecutively incubated with 10 equivalents of doxorubicin for 12 hours in 1x PBS buffer and

further purified by phenol chloroform extraction to remove excess doxorubicin. The loaded carrier motif was subjected to weak anionic exchange HPLC in a gradient of 1xPBS buffer with 5 % ACN and 1xPBS buffer including 1 M NaCl with 5 % ACN while detecting the doxorubicin fluorescence signal at 480 nm.[238] While the carrier is absorbed to the stationary HPLC phase, loaded doxorubicin inside the carrier is washed out and can be detected by the fluorescence detector. Irradiating the loaded carrier at 365 nm for 5 minutes at 37 °C and performing the

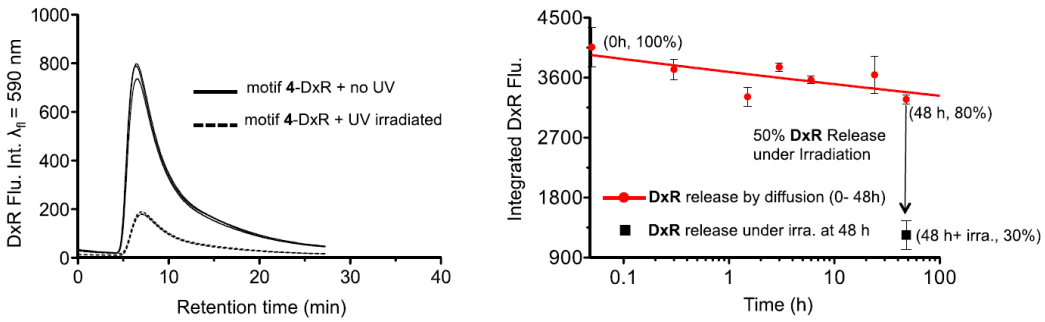

Fig. 91: Left: Doxorubicin autofluorescence revealed a doxorubicin loading and release efficiency and showed a 63 % decrease in fluorescence when the doxorubicin loaded carrier sequence is irradiated at 365 nm light for 5 minutes at 40 °C. Right: Doxorubicin diffusion out of the loaded carrier over time in 1 x PBS buffer. The experiment was performed by Dr. Deepak Prusty. The figure shows an adapted version of the figure found in reference[238].

same phenol/chloroform workup and HPLC run yields a 63 % fluorescence reduction compared to the fluorescence signal of the loaded carrier (fig. 91, left). Assuming 8 doxorubicin molecules per carrier as determined before, the decrease in fluorescence intensity corresponds to a number of 5 released doxorubicin molecules per carrier sequence upon isomerization to *cis*. Doxorubicin diffusion out of the carrier over time in 1 x PBS buffer showed a 20 % decrease in fluorescence intensity when left in the dark at 37 °C for 48 hours (fig. 91, right). This result indicates that the majority of doxorubicin molecules remains within the carrier sequence in buffer after intercalation and only 20 % of the molecules diffuse out of the structure over time. To prove the remaining doxorubicin inside the carrier, irradiation at 365 nm after 48 hours resulted in a further fluorescence intensity decrease, showing an additional 50 % photoinduced doxorubicin release after 48 hours.[238] The fluorescence decay and drop after irradiation proves retention of doxorubicin inside the carrier and a photoinduced release even after 48 hours, which is one of the main prerequisites for the HyApNc to function *in vivo*.

The 5'-lipid modified cMet targeting motif showed no significant decrease in binding affinity in direct comparison to the non-lipidated cMet aptamer in a competitive filter retention assay. While the lipidated cMet motif retained a binding affinity for the cMet receptor of IC_{50} = 46 nM, the non-lipidated cMet aptamer shows a binding affinity of IC_{50} = 56 nM under the same conditions.[238] A two-point mutant cMet aptamer did not reveal any target binding at all. These observations confirm no reduction in aptamer binding affinity through 5'-lipid tails when translated into micelle structures and therefore pave the way for an applicability of the motif without loss of target affinity.

The two moieties, cMet targeting aptamer and doxorubicin carrier motif, were both investigated separately tom prove their individual function. A combinatorial function has to be proven upon combination of both motifs in lipid-mediated hybrid aptamer nanocarriers.

5.2 Assembly and stability of micellar hybrid aptameric nanoconstructs

Assembly of the hybrid aptameric nanoconstructs was performed by mixing both lipid modified motifs in a 1:1 ratio, followed by heating the mixture to 90 °C and slowly cooling down to room temperature with a gradient of 1 °C per 5 minutes. Formation and structure of the micelles was monitored by STM, AFM and CryoEM. A spherical micellar structure was observed in all methods, indicating a successful micelle formation with an average particle size between 30 and 35 nm.[238] A FRET based assay using ATTO550 on the cMet aptamer motif 5'-end and Atto647N attached to the doxorubicin cafrrier 5'-end was utilized to find an optimum mixing ratio (fig. 92). Different mixing ratios exhibited a maximum FRET signal when using a 1:1 mixing ratio. Using this FRET signal for micelles mixed in a 1:1 ratio, dilution of the nanoconstructs reveald a disintegration of the particles below a critical micelle concentration of 400 nM.[238] Mixing the two motifs in a 1:1 ratio bears the advantage of retaining both core functionalities in equal amounts within the nanoconstructs to provide efficient cell targeting and a high doxorubicin load per micelle at the same time.

Successful formation of the hybrid aptamer nanocarriers above the critical micelle concentration was used to investigate the overall nuclease stability of the nanocarriers. The readily formed hybrid aptamer nanocamrriers HyApNc revealed a high stability against nucleases as tested in concentrated human blood serum and BSA.[238] The carriers showed a slow disintegration over time in both solutions but even after 12 hours more than 50 % of the

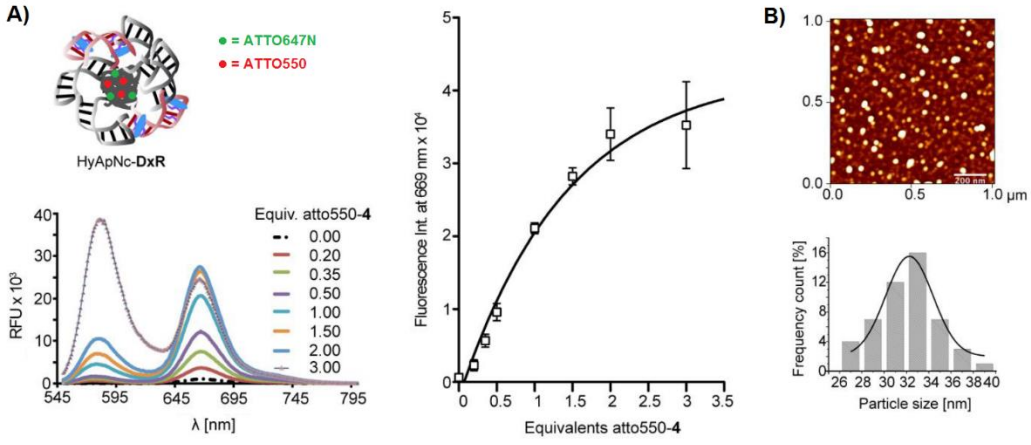

Fig. 92: Both motifs, cMet targeting unit and doxorubicin carrier, both labelled with ATTO550 and ATTO647 on each 5'-end, exhibit a maximum FRET efficiency at a mixing ratio of 1:1 or 1:1.5. STM and AFM images of the formed mixed micellar nanoconstructs indicate a nearly spherical shape of the formed HyApNc nanoconstructs. The experiments were performed by Dr. Deepak Prust. The figure shows an adapted version of the figure found in reference[238].

nanoconstructs still remained intact. When injected into human systemic blood circulation, the inherent dilution during circulation possibly prevents a translation of the system for therapeutic applications.

5.3 Cell internalization and photoinduced doxorubicin release induce cell death

Doxorubicin loaded HyApNc nanocarriers were used in combination with H1838 nsclc non small cell lung cancer cells to investigate the receptor-mediated cell internalization and photoinduced doxo-rubicin release efficiency. H1838 cells were reported to strongly overexpress cMet on their cell surface, therefore providing a useful cell line for cMet targeting. Introduction of the fluorescently labelled HyApNc including ATTO550 and ATTO647N was monitored by confocal microscopy (fig. 93, A).[238] ATTO550 and ATTO647N fluorescence as well as the resulting FRET signal of both dyes were monitored to follow position and stability of the nanoconstructs around or inside the cells. A FRET signal upon excitation of ATTO550 could be observed inside the cytosol after cell uptake, manifesting a successful cell uptake of the nanocarriers. Execution of the experiments at 4°C showed no cell internalization over time, thus indicating an endocytotic cell uptake pathway since endocyctotic cell uptake is not possible at low temperatures.[238]

Phototriggered doxorubicin release from the loaded HyApNc was also monitored by confocal microscopy making use of the doxorubicin self fluorescence (fig. 93, B+C). Free doxorubicin as a control already shows a diffusion into the cells and collocates inside the nucleus.[238] The

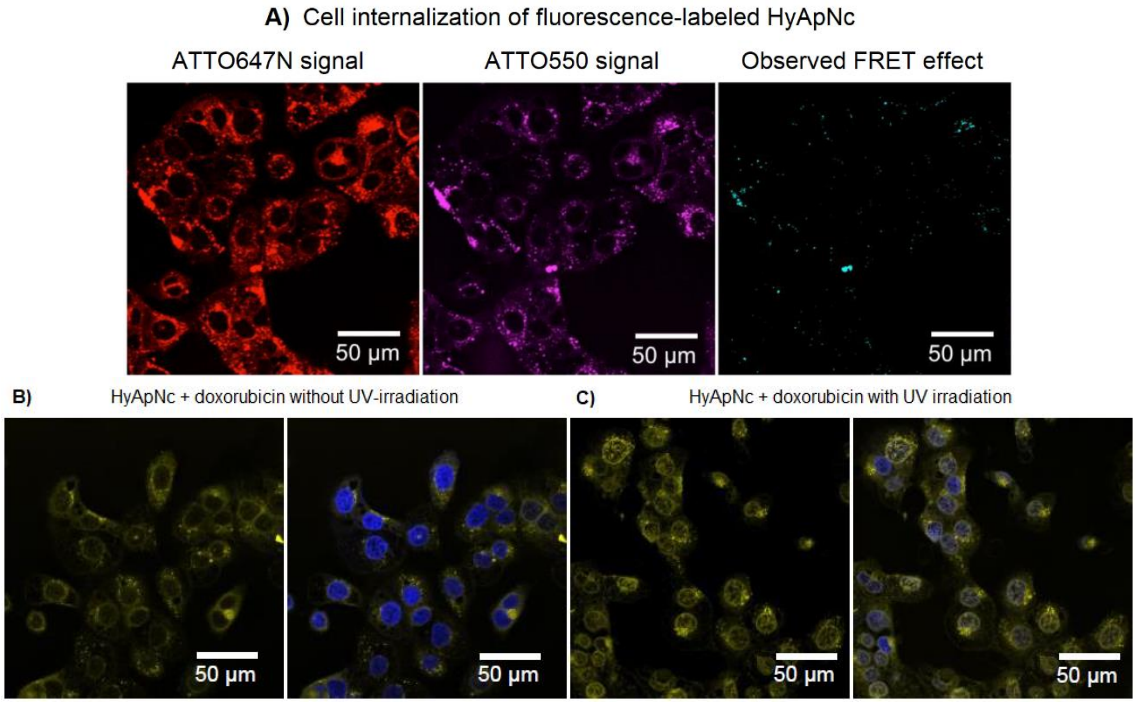

Fig. 93: A) Confocal microscopy reveals a cell internalization of the HyApNc construct into H1838 non small cell lung cancer cells as observed by fluorescence and FRET signals inside the cytosol. B) + C): Doxorubicin fluorescence of the doxorubicin loaded HyApNc inside the cell before (B) and after (C) UV irradiation. All confocal images were recorded by Dr. Deepak Prusty. The figure shows an adapted version of the figure found in reference[238].

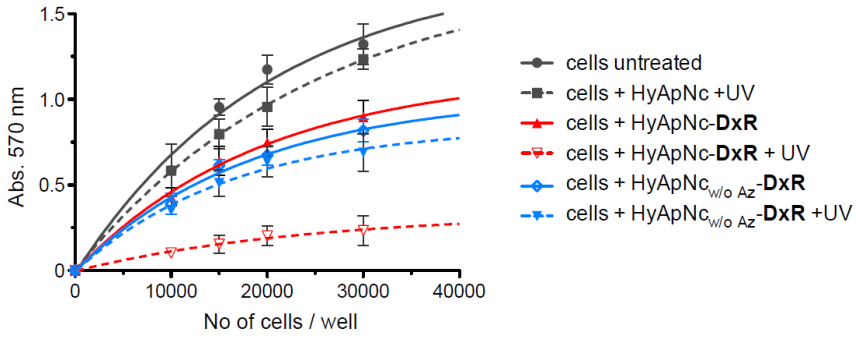

Fig. 94: MTT staining after incubation with doxorubicin loaded HyApNc in different cell amounts with and without UV irradiation. Addition of the doxorubicin loaded HyApNc without UV irradiation leads to 64 % cell survival after 24 hours while the doxorubicin loaded carrier reduces the cell survival rate down to 17 % after UV light irradiation. The experiments were performed by Dr. Deepak Prusty. The figure shows an adapted version of the figure found in reference[238].

doxorubicin loaded HyApNc exhibits a strong fluorescence mainly in the cytosol, indicating that doxorubicin is intercalated into to the carrier even inside the cytosol. Irradiation at 365 nm changes the doxorubicin fluorescence mainly to the nuclear region, indicating a release of doxorubicin and diffusion into the nucleus. This *in vitro* proof of concept demonstrates a general feasibility of doxorubicin loaded delivery into the cells and a phototriggered release of the payload within the target.

To further test a photoinduced cell viability upon release of the payload from the doxorubicin loaded HyApNc an MTT cell staining assay was performed.[238] Alive cells thereby express a higher MTT signal than dead cells, showing a cell viability in dependency on the observed MTT signal. Different cell amounts were grown with and wihout incubation with the doxorubicin loaded HyApNc as well as with and without 365 nm irradiation (fig. 94). Cells without HyApNc and doxorubicin only irradiated with UV light and cells with HyApNc irradiated with UV light in absence of doxorubicin showed cell survival rates comparable to the native untreated cells. Cells treated with doxorubicin loaded HyApNc in absence of UV light shows a drop in cell survival down to 64 % which might be caused by a partial doxorubicin diffusion from the nanoconstruct into the cycoplasm or partial disintegration of the construct inside the cell. UV exposure of these cells further decreases the cell survival rate down to 17 %, indicating an efficient photoinduced cell death. After 48 hours, cell viability significantly increases when using a doxorubicin loaded HyApNc without UV irradiation, showing a disintegration of the construct or a doxorubicin diffusion out of the carrier over time. While the unloaded carrier and pure UV irradiation do not reveal any significant effect on cell viability, the combination of doxorubicin and HyApNc proves an efficient photoinduced cell viability.

Although the doxorubicin delivery approach using HyApNc nanocarriers showed a successful doxorubicin deliver into cancer cells and a photoinduced cell viability *in vitro* in H1838 nsclc cells, a translation into mouse models or the use as a therapeutic system is highly limited through the overall micelle stability. Systemic dilution of the micelles possibly leads to a disintegration of the HyApNc, thus peventing an efficient delivery of doxorubicin into the cells. This issue could be improved by covalent crosslinking of the lipid chains within both motifs in the core structure to provide a higher HyApNc stability.

6. Conclusion and outlook

6.1 Summary and conclusions

The three main criteria for an ideal DNA photoswitch for use in long-term applications remain high conversion efficiencies between both stereo isomers, reversible photoswitching in visible light range while maintaining a high thermal *cis* state stability. Based on these three criteria, the systematic synthetic and spectroscopic development of new azobenzene and arylazopyrazole photochromes emerged a series of D-threoninol bound molecules with improved photophysical properties compared to the reported azobenzene series. While a tetra *ortho* fluorinated azobenzene phosphoramidite (TFAB) could not be obtained synthetically, azobenzenes with two *ortho* substituents in 2'- and 6'-position on the peripheral ring could be successfully synthesized and revealed visible light photoconversion from *trans* to *cis* and vice versa accompanied by retaining high thermal *cis* stabilities. Further synthetic development resulted in two azobenzene derivatives, 2',6'-difluoroazobenzene (DFAB) and 2',6'-dimethoxyazobenzene (DOAB), which could successfully be obtained as DMT-protected phosphoramidites and were consecutively implemented into a series of DNA strands. Beyond azobenzenes, two arylazopyrazole photochromes, *N*-methylarylazopyrazole (AAP1) and N-phenylarylazopyrazole (AAP2), could both be synthesized successfully as DMT-protected phosphoramidites and were also introduced into the same set of DNA strands with different lengths and positions.

All newly designed D-threoninol coupled photochromes revealed red-shifted response wavelengths further into visible light range compared to azobenzene as observed in empirical reversed-phase HPLC quantifications involving all D-threoninol bound photochromes as well as single modified 8-mer DNA strands. Determination of thermal stabilities showed half-life times between ten and several hundred hours at room temperature. Unfortunately, the most stable photochrome 2',6'-dichloroazobenzene (DCAB) could not be obtained successfully as a DMT-protected phosphoramidite.

Both arylazopyrazole photochromes AAP1 and AAP2 on the other hand revealed near-quantitative two-way isomerization between the *trans* and *cis* state. These two photochromes could be synthesized in high overall yields and successfully be translated from D-threoninol bound small molecules into a series of DNA strands with different lengths and GC-contents. In contrast to the DNA duplex stabilization observed for all azobenzene photochromes, arylazopyrazoles resulted in a duplex destabilization. While AAP1 does not significantly alter the native DNA duplex melting temperatures in *trans*, AAP2 showed a severe duplex destabilizing effect. AAP1 isomerization to *cis* significantly decreased the duplex melting

temperatures even at room temperature irradiation. The stabilizing effect of azobenzene and its derivatives upon DNA duplex introduction which yet resulted in the mandatory use of elevated irradiation temperatures could successfully be eliminated by the destabilizing effect of both arylazopyrazoles on DNA duplexes. Furthermore, the minimum synthetic load could be reduced significantly from one photoswitch per two base pairs (NNX-motif) to one photoswitch per three base pairs (NNNX-motif) while retaining room temperature photoswitching and offering a successful photoinduced duplex dissociation in strands with GC-contents above 50 %. The superior photoswitch-ing properties of AAP1 and AAP2 could further be proven in a series of melting curve and duplex hybridization experiments involving DNA hairpins and macromolecular double-stranded DNA nanoconstructs. Even DNA strands with GC-contents of 66 % could successfully decrease the melting temperature upon room temperature irradiation when modified with AAP1 or AAP2 moieties. Interestingly, using competitive strand displacement in DNA hairpins revealed a successful reversible hairpin opening and closing even when using an AAP1 NNNNX-motif with one photoswitch per four base pairs. Azobenzene modified release oligomers within the same systems did not result in any reversible hairpin opening and closing, possibly due to an increased duplex stabilization upon azobenzene intercalation. Cooperativity between the hybridizing hairpin stem regions in combination with photoswitch-modified opening oligomers revealed the complexity which requires a sophisticated design for introduction of photoswitches into complex DNA nanosystems.

Unfortunately, a successful translation of all newly designed photoswitches into higher order DNA systems could not be established. A macromolecular dsDNA [2]catenane system was designed to provide a prototype for investigating coherent and independent photoswitching properties using differently modified complementary sequences for a series of photochrome combinations. Structural investigations *via* AFM proved the successful structural assembly and, in combination with additional gel experiments, revealed a systemic interconversion between two different stalled states using non-modified complementary release oligomers. Photoswitch-modified release oligomers could not be tested within the system due to the described synthetic limitations.

All experiments proved that a sophisticated design of modified DNA sequences in combination with the chemical nature of photochromes, their amount and positions as well as the wise selection of photochrome combinations are absolutely required to achieve efficient photocontrolled DNA hybridizaion in macromolecular systems and cooperative effects when using a series of different photochrome types. Empirical development of photochromes facilitated the prediction of maximum response wave-lengths when translating a combination

of two or more small molecule photochromes into the same DNA system as resulted from multiple HPLC quantifications. Unfortunately, combina-torial photoswitching of multiple photochromes could not be investigated within the course of this thesis.

Further synthetic effort has to be performed to finally achieve coherently and independently addressable photochromes for multi-state DNA photoswitching systems. On the long road towards reaching this ultimate goal, arylazopyrazoles AAP1 and AAP2 prove valuable and versatile molecules, expanding the yet available toolbox of DNA photoswitches.

6.2 Future perspectives

Synthetic design and development of new azobenzene and arylazopyrazole based phosphoramidites constitutes a straight forward project with practically unlimited possibilities for introducing functional azobenzene and arylazopyrazole moieties into DNA backbones in different positional and numerous combinations. Further multicyclic and heterocyclic photochrome molecules beyond arylazopyrazoles have been reported during the time course of this project, potentially offering more versatile and promising candidates for the improvement of photocontrol over oligonucleotide duplexes.[261] Especially the development of photochromes with high conversion efficiencies back and forth in visible or even infrared light range still remains a highly ambitious goal, possibly offering deeper light penetration into living tissue. Heterocyclic molecules became the center of attention in this context as potent photochromes beyond azobenzenes. Future developments may target more towards the development of heterocyclic photochromes rather than using azobenzene based photochromes.

As proven in this abstract, sophisticated design and substitution of photochromic molecules in combination with oligonucleotide sequences facilitates the development of photoresponsive multi-state systems. Including UV-responsive photochromes, DNA nanotechnology applications switching between a multitude of different states become possible. This prevails one main prerequisite for the development of multi-state nano assembly lines, factories, data storage devices or nanomachines which are controlled by light. The vast complexity of such projects requires a multitude of orthogonal and independent photoswitches, thus enabling consecutive, orthogonal and independent photoswitching of multiple photochromes within the same system. A long road to success which still has to be gone. Since the accessible light range can be used from UV to visible light, also the development of Stenhouse adducts and other structurally different photoswitches might bring projects in this field along.

The ultimate goal still remains reversible light addressation of oligonucleotide duplex hybridization inside cells and living organisms for phototherapeutic applications. One of the main discoveries and developments in this field is the photocontrolled gene knockdown by photoresponsive antisense oligonucleotides,[262] the so-called antagomiRs, offering a photo-controlled gene regulation through the systematic introduction of photochromes. Also photoresponsive siRNAs could be of great interest. Furthermore, the use of photoresponsive aptamers *in vivo* affords a reversible photocontrol of receptor inhibition, thus potentially turning on and off signal cascades of special cellular receptors. This plays a key role in many disease models where receptor activities and signal cascades are suppressed or overexpressed. Optical control of receptors and metabolic

pathways has successfully been proven by D. Trauner by vision restoration in blind mice.[228] Further optically accessible receptors provide useful targets for future therapeutic projects. The developed lipid-mediated hybrid aptameric nanocarrier system presents a versatile tool for future developments using phototriggered lipid nanoparticles in combination with additional targeting moieties and further transporting systems instead of a doxorubicin carrier and anti cMet aptamers.

The possible combination of photochromes and functionalized oligonucleotides is virtually unlimited and even more than two functional motifs within a single photoresponsive micellar nanoconstruct are thinkable. Beyond the described phototriggered doxorubicin carrier, other physical triggers can be used to release molecules within a cell. Cancer cells usually exhibit lower pH values than non-diseased cells, facilitating a pH-triggered release mechanism for agents in acidic cellular environments. I-motif structures constitue pH-dependent triggerable secondary structures which can be used as inherent triggers to release molecules within cells with a low pH trigger. A pH triggered release mechanism inside cells does not necessitate any external stimulus and potentially only triggers in cells with low pH, preferably cancer cells. A hybrid lipid nanocarrier containing a targeting functionality combined with a pH trigger would include an automatic trigger for payload release inside cancer cells.

The use of light, despite all the discussed advantages, has its limitations concerning applicability in living systems and therapeutic areas since its penetration depth is highly limited and light cannot reach targets deep inside the human body without bringing light sources deeply into the body. Therefore, non light triggers have to be used to fully reach targets all over the human body. Heat and time triggered delivery systems or antisense oligonucleotides possibly lead to a time dependent back-relaxation of photochromes inside the oligonucleotides while circulating through the human body and might unfold its potency over time at the site of interest. As demonstrated by AAP1, a thermal back-relaxation by switching AAP1 modified oligomers into *cis* conformation in combination with a further functionality which is activated through AAP1 in *trans* conformation can be used to achieve different effects over time.

Another physical trigger which can penetrate the whole human body is electricity. Electricity can be used in antisense oligonucleotides in combination with electrochemically responsive moieties, thus leading to an electro-triggered DNA duplex formation or dissociation to control cellular and metabolic functions. Phenazines have been reported in this context to isomerize from an all over planar aromatic structure to a reduced non-planar structure containing two separated aromatic rings.[263-264] Both rings are connected by two amine moieties, thus leading to a bending of the molecular structure. The electric potential for a reversible electrochemical reduction of phenazines is rather low with +0.2 V and can easily be applied in the human body.

Theoretically, the planar aromatic phenazine and its derivatives attached to D-threoninol possibly intercalate between the stacked DNA base pairs analogous to azobenzene and lead to a duplex destabilization in its reduced form. Also, further molecules could be investigated in this context in future developments.

All described possibilities may be of high interest in future developments but any limitations for each described method have to be considered when developing systems including new triggers.

7. Experimental section

7.1 Materials and methods

Chemicals and devices

All chemical reactions were performed on air at room temperature with reagent grade purity chemicals ordered from ABCR, ACROS, Alfa Aesar, Fluorochem UK, Merck Millipore, Sigma Aldrich, TCI Chemicals and VWR. Special reaction conditions are stated in the corresponding procedures. Thin layer chromatography (TLC) was performed on aluminium coated silica gel plates. Purification of small molecule compounds via column chromatography was performed on an automated Interchim PuriFlash 430 flash chromatography column with a pressure of 10 bar. Pre-packed silica gel columns from Interchim and Grace were used with a particle size of 50 µm and 40 µm respectively and column sizes of 12 g, 25 g, 40 g and 80 g high purity silica.

All compounds were dried after isolation by a high vacuum pump with a maximum pressure up to $1 \cdot 10^{-2}$ millibar. NMR-spectra were measured on Bruker Advance 300 MHz, 400 MHz and 500 MHz NMR machines in deuterated solvents from ALFA or Sigma Aldrich at room temperature. The corresponding measurement frequencies for all NMR spectra are given in each synthesis procedure. Mass-spectra were measured on by the mass spectrometry department of the chemical institutes of the Univeristy of Bonn.

Preparative High Performance Liquid Chromatography (HPLC)

Purification of small molecules by preparative HPLC was done on an Agilent 1200 Series system by Agilent Technologies with a Gemini Preparative C18 column 30 x 75 mm 5 µm. HPLC-grade acetonitrile and Millipore water with 0.1 % formic acid were used as eluents.

Analytical High Performance Liquid Chromatography (HPLC)

Analysis and purification of small molecules and oligonucleotide-strands was performed on a semi-preparative Agilent 1100 Series HPLC system by Agilent Technologies. DNA and RNA analysis and workup were done with an Agilent Eclipse XDB-C18 column 4.5 x 150 mm and a particle size of 5 µm. Small molecule quantifications were done on a Nucleodur pentafluorophenylpropyl (PFP) column 150x2 mm with a particle size of 5 µm. Weak anionic exchange chromatography was performed on a TOSOH DNA-NPR column 4.5 x 75 mm with a particle size of 5 µm.

All buffers were prepared in Millipore water and HPLC grade solvents. Buffers were filtered through a 0.2 µm Nylon membrane filter and degassed *in vacuo* using an ultrasonic bath for 10 minutes before usage.

DNA synthesis and workup

If not further specified, all modified and unmodified DNA strands were synthesized either by Microsynth AG, Schützenstrasse 34, Balgach, Switzerland or in the Famulok group lab on an ABI Applied Biosystems 3400 DNA synthesizer on CPG (controlled pore glass) solid supports in 0.2 µmol scale. Further details are given in section 5.3.3.

UV/Vis-spectroscopy and melting curve analysis

All UV/Vis measurements and melting curves were performed on a JASCO V630 Bio Spectrophotometer with an automated 6-slot cuvette changer including a thermostat and Hellma Analytics ultra micro cuvettes 105.202_QS 10 mm with a minimum volume of 50 µL. Small molecule samples for UV/Vis spectroscopy were diluted by Millipore purity water and HPLC-grade acetonitrile. Standard scan range for all UV/Vis absorption measurements ranged from 220 nm to 650 nm. DNA samples were diluted in Millipore purity water and measured in the same wavelength range.

DNA melting curves were performed with the same technical equipment, but all oligonucleotide strands were diluted in 0.5 M NaCl solution. Melting curves were measured between 10 °C and 60 °C for 8-mer duplexes and between 20 °C and 80 °C for all other DNA strands. Melting temperatures were determined by use of the JASCO melting temperature software provided with the device.

Fluorescence Measurements

Fluorescence measurements were performed on an EnSpire Multimode Plate Reader by Perkin Elmer Inc. in flat-bottom 96 well OptiPlates or flat bottom 364 well ProxyPlates. Sample volumes, excitation wavelengths and emission wavelength ranges are given in the corresponding experimental procedures.

LCMS-measurements

Liquid chromatography mass spectrometry (LCMS) was performed on an esquire HCT series ESI mass spectrometer by Bruker Daltonics connected to an Agilent 1100 series HPLC system. All samples were separated on an Agilent Zorbax SB-C18 column 2.1x50mm with a flow rate of 0.4 mL/minute.

For separation and measurement of small molecules, a solution of 0.1 mg/mL of each sample was dissolved in 95/5 Millipore purity water and acetonitrile and filtered through a 0.2 µm PTFE filter membrane. All samples were separated by a gradient of 95/5 -> 0/100 acetonitrile and Millipore water containing 0.1 % formic acid. Oligonucleotide strands were diluted in Millipore

water in a concentration between 5 and 10 µM and separated by a gradient of 100/0 -> 80/20 TAE buffer containing 1 % hexafluoroisopropanol (HFIP) and acetonitrile.

Gel electrophoresis

Agarose gel chromatography was performed with High Resolution Agarose from Carl Roth GmbH (Germany) in horizontal gel electrophoresis chambers by Bio-Rad Laboratories GmbH (Germany) attached to an external power supply.

Polyacrylamide gel chromatography (PAGE) was performed using a Rotiphorese Sequenziergel 30 solution by Carl Roth GmbH containing 30% acrylamide in water. The PAGE gels were run in Mini Protean Tetra Cell Systems gel chambers by Bio-Rad Laboratories GmbH in Mini Protean Spacer Cells 10.1x8.2 cm.

Buffers and solvents

All buffers were mixed in Millipore purity water and filtered through a 0.2 µm cellulose sterile filter membrane before usage. Buffers for HPLC-purification- and quantification-runs were degassed for 10 minutes under reduced pressure after sterile filtration. The following buffers were used for all experiments and purifications:

Melting curves buffer:	0.5 M NaCl, pH = 7.0.
TAE-buffer:	40 mM Tris, 20 mM acetic acid, 1 mM EDTA, pH = 8.3.
TBE-buffer:	89 mM Tris, 89 mM boric acid, 2 mM EDTA, pH = 7.6.
TEAAc-buffer:	100 mM glacial acetic acid, 100 mM trimethylamine, pH = 7.0.
DA-buffer:	10 mM Tris, 50 mM NaCl, 10 mM $MgCl_2$, pH = 7.5.
WaxA-buffer:	20 mM Tris, pH = 9.0.
WaxB-buffer:	20 mM Tris, 1 M NaCl, pH = 9.0.

Atomic Force Microscopy

Atomic Force Microscopy was performed on a Nanowizard 3 instrument by JPK instruments on mica surfaces in intermittend contact mode in air (AC-mode) and liquid (Hyperdrive mode). All buffers, solvents and sample solutions were filtered through a 0.2 µm PTFE-filter before usage.

In AC-mode, the samples were immobilized in a marked area on a freshly cleaved mica-surface, which was obtained by removal of the top layer on the mica surface by a tape strip. Each sample in a concentration between 1 and 5 nM in 1xDA-buffer was incubated for 1 minute on the surface, followed by rinsing of the surface area three times with Millipore water and drying in an air flow. Samples were directly taken after this procedure.

LED-irradiation-machine

For all irradiation procedures, an irradiation machine specially designed for the working group Famulok by the electrical department of the University Bonn was used (fig. 95). The irradiation machine consists of several LEDs with a high light output and narrow bandwidths for irradiation of all samples with a distinct wavelength range. The technical details including wavelength (WL), bandwidth (BW) and other technical details for all LEDs are given below.

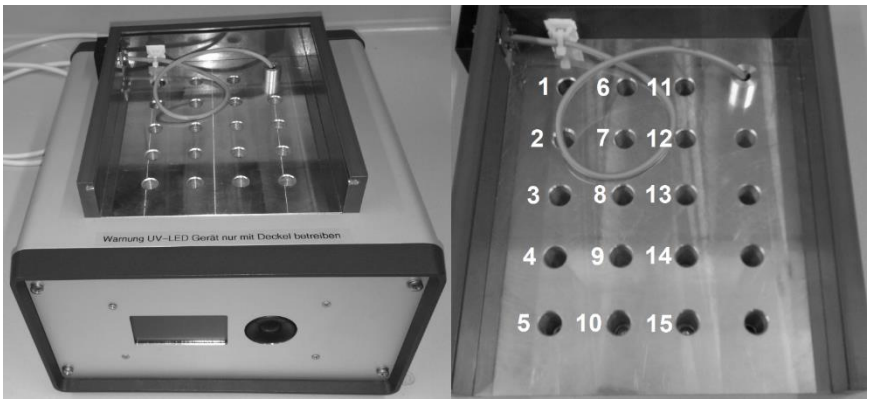

Fig. 95: LED irradiation machine used for all irradiation experiments. Complete closed apparatus (left) and open apparatus showing all slots for irradiation vials (right). Technical details for all irradiation LEDs are given in table 24 below.

Slot	LED	WL	BW	max. I	max. U	Output
1	UVTOP320-TO18-FW	325nm	10nm	20mA	6,2 V	180 mW
2	NICHIA NCSU033B	365nm	10nm	500mA	3,8 V	450 mW
3	NICHIA NCSU034B	385nm	10nm	500mA	3,7 V	540 mW
4	VL400-Emitter	400nm	10nm	500mA	3,6 V	350 mW
5	APG2C1-420	420nm	20nm	350mA	3,5 V	130 mW
6	VL440-Emitter	440nm	10nm	350mA	3,2 V	350 mW
7	Edixeon S Series royal blue	450nm	10nm	700mA	3,5 V	81 mW
8	APG2C3-470	470nm	10nm	700mA	4,0 V	30 lm
9	APG2C1-490	490nm	35nm	350mA	3,3 V	130 mW
10	APG2C1-505	505nm	35nm	350mA	3,5 V	130 mW
11	APG2C3-530	530nm	20nm	700mA	4,0 V	120 lm
12	APG2C3-590	590nm	20nm	700mA	2,8 V	36 lm
13	ELJ-630-628	630nm	20nm	350mA	2,5 V	70 mW
14	2 x UVTOP335-FW-SMD	340nm	10 nm	30mA	6,2 V	400 mW
15	2 x UVTOP345-FW-SMD	350nm	10 nm	30mA	6,2 V	400 mW

Tab. 24: Technical details for all irradiation LEDs built into the irradiation machine. LED type, output wavelengths (WL), bandwidth (BW) and maximum current and voltage are given for each implemented LED. The respective maximum light output is given in lumen (lm).

The LEDs were installed with digital time-, current- and temperature controlling devices. Temperature-control ranges from 20 °C to 100 °C and time-control between 1 millisecond and 9000 seconds. All wavelengths and bandwidths were chosen to cover the whole range of the visible light spectrum without large wavelength-gaps.

7.2 Synthetic procedures for all synthesized small molecules

7.2.1 Synthesis of azobenzene phosphoramidite[192]

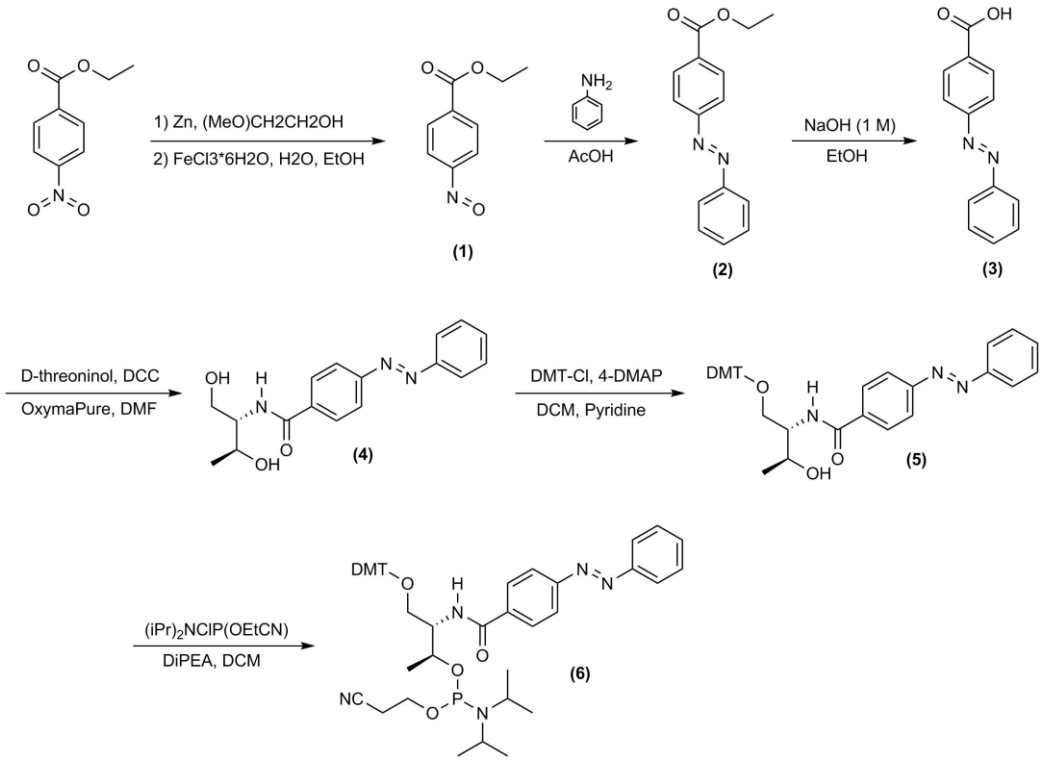

Ethyl-4-nitrosobenzoate (1)[250]

Ethyl-4-nitrobenzoate (100 g, 512 mmol) was dissolved in 1.25 L 2-methoxyethanol and mixed with NH_4Cl (54.6 g, 1.02 mol) dissolved in 250 mL distilled water. The resulting mixture was stirred for 15 minutes at room temperature, then cooled to 0 °C. Zinc-powder (100 g, 1.53 mol) was added slowly over 30 minutes at 0 °C and the reaction mixture was stirred at 0 °C for 1 hour, then warmed up to room temperature and stirring was continued for 24 hours. All solid residues were filtered off and rinsed twice with 50 ml of 2-methoxyethanol. A solution of $FeCl_3 \cdot 6H_2O$ (375 g, 1.37 mol) in 2 L water and 350 mL ethanol was prepared and cooled to 0 °C. The filtrate was added slowly to the prepared solution at 0 °C over 30 minutes and the resulting mixture was stirred for 1 hour at 0 °C. 500 mL ice cold water was added and the yellow precipitate was collected by filtration. The product was isolated by recrystallization from a 2:1 mixture of water and ethanol as a bright yellow solid (yield: 57.0 g, 62 %).

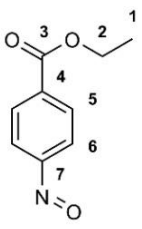

^{1}H-NMR (300 MHz, $CDCl_3$) δ [ppm] = 8.29 (dt, 2 H, $^3J_{6,5}$ = 8.5 Hz, $^4J_{6,6'}$ = 1.8 Hz, H_6), 7.98 (dt, 2 H, $^3J_{5,6}$ = 8.5 Hz, $^4J_{5,5'}$ = 1.8 Hz, H_5), 4.36 (q, 2 H, $^3J_{2,1}$ = 7.1 Hz, H_2), 1.36 (t, 3 H, $^3J_{1,2}$ = 7.1 Hz, H_1).

^{13}C-NMR (75 MHz, $CDCl_3$) δ [ppm] = 164.9 (C_3), 164.1 (C_7), 135.2 (C_5), 130.6 (C_6), 120.0 (C_4), 61.5 (C_2), 13.9 (C_1).

MS (ESI, positive) *m/z* (%) 179.1 (100) $[M]^+$, 149.0 (14) $[M\text{-}NO]^+$, 124.1 (54) $[C_7H_8O_2]^+$.

HRMS (ESI, positive) *m/z* calculated for $C_9H_9NO_3$: 179.0582, found: 179.0577.

Ethyl-4-carboxyazobenzene (2)[192]

Ethyl-4-nitrosobenzoate **(1)** (5.50 g, 30.7 mmol) and aniline (3.43 g, 3.4 mL, 36.8 mmol) were dissolved in 250 mL glacial acetic acid and the reaction mixture was stirred for 48 hours at room temperature. 150 mL water were added and the resulting mixture was neutralized with sodium bicarbonate. The resulting mixture was extracted twice with 250 mL ethyl acetate, the organic layer was washed subsequently with 300 mL water, 500 mL saturated sodium bicarbonate solution and 300 mL brine. The organic layer was dried over $MgSO_4$ and all solvents were removed *in vacuo*. The product was isolated by column chromatography (silica, eluent: cyclohexane) as a red solid (yield: 5.46 g, 70 %).

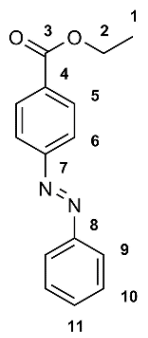

^{1}H-NMR (300 MHz, DMSO-d_6) δ [ppm] = 8.20 (dd, 2 H, $^3J_{5,6}$ = 8.7 Hz, $^4J_{5,5'}$ = 2.1 Hz, H_5), 7.95 (m, 4 H, H_6+H_9), 7.53 (m, 3 H, H_{10}+H_{11}), 4.44 (q, 2 H, $^3J_{2,1}$ = 7.1 Hz, H_2), 1.44 (t, 3 H, , $^3J_{1,2}$ = 7.1 Hz, H_1).

^{13}C-NMR (75 MHz, DMSO-d_6) δ [ppm] = 166.0 (C_3), 155.0 (C_4), 152.5 (C_7), 131.6 (C_8), 130.5 (C_{11}), 129.2 (C_5), 123.4 (C_9), 123.1 (C_{10}), 122.6 (C_6), 61.2 (C_2), 14.3 (C_1).

MS (ESI, negative) *m/z* (%) 255.1 (100) $[M+H]^+$.

HRMS (EI, 70 eV) *m/z* calculated for $C_{15}H_{15}N_2O_2$: 255.1128, found: 255.1133.

4-Carboxyazobenzene (3)[192]

Ethyl-4-carboxyazobenzene **(2)** (5.0 g, 19.7 mmol) was dissolved in 200 mL ethanol and 60 mL 2 M aqueous NaOH was added. The reaction mixture was stirred for 6 hours at room temperature, then 150 mL hydrochloric acid (1 M) was added. The reaction mixture was extracted two times with 250 mL ethyl acetate each, the combined organic layers were washed twice with 250 mL water and 250 mL brine and the organic layer was dried over $MgSO_4$. All solvents were removed *in vacuo* to yield a red solid (yield: 4.42 g, quant.).

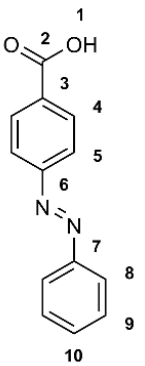

^{1}H-NMR (300 MHz, DMSO-d_6) δ [ppm] = 13.31 (s, 1 H, H_1), 8.18 (m, 2 H, H_4), 7.97 (m, 4 H, H_5+H_8), 7.63 (m, 3 H, H_9+H_{10}).

^{13}C-NMR (75 MHz, DMSO-d_6) δ [ppm] = 166.7 (C_2), 154.3 (C_3), 151.9 (C_6), 132.9 (C_7), 130.6 (C_{10}), 129.6 (C_4), 123.7 (C_8), 122.8 (C_9), 122.5 (C_5).

MS (ESI, negative) *m/z* (%) 225.0 (100) $[M\text{-}H]^-$.

HRMS (EI, 70 eV) *m/z* calculated for $C_{13}H_9N_2O_2$: 225.0659, found: 225.0652.

4-Carboxyazobenzene-D-threoninol ("AB") (4)[192]

4-Carboxyazobenzene **(3)** (10.0 g, 44.2 mmol), DCC (10.9 g, 53.0 mmol), OxymaPure (6.91 g, 48.6 mmol) and D-threoninol (5.11 g, 48.6 mmol) were mixed in 400 mL dry DMF under argon atmosphere. The reaction mixture was stirred for 24 hours under argon atmosphere at room temperature. All solids were filtered off and DMF was removed *in vacuo*. The product was isolated by column chromatography (silica, eluent: chloroform/methanol = 95/5) as a red solid (yield: 11.8 g, 85 %).

TLC (SiO_2, eluent: chloroform/methanol = 10:1) R_f = 0.32.

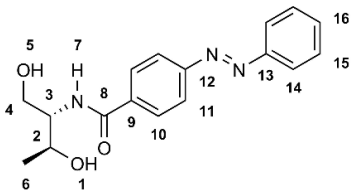

^{1}H-NMR (500 MHz, DMSO-d_6) δ [ppm] = 8.09-8.06 (m, 2 H, H_{10}), 7.95-7.91 (m, 5 H, H_{11}+H_{14}+H_{16}),7.63-7.58 (m, 3 H, H_{15}+H_7), 4.63-4.59 (m, 2 H, H_1+H_3), 3.96-3.91 (m, 2 H, H_4), 3.63-3.61 (m, 1 H, H_2), 3.53-3.51 (m, 1 H, H_5), 1.09 (d, 3 H, $^3J_{6,2}$ = 6.2 Hz, H_6).

^{13}C-NMR (125 MHz, DMSO-d_6) δ [ppm] = 166.0 (C_8), 153.4 (C_{12}), 152.1 (C_{13}), 137.2 (C_{16}), 132.1 (C_{15}), 129.7 (C_{10}), 128.8 (C_{14}), 122.9 (C_{11}), 122.4 (C_9), 65.1 (C_2), 60.7 (C_3), 57.1 (C_4), 20.4 (C_6).

MS (ESI, positive) *m/z* (%) 649.3 (14) $[2M+Na]^+$, 336.1 (100%) $[M+Na]^+$, 247.2 (18 %) $[M-C_4H_9O_2+Na]^{+\cdot}$.

HRMS (ESI, positive) *m/z* calculated for $C_{17}H_{19}N_3O_3Na$: 336.1319 $[M+Na]^+$, found: 336.1316 $[M+Na]^+$.

DMT-protected 4-carboxyazobenzene-D-threoninol (5)[192]

4-Carboxyazobenzene-D-threoninol **(4)** (1.0 g, 3.19 mmol) and 4-DMAP (19.6 mg, 0.16 mmol) were mixed in 20 mL dry pyridine under argon atmosphere and cooled to 0 °C. 4,4'-dimethoxytritylchloride (1.19 g, 3.51 mmol) was dissolved in 15 mL dry dichloromethane and added dropwise to the reaction mixture at 0 °C under argon atmosphere. The reaction mixture was warmed up to room temperature and stirred under argon atmosphere for 24 hours. All solvents were removed *in vacuo* and the product was isolated column chromatography (silica, eluent: cyclohexane/ethyl acetate = 1/1 with 3 % triethylamine) as a red foamy solid (yield: 0.84 g, 43%).

^{1}H-NMR (400 MHz, $CDCl_3$) δ [ppm] = 8.50-8.47 (m, 2 H, H_9), 7.91-7.85 (m, 2 H, H_{18}), 7.60-7.55 (m, 1 H, H_{15}), 7.60-7.41 (m, 2 H, H_{10}), 7.34-7.08 (m, 11 H, H_{13}+H_{14}+H_{19}+H_{20}+H_{22}), 6.86-6.68 (m, 4 H, H_{23}), 4.19-4.06 (m, 1 H, H_6), 3.70-3.65 (m, 6 H, H_{25}), 3.51-3.30 (m, 2 H, H_1+H_3), 1.85-1.81 (m, 2 H, H_4), 1.62-1.48 (m, 1 H, H_2), 1.28-0.96 (m, 3 H, H_5).

^{13}C-NMR (100 MHz, $CDCl_3$) δ [ppm] = 167.0 (C_7), 158.5 (C_{24}), 154.3 (C_{11}), 152.5 (C_{12}), 149.7 (C_{17}), 147.5 (C_{21}), 144.3 (C_{14}), 139.6 (C_{19}), 136.0 (C_9), 131.6 (C_{22}), 129.9 (C_{20}), 129.1 (C_{18}),

127.8 (C_{15}), 127.0 (C_{10}), 123.7 (C_8), 123.1 (C_{13}), 113.1 (C_{23}), 86.9 (C_{16}), 68.6 (C_4), 65.3 (C_2), 55.2 (C_{25}), 54.1 (C_3), 20.1 (C_5).

MS (ESI, positive) *m/z* (%) 638.3 (73) $[M+Na]^+$, 303.1 (100) $[DMT]^+$.

HRMS (ESI, positive) *m/z* calculated for $C_{38}H_{37}N_3O_5Na$: 638.2625, found: 638.2622.

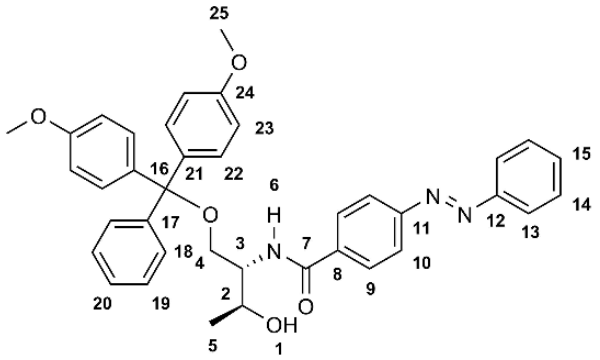

DMT-protected 4-carboxyazobenzene-D-threoninol phosphoramidite (6)[192]

DMT-protected 4-carboxyazobenzene-D-threoninol **(5)** (0.50 g, 0.81 mmol) was dissolved in 10 mL extra dry dichloromethane under argon atmosphere and the solution was cooled to 0 °C. DiPEA (0.15 mL, 0.89 mmol) was added dropwise to the solution and the reaction mixture was stirred for 10 minutes at 0 °C. 2-Cyanoethyl-*N*,*N*-diisopropylchlorophosophoramidite (0.20 mL, 0.89 mmol) was added dropwise to the reaction mixture at 0 °C under argon atmosphere and the reaction mixture was stirred for 10 minutes at 0 °C, then warmed up to room temperature and stirred for 2.5 hours. All solvents were removed *in vacuo*. The product was isolated *via* column chromatography (silica, eluent: cyclohexane/ethyl acetate = 1/1 with 3 % triethylamine) as a red foamy solid (yield: 0.41 g, 62 %).

^{1}H-NMR (300 MHz, DMSO-d_6) δ [ppm] = 7.96-7.88 (m, 3 H, H_8+H_{14}), 7.52-7.40 (m, 3 H, H_{17}+H_{19}), 7.33-7.13 (m, 10 H, H_9+H_{12}+H_{13}+H_{21}), 6.81-6.76 (m, 6 H, H_{18}+H_{22}), 4.48-4.36 (m, 1 H, H_5), 3.75-3.74 (m, 9 H, H_{24}+H_{28}+H_3), 3.57-3.48 (m, 2 H, H_4), 3.34-3.32 (m, 1 H, H_6), 3.04-2.98 (m, 1 H, H_6'), 2.86 (s, br, 1 H, H_2), 2.62-2.31 (m, 2 H, H_{29}), 1.34-0.96 (m, 15 H, H_1+H_{27}).

^{13}C-NMR (75 MHz, DMSO-d_6) δ [ppm] = 166.4 (C_6), 158.6 (C_{23}), 154.2 (C_{10}), 152.5 (C_{11}), 147.4 (C_{20}), 144.8 (C_{16}), 139.5 (C_{13}), 135.9 (C_{19}), 131.5 (C_8) 130.1 (C_{21}), 129.1 (C_{18}), 128.2 (C_{17}), 128.0 (C_{14}), 127.8 (C_9), 127.0 (C_{10}), 123.1 (C_{12}), 117.7 (C_{30}), 113.1 (C_{22}), 86.1 (C_{15}), 81.4 (C_2), 69.2 (C_4), 62.7 (C_{28}), 55.2 (C_3), 51.8 (C_{24}), 43.1 (C_{26}), 39.1 (C_{29}), 24.6 (C_{27}), 20.6 (C_1).

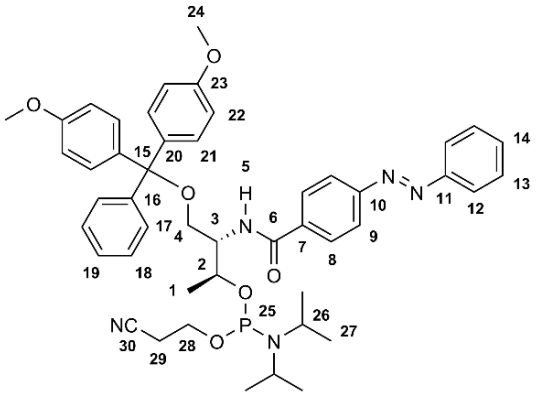

^{31}P-NMR: (162 MHz, $CDCl_3$) δ [ppm] = 148.7.

MS (ESI, positive) *m/z* (%) 838.4 (10) $[M+Na]^+$, 130.2 (100) $[C_6H_7N_2+Na]^+$.

HRMS (ESI, positive) *m/z* calculated for $C_{47}H_{54}N_5O_6PNa$: 838.3704, found: 838.3698.

7.2.2 Synthesis of 2',6'-dimethylazobenzene phosphoramidite[192]

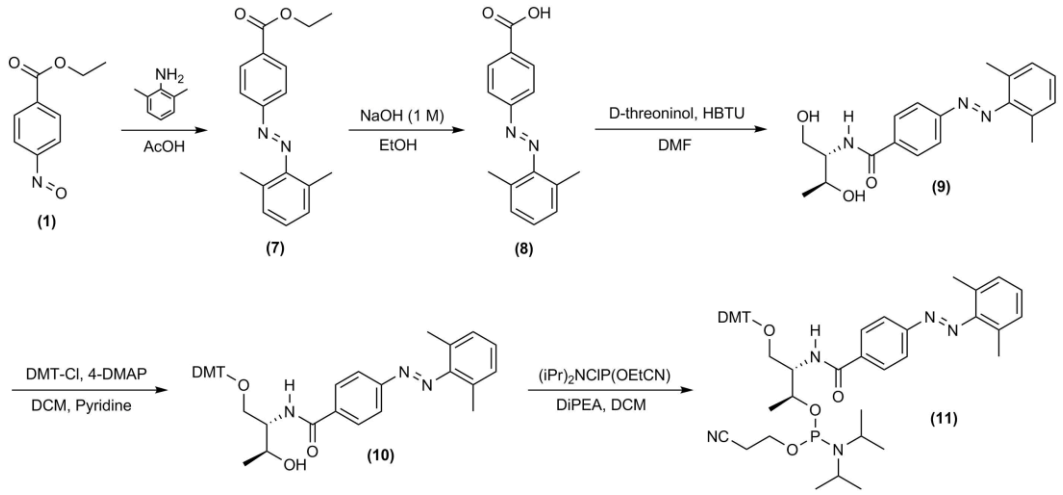

Ethyl-4-carboxy-2',6'-dimethylazobenzene (7)[192]

Ethyl-4-nitrosobenzoate **(1)** (40.41 g, 226 mmol) and 2,6-dimethylaniline (35.20 g, 36.0 mL, 290 mmol) were dissolved in 2 L glacial acetic acid. The reaction mixture was stirred for 48 hours at room temperature, then 500 mL water were added and the resulting mixture was neutralized with sodium carbonate. The mixture was extracted twice with 2 L ethyl acetate and the organic layer was washed subsequently with 2 L water, 2 L saturated sodium bicarbonate solution and 1 L brine. The organic layer was dried over $MgSO_4$ and all solvents were removed *in vacuo*. The product was isolated by column chromatography (silica, eluent: cyclohexane) as a red solid (yield: 46.0 g, 72 %).

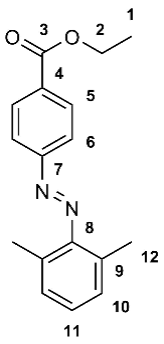

^{1}H-NMR (400 MHz, $CDCl_3$) δ [ppm] = 8.23 (m, 2 H, H_5), 7.93 (m, 2 H, H_6), 7.21 (m, 3 H, H_{10}+H_{11}), 4.46 (q, 2 H, $^3J_{2,1}$ = 7.1 Hz, H_2), 2.41 (s, 6 H, H_{12}), 1.46 (t, 3 H, $^3J_{1,2}$ = 7.1 Hz, H_1).

^{13}C-NMR (100 MHz, $CDCl_3$) δ [ppm] = 166.0 (C_3), 155.2 (C_7), 150.9 (C_8), 132.2 (C_4), 131.4 (C_5), 130.6 (C_{10}), 129.3 (C_9), 128.9 (C_{11}), 122.2 (C_6), 61.2 (C_2), 19.1 (C_{12}), 14.3 (C_1).

MS (ESI, positive) *m/z* (%) 283.1 $[M+H]^+$, 194.1 $[C_{11}H_{11}N_2+Na]^+$.

HRMS (ESI, positive) *m/z* calculated for $C_{17}H_{19}N_2O_2$: 283.1441, found: 283.1449.

4-Carboxy-2',6'-dimethylazobenzene (8)[192]

Ethyl-4-carboxy-2',6'-dimethylazobenzene **(7)** (3.69 g, 13.1 mmol) was dissolved in 130 mL ethanol. 40 mL 2 M aqueous NaOH solution was added and the reaction mixture was stirred for 6 hours at room temperature, then 90 mL 1 M hydrochloric acid was added. The reaction mixture was extracted two times with 150 mL ethyl acetate each, the combined organic layers were washed twice with 150 mL water and 150 mL brine and dried over $MgSO_4$. All solvents were removed *in vacuo* to yield the product as a red solid (yield: 3.28 g, 98 %).

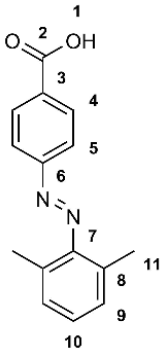

^{1}H-NMR (400 MHz, DMSO-d_6) δ [ppm] = 13.07 (s, br, 1 H, H_1), 8.15-8.12 (m, 2 H, H_4), 7.91-7.88 (m, 2 H, H_5), 7.24-7.15 (m, 3 H, H_9+H_{10}), 2.31 (s, 6 H, H_{11}).

^{13}C-NMR (100 MHz, DMSO-d_6) δ [ppm] = 165.9 (C_2), 153.8 (C_6), 149.5 (C_7), 132.0 (C_3), 130.0 (C_4), 129.8 (C_9), 128.5 (C_8), 128.3 (C_{10}), 121.3 (C_5), 17.9 (C_{11}).

MS (ESI, negative) *m/z* (%) 253.1 (100) $[M-H]^-$.

HRMS (ESI, negative) *m/z* calculated for $C_{15}H_{13}N_2O_2$: 253.0972, found: 253.0974.

4-Carboxy-2',6'-dimethylazobenzene-D-threoninol ("DMAB") (9)[192]

4-Carboxy-2',6'-dimethylazobenzene **(8)** (10.0 g, 39.3 mmol) and D-threoninol (4.96 g, 47.2 mmol) were dissolved in 250 mL extra dry DMF under argon atmosphere. HBTU (17.9 g, 47.2 mmol) was dissolved in 150 mL extra dry DMF and added dropwise to the reaction mixture. The resulting solution was stirred for 24 hours at room temperature under argon atmosphere, followed by filtering off all solids and removal of DMF *in vacuo*. The product was isolated by column chromatography (silica, eluent: $CHCl_3$/MeOH = 95/5) as a red solid (yield: 12.5 g, 93 %).

TLC (SiO_2, eluent: chloroform/methanol = 10/1) R_f = 0.30.

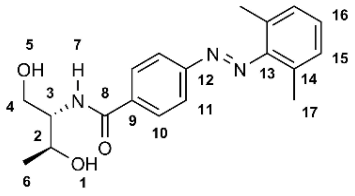

^{1}H-NMR (300 MHz, DMSO-d_6) δ [ppm] = 8.10-8.08 (m, 2 H, H_{10}), 7.94-7.89 (m, 3 H, H_7+H_{11}), 7.21-7.16 (m, 3 H, H_{15}+H_{16}), 4.66 (s, br, 2 H, H_1+H_3), 3.96 (m, 2 H, H_4), 3.63-3.61 (m, 1 H, H_2), 3.55-3.52 (m, 1 H, H_5) 2.34 (s, 6 H, H_{17}), 1.10 (s, 3 H, H_6).

^{13}C-NMR (75 MHz, DMSO-d_6) δ [ppm] = 165.9 (C_8), 153.6 (C_{12}), 150.4 (C_{13}), 137.0 (C_{16}), 130.6 (C_{15}), 129.2 (C_{10}), 128.9 (C_{14}), 128.7 (C_9), 121.9 (C_{11}), 64.9 (C_2), 60.5 (C_3), 56.9 (C_4), 20.3 (C_6), 18.6 (C_{17}).

MS (ESI, positive) *m/z* (%) 364.2 (100%) $[M+Na]^+$.

HRMS (ESI, positive) *m/z* calculated for $C_{19}H_{23}N_3O_3Na$: 364.1632 $[M+Na]^+$, found: 364.1635 $[M+Na]^+$.

DMT-protected 4-carboxy-2',6'-dimethylazobenzene-D-threoninol (10)[192]

4-Carboxy-2',6'-dimethylazobenzene-D-threoninol **(9)** (3.60 g, 10.54 mmol) and 4-DMAP (65 mg, 0.53 mmol) were mixed in 80 mL dry pyridine under argon atmosphere and cooled to 0 °C. 4,4'-dimethoxytritylchloride (3.93 g, 11.6 mmol) was dissolved in 60 mL dry dichloromethane and added dropwise to the reaction mixture at 0 °C under argon atmosphere. The mixture was warmed up to room temperature and stirred under argon atmosphere for 24 hours. All solvents were removed *in vacuo* and the product was isolated by column chromatography (silica, eluent: cyclohexane/ethyl acetate = 1/1 with 3 % triethylamine) as a red foamy solid (yield: 5.37 g, 79 %).

^{1}H-NMR (400 MHz, $CDCl_3$) δ [ppm] = 7.91-7.96 (m, 4 H, H_9+H_{19}), 7.11-7.40 (m, 9 H, H_9+H_{10}+H_{21}+H_{23}), 6.91-6.89 (m, 1 H, H_{15}), 6.77-6.81 (m, 6 H, H_{14}+H_{24}), 4.19-4.25 (m, 1 H, H_4), 4.12-4.15 (m, 1 H, H_4'), 3.74 (s, 6 H, H_{26}), 3.57-3.61 (m, 1 H, H_6), 3.46-3.16 (m, 3 H, H_1+H_2+H_3), 2.39 (s, 6 H, H_{16}), 1.17-1.22 (m, 3 H, H_5).

^{13}C-NMR (100 MHz, $CDCl_3$) δ [ppm] = 166.8 (C_7), 158.4 (C_{25}), 154.3 (C_{11}), 150.8 (C_{12}), 144.1 (C_{18}), 135.9 (C_{14}), 135.2 (C_{20}), 131.1 (C_9), 129.7 (C_{23}), 129.1 (C_{21}), 128.9 (C_{19}), 128.7 (C_{15}), 127.8 (C_{10}), 127.6 (C_8), 126.8 (C_{22}), 122.4 (C_{13}), 113.1 (C_{24}), 86.7 (C_{17}), 68.6 (C_4), 65.2 (C_2), 55.0 (C_{26}), 53.9 (C_3), 19.9 (C_5), 18.9 (C_{16}).

MS (ESI, positive) *m/z* (%) 666.3 (5) $[M+Na]^+$, 512.4 (14) $[C_{32}H_{34}NO_5]^+$, 449.4 (50) $[C_{26}H_{24}N_3O_3Na]^+$, 328.3 (100) $[C_{23}H_{20}O_2]^+$, 303.1 (52) $[DMT]^+$,

HRMS (ESI, positive) *m/z* calculated for $C_{40}H_{41}N_3O_5Na$: 666.2938, found: 666.2971.

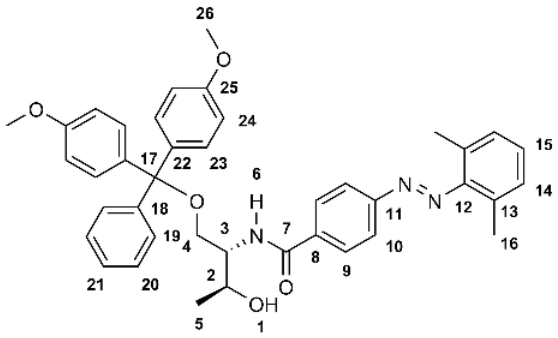

DMT-protected 4-carboxy-2',6'-dimethylazobenzene-D-threoninol phosphoramidite (11)[192]

DMT-protected 4-carboxy-2',6'-dimethylazobenzene-D-threoninol **(10)** (1.00 g, 1.55 mmol) was dissolved in 15 mL dry dichloromethane under argon atmosphere and the solution was cooled to 0 °C. DiPEA (0.29 mL, 1.70 mmol) was added dropwise to the solution and the reaction mixture was stirred for 10 minutes at 0 °C under argon atmosphere. 2-Cyanoethyl-*N*,*N*-diisopropylchloro-phosophoramidite (0.38 mL, 0.17 mmol) was added dropwise to the

reaction mixture at 0 °C and the reaction mixture was stirred for 10 minutes at 0 °C, then warmed up to room temperature and stirred for 2.5 hours under argon atmosphere. All solvents were removed *in vacuo* and the product was isolated *via* column chromatography (silica, eluent: cyclohexane/ethyl acetate = 1/1 with 3 % triethylamine) as a red foamy solid (yield: 1.06 g, 81 %).

^{1}H-NMR (400 MHz, CD_2Cl_2) δ [ppm] = 7.94-7.89 (m, 2 H, H_8), 7.65-7.39 (m, 2 H, H_{18}), 7.35-7.14 (m, 10 H, H_9+H_{13}+H_{19}+H_{22}), 7.03-6.91 (m, 1 H, H_{20}), 6.85-6.78 (m, 4 H, H_{23}), 6.60-6.41 (m, 1 H, H_{14}), 4.48-4.34 (m, 1 H, H_5), 3.87-3.67 (m, 7 H, H_{25}+H_2), 3.59-3.54 (m, 3 H, H_4), 3.38-3.20 (m, 2 H, H_{27}), 3.02-2.99 (m, 1 H, H_3), 2.62-2.38 (m, 6 H, H_{15}), 1.95-.1.93 (m, 1 H, H_{29}), 1.58 (s, 1 H, H_{29}'), 1.34-1.26 (m, 2 H, H_{30}), 1.24-0.94 (m, 15 H, H_1+H_{28}).

^{31}P-NMR: (100 MHz, CD_2Cl_2) δ [ppm] = 148.5.

MS (ESI, positive) *m/z* (%) 866.4 (100) $[M+Na]^+$, 303.1 (92) $[DMT]^+$.

HRMS (ESI, positive) *m/z* calculated for $C_{49}H_{58}N_5O_6PNa$: 866.4017 $[M+Na]^+$, found: 866.4011 $[M+Na]^+$.

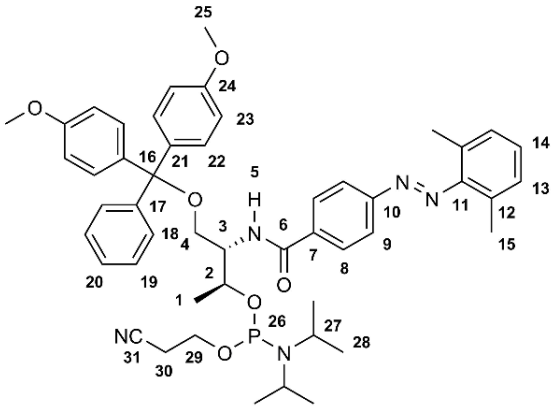

7.2.3 Synthesis of 2',6'-dimethyl-4'-methylthioazobenzene phosphoramidite[198]

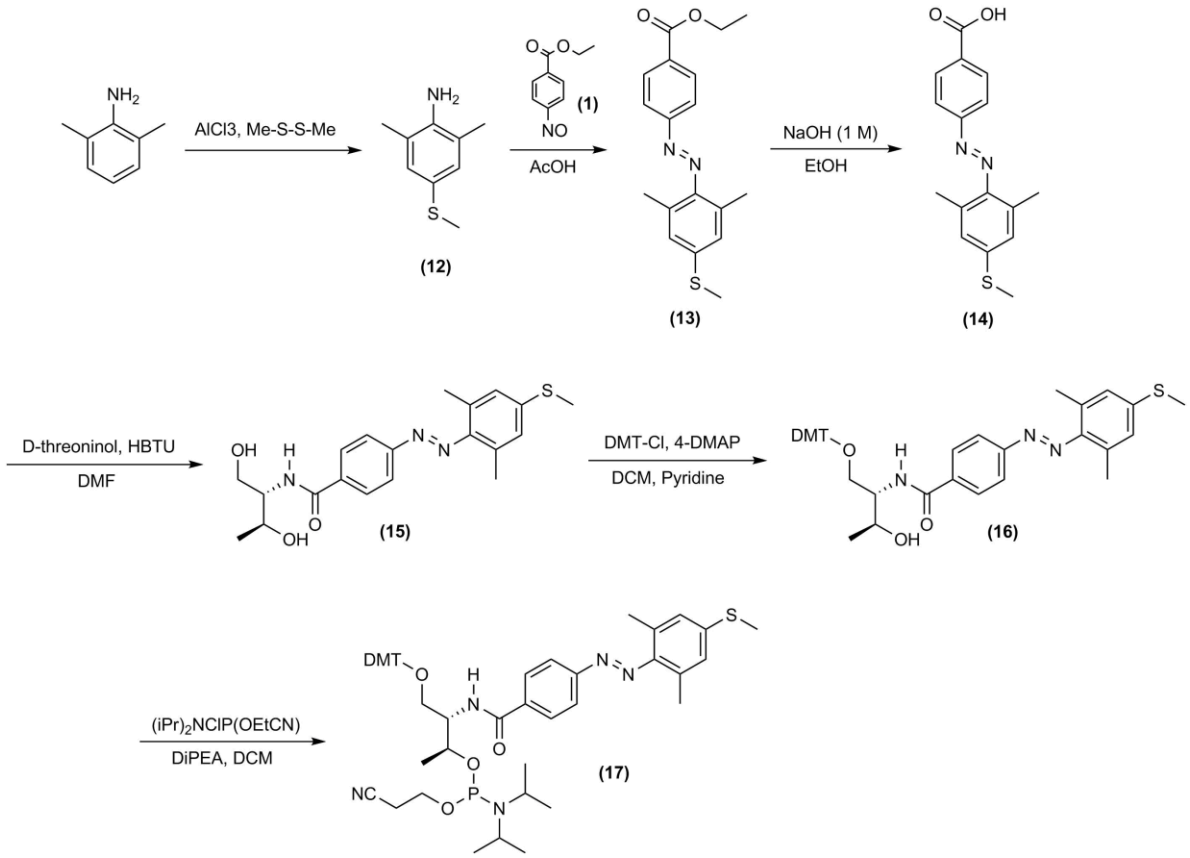

2,6-Dimethyl-4-methylthioaniline (12)[198]

2,6-Dimethylaniline (20.0 g, 165 mmol) and dry aluminium chloride (1.46 g, 10.9 mmol) were mixed and heated to 150 °C for 30 minutes. The reaction mixture was cooled to 100 °C and dimethyl-disulfide (15.5 g, 165 mmol) was added dropwise to the solution. The reaction mixture was refluxed for 16 hours, then cooled down to room temperature. The reaction mixture was quenched with 200 mL 1 M aqueous NaOH solution and extracted twice with 500 mL ethyl acetate. The combined organic layers were washed with 1 L brine and dried over $MgSO_4$. The product was isolated by column chromatography (silica, eluent: cyclohexane/ethyl acetate = 19/1) as a yellowish oil (yield: 12.85 g, 47 %).

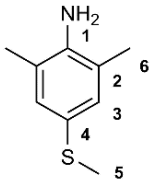

^{1}H-NMR (400 MHz, $CDCl_3$) δ [ppm] = 7.00 (s, 2H, H_3), 3.66 (s, br, 2 H, H_1), 2.42 (s, 3 H, H_5), 2,17 (s, 6 H, H_6).

^{13}C-NMR (100 MHz, $CDCl_3$) δ [ppm] = 141.3 (C_1), 129.8 (C_4), 124.7 (C_3), 122.3 (C_2), 18.8 (C_6), 17.4 (C_5).

MS (ESI, positive) *m/z* (%) 168.1 (100) $[M+H]^+$.

HRMS (ESI, positive) *m/z* calculated for $C_9H_{14}NS$: 168.0841, found: 168.0841.

Ethyl-4-carboy-2',6'-dimethyl-4'-methylthioazobenzene (13)[198]

Ethyl-4-nitrosobenzoate **(1)** (12.9 g, 71.7 mmol) and 2,6-dimethyl-4-methylthioaniline **(12)** (10.0 g, 59.8 mmol) were mixed in 350 mL glacial acetic acid and the reaction mixture was stirred for 24 hours at room temperature. 200 mL water was added and the resulting mixture was neutralized with sodium carbonate. The resulting crude mixture was extracted twice with 500 mL ethyl acetate, the combined organic layers were washed subsequently with 500 mL water, 500 mL saturated sodium bicarbonate solution and 500 mL brine. The organic layer was dried over $MgSO_4$ and all solvents were removed *in vacuo*. The product was isolated by column chromatography (silica, eluent: cyclohexane) as a red solid (yield: 10.0 g, 42 %).

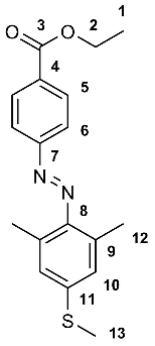

^{1}H-NMR (400 MHz, $CDCl_3$) δ [ppm] = 8.20 (m, 2 H, H_5), 7.87 (m, 2 H, H_6), 6.98 (s, 2 H, H_{10}), 4.43 (q, 2 H, $^3J_{2,1}$ = 7.1 Hz, H_2), 2.51 (s, 3 H, H_{13}), 2.46 (s, 6 H, H_{12}), 1.44 (t, 3 H, $^3J_{1,2}$ = 7.1 Hz, H_1).

^{13}C-NMR (100 MHz, $CDCl_3$) δ [ppm] = 165.8 (C_3), 155.3 (C_7), 147.2 (C_8), 140.5 (C_4), 133.3 (C_5), 130.3 (C_{10}), 126.1 (C_9), 123.2 (C_{11}), 121.9 (C_6), 61.0 (C_2), 19.8 (C_{12}), 15.0 (C_1), 14.1 (C_{13}).

MS (ESI, positive) *m/z* (%) 329.1 (100) $[M+H]^+$.

HRMS (ESI, positive) *m/z* calculated for $C_{18}H_{21}N_2O_2S$: 329.1318, found: 329.1310.

4-Carboxy-2',6'-dimethyl-4'-methylthioazobenzene (14)[198]

Ethyl-4-carboxy-2',6'-dimethyl-4'-methylthioazobenzene **(13)** (9.90 g, 30.1 mmol) was dissolved in 750 mL ethanol and 100 mL 2 M aqueous NaOH solution was added. The reaction mixture was stirred for 6 hours at room temperature, then 220 mL hydrochloric acid (1 M) was added. The reaction mixture was extracted twice with 300 mL ethyl acetate, the combined organic layers were washed twice with 100 mL water and 100 mL brine. The organic layer was dried over $MgSO_4$ and all solvents were

removed *in vacuo* to yield the product as a red solid (yield: 8.54 g, 94 %).

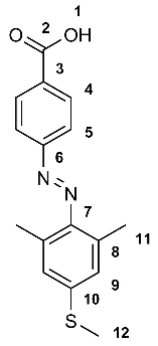

^{1}H-NMR (400 MHz, DMSO-d_6) δ [ppm] = 13.29 (s, br, 1 H, H_1), 8.16 (m, 2 H, H_4), 7.88 (m, 2 H, H_5), 7.06 (s, 2 H, H_9), 2.51 (s, 3 H, H_{12}), 2.40 (s, 6 H, H_{11}).

^{13}C-NMR (100 MHz, DMSO-d_6) δ [ppm] = 166.1 (C_2), 154.2 (C_6), 146.0 (C_7), 140.3 (C_3), 132.5 (C_4), 130.0 (C_9), 125.2 (C_8), 123.1 (C_{10}), 121.4 (C_5), 18.9 (C_{11}), 13.5 (C_{12}).

MS (ESI, negative) *m/z* (%) 299.1 (38) $[M-H]^-$, 166.0 (100) $[C_9H_{12}NS]^-$.

HRMS (ESI, negative) *m/z* calculated for $C_{16}H_{15}N_2O_2S$: 299.0849, found: 299.0855.

4-Carboxy-2',6'-dimethyl-4'-methylthioazobenzene-D-threoninol ("S-DMAB") (15)[198]

4-Carboxy-2',6'-dimethyl-4'-methylthioazobenzene **(14)** (1.74 g, 5.78 mmol), D-threoninol·HCl (0.90 g, 6.36 mmol) and NEt_3 (0.96 mL, 6.93 mmol) were dissolved in 35 mL dry DMF under argon atmosphere. HBTU (2.63 g, 6.93 mmol) was dissolved in 25 mL dry DMF and added dropwise to the reaction mixture. The resulting solution was stirred for 24 hours under argon atmosphere at room temperature, all solids were filtered off followed by removal of DMF *in vacuo*. The product was isolated by column chromatography (silica, eluent: $CHCl_3$/MeOH = 95/5) as a red solid (yield: 2.21 g, 99 %).

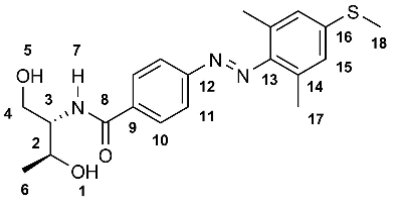

TLC (SiO_2, eluent: chloroform/methanol = 10/1) R_f = 0.28.

^{1}H-NMR (300 MHz, DMSO-d_6) δ [ppm] = 8.30-8.28 (m, 1 H, H_{10}), 8.15-8.05 (m, 3 H, H_{10}+H_{11}), 7.94-7.86 (m, 2 H, H_{15}), 4.67 (s, br, 2 H, H_3+H_7), 3.96-3.91 (m, 2 H, H_4), 3.50-3.65 (m, 2 H, H_5), 3.34 (s, br, 1 H, H_1), 2.52 (s, 3 H, H_{18}), 2.40 (s, 6 H, H_{17}), 1.09 (t, 3 H, $^3J_{6,2}$ = 6.4 Hz, H_6).

^{13}C-NMR (75 MHz, DMSO-d_6) δ [ppm] = 165.9 (C_8), 153.9 (C_{12}), 146.7 (C_{13}), 140.5 (C_{16}), 136.6 (C_{14}), 132.9 (C_{10}), 128.6 (C_{15}), 125.8 (C_{11}), 121.7 (C_9), 64.9 (C_4), 60.5 (C_2), 56.9 (C_3), 20.3 (C_{17}), 19.5 (C_6), 14.2 (C_{18}).

MS (ESI, positive) *m/z* (%) 388.2 (15) $[M+Na]^+$.

HRMS (ESI, positive) *m/z* calculated for $C_{20}H_{25}N_3O_3SH$: 388.1689 $[M+H]^+$, found: 388.1681 $[M+H]^+$.

DMT-protected 4-carboxy-2',6'-dimethyl-4'-methylthioazobenzene-D-threoninol (16)[198]

4-Carboxy-2',6'-dimethyl-4'-methylthioazobenzene-D-threoninol **(15)** (1.97 g, 5.08 mmol) and 4-DMAP (30 mg, 0.26 mmol) were dissolved in 30 mL dry pyridine under argon atmosphere and cooled to 0 °C. 4,4'-dimethoxytritylchloride (1.89 g, 5.59 mmol) was dissolved in 15 mL dry dichloromethane and the resulting solution was added dropwise to the reaction mixture at 0 °C under argon atmosphere. The reaction mixture was warmed up to room temperature and stirred under argon atmosphere for 24 hours. All solvents were removed *in vacuo* and the product was isolated by silica gel chromatography (eluent: cyclohexane/ethyl acetate = 1/1 with 3 % triethylamine) as a red foamy solid (yield: 2.23 g, 64 %).

^{1}H-NMR (500 MHz, $CDCl_3$) δ [ppm] = 8.57-7.62 (m, 4 H, H_9+H_{20}), 7.38-7.34 (m, 2 H, H_{21}), 7.28-7.13 (m, 6 H, H_{10}+H_{24}), 6.97 (s, 1 H, H_{22}), 6.89-6.74 (m, 6 H, H_{14}+H_{25}), 4.23-4.11 (m, 2 H, H_4), 3.75-3.72 (m, 9 H, H_{17}+H_{27}), 3.59-3.51 (m, 1 H, H_6), 3.42-3.36 (m, 1 H, H_3), 3.25-3.11 (m, 1 H, H_1), 2.49-2.37 (m, 6 H, H_{16}), 2.01-1.77 (m, 1 H, H_2), 1.21-1.18 (m, 3 H, H_5).

^{13}C-NMR (125 MHz, $CDCl_3$) δ [ppm] = 167.0 (C_7), 165.6 (C_{26}), 158.7 (C_{23}), 154.8 (C_{19}), 149.7 (C_{11}), 147.5 (C_{12}), 144.3 (C_{15}), 140.5 (C_{22}), 135.3 (C_9), 133.4 (C_{24}), 129.9 (C_{21}), 129.1 (C_{20}), 128.0 (C_{13}), 126.4 (C_{14}), 123.8 (C_{10}), 122.5 (C_8), 113.3 (C_{25}), 86.9 (C_{18}), 68.7 (C_4), 65.4 (C_{27}), 56.2 (C_2), 54.0 (C_3), 20.1 (C_{16}), 19.9 (C_5), 15.2 (C_{17}).

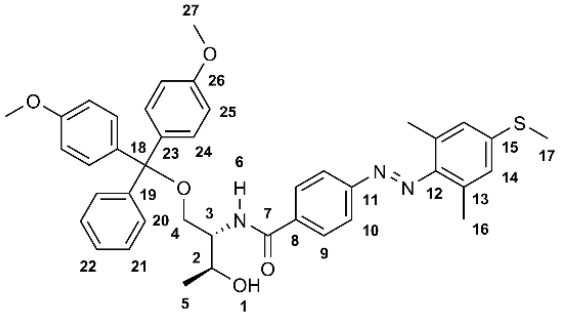

DMT-protected 4-carboxy-2',6'-dimethyl-4'-methylthioazobenzene-D-threoninol phosphoramidite (17)[198]

DMT-protected 4-carboxy-2',6'-dimethyl-4'-methylthioazobenzene-D-threoninol **(16)** (1.00 g, 1.45 mmol) was dissolved in 15 mL dry dichloromethane under argon atmosphere and the solution was cooled to 0 °C. DiPEA (0.28 mL, 1.60 mmol) was added dropwise to the solution and the reaction mixture was stirred for 10 minutes at 0 °C. 2-Cyanoethyl-*N*,*N*-diisopropylchlorophosophoramidite (0.36 mL, 1.60 mmol) was added dropwise to the reaction mixture at 0 °C and stirring was continued for 10 minutes at 0 °C, then warmed up to room temperature and stirred for 2.5 hours under argon atmosphere. All volatiles were removed *in vacuo* and the product was isolated *via* column chromatography (silica, eluent: cyclohexane/ethyl acetate = 1/1 with 3 % triethylamine) as a red foamy solid (yield: 0.91 g, 69 %).

^{1}H-NMR (300 MHz, DMSO-d_6) δ [ppm] = 8.30-7.80 (m, 3 H, H_8+H_{21}), 7.69-7.15 (m, 10 H, H_9+H_{19}+H_{20}+H_{23}), 7.02-6.64 (m, 6 H, H_{13}+H_{24}), 4.48-4.38 (m, 2 H, H_4), 3.81-3.75 (m, 7 H, H_5+H_{26}), 3.59-3.47 (m, 3 H, H_{16}), 3.35-2.95 (m, 2 H, H_{27}), 2.71-2.35 (m, 7 H, H_{15}+H_3), 1.95-1.92 (m, 1 H, H_2), 1.58-0.94 (m, 19 H, H_1+H_{28}+H_{29}+H_{30}).

^{31}P-NMR: (162 MHz, $CDCl_3$) δ [ppm] = 149.0, 148.7.

MS (ESI, positive) *m/z* (%) 912.4 (26) $[M+Na]^+$, 866.4 (10) $[M-CH_2S+Na]^+$, 303.1 (100) $[DMT]^+$.

HRMS (ESI, positive) *m/z* calculated for $C_{50}H_{60}N_5O_6PSNa$: 912.3894 $[M+Na]^+$, found: 912.3878 $[M+Na]^+$.

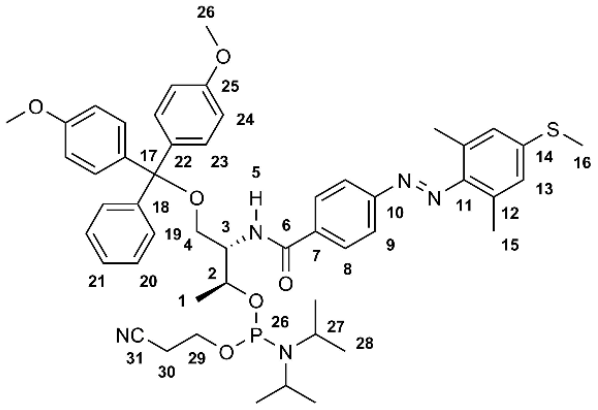

7.2.4 Synthesis of *ortho*-substituted azobenzenes ("azobenzene-library")

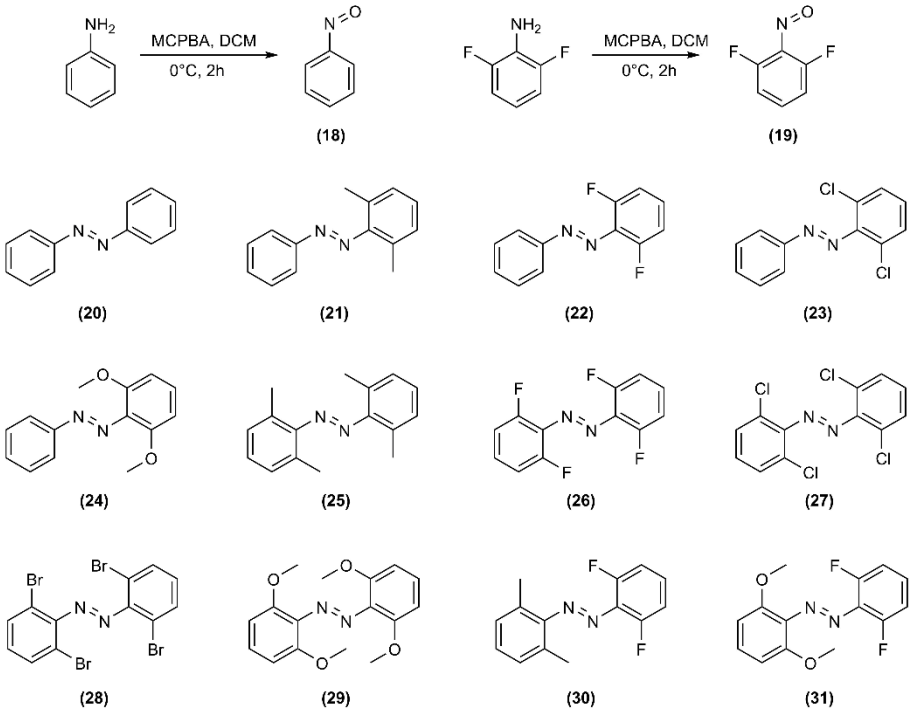

Nitrosobenzene (18)[251]

Aniline (100 g, 1.07 mol), 35 % H_2O_2 (146.15 g, 4.29 mol) and MoO_3 (15.46 g, 107 mmol) were mixed with a 108 mL 1 M aqueous KOH-solution, 300 mL methanol and 400 mL water. The reaction mixture was cooled to 4 °C and stirred for 20 hours, then extracted two times with 1 L ethyl acetate each. The combined organic layers were washed with 1 L water and 1 L brine. All solvents were removed under reduced pressure to yield the product as a brownish white solid (yield: 63.92 g, 56 %).

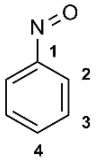

^{1}H-NMR (500 MHz, $CDCl_3$) δ [ppm] = 7.91-7.89 (m, 2 H, H_2), 7.72-7.69 (m, 1 H, H_4), 7.64-7.61 (m, 2 H, H_3).

^{13}C-NMR (125 MHz, $CDCl_3$) δ [ppm] = 165.8 (C_1), 135.5 (C_4), 129.3 (C_3), 120.9 (C_2).

MS (EI, 70 eV) *m/z* (%) 107.0 (63) $[M]^{+\cdot}$, 77.0 (100) $[C_6H_5]^+$.

2,6-Difluoro-nitrosobenzene (19)[252]

To a solution of 2,6-difluoroaniline (10.0 g, 77.4 mmol) in 400 mL dichloromethane a solution of MCPBA (38.19 g, 155 mmol) in 350 mL dichloromethane was added dropwise at 0 °C over 1.5 hours. The reaction mixture was continued stirring and warmed up slowly to room temperature over 2 hours. 300 mL dichloromethane was added and the reaction mixture was washed subsequently with two times 500 mL 2 % $Na_2S_2O_3$ solution, four times 500 mL saturated $NaHCO_3$ solution and twice with 300 mL water. All solids were filtered off and all

solvents were removed *in vacuo* to yield the product as a brownish white solid (yield: 10.31 g, 93 %).

^{1}H-NMR (300 MHz, $CDCl_3$) δ [ppm] = 7.68-7.58 (m, 1 H, H_4), 7.16-7.08 (m, 2 H, H_3).

^{19}F-NMR (100 MHz, $CDCl_3$) δ [ppm] = -130.5 (F_5).

^{13}C-NMR (75 MHz, $CDCl_3$) δ [ppm] = 151.4 (C_2), 137.0 (C_1), 129.0 (C_4), 112.8 (C_3).

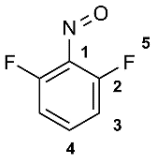

MS (EI, 70 eV) *m/z* (%) 143.1 (100) $[M]^{+\cdot}$, 113.1 (65) $[C_6H_3F_2]^+$, 63.1 (31) $[C_5H_3]^+$.

HRMS (EI, 70 eV) *m/z* calculated for $C_6H_3F_2NO$: 143.0183, found: 143.0183.

Azobenzene (20)[81]

Aniline (0.37 g, 4.0 mmol) was mixed with 2 g $KMnO_4$ and 2 g $CuSO_4$ in 40 mL dichloromethane and the reaction mixture was stirred for 24 hours at room temperature. All solids were filtered off and rinsed twice with 10 mL dichloromethane. Dichloromethane was removed under reduced pressure and the product was isolated *via* column chromatography (silica, eluent: cyclohexane) as a red solid (yield: 0.11 g, 15 %).

^{1}H-NMR (400.1 MHz, $CDCl_3$) δ [ppm] = 7.84 (d, 2 H, $^{3}J_{2,3}$ = 6.8 Hz, H_2), 7.43-7.34 (m, 3 H, H_3+H_4).

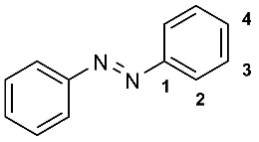

^{13}C-NMR (100.6 MHz, $CDCl_3$) δ [ppm] = 152.7 (C_1), 131.0 (C_4), 129.1 (C_3), 122.9 (C_2).

2,6-Dimethylazobenzene (21)

2,6-Dimethylaniline (1.36 g, 11.2 mmol) and nitrosobenzene **(18)** (1.0 g, 9.34 mmol) were dissolved in 80 mL glacial acetic acid and the reaction mixture was stirred for 24 hours at room temperature. 50 mL water were added and the mixture was neutralized with sodium bicarbonate. The crude reaction mixture was extracted twice with 100 mL ethyl acetate, the combined organic layers were collected and washed subsequently with 100 mL water, 200 mL saturated sodium bicarbonate solution and 100 mL brine, followed by drying over $MgSO_4$. All solvents were removed under reduced pressure and the product was isolated by column chromatography (silica, eluent: cyclohexane) as a red solid (yield: 1.20 g, 61 %).

^{1}H-NMR (400.1 MHz, $CDCl_3$) δ [ppm] = 7.82-7.79 (m, 2 H, H_7), 7.44-7.37 (m, 3 H, H_8+H_9), 7.04-7.01 (m, 3 H, H_3+H_4), 2.25 (s, 6H, H_5).

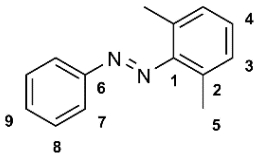

^{13}C-NMR (100.6 MHz, $CDCl_3$) δ [ppm] = 152.8 (C_6), 151.5 (C_1), 131.0 (C_9), 130.6 (C_3), 129.1 (C_8), 129.1 (C_4), 128.1 (C_2), 122.5 (C_7), 18.8 (C_5).

MS (EI, 70 eV) *m/z* (%) 210.1 (72) $[M]^{+\cdot}$, 105.1 (100) $[C_6H_5N_2]^+$, 77.0 (52) $[C_6H_5]^+$.

HRMS (EI, 70 eV) *m/z* (%) calculated for $C_{14}H_{13}N_2$ $[M-H]^+$: 209.1079, found: 209.1078.

2,6-Difluoroazobenzene (22)

Nitrosobenzene **(18)** (1.50 g, 14.0 mmol) and 2,6-difluoroaniline (2.17 g, 16.8 mmol) were dissolved in 150 mL glacial acetic acid and the reaction mixture was stirred for 24 hours at room temperature. 100 mL water was added, the mixture was neutralized with sodium bicarbonate and extracted twice with 100 mL ethyl acetate. The combined organic layers were washed subsequently with 150 mL water, 250 mL saturated bicarbonate solution and 150 mL brine. The remaining organic layer was dried over $MgSO_4$ and all solvents were removed under reduced pressure. The product was isolated by column chromatography (silica, eluent: cyclohexane) as a red oil (yield: 0.71 g, 19 %).

^{1}H-NMR (300 MHz, $CDCl_3$) δ [ppm] = 8.22-8.06 (m, 1 H, H_4), 7.86-7.82 (m, 1 H, H_9), 7.45-7.36 (m, 3 H, H_7+H_8), 7.22-7.15 (m, 1 H, H_8), 6.97-6.89 (m, 2 H, H_3).

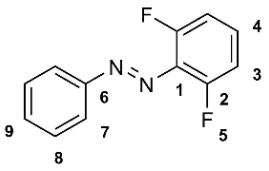

^{13}C-NMR (75 MHz, $CDCl_3$) δ [ppm] = 156.7 (C_2), 153.2 (C_6), 131.9 (C_1), 130.2 (C_9), 129.1 (C_8), 125.5 (C_7), 122.9 (C_4), 112.6 (C_3).

^{19}F-NMR (100 MHz, $CDCl_3$) δ [ppm] = -121.75 (F_5).

MS (EI, 70 eV) *m/z* (%) 218.0 (47) $[M]^{+\cdot}$, 198.1 (24) $[M-HF]^{+\cdot}$, 141.0 (16) $[C_6H_3F_2N_2]^+$, 105.0 (37) $[C_6H_5N_2]^+$, 77.0 (100) $[C_6H_5]^+$.

HRMS (EI, 70 eV) *m/z* calculated for $C_{12}H_8F_2N_2$: 218.0655, found: 218.0656.

2,6-Dichloroazobenzene (23)

2,6-Dichloroaniline (2.50 g, 14.20 mmol) and nitrosobenzene **(18)** (1.59 g, 17.05 mmol) were dissolved in a mixture of 130 mL glacial acetic acid and 13 mL trifluoroacetic acid and the reaction mixture was stirred for 24 hours at room temperature. 100 mL water was added and the mixture was neutralized with sodium bicarbonate, then extracted twice with 150 mL ethyl acetate. The combined organic layers were washed subsequently with 250 mL water, 250 mL saturated sodium bicarbonate solution, and 150 mL brine. All volatiles were removed under reduced pressure and the product was isolated by column chromatography (silica, eluent: cyclohexane/ethyl acetate = 19/1) as a red solid (yield: 30 mg, 1 %).

^{1}H-NMR (300 MHz, $CDCl_3$) δ [ppm] = 7.91-7.88 (m, 1 H, H_7), 7.50-7.47 (m, 2 H, H_7), 7.35 (d, 2 H, $^3J_{3,4}$ = 8.1 Hz, H_3), 7.18-7.11 (m, 3 H, H_8+H_9), 7.00-6.97 (m, 1 H, H_4).

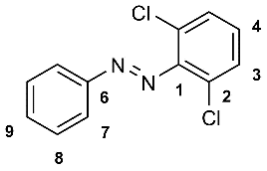

^{13}C-NMR (75 MHz, $CDCl_3$) δ [ppm] = 132.0 (C_6), 128.9 (C_1), 128.7 (C_4), 128.1 (C_9), 128.0 (C_8), 128.0 (C_3), 122.7 (C_7), 119.3 (C_2).

MS (EI, 70 eV) *m/z* (%) 250.0 (48) $[M]^{+\cdot}$, 144.9 (100) $[C_6H_3Cl_2]^+$, 105.0 (142) $[C_6H_5N_2]^+$, 77.0 (100) $[C_6H_5]^+$.

HRMS (EI, 70 eV) *m/z* calculated for $C_{12}H_8Cl_2N_2$: 250.0065, found: 250.0067.

2,6-Dimethoxyazobenzene (24)

2,6-Dimethoxyaniline **(69)** (2.57 g, 16.81 mmol) and nitrosobenzene **(18)** (1.50 g, 14.00 mmol) were dissolved in 150 mL glacial acetic acid and the reaction mixture was stirred for 24 hours at room temperature. 100 mL water was added, the mixture was neutralized with sodium carbonate and extracted twice with 150 mL ethyl acetate. The combined organic layers were washed subsequently with 150 mL water, 250 mL saturated sodium bicarbonate solution and 150 mL brine. The organic layer was dried over $MgSO_4$ and all solvents were removed under reduced pressure. The product was isolated by column chromatography (silica, eluent: cyclohexane) as a red solid (yield: 1.78 g, 52 %).

^{1}H-NMR (400.1 MHz, $CDCl_3$) δ [ppm] = 7.82-7.80 (m, 2 H, H_7), 7.43-7.36 (m, 3 H, H_8+H_9), 7.17 (t, 1 H, $^3J_{4,3}$ = 8.4 Hz, H_4), 6.59 (d, 2 H, $^3J_{3,4}$ = 8.5 Hz, H_3), 3.73 (s, 6 H, H_5).

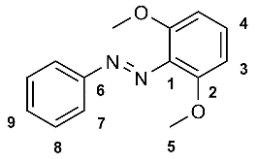

^{13}C-NMR (100.6 MHz, $CDCl_3$) δ [ppm] = 153.3 (C_6), 152.3 (C_2), 133.8 (C_1), 130.8 (C_9), 129.5 (C_8), 128.9 (C_7), 122.6 (C_4), 105.1 (C_3), 56.4 (C_5).

MS (EI) *m/z* (%) 242.1 (88) $[M]^{+\cdot}$, 165.0 (100) $[M\text{-}C_6H_5]^+$, 122.0 (62) $[C_7H_6O_2]^+$, 107.0 (69) $[C_7H_7O]^+$.

HRMS (EI) *m/z* (%) calculated for $C_{14}H_{14}N_2O_2$: 242.1055, found: 242.1057.

2,2',6,6'-Tetramethylazobenzene (25)[81]

2,6-Dimethylaniline (0.49 g, 4.0 mmol) was mixed with 2 g $KMnO_4$ and 2 g $CuSO_4$ in 40 mL dichloromethane. The reaction mixture was stirred for 24 hours at room temperature, followed by filtering off all solids and rinsing twice with 10 mL dichloromethane. All volatiles were removed under reduced pressure and the product was isolated by column chromatography (silica, eluent: cyclohexane) as a red solid (yield: 0.14 g, 15 %).

^{1}H-NMR (400.1 MHz, $CDCl_3$) δ [ppm] = 7.09-7.03 (m, 6 H, H_3+H_4), 2.33 (s, 12 H, H_5).

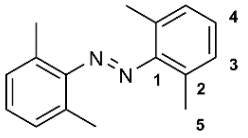

^{13}C-NMR (100.6 MHz, $CDCl_3$) δ [ppm] = 151.4 (C_1), 131.3 (C_3), 129.4 (C_2), 128.4 (C_4), 19.8 (C_5).

MS (EI, 70 eV) *m/z* (%) 238.0 (24) $[M]^{+\cdot}$, 104.9 (100) $[C_8H_9]^+$.

HRMS (EI, 70 eV) *m/z* calculated for $C_{16}H_{18}N_2$: 238.1470, found: 238.1464.

2,2',6,6'-Tetrafluoroazobenzene (26)[253]

2,6-Difluoroaniline (1.0 g, 7.75 mmol), $K_3Fe(CN)_6$ (10.2 g, 30.98 mmol) and KOH (0.87 g, 15.5 mmol) were mixed in 25 mL water and 25 mL ethanol and refluxed for 24 hours. All solids were filtered off and the reaction mixture was extracted twice with 50 mL ethyl acetate. The combined organic layers were washed with 50 mL water and all solvents were removed *in vacuo*. The product was isolated by column chromatography (silica, eluent: cyclohexane) as a red solid (yield: 0.18 g, 18 %).

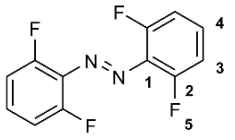

^{1}H-NMR (300 MHz, $CDCl_3$) δ [ppm] = 7.42-7.33 (m, 2 H, H_4), 7.10-7.02 (m, 4 H, H_3).

^{19}F-NMR (100 MHz, $CDCl_3$) δ [ppm] = -119.8 (F_5), -121.5 (F_5').

^{13}C-NMR (75 MHz, $CDCl_3$) δ [ppm] = 157.0 (C_2), 153.5 (C_1), 131.3 (C_4), 112.4 (C_3).

MS (EI, 70 eV) *m/z* (%) 254.0 (52) $[M]^{+\cdot}$, 140.9 (73) $[C_6H_3F_2N_2]^+$, 112.9 (100) $[C_6H_3F_2]^+$.

HRMS (EI, 70 eV) *m/z* calculated for $C_{12}H_6F_4N_2$: 254.0467, found: 254.0466.

2,2',6,6'-Tetrachloroazobenzene (27)[81]

2,6-Dichloroaniline (0.56 g, 4.0 mmol) was mixed with 2 g $KMnO_4$ and 2 g $CuSO_4$ in 40 mL dichloromethane. The reaction mixture was stirred for 24 hours at room temperature. All solids were filtered off and rinsed twice with 10 mL dichloromethane, followed by removal of dichloromethane under reduced pressure. The product was isolated by column chromatography (silica, eluent: cyclohexane) to yield a red solid (yield: 0.22 g, 17 %).

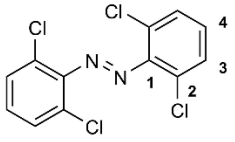

^{1}H-NMR (400 MHz, $CDCl_3$) δ [ppm] = 7.41-7.32 (m, 2 H, H_4), 7.22-7.06 (m, 4 H, H_3).

^{13}C-NMR (100 MHz, $CDCl_3$) δ [ppm] =129.6 (C_1), 129.4 (C_3), 129.1 (C_4), 127.3 (C_2).

MS (EI, 70 eV) *m/z* (%) 317.9 (30) $[M]^{+\cdot}$, 251.0 (20) $[M\text{-}Cl_2]^+$, 173.0 (93) $[C_6H_3Cl_2N_2]^+$, 145.0 (100) $[C_6H_3Cl_2]^+$, 109.0 (32) $[C_6H_2Cl]^+$.

HRMS (EI, 70 eV) *m/z* calculated for $C_{12}H_6Cl_4N_2$: 317.9285, found: 317.9284.

2,2',6,6'-Tetrabromoazobenzene (28)[81]

2,6-Dibromoaniline (1.0 g, 4.0 mmol) was mixed with 2 g $KMnO_4$ and 2 g $CuSO_4$ in 40 mL dichloromethane. The reaction mixture was stirred for 48 hours at room temperature. All solids were filtered off and rinsed with 10 mL dichloromethane, then dichloromethane was removed under reduced pressure. The product was isolated by column chromatography (silica, eluent: cyclohexane) to yield a red solid (yield: 0.38 g, 19 %).

^{1}H-NMR (600 MHz, $CDCl_3$) δ [ppm] = 7.59-7.62 (m, 4 H, H_3), 6.93-6.95 (m, 2 H, H_4).

^{13}C-NMR (150 MHz, $CDCl_3$) δ [ppm] = 146.2 (C_1), 132.2 (C_3), 126.8 (C_4), 113.3 (C_2).

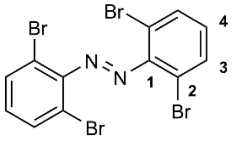

MS (EI, 70 eV) *m/z* (%) 493.7 (43) $[M]^{+\cdot}$, 260.8 (100) $[C_6H_3Br_2N_2]^+$, 232.8 (82) $[C_6H_3Br_2]^+$, 153.9 (20) $[C_6H_3Br]^+$, 75.0 (32) $[C_6H_3]^+$.

HRMS (EI, 70 eV) *m/z* (%) calculated for $C_{12}H_6Br_4N_2$: 493.7264, found: 493.7262.

2,2',6,6'-Tetramethoxyazobenzene (29)[81]

2,6-Dimethoxyaniline **(69)** (0.31 g, 2.0 mmol) was mixed with 1 g $KMnO_4$ and 1 g $CuSO_4$ in 20 mL dichloromethane. The reaction mixture was stirred for 24 hours at room temperature. All solids were filtered off and rinsed with 10 mL dichloromethane followed by removal of all solvents under reduced pressure. The product was isolated by column chromatography (silica, eluent: cyclohexane) as a red solid (yield: 0.11 g, 18 %).

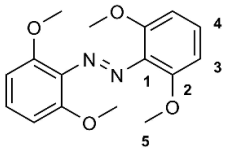

^{1}H-NMR (300 MHz, $CDCl_3$) δ [ppm] = 7.20-7.09 (m, 2 H, H_4), 6.64-6.62 (m, 4 H, H_3), 3.85 (s, 3 H, H_5), 3.81 (s, 3 H, H_5'), 3.77 (s, 6 H, H_5'').

^{13}C-NMR (75 MHz, $CDCl_3$) δ [ppm] = 154.3 (C_2), 152.3 (C_2'), 149.9 (C_1), 129.2 (C_4), 104.5 (C_3), 100.1 (C_3'), 56.5 (C_5), 56.5 (C_5').

MS (ESI, positive) *m/z* (%) 326.1 (73) $[M+Na]^+$, 303.1 (100) $[M+H]^+$.

HRMS (ESI, positive) *m/z* calculated for $C_{16}H_{18}N_2O_4H$: 303.1339, found: 303.1341.

2,6-Difluoro-2',6'-dimethylazobenzene (30)

2,6-Difluoro-nitrosobenzene **(19)** (2.0 g, 13.98 mmol) and 2,6-dimethylaniline (2.03 g, 16.77 mmol) were dissolved in 150 mL glacial acetic acid. The reaction mixture was stirred for 24 hours at room temperature, then 100 mL water was added and the mixture was neutralized with sodium bicarbonate. The crude mixture was extracted twice with 150 mL ethyl acetate and the combined organic layers were washed subsequently with 150 mL water, 250 mL saturated bicarbonate solution and 150 mL brine. The organic layer was dried over $MgSO_4$ and all solvents were removed under reduced pressure. The product was isolated by column chromatography (silica, eluent: cyclohexane) as a red solid (yield: 470 mg, 14 %).

^{1}H-NMR (300 MHz, $CDCl_3$) δ [ppm] = 7.23-7.17 (m, 1 H, H_4), 7.10-7.02 (m, 3 H, H_3+H_9), 6.98-6.90 (m, 2 H, H_8), 2.32 (s, 6 H, H_{10}).

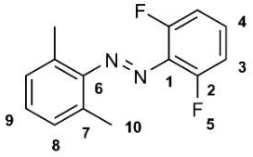

^{19}F-NMR (100 MHz, $CDCl_3$) δ [ppm] = -116.9 (F_5), -122.9 (F_5').

^{13}C-NMR (75 MHz, $CDCl_3$) δ [ppm] = 156.8 (C_2), 153.4 (C_1), 151.4 (C_6), 131.1 (C_8), 129.6 (C_7), 128.9 (C_9), 127.9 (C_4), 112.2 (C_3), 18.7 (C_{10}).

MS (EI, 70 eV) *m/z* (%) 246.1 (60) $[M]^{+\cdot}$, 105.0 (100) $[C_6H_5N_2]^+$.

HRMS (EI, 70 eV) *m/z* (%) calculated for $C_{14}H_{11}F_2N_2$ $[M-H]^+$: 245.0890, found: 245.0890.

2,6-Difluoro-2',6'-dimethoxyazobenzene (31)

2,6-Difluoro-nitrosobenzene **(19)** (1.50 g, 10.48 mmol) and 2,6-dimethoxyaniline **(69)** (1.93 g, 12.58 mmol) were dissolved in 120 mL glacial acetic acid and the reaction mixture was stirred for 24 hours at room temperature. 100 mL water was added and the reaction mixture was neutralized with sodium bicarbonate. The crude mixture was extracted twice with 100 mL ethyl acetate and the combined organic layers were washed subsequently with 100 mL water, 200 mL saturated sodium bicarbonate solution and 150 mL brine. The organic layer was dried over $MgSO_4$ and all solvents were removed under reduced pressure. The product was isolated by column chromatography (silica, eluent: cyclohexane) as a red solid (yield: 0.80 g, 27 %).

^{1}H-NMR (300 MHz, $CDCl_3$) δ [ppm] = 7.22-7.15 (m, 2 H, H_4+H_9), 6.95 (d, 2 H, $^{3}J_{3,4}$ = 8.4 Hz, H_3), 6.60 (d, 2 H, $^{3}J_{8,9}$ = 8.4 Hz, H_8), 3.77 (s, 6 H, H_{10}).

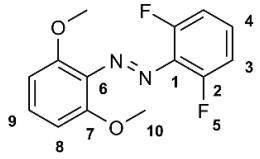

^{19}F-NMR (100 MHz, $CDCl_3$) δ [ppm] = -120.5 (F_5), -123.1 (F_5').

^{13}C-NMR (75 MHz, $CDCl_3$) δ [ppm] = 156.6 (C_2), 153.2 (C_7), 152.4 (C_1), 133.6 (C_6), 130.7 (C_9), 129.4 (C_4), 112.2 (C_3), 104.8 (C_8), 56.2 (C_{10}).

MS (EI, 70 eV) *m/z* (%) 278.0 (100) $[M]^{+\cdot}$, 165.0 (20) $[C_8H_9N_2O_2]^+$, 142.0 (93) $[C_6H_4F_2N_2]^+$, 122.0 (74) $[C_7H_6O_2]^+$, 107.0 (80) $[C_7H_7O]^+$, 77.0 (34) $[C_6H_5]^+$.

HRMS (EI, 70 eV) *m/z* calculated for $C_{14}H_{12}F_2N_2O_2$: 278.0867, found: 278.0866.

7.2.5 Attempted synthesis of 2,2',6,6'-tetrafluoroazobenzene phosphoramidite

First synthesis pathway]

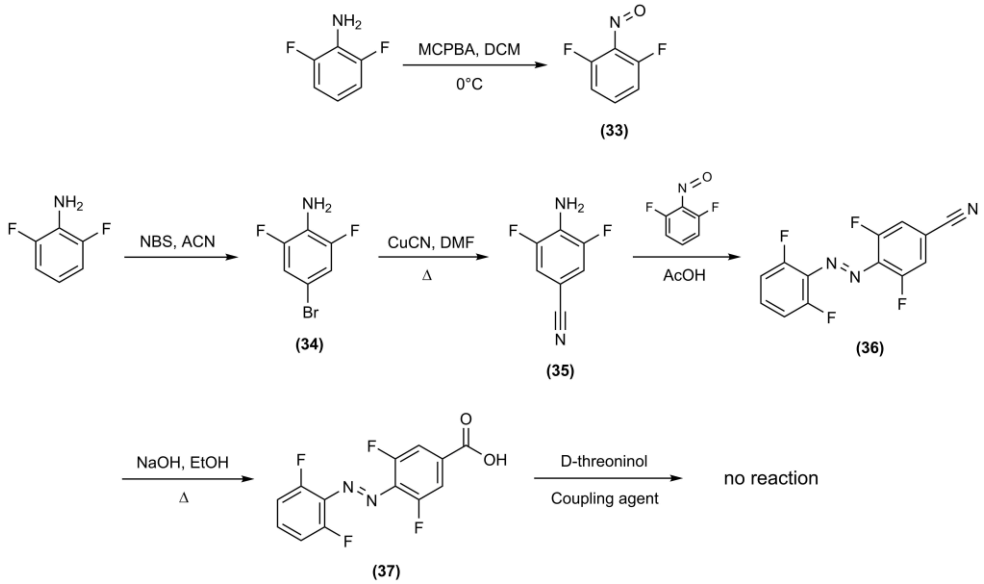

4-Bromo-2,6-difluoroaniline (32)[132]

2,6-Difluoroaniline (5.0 g, 38.7 mmol) and *N*-bromosuccinimide (7.58 g, 42.6 mmol) were dissolved in 100 mL acetonitrile and the reaction mixture was stirred for 24 hours at room temperature. 100 mL water and 100 mL cyclohexane were added, the organic layer was separated and dried over $MgSO_4$. All solvents were evaporated and the product was isolated by column chromatography (silica, eluent: dichloromethane/cyclohexane = 1/1) as a white brownish solid (yield: 7.26 g, 90 %).

^{1}H-NMR (400 MHz, $CDCl_3$) δ [ppm] = 6.92-6.90 (m, 2 H, H_4), 3.62 (s, br, H_1).

^{13}C-NMR (75 MHz, $CDCl_3$) δ [ppm] = 149.8 (C_3), 123.1 (C_2), 114.6 (C_4), 106.9 (C_5).

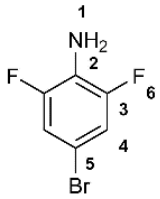

^{19}F-NMR: (162 MHz, $CDCl_3$) δ [ppm] = 130.9 (F_6).

MS (ESI, positive) *m/z* (%) 208.0 (100) $[M+H]^+$.

HRMS (ESI, positive) *m/z* calculated for $C_6H_5BrF_2N$: 207.9568, found: 207.9562.

4-Cyano-2,6-difluoroaniline (33)[132]

4-Bromo-2,6-difluoroaniline **(32)** (28.5 g, 137 mmol) and CuCN (36.8 g, 411 mmol) were mixed in 300 mL DMF and refluxed for 16 hours, then cooled down to room temperature and purged into 300 mL 12% aqueous ammonia. The crude mixture was extracted twice with 300 mL ethyl acetate, the combined organic layers were dried over $MgSO_4$ followed by evaporation of all solvents. The product was isolated by column chromatography (silica, eluent:

dichloromethane/cyclohexane = 1/1) as a white solid (yield: 13.4 g, 63 %).

^{1}H-NMR (400 MHz, $CDCl_3$) δ [ppm] = 7.08-7.05 (m, 2 H, H_4), 4.22 (s, br, 2H, H_1).

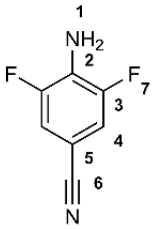

^{13}C-NMR (75 MHz, $CDCl_3$) δ [ppm] = 151.8 (C_3), 148.6 (C_2), 129.5 (C_6), 115.3 (C_5), 97.9 (C_4).

^{19}F-NMR (162 MHz, $CDCl_3$) δ [ppm] = -131.9 (F_7).

MS (ESI, positive) *m/z* (%) 155.0 (1) $[M+H]^+$, 111.0 (100) $[M-HCN-2HF+Na]^+$.

HRMS (ESI, positive) *m/z* (%) calculated for $C_7H_5F_2N_2$: 155.0415, found: 155.0422.

4-Cyano-2,2',6,6'-tetrafluoroazobenzene (34)

4-Cyano-2,6-difluoroaniline **(33)** (17.45 g, 122 mmol) and 2,6-difluoronitrosobenzene **(18)** (9.40 g, 61 mmol) were dissolved in 1.0 L glacial acetic acid and the reaction mixture was stirred for 48 hours at room temperature. 1.0 L water was added and the crude mixture was neutralized with sodium carbonate, followed by extraction with two times 1.0 L ethyl acetate. The combined organic layers were washed subsequently with 1.0 L water, 1.0 L saturated sodium hydrogen carbonate solution and 500 mL water. The organic phase was dried over $MgSO_4$, all solvents were removed under reduced pressure and the product was isolated by column chromatography (silica, eluent: cyclohexane/ethyl acetate = 9/1) as a yellow solid (yield: 3.42 g, 10 %).

^{1}H-NMR (500 MHz, $CDCl_3$) δ [ppm] = 7.66-7.44 (m, 1 H, H_3), 7.38-7.28 (m, 1 H, H_3'), 7.17-7.00 (m, 3 H, H_8+H_9).

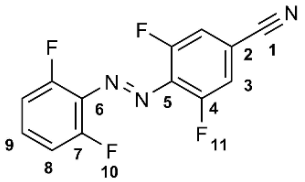

^{19}F-NMR: (125 MHz, $CDCl_3$) δ [ppm] = -113.8, -120.8.

MS (EI, 70 eV) *m/z* (%) 279.1 (100) $[M]^{+\cdot}$, 166.1 (12) $[C_7H_2F_2N_3]^+$, 141.1 (34) $[C_6H_3F_2N_2]^+$, 138.0 (19) $[C_7H_2F_2N]^+$, 113.0 (32) $[C_6H_3F_2]^+$.

4-Carboxy-2,2',6,6'-tetrafluoroazobenzene (35)

4-Cyano-2,2',6,6'-tetrafluoroazobenzene **(34)** (1.0 g, 3.58 mmol) was suspended in 40 mL 1 M aqueous NaOH and refluxed for 20 hours. The reaction mixture was cooled to room temperature, acidified with 45 mL 1 M hydrochloric acid and extracted with 200 mL ethyl acetate. The organic layer was washed with 100 mL water, dried over $MgSO_4$ and all volatiles were removed under reduced pressure. The product was isolated by column chromatography (silica, eluent: cyclohexane/ethyl acetate = 1/1) as a yellow solid (yield: 1.06 g, quant.).

^{1}H-NMR (500 MHz, DMSO-d_6) δ [ppm] = 11.21 (s, br, 1 H, H_1), 7.81-7.75 (m, 1 H, H_{10}), 7.58-7.50 (m, 2 H, H_4), 7.43-6.90 (m, 2 H, H_9).

^{13}C-NMR (500 MHz, DMSO-d_6) δ [ppm] = 155.5 (C_2), 153.5 (C_5), 153.5 (C_8), 133.9 (C_6), 131.3

(C_7), 127.0 (C_{10}), 120.7 (C_3), 114.0 (C_4), 113.1 (C_9).

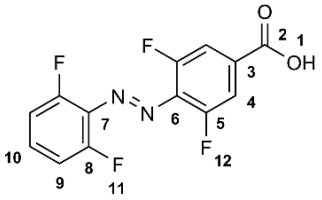

^{19}F-NMR (500 MHz, $CDCl_3$) δ [ppm] = -115.4, -123.0.

MS (EI, 70 eV) *m/z* (%) 298.0 (3) $[M]^{+\cdot}$, 270.0 (50) $[M\text{-}CO]^+$, 157.0 (18) $[C_7H_3F_2O_2]^+$, 141.0 (50) $[C_6H_3F_2N_2]^+$, 127.0 (100) $[C_6H_3F_2N]^+$, 113.0 (64) $[C_6H_3F_2]^+$, 100 (30) $[C_5H_2F_2]^+$.

Second synthesis pathway

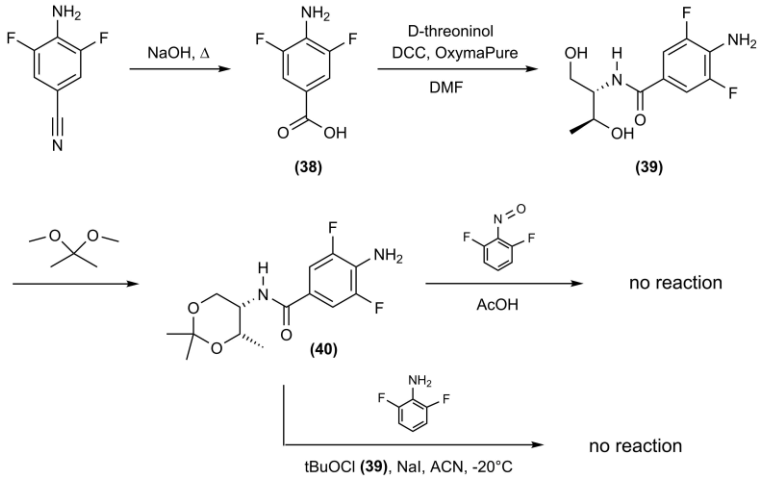

4-Carboxy-2,6-difluoroaniline (36)[132]

4-Cyano-2,6-difluoroaniline **(33)** (8.0 g, 51.9 mmol) was suspended in 300 mL 1 M aqueous NaOH solution and refluxed for 16 hours. 320 mL 1 M aqueous hydrochloric acid was added to form a white precipitate and the crude mixture was extracted with 500 mL ethyl acetate. The organic layer was separated, dried over $MgSO_4$ and all solvents were removed *in vacuo* to yield a white solid as the product (yield: 9.43 g, quant.).

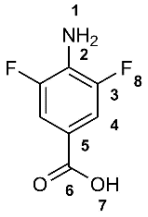

^{1}H-NMR (500 MHz, DMSO-d_6) δ [ppm] = 12.63 (s, br, 1 H, H_7), 7.40 (m, 2 H, H_4), 6.05 (s, br, 2 H, H_1).

^{13}C-NMR (125 MHz, DMSO-d_6) δ [ppm] = 166.5 (C_6), 151.2 (C_3), 131.1 (C_4), 116.1 (C_2), 112.8 (C_5).

^{19}F-NMR: (500 MHz, DMSO-d_6) δ [ppm] = -131.6 (F_8).

MS (ESI, negative) *m/z* (%) 172.0 (100) $[M\text{-}H]^-$, 128.0 (36) $[M\text{-}CO_2H]^-$, 108.0 $[C_6H_3FN]^-$.

HRMS (ESI, negative) *m/z* (%) calculated for $C_7H_4F_2NO_2$: 172.0216, found: 172.0226.

4-Carboxy-2,6-difluoroaniline-D-threoninol (37)

4-Carboxy-2',6'-difluoroaniline **(36)** (2.26 g, 13.0 mmol), D-threoninol (1.51 g, 14.3 mmol) and HBTU (5.44 g, 14.3 mmol) were dissolved in 150 mL DMF and the reaction mixture was stirred for 24 hours at room temperature under argon atmosphere. All solid residues were filtered off and rinsed with DMF followed by evaporation of DMF under reduced pressure. The

crude product was purified by column chromatography (silica, eluent: chloroform/methanol = 98/2) to yield a brownish white solid (yield: 3.01 g, 89 %).

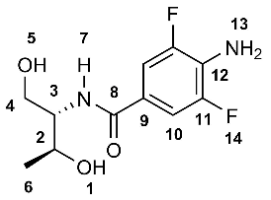

^{1}H-NMR (500 MHz, DMF-d_7) δ [ppm] = 7.57-7.50 (m, 1 H, H_7), 7.50-7.47 (m, 2 H, H_{10}), 5.74 (s, 2 H, H_{13}), 4.56-4.50 (m, 2 H, H_3+H_5), 3.86-3.83 (m, 2 H, H_4), 3.57-3.55 (m, 1 H, H_1), 3.45-3.43 (m, 1 H, H_2), 1.02 (d, 3 H, $^{3}J_{6,2}$ = 5.8 Hz, H_6).

^{13}C-NMR (125 MHz, DMF-d_7) δ [ppm] = 165.4 (C_8), 151.9 (C_{11}), 129.5 (C_9), 121.0 (C_{12}), 111.4 (C_{10}), 65.8 (C_2), 61.3 (C_4), 57.6 (C_3), 21.0 (C_6).

^{19}F-NMR: (500 MHz, DMSO-D_6) δ [ppm] = -131.5.

MS (EI, 70eV) *m/z* (%) 260.2 (10) $[M]^{+\cdot}$, 258.2 (14) $[M\text{-}H_2]^{+\cdot}$, 198.1 (16) $[C_9H_8F_2N_2O]^{+}$, 156.1 (100) $[C_7H_4F_2NO]^{+}$, 114.1 (40) $[C_6H_4F_2]^{+}$.

HRMS (EI, 70eV) *m/z* calculated for $C_{11}H_{14}F_2N_2O_3$: 260.0972, found: 260.0976.

Dimethylacetyl-4-carboxy-2,6-difluoroaniline-D-threoninol (38)[254]

4-Carboxy-2',6'-difluoroaniline-D-threoninol **(37)** (1.0 g, 3.48 mmol) and *p*-toluenesulfonic acid (75 mg, 0.1 eq) were dissolved in 40 mL acetone. 2,2-Dimethoxypropane (4.0 g, 34.8 mmol) was added dropwise to the solution and the reaction mixture was stirred for 24 hours at room temperature. Acetone was removed under reduced pressure and the crude product was purified by column chromatography (silica, eluent: cyclohexane/ethyl acetate = 1/1) to yield a white solid (yield: 0.68 g, 65 %).

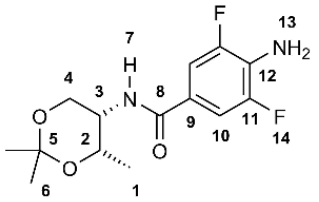

^{1}H-NMR (300 MHz, $CDCl_3$) δ [ppm] = 7.38-7.31 (m, 2 H, H_{10}), 6.66-6.63 (m, 1 H, H_7), 4.27-3.68 (m, 6 H, H_2+H_3+H_4+H_{13}), 1.52-1.40 (m, 6 H, H_6), 1.16-1.11 (d, 3 H, $^{3}J_{1,2}$ = 6.3 Hz, H_1).

^{19}F-NMR: (125 MHz, $CDCl_3$) δ [ppm] = -132.2.

MS (ESI, positive) *m/z* (%) 300.1 (4) $[M]^{+\cdot}$, 285.1 (10) $[M\text{-}CH_3]^{+}$, 198.0 (30) $[C_9H_8F_2N_2O]^{+}$, 156.0 (100) $[C_7H_4F_2NO]^{+}$.

HRMS (ESI, positive) *m/z* calculated for $C_{14}H_{18}F_2N_2O_3$: 300.1285, found: 300.1289.

***tert*-butylhypochlorite (39)[98]**

The following reaction was performed under exclusion of light and moisture! *tert*-Butanol (41.5 mL, 32.4 g, 437 mmol) and glacial acetic acid (25.0 mL, 26.25 g, 437 mmol) were mixed in a 1 L flask and cooled down to 0 °C. A 25 % aqueous NaOCl solution containing 12 % active chlorine (300 mL, 1.0 mol) was added in one portion and the resulting mixture was stirred vigorously for 15 minutes at 0 °C. The organic layer was separated and washed with 100 mL 10% aqueous $NaHCO_3$ solution and 100 mL water. The resulting colourless oily liquid was

collected as the pure product (42 g, 88 %).

^{1}H-NMR (300 MHz, $CDCl_3$) δ [ppm] = 1.26 (s, 9H, Me-*H*).

^{13}C-NMR (75 MHz, $CDCl_3$) δ [ppm] = 83.5, 26.4.

7.2.6 Synthesis of 2',6'-difluoroazobenzene phosphoramidite

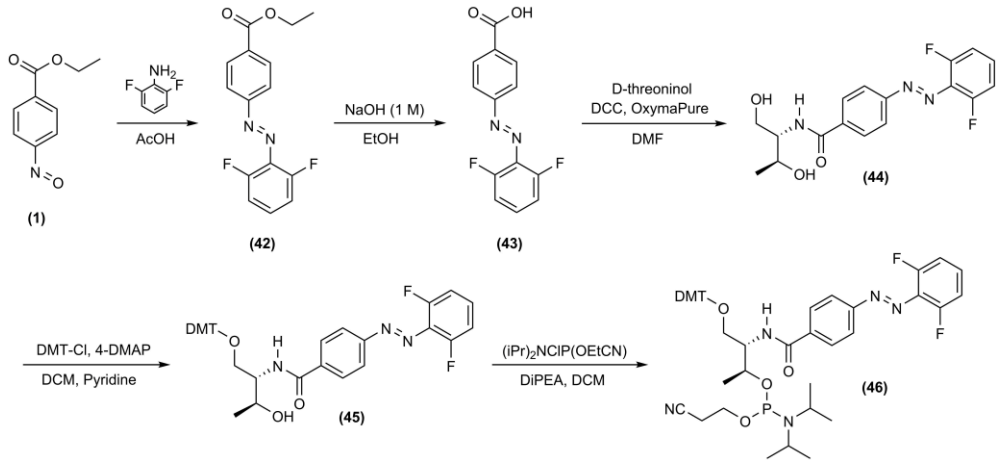

Ethyl-4-carboxy-2',6'-difluoroazobenzene (40)

Ethyl-4-nitrosobenzoate **(1)** (10.0 g, 55.8 mmol) and 2,6-difluoroaniline (14.4 g, 112 mmol) were dissolved in 400 mL glacial acetic acid and the reaction mixture was stirred for 24 hours at room temperature. 300 mL water was added and the resulting mixture was neutralized with sodium carbonate. The crude mixture was extracted twice with 500 mL ethyl acetate, the combined organic layers were washed subsequently with 500 mL water, 500 mL saturated sodium bicarbonate solution and 250 mL brine. The organic layer was dried over $MgSO_4$ and all solvents were removed *in vacuo*. The product was isolated by silica gel chromatography (eluent: cyclohexane) as a red solid (yield: 10.9 g, 67 %).

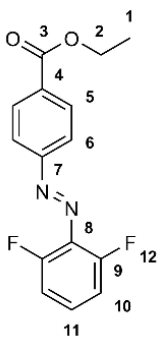

^{1}H-NMR (300 MHz, $CDCl_3$) δ [ppm] = 8.18-8.21 (m, 2 H, H_5), 7.94-7.96 (m, 2 H, H_6), 7.32-7.38 (m, 1 H, H_{11}), 7.03-7.07 (m, 2 H, H_{10}), 4.44 (q, 2 H, $^{3}J_{2,1}$ = 7.1 Hz, H_2), 1.44 (t, 3 H, $^{3}J_{1,2}$ = 7.1 Hz, H_1).

^{19}F-NMR: (162 MHz, $CDCl_3$) δ [ppm] = -121.0, -132.9.

^{13}C-NMR (75 MHz, $CDCl_3$) δ [ppm] = 165.8 (C_3), 156.9 (C_7), 155.4 (C_9), 132.9 (C_8), 131.1 (C_5), 130.5 (C_6), 122.6 (C_4), 118.2 (C_{10}), 112.7 (C_{11}), 61.3 (C_2), 14.2 (C_1).

MS (ESI, positive) *m/z* (%) 291.1 (100) $[M+H]^+$.

HRMS (ESI, positive) *m/z* (%) calculated for $C_{15}H_{13}F_2N_2O_2$: 291.0940, found: 291.0940.

4-Carboxy-2‘,6‘-difluoroazobenzene (41)

Ethyl-4-carboxy-2’,6’-difluoroazobenzene **(40)** (10.0 g, 34.5 mmol) was dissolved in 350 mL ethanol and 86 mL 1 M aqueous sodium hydroxide solution and the reaction mixture was stirred for 8 hours at room temperature. The mixture was acidified with 90 mL 1 M hydrochloric acid and extracted two times with 250 mL ethyl acetate. The combined organic layers were washed subsequently with 200 mL water and 100 mL brine, dried over $MgSO_4$ and all volatiles were removed under reduced pressure to yield the product as a red solid (yield: 6.62 g, 73 %).

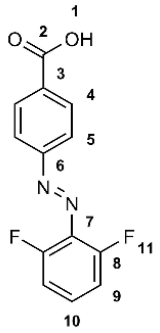

^{1}H-NMR (500 MHz, DMSO-d_6) δ [ppm] = 13.28 (s, 1 H, H_1), 8.16-8.13 (m, 2 H, H_5), 7.94-7.91 (m, 2 H, H_4), 7.62-7.56 (m, 1 H, H_{10}), 7.35-7.31 (m, 2 H, H_9).

^{13}C-NMR (125 MHz, DMSO-d_6) δ [ppm] = 167.0 (C_2), 156.5 (C_6), 155.1 (C_8), 134.2 (C_7), 133.1 (C_3), 131.2 (C_4), 123.0 (C_5), 118.8 (C_{10}), 113.7 (C_9).

^{19}F-NMR: (162 MHz, DMSO-d_6) δ [ppm] = -120.1 (F_{11}), -121.5 (F_{11}’).

MS (ESI, negative) *m/z* (%) 261.0 (100) $[M-H]^-$.

HRMS (ESI, negative) *m/z* calculated for $C_{13}H_7F_2N_2O_2$: 261.0470, found: 261.0476.

4-Carboxy-2‘,6‘-difluoroazobenzene-D-threoninol (“DFAB”) (42)

4-Carboxy-2’,6’-difluoroazobenzene **(41)** (1.0 g, 3.81 mmol), D-threoninol (0.44 g, 4.20 mmol) and HBTU (1.59 g, 4.20 mmol) were mixed in 40 mL DMF and the reaction mixture was stirred for 24 hours at room temperature under argon atmosphere. All solids were filtered off, DMF was removed under reduced pressure and the crude mixture was purified by column chromatography (silica, eluent: chloroform/methanol = 98/2) to yield a red solid (yield: 0.90 g, 69 %).

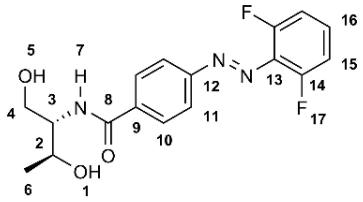

TLC (SiO_2, eluent: chloroform/methanol = 10/1) R_f = 0.28.

^{1}H-NMR (300 MHz, DMSO-d_6) δ [ppm] = 8.31-8.08 (m, 3 H, H_{10}+H_{16}), 8.01-7.92 (m, 2 H, H_{11}), 7.70-7.28 (m, 3 H, H_7+H_{15}), 4.53 (s, br, 2 H, H_1+H_5), 3.97-3.93 (m, 2 H, H_4), 3.67-3.49 (m, 2 H, H_2+H_3), 1.10-1.03 (m, 3 H, H_6).

^{13}C-NMR (75 MHz, DMSO-d_6) δ [ppm] = 165.8 (C_8), 162.3 (C_{12}), 153.7 (C_{14}), 137.9 (C_{13}), 128.8 (C_{10}), 127.1 (C_{16}), 124.4 (C_{16}’), 123.3 (C_{11}), 122.3 (C_{11}’), 119.0 (C_9), 109.7 (C_{15}), 65.0 (C_2), 60.5 (C_4), 57.0 (C_3), 20.2 (C_6).

^{19}F-NMR: (162 MHz, $CDCl_3$) δ [ppm] = -120.0, -121.5.

MS (ESI, positive) *m/z* (%) 721.2 (88) $[2M+Na]^+$, 372.1 (100) $[M+Na]^+$, 350.1 (86) $[M+H]^+$.

HRMS (ESI, positive) *m/z* (%) calculated for $C_{17}H_{17}F_2N_3O_3Na$:372.1130, found: 372.1135.

DMT-protected 4-carboxy-2‘,6‘-difluoroazobenzene-D-threoninol (43)

4-Carboxy-2’,6’-difluoroazobenzene-D-threoninol **(42)** (0.33 g, 0.95 mmol) and 4-DMAP (6 mg, 0.05 mmol) were dissolved in 8 mL dry pyridine under argon atmosphere and cooled to 0 °C. 4,4’-dimethoxytritylchloride (0.36 g, 1.05 mmol) was dissolved in 7 mL dry dichloromethane and added dropwise to the reaction mixture at 0 °C. The reaction mixture was warmed up to room temperature and stirred under argon atmosphere for 24 hours. All volatiles were removed *in vacuo* and the product was isolated by silica gel chromatography (eluent: cyclohexane/ethyl acetate = 1/1 with 3 % triethylamine) as a red foamy solid (yield: 0.42 g, 66 %).

^{1}H-NMR (300 MHz, $CDCl_3$) δ [ppm] = 8.47 (s, br, 1 H, H_9), 8.17-8.07 (m, 1 H, H_9’), 7.89-7.54 (m, 3 H, H_{19}+H_{21}), 7.33-6.65 (m, 15 H, H_{10}+H_{14}+H_{15}+H_{20}+H_{23}+H_{24}), 4.32-3.97 (m, 4 H, H_3+H_4+H_6), 3.69-3.64 (m, 6 H, H_{26}), 3.49-3.30 (m, 2 H, H_1+H_2), 1.29-1.06 (m, 3 H, H_5).

^{13}C-NMR (75 MHz, $CDCl_3$) δ [ppm] = 165.4 (C_7), 158.9 (C_{25}), 158.3 (C_{11}), 149.2 (C_{12}), 148.7 (C_{18}), 144.0 (C_{22}), 139.6 (C_{20}), 139.2 (C_{13}), 136.4 (C_{21}), 135.1 (C_9), 130.5 (C_{23}), 129.6 (C_{19}), 128.8 (C_{14}), 127.9 (C_{15}), 126.7 (C_{10}), 123.4 (C_8),

113.0 (C_{24}), 86.5 (C_{17}), 67.7 (C_4), 64.4 (C_2), 62.8 (C_3), 54.8 (C_{26}), 19.9 (C_5).

^{19}F-NMR: (162 MHz, $CDCl_3$) δ [ppm] = -119.4, -121.0.

MS (ESI, positive) *m/z* (%) 1325.5 (46) $[2M+Na]^+$, 674.3 (100) $[M+Na]^+$, 303.1 (60) $[DMT]^+$.

HRMS (ESI, positive) *m/z* calculated for $C_{38}H_{35}F_2N_3O_5Na$: 674.2437, found: 674.2441.

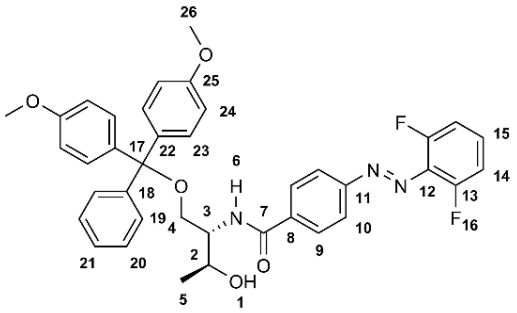

DMT-protected 4-carboxy-2‘,6‘-difluoroazobenzene-D-threoninol phosphoramidite (44)

DMT-protected 4-carboxy-2’,6’-difluoroazobenzene-D-threoninol **(43)** (0.97 g, 1.49 mmol) was dissolved in 15 mL dry dichloromethane under argon atmosphere and the solution was cooled to 0 °C. DiPEA (0.28 mL, 1.64 mmol) was added dropwise to the solution and the reaction mixture was stirred for 10 minutes at 0 °C. 2-Cyanoethyl-*N*,*N*-diisopropylchlorophosophoramidite (0.40 mL, 1.78 mmol) was added dropwise at 0 °C and the reaction mixture was stirred for 10 minutes at 0 °C, then warmed up to room temperature and stirred for 2.5 hours. All solvents were removed *in vacuo* and the product was isolated *via*

column chromatography (silica, eluent: cyclohexane/ethyl acetate = 1/1 with 3 % triethylamine) as a red foamy solid (yield: 0.75 g, 58 %).

^{1}H-NMR (500 MHz, CD_2Cl_2) δ [ppm] = 8.33-8.16 (m, 1 H, H_8), 8.02-7.93 (m, 1 H, $H_{8'}$), 7.50-7.00 (m, 13 H, H_5+H_9+H_{13}+H_{14}+H_{18}+H_{20}+H_{22}), 6.89-6.67 (m, 6 H, H_{19}+H_{23}),

4.50-4.36 (m, 1 H, H_3), 3.85-3.79 (m, 9 H, H_2+H_4+H_{25}), 3.62-3.54 (m, 2 H, H_{29}), 3.39-3.05 (m, 2 H, H_{30}), 2.64-2.43 (m, 2 H, H_{27}), 1.48 (s, 3 H, H_1), 1.39-1.01 (m, 12 H, H_{28}).

^{19}F-NMR (500 MHz, CD_2Cl_2) δ [ppm] = -115.1, -120.2, -121.7, -127.2.

^{31}P-NMR (500 MHz, CD_2Cl_2) δ [ppm] = 148.2.

MS (ESI, positive) *m/z* (%) 874.3 (100) $[M+Na]^+$, 303.1 (95) $[DMT]^+$.

HRMS (ESI, positive) *m/z* calculated for $C_{47}H_{52}F_2N_5O_6PNa$: 874.3515, found: 874.3478.

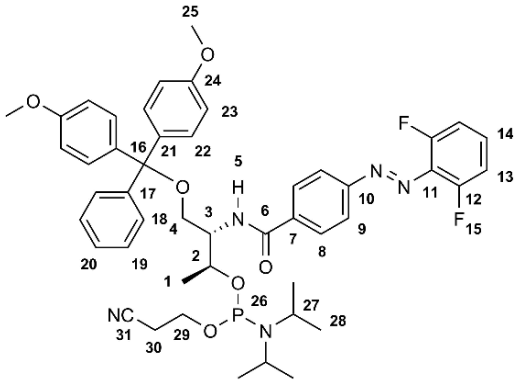

7.2.7 Synthesis of 2',4',6'-trifluoroazobenzene-D-threoninol

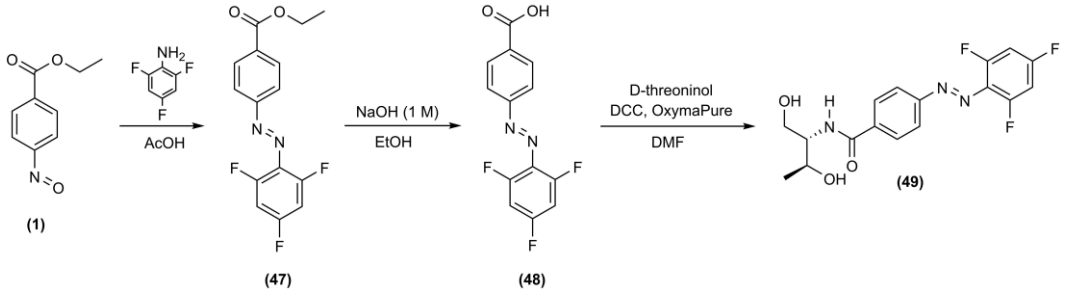

Ethyl-4-carboxy-2',4',6'-trifluoroazobenzene (45)

Ethyl-4-nitrosobenzoate **(1)** (3.05 g, 17.0 mmol) and 2,4,6-trifluoroaniline (3.0 g, 20.4 mmol) were dissolved in 150 mL glacial acetic acid and the reaction mixture was stirred for 24 hours at room temperature. 100 mL water was added, the resulting mixture was neutralized with sodium carbonate and extracted twice with 250 mL ethyl acetate. The combined organic layers were washed subsequently with 500 mL water, 500 mL saturated sodium bicarbonate solution and 100 mL brine. The organic layer was dried over $MgSO_4$ and all solvents were removed *in vacuo*. The product was isolated by column chromatography (silica, eluent: cyclohexane) as a red solid (yield: 1.80 g, 34 %).

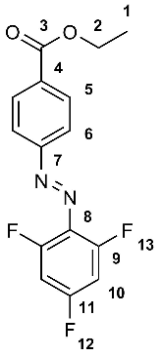

^{1}H-NMR (300 MHz, DMSO-d_6) δ [ppm] = 8.24-7.87 (m, 4 H, H_5+H_6), 7.45-7.39 (m, 1 H, $H_{10'}$), 6.96-6.90 (m, 1 H, H_{10}), 4.38-4.29 (m, 2 H, H_2), 1.35 (t, 3 H, $^3J_{1,2}$ = 7.1 Hz, H_1).

^{19}F-NMR: (100 MHz, DMSO-d_6) δ [ppm] = -102.41 (F_{12}) -116.6 ($F_{12'}$), -126.77 (F_{13}), -128.8 ($F_{13'}$),

^{13}C-NMR (75 MHz, DMSO-d_6) δ [ppm] = 164.9 (C_3), 154.8 (C_7), 135.4 (C_{11}), 132.5 (C_9), 130.9 (C_8), 130.5 (C_4), 122.5 (C_5), 120.6 (C_6), 100.1 (C_{10}), 61.2 (C_2), 14.0 (C_1).

MS (ESI, positive) *m/z* (%) 309.1 (12) $[M+H]^+$, 210.0 (50) $[C_{10}H_5F_3N_2]^+$,168.1 (100) $[C_6H_3F_2N+Na]^+$.

HRMS (ESI, positive) *m/z* calculated for $C_{16}H_{12}F_3N_2O_2$: 309.0845, found: 309.0844.

4-Carboxy-2',4',6'-trifluoroazobenzene (46)

Ethyl-4-carboxy-2',4',6'-trifluoroazobenzene **(45)** (1.70 g, 5.51 mmol) was dissolved in 50 mL ethanol and 27.6 mL 1 M aqueous sodium hydroxide and the mixture was stirred for 16 hours at room temperature. The reaction mixture was acidified with 30 mL 1 M hydrochloric acid and extracted two times with 100 mL ethyl acetate. The combined organic layers were washed subsequently with 100 mL water and 50 mL brine, dried over $MgSO_4$ and all volatiles were

removed under reduced pressure to remain a red solid as the product (yield: 1.05 g, 68 %).

^{1}H-NMR (300 MHz, DMSO-d_6) δ [ppm] = 13.06 (s, br, 1 H, H_1), 8.34-7.80 (m, 4 H, H_4+H_5), 7.44-6.85 (m, 2 H, H_9).

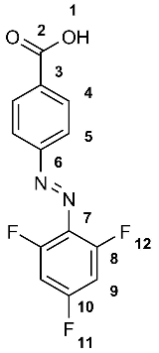

^{19}F-NMR: (100 MHz, DMSO-d_6) δ [ppm] = -117.2 (F_{11}), -120.5 (F_{12}).

^{13}C-NMR (75 MHz, DMSO-d_6) δ [ppm] = 166.7 (C_2), 155.1 (C_6), 132.7 (C_8), 130.6 (C_{10}), 124.9 (C_8), 123.7 (C_3) , 122.4 (C_4), 122.1 (C_5), 99.9 (C_9).

MS (EI, 70 eV) *m/z* (%) 280.1 (45) $[M]^{+\cdot}$, 121.1 (100) $[C_7H_5O_2]^+$, 65.1 (78) $[C_6H_5]^+$.

HRMS (EI, 70 eV) *m/z* calculated for $C_{13}H_7F_3N_2O_2$: 280.0460, found: 280.0460.

4-Carboxy-2‘,4‘,6‘-trifluoroazobenzene-D-threoninol (“DFAB-F”) (47)

4-Carboxy-2’,4’,6’-trifluoroazobenzene **(46)** (0.50 g, 1.78 mmol), D-threoninol (0.21 g, 1.96 mmol), DCC (0.37 g, 1.78 mmol) and OxymaPure (0.25 g, 1.78 mmol) were mixed in 18 mL dry DMF and stirred for 20 hours at room temperature under argon atmosphere. All solids were filtered off and rinsed with DMF, then DMF was removed under reduced pressure. The product was isolated by column chromatography (silica, eluent: chloroform/methanol = 98/2) to yield a red solid (yield: 0.55 g, 72 %).

TLC (SiO_2, eluent: chloroform/methanol = 10/1) R_f = 0.28.

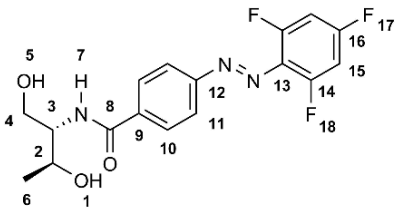

^{1}H-NMR (600 MHz, DMSO-d_6) δ [ppm] = 8.34-8.04 (m, 2 H, H_{10}), 7.95-7.80 (m, 2 H, H_{11}), 7.49-6.72 (m, 2 H, H_{15}), 4.62-4.50 (m, 1 H, H_7), 4.32-4.15 (m, 2 H, H_4), 4.03-3.83 (m, 2 H, H_2+H_5), 3.61-3.43 (m, 2 H, H_1+H_3), 1.36-1.22 (m, 3 H, H_6).

^{19}F-NMR: (162 MHz, DMSO-d_6) δ [ppm] = -103.0, -117.1, -117.5, -118.0.

^{13}C-NMR (150 MHz, DMSO-d_6) δ [ppm] = 165.9 (C_8), 158.7 (C_{16}), 154.3 (C_{14}), 128.8 (C_{12}), 125.9 (C_{12}’), 122.4 (C_{10}), 118.5 (C_{11}), 109.1 (C_9), 102.4 (C_{15}), 100.1 (C_{15}’), 65.1 (C_2), 62.6 (C_2‘), 60.7 (C_4), 57.1 (C_3), 20.4 (C_6), 14.0 (C_6’).

MS (ESI, positive) *m/z* (%) 390.1 (12) $[M+Na]^+$, 247.2 (100) $[M-2HF-H_2O+Na]^+$.

HRMS (ESI, positive) *m/z* calculated for $C_{17}H_{16}N_3F_3O_3Na$: 390.1036, found: 390.1037.

7.2.8 Synthesis of 4'-chloro-2',6'-difluoroazobenzene phosphoramidite

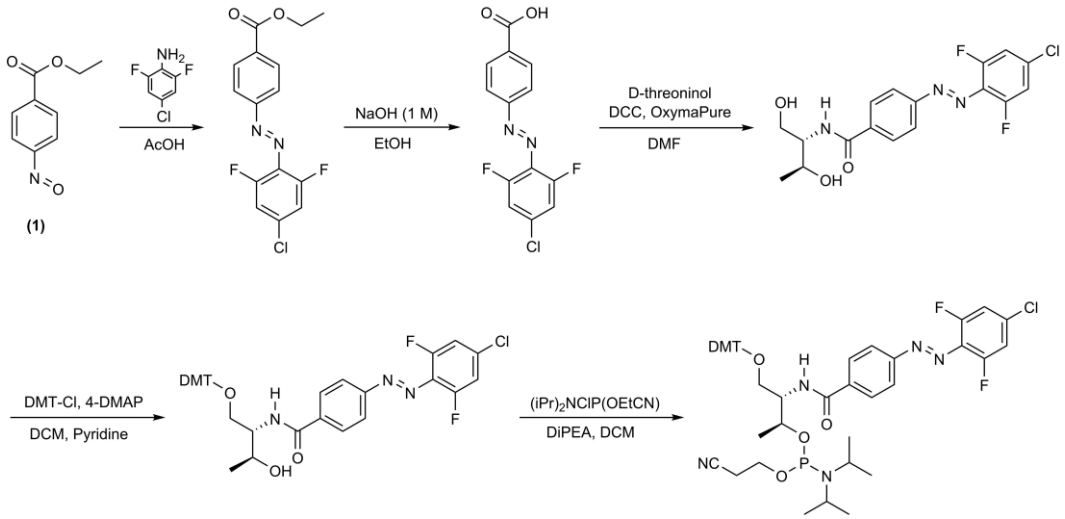

4-Chloro-2,6-difluoroaniline (48)[255]

2,6-Difluoroaniline (15.0 g, 116 mmol) and *N*-chlorosuccinimide (17.6 g, 128 mmol) were dissolved in 120 mL acetonitrile. The reaction mixture was refluxed for 20 hours, then poured into 300 mL 2 % aequous Na_2SO_3 solution. The aqueous mixture was extracted twice with 250 mL diethyl ether, the combined oranic layers were washed with 200 mL water and 200 mL brine and dried over $MgSO_4$. Diethyl ether was removed under reduced pressure and the product was isolated by column chromatography (silica, eluent: cyclohexane/ethyl acetate = 1/1) as a white solid (yield: 19.77 g, quant.).

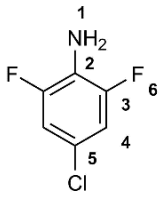

^{1}H-NMR (300 MHz, $CDCl_3$) δ [ppm] = 6.75-6.73 (m, 2 H, H_4), 3.65 (s, br, 2 H, H_1).

^{19}F-NMR: (100 MHz, $CDCl_3$) δ [ppm] = -131.0.

^{13}C-NMR (75 MHz, $CDCl_3$) δ [ppm] = 152.9 (C_3), 149.6 (C_5), 122.8 (C_2), 111.8 (C_4).

Ethyl-4-carboxy-4'-chloro-2',6'-difluoroazobenzene (49)

Ethyl-4-nitrosobenzoate **(1)** (2.0 g, 11.2 mmol) and 4-chloro-2,6-difluoroaniline **(48)** (2.08 g, 13.4 mmol) were dissolved in 100 mL glacial acetic acid. The reaction mixture was stirred for 24 hours at room temperature, followed by addition of 100 mL water. The resulting mixture was neutralized with sodium carbonate and extracted twice with 150 mL ethyl acetate. The combined organic layers were washed subsequently with 200 mL water, 300 mL saturated sodium bicarbonate solution and 100 mL brine. The organic layer was dried over $MgSO_4$ and all solvents were removed *in vacuo*. The product was isolated by column chromatography (silica, eluent: cyclohexane) as a red solid (yield: 0.55 g, 15 %).

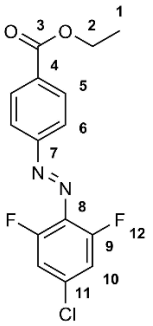

^{1}H-NMR (300 MHz, $CDCl_3$) δ [ppm] = 8.21-8.17 (m, 2 H, H_5), 7.96-7.92 (m, 2 H, H_6), 7.13-6.83 (m, 2 H, H_{10}), 4.45 (q, 2 H, $^{3}J_{2,1}$ = 7.1 Hz, H_2), 1.45 (t, 3 H, $^{3}J_{1,2}$ = 7.1 Hz, H_1).

^{19}F-NMR (100 MHz, $CDCl_3$) δ [ppm] = -111.9, -118.5.

^{13}C-NMR (75 MHz, $CDCl_3$) δ [ppm] = 165.4 (C_3), 157.3 (C_7), 155.0 (C_9), 153.8 (C_8), 136.1 (C_{11}), 132.8 (C_5), 130.2 (C_6), 122.3 (C_4), 113.6 (C_{10}), 61.0 (C_2), 13.9 (C_1).

4-Carboxy-4‘-chloro-2‘,6‘-difluoroazobenzene (50)

Ethyl-4-carboxy-4’-chloro-2’,6’-difluoroazobenzene **(49)** (0.41 g, 1.26 mmol) was mixed with 12 mL ethanol and 7.5 mL 1 M aqueous sodium hydroxide and the reaction mixture was stirred for 20 hours at room temperature followed by addition of 15 mL 1 M hydrochloric acid. The mixture was extracted two times with 200 mL ethyl acetate, the combined organic layers were washed subsequently with 300 mL water and 100 mL brine, dried over $MgSO_4$ and all volatiles were removed under reduced pressure to remain a red solid as the product (yield: 0.35 g, quant.).

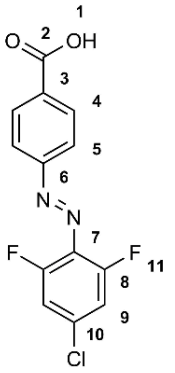

^{1}H-NMR (300 MHz, DMSO-d_6) δ [ppm] = 13.30 (s, br, 1 H, H_1), 8.37-8.10 (m, 2 H, H_4), 7.95-7.84 (m, 2 H, H_5), 7.66-7.59 (m, 1 H, H_9), 7.48-6.87 (m, 1 H, H_9’).

^{13}C-NMR (75 MHz, DMSO-d_6) δ [ppm] = 166.5 (C_2), 154.8 (C_6), 154.7 (C_8), 133.8 (C_7), 133.2 (C_{10}), 130.7 (C_4), 122.6 (C_3), 122.3 (C_5), 114.5 (C_9).

^{19}F-NMR: (100 MHz, $CDCl_3$) δ [ppm] = -118.8, -122.9.

MS (ESI, negative) *m/z* (%) 311.0 (100) $[M+O-H]^-$, 295.0 (54) $[M-H]^-$.

HRMS (ESI, negative) *m/z* calculated for $C_{13}H_6ClF_2N_2O_2$: 295.0091, found: 295.0077.

4-Carboxy-4‘-chloro-2‘,6‘-difluoroazobenzene-D-threoninol (“DFAB-Cl”) (51)

4-Carboxy-4’-chloro-2’,6’-difluoroazobenzene **(50)** (0.30 g, 1.01 mmol), D-threoninol (0.13 g, 1.21 mmol) and HBTU (0.46 g, 1.21 mmol) were mixed in 15 mL DMF and the reaction mixture was stirred for 24 hours at room temperature under argon atmosphere. All solid residuals were filtered off and DMF was removed under reduced pressure. The product was isolated by column chromatography (silica, eluent: chloroform/methanol = 98/2) to yield a red solid (yield: 0.42 g, quant.).

TLC (SiO_2, eluent: chloroform/methanol = 10/1) R_f = 0.28.

^{1}H-NMR (300 MHz, DMSO-d_6) δ [ppm] = 8.35-7.84 (m, 4 H, H_{10}+H_{11}), 7.71-6.93 (m, 3 H,

H_7+H_{15}), 4.63 (s, br, 1 H, H_5), 4.20-3.91 (m, 2 H, H_1+H_3), 3.66-3.49 (m, 3 H, H_2+H_4), 1.33-1.02 (m, 3 H, H_6).

^{13}C-NMR (75 MHz, DMSO-d_6) δ [ppm] = 165.7 (C_8), 162.3 (C_{12}), 153.7 (C_{14}),

138.1 (C_{13}), 130.7 (C_{16}), 128.8 (C_{16}'), 127.2 (C_{10}), 124.4 (C_{11}), 122.6 (C_{11}'), 119.1 (C_9), 109.6 (C_{15}), 64.9 (C_2), 60.5 (C_4), 57.0 (C_3), 20.2 (C_6).

^{19}F-NMR: (100 MHz, DMSO-d_6) δ [ppm] = -119.0, -123.2.

MS (ESI, positive) *m/z* (%) 789.2 (77) $[2M+Na]^+$, 406.1 (87) $[M+Na]^+$, 384.1 (100) $[M+H]^+$.

HRMS (ESI, positive) *m/z* calculated for $C_{17}H_{16}ClF_2N_3O_3H$: 384.0921, found: 384.0911.

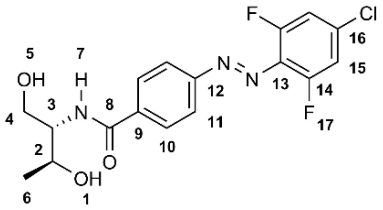

DMT-protected 4-carboxy-4'-chloro-2',6'-difluoroazobenzene-D-threoninol (52)

4-Carboxy-4'-chloro-2',6'-difluoroazobenzene-D-threoninol **(51)** (2.50 g, 6.51 mmol) and 4-DMAP (0.08 g, 0.6 mmol) were dissolved in 30 mL dry pyridine under argon atmosphere. The reaction mixture was cooled to 0 °C and 4,4'-dimethoxytritylchloride (2.43 g, 7.17 mmol) dissolved in 30 mL dry dichloromethane was added dropwise to the mixture. The reaction was warmed up to room temperature and stirred under argon atmosphere for 24 hours. All volatiles were removed *in vacuo* and the product was isolated by column chromatography (silica, eluent: cyclohexane/ethyl acetate = 1/1 with 3 % triethylamine) as a red foamy solid (yield: 1.80 g, 39 %).

^{1}H-NMR (300 MHz, DMSO-d_6) δ [ppm] = 8.37-7.83 (m, 7 H, H_{10}+H_{14}+H_{19}+H_{21}), 7.68-7.60 (m, 2 H, H_9), 7.45-7.17 (m, 5 H, H_{23}), 7.08-6.81 (m, 5 H, H_6+H_{24}), 4.24-4.17 (m, 1 H, H_3), 4.01-3.90 (m, 2 H, H_4), 3.72 (s, 6 H, H_{26}), 3.59-3.35 (m, 2 H, H_1+H_2), 1.34-1.21 (m, 3 H, H_5).

^{19}F-NMR: (100 MHz, DMSO-d_6) δ [ppm] = -112.49, -117.48, -118.80, -120.53, -122.96.

MS (ESI, positive) *m/z* (%) 734.2 (42) $[M-H+2Na]^+$, 708.2 (42) $[M+Na]^+$, 406.1 (100) $[M-DMT+Na]^+$.

HRMS (ESI, positive) *m/z* calculated for $C_{38}H_{34}ClF_2N_3O_5Na$: 708.2047, found: 708.2042.

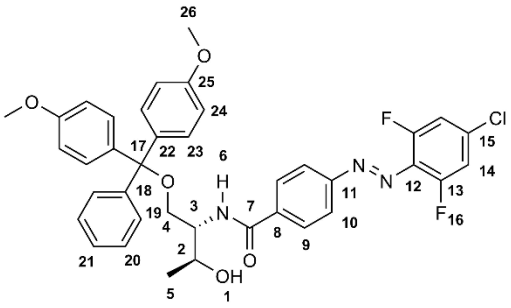

DMT-protected 4-carboxy-4‘-chloro-2‘,6‘-difluoroazobenzene-D-threoninol phosphoramidite (53)

DMT-protected 4-carboxy-4’-chloro-2’,6’-difluoroazobenzene-D-threoninol **(52)** (0.25 g, 0.36 mmol) was dissolved in 5 mL dry dichloromethane under argon atmosphere and the solution was cooled to 0 °C. DiPEA (0.08 mL, 0.44 mmol) was added dropwise to the solution and the reaction mixture was stirred for 10 minutes at 0 °C. 2-Cyanoethyl-*N*,*N*-diisopropylchlorophosophoramidite (0.10 mL, 0.44 mmol) was added dropwise to the reaction mixture at 0 °C and the reaction mixture was stirred for 10 minutes at 0 °C, then warmed up to room temperature and stirred for 2.5 hours. All solvents were removed *in vacuo*, the product was isolated *via* column chromatography (silica, eluent: cyclohexane/ethyl acetate = 1/1 with 3% triethylamine) as a red foamy solid (yield: 0.30 g, 92 %).

^{1}H-NMR (500 MHz, $CDCl_3$) δ [ppm] = 8.29-8.27 (m, 1 H, H_{20}), 7.95-7.63 (m, 2 H, H_9), 7.44-7.39 (m, 2 H, H_{13}), 7.32-7.10 (m, 9 H, H_8+H_{22}+H_{18}+H_{19}), 6.96-6.77 (m, 5 H, H_8+H_{23}), 6.66-6.26 (m, 1 H, H_5), 4.48-4.33 (m, 1 H, H_3), 3.77 (s, 6 H, H_{25}), 3.55-3.50 (m, 3 H, H_2+H_4), 3.35-3.23 (m, 2 H, H_{27}), 1.47-0.95 (m, 19 H, H_1+H_{28}+H_{29}+H_{30}).

^{19}F-NMR (500 MHz, $CDCl_3$) δ [ppm] = -111.75, -118.40, -119.30, -121.84.

^{31}P-NMR (500 MHz, $CDCl_3$) δ [ppm] = 148.40.

MS (ESI, positive) *m/z* (%) 908.3 (4) $[M+Na]^+$, 535.2 (7) $[C_{23}H_{28}ClF_2N_4O_3P+Na]^+$, 372.2 (31) $[C_{17}H_{14}ClF_2N_3O+Na]^+$, 370.2 (100) $[C_{17}H_{12}ClF_2N_3O+Na]^+$, 303.1 (30)]DMT}$^+$.

HRMS (ESI, positive) *m/z* calculated for $C_{47}H_{51}ClF_2N_5O_6PNa$: 908.3126, found: 908.3132.

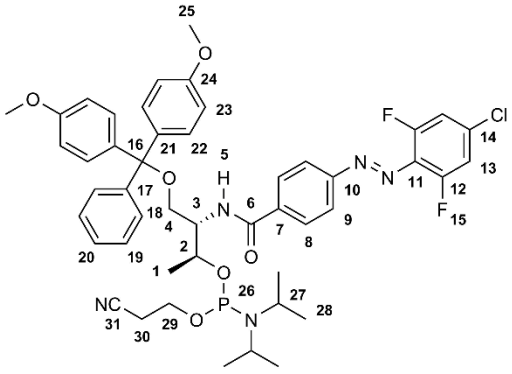

7.2.9 Synthesis of 4'-bromo-2',6'-difluoroazobenzene-D-threoninol

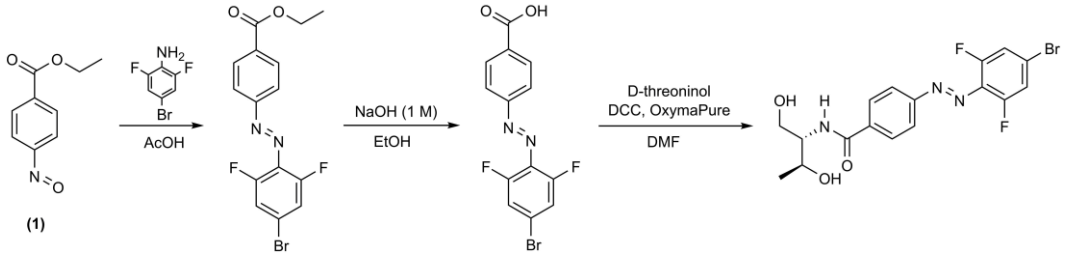

Ethyl-4'-bromo-4-carboxy-2',6'-difluoroazobenzene (54)

Ethyl-4-nitrosobenzoate **(1)** (1.0 g, 5.58 mmol) and 4-bromo-2,6-difluoroaniline **(32)** (1.74 g, 8.37 mmol) were mixed in 50 mL glacial acetic acid and stirred for 24 hours at room temperature. 30 mL water was added, the resulting mixture was neutralized with sodium carbonate and extracted with 150 mL ethyl acetate. The organic layer was washed subsequently with 200 mL saturated sodium bicarbonate solution and 100 mL brine. The organic layer was dried over $MgSO_4$ and all solvents were removed *in vacuo*. The product was isolated by column chromatography (silica, eluent: cyclohexane) as a red solid (yield: 0.65 g, 32 %).

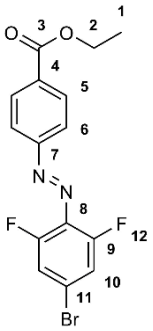

^{1}H-NMR (300 MHz, $CDCl_3$) δ [ppm] = 8.11-8.09 (m, 2 H, H_5), 7,86-7,83 (m, 2 H, H_6), 7,19-7,15 (m, 2 H, H_{10}), 4,37 (q, 2 H, $^3J_{2,1}$ = 7.1 Hz, H_2), 1,36 (t, 3 H, $^3J_{1,2}$ = 7.1 Hz, H_1).

^{13}C-NMR (75 MHz, $CDCl_3$) δ [ppm] = 165.4 (C_3), 157.2 (C_9), 155.0 (C_7), 153.7 (C_8), 132.8 (C_5), 130.2 (C_4), 123.2 (C_6), 122.4 (C_{10}), 116.5 (C_{11}), 61.0 (C_2), 13.9 (C_1).

^{19}F-NMR: (100 MHz, $CDCl_3$) δ [ppm] = -118.7 (F_{12}), -111.9 ($F_{12'}$).

MS (EI, 70 eV) *m/z* (%) 368.0 (40) $[M]^{+\cdot}$, 323.0 (10) $[M\text{-}C_2H_5O]^+$, 218.9 (22) $[M\text{-}C_9H_9O_2]^+$, 190.9 (20) $[C_6H_2BrF_2]^+$, 149.1 (100) $[C_9H_9O_2]^+$.

HRMS (EI, 70 eV) *m/z* calculated for $C_{15}H_{11}BrF_2N_2O_2$: 367.9972, found: 367.9972.

4-Carboxy-4'-bromo-2',6'-difluoroazobenzene (55)

Ethyl-4'-bromo-4-carboxy-2',6'-difluoroazobenzene **(54)** (2.35 g, 6.37 mmol) was dissolved in 70 mL ethanol and 40 mL 1 M aqueous NaOH solution and stirred for 24 hours at room temperature, followed by addition of 50 mL 1 M hydrochloric acid. The resulting mixture was extracted twice with 200 mL ethyl acetate. The combined organic layers were washed with 200 mL water and 200 mL brine and all volatiles were removed under reduced pressure. The product was isolated by column chromatography (silica, eluent: chloroform/methanol = 98/2) to yield a bright red solid (yield: 0.59 g, 27 %).

^{1}H-NMR (500 MHz, DMSO-d_6) δ [ppm] = 13.19 (s, br, 1 H, H_1), 8.39-8.14 (m, 3 H, H_4+H_5), 7.97-7.54 (m, 2 H, H_5+H_9), 7.39-6.97 (m, 1 H, H_9).

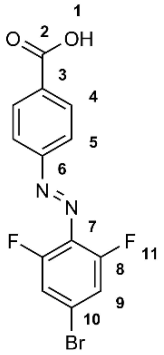

^{13}C-NMR (500 MHz, DMSO-d_6) δ [ppm] = 166.7 (C_2), 155.0 (C_8), 133.4 (C_6), 130.8 (C_7), 123.8 (C_4), 122.4 (C_3), 118.3 (C_5), 113.7 (C_9), 112.4 (C_{10}).

^{19}F-NMR (100 MHz, DMSO-d_6) δ [ppm] = -112.8, -119.2, -121.5, -123.3.

MS (EI, 70 eV) *m/z* (%) 339.9 (15) $[M]^{+\cdot}$, 262.0 (36) $[M\text{-}Br]^{+}$, 204.9 (56) $[C_6H_2BrF_2N]^{+}$, 167.0 (76) $[C_6H_2BrN]^{+}$, 121.0 (100) $[C_7H_5O_2]^{+}$.

HRMS (EI, 70 eV) *m/z* calculated for $C_{13}H_7BrF_2N_2O_2$: 339.9659, found: 339.9659.

4'-Bromo-4-carboxy-2',6'-difluoroazobenzene-D-threoninol ("DFAB-Br") (56)

4'-Bromo-4-carboxy-2',6'-difluoroazobenzene **(55)** (0.50 g, 1.47 mmol), D-threoninol (0.19 g, 1.76 mmol) and HBTU (0.67 g, 1.76 mmol) were mixed in 20 mL dry DMF. The reaction mixture was stirred for 24 hours at room temperature under argon atmosphere followed by filtering off all solids. DMF was removed under reduced pressure and the product was isolated by column chromatography (silica, eluent: chloroform/methanol = 98/2) to yield a red solid (yield: 0.55 g, 87 %).

TLC (SiO_2, eluent: chloroform/methanol = 10/1) R_f = 0.30.

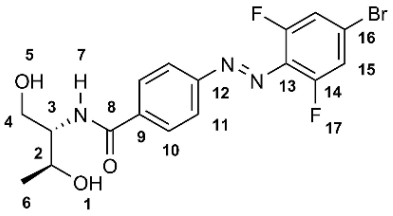

^{1}H-NMR (300 MHz, DMSO-d_6) δ [ppm] = 8.32-8.28 (m, 1 H, H_{10}), 8.17-7.69 (m, 4 H, H_{10}+H_{11}+H_{15}), 7.56-7.30 (m, 1 H, H_{15}), 4.63 (s, br, 1 H, H_7), 3.95-3.90 (m, 2 H, H_4), 3.63-3.23 (m, 3 H, H_1+H_3+H_5), 2.67-2.55 (m, 1 H, H_2), 1.33-1.04 (m, 3 H, H_6).

^{13}C-NMR (75 MHz, DMSO-d_6) δ [ppm] = 165.1 (C_8), 162.3 (C_8'), 148.9 (C_{14}), 140.6 (C_{12}), 130.7 (C_{13}), 128.9 (C_{13}'), 127.3 (C_{10}), 124.5 (C_{11}), 123.4 (C_{11}'), 122.0 (C_9), 119.1 (C_{15}), 109.6 (C_{16}), 64.9 (C_2), 60.4 (C_4), 57.2 (C_3), 20.2 (C_6).

^{19}F-NMR (100 MHz, DMSO-d_6) δ [ppm] = 68.71, 71.22,112.88, 115.97, 119.34, 120.63, 123.57.

MS/HRMS (EI, 70 eV): no target mass could be isolated

7.2.10 Synthesis of 4'-acetamido-2',6'-difluoroazobenzene-D-threoninol

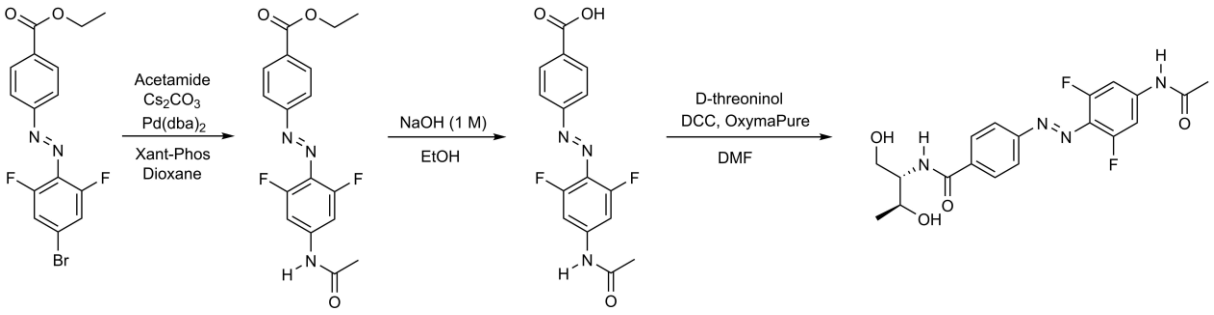

Ethyl-4'-acetamido-4-carboxy-2',6'-difluoroazobenzene (57)[132]

Ethyl-4'-bromo-4-carboxy-2',6'-difluoroazobenzene **(54)** (5.0 g, 13.5 mmol), acetamide (2.40 g, 40.6 mmol) and caesium carbonate (8.83 g, 27.1 mmol) were mixed in a flask with 140 mL dioxane and set under argon. Pd_2dba_3 (0.39 g, 0.68 mmol) and XantPhos (1.57 g, 2.71 mmol) were added under argon and the resulting reaction mixture was heated at 90 °C for 1 hour. After cooling to room temperature, 300 mL ethyl acetate were added and the resulting mixture was washed with 400 mL brine. The organic layer was dried over $MgSO_4$, all solids were filtered off and all solvents were removed *in vacuo*. The product was isolated by column chromatography (silica, eluent: cyclohexane/ethyl acetate = 9/1) as a red solid (yield: 3.20 g, 68 %).

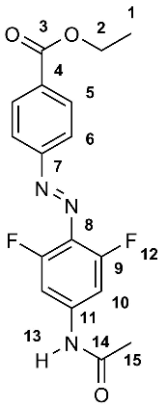

^{1}H-NMR (300 MHz, DMSO-d_6) δ [ppm] = 8.16-8.10 (m, 2 H, H_5), 7.99-7.87 (m, 2 H, H_6), 7.71-7.48 (m, 2 H, H_{12}), 7.27-7.05 (m, 1 H, H_{13}), 4.38-4.25 (m, 2 H, H_2), 2.12-2.02 (m, 3 H, H_{15}), 1.37-1.26 (m, 3 H, H_1).

^{19}F-NMR (100 MHz, DMSO-d_6) δ [ppm] = -117.88, -118.34.

MS (EI, 70 eV) *m/z* (%) 347.1 (100) $[M]^{+\cdot}$, 302.0 (15) $[M\text{-}C_2H_5O]^+$, 198.0 (62) $[C_8H_6F_2N_3O]^+$, 170.0 (52) $[C_8H_6F_2NO]^+$, 149.0 (57) $[C_9H_9O_2]^+$, 120.0 (33) $[C_7H_4O_2]^+$.

HRMS (EI, 70 eV) *m/z* calculated for $C_{17}H_{15}F_2N_3O_3$: 347.1081, found: 347.1079.

4'-Acetamido-4-carboxy-2',6'-difluoroazobenzene (58)

Ethyl-4'-acetamido-4-carboxy-2',6'-difluoroazobenzene **(57)** (0.38 g, 1.10 mmol) was dissolved in 5 mL ethanol and 5 mL 1 M aqueous NaOH and stirred for 10 hours at room temperature. The reaction mixture was acidified with 10 mL 1 M aqueous hydrochloric acid followed by extraction with 100 mL ethyl acetate. The organic layer was washed with 80 mL water and 80 mL brine. Evaporation of all solvents yielded the product as a red solid (yield: 0.35 g, quant.).

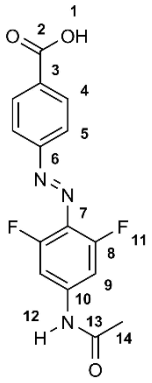

^{1}H-NMR (300 MHz, DMSO-d_6) δ [ppm] = 13.60 (s, br, 1 H, H_1), 8.14-7.87 (m, 2 H, H_4), 7.78-7.57 (m, 2 H, H_5), 7.54-7.36 (m, 3 H, H_9+H_{12}), 2.86-2.12 (m, 3 H, H_{14}).

^{13}C-NMR (75 MHz, DMSO-d_6) δ [ppm] = 169.6 (C_{13}), 162.3 (C_2), 155.2 (C_8), 142.8 (C_6), 130.5 (C_7), 127.8 (C_{10}), 127.3 (C_4), 124.5 (C_5), 119.1 (C_3), 109.6 (C_9), 14.1 (C_{14}).

^{19}F-NMR (100 MHz, DMSO-d_6) δ [ppm] = -117.8, -129.3.

4'-Acetamido-4-carboxy-2',6'-difluoroazobenzene-D-threoninol ("DFAB-Pep") (59)

4'-Acetamido-4-carboxy-2',6'-difluoroazobenzene **(58)** (0.35 g, 1.10 mmol), D-threoninol hydrochloride (0.19 g, 1.32 mmol), triethylamine (0.13 g, 1.32 mmol) and HBTU (0.46 g, 1.21 mmol) were mixed in 10 mL dry DMF. The reaction mixture was stirred for 24 hours at room temperature under argon atmosphere followed by filtering off all solid residuals. DMF was removed under reduced pressure and the product was isolated by column chromatography (silica, eluent: chloroform/methanol = 98/2) to yield a red solid (yield: 0.44 g, quant.).

TLC (SiO_2, eluent: chloroform/methanol = 10/1) R_f = 0.18.

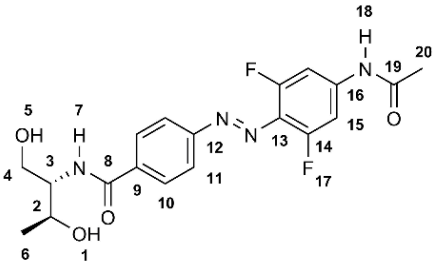

^{1}H-NMR (300 MHz, DMSO-d_6) δ [ppm] = 8.08-7.62 (m, 4 H, H_{10}+H_{11}), 7.54-7.00 (m, 2 H, H_{15}), 6.80-6.32 (m, 1 H, H_{18}), 4.61 (s, br, 1 H, H_7), 3.95-3.82 (m, 2 H, H_4), 3.61-3.50 (m, 2 H, H_3+H_5), 3.01-2.68 (m, 3 H, H_{20}), 2.12-1.83 (m, 2 H, H_1+H_2), 1.12-0.99 (m, 3 H, H_6).

^{19}F-NMR (100 MHz, DMSO-d_6) δ [ppm] = -117.3, -118.3.

MS (ESI, positive) *m/z* (%) 429.2 (100) $[M+Na]^+$, 387.1 (72) $[M-CH_2O+Na]^+$.

HRMS (ESI, positive) *m/z* calculated for $C_{19}H_{20}F_2N_4O_4Na$: 429.1345, found: 429.1349.

7.2.11 Synthesis of 2',6'-difluro-2,6-dimethylazobenzene-D-threoninol

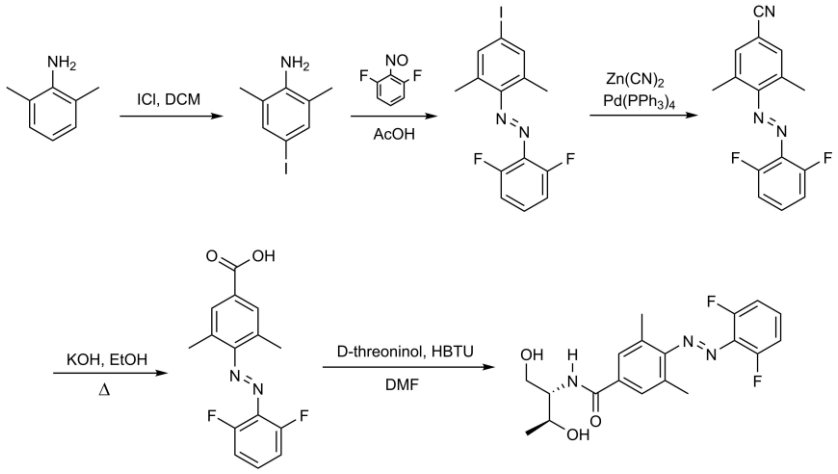

2,6-Dimethyl-4-iodoaniline (60)[256]

2,6-Dimethylaniline (20.0 g, 166 mmol) was mixed with $NaHCO_3$ (41.6 g, 248 mmol) and 230 mL methanol. ICl (29.4 g, 183 mmol) was dissolved in 180 mL dichloromethane and added dropwise to the reaction mixture followed by stirring for 16 hours at room temperature. The reaction mixture was quenched with 500 mL 2 % aqueous $Na_2S_2O_3$ solution, the organic layer was separated, dried over $MgSO_4$ and concentrated *in vacuo*. The product was isolated by column chromatography (silica, eluent: cyclohexane/ethyl acetate = 9/1) as a dark purple solid (yield: 39.78 g, 97 %).

^{1}H-NMR (500 MHz, $CDCl_3$) δ [ppm] = 7.24 (s, 2 H, H_4), 4.43 (s, br, 2 H, H_1), 2.13 (s, 6 H, H_6).

^{13}C-NMR (125 MHz, $CDCl_3$) δ [ppm] = 141.7 (C_2), 136.5 (C_4), 128.6 (C_3), 124.6 (C_5), 17.3 (C_6).

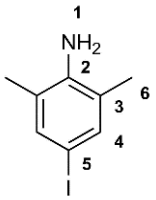

MS (ESI, positive) *m/z* (%) 248.0 (100) $[M+H]^+$.

HRMS (ESI, positive) *m/z* calculated for $C_8H_{11}IN$: 247.9931, found: 247.9925.

2',6'-Difluoro-2,6-dimethyl-4-iodoazobenzene (61)

2,6-Dimethyl-4-iodoaniline **(60)** (5.0 g, 20.2 mmol) and 2,6-difluoro-4-nitrosobenzene **(19)** (3.48 g, 24.3 mmol) were dissolved in 150 mL glacial acetic acid. The reaction mixture was stirred for 24 hours at room temperature, then 250 mL water was added and the mixture was neutralized with sodium carbonate. The resulting mixture was extracted twice with 500 mL ethyl acetate, the combined organic layers were washed subsequently with 250 mL water, 300 mL saturated sodium bicarbonate soltion and 200 mL brine. All solvents were removed *in vacuo* and the product was isolated by column chromatography (silica, eluent: cyclohexane/ethyl acetate = 19/1) as a red solid (yield: 1.61 g, 22 %).

^{1}H-NMR (300 MHz, $CDCl_3$) δ [ppm] = 7.42 (s, 2 H, H_2), 7.26-7.16 (m, 1 H, H_8), 6.97 (t, 2 H, $^{3}J_{7,8}$ = 8.5 Hz, H_7), 2.27 (s, 6H, H_{10}).

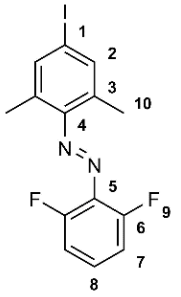

^{19}F-NMR: (100 MHz, $CDCl_3$) δ [ppm] = -116.9 (F_9), -122.4 (F_9').

^{13}C-NMR (75 MHz, $CDCl_3$) δ [ppm] = 156.8 (C_6), 153.4 (C_5), 150.6 (C_4), 137.7 (C_2), 133.3 (C_3), 130.0 (C_8), 112.3 (C_7), 95.2 (C_1), 18.4 (C_{10}).

MS (EI, 70 eV) *m/z* (%) 372.1 (98) $[M]^{+\cdot}$, 231.0 (100) $[M\text{-}CH_2I]^{+}$, 104.1 (44) $[C_8H_8]^{+}$.

HRMS (EI, 70 eV) *m/z* calculated for $C_{14}H_{10}F_2N_2I$ $[M\text{-}H]^{+\cdot}$: 370.9856, found: 370.9851.

4-Cyano-2',6'-difluoro-2,6-dimethylazobenzene (62)[257]

2',6'-Difluoro-2,6-dimethyl-4-iodoazobenzene **(61)** (1.0 g, 2.69 mmol), $Pd(PPh_3)_4$ (0.31 g, 0.27 mmol) and zinc cyanide (0.38 g, 3.22 mmol) were suspended in 10 mL dry DMF and heated at 90 °C for 16 hours. The reaction mixture was cooled to room temperature, poured into 20 mL 12 % aqueous ammonia solution and extracted with 150 mL ethyl acetate. The organic phase was washed with 50 mL saturated sodium bicarbonate solution and 50 mL brine, dried over $MgSO_4$ and all solvents were removed *in vacuo*. The product was isolated by silica gel chromatography (eluent: cyclohexane/ethyl acetate = 4/1) as a red solid (yield: 0.68 g, 93 %).

^{1}H-NMR (300 MHz, $CDCl_3$) δ [ppm] = 7.35-7.28 (m, 3 H, H_3+H_9), 7.03-6.95 (m, 2 H, H_8), 2.25 (s, 6 H, H_{11}).

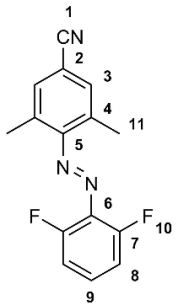

^{19}F-NMR: (100 MHz, $CDCl_3$) δ [ppm] = -116.9 (F_{10}), -122.0 (F_{10}').

^{13}C-NMR (75 MHz, $CDCl_3$) δ [ppm] = 156.9 (C_7), 154.3 (C_6), 153.4 (C_5), 132.3 (C_3), 131.3 (C_4), 131.0 (C_9), 118.3 (C_1), 112.4 (C_8), 111.5 (C_2), 18.0 (C_{11}).

MS (EI, 70 eV) *m/z* (%) 271.1 (84) $[M]^{+\cdot}$, 251.1 (10) $[M\text{-}HF]^{+}$, 208.1 (8) $[C_{14}H_{10}N_2]^{+}$, 183.1 (15) $[C_{11}H_9N_3]^{+}$, 158.1 (8) $[C_9H_8N_3]^{+}$, 141.1 (18) $[C_6H_3F_2N_2]^{+}$, 130.1 (100) $[C_9H_8N]^{+}$, 113.1 (24) $[C_6H_3F_2]^{+}$, 103.1 (19) $[C_8H_7]^{+}$.

HRMS (EI, 70 eV) *m/z* calculated for $C_{15}H_{11}F_2N_3$: 271.0921, found: 271.0918.

4-Carboxy-2',6'-difluoro-2,6-dimethylazobenzene (63)

4-Cyano-2',6'-difluoro-2,6-dimethylazobenzene **(62)** (0.25 g, 0.92 mmol) and potassium hydroxide (0.05 g, 0.92 mmol) were dissolved in 3 mL ethanol and the mixture was refluxed for 6 hours at 80 °C. The reaction mixture was cooled to room temperature, neutralized with 1 M aqueous hydrochloric acid and extracted with 50 mL ethyl acetate. The organic layer was

washed with 20 mL water and 20 mL brine, followed by evaporation of all solvents. The product was isolated by column chromatography (silica, eluent: chloroform/methanol = 19/1) as a red solid (yield: 0.32 g, quant.).

^{1}H-NMR (600 MHz, DMSO-d_6) δ [ppm] = 7.11 (s, br, 1 H, H_1), 7.75-7.69 (m, 1 H, H_{10}), 7.61-7.52 (m, 2 H, H_9), 2.33 (s, 6 H, H_{12}).

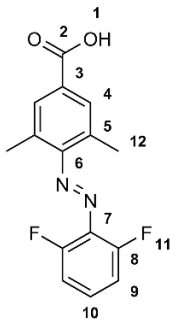

^{13}C-NMR (125 MHz, DMSO-d_6) δ [ppm] = 167.4 (C_2), 155.7 (C_8), 153.7 (C_6), 153.0 (C_7), 134.6 (C_3), 132.1 (C_4), 130.3 (C_5), 128.6 (C_{10}), 113.3 (C_9), 18.5 (C_{12}).

^{19}F-NMR: (125 MHz, $CDCl_3$) δ [ppm] = -118.7, -122.6, -126.4, 126.9.

MS (ESI, negative) *m/z* (%) 289.1 (100) $[M-H]^-$, 265.1 (78) $[C_{13}H_{11}F_2N_2O_2]^-$, 236.1 (51) $[C_{14}H_8N_2O_2]^-$, 221.1 (42) $[C_{13}H_5N_2O_2]^-$.

HRMS (ESI, negative) *m/z* calculated for $C_{15}H_{11}F_2N_2O_2$: 289.0794, found: 289.0780.

4-Carboxy-2‘,6‘-difluoro-2,6-dimethylazobenzene-D-threoninol (“DMDFAB”) (64)

4-Carboxy-2’,6’-difluoro-2,6-dimethylazobenzene **(63)** (0.10 g, 0.35 mmol), D-threoninol (0.04 g, 0.38 mmol) and HBTU (0.16 g, 0.41 mmol) were mixed in 5 mL DMF. The reaction mixture was stirred for 24 hours at room temperature under argon atmosphere followed by filtering off all solid residues and evaporation of DMF under reduced pressure. The product was isolated by column chromatography (silica, eluent: chloroform/methanol = 98/2) to yield a red solid (yield: 0.01 g, 8 %).

TLC (SiO_2, eluent: chloroform/methanol = 10/1) R_f = 0.31.

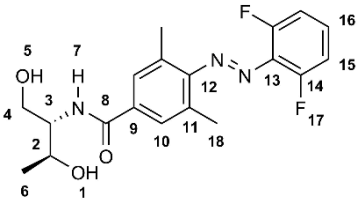

^{1}H-NMR (300 MHz, DMSO-d_6) δ [ppm] = 7.78-7.67 (m, 2 H, H_{10}), 7.60-7.48 (m, 1 H, H_{15}), 7.42-7.33 (m, 1 H, H_{15}’), 7.14-6.89 (m, 1 H, H_{16}), 4.60-4.51 (m, 2 H, H_3+H_7), 3.93-3.90 (m, 2 H, H_4), 3.62-3.42 (m, 3 H, H_1+H_2+H_5), 2.35 (s, 4 H, H_{18}), 1.97 (s, 2 H, H_{18}’), 1.07-1.01 (m, 3 H, H_6).

^{13}C-NMR (75 MHz, DMSO-d_6) δ [ppm] = 166.0 (C_8), 155.7 (C_{14}), 153.7 (C_{12}), 152.8 (C_{13}), 135.2 (C_9), 132.1 (C_{10}), 130.4 (C_{11}), 128.4 (C_{16}), 113.3 (C_{15}), 65.0 (C_2), 60.7 (C_4), 56.9 (C_3), 20.4 (C_6), 18.5 (C_{18}).

^{19}F-NMR (125 MHz, DMSO-d_6) δ [ppm] = -117.8, -122.4, -123.0, -127.0.

MS (ESI, positive) *m/z* (%) 378.2 (68) $[M+H]^+$, 400.1 (100) $[M+Na]^+$, 777.3 (64) $[2M+Na]^+$.

HRMS (ESI, positive) *m/z* calculated for $C_{19}H_{22}F_2N_3O_3$: 378.1624, found: 378.1634.

7.2.12 Synthesis of 2',6'-dichloroazobenzene-D-threoninol

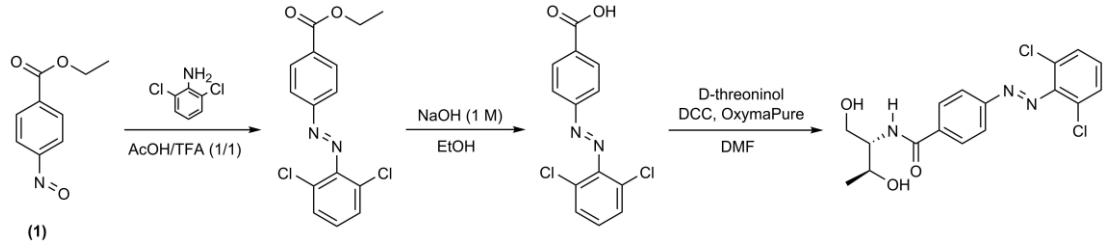

Ethyl-4-carboxy-2',6'-dichloroazobenzene (65)

Ethyl-4-nitrosobenzoate **(1)** (2.0 g, 11.2 mmol) and 2,6-dichloroaniline (2.17 g, 13.4 mmol) were dissolved in a mixture of 70 mL acetic acid and 50 mL trifluoroacetic acid and stirred for 24 hours at room temperature. 200 mL water was added, the resulting mixture was neutralized with sodium carbonate and extracted twice with 200 mL ethyl acetate. The combined organic layers were washed subsequently with 250 mL water, 250 mL saturated sodium bicarbonate solution and 200 mL brine. The organic layer was dried over $MgSO_4$ and all solvents were removed *in vacuo*. The product was isolated by column chromatography (silica, eluent: cyclohexane) as a red solid (yield: 1.20 g, 33 %).

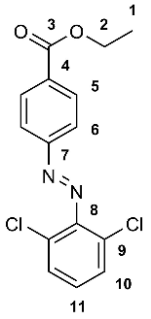

^{1}H-NMR (500 MHz, $CDCl_3$) δ [ppm] = 8.31-8.69 (m, 2 H, H_5), 7.67-8.19 (m, 5 H, H_6+H_{10}+H_{11}).

^{13}C-NMR (125 MHz, $CDCl_3$) δ [ppm] = 165.6 (C_3), 150.7 (C_7), 146.8 (C_8), 133.5 (C_5), 131.0 (C_{10}), 130.1 (C_{11}), 125.2 (C_4), 122.4 (C_9), 119.4 (C_6), 61.6 (C_2), 14.2 (C_1).

MS (EI, 70 eV) *m/z* (%) no target mass could be isolated.

4-Carboxy-2',6'-dichloroazobenzene (66)

Ethyl-4-carboxy-2',6'-dichloroazobenzene **(65)** (3.0 g, 9.28 mmol) was dissolved in 45 mL ethanol and 45 mL 1 M aqueous NaOH solution and stirred for 20 hours at room temperature. The reaction mixture was acidified with 60 mL 1 M aqueous hydrochloric acid and extracted twice with 200 mL ethyl acetate. The combined organic layers were washed with 200 mL water and 100 mL brine, followed by evaporation of all solvents. Column chromatography (silica, eluent: chloroform/methanol = 98/2) was performed to yield a red solid (yield: 0.86 g, 32 %).

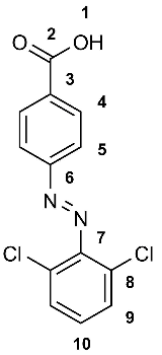

^{1}H-NMR (300 MHz, DMSO-d_6) δ [ppm] = 13.32 (s, 1 H, H_1), 8.21-8.17 (m, 2 H, H_4), 8.01-7.97 (m, 2 H, H_5), 7.67-7.65 (m, 2 H, H_9), 7.48-7.43 (m, 1 H, H_{10}).

^{13}C-NMR (75 MHz, DMSO-d_6) δ [ppm] = 166.49 (C_2), 153.83 (C_6), 147.39 (C_7), 134.26 (C_4), 130.83 (C_9), 130.20 (C_{10}), 129.59 (C_3), 125.55 (C_8), 122.71 (C_5).

MS (ESI, positive) *m/z* (%) 295.0 (5) $[M+Na]^+$, 225.2 (100) $[M-Cl_2+H]^+$.

HRMS (ESI, positive) *m/z* (%) calculated for $C_{13}H_8Cl_2N_2O_2$: 295.0036, found: 295.0027.

4-Carboxy-2‘,6‘-dichloroazobenzene-D-threoninol (“DCAB”) (67)

4-Carboxy-2’,6’-dichloroazobenzene **(66)** (0.10 g, 0.34 mmol), D-threoninol (0.04 g, 0.41 mmol), DCC (0.08 g, 0.37 mmol) and OxymaPure (0.05 g, 0.37 mmol) were mixed in 3.5 mL dry DMF. The reaction mixture was stirred for 24 hours at room temperature under argon atmosphere. All solids were filtered off and DMF was removed under reduced pressure. A small product fraction was isolated by preparative HPLC chromatography (C18, eluent: acetonitrile/water in different gradients) to yield a red solid (yield: 0.04 g, 31 %).

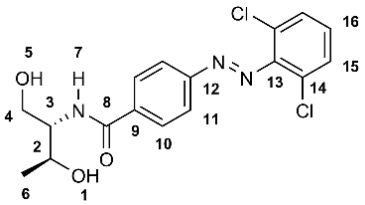

TLC (SiO_2, eluent: chloroform/methanol = 10/1) R_f = 0.26.

MS (ESI, positive) *m/z* (%) 787.1 (20) $[2M+Na]^+$, 404.0 (100) $[M+Na]^+$, 306.3 (15) $[C_{16}H_{15}N_2O_3+Na]^+$.

HRMS (ESI, positive) *m/z* calculated for $C_{17}H_{17}Cl_2N_3O_3Na$: 404.0539, found: 404.0541.

7.2.13 Synthesis of 2',6'-dimethoxyazobenzene-D-threoninol phosphoramidite

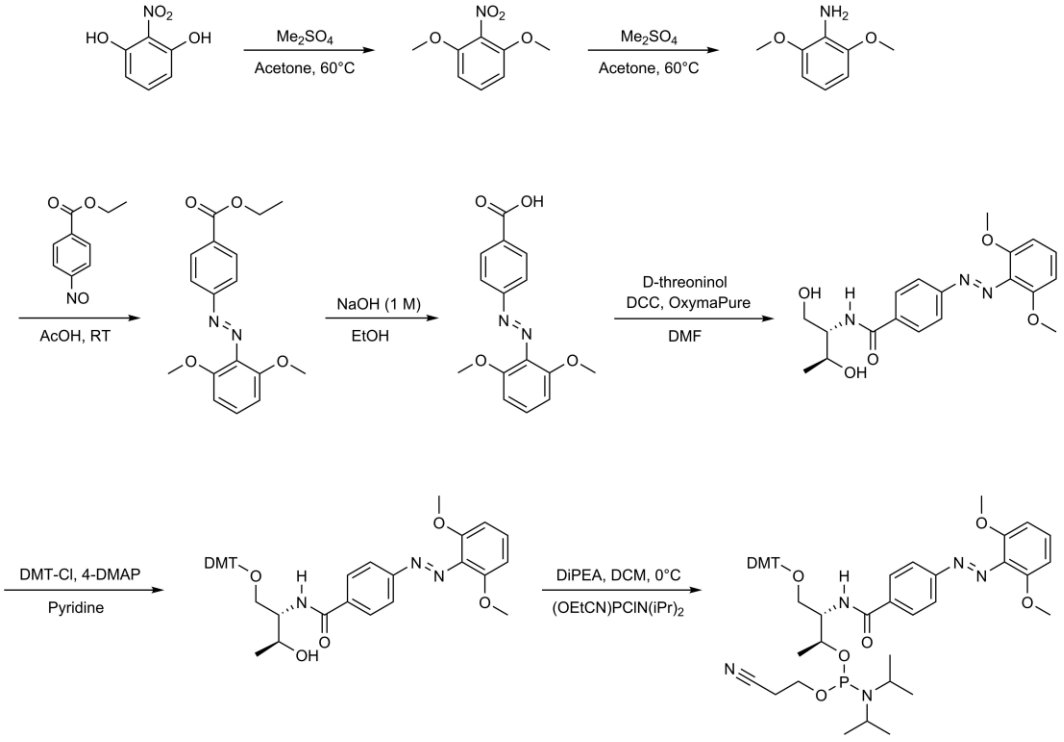

1,3-Dimethoxy-2-nitrobenzene (68)[258]

2-Nitroresorcinol (10.0 g, 64.5 mmol) and sodium carbonate (34.2 g, 322 mmol) were dissolved in 600 mL acetone. Dimethylsulfate (24.4 g, 193 mmol) was added dropwise and the reaction mixture was heated to 60 °C for 2.5 hours, then cooled down to room temperature and acetone was removed by distillation. The remaining aqueous layer was extracted three times with 500 mL dichloromethane. The combined organic layers were dried over $MgSO_4$ followed by removal of dichloromethane under reduced pressure. The remaining yellowish white solid was isolated as the product (yield: 11.58 g, 98 %).

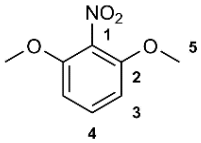

^{1}H-NMR (500 MHz, $CDCl_3$) δ [ppm] = 7.34 (t, 1 H, $^3J_{4,3}$ = 8.5 Hz, H_4), 6.63 (d, 2 H, $^3J_{3,4}$ = 8.5 Hz, H_3), 3.87 (s, 6 H, H_5).

^{13}C-NMR (166 MHz, $CDCl_3$) δ [ppm] = 151.9 (C_2), 131.1 (C_4), 131.1 (C_1), 104.5 (C_3), 56.5 (C_5).

MS (EI, 70 eV) *m/z* (%) 183.1 $[M]^{+\cdot}$, 136.0 (50) $[M\text{-}NO_2]^+$, 107.0 (46) $[C_7H_7O]^+$.

HRMS (EI, 70 eV) *m/z* calculated for $C_8H_9NO_4$: 183.0532, found: 183.0532.

1,3-Dimethoxyaniline (69)[258]

1,3-Dimethoxy-2-nitrobenzene **(68)** (7.5 g, 41.0 mmol) was dissolved in 200 mL glacial acetic acid, 200 mL ethanol and 100 mL water. Iron powder (13.7 g, 246 mmol) was added in small portions and the resulting mixture was heated to 90 °C for 20 hours under argon atmosphere.

The reaction mixture was cooled to room temperature, then extracted twice with 250 mL ethyl acetate. The combined organic layers were dried over $MgSO_4$, filtered and all volatiles were removed *in vacuo*. The resulting brownish white solid was isolated as the product (yield: 5.77 g, 92 %).

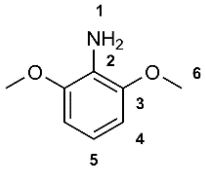

^{1}H-NMR (500 MHz, $CDCl_3$) δ [ppm] = 6.72-6.69 (m, 1 H, H_5), 6.55 (d, 2 H, $^3J_{4,5}$ = 8.3 Hz, H_4), 3.87 (s, 6 H, H_6), 3.84 (s, br, 2 H, H_1).

^{13}C-NMR (166 MHz, $CDCl_3$) δ [ppm] = 147.6 (C_3), 125.3 (C_2), 117.1 (C_5), 104.1 (C_4), 55.9 (C_6).

MS (ESI, positive) *m/z* (%) 182.1 (63) $[M+Na]^+$, 154.1 (100) $[M+H]^+$.

HRMS (ESI, positive) *m/z* calculated for $C_8H_{12}NO_2$: 154.0863, found: 154.0871.

Ethyl-4-carboxy-2‘,6‘-dimethoxyazobenzene (70)

1,3-Dimethoxyaniline **(69)** (5.0 g, 32.6 mmol) and ethyl-4-nitrosobenzoate (5.85 g, 32.6 mmol) were dissolved in 300 mL glacial acetic acid. The reaction mixture was stirred for 24 hours at room temperature, then neutralized with sodium carbonate and extracted two times with 300 mL ethyl acetate. The combined organic layers were washed subsequently with 300 mL water, 300 mL saturated sodium bicarbonate solution and 150 mL brine. The organic layer was dried over $MgSO_4$ and all volatiles were removed under reduced pressure. The product was isolated by column chromatography (silica, eluent: cyclohexane/ethyl acetate = 95/5) as a red solid (yield: 2.08 g, 20 %).

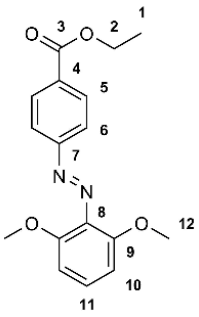

^{1}H-NMR (500 MHz, $CDCl_3$) δ [ppm] = 8.19-8.17 (m, 2 H, H_5), 7.92-7.90 (m, 2 H, H_6), 7.31 (t, 1 H, $^3J_{11,10}$ = 8.5 Hz, H_{11}), 6.70 (d, 2 H, $^3J_{10,11}$ = 8.4 Hz, H_{10}), 4.43 (q, 2 H, $^3J_{2,1}$ = 7.1 Hz, H_2), 3.86 (s, 6 H, H_{12}), 1.43 (t, 3 H, $^3J_{1,2}$ = 7.1 Hz, H_1).

^{13}C-NMR (166 MHz, $CDCl_3$) δ [ppm] = 166.1 (C_3), 155.7 (C_7), 152.9 (C_9), 133.4 (C_8), 131.9 (C_4), 130.9 (C_{11}), 130.5 (C_5), 122.3 (C_6), 105.1 (C_{10}), 61.2 (C_2), 56.5 (C_{12}), 14.3 (C_1).

MS (ESI, positive) *m/z* (%) 337.1 (81) $[M+Na]^+$, 315.1 (100) $[M+H]^+$.

HRMS (EI, 70 eV) *m/z* calculated for $C_{17}H_{19}N_2O_4$: 315.1339, found: 315.1363.

4-Carboxy-2‘,6‘-dimethoxyazobenzene (71)

Ethyl-4-carboxy-2’,6’-dimethoxyazobenzene **(70)** (1.67 g, 5.31 mmol) was dissolved in 25 mL 1 M aqueous NaOH and 25 mL ethanol. The reaction mixture was stirred for 3 hours at room temperature, then 30 mL 1 M aqueous hydrochloric acid was added and the mixture was extracted twice with

150 mL ethyl acetate. The combined organic layers were washed with 200 mL brine and dried over $MgSO_4$. All solvents were removed under reduced pressure to yield the product as a red solid (yield: 1.50 g, quant.).

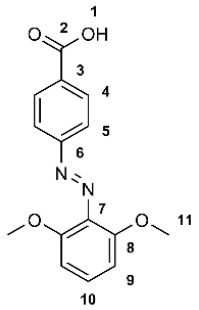

^{1}H-NMR (500 MHz, DMSO-d_6) δ [ppm] = 10.17 (s, br, 1 H, H_1), 8.13-8.11 (m, 2 H, H_4), 7.83-7.80 (m, 2 H, H_5), 7.36-7.33 (m, 1 H, H_{10}), 6.83-6.80 (m, 2 H, H_9), 3.76 (s, 6 H, H_{11}).

^{13}C-NMR (125 MHz, DMSO-d_6) δ [ppm] = 167.2 (C_2), 155.4 (C_6), 152.3 (C_8), 133.3 (C_7), 133.0 (C_3), 131.0 (C_{10}), 130.9 (C_4), 122.5 (C_5), 105.7 (C_9), 56.7 (C_{11}).

MS (ESI, positive) *m/z* (%) 287.1 (100) $[M+H]^+$.

HRMS (ESI, positive) *m/z* calculated for $C_{15}H_{15}N_2O_4$: 287.1032, found: 287.1032.

4-Carboxy-2‘,6‘-dimethoxyazobenzene-D-threoninol (“DOAB”) (72)

4-Carboxy-2’,6’-dimethoxyazobenzene **(71)** (0.70 g, 2.45 mmol), D-threoninol (0.31 g, 2.93 mmol), DCC (0.55 g, 2.69 mmol) and OxymaPure (0.38 g, 2.69 mmol) were dissolved in 25 mL dry DMF. The reaction mixture was stirred for 24 hours at room temperature under argon atmosphere. All solid residues were filtered off followed by removal of DMF *in vacuo*. The crude product was purified by column chromatography (silica, eluent: chloroform/methanol = 98/2) to yield a red solid (yield: 0.81 g, 88 %).

TLC (SiO_2, eluent: chloroform/methanol = 10/1) R_f = 0.28.

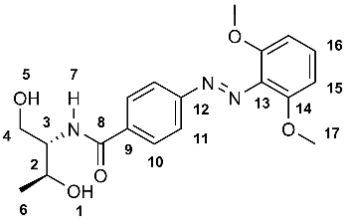

^{1}H-NMR (500 MHz, DMSO-d_6) δ [ppm] = 7.90-8.30 (m, 2 H, H_{10}), 7.71-7.82 (m, 2 H, H_{11}), 7.06-7.35 (m, 1 H, H_{16}), 6.55-6.85 (m, 2 H, H_{15}), 4.53-4.66 (m, 1 H, H_3), 3.77-3.95 (m, 1 H, H_2), 3.75 (s, 3 H, H_1+H_5+H_7), 3.42-3.65 (m, 2 H, H_4), 3.35 (s, 6 H, H_{17}), 1.01-1.22 (m, 3 H, H_6).

^{13}C-NMR (125 MHz, DMSO-d_6) δ [ppm] = 166.4 (C_8), 154.3 (C_{12}), 152.2 (C_{12}’), 148.1 (C_{16}), 137.2 (C_{14}), 133.4 (C_{14}’), 130.6 (C_{13}), 129.0 (C_{13}’), 128.1 (C_{10}), 122.3 (C_{11}), 117.8 (C_9), 105.7 (C_{15}), 104.8 (C_{15}’), 79.6 (C_2), 65.4 (C_4), 60.9 (C_4’), 57.4 (C_3), 56.7 (C_{17}), 56.1 (C_{17}’), 20.7 (C_6).

MS (ESI, positive) *m/z* (%) 769.3 (50) $[2M+Na]^+$, 396.2 (65) $[M+Na]^+$, 374.2 (100) $[M+H]^+$.

HRMS (ESI, positive) *m/z* calculated for $C_{19}H_{23}N_3O_5H$: 374.1710, found: 374.1697.

DMT-protected 4-carboxy-2‘,6‘-dimethoxyazobenzene-D-threoninol (73)

4-Carboxy-2’,6’-dimethoxyazobenzene-D-threoninol **(72)** (3.20 g, 8.57 mmol) and 4-DMAP (0.12 g, 0.86 mmol) were dissolved in 60 mL dry pyridine under argon atmosphere and cooled to 0 °C. DMT-chloride (3.48 g, 10.3 mmol) was dissolved in 30 mL dry pyridine and added

dropwise to the reaction mixture under argon atmosphere. The mixture was warmed up to room temperature and stirring was continued for 24 hours under argon atmosphere. All solvents were removed *in vacuo* followed by purification *via* column chromatography (silica, eluent: cyclohexane/ethyl acetate = 1/1 with 3 % triethylamine) to yield the product as a red solid (yield: 1.91 g, 32 %).

^{1}H-NMR (500 MHz, DMSO-d_6) δ [ppm] = 8.20-7.58 (m, 4 H, H_9+H_{19}), 7.42-7.06 (m, 9 H, H_{10}+H_{20}+H_{21}+H_{23}), 6.89-6.80 (m, 6 H, H_{14}+H_{24}), 6.57-6.55 (m, 1 H, H_{15}), 4.62-4.50 (m, 1 H, H_6), 4.20-3.98 (m, 2 H, H_4), 3.76 (s, 3 H, H_{16}), 3.71 (s, 6 H, H_{26}), 3.64 (s, 3 H, H_{16}'), 3.27-3.16 (m, 1 H, Hx), 3.08-2.88 (m, 1 H, Hx), 1.77-1.58 (m, 1 H, Hx), 1.06-0.97 (m, 3 H, Hx).

^{13}C-NMR (125 MHz, DMSO-d_6) δ [ppm] = 171.1 (C_7), 163.2 (C_{25}), 159.1 (C_{11}), 156.9 (C_{13}), 152.8 (C_{22}), 150.3 (C_{18}), 141.9 (C_{12}), 141.1 (C_{15}), 138.5 (C_9), 137.2 (C_{23}), 134.9 (C_{20}), 133.8 (C_{19}), 132.9 (C_{10}), 122.6 (C_8), 118.3 (C_{24}), 110.4 (C_{14}), 90.4 (C_{17}), 70.5 (C_4), 68.2 (C_2), 61.4 (C_{16}), 60.8 (C_{16}'), 60.2 (C_{26}), 52.7 (C_3), 25.6 (C_5).

MS (ESI, positive) *m/z* (%) 1373.6 (20) $[2M+Na]^+$, 698.3 (56) $[M+Na]^+$.

HRMS (ESI, positive) *m/z* calculated for $C_{40}H_{41}N_3O_7Na$: 698.2837, found: 698.2820.

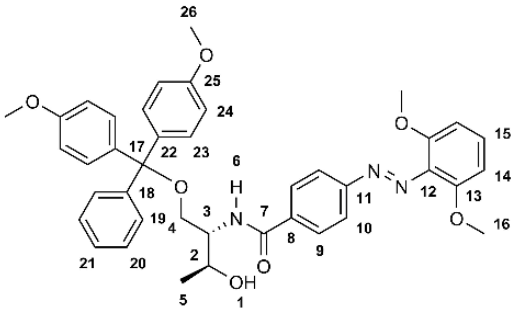

DMT-protected 4-carboxy-2',6'-dimethoxyazobenzene-D-threoninol phosphoramidite (74)

DMT-protected 4-carboxy-2',6'-dimethoxyazobenzene-D-threoninol **(73)** (0.50 g, 0.74 mmol) was dissolved in 7.5 mL dry dichloromethane under argon atmosphere and cooled to 0 °C. DIPEA (0.12 g, 0.89 mmol) was added under argon atmosphere, followed by addition of 2-cyanoethyl-*N*,*N*-diisopropylchlorophosphoramidite (0.21 g, 0.89 mmol). The reaction mixture was stirred for 15 minutes at 0 °C, then warmed up to room temperature and stirring was continued for 1 hour at room temperature under argon atmosphere. All solvents were removed *in vacuo* and the product was isolated by column chromatography (silica, eluent: cyclohexane/ethyl acetate = 1/1 with 3 % triethylamine) as a red foamy solid (yield: 0.50 g, 77 %).

^{31}P-NMR (125 MHz, CD_2Cl_2) δ [ppm] = 148.6, 147.9, 147.1.

MS (ESI, positive) *m/z* (%) 892.4 (1) $[M+Na]^+$, 876.4 (1) $[M+H]^+$, 303.1 (100) $[DMT]^+$.

HRMS (ESI, positive) *m/z* calculated for $C_{49}H_{59}N_5O_8P$: 876.4096, found: 876.4094.

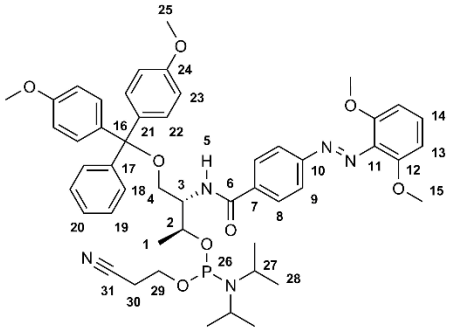

7.2.14 Synthesis of substituted arylazopyrazoles (“arylazopyrazole-library”)

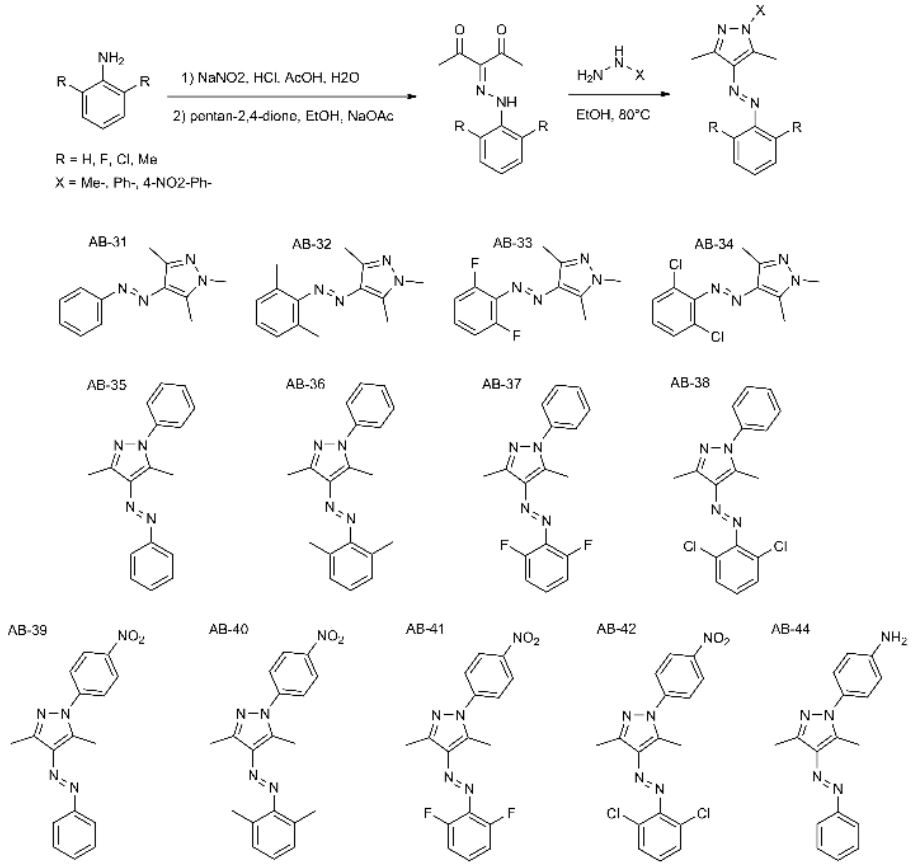

3-(2-Phenylhydrazono)pentane-2,4-dione (75)[136]

A solution of aniline (3.00 g, 32.2 mmol) in 40 mL glacial acetic acid and 8 mL 12 % aqueous hydrochloric acid was prepared. $NaNO_2$ (2.67 g, 38.6 mmol) was dissolved in 12 mL water and the solution was added dropwise to the prepared solution at 0 °C and stirred for 1 hour at 0 °C. A suspension of 2,4-pentanedione (4.19 g, 41.5 mmol) and NaOAc (7.92 g, 96.6 mmol) in 35 mL ethanol and 20 mL water was prepared and the reaction mixture was added dropwise to the suspension, forming a yellow precipitate. The resulting mixture was stirred for 1 hour at room temperature, the yellow precipitate was collected by filtration and rinsed with 20 mL of a 1:1 mixture of water and ethanol followed by rinsing with 10 mL cyclohexane. All solvents were removed *in vacuo* to yield a bright yellow solid as the product (5.52 g, 84 %).

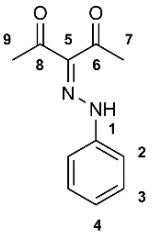

^{1}H-NMR (300 MHz, $CDCl_3$) δ [ppm] = 14.63 (s, br, 1 H, H_1), 7.32 (m, 4 H, H_2+H_3), 7.12-7.09 (m, 1 H, H_4), 2.51 (s, 3 H, H_7), 2.39 (s, 3 H, H_9).

^{13}C-NMR (75 MHz, $CDCl_3$) δ [ppm] = 197.5 (C_6), 196.7 (C_8), 141.1 (C_1), 132.8 (C_4), 129.3 (C_3), 125.5 (C_2), 115.9 (C_5), 31.3 (C_7), 26.2 (C_9).

MS (ESI, positive) *m/z* (%) 205.1 (100) $[M+H]^+$, 187.1 (27) $[C_{11}H_{11}N_2O]^+$, 162.1 (77) $[C_9H_9N_2O+H]^+$.

HRMS (ESI, positive) *m/z* calculated for C11H12N2O2H: 205.0972, found: 205.0965.

3-(2-(2,6-Dimethylphenyl)hydrazono)pentane-2,4-dione (76)

A solution of 2,6-dimethylaniline (3.90 g, 32.2 mmol) in 40 mL glacial acetic acid and 8 mL 12 % aqueous hydrochloric acid was prepared. $NaNO_2$ (2.67 g, 38.6 mmol) was dissolved in 12 mL water and added dropwise to the prepared solution at 0 °C, followed by stirring for 1 hour at 0 °C. A suspension of 2,4-pentanedione (4.19 g, 41.5 mmol) and NaOAc (7.92 g, 96.6 mmol) in 35 mL ethanol and 20 mL water was prepared and the reaction mixture was added dropwise to the suspension, forming a bright red solution. The resulting solution was stirred for 1 hour at room temperature and extracted twice with 100 mL ethyl acetate. The combined organic layers were washed with 100 mL water and 100 mL brine, dried over $MgSO_4$, followed by filtering off all solids and removal of ethyl acetate under reduced pressure. The product was isolated as a bright yellow solid (5.12 g, 68 %).

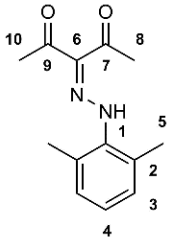

^{1}H-NMR (500 MHz, $CDCl_3$) δ [ppm] = 14.96 (s, br, 1 H, H_1), 7.12-7.06 (m, 3 H, H_3+H_4), 2.62 (s, 3 H, H_8), 2.45 (s, 6 H, H_5), 2.40 (s, 3 H, H_{10}).

^{13}C-NMR (125 MHz, $CDCl_3$) δ [ppm] = 197.7 (C_7), 197.2 (C_9), 138.0 (C_1), 133.6 (C_6), 129.8 (C_2), 129.7 (C_4), 126.4 (C_3), 31.6 (C_8), 27.0 (C_{10}), 19.5 (C_5).

MS (ESI, positive) *m/z* (%) 233.1 (100) $[M+H]^+$, 121.1 (39) $[C_8H_{11}N]^+$.

HRMS (EI, 70 eV) *m/z* calculated for $C_{13}H_{17}N_2O_2$: 233.1285, found: 233.1291.

3-(2-(2,6-Dichlorophenyl)hydrazono)pentane-2,4-dione (77)

A solution of 2,6-dichloroaniline (5.22 g, 32.2 mmol) in 40 mL glacial acetic acid and 8 mL 12 % aqueous hydrochloric acid was prepared. $NaNO_2$ (2.67 g, 38.6 mmol) was dissolved in 12 mL water, added dropwise to the prepared solution at 0 °C and stirred for 1 hour at 0 °C. A suspension of 2,4-pentanedione (4.19 g, 41.5 mmol) and NaOAc (7.92 g, 96.6 mmol) in 35 mL ethanol and 20 mL water was prepared and the reaction mixture was added dropwise to the suspension, forming a yellow precipitate. The resulting mixture was stirred for 1 hour at room temperature, the yellow precipitate was collected by filtration and rinsed with 20 mL of a 1:1-mixture of water and ethanol followed by 10 mL cyclohexane. All solvents were removed *in vacuo* to yield a yellow solid (4.84 g, 55 %).

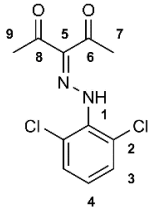

^{1}H-NMR (300 MHz, $CDCl_3$) δ [ppm] = 14.53 (s, br, 1 H, H_1), 7.39 (d, 2 H, $^3J_{3,4}$ = 8.1 Hz, H_3), 7.12 (m, 1 H, H_4), 2.62 (s, 3 H, H_7), 2.43 (s, 3 H, H_9).

^{13}C-NMR (75 MHz, $CDCl_3$) δ [ppm] = 198.1 (C_6), 197.4 (C_8), 135.3 (C_5), 134.4 (C_1), 129.6 (C_3), 127.4 (C_4), 126.6 (C_2), 31.6 (C_7), 26.7 (C_9).

MS (ESI, positive) *m/z* (%) 301.1 (55) $[M+Na]^+$, 273.1 (43) $[M+H]^+$, 160.9 (100) $[C_6H_5Cl_2N]^+$.

HRMS (ESI, positive) *m/z* calculated for $C_{11}H_{10}Cl_2N_2O_2H$: 273.0192, found: 273.0183.

3-(2-(2,6-Difluorophenyl)hydrazono)pentane-2,4-dione (78)

A solution of 2,6-difluoroaniline (4.16 g, 32.2 mmol) in 40 mL glacial acetic acid and 8 mL 12 % aqueous hydrochloric acid was prepared. $NaNO_2$ (2.67 g, 38.6 mmol) was dissolved in 12 mL water and the solution was added dropwise to the prepared solution at 0 °C, followed by stirring for 1 hour at 0 °C. A suspension of 2,4-pentanedione (4.19 g, 41.5 mmol) and NaOAc (7.92 g, 96.6 mmol) in 35 mL ethanol and 20 mL water was prepared and the reaction mixture was added dropwise to the suspension, forming a yellow precipitate. The resulti-ng mixture was stirred for 1 hour at room temperature, the yellow precipitate was collected by filtration and rinsed with 20 mL of a 1:1-mixture of water and ethanol followed by 10 mL cyclohexane. All solvents were removed *in vacuo* to yield a bright orange solid (6.06 g, 78 %).

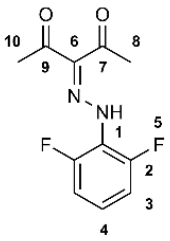

^{1}H-NMR (300 MHz, $CDCl_3$) δ [ppm] = 14.34 (s, br, 1 H, H_1), 7.07-6.89 (m, 3 H, H_3+H_4), 2.53 (s, 3 H, H_8), 2.35 (s, 3 H, H_{10}).

^{19}F-NMR (162 MHz, $CDCl_3$) δ [ppm] = -124.6 (F_5).

^{13}C-NMR (75 MHz, $CDCl_3$) δ [ppm] = 197.7 (C_7), 197.1 (C_9), 155.5 (C_6), 152.1 (C_2), 134.7 (C_1), 125.1 (C_4), 112.3 (C_3), 31.2 (C_{10}), 26.0 (C_8).

MS (ESI, positive) *m/z* (%) 241.1 (79) $[M+H]^+$, 203.9 (51) $[C_{11}H_{12}N_2O_2]^+$.

HRMS (ESI, positive) *m/z* calculated for $C_{11}H_{10}F_2N_2O_2H$: 241.0783, found: 241.0777.

(*E*)-1,3,5-Trimethyl-4-(phenyldiazenyl)-1*H*-pyrazole (79)[136]

N-Methylhydrazine (1.00 g, 4.90 mmol) was added dropwise to a solution of 3-(2-phenylhydrazono)pentane-2,4-dione **(75)** (1.00 g, 4.90 mmol) in 25 mL ethanol. The reaction mixture was refluxed for 3 hours at 80 °C, cooled to room temperature and all solvents were removed *in vacuo*. The product was isolated as the remaining bright yellow solid (0.93 g, 89 %).

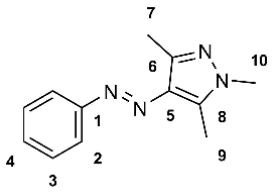

^{1}H-NMR (300 MHz, $CDCl_3$) δ [ppm] = 7.80-7.76 (m, 2 H, H_3), 7.48-7.42 (m, 2 H, H_2), 7.38-7.33 (m, 1 H, H_4), 3.75 (s, 3 H, H_{10}), 2.56 (s, 3 H, H_9), 2.51 (s, 3 H, H_7).

^{13}C-NMR (75 MHz, $CDCl_3$) δ [ppm] = 153.2 (C_1), 142.0 (C_8), 138.4 (C_5), 134.7 (C_6), 128.9 (C_4), 128.5 (C_3), 121.4 (C_2), 35.6 (C_{10}), 13.5 (C_9), 9.6 (C_7).

MS (EI, 70 eV) *m/z* (%) 214.1 (90) $[M]^{+\cdot}$, 137.1 (100) $[M-C_6H_5]^+$, 109.1 (78) $[M-C_6H_5N_2]^+$.

HRMS (EI, 70 eV) *m/z* calculated for $C_{12}H_{14}N_4$: 214.1218, found: 214.1223.

(*E*)-1,3,5-Trimethyl-4-((2,6-dimethylphenyl)diazenyl)-1*H*-pyrazole (80)

N-Methylhydrazine (0.26 mL, 5.00 mmol) was added dropwise to a solution of 3-(2-(2,6-dimethylphenyl)hydrazono)pentane-2,4-dione **(76)** (1.16 g, 5.00 mmol) in 25 mL ethanol. The

reaction mixture was refluxed for 3 hours at 80 °C, cooled to room temperature and all solvents were removed *in vacuo*. The product was isolated as the remaining bright yellow solid (1.12 g, 93 %).

^{1}H-NMR (300 MHz, $CDCl_3$) δ [ppm] = 7.02-6.98 (m, 3 H, H_3+H_4), 3.69 (s, 3 H, H_{11}), 2.45 (s, 3 H, H_{10}), 2.39 (s, 3 H, H_8), 2.26 (s, 6 H, H_5).

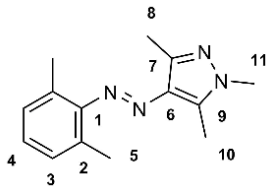

^{13}C-NMR (75 MHz, $CDCl_3$) δ [ppm] = 151.5 (C_7), 141.3 (C_1), 138.4 (C_6), 135.4 (C_9), 130.0 (C_3), 128.7 (C_2), 126.7 (C_4), 35.5 (C_{11}), 18.9 (C_5), 13.6 (C_{10}), 9.5 (C_8).

MS (EI, 70 eV) *m/z* (%) 242.2 (84) $[M]^{+\cdot}$, 227.1 (16) $[M\text{-}CH_3]^+$, 213.1 (37) $[M\text{-}CH_2N]^{+\cdot}$, 199.1 (34) $[M\text{-}CH_2N_2]^+$, 137.1 (100) $[C_6H_9N_4]^+$, 109.1 (98) $[C_6H_9N_2]^+$.

HRMS (EI, 70 eV) *m/z* calculated for $C_{14}H_{18}N_4$: 242.1531, found: 242.1530.

(*E*)-1,3,5-Trimethyl-4-((2,6-dichlorophenyl)diazenyl)-1*H*-pyrazole (81)

N-Methylhydrazine (0.26 mL, 5.00 mmol) was added dropwise to a solution of 3-(2-(2,6-dichlorophenyl)hydrazono)pentane-2,4-dione **(77)** (1.37 g, 5.00 mmol) in 25 mL ethanol. The reaction mixture was refluxed for 3 hours at 80 °C, cooled to room temperature and all solvents were removed *in vacuo*. The product was isolated as the remaining bright yellow solid (0.84 g, 60 %).

^{1}H-NMR (300 MHz, $CDCl_3$) δ [ppm] = 7.22-7.19 (m, 2 H, H_3), 6.97-6.92 (m, 1 H, H_4), 3.63 (s, 3 H, H_{10}), 2.40 (s, 3 H, H_9), 2.33 (s, 3 H, H_7).

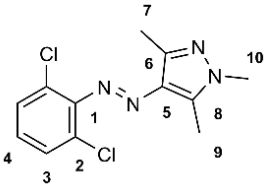

^{13}C-NMR (75 MHz, $CDCl_3$) δ [ppm] = 176.1 (C_6), 148.3 (C_1), 142.4 (C_5), 139.8 (C_8), 135.4 (C_3), 128.6 (C_4), 127.1 (C_2), 35.6 (C_{10}), 13.3 (C_9), 9.5 (C_7).

MS (EI, 70 eV) *m/z* (%) 282.0 (16) $[M]^{+\cdot}$, 247.1 (16) $[M\text{-}Cl]^+$, 161.0 (100) $[C_5H_3Cl_2N_2]^+$, 137.1 (45) $[M\text{-}C_6H_3Cl_2]^+$, 109.1 (30) $[C_6H_9N_2]^+$, 77.1 (73) $[C_6H_5]^+$.

HRMS (EI, 70 eV) *m/z* calculated for $C_{12}H_{12}Cl_2N_4$: 282.0439, found: 282.0439.

(*E*)-1,3,5-Trimethyl-4-((2,6-difluorophenyl)diazenyl)-1*H*-pyrazole (82)

N-Methylhydrazine (0.26 mL, 5.00 mmol) was added dropwise to a solution of 3-(2-(2,6-difluorophenyl)hydrazono)pentane-2,4-dione **(78)** (1.20 g, 5.00 mmol) in 25 mL ethanol. The reaction mixture was refluxed for 3 hours at 80 °C, cooled to room temperature and all solvents were removed *in vacuo*. The product was isolated as the remaining bright orange solid (yield: 0.87 g, 70 %).

^{1}H-NMR (300 MHz, $CDCl_3$) δ [ppm] = 7.22-7.11 (m, 1 H, H_4), 6.99-6.90 (m, 2 H, H_3), 3.74 (s, 3 H, H_{11}), 2.51 (s, 3 H, H_{10}), 2.45 (s, 3 H, H_8).

^{19}F-NMR (100 MHz, $CDCl_3$) δ [ppm] = -123.4 (F_5).

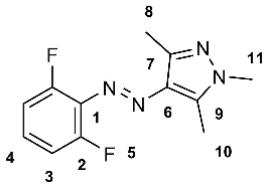

^{13}C-NMR (75 MHz, $CDCl_3$) δ [ppm] = 157.1 (C_2), 153.7 (C_7), 142.0 (C_1), 139.4 (C_8), 136.2 (C_9), 127.9 (C_4), 112.0 (C_3), 35.6 (C_{11}), 13.4 (C_{10}), 9.4 (C_8).

MS (EI, 70 eV) *m/z* (%) 250.1 (100) $[M]^{+\cdot}$, 137.1 (72) $[M\text{-}C_6H_3F_2]^+$, 109.1 (69) $[M\text{-}C_6H_3F_2N_2]^+$.

HRMS (EI, 70 eV) *m/z* calculated for $C_{12}H_{12}F_2N_4$: 250.1030, found: 250.1032.

(*E*)-1-Phenyl-3,5-dimethyl-4-(phenyldiazenyl)-1*H*-pyrazole (83)

N-Phenylhydrazine (0.46 mL, 4.90 mmol) was added dropwise to a solution of 3-(2-phenylhydrazono)pentane-2,4-dione **(75)** (1.00 g, 4.90 mmol) in 25 mL ethanol. The reaction mixture was refluxed for 3 hours at 80 °C, cooled to room temperature and all solvents were removed *in vacuo*. The product was isolated as the remaining bright orange solid (1.31 g, 97 %).

^{1}H-NMR (300 MHz, $CDCl_3$) δ [ppm] = 7.75-7.71 (m, 2 H, H_{11}), 7.42-7.26 (m, 8 H, H_2+H_3+H_4+H_{12}+H_{13}), 2.55 (s, 3 H, H_7), 2.51 (s, 3 H, H_9).

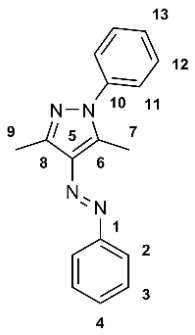

^{13}C-NMR (75 MHz, $CDCl_3$) δ [ppm] = 153.2 (C_8), 143.5 (C_1), 138.7 (C_{10}), 135.8 (C_5), 129.2 (C_6), 128.9 (C_3), 128.6 (C_{12}), 127.7 (C_4+C_{11}), 124.5 (C_{13}), 121.5 (C_2), 13.7 (C_9), 11.0 (C_7).

MS (EI, 70 eV) *m/z* (%) 276.2 (100) $[M]^{+\cdot}$, 199.1 (72) $[M\text{-}C_6H_5]^+$, 171.1 (53) $[M\text{-}C_6H_5N_2]^+$, 108.1 (70) $[C_5H_6N_3]^+$, 77.1 (73) $[C_6H_5]^+$.

HRMS (EI, 70 eV) *m/z* calculated for $C_{17}H_{16}N_4$: 276.1375, found: 276.1375.

(*E*)-1-Phenyl-3,5-dimethyl-4-((2,6-dimethylphenyl)diazenyl)-1*H*-pyrazole (84)

N-Phenylhydrazine (0.49 mL, 5.00 mmol) was added dropwise to a solution of 3-(2-(2,6-dimethylphenyl)hydrazono)pentane-2,4-dione **(76)** (1.16 g, 5.00 mmol) in 25 mL ethanol. The reaction mixture was refluxed for 3 hours at 80 °C, cooled to room temperature and all solvents were removed *in vacuo*. The product was isolated as the remaining bright orange solid (1.42 g, 93 %).

^{1}H-NMR (300 MHz, $CDCl_3$) δ [ppm] = 7.53-7.51 (m, 4 H, H_{12}+H_{13}), 7.46-7.41 (m, 1 H, H_4), 7.15-7.12 (m, 3 H, H_3+H_{14}), 2.64 (s, 3 H, H_8), 2.60 (s, 3 H, H_{10}), 2.42 (s, 6 H, H_5).

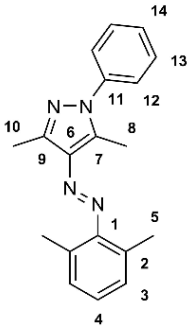

^{13}C-NMR (75 MHz, $CDCl_3$) δ [ppm] = 151.5 (C_9), 142.8 (C_1), 138.7 (C_{11}), 136.4 (C_6), 130.2 (C_7), 128.9 (C_3), 128.8 (C_{13}), 127.8 (C_2), 127.0 (C_4), 124.6 (C_{14}), 119.8 (C_{12}), 19.0 (C_5), 13.9 (C_{10}), 10.9 (C_8).

MS (EI, 70 eV) *m/z* (%) 304.2 (30) $[M]^{+\cdot}$, 275.1 (17) $[M\text{-}C_2H_5]^+$, 199.1 (28) $[M\text{-}C_8H_9]^+$, 187.1 (45) $[M\text{-}C_8H_7N]^+$, 171.1 (44) $[M\text{-}C_8H_9N_2]^+$, 137.1 (82) $[C_6H_9N_4]^+$, 108.1 (100) $[C_5H_6N_3]^+$, 105.1 (52) $[C_8H_9]^+$, 77.1 (98) $[C_6H_5]^+$.

HRMS (EI, 70 eV) *m/z* calculated for $C_{19}H_{20}N_4$: 304.1688, found: 304.1687.

(*E*)-1-Phenyl-3,5-dimethyl-4-((2,6-dichlorophenyl)diazenyl)-1*H*-pyrazole (85)

N-Phenylhydrazine (0.49 mL, 5.00 mmol) was added dropwise to a solution of 3-(2-(2,6-dichlorophenyl)hydrazono)pentane-2,4-dione **(77)** (1.37 g, 5.00 mmol) in 25 mL ethanol. The reaction mixture was refluxed for 3 hours at 80 °C, cooled to room temperature and all solvents were removed *in vacuo*. The product was isolated as the remaining bright orange solid (1.22 g, 71 %).

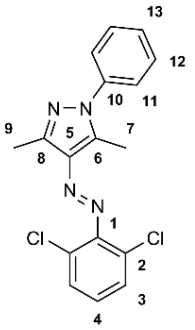

^{1}H-NMR (300 MHz, $CDCl_3$) δ [ppm] = 7.40-7.36 (m, 3 H, H_4+H_{11}), 7.34-7.29 (m, 1 H, H_{13}), 7.14-7.07 (m, 1 H, H_3), 7.04-6.98 (m, 1 H, H_3), 6.80-6.57 (m, 2 H, H_{12}), 2.52 (s, 2 H, H_7), 2.48 (s, 2 H, H_9), 1.93 (s, 1 H, H_7), 1.90 (s, 1 H, H_9).

^{13}C-NMR (75 MHz, $CDCl_3$) δ [ppm] = 148.4 (C_8), 143.7 (C_1), 140.3 (C_{10}), 138.4 (C_5), 128.9 (C_6), 128.7 (C_6'), 128.0 (C_3), 127.3 (C_{12}), 124.6 (C_4), 120.9 (C_{13}), 114.8 (C_{11}), 113.2 (C_2), 112.1 (C_2'), 20.5 (C_7), 13.6 (C_7'), 10.9 (C_9).

MS (EI, 70 eV) *m/z* (%) 344.1 (4) $[M]^{+\cdot}$, 309.1 (6) $[M\text{-}Cl]^+$, 199.1 (8) $[M\text{-}C_6H_3Cl_2]^+$, 171.1 (32) $[M\text{-}C_6H_3F_2N_2]^+$, 108.1 (100) $[C_5H_6N_3]^+$, 92.0 (36) $[C_5H_4N_2]^+$, 77.1 (52) $[C_6H_5]^+$.

HRMS (EI, 70 eV) *m/z* calculated for $C_{17}H_{14}Cl_2N_4$: 344.0596, found: 344.0597.

(*E*)-1-Phenyl-3,5-dimethyl-4-((2,6-difluorophenyl)diazenyl)-1*H*-pyrazole (86)

N-Phenylhydrazine (0.49 mL, 5.00 mmol) was added dropwise to a solution of 3-(2-(2,6-difluorophenyl)hydrazono)pentane-2,4-dione **(78)** in 25 mL ethanol. The reaction mixture was refluxed for 3 hours at 80 °C, cooled to room temperature and all solvents were removed *in vacuo*. The product was isolated as the remaining bright orange solid (1.23 g, 79 %).

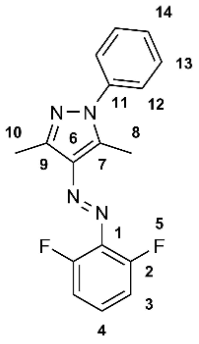

^{1}H-NMR (300 MHz, $CDCl_3$) δ [ppm] = 7.42-7.32 (m, 5 H, H_4+H_{12}+H_{13}), 7.14-7.09 (m, 1 H, H_{14}), 6.93-6.87 (m, 2 H, H_3), 2.53 (s, 3 H, H_8), 2.43 (s, 3 H, H_{10}).

^{13}C-NMR (75 MHz, $CDCl_3$) δ [ppm] = 157.1 (C_2), 153.7 (C_9), 143.4 (C_1), 139.9 (C_{11}), 138.5 (C_6), 137.3 (C_7), 128.9 (C_{13}), 128.1 (C_{14}), 127.9 (C_{12}), 124.5 (C_4), 111.8 (C_3), 13.7 (C_{10}), 10.9 (C_8).

^{19}F-NMR (100 MHz, $CDCl_3$) δ [ppm] = -123.2 (F_5).

MS (EI, 70 eV) *m/z* (%) 312.1 (46) $[M]^{+\cdot}$, 205.1 (54) $[M\text{-}C_6H_3N_2]^+$, 199.1 (26) $[M\text{-}C_6H_3F_2]^+$, 171.1 (27) $[M\text{-}C_6H_3F_2N_2]^+$, 148.1 (100) $[C_7H_8N_4]^+$, 108.1 (67) $[C_5H_6N_3]^+$, 92.0 (96) $[C_5H_4N_2]^+$, 77.1 (76) $[C_6H_5]^+$.

HRMS (EI, 70 eV) *m/z* calculated for $C_{17}H_{14}F_2N_4$: 312.1187, found: .312.1187.

(*E*)-1-(4-Nitrophenyl)-3,5-dimethyl-4-(phenyldiazenyl)-1*H*-pyrazole (87)

N-(4-Nitrophenyl)-hydrazine (0.77 g, 5.00 mmol) was added dropwise to a solution of 3-(2-phenylhydrazono)pentane-2,4-dione **(75)** (1.02 g, 5.00 mmol) in 25 mL ethanol. The reaction mixture was refluxed for 3 hours at 80 °C, cooled to room temperature and all solvents were removed *in vacuo*. The product was isolated as the remaining bright orange solid (1.13 g, 70 %).

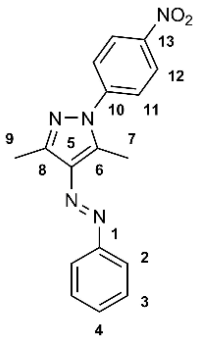

^{1}H-NMR (600 MHz, $CDCl_3$) δ [ppm] = 8.37-8.39 (m, 2 H, H_{12}), 7.82-7.84 (m, 2 H, H_{11}), 7.76-7.78 (m, 2 H, H_3), 7.48-7.51 (m, 2 H, H_2), 7.43-7.45 (m, 1 H, H_4), 2.79 (s, 3 H, H_7), 2.60 (s, 3 H, H_9).

^{13}C-NMR (150 MHz, $CDCl_3$) δ [ppm] = 153.3 (C_8), 146.2 (C_1), 145.1 (C_{13}), 144.1 (C_{10}), 139.6 (C_5), 137.1 (C_6), 130.1 (C_3), 129.0 (C_4), 124.8 (C_{11}), 124.0 (C_2), 122.0 (C_{12}), 14.2 (C_9), 11.8 (C_7).

MS (EI, 70 eV) *m/z* (%) 321.1 (80) $[M]^{+\cdot}$, 291.1 (38) $[M\text{-}NO]^+$, 274.1 (22) $[M\text{-}HNO_2]^+$, 244.1 (100) $[M\text{-}C_6H_5]^+$, 216.1 (51) $[M\text{-}C_6H_5N_2]^+$, 186.1 (28) $[C_{10}H_{10}N_4]^+$, 170.1 (38) $[C_{11}H_{10}N_2]^+$, 151.0 (16) $[C_6H_5N_3O_2]^+$, 122.0 (22) $[C_6H_4NO_2]^+$, 92.0 (96) $[C_5H_4N_2]^+$, 77.1 (76) $[C_6H_5]^+$.

HRMS (EI, 70 eV) *m/z* calculated for $C_{17}H_{15}N_5O_2$: 321.1226, found: 321.1227.

(*E*)-1-(4-Nitrophenyl)-3,5-dimethyl-4-((2,6-dimethylphenyl)diazenyl)-1*H*-pyrazole (88)

N-(4-Nitrophenyl)-hydrazine (0.77 g, 5.00 mmol) was added dropwise to a solution of 3-(2-(2,6-dimethylphenyl)hydrazono)pentane-2,4-dione **(76)** (1.16 g, 5.00 mmol) in 25 mL ethanol. The reaction mixture was refluxed for 3 hours at 80 °C, cooled to room temperature and all solvents were removed *in vacuo*. The product was isolated as the remaining bright orange solid (1.28 g, 73 %).

H-NMR (600 MHz, $CDCl_3$) δ [ppm] = 8.38-8.40 (m, 2 H, H_{13}), 7.77-7.79 (m, 2 H, H_{12}), 7.11-7.14 (m, 3 H, H_3+H_4), 2.75 (s, 3 H, H_8), 2.58 (s, 3 H, H_{10}), 2.41 (s, 6 H, H_5).

^{13}C-NMR (150 MHz, $CDCl_3$) δ [ppm] = 151.5 (C_9), 146.3 (C_1), 144.4 (C_{14}), 139.7 (C_{11}), 137.7 (C_6), 136.9 (C_7), 130.8 (C_3), 129.2 (C_2), 127.8 (C_4), 124.9 (C_{12}), 124.1 (C_{13}), 19.5 (C_5), 14.4 (C_{10}), 11.6 (C_8).

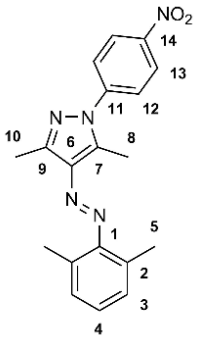

MS (EI, 70 eV) *m/z* (%) 349.1 (6) $[M]^{+\cdot}$, 320.1 (4) $[M\text{-}C_2H_5]^+$, 262.1 (7) $[C_{16}H_{14}N_4]^+$, 232.1 (52) $[C_{11}H_{12}N_4O_2]^+$, 217.1 (22) $[M\text{-}C_8H_8N_2]^+$, 193.1 (100) $[C_{11}H_{10}N_2\text{+Na}]^+$, 120.1 (77) $[C_8H_{10}N]^+$.

HRMS (EI, 70 eV) *m/z* calculated for $C_{19}H_{19}N_5O_2$: 349.1539, found: 349.1537.

(*E*)-1-(4-Nitrophenyl)-3,5-dimethyl-4-((2,6-dichlorophenyl)diazenyl)-1*H*-pyrazole (89)

N-(4-Nitrophenyl)-hydrazine (0.77 g, 5.00 mmol) was added dropwise to a solution of 3-(2-(2,6-dichlorophenyl)hydrazono)pentane-2,4-dione **(77)** (1.37 g, 5.00 mmol) in 25 mL ethanol. The reaction mixture was refluxed for 3 hours at 80 °C, cooled to room temperature and all solvents were removed *in vacuo*. The product was isolated as the remaining bright orange solid (1.61 g, 83 %).

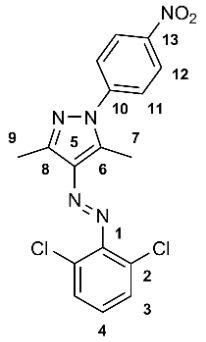

^{1}H-NMR (600 MHz, $CDCl_3$) δ [ppm] = 8.39-8.41 (m, 2 H, H_{12}), 7.76-7.78 (m, 2 H, H_3), 7.40-7.42 (m, 2 H, H_{11}), 7.15-7.18 (m, 1 H, H_4), 2.77 (s, 3 H, H_9), 2.59 (s, 3 H, H_7).

^{13}C-NMR (150 MHz, $CDCl_3$) δ [ppm] = 148.4 (C_8), 146.5 (C_1), 145.2 (C_{13}), 143.9 (C_{10}), 141.3 (C_5), 137.7 (C_6), 129.1 (C_3), 128.0 (C_4), 127.3 (C_{11}), 124.9 (C_2), 124.3 (C_{12}), 14.2 (C_9), 11.6 (C_7).

MS (EI, 70 eV) *m/z* (%) 389.0 (45) $[M]^{+\cdot}$, 354.1 (63) $[M\text{-Cl}]^+$, 324.1 (6) $[M\text{-ClNO}]^+$, 244.1 (100) $[M\text{-}C_6H_3Cl_2]^+$, 216.1 (58) $[M\text{-}C_6H_3Cl_2N_2]^+$, 170.1 (34) $[M\text{-}C_6H_2Cl_2N_2\text{-}NO_2]^+$, 108.1 (41) $[C_5H_6N_3]^+$.

HRMS (EI, 70 eV) *m/z* calculated for $C_{17}H_{13}Cl_2N_5O_2$: 389.0446, found: 389.0443.

(*E*)-1-(4-Nitrophenyl)-3,5-dimethyl-4-((2,6-difluorophenyl)diazenyl)-1*H*-pyrazole (90)

N-(4-Nitrophenyl)-hydrazine (0.77 g, 5.00 mmol) was added dropwise to a solution of 3-(2-(2,6-difluorophenyl)hydrazono)pentane-2,4-dione **(78)** (1.20 g, 5.00 mmol) in 25 mL ethanol. The reaction mixture was refluxed for 3 hours at 80 °C, cooled to room temperature and all solvents were removed *in vacuo*. The product was isolated as the remaining bright orange solid (1.48 g, 83 %).

^{1}H-NMR (600 MHz, $CDCl_3$) δ [ppm] = 8.38-8.40 (m, 2 H, H_{13}), 7.76-7.78 (m, 2 H, H_{12}), 7.25-7.28 (m, 1 H, H_4), 7.01-7.04 (m, 2 H, H_3), 2.76 (s, 3 H, H_{10}), 2.56 (s, 3 H, H_8).

^{13}C-NMR (150 MHz, $CDCl_3$) δ [ppm] = 156.6 (C_2), 154.9 (C_9), 146.4 (C_1), 144.9 (C_{14}), 144.0 (C_{11}), 140.8 (C_6), 138.5 (C_7), 131.8 (C_{12}), 129.1 (C_{13}), 124.9 (C_4), 124.2 (C_4'), 112.4 (C_3), 14.2 (C_{10}), 11.6 (C_8).

MS (EI, 70 eV) *m/z* (%) 357.1 (100) $[M]^{+\cdot}$, 337.1 (10) $[M\text{-}HF]^{+\cdot}$, 327.1 (19) $[M\text{-}NO]^{+}$, 244.1 (77) $[M\text{-}C_6H_3F_2]^{+}$, 216.1 (55) $[M\text{-}C_6H_3F_2N_2]^{+}$, 170.1 (27) $[M\text{-}C_6H_2F_2N_2\text{-}NO_2]^{+}$, 122.0 (18) $[C_6H_4NO_2]^{+}$, 108.1 (12) $[C_5H_6N_3]^{+}$.

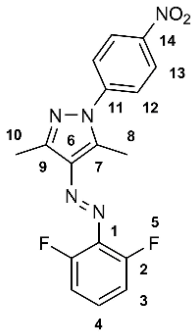

HRMS (EI, 70 eV) *m/z* calculated for $C_{17}H_{13}F_2N_5O_2$: 357.1037, found: 357.1037.

(*E*)-1-(4-Aminophenyl)-3,5-dimethyl-4-(phenyldiazenyl)-1*H*-pyrazole (91)[259]

(*E*)-1-(4-Nitrophenyl)-3,5-dimethyl-4-(phenyldiazenyl)-1*H*-pyrazole **(87)** (0.50 g, 1.56 mmol) was dissolved in 30 mL DMF. $Na_2S{\cdot}H_2O$ (0.38 g, 3.90 mmol) was dissolved in 37.5 mL H_2O and the solution was added dropwise to the first solution. The resulting reaction mixture was heated to 90 °C for 5 hours, then cooled to room temperature and diluted with 100 mL water. The reaction mixture was extracted twice with 100 mL dichloromethane, the combined organic layers were dried over $MgSO_4$ and all solvents were removed *in vacuo* to yield the product as a bright yellow solid (0.41 g, 90 %).

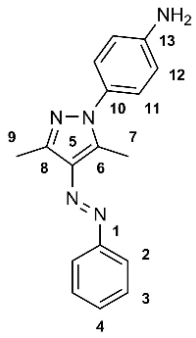

^{1}H-NMR (600 MHz, $CDCl_3$) δ [ppm] = 7.76-7.82 (m, 2 H, H_3), 7.46-7.48 (m, 2 H, H_{11}), 7.34-7.39 (m, 1 H, H_4), 7.22-7.24 (m, 2 H, H_2), 6.75-6.76 (m, 2 H, H_{12}), 2.57-2.60 (m, 6 H, H_7+H_9).

^{13}C-NMR (150 MHz, $CDCl_3$) δ [ppm] = 153.6 (C_8), 146.3 (C_1), 143.4 (C_{13}), 139.0 (C_{10}), 135.7 (C_5), 130.1 (C_6), 129.3 (C_3), 128.9 (C_4), 126.4 (C_{12}), 121.8 (C_2), 115.1 (C_{11}), 13.9 (C_9), 11.2 (C_7).

MS (ESI, positive) *m/z* (%) 605.3 (66) $[2M+Na]^{+}$, 314.1 (100) $[M+Na]^{+}$, 225.1 (65) $[C_{13}H_{13}N_4]^{+}$.

HRMS (ESI, positive) m/z calculated for $C_{17}H_{17}N_5Na$: 314.1376, found: 314.1375.

7.2.15 Synthesis of *N*-methyl-arylazopyrazole phosphoramidite

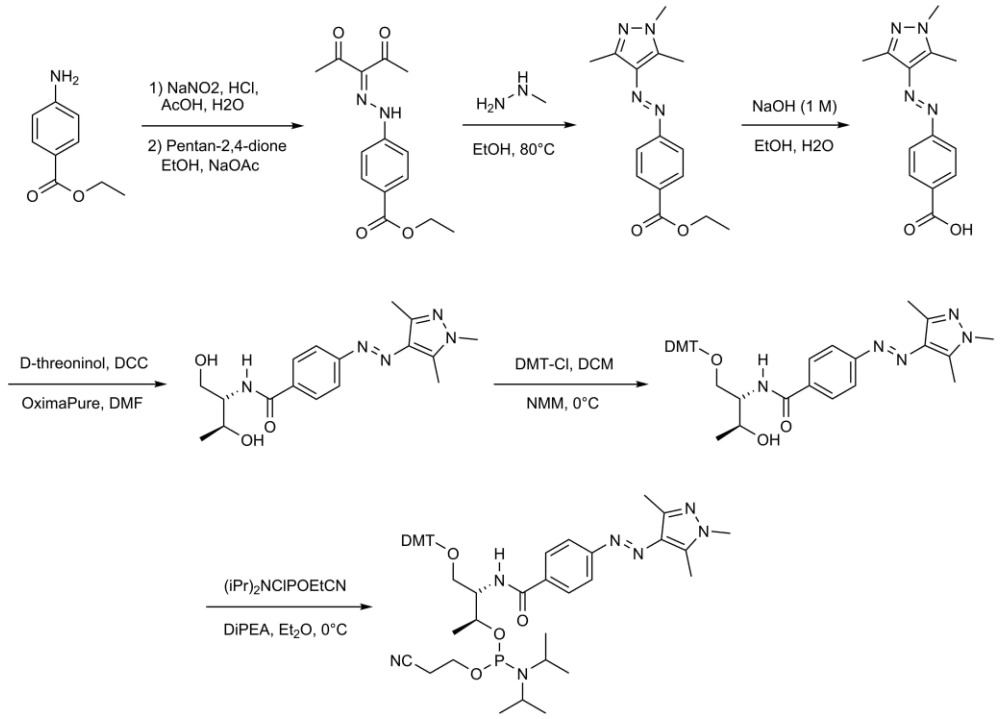

Ethyl-4-(2-(2,4-dioxopentan-3-ylidene)hydrazono)benzoate (92)

A solution of ethyl-4-aminobenzoate (12.2 g, 74.0 mmol) in 100 mL glacial acetic acid and 17 mL 12 % aqueous hydrochloric acid was prepared. $NaNO_2$ (6.10 g, 88.8 mmol) was dissolved in 25 mL water, the solution was added dropwise to the prepared solution at 0 °C and the reaction mixture was stirred for 1 hour at 0 °C. A suspension of 2,4-pentanedione (9.80 mL, 100 mmol) and NaOAc (18.1 g, 220 mmol) in 70 mL ethanol and 40 mL water was prepared and the reaction mixture was added dropwise to the suspension. The resulting mixture was stirred for 1 hour at room temperature, followed by removal of all solvents *in vacuo*. The product was isolated by column chromatography (silica, eluent: cyclohexane/ethyl acetate = 1/1) as a bright yellow solid (yield: 20.4 g, quant.).

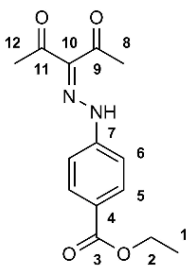

^{1}H-NMR (400 MHz, $CDCl_3$) δ [ppm] = 14.56 (s, br, 1 H, H_7), 8.09-8.06 (m, 2 H, H_5), 7.43-7.39 (m, 2 H, H_6), 4.40 (q, 2 H, $^3J_{2,1}$ = 7.1 Hz, H_2), 2.60 (s, 3 H, H_{12}), 2.49 (s, 3 H, H_8), 1.41 (t, 3 H, $^3J_{1,2}$ = 7.1 Hz, H_1).

^{13}C-NMR (100 MHz, $CDCl_3$) δ [ppm] = 198.3 (C_{11}), 196.9 (C_9), 165.8 (C_3), 145.0 (C_7), 134.1 (C_5), 131.3 (C_6), 127.3 (C_4), 115.6 (C_{10}), 61.0 (C_2), 31.7 (C_{12}), 26.6 (C_8), 14.3 (C_1).

MS (ESI, positive) *m/z* (%) 299.1 (100) $[M+Na]^+$.

HRMS (ESI, positive) *m/z* calculated for $C_{14}H_{16}N_2O_4Na$: 299.1002, found: 299.1004.

Ethyl-4-((*E*)-(1,3,5-trimethyl-1*H*-pyrazol-4-yl)diazenyl)benzoate (93)

Ethyl-4-(2-(2,4-dioxopentan-3-ylidene)hydrazono)benzoate **(92)** (1.50 g, 5.43 mmol) was dissolved in 30 mL ethanol. *N*-Methylhydrazine (0.28 mL, 5.43 mmol) was added dropwise to the solution at room temperature and the reaction mixture was refluxed for 3 hours. All solvents were removed *in vacuo* and the product was isolated by column chromatography (silica, eluent: cyclohexane/ethyl acetate = 1/1) as a bright orange solid (1.55 g, quant.).

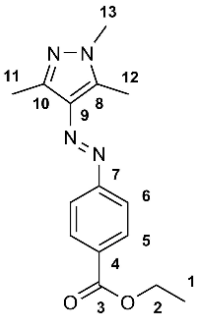

^{1}H-NMR (400 MHz, $CDCl_3$) δ [ppm] = 8.14-8.11 (m, 2 H, H_5), 7.81-7.78 (m, 2 H, H_6), 4.43 (q, 2 H, $^{3}J_{2,1}$ = 7.1 Hz, H_2), 3.78 (s, 3 H, H_{13}), 2.58 (s, 3 H, H_{11}), 2.51 (s, 3 H, H_{12}), 1.44 (t, 3 H, $^{3}J_{1,2}$ = 7.1 Hz, H_1).

^{13}C-NMR (100 MHz, $CDCl_3$) δ [ppm] = 166.2 (C_3), 156.2 (C_{10}), 142.6 (C_7), 139.7 (C_9), 135.4 (C_8), 130.5 (C_5), 130.4 (C_6), 121.5 (C_4), 61.0 (C_2), 36.0 (C_{13}), 14.3 (C_1), 13.9 (C_{11}), 9.9 (C_{12}).

MS (EI, 70 eV) *m/z* (%) 595.3 (27) $[2M+Na]^+$, 309.1 (100) $[M+Na]^+$.

HRMS (EI, 70 eV) *m/z* calculated for $C_{15}H_{18}N_4O_2Na$: 309.1322, found: 309.1323.

4-((*E*)-(1,3,5-Trimethyl-1*H*-pyrazol-4-yl)diazenyl)benzoic acid (94)

Ethyl-4-((*E*)-(1,3,5-trimethyl-1*H*-pyrazol-4-yl)diazenyl)benzoate **(93)** (7.50 g, 26.2 mmol) was dissolved in 1.2 L ethanol and 130 mL 1 M aqueous NaOH. The reaction mixture was stirred for 24 hours at room temperature, acidified with 1 M aqueous hydrochloric acid and extracted three times with 500 mL ethyl acetate. The combined organic layers were washed with 1 L water and 500 mL brine, dried over $MgSO_4$, filtered and all solvents were removed *in vacuo*. The product was isolated by column chromatography (silica, eluent: chloroform/methanol = 95/5) as a bright orange solid (6.75 g, quant.).

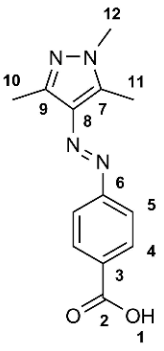

^{1}H-NMR (400 MHz, DMSO-d_6) δ [ppm] = 13.04 (s, br, 1 H, H_1), 8.06-8.03 (m, 2 H, H_4), 7.79-7.76 (m, 2H, H_5), 3.73 (s, 3 H, H_{12}), 2.54 (s, 3 H, H_{10}), 2.36 (s, 3 H, H_{11}).

^{13}C-NMR (100 MHz, DMSO-d_6) δ [ppm] = 166.9 (C_2), 155.6 (C_9), 140.7 (C_6), 134.8 (C_8), 131.0 (C_7), 130.5 (C_4), 121.4 (C_5), 36.0 (C_{12}), 13.8 (C_{10}), 9.5 (C_{11}).

MS (ESI, negative) *m/z* (%) 342.1 (23) $[M+CHCl_2-H]^-$, 257.1 (100) $[M-H]^-$, 213.1 (17) $[M-CO_2H]^-$.

HRMS (ESI, negative) *m/z* calculated for $C_{13}H_{13}N_4O_2$: 257.1044, found: 257.1028.

4-((*E*)-(1,3,5-Trimethyl-1*H*-pyrazol-4-yl)diazenyl)carboxy-D-threoninol ("AAP1") (95)

4-((*E*)-(1,3,5-Trimethyl-1*H*-pyrazol-4-yl)diazenyl)benzoic acid **(94)** (5.0 g, 19.4 mmol), D-threoninol (2.44 g, 23.2 mmol), DCC (4.79 g, 23.2 mmol) and OxymaPure (3.30 g, 23.2 mmol)

were dissolved in 180 mL dry DMF and the reaction mixture was stirred for 24 hours at room temperature under argon atmosphere. All solid residues were filtered off, DMF was removed *in vacuo* and the crude product was purified by column chromatography (silica, eluent: chloroform/methanol = 98/2) as a bright orange solid (4.76 g, 71 %).

TLC (SiO_2, eluent: chloroform/methanol = 10/1) R_f = 0.30.

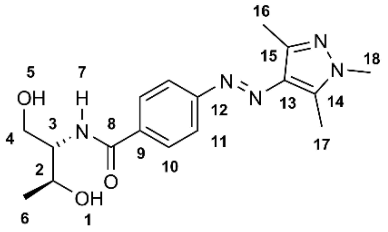

^{1}H-NMR (400 MHz, DMSO-d_6) δ [ppm] = 8.01-7.98 (m, 2 H, H_{10}), 7.83-7.75 (m, 3 H, H_7+H_{11}), 4.64-4.60 (m, 2 H, H_3+H_5), 3.95-3.89 (m, 2 H, H_4), 3.74 (s, 3 H, H_{18}), 3.64-3.58 (m, 1 H, H_2), 3.53-3.48 (m, 1 H, H_1), 2.56 (s, 3 H, H_{16}), 2.38 (s, 3 H, H_{17}), 1.08 (d, 3 H, $^3J_{6,2}$ = 6.2 Hz, H_6).

^{13}C-NMR (100 MHz, DMSO-d_6) δ [ppm] = 166.0 (C_8), 154.5 (C_{15}), 140.6 (C_{12}), 140.3 (C_{13}), 135.1 (C_{14}), 134.7 (C_{10}), 128.5 (C_{10}), 121.1 (C_{11}), 64.9 (C_4), 60.5 (C_2), 56.9 (C_3), 36.0 (C_{16}), 20.3 (C_6), 13.9 (C_{16}), 9.6 (C_{17}).

MS (ESI, positive) *m/z* (%) 713.4 (35) $[2M+Na]^+$, 368.2 (45) $[M+Na]^+$, 346.2 $[M+H]^+$.

HRMS (ESI, positive) *m/z* calculated for $C_{17}H_{23}N_5O_3H$: 346.1874, found: 346.1876.

DMT-protected 4-((*E*)-(1,3,5-trimethyl-1*H*-pyrazol-4-yl)diazenyl)carboxy-D-threoninol (96)

4-((*E*)-(1,3,5-Trimethyl-1*H*-pyrazol-4-yl)diazenyl)carboxy-D-threoninol **(95)** (0.91 g, 2.64 mmol) was dissolved in 30 mL dry dichloromethane. DMT-chloride (0.89 g, 2.64 mmol) was dissolved in 20 mL dry dichloromethane and added dropwise to the first solution under argon atmosphere over 20 minutes. The reaction mixture was stirred for 1 hour under argon atmosphere at room temperature, then *N*-methylmorpholine (0.27 g, 2.64 mmol) was added dropwise to the solution under argon atmosphere and stirring was continued for 24 hours at room temperature under argon atmosphere. All solvents were removed under reduced pressure and the product was isolated by column chromatography (silica, eluent: cyclohexane/ethyl acetate = 1/1 with 3 % triethylamine) as a bright orange solid (0.82 g, 47 %).

^{1}H-NMR (500 MHz, DMSO-d_6) δ [ppm] = 7.73-7.81 (m, 4 H, H_9+H_{20}), 7.33-7.36 (m, 2 H, H_{10}), 7.11-7.24 (m, 7 H, H_{21}+H_{22}+H_{24}), 6.72-6.75 (m, 4 H,H_{25}), 5.23 (s, 1 H, H_6), 4.12-4.15 (m, 1 H, H_3), 3.99-4.05 (m, 1 H, H_2), 3.66-3.69 (m, 9 H, H_{17}+H_{27}), 3.55-3.57 (m, 1 H, H_1), 3.25-3.40 (m, 2 H, H_4), 2.49 (s, 3 H, H_{15}), 2.38 (s, 3 H, H_{16}), 1.11-1.16 (m, 3 H, H_5).

^{13}C-NMR (125 MHz, DMSO-d_6) δ [ppm] = 167.3 (C_7), 159.1 (C_{26}), 155.9 (C_{14}), 145.1 (C_{11}), 142.5 (C_{19}), 140.3 (C_{23}), 136.0 (C_{12}), 135.9 (C_{13}), 135.7 (C_{22}), 135.0 (C_9), 130.3 (C_{24}), 128.3 (C_{21}), 128.2 (C_{20}), 127.3 (C_{10}), 122.0 (C_8), 113.6 (C_{25}), 87.0 (C_{18}), 68.5 (C_4), 65.0(C_2), 55.6 (C_3), 54.9 (C_{27}), 36.3 (C_{17}), 20.5 (C_5), 14.1 (C_{15}), 10.1 (C_{16}).

MS (ESI, positive) *m/z* (%) 670.3 (100) $[M+Na]^+$, 368.2 (92) $[M-DMT+Na]^+$, 343.1 (61) $[C_{17}H_{21}N_5O_3]^+$, 303.1 (32) $[DMT]^+$.

HRMS (ESI, positive) *m/z* calculated for $C_{38}H_{41}N_5O_5Na$: 670.3000, found: 670.2998.

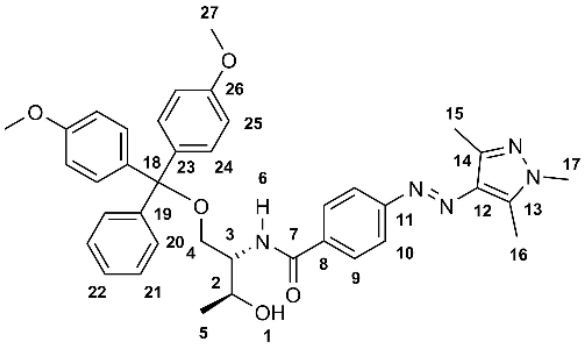

DMT-protected 4-((*E*)-(1,3,5-trimethyl-1*H*-pyrazol-4-yl)diazenyl)carboxy-D-threoninol phosphoramidite (97)

DMT-protected 4-((*E*)-(1,3,5-trimethyl-1*H*-pyrazol-4-yl)diazenyl)carboxy-D-threoninol **(96)** (1.0 g, 1.54 mmol) was dissolved in 15 mL dry diethyl ether under argon atmosphere and the reaction mixture was cooled to 0 °C. DiPEA (0.24 g, 1.85 mmol) was added dropwise at 0 °C followed by dropwise addition of 2-cyanoethyl-*N*,*N*-diisopropylchlorophosporamidite (0.44 g, 1.85 mmol). The reaction mixture was stirred for 15 minutes at 0 °C followed by evaporation of all solvents. The product was isolated by column chromatography (silica, eluent: cyclohexane/ethyl acetate = 1/1) as a bright orange solid (0.92 g, 69 %).

^{1}H-NMR (300 MHz, DMSO-d_6) δ [ppm] = 7.86-7.69 (m, 4 H, H_8+H_{19}), 7.46-7.40 (m, 2 H, H_9), 7.32-7.19 (m, 7 H, H_{20}+H_{21}+H_{23}), 6.82-6.78 (m, 4 H, H_{24}), 4.47-4.30 (m, 1 H, H_5), 4.18-3.98 (m, 1 H, H_3), 3.79-3.71 (m, 8 H, H_{26}+H_{30}), 3.64-3.45 (m, 5 H, H_{16}+H_{28}), 3.33-3.27 (m, 1 H, H_2), 3.04 (s, br, 2H, H_4), 2.56 (s, 3 H, H_{14}), 2.44 (s, 3 H, H_{15}), 1.50-0.96 (m, 17 H, H_1+H_{29}+H_{31}).

^{31}P-NMR (75 MHz, DMSO-d_6) δ [ppm] = 148.4, 140.8.

MS (ESI, positive) *m/z* (%) 870.4 (18) $[M+Na]^+$, 459.2 (100) $[C_{22}H_{32}N_6O_3P]^+$, 441.2 (78) $[C_{23}H_{34}N_6O_5P]^+$.

HRMS (ESI, positive) *m/z* calculated for $C_{47}H_{58}N_7O_6PNa$: 870.4078, found: 870.4081.

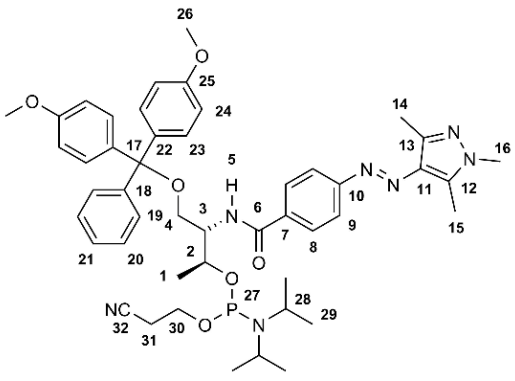

7.2.16 Synthesis of *N*-phenyl-arylazopyrazole phosphoramidite

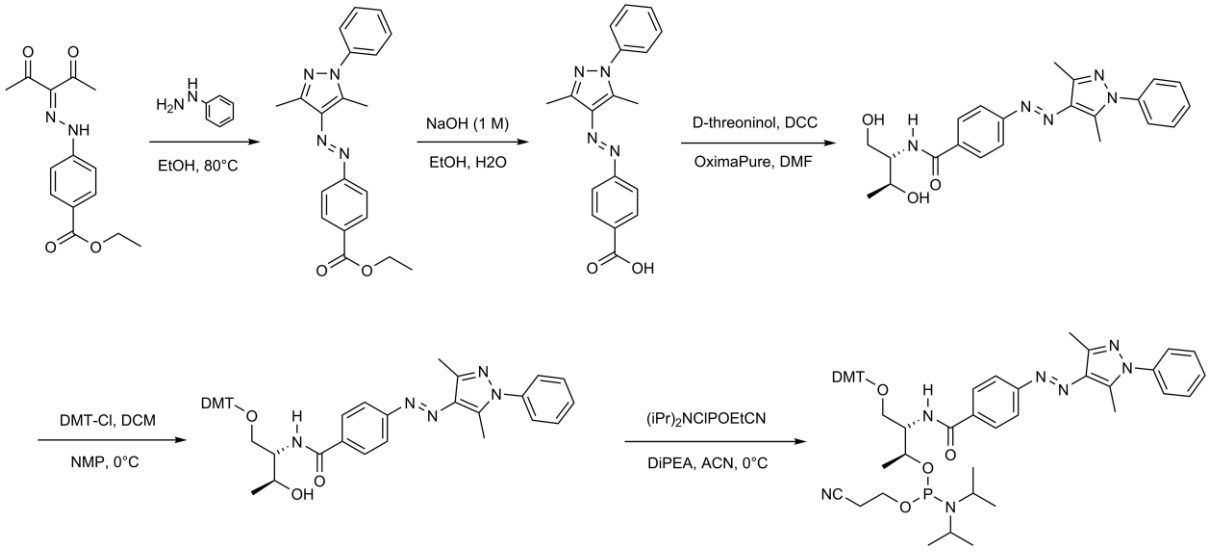

Ethyl-4-((*E*)-(1-Phenyl-3,5-dimethyl-1*H*-pyrazol-4-yl)diazenyl)benzoate (98)

Ethyl-4-(2-(2,4-dioxopentan-3-ylidene)hydrazono)benzoate **(92)** (7.50 g, 27.0 mmol) was dissolved in 150 mL ethanol. *N*-Phenylhydrazine (2.31 mL, 27.0 mmol) was added dropwise to the solution at room temperature and the reaction mixture was refluxed for 3 hours. The reaction mixture was cooled to room temperature and all solvents were removed *in vacuo*. The product was isolated by column chromatography (silica, eluent: cyclohexane/ethyl acetate = 1/1) as a bright orange solid (9.40 g, quant.).

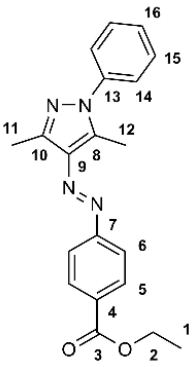

^{1}H-NMR (500 MHz, DMSO-d_6) δ [ppm] = 8.11-8.09 (m, 2 H, H_5), 7.87-7.86 (m, 2 H, H_{14}), 7.63-7.47 (m, 5 H, H_6+H_{15}+H_{16}), 4.36 (q, 2 H, $^{3}J_{2,1}$ = 7.1 Hz, H_2), 2.65 (s, 3 H, H_{11}), 2.49 (s, 3 H, H_{12}), 1.35 (t, 3 H, $^{3}J_{1,2}$ = 7.1 Hz, H_1).

^{13}C-NMR (166 MHz, DMSO-d_6) δ [ppm] = 165.7 (C_3), 156.1 (C_{10}), 142.9 (C_7), 141.5 (C_{13}), 139.0 (C_9), 136.4 (C_8), 130.9 (C_5), 130.8 (C_{15}), 129.8 (C_{16}), 128.7 (C_{14}), 125.1 (C_6), 122.2 (C_4), 61.4 (C_2), 14.7 (C_1), 14.6 (C_{11}), 11.5 (C_{12}).

MS (EI, 70 eV) *m/z* (%) 719.3 (55) $[2M+Na]^+$, 371.1 (100) $[M-Na]^+$, 349.2 (42) $[M+H]^+$.

HRMS (EI, 70 eV) *m/z* calculated for $C_{20}H_{20}N_4O_2Na$: 371.1478, found: 371.1465.

4-((*E*)-(1-Phenyl-3,5-dimethyl-1*H*-pyrazol-4-yl)diazenyl)benzoic acid (99)

Ethyl-4-((*E*)-(1-Phenyl-3,5-dimethyl-1*H*-pyrazol-4-yl)diazenyl)benzoate **(98)** (9.20 g, 26.4 mmol) was dissolved in 120 mL ethanol. 130 mL 1 M aqueous sodium hydroxide was added and the reaction mixture was stirred for 24 hours at room temperature, then acidified with 1 M hydrochloric acid followed by extraction twice with 250 mL ethyl acetate. The

combined organic layers were washed with 250 mL water and dried over $MgSO_4$. All solvents were removed *in vacuo* and the product was isolated by column chromatography (silica, eluent: chloroform/methanol = 95/5) as a bright orange solid (7.13 g, 85 %).

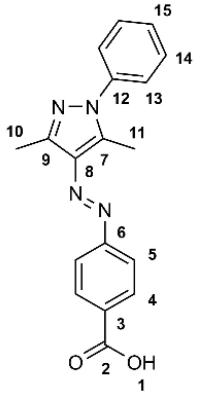

^{1}H-NMR (500 MHz, DMSO-d_6) δ [ppm] = 13.09 (s, br, 1 H, H_1), 8.11 (d, 2 H, $^3J_{4,5}$ = 8.5 Hz, H_4), 7.87 (d, 2 H, $^3J_{13,14}$ = 8.4 Hz, H_{13}), 7.64-7.49 (m, 5 H, H_5+H_{14}+H_{15}), 2.67 (s, 3 H, H_{10}), 2.50 (s, 3 H, H_{11}).

^{13}C-NMR (125 MHz, DMSO-d_6) δ [ppm] = 167.3 (C_2), 155.9 (C_9), 142.9 (C_6), 141.3 (C_{12}), 139.0 (C_8), 136.4 (C_7), 131.8 (C_4), 131.0 (C_{14}), 129.8 (C_{15}), 128.7 (C_{13}), 125.1 (C_5), 122.0 (C_3), 14.6 (C_{10}), 11.5 (C_{11}).

MS (ESI, negative) *m/z* (%) 319.1 (100) $[M-H]^-$.

HRMS (ESI, negative) *m/z* calculated for $C_{18}H_{15}N_4O_2$: 319.1200, found: 319.1190.

4-((*E*)-(1-Phenyl-3,5-dimethyl-1*H*-pyrazol-4-yl)diazenyl)carboxy-D-threoninol ("AAP2") (100)

4-((*E*)-(1-Phenyl-3,5-dimethyl-1*H*-pyrazol-4-yl)diazenyl)benzoic acid **(99)** (5.0 g, 15.6 mmol), DCC (3.87 g, 18.7 mmol), OxymaPure (2.66 g, 18.7 mmol) and D-threoninol (1.97 g, 18.7 mmol) were dissolved in 150 mL dry DMF under argon atmosphere and stirred for 24 hours at room temperature. All solids were filtered off and rinsed with DMF followed by removal of DMF *in vacuo*. The product was isolated by column chromatography (silica, eluent: chloroform/methanol = 98/2) as a bright orange solid (3.81 g, 50 %).

TLC (SiO_2, eluent: chloroform/methanol = 10/1) R_f = 0.38.

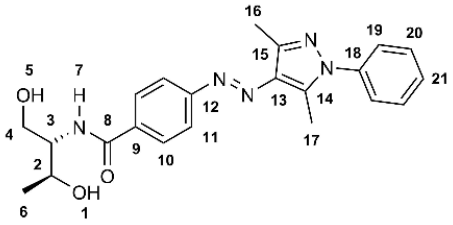

^{1}H-NMR (500 MHz, DMSO-d_6) δ [ppm] = 8.06-8.04 (m, 2 H, H_{10}), 7.87-7.83 (m, 3 H, H_{19}+H_{21}), 7.64-7.57 (m, 4 H, H_{11}+H_{20}), 7.51-7.48 (m, 1 H, H_7), 4.66-4.63 (m, 2 H, H_3+H_5), 3.97-3.94 (m, 2 H, H_4), 3.66-3.62 (m, 1 H, H_2), 3.54-3.52 (m, 1 H, H_1), 2.67 (s, 3 H, H_{16}), 2.51 (s, 3 H, H_{17}), 1.18-1.09 (m, 3 H, H_6).

^{13}C-NMR (125 MHz, DMSO-d_6) δ [ppm] = 166.4 (C_8), 154.8 (C_{15}), 142.8 (C_{12}), 141.0 (C_{18}), 139.0 (C_{13}), 136.2 (C_{14}), 136.0 (C_{10}), 129.8 (C_{20}), 129.0 (C_{21}), 125.0 (C_{19}), 121.7 (C_{11}), 79.6 (C_9), 65.4 (C_4), 61.0 (C_2), 57.3 (C_3), 20.7 (C_6), 14.6 (C_{16}), 11.5 (C_{17}).

MS (ESI, positive) *m/z* (%) 837.4 (82) $[2M+Na]^+$, 430.2 (100) $[M+Na]^+$, 408.2 (14) $[M+H]^+$.

HRMS (ESI, positive) *m/z* calculated for $C_{22}H_{26}N_5O_3$: 408.2030, found: 408.2034.

DMT-protected 4-((*E*)-(1-Phenyl-3,5-dimethyl-1*H*-pyrazol-4-yl)diazenyl)carboxy-D-threoninol (101)

4-((*E*)-(1-Phenyl-3,5-dimethyl-1*H*-pyrazol-4-yl)diazenyl)carboxy-D-threoninol **(100)** (1.0 g, 2.45 mmol) was dissolved in 20 mL dry dichloromethane under argon atmosphere. DMT-chloride (0.83 g, 2.45 mmol) was dissolved in 10 mL dry dichloromethane and added dropwise to the first solution under argon atmosphere over 30 minutes. The reaction mixture was stirred for 30 minutes at room temperature under argon atmosphere. A gentle argon flow was attached to the reaction mixture and *N*-methylpyrrolidine (0.19 mL, 1.96 mmol) was added very slowly dropwise to the solution over 30 minutes. The reaction mixture was stirred for 24 hours at room temperature under argon atmosphere followed by evaporation of all solvents. The product was isolated by column chromatography (silica, eluent: cyclohexane/ethyl acetate/triethylamine = 50/50/3%) as a bright orange solid (0.45 g, 25%).

^{1}H-NMR (500 MHz, $CDCl_3$) δ [ppm] = 8.14-8.15 (m, 1 H, H_{20}), 8.06-8.09 (m, 2 H, H_9), 7.86-7.88 (m, 2 H, H_{23}), 7.61-7.63 (m, 2 H, H_{18}), 7.55-7.58 (m, 2 H, H_{19}), 7.46-7.49 (m, 1 H, H_{25}), 7.40-7.43 (m, 2 H, H_{10}) 7.25-7.28 (m, 6 H, H_{24}+H_{27}), 7.17-7.20 (m, 1 H, H_6), 6.82-6.86 (m, 4 H, H_{28}), 4.62-4.62 (m, 1 H, H_6), 4.16-4.19 (m, 1 H, H_3), 4.04-4.08 (m, 1 H, H_2), 3.71 (s, 6 H, H_{30}), 3.25-3.28 (m, 1 H, H_4), 3.00-3.03 (m, 1 H, H_4'), 2.66 (s, 3 H, H_{15}), 2.50 (s, 3 H, H_{16}), 1.03-1.05 (m, 3 H, H_5).

^{13}C-NMR (125 MHz, $CDCl_3$) δ [ppm] = 175.5 (C_7), 171.2 (C_{29}), 163.2 (C_{14}), 159.7 (C_{11}), 150.4 (C_{22}), 147.6 (C_{26}), 145.8 (C_{17}), 143.8 (C_{12}), 141.1 (C_{13}), 141.0 (C_{24}), 140.6 (C_{25}), 134.9 (C_9), 134.6 (C_{27}), 134.5 (C_{23}), 133.8 (C_{19}), 132.9 (C_{18}), 131.8 (C_{10}), 129.8 (C_{20}), 126.5 (C_8), 118.3 (C_{28}), 90.4 (C_{21}), 70.5 (C_4), 68.3 (C_2), 65.0 (C_3), 60.2 (C_{30}), 25.6 (C_{15}), 19.3 (C_5), 16.2 (C_{16}).

MS (ESI, positive) *m/z* (%) 1442.7 (24) $[2M+Na]^+$, 732.4 (100) $[M+Na]^+$.

HRMS (ESI, positive) *m/z* calculated for $C_{43}H_{43}N_5O_5Na$: 732.3156, found: 732.3142.

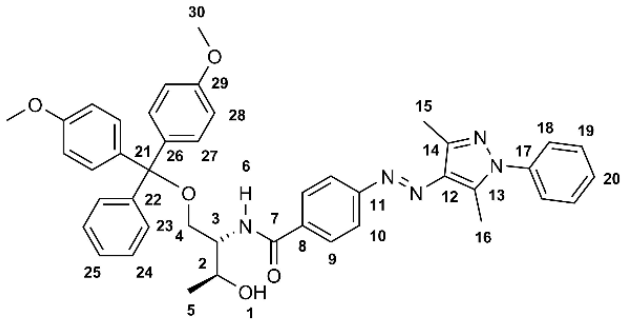

DMT-protected 4-((*E*)-(1-phenyl-3,5-dimethyl-1*H*-pyrazol-4-yl)diazenyl)carboxy-D-threoninol phosphoramidite (102)

DMT-protected 4-((*E*)-(1-Phenyl-3,5-dimethyl-1*H*-pyrazol-4-yl)diazenyl)carboxy-D-threoninol **(101)** (1.0 g, 1.41 mmol) was dissolved in 14 mL dry acetonitrile under argon atmosphere and cooled to 0 °C. DiPEA (0.22 g, 1.69 mmol) was added dropwise followed by dropwise addition of 2-cyanoethyl-*N*,*N*-diisopropylchlorophosporamidite (0.40 g, 1.69 mmol). The reaction mixture was stirred for ten minutes at 0 °C followed by evaporation of all solvents. The product was isolated by column chromatography (silica, eluent: cyclohexane/ethyl acetate = 1/1) as a bright orange solid (1.08 g, 82 %).

^{1}H-NMR (300 MHz, CD_3CN) δ [ppm] = 7.94-7.85 (m, 4 H, H_8+H_{17}), 7.54-7.41 (m, 7 H, H_{19}+H_{22}+H_{27}), 7.31-7.18 (m, 8 H, H_{23}+H_{26}), 6.85-6.74 (m, 5 H, H_9+H_{18}+H_{24}), 4.41-4.19 (m, 1 H, H_5), 4.14-4.03 (m, 1 H, H_3), 3.72 (s, 6 H, H_{29}), 3.61-3.55 (m, 2 H, H_{31}), 3.39-3.30 (m, 2 H, H_2), 3.25-3.18 (m, 1 H, Hx), 2.62 (s, 3 H, H_{14}), 2.50 (s, 3 H, H_{15}), 1.41.1.07 (m, 17 H, H_1+H_{32}+H_{34}).

^{31}P-NMR (75 MHz, CD_3CN) δ [ppm] = 181.8, 148.5, 141.2.

MS (ESI, positive) *m/z* (%) 932.4 (10) $[M+Na]^+$, 849.3 (100) $[M-CH_3+OH]^+$, 467.2 (48) $[C_{20}H_{25}N_6O_4P]^+$.

HRMS (ESI, positive) *m/z* calculated for $C_{52}H_{60}N_7O_6PNa$: 932.4235, found: 932.4238.

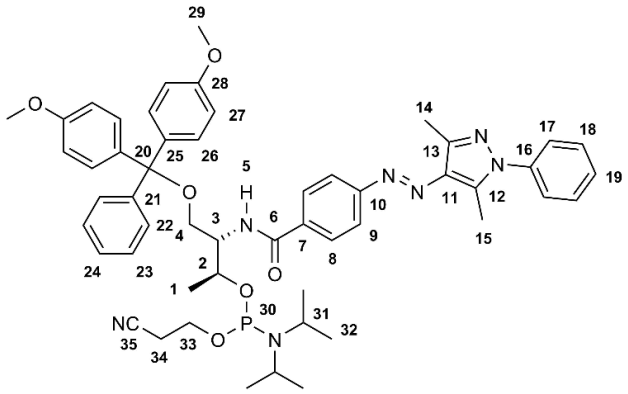

7.2.17 Synthesis of *N*-(4-nitrophenyl)-arylazopyrazole-D-threoninol ("AAP3")

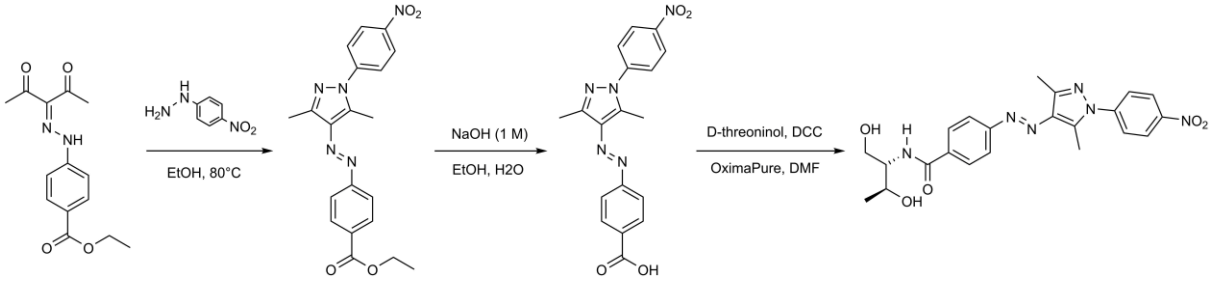

Ethyl-4-((*E*)-(1-(4-nitrophenyl)-3,5-dimethyl-1*H*-pyrazol-4-yl)diazenyl)benzoate (103)

Ethyl-4-(2-(2,4-dioxopentan-3-ylidene)hydrazono)benzoate **(92)** (2.0 g, 7.24 mmol) was dissolved in 40 mL ethanol. 4-Nitrophenylhydrazine (1.11 g, 7.24 mmol) was added portionwise to the solution and the reaction mixture was refluxed for 3 hours. All solvents were removed *in vacuo* and the product was isolated by column chromatography (silica, eluent: cyclohexane/ethyl acetate = 1/1) as a bright orange solid (2.30 g, 81 %).

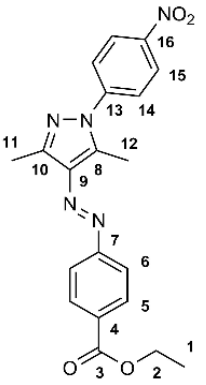

^{1}H-NMR (600 MHz, C_6D_6) δ [ppm] = 8.32-8.34 (m, 2 H, H_{15}), 7.87-7.90 (m, 2 H, H_5), 7.74-7.76 (m, 2 H, H_{14}), 7.02-7.04 (m, 2 H, H_6), 4.17 (q, 2 H, $^{3}J_{2,1}$ = 7.1 Hz, H_2) , 2.67 (s, 3 H, H_{12}) , 2.16 (s, 3 H, H_{11}) , 1.05 (t, 3 H, $^{3}J_{1,2}$ = 7.1 Hz, H_1).

^{13}C-NMR (150 MHz, C_6D_6) δ [ppm] = 166.2 (C_3), 156.9 (C_{10}), 146.8 (C_{16}), 145.2 (C_{13}), 144.1 (C_7), 141.3 (C_9), 138.3 (C_8), 132.5 (C_5), 131.4 (C_{14}), 128.7 (C_6), 125.0 (C_3), 124.0 (C_4), 122.6 (C_{15}), 61.5 (C_2), 15.1 (C_1), 14.7 (C_{11}), 11.8 (C_{12}).

MS (ESI, positive) *m/z* (%) 416.1 (47) $[M+Na]^+$, 381.3 (24) $[C_{19}H_{19}N_5O_4]^+$, 305.1 (28) $[C_{17}H_{15}N_5O]^+$, 299.1 (100) $[C_{17}H_{16}N_4+Na]^+$.

HRMS (ESI, positive) *m/z* calculated for $C_{20}H_{19}N_5O_4Na$: 416.1329, found: 416.1336.

4-((*E*)-(1-(4-Nitrophenyl)-3,5-dimethyl-1*H*-pyrazol-4-yl)diazenyl)benzoic acid (104)

Ethyl-4-((*E*)-(1-(4-nitrophenyl)-3,5-dimethyl-1*H*-pyrazol-4-yl)diazenyl)benzoate **(103)** (1.00 g, 2.54 mmol) was dissolved in 18 mL ethanol and 7 mL 1 M aqueous NaOH solution and the reaction mixture was stirred for 24 hours at room temperature. The mixture was acidified with 1 M aqueous hydrochloric acid and extracted twice with 100 mL ethyl acetate. The combined organic layers were washed with 150 mL water and 100 mL brine followed by evaporation of all solvents. The product was isolated by column chromatography (silica, eluent: chloroform/methanol = 95/5) as a bright orange solid (0.75 g, 81 %).

^{1}H-NMR (500 MHz, $CDCl_3$) δ [ppm] = 9.47 (s, br, 1 H, H_1), 8.39-8.41 (m, 2 H, H_{14}), 8.16-8.18 (m, 2 H, H_4), 7.85-7.87 (m, 2 H, H_5), 7.76-7.79 (m, 2 H, H_{13}), 2.81 (s, 3 H, H_{11}), 2.61 (s, 3 H, H_{10}).

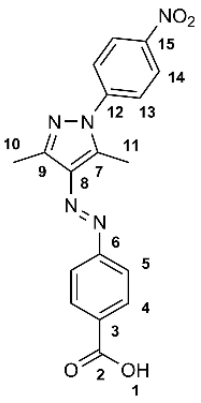

^{13}C-NMR (125 MHz, $CDCl_3$) δ [ppm] = 166.1 (C_2), 155.9 (C_9), 146.4 (C_6), 145.1 (C_{15}), 143.9 (C_{12}), 140.6 (C_6), 137.3 (C_7), 131.3 (C_4), 130.5 (C_3), 124.9 (C_{13}), 124.2 (C_5), 121.8 (C_{14}), 14.3 (C_{10}), 11.8 (C_{11}).

MS (ESI, negative) *m/z* (%) 364.1 (100) $[M-H]^-$.

HRMS (ESI, negative) *m/z* calculated for $C_{18}H_{14}N_5O_4$: 364.1051, found: 364.1033.

4-((*E*)-(1-(4-Nitrophenyl)-3,5-dimethyl-1*H*-pyrazol-4-yl)diazenyl)carboxy-D-threoninol ("AAP3") (105)

4-((*E*)-(1-(4-Nitrophenyl)-3,5-dimethyl-1*H*-pyrazol-4-yl)diazenyl)benzoic acid **(104)** (0.71 g, 1.94 mmol), DCC (0.48 g, 2.32 mmol), OxymaPure (0.30 g, 2.13 mmol) and D-threoninol (0.22 g, 2.13 mmol) were mixed in 20 mL dry DMF under argon atmosphere and stirred for 24 hours. All solid residuals were filtered off and rinsed with DMF followed by removal of DMF *in vacuo*. A small product fraction was isolated by preparative HPLC (C18, eluent: acetonitrile and water in different gradients) as a bright orange solid (10 mg, 1 %).

^{1}H-NMR/^{13}C-NMR: not possible.

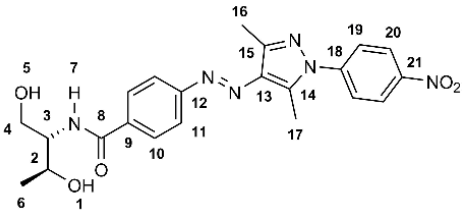

MS (ESI, positive) *m/z* (%) 475.2 (22) $[M+Na]^+$, 431 (100) $[M-NO_2+Na]^+$, 358.1 (44) $[C_{17}H_{15}N_5O_3+Na]^+$, 306.3 (32) $[C_{17}H_{16}N_5O]^+$.

HRMS (ESI, positive) *m/z* calculated for $C_{22}H_{24}N_6O_5Na$: 475.1700, found: 475.1715.

7.2.18 Synthesis of 5-dodecyne-2'-deoxyuridine phosphoramidite ("Lipid")

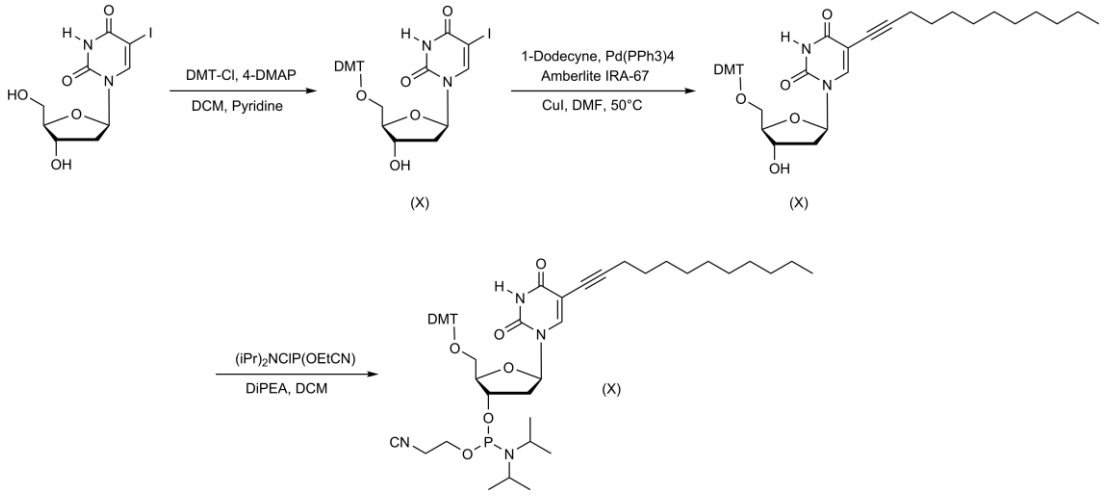

DMT-protected 5-iodo-2'-deoxyuridine (106)[260]

5-Iodo-2'-deoxyuridine (5.0 g, 14.1 mmol) and 4-DMAP (85 mg, 0.7 mmol) were dissolved in 80 mL dry pyridine under argon atmosphere. DMT-chloride (5.74 g, 16.9 mmol) was dissolved in dry dichloromethane and the solution was added dropwise to the first solution under argon atmosphere at room temperature over 30 minutes. The reaction mixture was stirred for 16 hours followed by removal of all volatiles under reduced pressure. The product was isolated by column chromatography (silica, eluent: cyclohexane/ethyl acetate = 1/1 with 3 % triethylamine) as a yellowish white solid (yield: 3.0g, 32 %).

^{1}H-NMR (500 MHz, CD_2Cl_2) δ [ppm] = 9.55 (s, br, 1 H, H_8), 8.15 (s, 1 H, H_{11}), 7.49-7.47 (m, 2 H, H_{14}), 7.40-7.26 (m, 7 H, H_{15}+H_{16}+H_{18}), 6.91-6.89 (m, 4 H, H_{19}), 6.33-6.30 (m, 1 H, H_1), 4.14 (q, 2 H, H_3+H_6), 3.82 (s, 6 H, H_{21}), 3.40-3.39 (m, 2 H, H_5), 2.59-2.49 (m, 2 H, H_2), 2.35-2.30 (m, 1 H, H_4).

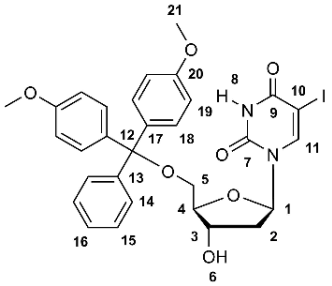

^{13}C-NMR (125 MHz, CD_2Cl_2) δ [ppm] = 170.9 (C_{11}), 160.3 (C_7), 158.8 (C_{20}), 150.1 (C_9), 144.5 (C_{13}), 135.6 (C_{17}), 130.1 (C_{16}), 128.1 (C_{18}), 127.0 (C_{19}), 113.3 (C_{14}), 86.6 (C_4), 85.7 (C_1), 72.3 (C_{21}), 68.4 (C_3), 63.6 (C_{10}), 60.3 (C_{12}), 55.3 (C_5), 41.3 (C_2).

MS (ESI, positive) *m/z* (%) 679.1 (48%) $[M+Na]^+$, 303.1 (100%) $[DMT]^+$.

HRMS (ESI, positive) *m/z* calculated for $C_{30}H_{29}IN_2O_7Na$: 679.0912 $[M+Na]^+$, found: 679.0900 $[M+Na]^+$.

DMT-protected 5-dodecynyl-2'-deoxyuridine (107)[260]

DMT-protected 5-iodo-2'-deoxyuridine **(106)** (1.0 g, 1.52 mmol), $Pd(PPh_3)_4$ (176 mg, 0.15 mmol) and CuI (57 mg, 0.30 mmol) were dried for 30 minutes. 12.5 mL dry DMF was added under argon atmosphere, followed by Amberlite IRA67 (2.5 g) and 1-dodecyne (0.76 g, 4.56 mmol). The reaction mixture was stirred for 20 hours at room temperature under argon atmosphere. All solids were filtered off and rinsed with 10 mL of a 1:1 methanol dichloromethane mixture. All solvents were removed under reduced pressure and the product was isolated by column chromatography (silica, eluent: cyclohexane/ethyl acetate = 1/1) as a white solid (yield: 0.50 g, 47 %).

^{1}H-NMR (500 MHz, CD_2Cl_2) δ [ppm] = 7.94-7.96 (m, 2 H, H_{26}), 7.21-7.48 (m, 8 H, H_8+H_{27}+H_{28}+H_{30}), 6.84-6.86 (m, 4 H, H_{31}), 6.24-6.30 (m, 1 H, H_{11}), 4.53-4.55 (m, 1 H, H_1), 4.06-4.08 (m, 1 H, H_3), 3.78 (s, 6 H, H_{33}), 3.31-3.47 (m, 2 H, H_5), 2.56-2.59 (m, 1 H, H_2), 2.42-2.48 (m, 1 H, H_2'),2.24-2.29 (m, 1 H, H_4), 2.05-2.21 (m, 1 H, H_4), 1.18-1.43 (m, 19 H, H_{15}-H_{23}), 0.87-0.90 (m, 2 H, H_{14}).

^{13}C-NMR (125 MHz, CD_2Cl_2) δ [ppm] = 162.1 (C_7), 158.7 (C_{32}), 149.5 (C_9), 144.7 (C_{11}), 141.7 (C_{27}), 135.6 (C_{25}), 130.0 (C_{29}), 128.0 (C_{28}), 127.9 (C_{30}), 126.8 (C_{31}), 113.2 (C_{26}), 100.8 (C_{13}), 95.1 (C_{12}), 86.5 (C_4), 85.5 (C_1), 72.3 (C_{33}), 70.7 (C_3), 63.6 (C_{24}), 57.9 (C_{10}), 55.2 (C_5), 45.3 (C_{14}), 41.3 (C_2), 31.9 ($C_{15\text{-}23}$), 29.6 ($C_{15\text{-}23}$), 29.5 ($C_{15\text{-}23}$), 29.3 ($C_{15\text{-}23}$), 29.1 ($C_{15\text{-}23}$), 28.5 ($C_{15\text{-}23}$), 22.7 ($C_{15\text{-}23}$), 19.4 ($C_{15\text{-}23}$), 13.9 ($C_{15\text{-}23}$).

MS (ESI, positive) *m/z* (%) 717.4 (95%) $[M+Na]^+$, 303.1 (100 %) $[DMT]^+$.

HRMS (ESI, positive) *m/z* calculated for $C_{42}H_{50}N_2O_7Na$: 717.3510 $[M+Na]^+$, found: 717.3500 $[M+Na]^+$.

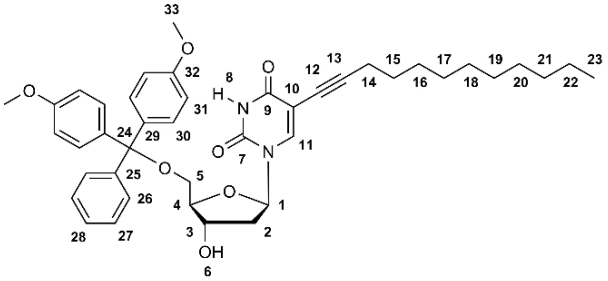

DMT-protected 5-dodecynyl-2'-deoxyuridine phosphoramidite (108)[260]

DMT-protected 5-dodecynyl-2'-deoxyuridine **(107)** (0.5 g, 0.72 mmol) was dissolved in 7 mL dry dichloromethane under argon atmosphere and the solution was cooled to 0 °C. DiPEA (0.10 g, 0.80 mmol) was added dropwise to the solution and the reaction mixture was stirred for 10 minutes at 0 °C. 2-Cyanoethyl-*N*,*N*-diisopropylchlorophosophoramidite (0.19 g, 0.80 mmol) was added dropwise to the reaction mixture at 0 °C and stirring was continued for

10 minutes at 0 °C, then the mixture was warmed up to room temperature. Stirring was continued for 2.5 hours followed by evaporation of all solvents *in vacuo*. The product was isolated *via* column chromatography (silica, eluent: cyclohexane/ethyl acetate = 1/1 with 3% triethylamine) as a white foamy solid (yield 0.5 g, 78 %).

^{1}H-NMR (400 MHz, CD_2Cl_2) δ [ppm] = 8.72 (s, br, 1 H, H_7), 7.94-7.98 (m, 1 H, H_{27}), 7.46-7.49 (m, 2 H, H_{25}), 7.30-7.39 (m, 6 H, H_{26}+H_{29}), 7.22-7.26 (m, 1 H, H_3), 6.84-6.88 (m, 4 H, H_{30}), 6.25-6.29 (m, 1 H, H_{10}), 4.61-4.65 (m, 1 H, H_1), 4.16-4.22 (m, 1 H, H_{36}), 3.58-3.79 (m, 9 H, H_5+H_{32}+H_{36}), 3.33-3.38 (m, 3 H, H_{37}+H_3), 2.48-2.65 (m, 3 H, H_2+H_{34}), 2.28-2.33 (m, 1 H, H_{34}), 2.06-2.11 (m, 2 H, H_4), 1.17-1.29 (m, 25 H, $H_{14\text{-}22}$+H_{35}), 1.11 (d, 3 H, H_{35}), 0.90 (t, 3 H, H_{35}).

^{31}P-NMR: (162 MHz, CD_2Cl_2) δ [ppm] = 149.3 (P_{33}).

MS (ESI, positive) *m/z* (%) 917.5 (17) $[M+Na]^+$, 895.5 (29) $[M+H]^+$, 303.1 (100) $[DMT]^+$.

HRMS (ESI, positive) *m/z* calculated for $C_{51}H_{67}N_4O_8PH$: 895.4769, found: 895.4773.

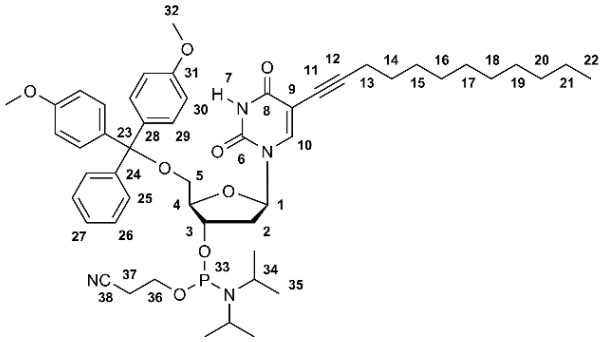

7.3 UV/Vis spectra of all synthesized photochrome molecules

UV/Vis spectroscopy was performed on a JASCO V630 Bio spectrophotometer in Hellma Analytics Suprasil QS precision cuvettes with a sample volume of 100 µL and a concentration of c = 25 µM in a mixture of 1:1 acetonitrile and Millipore water. Each sample was irradiated for 5 minutes at room temperature at a given wavelength with maximum intensity to fully reach the wavelength-dependent photostationary state (PSS). For each set of UV/Vis absorption spectra, the relative change of intensity at the absorption maximum was calculated to yield a qualitative wavelength-dependent irradiation scan profile. The highest absorption maximum was normalized to 1 in each irradiation scan profile, all other values are given in respect to the normalized maximum value.

7.3.1 UV/Vis spectra of all synthesized azobenzene molecules

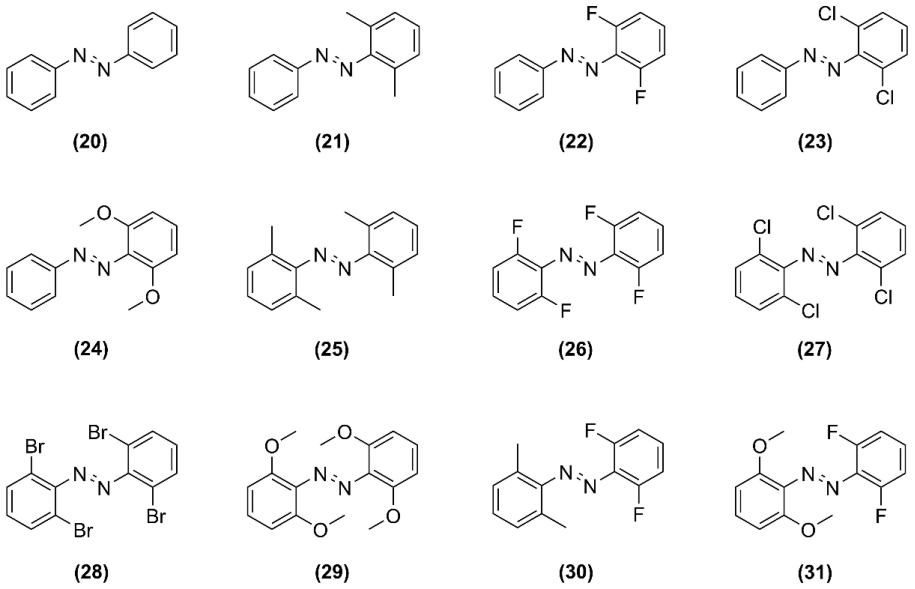

Fig. 96: Azobenzene molecules investigated *via* UV/Vis-spectroscopy to determine the absorption maxima as well as the minimum and maximum converting irradiation wavelengths.

Azobenzene **(20)**

UV/vis absorption spectra after irradiation with each available wavelength (left) and the resulting change in absorption intensity at the absorption maximum upon irradiation (right).

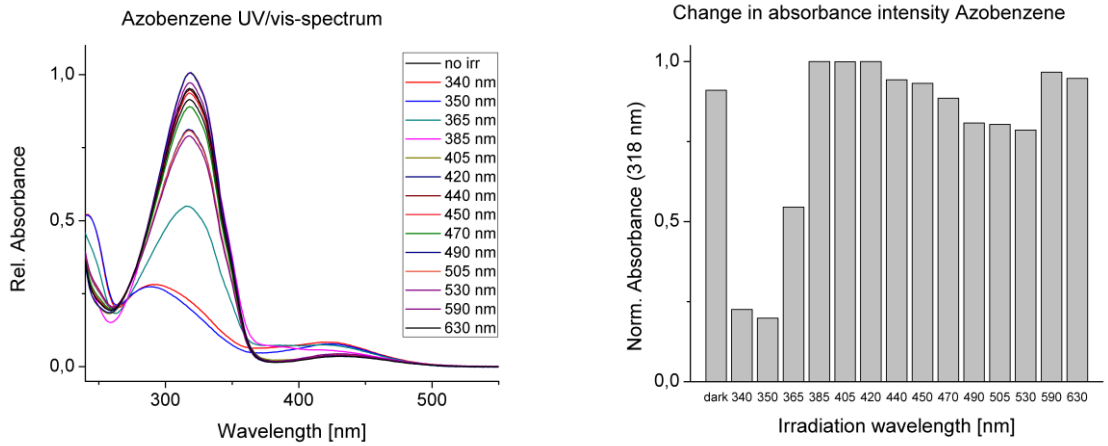

Normalized, wavelength dependent absorption intensity values at the absorption maximum:

Wave-length	**dark**	**340 nm**	**350 nm**	**365 nm**	**385 nm**	**405 nm**	**420 nm**	**440 nm**	**450 nm**	**470 nm**	**490 nm**	**505 nm**	**530 nm**	**590 nm**	**630 nm**
I(318 nm)	0.91	0.23	0.20	0.55	1.00	1.00	1.00	0.94	0.93	0.89	0.81	0.80	0.79	0.97	0.95

2,6-Dimethylazobenzene **(21)**

UV/vis absorption spectra after irradiation with each available wavelength (left) and the resulting change in absorption intensity at the absorption maximum upon irradiation (right).

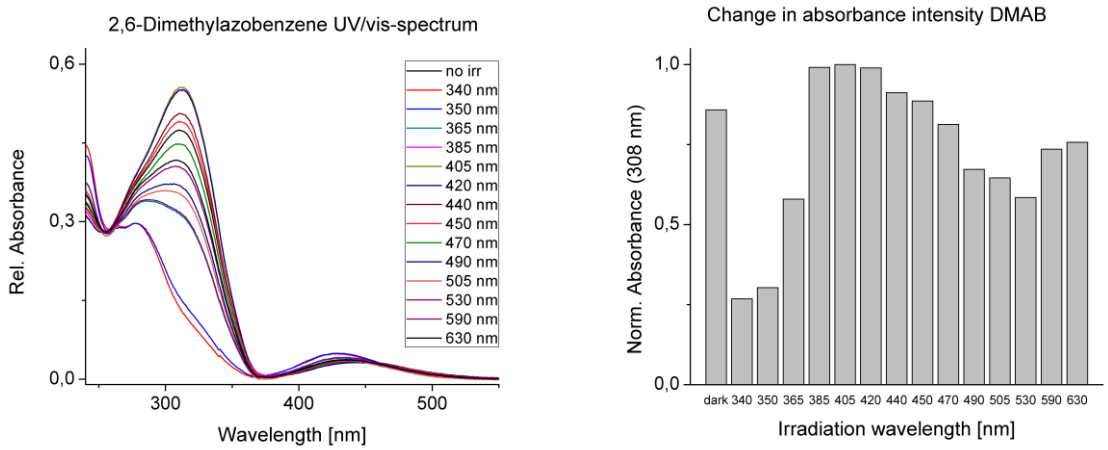

Normalized, wavelength dependent absorption intensity values at the absorption maximum:

Wave-length	**dark**	**340 nm**	**350 nm**	**365 nm**	**385 nm**	**405 nm**	**420 nm**	**440 nm**	**450 nm**	**470 nm**	**490 nm**	**505 nm**	**530 nm**	**590 nm**	**630 nm**
I(308 nm)	0.86	0.27	0.30	0.58	0.99	1.00	0.99	0.91	0.89	0.81	0.67	0.65	0.58	0.74	0.76

2,6-Difluoroazobenzene **(22)**

UV/vis absorption spectra after irradiation with each available wavelength (left) and the resulting change in absorption intensity at the absorption maximum upon irradiation (right).

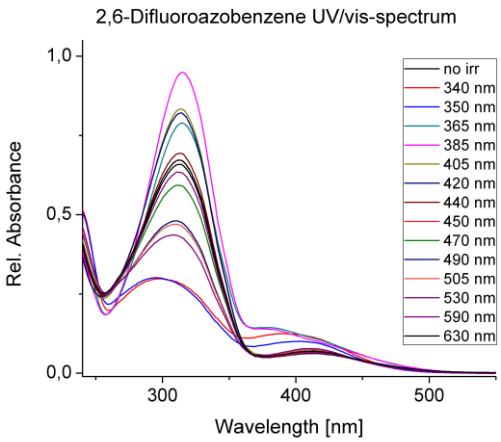

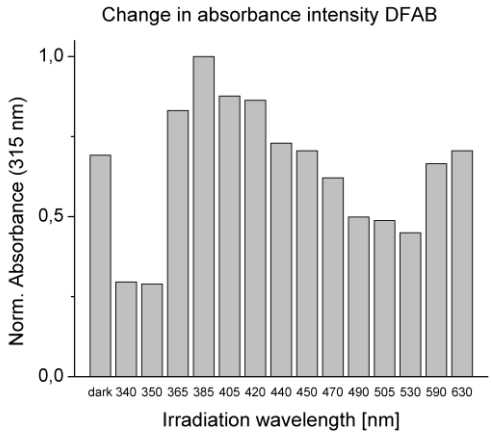

Normalized, wavelength dependent absorption intensity values at the absorption maximum:

Wave-length	**dark**	**340 nm**	**350 nm**	**365 nm**	**385 nm**	**405 nm**	**420 nm**	**440 nm**	**450 nm**	**470 nm**	**490 nm**	**505 nm**	**530 nm**	**590 nm**	**630 nm**
I(315 nm)	0.69	0.30	0.29	0.83	1.00	0.88	0.86	0.73	0.71	0.62	0.50	0.49	0.45	0.67	0.71

2,6-Dichloroazobenzene **(23)**

UV/vis absorption spectra after irradiation with each available wavelength (left) and the resulting change in absorption intensity at the absorption maximum upon irradiation (right).

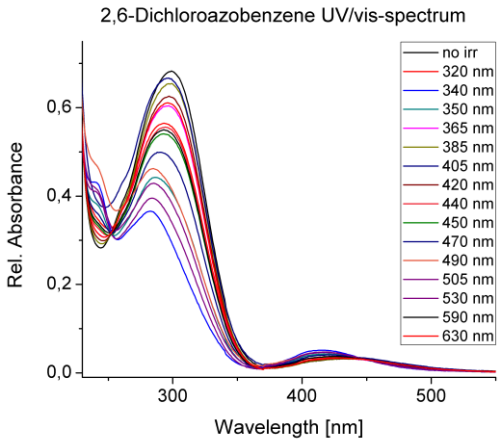

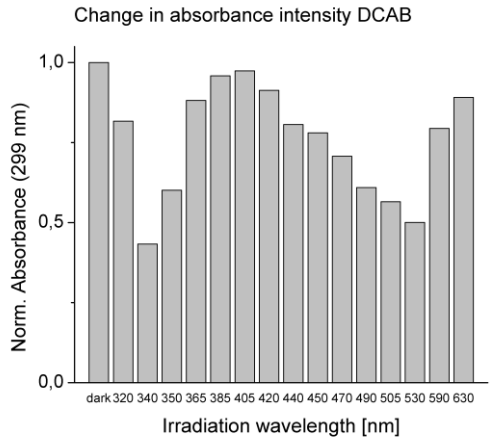

Normalized, wavelength dependent absorption intensity values at the absorption maximum:

Wave-length	**dark**	**320 nm**	**340 nm**	**350 nm**	**365 nm**	**385 nm**	**405 nm**	**420 nm**	**440 nm**	**450 nm**	**470 nm**	**490 nm**	**505 nm**	**530 nm**	**590 nm**	**630 nm**
I(299 nm)	1.00	0.82	0.43	0.60	0.88	0.96	0.97	0.91	0.81	0.78	0.71	0.61	0.56	0.50	0.79	0.89

2,6-Dimethoxyazobenzene **(24)**

UV/vis absorption spectra after irradiation with each available wavelength (left) and the resulting change in absorption intensity at the absorption maximum upon irradiation (right).

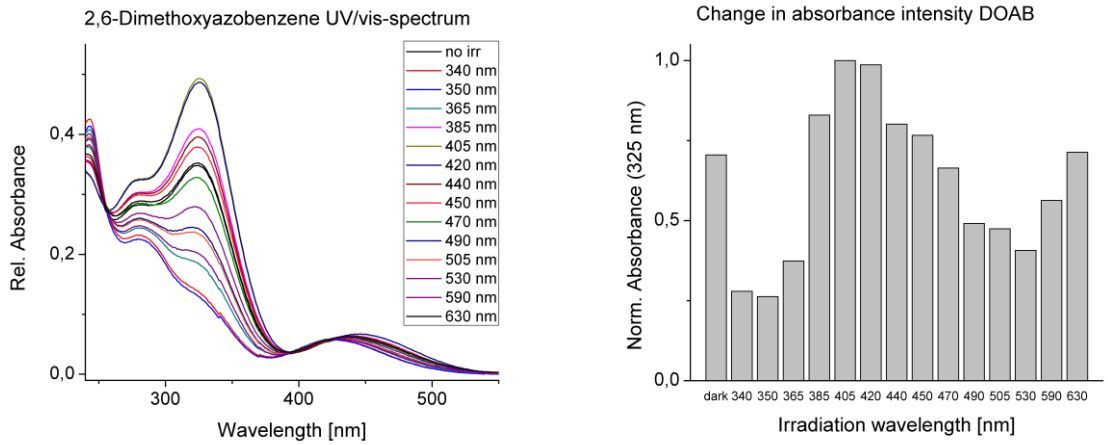

Normalized, wavelength dependent absorption intensity values at the absorption maximum:

Wave-length	**dark**	**340 nm**	**350 nm**	**365 nm**	**385 nm**	**405 nm**	**420 nm**	**440 nm**	**450 nm**	**470 nm**	**490 nm**	**505 nm**	**530 nm**	**590 nm**	**630 nm**
I(325 nm)	0.71	0.28	0.26	0.37	0.83	1.00	0.99	0.80	0.77	0.66	0.49	0.47	0.41	0.56	0.71

2,2‘,6,6‘-Tetramethylazobenzene **(25)**

UV/vis absorption spectra after irradiation with each available wavelength (left) and the resulting change in absorption intensity at the absorption maximum upon irradiation (right).

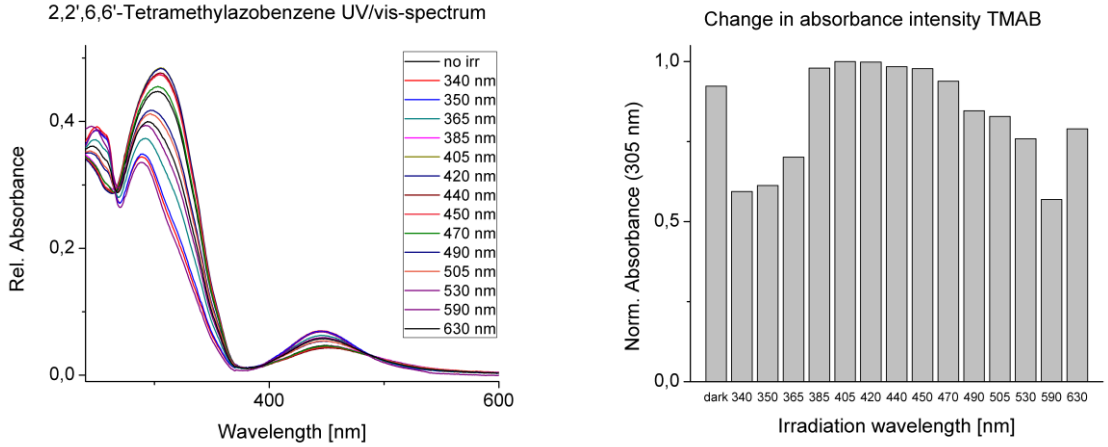

Normalized, wavelength dependent absorption intensity values at the absorption maximum:

Wave-length	**dark**	**340 nm**	**350 nm**	**365 nm**	**385 nm**	**405 nm**	**420 nm**	**440 nm**	**450 nm**	**470 nm**	**490 nm**	**505 nm**	**530 nm**	**590 nm**	**630 nm**
I(305 nm)	0.92	0.59	0.61	0.70	0.98	1.00	1.00	0.98	0.98	0.94	0.85	0.83	0.76	0.57	0.79

2,2‘,6,6‘-Tetrafluoroazobenzene **(26)**

UV/vis absorption spectra after irradiation with each available wavelength (left) and the resulting change in absorption intensity at the absorption maximum upon irradiation (right).

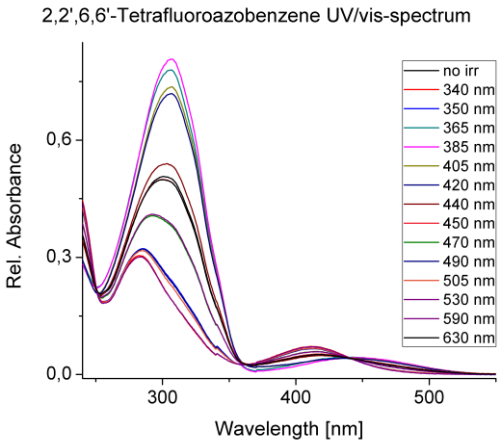

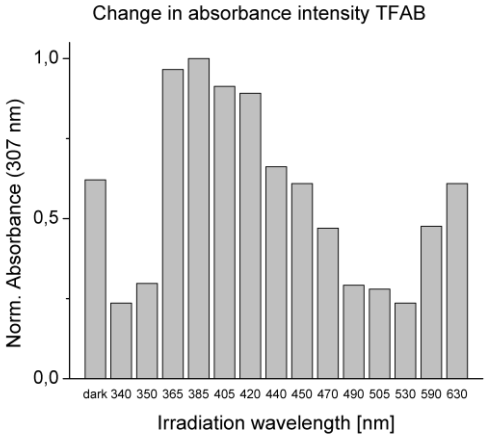

Normalized, wavelength dependent absorption intensity values at the absorption maximum:

Wave-length	**dark**	**340 nm**	**350 nm**	**365 nm**	**385 nm**	**405 nm**	**420 nm**	**440 nm**	**450 nm**	**470 nm**	**490 nm**	**505 nm**	**530 nm**	**590 nm**	**630 nm**
I(307 nm)	0.62	0.24	0.30	0.97	1.00	0.91	0.89	0.66	0.61	0.47	0.29	0.28	0.24	0.48	0.61

2,2‘,6,6‘-Tetrachloroazobenzene **(27)**

UV/vis absorption spectra after irradiation with each available wavelength (left) and the resulting change in absorption intensity at the absorption maximum upon irradiation (right).

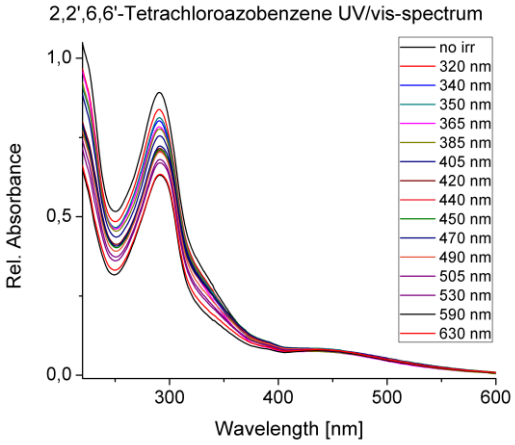

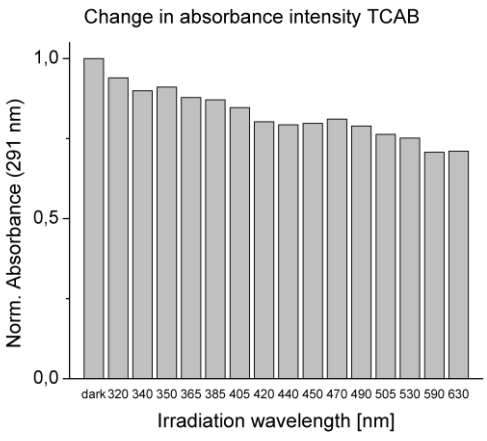

Normalized, wavelength dependent absorption intensity values at the absorption maximum:

Wave-length	**dark**	**320 nm**	**340 nm**	**350 nm**	**365 nm**	**385 nm**	**405 nm**	**420 nm**	**440 nm**	**450 nm**	**470 nm**	**490 nm**	**505 nm**	**530 nm**	**590 nm**	**630 nm**
I(291 nm)	1.00	0.94	0.90	0.91	0.88	0.87	0.85	0.80	0.79	0.80	0.81	0.79	0.76	0.75	0.71	0.71

2,2',6,6'-Tetrabromoazobenzene **(28)**

UV/vis absorption spectra after irradiation with each available wavelength (left) and the resulting change in absorption intensity at the absorption maximum upon irradiation (right).

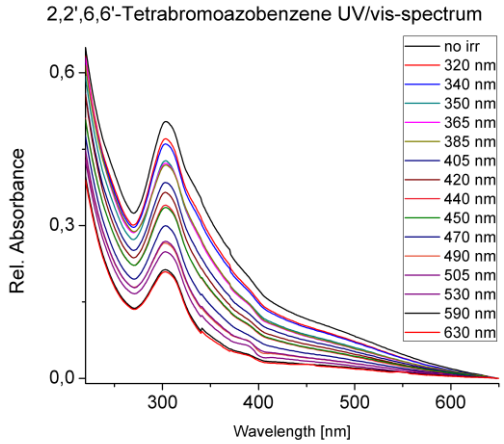

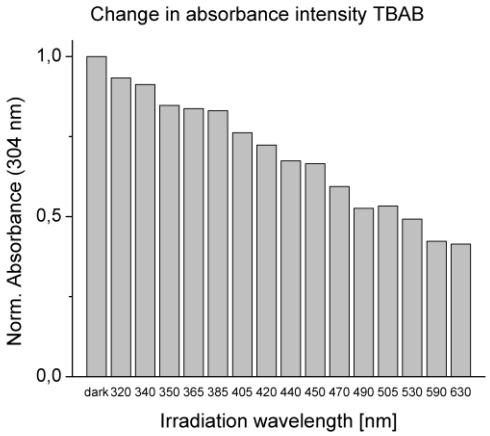

Normalized, wavelength dependent absorption intensity values at the absorption maximum:

Wave-length	**dark**	**320 nm**	**340 nm**	**350 nm**	**365 nm**	**385 nm**	**405 nm**	**420 nm**	**440 nm**	**450 nm**	**470 nm**	**490 nm**	**505 nm**	**530 nm**	**590 nm**	**630 nm**
I(304 nm)	1.00	0.93	0.91	0.85	0.84	0.83	0.76	0.72	0.67	0.66	0.59	0.53	0.53	0.49	0.42	0.41

2,2',6,6'-Tetramethoxyazobenzene **(29)**

UV/vis absorption spectra after irradiation with each available wavelength (left) and the resulting change in absorption intensity at the absorption maximum upon irradiation (right).

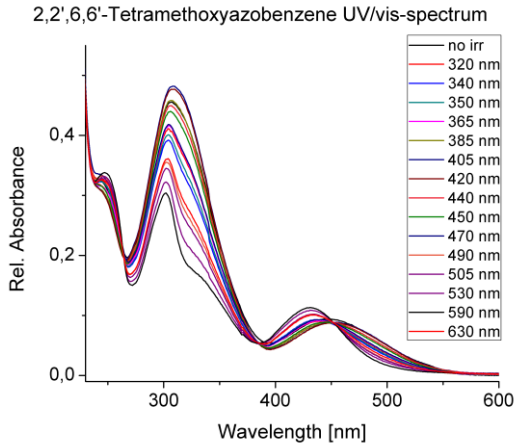

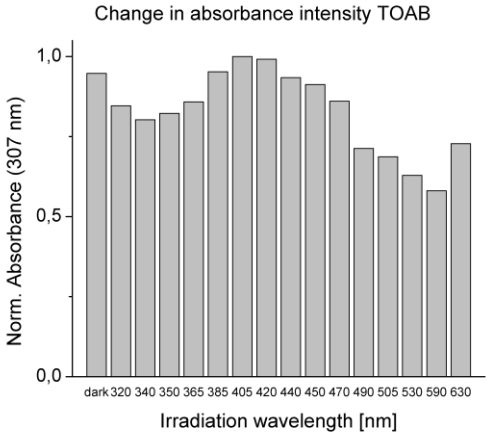

Normalized, wavelength dependent absorption intensity values at the absorption maximum:

Wave-length	**dark**	**320 nm**	**340 nm**	**350 nm**	**365 nm**	**385 nm**	**405 nm**	**420 nm**	**440 nm**	**450 nm**	**470 nm**	**490 nm**	**505 nm**	**530 nm**	**590 nm**	**630 nm**
I(307 nm)	0.95	0.85	0.80	0.82	0.86	0.95	1.00	0.99	0.93	0.91	0.86	0.71	0.69	0.63	0.58	0.73

2,6-Dimethyl-2',6'-difluoroazobenzene **(30)**

UV/vis absorption spectra after irradiation with each available wavelength (left) and the resulting change in absorption intensity at the absorption maximum upon irradiation (right).

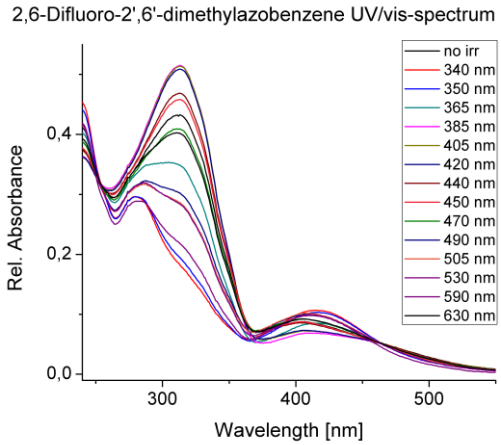

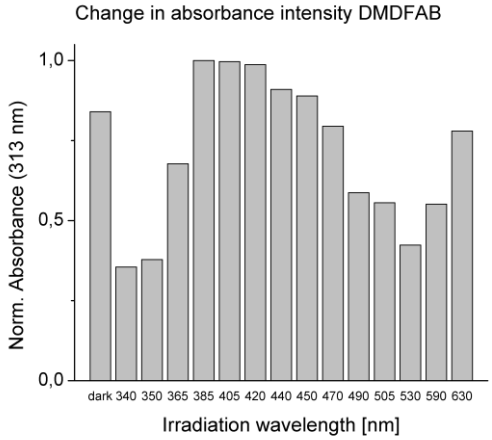

Normalized, wavelength dependent absorption intensity values at the absorption maximum:

Wave-length	**dark**	**340 nm**	**350 nm**	**365 nm**	**385 nm**	**405 nm**	**420 nm**	**440 nm**	**450 nm**	**470 nm**	**490 nm**	**505 nm**	**530 nm**	**590 nm**	**630 nm**
I(313 nm)	0.84	0.35	0.38	0.68	1.00	1.00	0.99	0.91	0.90	0.79	0.59	0.56	0.42	0.55	0.78

2,6-Dimethoxy-2',6'-difluoroazobenzene **(31)**

UV/vis absorption spectra after irradiation with each available wavelength (left) and the resulting change in absorption intensity at the absorption maximum upon irradiation (right).

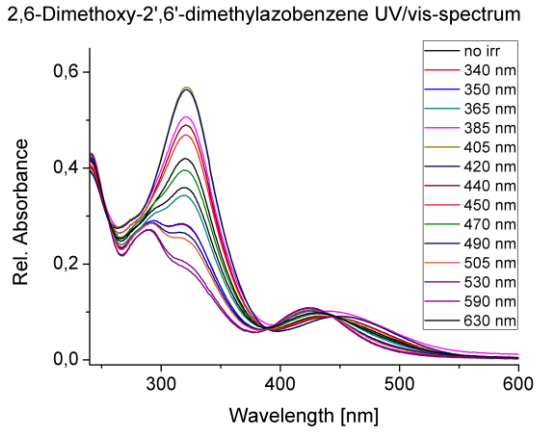

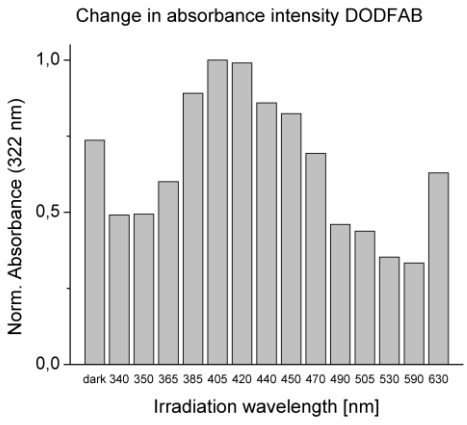

Normalized, wavelength dependent absorption intensity values at the absorption maximum:

Wave-length	**dark**	**340 nm**	**350 nm**	**365 nm**	**385 nm**	**405 nm**	**420 nm**	**440 nm**	**450 nm**	**470 nm**	**490 nm**	**505 nm**	**530 nm**	**590 nm**	**630 nm**
I(322 nm)	0.74	0.49	0.49	0.60	0.89	1.00	0.99	0.86	0.82	0.69	0.46	0.44	0.35	0.33	0.63

7.3.2 UV/Vis spectra of all synthesized arylazopyrazole molecules

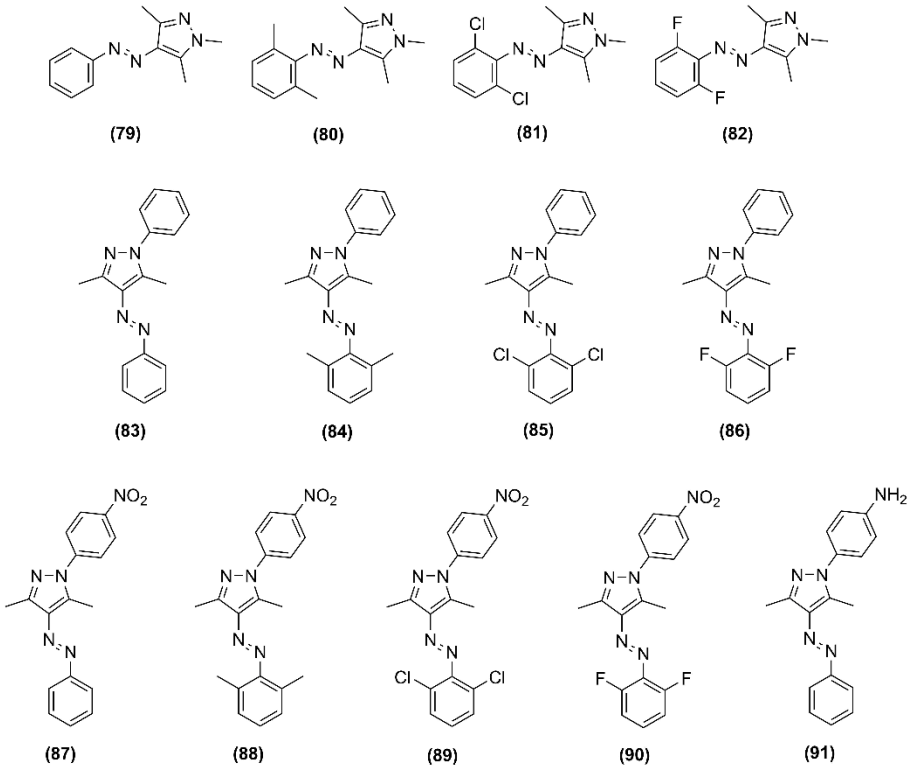

Fig. 97: Arylazopyrazole molecules investigated *via* UV/Vis-spectroscopy to determine the absorption maxima as well as the minimum and maximum converting irradiation wavelengths.

Phenyl-AAP1 **(79)**

UV/vis absorption spectra after irradiation with each available wavelength (left) and the resulting change in absorption intensity at the absorption maximum upon irradiation (right).

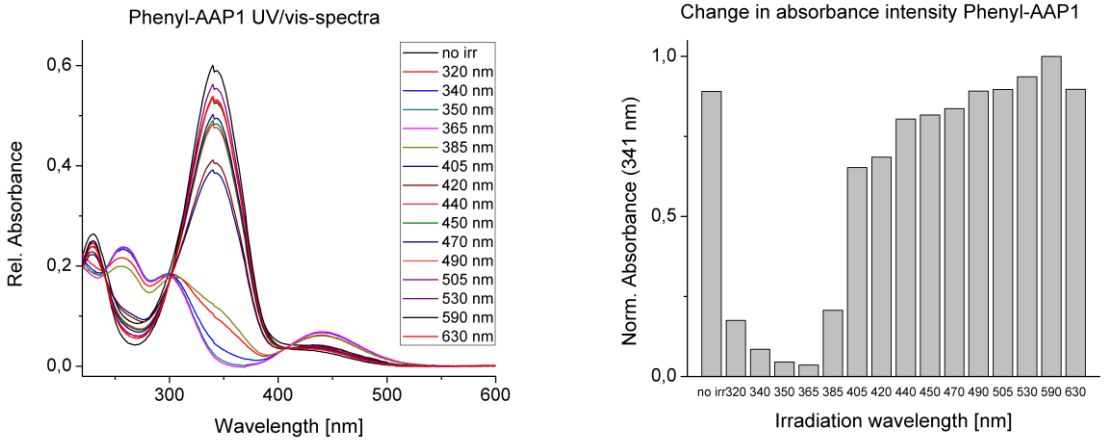

Normalized, wavelength dependent absorption intensity values at the absorption maximum:

Wave-length	**dark**	**320 nm**	**340 nm**	**350 nm**	**365 nm**	**385 nm**	**405 nm**	**420 nm**	**440 nm**	**450 nm**	**470 nm**	**490 nm**	**505 nm**	**530 nm**	**590 nm**	**630 nm**
I(341 nm)	0.89	0.18	0.08	0.05	0.04	0.21	0.65	0.69	0.80	0.82	0.84	0.89	0.90	0.94	1.00	0.90

2’,6’-Dimethyl-AAP1 **(80)**

UV/vis absorption spectra after irradiation with each available wavelength (left) and the resulting change in absorption intensity at the absorption maximum upon irradiation (right).

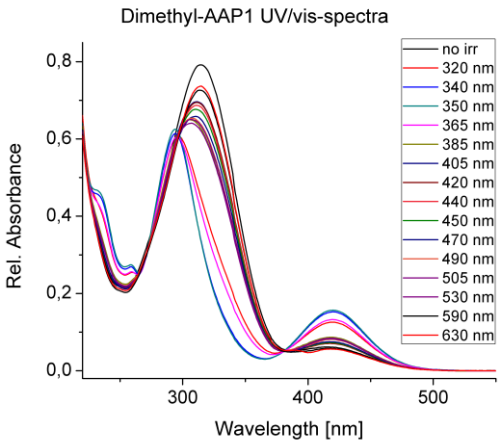

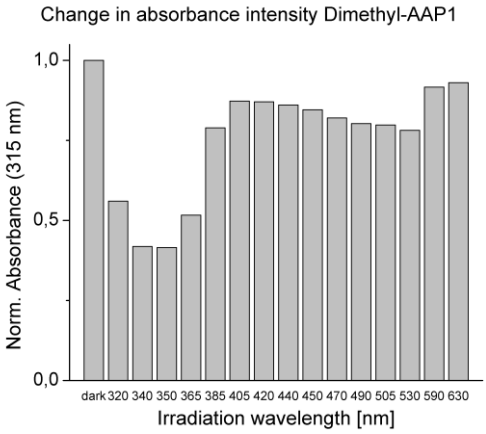

Normalized, wavelength dependent absorption intensity values at the absorption maximum:

Wave-length	**dark**	**320 nm**	**340 nm**	**350 nm**	**365 nm**	**385 nm**	**405 nm**	**420 nm**	**440 nm**	**450 nm**	**470 nm**	**490 nm**	**505 nm**	**530 nm**	**590 nm**	**630 nm**
I(315 nm)	1.00	0.56	0.42	0.42	0.52	0.79	0.87	0.87	0.86	0.85	0.82	0.80	0.80	0.78	0.92	0.93

2’,6’-Dichloro-AAP1 **(81)**

UV/vis absorption spectra after irradiation with each available wavelength (left) and the resulting change in absorption intensity at the absorption maximum upon irradiation (right).

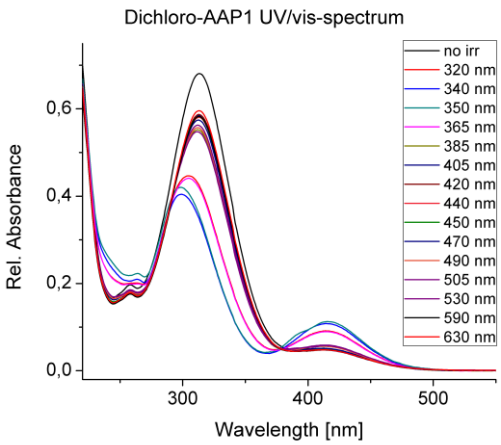

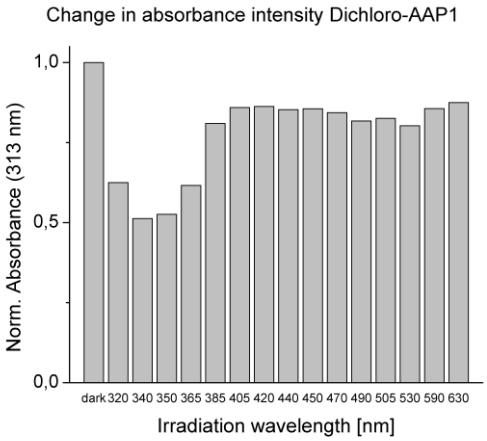

Normalized, wavelength dependent absorption intensity values at the absorption maximum:

Wave-length	**dark**	**320 nm**	**340 nm**	**350 nm**	**365 nm**	**385 nm**	**405 nm**	**420 nm**	**440 nm**	**450 nm**	**470 nm**	**490 nm**	**505 nm**	**530 nm**	**590 nm**	**630 nm**
I(313 nm)	1.00	0.62	0.51	0.53	0.62	0.81	0.86	0.86	0.85	0.86	0.84	0.82	0.83	0.80	0.86	0.87

2',6'-Difluoro-AAP1 **(82)**

UV/vis absorption spectra after irradiation with each available wavelength (left) and the resulting change in absorption intensity at the absorption maximum upon irradiation (right).

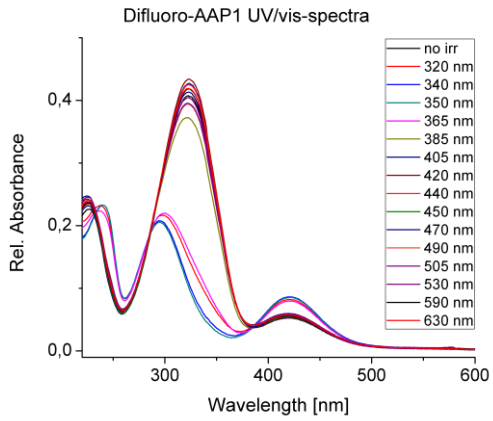

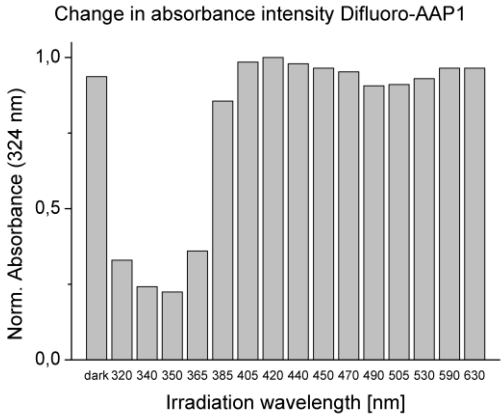

Normalized, wavelength dependent absorption intensity values at the absorption maximum:

Wave-length	**dark**	**320 nm**	**340 nm**	**350 nm**	**365 nm**	**385 nm**	**405 nm**	**420 nm**	**440 nm**	**450 nm**	**470 nm**	**490 nm**	**505 nm**	**530 nm**	**590 nm**	**630 nm**
I(324 nm)	0.94	0.33	0.24	0.22	0.36	0.86	0.99	1.00	0.98	0.96	0.95	0.91	0.91	0.93	0.97	0.97

Phenyl-AAP2 **(83)**

UV/vis absorption spectra after irradiation with each available wavelength (left) and the resulting change in absorption intensity at the absorption maximum upon irradiation (right).

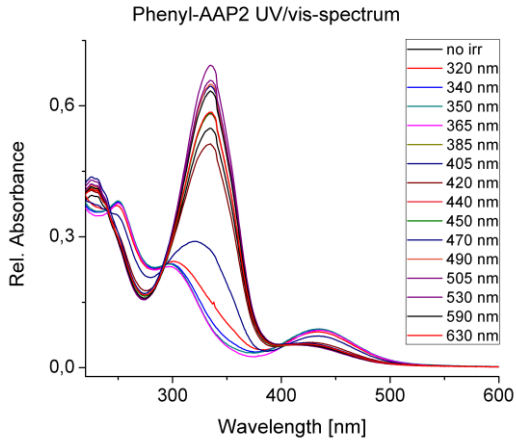

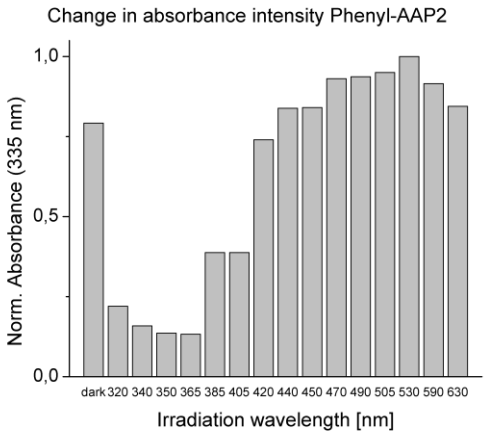

Normalized, wavelength dependent absorption intensity values at the absorption maximum:

Wave-length	**dark**	**320 nm**	**340 nm**	**350 nm**	**365 nm**	**385 nm**	**405 nm**	**420 nm**	**440 nm**	**450 nm**	**470 nm**	**490 nm**	**505 nm**	**530 nm**	**590 nm**	**630 nm**
I(335 nm)	0.79	0.22	0.16	0.14	0.13	0.39	0.39	0.74	0.84	0.84	0.93	0.94	0.95	1.00	0.91	0.84

2’,6’-Dimethyl-AAP2 **(84)**

UV/vis absorption spectra after irradiation with each available wavelength (left) and the resulting change in absorption intensity at the absorption maximum upon irradiation (right).

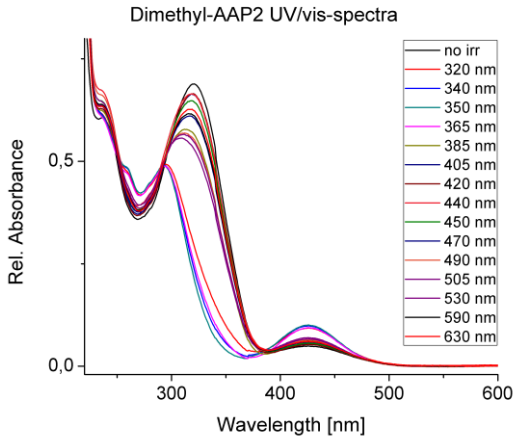

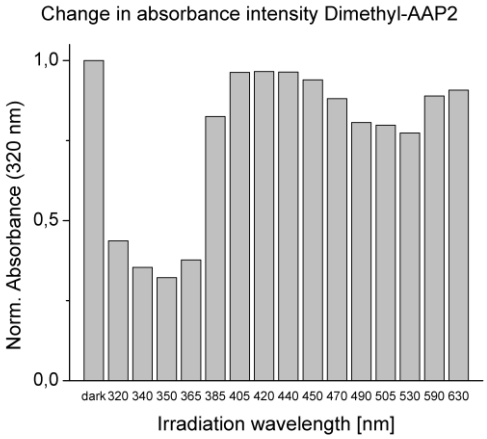

Normalized, wavelength dependent absorption intensity values at the absorption maximum:

Wave-length	**dark**	**320 nm**	**340 nm**	**350 nm**	**365 nm**	**385 nm**	**405 nm**	**420 nm**	**440 nm**	**450 nm**	**470 nm**	**490 nm**	**505 nm**	**530 nm**	**590 nm**	**630 nm**
I(320 nm)	1.00	0.44	0.36	0.32	0.38	0.83	0.96	0.97	0.96	0.94	0.88	0.81	0.80	0.77	0.89	0.91

2’,6’-Dichloro-AAP2 **(85)**

UV/vis absorption spectra after irradiation with each available wavelength (left) and the resulting change in absorption intensity at the absorption maximum upon irradiation (right).

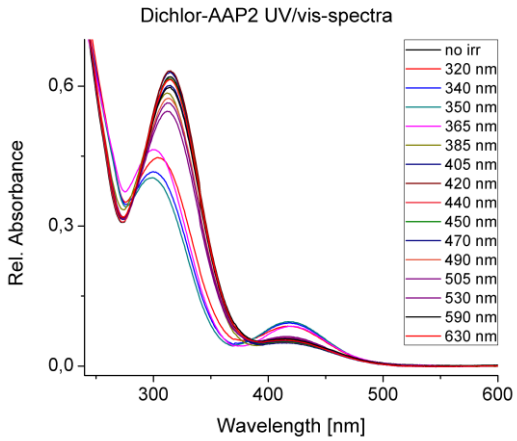

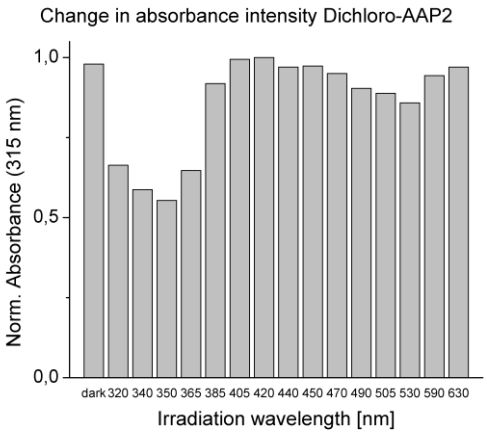

Normalized, wavelength dependent absorption intensity values at the absorption maximum:

Wave-length	**dark**	**320 nm**	**340 nm**	**350 nm**	**365 nm**	**385 nm**	**405 nm**	**420 nm**	**440 nm**	**450 nm**	**470 nm**	**490 nm**	**505 nm**	**530 nm**	**590 nm**	**630 nm**
I(315 nm)	0.98	0.66	0.59	0.55	0.65	0.92	0.99	1.00	0.97	0.97	0.95	0.90	0.89	0.86	0.94	0.97

2',6'-Difluoro-AAP2 **(86)**

UV/vis absorption spectra after irradiation with each available wavelength (left) and the resulting change in absorption intensity at the absorption maximum upon irradiation (right).

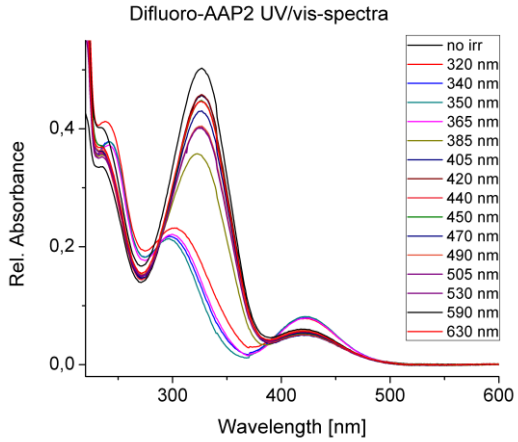

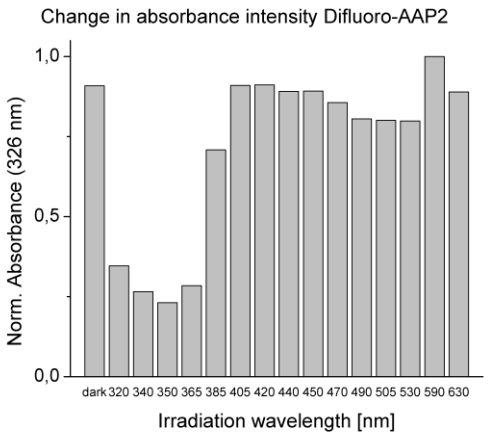

Normalized, wavelength dependent absorption intensity values at the absorption maximum:

Wave-length	**dark**	**320 nm**	**340 nm**	**350 nm**	**365 nm**	**385 nm**	**405 nm**	**420 nm**	**440 nm**	**450 nm**	**470 nm**	**490 nm**	**505 nm**	**530 nm**	**590 nm**	**630 nm**
I(326 nm)	0.91	0.35	0.27	0.23	0.28	0.71	0.91	0.91	0.89	0.89	0.86	0.81	0.80	0.80	1.00	0.89

Phenyl-AAP3 **(87)**

UV/vis absorption spectra after irradiation with each available wavelength (left) and the resulting change in absorption intensity at the absorption maximum upon irradiation (right).

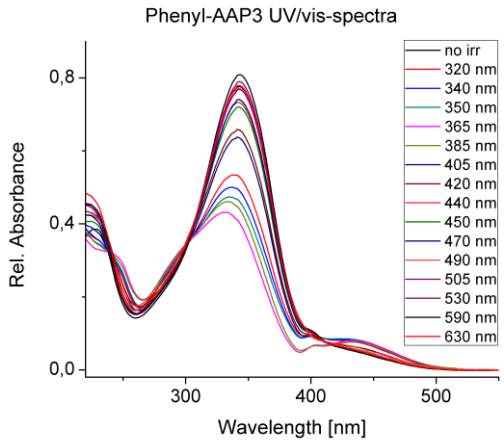

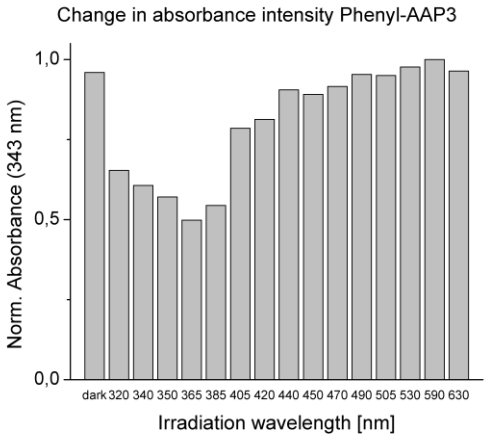

Normalized, wavelength dependent absorption intensity values at the absorption maximum:

Wave-length	**dark**	**320 nm**	**340 nm**	**350 nm**	**365 nm**	**385 nm**	**405 nm**	**420 nm**	**440 nm**	**450 nm**	**470 nm**	**490 nm**	**505 nm**	**530 nm**	**590 nm**	**630 nm**
I(343 nm)	0.96	0.65	0.61	0.57	0.50	0.54	0.79	0.81	0.90	0.89	0.92	0.95	0.95	0.98	1.00	0.96

2’,6’-Dimethyl-AAP3 **(88)**

UV/vis absorption spectra after irradiation with each available wavelength (left) and the resulting change in absorption intensity at the absorption maximum upon irradiation (right).

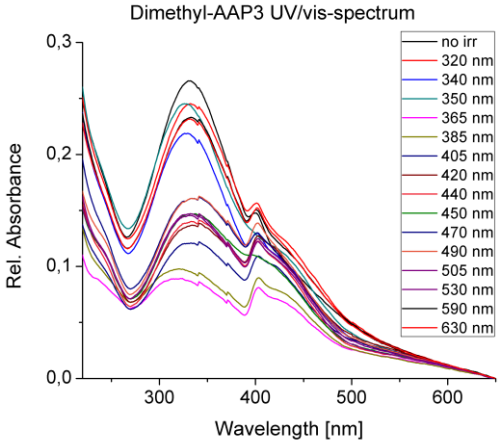

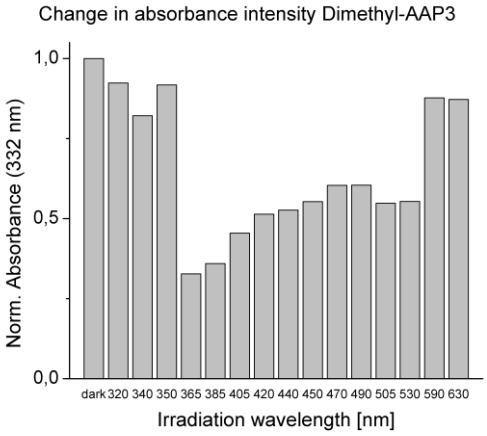

Normalized, wavelength dependent absorption intensity values at the absorption maximum:

Wave-length	**dark**	**320 nm**	**340 nm**	**350 nm**	**365 nm**	**385 nm**	**405 nm**	**420 nm**	**440 nm**	**450 nm**	**470 nm**	**490 nm**	**505 nm**	**530 nm**	**590 nm**	**630 nm**
I(332 nm)	1.00	0.92	0.82	0.92	0.33	0.36	0.45	0.51	0.53	0.55	0.60	0.60	0.55	0.55	0.88	0.87

2’,6’-Dichloro-AAP3 **(89)**

UV/vis absorption spectra after irradiation with each available wavelength (left) and the resulting change in absorption intensity at the absorption maximum upon irradiation (right).

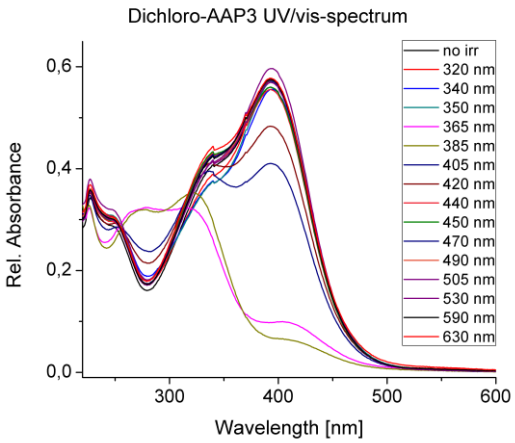

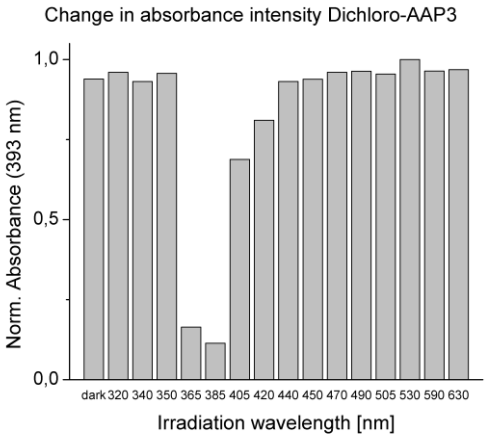

Normalized, wavelength dependent absorption intensity values at the absorption maximum:

Wave-length	**dark**	**320 nm**	**340 nm**	**350 nm**	**365 nm**	**385 nm**	**405 nm**	**420 nm**	**440 nm**	**450 nm**	**470 nm**	**490 nm**	**505 nm**	**530 nm**	**590 nm**	**630 nm**
I(393 nm)	0.94	0.96	0.93	0.96	0.16	0.11	0.69	0.81	0.93	0.94	0.96	0.96	0.95	1.00	0.96	0.97

2',6'-Difluoro-AAP3 **(90)**

UV/vis absorption spectra after irradiation with each available wavelength (left) and the resulting change in absorption intensity at the absorption maximum upon irradiation (right).

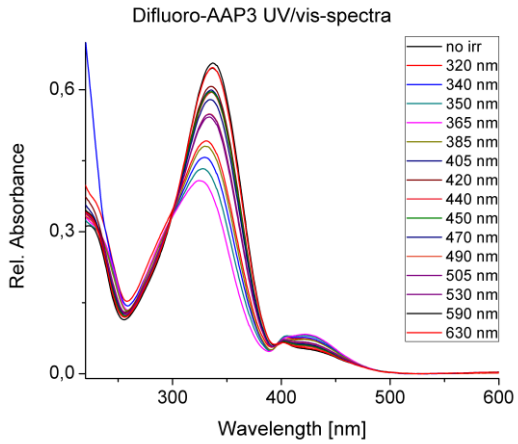

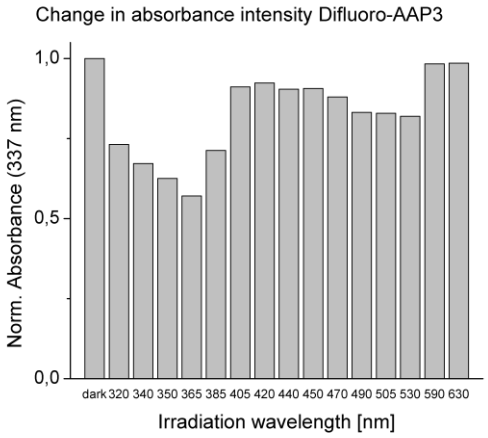

Normalized, wavelength dependent absorption intensity values at the absorption maximum:

Wave-length	**dark**	**320 nm**	**340 nm**	**350 nm**	**365 nm**	**385 nm**	**405 nm**	**420 nm**	**440 nm**	**450 nm**	**470 nm**	**490 nm**	**505 nm**	**530 nm**	**590 nm**	**630 nm**
I(337 nm)	1.00	0.73	0.67	0.63	0.57	0.71	0.91	0.92	0.90	0.91	0.88	0.83	0.83	0.82	0.98	0.99

Phenyl-Amino-AAP3 **(91)**

UV/vis absorption spectra after irradiation with each available wavelength (left) and the resulting change in absorption intensity at the absorption maximum upon irradiation (right).

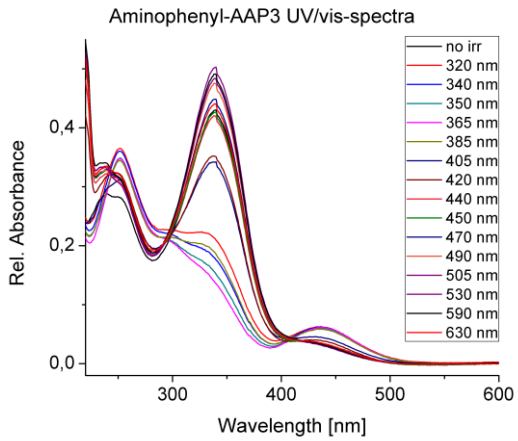

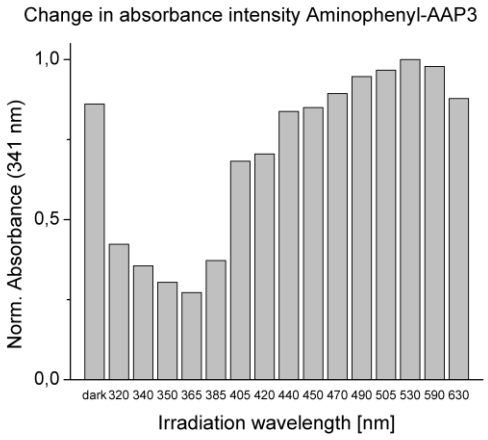

Normalized, wavelength dependent absorption intensity values at the absorption maximum:

Wave-length	**dark**	**320 nm**	**340 nm**	**350 nm**	**365 nm**	**385 nm**	**405 nm**	**420 nm**	**440 nm**	**450 nm**	**470 nm**	**490 nm**	**505 nm**	**530 nm**	**590 nm**	**630 nm**
I(341 nm)	0.86	0.42	0.36	0.30	0.27	0.37	0.68	0.70	0.84	0.85	0.89	0.95	0.97	1.00	0.98	0.88

7.3.3 UV/Vis spectra of all synthesized D-threoninol bound photochromes

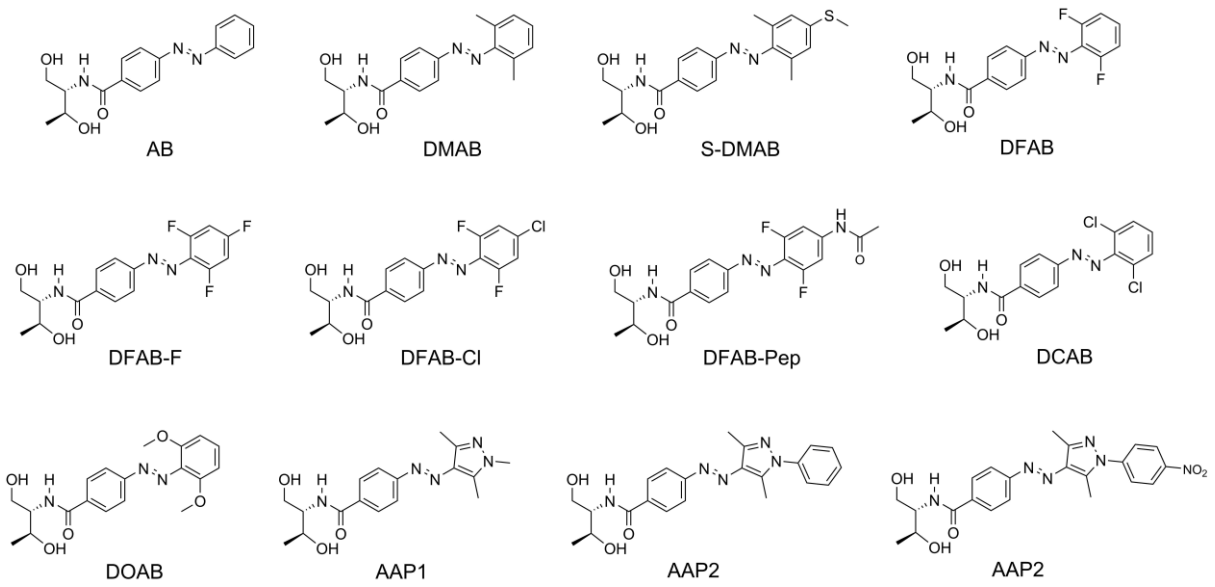

Fig. 98: D-threoninol bound azobenzene and arylazopyraole molecules investigated *via* UV/Vis-spectroscopy to determine the absorption maxima as well as the minimum and maximum converting irradiation wavelengths.

Azobenzene-D-threoninol (AB) **(4)**

UV/vis absorption spectra after irradiation with each available wavelength (left) and the resulting change in absorption intensity at the absorption maximum upon irradiation (right).

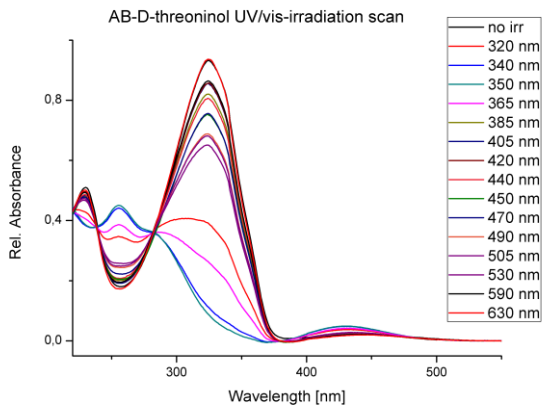

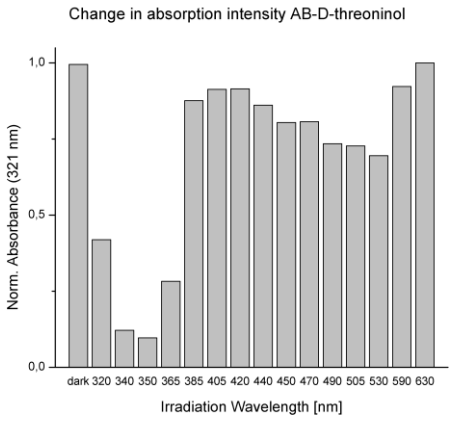

Normalized, wavelength dependent absorption intensity values at the absorption maximum:

Wave-length	dark	320 nm	340 nm	350 nm	365 nm	385 nm	405 nm	420 nm	440 nm	450 nm	470 nm	490 nm	505 nm	530 nm	590 nm	630 nm
I(321 nm)	0.99	0.42	0.12	0.10	0.28	0.88	0.91	0.91	0.86	0.80	0.81	0.73	0.73	0.69	0.92	1.00

2',6'-Dimethylazobenzene-D-threoninol (DMAB) **(9)**

UV/vis absorption spectra after irradiation with each available wavelength (left) and the resulting change in absorption intensity at the absorption maximum upon irradiation (right).

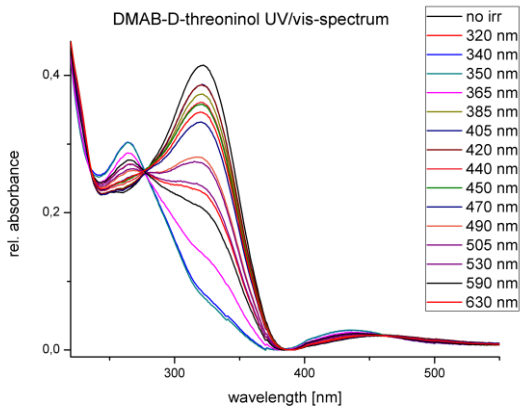

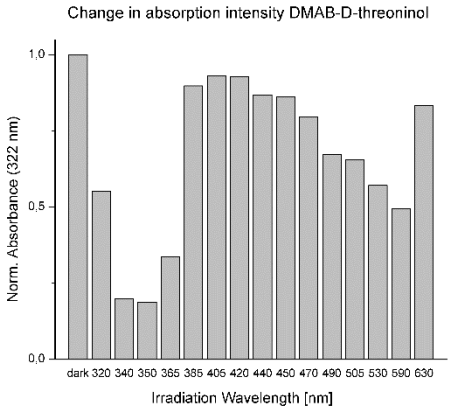

Normalized, wavelength dependent absorption intensity values at the absorption maximum:

Wave-length	**dark**	**320 nm**	**340 nm**	**350 nm**	**365 nm**	**385 nm**	**405 nm**	**420 nm**	**440 nm**	**450 nm**	**470 nm**	**490 nm**	**505 nm**	**530 nm**	**590 nm**	**630 nm**
I(322 nm)	1.00	0.55	0.20	0.19	0.34	0.90	0.93	0.93	0.87	0.86	0.80	0.67	0.65	0.57	0.50	0.83

4'-Methylthio-2',6'-dimethylazobenzene-D-threoninol (S-DMAB) **(15)**

UV/vis absorption spectra after irradiation with each available wavelength (left) and the resulting change in absorption intensity at the absorption maximum upon irradiation (right).

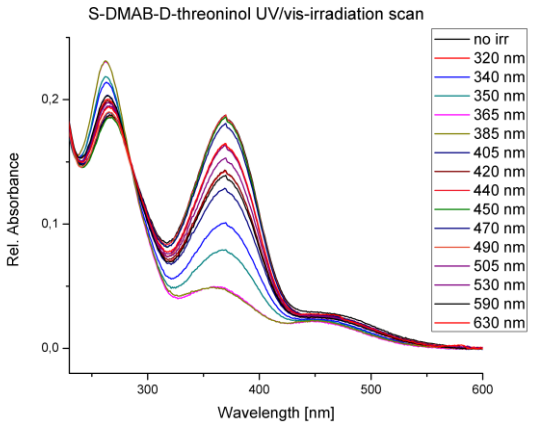

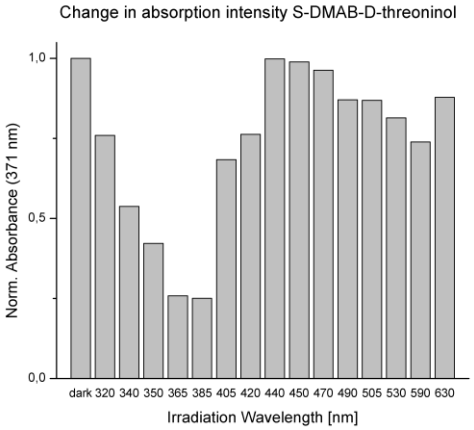

Normalized, wavelength dependent absorption intensity values at the absorption maximum:

Wave-length	**dark**	**320 nm**	**340 nm**	**350 nm**	**365 nm**	**385 nm**	**405 nm**	**420 nm**	**440 nm**	**450 nm**	**470 nm**	**490 nm**	**505 nm**	**530 nm**	**590 nm**	**630 nm**
I(371 nm)	1.00	0.76	0.53	0.42	0.26	0.25	0.68	0.76	1.00	0.99	0.96	0.87	0.87	0.81	0.74	0.88

2’,6’-Difluoroazobenzene-D-threoninol (DFAB) **(42)**

UV/vis absorption spectra after irradiation with each available wavelength (left) and the resulting change in absorption intensity at the absorption maximum upon irradiation (right).

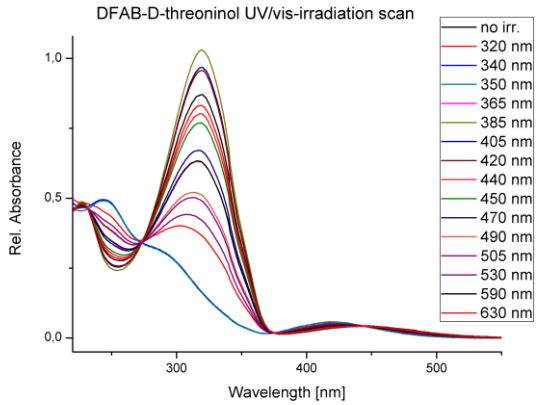

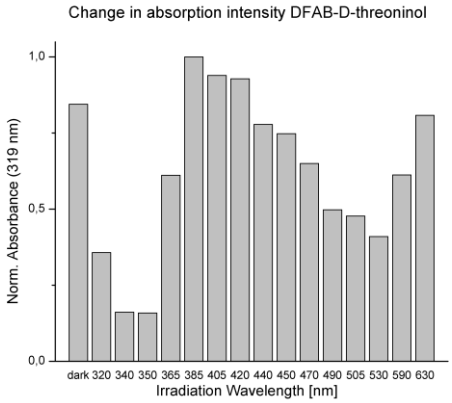

Normalized, wavelength dependent absorption intensity values at the absorption maximum:

Wave-length	**dark**	**320 nm**	**340 nm**	**350 nm**	**365 nm**	**385 nm**	**405 nm**	**420 nm**	**440 nm**	**450 nm**	**470 nm**	**490 nm**	**505 nm**	**530 nm**	**590 nm**	**630 nm**
I(319 nm)	0.84	0.36	0.16	0.16	0.61	1.00	0.94	0.93	0.78	0.75	0.65	0.50	0.48	0.41	0.61	0.81

2’,4’,6’-Trifluoroazobenzene-D-threoninol (DFAB-F) **(47)**

UV/vis absorption spectra after irradiation with each available wavelength (left) and the resulting change in absorption intensity at the absorption maximum upon irradiation (right).

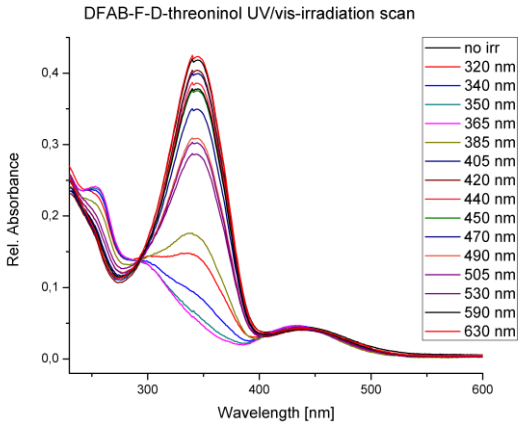

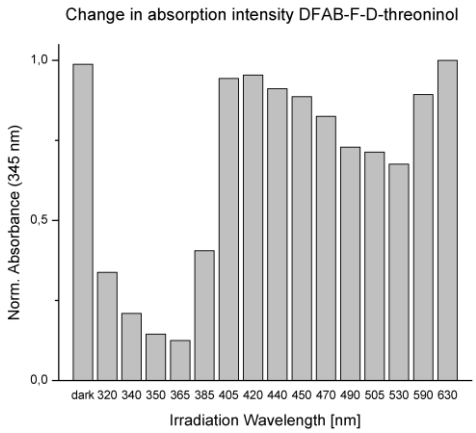

Normalized, wavelength dependent absorption intensity values at the absorption maximum:

Wave-length	**dark**	**320 nm**	**340 nm**	**350 nm**	**365 nm**	**385 nm**	**405 nm**	**420 nm**	**440 nm**	**450 nm**	**470 nm**	**490 nm**	**505 nm**	**530 nm**	**590 nm**	**630 nm**
I(345 nm)	0.99	0.34	0.21	0.14	0.12	0.41	0.94	0.95	0.91	0.89	0.83	0.73	0.71	0.68	0.89	1.00

4’-Chloro-2’,6’-difluoroazobenzene-D-threoninol (DFAB-Cl) **(51)**

UV/vis absorption spectra after irradiation with each available wavelength (left) and the resulting change in absorption intensity at the absorption maximum upon irradiation (right).

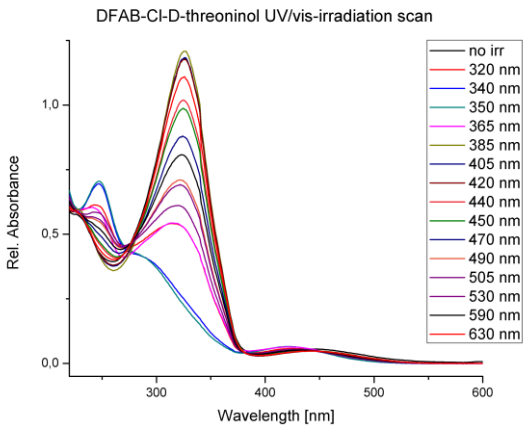

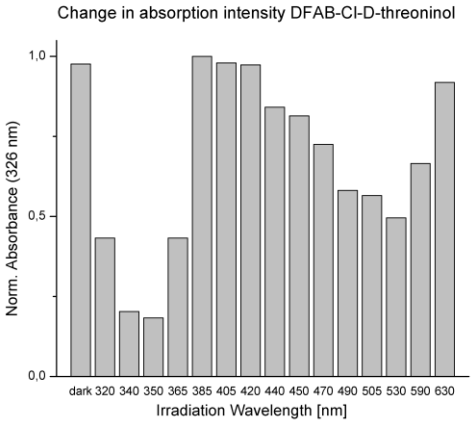

Normalized, wavelength dependent absorption intensity values at the absorption maximum:

Wave-length	**dark**	**320 nm**	**340 nm**	**350 nm**	**365 nm**	**385 nm**	**405 nm**	**420 nm**	**440 nm**	**450 nm**	**470 nm**	**490 nm**	**505 nm**	**530 nm**	**590 nm**	**630 nm**
I(326 nm)	0.98	0.43	0.20	0.18	0.43	1.00	0.98	0.97	0.84	0.81	0.73	0.58	0.57	0.50	0.67	0.92

4’-Acetamido-2’,6’-difluoroazobenzene-D-threoninol (DFAB-Pep) **(59)**

UV/vis absorption spectra after irradiation with each available wavelength (left) and the resulting change in absorption intensity at the absorption maximum upon irradiation (right).

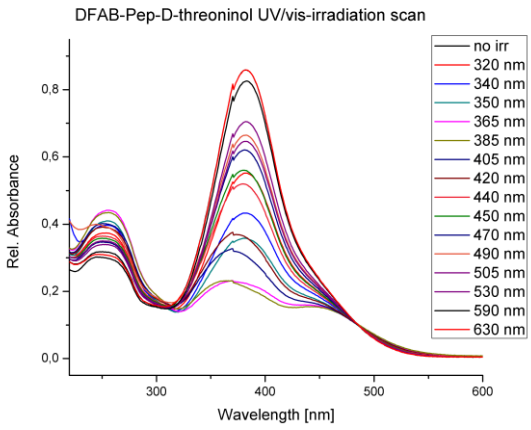

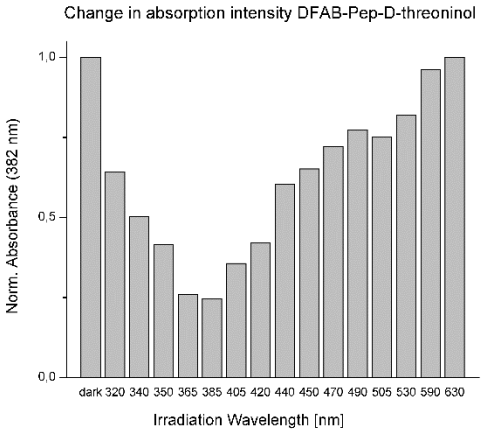

Normalized, wavelength dependent absorption intensity values at the absorption maximum:

Wave-length	**dark**	**320 nm**	**340 nm**	**350 nm**	**365 nm**	**385 nm**	**405 nm**	**420 nm**	**440 nm**	**450 nm**	**470 nm**	**490 nm**	**505 nm**	**530 nm**	**590 nm**	**630 nm**
I(382 nm)	1.00	0.64	0.50	0.42	0.26	0.25	0.36	0.42	0.60	0.65	0.72	0.77	0.75	0.82	0.96	1.00

2',6'-Dichloroazobenzene-D-threoninol (DCAB) **(67)**

UV/vis absorption spectra after irradiation with each available wavelength (left) and the resulting change in absorption intensity at the absorption maximum upon irradiation (right).

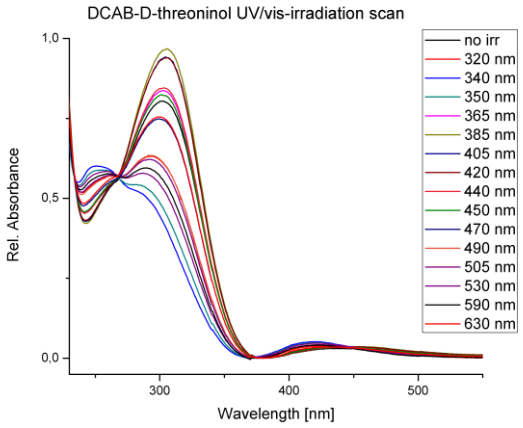

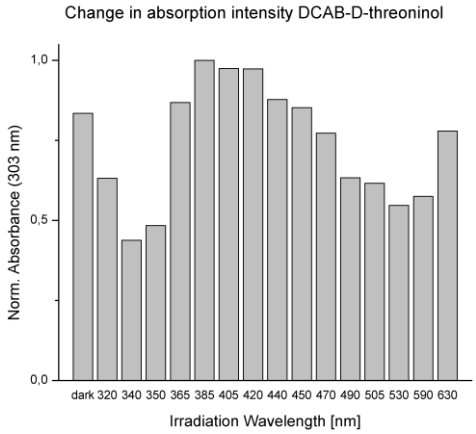

Normalized, wavelength dependent absorption intensity values at the absorption maximum:

Wave-length	**dark**	**320 nm**	**340 nm**	**350 nm**	**365 nm**	**385 nm**	**405 nm**	**420 nm**	**440 nm**	**450 nm**	**470 nm**	**490 nm**	**505 nm**	**530 nm**	**590 nm**	**630 nm**
I(303 nm)	0.83	0.63	0.44	0.48	0.87	1.00	0.97	0.97	0.88	0.85	0.77	0.63	0.62	0.55	0.58	0.78

2',6'-Dimethoxyazobenzene-D-threoninol (DOAB) **(72)**

UV/vis absorption spectra after irradiation with each available wavelength (left) and the resulting change in absorption intensity at the absorption maximum upon irradiation (right).

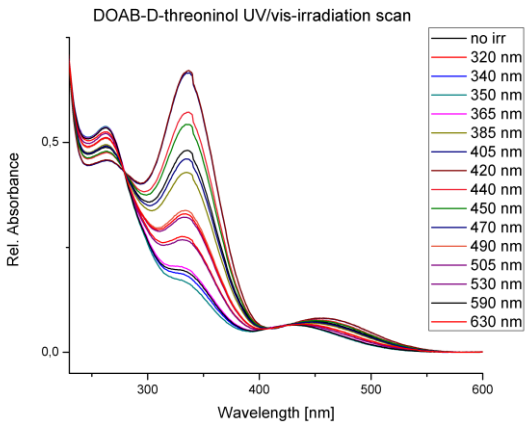

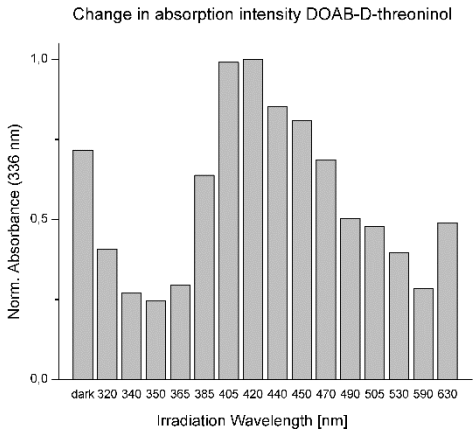

Normalized, wavelength dependent absorption intensity values at the absorption maximum:

Wave-length	**dark**	**320 nm**	**340 nm**	**350 nm**	**365 nm**	**385 nm**	**405 nm**	**420 nm**	**440 nm**	**450 nm**	**470 nm**	**490 nm**	**505 nm**	**530 nm**	**590 nm**	**630 nm**
I(336 nm)	0.72	0.41	0.27	0.25	0.29	0.64	0.99	1.00	0.85	0.81	0.69	0.50	0.48	0.40	0.28	0.49

Methyl-arylazopyrazole-D-threoninol (AAP1) **(95)**

UV/vis absorption spectra after irradiation with each available wavelength (left) and the resulting change in absorption intensity at the absorption maximum upon irradiation (right).

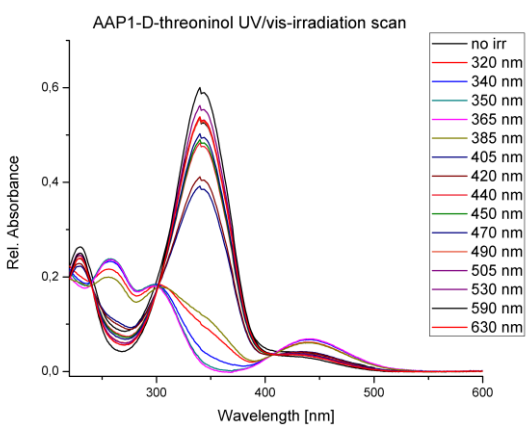

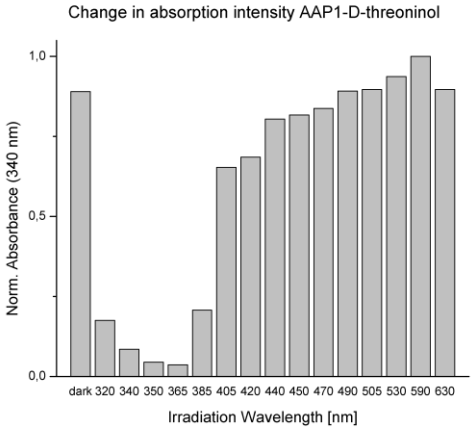

Normalized, wavelength dependent absorption intensity values at the absorption maximum:

Wave-length	**dark**	**320 nm**	**340 nm**	**350 nm**	**365 nm**	**385 nm**	**405 nm**	**420 nm**	**440 nm**	**450 nm**	**470 nm**	**490 nm**	**505 nm**	**530 nm**	**590 nm**	**630 nm**
I(341 nm)	0.89	0.18	0.09	0.05	0.04	0.21	0.65	0.69	0.80	0.82	0.84	0.89	0.90	0.94	1.00	0.90

Phenyl-arylazopyrazole-D-threoninol (AAP2) **(100)**

UV/vis absorption spectra after irradiation with each available wavelength (left) and the resulting change in absorption intensity at the absorption maximum upon irradiation (right).

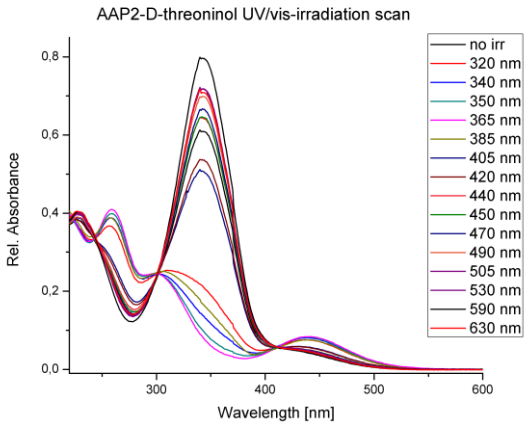

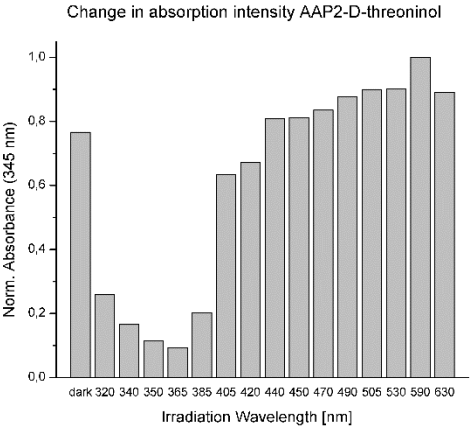

Normalized, wavelength dependent absorption intensity values at the absorption maximum:

Wave-length	**dark**	**320 nm**	**340 nm**	**350 nm**	**365 nm**	**385 nm**	**405 nm**	**420 nm**	**440 nm**	**450 nm**	**470 nm**	**490 nm**	**505 nm**	**530 nm**	**590 nm**	**630 nm**
I(341 nm)	0.77	0.26	0.17	0.12	0.09	0.20	0.63	0.67	0.81	0.81	0.84	0.88	0.90	0.90	1.00	0.89

4’-Nitrophenyl-arylazopyrazole-D-threoninol (AAP3) **(105)**

UV/vis absorption spectra after irradiation with each available wavelength (left) and the resulting change in absorption intensity at the absorption maximum upon irradiation (right).

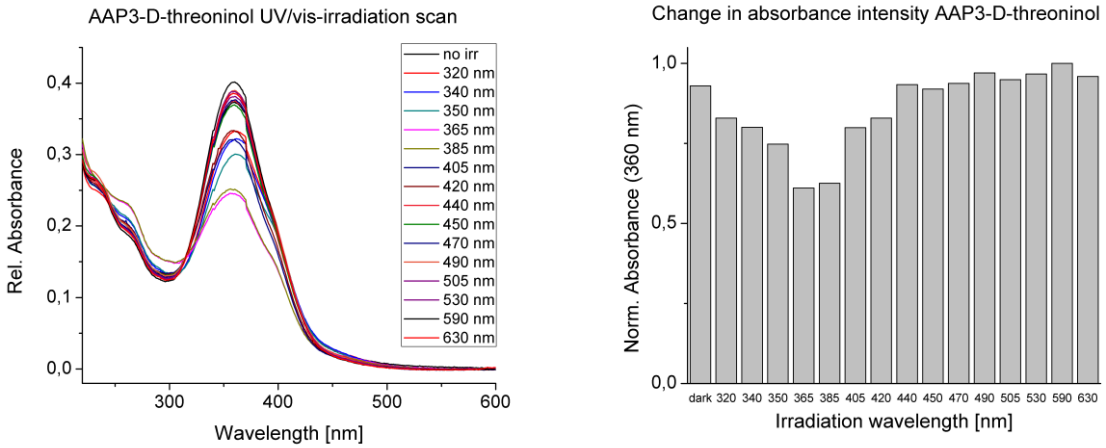

Normalized, wavelength dependent absorption intensity values at the absorption maximum:

Wave-length	**dark**	**320 nm**	**340 nm**	**350 nm**	**365 nm**	**385 nm**	**405 nm**	**420 nm**	**440 nm**	**450 nm**	**470 nm**	**490 nm**	**505 nm**	**530 nm**	**590 nm**	**630 nm**
I(360 nm)	0.93	0.83	0.80	0.75	0.61	0.63	0.80	0.83	0.93	0.92	0.94	0.97	0.95	0.97	1.00	0.96

7.3.4 Extinction coefficient calculation for D-threoninol bound photoswitches

The introduction of photoresponsive moieties into oligonucleotides necessitates a correction of each extinction coefficient for the maximum absorbance of oligonucleotides λ = 260 nm. Extinction coefficients at λ = 260 nm for all D-threoninol bound photoswitches were determined from the recorded UV/Vis spectra to permit a calculation of concentrations for modified oligonucleotides. From the absorption value at λ = 260 nm for each dark adapted sample, the extinction coefficient was calculated following the Lambert-Beer-law:

$$E = lg\left(\frac{I_0}{I}\right) = \varepsilon cd$$

The ectinction coefficient ε results as:

$$\varepsilon = \frac{E}{cd}$$

Using a cuvette length d = 1 cm, the absorption values and extinction coefficients depending on the concentrations were determined as given below.

Azobenzene	Concentration	Abs. (260 nm)	ε (260 nm)
AB	50 µM	0.182	3640
DMAB	50 µM	0.405	8100
S-DMAB	50 µM	0.181	3620
DFAB	50 µM	0.278	5560
DOAB	50 µM	0.487	9740
AAP1	25 µM	0.095	3800
AAP2	25 µM	0.234	9360

The calculated extinction coefficients were used for all concentration calculations of the synthesized modified oligonucleotides.

7.4 DNA synthesis and purification

7.4.1 Synthesis and purification of modified DNA strands

Coupling conditions

Modified and non-modified DNA strands were synthesized using an ABI Applied Biosystems 3400 DNA synthesizer with the following settings and chemicals:

Activator: 5-(Ethylthio)-1H-tetrazole (ETT).

Cap Mix A: 80 % tetrahydrofuran, 10 % acetic anhydride, 10 % pyridine.

Cap Mix B: 84 % tetrahydrofuran, 16 % 1-methylimidazole.

Oxidizer: 0.02 M Iodine in 70 % tetrahydrofuran, 20 % pyridine and 10 % water.

DNA synthesis grade acetonitrile was used for dissolving custom phosphoramidites to a 0.2 M solution. The coupling time for all custom phosphoramidites was 600 seconds. The terminal DMT group was not cleaved from the 5'-end of each oligonucleotide after each DNA synthesis. All synthesized DNA strands were deprotected and released from the solid support by heating the solid support in a 25 % aqueous ammonia solution at 55 °C for 16 hours. The resulting dispersion was centrifuged for 5 minutes at 15000 rpm, the supernatant was separated from the solid residues using spin filtration columns and lyophilised overnight in an Eppendorf Concentrator at 40 °C. The remaining crude DNA product was dissolved in 200 µL Millipore water and purified via reversed phase HPLC on an Eclipse XDB C18 column with a solvent gradient of 0-30% acetonitrile and water. The target fractions were evaporated and further worked up by manual 5'-DMT deprotection.

Manual DMT-deprotection of 5*-DMT-groups

5'-DMT deprotection of all DNA strands was performed with the collected fractions from HPLC purification. The following deprotection procedure was used:

Waters SepPak C18 classic columns were conditioned with 4 mL acetonitrile, followed by 4 mL 0.1 M TEAAc buffer. The target HPLC fractions were dissolved in 1 mL Millipore water, loaded on the column and the loading process was repeated three times. The column was flushed with 4mL Millipore water, 4 mL 2 % trifluoroacetic acid and 4 mL Millipore water, followed by elution and collection of the DNA with 2 mL acetonitrile and water in a1:1 mixture. The collected DNA solution was dried by lyophilisation and further subjected to LCMS analysis (see chapter 7.4.2).

7.4.2 LCMS results for all modified oligonucleotides

LCMS analysis for all modified oligonucleotide strands was performed on an Agilent 1100 Series HPLC system in line with an Esquire HCT ESI-MS system by Bruker Daltonics in standard enhanced mode with alternating charge. 5 µL 10 µM sample solution of each oligonucleotide dissolved in Millipore water were used for injection and separated on an Agilent Zorbax SB-C18 column (2.1x50 mm) with a gradient of 3 % to 20 % LCMS-grade acetonitrile in 0.1 M LCMS-grade TEAAc buffer containing 2 % 1,1,1,3,3,3-hexafluoro isopropanol (HFIP). The absorbance at λ = 260 nm was detected and a mass spectrum for every detected area was processed. The relative masses were determined *via* deconvolution of the resulting ESI mass spectra.

Azobenzene-modified DNA strands

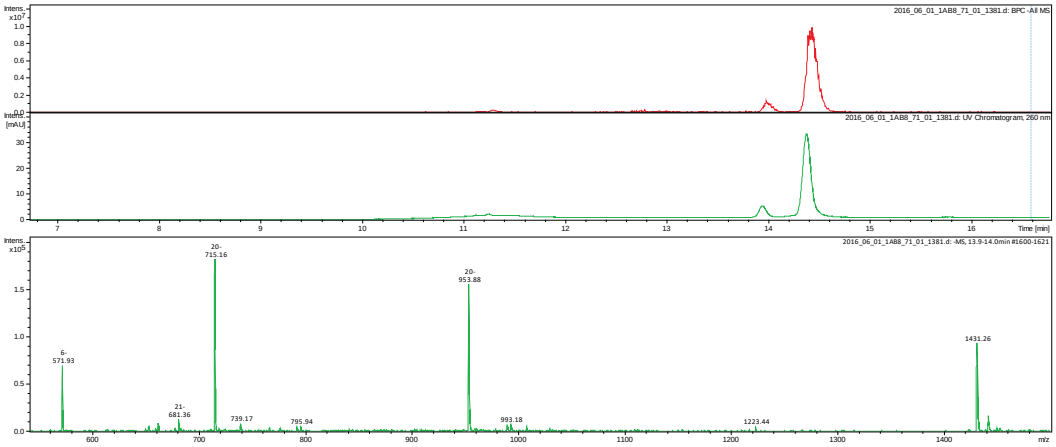

Fig. 99: UV absorption trace at 260 nm (top) and the mass spectra corresponding to each absorption maxima (bottom) were recorded and deconvoluted to determine each oligonucleotide mass. Full chromatograms and mass spectra are given in the attachments (chapter 10.2).

Sequence	Modification	Mass calculated	Mass found
5'-GAATXGGTG-3' (A)	X = AB	2864.79	2864.65
5'-GAXATGGXTG-3' (B)	X = AB	3239.89	3239.77
5'-GAXATXGGXTG-3' (C)	X = AB	3614.98	3614.87
5'-CACCATXTCCGGT-3' (D)	X = AB	3956.49	3956.20
5'-CACXCATTCCXGGT-3' (E)	X = AB	4331.59	4331.48
5'-CACXCATXTCCXGGT-3' (F)	X = AB	4706.69	4706.36
5'-TCCXCCAXGCAXTCG-3' (I)	X = AB	4691.67	4691.45
5'-CCXGATXGCTXGT-3' (J)	X = AB	4144.32	4144.20
5'-GGXAATXGGTXGA-3' (K)	X = AB	4257.40	4257.20

2‘,6‘-Dimethylazobenzene-modified DNA strands

Sequence	Modification	Mass calculated	Mass found
5’-GAATXGGTG-3’ (A)	X = DMAB	2892.82	2892.67
5’-GAXATGGXTG-3’ (B)	X = DMAB	3295.94	3295.75
5’-GAXATXGGXTG-3’ (C)	X = DMAB	3699.07	3698.87
5’-CACCATXTCCGGT-3’ (D)	X = DMAB	3984.52	3984.25
5’-CACXCATTCCXGGT-3’ (E)	X = DMAB	4387.65	4387.14
5’-CACXCATXTCCXGGT-3’ (F)	X = DMAB	4790.77	4790.65
5‘-TCCXCCAXGCAXTCG-3‘ (I)	X = DMAB	4775.76	4775.44
5‘-CCXGATXGCTXGT-3‘ (J)	X = DMAB	4228.40	4228.41
5‘-GGXAATXGGTXGA-3‘ (K)	X = DMAB	4341.49	4341.58

4‘-Methylthio-2‘,6‘-dimethylazobenzene-modified DNA strands

Sequence	Modification	Mass calculated	Mass found
5’-GAATXGGTG-3’ (A)	X = S-DMAB	2938.81	2938.53
5’-GAXATGGXTG-3’ (B)	X = S-DMAB	3387.92	3387.66
5’-GAXATXGGXTG-3’ (C)	X = S-DMAB	3837.04	3836.90
5’-CACCATXTCCGGT-3’ (D)	X = S-DMAB	4030.51	4029.64
5’-CACXCATTCCXGGT-3’ (E)	X = S-DMAB	4479.63	4479.34
5’-CACXCATXTCCXGGT-3’ (F)	X = S-DMAB	4928.74	4928.74
5‘-TCCXCCAXGCAXTCG-3‘ (I)	X = S-DMAB	4913.73	4913.63
5‘-CCXGATXGCTXGT-3‘ (J)	X = S-DMAB	4366.37	4366.65
5‘-GGXAATXGGTXGA-3‘ (K)	X = S-DMAB	4479.46	4479.92

2’,6’-Difluoroazobenzene-modified DNA strands

Sequence	Modification	Mass calculated	Mass found
5’-GAATXGGTG-3’ (A)	X = DFAB	2900.77	2900.92
5’-CACCATXTCCGGT-3’ (D)	X = DFAB	3992.47	3992.39

2’,6’-Dimethoxyazobenzene-modified DNA strands

Sequence	Modification	Mass calculated	Mass found
5’-GAATXGGTG-3’ (A)	X = DOAB	2924.81	2924.47
5’-CACCATXTCCGGT-3’ (D)	X = DOAB	4016.52	4015.99

N-methyl-arylazopyrazole-modified DNA strands

Sequence	Modification	Mass calculated	Mass found
5’-GAATXGGTG-3’ (A)	X = AAP1	2896.82	2896.79
5’-GAXATGGXTG-3’ (B)	X = AAP1	3303.96	3303.87
5’-GAXATXGGXTG-3’ (C)	X = AAP1	3711.10	3711.25
5’-CACCATXTCCGGT-3’ (D)	X = AAP1	3988.53	3988.19
5’-CACXCATTCCXGGT-3’ (E)	X = AAP1	4395.66	4395.48
5’-CACXCATXTCCXGGT-3’ (F)	X = AAP1	4802.80	4803.00
5’-CACCXATTCXCAGT-3’ (G)	X = AAP1	4379.68	4379.78
5’-CACXCATXTCCXAGT-3’ (H)	X = AAP1	4786.82	4787.29
5‘-TCCXCCAXGCAXTCG-3‘ (I)	X = AAP1	4787.79	4787.41
5‘-CCXGATXGCTXGT-3‘ (J)	X = AAP1	4240.43	4240.19
5‘-GGXAATXGGTXGA-3‘ (K)	X = AAP1	4353.52	4353.23
5‘-TCCCXCAGCXATCG-3‘ (L)	X = AAP1	4380.68	4380.39
5’-CACCXATTCXCGGT-3’ (M)	X = AAP1	4395.68	4395.39

N-pheny-arylazopyrazole-modified DNA strands

Sequence	Modification	Mass calculated	Mass found
5’-GAATXGGTG-3’ (A)	X = AAP2	2958.84	2958.83
5’-GAXATGGXTG-3’ (B)	X = AAP2	3427.99	3427.90
5’-GAXATXGGXTG-3’ (C)	X = AAP2	3897.14	3897.11
5’-CACCATXTCCGGT-3’ (D)	X = AAP2	4050.54	4050.19
5’-CACXCATTCCXGGT-3’ (E)	X = AAP2	4519.69	4519.46
5’-CACXCATXTCCXGGT-3’ (F)	X = AAP2	4988.85	4988.77
5’-CACCXATTCXCAGT-3’ (G)	X = AAP2	4503.70	4504.15
5’-CACXCATXTCCXAGT-3’ (H)	X = AAP2	4972.85	4973.26
5‘-TCCXCCAXGCAXTCG-3‘ (I)	X = AAP2	4973.83	4973.90
5‘-CCXGATXGCTXGT-3‘ (J)	X = AAP2	4426.48	4426.49
5‘-GGXAATXGGTXGA-3‘ (K)	X = AAP2	4539.56	4540.02
5‘-TCCCXCAGCXATCG-3‘ (L)	X = AAP2	4504.70	4504.26
5’-CACCXATTCXCGGT-3’ (M)	X = AAP2	4519.70	4519.59

7.4.3 Proof of reversible isomerization for all modifications in DNA strands

Introduction of photoresponsive modifications was proven by reversible switching measurements. All modified 8-mer DNA strands containing a single modifictions in the sequence 5'-GAATXGGTG-3' (X = AB, DMAB, S-DMAB, DFAB, DOAB, AAP1 or AAP2) were diluted in a stem solution of 1 mL with Millipore water to a concentration of 5 µM. The stem solutions were alternatingly irradiated with the wavelengths corresponding to the maximum *cis* and *trans* coverting wavelengths for 5 minutes with maximum intensity at room temperature. After each irradiation step, an aliquot of the solution was measured in a JASCO V630 Bio UV/Vis spectrometer with a detection range between 220 nm and 650 nm. The resulting spectra and corresponding irradiation wavelengths for each individual measurement are given below.

Reversible switching of azobenzene-modified 8-mer DNA

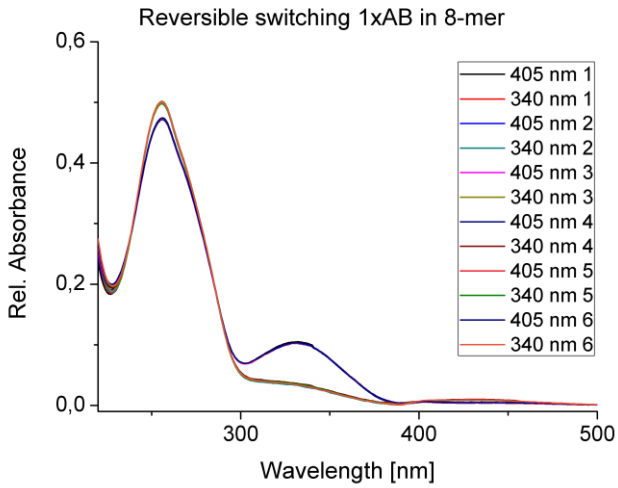

UV/Vis-spectra of the sequence 5'-GAATXGGTG-3' with X = Azobenzene (AB) after 5 minutes alternating irradiation with the maximum *trans*- and *cis*-converting wavelengths at room temperature. A UV/Vis-spectrum was recorded after each irradiation step.

Excitation wavelength *trans* isomer: 405 nm.

Excitation wavelength *cis* isomer: 340 nm.

Reversible switching of 2',6'-dimethylazobenzene-modified 8-mer DNA

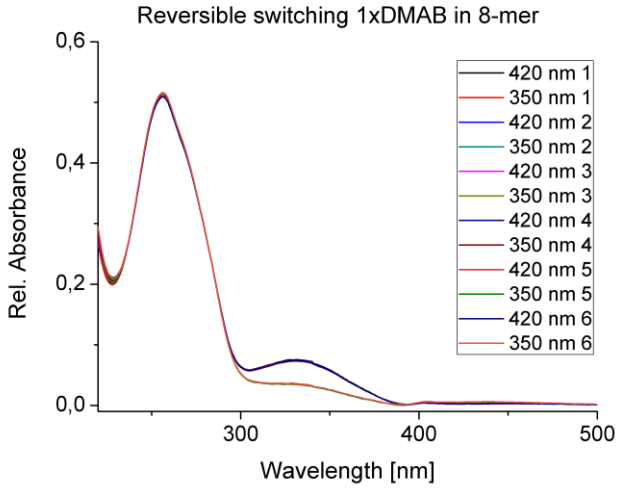

UV/Vis-spectra of the sequence 5'-GAATXGGTG-3' with X = 2',6'-Dimethylazobenzene (DMAB) after 5 minutes alternating irradiation with the maximum *trans*- and *cis*-converting wavelengths at room temperature. A UV/Vis-spectrum was recorded after each irradiation step.

Excitation wavelength *trans* isomer: 420 nm.

Excitation wavelength *cis* isomer: 350 nm.

Reversible switching of 2',6'-dimethyl-4'-methylthioazobenzene-modified 8-mer DNA

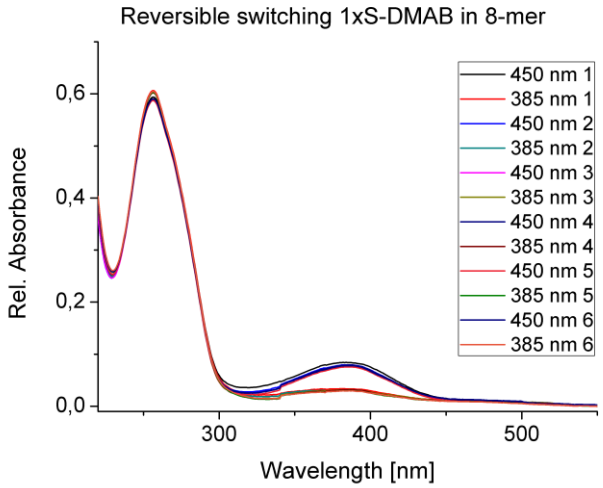

UV/Vis-spectra of the sequence 5'-GAATXGGTG-3' with X = 2',6'-Dimethyl-4'-methylthioazobenzene (S-DMAB) after 5 minutes alternating irradiation with the maximum *trans*- and *cis*-converting wavelengths at room temperature. A UV/Vis-spectrum was recorded after each irradiation step.

Excitation wavelength *trans* isomer: 450 nm.

Excitation wavelength *cis* isomer: 385 nm.

Reversible switching of 2',6'-difluoroazobenzene-modified 8-mer DNA

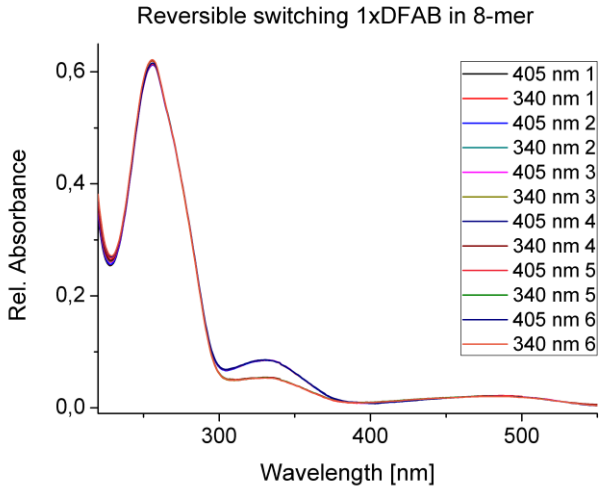

UV/Vis-spectra of the sequence 5'-GAATXGGTG-3' with X = 2',6'-Difluoroazobenzene (DFAB) after 5 minutes alternating irradiation with the maximum *trans*- and *cis*-converting wavelengths at room temperature. A UV/Vis-spectrum was recorded after each irradiation step.

Excitation wavelength *trans* isomer: 405 nm.

Excitation wavelength *cis* isomer: 340 nm.

Reversible switching of 2',6'-dimethoxyazobenzene-modified 8-mer DNA

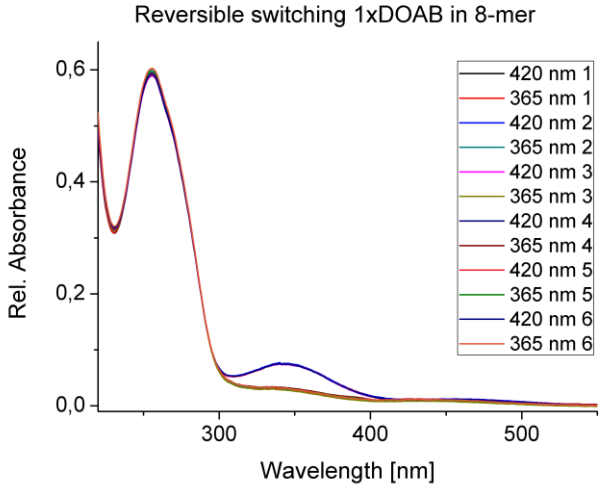

UV/Vis-spectra of the sequence 5'-GAATXGGTG-3' with X = 2',6'-Dimethoxyazobenzene (DOAB) after 5 minutes alternating irradiation with the maximum *trans*- and *cis*-converting wavelengths at room temperature. A UV/Vis-spectrum was recorded after each irradiation step.

Excitation wavelength *trans* isomer: 420 nm.

Excitation wavelength *cis* isomer: 365 nm.

Reversible switching of *N*-methylarylazopyrazole-modified 8-mer DNA

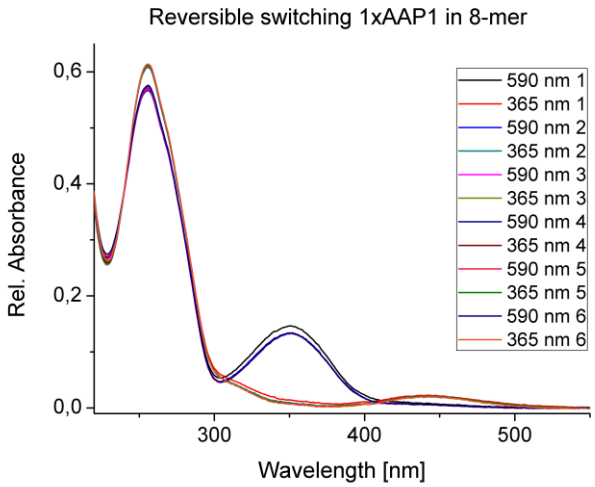

UV/Vis-spectra of the sequence 5'-GAATXGGTG-3' with X = *N*-Methylarylazopyrazole (AAP1) after 5 minutes alternating irradiation with the maximum *trans*- and *cis*-converting wavelengths at room temperature. A UV/Vis-spectrum was recorded after each irradiation step.

Excitation wavelength *trans* isomer: 590 nm.

Excitation wavelength *cis* isomer: 365 nm.

Reversible switching of *N*-phenylarylazopyrazole-modified 8-mer DNA

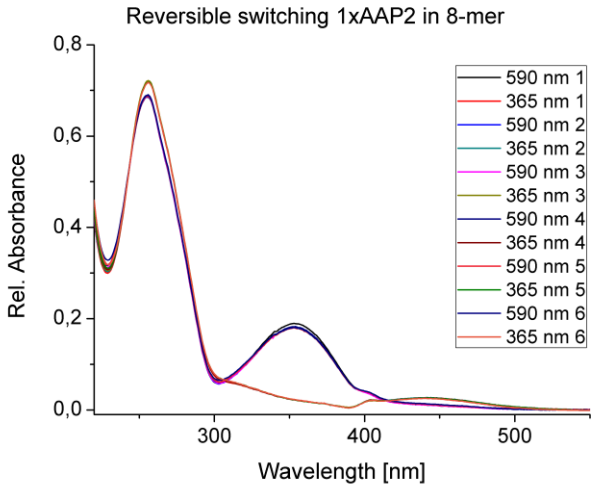

UV/Vis-spectra of the sequence 5'-GAATXGGTG-3' with X = *N*-Phenylarylazopyrazole (AAP2) after 5 minutes alternating irradiation with the maximum *trans*- and *cis*-converting wavelengths at room temperature. A UV/Vis-spectrum was recorded after each irradiation step.

Excitation wavelength *trans* isomer: 590 nm.

Excitation wavelength *cis* isomer: 365 nm.

7.5 Determination of conversion efficiencies *via* HPLC quantification

7.5.1 Reversed-phase HPLC quantification of D-threoninol coupled photochromes

Separation of both *cis* and *trans* isomer for all D-threoninol bound azobenzene-molecules was performed on a Nucleodur PFP (PentaFluorophenylPropyl) 4.6x150 mm column with different gradients of acetonitrile and water. The sample of the corresponding azobenzene or arylazopyrazole was dissolved in a 1:1 mixture of Millipore water and acetonitrile and irradiated for 5 minutes at room temperature with each available wavelength. After irradiation, the samples were immediately injected into the HPLC for separation of both *cis* and *trans* isomers while the absorption of the isosbestic point was measured. Each fraction of *cis* and *trans* isomer was determined by integration of the corresponding signals in the chromatogram. Each measurement was performed in dublets, the calculated standard deviation is given for each irradiation wavelength.

Azobenzene-D-threoninol (AB)

Sample: Azobenzene-D-threoninol, 10 µM, 20 µL injection for each measurement.

Gradient: ACN/H_2O = 40/60 -> 80/20 in 15 minutes, flow-rate: 0.5 mL/min.

Detection: λ = 282 nm.

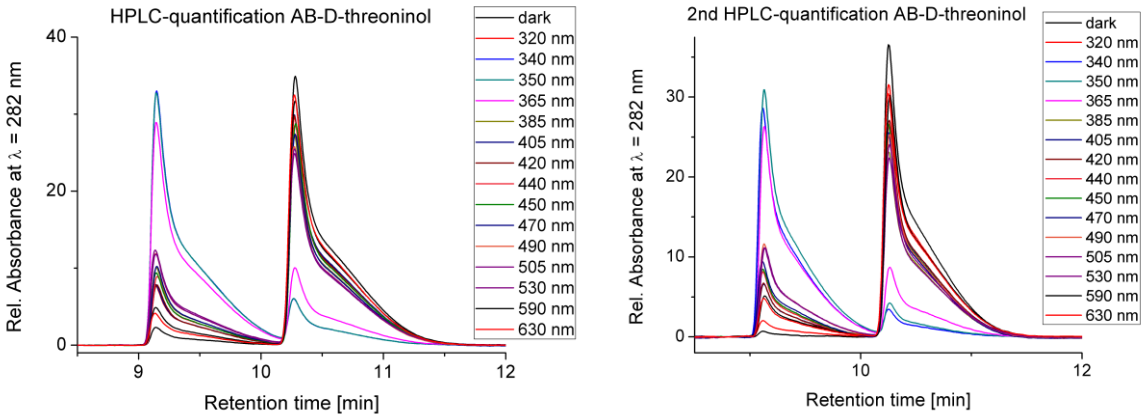

Wavelength dependent *cis*-percentage calculated from integrated peak areas:

Wavelength	Dark	320 nm	340 nm	350 nm	365 nm	385 nm	405 nm	420 nm	440 nm	450 nm	470 nm	490 nm	505 nm	530 nm	590 nm	630 nm
***cis*-fraction [%]**	3.63 ± 2.13	12.87 ± 7.11	85.87 ± 2.42	85.30 ± 1.90	73.43 ± 0.60	25.14 ± 0.16	19.31 ± 0.38	19.13 ± 0.42	22.26 ± 0.15	23.12 ± 0.15	25.77 ± 0.15	30.22 ± 0.14	30.51 ± 0.39	32.06 ± 0.28	13.37 ± 0.88	11.86 ± 1.38

2',6'-Dimethylazobenzene-D-threoninol (DMAB)

Sample: 2',6'-Dimethylazobenzene-D-threoninol, 10 µM, 20 µL injection for each measurement.

Gradient: ACN/H_2O = 40/60 -> 80/20 in 15 minutes, flow-rate: 0.5 mL/min.

Detection: λ = 277 nm.

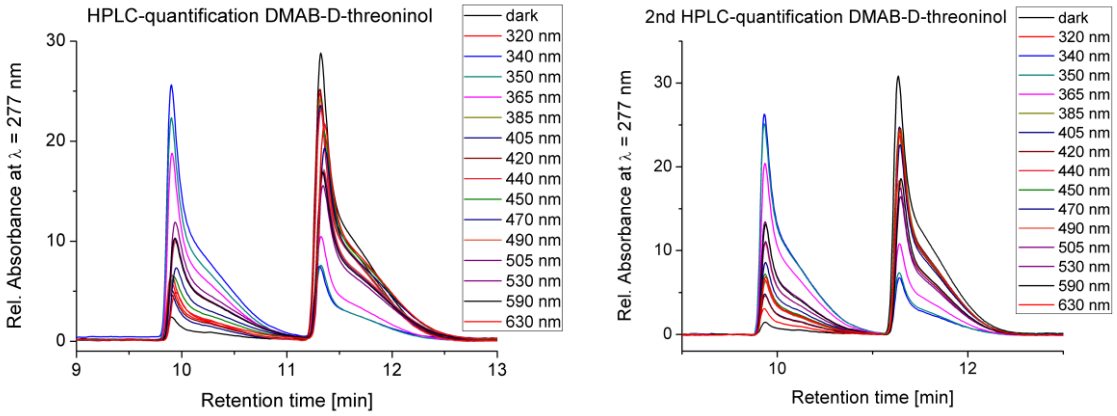

Wavelength dependent *cis*-percentage calculated from integrated peak areas:

Wave-length	dark	320 nm	340 nm	350 nm	365 nm	385 nm	405 nm	420 nm	440 nm	450 nm	470 nm	490 nm	505 nm	530 nm	590 nm	630 nm
***cis*-fraction [%]**	6.52 ± 2.02	14.84 ± 4.42	76.55 ± 1.88	74.86 ± 1.99	63.44 ± 1.02	20.19 ± 0.68	15.79 ± 0.32	16.36 ± 1.08	21.07 ± 0.51	22.72 ± 0.80	26.88 ± 0.46	35.92 ± 0.01	37.21 ± 0.23	42.84 ± 0.73	38.55 ± 1.46	19.87 ± 1.04

4'-Methylthio-2',6'-dimethylazobenzene-D-threoninol (S-DMAB)

Sample: 4'-Methylthio-2',6'-dimethylazobenzene-D-threoninol, 10 µM, 20 µL injection.

Gradient: ACN/H_2O = 40/60 -> 80/20, flow-rate: 0.5 mL/min.

Detection: λ = 288 nm.

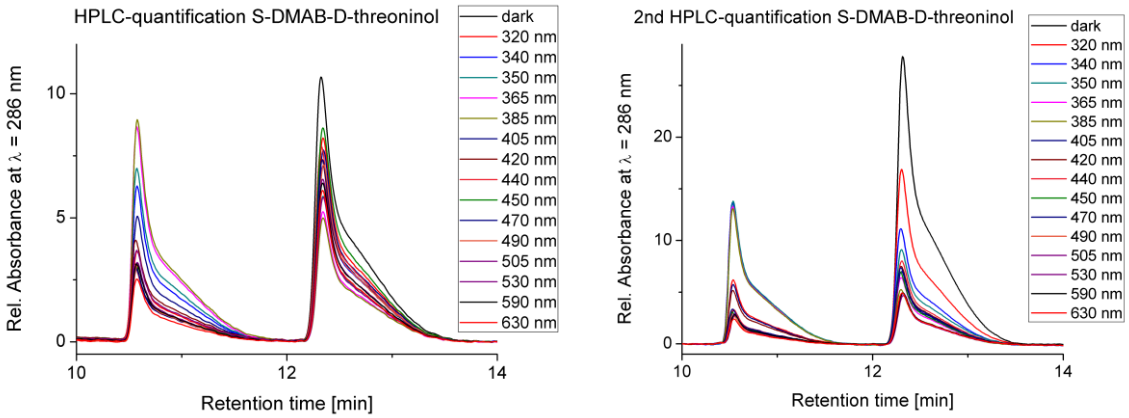

Wavelength dependent *cis*-percentage calculated from integrated peak areas:

Wave-length	dark	320 nm	340 nm	350 nm	365 nm	385 nm	405 nm	420 nm	440 nm	450 nm	470 nm	490 nm	505 nm	530 nm	590 nm	630 nm
***cis*-fraction [%]**	15.43 ± 6.24	27.12 ± 1.79	48.61 ± 4.21	54.84 ± 2.88	62.90 ± 3.27	65.93 ± 4.49	40.38 ± 3.03	37.05 ± 2.09	27.13 ± 0.22	26.81 ± 1.70	28.43 ± 0.82	30.29 ± 2.32	34.34 ± 0.78	34.83 ± 0.90	33.05 ± 1.72	29.00 ± 1.03

2’,6’-Difluoroazobenzene-D-threoninol (DFAB)

Sample: Azobenzene-D-threoninol, 10 µM, 20 µL injection for each measurement.

Gradient: ACN/H_2O = 25/75 -> 45/55 in 15 minutes, flow-rate: 0.5 mL/min.

Detection: λ = 274 nm.

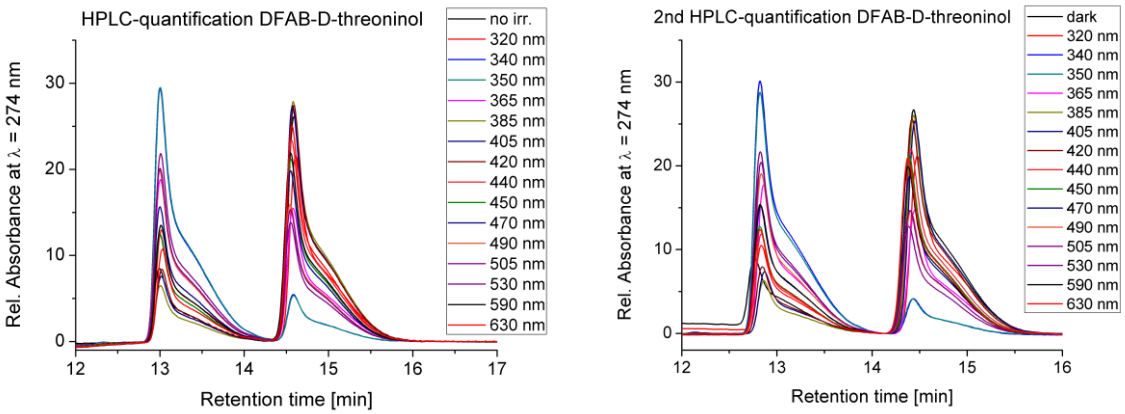

Wavelength dependent *cis*-percentage calculated from integrated peak areas:

Wave-length	dark	320 nm	340 nm	350 nm	365 nm	385 nm	405 nm	420 nm	440 nm	450 nm	470 nm	490 nm	505 nm	530 nm	590 nm	630 nm
***cis*-fraction [%]**	24.73 ± 1.47	34.40 ± 1.56	85.93 ± 2.60	85.56 ± 2.03	53.48 ± 0.04	18.24 ± 0.34	20.94 ± 0.48	22.52 ± 0.20	33.26 ± 0.31	35.91 ± 0.25	42.92 ± 0.49	54.53 ± 0.65	55.97 ± 0.89	60.55 ± 1.04	39.28 ± 2.86	32.11 ± 3.69

2’,4’,6’-Trifluoroazobenzene-D-threoninol (DFAB-F)

Sample: Azobenzene-D-threoninol, 10 µM, 20 µL injection for each measurement.

Gradient: ACN/H_2O = 25/75 -> 45/55, flow-rate: 0.5 mL/min.

Detection: λ = 292 nm.

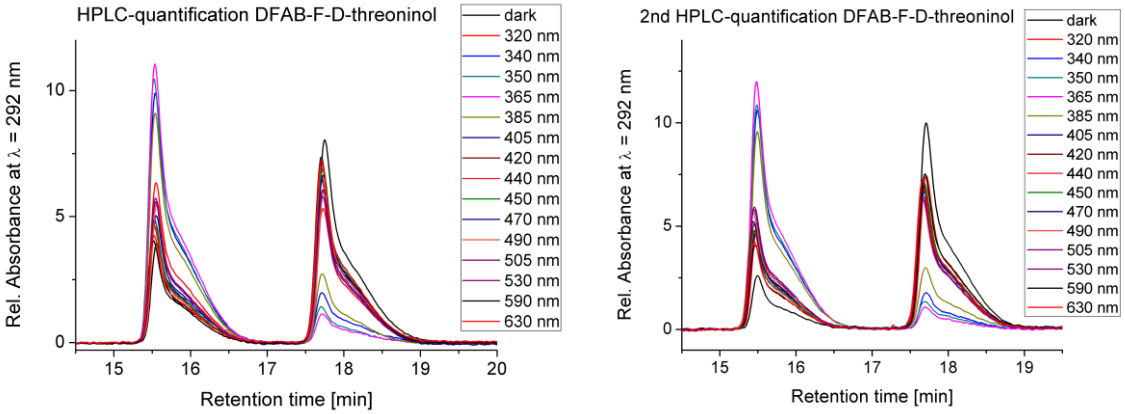

Wavelength dependent *cis*-percentage calculated from integrated peak areas:

Wave-length	dark	320 nm	340 nm	350 nm	365 nm	385 nm	405 nm	420 nm	440 nm	450 nm	470 nm	490 nm	505 nm	530 nm	590 nm	630 nm
***cis*-fraction [%]**	25.77 ± 5.50	45.67 ± 7.08	82.42 ± 1.35	87.18 ± 0.39	90.09 ± 0.47	75.45 ± 1.72	41.48 ± 0.40	40.48 ± 0.21	38.53 ± 0.06	39.54 ± 0.17	42.05 ± 0.17	46.05 ± 0.20	46.27 ± 0.04	47.78 ± 0.59	34.09 ± 0.09	36.33 ± 0.16

4’-Chloro-2’,6’-difluoroazobenzene-D-threoninol (DFAB-Cl)

Sample: Azobenzene-D-threoninol, 10 µM, 20 µL injection for each measurement.

Gradient: ACN/H_2O = 25/75 -> 45/55 in 15 minutes, flow-rate: 0.5 mL/min.

Detection: λ = 278 nm.

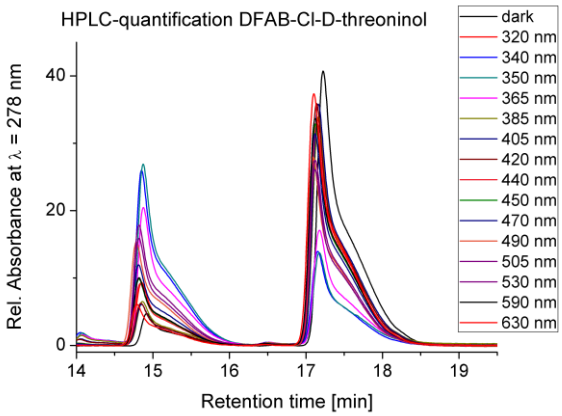

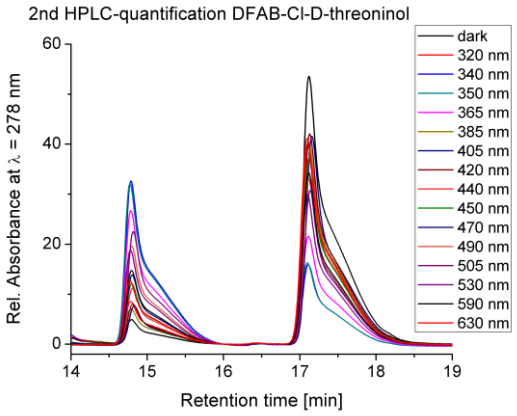

Wavelength dependent *cis*-percentage calculated from integrated peak areas:

Wave-length	dark	320 nm	340 nm	350 nm	365 nm	385 nm	405 nm	420 nm	440 nm	450 nm	470 nm	490 nm	505 nm	530 nm	590 nm	630 nm
***cis*-fraction [%]**	8.75 ± 0.93	18.82 ± 2.27	65.73 ± 1.82	65.22 ± 1.30	53.91 ± 0.76	15.21 ± 0.95	14.42 ± 0.11	14.87 ± 0.28	21.30 ± 0.45	22.76 ± 0.49	27.44 ± 0.77	35.17 ± 0.78	36.34 ± 0.89	40.54 ± 1.14	25.44 ± 3.25	17.86 ± 4.53

2’,6’-Dichloroazobenzene-D-threoninol (DCAB)

Sample: Azobenzene-D-threoninol, 10 µM, 20 µL injection for each measurement.

Gradient: ACN/H_2O = 25/75 -> 45/55 in 15 minutes, flow-rate: 0.5 mL/min.

Detection: λ = 268 nm.

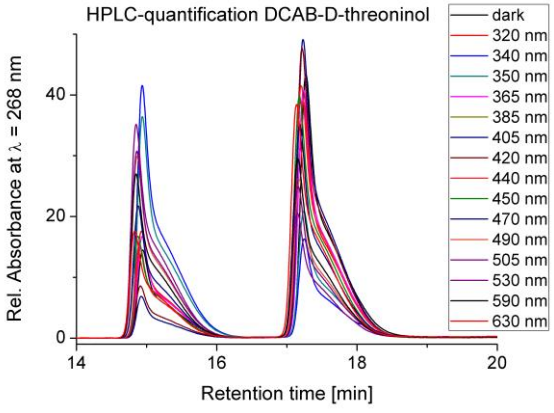

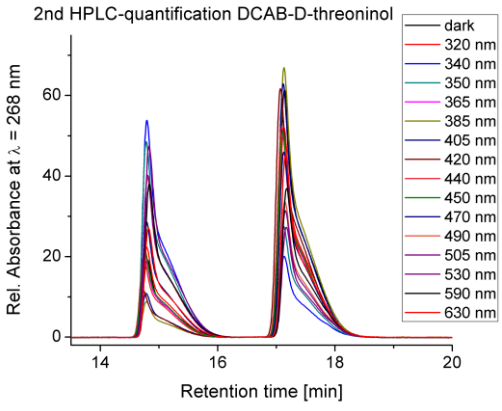

Wavelength dependent *cis*-percentage calculated from integrated peak areas:

Wave-length	dark	320 nm	340 nm	350 nm	365 nm	385 nm	405 nm	420 nm	440 nm	450 nm	470 nm	490 nm	505 nm	530 nm	590 nm	630 nm
***cis*-fraction [%]**	23.61 ± 0.64	29.59 ± 0.47	70.87 ± 0.91	62.21 ± 0.42	28.05 ± 0.05	11.42 ± 0.46	12.95 ± 1.08	15.13 ± 0.12	26.07 ± 0.05	28.77 ± 0.08	37.05 ± 0.18	52.37 ± 0.37	54.27 ± 0.64	61.84 ± 0.41	47.96 ± 1.52	33.38 ± 2.79

2’,6’-Dimethoxyazobenzene-D-threoninol (DOAB)

Sample: Azobenzene-D-threoninol, 10 µM, 20 µL injection for each measurement.

Gradient: ACN/H_2O = 15/85 -> 25/75 in 15 minutes, flow-rate: 0.5 mL/min.

Detection: λ = 279 nm.

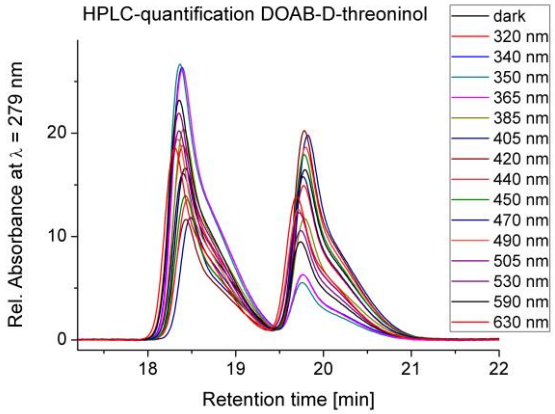

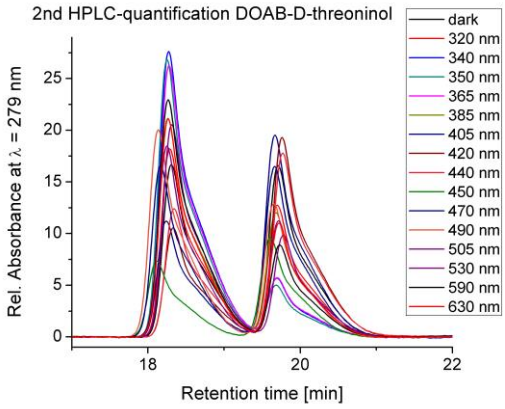

Wavelength dependent *cis*-percentage calculated from integrated peak areas:

Wave-length	dark	320 nm	340 nm	350 nm	365 nm	385 nm	405 nm	420 nm	440 nm	450 nm	470 nm	490 nm	505 nm	530 nm	590 nm	630 nm
***cis*-fraction [%]**	48.90 ± 0.08	56.23 ± 1.47	80.72 ± 1.72	82.75 ± 0.82	80.37 ± 0.92	62.63 ± 0.48	35.75 ± 0.02	34.76 ± 0.55	40.21 ± 0.37	42.67 ± 0.30	49.25 ± 0.19	60.07 ± 0.49	61.28 ± 0.25	66.36 ± 0.14	70.48 ± 0.78	60.74 ± 4.30

Methylarylazopyrazole-D-threoninol (AAP1)

Sample: Azobenzene-D-threoninol, 10 µM, 20 µL injection for each measurement.

Gradient: ACN/H_2O = 25/75 -> 45/55 in 15 minutes, flow-rate: 0.5 mL/min.

Detection: λ = 301 nm.

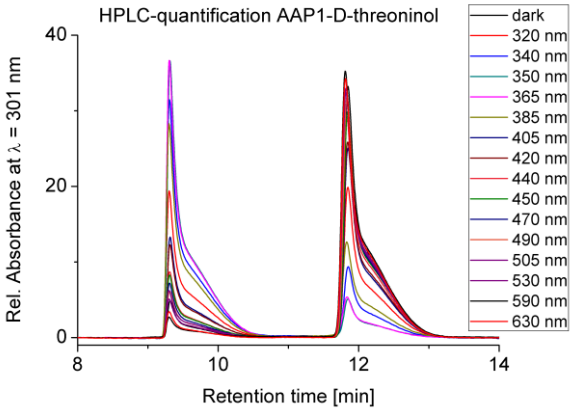

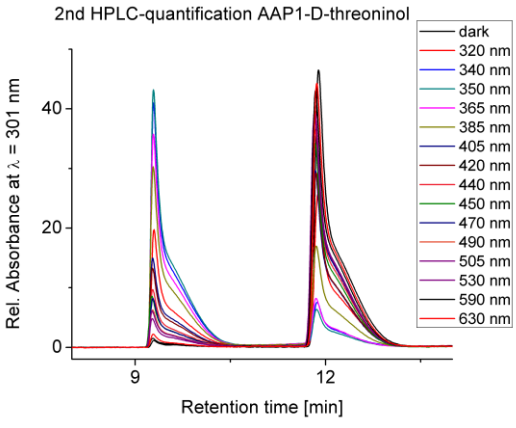

Wavelength dependent *cis*-percentage calculated from integrated peak areas:

Wave-length	dark	320 nm	340 nm	350 nm	365 nm	385 nm	405 nm	420 nm	440 nm	450 nm	470 nm	490 nm	505 nm	530 nm	590 nm	630 nm
***cis*-fraction [%]**	6.76 ± 4.36	42.50 ± 3.04	77.00 ± 3.45	84.11 ± 0.57	80.73 ± 3.27	62.32 ± 2.38	30.94 ± 0.16	28.83 ± 0.24	19.76 ± 0.64	18.94 ± 0.58	16.30 ± 0.19	13.56 ± 0.69	13.34 ± 1.04	11.21 ± 0.81	5.53 ± 2.06	6.03 ± 1.71

Phenylarylazopyrazole-D-threoninol (AAP2)

Sample: Azobenzene-D-threoninol, 10 µM, 20 µL injection for each measurement.

Gradient: ACN/H_2O = 25/75 -> 45/55 in 15 minutes, flow-rate: 0.5 mL/min.

Detection: λ = 301 nm.

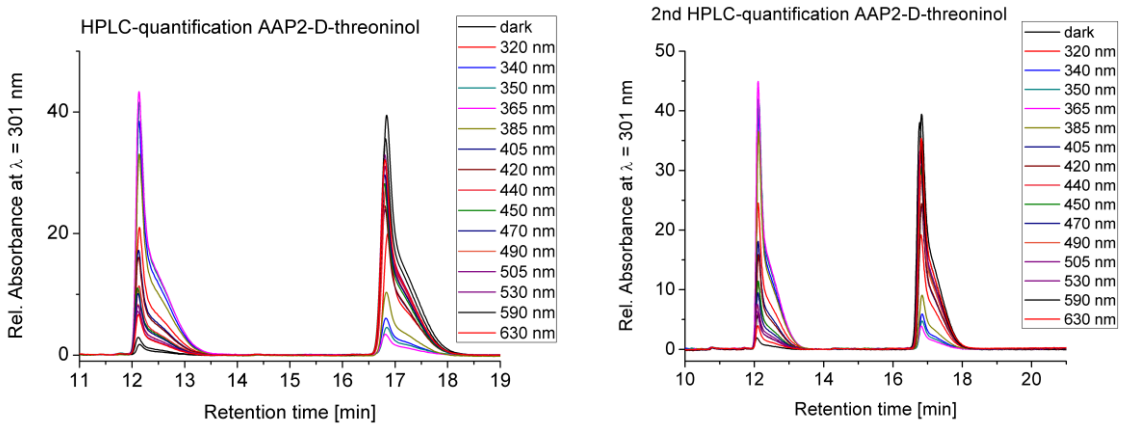

Wavelength dependent *cis*-percentage calculated from integrated peak areas:

Wave-length	**dark**	**320 nm**	**340 nm**	**350 nm**	**365 nm**	**385 nm**	**405 nm**	**420 nm**	**440 nm**	**450 nm**	**470 nm**	**490 nm**	**505 nm**	**530 nm**	**590 nm**	**630 nm**
***cis*-fraction [%]**	7.92 ± 4.04	49.53 ± 2.26	84.31 ± 0.37	87.76 ± 0.40	90.69 ± 0.18	75.67 ± 1.45	38.39 ± 0.21	35.67 ± 0.42	25.09 ± 0.50	24.42 ± 0.74	22.21 ± 0.62	18.40 ± 0.37	17.71 ± 0.79	15.03 ± 0.77	5.29 ± 1.22	12.05 ± 3.18

Comparison of wavelength-dependent *cis*-fraction of all D-threoninol-bound small molecules

Each individual quantification of wavelength dependent *cis* fractions permits the direct comparison of switching properties for all synthesized D-threoninol bound small molecules. All *cis* fractions derived from the individual quantification steps are given below.

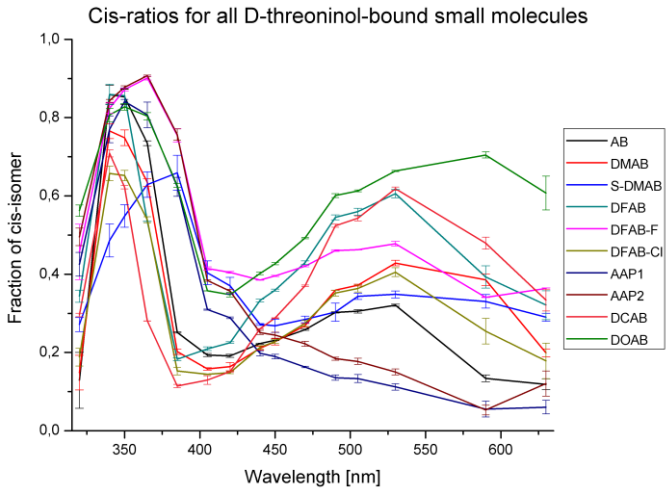

Cis percentage values calculated for all synthesized D-threoninol bound small molecules:

WL [nm]	AB	DMAB	S-DMAB	DFAB	DFAB-F	DFAB-Cl	AAP1	AAP2	DCAB	DOAB
dark	3.63 ± 2.13	6.52 ± 2.02	15.43 ± 6.24	24.73 ± 1.47	25.77 ± 5.50	8.75 ± 0.93	6.76 ± 4.36	7.92 ± 4.04	23.61 ± 0.64	48.90 ± 0.08
320 nm	12.87 ± 7.11	14.84 ± 4.42	27.12 ± 1.79	34.40 ± 1.56	45.67 ± 7.08	18.82 ± 2.27	42.50 ± 3.04	49.53 ± 2.26	29.59 ± 0.47	56.23 ± 1.47
340 nm	85.87 ± 2.42	76.55 ± 1.88	48.61 ± 4.21	85.93 ± 2.60	82.42 ± 1.35	65.73 ± 1.82	77.00 ± 3.45	84.31 ± 0.37	70.87 ± 0.91	80.72 ± 1.72
350 nm	85.30 ± 1.90	74.86 ± 1.99	54.84 ± 2.88	85.56 ± 2.03	87.18 ± 0.39	65.22 ± 1.30	84.11 ± 0.57	87.76 ± 0.40	62.21 ± 0.42	82.75 ± 0.82
365 nm	73.43 ± 0.60	63.44 ± 1.02	62.90 ± 3.27	53.48 ± 0.04	90.09 ± 0.47	53.91 ± 0.76	80.73 ± 3.27	90.69 ± 0.18	28.05 ± 0.05	80.37 ± 0.92
385 nm	25.14 ± 0.16	20.19 ± 0.68	65.93 ± 4.49	18.24 ± 0.34	75.45 ± 1.72	15.21 ± 0.95	62.32 ± 2.38	75.67 ± 1.45	11.42 ± 0.46	62.63 ± 0.48
405 nm	19.31 ± 0.38	15.79 ± 0.32	40.38 ± 3.03	20.94 ± 0.48	41.48 ± 0.40	14.42 ± 0.11	30.94 ± 0.16	38.39 ± 0.21	12.95 ± 1.08	35.75 ± 0.02
420 nm	19.13 ± 0.42	16.36 ± 1.08	37.05 ± 2.09	22.52 ± 0.20	40.48 ± 0.21	14.87 ± 0.28	28.83 ± 0.24	35.67 ± 0.42	15.13 ± 0.12	34.76 ± 0.55
440 nm	22.26 ± 0.15	21.07 ± 0.51	27.13 ± 0.22	33.26 ± 0.31	38.53 ± 0.06	21.30 ± 0.45	19.76 ± 0.64	25.09 ± 0.50	26.07 ± 0.05	40.21 ± 0.37
450 nm	23.12 ± 0.15	22.72 ± 0.80	26.81 ± 1.70	35.91 ± 0.25	39.54 ± 0.17	22.76 ± 0.49	18.94 ± 0.58	24.42 ± 0.74	28.77 ± 0.08	42.67 ± 0.30
470 nm	25.77 ± 0.15	26.88 ± 0.46	28.43 ± 0.82	42.92 ± 0.49	42.05 ± 0.17	27.44 ± 0.77	16.30 ± 0.19	22.21 ± 0.62	37.05 ± 0.18	49.25 ± 0.19
490 nm	30.22 ± 0.14	35.92 ± 0.01	30.29 ± 2.32	54.53 ± 0.65	46.05 ± 0.20	35.17 ± 0.78	13.56 ± 0.69	18.40 ± 0.37	52.37 ± 0.37	60.07 ± 0.49
505 nm	30.51 ± 0.39	37.21 ± 0.23	34.34 ± 0.78	55.97 ± 0.89	46.27 ± 0.04	36.34 ± 0.89	13.34 ± 1.04	17.71 ± 0.79	54.27 ± 0.64	61.28 ± 0.25
530 nm	32.06 ± 0.28	42.84 ± 0.73	34.83 ± 0.90	60.55 ± 1.04	47.78 ± 0.59	40.54 ± 1.14	11.21 ± 0.81	15.03 ± 0.77	61.84 ± 0.41	66.36 ± 0.14
590 nm	13.37 ± 0.88	38.55 ± 1.46	33.05 ± 1.72	39.28 ± 2.86	34.09 ± 0.09	25.44 ± 3.25	5.53 ± 2.06	5.29 ± 1.22	47.96 ± 1.52	70.48 ± 0.78
630 nm	11.86 ± 1.38	19.87 ± 1.04	29.00 ± 1.03	32.11 ± 3.69	36.33 ± 0.16	17.86 ± 4.53	6.03 ± 1.71	12.05 ± 3.18	33.38 ± 2.79	60.74 ± 4.30

7.5.2 Reversed-phase HPLC quantification of modified oligonucleotides

Separation of both *cis* to *trans* ratio for modified oligonucleotides was performed on an Agilent Eclipse SDB C18 4.6x150 mm reversed phase column with different gradients of acetonitrile and 0.1 M TEAAc buffer. All DNA strands were directly injected into the HPLC column upon irradiation and both *cis* and *trans* isomers were separated. The absorption at λ = 260 nm was recorded, integration of the corresponding signalsresults in the corresponding fraction of *cis* and *trans* isomer. Integral limits and values are given for each chromatogram.

Azobenzene-modified 8-mer DNA (AB)

Sample: 5'-GAATXGGTG-3' with X = Azobenzene (AB), 10 µM solution in H_2O, 20 µL injection for each measurement.

Gradient: ACN/0.1 M TEAAC = 5/95 -> 25/75 in 20 minutes, flow-rate: 1 mL/min.

Detection: λ = 260 nm.

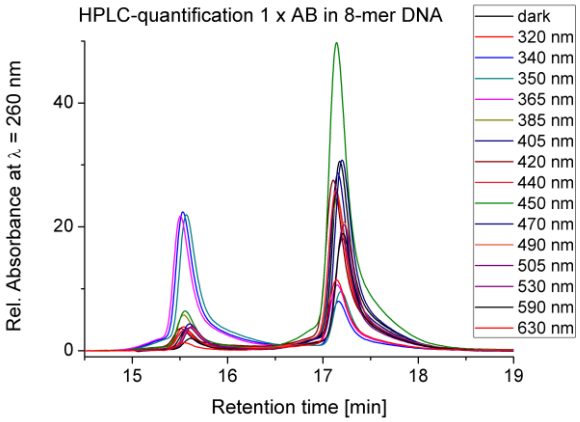

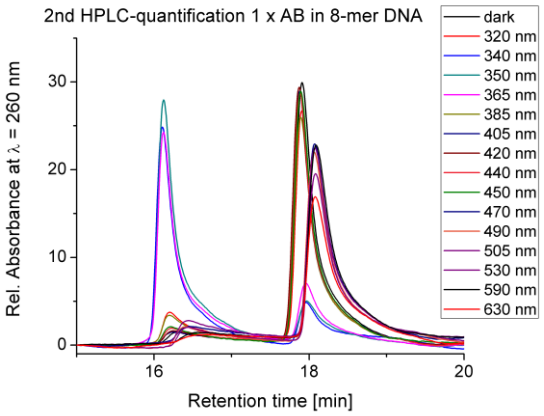

Wavelength dependent *cis*-percentage calculated from integrated peak areas:

Wave-length	**dark**	**320 nm**	**340 nm**	**350 nm**	**365 nm**	**385 nm**	**405 nm**	**420 nm**	**440 nm**	**450 nm**	**470 nm**	**490 nm**	**505 nm**	**530 nm**	**590 nm**	**630 nm**
***cis*-fraction [%]**	10.49 ± 0.41	17.22 ± 2.49	72.94 ± 2.58	72.76 ± 5.54	68.21 ± 4.05	18.94 ± 0.06	10.75 ± 0.52	13.44 ± 2.12	12.20 ± 0.74	11.91 ± 0.40	13.53 ± 2.78	13.51 ± 2.07	16.75 ± 1.45	14.76 ± 2.18	10.79 ± 1.35	11.62 ± 0.99

2',6'-Dimethylazobenzene-modified 8-mer DNA (DMAB)

Sample: 5'-GAATXGGTG-3' with X = 2',6'-Dimethylazobenzene (DMAB), 10 µM solution in H_2O, 20 µL injection for each measurement.

Gradient: ACN/0.1 M TEAAC = 15/85 -> 25/75 in 20 minutes, flow-rate: 1 mL/min.

Detection: λ = 260 nm.

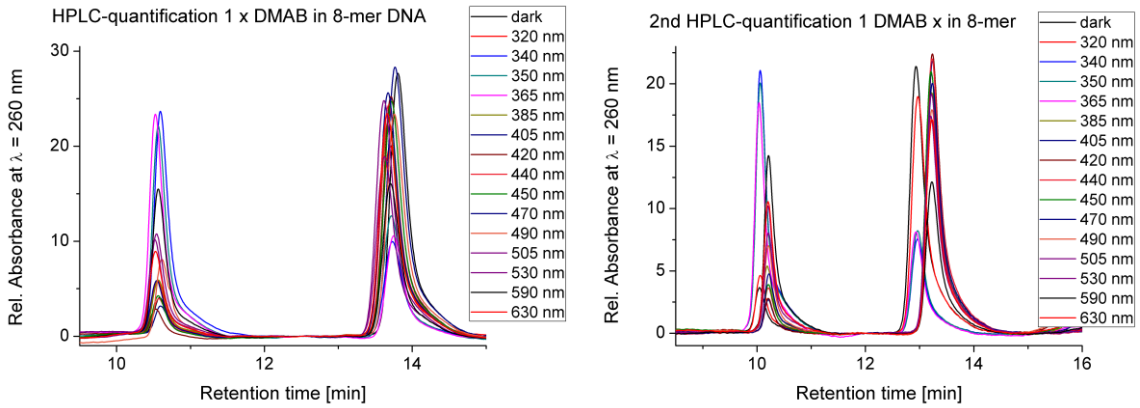

Wavelength dependent *cis*-percentage calculated from integrated peak areas:

Wave-length	dark	320 nm	340 nm	350 nm	365 nm	385 nm	405 nm	420 nm	440 nm	450 nm	470 nm	490 nm	505 nm	530 nm	590 nm	630 nm
***cis*-fraction [%]**	10.51 ± 1.10	16.85 ± 1.56	68.01 ± 1.91	66.08 ± 1.56	63.58 ± 2.52	17.73 ± 0.23	8.43 ± 0.14	6.88 ± 1.54	11.09 ± 0.03	11.43 ± 1.22	15.15 ± 0.33	22.03 ± 1.19	24.73 ± 0.10	31.15 ± 0.07	45.86 ± 2.38	27.83 ± 4.84

4'-Methylthio-2',6'-dimethylazobenzene-modified 8-mer DNA (S-DMAB)

Sample: 5'-GAATXGGTG-3' with X = 4'-Methylthio-2',6'-dimethylazobenzene (S-DMAB), 10 µM solution in H_2O, 20 µL injection for each measurement.

Gradient: ACN/0.1 M TEAAC = 5/95 -> 25/75 in 20 minutes, flow-rate: 1 mL/min.

Detection: λ = 260 nm.

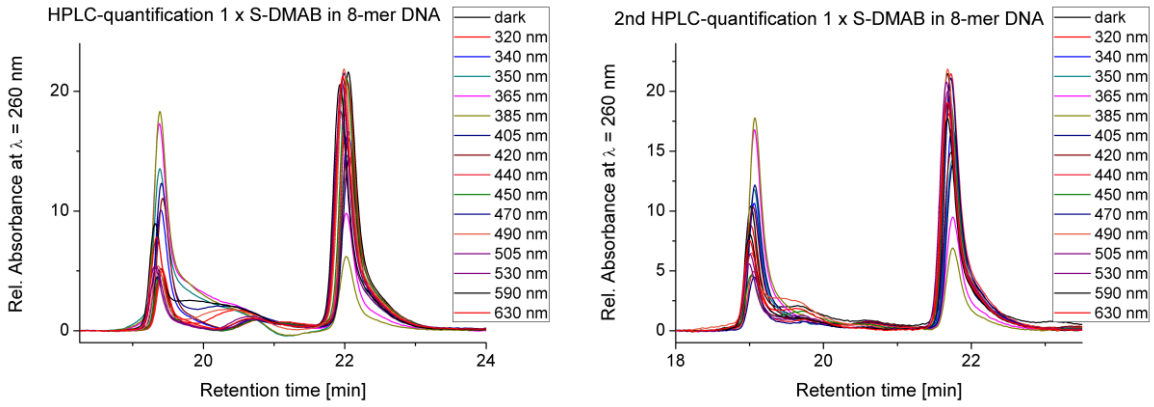

Wavelength dependent *cis*-percentage calculated from integrated peak areas:

Wave-length	dark	320 nm	340 nm	350 nm	365 nm	385 nm	405 nm	420 nm	440 nm	450 nm	470 nm	490 nm	505 nm	530 nm	590 nm	630 nm
***cis*-fraction [%]**	24.97 ± 9.19	25.37 ± 6.20	33.79 ± 1.06	47.15 ± 5.82	62.87 ± 3.12	73.04 ± 3.46	44.15 ± 0.36	36.56 ± 1.44	17.52 ± 2.11	19.81 ± 5.46	16.08 ± 1.75	27.38 ± 5.98	19.96 ± 3.01	22.66 ± 3.70	33.35 ± 1.81	27.77 ± 4.87

2',6'-Difluoroazobenzene-modified 8-mer DNA (DFAB)

Sample: 5'-GAATXGGTG-3' with X = 2',6'-Difluoroazobenzene (DFAB), 10 µM solution in H_2O, 20 µL injection for each measurement.

Gradient: ACN/0.1 M TEAAC = 13/87 -> 18/82 in 20 minutes, flow-rate: 1 mL/min.

Detection: λ = 260 nm.

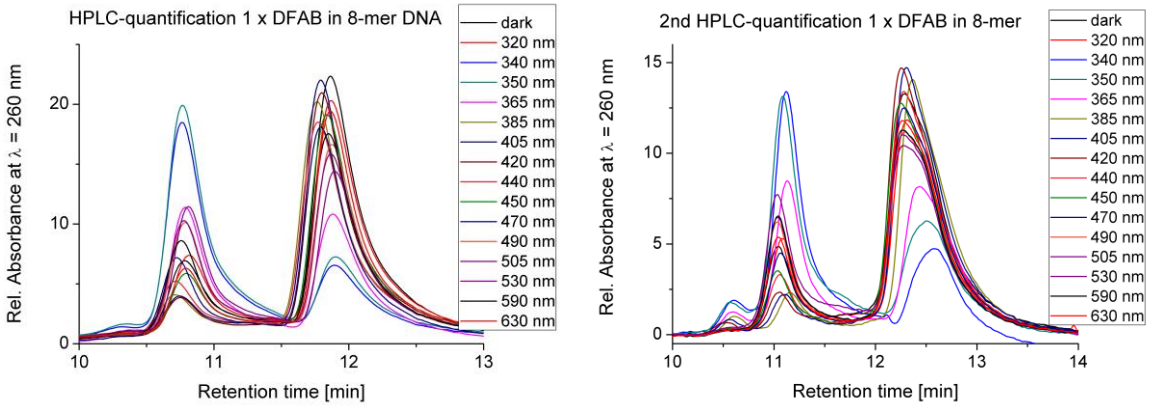

Wavelength dependent *cis*-percentage calculated from integrated peak areas:

Wave-length	**dark**	**320 nm**	**340 nm**	**350 nm**	**365 nm**	**385 nm**	**405 nm**	**420 nm**	**440 nm**	**450 nm**	**470 nm**	**490 nm**	**505 nm**	**530 nm**	**590 nm**	**630 nm**
***cis*-fraction [%]**	23.24 ± 2.34	25.39 ± 2.16	69.90 ± 1.92	62.91 ± 4.61	45.12 ± 3.41	17.57 ± 3.16	16.97 ± 3.41	17.29 ± 1.67	20.36 ± 4.03	21.84 ± 3.82	24.64 ± 4.17	32.00 ± 5.19	33.09 ± 5.33	38.34 ± 4.41	30.26 ± 2.77	24.95 ± 1.52

2',6'-Dimethoxyazobenzene-modified 8-mer DNA (DOAB)

Sample: 5'-GAATXGGTG-3' with X = 2',6'-Dimethoxyazobenzene (DOAB), 10 µM solution in H_2O, 20 µL injection for each measurement.

Gradient: ACN/0.1 M TEAAC = 10/90 -> 20/80 in 20 minutes, flow-rate: 1 mL/min.

Detection: λ = 260 nm.

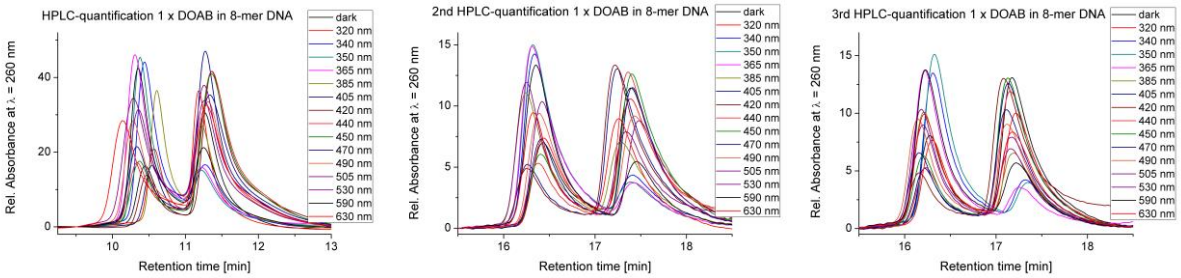

Wavelength dependent *cis*-percentage calculated from integrated peak areas:

Wave-length	**dark**	**320 nm**	**340 nm**	**350 nm**	**365 nm**	**385 nm**	**405 nm**	**420 nm**	**440 nm**	**450 nm**	**470 nm**	**490 nm**	**505 nm**	**530 nm**	**590 nm**	**630 nm**
***cis*-fraction [%]**	35.13 ± 0.64	38.69 ± 1.27	70.73 ± 0.57	73.58 ± 1.07	74.73 ± 0.47	57.18 ± 0.35	27.61 ± 0.23	25.84 ± 0.31	28.22 ± 0.77	30.86 ± 0.52	36.74 ± 0.69	47.43 ± 1.32	49.87 ± 0.06	56.20 ± 0.47	66.65 ± 0.18	49.30 ± 1.38

N-Methylarylazopyrazole-modified 8-mer DNA (AAP1)

Sample: 5'-GAATXGGTG-3' with X = *N*-Methylarylazopyrazole (AAP1), 10 µM solution in H_2O, 20 µL injection for each measurement.

Gradient: ACN/0.1 M TEAAC = 5/95 -> 25/75 in 20 minutes, flow-rate: 1 mL/min.

Detection: λ = 260 nm.

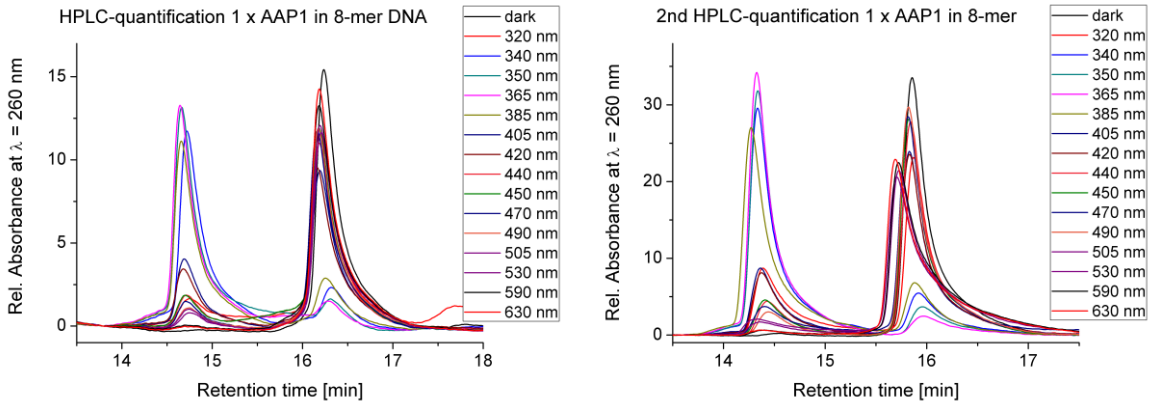

Wavelength dependent *cis*-percentage calculated from integrated peak areas:

Wave-length	dark	320 nm	340 nm	350 nm	365 nm	385 nm	405 nm	420 nm	440 nm	450 nm	470 nm	490 nm	505 nm	530 nm	590 nm	630 nm
***cis*-fraction [%]**	4.53 ± 4.01	25.22 ± 6.29	81.20 ± 2.21	86.65 ± 1.19	88.87 ± 0.77	77.28 ± 0.89	29.05 ± 0.50	26.75 ± 0.11	16.53 ± 1.61	16.26 ± 0.92	12.61 ± 3.89	8.26 ± 2.05	8.83 ± 4.26	6.05 ± 3.39	3.52 ± 0.36	4.55 ± 0.66

N-Phenylarylazopyrazole-modified 8-mer DNA (AAP2)

Sample: 5'-GAATXGGTG-3' with X = *N*-Phenylarylazopyrazole (AAP2), 10 µM solution in H_2O, 20 µL injection for each measurement.

Gradient: ACN/0.1 M TEAAC = 10/90 -> 30/70 in 20 minutes, flow-rate: 1 mL/min.

Detection: λ = 260 nm.

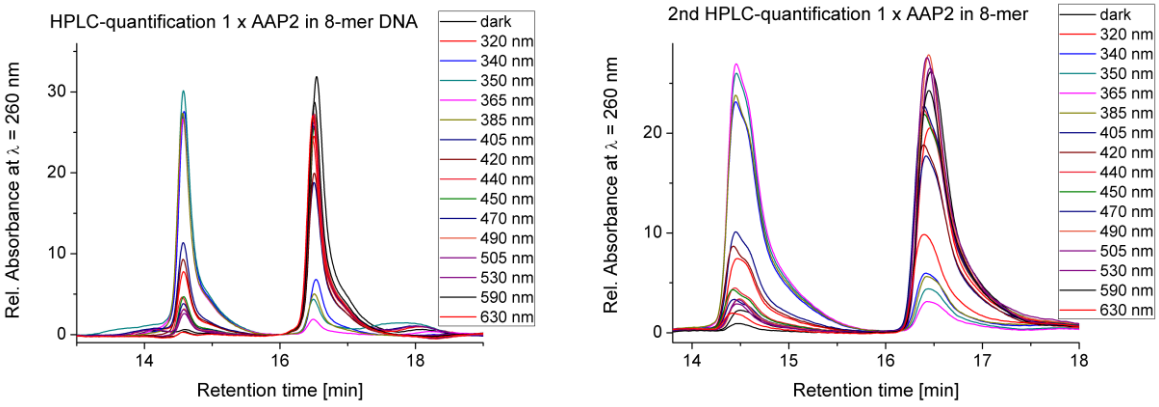

Wavelength dependent *cis*-percentage calculated from integrated peak areas:

Wave-length	dark	320 nm	340 nm	350 nm	365 nm	385 nm	405 nm	420 nm	440 nm	450 nm	470 nm	490 nm	505 nm	530 nm	590 nm	630 nm
***cis*-fraction [%]**	5.75 ± 2.33	25.29 ± 0.47	78.00 ± 1.83	83.79 ± 0.39	90.61 ± 2.99	80.57 ± 3.63	35.50 ± 0.88	29.90 ± 0.25	14.37 ± 1.69	13.99 ± 1.50	11.09 ± 1.46	9.31 ± 1.76	10.29 ± 0.07	8.01 ± 1.72	2.52 ± 1.08	8.41 ± 5.93

Comparison of wavelength-dependent *cis* fraction of all modified 8-mer DNA strands

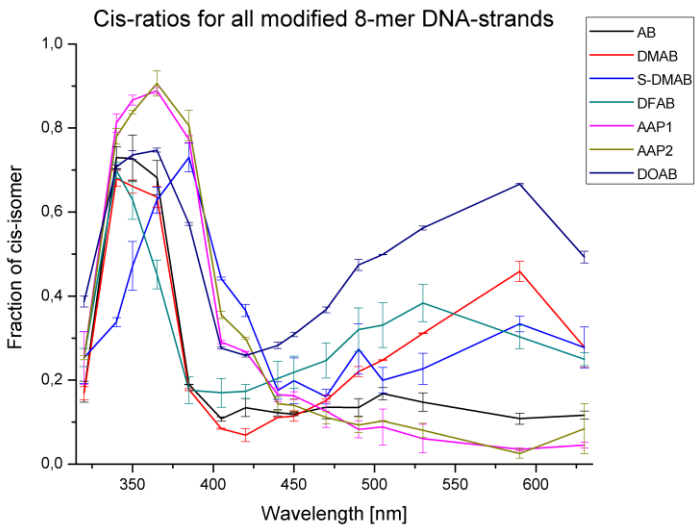

Cis-percentage calculated for all modified 8-mer DNA strands:

WL [nm]	AB	DMAB	S-DMAB	DFAB	DOAB	AAP1	AAP2
dark	10.49 ± 0.41	10.51 ± 1.10	24.97 ± 9.19	23.24 ± 2.34	35.13 ± 0.64	4.53 ± 4.01	5.75 ± 2.33
320 nm	17.22 ± 2.49	16.85 ± 1.56	25.37 ± 6.20	25.39 ± 2.16	38.69 ± 1.27	25.22 ± 6.29	25.29 ± 0.47
340 nm	72.94 ± 2.58	68.01 ± 1.91	33.79 ± 1.06	69.90 ± 1.92	70.73 ± 0.57	81.20 ± 2.21	78.00 ± 1.83
350 nm	72.76 ± 5.54	66.08 ± 1.56	47.15 ± 5.82	62.91 ± 4.61	73.58 ± 1.07	86.65 ± 1.19	83.79 ± 0.39
365 nm	68.21 ± 4.05	63.58 ± 2.52	62.87 ± 3.12	45.12 ± 3.41	74.73 ± 0.47	88.87 ± 0.77	90.61 ± 2.99
385 nm	18.94 ± 0.06	17.73 ± 0.23	73.04 ± 3.46	17.57 ± 3.16	57.18 ± 0.35	77.28 ± 0.89	80.57 ± 3.63
405 nm	10.75 ± 0.52	8.43 ± 0.14	44.15 ± 0.36	16.97 ± 3.41	27.61 ± 0.23	29.05 ± 0.50	35.50 ± 0.88
420 nm	13.44 ± 2.12	6.88 ± 1.54	36.56 ± 1.44	17.29 ± 1.67	25.84 ± 0.31	26.75 ± 0.11	29.90 ± 0.25
440 nm	12.20 ± 0.74	11.09 ± 0.03	17.52 ± 2.11	20.36 ± 4.03	28.22 ± 0.77	16.53 ± 1.61	14.37 ± 1.69
450 nm	11.91 ± 0.40	11.43 ± 1.22	19.81 ± 5.46	21.84 ± 3.82	30.86 ± 0.52	16.26 ± 0.92	13.99 ± 1.50
470 nm	13.53 ± 2.78	15.15 ± 0.33	16.08 ± 1.75	24.64 ± 4.17	36.74 ± 0.69	12.61 ± 3.89	11.09 ± 1.46
490 nm	13.51 ± 2.07	22.03 ± 1.19	27.38 ± 5.98	32.00 ± 5.19	47.43 ± 1.32	8.26 ± 2.05	9.31 ± 1.76
505 nm	16.75 ± 1.45	24.73 ± 0.10	19.96 ± 3.01	33.09 ± 5.33	49.87 ± 0.06	8.83 ± 4.26	10.29 ± 0.07
530 nm	14.76 ± 2.18	31.15 ± 0.07	22.66 ± 3.70	38.34 ± 4.41	56.20 ± 0.47	6.05 ± 3.39	8.01 ± 1.72
590 nm	10.79 ± 1.35	45.86 ± 2.38	33.35 ± 1.81	30.26 ± 2.77	66.65 ± 0.18	3.52 ± 0.36	2.52 ± 1.08
630 nm	11.62 ± 0.99	27.83 ± 4.84	27.77 ± 4.87	24.95 ± 1.52	49.30 ± 1.38	4.55 ± 0.66	8.41 ± 5.93

7.6 Melting curve analysis

7.6.1 Melting curves of unmodified DNA duplexes

Melting curves were performed in a volume of 200 µL of a 0.5 M NaCl solution in Millipore water. 8-mer duplexes were diluted to a concentration of 3 µM 8-mer strand plus 3 µM 8-mer antisense strand and 2 µM 12-mer strand plus 2 µM 12-mer antisense strand. Melting curves were performed with a ramp rate of 1 °C/minute in a range between 10 °C and 60 °C for 8-mer duplexes and a range between 20 °C and 80 °C for 12-mer duplexes. Determination of melting temperatures T_m was done *via* the JASCO spectra analysis software by fitting all melting curves with a second derivative fit curve.

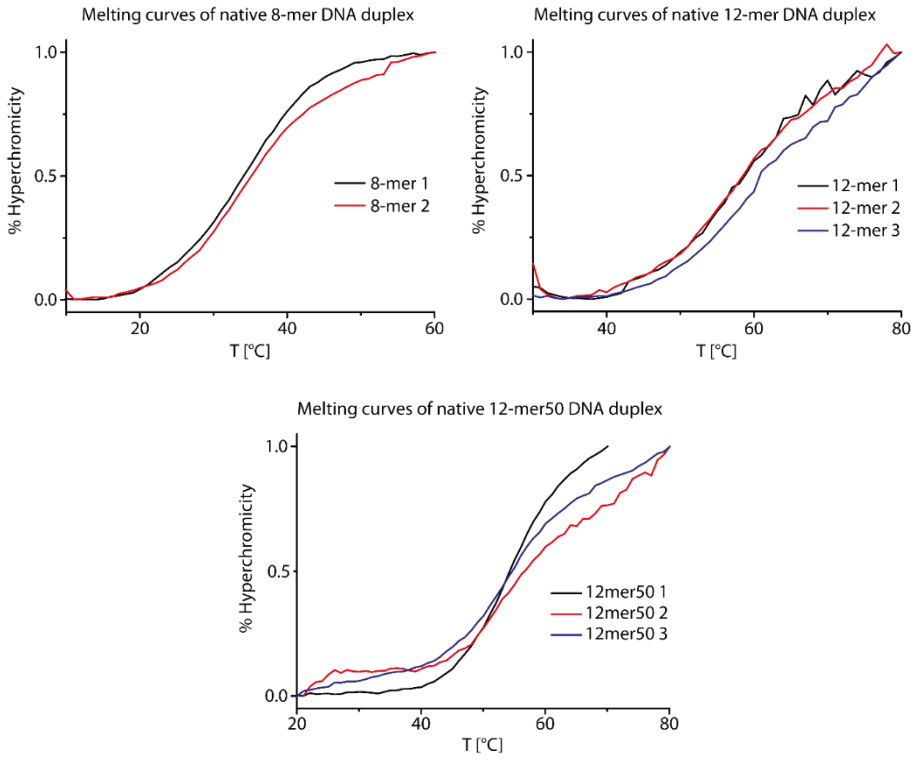

Melting curves recorded for the three unmodified DNA duplexes given below.The melting temperatures were determined as follows:

<u>Melting temperatures of unmodified DNA duplexes (error = SD):</u>

Native 8-mer duplex 5'-GAATGGTG-3' and complement (n = 2): 33.9 °C ± 0.1 °C

Native 12-mer duplex 5'-CACCATTCCGGT-3' and complement (n = 3): 59.4 °C ± 0.2 °C

Native 12-mer50 duplex 5'-CACCATTCCAGT-3' and complement (n = 3): 54.6 °C ± 0.3 °C

7.6.2 Melting curves of modified 8-mer DNA duplexes

The following modified 8-mer duplexes with X as a given modification were used with the unmodified complementary strand:

A) 5'-GAATXGGTG-3'

B) 5'-GAXATGGXTG-3'

C) 5'-GAXATXGGXTG-3'

Melting curves of azobenzene-modified 8-mer DNA sequences A, B and C with X = AB.

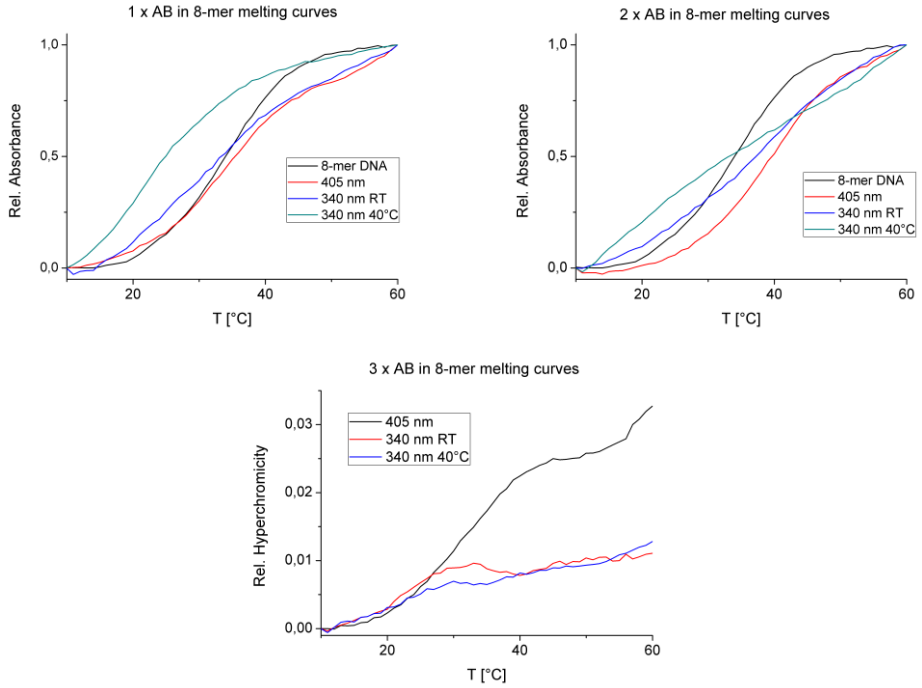

The melting temperatures after each irradiation step were determined as follows (n = 3, error = SD):

Mod.	405 nm	350 nm	350 nm 40 °C
T_m (A) [°C]	35.38 ± 1.89	28.03 ± 1.23	22.89 ± 0.53
T_m (B) [°C]	38.95 ± 0.25	32.70 ± 3.40	18.77 ± 1.40
T_m (C) [°C]	32.74 ± 1.05	21.03 ± 0.82	18.33 ± 2.04

Melting curves of 2',6'-dimethylazobenzene-modified 8-mer DNA sequences A, B and C with X = DMAB:

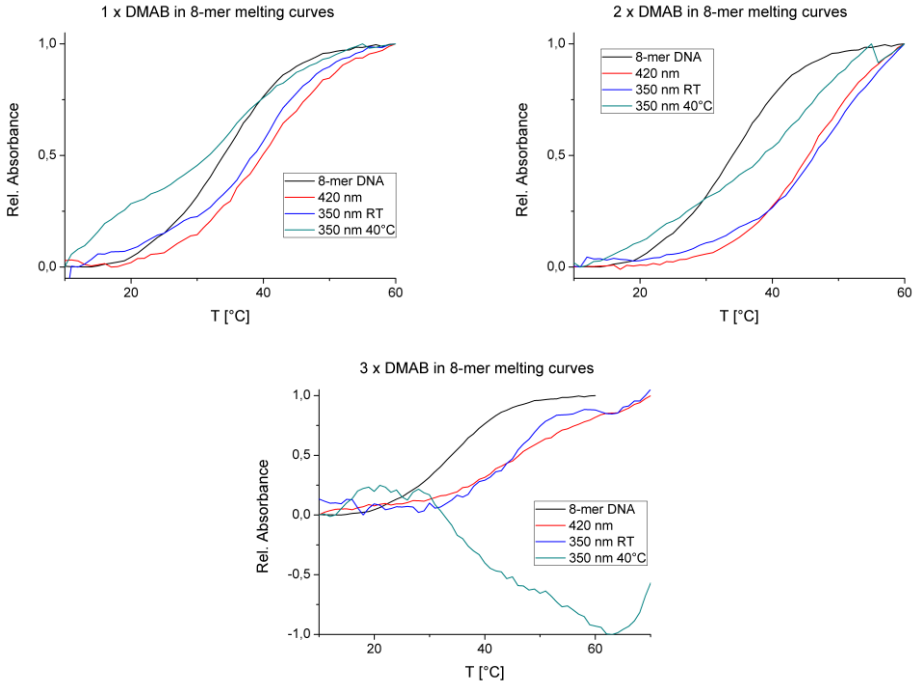

The melting temperatures after each irradiation step were determined as follows (n = 3, error = SD):

Mod.	420 nm	350 nm	350 nm 40 °C
T_m (A) [°C]	40.26 ± 0.53	40.27 ± 0.37	40.79 ± 1.93
T_m (B) [°C]	47.09 ± 0.84	48.59 ± 0.45	47.81 ± 2.04
T_m (C) [°C]	46.54 ± 0.98	44.94 ± 0.39	N/A

Melting curves of 4’-methylthio-2’,6’-dimethylazobentene-modified 8-mer DNA sequences A, B and C with X = S-DMAB:

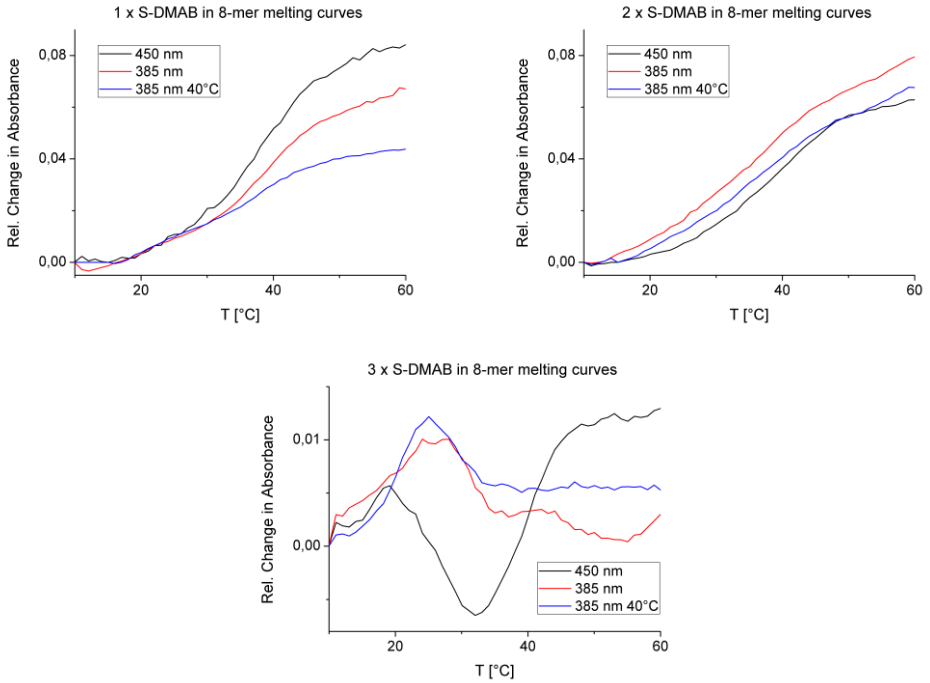

The melting temperatures after each irradiation step were determined as follows (n = 3, error = SD):

Mod.	450 nm	385 nm	385 nm 40 °C
T_m (A) [°C]	38.25 ± 0.39	38.48 ± 0.09	37.62 ± 1.53
T_m (B) [°C]	39.09 ± 0.82	38.49 ± 3.23	36.10 ± 0.45
T_m (C) [°C]	39.77 ± 1.53	16.91 ± 2.20	17.05 ± 2.29

Melting curves of 2’,6’-difluoroazobenzene-modified 8-mer DNA sequence A with X = DFAB:

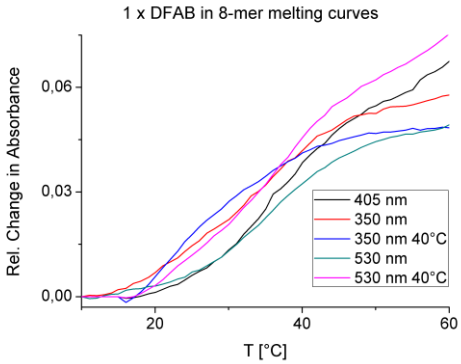

The melting temperatures after each irradiation step were determined as follows (n = 3, error = SD):

Mod.	405 nm	350 nm	350 nm 40 °C	530 nm	530 nm 40 °C
T_m (A) [°C]	36.82 ± 0.38	32.10 ± 0.26	22.96 ± 0.36	34.87 ± 0.96	33.99 ± 0.71

Melting curves of 2',6'-dimethoxylazobenzene-modified 8-mer DNA sequence A with X = DOAB:

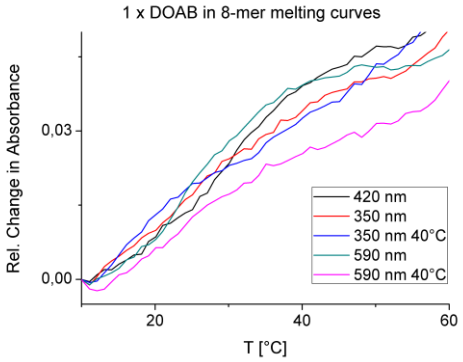

The melting temperatures after each irradiation step were determined as follows (n = 3, error = SD):

Mod.	420 nm	350 nm	350 nm 40 °C	590 nm	590 nm 40 °C
T_m (A) [°C]	28,44 ± 3,01	16,42 ± 1,16	16,66 ± 0,51	25,14 ± 0,50	21,52 ± 0,79

Melting curves of *N*-methyl-arylazopyrazole-modified 8-mer DNA sequences A, B and C with X = AAP1:

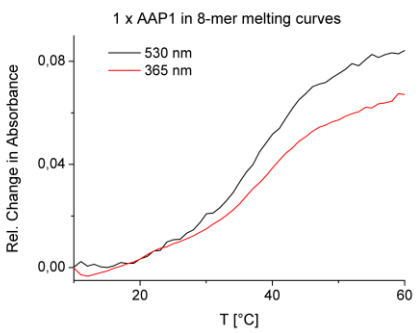

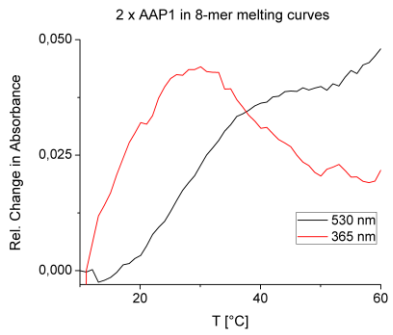

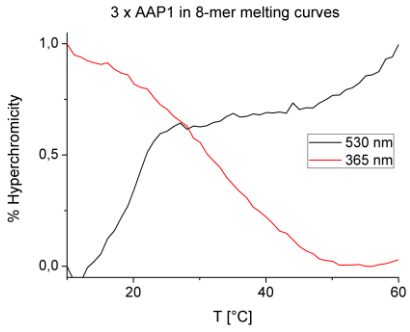

The melting temperatures after each irradiation step were determined as follows (n = 3, error = SD):

Mod.	590 nm	365 nm
T_m (A) [°C]	30.27 ± 0.56	21.66 ± 1.32
T_m (B) [°C]	26.06 ± 1.85	N/A
T_m (C) [°C]	19.57 ± 0.38	N/A

Melting curves of *N*-phenyl-arylazopyrazole-modified 8-mer DNA sequence A with X = AAP2:

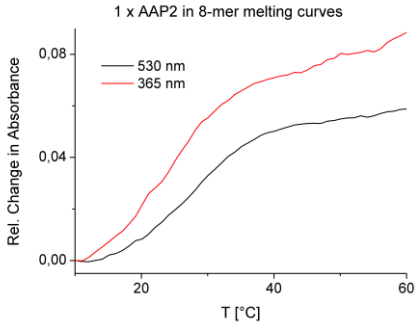

The melting temperatures after each irradiation step were determined as follows (n = 3, error = SD):

Mod.	590 nm	365 nm
T_m (A) [°C]	26.91 ± 0.64	22.09 ± 1.29

7.6.3 Melting curves of modified 12-mer DNA duplexes

The following modified 8-mer duplexes with X = modification were used with the unmodified complementary strand:

D) 5'-CAC CAT X TCC GGT-3'

E) 5'-CAC X CAT TCC X GGT-3'

F) 5'-CAC X CAT X TCC X GGT-3'

G) 5'-CAC CXAT TCXC AGT-3'

H) 5'-CAC X CAT X TCC X AGT-3'

Melting curves of azobenzene-modified 12-mer DNA sequences D, E and F with X = AB:

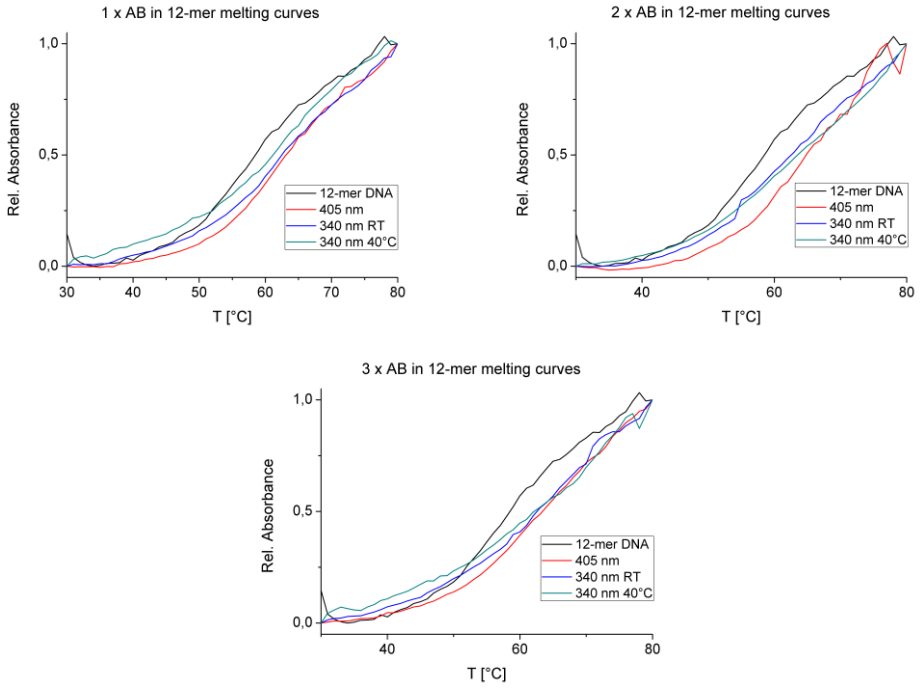

The melting temperatures after each irradiation step were determined as follows (n = 3, error = SD):

Mod.	405 nm	350 nm	350 nm 40 °C
T_m (D) [°C]	65.31 ± 1.10	65.01 ± 0.27	64.65 ± 2.53
T_m (E) [°C]	65.30 ± 1.70	64.46 ± 1.80	63.05 ± 3.96
T_m (F) [°C]	66.45 ± 1.63	64.68 ± 1.18	58.69 ± 1.40

Melting curves of 2',6'-dimethylazobenzene-modified 12-mer DNA sequences D, E and F with X = DMAB:

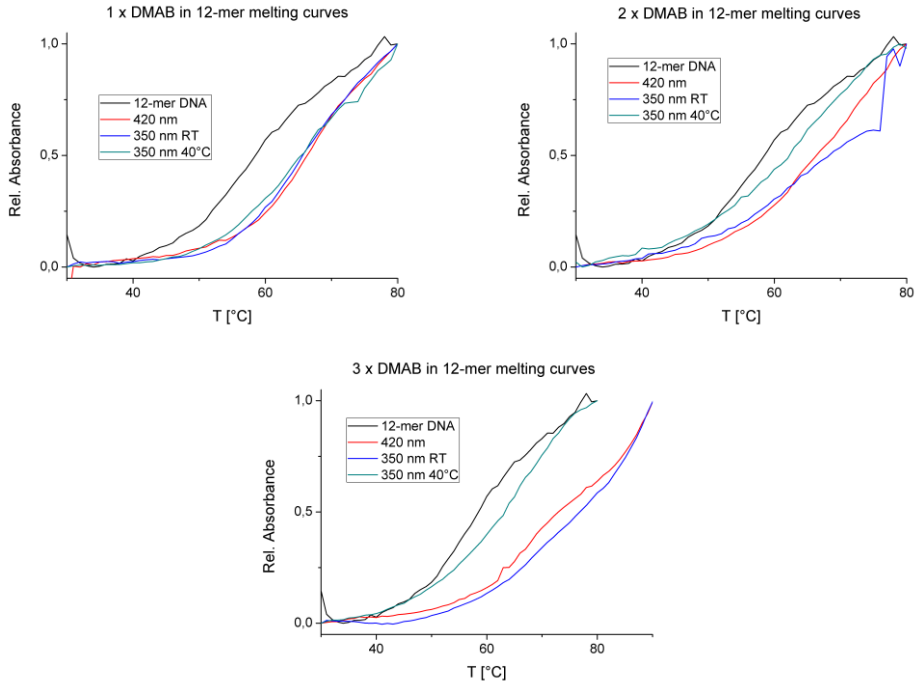

The melting temperatures after each irradiation step were determined as follows (n = 3, error = SD):

Mod.	420 nm	350 nm	350 nm 40 °C
T_m (D) [°C]	66.48 ± 0.55	66.74 ± 0.19	67.05 ± 3.21
T_m (E) [°C]	69.96 ± 4.59	67.95 ± 3.73	67.87 ± 4.56
T_m (F) [°C]	72.13 ± 2.06	72.56 ± 3.79	64.61 ± 10.81

Melting curves of 4'-methylthio-2',6'-dimethylazobenzene-modified 12-mer DNA sequences D, E and F with X = S-DMAB:

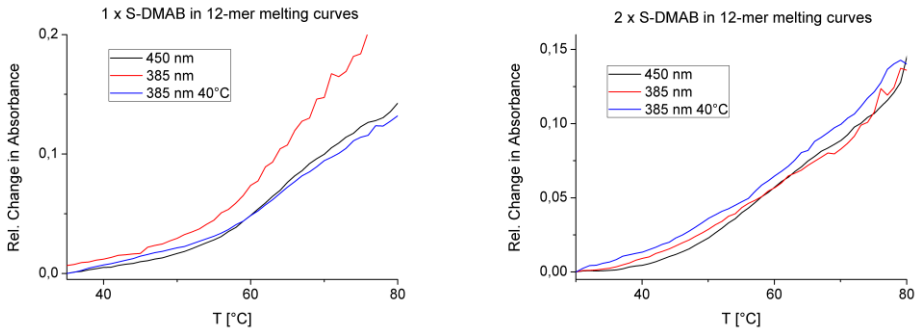

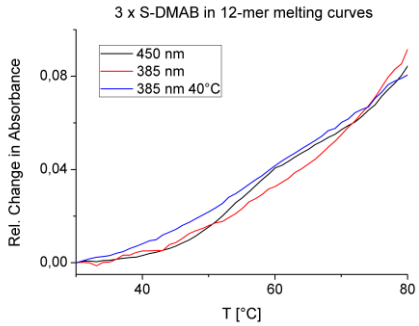

The melting temperatures after each irradiation step were determined as follows (n = 3, error = SD):

Mod.	450 nm	385 nm	385 nm 40 °C
T_m (D) [°C]	64.72 ± 0.99	66.34 ± 0.21	66.62 ± 0.36
T_m (E) [°C]	64.67 ± 1.27	60.63 ± 1.10	59.64 ± 2.92
T_m (F) [°C]	59.23 ± 2.45	59.75 ± 4.92	61.58 ± 5.01

Melting curves of 2',6'-difluoroazobenzene-modified 12-mer DNA sequence D with X = DFAB:

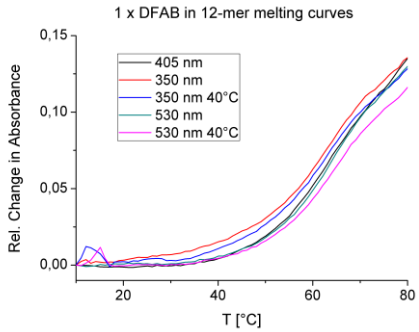

The melting temperatures after each irradiation step were determined as follows (n = 3, error = SD):

Mod.	405 nm	350 nm	350 nm 40 °C	530 nm	530 nm 40 °C
T_m (D) [°C]	63,48 ± 0,37	63,37 ± 0,31	64,26 ± 1,44	64,29 ± 0,46	65,34 ± 0,35

Melting curves of 2',6'-dimethoxyazobenzene-modified 12-mer DNA sequence D with X = DOAB:

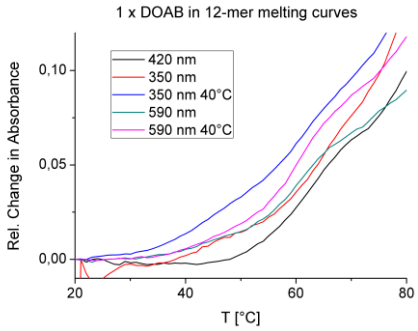

The melting temperatures after each irradiation step were determined as follows (n = 3, error = SD):

Mod.	420 nm	350 nm	350 nm 40 °C	590 nm	590 nm 40 °C
T_m (D) [°C]	62,82 ± 0,81	63,79 ± 1,52	65,06 ± 0,91	61,82 ± 0,59	62,94 ± 1,52

Melting curves of *N*-methylarylazopyrazole-modified 12-mer DNA sequences D, E and F with X = AAP1:

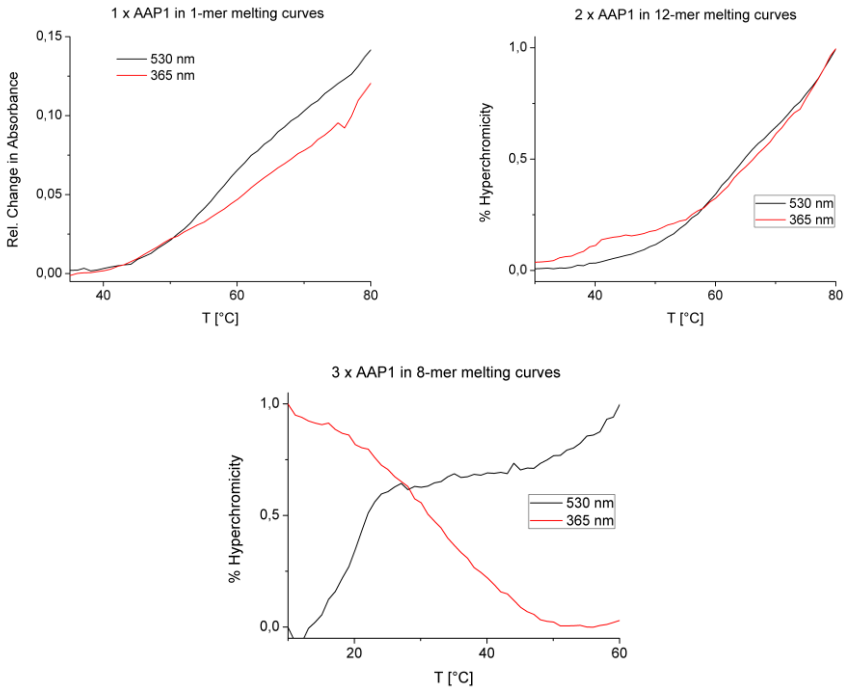

The melting temperatures after each irradiation step were determined as follows (n = 3, error = SD):

Mod.	590 nm	365 nm
T_m (D) [°C]	60.55 ± 1.31	62.70 ± 1.43
T_m (E) [°C]	62.85 ± 0.29	N/A
T_m (F) [°C]	57.64 ± 3.49	N/A

Melting curves of *N*-phenylarylazopyrazole-modified 12-mer DNA sequences D, E and F with X = AAP2:

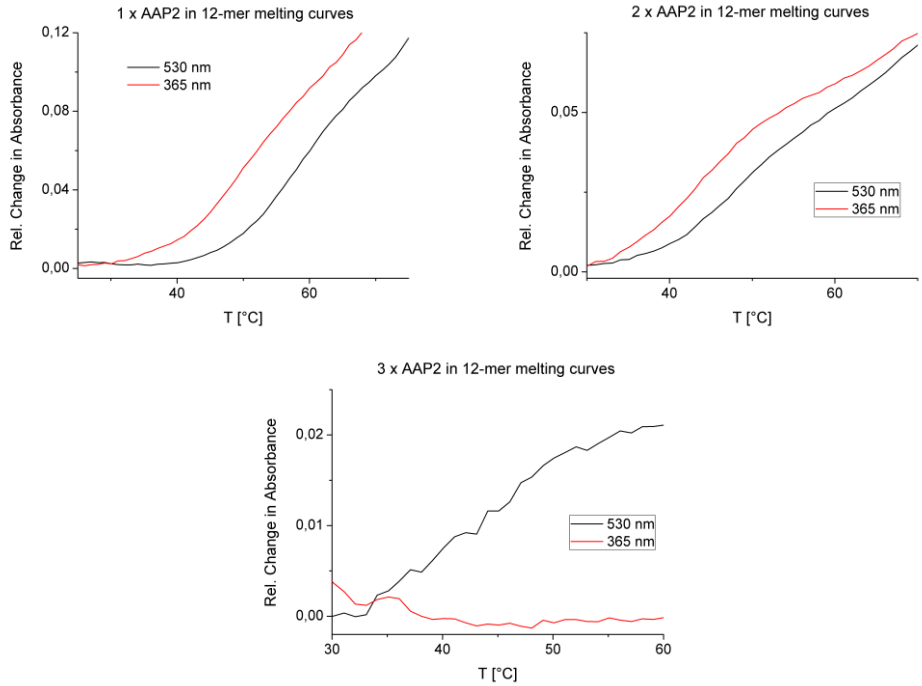

The melting temperatures after each irradiation step were determined as follows (n = 3, error = SD):

Mod.	590 nm	365 nm
T_m (D) [°C]	57.88 ± 1.08	54.17 ± 0.17
T_m (E) [°C]	52.30 ± 1.11	43.82 ± 0.78
T_m (F) [°C]	43.77 ± 0.83	N/A

Melting curves of *N*-methyl-arylazopyrazole-modified 12-mer50 DNA sequences G and H with X = AAP1:

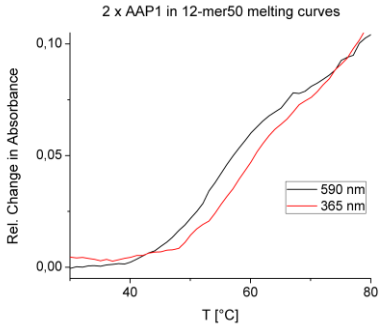

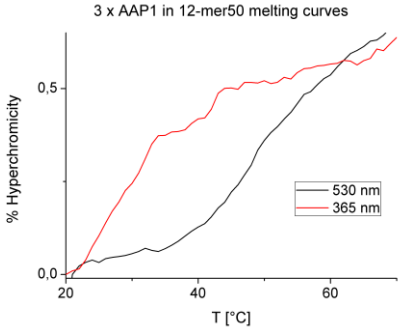

The melting temperatures after each irradiation step were determined as follows (n = 3, error = SD):

Mod.	590 nm	365 nm
T_m (G) [°C]	54.67 ± 0.93	58.21 ± 0.52
T_m (H) [°C]	48.44 ± 2.83	26.83 ± 0.79

Melting curves of *N*-phenyl-arylazopyrazole-modified 12-mer50 DNA sequences G and H with X = AAP2:

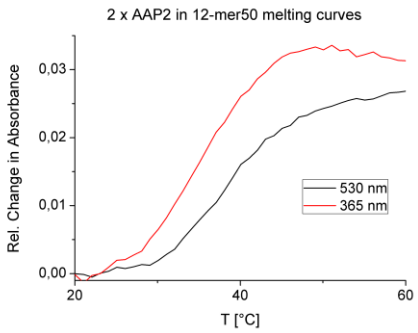

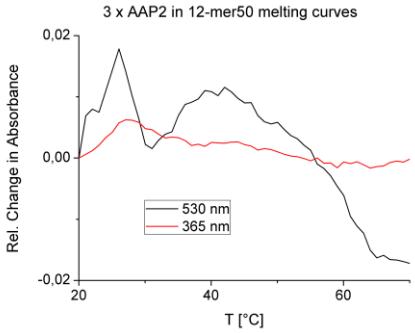

The melting temperatures after each irradiation step were determined as follows (n = 3, error = SD):

Mod.	590 nm	365 nm
T_m (G) [°C]	38.07 ± 1.22	35.52 ± 0.39
T_m (H) [°C]	N/A	N/A

7.6.4 Melting curves of modified release-oligomer DNA duplexes

In addition to the modified 8-mer and 12-mer sequences described in chapter 7.6.1, another 12-mer sequence with 66 % GC-content and two 10-mer sequences were used for additional melting curve measurements for further use in a catenane system.

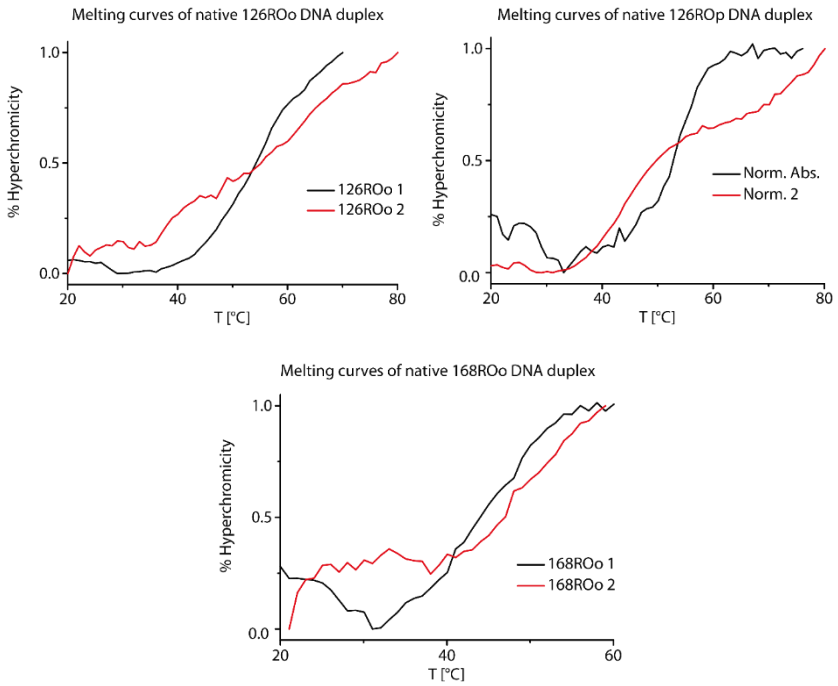

Melting points of unmodified DNA duplexes, n = 2, error = SD:

Native 168ROo duplex 5'-TCC CCA GCA TCG-3' and complement:	63.8 °C ± 1.1 °C
Native 126ROo duplex 5'-CCG ATG CTG T-3' and complement:	53.9 °C ± 0.2 °C
Native 126ROp duplex 5'-GGA ATG GTG A-3' and complement:	44.3 °C ± 0.1 °C

The following sequences with X = modification were used:

I) 5'-TCC X CCA X GCA X TCG-3' (168ROo)

J) 5'-CC X GAT X GCT X GT-3' (126ROo)

K) 5'-GG X AAT X GGT X GA-3' (126ROp)

Melting curves of azobenzene-modified DNA sequences I, J and K with X = AB:

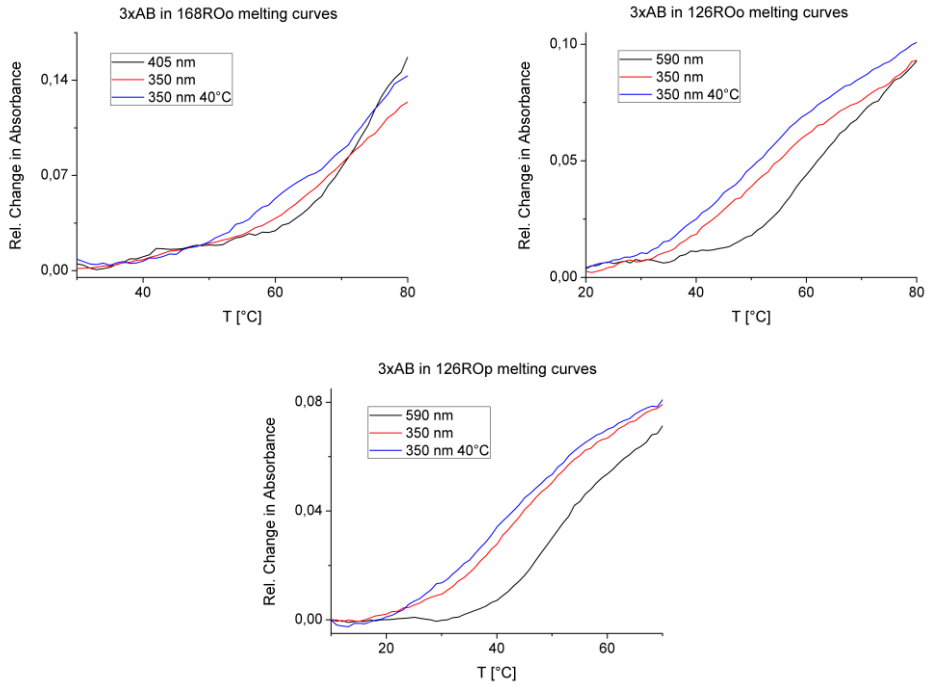

The melting temperatures after each irradiation step were determined as follows (n = 3, error = SD):

Mod.	405 nm	350 nm	350 nm 40 °C
T_m (I) [°C]	74.34 ± 1.11	73.38 ± 1.94	64.30 ± 10.10
T_m (J) [°C]	62.17 ± 1.09	56.45 ± 3.44	53.35 ± 2.23
T_m (K) [°C]	52.24 ± 1.72	45.51 ± 0.57	43.62 ± 1.27

Melting curves of 2',6'-dimethylazobenzene-modified DNA sequences I, J and K with X = DMAB:

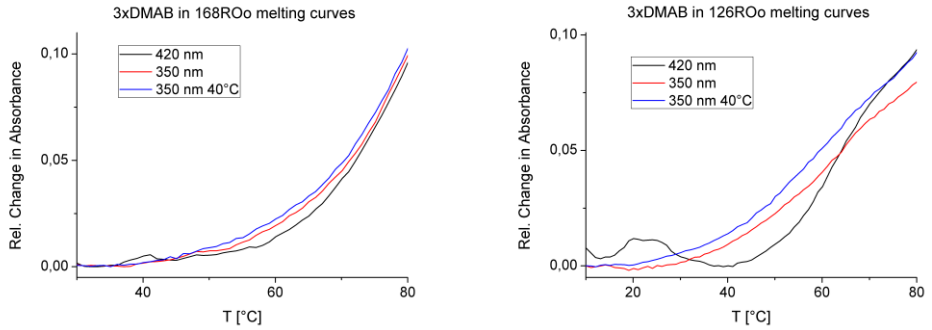

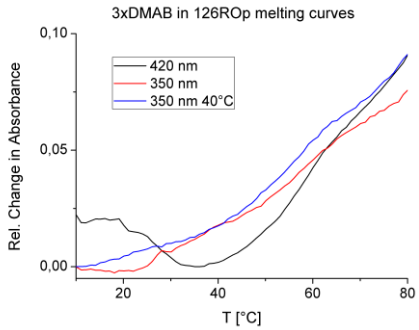

The melting temperatures after each irradiation step were determined as follows (n = 3, error = SD):

Mod.	420 nm	350 nm	350 nm 40 °C
T_m (I) [°C]	82.19 ± 4.38	79.15 ± 1.50	56.44 ± 15.18
T_m (J) [°C]	65.02 ± 1.16	66.89 ± 1.17	64.26 ± 1.84
T_m (K) [°C]	59.60 ± 1.28	63.09 ± 2.88	53.30 ± 1.79

Melting curves of 4’-methylthio-2’,6’-dimethylazobenzene-modified DNA sequences with X = S-DMAB:

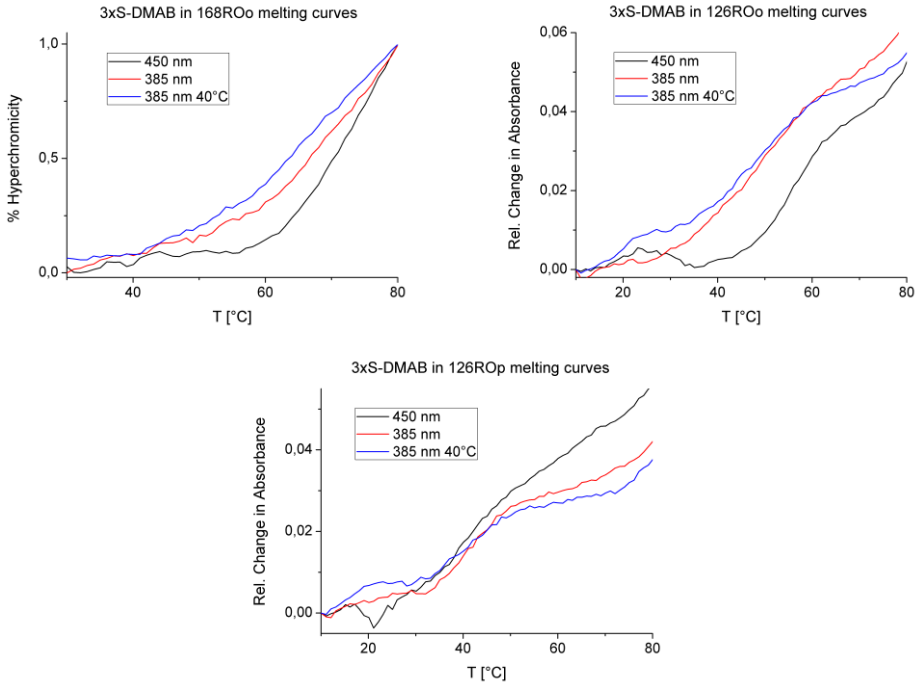

The melting temperatures after each irradiation step were determined as follows (n = 3, error = SD):

Mod.	450 nm	385 nm	385 nm 40 °C
T_m (I) [°C]	71.05 ± 3.63	68.38 ± 0.88	67.90 ± 1.30
T_m (J) [°C]	54.53 ± 1.35	47.32 ± 1.38	51.47 ± 3.43
T_m (K) [°C]	41.44 ± 0.25	41.48 ± 0.73	44.44 ± 2.10

Melting curves of *N*-methyl-arylazopyrazole-modified DNA sequences J and K with X = AAP1:

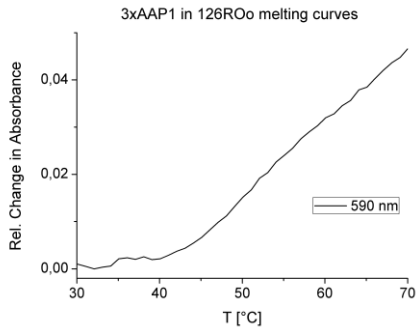

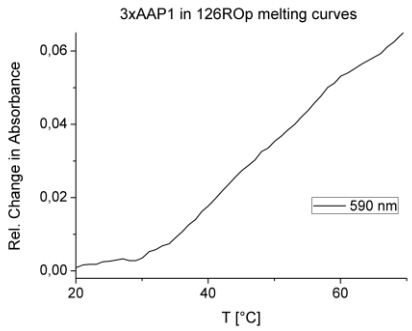

The melting temperatures after each irradiation step were determined as follows (n = 3, error = SD):

Mod.	590 nm
T_m (J) [°C]	54.11 ± 1.87
T_m (K) [°C]	45.48 ± 3.62

Further melting curves with the same sequences and modifications have been measured in chapter 7.6.5 as reversible melting curve measurements.

Melting curves of *N*-phenyl-arylazopyrazole-modified DNA-sequences J and K with X = AAP2:

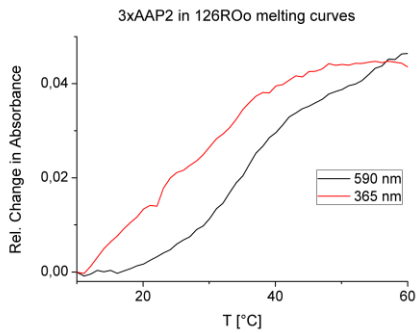

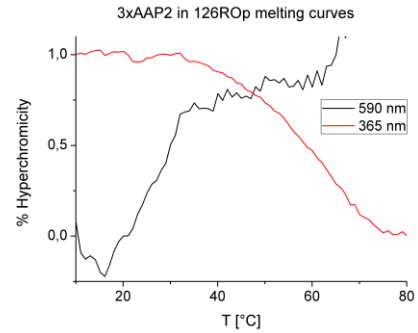

The melting temperatures after each irradiation step were determined as follows (n = 3, error = SD):

Mod.	590 nm	365 nm
T_m (J) [°C]	40.35 ± 2.72	21.66 ± 1.09
T_m (K) [°C]	36.24 ± 0.32	no MP

7.6.5 Reversible melting curve measurements

The following modified duplexes with X = modification were used with the complementary strand. Melting curves were recorded in forward mode, then the sample was cooled down to 20 °C and re-hybridized for 30 minutes before starting the next melting curve.

The following sequences with X = modification were used:

A) 5'-GAATXGGTG-3'

B) 5'-GAXATGGXTG-3'

C) 5'-GAXATXGGXTG-3'

D) 5'-CAC CAT X TCC GGT-3'

E) 5'-CAC X CAT TCC X GGT-3'

F) 5'-CAC X CAT X TCC X GGT-3'

G) 5'-CAC CXAT TCXC AGT-3'

H) 5'-CAC X CAT X TCC X AGT-3'

I) 5'-TCC X CCA X GCA X TCG-3'

J) 5'-CC X GAT X GCT X GT-3'

K) 5'-GG X AAT X GGT X GA-3'

L) 5'-TCC CXCA GCXA TCG-3'

M) 5'-CAC CXAT TCXC GGT-3'

Reversible melting curves of *N*-methyl-arylazopyrazole-modified 8-mer DNA-sequences A; B and C with X = AAP1:

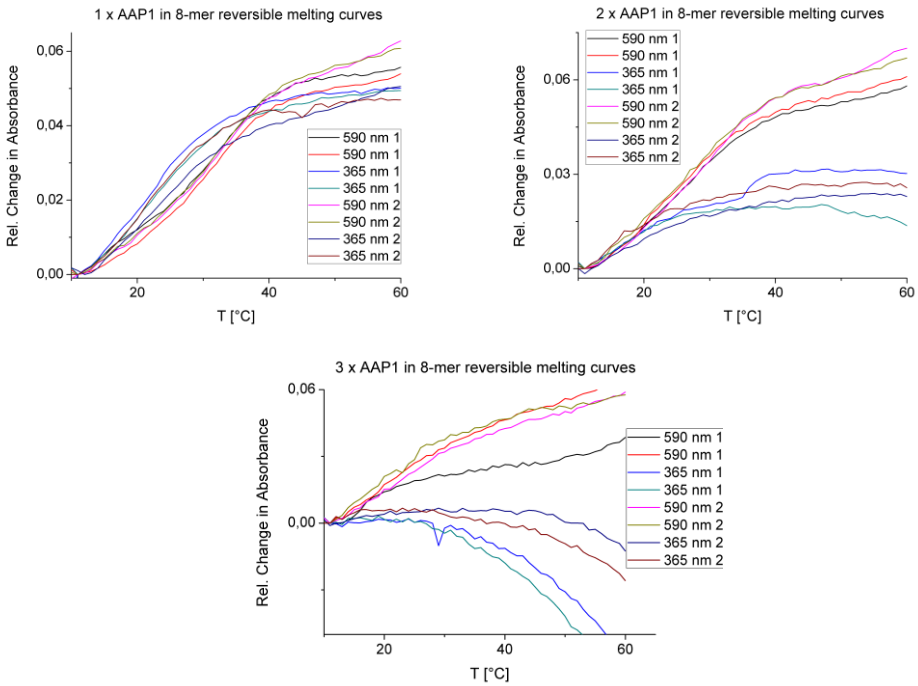

The melting temperatures after each irradiation step were determined as follows (n = 3, error = SD):

Mod.	590 nm1	365 nm 1	590 nm 2	365 nm 2
T_m (A) [°C]	30.53 ± 1.15	21.95 ± 0.93	30.87 ± 0.19	22.50 ± 0.88
T_m (B) [°C]	25.21 ± 0.25	18.28 ± 0.22	26.77 ± 0.92	16.15 ± 0.16
T_m (C) [°C]	18.53 ± 0.20	N/A	20.72 ± 1.10	N/A

Reversible melting curves of *N*-methyl-arylazopyrazole-modified 12-mer DNA-sequences D, E and F with X = AAP1:

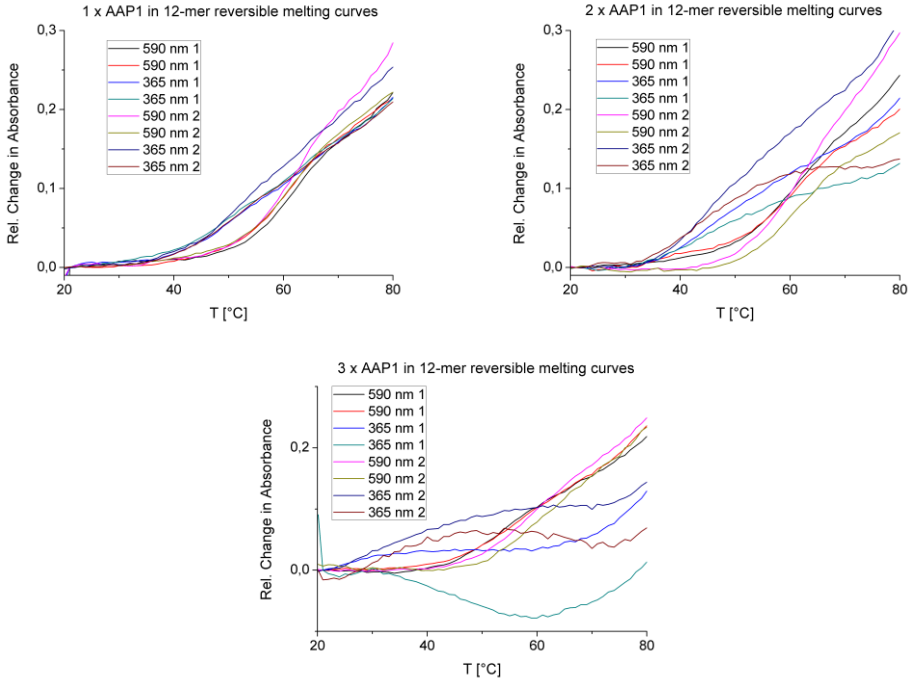

The melting temperatures after each irradiation step were determined as follows (n = 3, error = SD):

Mod.	590 nm1	365 nm 1	590 nm 2	365 nm 2
T_m (D)	61.60 ± 0.41	60.38 ± 0.17	62.59 ± 0.29	58.92 ± 0.71
T_m (E)	61.66 ± 0.36	49.24 ± 1.71	62.80 ± 1.18	48.20 ± 3.20
T_m (F)	57.99 ± 1.35	25.90 ± 0.01	62.71 ± 0.70	31.67 ± 0.19

Reversible melting curves of *N*-phenyl-arylazopyrazole-modified 8-mer DNA-sequences A, B and C with X = AAP2:

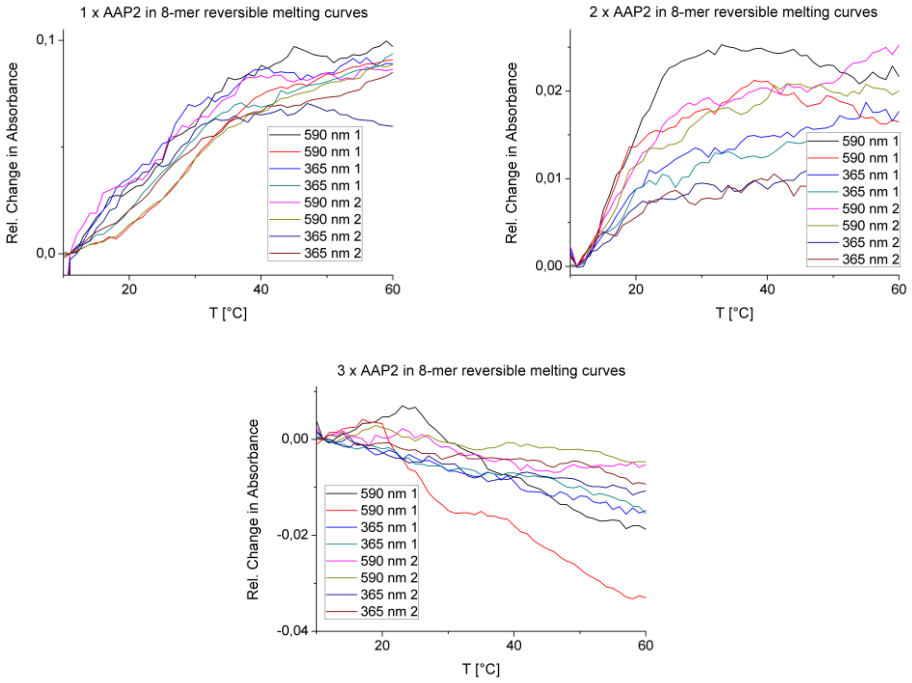

The melting temperatures after each irradiation step were determined as follows (n = 3, error = SD):

Mod.	590 nm1	365 nm 1	590 nm 2	365 nm 2
T_m (A) [°C]	27.60 ± 1.73	20.76 ± 4.00	27.04 ± 0.47	19.49 ± 3.94
T_m (B) [°C]	17.53 ± 0.98	17.71 ± 0.77	17.83 ± 0.95	16.81 ± 0.38
T_m (C) [°C]	N/A	N/A	N/A	N/A

Reversible melting curves of *N*-phenyl-arylazopyrazole-modified 12-mer DNA-sequences D, E and F with X = AAP2:

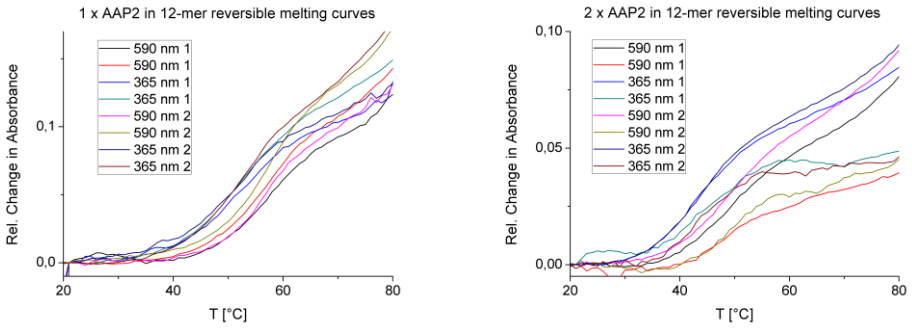

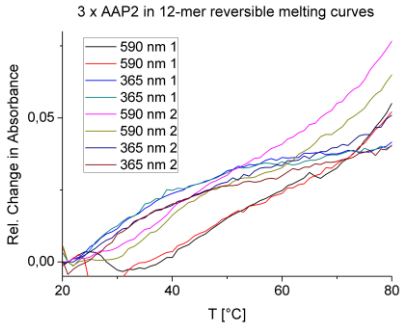

The melting temperatures after each irradiation step were determined as follows (n = 3, error = SD):

Mod.	590 nm1	365 nm 1	590 nm 2	365 nm 2
T_m (D) [°C]	57.75 ± 0.23	53.10 ± 0.15	58.05 ± 0.18	52.63 ± 0.63
T_m (E) [°C]	50.42 ± 0.39	44.73 ± 0.59	49.80 ± 0.72	44.19 ± 0.03
T_m (F) [°C]	44.79 ± 2.38	24.48 ± 0.56	42.14 ± 1.87	N/A

Reversible melting curves of 2 x *N*-methyl-arylazopyrazole (X = AAP1) and 2 x *N*-phenyl-arylazopyrazole (X = AAP2) in 12-mer DNA-sequence M:

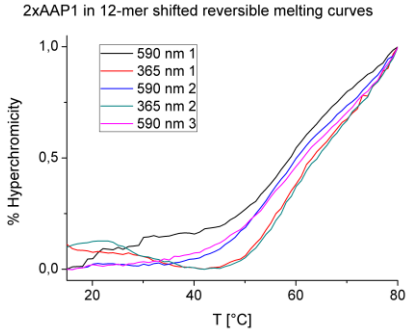

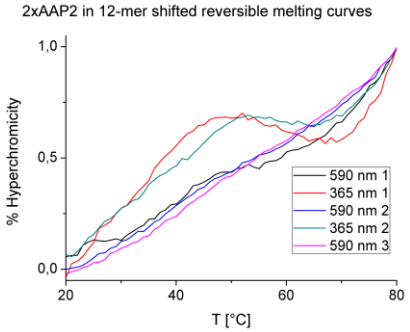

The melting temperatures after each irradiation step were determined as follows (n = 2, error = SD):

Mod.	590 nm 1	365 nm 1	590 nm 2	365 nm 2	590 nm 3
T_m (M, AAP1) [°C]	55.27 ± 3.76	59.13 ± 0.45	57.57 ± 0.29	60.55 ± 0.47	60.45 ± 1.00
T_m (M, AAP2) [°C]	36.93 ± 2.42	31.05 ± 3.60	38.71 ± 0.44	34.40 ± 1.22	42.37 ± 2.03

Reversible melting curves of 3 x *N*-methyl-arylazopyrazole (X = AAP1) in DNA-sequences J and K:

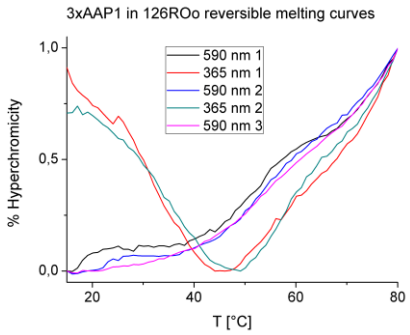

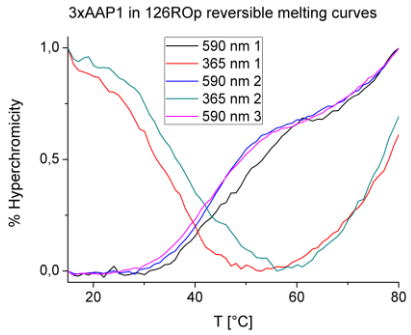

The melting temperatures after each irradiation step were determined as follows (n = 3, error = SD):

Mod.	590 nm 1	365 nm 1	590 nm 2	365 nm 2	590 nm 3
T_m (J) [°C]	53.01 ± 1.59	56.72 ± 1.91	56.18 ± 0.60	58.72 ± 0.12	54.54 ± 1.42
T_m (K) [°C]	46.96 ± 0.30	N/A	43.45 ± 0.82	N/A	44.01 ± 0.67

Reversible melting curves of 2 x *N*-methyl-arylazopyrazole (X = AAP1) and 2 x *N*-phenyl-arylazopyrazole (X = AAP2) in DNA-sequence L:

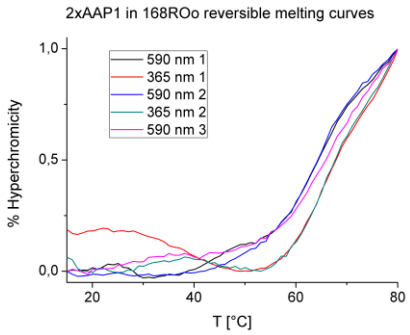

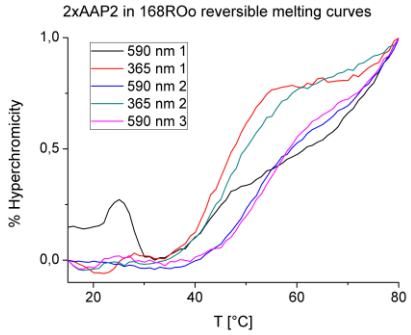

The melting temperatures after each irradiation step were determined as follows (n = 3, error = SD):

Mod.	590 nm 1	365 nm 1	590 nm 2	365 nm 2	590 nm 3
T_m (L, AAP1) [°C]	66.05 ± 1.35	65.81 ± 0.37	65.14 ± 0.78	66.26 ± 0.15	65.69 ± 1.55
T_m (L, AAP2) [°C]	38.26 ± 3.32	43.65 ± 3.33	50.83 ± 1.01	47.92 ± 0.69	53.71 ± 1.58

Reversible melting curves of 3 x *N*-methyl-arylazopyrazole (X = AAP1) and 3 x *N*-phenyl-arylazopyrazole (X = AAP2) in DNA-sequence I:

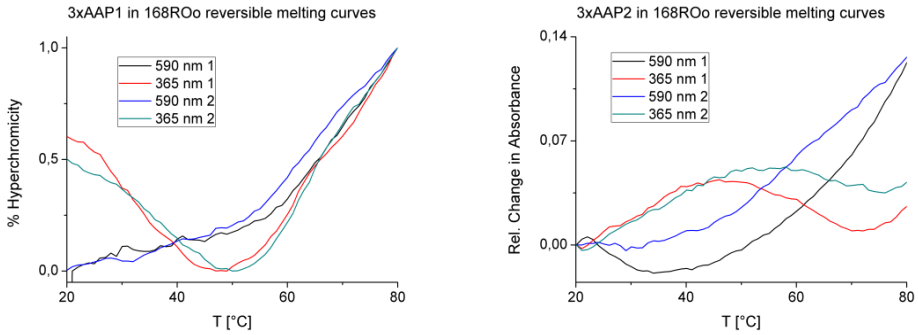

The melting temperatures after each irradiation step were determined as follows (n = 3, error = SD):

Mod.	590 nm 1	365 nm 1	590 nm 2	365 nm 2
T_m (I, AAP1) [°C]	68.23 ± 3.99	62.57 ± 0.56	66.82 ± 3.13	66.68 ± 1.75
T_m (I, AAP2) [°C]	70.97 ± 3.13	30.63 ± 1.86	61.77 ± 2.76	33.16 ± 0.34

7.7 Determination of thermal stabilities

7.7.1 Determination of thermal stabilities for D-threoninol bound photochromic molecules

Thermal stabilities of D-threoninol bound small molecules were determined by irradiating all samples with the wavelengths corresponding to each maximum *cis* switching effect for 5 minutes. Irradiation for room temperature measurements were carried out at room temperature, irradiation for 40 °C and 60 °C measurements were carried out at 40 °C and 60 °C. Each sample was left in the dark at the given temperature and UV/Vis spectra were recorded after predefined time peiods. The relative change of each absorption maximum was plotted against the time period each sample was left at the given temperature. A logarithmic fit of each plot allows the calculation of half-life times *via* the equation

$$y = y_0 + A_1 \cdot \exp(-(x - x_0)/t_1)$$

wheras y resembles the intensity of absorbance for a given time x while y_0 is the initial absorbance at the time point x_0. Solving the equation for x and insertion of the half maximum change in absorbance $(y-y_0)/2$ leads to the calculation of all half-life times for a given temperature.

$$ln\left(\frac{y-y_0}{A_1}\right) = (-(x - x_0)/t_1) \Leftrightarrow$$

$$\left(-(x - x_0)\right) = ln\left(\frac{y-y_0}{A_1}\right) \cdot t_1 \Leftrightarrow$$

$$x = -ln\left(\frac{y - y_0}{A_1}\right) \cdot t_1 - x_0$$

The themal half-life times were determined as follows:

Sample	Irr.-WL	Abs.-max.	$t_{1/2}$ (20 °C)	$t_{1/2}$ (40 °C)	$t_{1/2}$ (60 °C)
AB	340 nm	325 nm	N/A	42.9 hours	N/A
DMAB	340 nm	316 nm	N/A	N/A	87.5 hours
S-DMAB	385 nm	370 nm	N/A	N/A	4.1 hours
DFAB	340 nm	318 nm-	N/A	N/A	36.7 hours
DFAB-F	365 nm	346 nm	N/A	N/A	47.1 hours
DFAB-Cl	350 nm	325 nm	N/A	85.0 hours	N/A
DCAB	340 nm	307 nm	N/A	N/A	143.0 hours
DOAB	350 nm	341 nm	N/A	96.1 hours	13.4 hours
AAP1	365 nm	341 nm	14.0 hours	4.2 hours	N/A
AAP2	365 nm	341 nm	108.8 hours	22.0 hours	N/A

Thermal stability AB-D-threoninol 40 °C

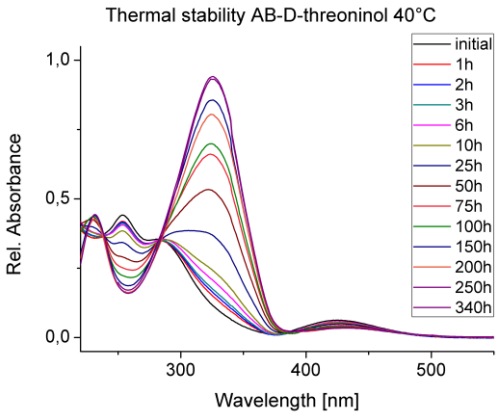

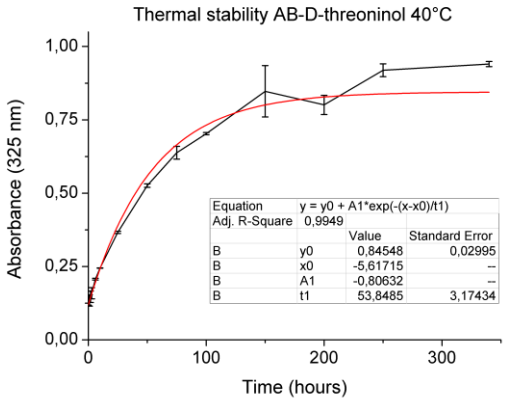

UV/vis-spectra of AB-D-threoninol in *cis* recorded after defined time intervals after leaving the sample in the dark at 40°C (left). Plotting the absorbance at 325 nm against time allows calculation of the half-life time (right).

Sample: AB-D-threoninol, 50 µM dissolved in a 1:1 mixture of Millipore water and acetonitrile.

Half-life time calculated: 42.9 hours (n = 2).

Thermal stability DMAB-D-threoninol 60 °C

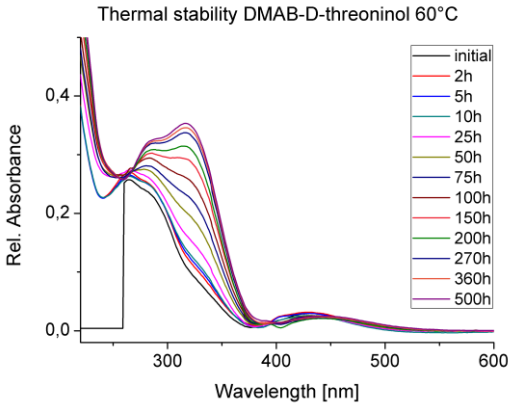

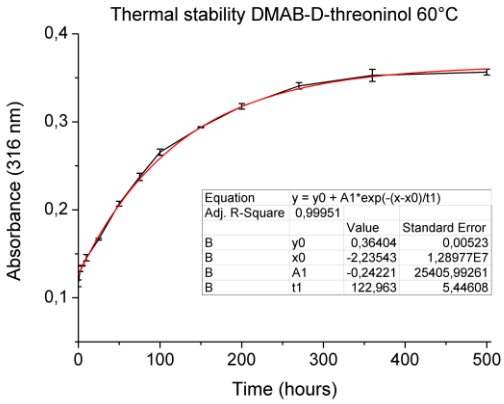

UV/vis-spectra of DMAB-D-threoninol in *cis* recorded after defined time intervals after leaving the sample in the dark at 60°C (left). Plotting the absorbance at 316 nm against time allows calculation of the half-life time (right).

Sample: DMAB-D-threoninol, 50 µM dissolved in a 1:1 mixture of Millipore water and acetonitrile.

Half-life time calculated: 87.5 hours (n = 2).

Thermal stability S-DMAB-D-threoninol 60 °C

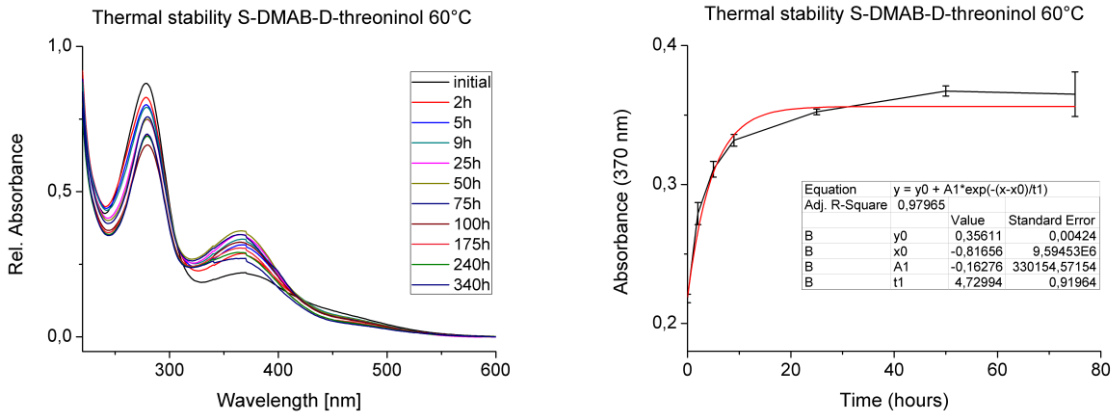

UV/vis-spectra of S-DMAB-D-threoninol in *cis* recorded after defined time intervals after leaving the sample in the dark at 60°C (left). Plotting the absorbance at 370 nm against time allows calculation of the half-life time (right).

Sample: S-DMAB-D-threoninol, 50 µM dissolved in a 1:1 mixture of Millipore water and acetonitrile.

Half-life time calculated: 4.1 hours (n = 2).

Thermal stability AAP1-D-threoninol 20 °C

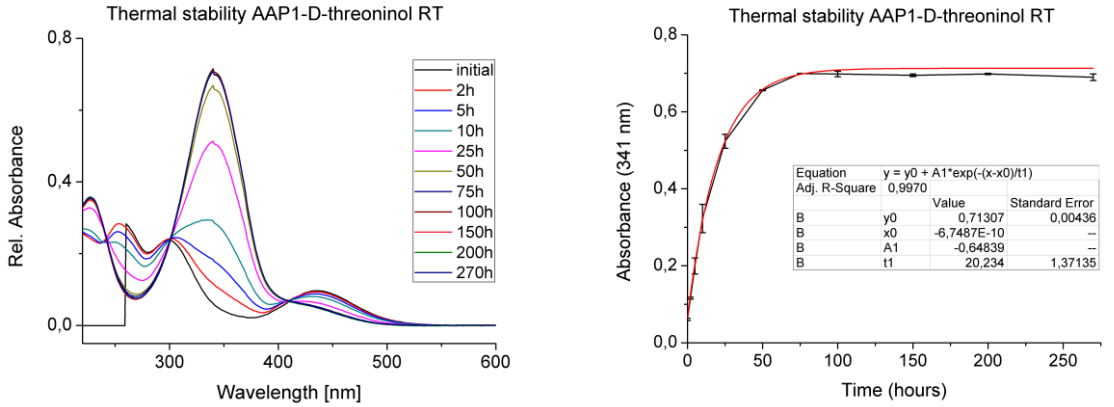

UV/vis-spectra of AAP1-D-threoninol in *cis* recorded after defined time intervals after leaving the sample in the dark at 20°C (left). Plotting the absorbance at 341 nm against time allows calculation of the half-life time (right).

Sample: AAP1-D-threoninol, 12.5 µM dissolved in a 1:1 mixture of Millipore water and acetonitrile.

Half-life time calculated: 14.0 hours (n = 2).

Thermal stability AAP1-D-threoninol 40 °C

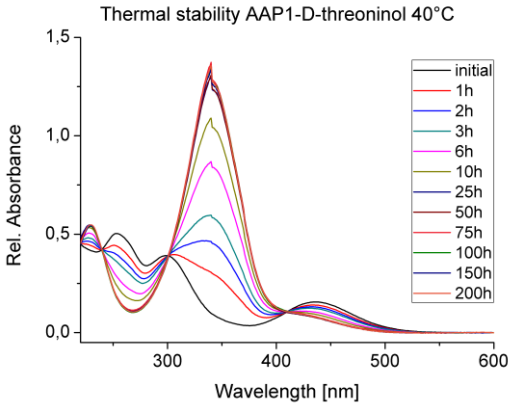

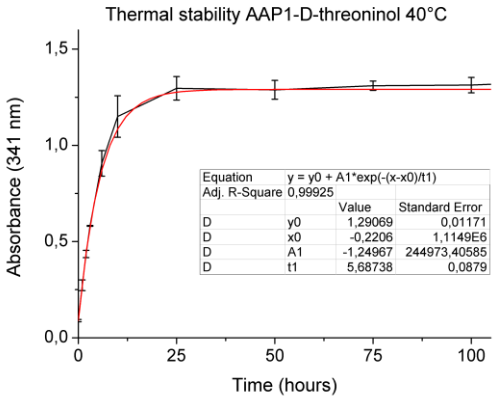

UV/vis-spectra of AAP1-D-threoninol in *cis* recorded after defined time intervals after leaving the sample in the dark at 40°C (left). Plotting the absorbance at 341 nm against time allows calculation of the half-life time (right).

Sample: AAP1-D-threoninol, 25 µM dissolved in a 1:1 mixture of Millipore water and acetonitrile.

Half-life time calculated: 4.2 hours (n = 2).

Thermal stability AAP2-D-threoninol 20 °C

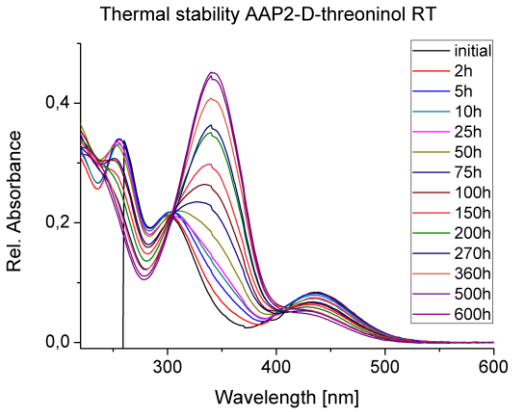

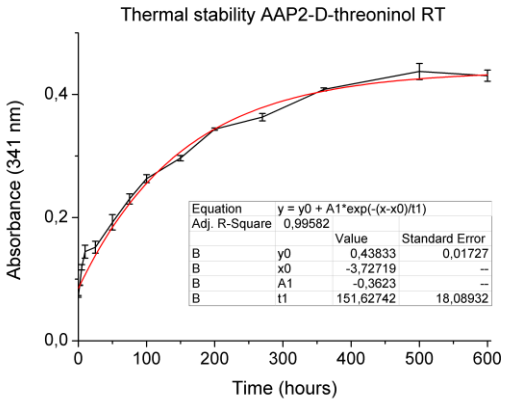

UV/vis-spectra of AAP2-D-threoninol in *cis* recorded after defined time intervals after leaving the sample in the dark at 20°C (left). Plotting the absorbance at 341 nm against time allows calculation of the half-life time (right).

Sample: AAP2-D-threoninol, 12.5 µM dissolved in a 1:1 mixture of Millipore water and acetonitrile.

Half-life time calculated: 108.8 hours (n = 2).

Thermal stability AAP2-D-threoninol 40 °C

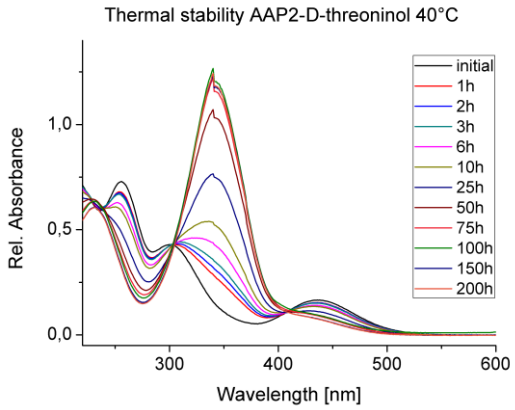

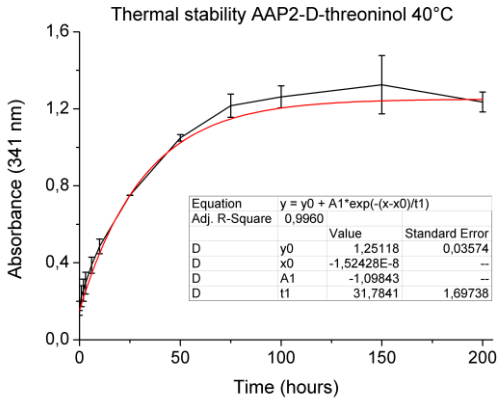

UV/vis-spectra of AAP2-D-threoninol in *cis* recorded after defined time intervals after leaving the sample in the dark at 40°C (left). Plotting the absorbance at 341 nm against time allows calculation of the half-life time (right).

Sample: AAP2-D-threoninol, 25 µM dissolved in a 1:1 mixture of Millipore water and acetonitrile.

Half-life time calculated: 22.0 hours (n = 2).

Thermal stability DFAB-D-threoninol 60 °C

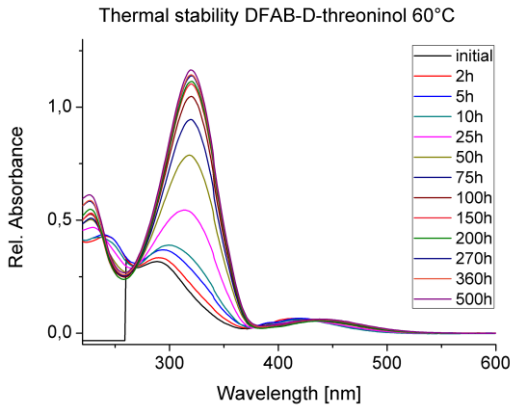

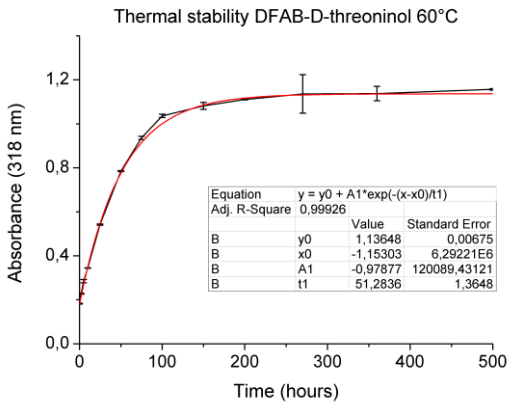

UV/vis-spectra of DFAB-D-threoninol in *cis* recorded after defined time intervals after leaving the sample in the dark at 60°C (left). Plotting the absorbance at 318 nm against time allows calculation of the half-life time (right).

Sample: DFAB-D-threoninol, 50 µM dissolved in a 1:1 mixture of Millipore water and acetonitrile.

Half-life time calculated: 36.7 hours (n = 2).

Thermal stability DFAB-F-D-threoninol 60 °C

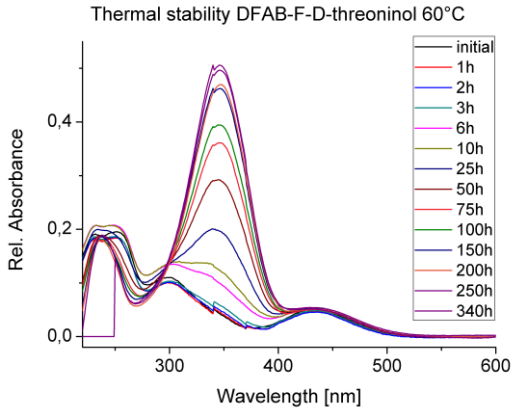

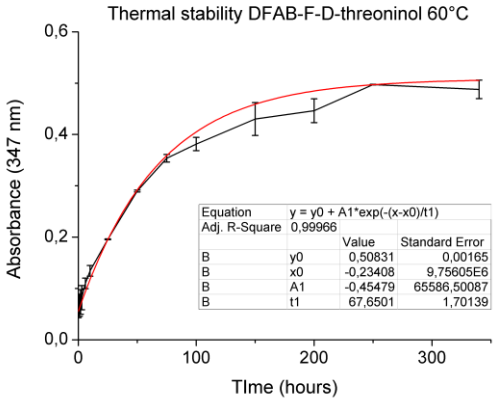

UV/vis-spectra of DFAB-F-D-threoninol in *cis* recorded after defined time intervals after leaving the sample in the dark at 60°C (left). Plotting the absorbance at 347 nm against time allows calculation of the half-life time (right).

Sample: DFAB-F-D-threoninol, 50 µM dissolved in a 1:1 mixture of Millipore water and acetonitrile.

Half-life time calculated: 47.1 hours (n = 2).

Thermal stability DFAB-Cl-D-threoninol 40 °C

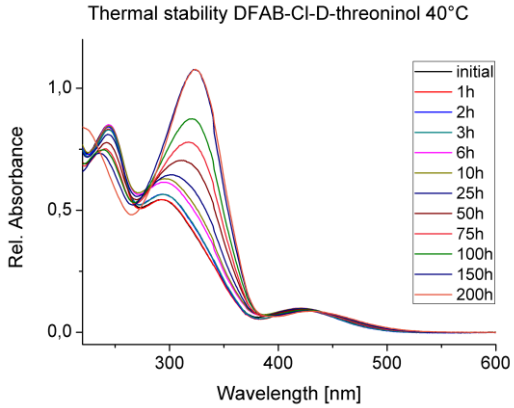

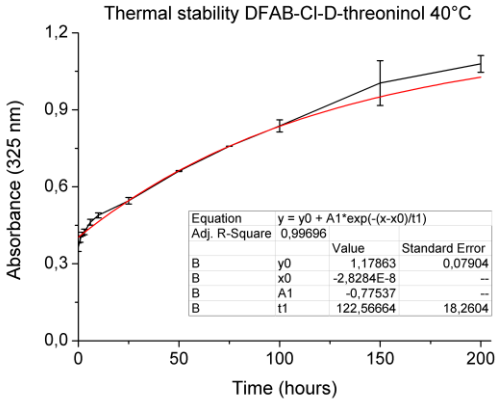

UV/vis-spectra of DFAB-Cl-D-threoninol in *cis* recorded after defined time intervals after leaving the sample in the dark at 40°C (left). Plotting the absorbance at 325 nm against time allows calculation of the half-life time (right).

Sample: DFAB-Cl-D-threoninol, 50 µM dissolved in a 1:1 mixture of Millipore water and acetonitrile.

Half-life time calculated: 85.0 hours (n = 2).

Thermal stability DOAB-D-threoninol 40 °C

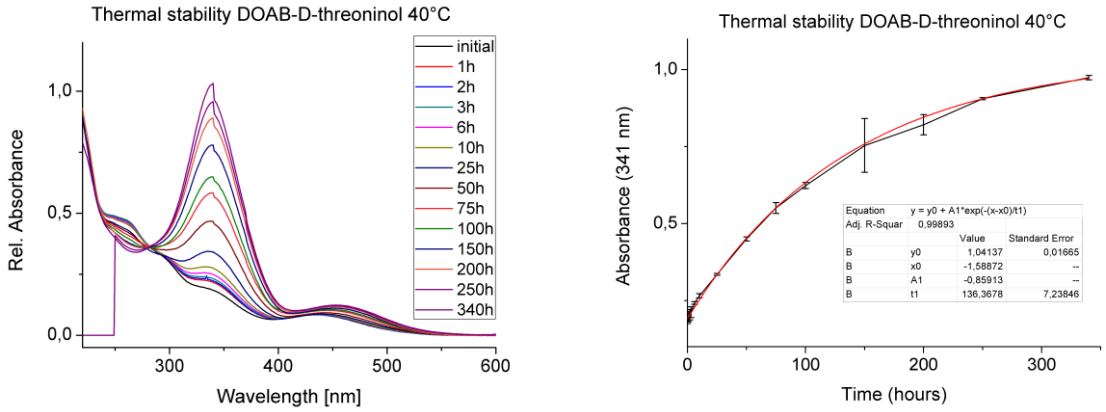

UV/vis-spectra of DOAB-D-threoninol in *cis* recorded after defined time intervals after leaving the sample in the dark at 40°C (left). Plotting the absorbance at 341 nm against time allows calculation of the half-life time (right).

Sample: DOAB-D-threoninol, 50 µM dissolved in a 1:1 mixture of Millipore water and acetonitrile.

Half-life time calculated: 96.1 hours (n = 2).

Thermal stability DOAB-D-threoninol 60 °C

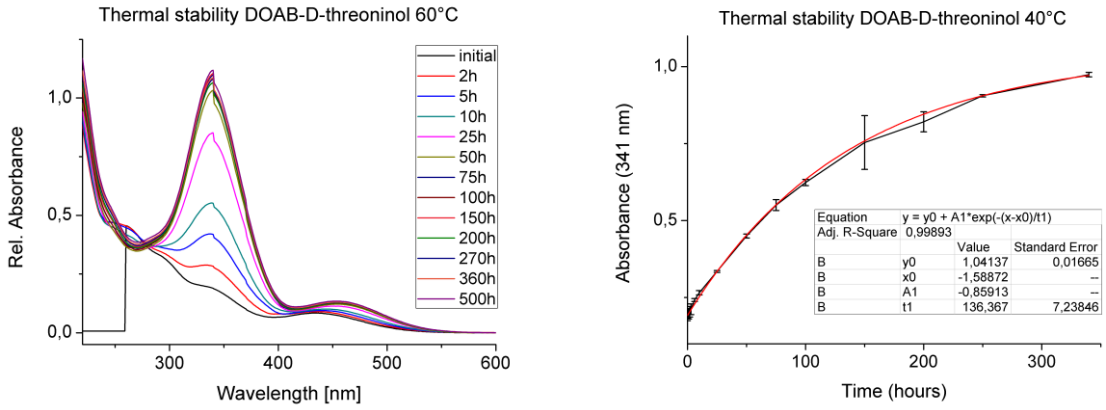

UV/vis-spectra of DOAB-D-threoninol in *cis* recorded after defined time intervals after leaving the sample in the dark at 60°C (left). Plotting the absorbance at 341 nm against time allows calculation of the half-life time (right).

Sample: DOAB-D-threoninol, 50 µM dissolved in a 1:1 mixture of Millipore water and acetonitrile.

Half-life time calculated: 13.4 hours (n = 2).

Thermal stability DCAB-D-threoninol 60 °C

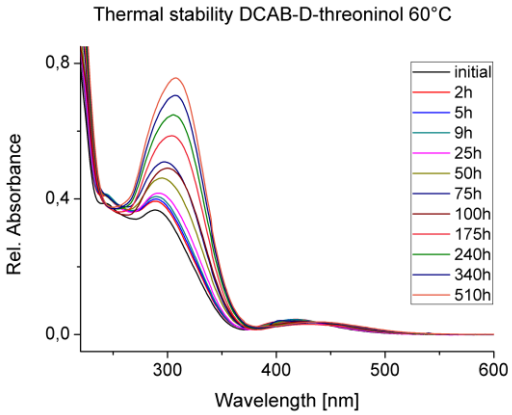

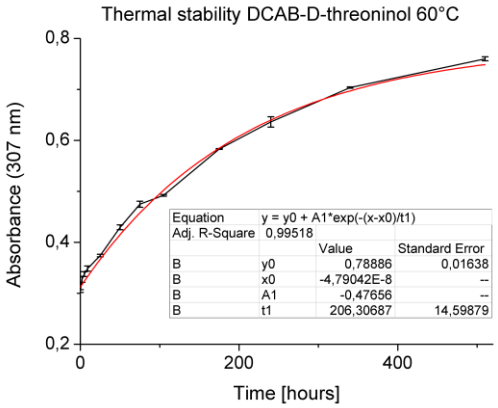

UV/vis-spectra of DCAB-D-threoninol in *cis* recorded after defined time intervals after leaving the sample in the dark at 60°C (left). Plotting the absorbance at 307 nm against time allows calculation of the half-life time (right).

Sample: DCAB-D-threoninol, 25 µM dissolved in a 1:1 mixture of Millipore water and acetonitrile.

Half-life time calculated: 143.0 hours (n = 2).

7.7.2 D-threoninol bound small molecules melting curves

Small molecules melting curves were performed for AAP1-D-threoninol and AAP2-D-threoninol. Solutions containing 25 µM of each sample in 500 µL of a 19:1 mixture of Millipore water and acetonitrile. A temperature gradient was applied starting from 20 °C to 80 °C with a gradient of 1 °C per minute while detecting the absorbance at the absorption maximum λ = 341 nm. Several cycles were run to monitor the change in absorbance.

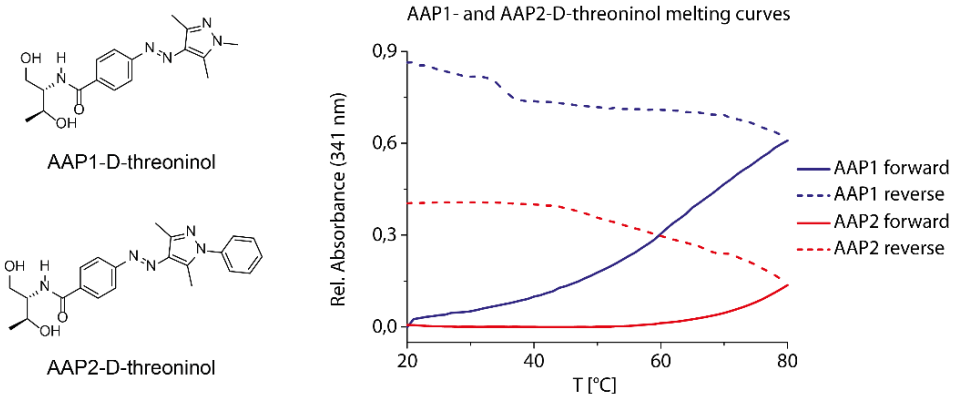

Fig. 100: Forward and reverse small molecule melting curves of AAP1-D-threoninol and AAP2-D-threoninol with an applied thermal gradient of 1°C per minute. Absorbance was recorded at the isosbestic point at λ = 341 nm.

AAP1-D-threoninol in *cis* conformation shows a constant increase in absorption intensity at the absorption maximum over a constant temperature gradient, indicating a fast back relaxation into *trans* conformation even at lower temperatures. The increase in absorption intensity becomes more significant with increasing temperatures, indicating a rapid back relaxation of the *cis* state into *trans* conformation.

AAP2-D-threoninol in *cis* conformation on the other hand exhibits no significant increase in absorption intensity below 55 °C, indicating a high thermal stability of the *cis* state below this tempera-ture. Above 55 °C, a constant increase in absorption intensity indicates a slow back relaxation of the *cis* state into *trans* conformation.

7.8 Assembly of higher order dsDNA systems

7.8.1 Assembly of circular dsDNA structures

All double-stranded DNA constructs were assembled by the following setup:

4 µM (8 µL) of each single strand was mixed in a total volume of 180 µL containing 20 mM NaCl (4 µL 1 M NaCl solution) and the sample mixtures were assembled on a thermocycler. The assembly started by heating the sample solutions with all single strands to 60 °C for 5 minutes followed by consecutive cooldown with a gradient of 3 °C in 5:25 minutes in each step down to 15 °C. After cooldown to 15 °C, 20 µL of 10x T4 ligase buffer was added followed by addition of 1 µL T4 ligase. The sample solutions were ligated overnight at 15 °C and ligation process was monitored by 6 % PAGE gel electrophoresis.

The base sequences corresponding to all single strands for each construct are given below.

7.8.1.1 Assembly of a double-stranded 126 bp ring structure

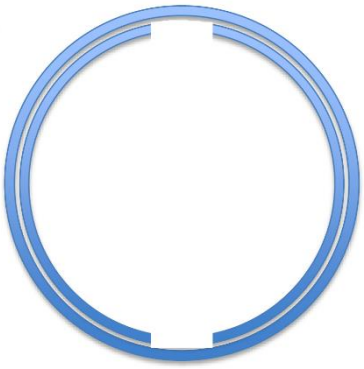

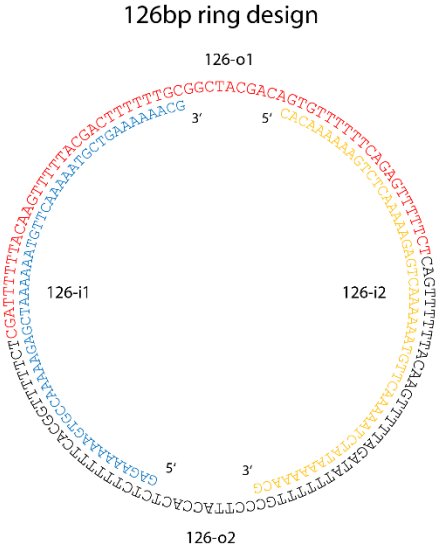

The double-stranded 126 bp ring structure was assembled *via* the previously described procedure using the following DNA strands:

Name	Sequence
126-i1	5‘-AGAGAAAAAAGTGCCAAAAAGAGCTAAAAAATGTTCAAAAATGCTGAAAAAACGC-3’
126-i2	5‘-TCACAAAAAAGTCTCAAAAAGAGTCAAAAAATGTTCAAAAATCTATAAAAAACGG-3‘
126-o1	5‘-Phos-TCTTTTTGAGACTTTTTTGTGACAGCATCGGCGTTTTTTCAGCATTTTTGAAC-ATTTTTTAGC-3‘
126-o2	5‘-Phos-TCTTTTTGGCACTTTTTTCTCTCACCATTCCCGTTTTTTATAGATTTTTGAACA-TTTTTTGAC-3‘

7.8.1.2 Assembly of double-stranded 168 bp ring structures

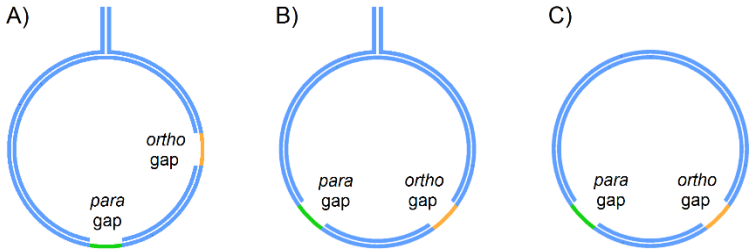

Three different double-stranded 168 ring constructs containing a 13-mer single-stranded gap in *ortho* position and a single-stranded 13-mer gap in *para* position were assembled following the procedure given in 7.8.1. The base sequences corresponding to all single strands for each construct are given below.

<u>168 bp ring containing two non-symmetric gaps (A)</u>

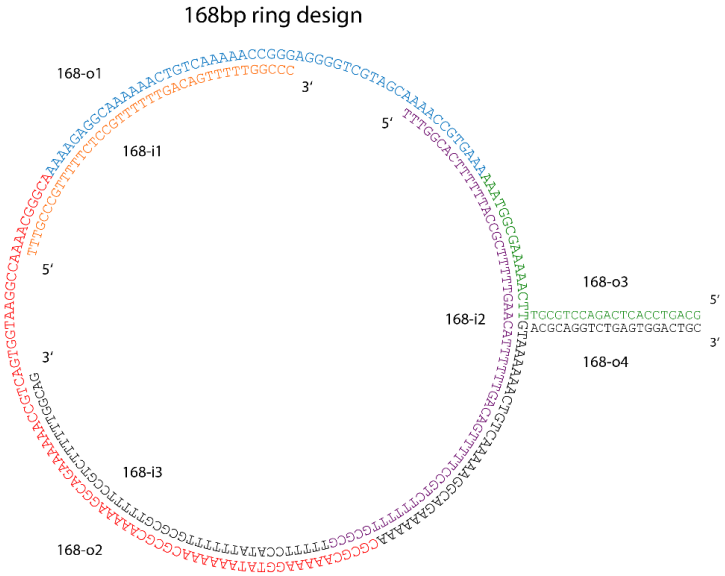

The double-stranded 168 bp ring structure containing two non-symmetric gaps (A) was assembled *via* the previously described procedure using the following DNA strands:

Name	Sequence
168-i1	5’-TTTTGAACATTTTTCTCCGTTTTTTGACAGTTTTTGGCCCT-3’
168-i2	5’-TTTTGGCACTTTTTTACCGCTTTTTGAACATTTTTTGACAGTTTTTCCGTCTTTTTTT-GCGCG-3’
168-i3	5’-Phos-TTTTTCCATATTTTTTGCGCGTTTTTCCGTCTTTTTTTGGCAGT-3’
168-o1	5’-Phos-AAAGTGCCAAAACGATGCTGGGGAGGGCCAAAAACTGTCAAAAAACGGAG-AAAAATGTT-3’
168-o2	5’-Phos-CAAAACCGGAATGGTGACTGCCAAAAAAGACGGAAAAACGCGCAAAAAAT-ATGGAAAAACGCGC-3’
168-o3	5’-GCAGTCCACTCAGACCTGCGTTTCAAAAAGCGGTAAA-3’
168-o4	5’-Phos-AAAAAAGACGGAAAAACTGTCAAAAAATGACGCAGGTCTGAGTGGACTGC-3’

168 bp ring shifted containing two symmetric gaps (B)

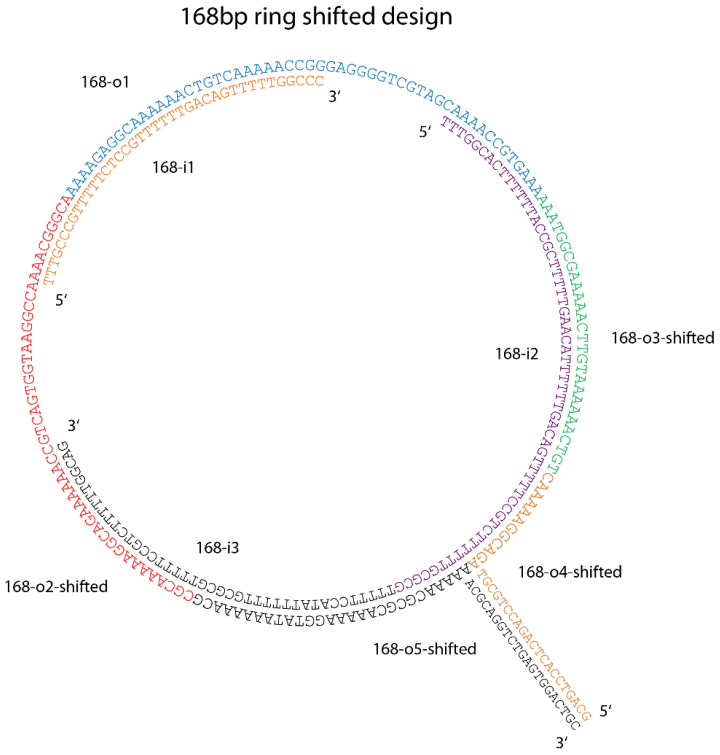

The double-stranded 168 bp ring structure containing two symmetric gaps and a double-stranded overhang (B) was assembled *via* the previously described procedure using the following DNA strands:

Name	**Sequence**
168-i1	5'-TTTTGAACATTTTTCTCCGTTTTTTGACAGTTTTTGGCCCT-3'
168-i2	5'-TTTTGGCACTTTTTTACCGCTTTTTGAACATTTTTTGACAGTTTTTCCGTCTTTTTTG-CGCG-3'
168-i3	5'-Phos-TTTTTCCATATTTTTTGCGCGTTTTTCCGTCTTTTTTGGCAGT-3'
168-o1	5'-Phos-AAAGTGCCAAAACGATGCTGGGGAGGGCCAAAAACTGTCAAAAAACGGAG-AAAAATGTT-3'
168-o2-shift	5'-Phos-ACGGGCAAAACCGGAATGGTGACTGCCAAAAAAGACGGAAAAACGC-3'
168-o3-shift	5'-Phos-TGTCAAAAAATGTTCAAAAAGCGGTAAA-3'
168-o4-shift	5'-GCAGTCCACTCAGACCTGCGTAGACGGAAAAAC-3'
168-o5-shift	5'-Phos-GCAAAAAATATGGAAAAACGCGCAAAAAACGCAGGTCTGAGTGGACTGC-3'

168 bp ring truncated containing two symmetric gaps and no overhang (C)

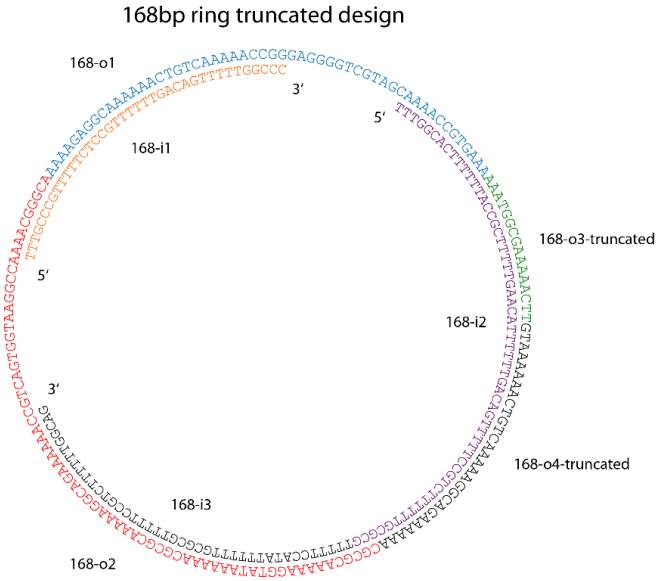

The double-stranded 168 bp ring structure containing two gaps and no double-stranded overhang (C) was assembled *via* the previously described procedure using the following DNA strands:

Name	**Sequence**
168-i1	5'-TTTTGAACATTTTTCTCCGTTTTTTGACAGTTTTTGGCCCT-3'
168-i2	5'-TTTTGGCACTTTTTTACCGCTTTTTGAACATTTTTTGACAGTTTTTCCGTCTTTTTT-GCGCG-3'
168-i3	5'-Phos-TTTTTCCATATTTTTTGCGCGTTTTTCCGTCTTTTTTGGCAGT-3'
168-o1	5'-Phos-AAAGTGCCAAAACGATGCTGGGGAGGGCCAAAAACTGTCAAAAAACGGAG-AAAAATGTT-3'
168-o2	5'-Phos-CAAAACCGGAATGGTGACTGCCAAAAAAGACGGAAAAACGCGCAAAAAAT-ATGGAAAAACGCGC-3'
168-o3-trunc	5'-Phos-TTCAAAAAGCGGTAAA-3'
168-o4-trunc	5'-Phos-AAAAAAGACGGAAAAACTGTCAAAAAATG-3'

7.8.2 Assembly of a non-symmetric two-state dsDNA [2]catenane system

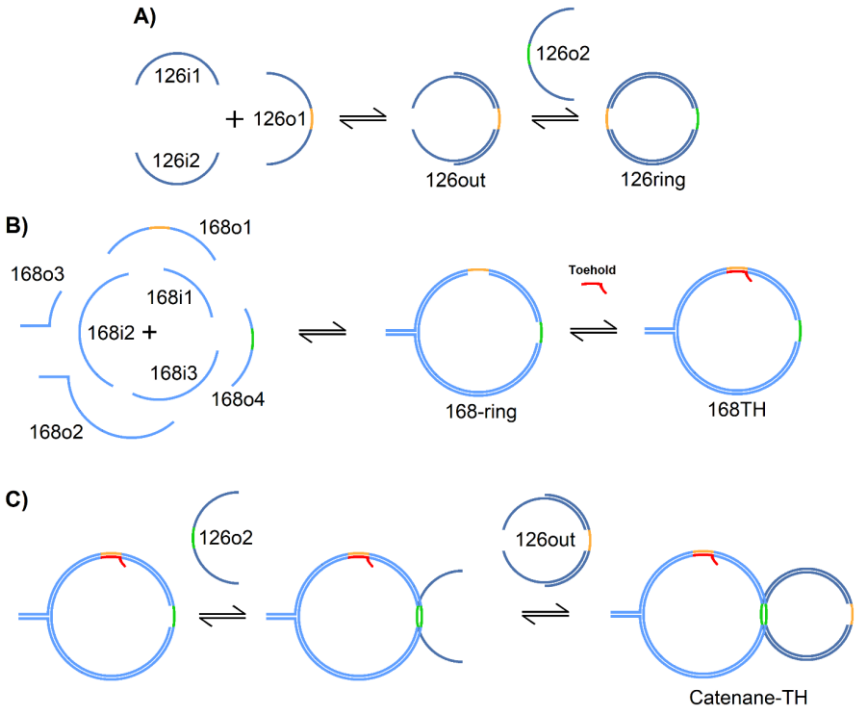

Fig. 101: Assembly of a two-state DNA [2]catenane system. Starting from the separate assembly of 126out (A) and the 168 bp ring (B), the 168 bp ring's *ortho* gap was blocked with a toehold oligomer (B), followed by hybridization of 126o2 to the *para* gap of the 168 bp ring (C). Consecutive hybridization of the 126out construct to the hybridized 126o2 oligomer and ligation of all oligomers leads to the [2]catenane product Catenane-TH (C). Addition of the complementary toehold oligomer facilitates the isolation of the free [2]catenane.

The [2]catenane system was assembled as follows:

The outer construct of the 126 bp ring (126out) was assembled *via* the following setup:

Strand	Concentration	Volume	Final concentration
126i1	100 µM	8 µL	4 µM
126i2	100 µM	8 µL	4 µM
126o2	100 µM	8 µL	4 µM
126RO-TH	100 µM	8 µL	4 µM
10xDA buffer		20 µL	1x buffer
Water		148 µL	200 µL total volume

All DNA strands, the 10x DA buffer and water were mixed, heated to 60 °C and slowly cooled down to 15 °C in a thermocycler (33 °C per hour). A 4.6 µM solution of the 168 bp ring construct (21.7 µL) in 1x DA buffer was mixed with 1.2 equivalents of 126o1 (1.2 µL, 100 µM), 8 µL 10x DA buffer and 69 µL water and the mixture was incubated for 4 hours at room temperature to yield a 1 µM solution of the 168 bp ring with 126o1 attached. 90 µL of the 168 bp construct

(1 µM) were mixed with 90 µL of the assembled construct 126out (1 µM) and the resulting mixture was incubated at 15 °C for 16 hours followed by a ligation step using 19 µL 10x T4 ligation buffer and 1 µL T4 DNA ligase. The crude [2]catenane assembly was purified by weak anionic exchange HPLC or freeze and squeeze gel extraction to yield the pure [2]catenane product.

126bp-ring containing two gaps

The following DNA strands were used for the assembly of the 126 bp ring construct:

Name	**Sequence**
126-i1	5‘-Cy5-AGAGAAAAAAGTGCCAAAAAGAGCTAAAAAATGTTCAAAAATGCTGAAAAAA-CGC-3’
126-i2	5‘-TAMRA-TCACAAAAAAGTCTCAAAAAGAGTCAAAAAATGTTCAAAAATCTATAAAA-AACGG-3‘
126-o1	5‘-Phos-TCTTTTTGAGACTTTTTTGTGACAGCATCGGCGTTTTTTCAGCATTTTTGAA-CATTTTTTAGC-3‘
126-o2	5‘-Phos-TCTTTTTGGCACTTTTTTCTCTCACCATTCCCGTTTTTTATAGATTTTTGAAC-ATTTTTTGAC-3‘

168 bp ring containing two non-symmetric gaps and a fluorophore quencher pair

The following DNA strands were used for the assembly of the 168 bp ring construct:

Name	**Sequence**
168-i1	5’-TTTTGAACATTTTTCTCCGTTTTTTGACAGTTTTTGGCCCT-BHQ2-3’
168-i2	5’-TTTTGGCACTTTTTTACCGCTTTTTGAACATTTTTTGACAGTTTTTCCGTCTTTTTT-GCGCG-3’
168-i3	5’-Phos-TTTTTCCATATTTTTTGCGCGTTTTTCCGTCTTTTTTGGCAGT-BHQ3-3’
168-o1	5’-Phos-AAAGTGCCAAAACGATGCTGGGGAGGGCCAAAAACTGTCAAAAAACGGAG-AAAAATGTT-3’
168-o2	5’-Phos-CAAAACCGGAATGGTGACTGCCAAAAAAGACGGAAAAACGCGCAAAAAAT-ATGGAAAAACGCGC-3’
168-o3	5’-GCAGTCCACTCAGACCTGCGTTTCAAAAAGCGGTAAA-3’
168-o4	5’-Phos-AAAAAAGACGGAAAAACTGTCAAAAAATGACGCAGGTCTGAGTGGACTGC-3’

Toehold oligomer sequences used for the catenane assembly

The following DNA sequences were used as toehold oligomers during the assembly:

Name	**Sequence**
Toehold	5‘-GGACTAGGCTCCCCAGCATCG-3‘
Toehold comp	5‘-CGATGCTGGGGAGCCTAGTCC-3'

7.9 Gel electrophoresis measurements

7.9.1 Investigation of switching efficiencies in a circular 168bp dsDNA system

A double-stranded 168 bp DNA ring construct with two gaps and a double-stranded 20-mer overhang was used to determine the switching efficiencies of different modified DNA strands. For all quantifications, 1 µM ring construct was mixed with the corresponding modified release-oligomers in 2 µM concentration and incubated for one hour at room temperature. The samples were irradiated for 5 minutes under the conditions given below, then subjected to a 6 % PAGE gel and run at 200 V for 45 minutes at 4 °C. The modified release-oligomers used for each quantification is given in the corresponding quantification step. A GeneRuler Ultra Low Range DNA ladder was used and all gels were stained with an ethidiumbromide solution.

Unmodified release-oligomers in 168-ring construct *ortho* (left) and *para* (right)

Sample: 1 µM 168 bp ring construct + 2 µM unmodified release oligomers (2 eq.).

Gel conditions: 6 % PAGE, 200 V, 45 minutes, 4°C.

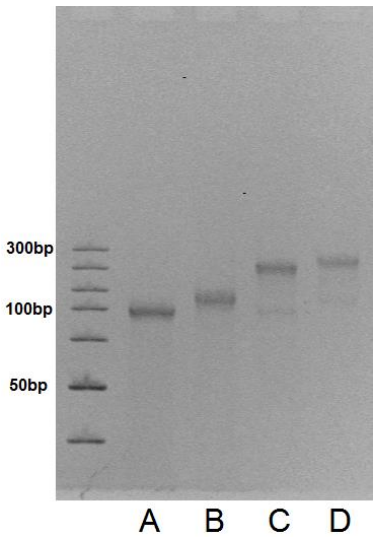

A: 168 bp ring without release oligomers

B: 168 bp ring with release oligomer *ortho*

C: 168 bp ring with release oligomer *para*

D: 168 bp ring with release oligomers *ortho* and *para*

Release oligomer *ortho*: 5’-TCC CCA GCA TCG-3’

Release oligomer *para*: 5’-CAC CAT TCC GGT-3’

Azobenzene 168 *ortho* (left) and *para* (right) release-oligomers, room temperature irradiation

Sample: 1 µM 168 bp ring construct + 2 µM release oligomers (2 eq.).

Gel conditions: 6 % PAGE, 200 V, 45 minutes, 4°C.

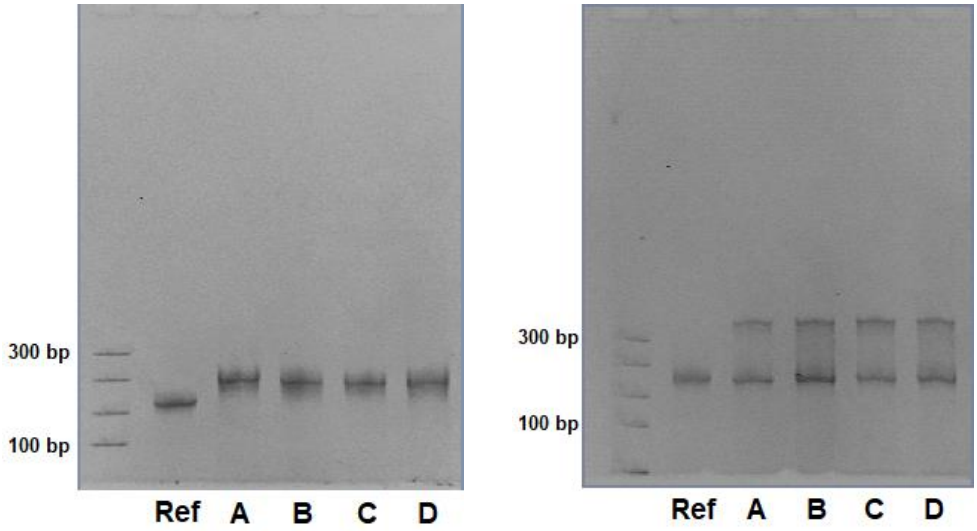

Ref: 168 bp ring without release oligomers.

Left: 168 bp ring with modified release oligomer *ortho* after irradiation into *trans* conformation (lanes A and C) and after irradiation into *cis* conformation (lanes B and D).

Right: 168 bp ring with modified release oligomer *para* after irradiation into *trans* conformation (lanes A and C) and after irradiation into *cis* conformation (lanes B and D).

Release oligomer *ortho*: 5'-TCC X CCA X GCA X TCG-3' with X = AB.

Release oligomer *para*: 5'-CAC X CAT X TCC X GGT-3' with X = AB.

The samples were irradiated alternatingly with 405 nm (lanes A and C) and 350 nm (lanes B and D) for 5 minutes at room temperature in consecutive irradiation steps before running the gel.

Azobenzene 168 *ortho* (left) and *para* (right) release-oligomers, 40 °C irradiation

Sample: 1 µM 168 bp ring construct + 2 µM release oligomers (2 eq.).

Gel conditions: 6 % PAGE, 200 V, 45 minutes, 4°C.

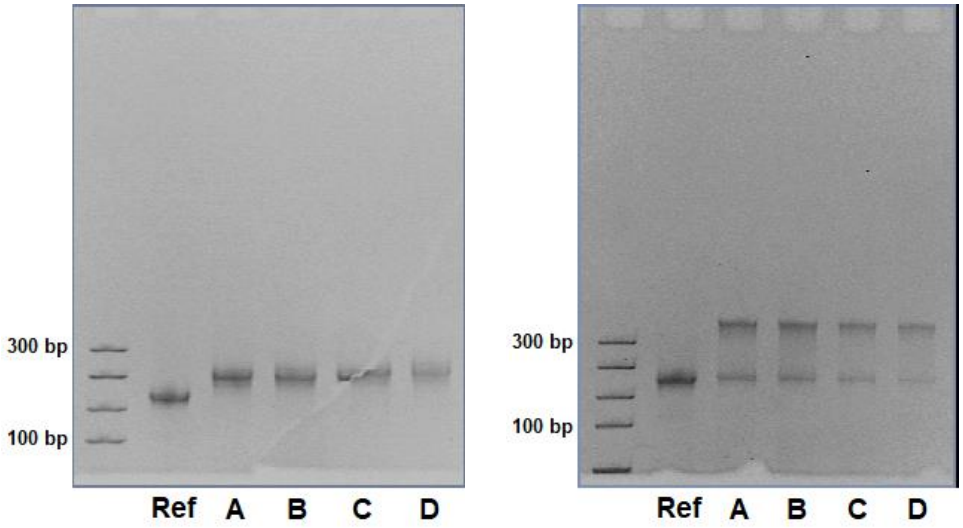

Ref: 168 bp ring without release oligomers.

Left: 168 bp ring with modified release oligomer *ortho* after irradiation into *trans* conformation (lanes A and C) and after irradiation into *cis* conformation (lanes B and D).

Right: 168 bp ring with modified release oligomer *para* after irradiation into *trans* conformation (lanes A and C) and after irradiation into *cis* conformation (lanes B and D).

Release oligomer *ortho*: 5'-TCC X CCA X GCA X TCG-3' with X = AB.

Release oligomer *para*: 5'-CAC X CAT X TCC X GGT-3' with X = AB.

The samples were irradiated alternatingly with 405 nm (lanes A and C) and 350 nm (lanes B and D) for 5 minutes at 40 °C and directly cooled down to room temperature in consecutive irradiation steps before running the gel.

DMAB 168 *ortho* (left) and *para* (right) release-oligomers, room temperature irradiation

Sample: 1 µM 168 bp ring construct + 2 µM release oligomers (2 eq.).

Gel conditions: 6 % PAGE, 200 V, 45 minutes, 4°C.

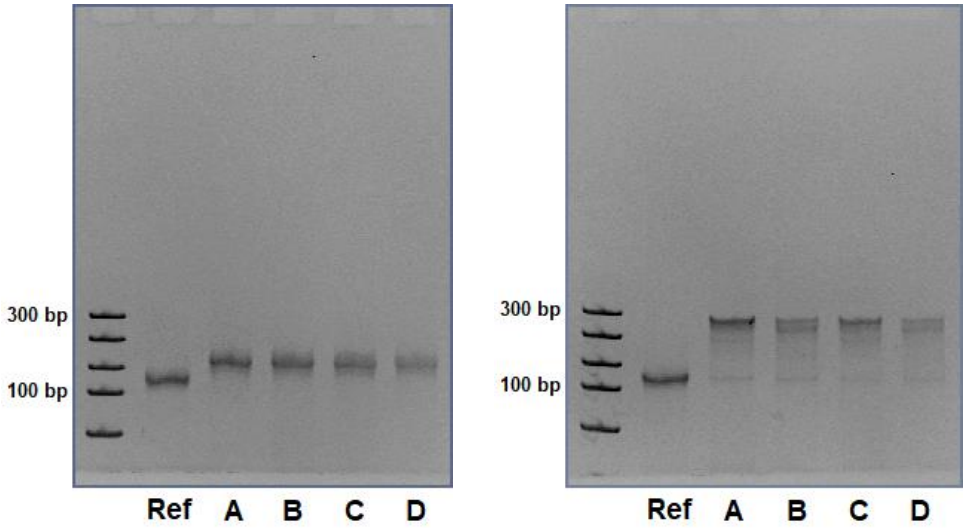

Ref: 168 bp ring without release oligomers.

Left: 168 bp ring with modified release oligomer *ortho* after irradiation into *trans* conformation (lanes A and C) and after irradiation into *cis* conformation (lanes B and D).

Right: 168 bp ring with modified release oligomer *para* after irradiation into *trans* conformation (lanes A and C) and after irradiation into *cis* conformation (lanes B and D).

Release oligomer *ortho*: 5'-TCC X CCA X GCA X TCG-3' with X = DMAB.

Release oligomer *para*: 5'-CAC X CAT X TCC X GGT-3' with X = DMAB.

The samples were irradiated alternatingly with 420 nm (lanes A and C) and 350 nm (lanes B and D) for 5 minutes at room temperature in consecutive irradiation steps before running the gel.

DMAB 168 *ortho* (left) and *para* (right) release-oligomers, 40 °C irradiation

Sample: 1 µM 168 bp ring construct + 2 µM release oligomers (2 eq.).

Gel conditions: 6 % PAGE, 200 V, 45 minutes, 4°C.

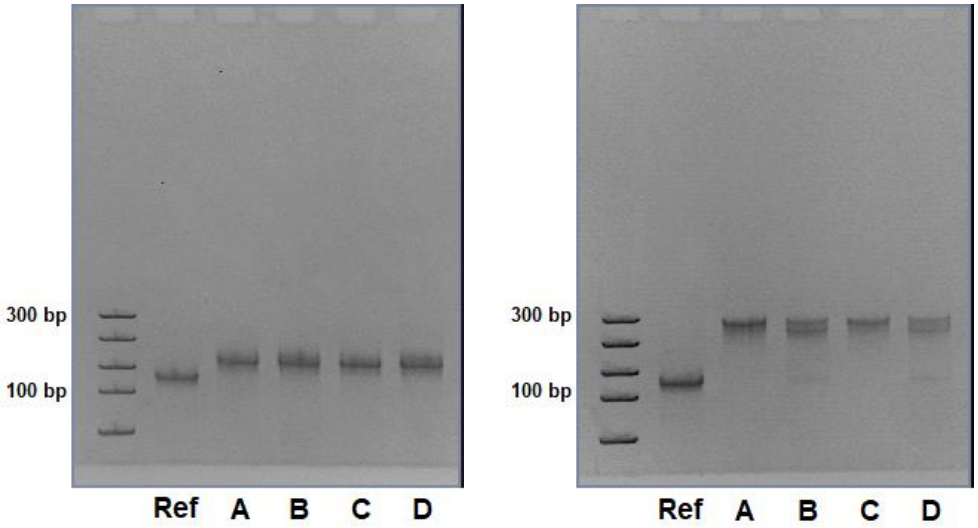

Ref: 168 bp ring without release oligomers.

Left: 168 bp ring with modified release oligomer *ortho* after irradiation into *trans* conformation (lanes A and C) and after irradiation into *cis* conformation (lanes B and D).

Right: 168 bp ring with modified release oligomer *para* after irradiation into *trans* conformation (lanes A and C) and after irradiation into *cis* conformation (lanes B and D).

Release oligomer *ortho*: 5'-TCC X CCA X GCA X TCG-3' with X = DMAB.

Release oligomer *para*: 5'-CAC X CAT X TCC X GGT-3' with X = DMAB.

The samples were irradiated alternatingly with 420 nm (lanes A and C) and 350 nm (lanes B and D) for 5 minutes at 40 °C in consecutive irradiation steps before running the gel.

S-DMAB 168 *ortho* (left) and *para* (right) release-oligomers, room temperature irradiation

Sample: 1 µM 168 bp ring construct + 2 µM release oligomers (2 eq.).

Gel conditions: 6 % PAGE, 200 V, 45 minutes, 4°C.

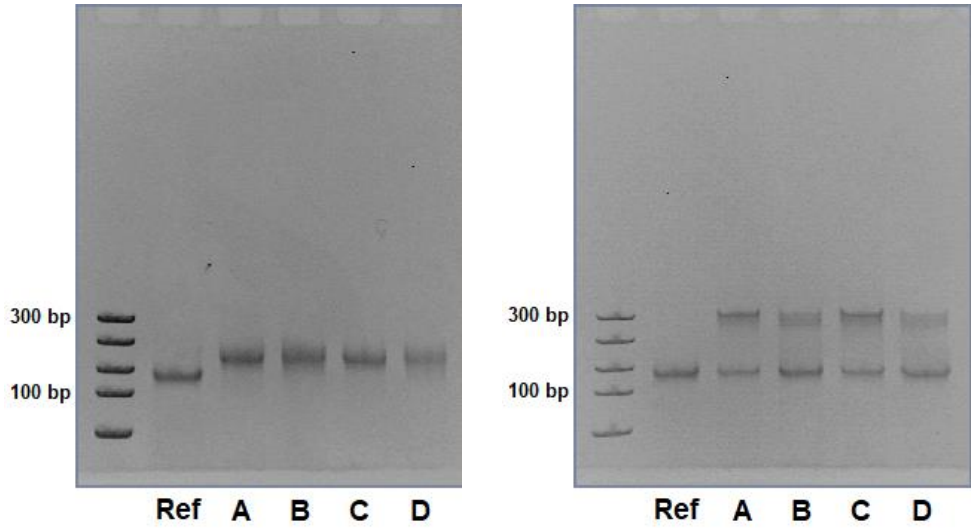

Ref: 168 bp ring without release oligomers.

Left: 168 bp ring with modified release oligomer *ortho* after irradiation into *trans* conformation (lanes A and C) and after irradiation into *cis* conformation (lanes B and D).

Right: 168 bp ring with modified release oligomer *para* after irradiation into *trans* conformation (lanes A and C) and after irradiation into *cis* conformation (lanes B and D).

Release oligomer *ortho*: 5'-TCC X CCA X GCA X TCG-3' with X = S-DMAB.

Release oligomer *para*: 5'-CAC X CAT X TCC X GGT-3' with X = S-DMAB.

The samples were irradiated alternatingly with 450 nm (lanes A and C) and 385 nm (lanes B and D) for 5 minutes at room temperature in consecutive irradiation steps before running the gel.

S-DMAB 168 *ortho* (left) and *para* (right) release-oligomers, 40 °C irradiation

Sample: 1 µM 168 bp ring construct + 2 µM release oligomers (2 eq.).

Gel conditions: 6 % PAGE, 200 V, 45 minutes, 4°C.

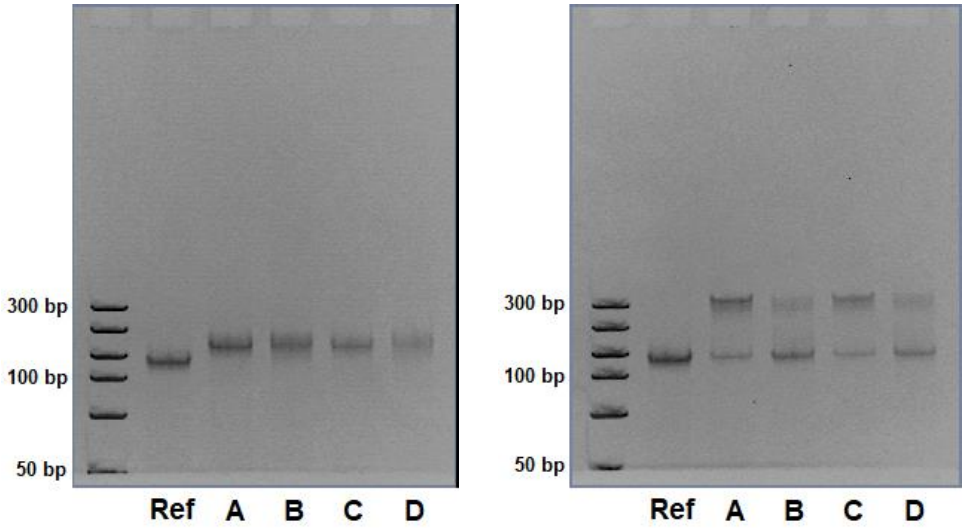

Ref: 168 bp ring without release oligomers.

Left: 168 bp ring with modified release oligomer *ortho* after irradiation into *trans* conformation (lanes A and C) and after irradiation into *cis* conformation (lanes B and D).

Right: 168 bp ring with modified release oligomer *para* after irradiation into *trans* conformation (lanes A and C) and after irradiation into *cis* conformation (lanes B and D).

Release oligomer *ortho*: 5'-TCC X CCA X GCA X TCG-3' with X = S-DMAB.

Release oligomer *para*: 5'-CAC X CAT X TCC X GGT-3' with X = S-DMAB.

The samples were irradiated alternatingly with 450 nm (lanes A and C) and 385 nm (lanes B and D) for 5 minutes at 40 °C in consecutive irradiation steps before running the gel.

AAP1 168 *ortho* (left) and *para* (right) release-oligomers, room temperature irradiation

Sample: 1 µM 168 bp ring construct + 2 µM release oligomers (2 eq.).

Gel conditions: 6 % PAGE, 200 V, 45 minutes, 4°C.

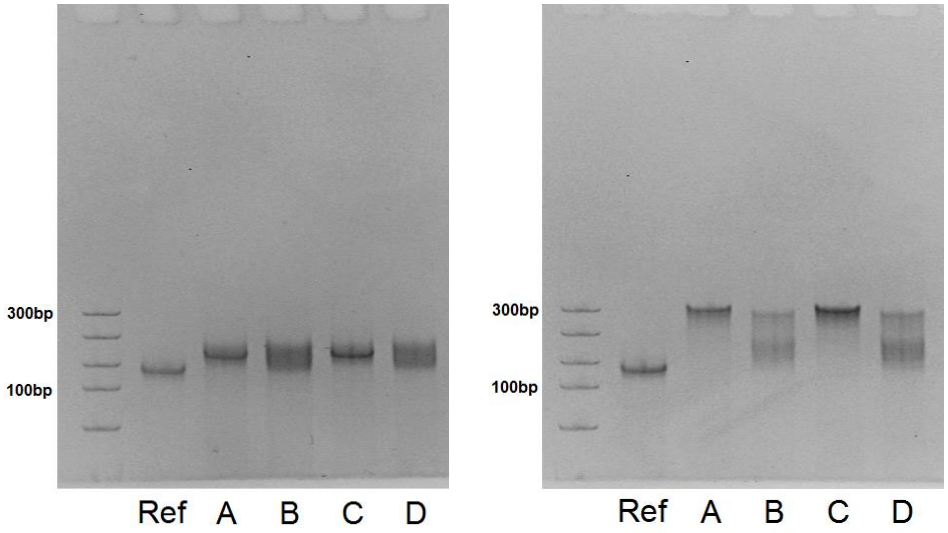

Ref: 168 bp ring without release oligomers.

Left: 168 bp ring with modified release oligomer *ortho* after irradiation into *trans* conformation (lanes A and C) and after irradiation into *cis* conformation (lanes B and D).

Right: 168 bp ring with modified release oligomer *para* after irradiation into *trans* conformation (lanes A and C) and after irradiation into *cis* conformation (lanes B and D).

Release oligomer *ortho*: 5'-TCC X CCA X GCA X TCG-3' with X = AAP1.

Release oligomer *para*: 5'-CAC X CAT X TCC X GGT-3' with X = AAP1.

The samples were irradiated alternatingly with 590 nm (lanes A and C) and 350 nm (lanes B and D) for 5 minutes at room temperature in consecutive irradiation steps before running the gel.

AAP1 168 *ortho* (left) and *para* (right) release-oligomers, 40 °C irradiation

Sample: 1 µM 168 bp ring construct + 2 µM release oligomers (2 eq.).

Gel conditions: 6 % PAGE, 200 V, 45 minutes, 4°C.

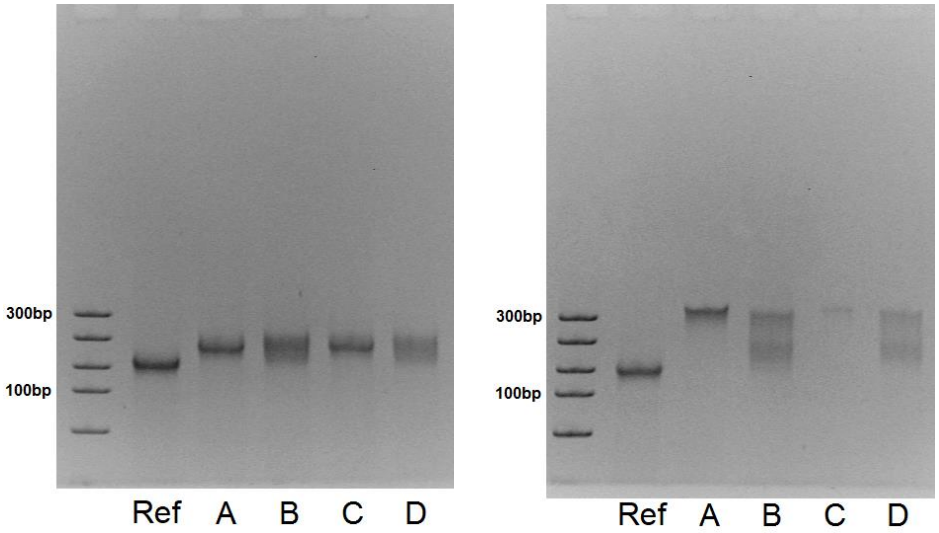

Ref: 168 bp ring without release oligomers.

Left: 168 bp ring with modified release oligomer *ortho* after irradiation into *trans* conformation (lanes A and C) and after irradiation into *cis* conformation (lanes B and D).

Right: 168 bp ring with modified release oligomer *para* after irradiation into *trans* conformation (lanes A and C) and after irradiation into *cis* conformation (lanes B and D).

Release oligomer *ortho*: 5'-TCC X CCA X GCA X TCG-3' with X = AAP1.

Release oligomer *para*: 5'-CAC X CAT X TCC X GGT-3' with X = AAP1.

The samples were irradiated alternatingly with 590 nm (lanes A and C) and 350 nm (lanes B and D) for 5 minutes at 40 °C in consecutive irradiation steps before running the gel.

AAP2 168 *ortho* (left) and *para* (right) release-oligomers, room temperature irradiation

Sample: 1 µM 168 bp ring construct + 2 µM release oligomers (2 eq.).

Gel conditions: 6 % PAGE, 200 V, 45 minutes, 4°C.

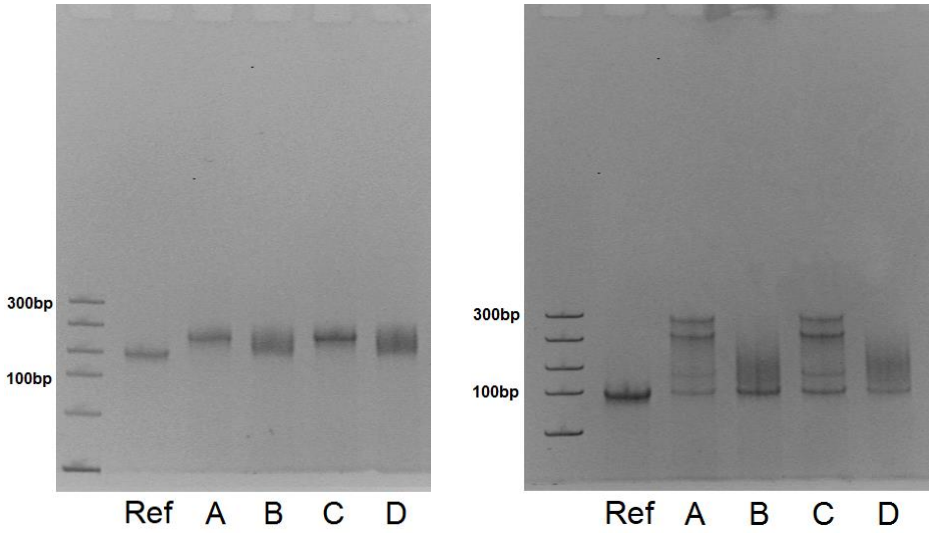

Ref: 168 bp ring without release oligomers.

Left: 168 bp ring with modified release oligomer *ortho* after irradiation into *trans* conformation (lanes A and C) and after irradiation into *cis* conformation (lanes B and D).

Right: 168 bp ring with modified release oligomer *para* after irradiation into *trans* conformation (lanes A and C) and after irradiation into *cis* conformation (lanes B and D).

Release oligomer *ortho*: 5'-TCC X CCA X GCA X TCG-3' with X = AAP2.

Release oligomer *para*: 5'-CAC X CAT X TCC X GGT-3' with X = AAP2.

The samples were irradiated alternatingly with 590 nm (lanes A and C) and 350 nm (lanes B and D) for 5 minutes at room temperature in consecutive irradiation steps before running the gel.

AAP2 168 *ortho* (left) and *para* (right) release-oligomers, 40 °C irradiation

Sample: 1 µM 168 bp ring construct + 2 µM release oligomers (2 eq.).

Gel conditions: 6 % PAGE, 200 V, 45 minutes, 4°C.

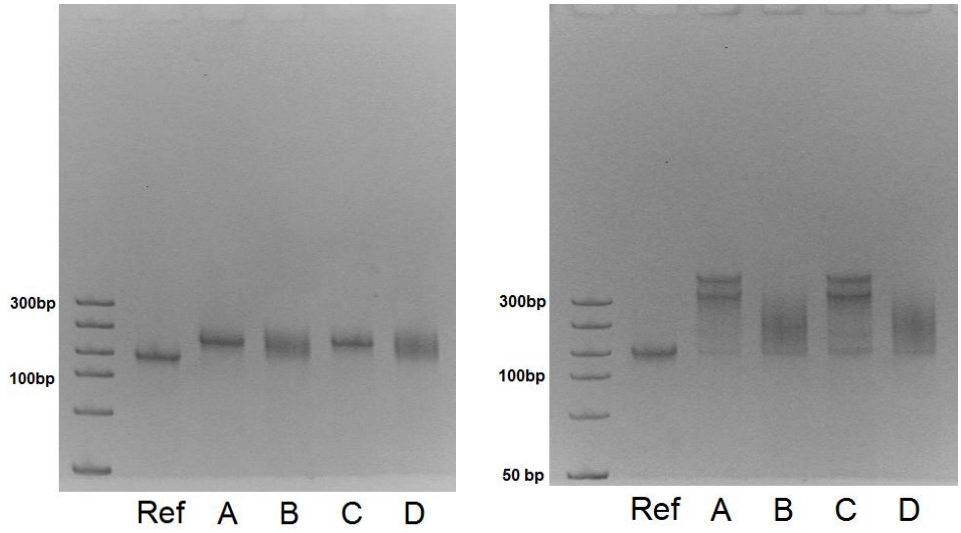

Ref: 168 bp ring without release oligomers.

Left: 168 bp ring with modified release oligomer *ortho* after irradiation into *trans* conformation (lanes A and C) and after irradiation into *cis* conformation (lanes B and D).

Right: 168 bp ring with modified release oligomer *para* after irradiation into *trans* conformation (lanes A and C) and after irradiation into *cis* conformation (lanes B and D).

Release oligomer *ortho*: 5'-TCC X CCA X GCA X TCG-3' with X = AAP2.

Release oligomer *para*: 5'-CAC X CAT X TCC X GGT-3' with X = AAP2.

The samples were irradiated alternatingly with 590 nm (lanes A and C) and 350 nm (lanes B and D) for 5 minutes at 40 °C in consecutive irradiation steps before running the gel.

7.10 Fluorophore quenching experiments

7.10.1 Fluorophore and quencher bleaching tests

Fluorescence-studies involving fluorophores and quenchers have to be tested on bleaching effects. Since a range of the absorption spectrum of fluorophores and quenchers are overlapping with the excitation wavelengths of both fluorophore and quencher, any bleaching effects that can occur during the irradiation process have to be excluded. All fluorophores were tested on bleaching effects by irradiating a 1 µM solution of the modified oligonucleotide 5'-Flu-GAATGGTG-3' in Millipore water and recording the remaining fluorescence intensity. Photobleaching of the quenchers were performed by use of the DNA duplex 5'-Flu-GAATGGTG-3' and 5'-CACCATTC-Que-3'. The DNA strand containing the quencher was irradiated in millipore water, then mixed with the complementary strand containing the fluorophore to yield a 1 µM solution of the duplex. The remaining fluorophore intensity of the duplex was measured.

Remaining fluorescence intensities for the fluorophore quencher pair Cy5.5 and BHQ3 are given in fig. 102 and 103.

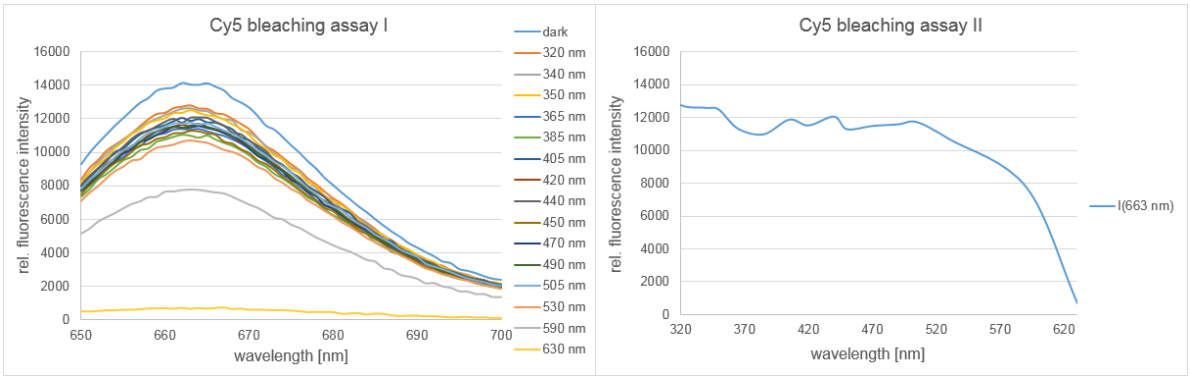

Fig. 102: Bleaching test for Cy5.5 Fluorescence intensites (left) for irradiation with all available wavelengths and fluorescence intensities at λ = 663 nm (right).

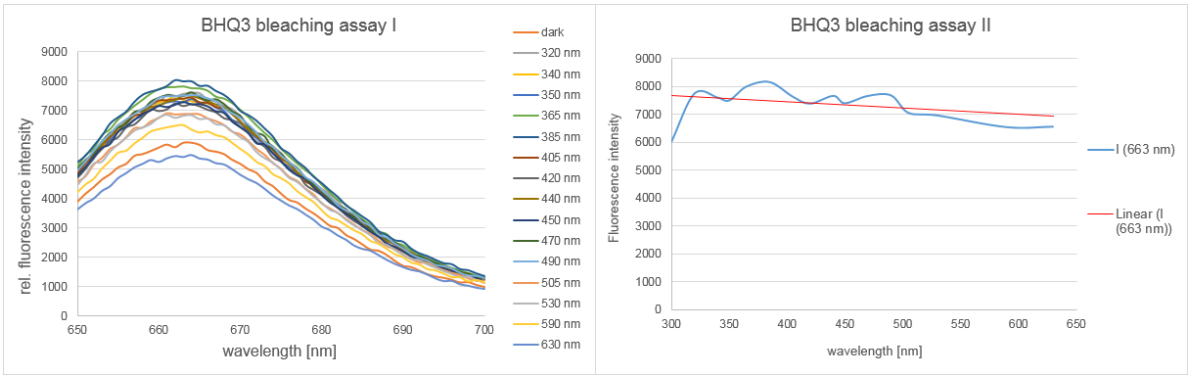

Fig. 103: Bleaching test for BHQ3. Fluorescence intensites (left) for the DNA duplex after irradiation with all available wavelengths and fluorescence intensities at λ = 663 nm (right).

7.10.2 Hairpin design and assembly

Two different hairpin constructs were designed to determine the strand displacement efficiency of modified release-oligomers. Both constructs resemble the design of *ortho* and *para* gaps in the non-symmetric two-state dsDNA catenane system. The designs and the corresponding strands for the assembly are depicted below.

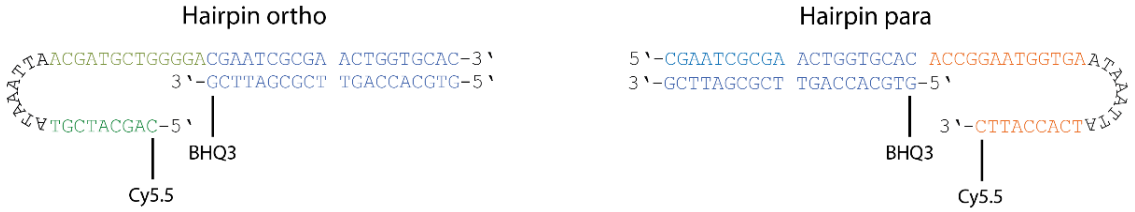

Hairpin *ortho*

The following DNA strands were used for the assembly of hairpin *ortho*:

Name	**Sequence**
HP *ortho*	5'-Cy5.5-AGCATCGTATAAATTAACGATGCTGGGGACGAATCGCGAACTGGTGCAC-3'
HP *ortho* comp	3'-BHQ3-GCTTAGCGCTTGACCACGTG-5'

Hairpin *para*

The following DNA strands were used for the assembly of hairpin *para*:

Name	**Sequence**
HP para	5'-CGAATCGCGAACTGGTGCACACCGGAATGGTGAATAAATTATCACCATT-Cy5.5-3'
HP para comp	3'-GCTTAGCGCTTGACCACGTG-BHQ3-5'

Both hairpins were assembled using the following setup:

Strand	**Concentration**	**Volume**	**Final concentration**
HP ortho/para	100 µM	8 µL	4 µM
HP ortho/para comp.	100 µM	8 µL	4 µM
10x DA buffer		20 µL	1x
Water		164 µL	Total volume: 200 µL

The two hairpin strands, the 10x DA buffer and water were mixed and heated to 60 °C for 5 minutes in a thermocycler, followed by cooling down the mixture with a temperature gradient of 33 °C per hour down to 15 °C. The samples were stored at 4 °C and warmed up to room temperature before usage.

7.10.3 Fluorophore quenching experiments of both hairpins with modified release oligomers

All hairpin experiments were executed in 1x DA buffer in a concentration of 1 µM hairpin and 2 µM release oligomer. All measurements involving modified release-oligomers were compared and normalized to the same experiment with unmodified release-oligomers. Modified release oligomers were irradiated to *trans* conformation via the corresponding wavelength and incubated for 30 minutes at room temperature in order to achieve a complete hybridization before irradiating the system to *cis* conformation. The following release oligomers were used for hairpin opening:

RO *ortho* sh: 5'-TCC CXCA GCXA TCG-3'

RO *ortho*: 5'-TCC X CCA X GCA X TCG-3'

RO *para* sh: 5'-CAC CXAT TCXC GGT-3'

RO *para*: 5'-CAC X CAT X TCC X GGT-3'

Hairpin *ortho* with AB-, DMAB- and S-DMAB-modified release oligomers

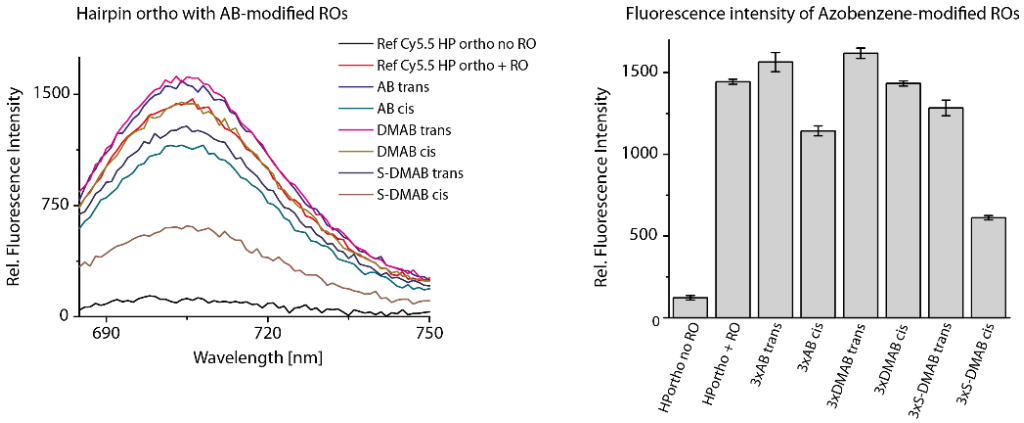

Hairpin opening experiment of hairpin *ortho* with unmodified and modified release oligomers. As modified release oligomers, the sequence 5'-TCC X CCA X GCA X TCG-3' was used with X = AB, DMAB or S-DMAB. Each mixture of hairpin and modified release oligomer was irradiated with the maximum *trans*- and *cis*-converting irradiation wavelength for 5 minutes at room temperature before measurement.

Fluorescence intensity at 705 nm was monitored for each individual measurement.

Hairpin *ortho* with AB-, DMAB- and S-DMAB-modified release oligomers

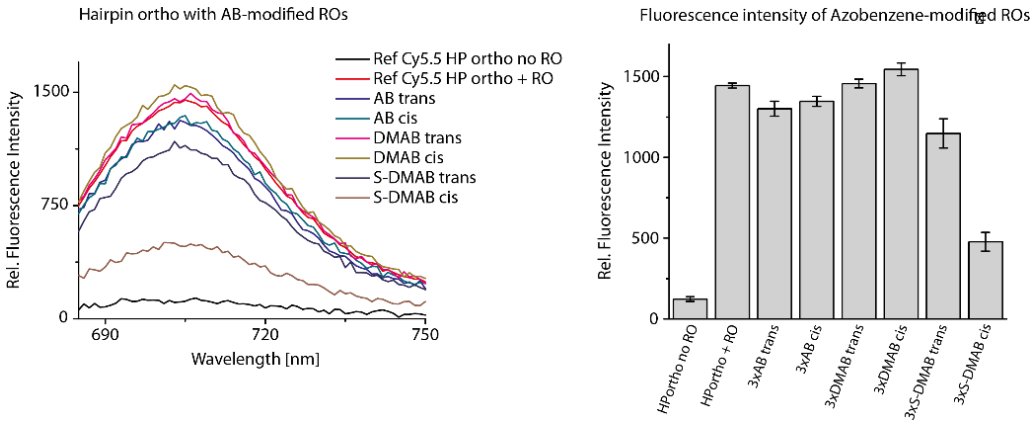

Hairpin opening experiment of hairpin *ortho* with unmodified and modified release oligomers. As modified release oligomers, the sequence 5'-TCC X CCA X GCA X TCG-3' was used with X = AB, DMAB or S-DMAB. Each mixture of hairpin *ortho* and modified release oligomer was irradiated with the maximum *trans*- and *cis*-converting irradiation wavelength for 5 minutes at 40 °C before measurement.

Fluorescence intensity at 705 nm was monitored for each individual measurement.

Hairpin *para* with AB-, DMAB- and S-DMAB-modified release oligomers

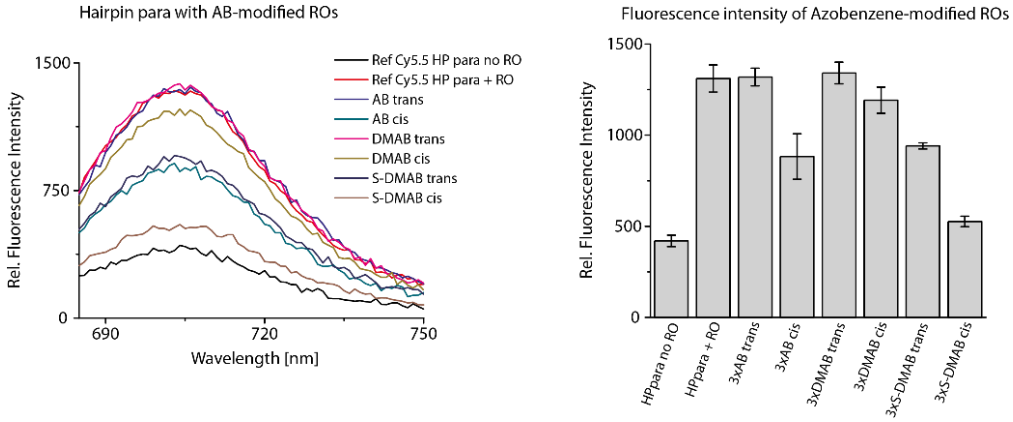

Hairpin opening experiment of hairpin *para* with unmodified and modified release oligomers. As modified release oligomers, the sequence 5'-CAC X CAT X TCC X GGT-3' was used with X = AB, DMAB or S-DMAB. Each mixture of hairpin *para* and modified release oligomer was irradiated with the maximum *trans*- and *cis*-converting irradiation wavelength for 5 minutes at room temperature before measurement.

Fluorescence intensity at 705 nm was monitored for each individual measurement.

Hairpin *para* with AB-, DMAB- and S-DMAB-modified release oligomers

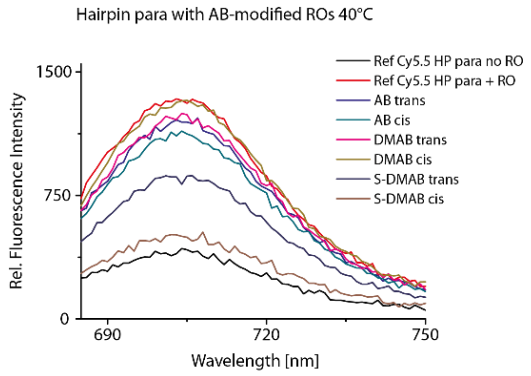

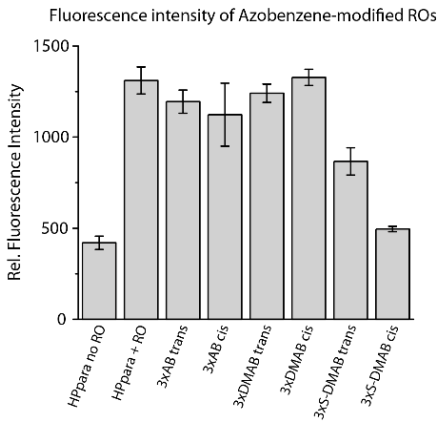

Hairpin opening experiment of hairpin *para* with unmodified and modified release oligomers. As modified release oligomers, the sequence 5'-CAC X CAT X TCC X GGT-3' was used with X = AB, DMAB or S-DMAB. Each mixture of hairpin *para* and modified release oligomer was irradiated with the maximum *trans*- and *cis*-converting irradiation wavelength for 5 minutes at 40 °C before measurement.

Fluorescence intensity at 705 nm was monitored for each individual measurement.

Hairpin *ortho* with AAP1-modified release oligomers

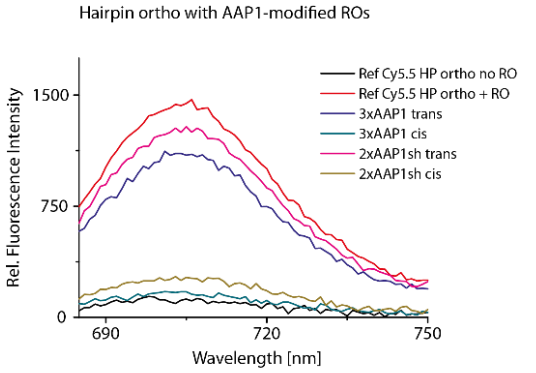

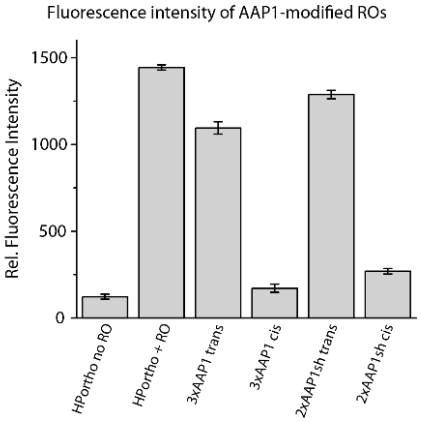

Hairpin opening experiment of hairpin *ortho* with unmodified and modified release oligomers. As modified release oligomers, the sequences 5'-TCC X CCA X GCA X TCG-3' and 5'-TCC CXCA GCXA TCG-3' (sh) were used with X = AAP1. Each mixture of hairpin *ortho* and modified release oligomer was irradiated with the maximum *trans*- and *cis*-converting irradiation wavelength for 5 minutes at room temperature before measurement.

Fluorescence intensity at 705 nm was monitored for each individual measurement.

Hairpin *para* with AAP1-modified release oligomers

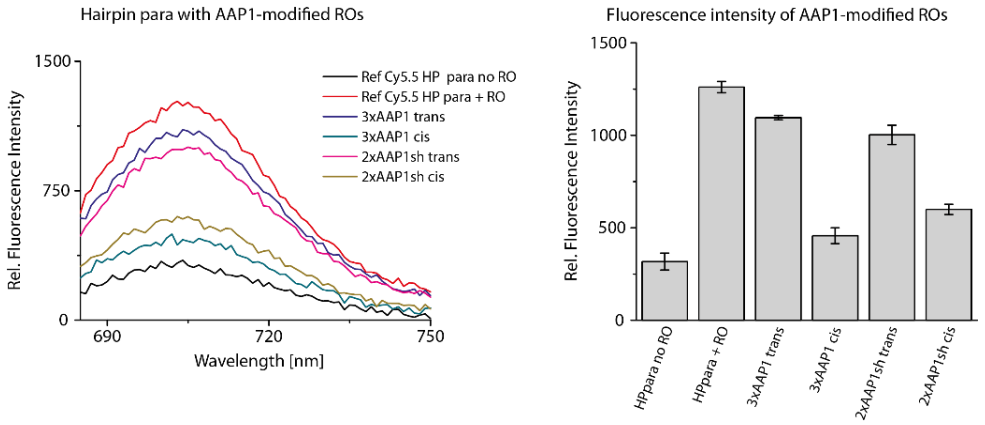

Hairpin opening experiment of hairpin *para* with unmodified and modified release oligomers. As modified release oligomers, the sequences 5'-CAC X CAT X TCC X GGT-3' and 5'-CAC CXAT TCXC GGT-3' (sh) were used with X = AAP1. Each mixture of hairpin *para* and modified release oligomer was irradiated with the maximum *trans*- and *cis*-converting irradiation wavelength for 5 minutes at room temperature before measurement.

Fluorescence intensity at 705 nm was monitored for each individual measurement.

Hairpin *ortho* with AAP2-modified release oligomers

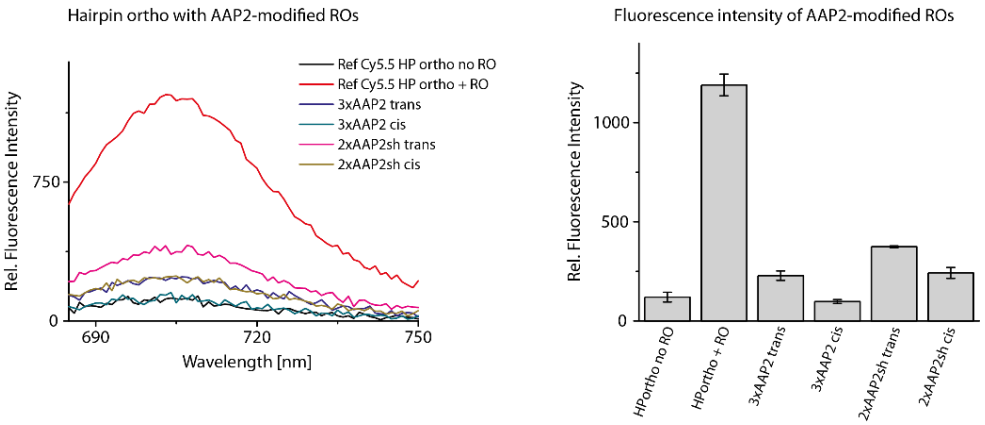

Hairpin opening experiment of hairpin *ortho* with unmodified and modified release oligomers. As modified release oligomers, the sequences 5'-TCC X CCA X GCA X TCG-3' and 5'-TCC CXCA GCXA TCG-3' (sh) were used with X = AAP2. Each mixture of hairpin *ortho* and modified release oligomer was irradiated with the maximum *trans*- and *cis*-converting irradiation wavelength for 5 minutes at room temperature before measurement.

Fluorescence intensity at 705 nm was monitored for each individual measurement.

Hairpin *para* with AAP2-modified release oligomers

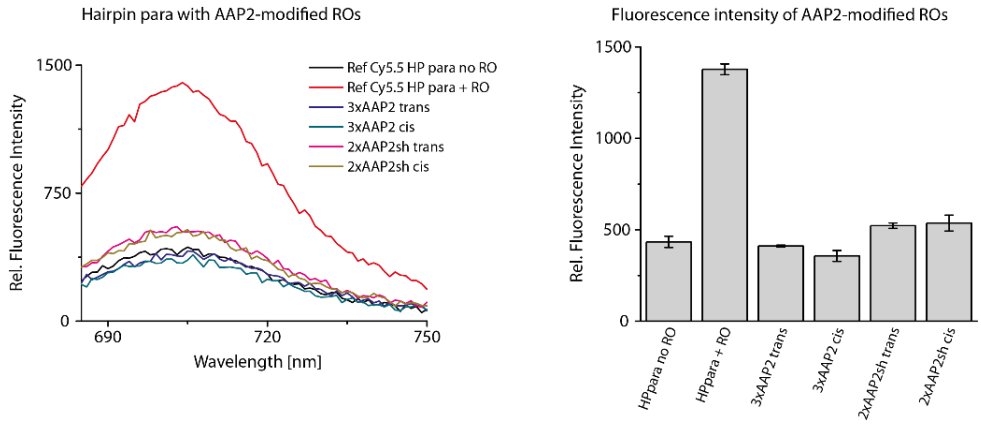

Hairpin opening experiment of hairpin *para* with unmodified and modified release oligomers. As modified release oligomers, the sequences 5'-CAC X CAT X TCC X GGT-3' and 5'-CAC CXAT TCXC GGT-3' (sh) were used with X = AAP2. Each mixture of hairpin *para* and modified release oligomer was irradiated with the maximum *trans*- and *cis*-converting irradiation wavelength for 5 minutes at room temperature before measurement.

Fluorescence intensity at 705 nm was monitored for each individual measurement.

7.10.4 Reversible hairpin switching with modified release-oligomers

Reversible opening and closing of hairpins were performed under the same conditions as described before. The hairpins were mixed with modified release oligomers and irradiated to *trans* conformation with the corresponding wavelength followed by incubation for 30 minutes at room temperature before irradiating the system to *cis* conformation. These successive steps were repeated for 5 irradiation cycles. Cy5.5 fluorescence intensity was monitored after each irradiation and hybridization step.

Reversible hairpin switching *ortho* with 2xAAP1sh

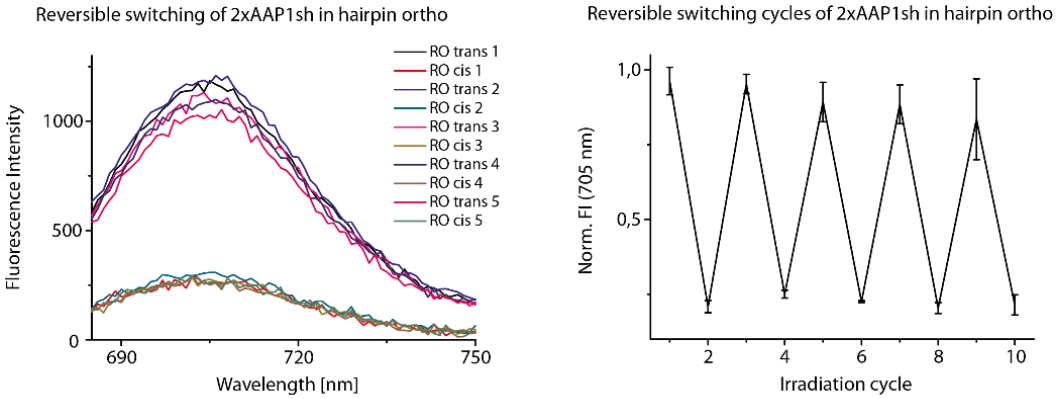

Reversible opening and closing of hairpin *ortho* using the modified sequence 5'-TCC CXCA GCXA TCG-3' with X = AAP1. The mixture of hairpin *ortho* and modified release oligomer was irradiated alternatingly in consecutive irradiation cycles with the maximum *trans*- and *cis*-converting irradiation wavelengths for 5 minutes at room temperature. After irradiation into *trans* conformation, the sample was left in the dark for 30 minutes at room temperature. After each irradiation and hybridization step, the fluorescence intensity was measured (left) and the fluorescence intensity at 705 nm was plotted (right).

Reversible hairpin switching *ortho* with 3xAAP1

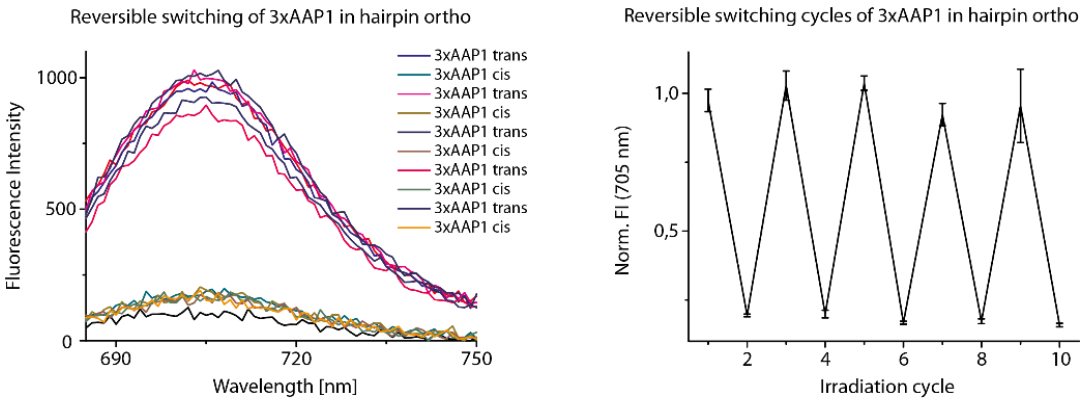

Reversible opening and closing of hairpin *ortho* using the modified sequence 5'-TCC X CCA X GCA X TCG-3' with X = AAP1. The mixture of hairpin *ortho* and modified release oligomer was irradiated alternatingly in consecutive irradiation cycles with the maximum *trans*- and *cis*-converting irradiation wavelengths for 5 minutes at room temperature. After irradiation into *trans* conformation, the sample was left in the dark for 30 minutes at room temperature. After each irradiation and hybridization step, the fluorescence intensity was measured (left) and the fluorescence intensity at 705 nm was plotted (right).

Reversible hairpin switching *para* 2xAAP1sh

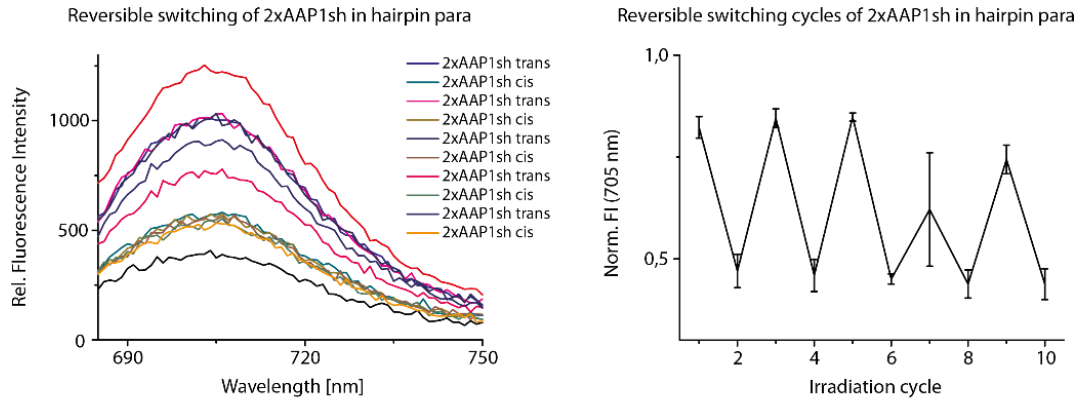

Reversible opening and closing of hairpin *para* using the modified sequence 5'-CAC CXAT TCXC GGT-3' with X = AAP1. The mixture of hairpin *para* and modified release oligomer was irradiated alternatingly in consecutive irradiation cycles with the maximum *trans*- and *cis*-converting irradiation wavelengths for 5 minutes at room temperature. After irradiation into *trans* conformation, the sample was left in the dark for 30 minutes at room temperature. After each irradiation and hybridization step, the fluorescence intensity was measured (left) and the fluorescence intensity at 705 nm was plotted (right).

Reversible hairpin switching *para* 3xAAP1

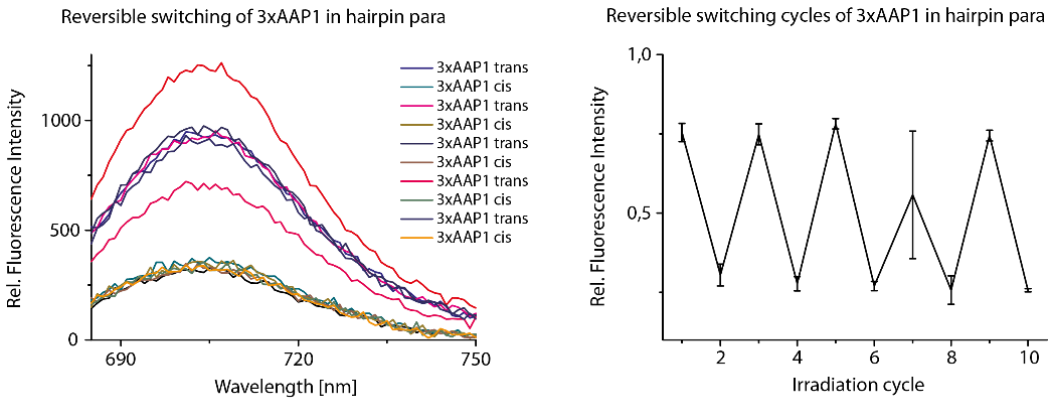

Reversible opening and closing of hairpin *para* using the modified sequence 5'-CAC X CAT X TCC X GGT-3' with X = AAP1. The mixture of hairpin *para* and modified release oligomer was irradiated alternatingly in consecutive irradiation cycles with the maximum *trans*- and *cis*-converting irradiation wavelengths for 5 minutes at room temperature. After irradiation into *trans* conformation, the sample was left in the dark for 30 minutes at room temperature. After each irradiation and hybridization step, the fluorescence intensity was measured (left) and the fluorescence intensity at 705 nm was plotted (right).

7.11 Atomic Force Microscopy data (AFM)

7.11.1 AFM pictures for dsDNA rings and the non-symmetric dsDNA [2]catenane system

The following AFM pictures were recorded by Johannes Weigandt using the 168 bp ring system and [2]catenane samples assembled and purified as described before (chapter 7.8.2).

168 bp ring system structural proof via AC-mode

Sample: 168 bp ring (chapter 7.8.1.2) 1 nM with 1 nM polyornithine.

Mode: AC, intermittent contanct, wide (left) and close-up (right) picture.

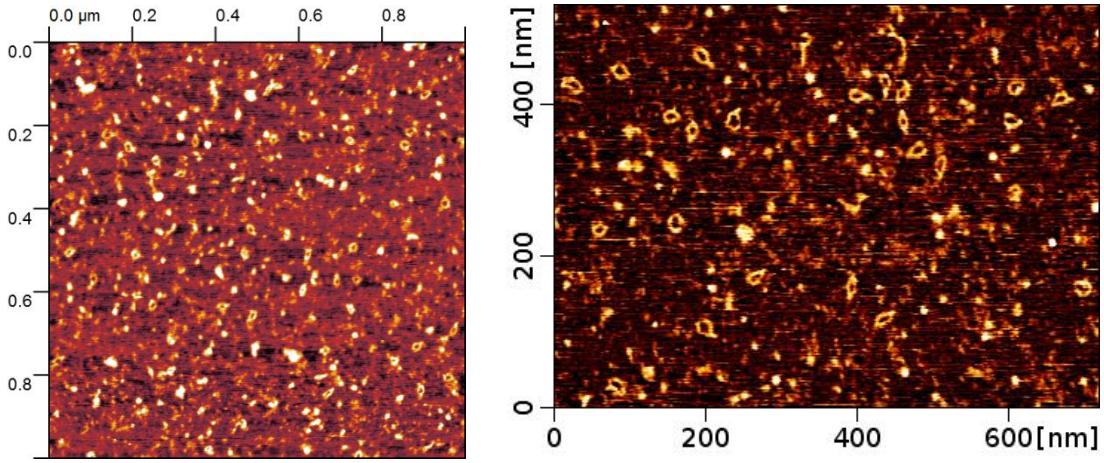

The AFM images reveal the circular structure of the 168 bp DNA ring (left) as well as the double-stranded overhang in the close up image (right).

[2]Catenane system structural proof via AC-mode

Sample: [2]catenane containing all four oligomers complementary to the four gaps, 1 nM with 1 nM polyornithine.

Mode: AC, intermittent contanct, wide (left) and close-up (right) picture.

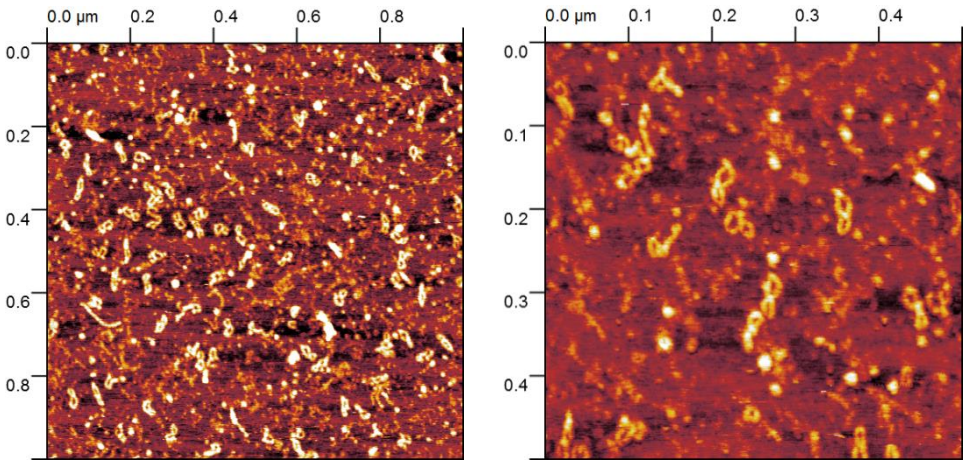

The AFM images show the two rings of the [2]catenane structure containing all four oligomers

Complementary to all four gaps. The close up image (right) shows different orientations of the double-stranded overhang.

[2]Catenane *ortho* conformation structural proof via AC-mode

Sample: [2]catenane containing 2 equivalents of the *para* release oligomer, 1 nM with 1 nM polyornithine. Mode: AC, intermittent contanct, wide (left) and close-up (right) picture.

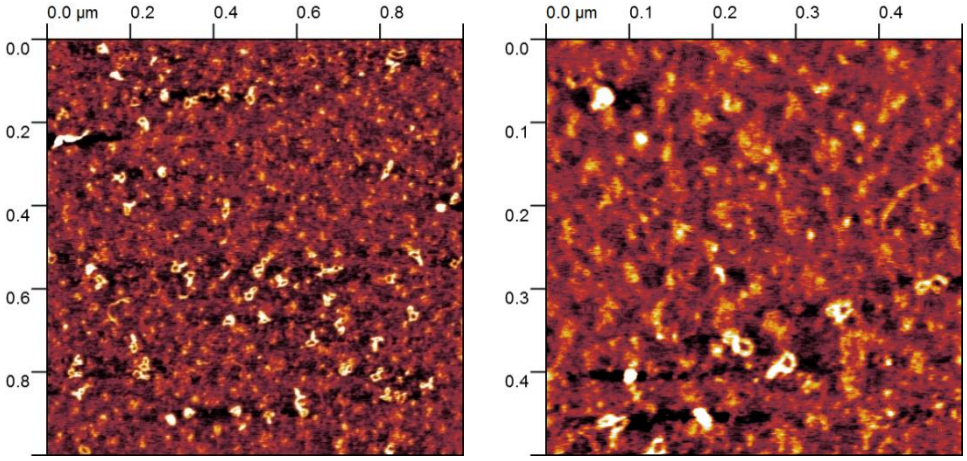

Both images show the [2]catenane structure in *ortho* conformation containing oligomers complementary to the para gaps. The right image reveals the double-stranded overhand in the preferred *ortho* orientation.

[2]Catenane *para* conformation structural proof via AC-mode

Sample: [2]catenane containing 2 equivalents of the *ortho* release oligomer, 1 nM with 1 nM polyornithine.

Mode: AC, intermittent contanct, wide (left) and close-up (right) picture.

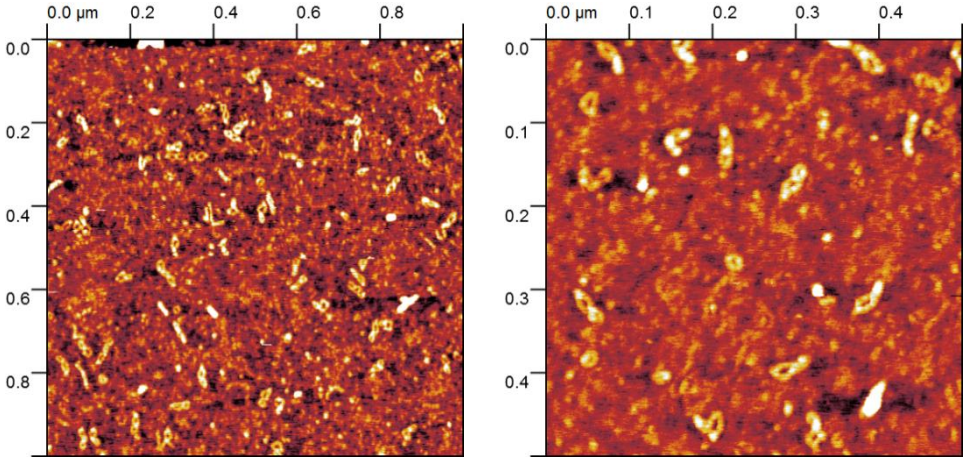

The AFM images show the [2]catenane structure in *para* conformation containing oligomers in both ortho gaps. The double-stranded overhang can be observed in *para* orientation as visible in the close up image (right).

8. Literature

[1] C. Brieke, F. Rohrbach, A. Gottschalk, G. Mayer, A. Heckel, *Angew. Chem. Int. Ed.* **2012**, *51*, 8446–8476.

[2] M. Irie, T. Fukaminato, K. Matsuda, S. Kobatake, *Chem. Rev.* **2014**, *114*, 12174-12277.

[3] H. A. Qu, Q. C. Wang, Q. W. Zhang, X. Ma, H. Tian, *Chem. Rev.* **2015**, *115*, 7543-7588.

[4] E. Merino, M. Ribagorda, *Beilstein J. Org. Chem.* **2012,** *8,* 1071–1090.

[5] E. Orgiu. P. Samori, *Adv. Mat.* **2014**, *26*, 1827-1845

[6] J. M. Abendroth, O. S. Bushuyev O. S. P. S. Weiss, C. J. Barrett, *ACS Nano* **2015**, *9*, 7746-7768.

[7] W.Szymanski, J. M. Bieerle, H. A. V. Kistemaker, W. A. Velema, B. L. Feringa, *Chem. Rev.* **2013**, *113*, 6114-6178.

[8] Y. Kamiya, H. Asanuma, *Acc. Chem. Res.* **2014**, *47*, 1663-1672.

[9] F. Zhang, J. Nangreave, Y. Liu, H. Yan, *J. Am. Chem. Soc.* **2014**, *136*, 11198−11211.

[10] S.-S. Jester, M. Famulok, *Acc. Chem. Res.* **2014**, *47* (6), 1700–1709.

[11] F. Wang, X. Liu, I. Willner, *Angew. Chem. Int. Ed.* **2015**, *54*, 1098–1129.

[12] A. A. Beharry, G. A. Woolley, *Chem. Soc. Rev.* **2011**, *40*, 4422–4437.

[13] W. A. Velema, W. Szymanski, B. L. Feringa, *J. Am. Chem. Soc.* **2014**, *136*, 2178−2191.

[14] A. S. Lubbe, W. Szymanski, B. L. Feringa, *Chem. Soc. Rev.* **2017**, *46*, 1052-1079.

[15] M. Dong, A. Babalhavaeji, S. Samanta, A. A. Beharry, G. A. Woolley, *Acc. Chem. Res.* **2015**, *48*, 2662-2670.

[16] D. Bléger, S. Hecht, *Angew. Chem. Int. Ed.* **2015**, *54*, 11338-11349.

[17] C. E. Weston, R. D. Richardson, P. R. Haycock, A. J. White, M. J. Fuchter, *J. Am. Chem. Soc.* **2014**, *136*, 11878-11881.

[18] J. Calbo, C. E. Weston, A. J. P. White, H. S. Rzepa, J. Contreras-García, M. J. Fuchter, *J. Am. Chem. Soc.* **2017**, *139*, 1261-1274.

[19] A. Einstein, *Phys. Z.* **1917**, *18*, 121-128.

[20] V. Balzani, A. Cerroni, A. Juris, *Photochemistry and Photophysics: Concepts, Research, Applications*, Wiley VCH (Weinheim), **2014,** 5-7.

[21] K.-H. Ng, “Non-Ionizing Radiations - Sources, Biological Effects, Emissions and Exposures”, Proceedings of the International Conference on Non-Ionizing Radiation at UNITEN (ICNIR2003) **2003**, 1-16.

[22] M. Planck, *Annalen der Physik* **1901**, *309* (3), 564-566.

[23] V. Balzani, A. Cerroni, A. Juris, *Photochemistry and Photophysics: Concepts, Research, Applications*, Wiley VCH (Weinheim), **2014,** 55-67.

[24] G. Wedler, *Lehrbuch der Physikalischen Chemie*, Wiley VCH (Weinheim), **2004**, 600ff.

[25] T. G. Mayerhöfer, H. Mutschke, J. Popp, *ChemPhysChem* **2016**, *17*, 1948-1955. [26]A. S. Coolidge, H. M. James, R. D. Present, *The Journal of Chemical Physics* **1936**, *4*, 193-211.

[27] J. Franck, E. G. Dymond, *Trans. Faraday Soc.* **1926**, *21*, 536-542.

[28] E. U. Condon, *Phys. Rev.* **1928**, *32*, 858-872.

[29] G. Wedler, *Lehrbuch der Physikalischen Chemie*, Wiley VCH (Weinheim), **2004**, 631ff.

[30] S. Ji, *Molecular Theory of the Living Cell*, Springer Science and Business Media **2012**, *p. 19*.

[31] M. Born, J. R. Oppenheimer, *Annalen der Physik* **1927**, *389* (20), 457-484.

[32] G. Wedler, *Lehrbuch der Physikalischen Chemie*, Wiley VCH (Weinheim), **2004**, 667.

[33] V. Balzani, A. Cerroni, A. Juris, *Photochemistry and Photophysics: Concepts, Research, Applications*, Wiley VCH (Weinheim), **2014,** 68-81.

[34] D. E. McCumber, Phys. Rev. 1964,136, A954 – Published 16 November 1964

[35] V. Balzani, A. Cerroni, A. Juris, *Photochemistry and Photophysics: Concepts, Research, Applications*, Wiley VCH (Weinheim), **2014,** 8-10.

[36] A. M. Brouwer, *Pure Appl. Chem.* **2011**, *83* (12), 2213–2228.

[37] R. I. Ghauharali, G. J. Brakenhoff, *Journal of Microscopy* **2001**, *198*, 88-100.

[38] H. Dürr, H. Bouas-Laurent, *Photochromism: Molecules and Systems*, Elsevier Science (Amsterdam), **2003**, 1-63.

[39] M. Kathan, S. Hecht, *Chem. Soc. Rev.* **2017**, *46*, 5536-5550.

[40] C. Bastianelli, V. Caia, G. Cum, R. Gallo, V. Mancini, *J. Chem. Soc. Perkin Trans* **1991**, 2, 679-683.

[41] S. J. Wezenberg, B. L. Feringa, *Org. Lett.* **2017**, *19*, 324-327.

[42] H. Rau, *Angew. Chem.* **1973**, *85* (6), 248-258.

[43] Z. Sekkat, W. Knoll, *Photoreactive Organic Thin Films*, Academic Press (London), **2002**, 3- 47.

[44] R. H. El Halabieh, O. Mermut, C. J. Barrett, *Pure Appl. Chem.* **2004**, *76* (7-8), 1445-1465.

[45] J. García-Amorós, D. Velasco, *Beilstein J. Org. Chem.* **2012**, *8*, 1003-1017.

[46] S. Wiedbrauk, H. Dube, *Tetrahedron Letters* **2015**, *56*, 4266-4274.

[47] S. Wiedbrauk, B. Maerz, E. Samoylova, A. Reiner, F. Trommer, P. Mayer, W. Zinth, H. Dube, *J. Am. Chem. Soc.* **2016**, *138*, 12219-12227.

[48] S. Kitzig, M. Thilemann, T. Cordes, K. Rück-Braun, *ChemPhysChem* **2016**, *17*, 1252-1263.

[49] H. Tian, S. Yang, *Chem. Soc. Rev.* **2004**, *33*, 85-97.

[50] T. Kudernac, S. J. van der Molen, B. J. van Wees, B. L. Feringa, *Chem. Commun.* **2006**, 3597- 3599.

[51] C. Sarter, M. Heimes, A. Jäschke, *Beilstein J. Org. Chem.* **2016**, *12*, 1103-1110.

[52] Y. Yokoyama, *Chem. Rev.* **2000**, *100*, 1717-1739. [53] H. Port, P. Gärtner, M. Hennrich, I. Ramsteiner, T. Schöck, *Mol. Cryst. Liq. Cryst.* **2005**, 430, 15-21.

[54] F. Renth, R. Siewertsen, F. Temps, *International Reviews in Physical Chemistry* **2013**, *32* (1), 1-38.

[55] G. Berkovic, K. Krongauz, V. Weiss, *Chem. Rev.* **2000**, *100*, 1741-1753.

[56] R. Klajn, *Chem. Soc. Rev.* **2014**, *43*, 148-184.

[57] P. Raster, A. Schmidt, M. Rambow, N. Kuzmanovic, B. König, G. Hilt, *Chem. Commun.* **2014**, *50*, 1864-1866.

[58] S. Helmy, S. Oh, S. A. Leibfarth, C. J. Hawker, J. R. de Alaniz, *J. Org. Chem.* **2014**, *79*, 11316-11329.

[59] S. Jia, J. D. Du, A. Hawley, W.-K. Fong, B. Graham, B. J. Boyd, *Langmuir* **2017**, *33*, 2215-2221.

[60] A. Noble, *Annalen der Chemie und Pharmacie* **1856**, *98* (2), 253-256.

[61] J. Griffiths, *Chem. Soc. Rev.* **1972**, *1*, 481-493.

[62] H. M. Dhammika Bandara, S. C. Burdette, *Chem. Soc. Rev.* **2012**, *41*, 1809-1825.

[63] J. M. Robertson, *J. Chem. Soc.* **1939**, 232-236.

[64] G. S. Hartley, R. J. W. Le Fèvre. *J. Chem. Soc.* **1939**, *0*, 531-535.

[65] G. S. Hartley, *Nature* **1937**, *140, 281.*

[66] G. S. Hartley, *J. Chem. Soc.* **1938**, 633.

[67] H. Rau, E. Lueddecke, *J. Am. Chem. Soc.* **1982**, *104*, 1616-1620.

[68] A. R. Dias, M. E: Minas de Piedade, J. A. Martinho de Simoes, J. A. Simoni, C. Teixeira, H. P. Diogo, *J. Chem. Thermoynamics* **1992**, *24*, 439-447.

[69] H. Rau, G. Kortüm, *Berichte der Bunsengesellschaft für physikalische Chemie* **1967**, *71* (7), 664-668.

[70] E. Merino, M. Ribagorda, *Beilstein J. Org. Chem.* **2012**, *8*, 1071-1090.

[71] Figure reference: H. Nishioka, X. Liang, H. Asanuma, *Chem. Eur. J.* **2010**, *16*, 2054-2062.

[72] I. Mita, K. Horie, K. Hirao, *Macromolecules* **1989**, *22*, 558-563.

[73] T. Schultz, J. Quenneville, B. Levine, A. Toniolo, T. J. Martinez, S. Lochbrunner, M. Schmitt, J. P. Shaffer, M. Z. Zgierski, A. Stolow, *J. Am. Chem. Soc.* **2003**, *125* (27), 8098-8099.

[74] A. Cembran, F. Bernardi, M. Garavelli, L. Gagliardi, G. Orlandi, *J. Am. Chem. Soc.* **2004**, *126* (10), 3234-3243.

[75] M. Quick, A. L. Dobryakov, M. Gerecke, C. Richter, F. Berndt, I. N. Ioffe, A. A. Granovsky, R. Mahrwald, N. P. Ernsting, S. A. Kovalenko, *J. Phys. Chem. B* **2014**, *118*, 8756-8771.

[76] T.-T. Yin, Z.-X. Zhao, H.-X. Zhang, *RSC Adv.* **2016**, *6*, 79879-79889.

[77] F. Hamon, F. Djedaini-Pilard, F. Barbot, C. Len, *Tetrahedron* **2009**, *65*, 10105–10123.

[78] E. Merino, *Chem. Soc. Rev.* **2011**, *40*, 3835–3853.

[79] S. Wawzonek, T. W. McIntyre, *J. Electrochem. Soc.* **1972**, *119* (10), 1350-1351.

[80] H. K. Hombrecher, K. Lüdtke, *Tetrahedron* **1993**, *49* (42), 9489-9494.

[81] N. A. Noureldin, J. W. Bellegarde, *Synthesis* **1999**, *6*, 939-942.

[82] S. M. Mehta, M. V. Makilwala, *J. Am. Chem. Soc.* **1952**, *74* (2), 563-564.

[83] E. S. Bacon, D. H. Richardson, *J. Chem. Soc.* **1932**, 0, 884-888.

[84] R. F. Nystrom, W. G. Brown, *J. Am. Chem. Soc.* **1948**, *70* (11), 3738-3740.

[85] W. Tadros, M. S. Ishak, E. Bassili, *J. Chem. Soc.* **1959**, *0*, 627-630.

[86] H. T. Clarke, W. R. Kirner, *Org. Synth.* **1922**, *2*, 47-49.

[87] I. Svele and H. Zollinger, Top. Curr. Chem., 1983, 112, 1.

[88] C. A. Hunter, L. D. Sarson, *Tetrahedron* **1996**, *37* (5), 699-702.

[89] K. Ueno, S. Akiyoshi, *J. Am. Chem. Soc.* **1954**, *76* (14), 3670-3672.

[90] Y. Ogata, Y. Takagi, *J. Am. Chem. Soc.* **1958**, *80* (14), 3591-3595.

[91] B.-C. Yu, Y. Shirai, J. M. Tour, *Tetrahedron* **2006**, *62* (44), 10303-10310.

[92] D. H. R. Barton, D. J. Lester, S. V. Ley, *J. Chem. Soc.*, *Perkin Trans. 1* **1980**, 1212-1217.

[93] L.-S. Bai, X.-M. Gao, X. Zhang, F.-F. Sun, N. Ma, *Tetrahedron Letters* **2014**, *55* (33), 4545-4548.

[94] W. E. Bachmann, *J. Am. Chem. Soc.* **1931**, *53* (4), 1524-1531.

[95] A. Saini, S. Kumar, J. S. Sandhu, *Synlett* **2006**, 395-398.

[96] S. Ishiro, M. Shigenori, *Bull. Chem. Soc. Jpn.* **1976**, *49*, 2294-2297.

[97] R. Zhao, C. Tan, Y. Xie, C. Gao, H, Liu, Y. Jiang, *Tetrahedron Letters* **2011**, *52*, 3805–3809.

[98] Y. Takeda, S. Okumura, S. Minakata, *Synthesis* **2013**, *45*, 1029–1033.

[99] G. W. Gribble, P. D. Lord, J. Skotnicki, S. E. Dietz, J. T. Eaton, J. Johnson, *J. Am. Chem. Soc.* **1974**, *96* (25), 7812-7814.

[100] O. Yoshiro, N. Yoshiaki, I. Morio, *Bull. Chem. Soc. Jpn.* **1981**, *54* (9), 2853-2854.

[101] E. Drug, M. Gozin, *J. Am. Chem. Soc.* **2007**, *129* (45), 13784-13785.

[102] X. Àlvarez Micó, T. Ziegler, L. R. Subramanian, *Angew. Chem.* **2004**, *116* (11), 1424-1427.

[103] H. Rau, *Azo compounds*, in H. Dürr, H. Bouas-Laurent, *Photochromism: Molecules and Systems*, Elsevier (Amsterdam), **1990**, 165-188.

[104] H. Rau, *Photoisomerization of Benzenes*, in Z. Sekkat, W. Knoll, *Photoreactive Organic Thin Films*, Elsevier (Berlin), **2002**, 3-38.

[105] K. G. Yager, C. J. Barrett, *Polymeric Nanostructures and their Applications,* American Scientific Publishers **2006**, *8*, 1-38.

[106] P. Bortolus, S. Monti, *J. Phys. Chem.* **1979**, *83* (6), 648-651.

[107] K. G. Yager, C. J. Barrett, *Journal of Photochemistry and Photobiology A: Chemistry* **2006**, *182*, 250–261. [108] A. F. Holleman, E. Wiberg, *Lehrbuch der Anorganischen Chemie*, DeGruyter (Berlin), **2007**, 688-689.

[109] E. McNellis, J. Meyer, A. D. Baghi, K. Reuter, *Phys. Rev. B* **2009**, *80* (035414), 1-10.

[110] I. Bridgeman, A. T. Peters, *Journal of the Society of Dyers and Colourists* **1970**, *86* (12), 519-524.

[111] O. S. Bushuyev, T. A. Singleton, C. J. Barrett, *Adv. Mater.* **2013**, *25*, 1796-1800.

[112] H. M. D. Bandara, S. C. Burdette, *Chem. Soc. Rev.* **2012**, *41*, 1809–1825.

[113] B. Buttingsrud, B. K. Alsberg, P.-O. Astrand, *Phys. Chem. Chem. Phys.* **2007**, *9*, 2226-2233.

[114] R. Siewertsen, H. Neumann, B. Buchheim-Stehn, R. Herges, C. Na ther, F. Renth, F. Temps, *J. Am. Chem. Soc.* **2009**, *131*, 15594–15595.

[115] O. Carstensen, J. Sielk, J. B. Schönborn, G. Granucci, B. Hartke, *J. Chem. Phys.* **2010**, *133* (124305), 1-12.

[116] M. Böckmann, N. L. Doltsinis, D. Marx, *Angew. Chem.* **2010**, *122*, 3454 –3456.

[117] Y. Yang, R. P. Hughes, I. Aprahamian, *J. Am. Chem. Soc.* **2012**, *134* (37), 15221−15224.

[118] Y. Yang, R. P. Hughes, I. Aprahamian, *J. Am. Chem. Soc.* **2014**, *136* (38), 13190−13193.

[119] S. Samanta, H. I. Qureshi, G. A. Woolley, *Beilstein J. Org. Chem.* **2012**, *5*, 2184-2190.

[120] M. A. Kienzler, A. Reiner, E. Trautman, S. Yoo, D. Trauner, E. Y. Isacoff, *J. Am. Chem. Soc.* **2013**, *135*, 17683−17686.

[121] C. Polini, W. Szymanski, L. Hou, W. R. Browne, B. L. Feringa, *Chem. Eur. J.* **2014**, 20, 946-951.

[122] O. Sadovski, A. A. Beharry, F. Zhang, G. A: Woolley, *Angew. Chem.* **2009**, *121*, 1512–1514.

[123] A. A. Beharry, G. A. Woolley, *Chem. Soc. Rev.*, **2011**, *40*, 4422–4437.

[124] H. A. Wegner, *Angew. Chem. Int. Ed.* **2012**, *51*, 4787–4788.

[125] M. Dong, A. Babalhavaeji, S. Samanta, A. A. Beharry, G. A. Woolley, *Acc. Chem. Res.* **2015**, *48*, 2662−2670.

[126] J. Pang, Z. Tian, J. Ma, *Chem. Phys. Lett.* **2014**, *613*, 110-114.

[127] M. J. Hansen, M. M. Lerch, W. Szymanski, B. L. Feringa, *Angew. Chem. Int. Ed.* **2016**, *55*, 13514 –13518.

[128] A. A. Beharry, O. Sadovski, G. A. Woolley, *J. Am. Chem. Soc.* **2011**, *133*, 19684–19687.

[129] S. Samanta, A. A. Beharry, O. Sadovski, T. M. McCormick, A. Babalhavaeji, V. Tropepe, G. A. Woolley, *J. Am. Chem. Soc.* **2013**, 135, 9777-9784.

[130] S. Samanta, T. McCormick, S. K. Schmidt, D. S. Seferos, G. A. Woolley, *Chem. Commun.* **2013**, *49*, 10314--10316.

[131] S. Samanta, A. Babalhavaeji, M. Dong, G. A. Woolley, *Angew. Chem.* **2013**, *125*, 14377–14380.

[132] D. Bléger, J. Schwarz, A. M. Brouwer, S. Hecht, *J. Am. Chem. Soc.* **2012**, *134*, 20597-20600.

[133] C. Knie, M. Utecht, F. Zhao, H. Kulla, S. Kovalenko, A. M. Brouwer, P. Saalfrank, S. Hecht, D. Bléger, *Chem. Eur. J*. **2014**, *20*, 16492–16501.

[134] D. Bléger, S. Hecht, *Angew. Chem. Int. Ed.* **2015**, *54*, 2–14.

[135] O. S. Bushuyev, A. Tomberg, T. Friscic, C. J. Barrett, *J. Am. Chem. Soc.* **2013**, *135*, 12556−12559.

[136] C. E. Weston, R. D. Richardson, P. R. Haycock, A. J. P. White, M. J. Fuchter, *J. Am. Chem. Soc.* **2014**, *136*, 11878-11881.

[137] Y.-T. Wang. X.-Y. Liu, G. Cui, W.-H. Fang, W. Thiel, *Angew. Chem. Int. Ed.* **2016**, *55*, 14009-14013.

[138] L. Stricker, E.-C. Fritz, M. Peterlechner, N. L. Doltsinis, B. J. Ravoo, *J. Am. Chem. Soc.* **2016**, *138*, 4547-4554.

[139] J. Moratz, L. Stricker, S. Engel, B. J. Ravoo, *Macromol. Rapid Commun.* **2017**, *1700256*, 1-5.

[140] J. Calbo, C. E. Weston, A. J. P. White, H. S. Rzepa, J. Contreras-García, M. J. Fuchter, *J. Am. Chem. Soc.* **2017**, *139*, 1261-1274.

[141] R. Göstl, A. Senf, S. Hecht, *Chem. Soc. Rev.,* **2014**, *43*, 1982-1996.

[142] J. S. Park et al., *J. Am. Chem. Soc.* **2013**, *135*, 16988−16996.

[143] J. D. Watson, F. C. H. Crick, *Cold Spring Harb Symp Quant Biol* **1953**, *18*. 123-131.

[144] G. M. Blackburn, M. J. Gait, D. Loakes, D. M. Williams, *Nucleic Acids in Chemistry and Biology*, RSC Publishing (Cambridge), **2006**.

[144a] Structures adapted from protein data bank. PDB-IDs: 213D, 1BNA, 3IRQ.

[145] E. T. Kool, *Chem. Rev.* **1997,** *97*, 1473-1487.

[146] R. W. Holley, J. Apgar, G. A. Everett, J. T. Madison, M. Marquisee, S. H. Merrill, J. R. Penswick, A. Zamir, *Science* **1965**, *147*, 1462-1465.

[147] I. Tinoco Jr., C. Bustamante, *J. Mol. Biol.* **1999**, *293*, 271-281.

[148] D. L. Beveridge, T. E. Cheatham III., M. Mezei, *J. Biosci.* **2012**, *37* (3), 379–397.

[149] R. E. Franklin, R. G. Gosling, *Acta Cryst.* **1953**, *6*, 673-677.

[150] F. M. Pohl, T. M. Jovin, *J Mol Biol.* **1972**, *67* (3), 375-96.

[151] K. Liu, H. T. Miles, J. Frazier, V. Sasisekharan, *Biochemistry* **1993**, *32* (44), 11802–11809.

[152] N. G. A. Abrescia, A. Thompson, T. Huynh-Dinh, J. A. Subirana, *Proc. Nat. Acad. Sci.* **2002**, *99* (5), 2806-2811.

[153] R. E. Johnson, L. Prakash, S. Prakash, *Proc. Nat. Acad. Sci.* **2005**, *102* (30), 10466-10471.

[154] S. Burge, G. N. Parkinson, P. Hazel, A. K. Todd, S. Neidle, *Nucleic Acids Research* **2006**, *34* (19), 5402–5415.

[155] J. L. Huppert, S. Balasubramanian, *Nucleic Acids Research* **2005**, *33* (9), 2908–2916.

[156] J.-L. Leroy, M. Guéron, J.-L. Mergny, C. Hélène, *Nucleic Acids Research* **1994**, *22* (9), 1600-1606.

[157] H. A. Day, P. Pavlou, Z. A. E. Waller, *Bioorg. Med. Chem.* **2014**, *22*, 4407–4418.

[158] J. C. Lee, R. R. Gutell, *J. Mol. Biol.* **2004**, *344*, 1225–1249.

[159] D. K. Hendrix, S. E. Brenner, S. R. Holbrook, *Quarterly Reviews of Biophysics* **2005**, *38* (3), 221–243.

[160] J. SantaLucia, D. Hicks, *Annu. Rev. Biophys. Biomol. Struct.* **2004**, *33*, 415–440.

[161] K. J. Breslauer, R. Frank, H. Blöcker, L. A. Marky, *Proc. Natl. Acad. Sci.* **1986**, *83*, 3746-3750.

[162] J. SantaLucia, H. T. Allawi, P. A. Seneviratne, *Biochemistry* **1996,** *35*, 3555-3562.

[163] T. Xia, J. SantaLucia, M. E. Burkard, R. Kierzek, S. J. Schroeder, X. Jiao, C. Cox, D. H. Turner, *Biochemistry* **1998,** *37,* 14719-14735.

[164] J. SantaLucia, *Proc. Natl. Acad. Sci.* **1998**, *95*, 1460–1465.

[165] R. Owczarzy, Y. You, B. G. Moreira, J. A. Manthey, L. Huang, M. A. Behlke, J. A. Walder, *Biochemistry* **2004,** *43,* 3537-3554.

[166] R. Owzcarzy, *Biophys. Chem.* **2005**, *117*, 207–215.

[167] R. Owczarzy, B. G. Moreira, Y. You, M. A. Behlke, J. A. Walder, *Biochemistry* **2008,** *47,* 5336–5353.

[168] G. F: Deleavey, M. J. Damha, *Chemistry & Biology* **2012**, *19*, 937-954.

[169] S. L. Beaucage, R. P. Iyer, *Tetrahedron* **1992**, *48* (12), 2223~2311.

[170] C. B. Reese, *Org. Biomol. Chem.* **2005**, *3*, 3851-3868.

[171] S. Danishefsky, M. Hirama, *J. Am. Chem. Soc.* **1977**, 99 (23), 7741-7743.

[172] J. C. Schulhof, R. Teoule, *Nucleic Acid Research* **1987**, *15* (2), 397-416.

[173] S. A. Scaringe, C. Francklyn, N. Usman, *Nucleic Acid Research* 1990, *18* (18), 5433-5441.

[174] J. H. Boal, A. Wilk, N. Harindranath, E. E. Max, *Nucleic Acids Research* **1996**, *24* (15), 3115–3117.

[175] Y. S. Sanghvi, *Current Protocols in Nucleic Acid Chemistry* **2011**, 4.1.1-4.1.22.

[176] H. Kashida, X. Liang, H. Asanuma, *Current Organic Chemistry* **2009**, *13,* 1065-1084.

[177] H. Kashida, T. Fujii, H. Asanuma, *Org. Biomol. Chem.* **2008**, *6* (16), 2892-2896.

[178] H. Asanuma, T. Takarada, T. Yoshida, D. Tamaru, X. Liang, M. Komiyama, *Angew. Chem.* **2001**, *113* (14), 2743-2745.

[179] R. Yamashige, M. Kimoto, Y. Takezawa, A. Sato, T. Mitsui, S. Yokoyama, I. Hirao, *Nucleic Acids Res.* **2012**, *40* (6), 2793–2806.

[180] D. A. Malyshev, K. Dhami, T. Lavergne, T. Chen, N. Dai, J. M. Foster, I. R. Corre, F. E. Romesberg, *Nature* **2014**, *509*, 385-402.

[181] J. Gierlich, G. A. Burley, P. M. E. Gramlich, D. M. Hammond, T. Carell, *Org. Lett.* **2006**, *8* (17), 3639-3642.

[182] H. Asanuma, T. Ito, M. Komiyama, *Tetrahedron Letters* **1998**, 9015-9018.

[183] H. Asanuma, T. Ito, T. Yoshida et al., *Angew. Chem. Int. Ed.* **1999**, *38* (16), 2393-2395.

[184] X. Liang, T. Yoshida, H. Asanuma, M. Komiyama, *Nucleic Acids Symposium* **2000**, *44*, 277-278.

[185] X. Liang, H. Asanuma, *J. Am. Chem. Soc.* **2002**, *124* (9), 1877-1883.

[186] H. Asanuma, D. Matsunaga, M. Liu, X. Liang, J. Jhao, M. Komiyama, *Nucleic Acids Research* **2003**, *3*, 117-118.

[187] H. Asanuma, D. Matsunaga, M. Komiyama, *Nucleic Acids Symposium* **2005**, *49*, 35-36.

[188] X. Liang, T. Mochizuki, H. Asanuma, *Small* **2009**, *5* (15), 1761–1768.

[189] T. Fujii, H. Kashida, H. Asanuma, *Chem. Eur. J.* **2009**, *15*, 10092 – 10102.

[190] H. Ito, X. Liang, H. Nishioka, H. Asanuma, *Org. Biomol. Chem.* **2010**, *8*, 5519–5524.

[191] Y. Nakasone, H. Ooi, Y. Kamiya, H. Asanuma, M. Terazima, *J. Am. Chem. Soc.* **2016**, *138* (29), 9001–9004.

[192] H. Asanuma, X. Liang, H. Nishioka, D. Matsunaga, M. Liu, M. Komiyama, *Nature Protocols* **2007**, 2 (1), 203-212.

[193] X. Liang, H. Nishioka, T. Mochizuki, H. Asanuma, *J. Mater. Chem.* **2010**, *20*, 575–581.

[194] Y. Kamiya, H. Asanuma, *Acc. Chem. Res.* **2014**, *47* (6), 1663-1672.

[195] H. Nishioka, H. Kashida, M. Komiyama, X. Liang, H. Asanuma, *Nucleic Acids Symposium* **2006**, *50*, 85-86.

[196] H. Nishioka, X. Liang, H. Kashida, H, Asanuma, *Chem. Commun.* **2007**, 4354–4356.

[197] H. Nishioka, X. Liang, H. Asanuma, *Chem. Eur. J.* **2010**, *16*, 2054–2062.

[198] H. Nishioka, X. Liang, T. Kato, H. Asanuma, *Angew. Chem. Int. Ed.* **2012**, *51*, 1165 – 1168.

[199] Y. Kamiya, T, Takagi, H, Ooi, H, Ito, X. Liang, H. Asanuma, *ACS Synth. Biol.* **2015**, *4* (4), 365-370.

[200] T. Goldau, K. Murayama, C. Brieke, H. Asanuma, A. Heckel, *Chem. Eur. J.* **2015**, *21*, 17870–17876.

[201] T. Goldau, K. Murayama, C. Brieke, S. Steinwand, P. Mondal, M. Biswas, I. Burghardt, J. Wachtveitl, H. Asanuma, A. Heckel, *Chem. Eur. J.* **2015**, *21*, 2845-2854.

[202] B. Kou, X. Guo, S.-J. Xiao, X. Liang, *Small* **2013**, *9* (23), 3939-3943.

[203] F. Wang, X. Liu, I. Willner, *Angew. Chem. Int. Ed.* **2015**, *54*, 1098–1129.

[204] J. M. Abendroth, O. S. Bushuyev, P. S. Weiss, C. J. Barrett, *ACS Nano* **2015**, *9* (8), 7746–7768.

[205] S. E. Cakmak, D. A. Leigh, C. T. McTernan, A. L. Nussbaumer, *Chem. Rev.* **2015**, *115*, 10081−10206.

[206] D. Han, J. Huang, Z. Zhu, Q. Yuan, M. You, Y. Chenab, W. Tan, *Chem. Commun.* **2011**, *47*, 4670–4672.

[207] T. Takenaka, M. Endo, Y. Suzuki, Y. Yang, T. Emura, K. Hidaka, T. Kato, T. Miyata, K. Namba, H. Sugiyama, *Chem. Eur. J.* **2014**, *20*, 14951 – 14954.

[208] X. Wang, Z. Li, Y. Yang, X. Gong, Y. Liao, X. Xie, *Langmuir* **2015**, *31*, 5456−5463.

[209] Y. Yang, M. Endo, K. Hidaka, H. Sugiyama, *J. Am. Chem. Soc.* **2012**, *134*, 20645−20653.

[210] X. Liang, H. Nishioka, N. Takenaka, H. Asanuma, *ChemBioChem* **2008**, *9*, 702-705.

[211] H. Kang, H. Liu, J. A. Phillips, Z. Cao, Y. Kim, Y. Chen, Z. Yang, J. Li, W. Tan, *Nano Lett.* **2009***, 9* (7), 2690-2696.

[212] A. Kuzyk, Y. Yang, X. Duan, S. Stoll, A. O. Govorov, H. Sugiyama, M. Endo, N. Liu, *Nat. Comm.* **2016**, *10591*, 1-6.

[213] F. Lohmann, D. Ackermann, M. Famulok, *J. Am. Chem. Soc.* **2012**, *134*, 11884−11887.

[214] F. Lohmann, J. Weigandt, J. Valéro, M. Famulok, *Angew. Chem. Int. Ed.* **2014**, *126*, 1-6.

[215] J. Weigandt, C.-L. Chung, S.-S. Jester, M. Famulok, *Angew. Chem. Int. Ed.* **2016**, *55*, 5512–5516.

[216] M. M. Lerch, M. J. Hansen, W. A. Velema, W. Szymanski, B. L. Feringa, *Nat. Comm.* **2016**, *12054*, 1-10.

[217] G. Meister, T. Tuschel, *Nature* **2004**, *431*, 343-349.

[218] J. K. Watts, D. R. Corey, *J. Pathol.* **2012**, *226*, 365–379.

[219] X. Tang, I. J. Dmochowski, *Mol. BioSyst.* **2007**, *3*, 100–110.

[220] A. A. Beharry, L. Wong, V. Tropepe, G. A. Woolley, *Angew. Chem. Int. Ed.* **2011**, *50*, 1325-1327.

[221] J. Wachtveitl, A. Zumbusch, *ChemBioChem* **2011**, *12*, 1169–1170.

[222] J. Broichhagen, J. A. Frank, D. Trauner, *Acc. Chem. Res.* **2015**, *48*, 1947−1960.

[223] M. M. Lerch, M. J. Hansen, G. M. van Dam, W. Szymanski, B. L. Feringa, *Angew. Chem. Int. Ed.* **2016**, *55*, 10978–10999.

[224] J. Broichhagen, M. Schönberger, S. C. Cork, J. A. Frank, P. Marchetti, M. Bugliani, A.M. J. Shapiro, S. Trapp, G. A. Rutter, D. J. Hodson, D. Trauner, *Nat. Comm.* **2014**, *5* (5116), 1-11.

[225] J. Broichhagen, T. Podewin, H. Meyer-Berg, Y. von Ohlen, N. R. Johnston, B. J. Jones, S. R. Bloom, G. A. Rutter, A. Hoffmann-Röder, D. J. Hodson, D. Trauner, *Angew. Chem. Int. Ed.* **2015**, *54*, 15565 –15569.

[226] M. Schönberger, M. Althaus, M. Fronius, W. Clauss, D. Trauner, *Nat. Chem.* **2014**, *6*, 712-719.

[227] M. Borowiak, W. Nahaboo, M. Reynders, K. Nekolla, P. Jalinot, J. Hasserodt, M. Rehberg, M. Delattre, S. Zahler, A. Vollmar, D. Trauner, O. Thorn-Seshold, *Cell* **2015**, *162* (2), 403-411.

[228] A. Polosukhina, J. Litt, I. Tochitsky, J. Nemargut, Y. Sychev, I. De Kouchkovsky, T. Huang, K. Borges, D. Trauner, R. N. Van Gelder, R. H. Kramer, *Neuron* **2012**, *75*, 271–282.

[229] I. Tochitsky, A. Polosukhina, V. E. Degtyar, N. Gallerani, C. M. Smith, A. Friedman, R. N. Van Gelder, D. Trauner, D. Kaufer, R. H. Kramer, *Neuron* **2014**, *81*, 800–813.

[230] L. Laprell, K. Hüll, P. Stawski, C. Schöm, S. Michalakis, M. Biel, M. P. Sumser, D. Trauner, *ACS Chem. Neurosci.* **2016**, *7*, 15−20.

[231] J. A. Frank, D. A. Yushchenko, D. J Hodson, N. Lipstein, J. Nagpal, G. A. Rutter, J.-S. Rhee, A. Gottschalk, N. Brose, C. Schultz, D. Trauner, *Nat. Chem. Biol.* **2016**, *2141*, 1-8.

[232] O. Akil, R. P. Seal, K. Burke, C. Wang, A. Alemi, M. During, R. H. Edwards, L. R. Lustig, *Neuron* **2012**, *75*, 283–293.

[233] D. B. Amabilino, J. F. Stoddart, *Chem. Rev.* **1995**, *95*, 2725-2828.

[234] J. F. Stoddart, *Chem. Soc. Rev.* **2009**, *38*, 1802-1844.

[235] G. Rasched, D. Ackermann, T. L. Schmidt, P. Broekmann, A. Heckel, M. Famulok, *Angew. Chem. Int. Ed.* **2008**, *47*, 967-970.

[236] D. Ackermann, T. L. Schmidt, J. S. Hannam, C. S. Purohit, A. Heckel, M. Famulok, *Nat. Nanotechnol.* **2010**, *5*, 436-442.

[237] V. Adam, D. K. Prusty, M. Centola, J. Hannam, M. Škugor, B. Klöckner, J. Valéro, M. Famulok, *Chem. Eur. J.* **2018**, *24* (5), 1062-1066.

[238] D. K. Prusty, V. Adam, R. Zadegan, S. Irsen, M. Famulok, *Nat. Comm.* **2018**, *9* (535), 1-14.

[239] O. C. Farokhzad, J. Cheng, B. A. Teply, I. Sherifi, S. Jon, P. W. Kantoff, J. P. Richie, R. Langer, *Proc. Natl Acad. Sci.* **2006**, *103*, 6315–6320.

[240] S. Dhar, F. X. Gu, R. Langer, O. C. Farokhzad, S. J. Lippard, *Proc. Natl Acad. Sci.* **2008**, *105* (40), 17356–17361.

[241] H. Xing, L. Tang, X. Yang, K. Hwang, W. Wang, Q. Yin et al., *J. Mater. Chem. B* **2013**, *1* (39), 5288-5297.

[242] W. Alshear, H. Hillaireau, J. Vergnaud, S. Ismail, E. Fattal, *Bioconjugate Chem.* **2015**, *26* (7),1307-1313.

[243] J. M. Cullen, R. T. Miller, *Expert Opin. Drug. Metab. Toxicol.* **2005**, *5*, 241-247.

[244] D. S. Alberts, A. Belforge, *Semin. Oncol.* **2006**, *33*, 8-17.

[245] A. Boltz, B. Piater, L. Toleikis, R. Guenther, H. Kolmar, B. Hock, *J. Biol. Chem.* **2011**, *286* (24), 21896-21905.

[246] J. L. Vinkenborg, G. Mayer, M. Famulok, *Angew. Chem. Int. Ed.* **2012**, 36, 9176-9180.

[247] A. Wochner, M. Menger, D. Orgel, B. Cech, M. Rimmele, V. A. Erdmann, J. Glökler, *Anal. Biochem.* **2008**, *373*, 34-42.

[248] L. Meng, L. Yang, X. Zhao, L. Zhang, H. Zhu, C. Liu, W. Tan, *PLoS One* **2012**, *7* (4), 1-8.

[249] O. Bayacloglu, C. H. Stuart, G. Kulik, W. H. Gmeiner, *Molecular Therapy - Nucleic Acids* **2013**, *2* (107), 1-8.

[250] J. Juodaityte, N. Sewald, *J. Biotechnol.* **2004**, *112*, 127-138.

[251] A. Defoin, *Synthesis* **2004**, *5*, 706-710.

[252] M. E. Jung, T. A. Dong, X. Cai, *Tetrahedron Letters* **2011**, *52*, 2533-2535.

[253] E. Leyva, C. Medina, E. Moctezuma, S. Leyva, *Can. J. Chem.* **2004**, *82*, 1712-1715.

[254] P. C. Bulman Page, B. R. Buckley, G. A. Rassias, A. J. Blacker, *Eur. J. Org. Chem.* **2006**, 803-813.

[255] M. C. Davis, *Synth. Comm.* **2009**, 39, 1100-1108.

[256] R. Johnsson, A. Meijer, U. Ellervik, *Tetrahedron* **2005**, *61*, 11657-11663.

[257] D. T. Cohen, S. L. Buchwald, *Org. Lett.* **2015**, *17* (2), 202-205.

[258] A. Ghinet, B. Rigo, J.-P. Hénichart et al., *Bioorg. Med. Chem.* **2011**, *19*, 6042-6054.

[259] L. Hamryszak, H. Janeczek, E. Schab-Balcerzak, *J. Mol. Liq.* **2012**, *165*, 12-20.

[260] M. Kwak, I. J. Minten, D.-M. Anaya et al., *J. Am. Chem. Soc.* **2010**, *132*, 7834-7835.

[261] M. Dong. A. Babalhavaeji, C. V. Collins, K. Jarrah, O. Sadovski, Q. Dai, G. A. Woolley, *J. Am. Chem. Soc.* **2017**, *139* (38), 13483-13486.

[262] I. J. Dmochowski, X. Tang, *Biotechniques* **2007**, *43* (2), 161-171.

[263] L. T. Kubota, L. Gorton, *Electroanalysis* **1999**, *10* (11), 719-728.

[264] M. M. Barsan, E. M. Pinto, C. M. A. Brett, *Electrochimica Acta* **2008**, *53*, 3973-3982.

9. Appendix I

9.1 List of commonly used abbreviations

AAP1	*N*-methyl-arylazopyrazole
AAP2	*N*-phenyl-arylazopyrazole
AAP3	*N*-4-nitrophenyl-arylazopyrazole
AB	azobenzene
ACN	acetonitrile
AFM	Atomic Force Microscopy
AMP	adenosine monophosphate
ATP	adenosine triphosphate
BHQ3	Blackhole quencher 3
Cap A	capping mix A for solid phase DNA synthesis
Cap B	capping mix B for solid phase DNA synthesis
CPG	controlled pore glass
Cy5.5	Cyanine 5.5
DCAB	2‘,6‘-dichloroazobenzene
DCM	dichloromethane
DFAB	2’,6’-difluoroazobenzene
DFAB-F	2‘,4‘,6‘-trifluoroazobenzene
DFAB-Br	4‘-bromo-2‘,6‘-difluoroazobenzene
DFAB-Cl	4‘-chloro-2‘,6‘-difluoroazobenzene
DFAB-Pep	4‘-acetamido-2‘,6‘-difluoroazobenzene
DNA	deoxyribonucleic acid
DMAB	2’,6’-dimethylazobenzene
DMDFAB	2,6-difluoro-2‘,6‘-dimethylazobenzene
DMSO	dimethylsulfoxide
DMT-Cl	4,4’-dimethoxytritylchloride
DNA	deoxyribonucleic acid
DOAB	2‘,6‘-dimethoxyazobenzene
Dox (DxR)	doxorubicin

HEPES	2-(4-(2-hydroxyethyl)-1-piperazinyl)ethansulfonic acid
HOMO	highest occupied molecular orbital
HPLC	high performance liquid chromatography
LCMS	liquid chromatography mass spectrometry
LUMO	lowest unoccupied molecular orbital
MO	molecular orbital
MS	mass spectrometry
NMM	*N*-methyl morpholine
NMPi	*N*-methyl pyrrolidine
NMR	nuclear magnetic resonance
PA	phosphoramidite
PBS	phosphate buffered saline
RNA	ribonucleic acid
SD	Standard deviation
SELEX	systematic evolution of ligands by exponential enrichtment
ssDNA/RNA	single-stranded DNA/RNA
TBAB	2,2’,6,6’-tetrabromoazobenzene
TCA	trichloroacetic acid
TCAB	2,2’,6,6’-tetrachloroazobenzene
TEAAc	triethylammonium acetate
TFA	trifluoroacetic acid
TFAB	2,2’,6,6’-tetrafluoroazobenzene
TLC	thin layer chromatography
TMAB	2,2',6,6'-tetramethoxyazobenzene
TOAB	2,2’,6,6’-tetramethoxyazobenzene
UV/Vis	ultraviolet and visible light

9.2 List of illustrations

9.3 List of tables

10. Attachments

10.1 NMR and mass spectra of synthesized compounds

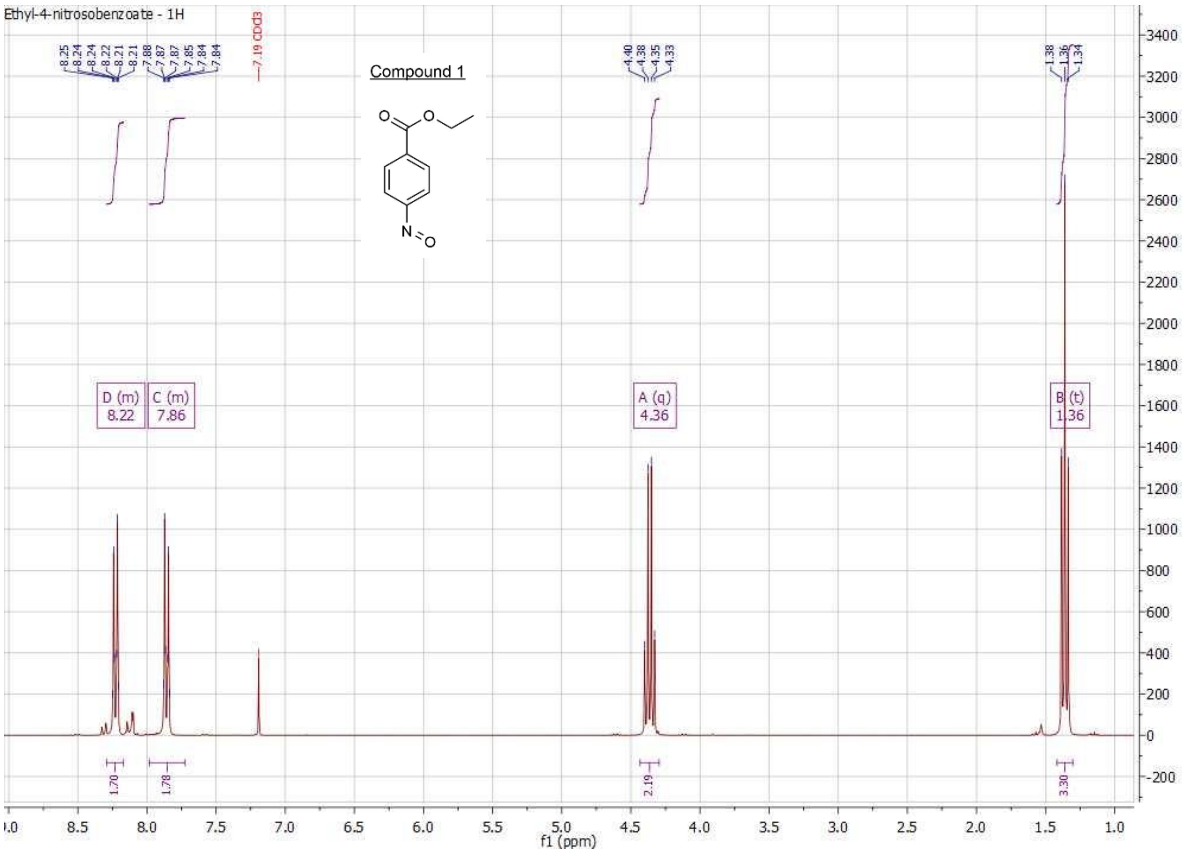
Ethyl-4-nitrosobenzoate - 1H
Compound 1
D (m) 8.22
C (m) 7.86
A (q) 4.36
B (t) 1.36
f1 (ppm)

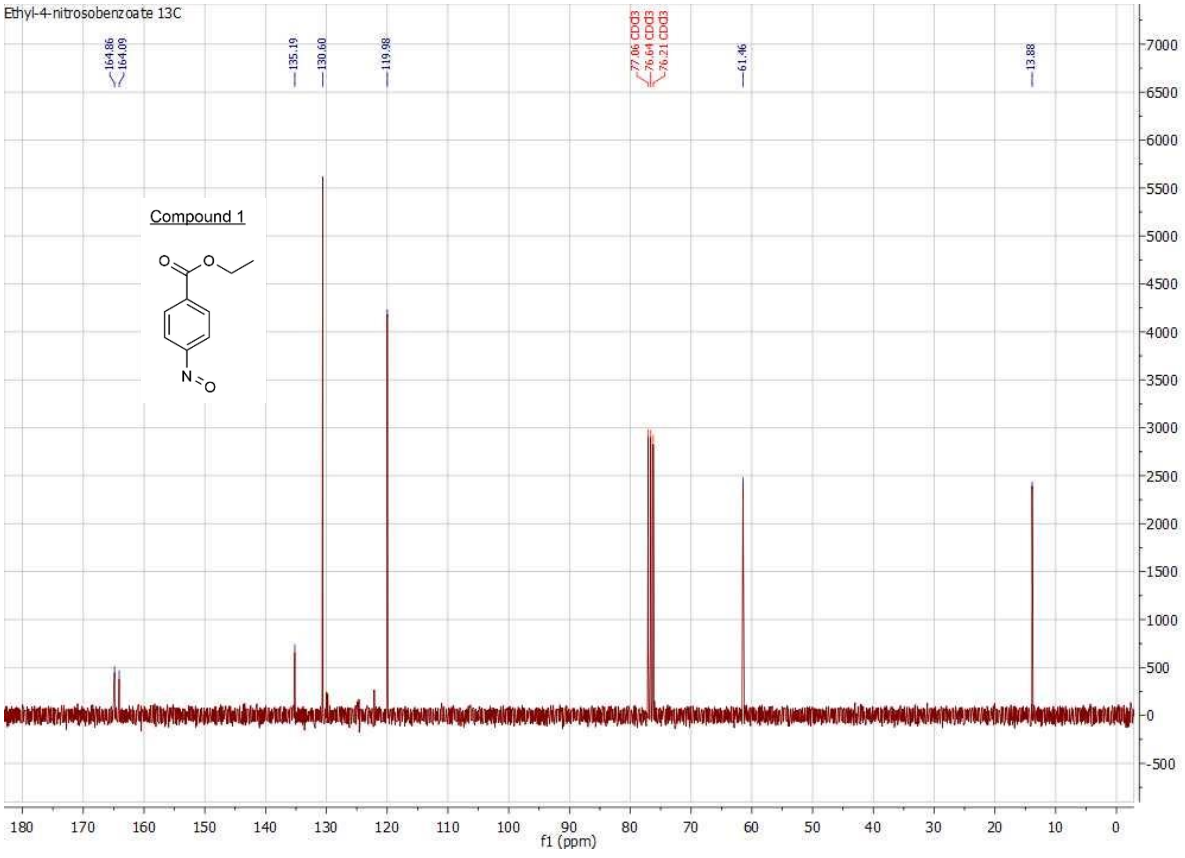
Ethyl-4-nitrosobenzoate 13C
Compound 1
f1 (ppm)

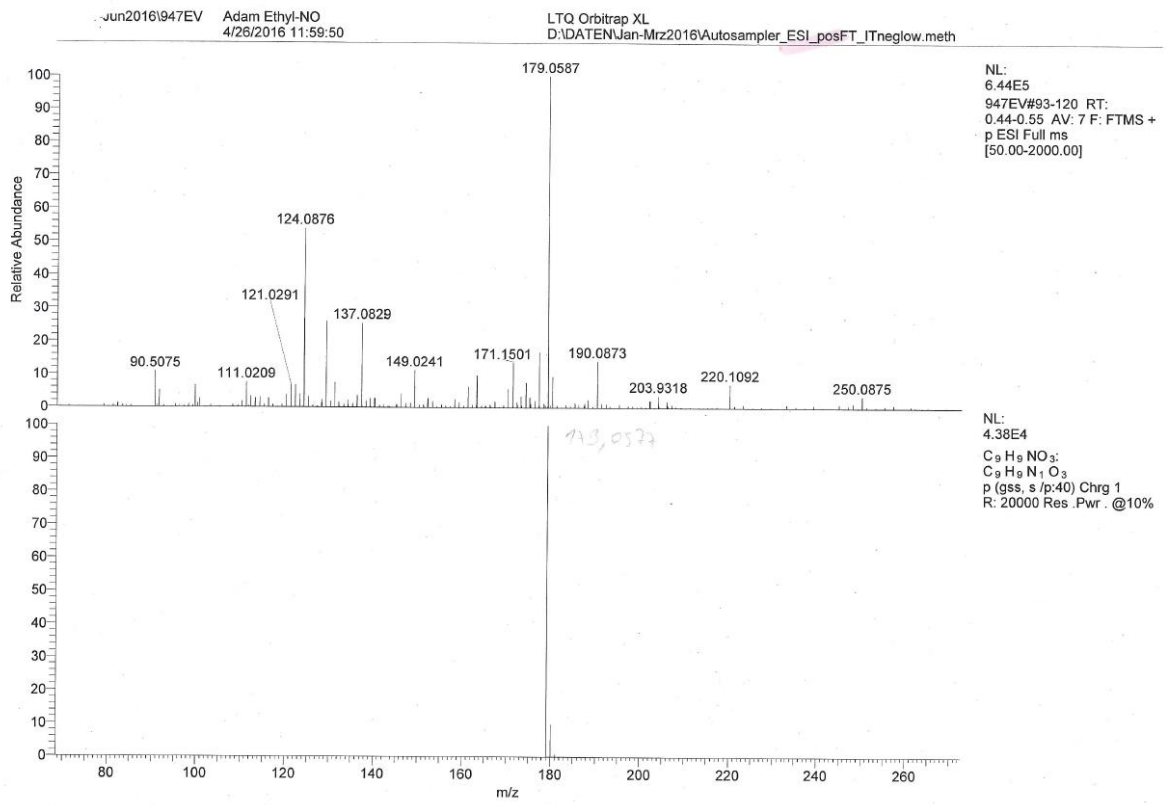
Jun2016\947EV Adam Ethyl-NO
4/26/2016 11:59:50
LTQ Orbitrap XL
D:\DATEN\Jan-Mrz2016\Autosampler_ESI_posFT_ITneglow.meth
NL:
6.44E5
947EV#93-120 RT:
0.44-0.55 AV: 7 F: FTMS +
p ESI Full ms
[50.00-2000.00]
179.0587
124.0876
121.0291
137.0829
90.5075
111.0209
149.0241
171.1501
190.0873
203.9318
220.1092
250.0875
Relative Abundance
NL:
4.38E4
C9 H9 NO3:
C9 H9 N1 O3
p (gss, s /p:40) Chrg 1
R: 20000 Res .Pwr . @10%
179.0577
m/z

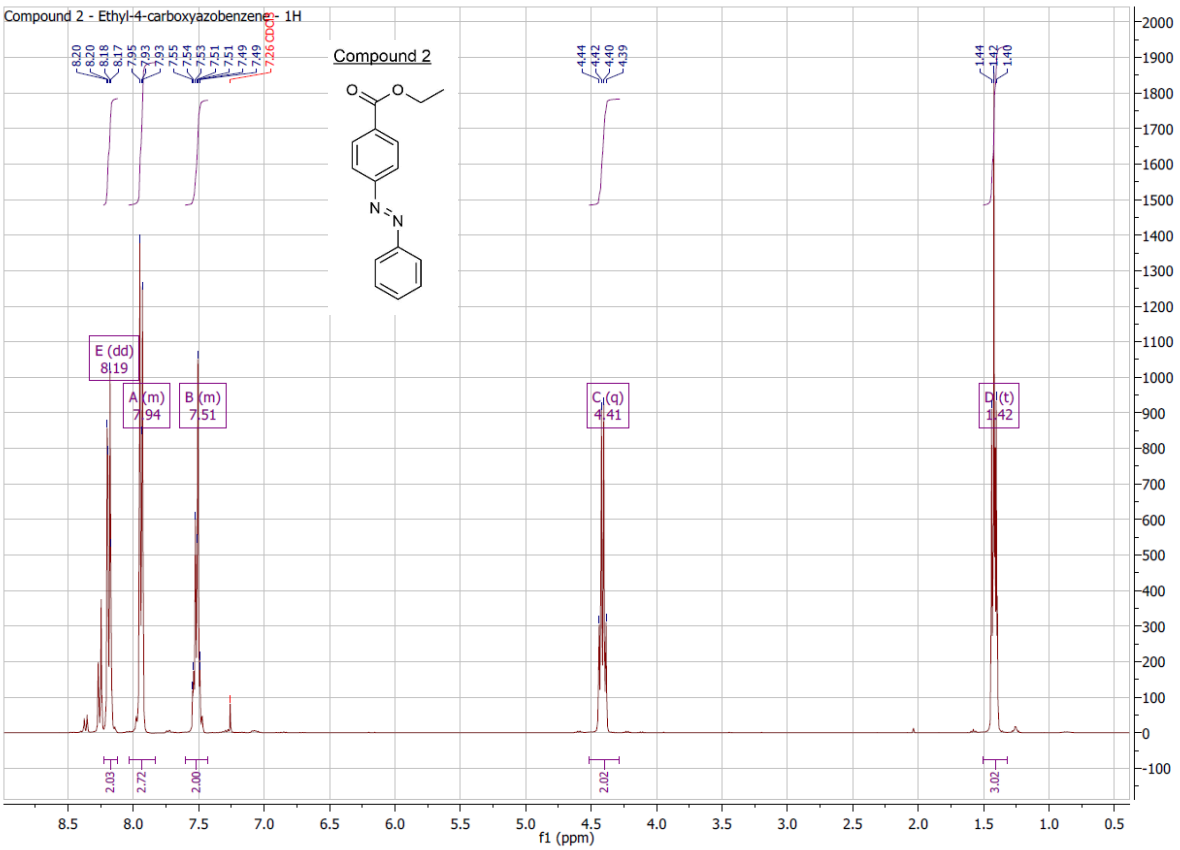
Compound 2 - Ethyl-4-carboxyazobenzene - 1H
Compound 2
E (dd)
8.19
A (m)
7.94
B (m)
7.51
C (q)
4.41
D (t)
1.42
f1 (ppm)

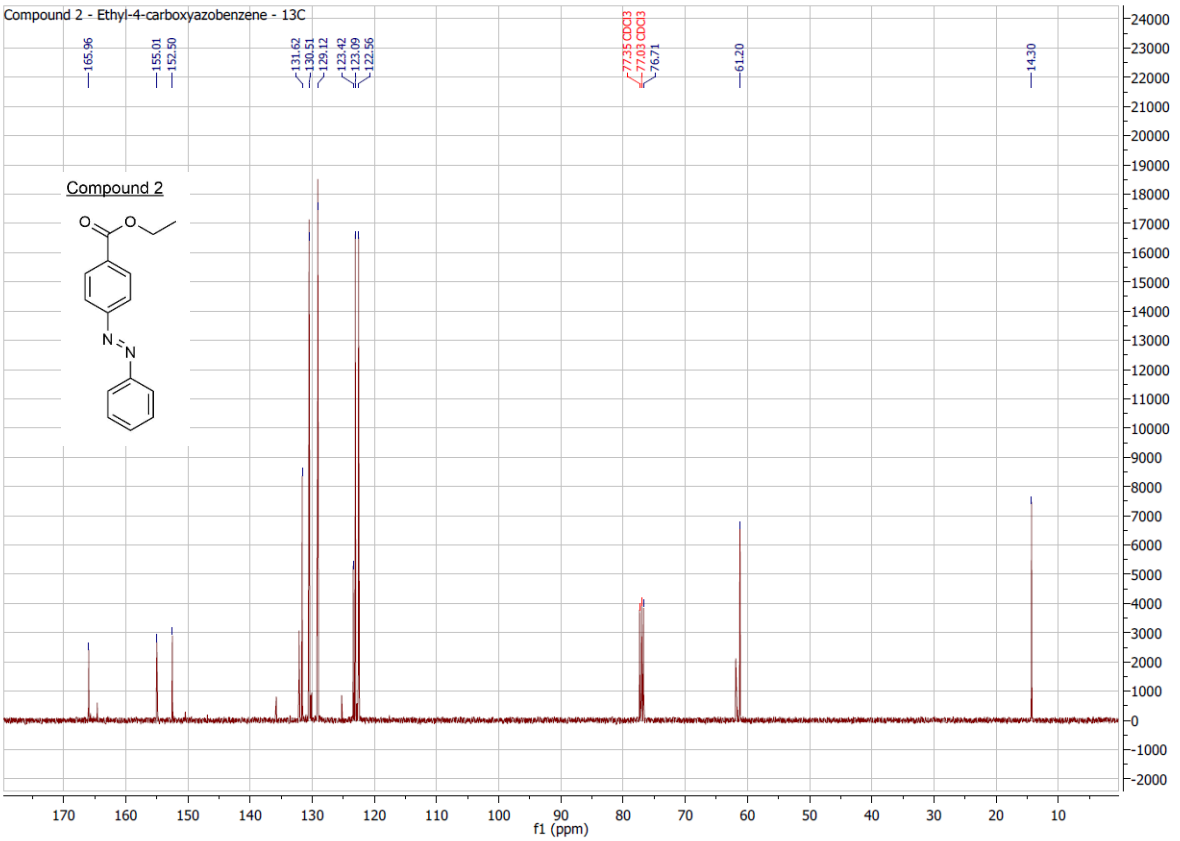
Compound 2 - Ethyl-4-carboxyazobenzene - 13C
Compound 2
f1 (ppm)

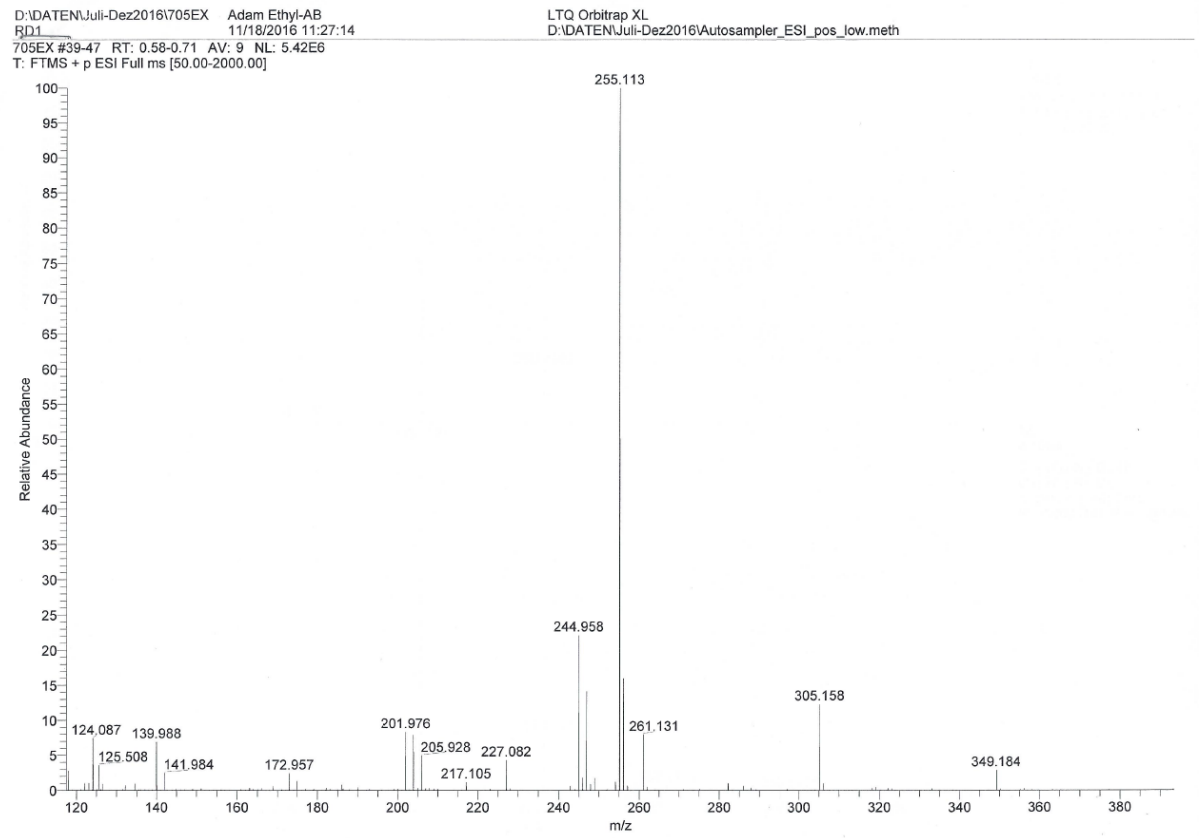
D:\DATEN\Juli-Dez2016\705EX Adam Ethyl-AB
RD1 11/18/2016 11:27:14
LTQ Orbitrap XL
D:\DATEN\Juli-Dez2016\Autosampler_ESI_pos_low.meth
705EX #39-47 RT: 0.58-0.71 AV: 9 NL: 5.42E6
T: FTMS + p ESI Full ms [50.00-2000.00]
Relative Abundance
m/z
255.113
244.958
305.158
261.131
201.976
205.928
227.082
124.087
139.988
125.508
141.984
172.957
217.105
349.184

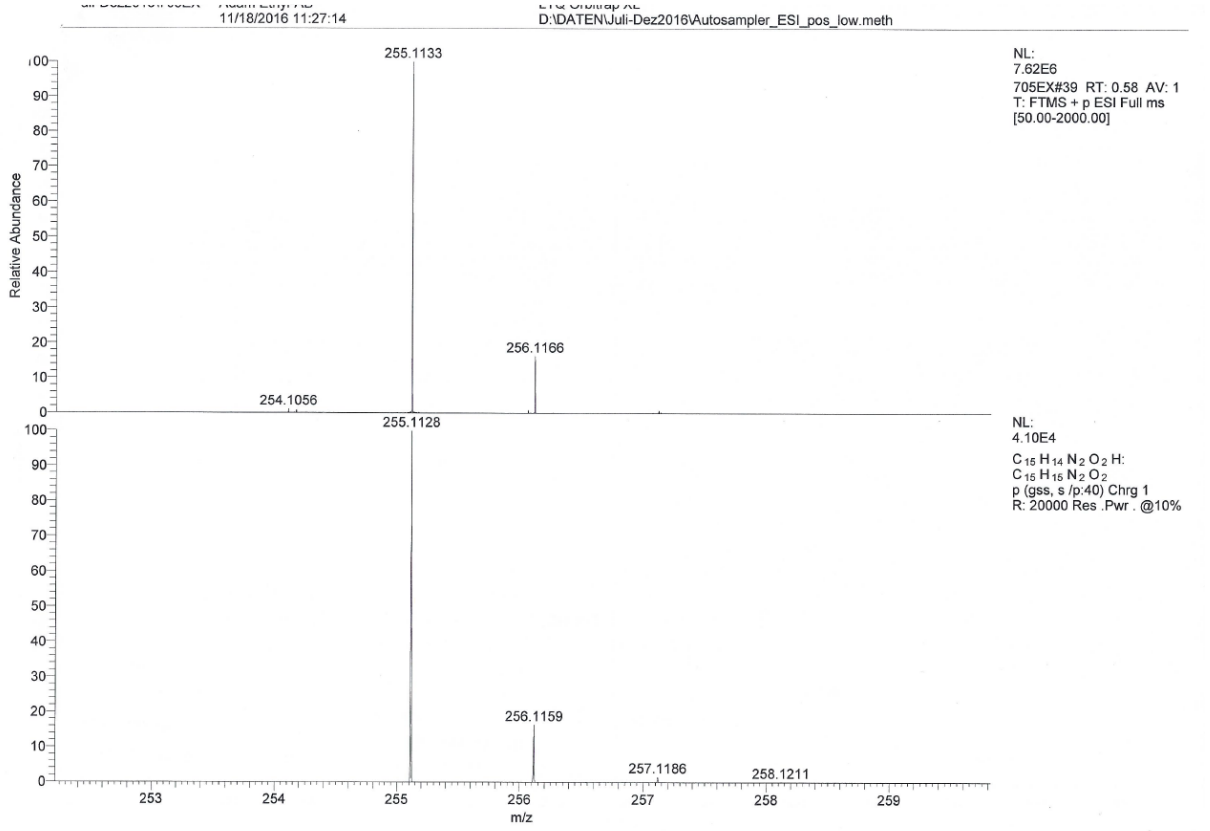
11/18/2016 11:27:14
D:\DATEN\Juli-Dez2016\Autosampler_ESI_pos_low.meth
NL:
7.62E6
705EX#39 RT: 0.58 AV: 1
T: FTMS + p ESI Full ms
[50.00-2000.00]
255.1133
256.1166
254.1056
NL:
4.10E4
C15 H14 N2 O2 H:
C15 H15 N2 O2
p (gss, s /p:40) Chrg 1
R: 20000 Res .Pwr . @10%
255.1128
256.1159
257.1186
258.1211
Relative Abundance
m/z

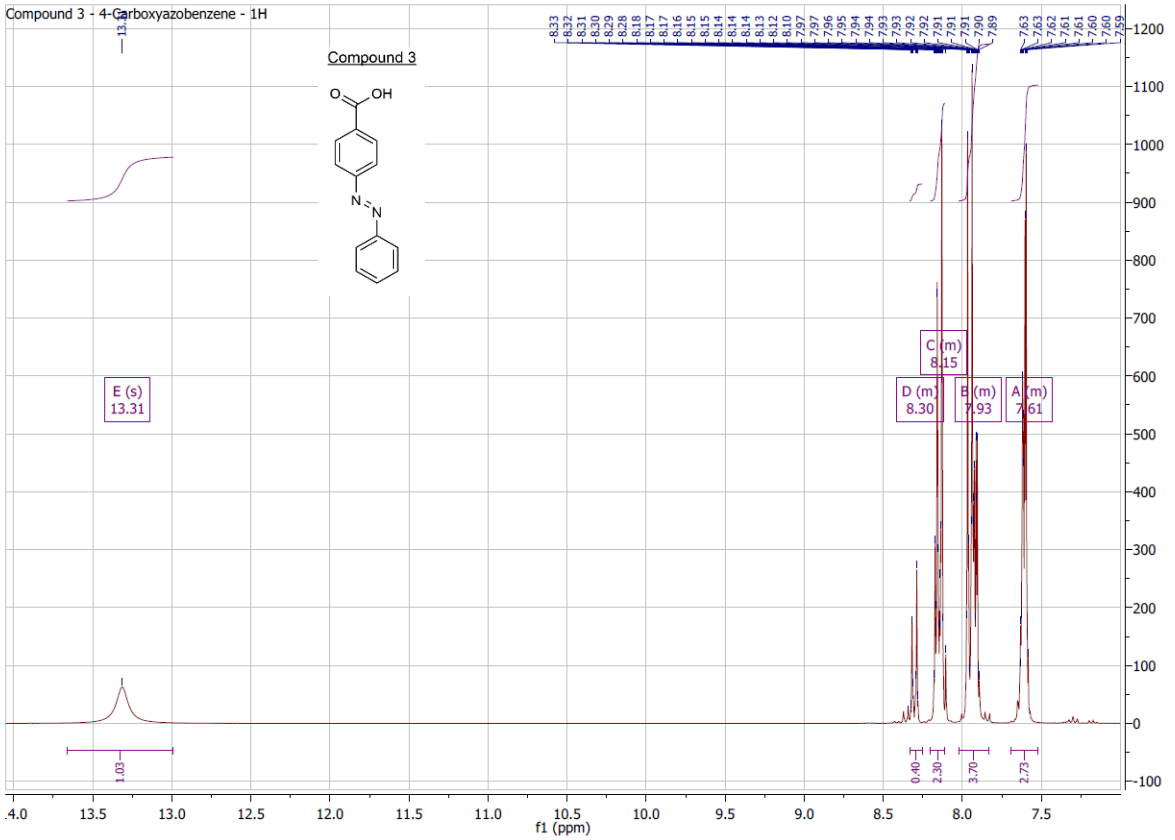
Compound 3 - 4-Carboxyazobenzene - 1H
Compound 3
E (s)
13.31
C (m)
8.15
D (m)
8.30
B (m)
7.93
A (m)
7.61
f1 (ppm)

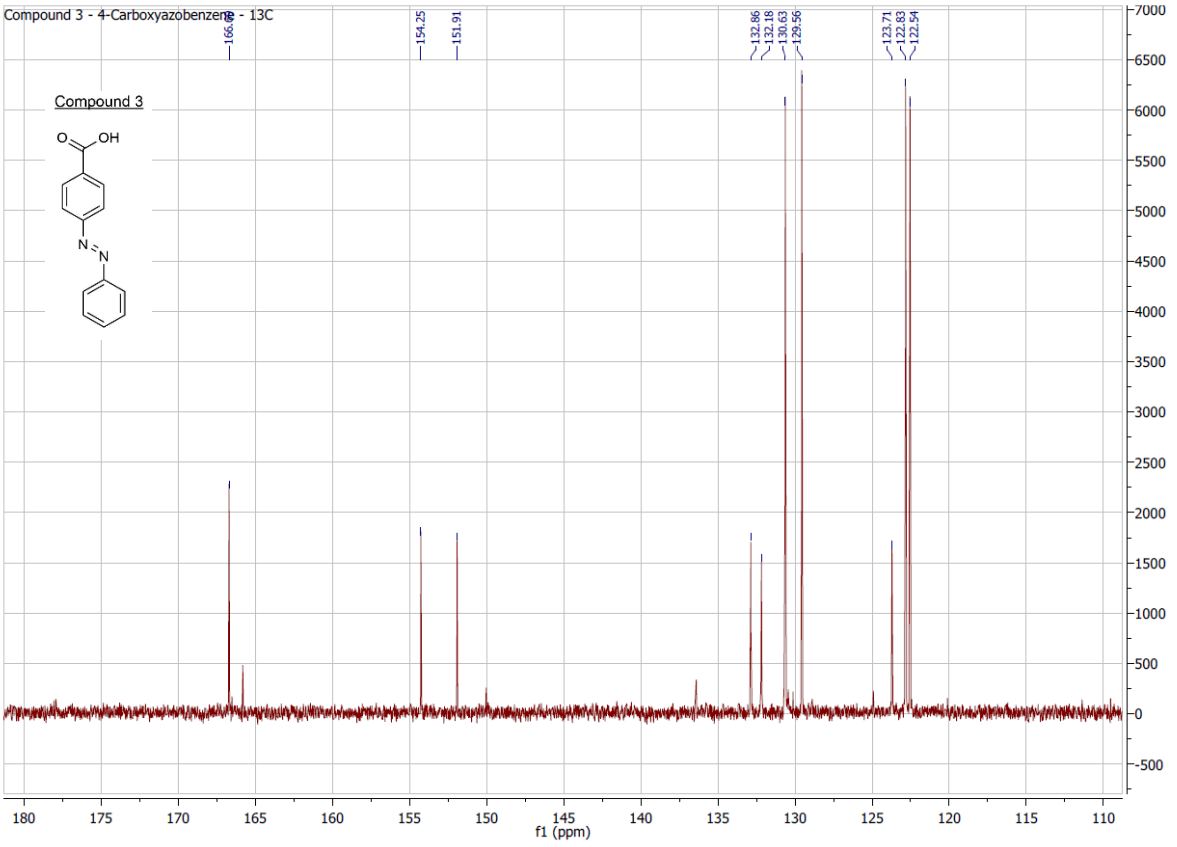
Compound 3 - 4-Carboxyazobenzene - 13C
Compound 3
f1 (ppm)

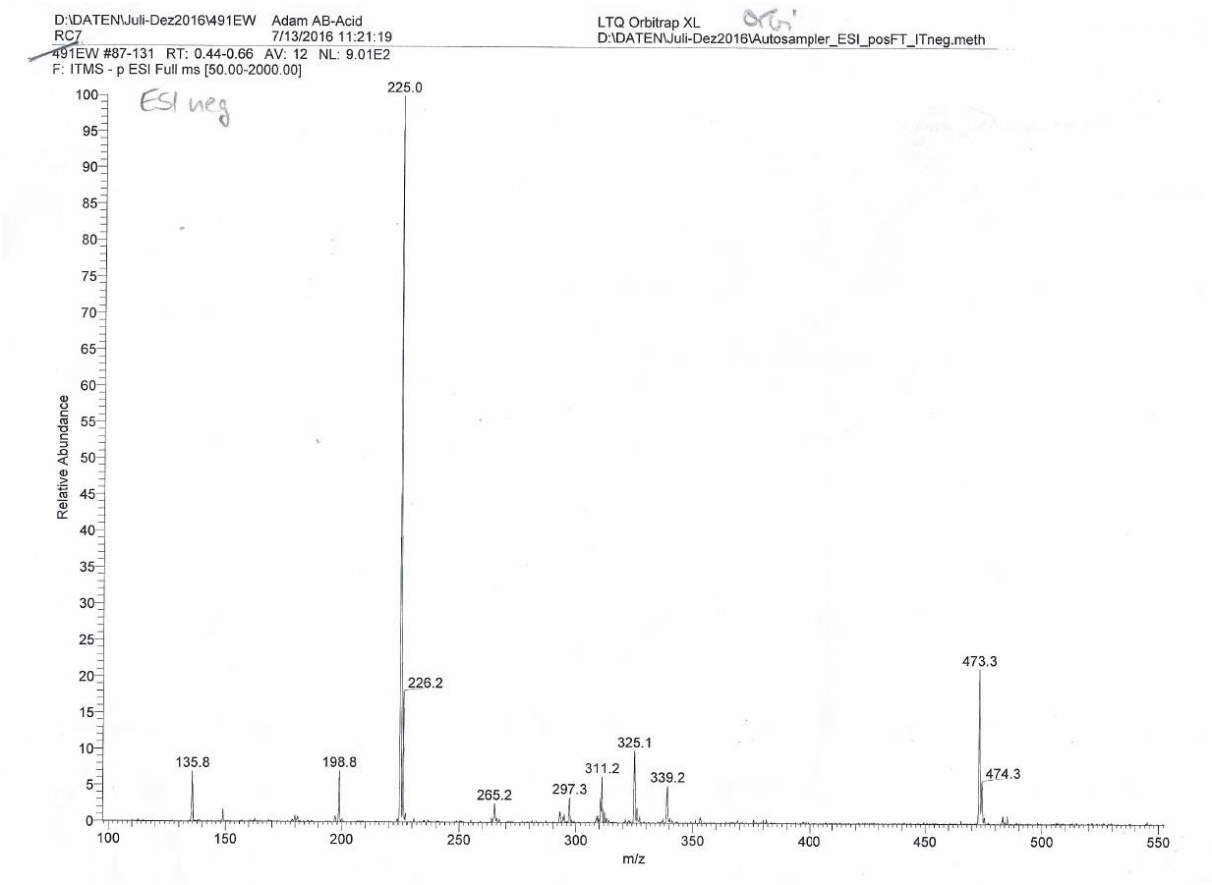
D:\DATEN\Juli-Dez2016\491EW Adam AB-Acid
RC7 7/13/2016 11:21:19
491EW #87-131 RT: 0.44-0.66 AV: 12 NL: 9.01E2
F: ITMS - p ESI Full ms [50.00-2000.00]
LTQ Orbitrap XL
D:\DATEN\Juli-Dez2016\Autosampler_ESI_posFT_ITneg.meth
ESI neg
Relative Abundance
m/z
225.0
226.2
135.8
198.8
265.2
297.3
311.2
325.1
339.2
473.3
474.3

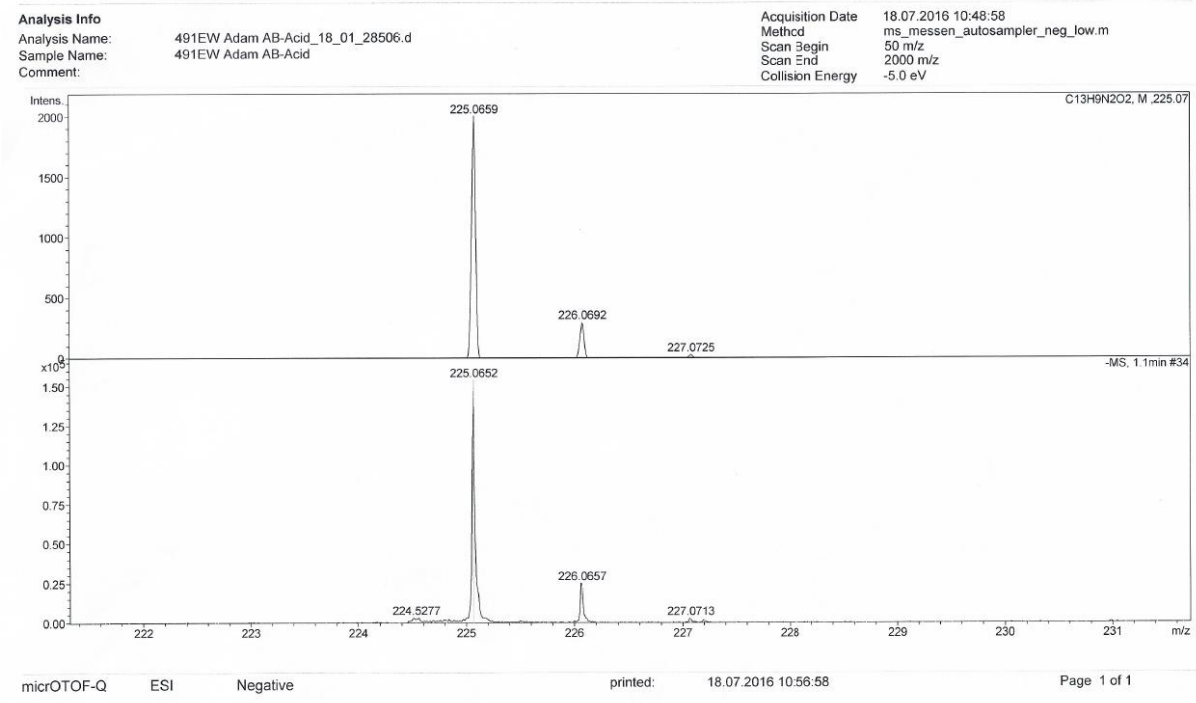
Analysis Info
Analysis Name: 491EW Adam AB-Acid_18_01_28506.d
Sample Name: 491EW Adam AB-Acid
Comment:
Acquisition Date 18.07.2016 10:48:58
Method ms_messen_autosampler_neg_low.m
Scan Begin 50 m/z
Scan End 2000 m/z
Collision Energy -5.0 eV
Intens.
C13H9N2O2, M ,225.07
225.0659
226.0692
227.0725
x10
-MS, 1.1min #34
225.0652
226.0657
224.5277
227.0713
m/z
micrOTOF-Q ESI Negative
printed: 18.07.2016 10:56:58
Page 1 of 1

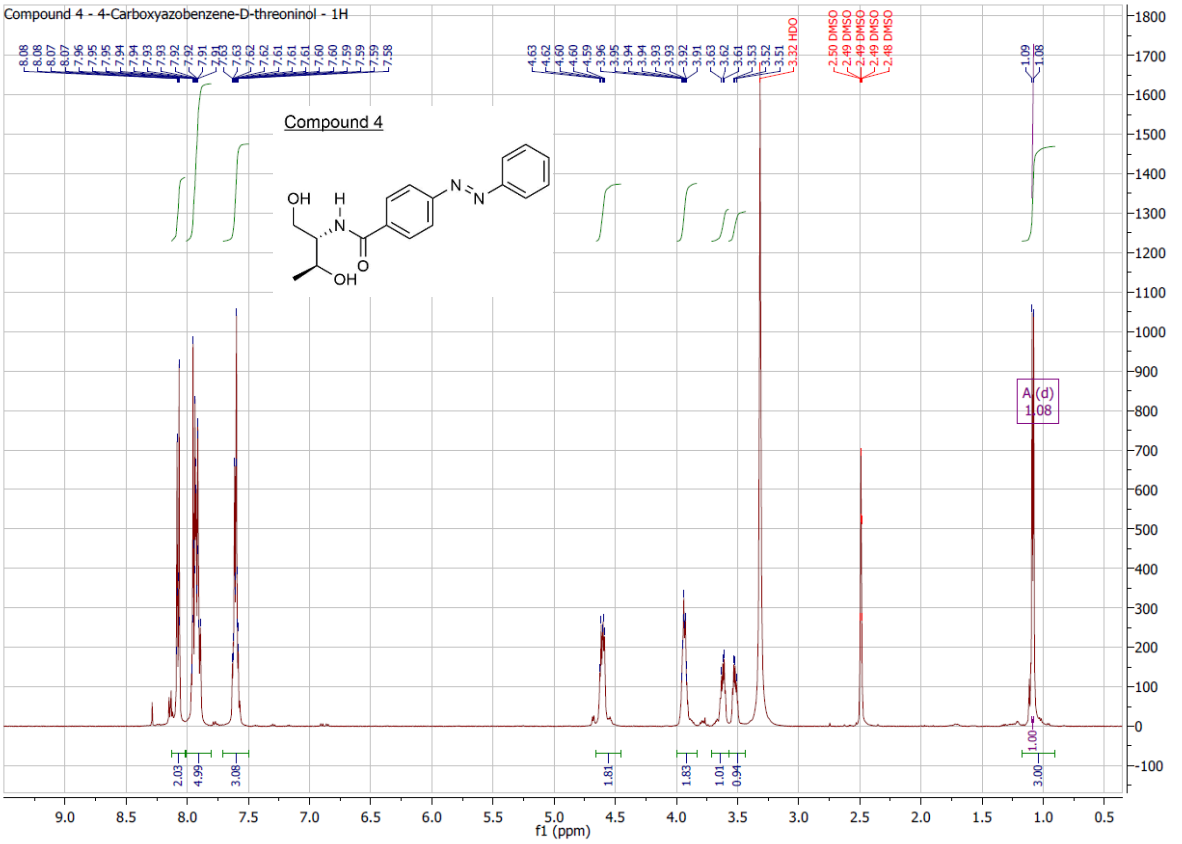
Compound 4 - 4-Carboxyazobenzene-D-threoninol - 1H
Compound 4
f1 (ppm)

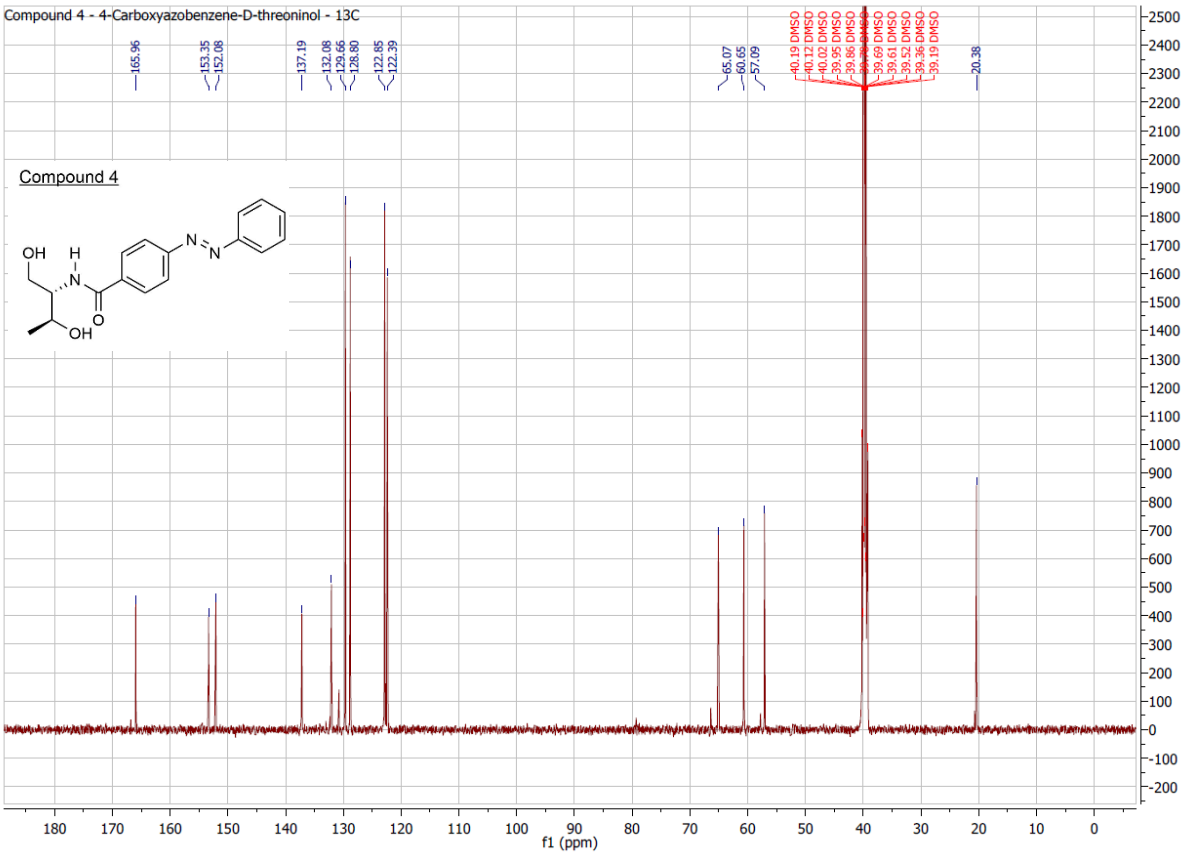
Compound 4 - 4-Carboxyazobenzene-D-threoninol - 13C
Compound 4
f1 (ppm)

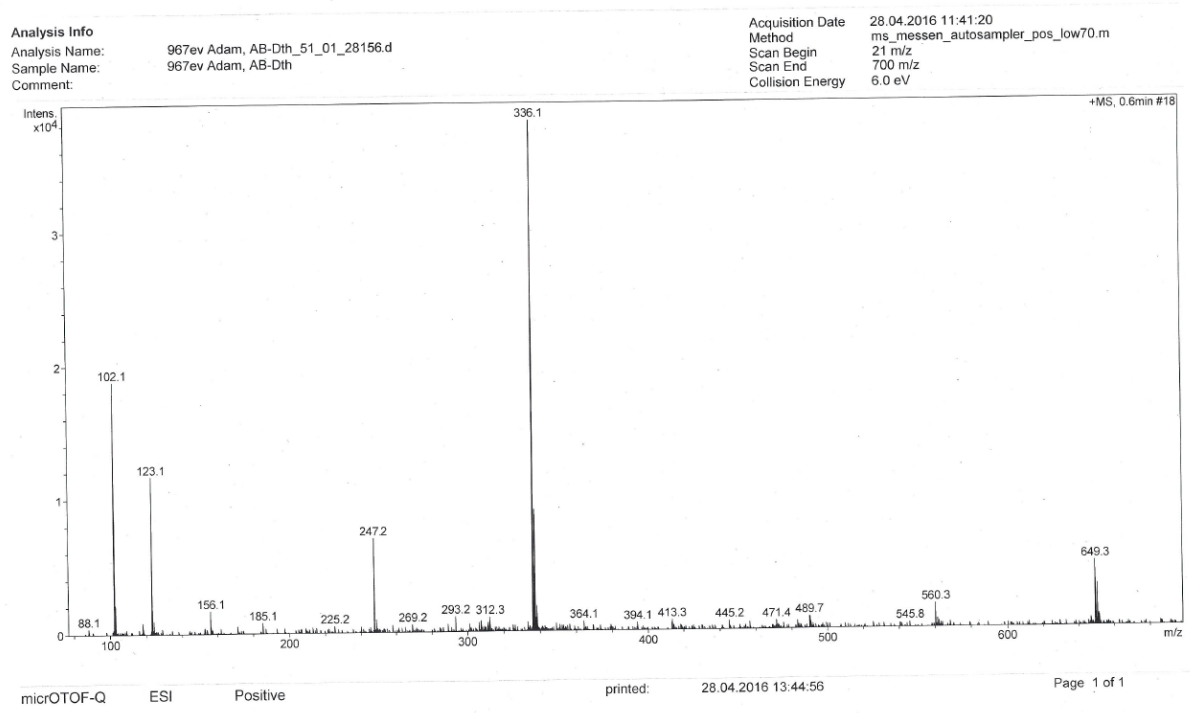
Analysis Info
Analysis Name: 967ev Adam, AB-Dth_51_01_28156.d
Sample Name: 967ev Adam, AB-Dth
Comment:
Acquisition Date 28.04.2016 11:41:20
Method ms_messen_autosampler_pos_low70.m
Scan Begin 21 m/z
Scan End 700 m/z
Collision Energy 6.0 eV
+MS, 0.6min #18
Intens.
x10^4
336.1
102.1
123.1
247.2
649.3
560.3
156.1
185.1
225.2
269.2
293.2
312.3
364.1
394.1
413.3
445.2
471.4
489.7
545.8
88.1
m/z
micrOTOF-Q ESI Positive
printed: 28.04.2016 13:44:56
Page 1 of 1

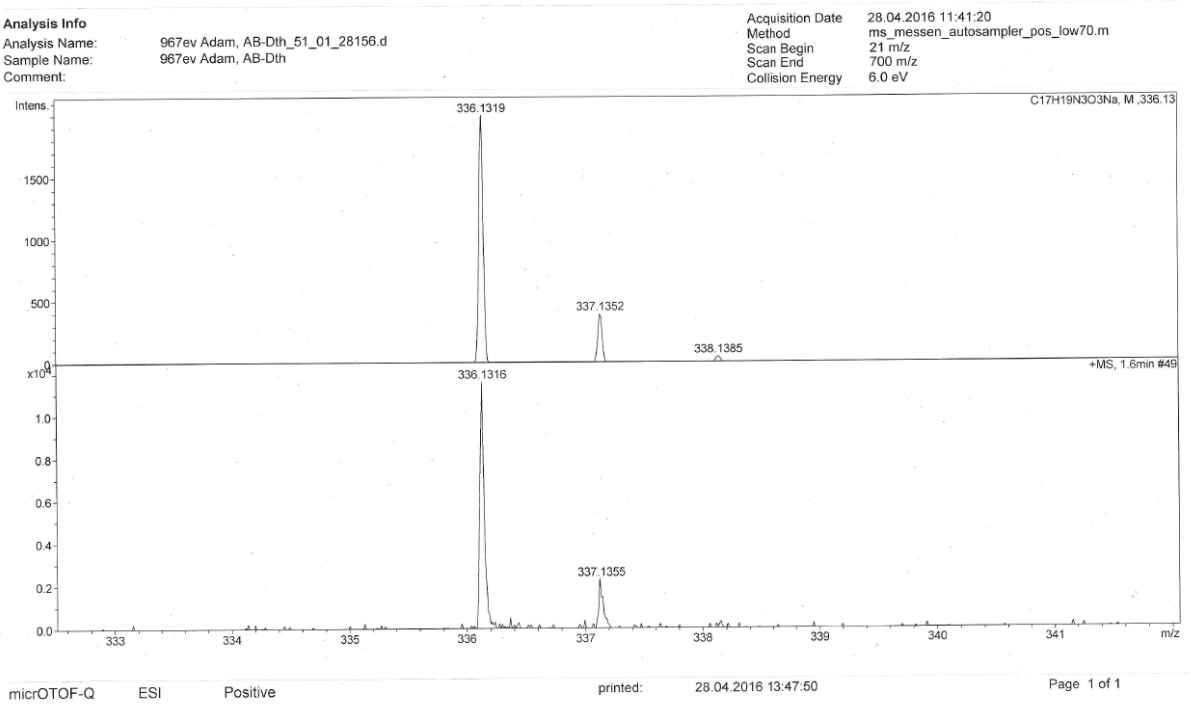
Analysis Info
Analysis Name: 967ev Adam, AB-Dth_51_01_28156.d
Sample Name: 967ev Adam, AB-Dth
Comment:
Acquisition Date 28.04.2016 11:41:20
Method ms_messen_autosampler_pos_low70.m
Scan Begin 21 m/z
Scan End 700 m/z
Collision Energy 6.0 eV
C17H19N3O3Na, M ,336.13
Intens.
336.1319
337.1352
338.1385
+MS, 1.6min #49
x10^4
336.1316
337.1355
m/z
micrOTOF-Q ESI Positive
printed: 28.04.2016 13:47:50
Page 1 of 1

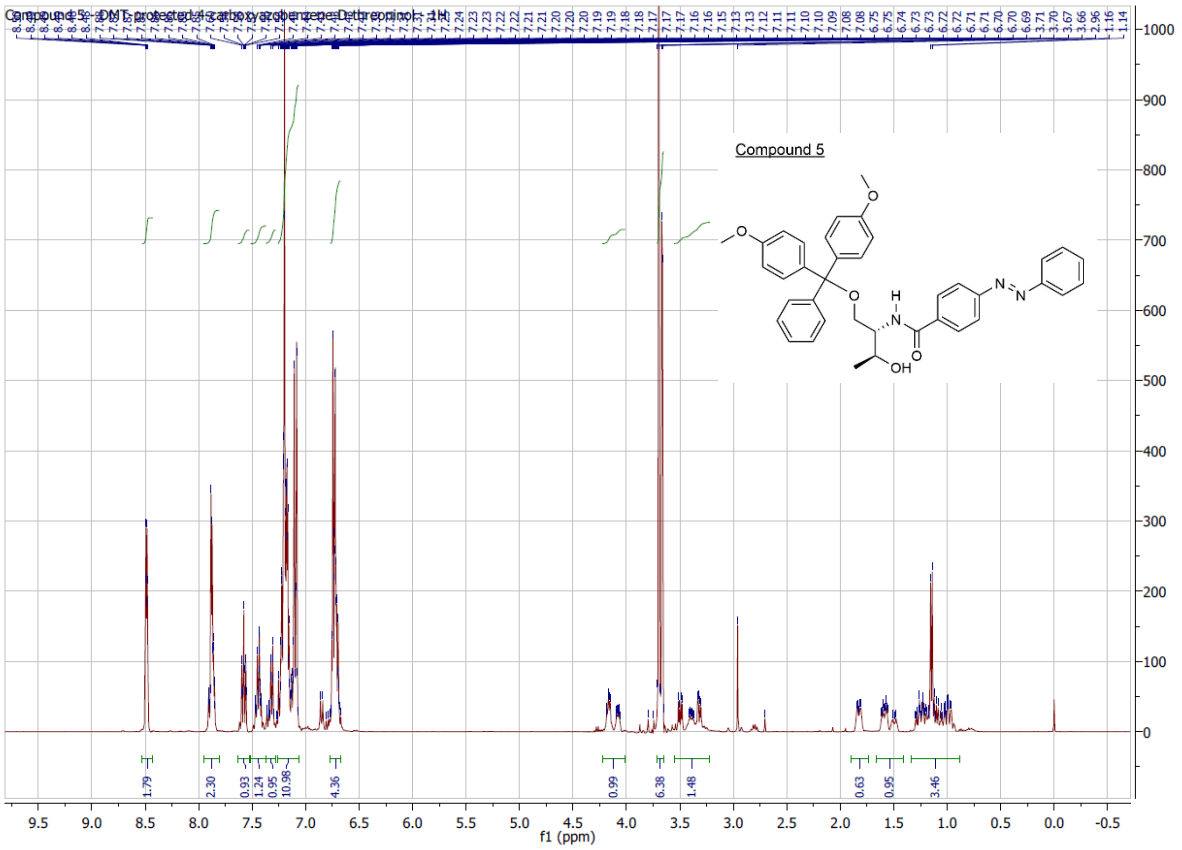
Compound 5 - DMT-protected 4-carboxyazobenzene-D-threoninol - 1H
Compound 5
f1 (ppm)

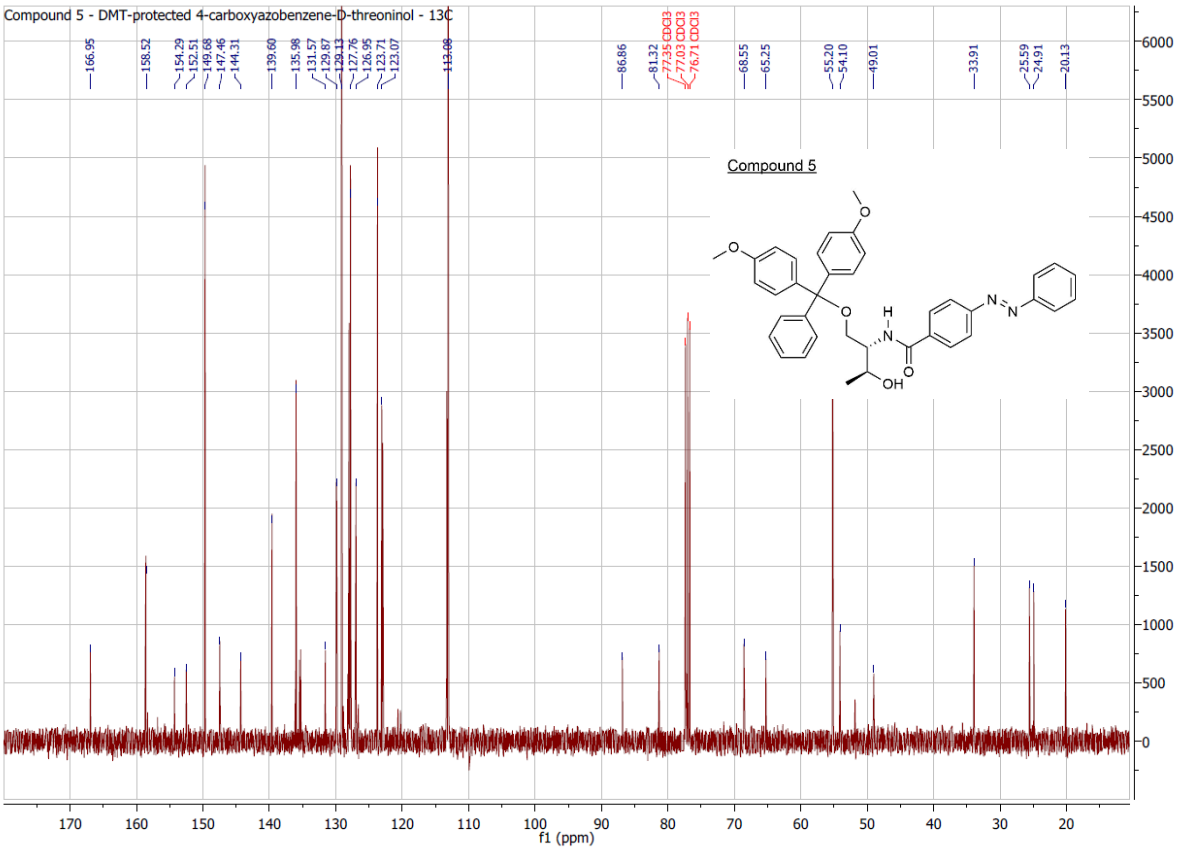
Compound 5 - DMT-protected 4-carboxyazobenzene-D-threoninol - 13C
Compound 5
f1 (ppm)

Analysis Info

Analysis Name: 446ER Adam VA-114_61_01_24269.d
Sample Name: 446ER Adam VA-114
Comment:

Acquisition Date 7/8/2014 10:44:19 AM
Method ms_messen_autosampler_pos_low.m
Scan Begin 50 m/z
Scan End 2000 m/z
Collision Energy 6.0 eV

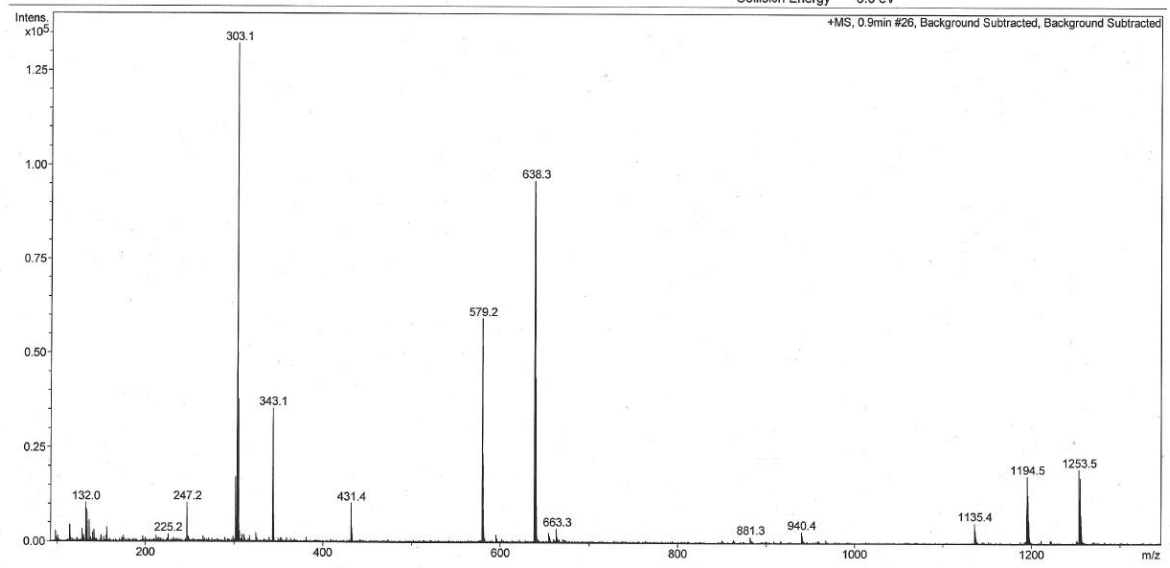

micrOTOF-Q ESI Positive printed: 7/8/2014 11:06:16 AM Page 1 of 1

Analysis Info

Analysis Name: 446ER Adam VA-114_61_01_24269.d
Sample Name: 446ER Adam VA-114
Comment:

Acquisition Date 7/8/2014 10:44:19 AM
Method ms_messen_autosampler_pos_low.m
Scan Begin 50 m/z
Scan End 2000 m/z
Collision Energy 6.0 eV

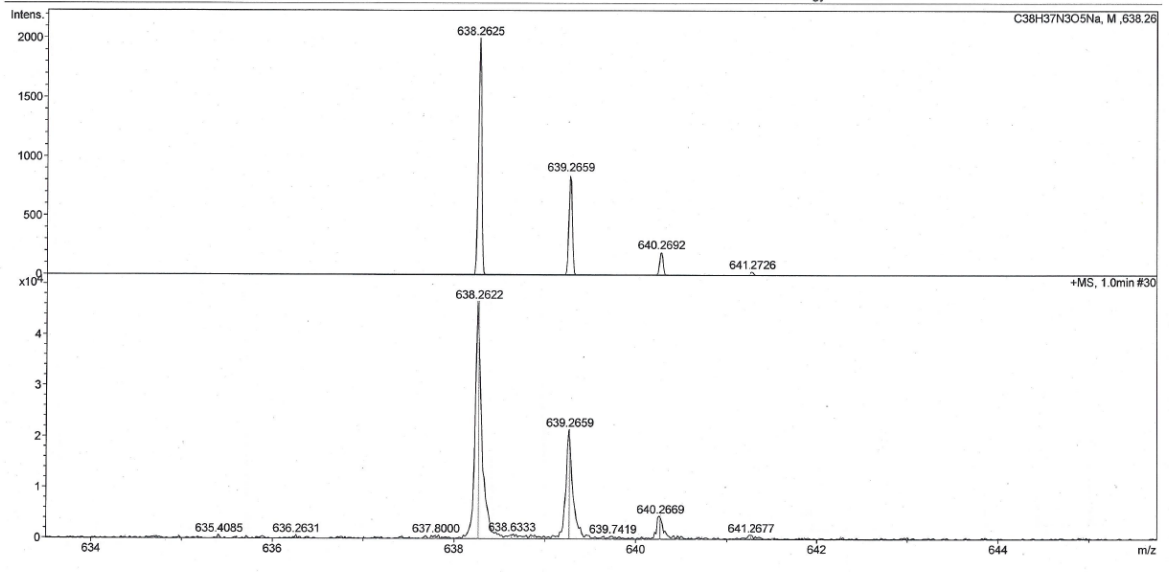

micrOTOF-Q ESI Positive printed: 7/8/2014 11:05:20 AM Page 1 of 1

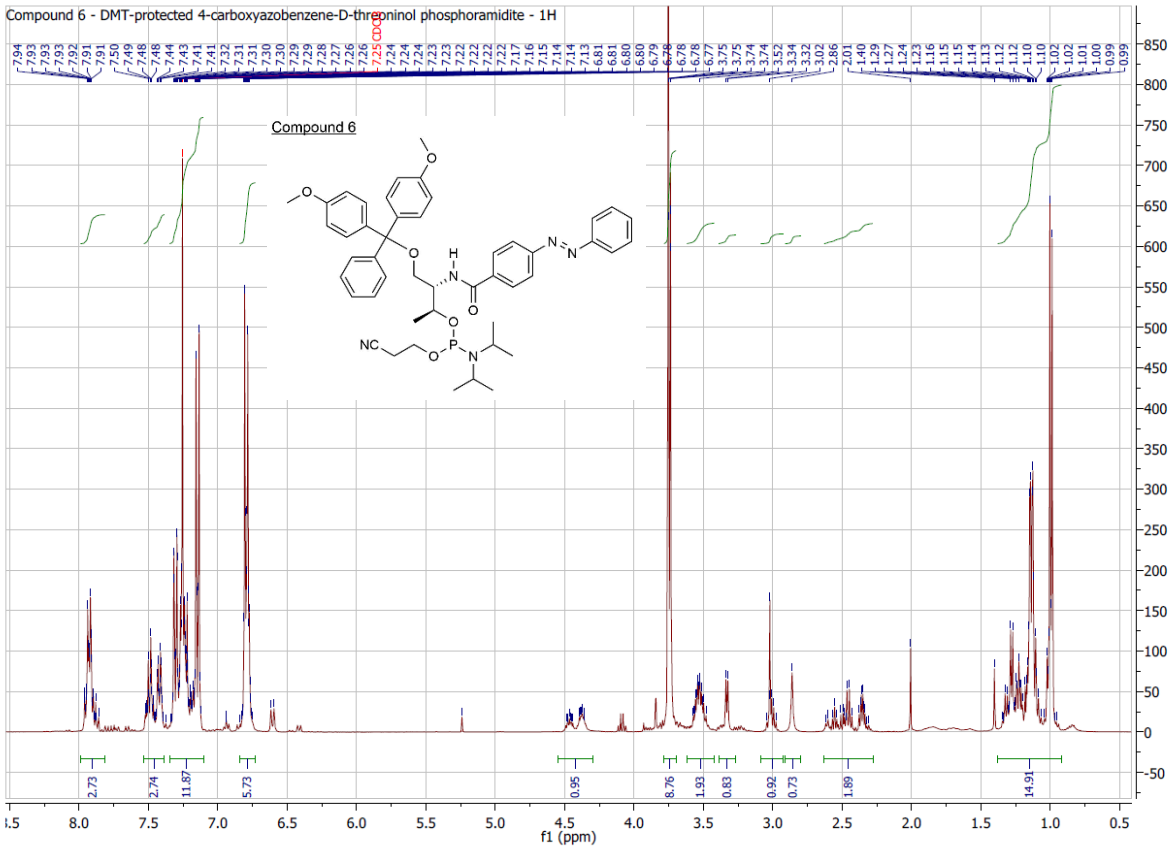
Compound 6 - DMT-protected 4-carboxyazobenzene-D-threoninol phosphoramidite - 1H
Compound 6
f1 (ppm)

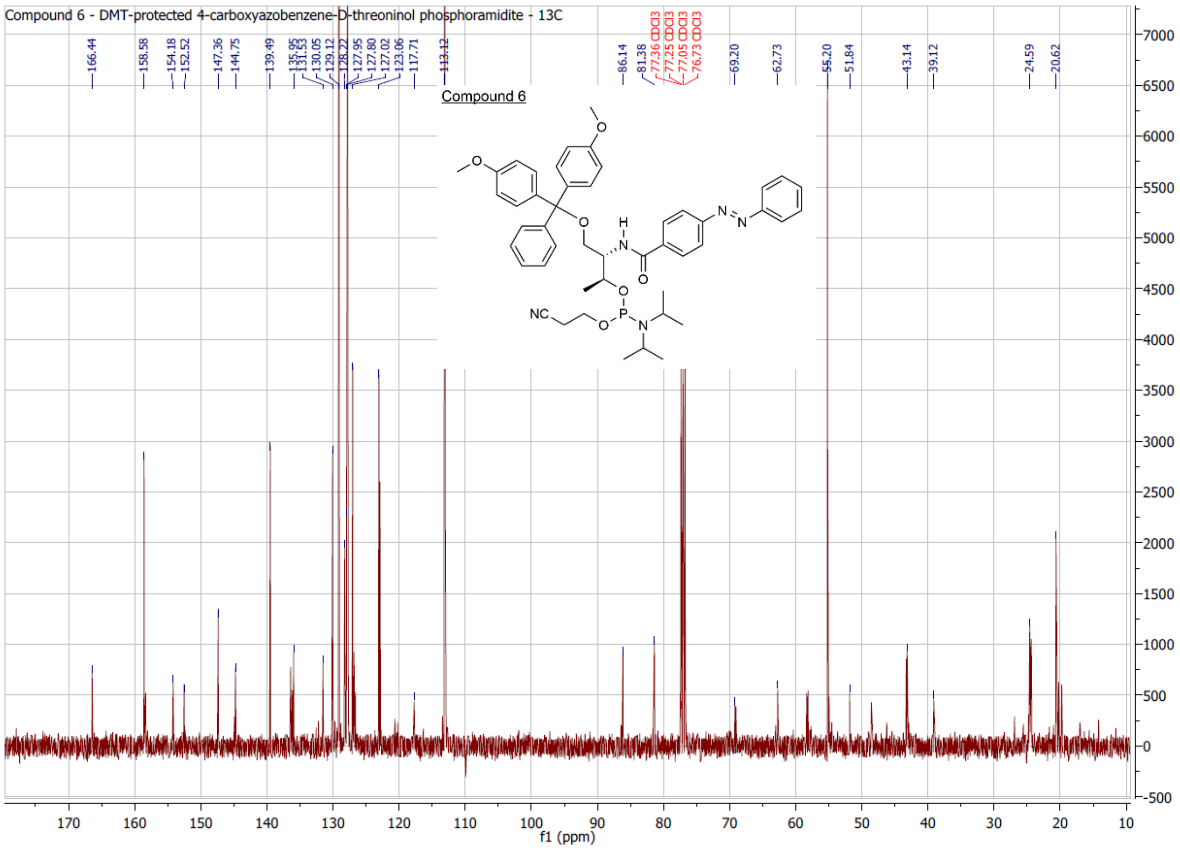
Compound 6 - DMT-protected 4-carboxyazobenzene-D-threoninol phosphoramidite - 13C
Compound 6
f1 (ppm)

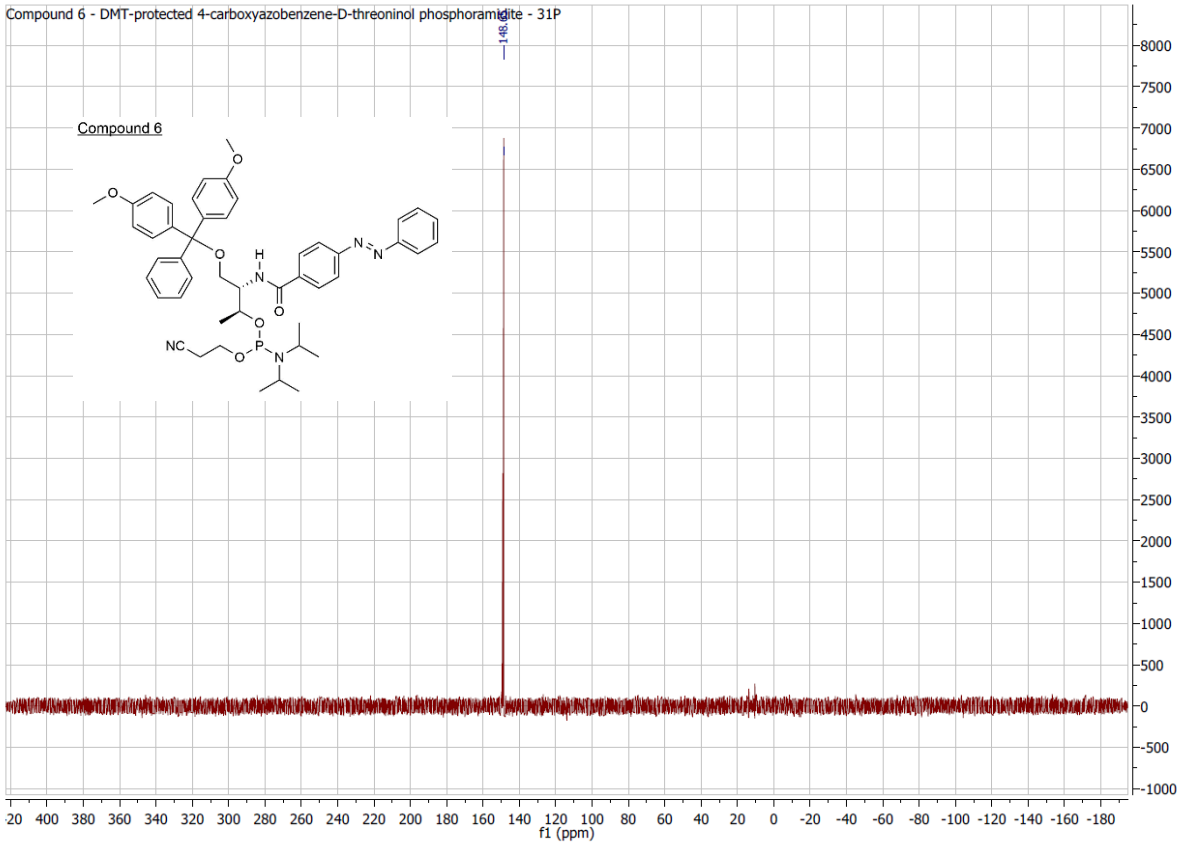
Compound 6 - DMT-protected 4-carboxyazobenzene-D-threoninol phosphoramidite - 31P
Compound 6
f1 (ppm)

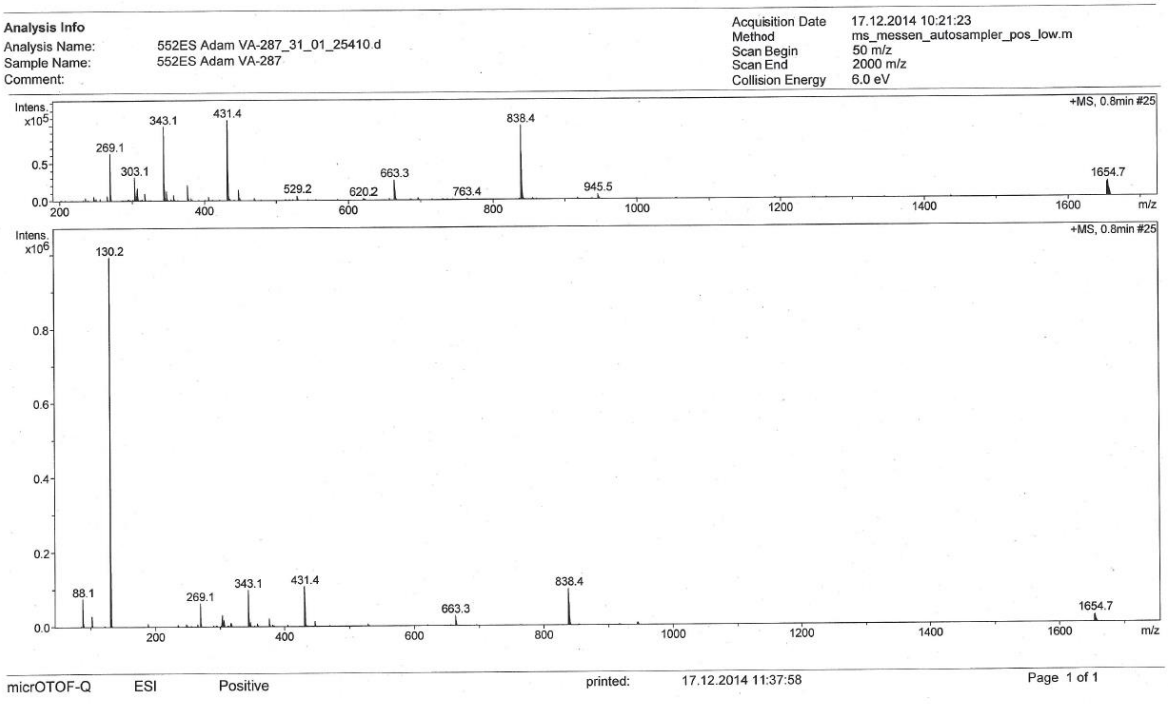
Analysis Info
Analysis Name: 552ES Adam VA-287_31_01_25410.d
Sample Name: 552ES Adam VA-287
Comment:
Acquisition Date 17.12.2014 10:21:23
Method ms_messen_autosampler_pos_low.m
Scan Begin 50 m/z
Scan End 2000 m/z
Collision Energy 6.0 eV
+MS, 0.8min #25
130.2
88.1
269.1
303.1
343.1
431.4
529.2
620.2
663.3
763.4
838.4
945.5
1654.7
m/z
micrOTOF-Q ESI Positive
printed: 17.12.2014 11:37:58
Page 1 of 1

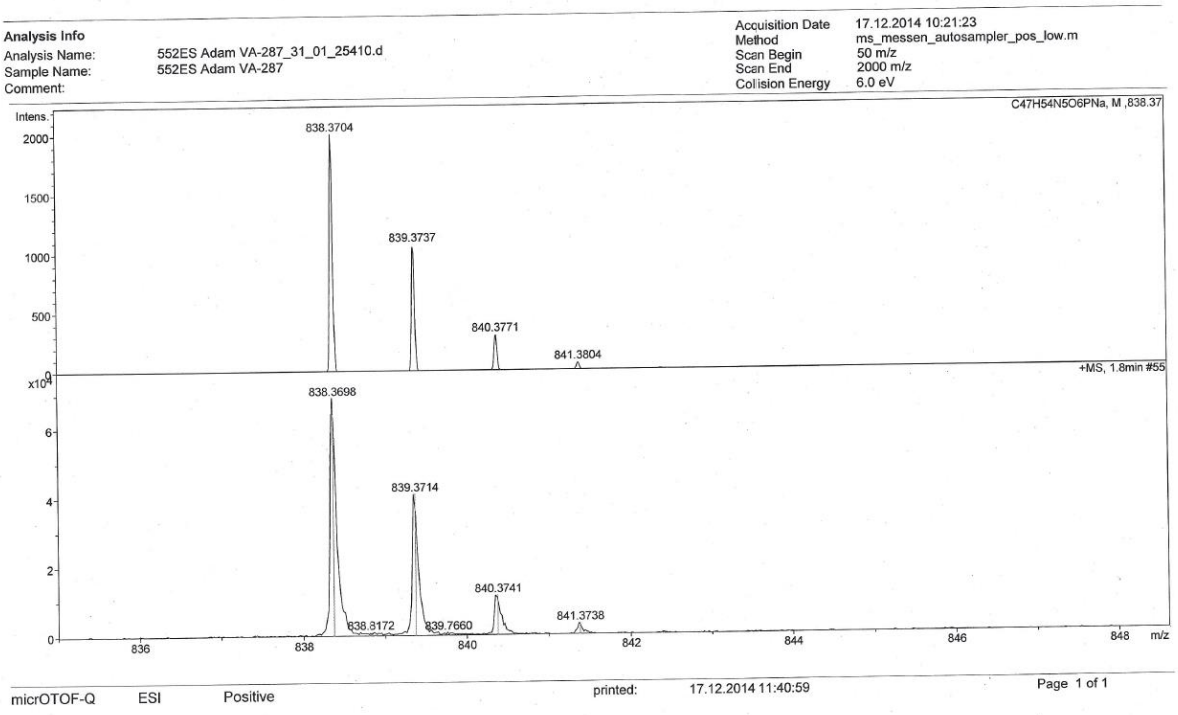
Analysis Info
Analysis Name: 552ES Adam VA-287_31_01_25410.d
Sample Name: 552ES Adam VA-287
Comment:
Accuisition Date 17.12.2014 10:21:23
Method ms_messen_autosampler_pos_low.m
Scan Begin 50 m/z
Scan End 2000 m/z
Collision Energy 6.0 eV
C47H54N5O6PNa, M ,838.37
Intens.
838.3704
839.3737
840.3771
841.3804
+MS, 1.8min #55
x10^4
838.3698
839.3714
840.3741
841.3738
838.3172
839.7660
m/z
micrOTOF-Q ESI Positive
printed: 17.12.2014 11:40:59
Page 1 of 1

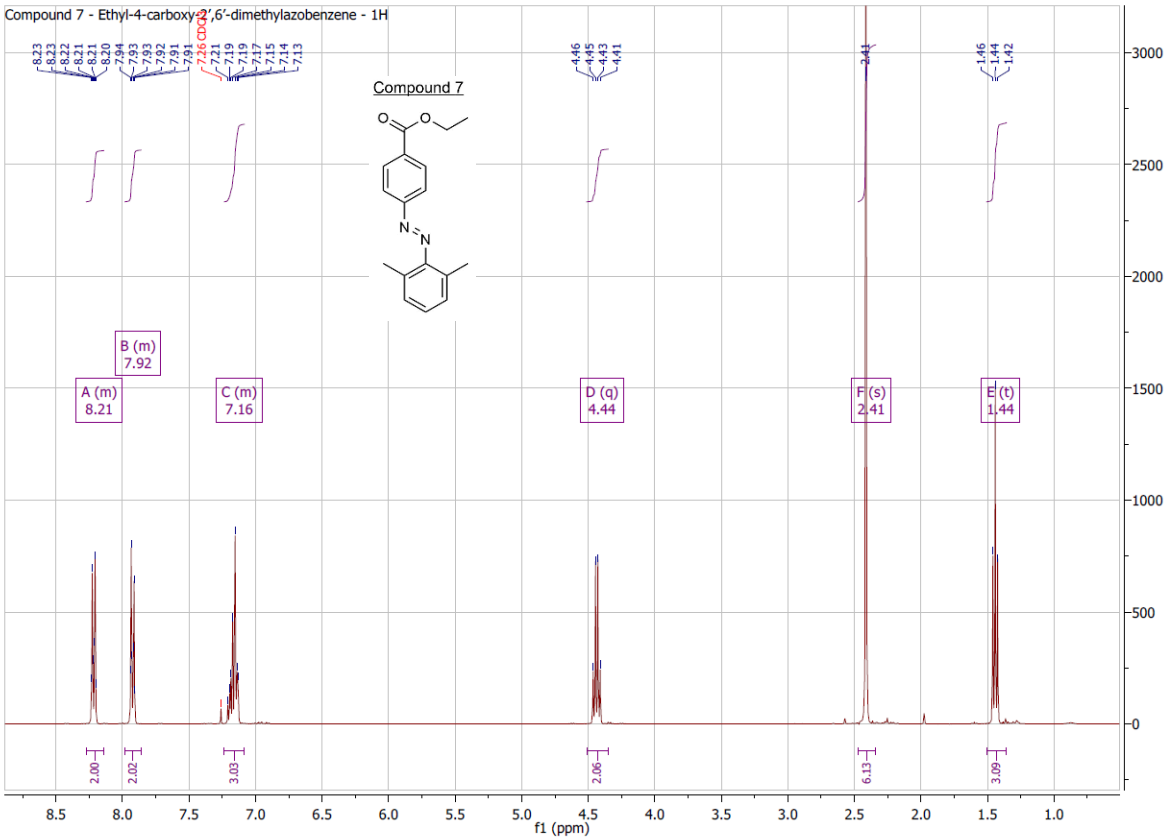
Compound 7 - Ethyl-4-carboxy-2′,6′-dimethylazobenzene - 1H
Compound 7
B (m)
7.92
A (m)
8.21
C (m)
7.16
D (q)
4.44
F (s)
2.41
E (t)
1.44
f1 (ppm)

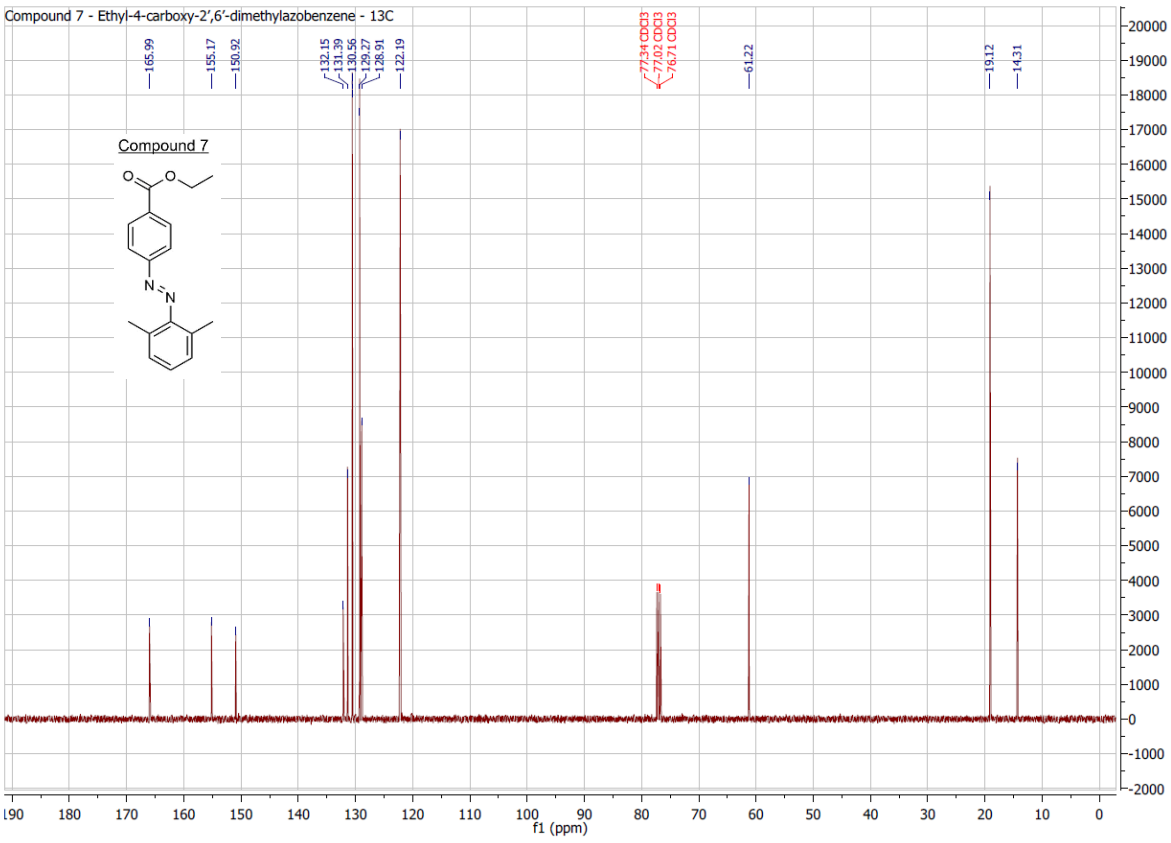
Compound 7 - Ethyl-4-carboxy-2′,6′-dimethylazobenzene - 13C
Compound 7
f1 (ppm)

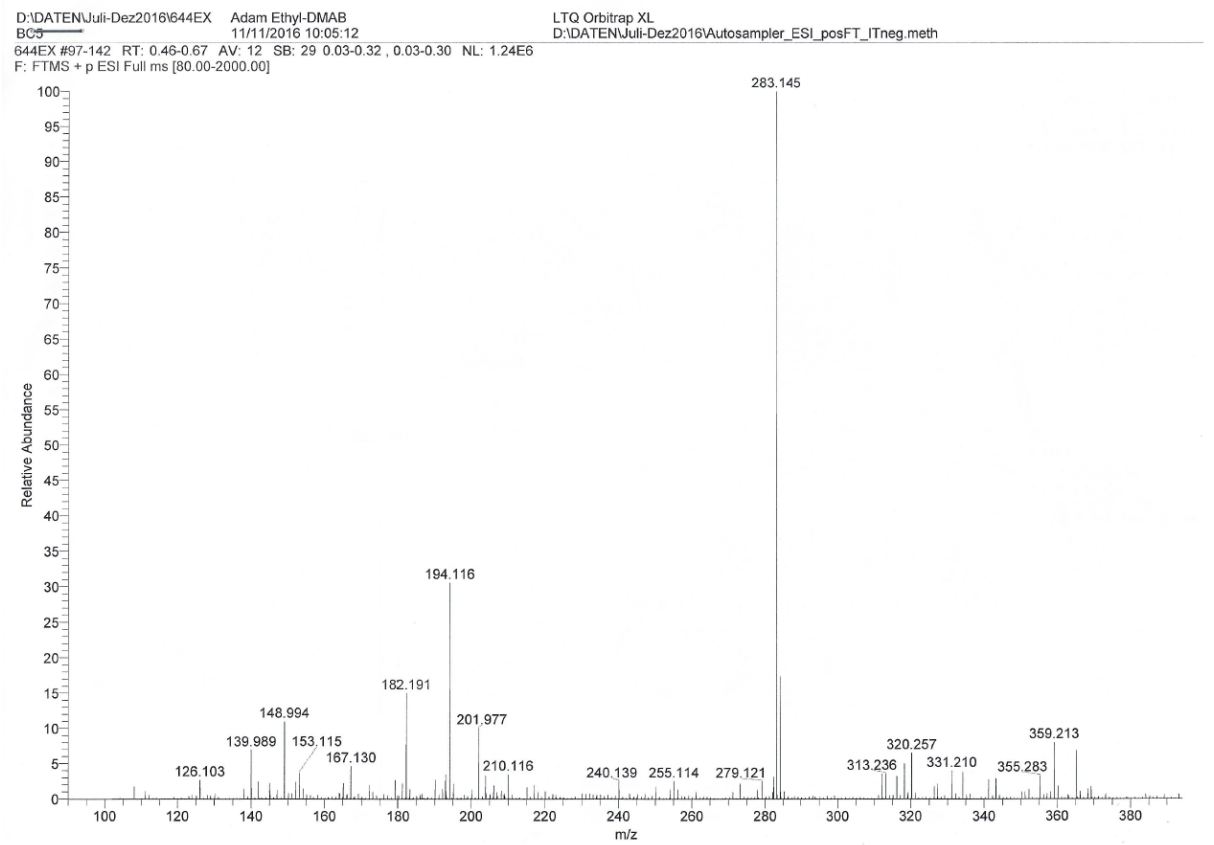
D:\DATEN\Juli-Dez2016\644EX Adam Ethyl-DMAB
11/11/2016 10:05:12
LTQ Orbitrap XL
D:\DATEN\Juli-Dez2016\Autosampler_ESI_posFT_ITneg.meth
644EX #97-142 RT: 0.46-0.67 AV: 12 SB: 29 0.03-0.32 , 0.03-0.30 NL: 1.24E6
F: FTMS + p ESI Full ms [80.00-2000.00]
283.145
194.116
182.191
148.994
201.977
139.989
153.115
167.130
126.103
210.116
240.139
255.114
279.121
313.236
320.257
331.210
355.283
359.213
Relative Abundance
m/z

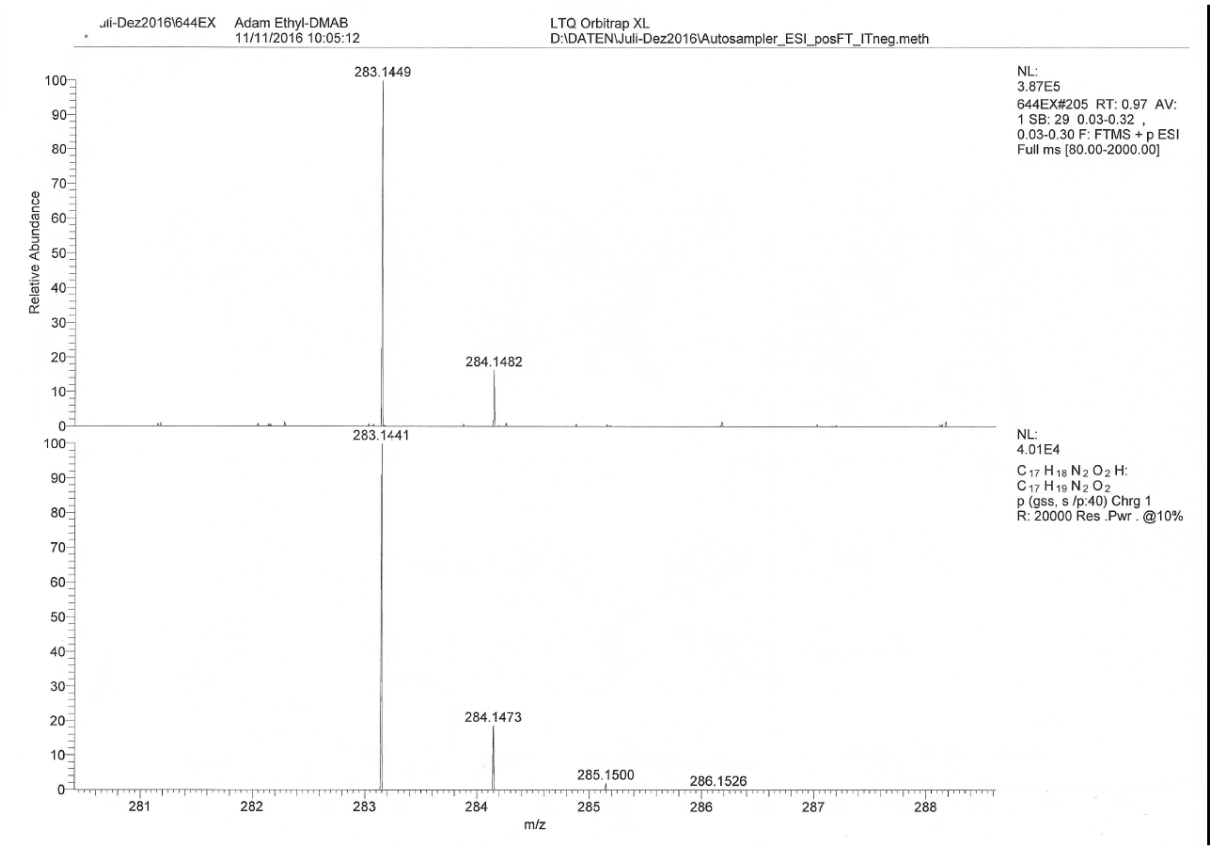
Juli-Dez2016\644EX Adam Ethyl-DMAB
11/11/2016 10:05:12
LTQ Orbitrap XL
D:\DATEN\Juli-Dez2016\Autosampler_ESI_posFT_ITneg.meth
283.1449
284.1482
NL:
3.87E5
644EX#205 RT: 0.97 AV:
1 SB: 29 0.03-0.32 ,
0.03-0.30 F: FTMS + p ESI
Full ms [80.00-2000.00]
283.1441
284.1473
285.1500
286.1526
NL:
4.01E4
C17 H18 N2 O2 H:
C17 H19 N2 O2
p (gss, s /p:40) Chrg 1
R: 20000 Res .Pwr . @10%
Relative Abundance
m/z

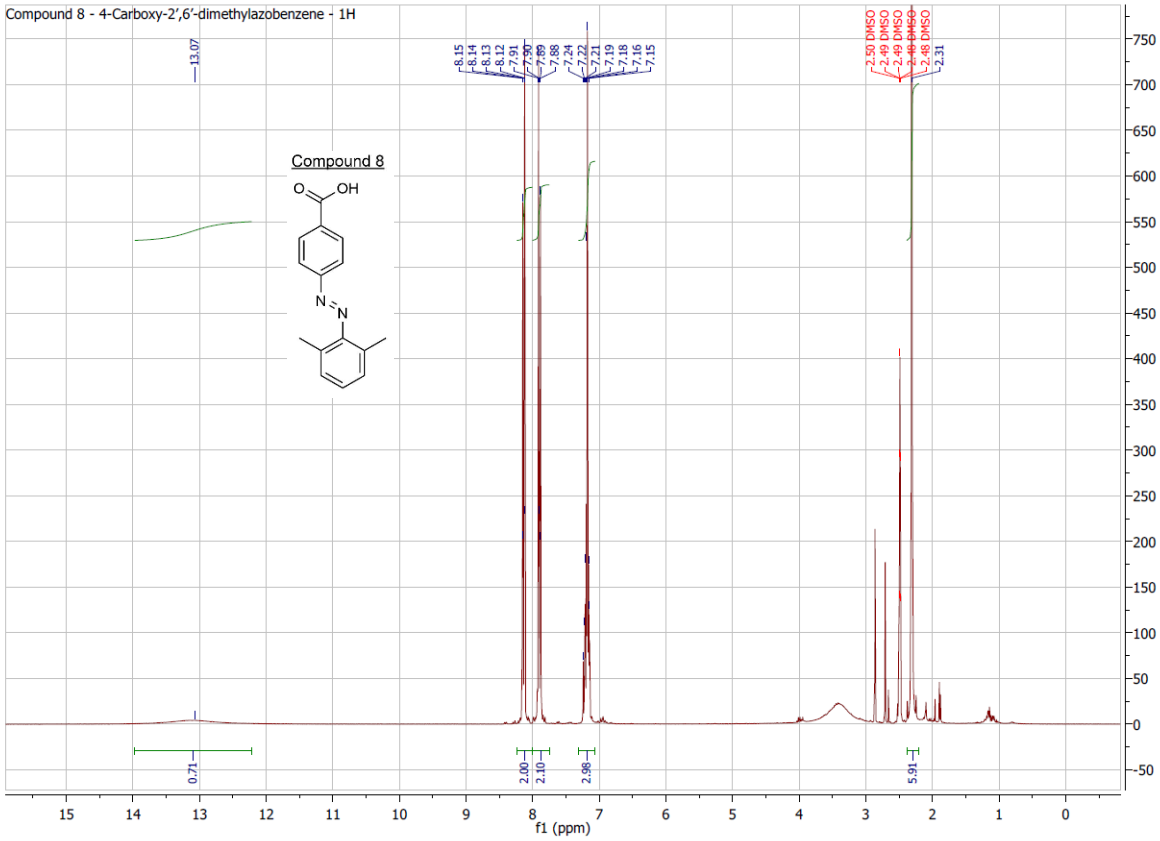
Compound 8 - 4-Carboxy-2',6'-dimethylazobenzene - 1H
Compound 8
f1 (ppm)

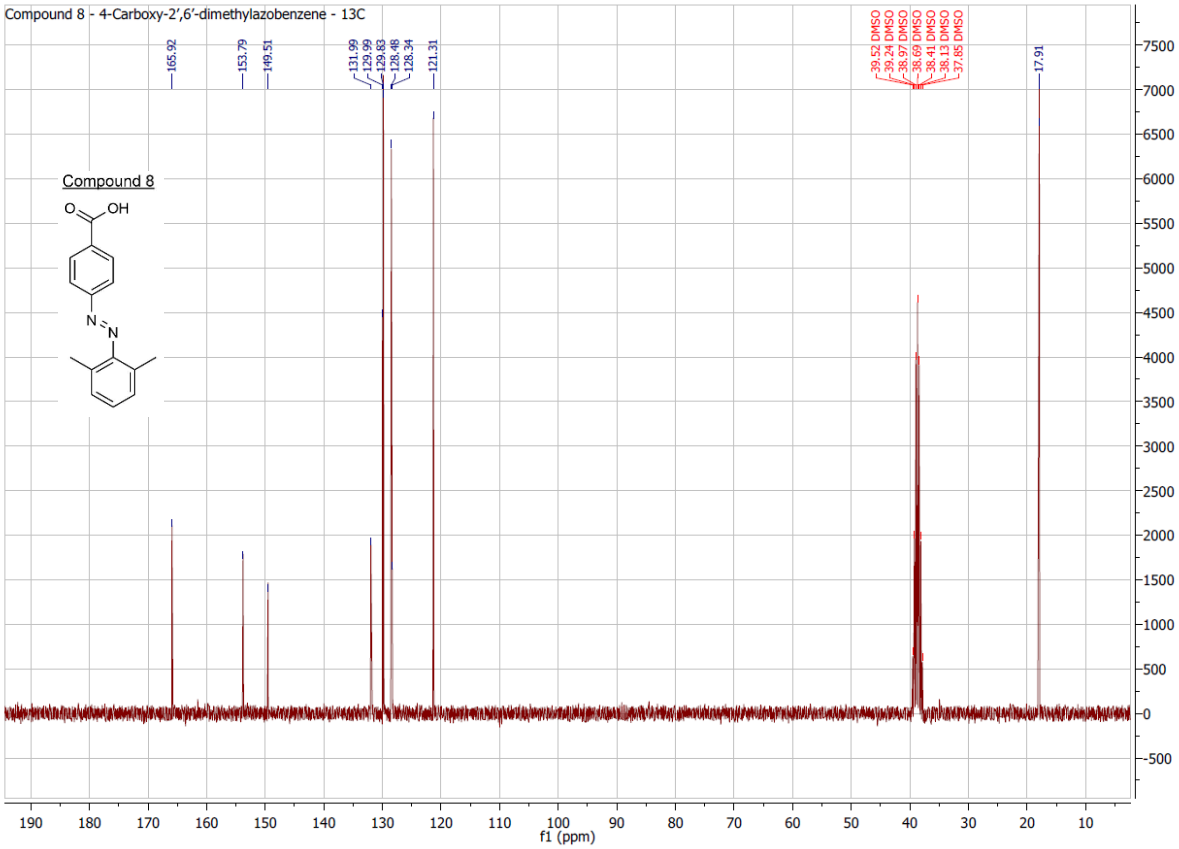
Compound 8 - 4-Carboxy-2',6'-dimethylazobenzene - 13C
Compound 8
f1 (ppm)

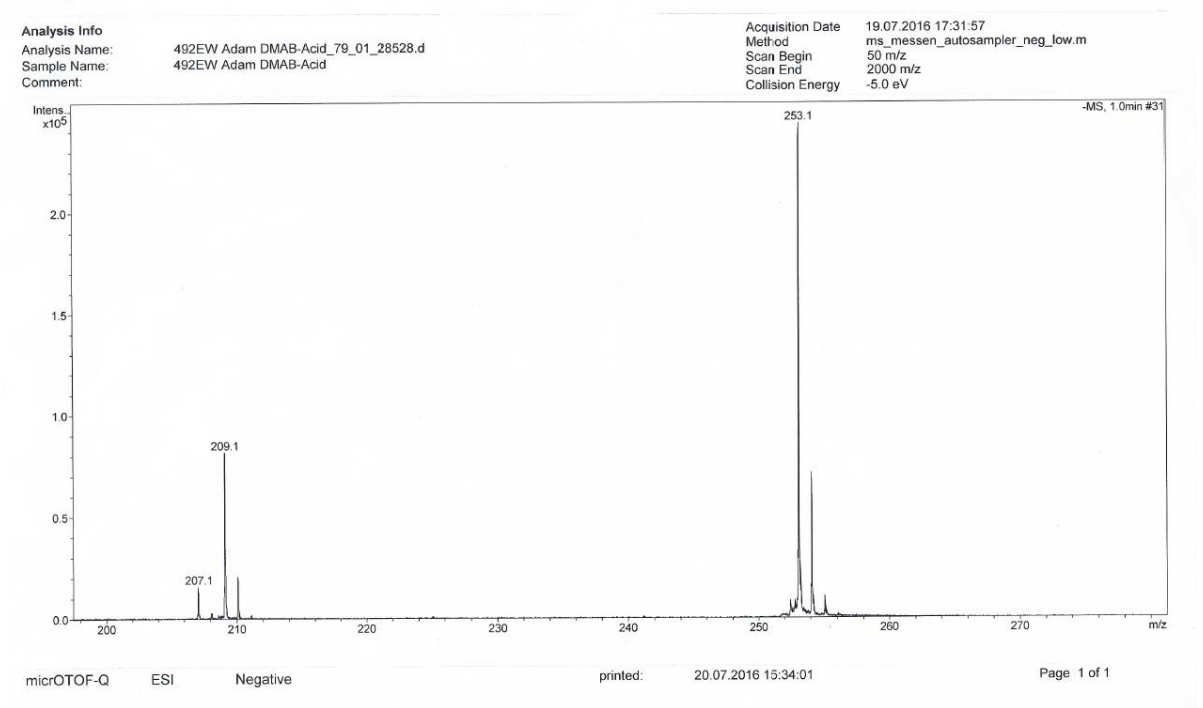
Analysis Info
Analysis Name: 492EW Adam DMAB-Acid_79_01_28528.d
Sample Name: 492EW Adam DMAB-Acid
Comment:
Acquisition Date 19.07.2016 17:31:57
Method ms_messen_autosampler_neg_low.m
Scan Begin 50 m/z
Scan End 2000 m/z
Collision Energy -5.0 eV
Intens. x10^5
-MS, 1.0min #31
253.1
209.1
207.1
m/z
micrOTOF-Q ESI Negative
printed: 20.07.2016 15:34:01
Page 1 of 1

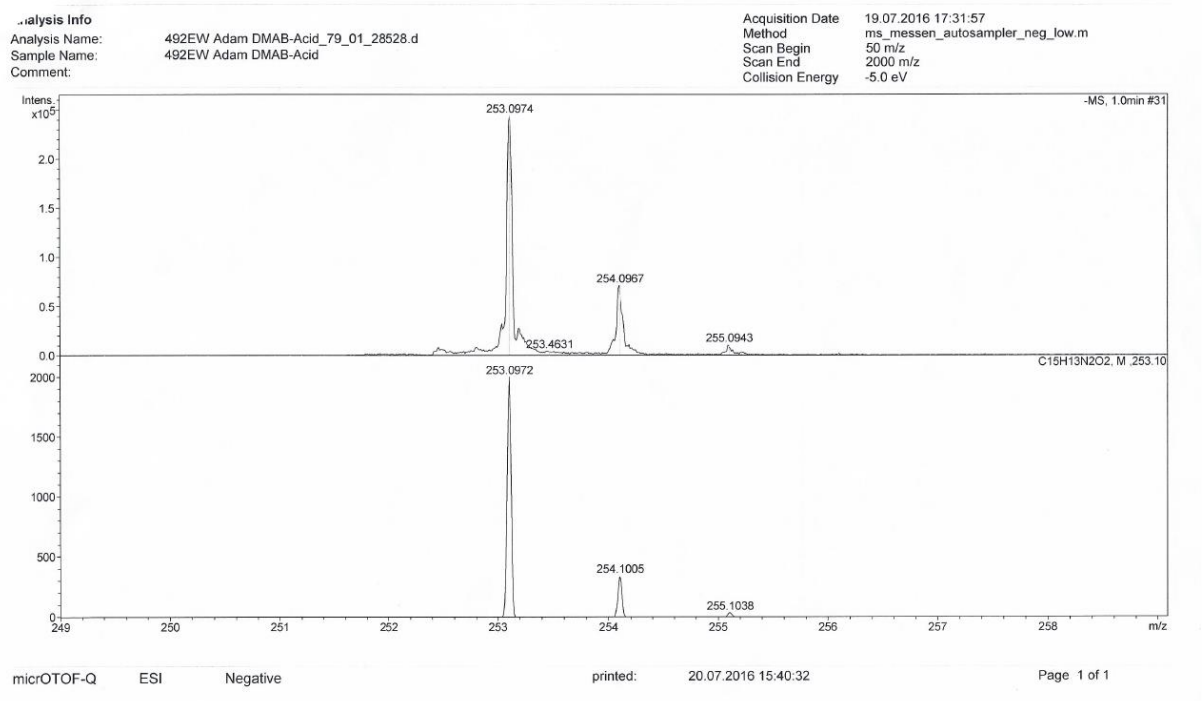
Analysis Info
Analysis Name: 492EW Adam DMAB-Acid_79_01_28528.d
Sample Name: 492EW Adam DMAB-Acid
Comment:
Acquisition Date 19.07.2016 17:31:57
Method ms_messen_autosampler_neg_low.m
Scan Begin 50 m/z
Scan End 2000 m/z
Collision Energy -5.0 eV
Intens. x10^5
-MS, 1.0min #31
253.0974
254.0967
253.4631
255.0943
C15H13N2O2, M ,253.10
253.0972
254.1005
255.1038
m/z
micrOTOF-Q ESI Negative
printed: 20.07.2016 15:40:32
Page 1 of 1

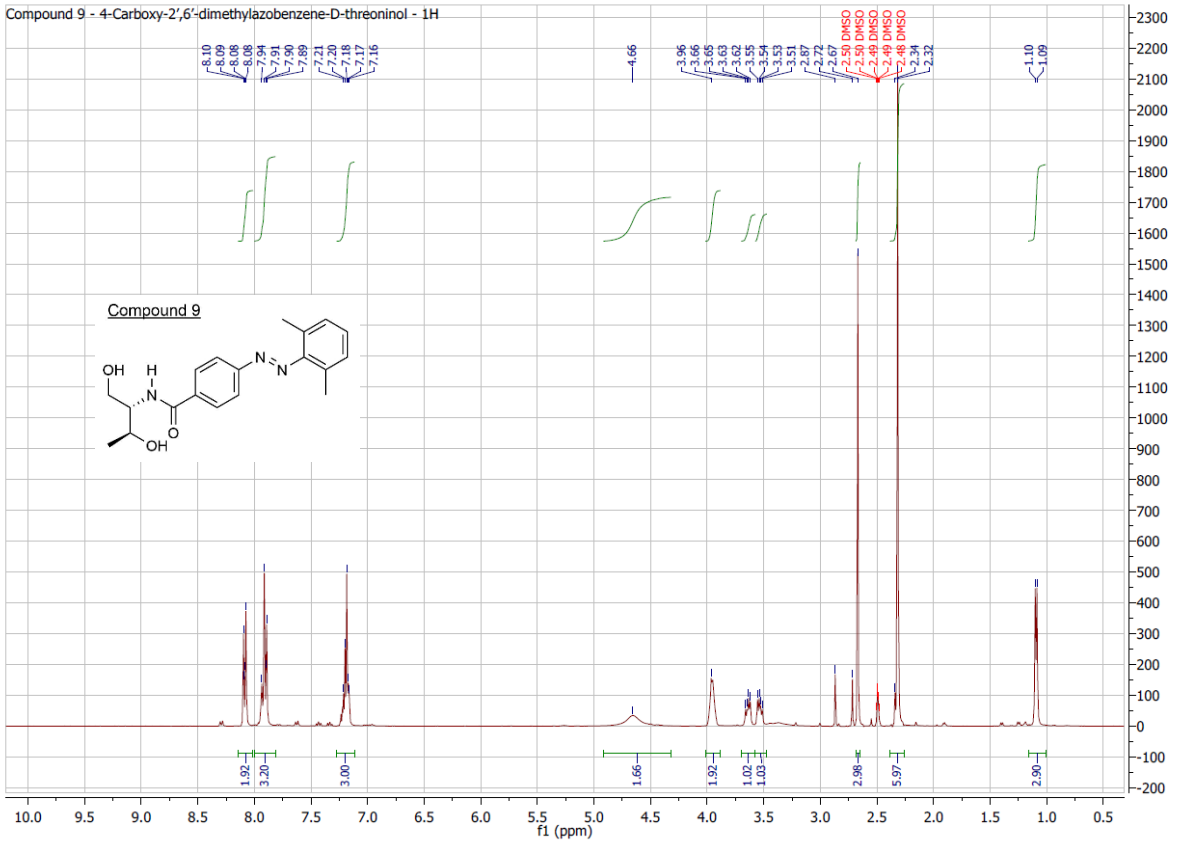
Compound 9 - 4-Carboxy-2′,6′-dimethylazobenzene-D-threoninol - 1H
Compound 9
f1 (ppm)

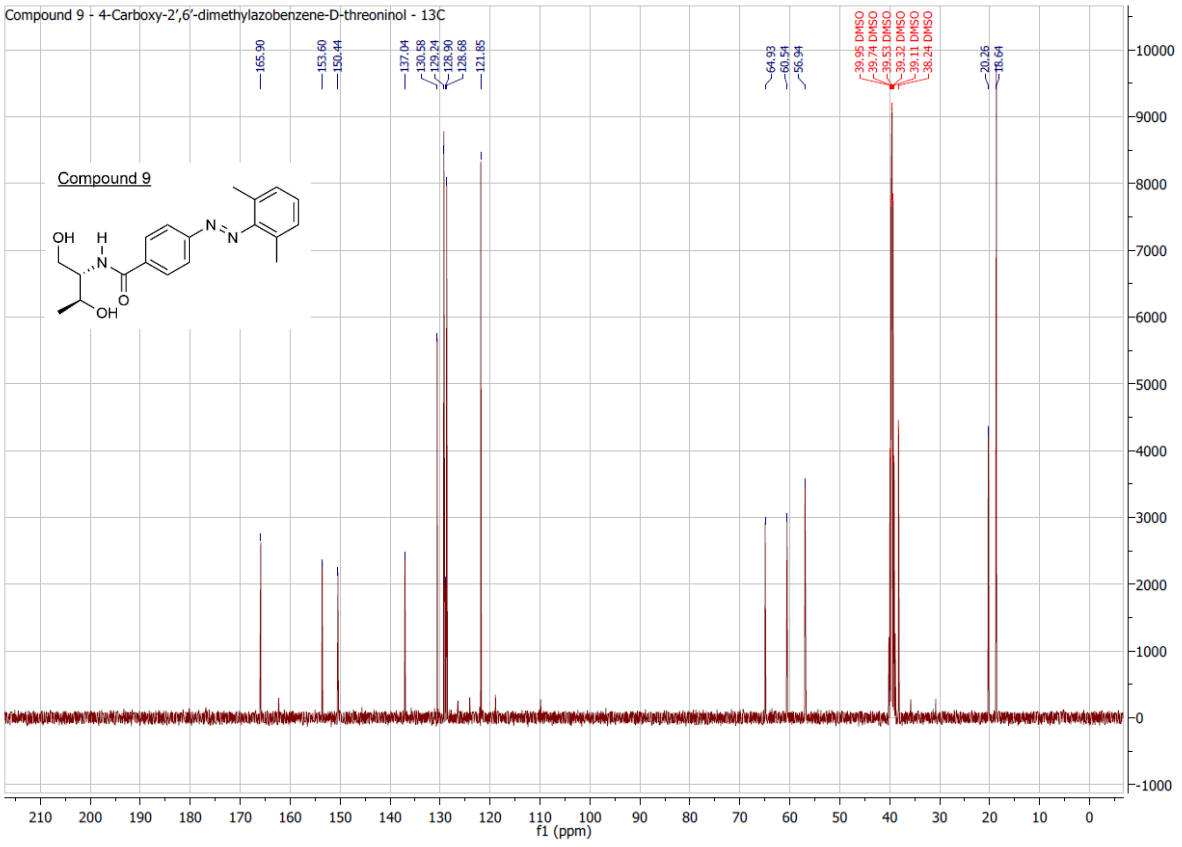
Compound 9 - 4-Carboxy-2′,6′-dimethylazobenzene-D-threoninol - 13C
Compound 9
f1 (ppm)

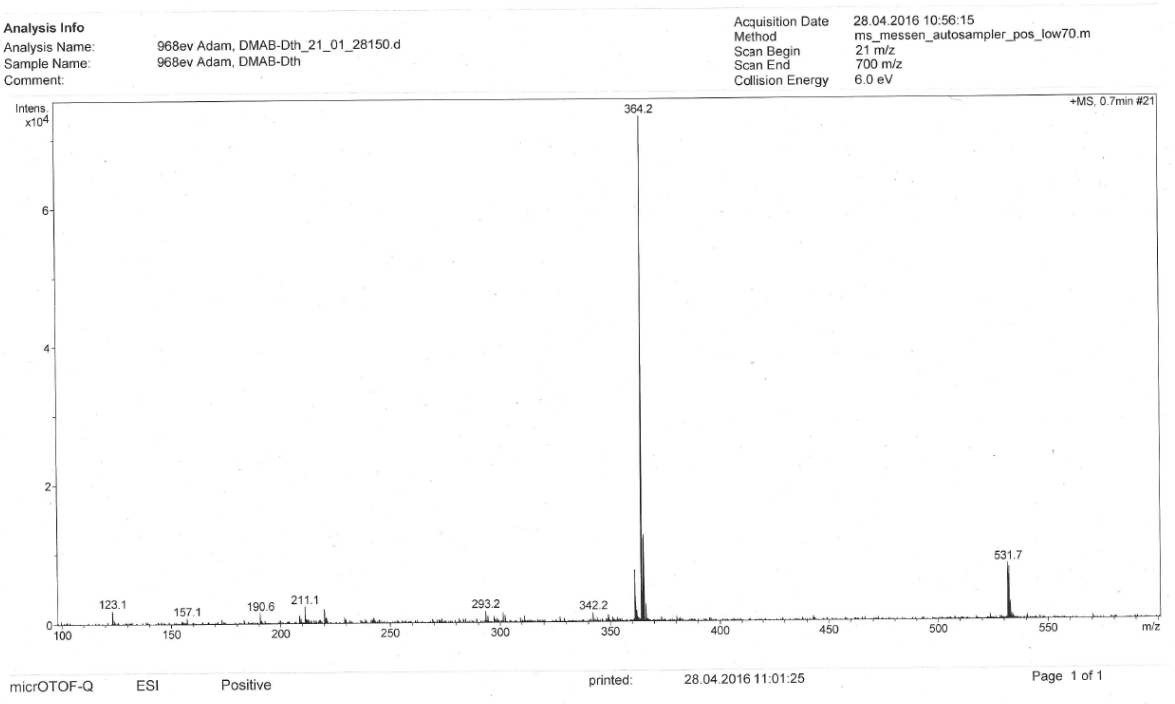
Analysis Info
Analysis Name: 968ev Adam, DMAB-Dth_21_01_28150.d
Sample Name: 968ev Adam, DMAB-Dth
Comment:
Acquisition Date 28.04.2016 10:56:15
Method ms_messen_autosampler_pos_low70.m
Scan Begin 21 m/z
Scan End 700 m/z
Collision Energy 6.0 eV
Intens.
x10^4
+MS, 0.7min #21
364.2
531.7
123.1
157.1
190.6
211.1
293.2
342.2
m/z
micrOTOF-Q ESI Positive
printed: 28.04.2016 11:01:25
Page 1 of 1

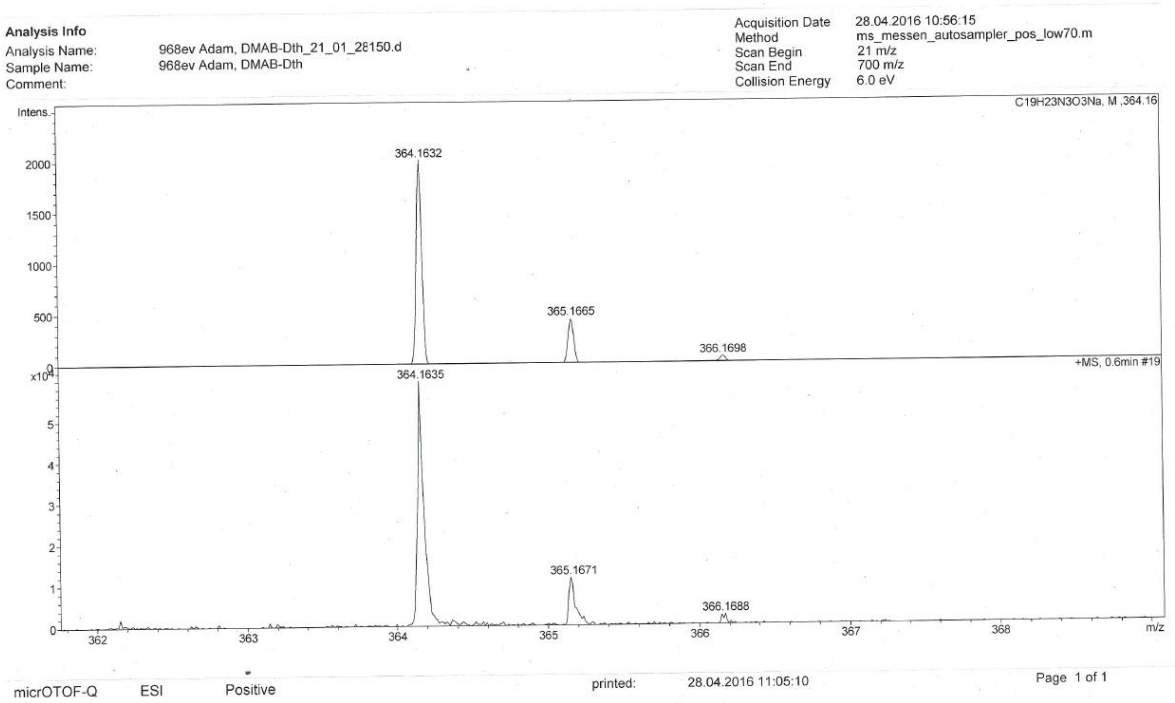
Analysis Info
Analysis Name: 968ev Adam, DMAB-Dth_21_01_28150.d
Sample Name: 968ev Adam, DMAB-Dth
Comment:
Acquisition Date 28.04.2016 10:56:15
Method ms_messen_autosampler_pos_low70.m
Scan Begin 21 m/z
Scan End 700 m/z
Collision Energy 6.0 eV
Intens.
C19H23N3O3Na, M ,364.16
364.1632
365.1665
366.1698
x10^4
+MS, 0.6min #19
364.1635
365.1671
366.1688
m/z
micrOTOF-Q ESI Positive
printed: 28.04.2016 11:05:10
Page 1 of 1

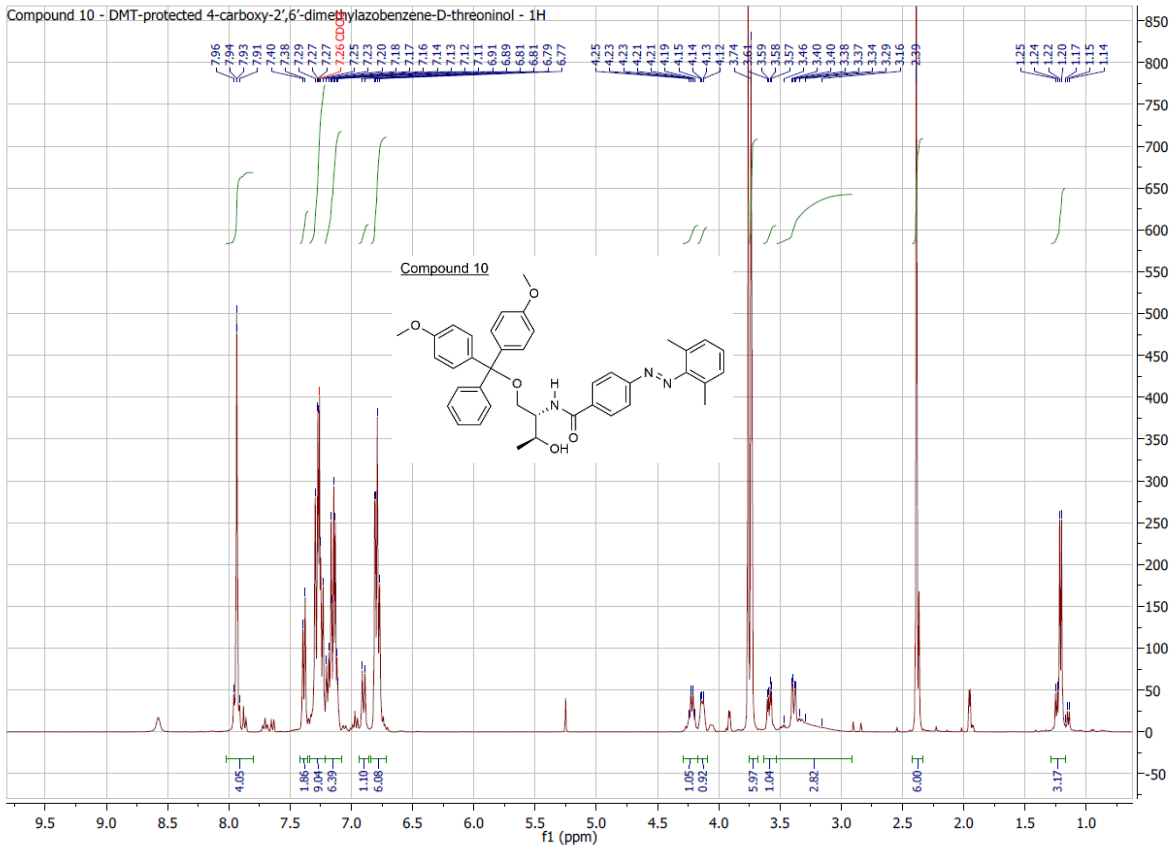
Compound 10 - DMT-protected 4-carboxy-2',6'-dimethylazobenzene-D-threoninol - 1H
Compound 10
f1 (ppm)

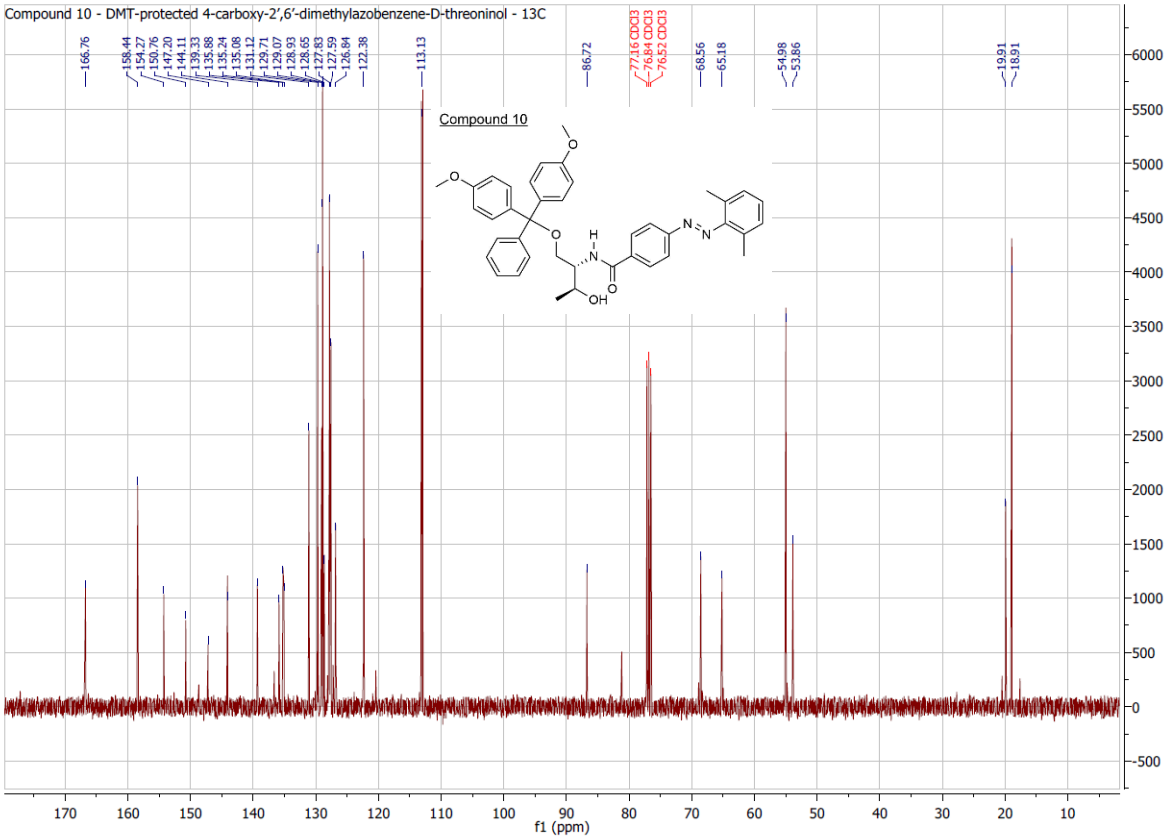
Compound 10 - DMT-protected 4-carboxy-2',6'-dimethylazobenzene-D-threoninol - 13C
Compound 10
f1 (ppm)

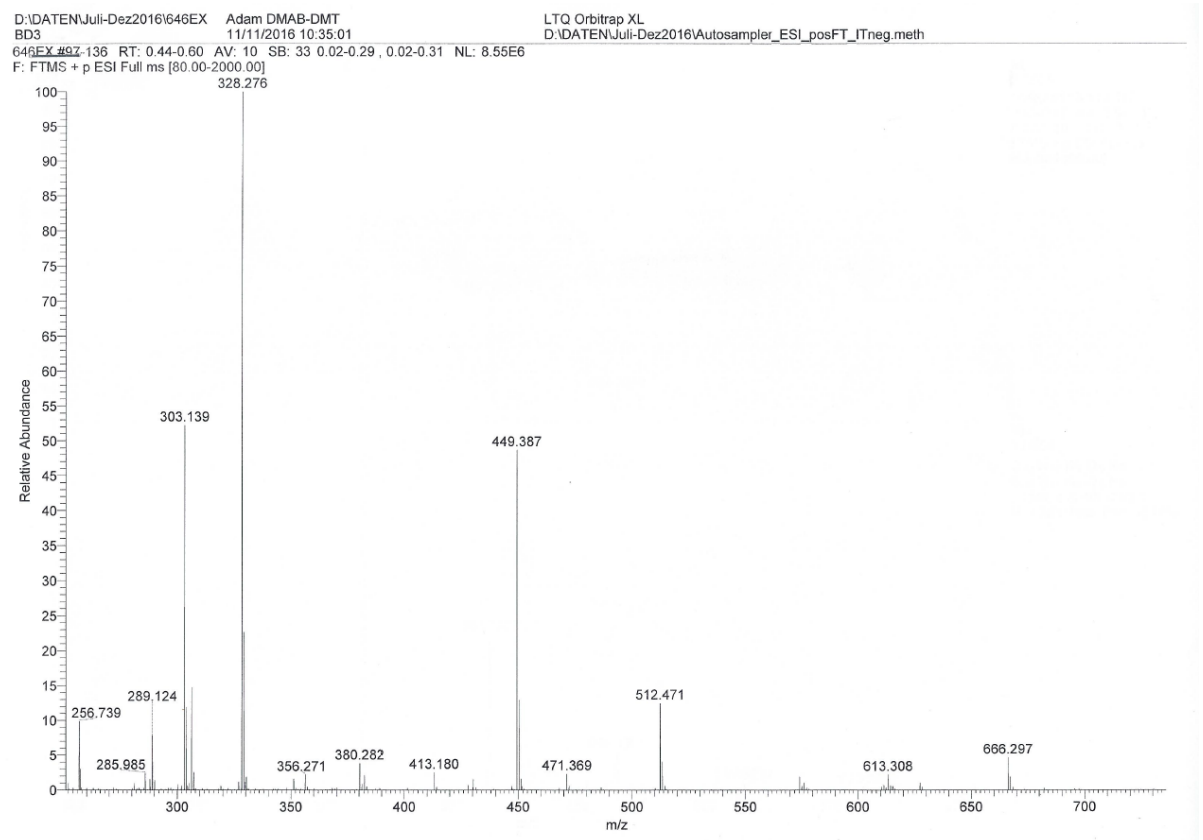
D:\DATEN\Juli-Dez2016\646EX Adam DMAB-DMT
BD3 11/11/2016 10:35:01
LTQ Orbitrap XL
D:\DATEN\Juli-Dez2016\Autosampler_ESI_posFT_ITneg.meth
646EX #97-136 RT: 0.44-0.60 AV: 10 SB: 33 0.02-0.29 , 0.02-0.31 NL: 8.55E6
F: FTMS + p ESI Full ms [80.00-2000.00]
328.276
303.139
449.387
289.124
256.739
512.471
666.297
285.985
356.271
380.282
413.180
471.369
613.308
Relative Abundance
m/z

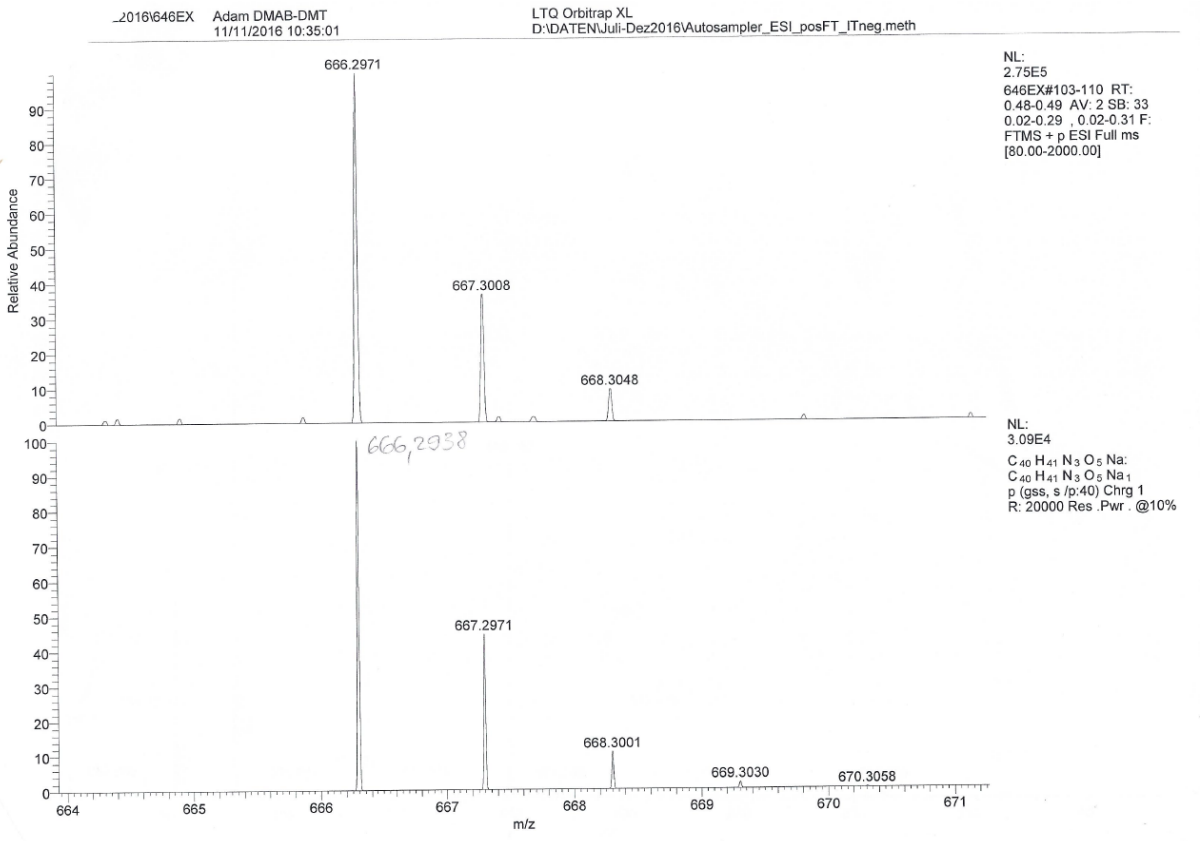
_2016\646EX Adam DMAB-DMT
11/11/2016 10:35:01
LTQ Orbitrap XL
D:\DATEN\Juli-Dez2016\Autosampler_ESI_posFT_ITneg.meth
NL:
2.75E5
646EX#103-110 RT:
0.48-0.49 AV: 2 SB: 33
0.02-0.29 , 0.02-0.31 F:
FTMS + p ESI Full ms
[80.00-2000.00]
666.2971
667.3008
668.3048
NL:
3.09E4
C40 H41 N3 O5 Na:
C40 H41 N3 O5 Na1
p (gss, s /p:40) Chrg 1
R: 20000 Res .Pwr . @10%
666,2938
667.2971
668.3001
669.3030
670.3058
Relative Abundance
m/z

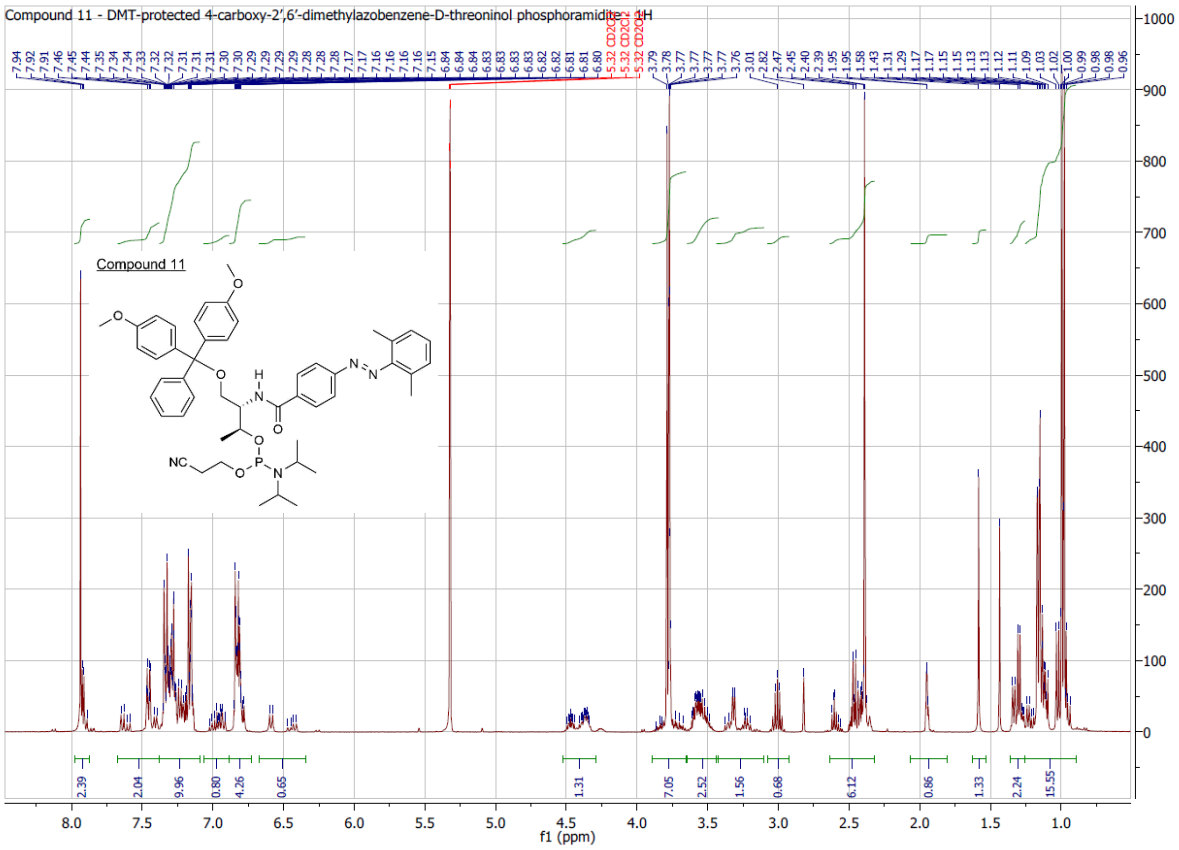
Compound 11 - DMT-protected 4-carboxy-2′,6′-dimethylazobenzene-D-threoninol phosphoramidite - 1H
Compound 11
f1 (ppm)

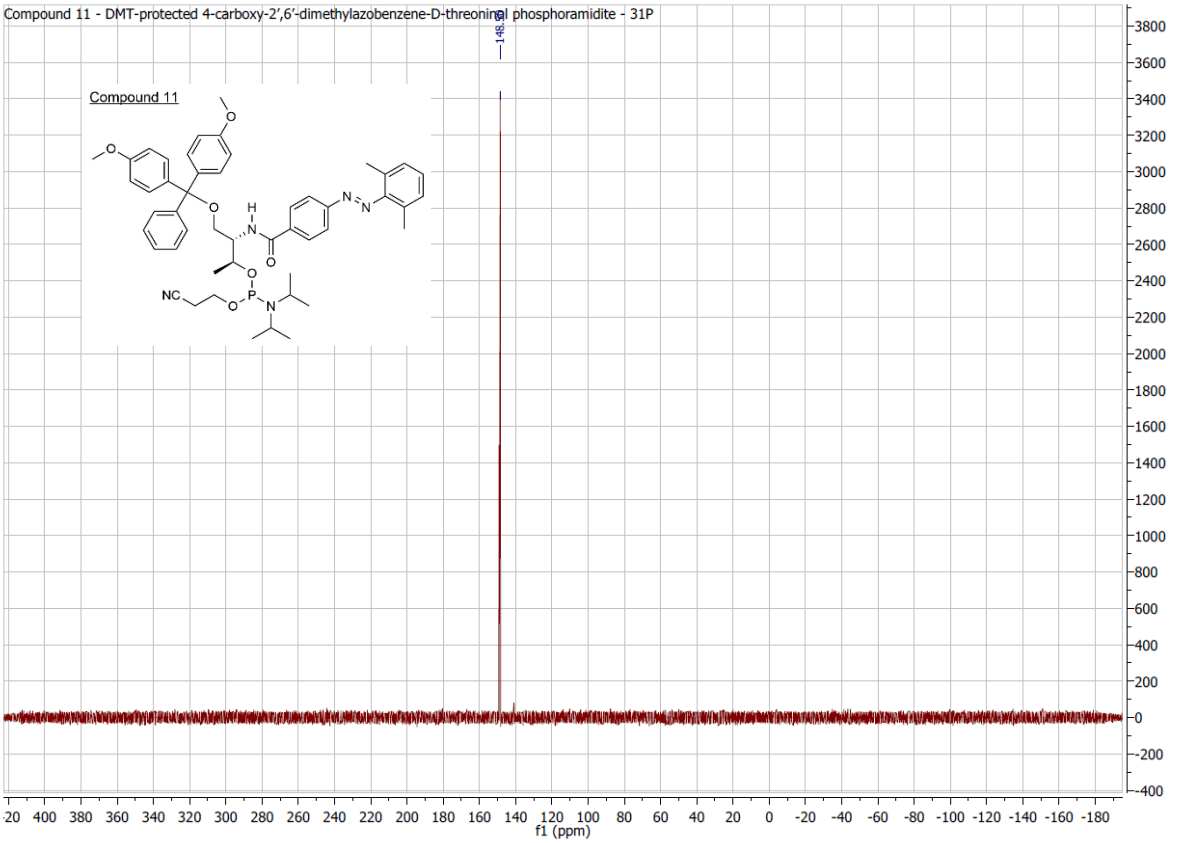
Compound 11 - DMT-protected 4-carboxy-2′,6′-dimethylazobenzene-D-threoninol phosphoramidite - 31P
Compound 11
f1 (ppm)

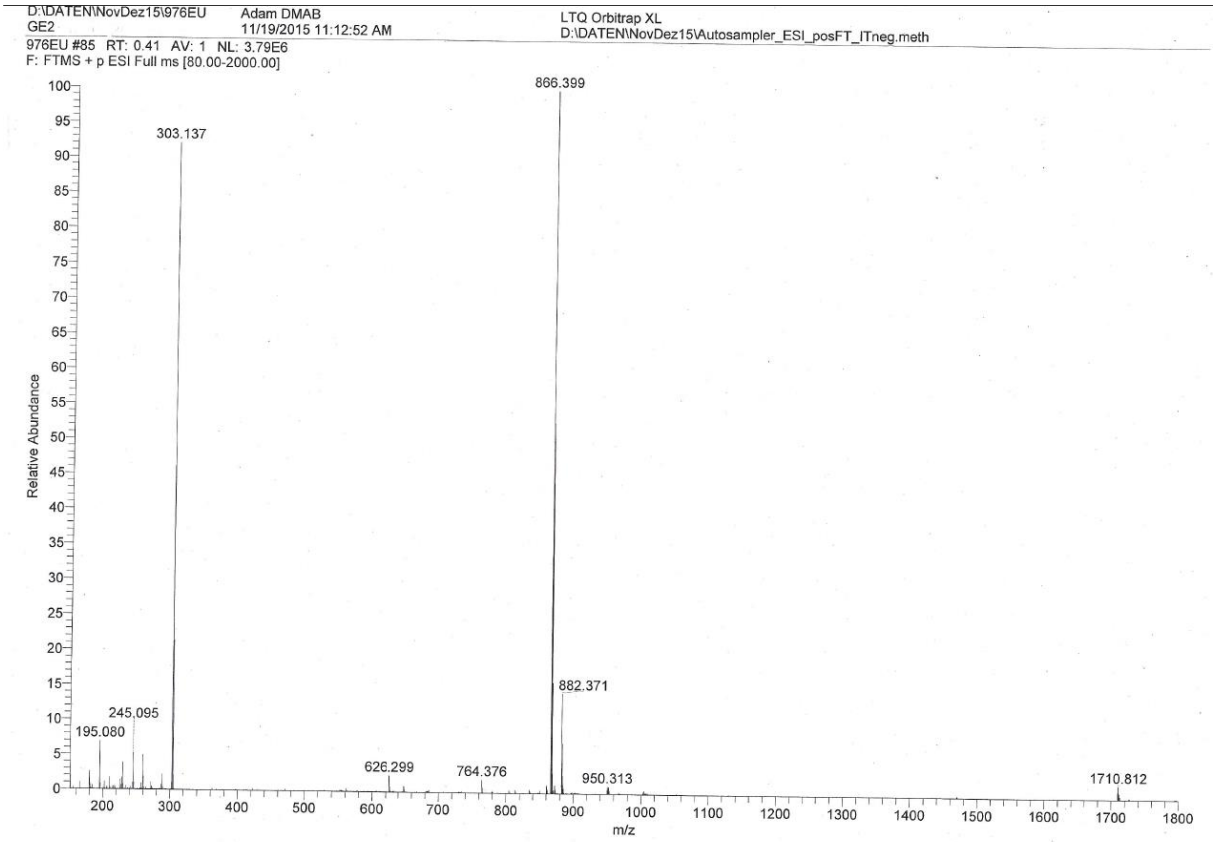
D:\DATEN\NovDez15\976EU
GE2
Adam DMAB
11/19/2015 11:12:52 AM
LTQ Orbitrap XL
D:\DATEN\NovDez15\Autosampler_ESI_posFT_ITneg.meth
976EU #85 RT: 0.41 AV: 1 NL: 3.79E6
F: FTMS + p ESI Full ms [80.00-2000.00]
866.399
303.137
882.371
245.095
195.080
626.299
764.376
950.313
1710.812
Relative Abundance
m/z

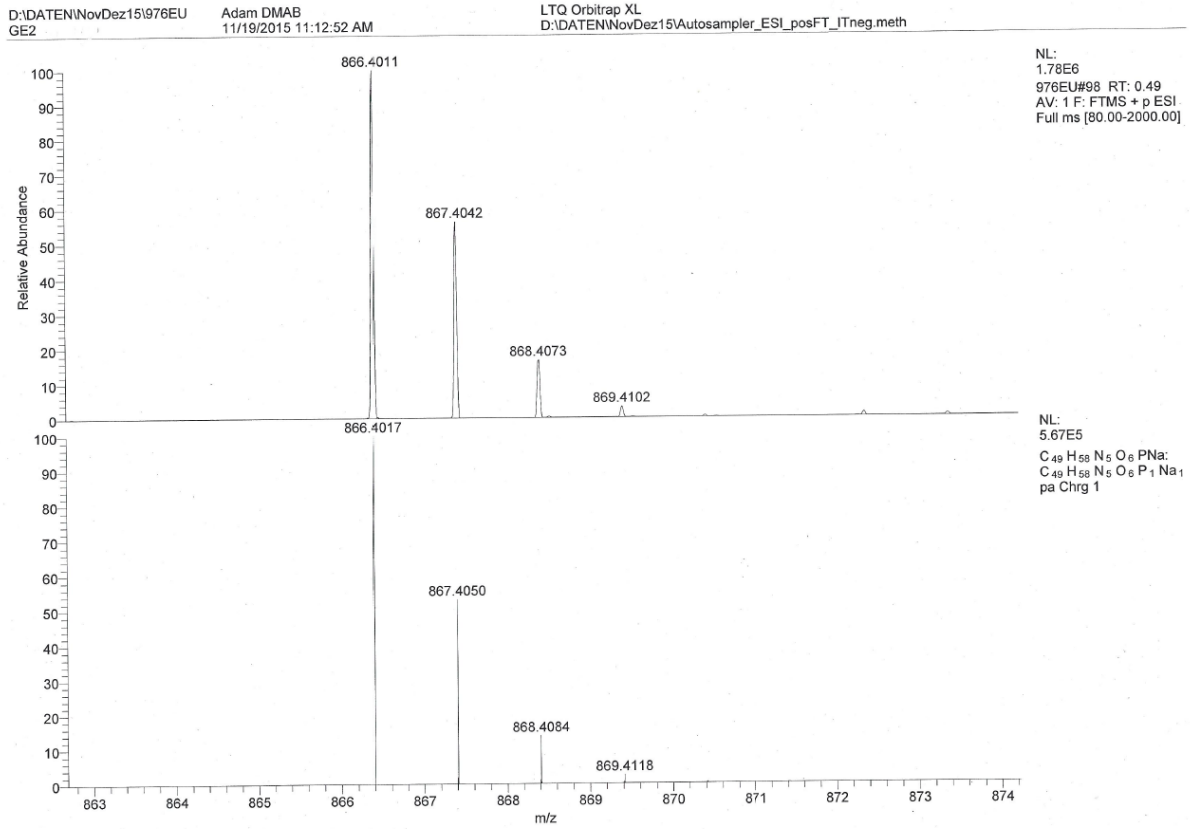
D:\DATEN\NovDez15\976EU
GE2
Adam DMAB
11/19/2015 11:12:52 AM
LTQ Orbitrap XL
D:\DATEN\NovDez15\Autosampler_ESI_posFT_ITneg.meth
NL:
1.78E6
976EU#98 RT: 0.49
AV: 1 F: FTMS + p ESI
Full ms [80.00-2000.00]
866.4011
867.4042
868.4073
869.4102
NL:
5.67E5
C49 H58 N5 O6 PNa:
C49 H58 N5 O6 P1 Na1
pa Chrg 1
866.4017
867.4050
868.4084
869.4118
Relative Abundance
m/z

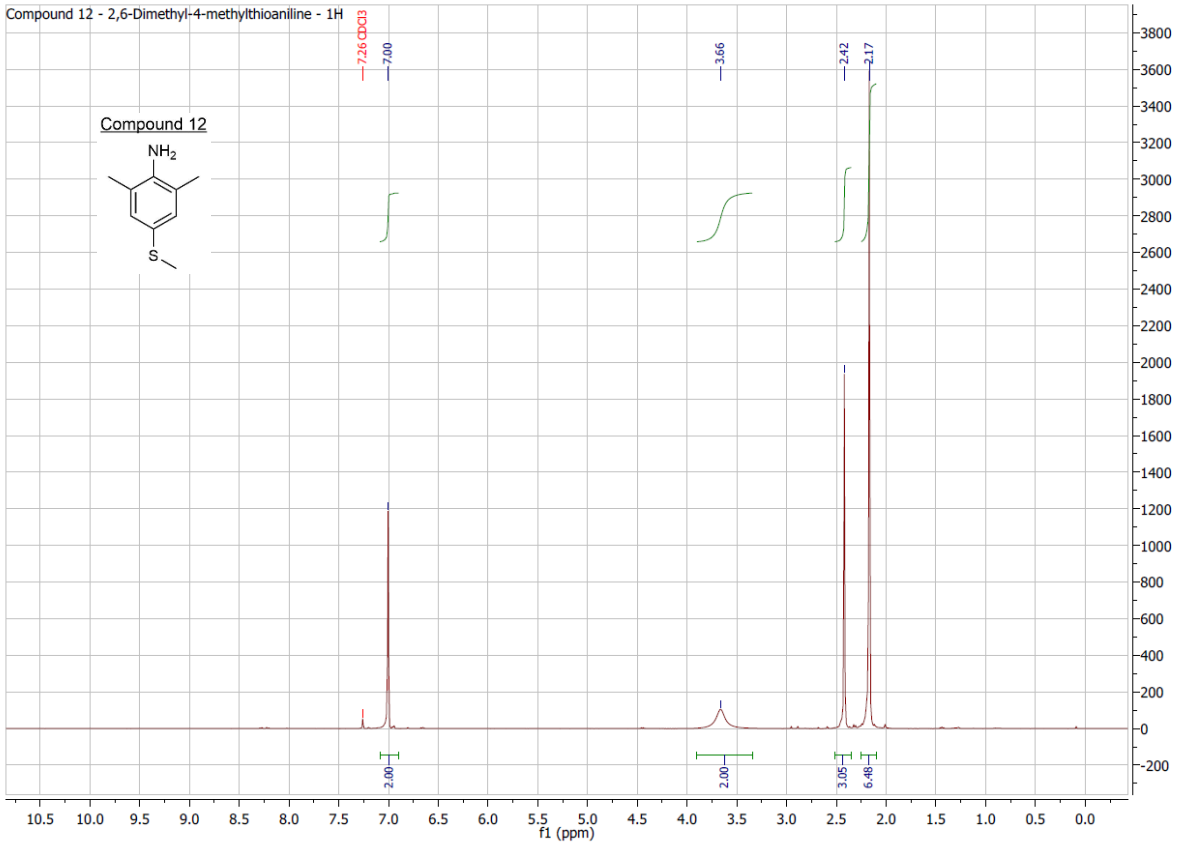
Compound 12 - 2,6-Dimethyl-4-methylthioaniline - 1H
Compound 12
NH2
S
7.26 CDCl3
7.00
3.66
2.42
2.17
2.00
2.00
3.05
6.48
f1 (ppm)

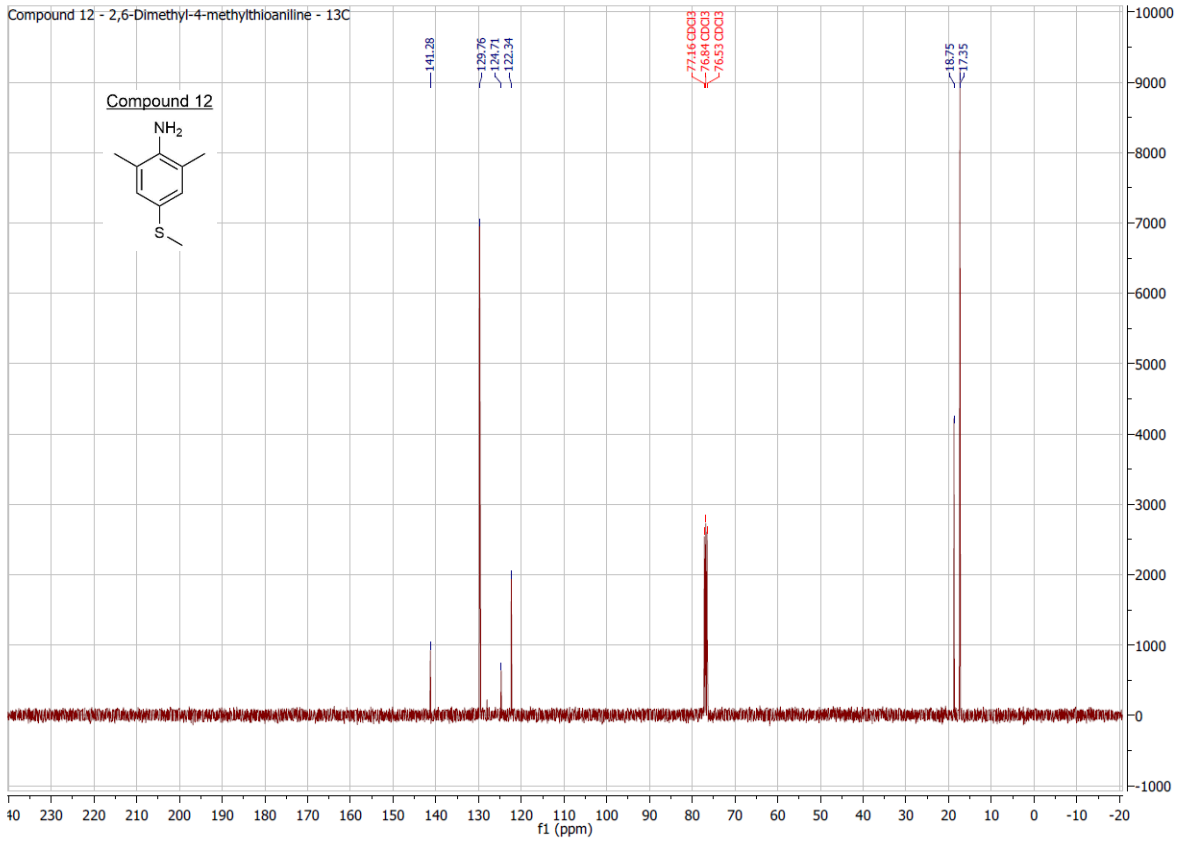
Compound 12 - 2,6-Dimethyl-4-methylthioaniline - 13C
Compound 12
NH2
S
141.28
129.76
124.71
122.34
77.16 CDCl3
76.84 CDCl3
76.53 CDCl3
18.75
17.35
f1 (ppm)

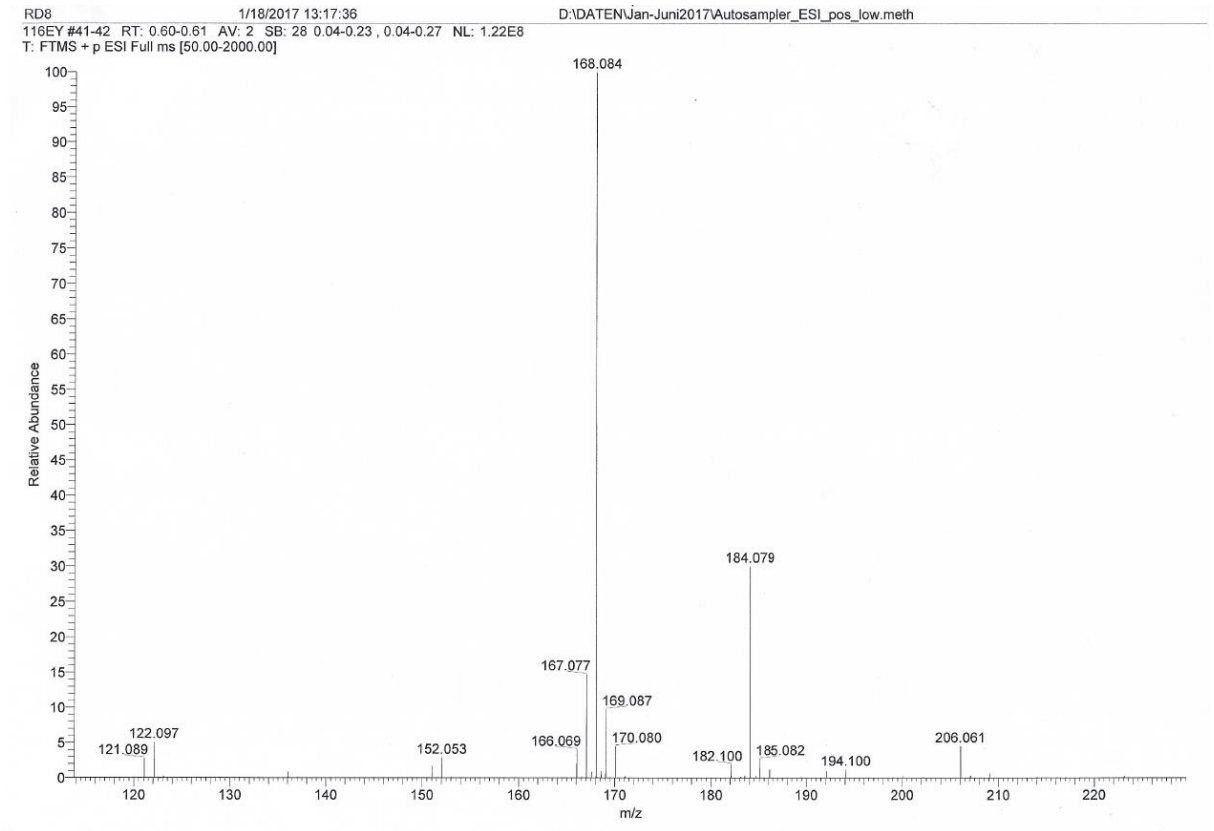
RD8 1/18/2017 13:17:36 D:\DATEN\Jan-Juni2017\Autosampler_ESI_pos_low.meth
116EY #41-42 RT: 0.60-0.61 AV: 2 SB: 28 0.04-0.23 , 0.04-0.27 NL: 1.22E8
T: FTMS + p ESI Full ms [50.00-2000.00]
168.084
184.079
167.077
169.087
122.097
121.089
152.053
166.069
170.080
182.100
185.082
194.100
206.061
Relative Abundance
m/z

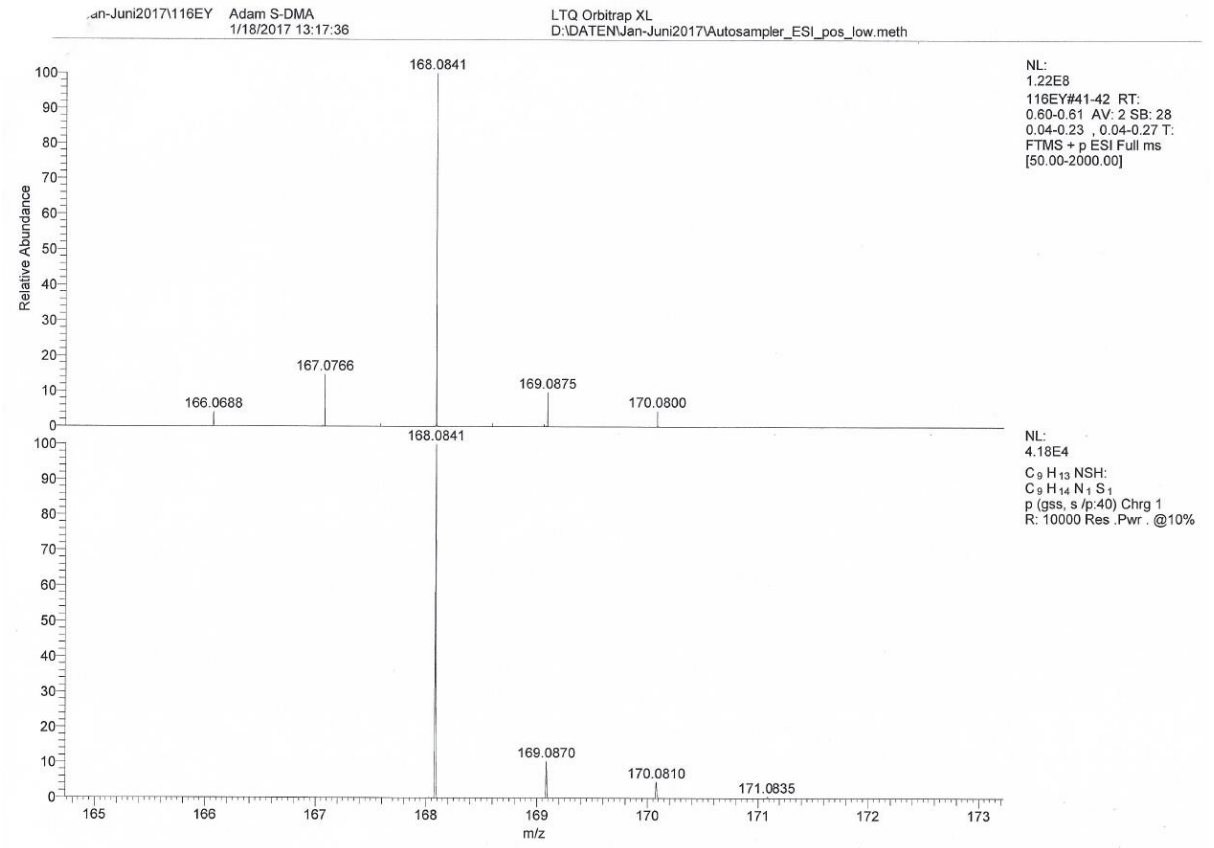
Jan-Juni2017\116EY Adam S-DMA 1/18/2017 13:17:36
LTQ Orbitrap XL D:\DATEN\Jan-Juni2017\Autosampler_ESI_pos_low.meth
168.0841
167.0766
169.0875
166.0688
170.0800
NL: 1.22E8 116EY#41-42 RT: 0.60-0.61 AV: 2 SB: 28 0.04-0.23 , 0.04-0.27 T: FTMS + p ESI Full ms [50.00-2000.00]
NL: 4.18E4 C9 H13 NSH: C9 H14 N1 S1 p (gss, s /p:40) Chrg 1 R: 10000 Res .Pwr . @10%
169.0870
170.0810
171.0835
Relative Abundance
m/z

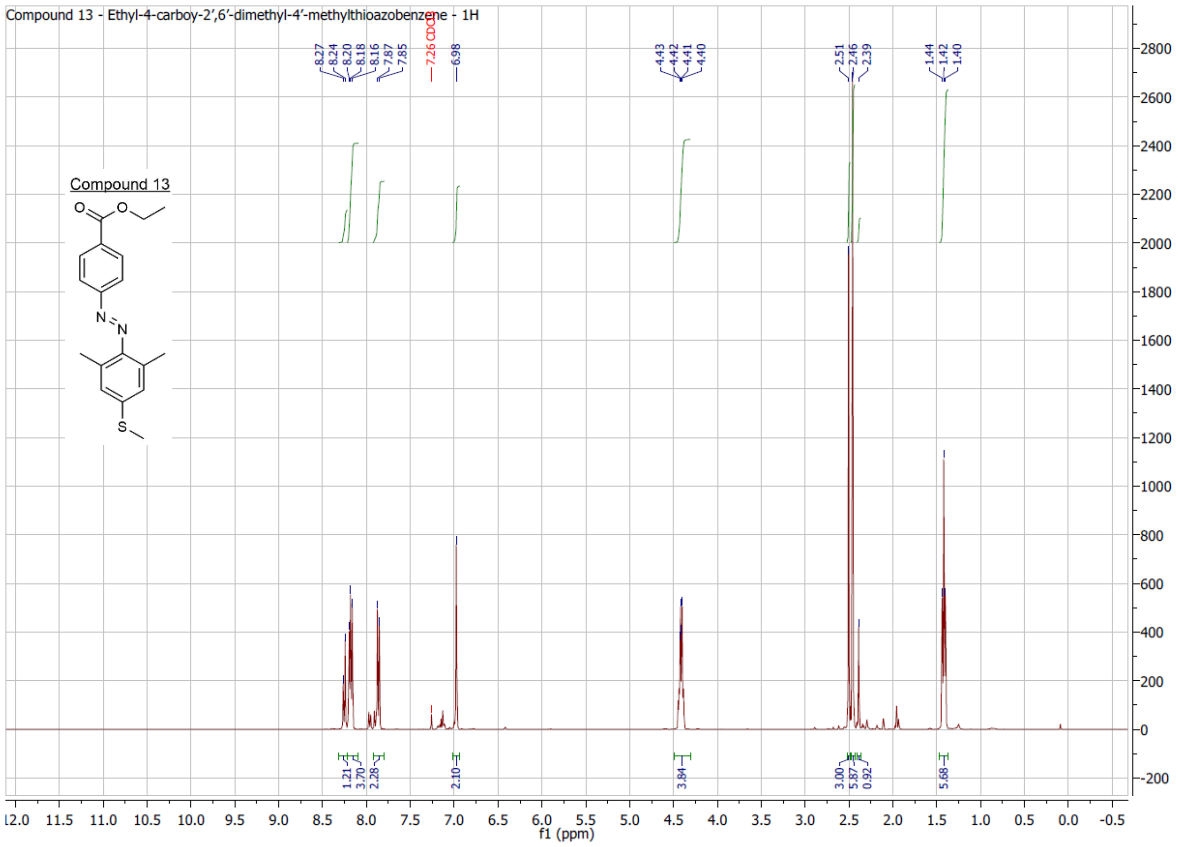
Compound 13 - Ethyl-4-carboy-2',6'-dimethyl-4'-methylthioazobenzene - 1H
Compound 13
f1 (ppm)

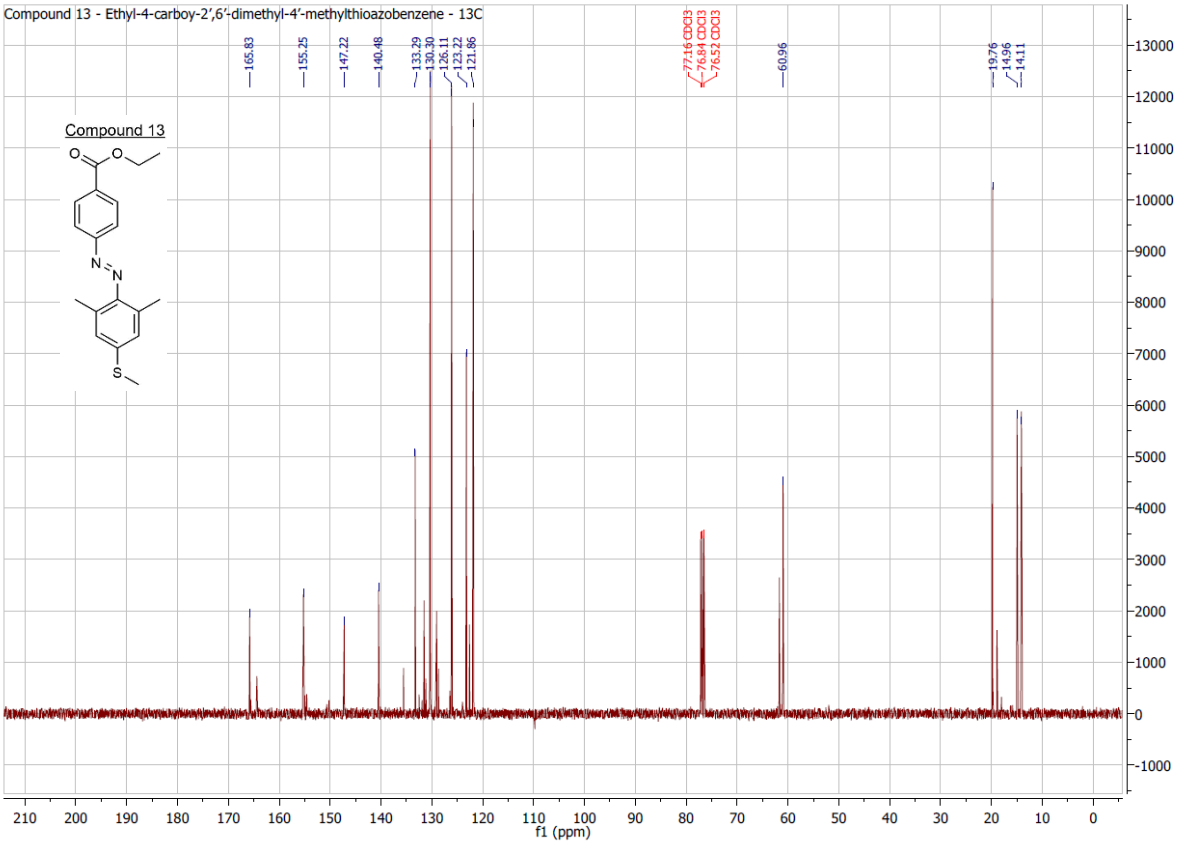
Compound 13 - Ethyl-4-carboy-2',6'-dimethyl-4'-methylthioazobenzene - 13C
Compound 13
f1 (ppm)

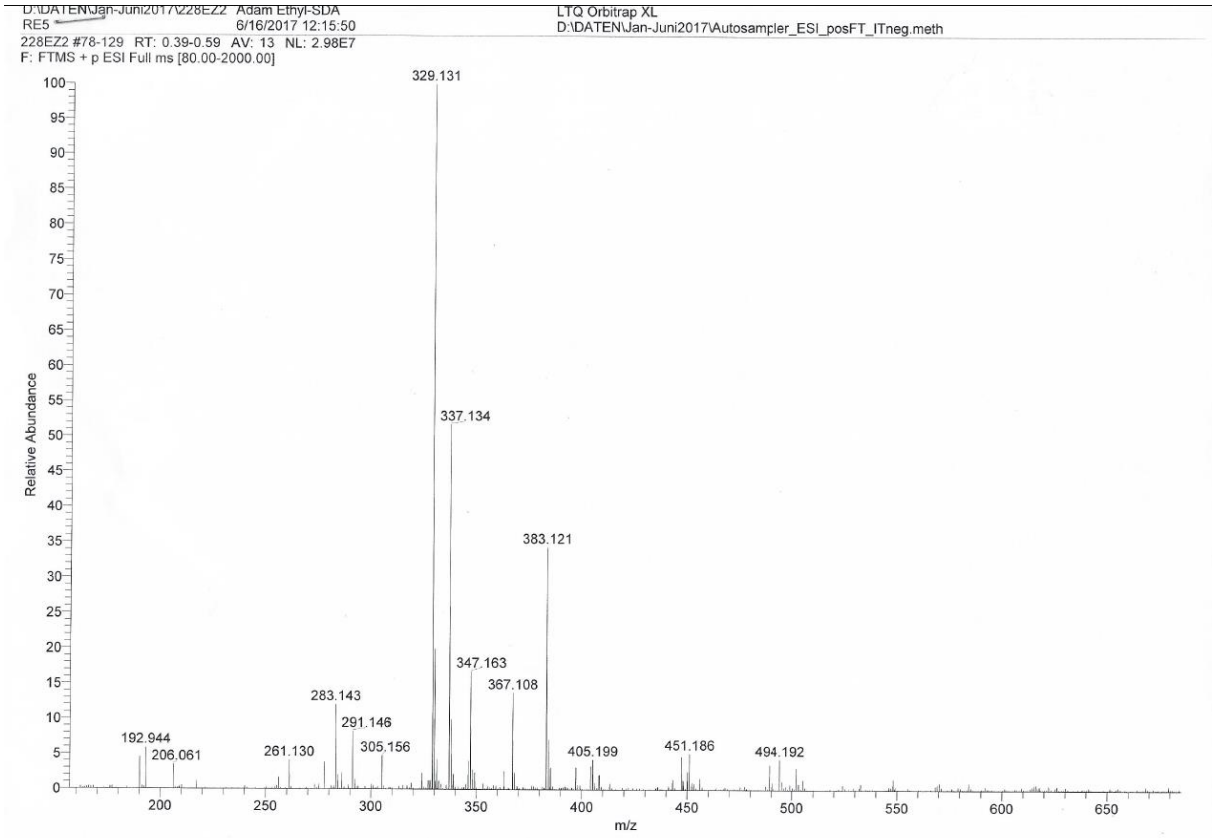
D:\DATEN\Jan-Juni2017\228EZ2 Adam Ethyl-SDA
RE5 6/16/2017 12:15:50
228EZ2 #78-129 RT: 0.39-0.59 AV: 13 NL: 2.98E7
F: FTMS + p ESI Full ms [80.00-2000.00]
LTQ Orbitrap XL
D:\DATEN\Jan-Juni2017\Autosampler_ESI_posFT_ITneg.meth
329.131
337.134
383.121
347.163
367.108
283.143
291.146
305.156
192.944
206.061
261.130
405.199
451.186
494.192
Relative Abundance
m/z

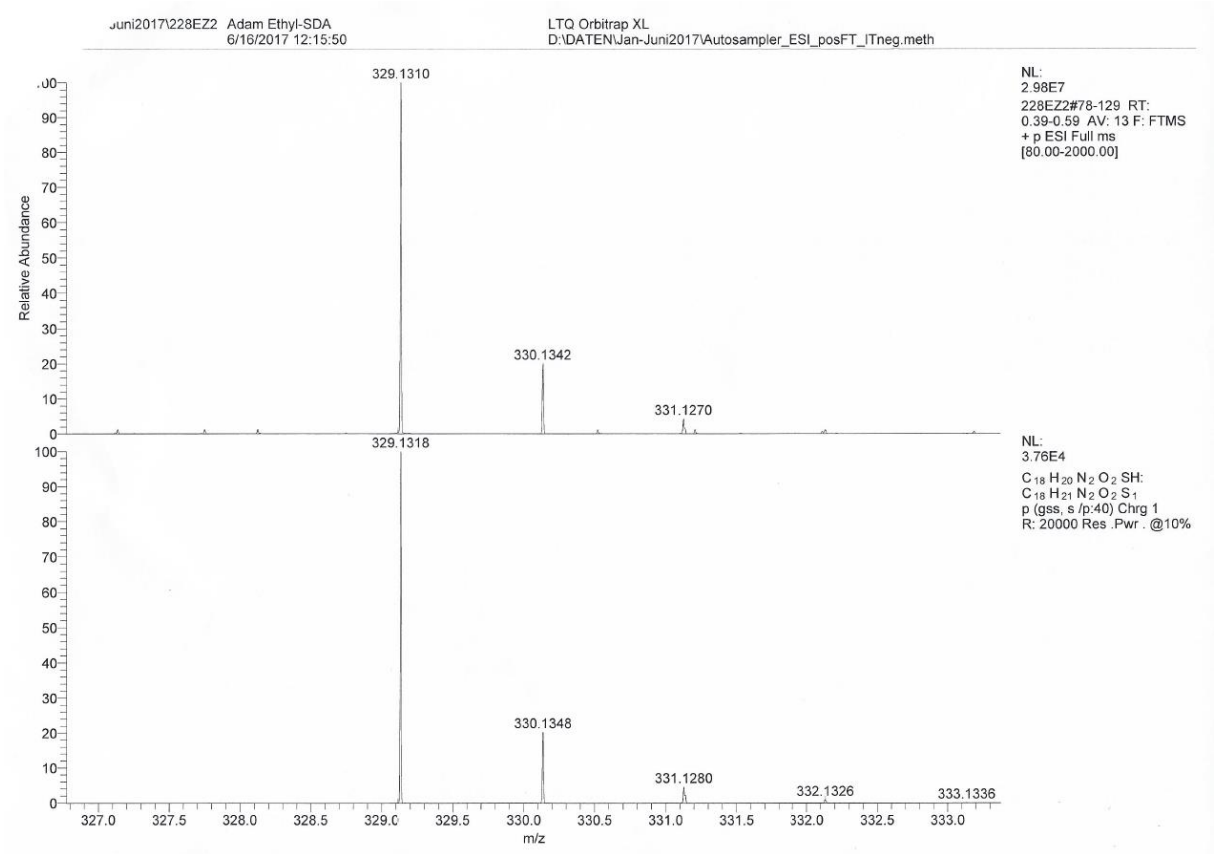
Juni2017\228EZ2 Adam Ethyl-SDA
6/16/2017 12:15:50
LTQ Orbitrap XL
D:\DATEN\Jan-Juni2017\Autosampler_ESI_posFT_ITneg.meth
329.1310
330.1342
331.1270
NL:
2.98E7
228EZ2#78-129 RT:
0.39-0.59 AV: 13 F: FTMS
+ p ESI Full ms
[80.00-2000.00]
329.1318
330.1348
331.1280
332.1326
333.1336
NL:
3.76E4
C18 H20 N2 O2 SH:
C18 H21 N2 O2 S1
p (gss, s /p:40) Chrg 1
R: 20000 Res .Pwr . @10%
Relative Abundance
m/z

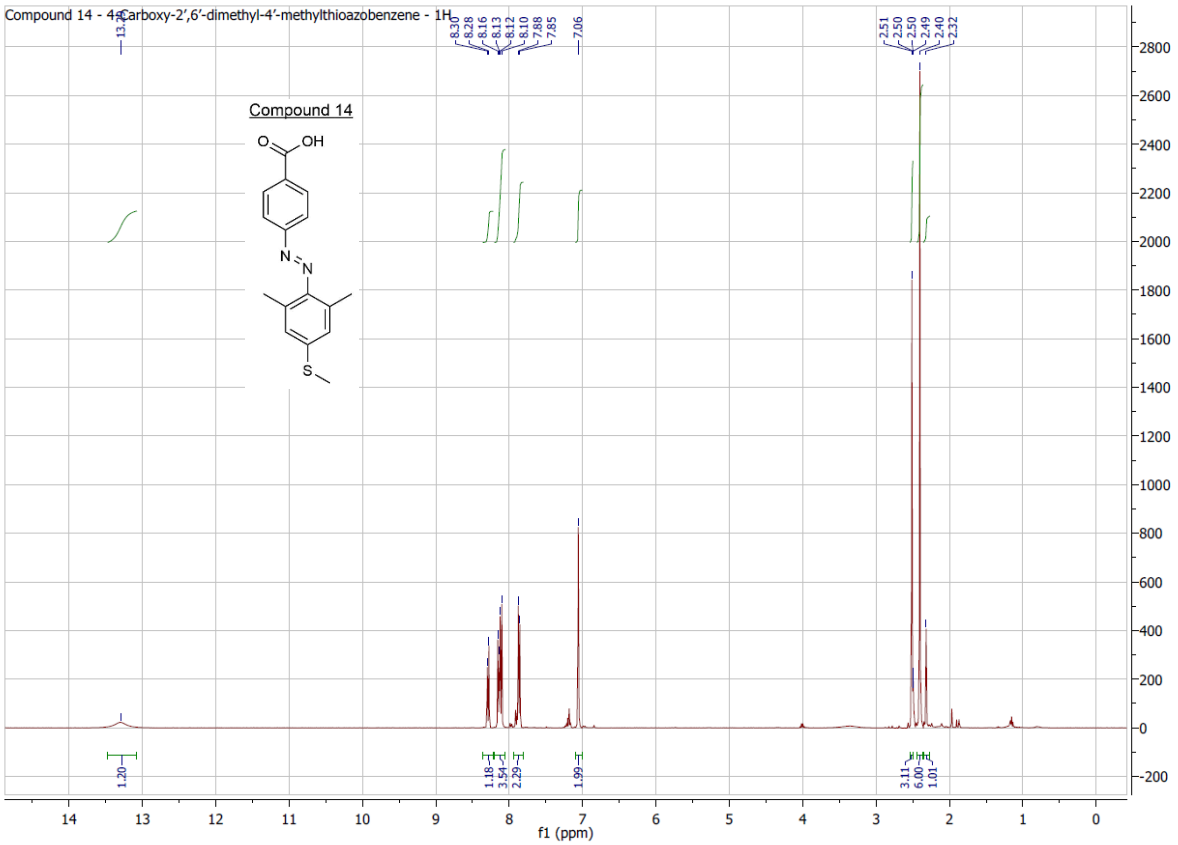
Compound 14 - 4-Carboxy-2′,6′-dimethyl-4′-methylthioazobenzene - 1H
Compound 14
f1 (ppm)

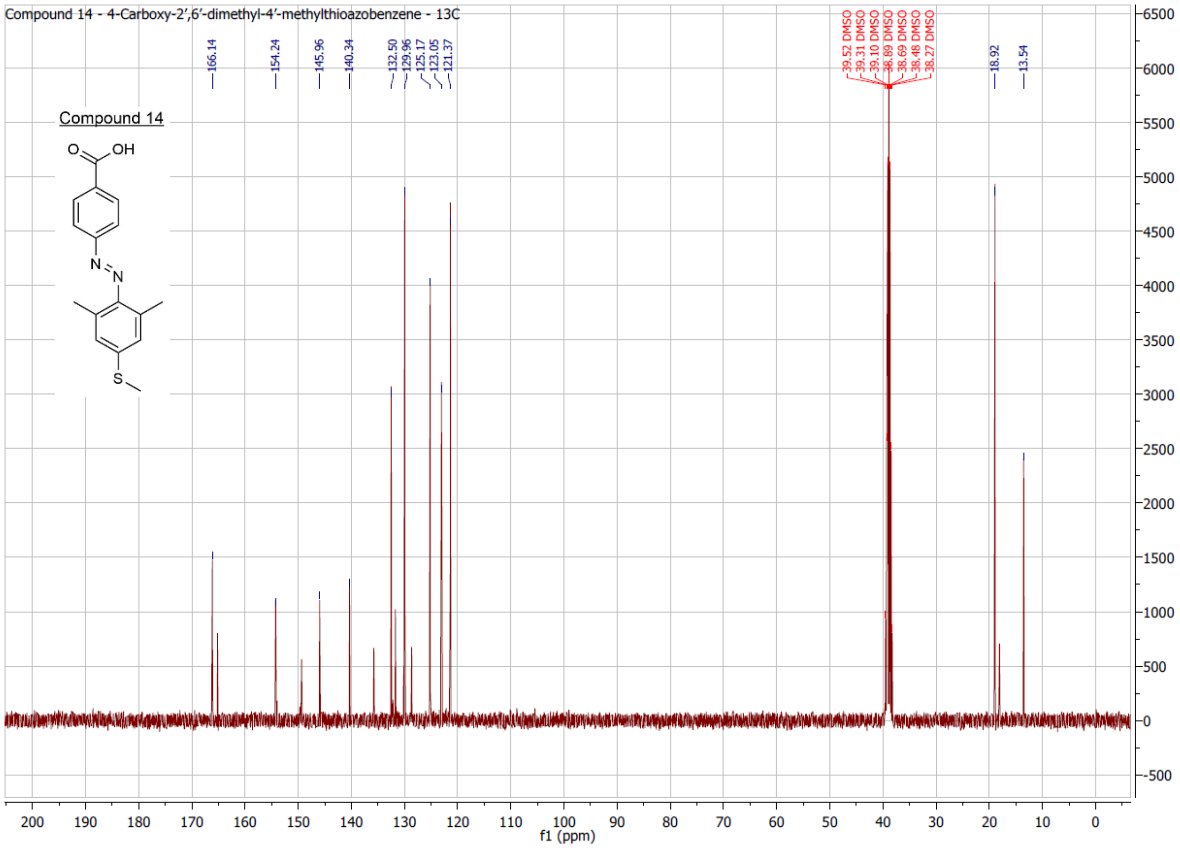
Compound 14 - 4-Carboxy-2′,6′-dimethyl-4′-methylthioazobenzene - 13C
Compound 14
f1 (ppm)

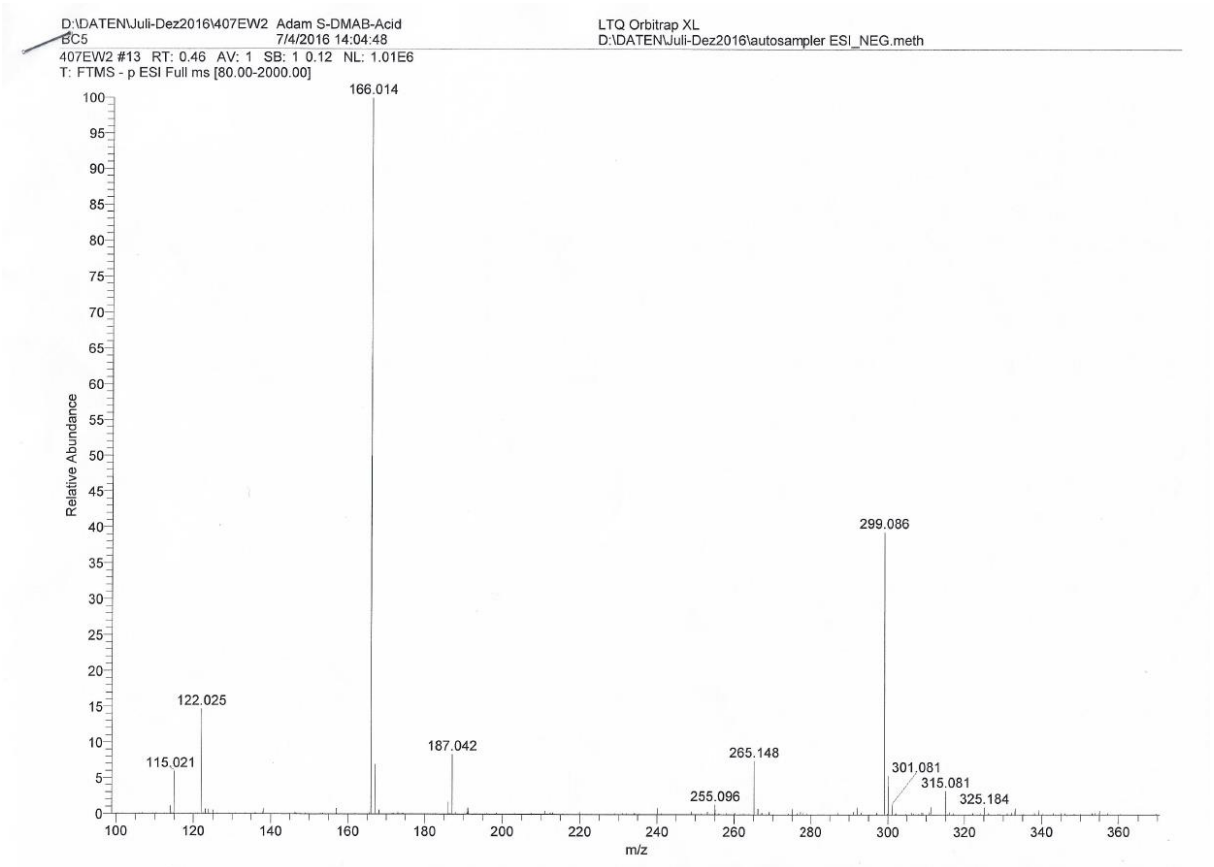
D:\DATEN\Juli-Dez2016\407EW2 Adam S-DMAB-Acid
BC5 7/4/2016 14:04:48
LTQ Orbitrap XL
D:\DATEN\Juli-Dez2016\autosampler ESI_NEG.meth
407EW2 #13 RT: 0.46 AV: 1 SB: 1 0.12 NL: 1.01E6
T: FTMS - p ESI Full ms [80.00-2000.00]
166.014
299.086
122.025
115.021
187.042
265.148
255.096
301.081
315.081
325.184
Relative Abundance
m/z

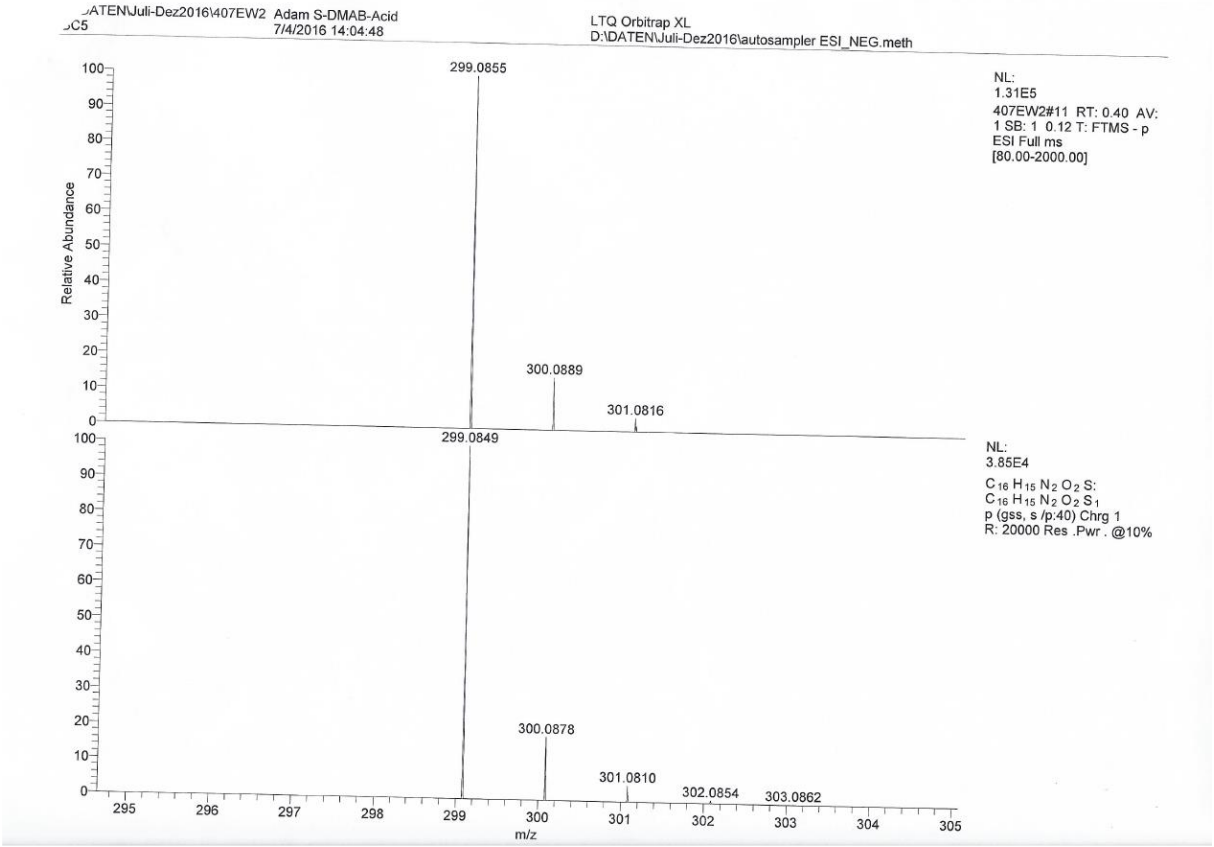
ATEN\Juli-Dez2016\407EW2 Adam S-DMAB-Acid
C5 7/4/2016 14:04:48
LTQ Orbitrap XL
D:\DATEN\Juli-Dez2016\autosampler ESI_NEG.meth
299.0855
300.0889
301.0816
NL:
1.31E5
407EW2#11 RT: 0.40 AV: 1 SB: 1 0.12 T: FTMS - p ESI Full ms [80.00-2000.00]
299.0849
300.0878
301.0810
302.0854
303.0862
NL:
3.85E4
C16 H15 N2 O2 S:
C16 H15 N2 O2 S1
p (gss, s /p:40) Chrg 1
R: 20000 Res .Pwr . @10%
Relative Abundance
m/z

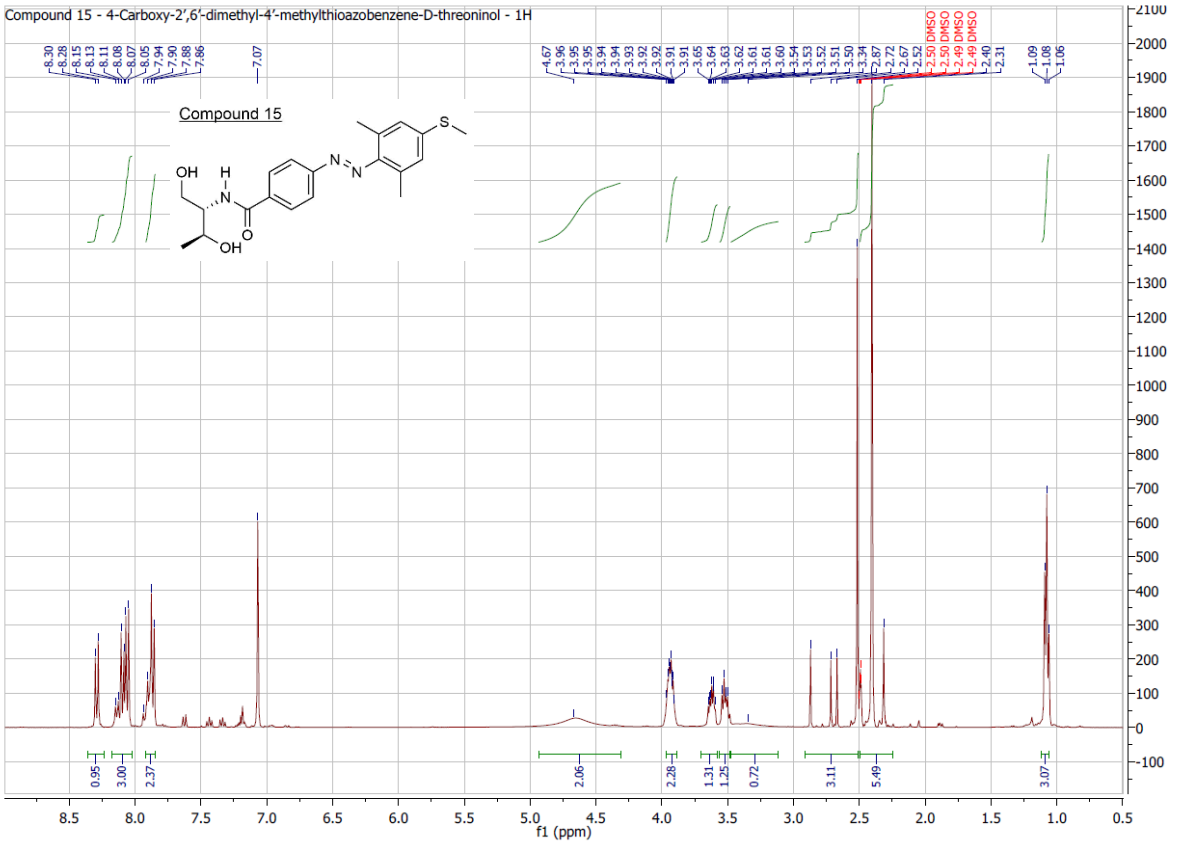
Compound 15 - 4-Carboxy-2′,6′-dimethyl-4′-methylthioazobenzene-D-threoninol - 1H
Compound 15
f1 (ppm)

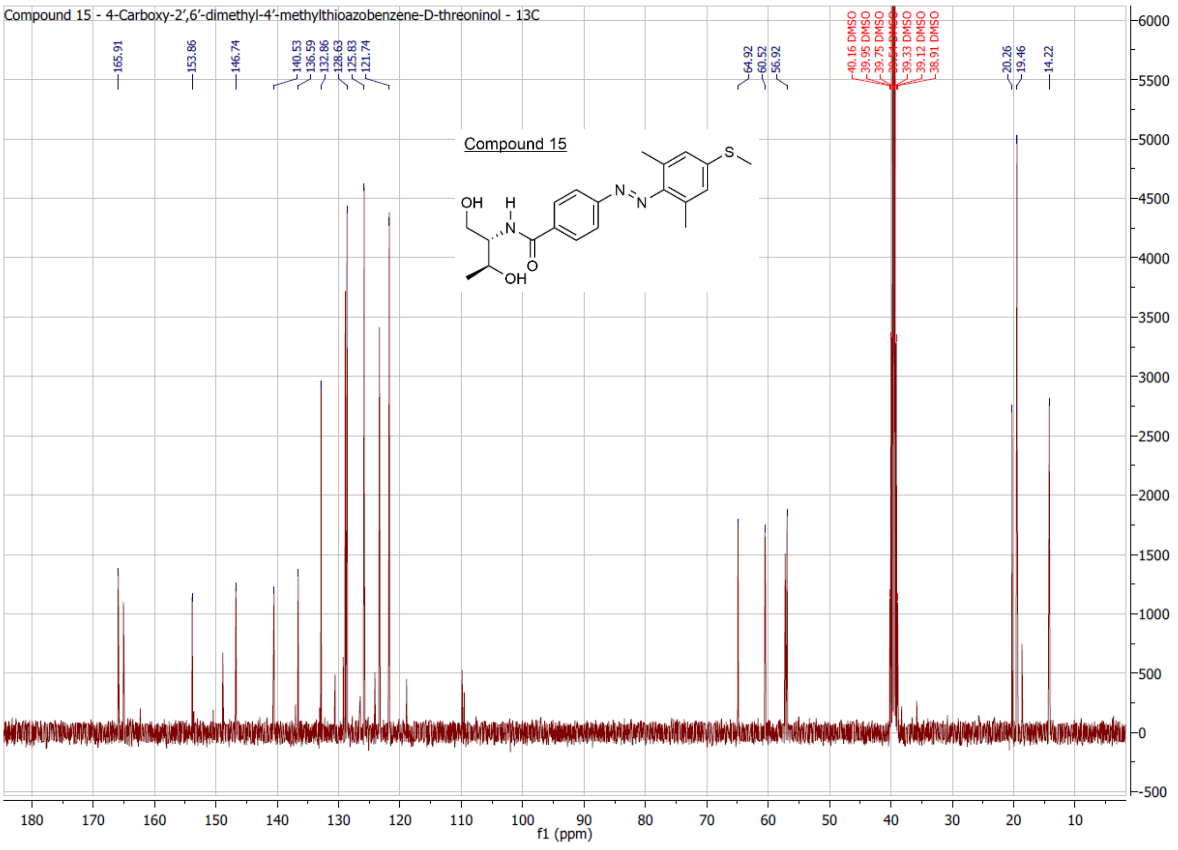
Compound 15 - 4-Carboxy-2′,6′-dimethyl-4′-methylthioazobenzene-D-threoninol - 13C
Compound 15
f1 (ppm)

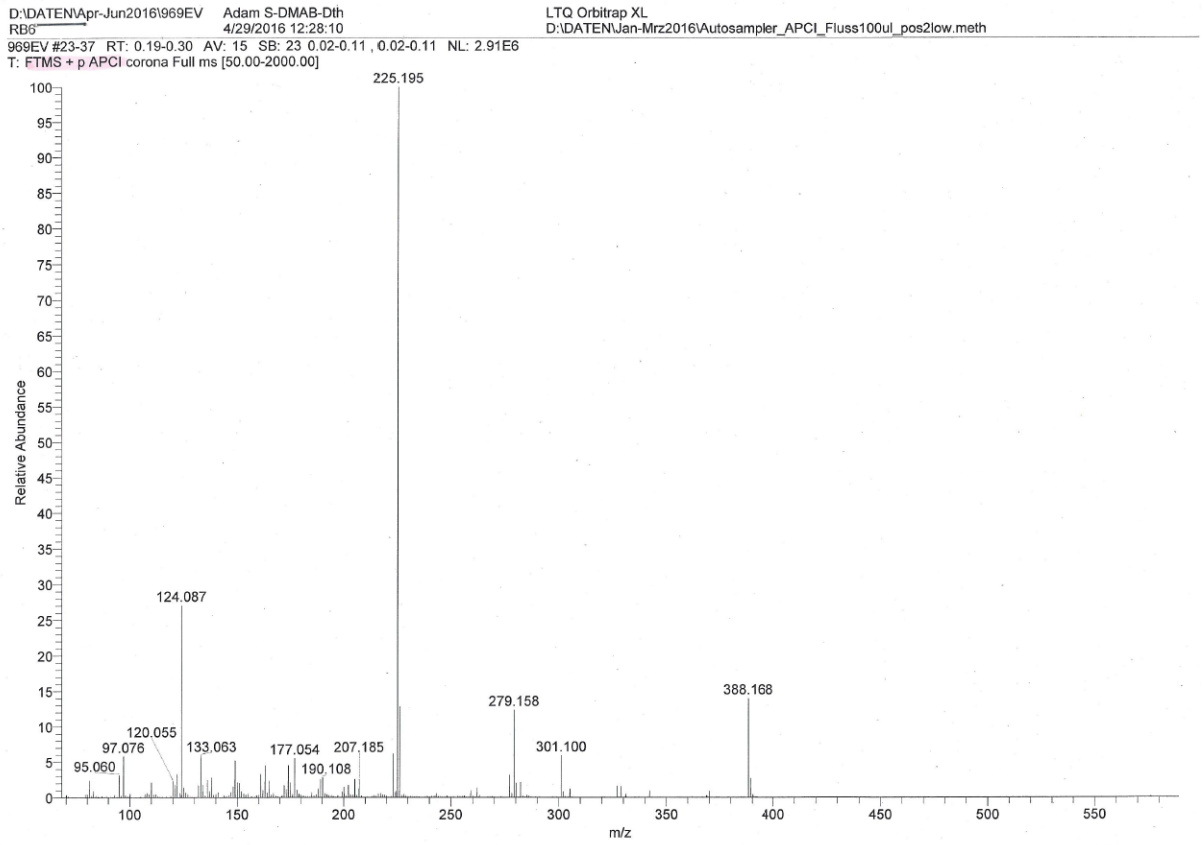
D:\DATEN\Apr-Jun2016\969EV
RB6
Adam S-DMAB-Dth
4/29/2016 12:28:10
LTQ Orbitrap XL
D:\DATEN\Jan-Mrz2016\Autosampler_APCI_Fluss100ul_pos2low.meth
969EV #23-37 RT: 0.19-0.30 AV: 15 SB: 23 0.02-0.11 , 0.02-0.11 NL: 2.91E6
T: FTMS + p APCI corona Full ms [50.00-2000.00]
225.195
124.087
279.158
388.168
120.055
97.076
133.063
177.054
207.185
301.100
95.060
190.108
Relative Abundance
m/z

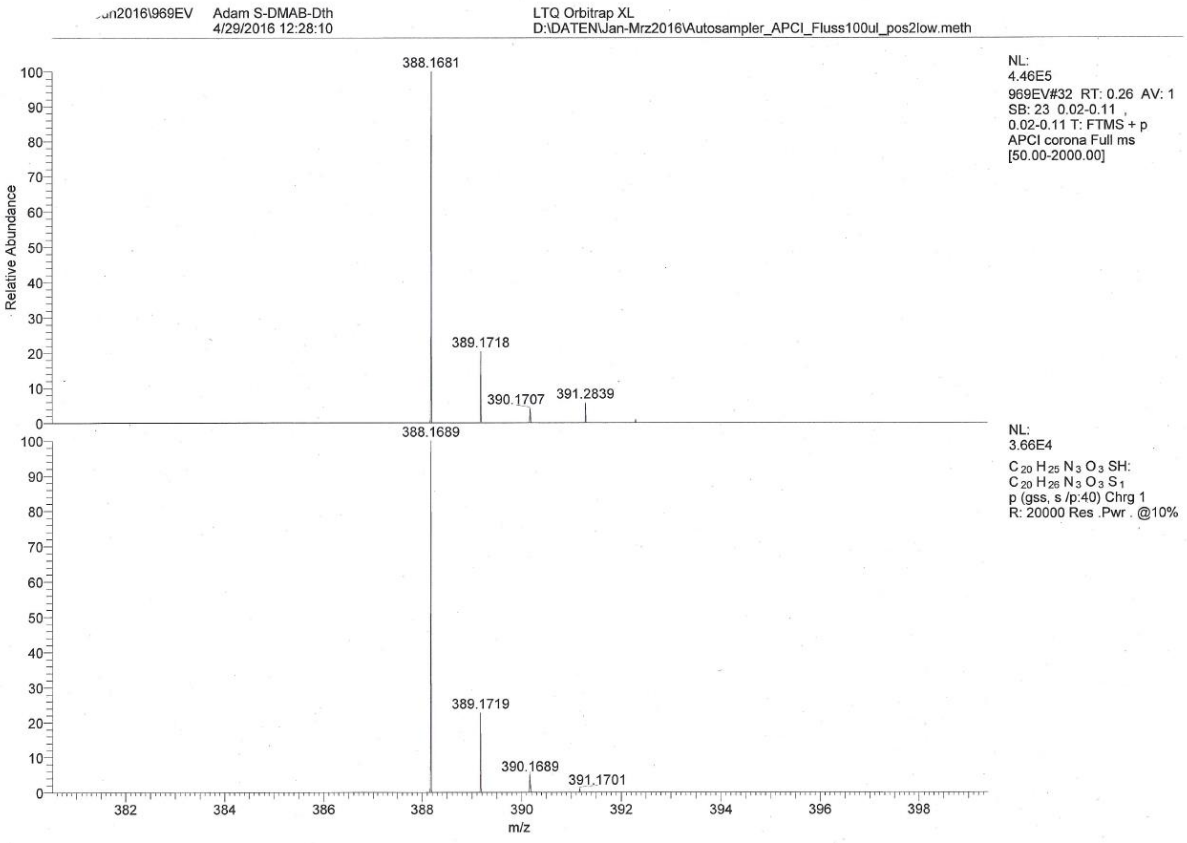
Adam S-DMAB-Dth
4/29/2016 12:28:10
LTQ Orbitrap XL
D:\DATEN\Jan-Mrz2016\Autosampler_APCI_Fluss100ul_pos2low.meth
388.1681
389.1718
390.1707
391.2839
NL:
4.46E5
969EV#32 RT: 0.26 AV: 1
SB: 23 0.02-0.11 ,
0.02-0.11 T: FTMS + p
APCI corona Full ms
[50.00-2000.00]
388.1689
389.1719
390.1689
391.1701
NL:
3.66E4
C20 H25 N3 O3 SH:
C20 H26 N3 O3 S1
p (gss, s /p:40) Chrg 1
R: 20000 Res .Pwr . @10%
Relative Abundance
m/z

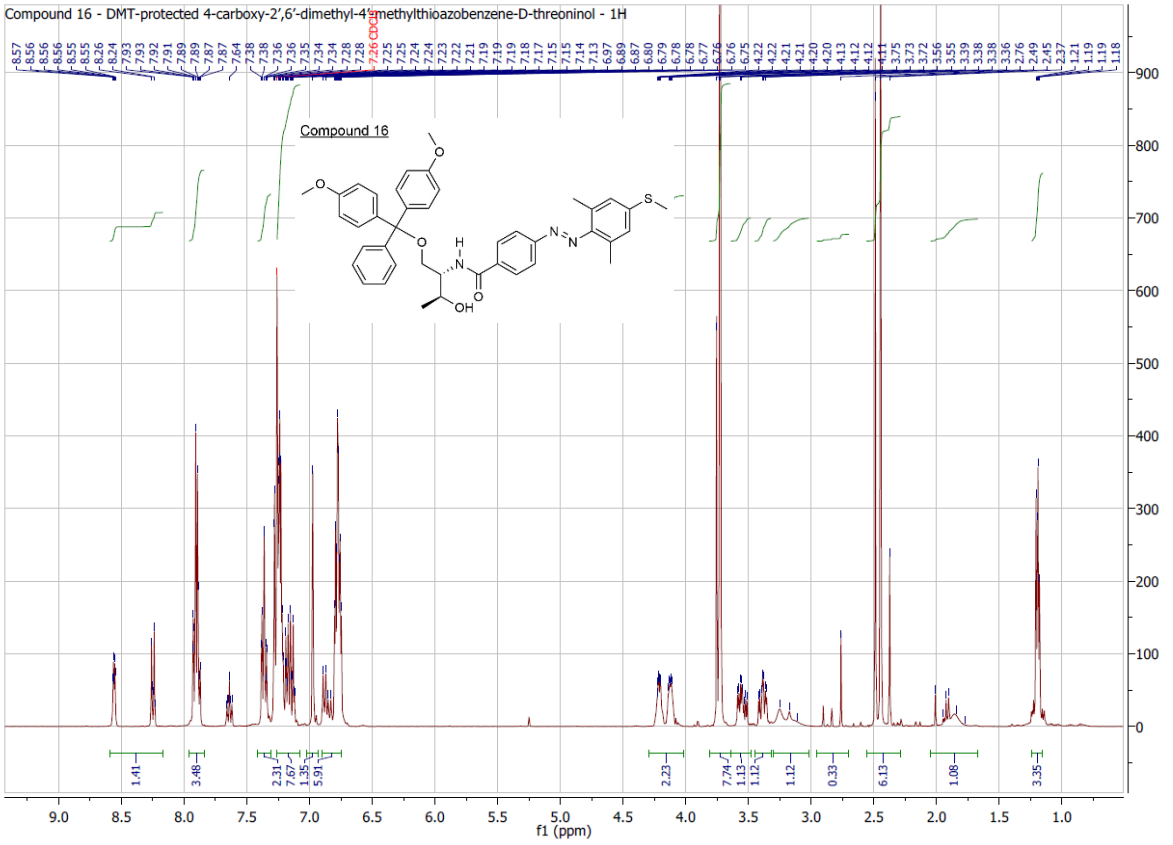
Compound 16 - DMT-protected 4-carboxy-2′,6′-dimethyl-4′-methylthioazobenzene-D-threoninol - 1H
Compound 16
f1 (ppm)

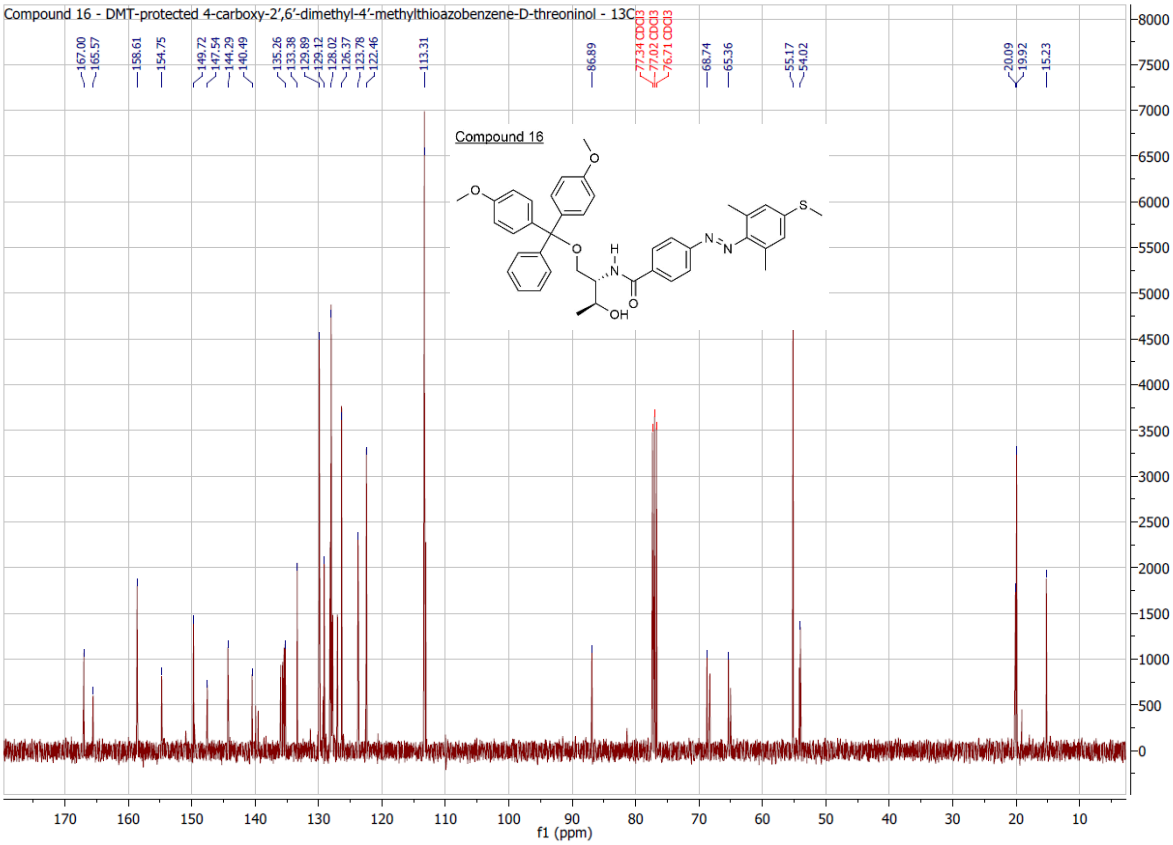
Compound 16 - DMT-protected 4-carboxy-2′,6′-dimethyl-4′-methylthioazobenzene-D-threoninol - 13C
Compound 16
f1 (ppm)

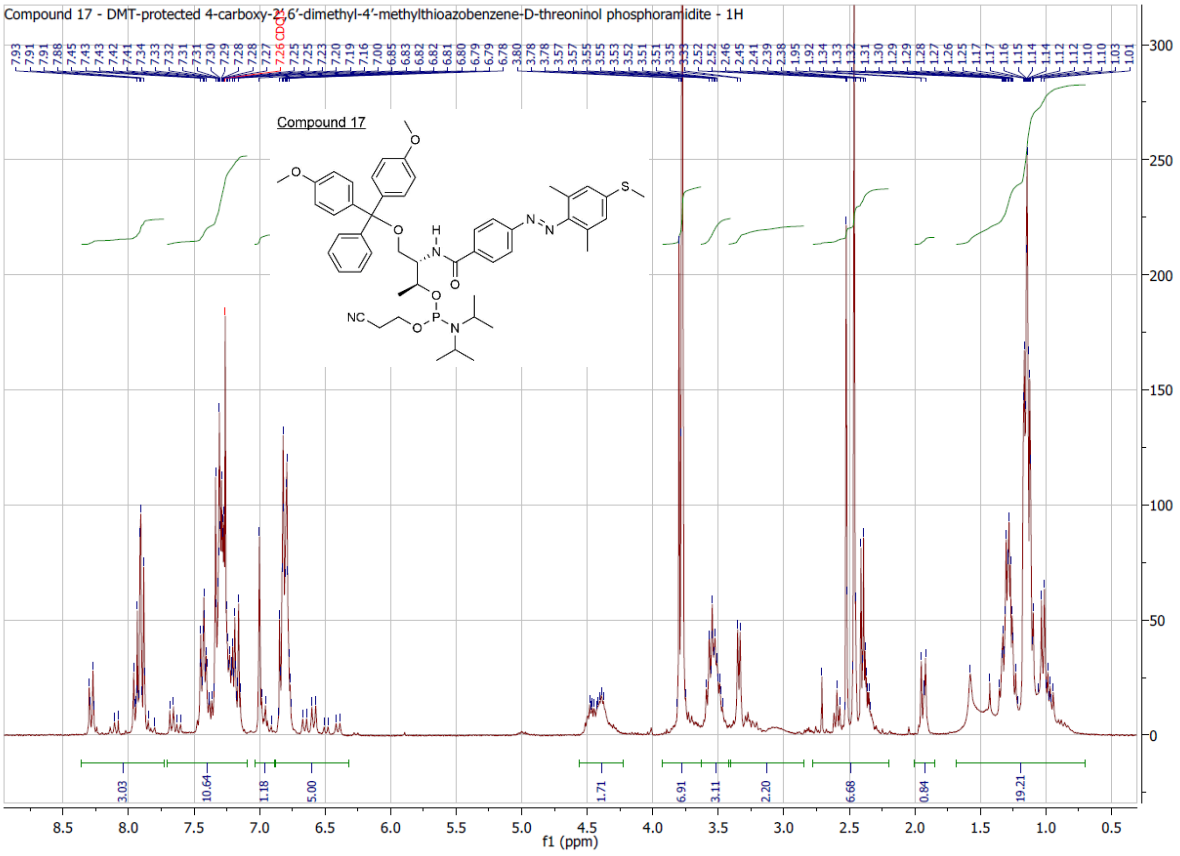
Compound 17 - DMT-protected 4-carboxy-2',6'-dimethyl-4'-methylthioazobenzene-D-threoninol phosphoramidite - 1H
Compound 17
f1 (ppm)

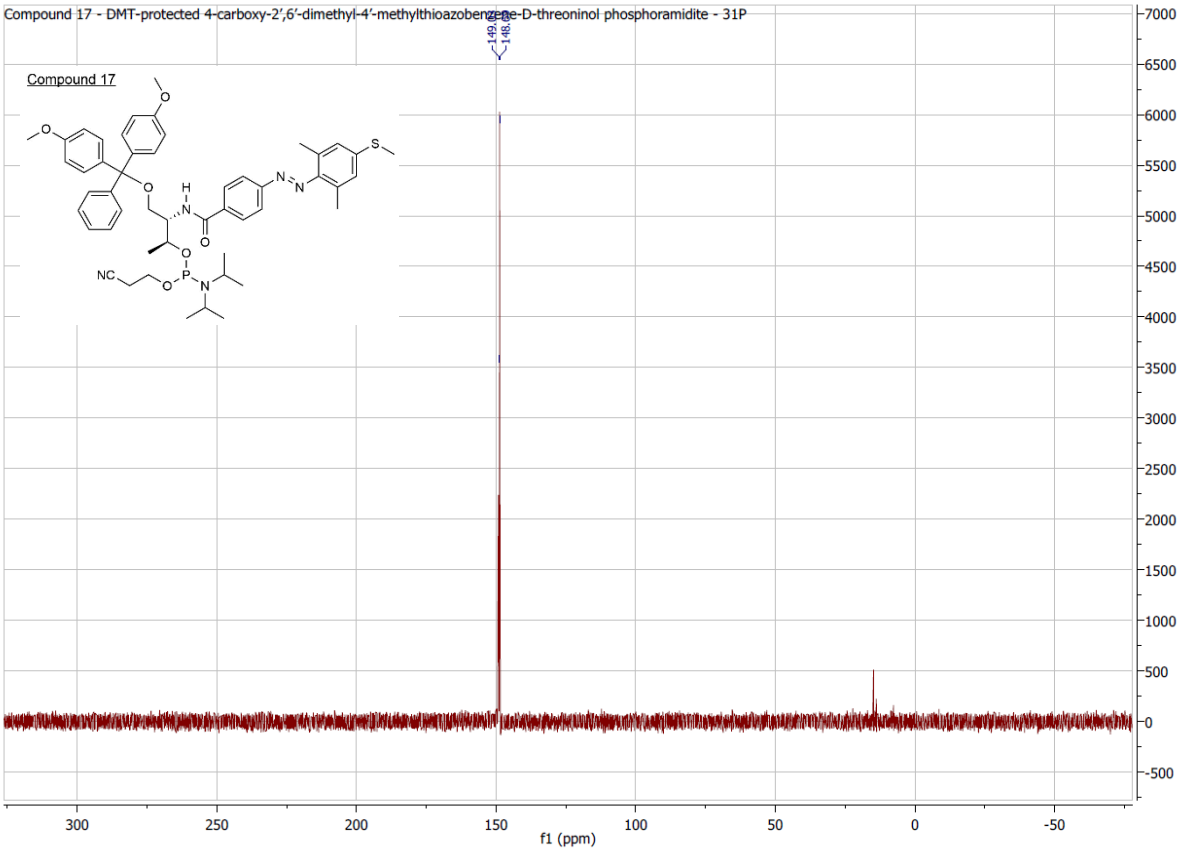
Compound 17 - DMT-protected 4-carboxy-2',6'-dimethyl-4'-methylthioazobenzene-D-threoninol phosphoramidite - 31P
Compound 17
f1 (ppm)

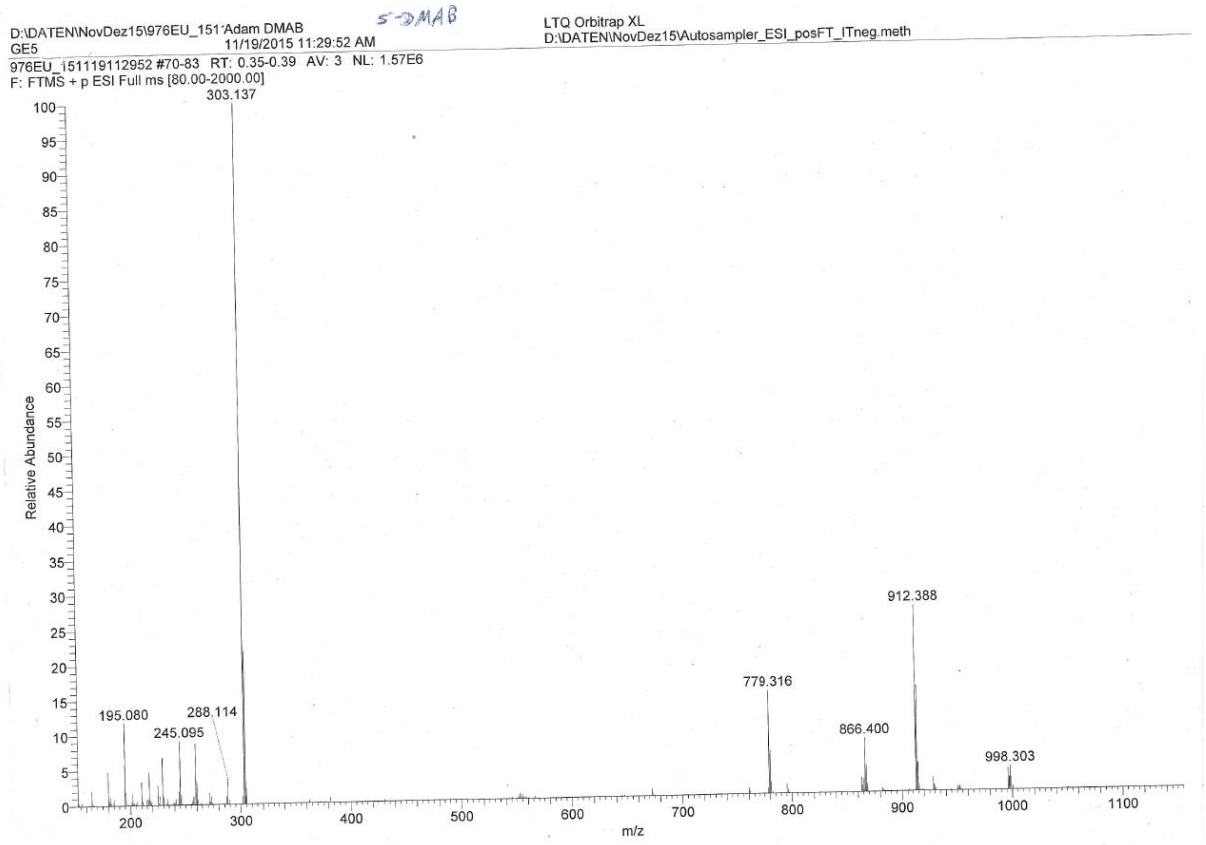
D:\DATEN\NovDez15\976EU_151 Adam DMAB
GE5
11/19/2015 11:29:52 AM
5-DMAB
LTQ Orbitrap XL
D:\DATEN\NovDez15\Autosampler_ESI_posFT_ITneg.meth
976EU_151119112952 #70-83 RT: 0.35-0.39 AV: 3 NL: 1.57E6
F: FTMS + p ESI Full ms [80.00-2000.00]
303.137
912.388
779.316
866.400
998.303
195.080
288.114
245.095
Relative Abundance
m/z

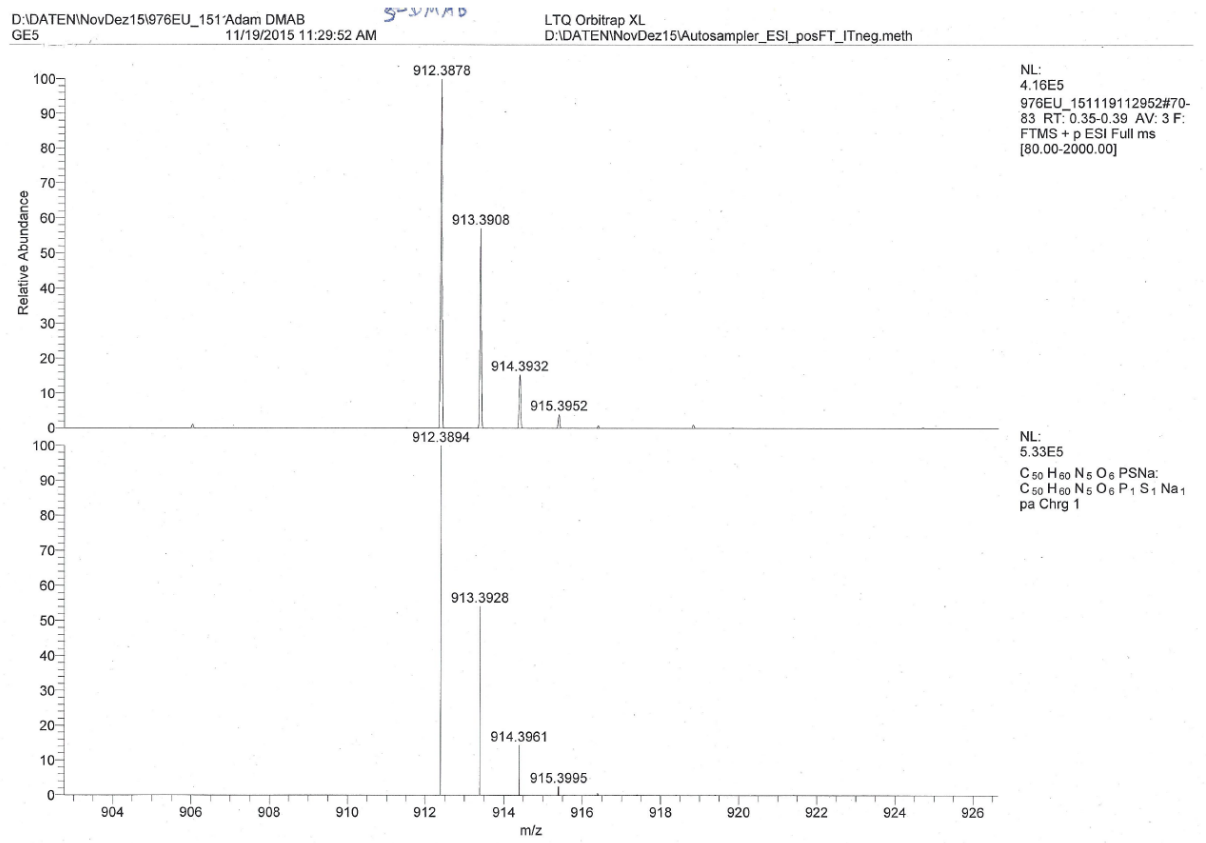
D:\DATEN\NovDez15\976EU_151 Adam DMAB
GE5
11/19/2015 11:29:52 AM
5-DMAB
LTQ Orbitrap XL
D:\DATEN\NovDez15\Autosampler_ESI_posFT_ITneg.meth
912.3878
913.3908
914.3932
915.3952
912.3894
913.3928
914.3961
915.3995
NL:
4.16E5
976EU_151119112952#70-83 RT: 0.35-0.39 AV: 3 F: FTMS + p ESI Full ms [80.00-2000.00]
NL:
5.33E5
C50 H60 N5 O6 PSNa:
C50 H60 N5 O6 P1 S1 Na1
pa Chrg 1
Relative Abundance
m/z

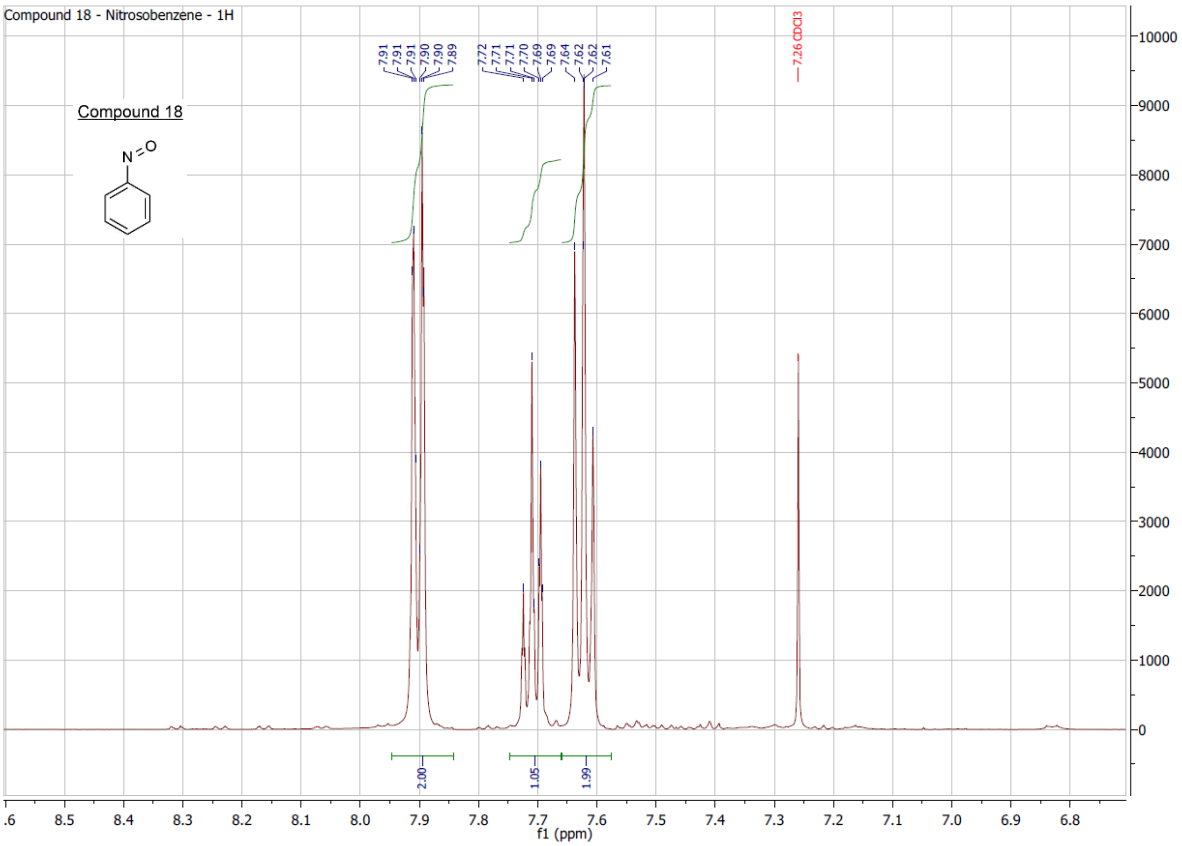
Compound 18 - Nitrosobenzene - 1H
Compound 18
7.91
7.91
7.91
7.90
7.90
7.89
7.72
7.71
7.71
7.70
7.69
7.64
7.62
7.62
7.61
7.26 CDCl3
2.00
1.05
1.99
f1 (ppm)

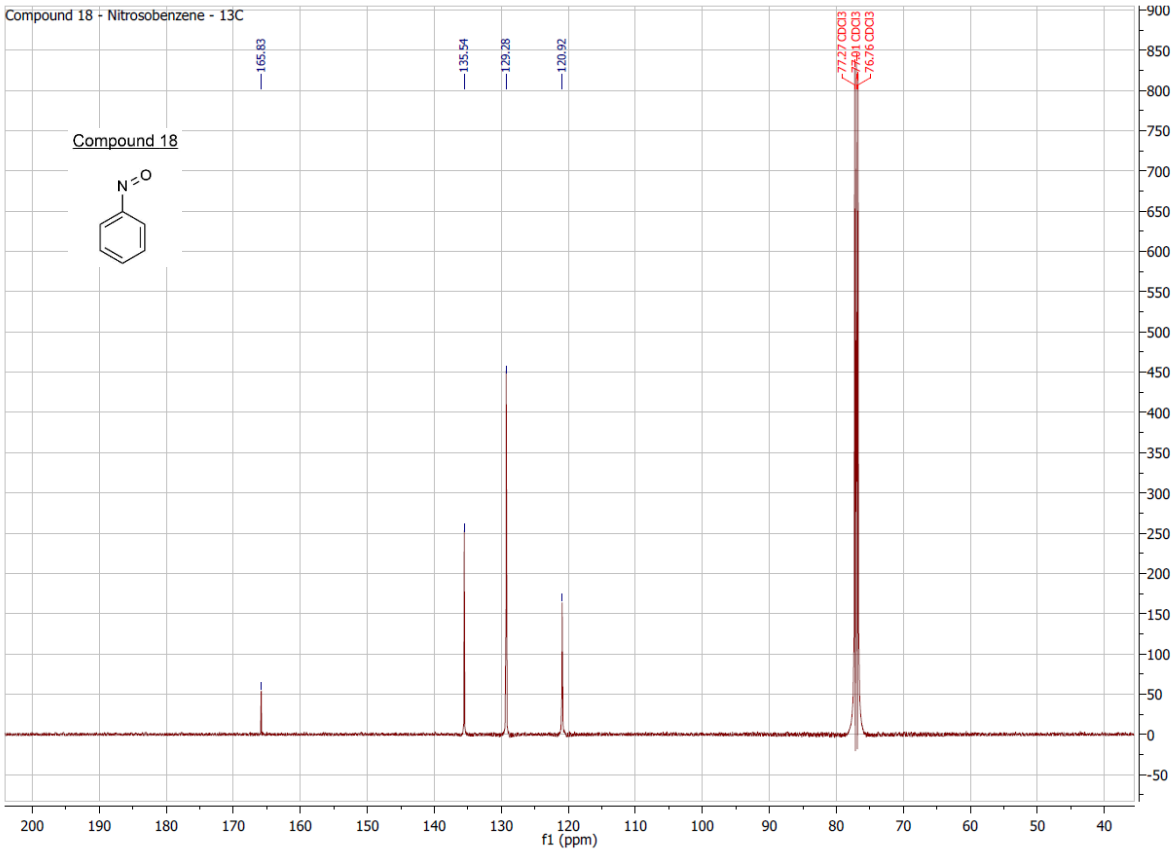
Compound 18 - Nitrosobenzene - 13C
Compound 18
165.83
135.54
129.28
120.92
77.27 CDCl3
77.01 CDCl3
76.76 CDCl3
f1 (ppm)

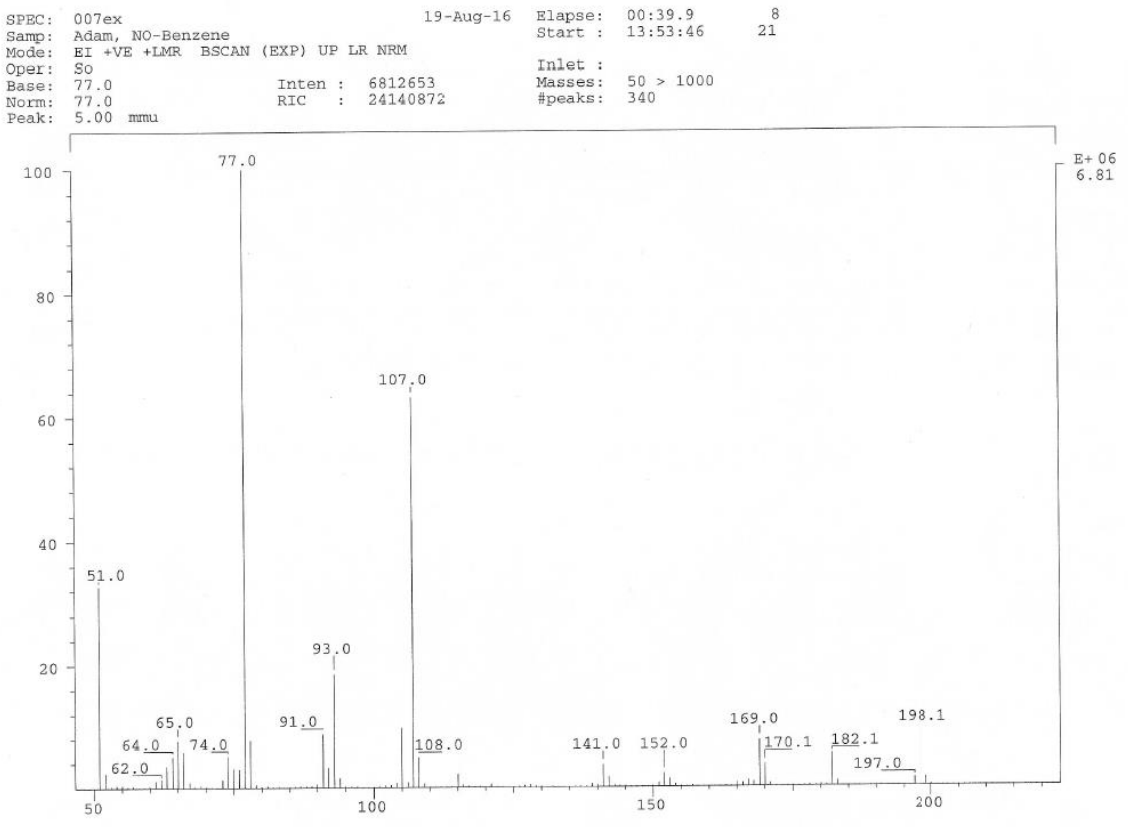
SPEC: 007ex
19-Aug-16
Elapse: 00:39.9 8
Samp: Adam, NO-Benzene
Start : 13:53:46 21
Mode: EI +VE +LMR BSCAN (EXP) UP LR NRM
Oper: So
Inlet :
Base: 77.0 Inten : 6812653
Masses: 50 > 1000
Norm: 77.0 RIC : 24140872
#peaks: 340
Peak: 5.00 mmu
E+ 06
6.81
100
80
60
40
20
77.0
107.0
51.0
93.0
65.0
91.0
64.0
74.0
108.0
62.0
141.0
152.0
169.0
198.1
170.1
182.1
197.0
50
100
150
200

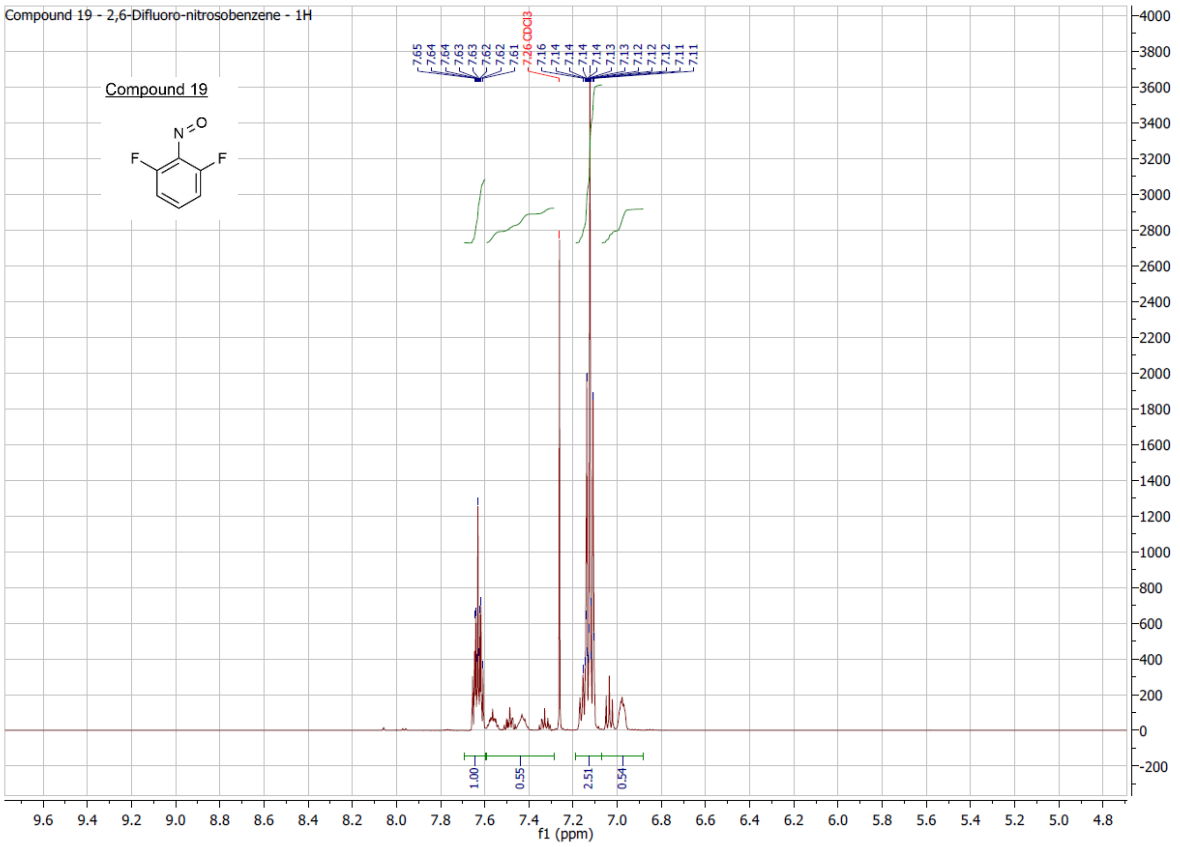
Compound 19 - 2,6-Difluoro-nitrosobenzene - 1H
Compound 19
7.65
7.64
7.64
7.63
7.63
7.62
7.62
7.61
7.26 CDCl3
7.16
7.14
7.14
7.14
7.14
7.13
7.12
7.12
7.12
7.11
7.11
1.00
0.55
2.51
0.54
f1 (ppm)

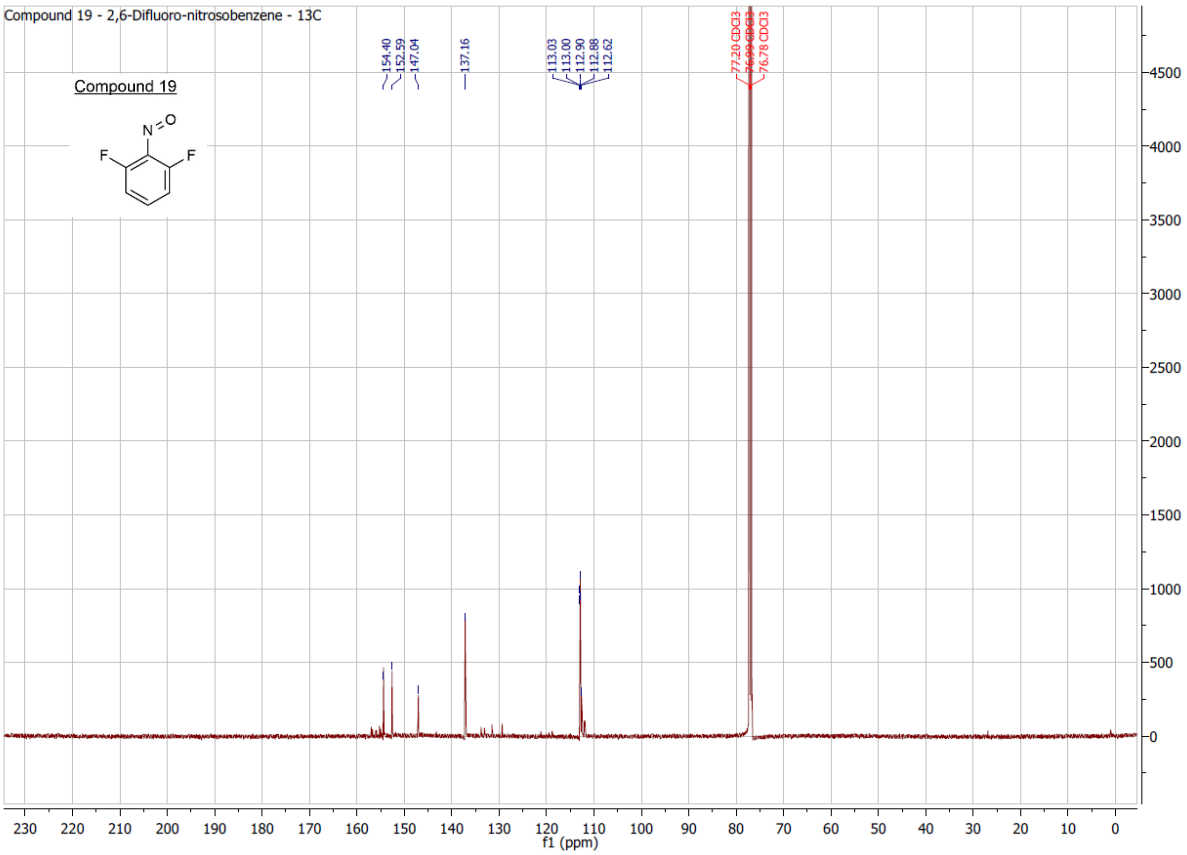
Compound 19 - 2,6-Difluoro-nitrosobenzene - 13C
Compound 19
154.40
152.59
147.04
137.16
113.03
113.00
112.90
112.88
112.62
77.20 CDCl3
76.78 CDCl3
f1 (ppm)

SPEC: 227ez 16-Jun-17 Elapse: 00:52.9 12
Samp: Adam, DFA-NO Start : 09:50:42 13
Mode: EI +VE +LMR BSCAN (EXP) UP LR NRM
Oper: So Inlet :
Base: 143.1 Inten : 2960037 Masses: 50 > 1000
Norm: 143.1 RIC : 9104375 #peaks: 133
Peak: 5.00 mmu

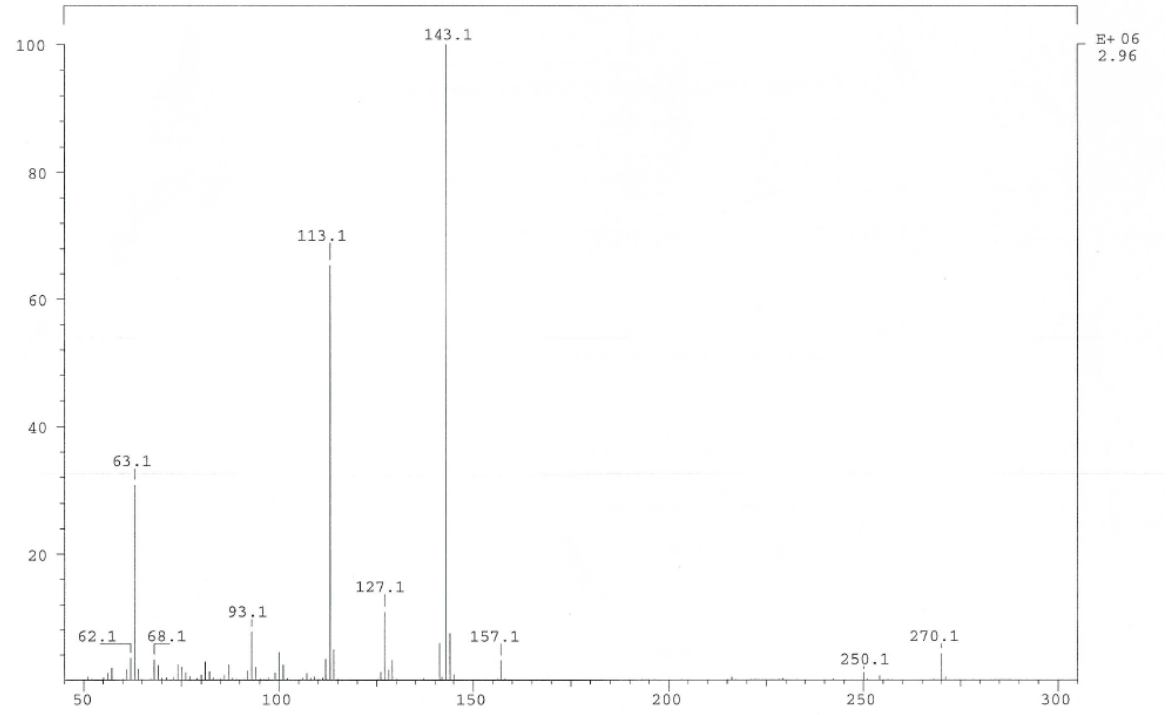

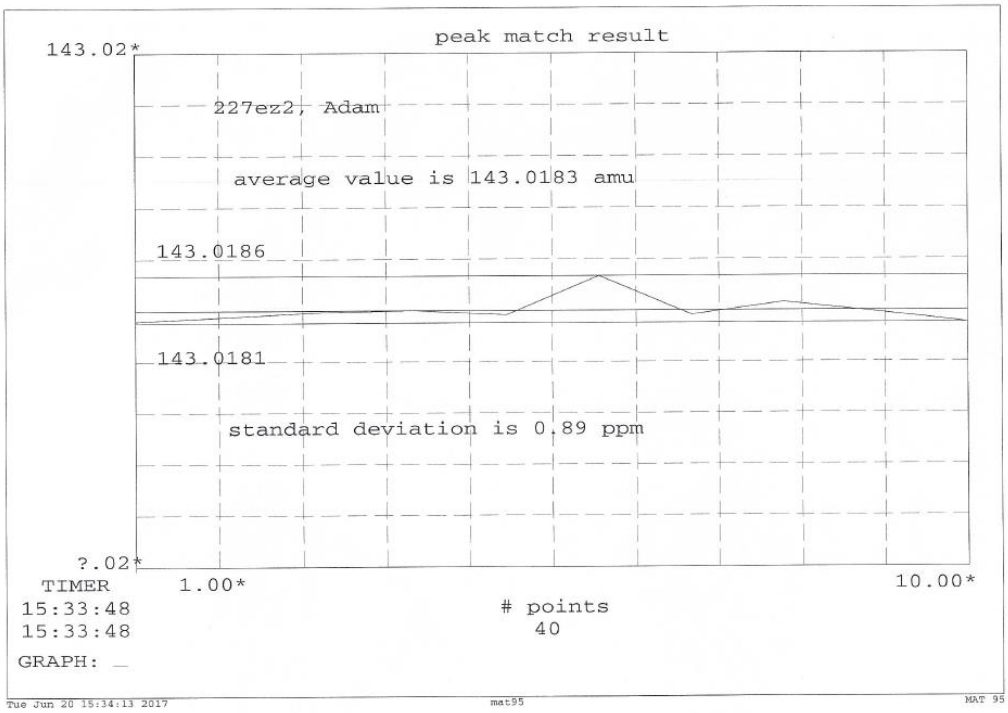

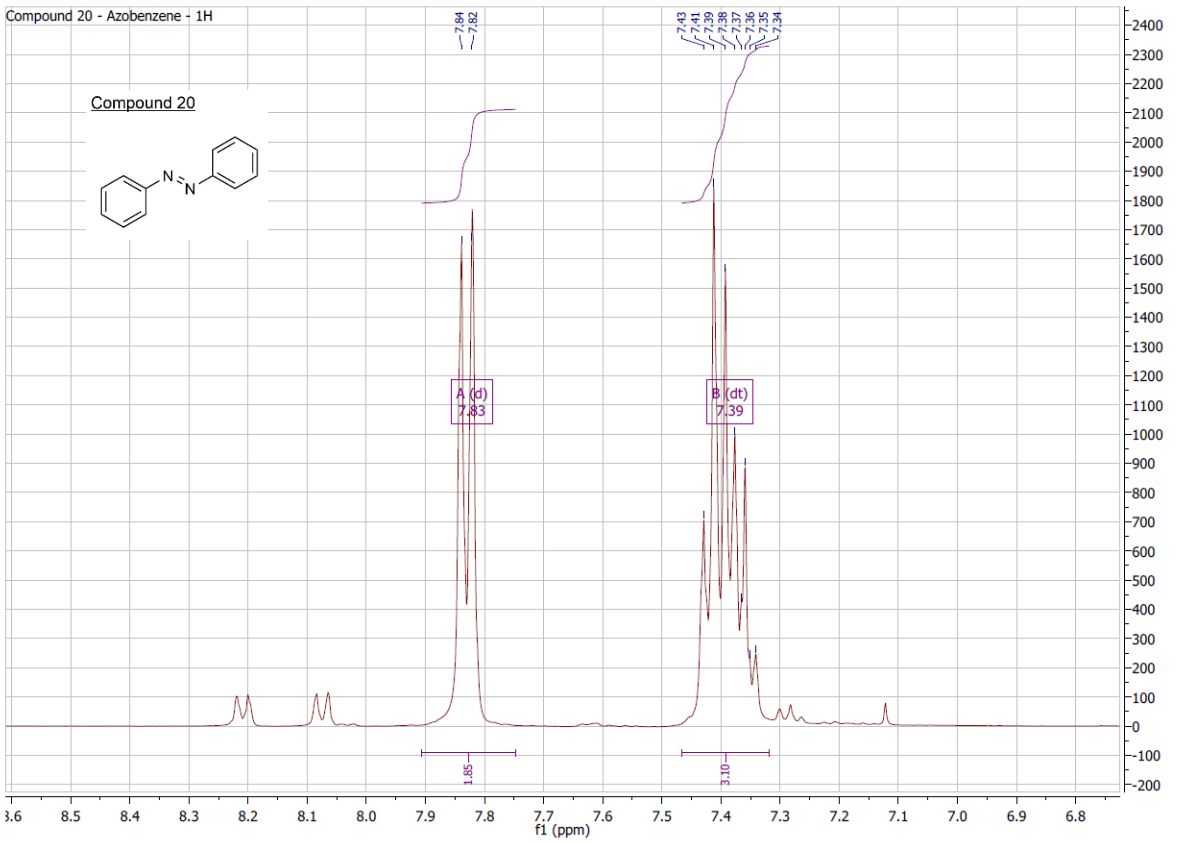
Compound 20 - Azobenzene - 1H
Compound 20
7.84
7.82
7.43
7.41
7.39
7.38
7.37
7.36
7.35
7.34
A (d)
7.83
B (dt)
7.39
1.85
3.10
f1 (ppm)

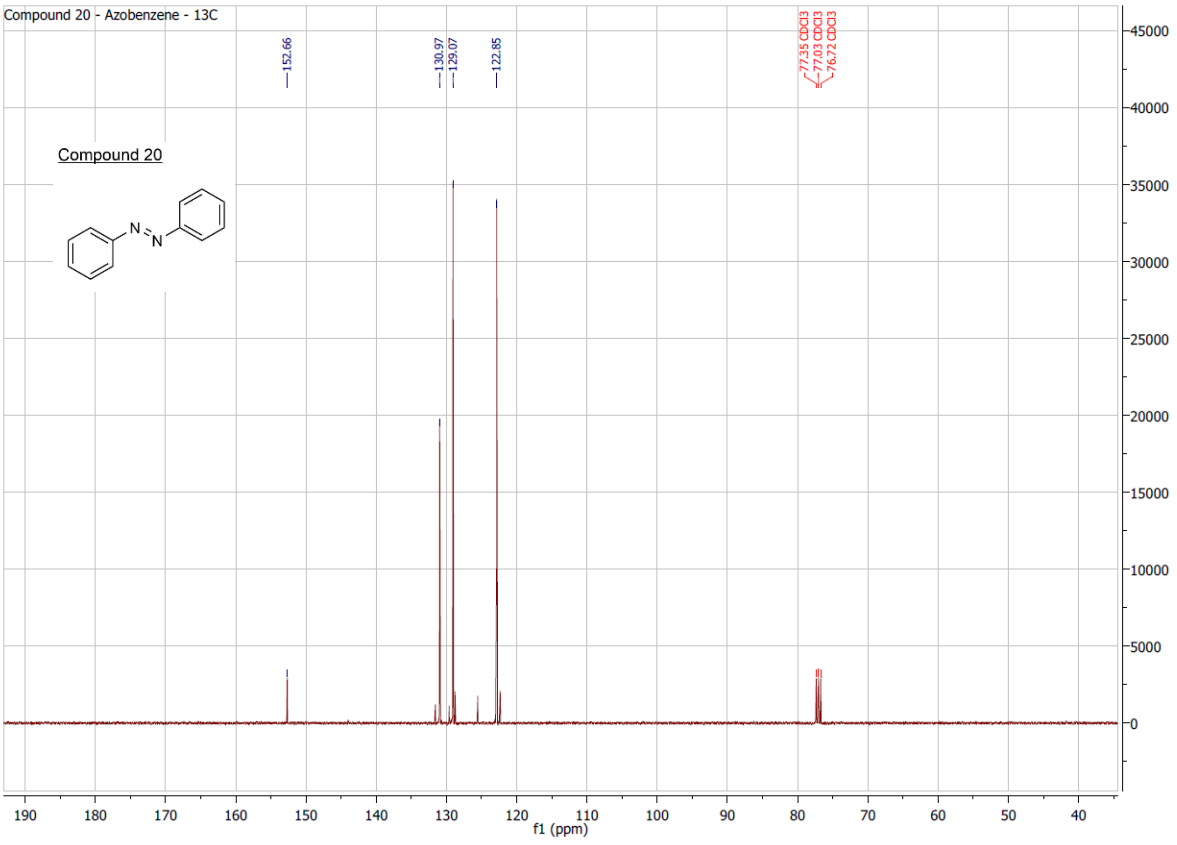
Compound 20 - Azobenzene - 13C
Compound 20
152.66
130.97
129.07
122.85
77.35 CDCl3
77.03 CDCl3
76.72 CDCl3
f1 (ppm)

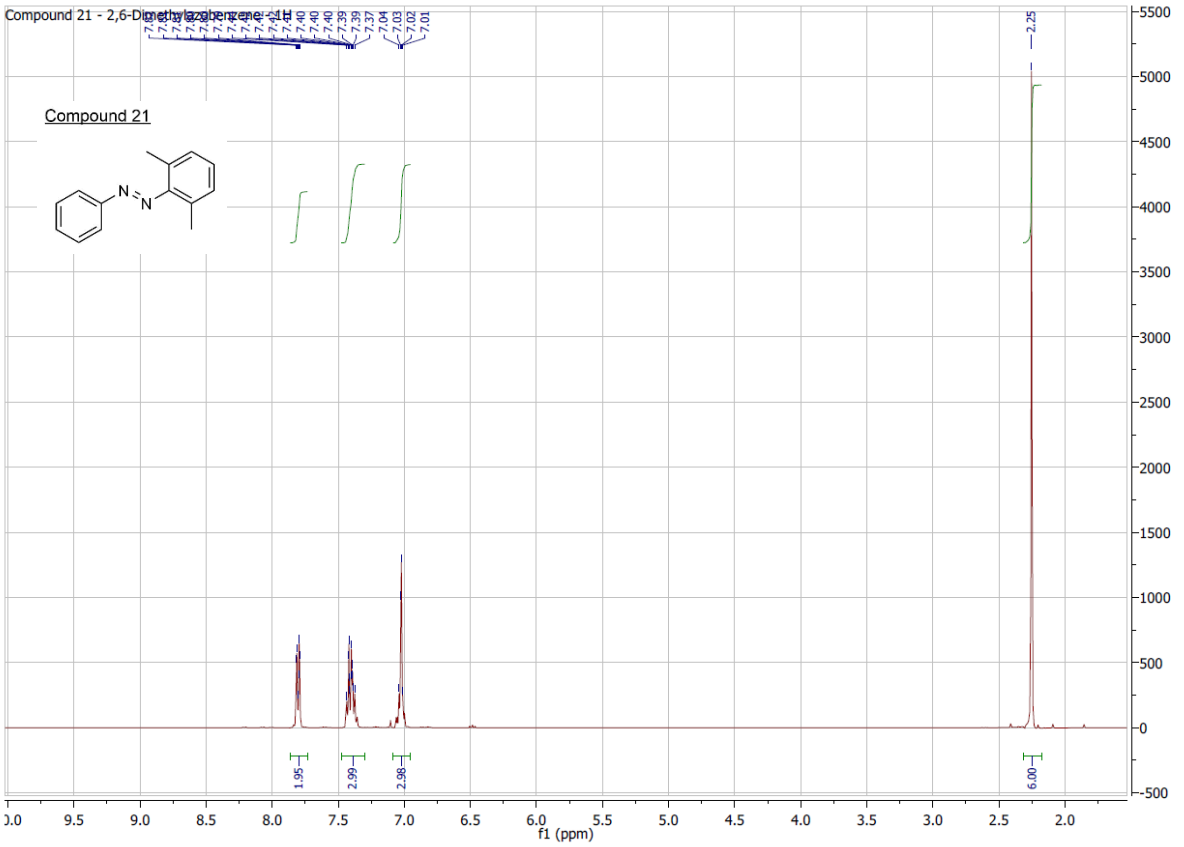
Compound 21 - 2,6-Dimethylazobenzene - 1H
Compound 21
7.41
7.40
7.40
7.40
7.39
7.39
7.37
7.04
7.03
7.02
7.01
2.25
1.95
2.99
2.98
6.00
f1 (ppm)

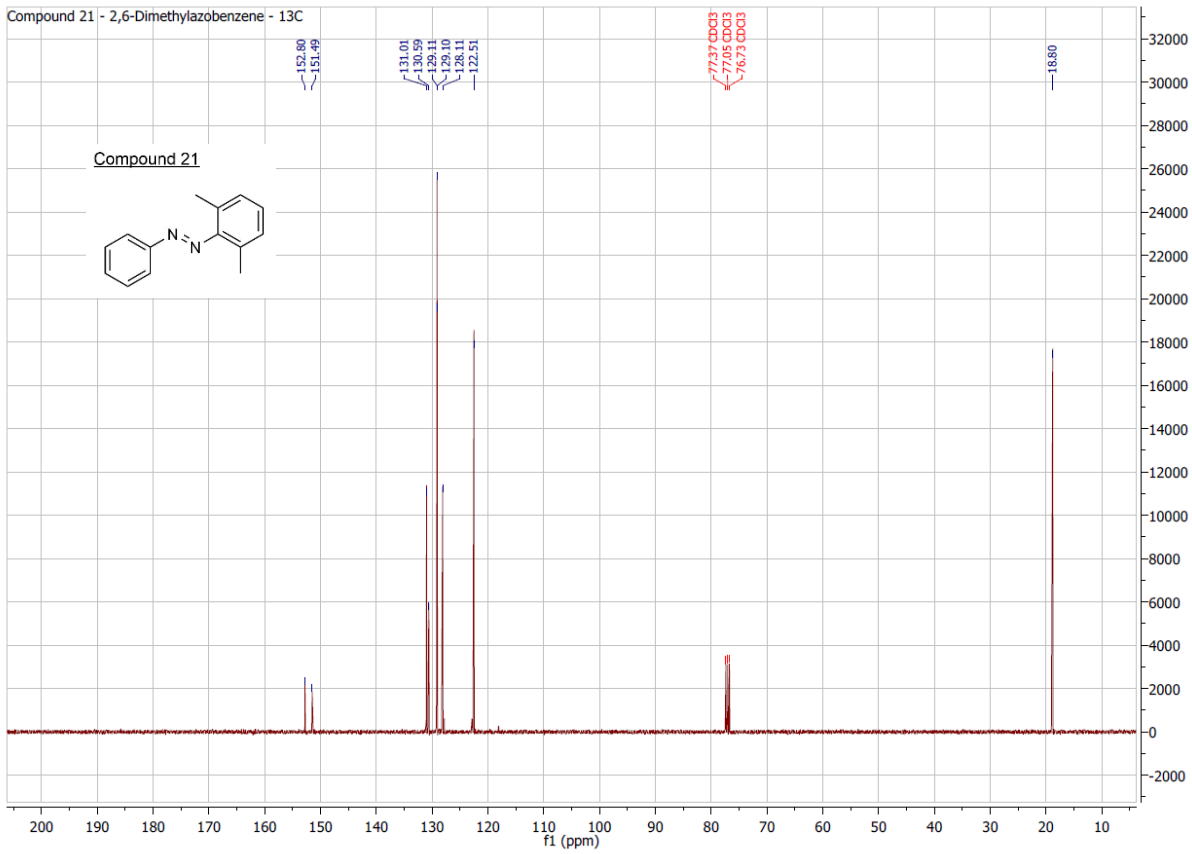
Compound 21 - 2,6-Dimethylazobenzene - 13C
Compound 21
152.80
151.49
131.01
130.59
129.11
129.10
128.11
122.51
77.37 CDCl3
77.05 CDCl3
76.73 CDCl3
18.80
f1 (ppm)

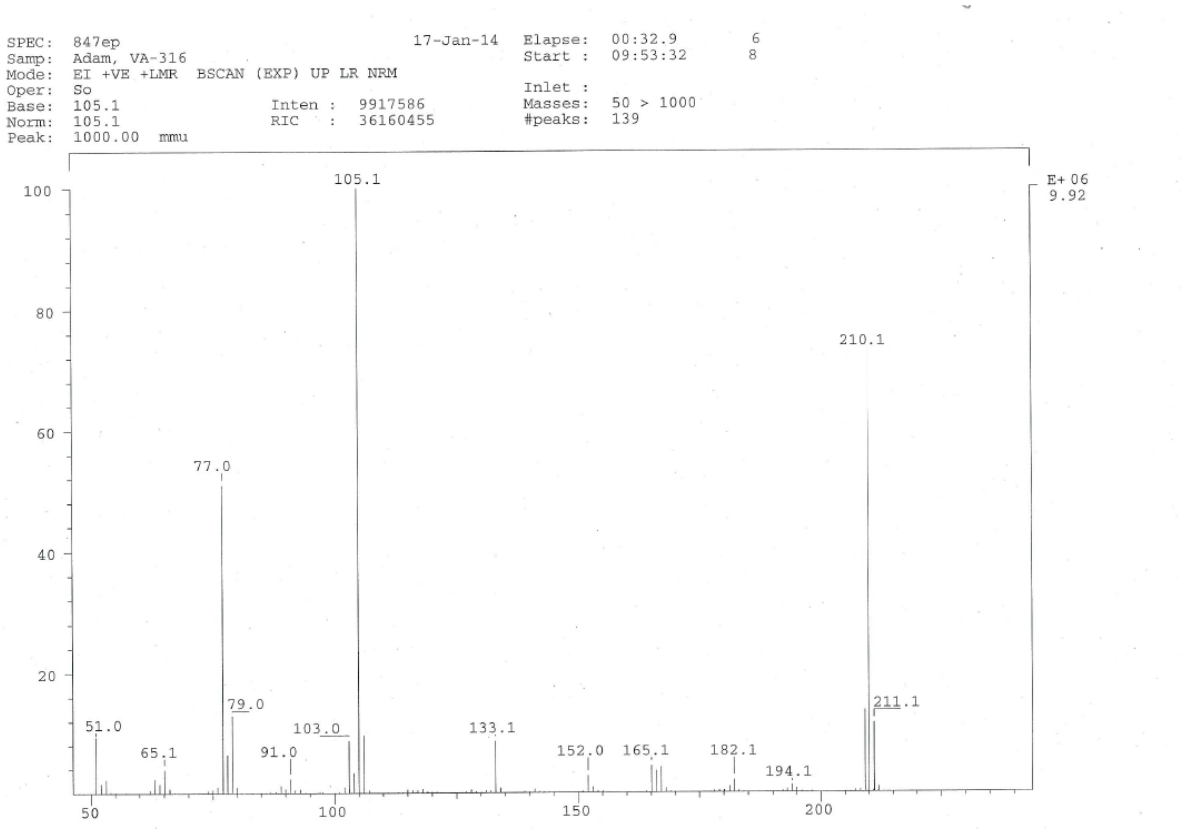
SPEC: 847ep
Samp: Adam, VA-316
Mode: EI +VE +LMR BSCAN (EXP) UP LR NRM
Oper: So
Base: 105.1
Norm: 105.1
Peak: 1000.00 mmu
17-Jan-14
Inten : 9917586
RIC : 36160455
Elapse: 00:32.9 6
Start : 09:53:32 8
Inlet :
Masses: 50 > 1000
#peaks: 139
E+06
9.92
105.1
210.1
77.0
79.0
211.1
51.0
103.0
133.1
65.1
91.0
152.0
165.1
182.1
194.1
100
80
60
40
20
50
100
150
200

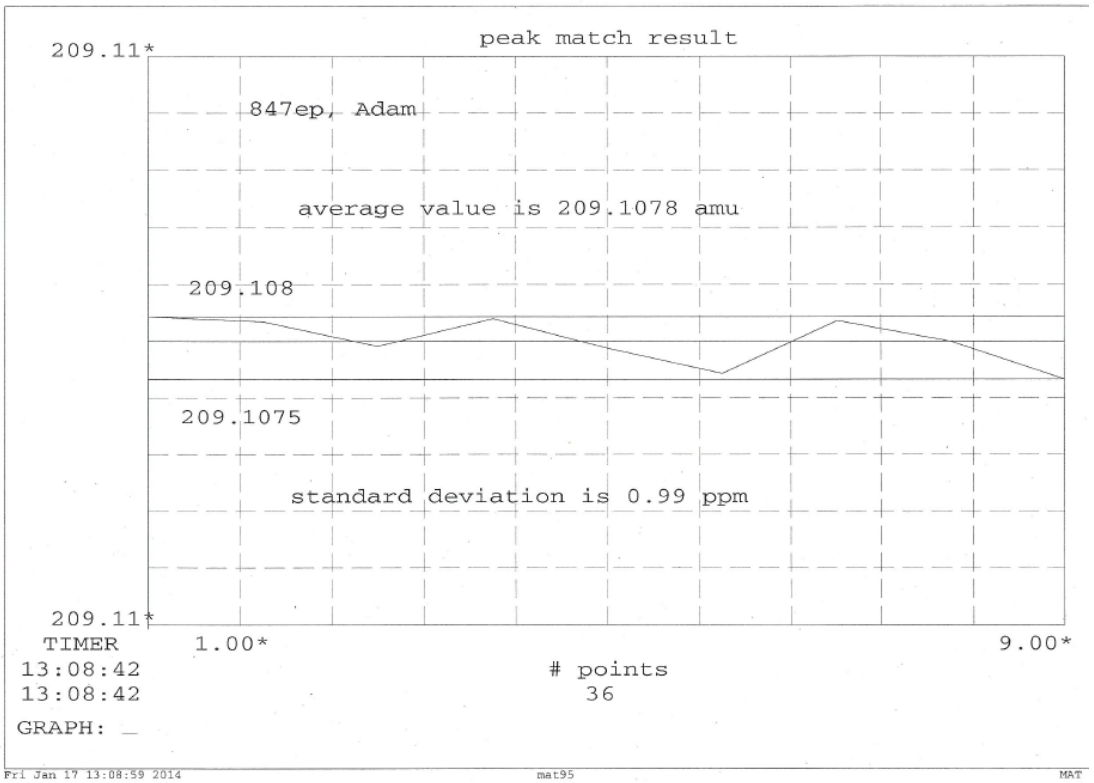
peak match result
209.11*
847ep, Adam
average value is 209.1078 amu
209.108
209.1075
standard deviation is 0.99 ppm
209.11*
TIMER
1.00*
9.00*
13:08:42
13:08:42
points
36
GRAPH:
Fri Jan 17 13:08:59 2014
mat95
MAT

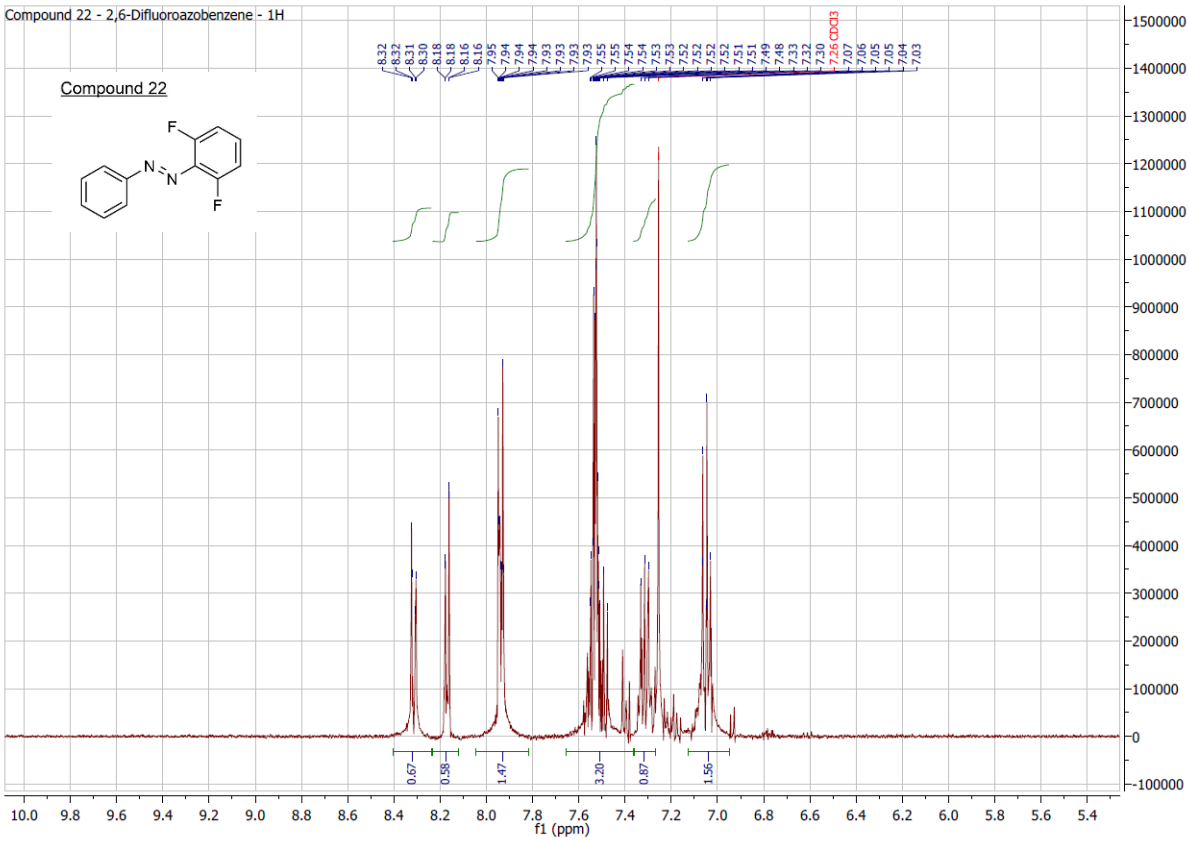
Compound 22 - 2,6-Difluoroazobenzene - 1H
Compound 22
F
N
N
F
8.32
8.32
8.31
8.30
8.18
8.18
8.16
8.16
7.95
7.94
7.94
7.93
7.93
7.93
7.93
7.55
7.55
7.54
7.54
7.53
7.53
7.52
7.52
7.52
7.52
7.51
7.51
7.49
7.48
7.33
7.32
7.30
7.26 CDCl3
7.07
7.06
7.05
7.05
7.04
7.03
0.67
0.58
1.47
3.20
0.87
1.56
f1 (ppm)

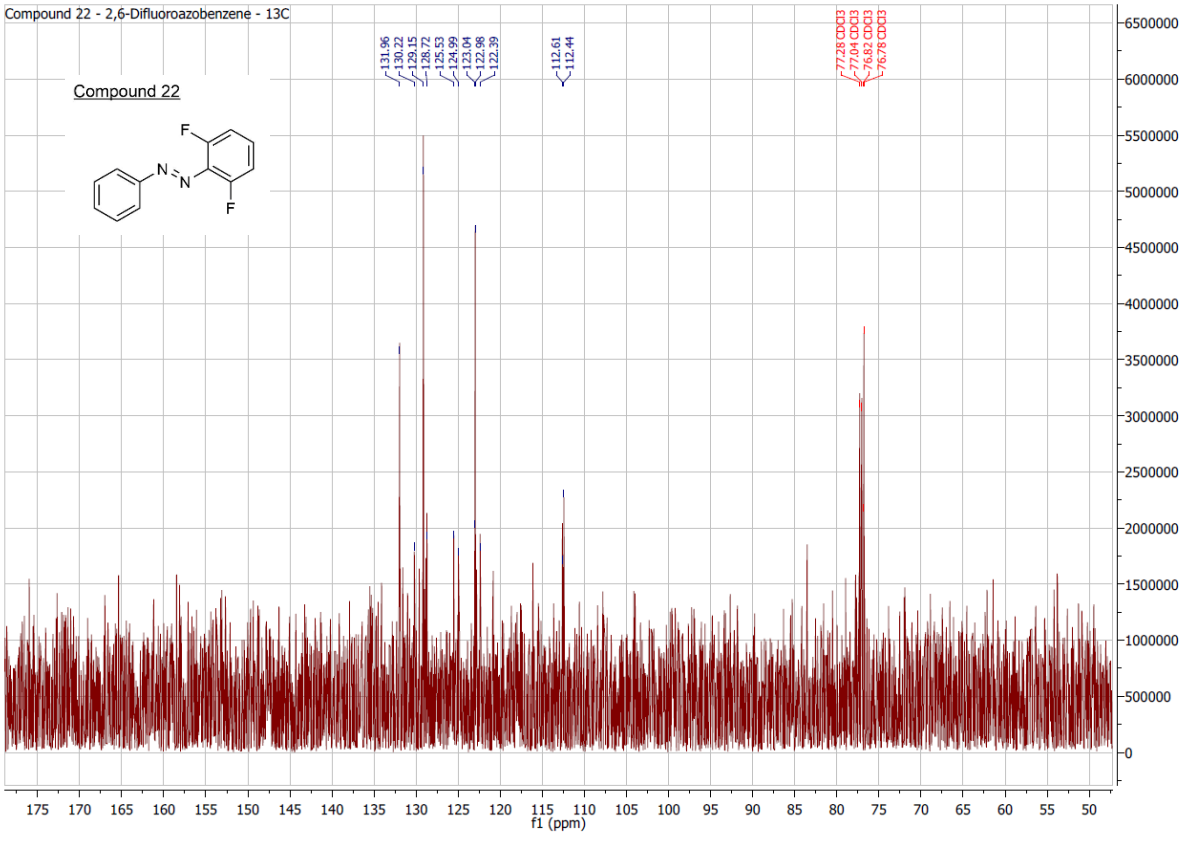
Compound 22 - 2,6-Difluoroazobenzene - 13C
Compound 22
F
N
N
F
131.96
130.22
129.15
128.72
125.53
124.99
123.04
122.98
122.39
112.61
112.44
77.28 CDCl3
77.04 CDCl3
76.82 CDCl3
76.78 CDCl3
f1 (ppm)

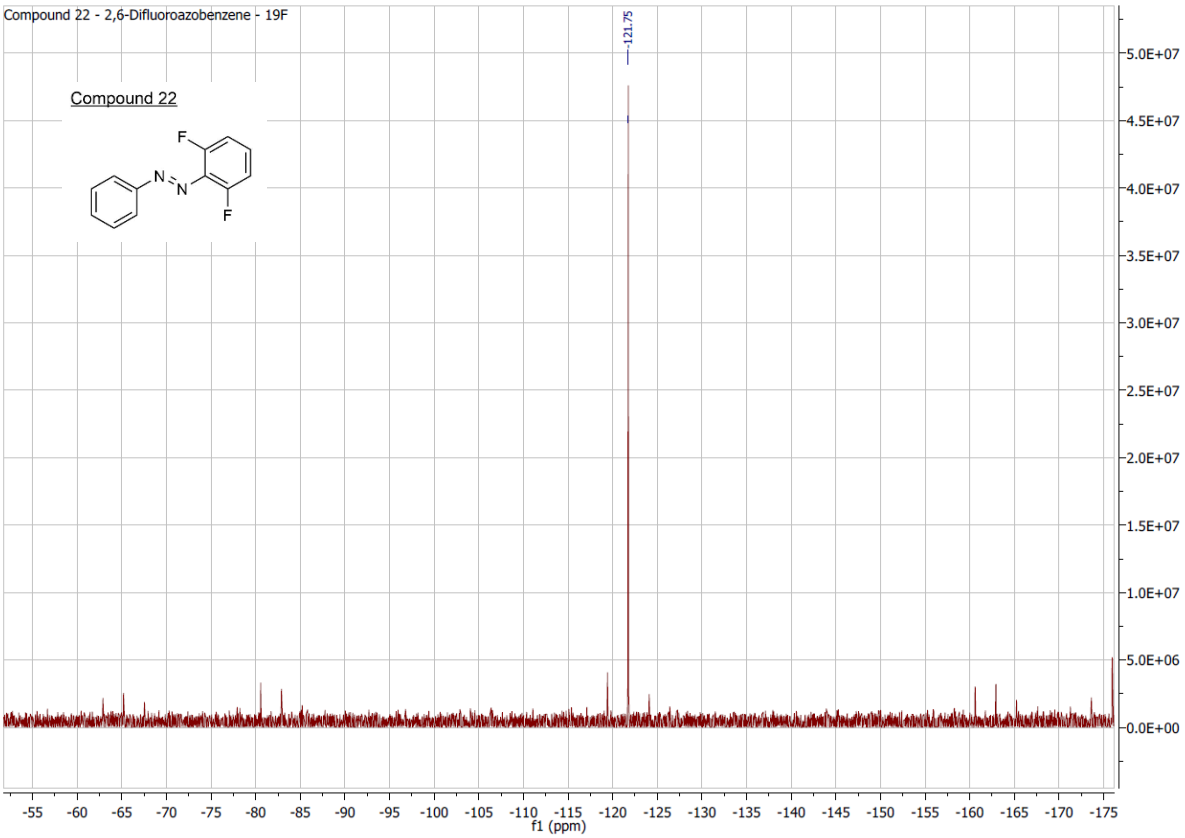
Compound 22 - 2,6-Difluoroazobenzene - 19F
Compound 22
F
N
N
F
-121.75
5.0E+07
4.5E+07
4.0E+07
3.5E+07
3.0E+07
2.5E+07
2.0E+07
1.5E+07
1.0E+07
5.0E+06
0.0E+00
-55 -60 -65 -70 -75 -80 -85 -90 -95 -100 -105 -110 -115 -120 -125 -130 -135 -140 -145 -150 -155 -160 -165 -170 -175
f1 (ppm)

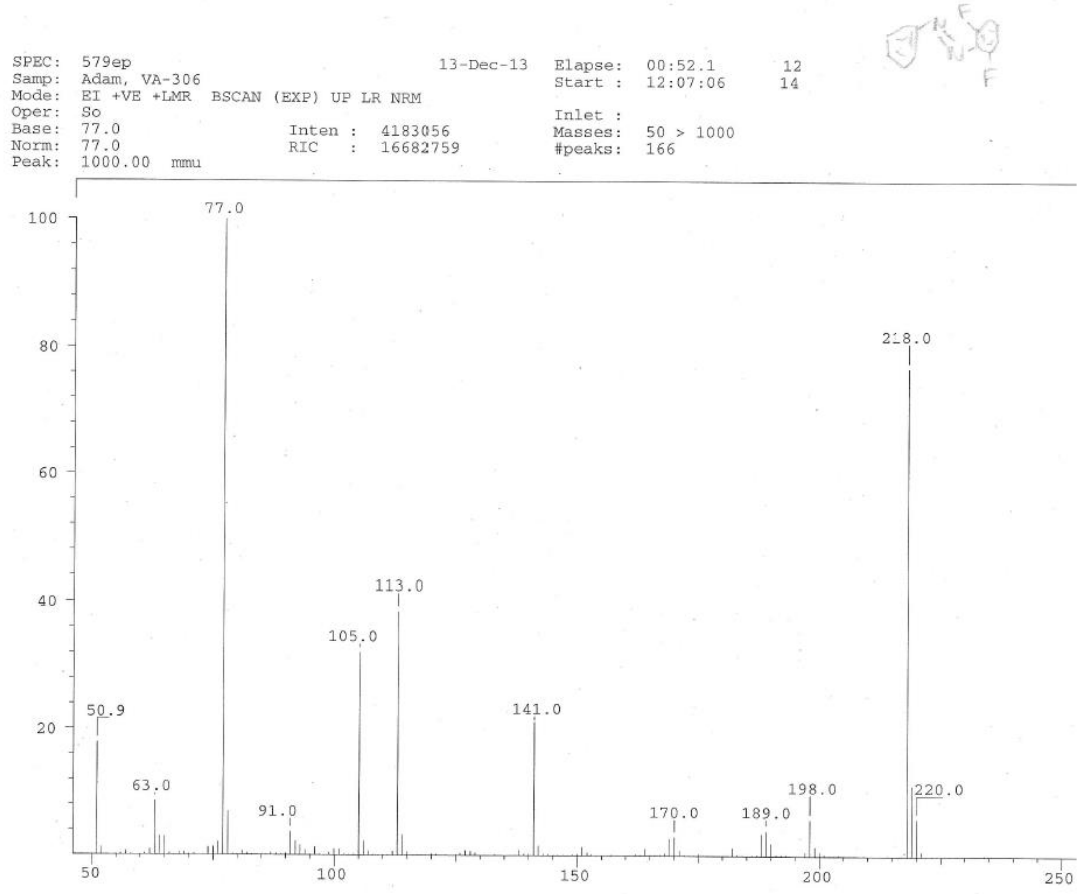
SPEC: 579ep
Samp: Adam, VA-306
Mode: EI +VE +LMR BSCAN (EXP) UP LR NRM
Oper: So
Base: 77.0
Norm: 77.0
Peak: 1000.00 mmu
13-Dec-13
Inten : 4183056
RIC : 16682759
Elapse: 00:52.1 12
Start : 12:07:06 14
Inlet :
Masses: 50 > 1000
#peaks: 166
77.0
218.0
113.0
105.0
50.9
141.0
63.0
91.0
198.0
220.0
170.0
189.0
100
80
60
40
20
50
100
150
200
250

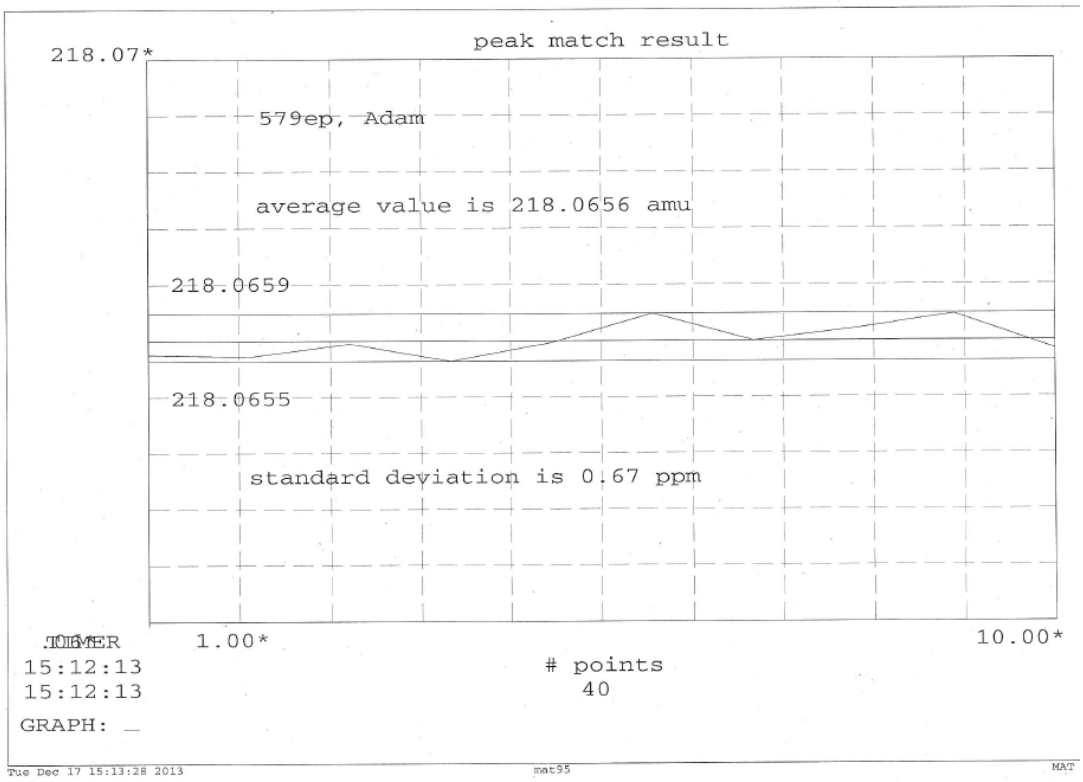
peak match result
218.07*
579ep, Adam
average value is 218.0656 amu
218.0659
218.0655
standard deviation is 0.67 ppm
1.00*
10.00*
15:12:13
15:12:13
points
40
GRAPH:
Tue Dec 17 15:13:28 2013
mat95
MAT

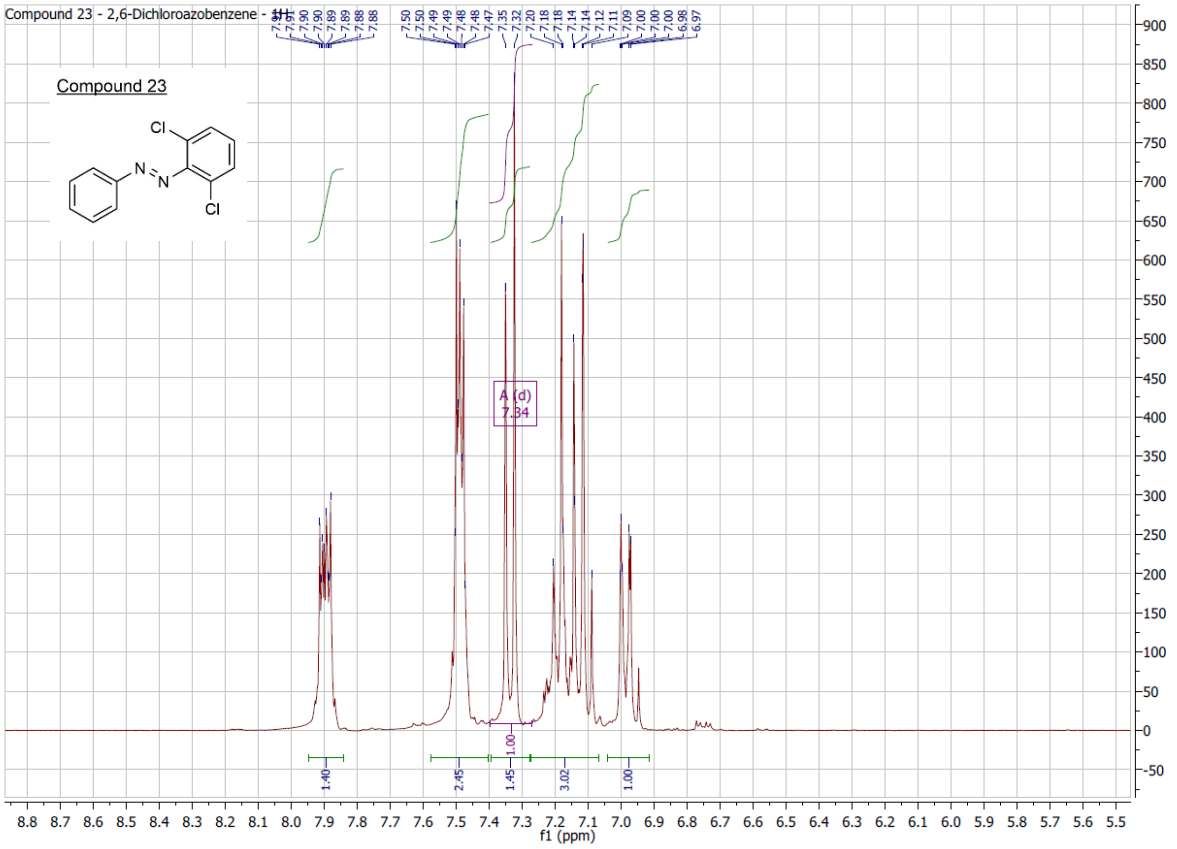
Compound 23 - 2,6-Dichloroazobenzene - 1H
Compound 23
Cl
N
N
Cl
A (d)
7.34
1.00
1.40
2.45
1.45
3.02
1.00
f1 (ppm)

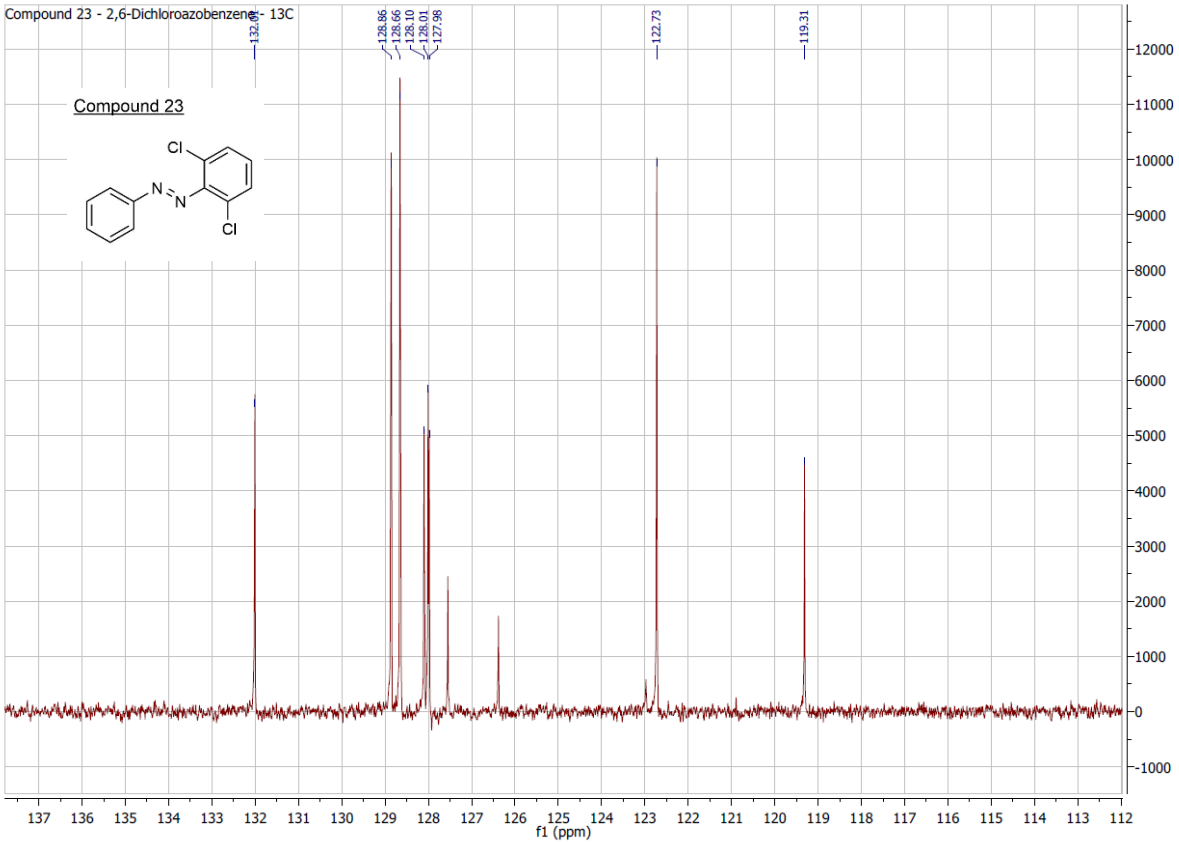
Compound 23 - 2,6-Dichloroazobenzene - 13C
132.46
128.86
128.66
128.10
128.01
127.98
122.73
119.31
Compound 23
Cl
N
N
Cl
f1 (ppm)

SPEC: 684es 22-Jan-15 Elapse: 00:52.4 11
Samp: Adam, VA-299 Start : 10:52:14 12
Mode: EI +VE +LMR BSCAN (EXP) UP LR NRM
Oper: So Inlet :
Base: 77.0 Inten : 5003776 Masses: 50 > 1000
Norm: 77.0 RIC : 23392186 #peaks: 145
Peak: 5.00 mmu

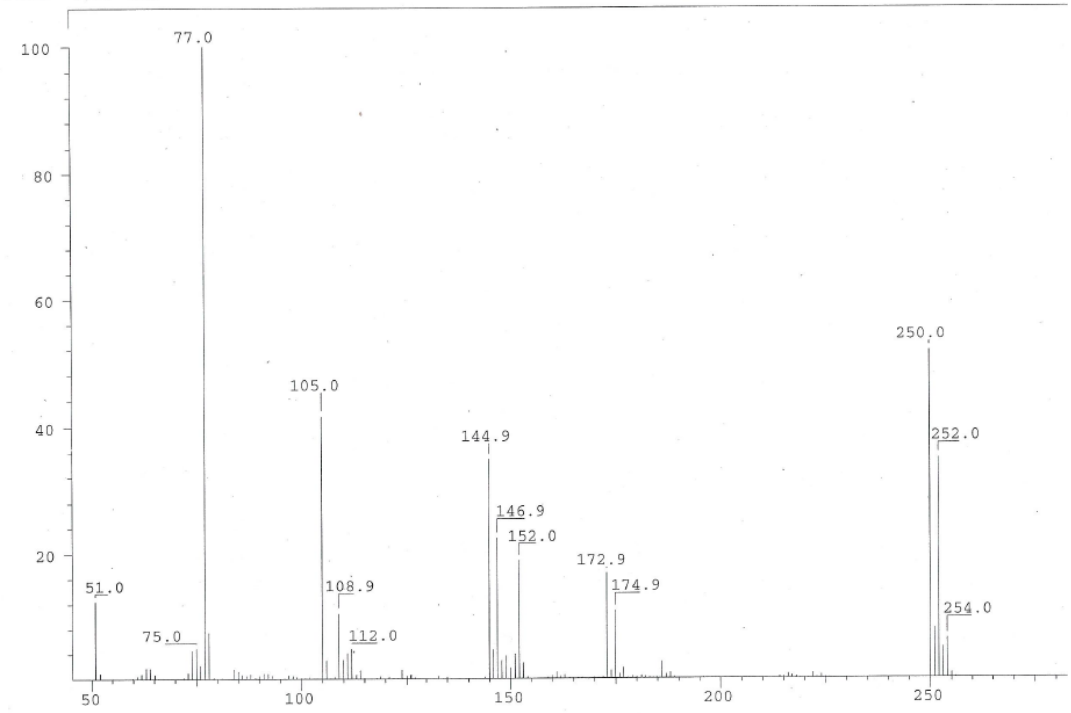

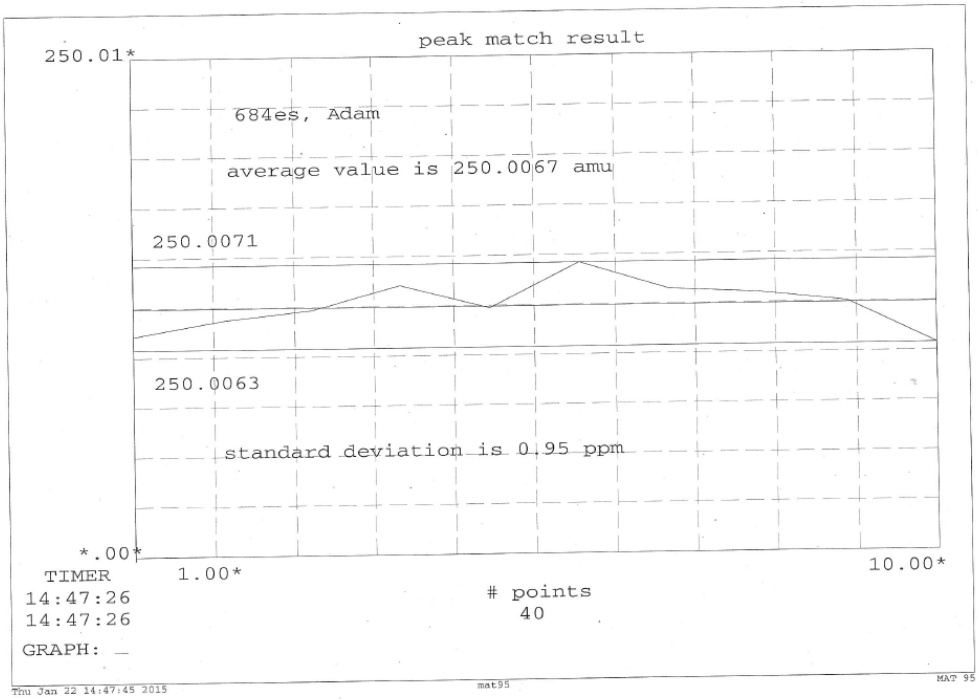

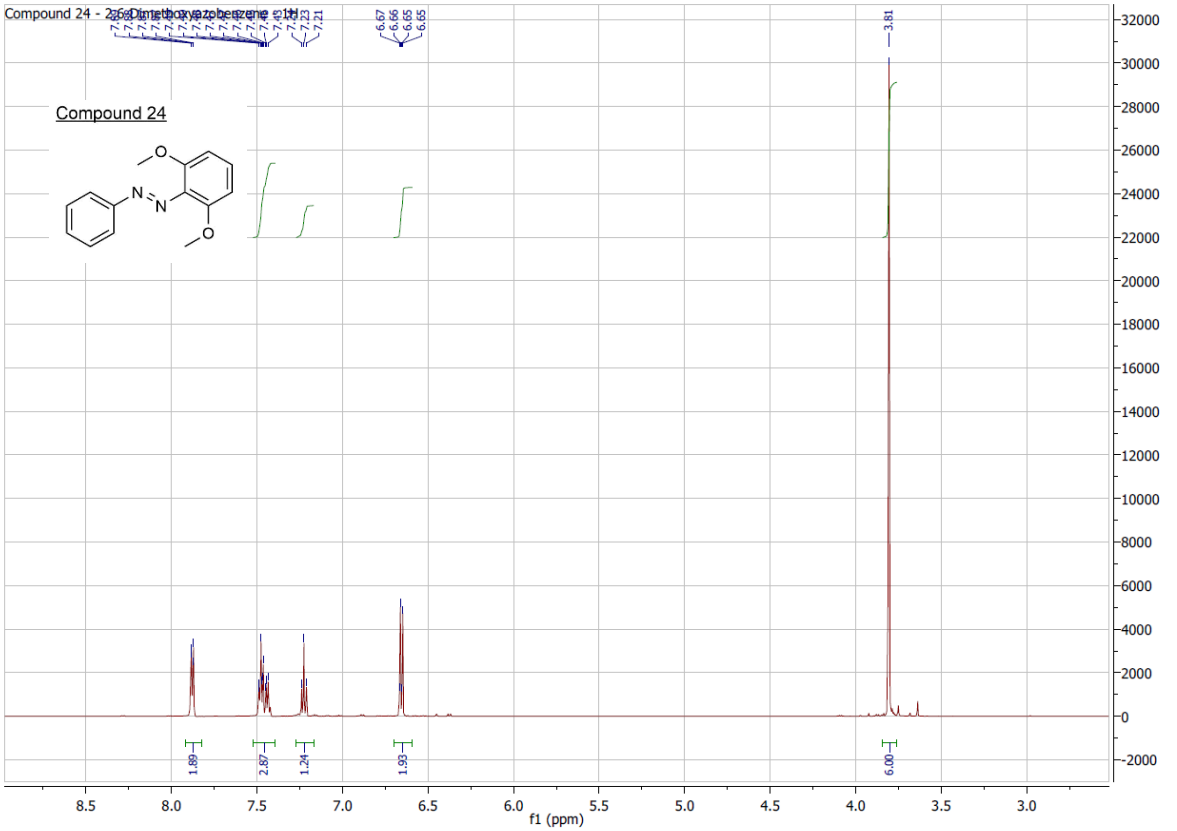
Compound 24 - 2,6-Dimethoxyazobenzene - 1H
Compound 24
7.45
7.23
7.21
6.67
6.66
6.65
6.65
3.81
1.89
2.67
1.24
1.93
6.00
f1 (ppm)

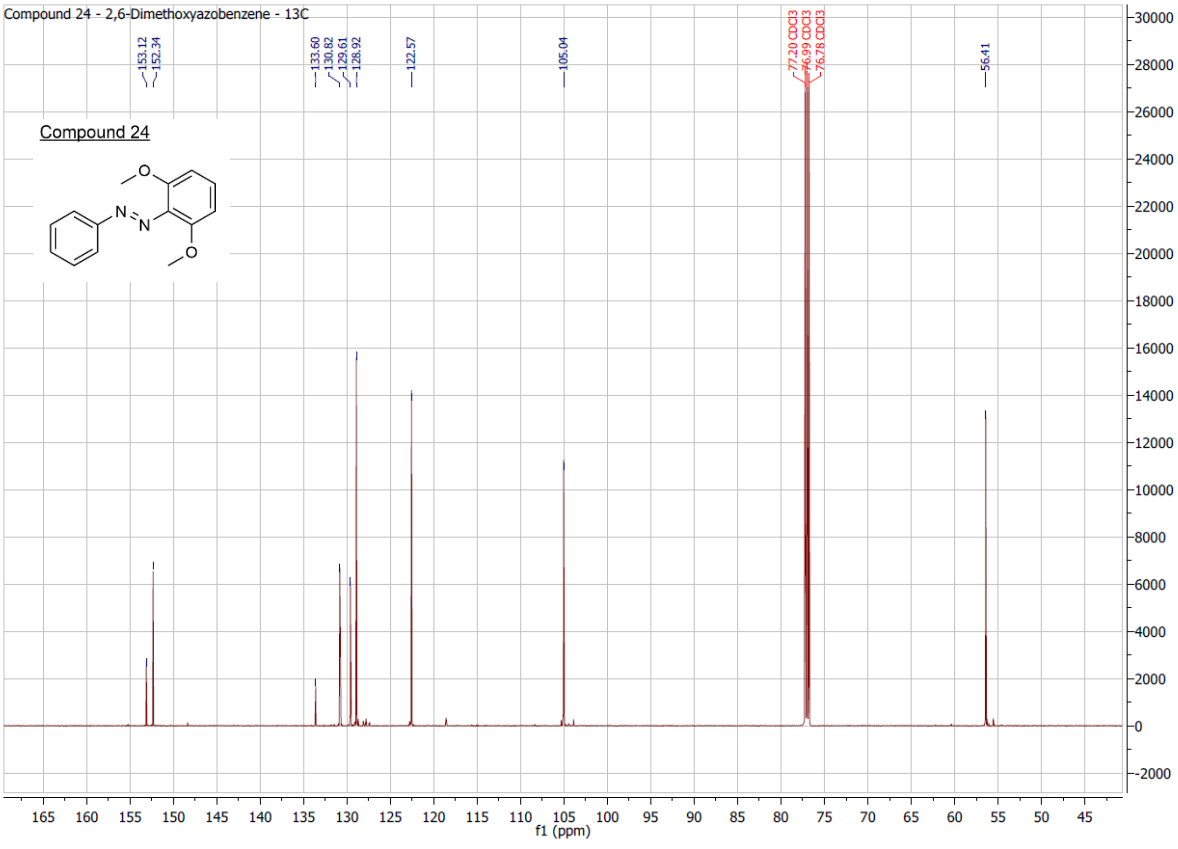
Compound 24 - 2,6-Dimethoxyazobenzene - 13C
Compound 24
153.12
152.34
133.60
130.82
129.61
128.92
122.57
106.04
77.20 CDCl3
76.99 CDCl3
76.78 CDCl3
56.41
f1 (ppm)

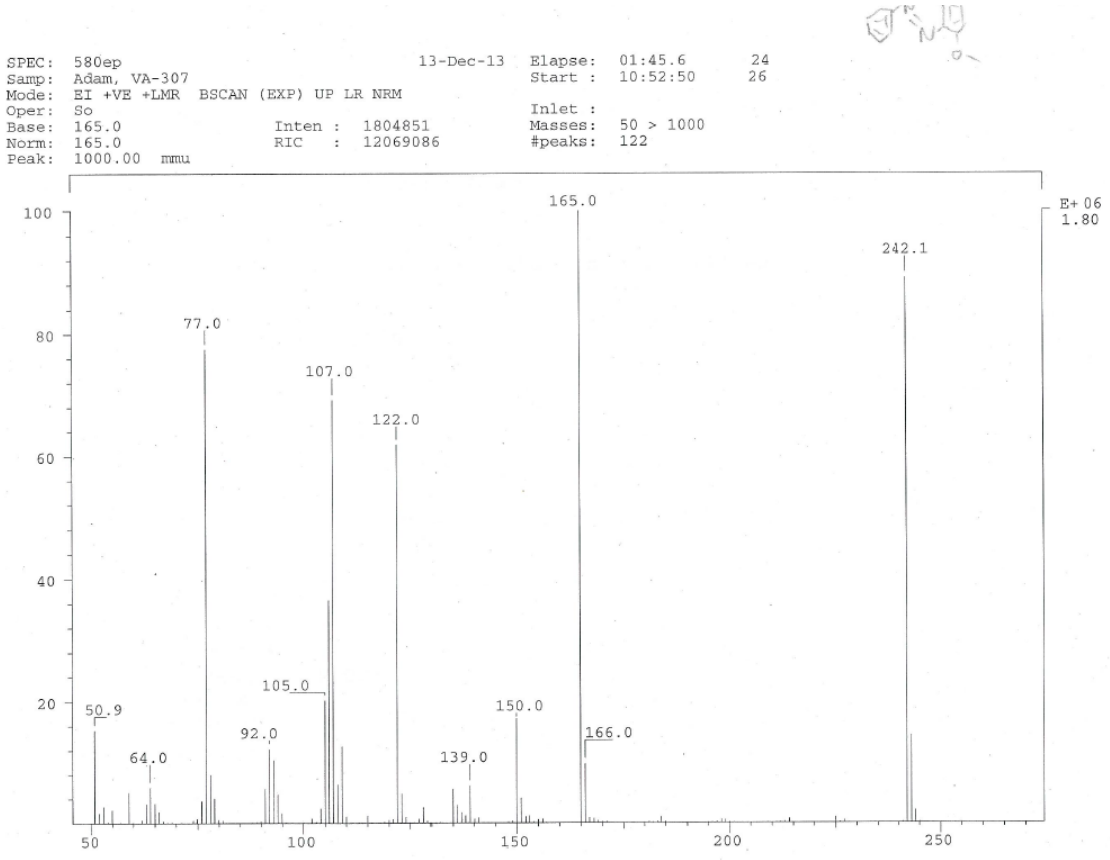
SPEC: 580ep
Samp: Adam, VA-307
Mode: EI +VE +LMR BSCAN (EXP) UP LR NRM
Oper: So
Base: 165.0
Norm: 165.0
Peak: 1000.00 mmu
13-Dec-13
Inten : 1804851
RIC : 12069086
Elapse: 01:45.6 24
Start : 10:52:50 26
Inlet :
Masses: 50 > 1000
#peaks: 122
E+06
1.80
165.0
242.1
77.0
107.0
122.0
105.0
50.9
92.0
64.0
150.0
166.0
139.0
100
80
60
40
20
50
100
150
200
250

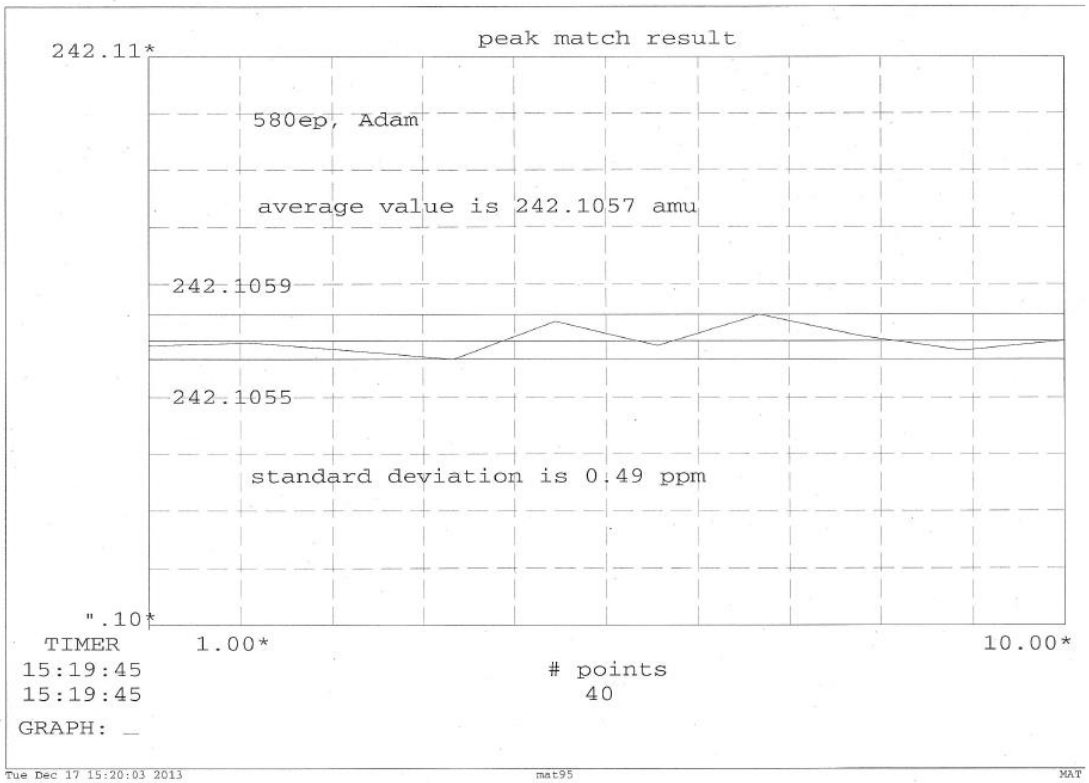
peak match result
242.11*
580ep, Adam
average value is 242.1057 amu
242.1059
242.1055
standard deviation is 0.49 ppm
".10*
TIMER
1.00*
10.00*
15:19:45
15:19:45
points
40
GRAPH:
Tue Dec 17 15:20:03 2013
mat95
MAT

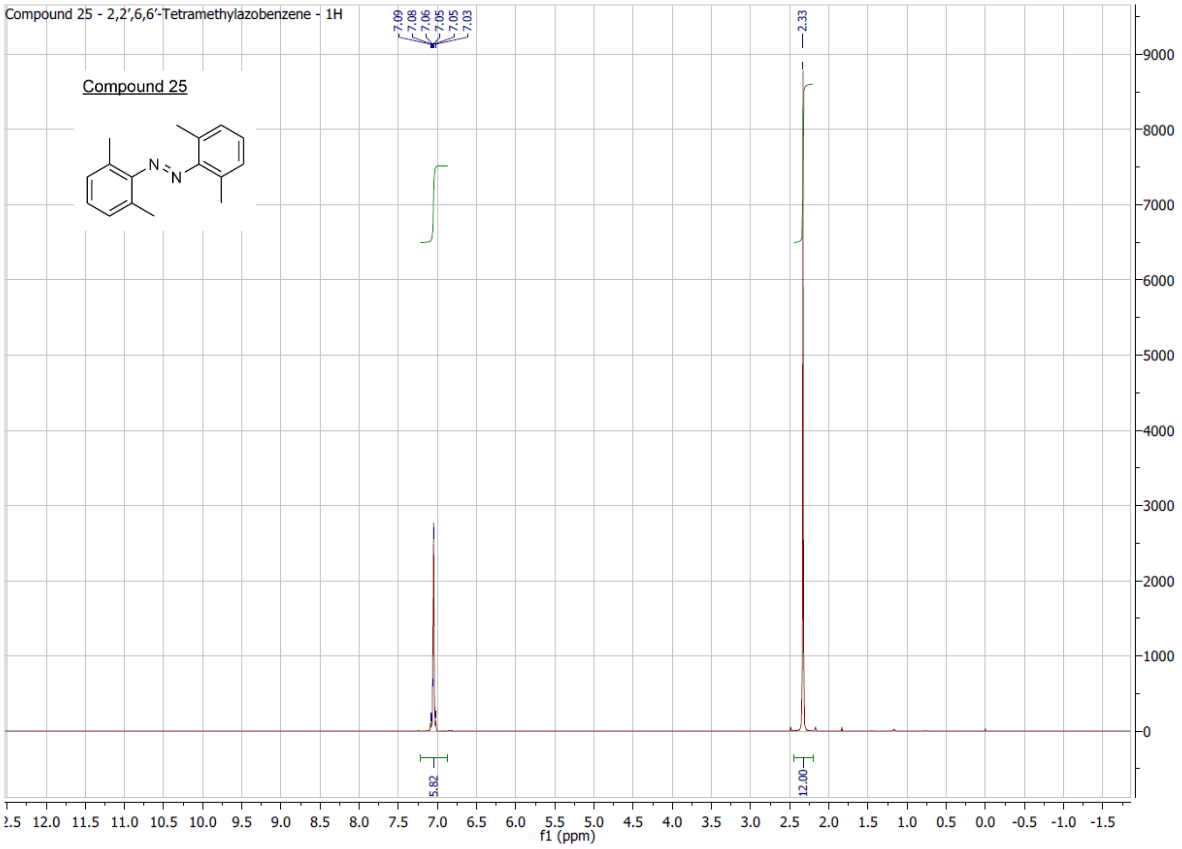
Compound 25 - 2,2',6,6'-Tetramethylazobenzene - 1H
Compound 25
7.09
7.08
7.06
7.05
7.05
7.03
2.33
5.82
12.00
f1 (ppm)

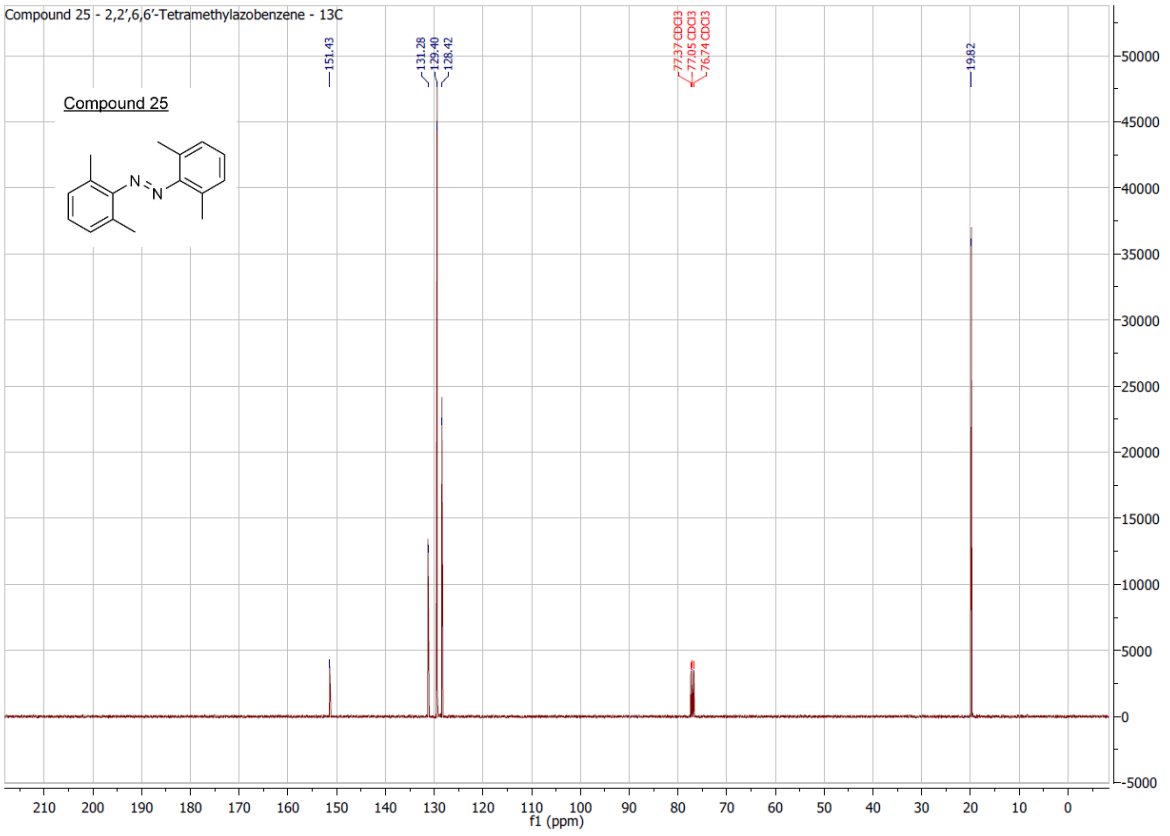
Compound 25 - 2,2',6,6'-Tetramethylazobenzene - 13C
Compound 25
151.43
131.28
129.40
128.42
77.37 CDCl3
77.05 CDCl3
76.74 CDCl3
19.82
f1 (ppm)

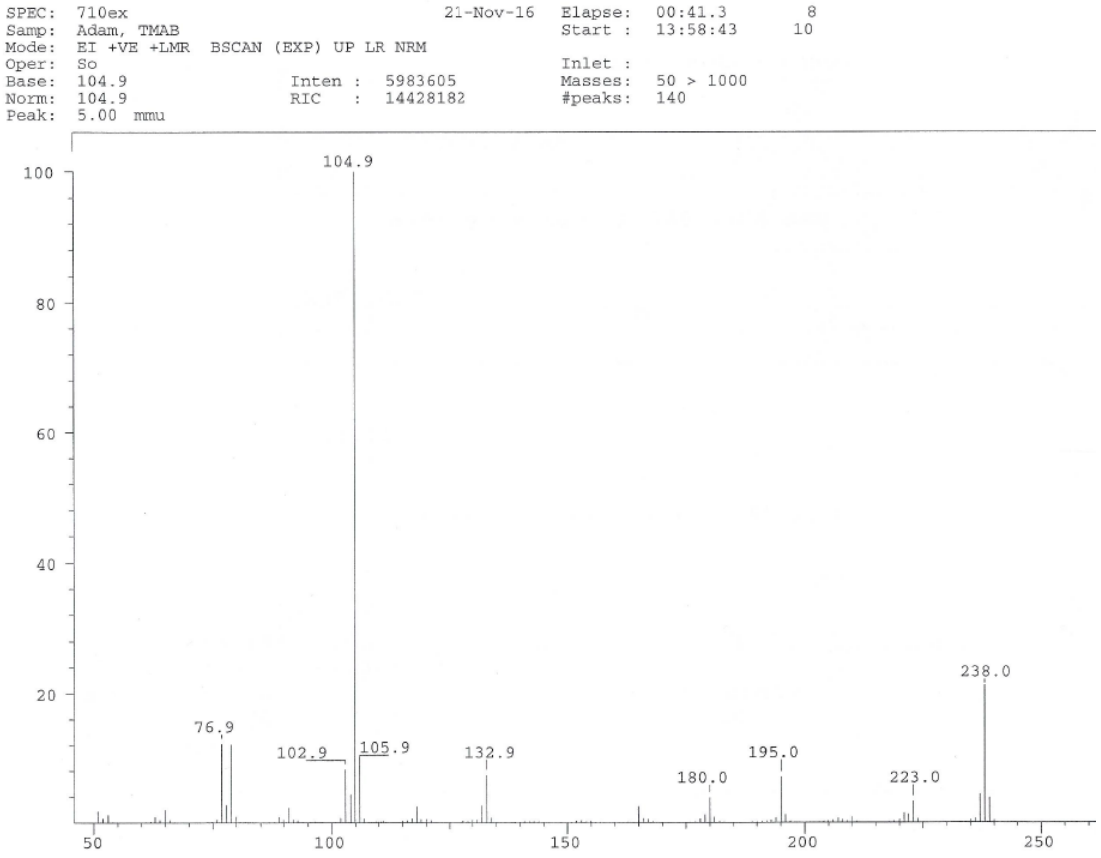
SPEC: 710ex 21-Nov-16 Elapse: 00:41.3 8
Samp: Adam, TMAB Start : 13:58:43 10
Mode: EI +VE +LMR BSCAN (EXP) UP LR NRM
Oper: So Inlet :
Base: 104.9 Inten : 5983605 Masses: 50 > 1000
Norm: 104.9 RIC : 14428182 #peaks: 140
Peak: 5.00 mmu
104.9
238.0
76.9
102.9
105.9
132.9
195.0
180.0
223.0

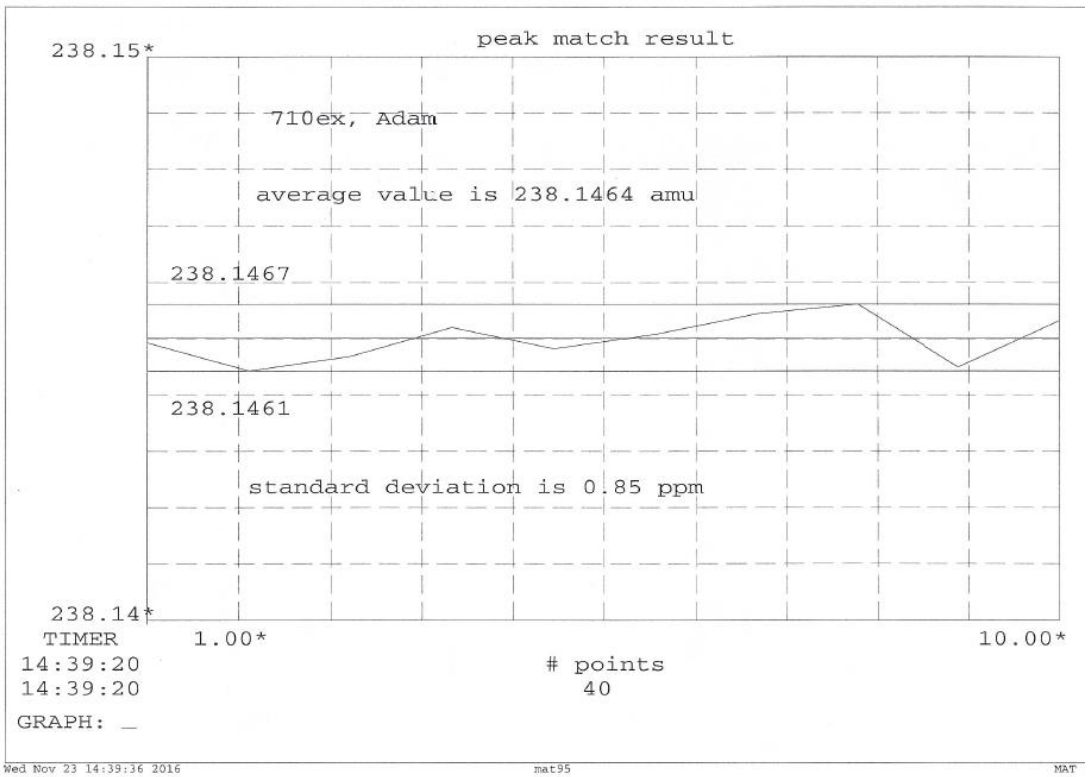
peak match result
238.15*
710ex, Adam
average value is 238.1464 amu
238.1467
238.1461
standard deviation is 0.85 ppm
238.14*
TIMER 1.00* 10.00*
14:39:20 # points
14:39:20 40
GRAPH: _
Wed Nov 23 14:39:36 2016 mat95 MAT

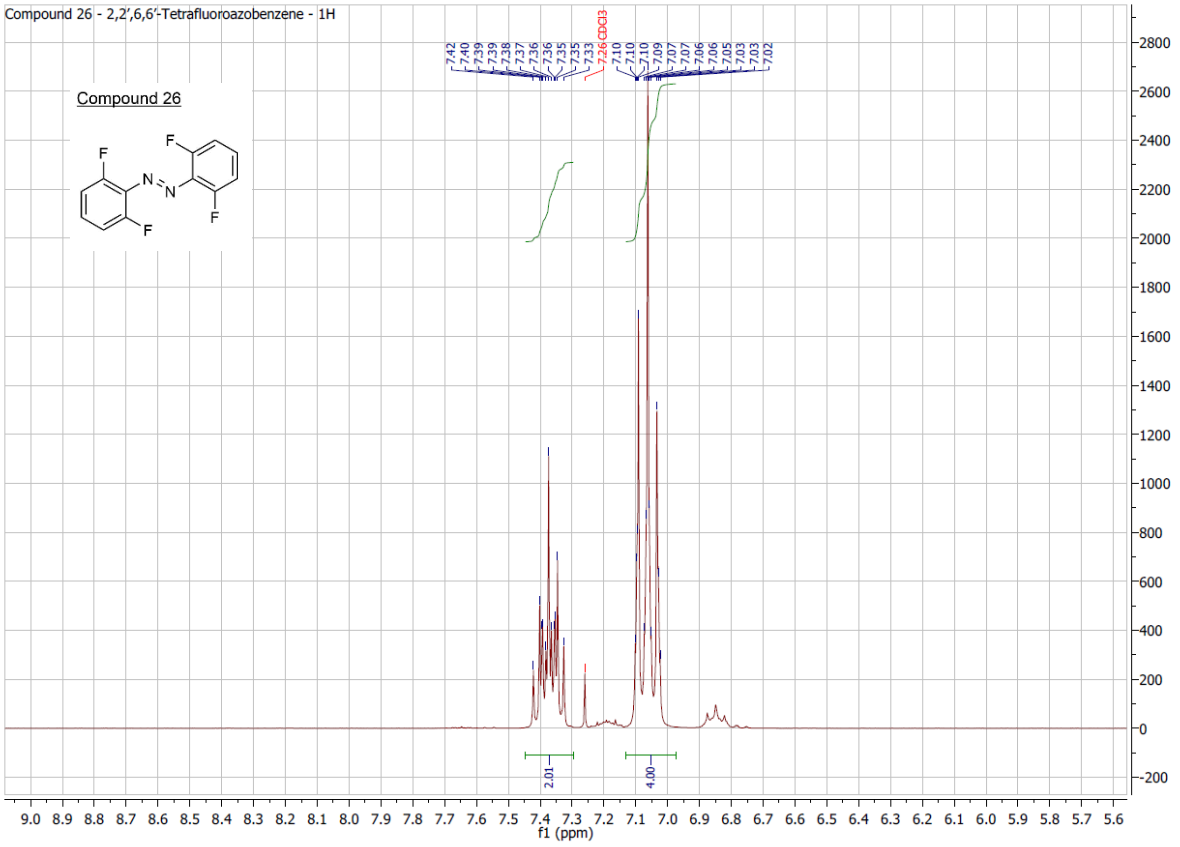
Compound 26 - 2,2',6,6'-Tetrafluoroazobenzene - 1H
Compound 26
F
F
N
N
F
F
7.42
7.40
7.39
7.38
7.37
7.36
7.36
7.35
7.35
7.33
7.26 CDCl3
7.10
7.10
7.10
7.09
7.07
7.07
7.07
7.06
7.06
7.05
7.03
7.03
7.02
2.01
4.00
f1 (ppm)

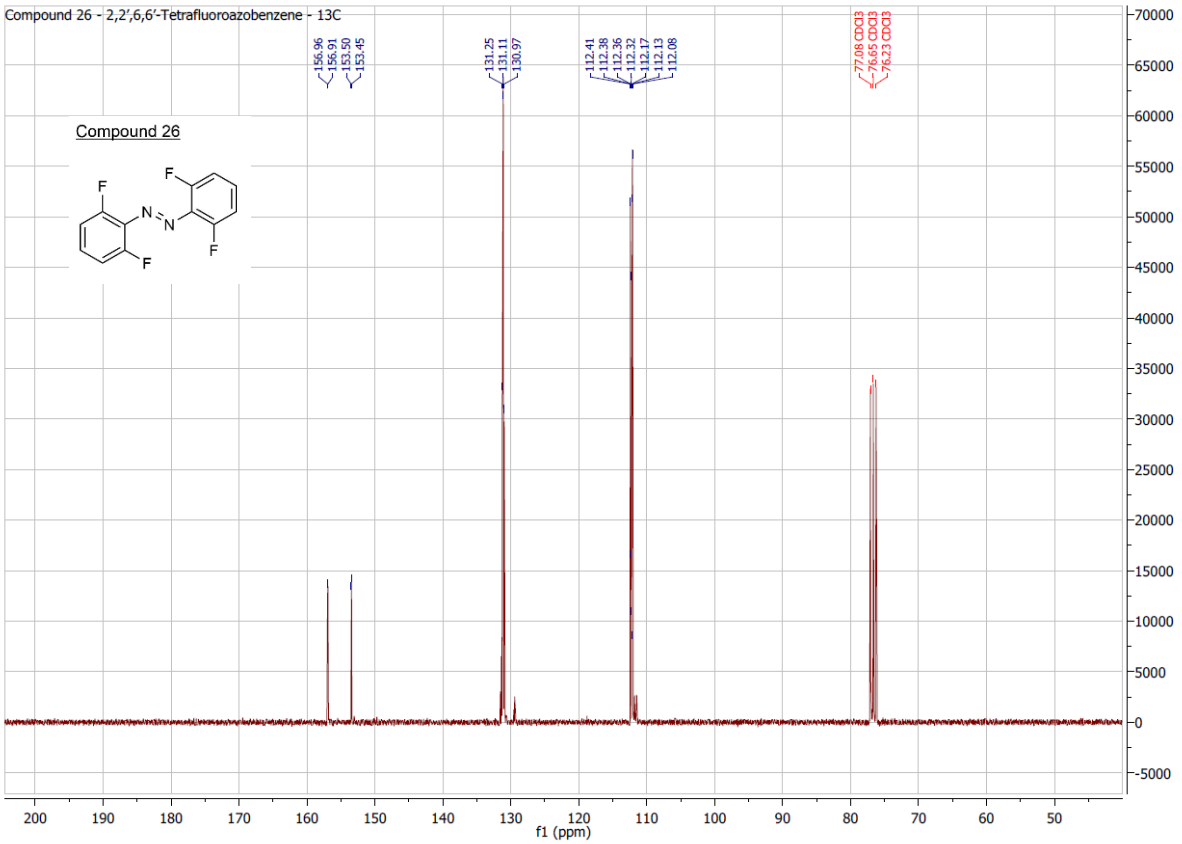
Compound 26 - 2,2',6,6'-Tetrafluoroazobenzene - 13C
Compound 26
F
F
N
N
F
F
156.96
156.91
153.50
153.45
131.25
131.11
130.97
112.41
112.38
112.36
112.32
112.17
112.13
112.08
77.08 CDCl3
76.65 CDCl3
76.23 CDCl3
f1 (ppm)

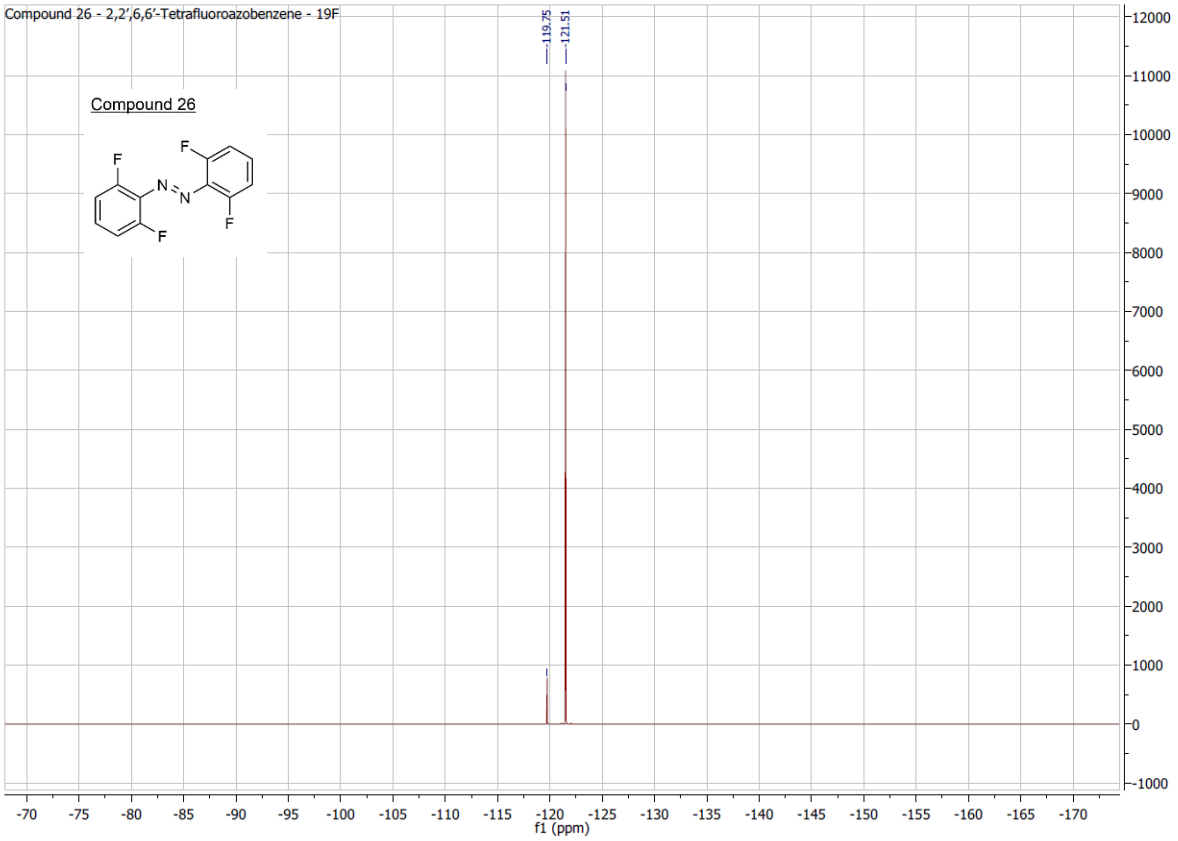
Compound 26 - 2,2',6,6'-Tetrafluoroazobenzene - 19F
Compound 26
F
F
N
N
F
F
-119.75
-121.51
12000
11000
10000
9000
8000
7000
6000
5000
4000
3000
2000
1000
0
-1000
-70 -75 -80 -85 -90 -95 -100 -105 -110 -115 -120 -125 -130 -135 -140 -145 -150 -155 -160 -165 -170
f1 (ppm)

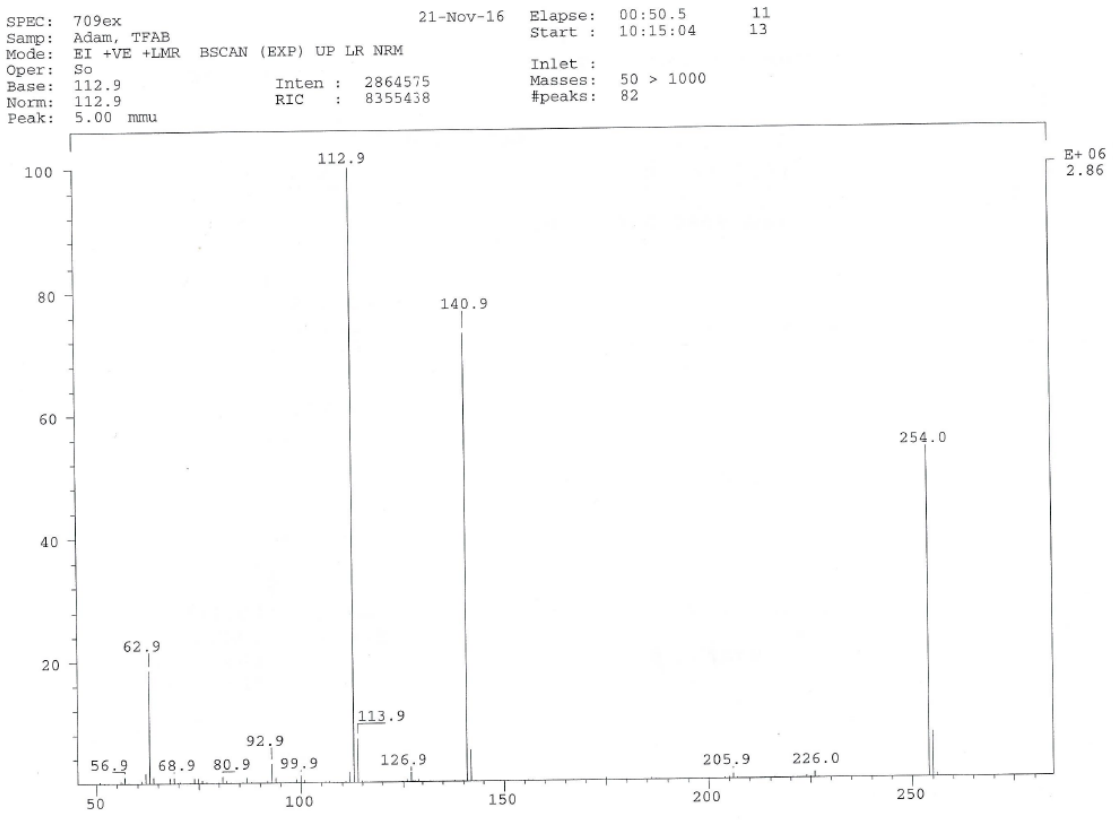
SPEC: 709ex
Samp: Adam, TFAB
Mode: EI +VE +LMR BSCAN (EXP) UP LR NRM
Oper: So
Base: 112.9
Norm: 112.9
Peak: 5.00 mmu
21-Nov-16
Inten : 2864575
RIC : 8355438
Elapse: 00:50.5 11
Start : 10:15:04 13
Inlet :
Masses: 50 > 1000
#peaks: 82
E+ 06
2.86
112.9
140.9
254.0
62.9
113.9
92.9
56.9
68.9
80.9
99.9
126.9
205.9
226.0
100
80
60
40
20
50
100
150
200
250

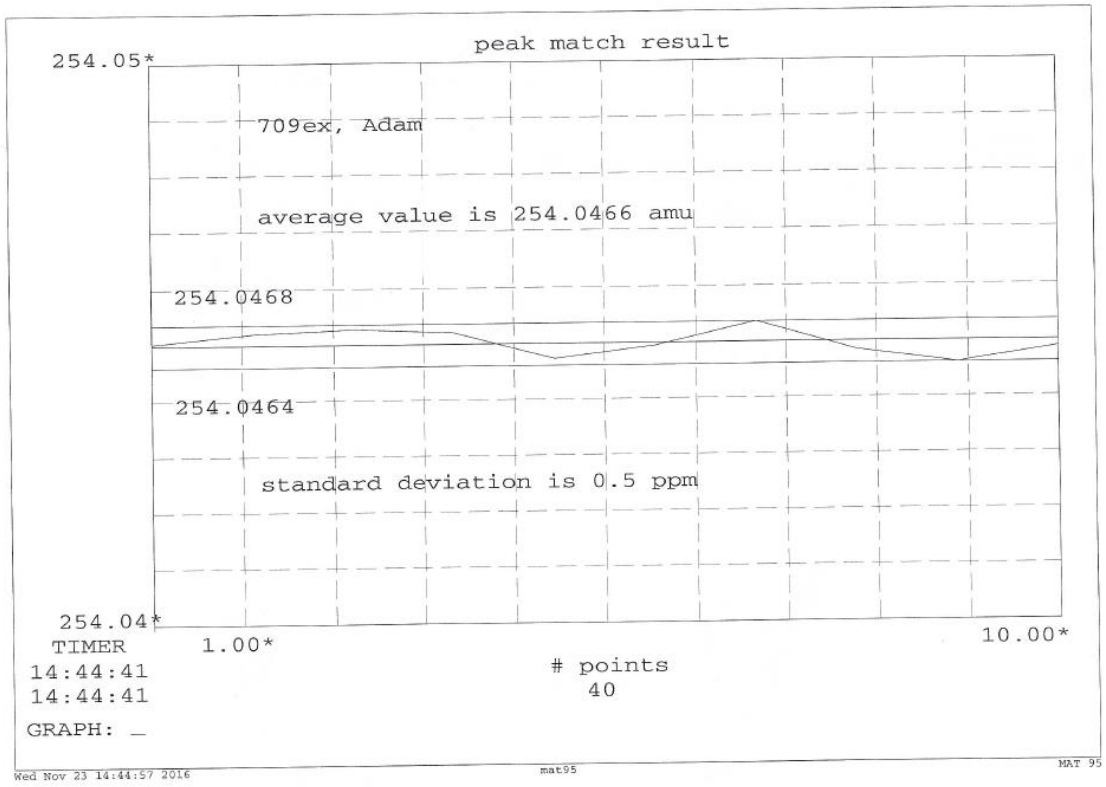
peak match result
254.05*
709ex, Adam
average value is 254.0466 amu
254.0468
254.0464
standard deviation is 0.5 ppm
254.04*
TIMER
14:44:41
14:44:41
1.00*
10.00*
points
40
GRAPH: _
Wed Nov 23 14:44:57 2016
mat95
MAT 95

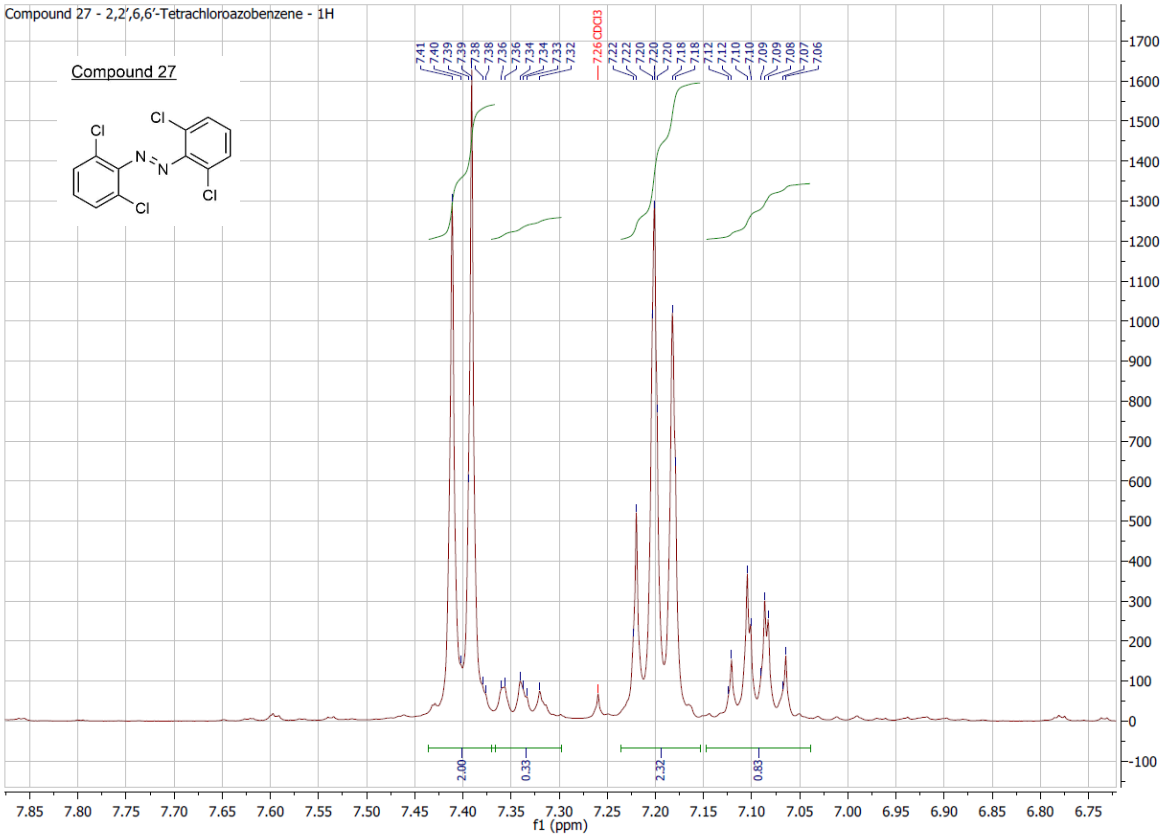
Compound 27 - 2,2',6,6'-Tetrachloroazobenzene - 1H
Compound 27
Cl
Cl
N
N
Cl
Cl
7.41
7.40
7.39
7.39
7.38
7.38
7.36
7.36
7.34
7.34
7.33
7.32
7.26 CDCl3
7.22
7.22
7.20
7.20
7.20
7.18
7.18
7.12
7.12
7.10
7.10
7.09
7.09
7.08
7.07
7.06
2.00
0.33
2.32
0.83
f1 (ppm)

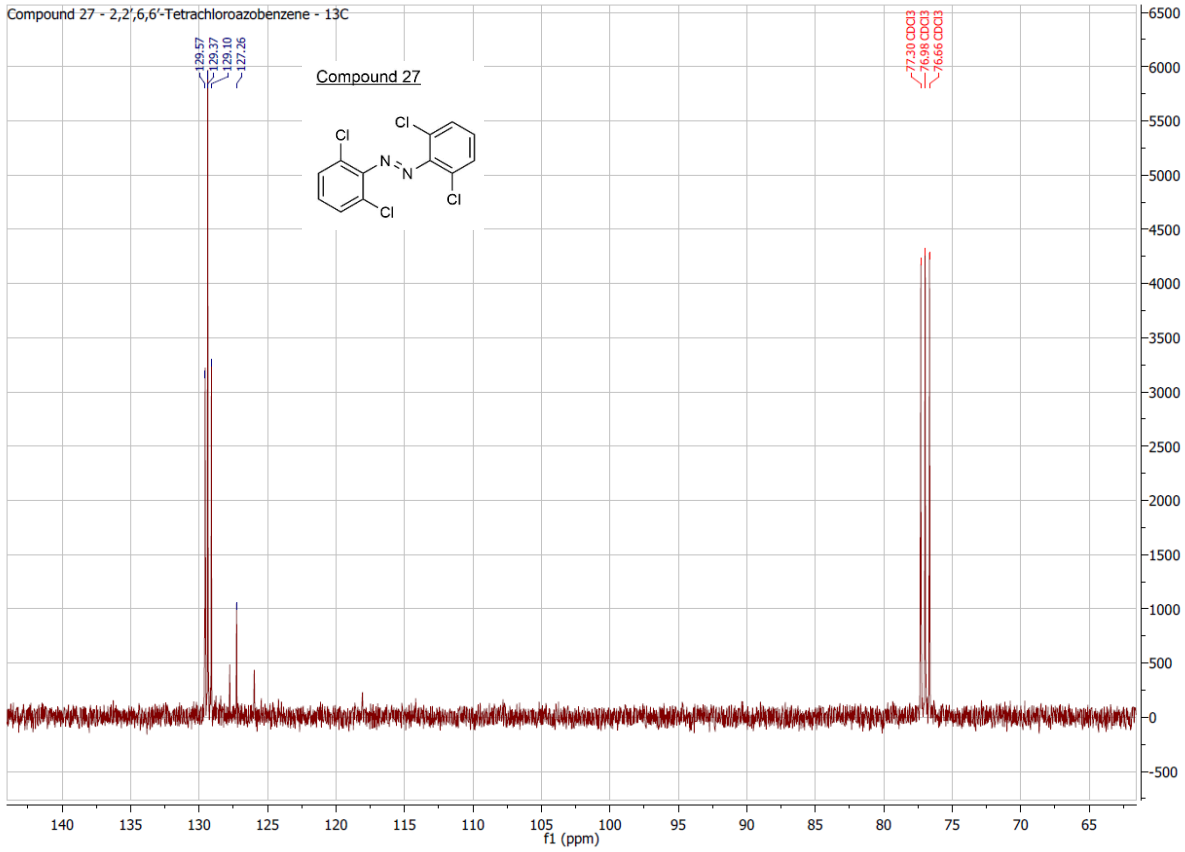
Compound 27 - 2,2',6,6'-Tetrachloroazobenzene - 13C
Compound 27
Cl
Cl
N
N
Cl
Cl
129.57
129.37
129.10
127.26
77.30 CDCl3
76.98 CDCl3
76.66 CDCl3
f1 (ppm)

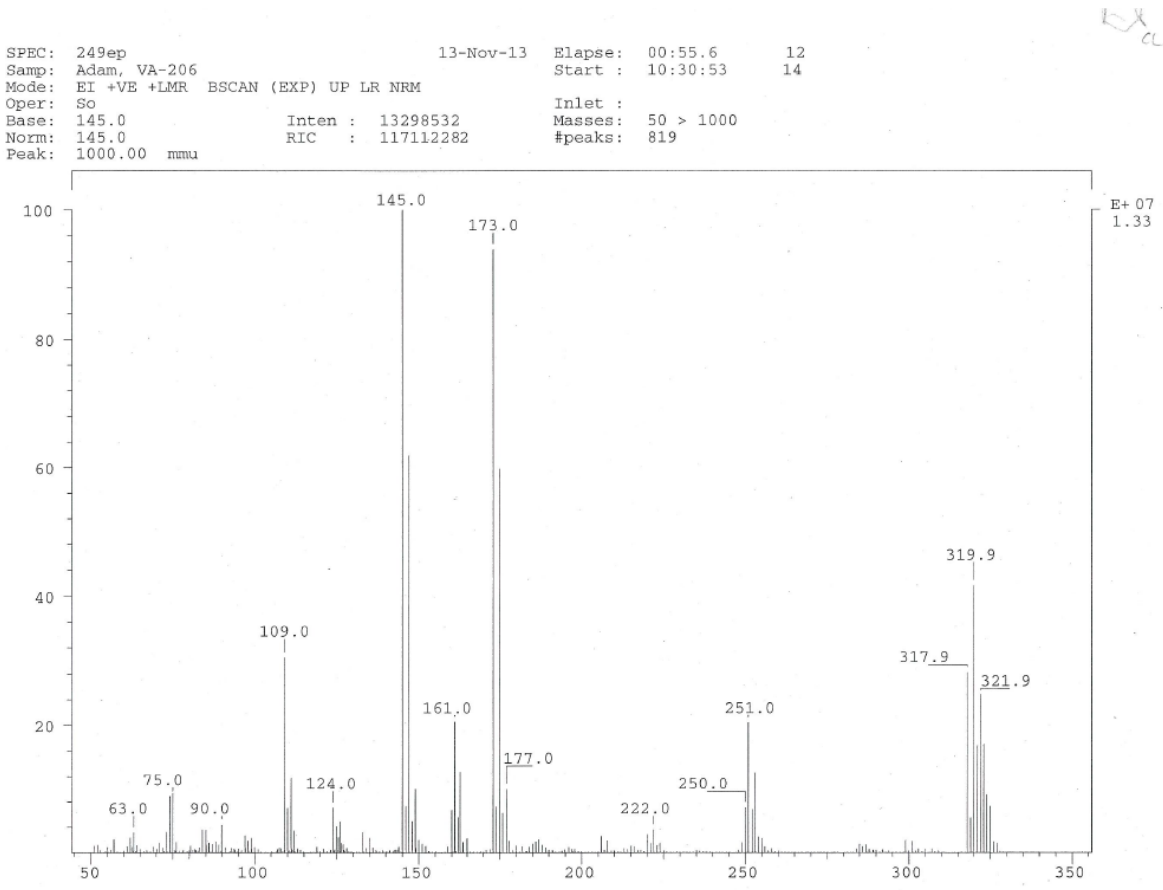
SPEC: 249ep 13-Nov-13 Elapse: 00:55.6 12
Samp: Adam, VA-206 Start : 10:30:53 14
Mode: EI +VE +LMR BSCAN (EXP) UP LR NRM
Oper: So Inlet :
Base: 145.0 Inten : 13298532 Masses: 50 > 1000
Norm: 145.0 RIC : 117112282 #peaks: 819
Peak: 1000.00 mmu
E+ 07
1.33
145.0
173.0
319.9
109.0
317.9
321.9
161.0
251.0
177.0
75.0
124.0
250.0
63.0
90.0
222.0

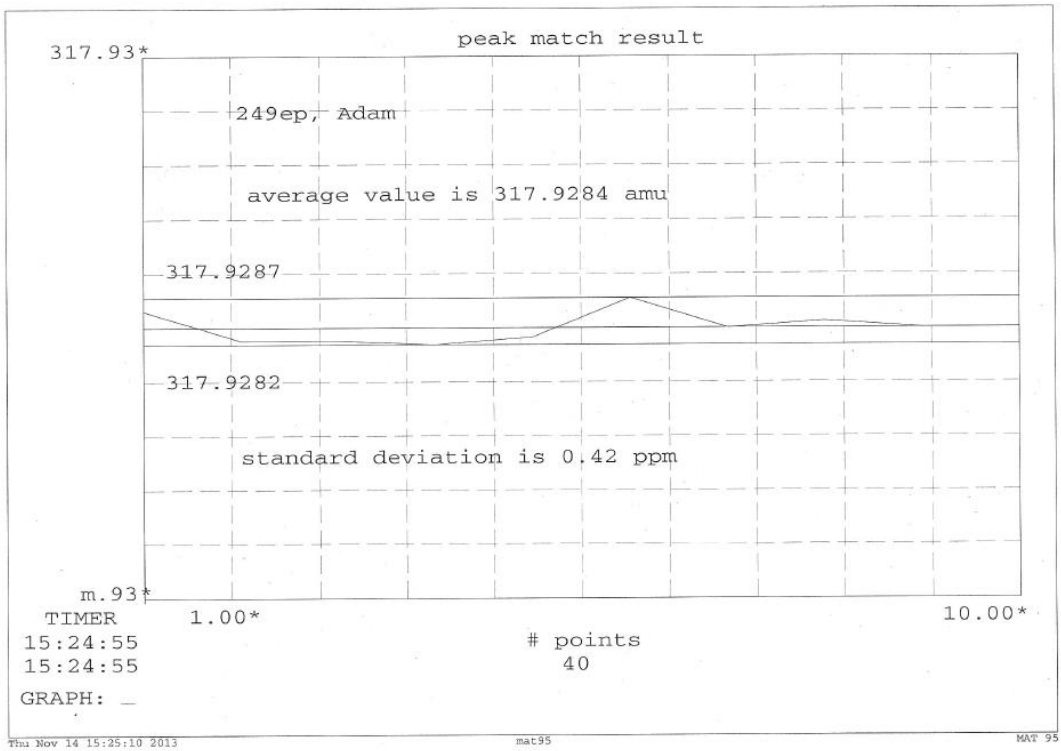
peak match result
317.93*
249ep, Adam
average value is 317.9284 amu
317.9287
317.9282
standard deviation is 0.42 ppm
m.93*
TIMER
1.00*
10.00*
15:24:55
15:24:55
points
40
GRAPH:
Thu Nov 14 15:25:10 2013
mat95
MAT 95

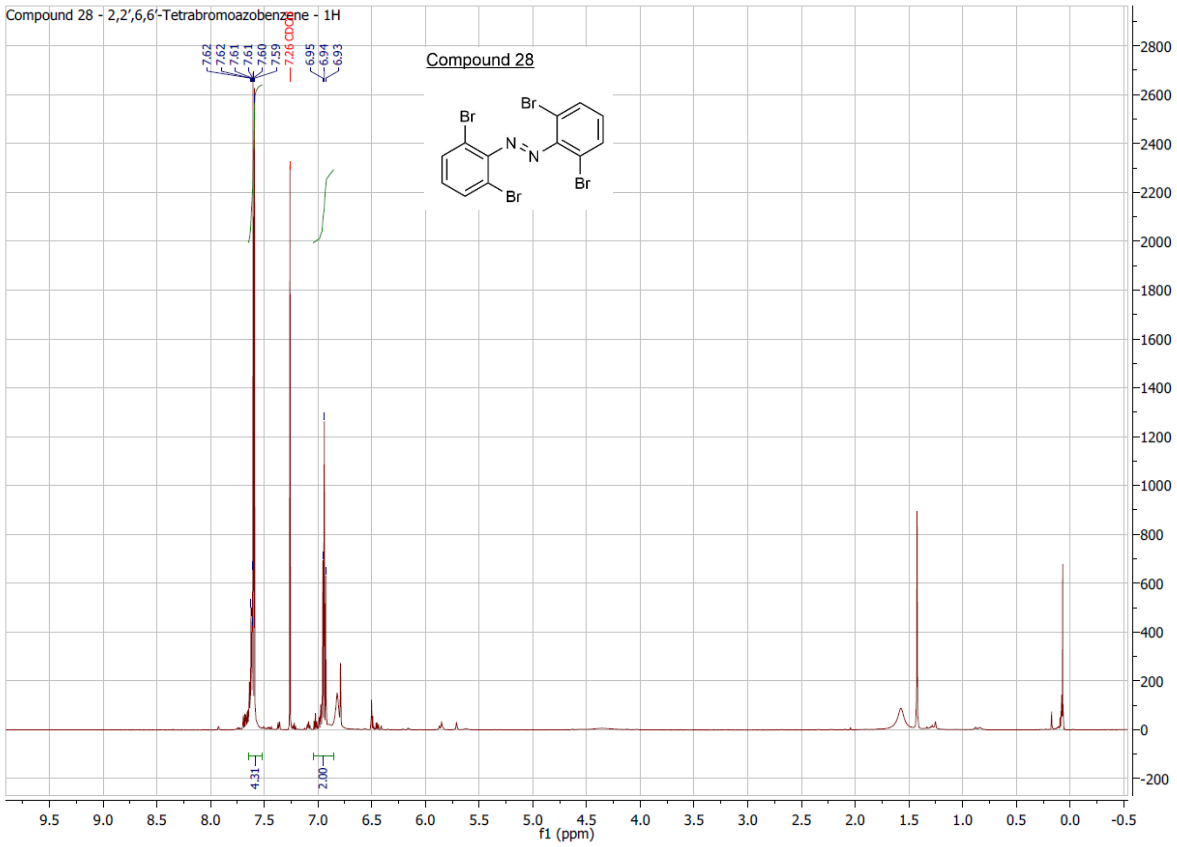
Compound 28 - 2,2′,6,6′-Tetrabromoazobenzene - 1H
Compound 28
7.62
7.62
7.61
7.61
7.60
7.59
7.26 CDCl3
6.95
6.94
6.93
4.31
2.00
f1 (ppm)

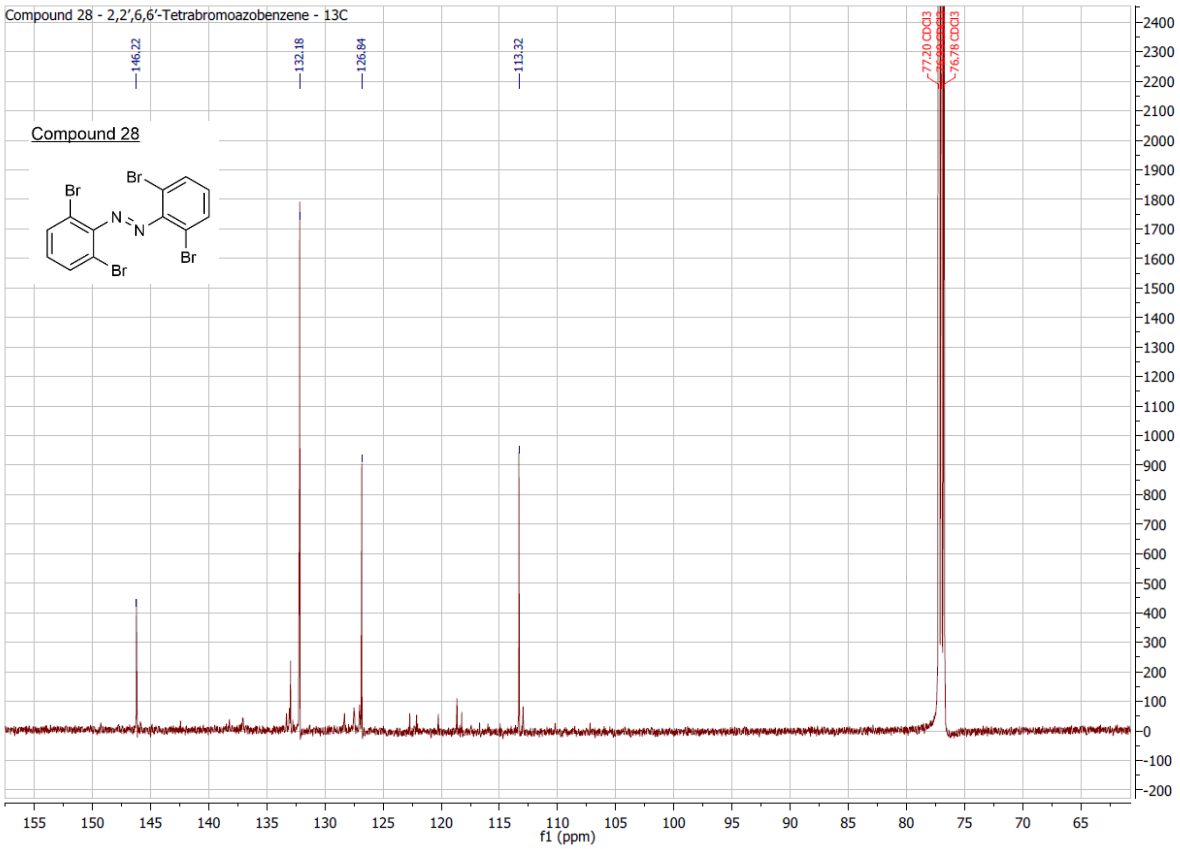
Compound 28 - 2,2′,6,6′-Tetrabromoazobenzene - 13C
Compound 28
146.22
132.18
126.84
113.32
77.20 CDCl3
76.78 CDCl3
f1 (ppm)

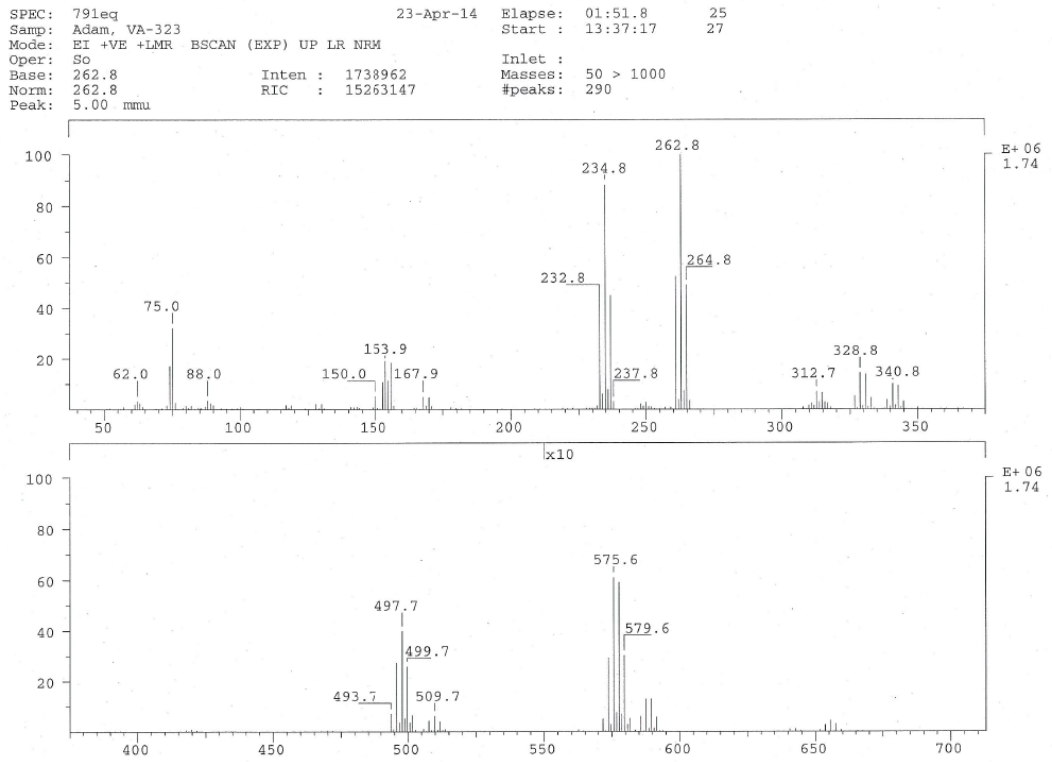
SPEC: 791eq 23-Apr-14 Elapse: 01:51.8 25
Samp: Adam, VA-323 Start : 13:37:17 27
Mode: EI +VE +LMR BSCAN (EXP) UP LR NRM
Oper: So Inlet :
Base: 262.8 Inten : 1738962 Masses: 50 > 1000
Norm: 262.8 RIC : 15263147 #peaks: 290
Peak: 5.00 mmu
E+ 06
1.74
262.8
234.8
264.8
232.8
75.0
153.9
328.8
62.0
88.0
150.0
167.9
237.8
312.7
340.8
x10
575.6
497.7
579.6
499.7
493.7
509.7

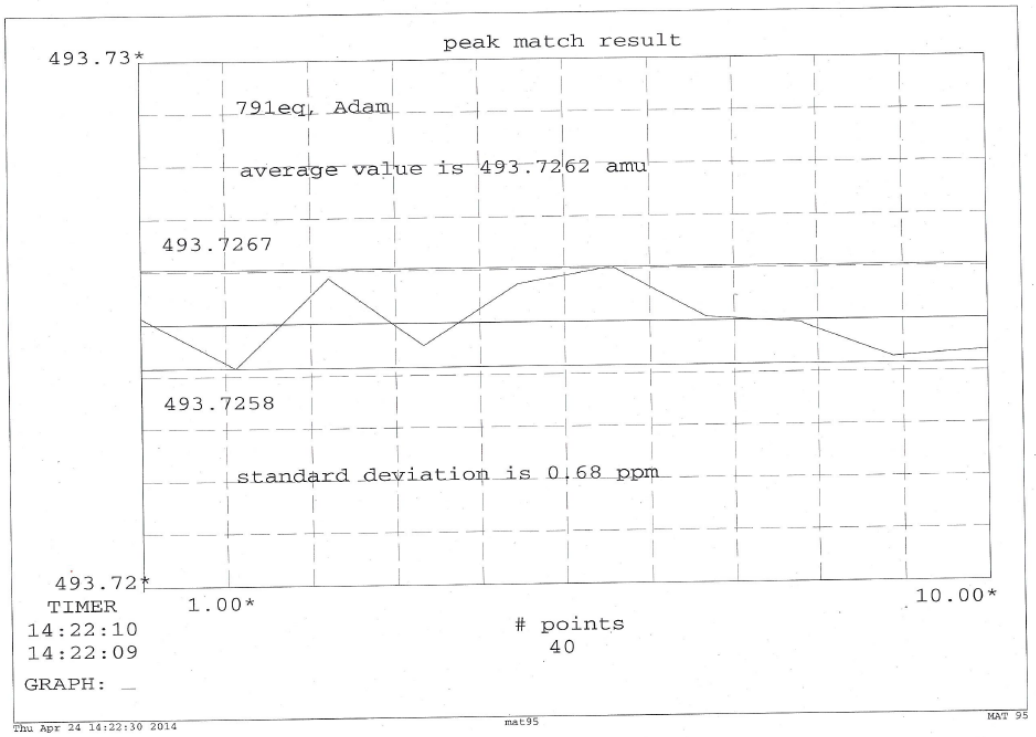
peak match result
493.73*
791eq, Adam
average value is 493.7262 amu
493.7267
493.7258
standard deviation is 0.68 ppm
493.72*
TIMER
14:22:10
14:22:09
GRAPH:
1.00*
10.00*
points
40
Thu Apr 24 14:22:30 2014
mat95
MAT 95

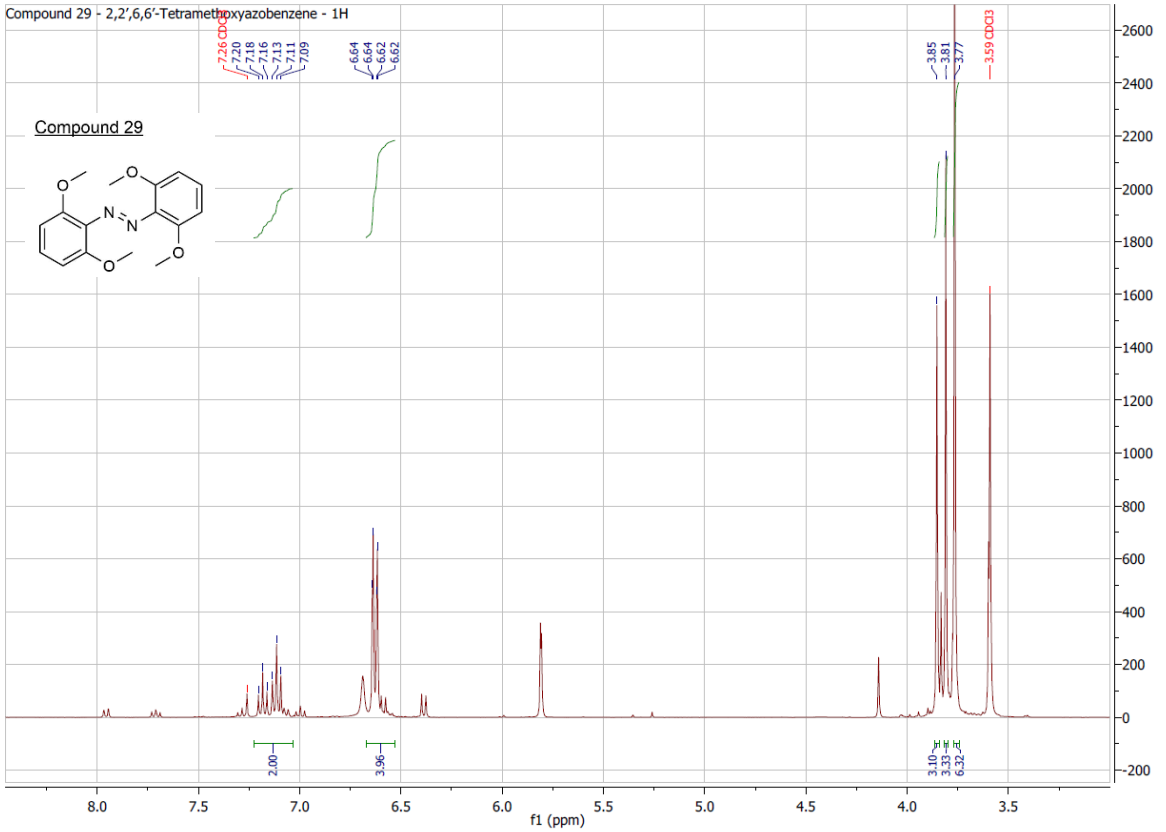
Compound 29 - 2,2',6,6'-Tetramethoxyazobenzene - 1H
Compound 29
7.26 CDCl3
7.20
7.18
7.16
7.13
7.11
7.09
6.64
6.64
6.62
6.62
3.85
3.81
3.77
3.59 CDCl3
2.00
3.96
3.10
3.33
6.32
f1 (ppm)

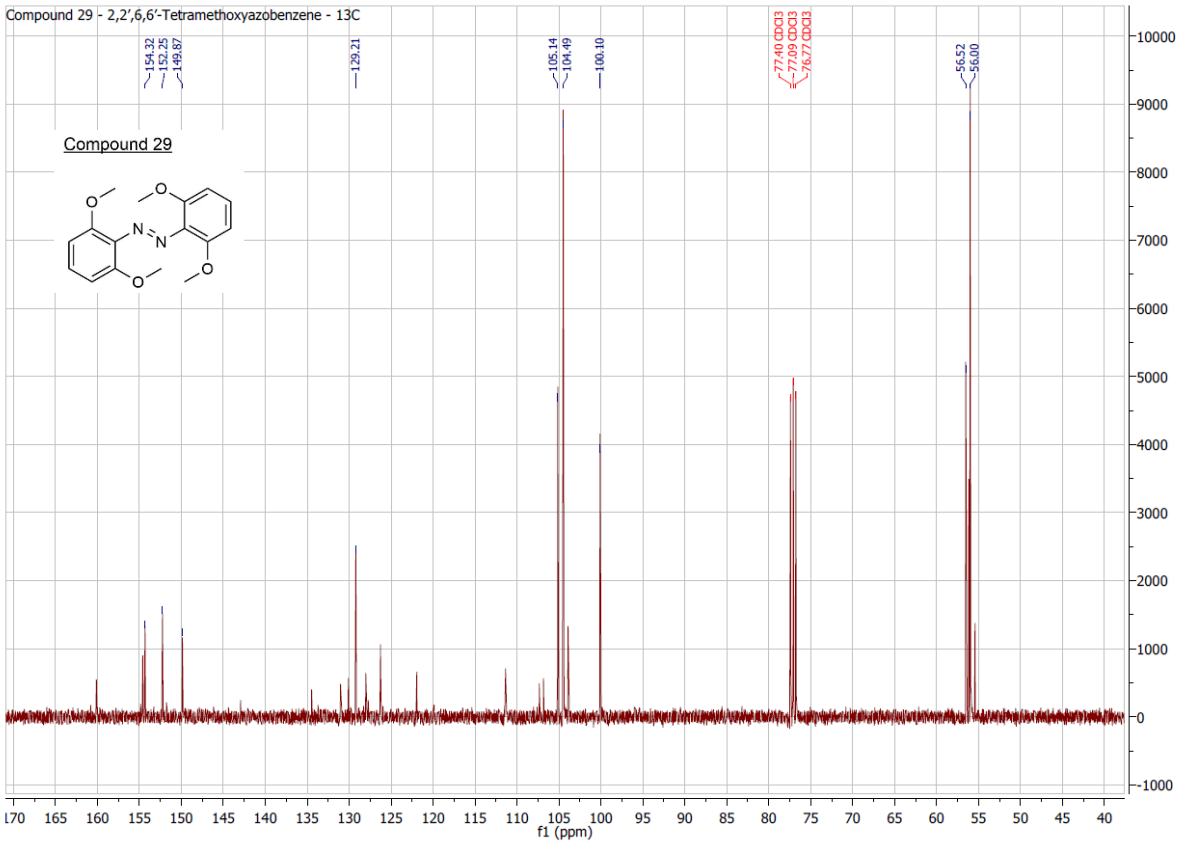
Compound 29 - 2,2',6,6'-Tetramethoxyazobenzene - 13C
Compound 29
154.32
152.25
149.87
129.21
105.14
104.49
100.10
77.40 CDCl3
77.09 CDCl3
76.77 CDCl3
56.52
56.00
f1 (ppm)

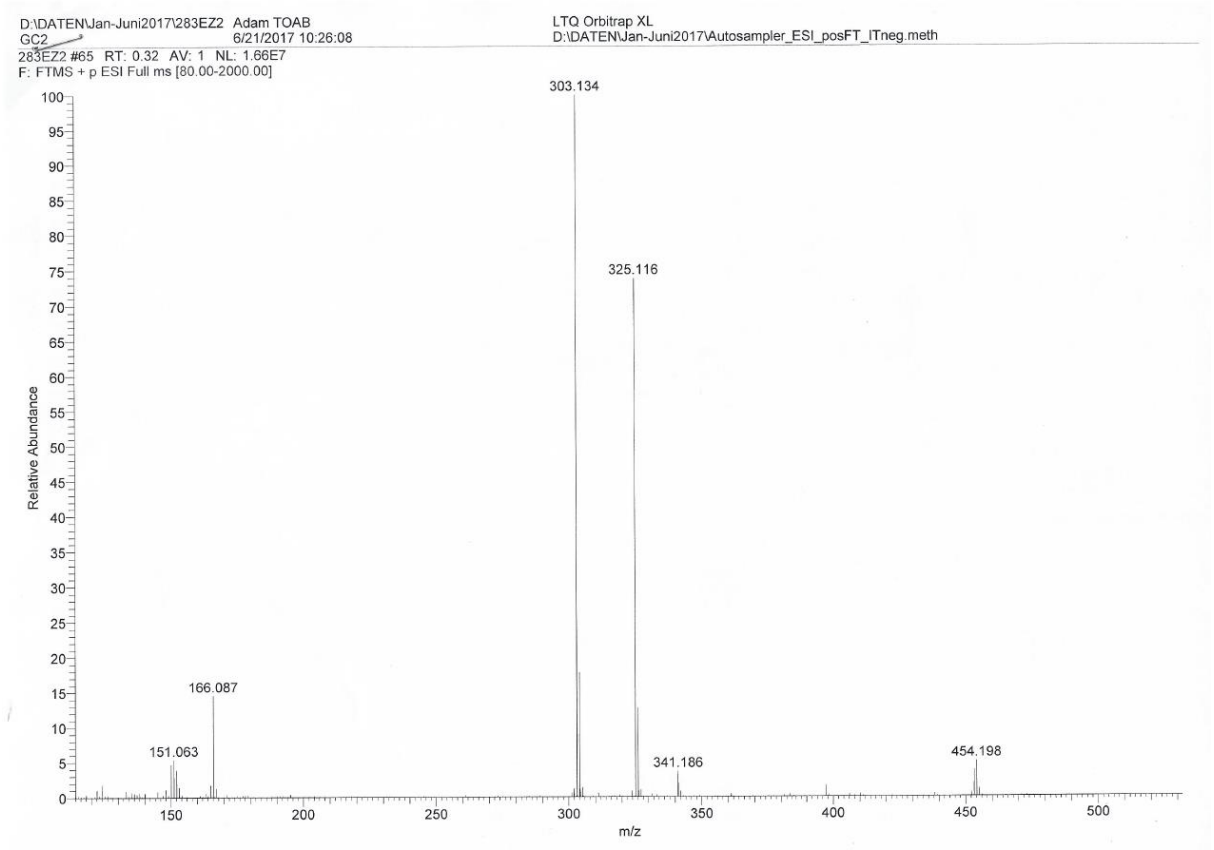
D:\DATEN\Jan-Juni2017\283EZ2 Adam TOAB
GC2 6/21/2017 10:26:08
283EZ2 #65 RT: 0.32 AV: 1 NL: 1.66E7
F: FTMS + p ESI Full ms [80.00-2000.00]
LTQ Orbitrap XL
D:\DATEN\Jan-Juni2017\Autosampler_ESI_posFT_ITneg.meth
303.134
325.116
166.087
151.063
341.186
454.198
Relative Abundance
m/z

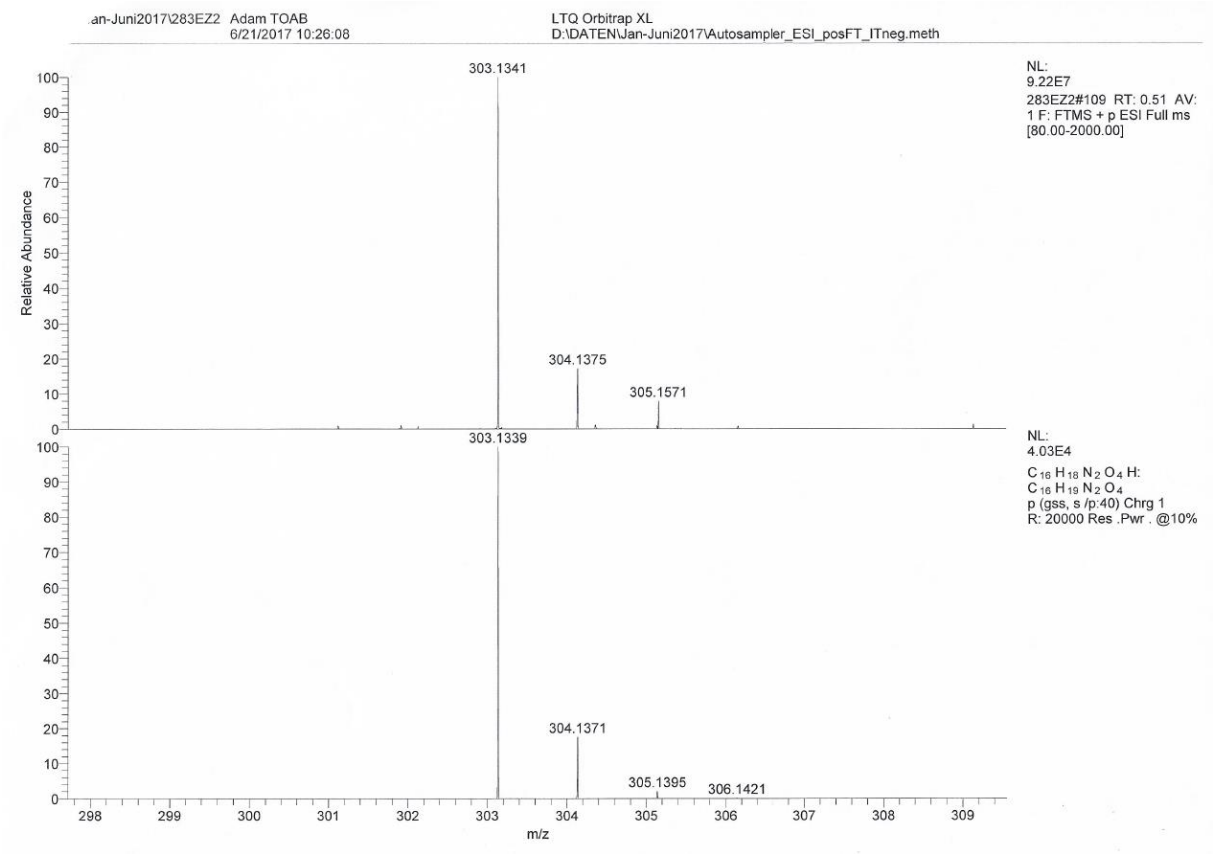
an-Juni2017\283EZ2 Adam TOAB
6/21/2017 10:26:08
LTQ Orbitrap XL
D:\DATEN\Jan-Juni2017\Autosampler_ESI_posFT_ITneg.meth
303.1341
304.1375
305.1571
NL:
9.22E7
283EZ2#109 RT: 0.51 AV:
1 F: FTMS + p ESI Full ms
[80.00-2000.00]
303.1339
304.1371
305.1395
306.1421
NL:
4.03E4
C16 H18 N2 O4 H:
C16 H19 N2 O4
p (gss, s /p:40) Chrg 1
R: 20000 Res .Pwr . @10%
Relative Abundance
m/z

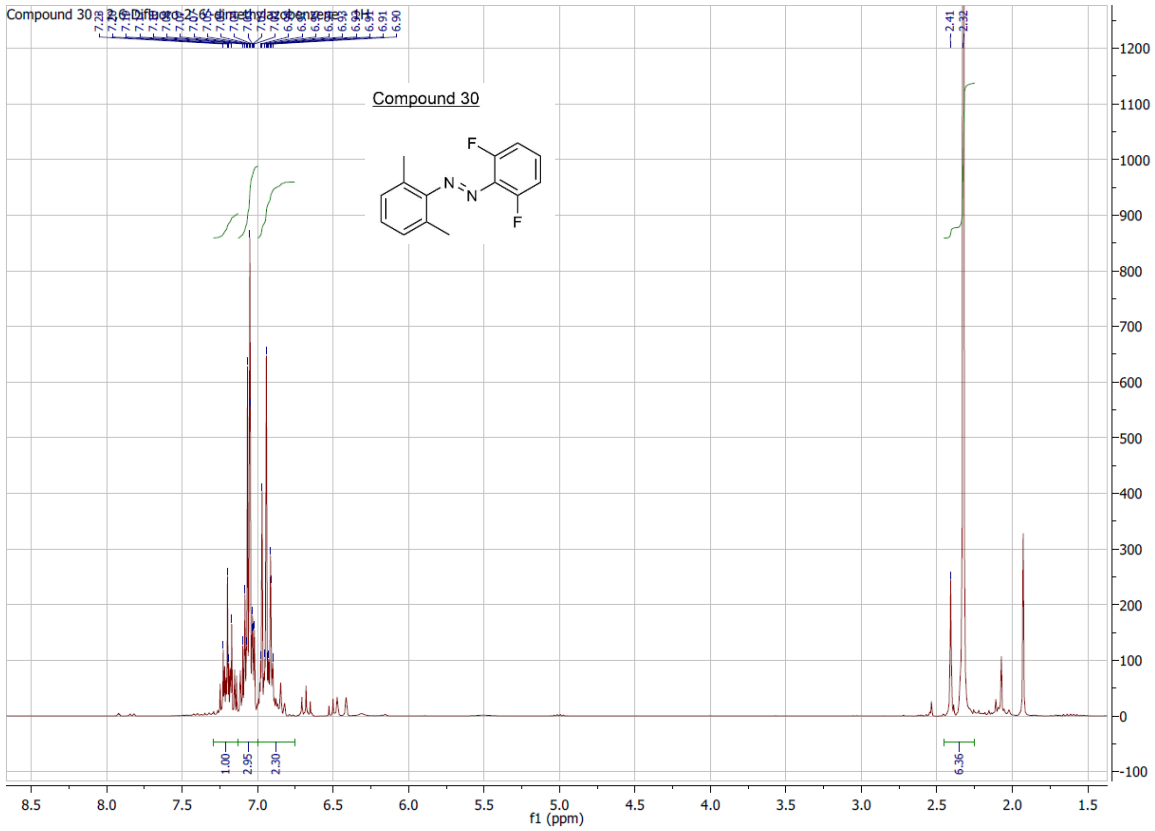
Compound 30 - 2,6-Difluoro-2',6'-dimethylazobenzene - 1H
Compound 30
F
N
N
F
1.00
2.95
2.30
6.36
f1 (ppm)

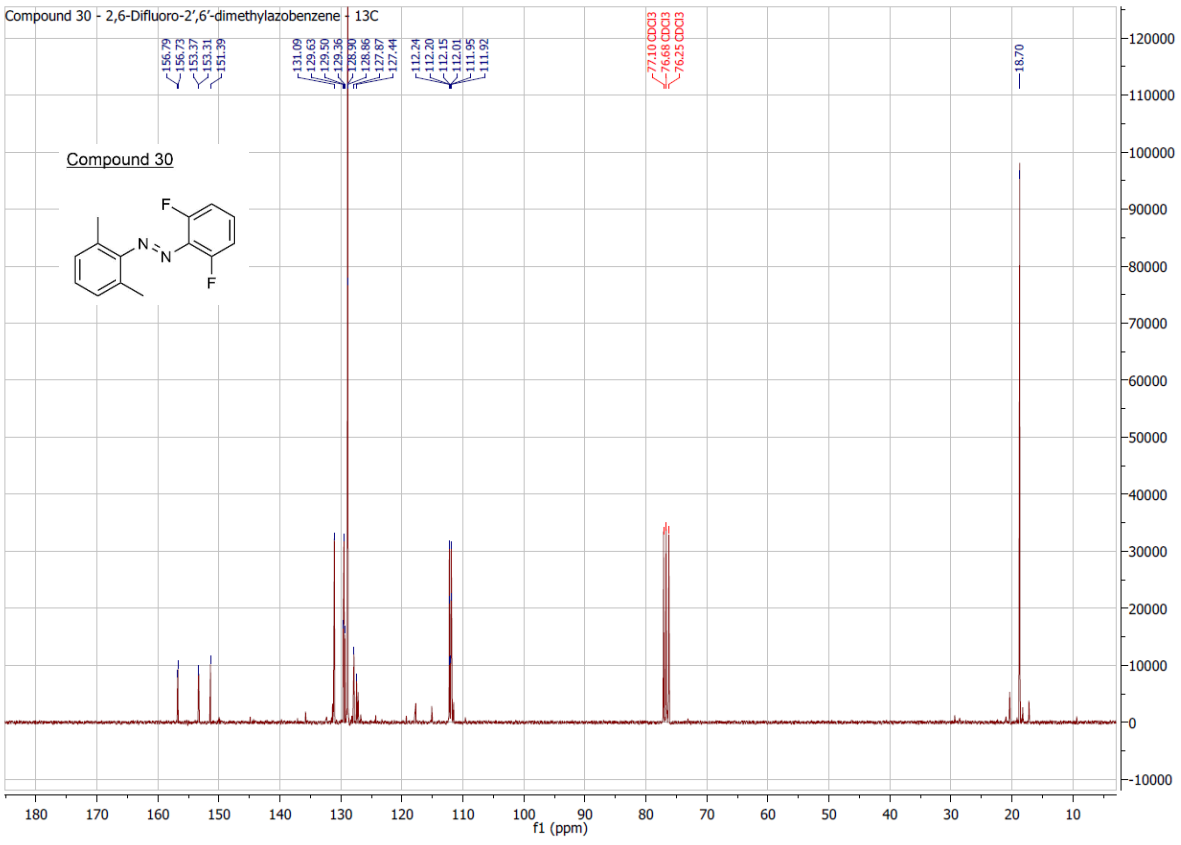
Compound 30 - 2,6-Difluoro-2',6'-dimethylazobenzene - 13C
Compound 30
F
N
N
F
f1 (ppm)

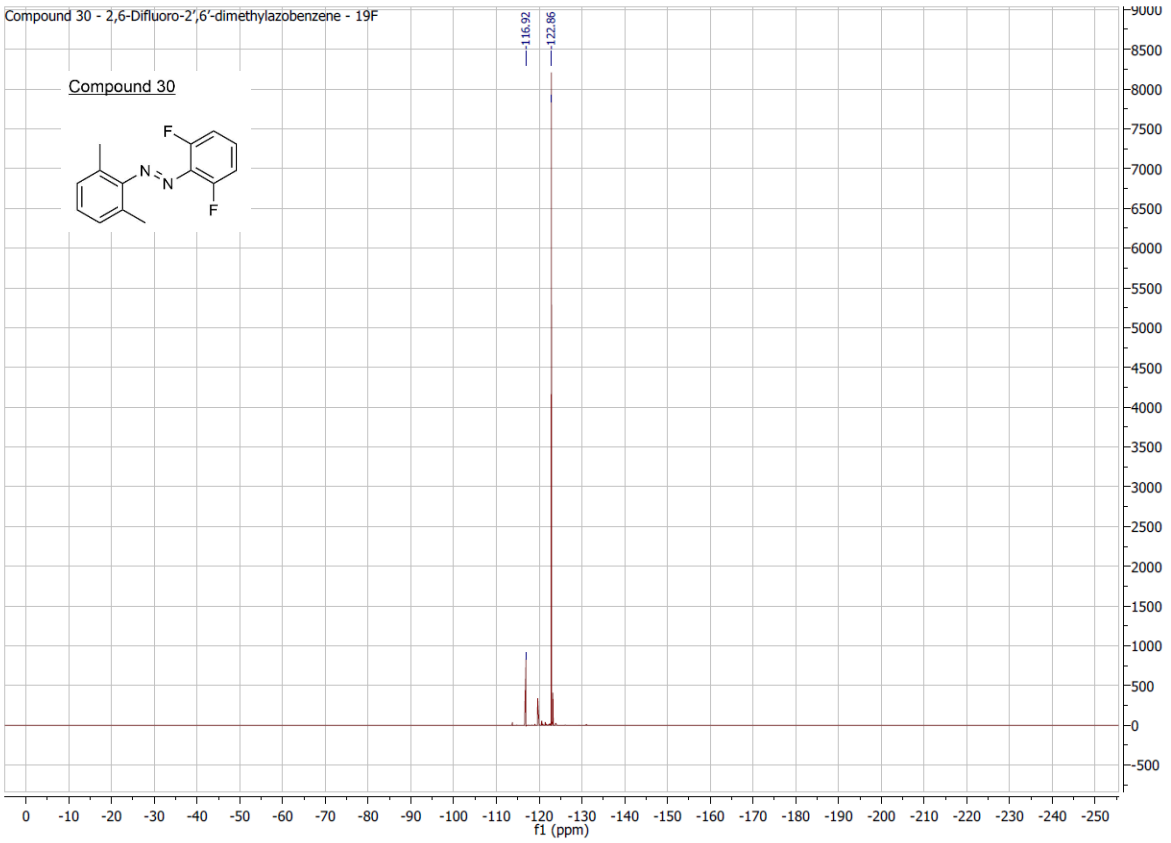
Compound 30 - 2,6-Difluoro-2',6'-dimethylazobenzene - 19F
Compound 30
F
N
N
F
116.92
122.86
f1 (ppm)

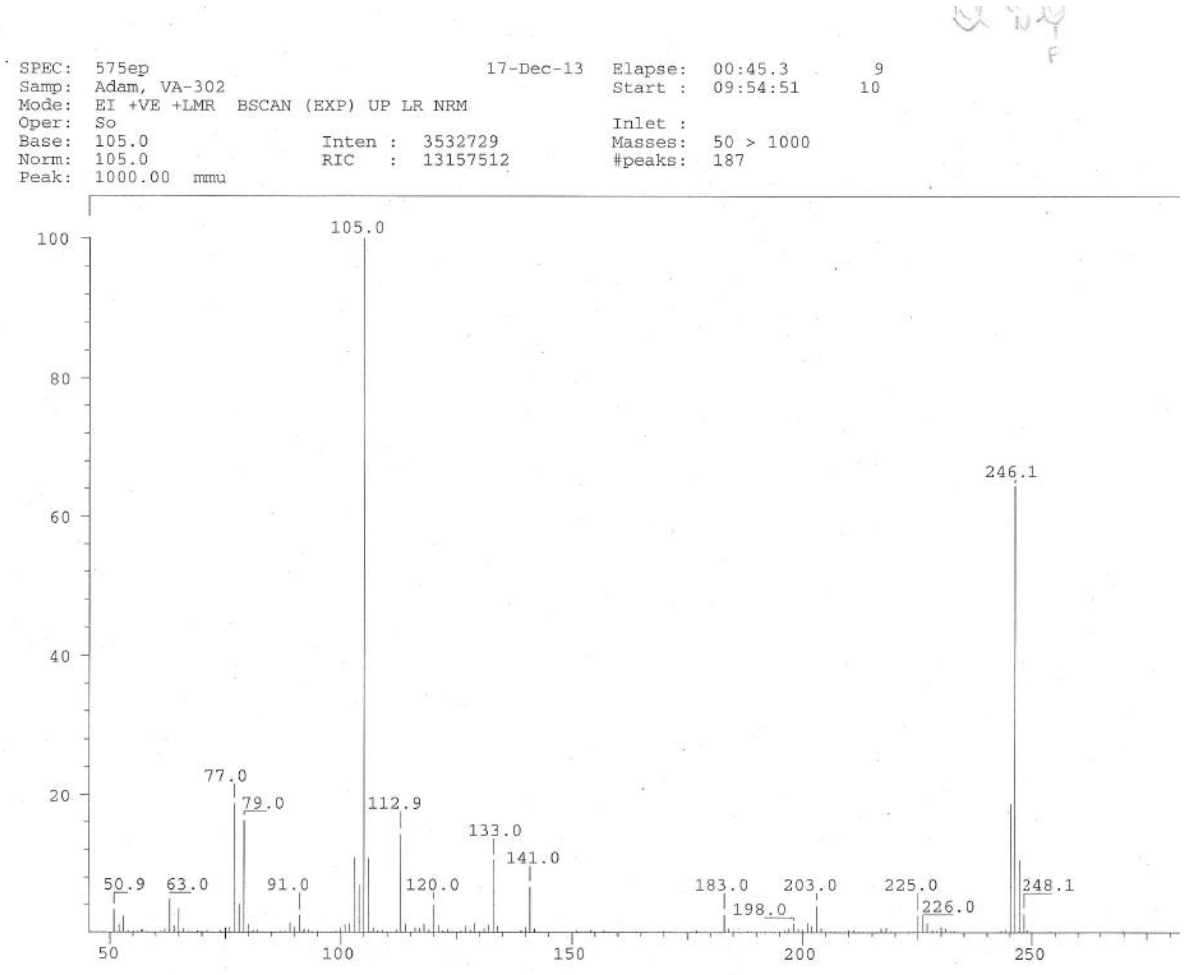
SPEC: 575ep 17-Dec-13 Elapse: 00:45.3 9
Samp: Adam, VA-302 Start : 09:54:51 10
Mode: EI +VE +LMR BSCAN (EXP) UP LR NRM
Oper: So Inlet :
Base: 105.0 Inten : 3532729 Masses: 50 > 1000
Norm: 105.0 RIC : 13157512 #peaks: 187
Peak: 1000.00 mmu
105.0
246.1
77.0
79.0
112.9
133.0
141.0
50.9
63.0
91.0
120.0
183.0
198.0
203.0
225.0
226.0
248.1

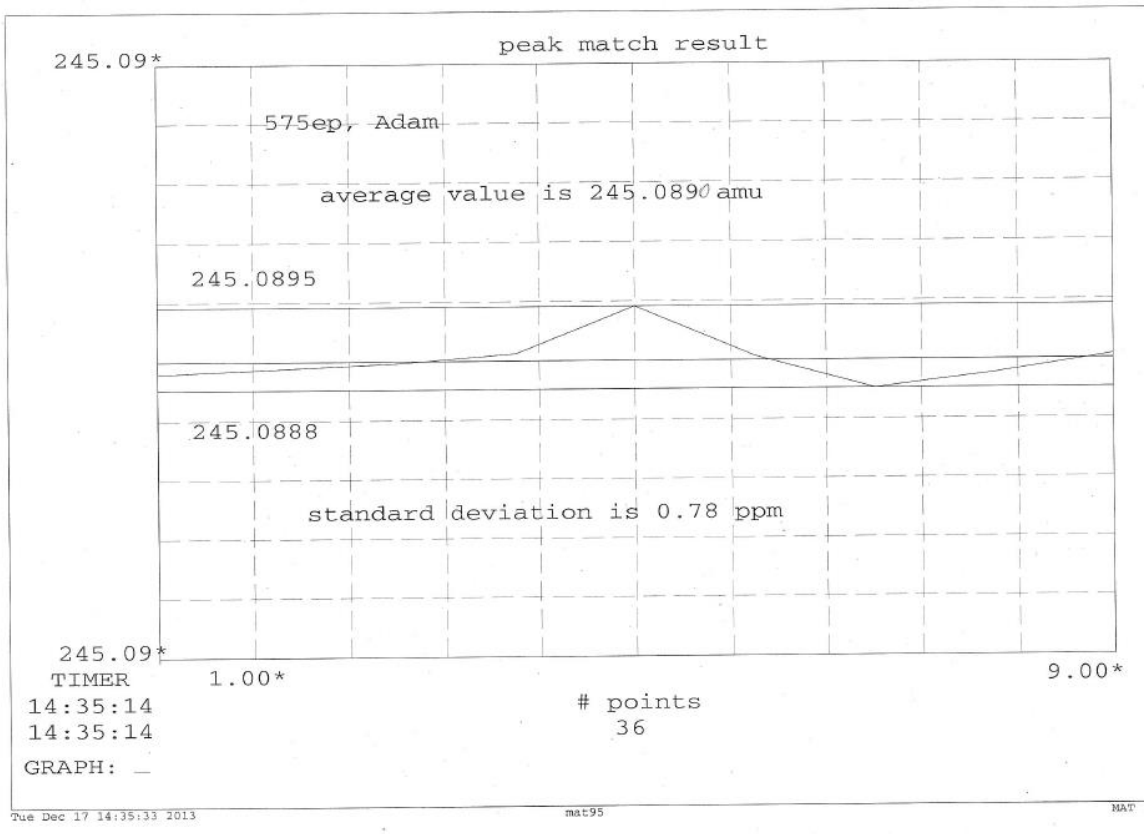
peak match result
245.09*
575ep, Adam
average value is 245.0890 amu
245.0895
245.0888
standard deviation is 0.78 ppm
245.09*
TIMER
1.00*
9.00*
14:35:14
14:35:14
points
36
GRAPH: _
Tue Dec 17 14:35:33 2013
mat95
MAT

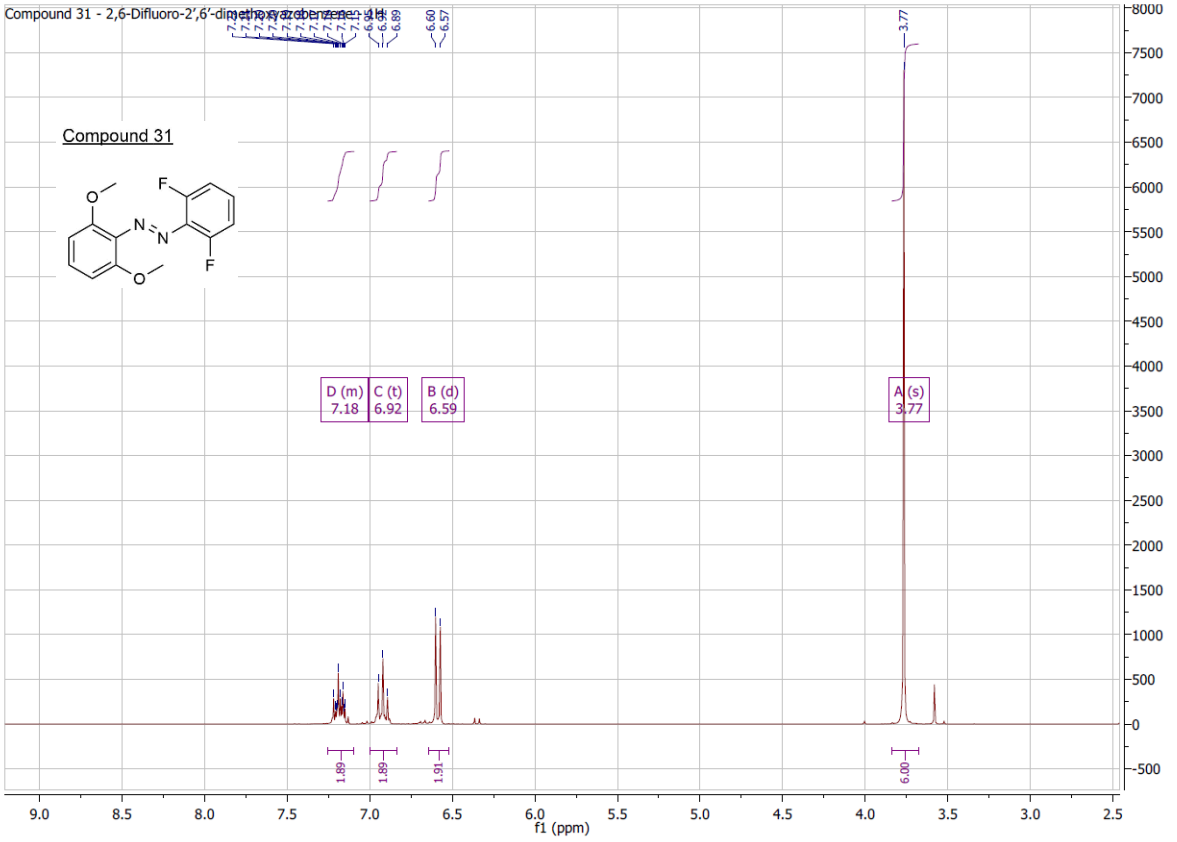
Compound 31 - 2,6-Difluoro-2′,6′-dimethoxyazobenzene - 1H
Compound 31
D (m) 7.18
C (t) 6.92
B (d) 6.59
A (s) 3.77
f1 (ppm)

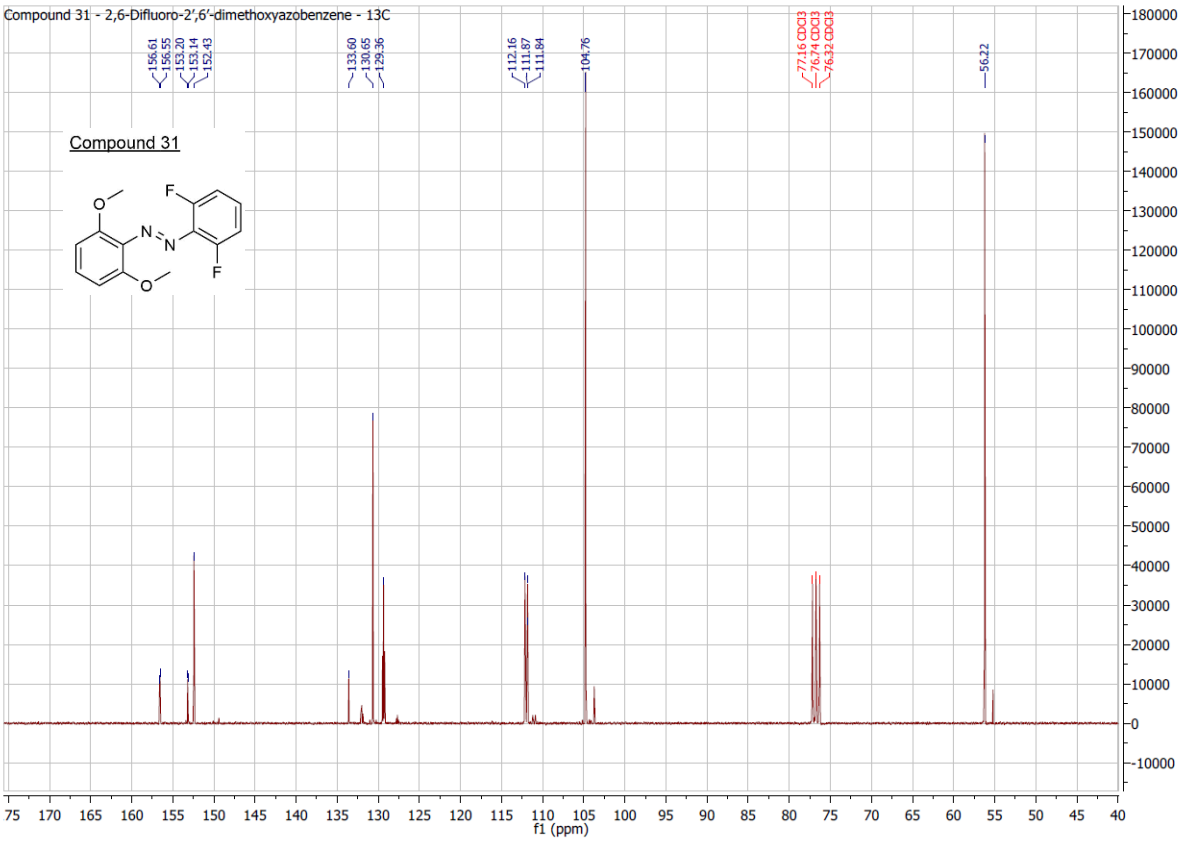
Compound 31 - 2,6-Difluoro-2′,6′-dimethoxyazobenzene - 13C
Compound 31
f1 (ppm)

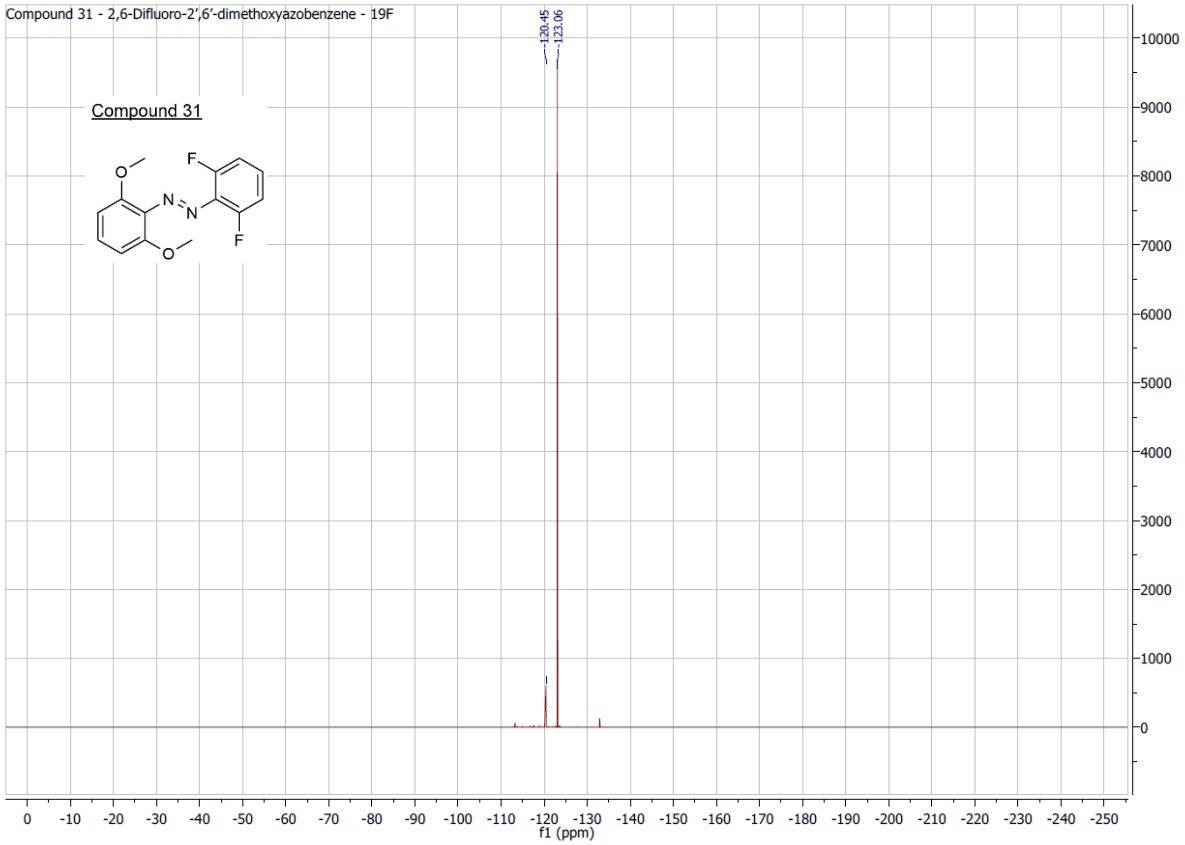
Compound 31 - 2,6-Difluoro-2',6'-dimethoxyazobenzene - 19F
120.45
123.06
Compound 31
O
F
N
N
O
F
10000
9000
8000
7000
6000
5000
4000
3000
2000
1000
0
0 -10 -20 -30 -40 -50 -60 -70 -80 -90 -100 -110 -120 -130 -140 -150 -160 -170 -180 -190 -200 -210 -220 -230 -240 -250
f1 (ppm)

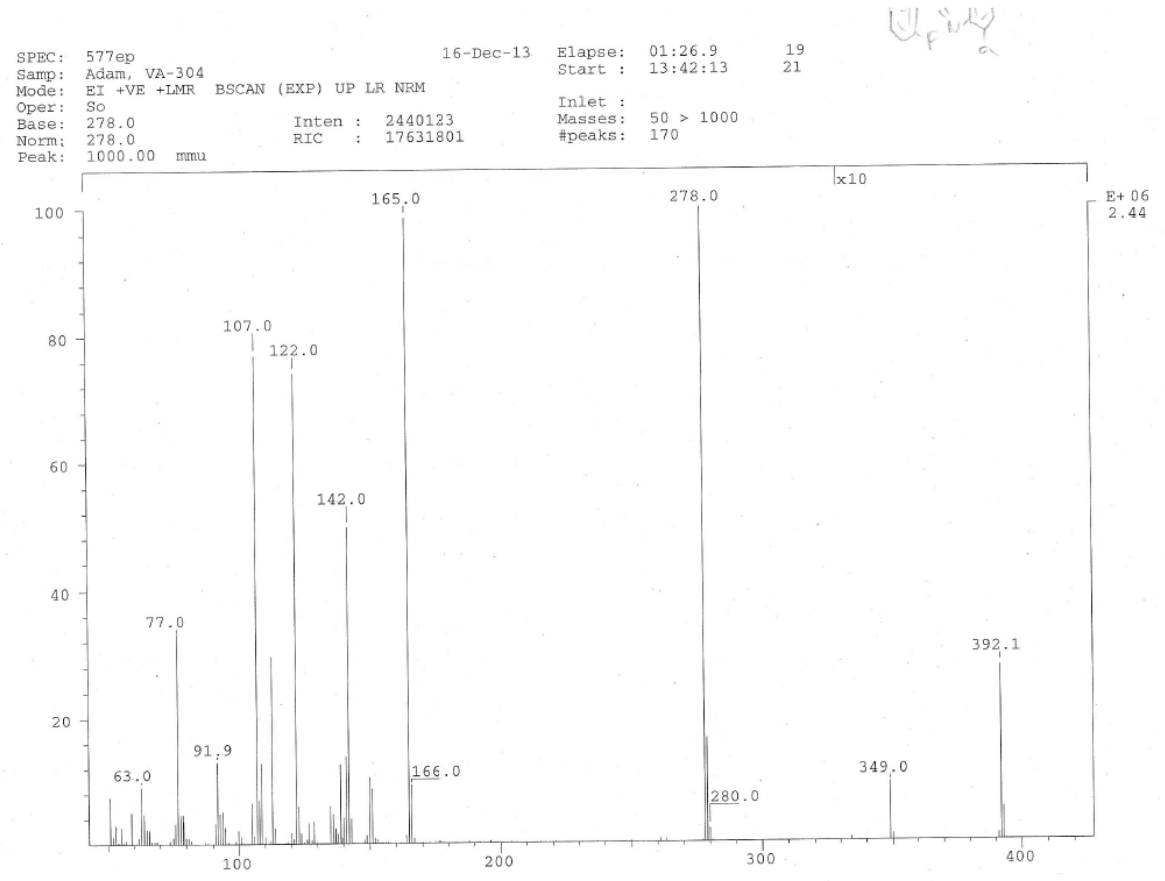
SPEC: 577ep
Samp: Adam, VA-304
Mode: EI +VE +LMR BSCAN (EXP) UP LR NRM
Oper: So
Base: 278.0
Norm: 278.0
Peak: 1000.00 mmu
16-Dec-13
Inten : 2440123
RIC : 17631801
Elapse: 01:26.9 19
Start : 13:42:13 21
Inlet :
Masses: 50 > 1000
#peaks: 170
x10
E+06
2.44
165.0
278.0
107.0
122.0
142.0
77.0
91.9
63.0
166.0
280.0
349.0
392.1
100
80
60
40
20
100
200
300
400

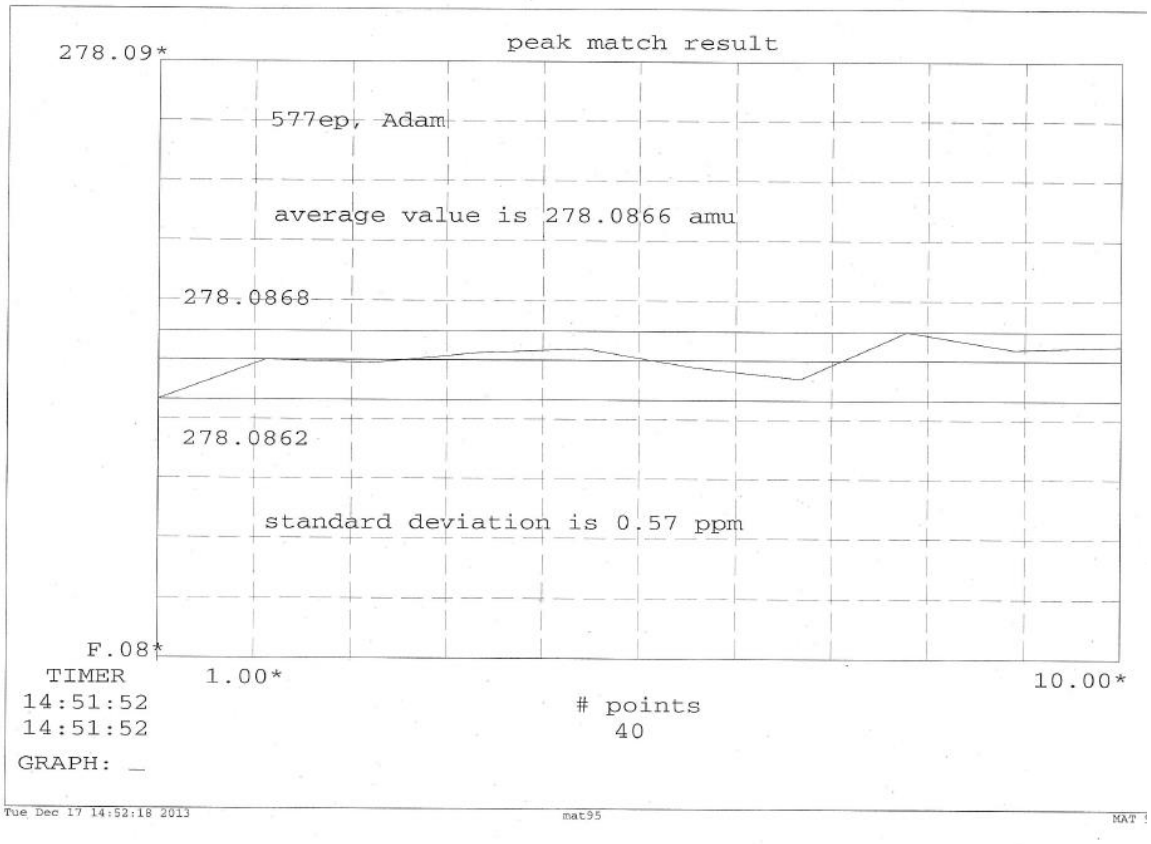
peak match result
278.09*
577ep, Adam
average value is 278.0866 amu
278.0868
278.0862
standard deviation is 0.57 ppm
F.08*
TIMER
1.00*
10.00*
14:51:52
14:51:52
points
40
GRAPH: _
Tue Dec 17 14:52:18 2013
mat95

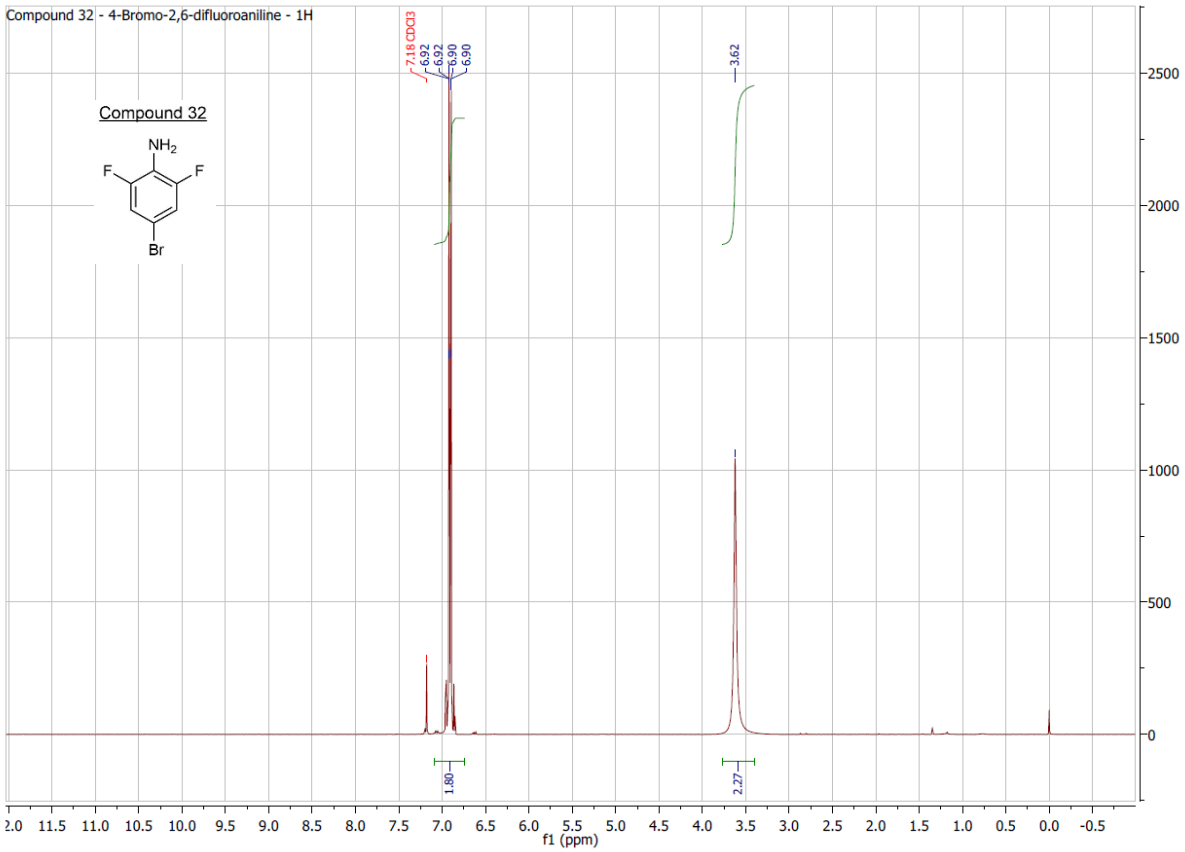
Compound 32 - 4-Bromo-2,6-difluoroaniline - 1H
Compound 32
NH2
F
F
Br
7.18 CDCl3
6.92
6.92
6.90
6.90
3.62
1.80
2.27
f1 (ppm)

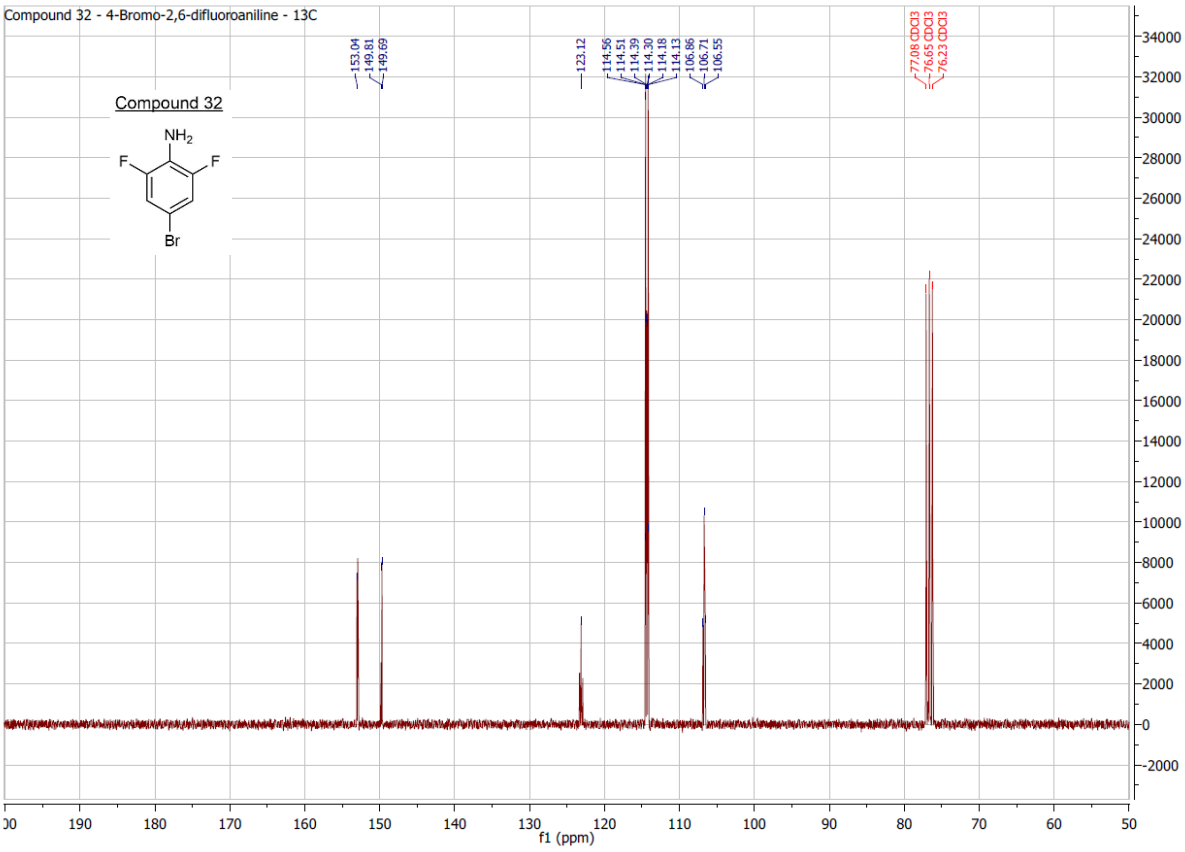
Compound 32 - 4-Bromo-2,6-difluoroaniline - 13C
Compound 32
NH2
F
F
Br
153.04
149.81
149.69
123.12
114.56
114.51
114.39
114.30
114.18
114.13
106.86
106.71
106.55
77.08 CDCl3
76.65 CDCl3
76.23 CDCl3
f1 (ppm)

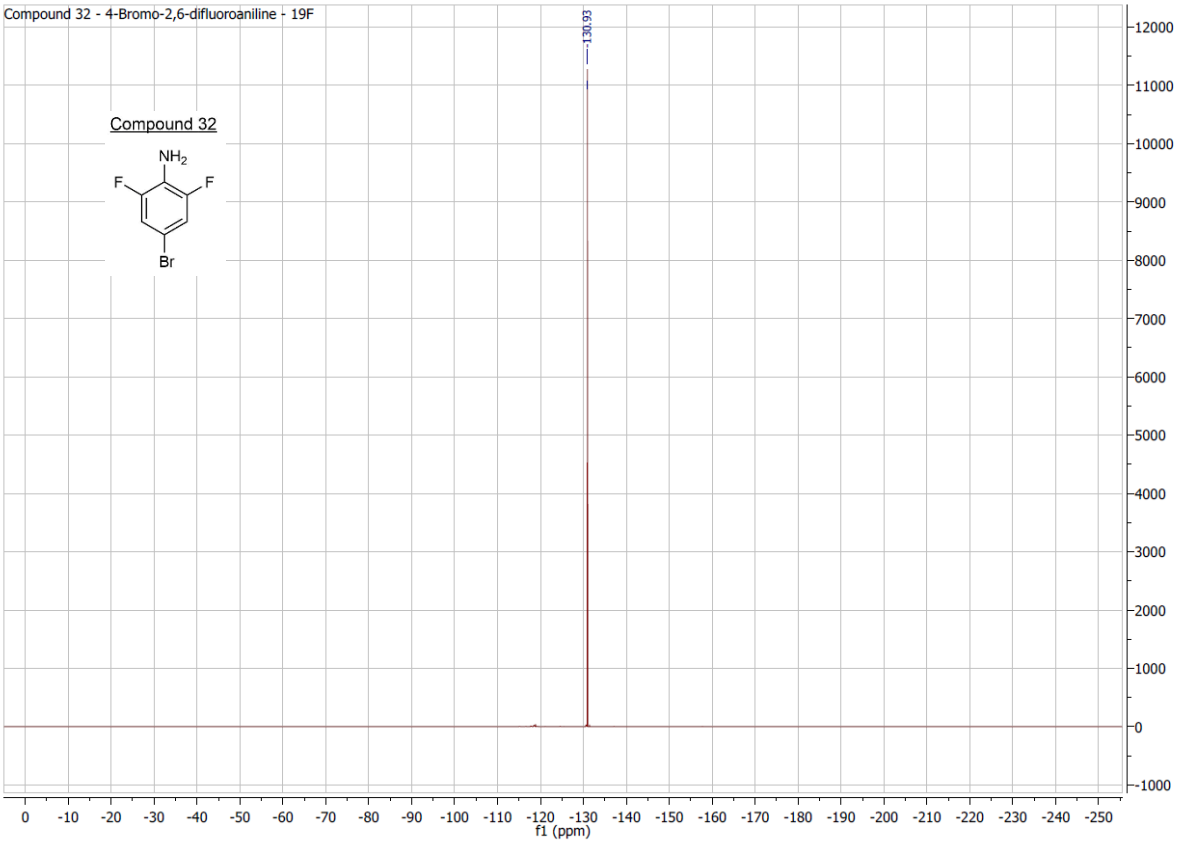
Compound 32 - 4-Bromo-2,6-difluoroaniline - 19F
-130.93
Compound 32
NH2
F
F
Br
f1 (ppm)

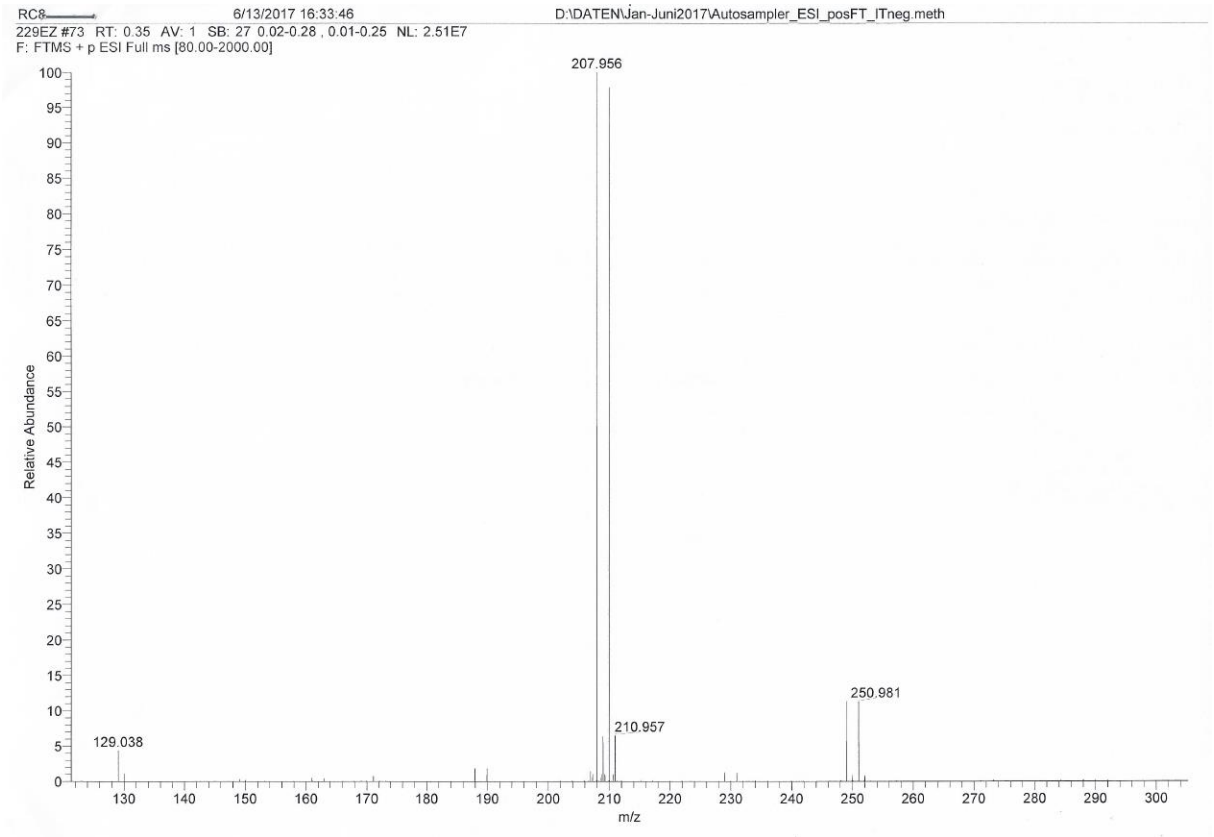
RC8
6/13/2017 16:33:46
D:\DATEN\Jan-Juni2017\Autosampler_ESI_posFT_ITneg.meth
229EZ #73 RT: 0.35 AV: 1 SB: 27 0.02-0.28 , 0.01-0.25 NL: 2.51E7
F: FTMS + p ESI Full ms [80.00-2000.00]
207.956
250.981
210.957
129.038
Relative Abundance
m/z

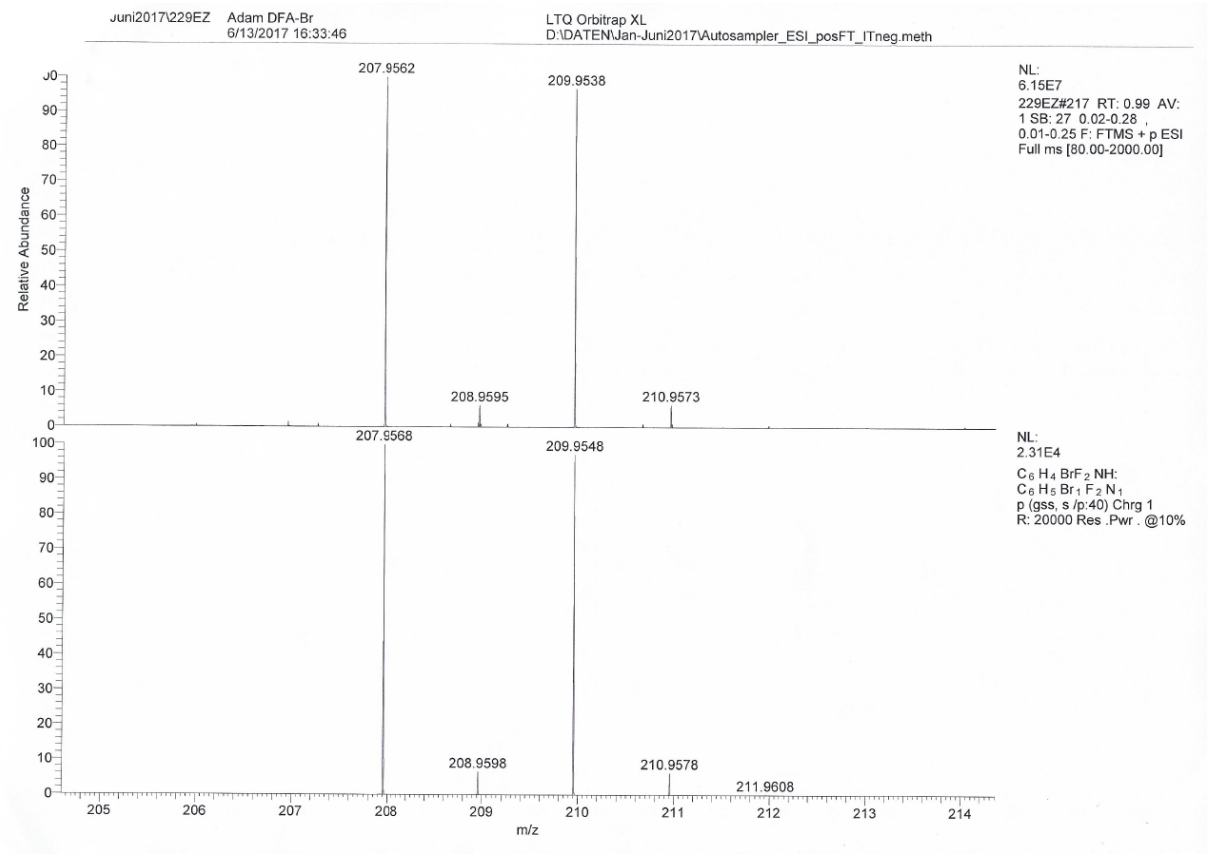
Juni2017\229EZ Adam DFA-Br
6/13/2017 16:33:46
LTQ Orbitrap XL
D:\DATEN\Jan-Juni2017\Autosampler_ESI_posFT_ITneg.meth
207.9562
209.9538
208.9595
210.9573
NL:
6.15E7
229EZ#217 RT: 0.99 AV:
1 SB: 27 0.02-0.28 ,
0.01-0.25 F: FTMS + p ESI
Full ms [80.00-2000.00]
207.9568
209.9548
208.9598
210.9578
211.9608
NL:
2.31E4
C6 H4 BrF2 NH:
C6 H5 Br1 F2 N1
p (gss, s /p:40) Chrg 1
R: 20000 Res .Pwr . @10%
Relative Abundance
m/z

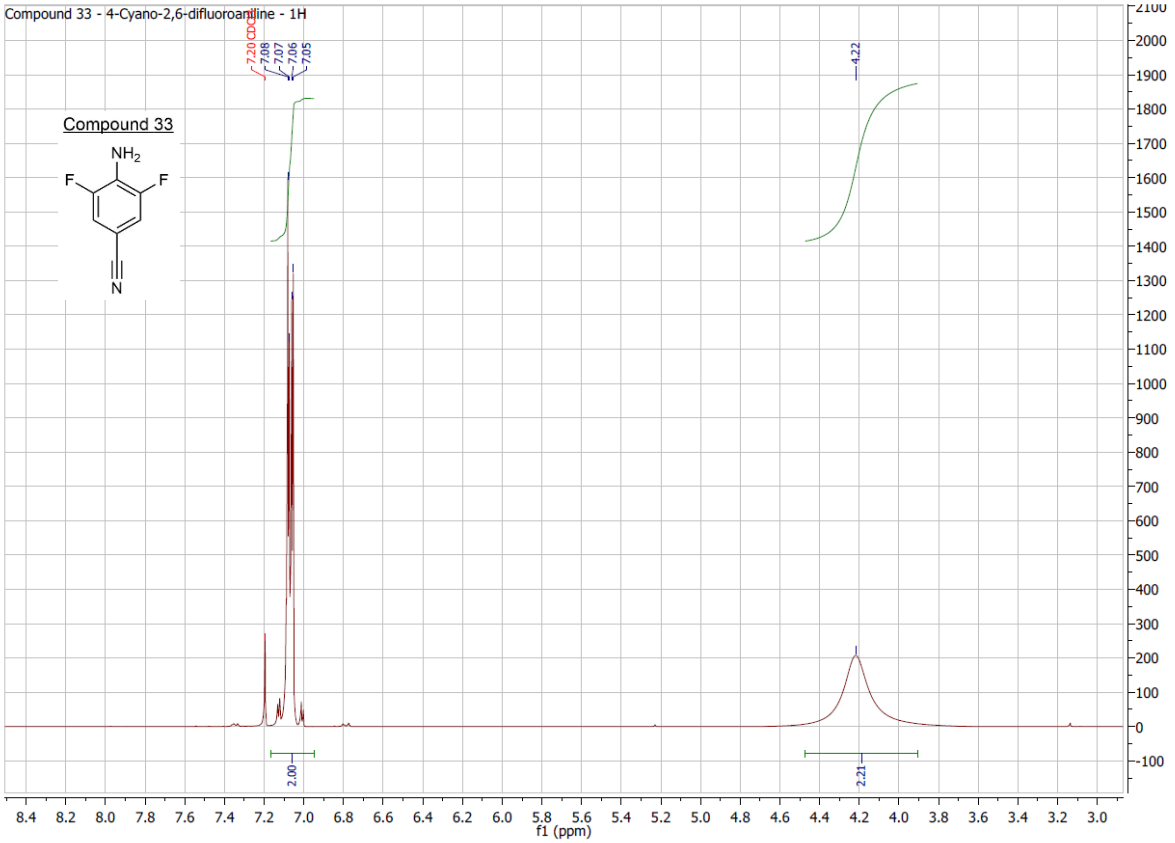
Compound 33 - 4-Cyano-2,6-difluoroaniline - 1H
Compound 33
NH2
F
F
N
7.20 CDCl3
7.08
7.07
7.06
7.05
4.22
2.00
2.21
f1 (ppm)

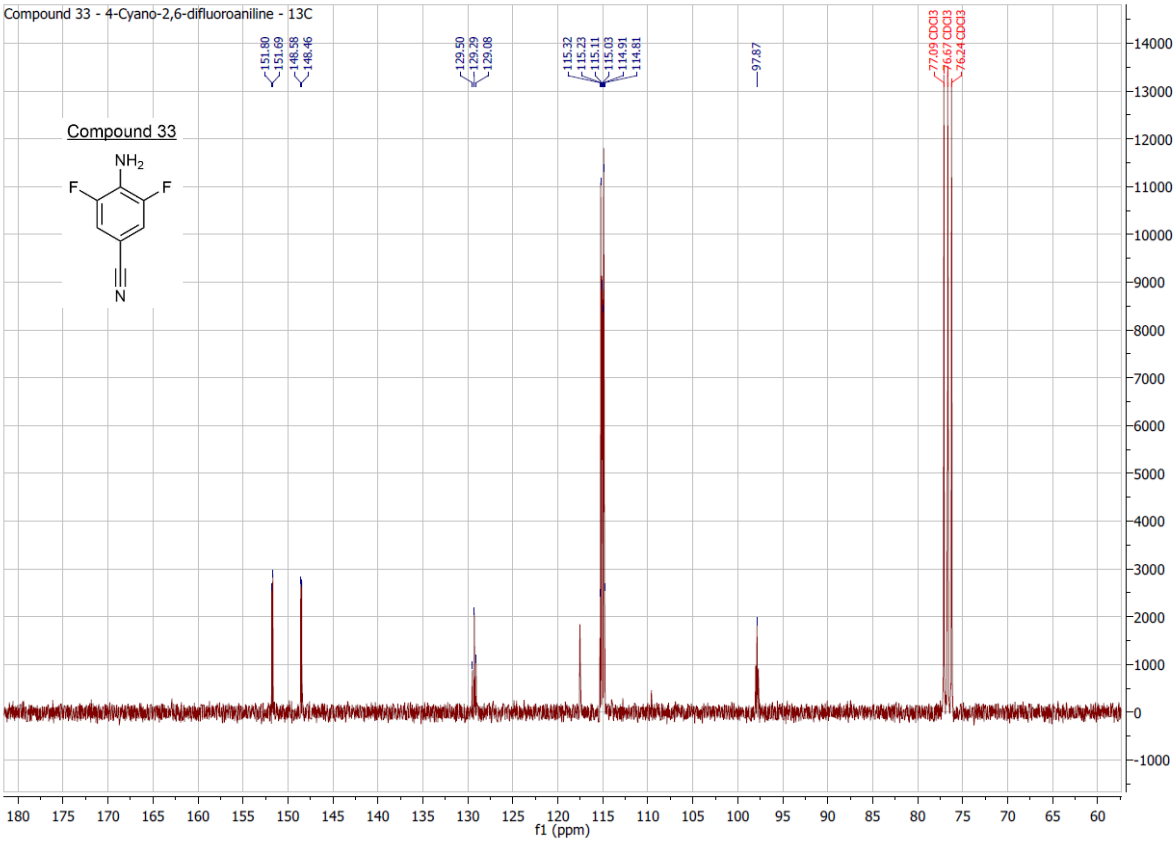
Compound 33 - 4-Cyano-2,6-difluoroaniline - 13C
Compound 33
NH2
F
F
N
151.80
151.69
148.58
148.46
129.50
129.29
129.08
115.32
115.23
115.11
115.03
114.91
114.81
97.87
77.09 CDCl3
76.67 CDCl3
76.24 CDCl3
f1 (ppm)

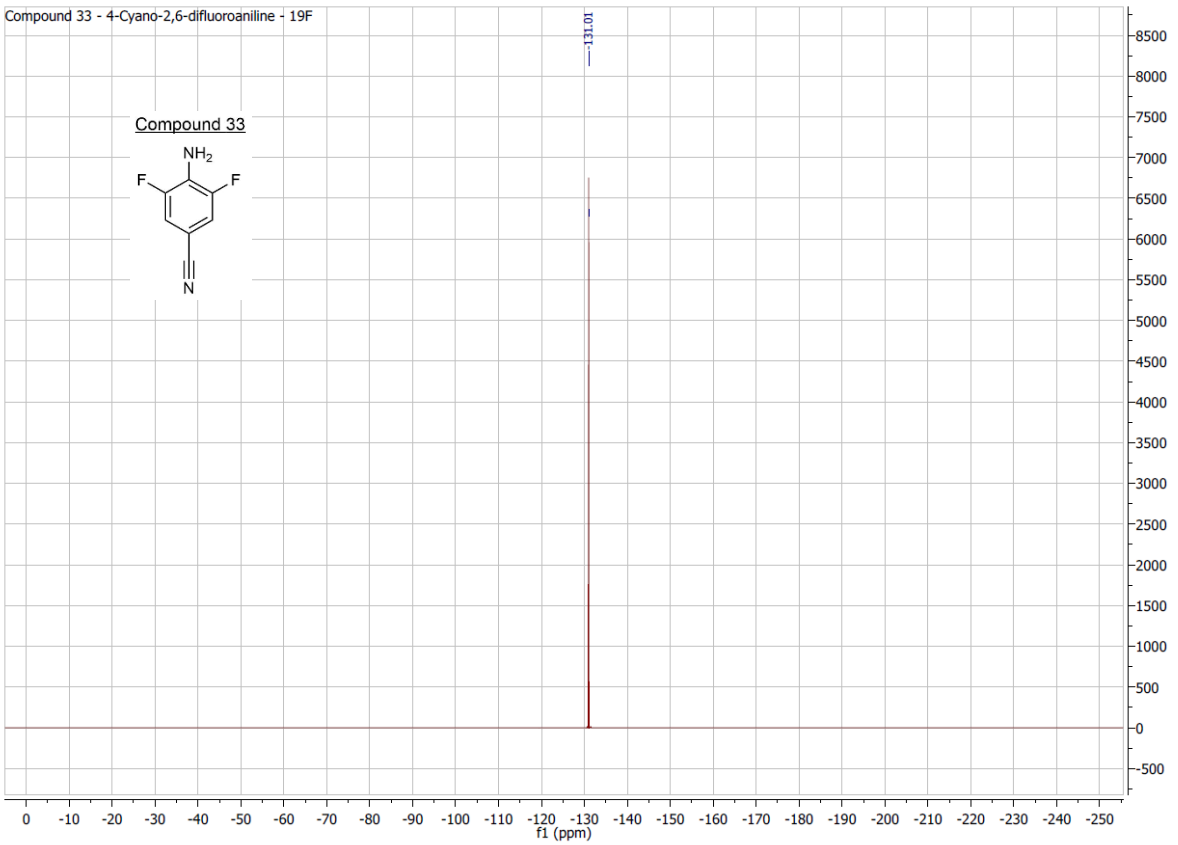
Compound 33 - 4-Cyano-2,6-difluoroaniline - 19F
131.01
Compound 33
NH2
F
F
N
f1 (ppm)

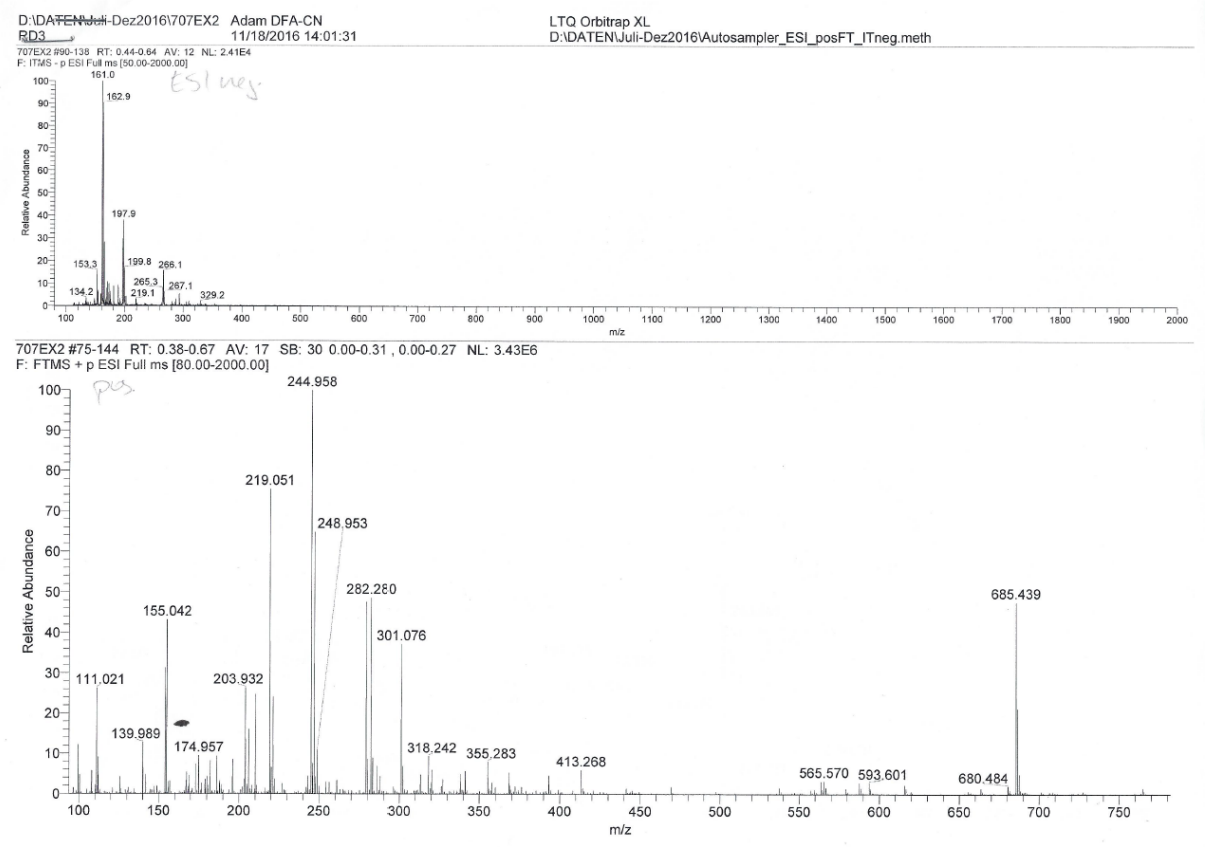
D:\DATEN\Juli-Dez2016\707EX2 Adam DFA-CN
RD3
11/18/2016 14:01:31
LTQ Orbitrap XL
D:\DATEN\Juli-Dez2016\Autosampler_ESI_posFT_ITneg.meth
707EX2 #90-138 RT: 0.44-0.64 AV: 12 NL: 2.41E4
F: ITMS - p ESI Full ms [50.00-2000.00]
ESI neg.
Relative Abundance
m/z
707EX2 #75-144 RT: 0.38-0.67 AV: 17 SB: 30 0.00-0.31 , 0.00-0.27 NL: 3.43E6
F: FTMS + p ESI Full ms [80.00-2000.00]
pos.
244.958
219.051
248.953
282.280
685.439
155.042
301.076
111.021
203.932
139.989
174.957
318.242
355.283
413.268
565.570
593.601
680.484
Relative Abundance
m/z

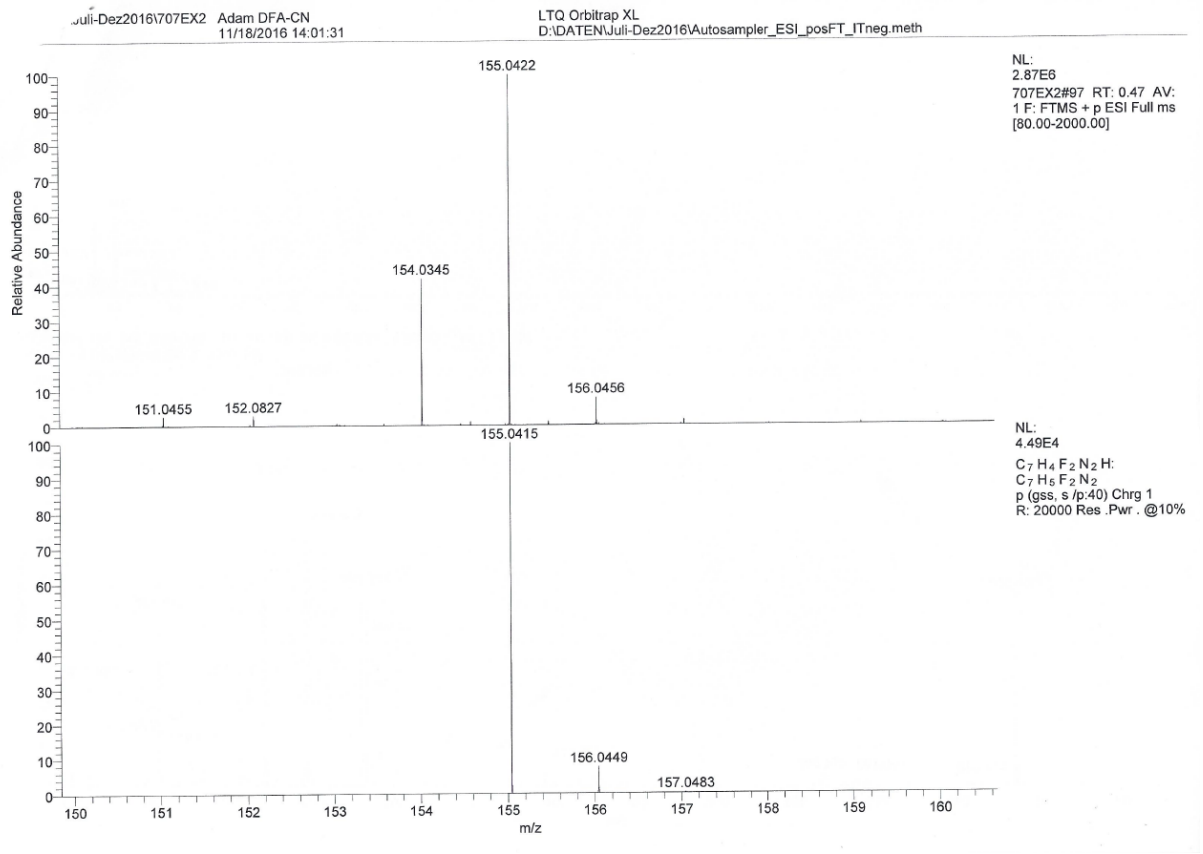
Juli-Dez2016\707EX2 Adam DFA-CN
11/18/2016 14:01:31
LTQ Orbitrap XL
D:\DATEN\Juli-Dez2016\Autosampler_ESI_posFT_ITneg.meth
NL:
2.87E6
707EX2#97 RT: 0.47 AV:
1 F: FTMS + p ESI Full ms
[80.00-2000.00]
155.0422
154.0345
156.0456
151.0455
152.0827
Relative Abundance
NL:
4.49E4
C7 H4 F2 N2 H:
C7 H5 F2 N2
p (gss, s /p:40) Chrg 1
R: 20000 Res .Pwr . @10%
155.0415
156.0449
157.0483
m/z

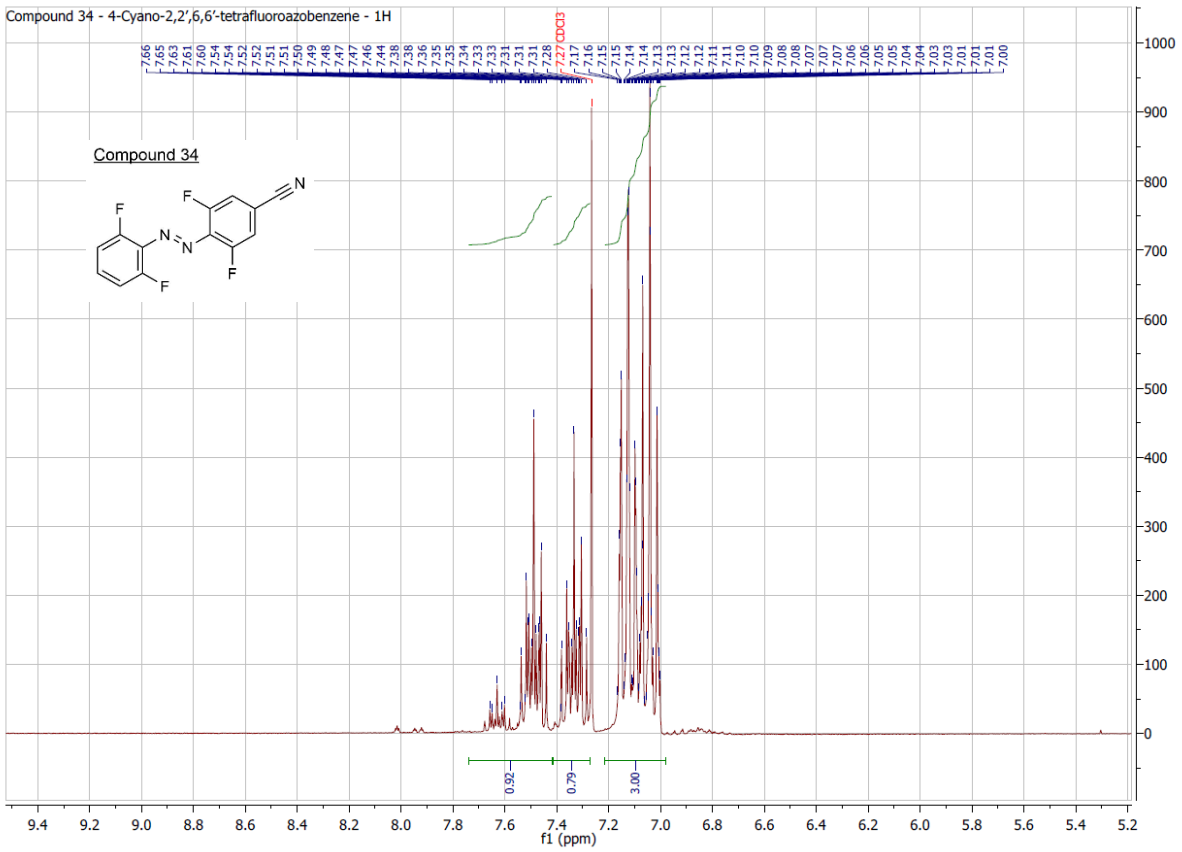
Compound 34 - 4-Cyano-2,2',6,6'-tetrafluoroazobenzene - 1H
Compound 34
0.92
0.79
3.00
f1 (ppm)

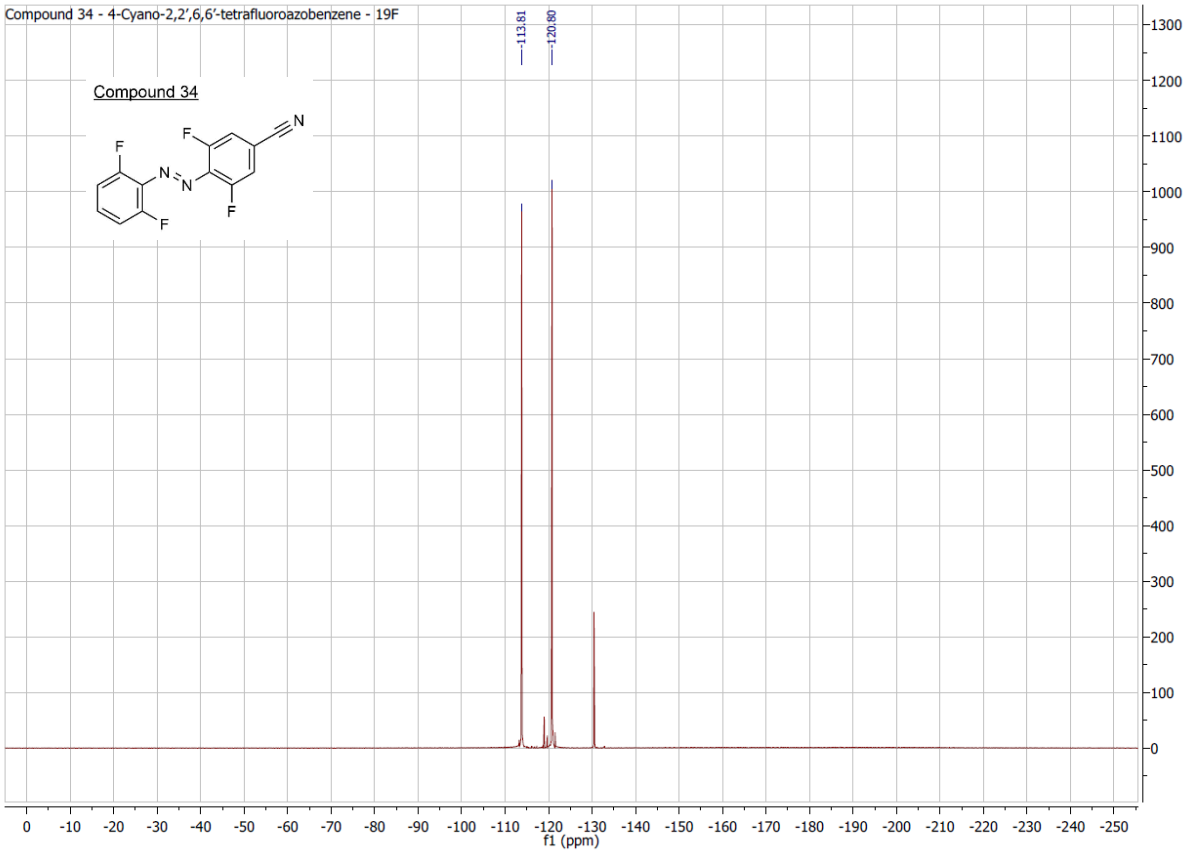
Compound 34 - 4-Cyano-2,2',6,6'-tetrafluoroazobenzene - 19F
113.81
120.80
Compound 34
f1 (ppm)

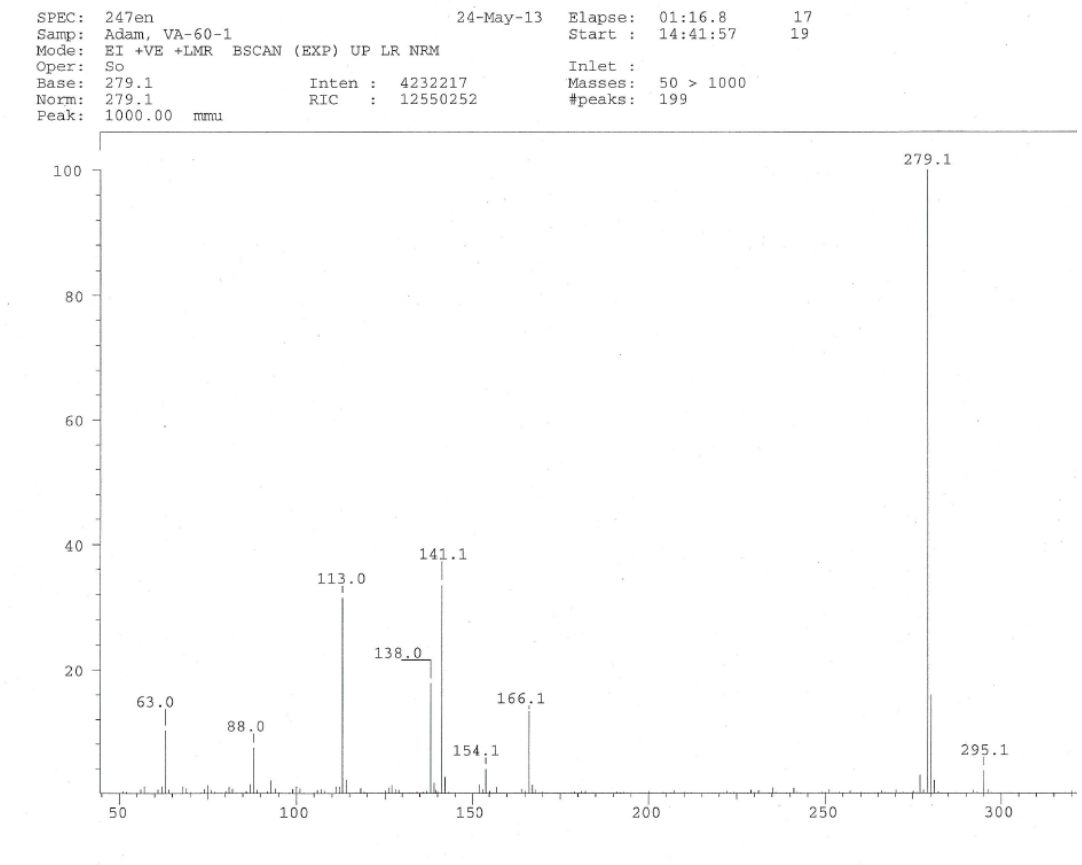
SPEC: 247en 24-May-13 Elapse: 01:16.8 17
Samp: Adam, VA-60-1 Start : 14:41:57 19
Mode: EI +VE +LMR BSCAN (EXP) UP LR NRM
Oper: So Inlet :
Base: 279.1 Inten : 4232217 Masses: 50 > 1000
Norm: 279.1 RIC : 12550252 #peaks: 199
Peak: 1000.00 mmu
279.1
141.1
113.0
138.0
63.0
88.0
166.1
154.1
295.1
100
80
60
40
20
50
100
150
200
250
300

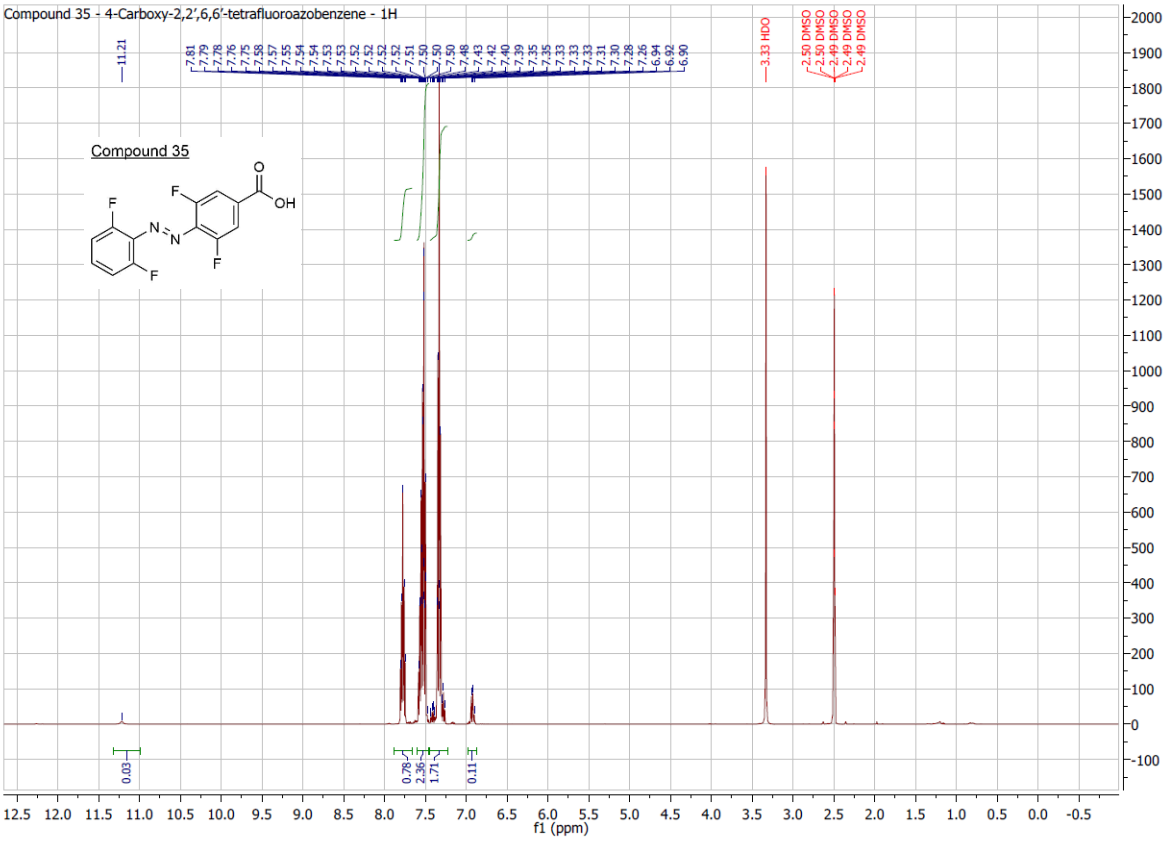
Compound 35 - 4-Carboxy-2,2',6,6'-tetrafluoroazobenzene - 1H
Compound 35
f1 (ppm)

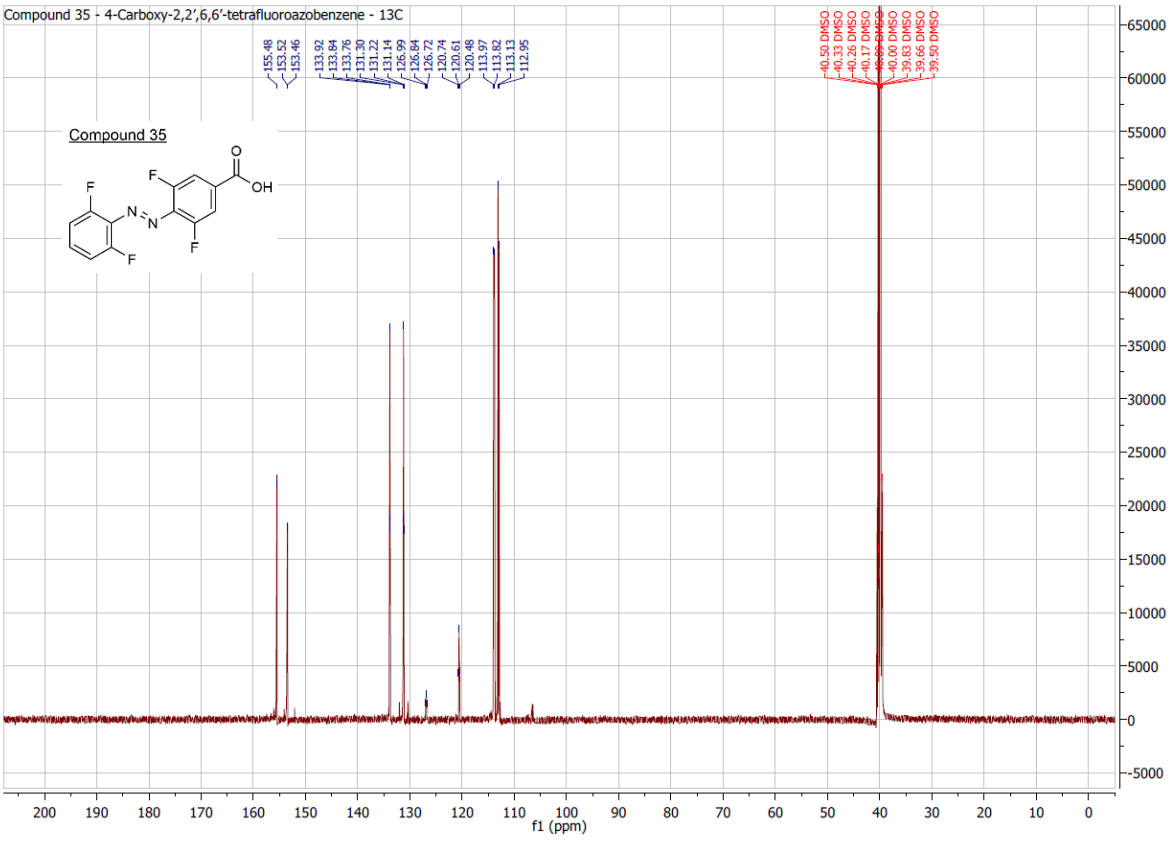
Compound 35 - 4-Carboxy-2,2',6,6'-tetrafluoroazobenzene - 13C
Compound 35
f1 (ppm)

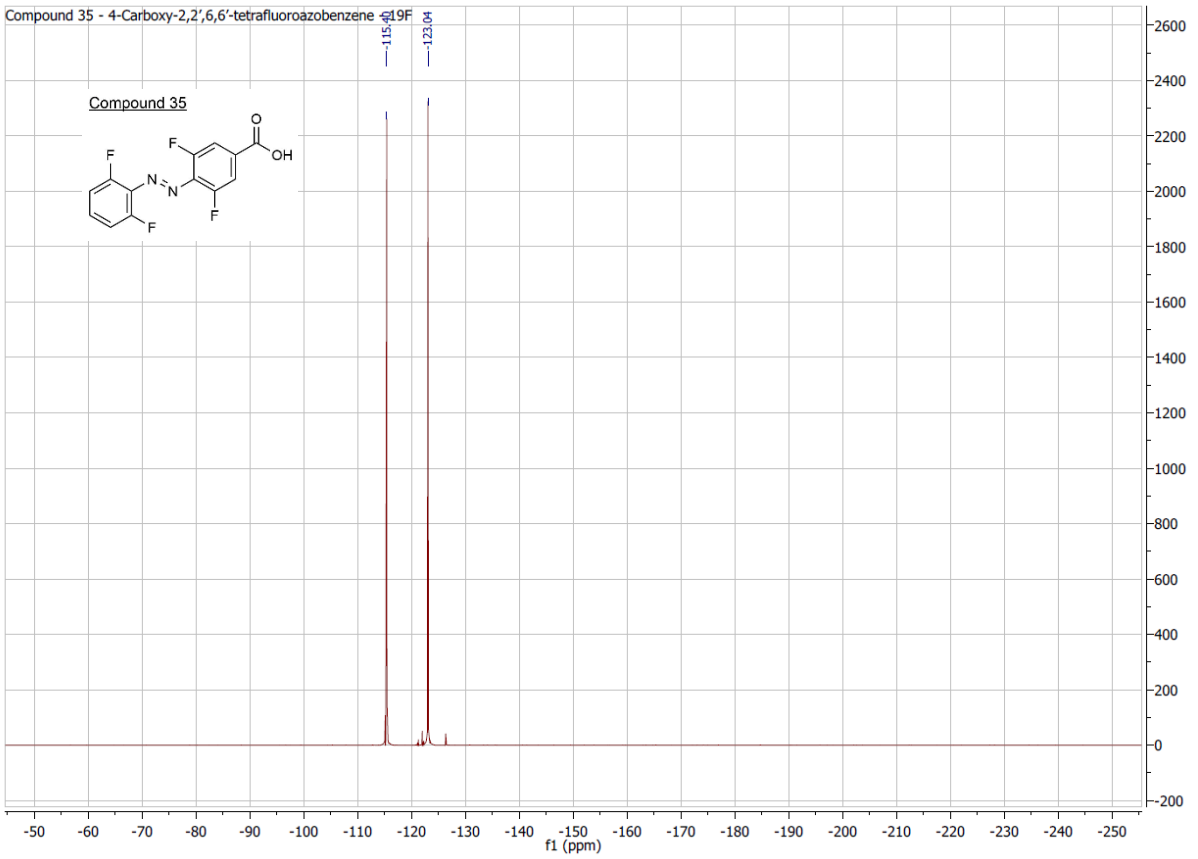
Compound 35 - 4-Carboxy-2,2',6,6'-tetrafluoroazobenzene - 19F
-115.41
-123.04
Compound 35
F
F
N
N
F
F
O
OH
2600
2400
2200
2000
1800
1600
1400
1200
1000
800
600
400
200
0
-200
-50 -60 -70 -80 -90 -100 -110 -120 -130 -140 -150 -160 -170 -180 -190 -200 -210 -220 -230 -240 -250
f1 (ppm)

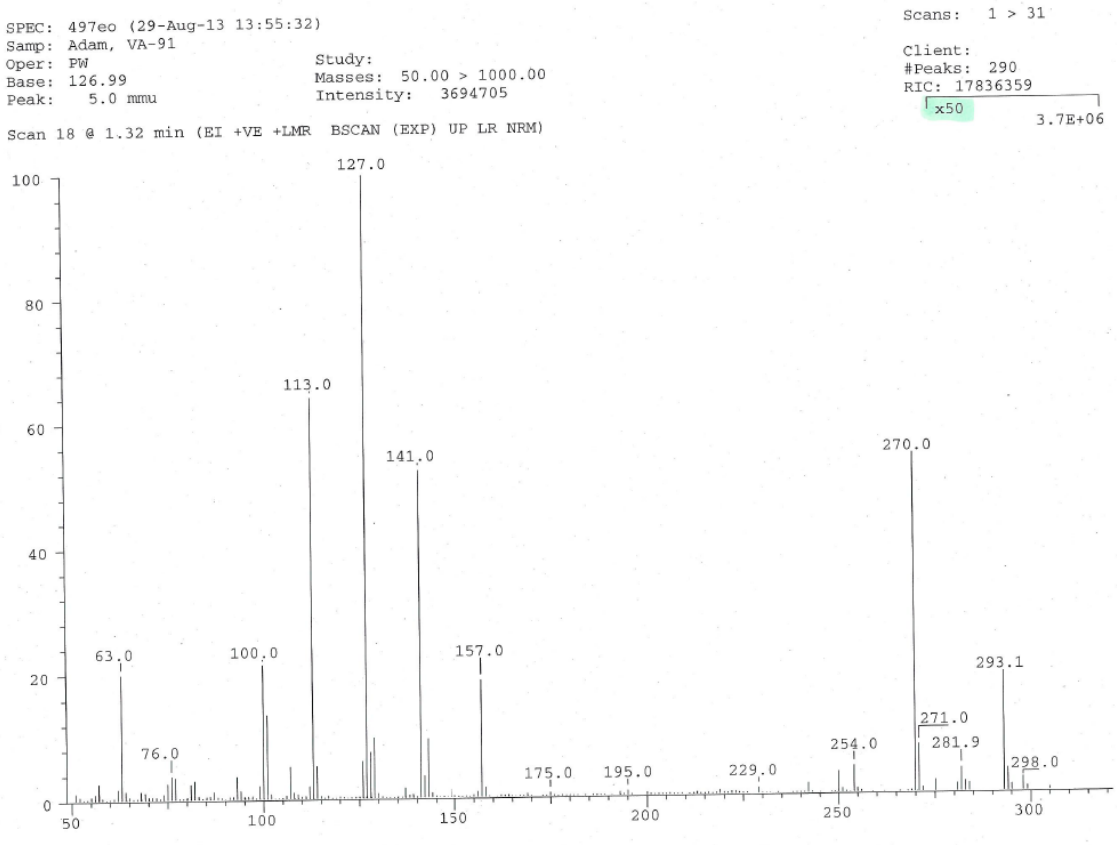
SPEC: 497eo (29-Aug-13 13:55:32)
Samp: Adam, VA-91
Oper: PW
Base: 126.99
Peak: 5.0 mmu
Study:
Masses: 50.00 > 1000.00
Intensity: 3694705
Scans: 1 > 31
Client:
#Peaks: 290
RIC: 17836359
x50
3.7E+06
Scan 18 @ 1.32 min (EI +VE +LMR BSCAN (EXP) UP LR NRM)
127.0
113.0
141.0
270.0
63.0
100.0
157.0
293.1
271.0
281.9
254.0
298.0
76.0
175.0
195.0
229.0
100
80
60
40
20
0
50
100
150
200
250
300

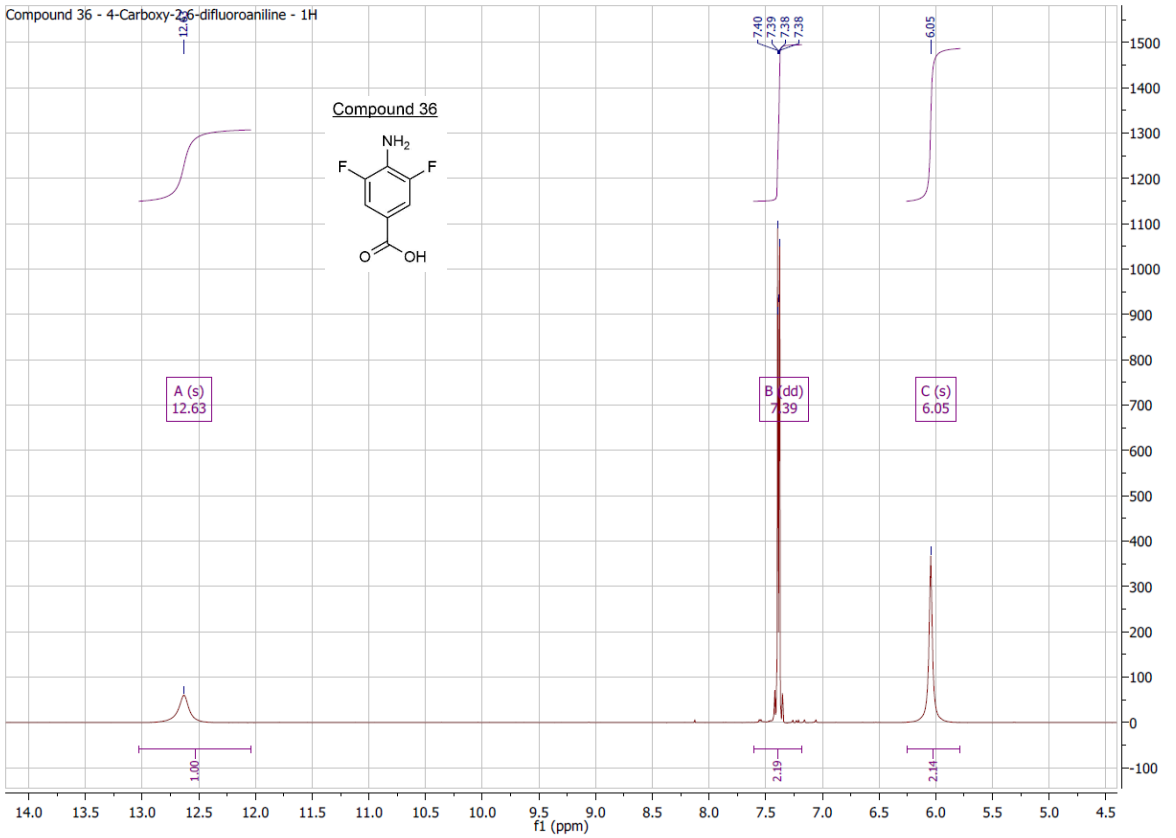
Compound 36 - 4-Carboxy-2,6-difluoroaniline - 1H
Compound 36
A (s)
12.63
B (dd)
7.39
C (s)
6.05
f1 (ppm)

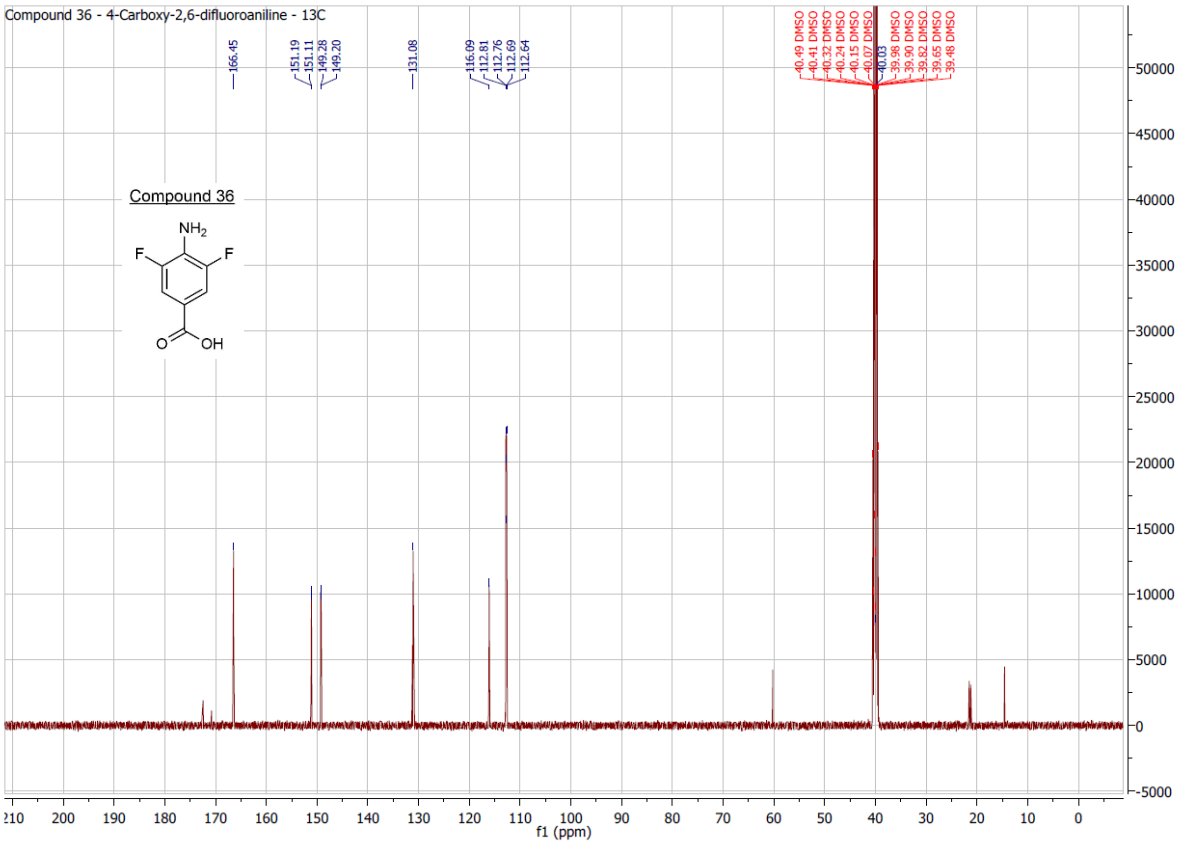
Compound 36 - 4-Carboxy-2,6-difluoroaniline - 13C
Compound 36
f1 (ppm)

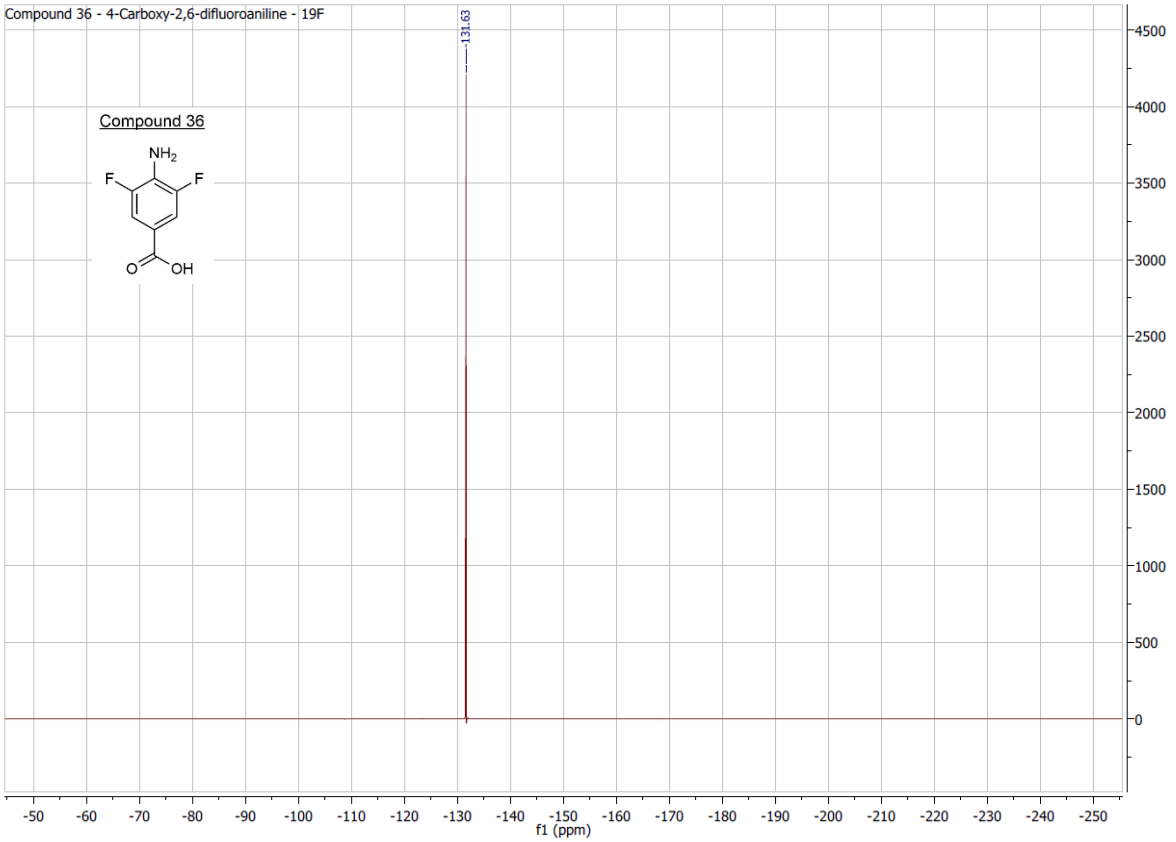
Compound 36 - 4-Carboxy-2,6-difluoroaniline - 19F
131.63
Compound 36
NH2
F
F
O
OH
4500
4000
3500
3000
2500
2000
1500
1000
500
0
-50 -60 -70 -80 -90 -100 -110 -120 -130 -140 -150 -160 -170 -180 -190 -200 -210 -220 -230 -240 -250
f1 (ppm)

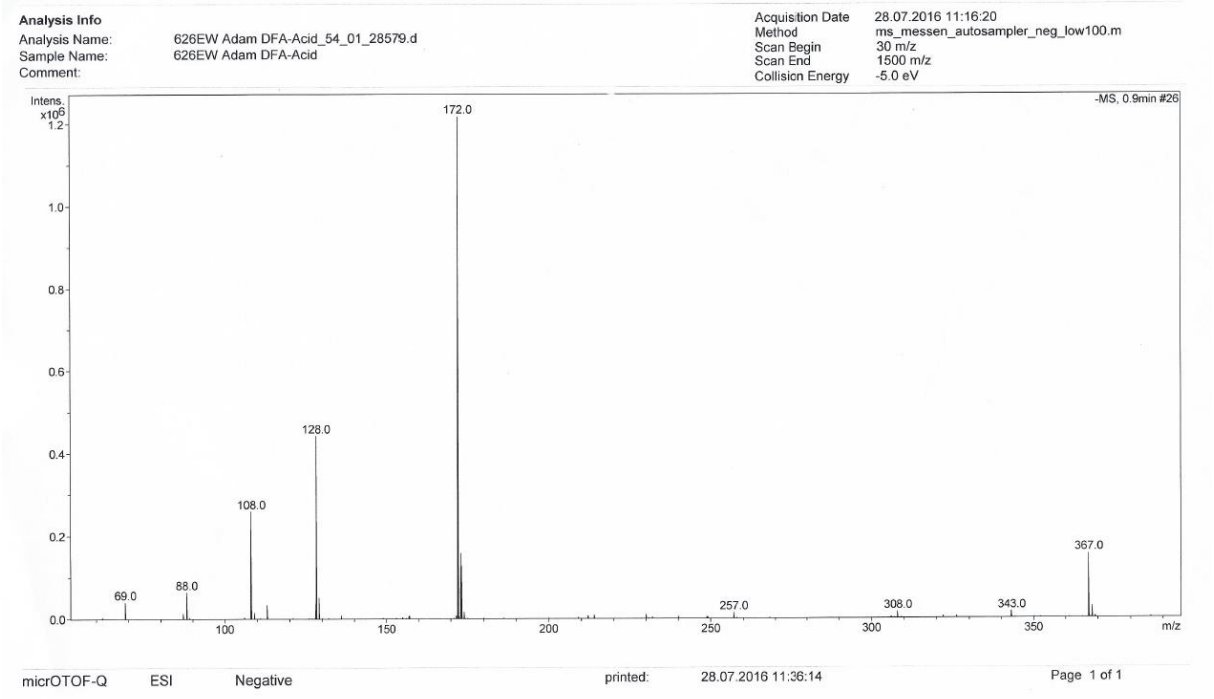
Analysis Info
Analysis Name: 626EW Adam DFA-Acid_54_01_28579.d
Sample Name: 626EW Adam DFA-Acid
Comment:
Acquisition Date 28.07.2016 11:16:20
Method ms_messen_autosampler_neg_low100.m
Scan Begin 30 m/z
Scan End 1500 m/z
Collision Energy -5.0 eV
Intens.
x10^6
-MS, 0.9min #26
172.0
128.0
108.0
88.0
69.0
257.0
308.0
343.0
367.0
m/z
micrOTOF-Q ESI Negative
printed: 28.07.2016 11:36:14
Page 1 of 1

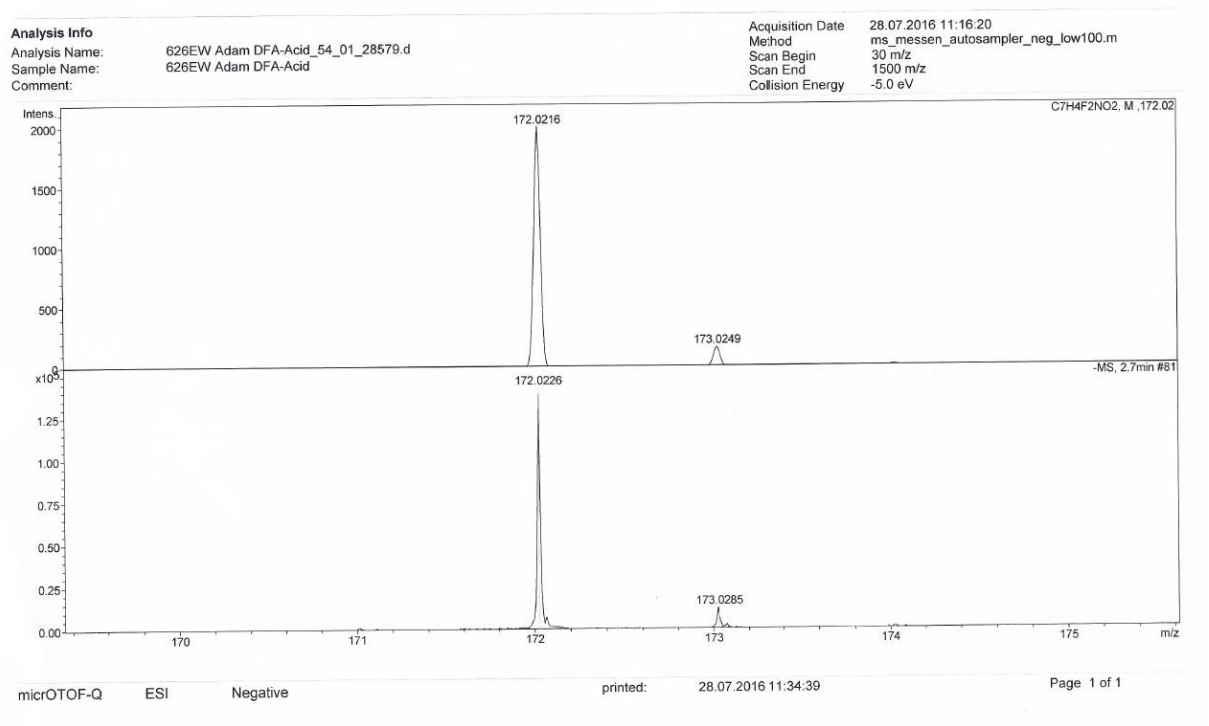
Analysis Info
Analysis Name: 626EW Adam DFA-Acid_54_01_28579.d
Sample Name: 626EW Adam DFA-Acid
Comment:
Acquisition Date 28.07.2016 11:16:20
Method ms_messen_autosampler_neg_low100.m
Scan Begin 30 m/z
Scan End 1500 m/z
Collision Energy -5.0 eV
Intens.
C7H4F2NO2, M ,172.02
172.0216
173.0249
-MS, 2.7min #81
x10
172.0226
173.0285
m/z
micrOTOF-Q ESI Negative
printed: 28.07.2016 11:34:39
Page 1 of 1

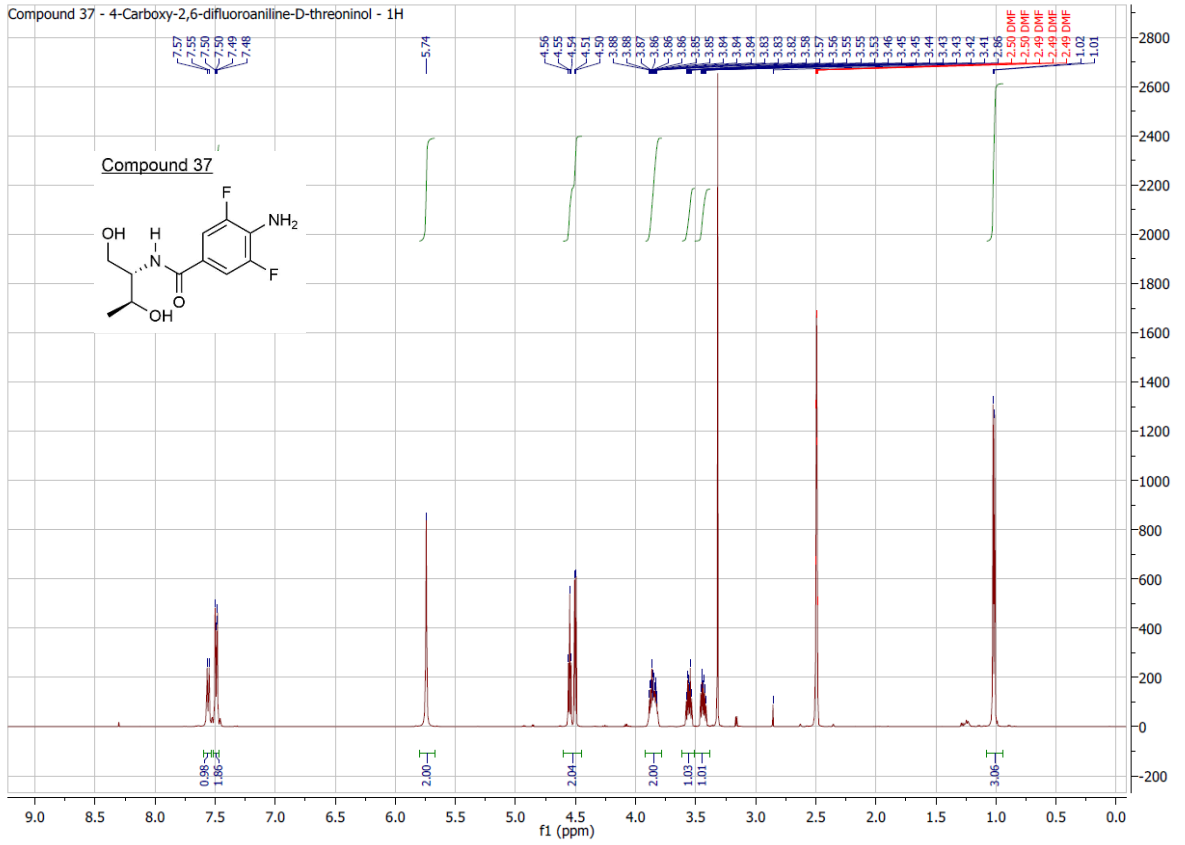
Compound 37 - 4-Carboxy-2,6-difluoroaniline-D-threoninol - 1H
Compound 37
f1 (ppm)

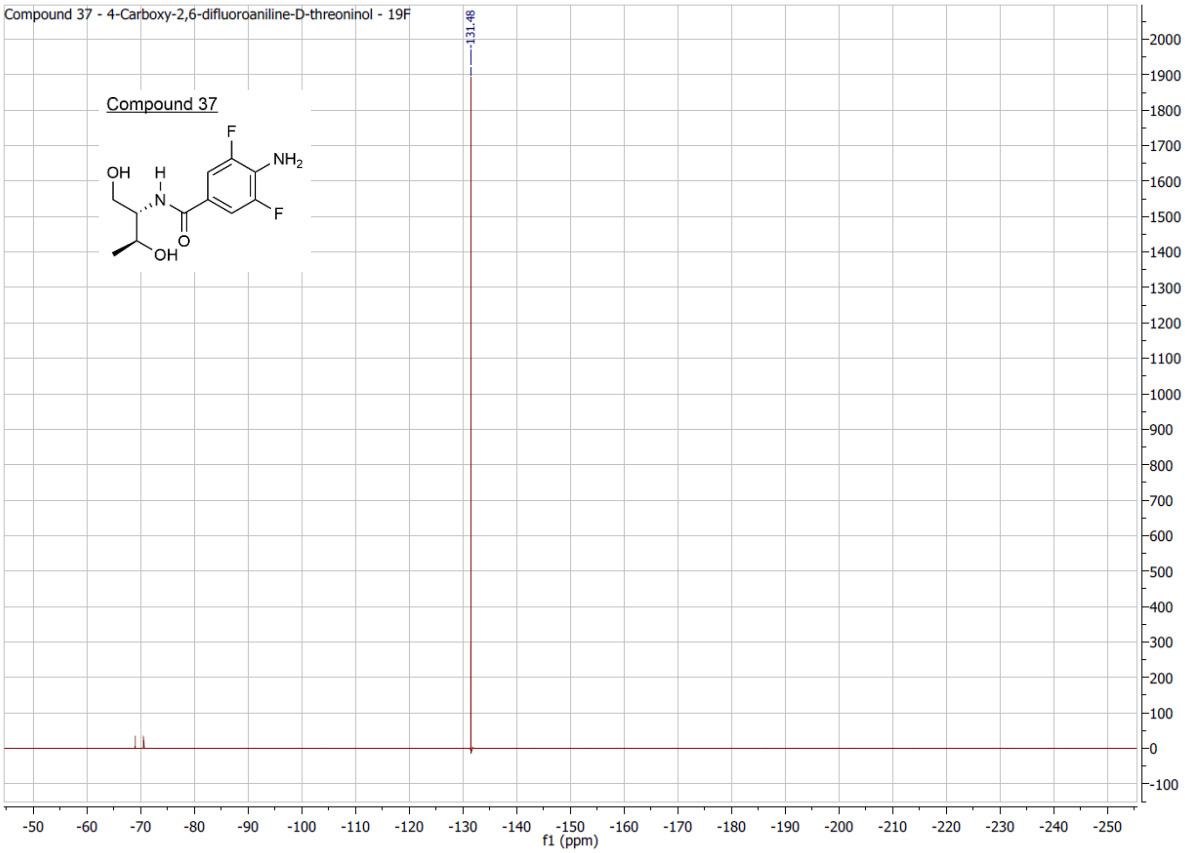
Compound 37 - 4-Carboxy-2,6-difluoroaniline-D-threoninol - 19F
Compound 37
f1 (ppm)

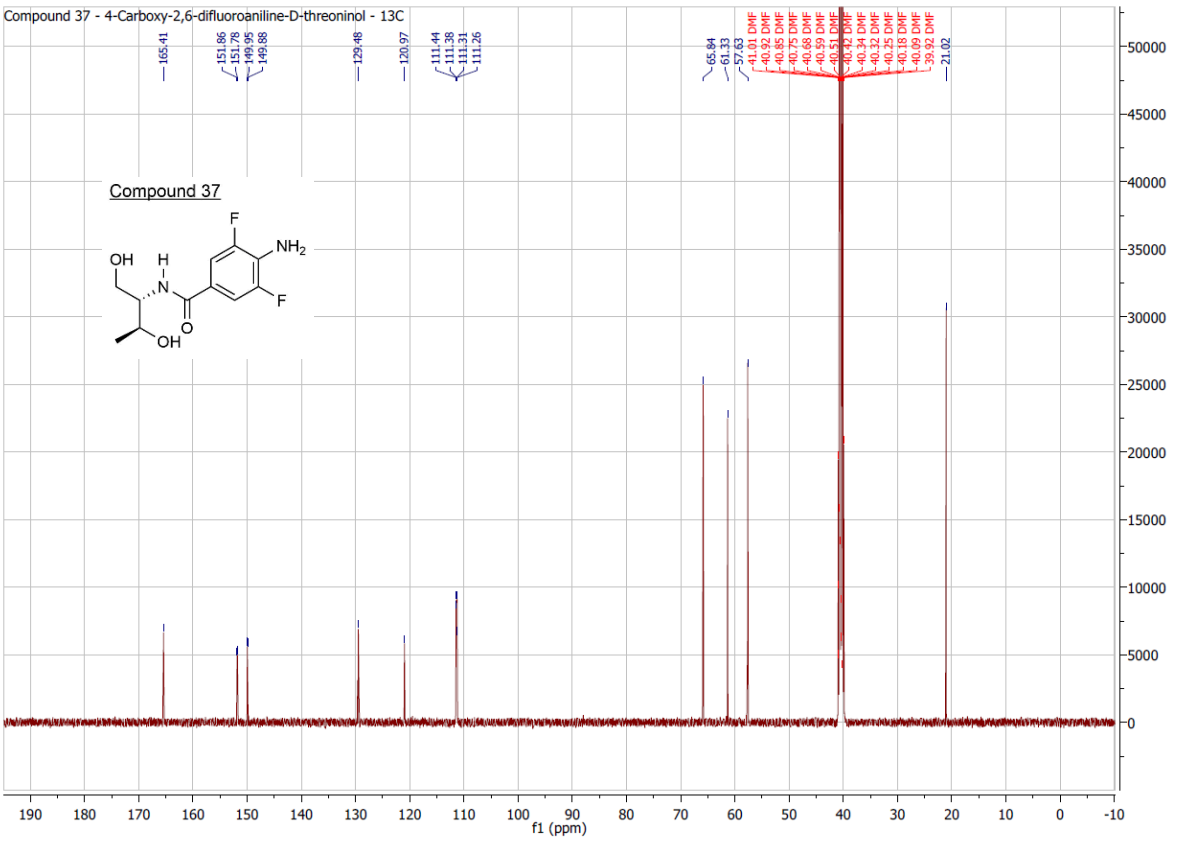

SPEC: 047ep 24-Oct-13 Elapse: 02:01.5 28
Samp: Adam, VA153-3 Start : 09:55:00 35
Mode: EI +VE +LMR BSCAN (EXP) UP LR NRM
Oper: So Inlet :
Base: 156.1 Inten : 56369664 Masses: 50 > 1000
Norm: 156.1 RIC : 262620245 #peaks: 896
Peak: 1000.00 mmu

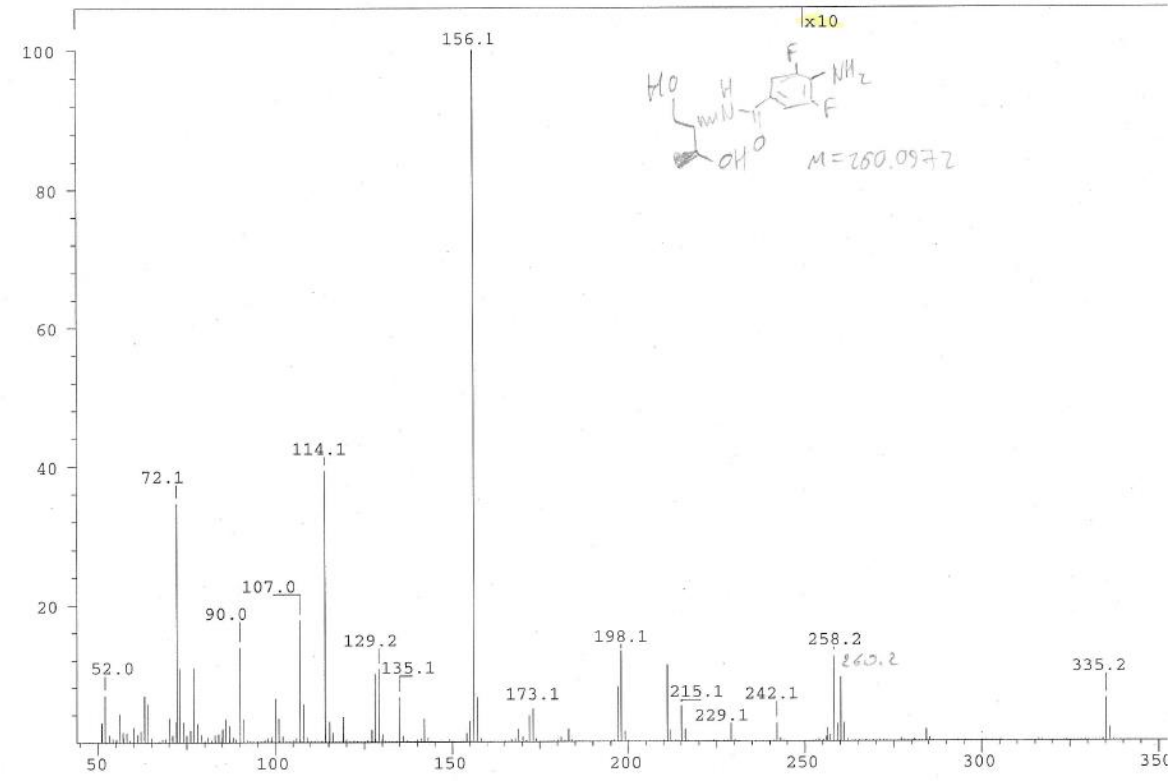

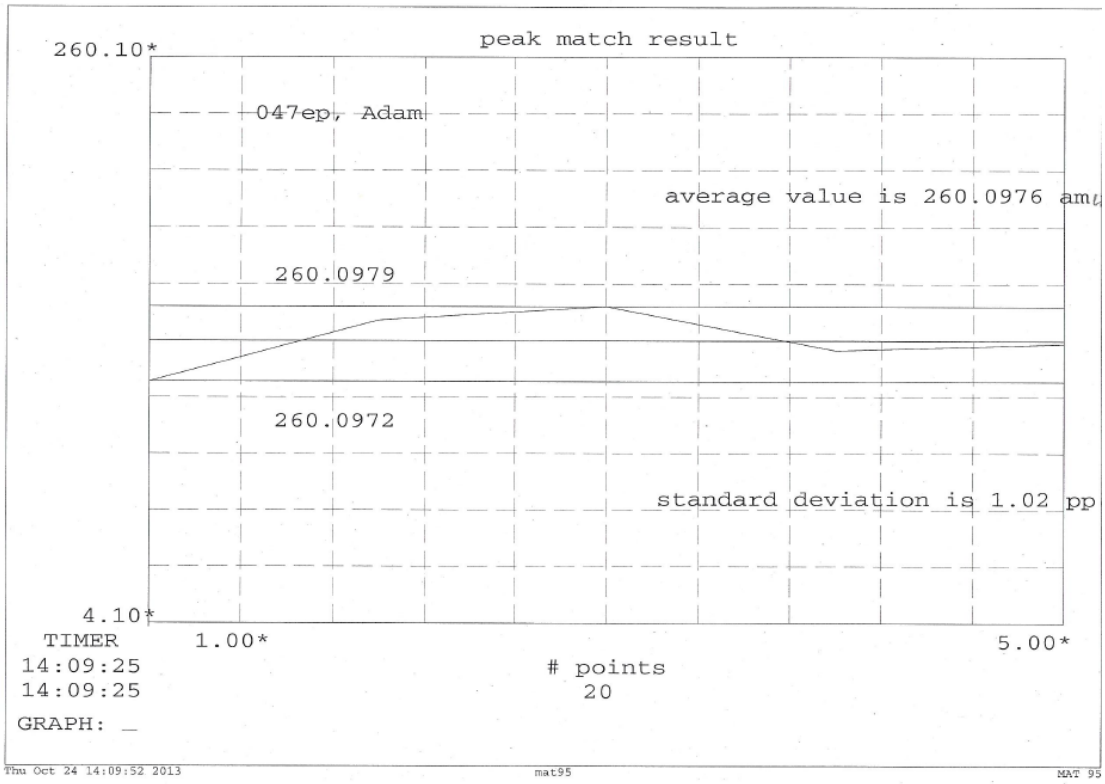
peak match result
260.10*
047ep, Adam
average value is 260.0976 am
260.0979
260.0972
standard deviation is 1.02 pp
4.10*
TIMER
1.00*
5.00*
14:09:25
14:09:25
points
20
GRAPH: _
Thu Oct 24 14:09:52 2013
mat95
MAT 95

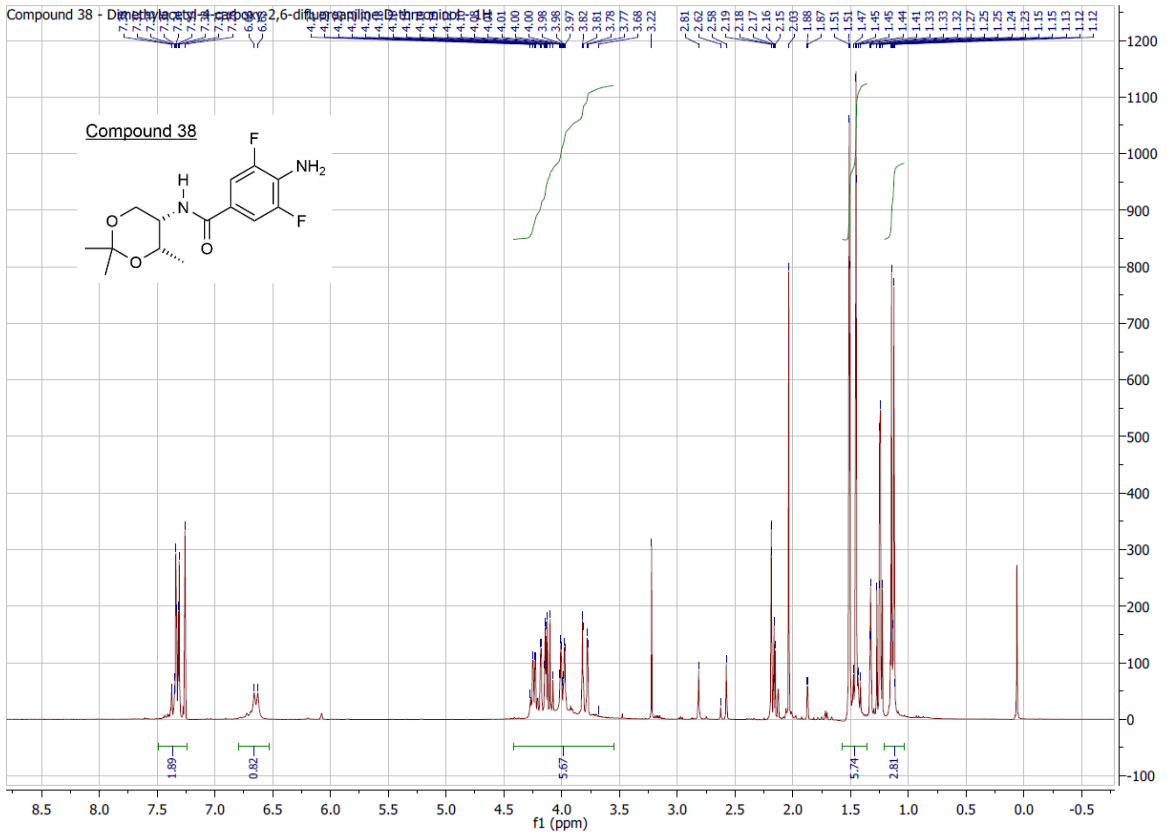
Compound 38 - Dimethylacetyl-4-carboxy-2,6-difluoroaniline-D-threoninol - 1H
Compound 38
F
NH2
H
N
O
O
O
F
1.89
0.82
5.67
5.74
2.81
f1 (ppm)

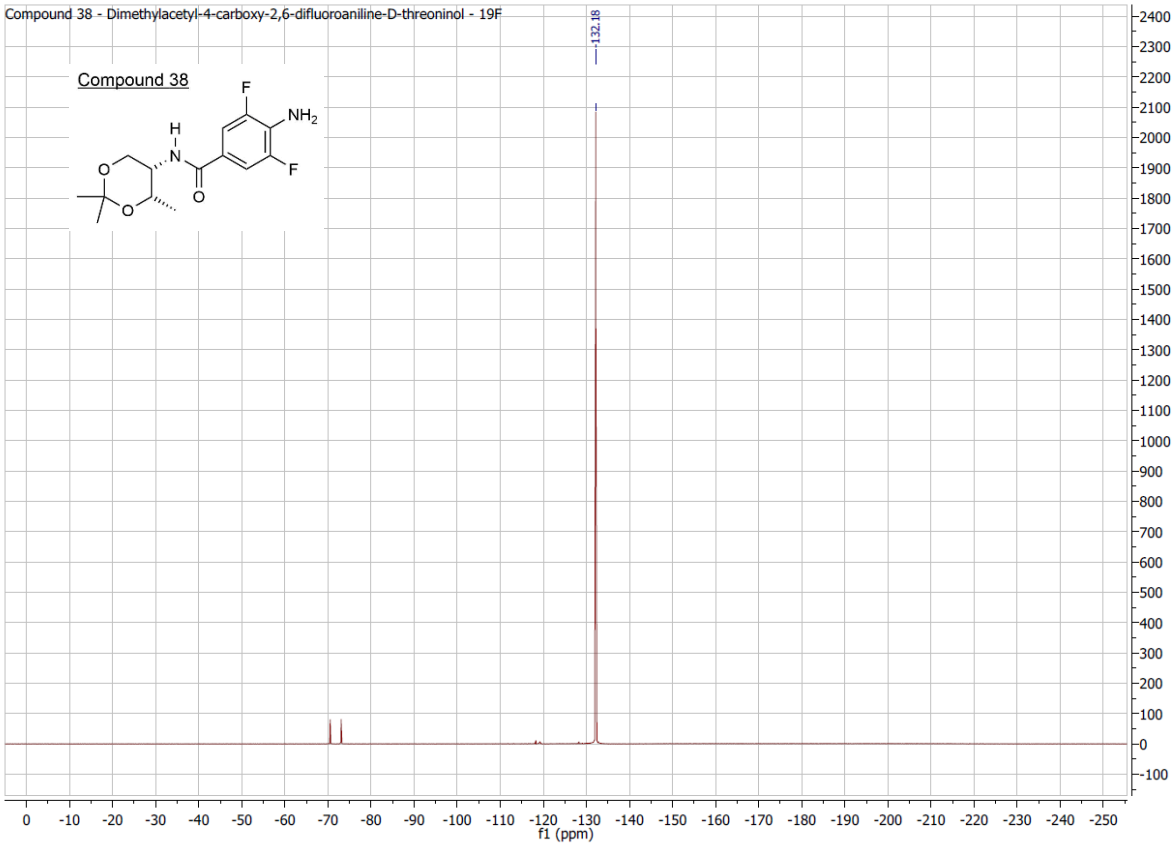
Compound 38 - Dimethylacetyl-4-carboxy-2,6-difluoroaniline-D-threoninol - 19F
-132.18
Compound 38
F
NH2
H
N
O
O
O
F
f1 (ppm)

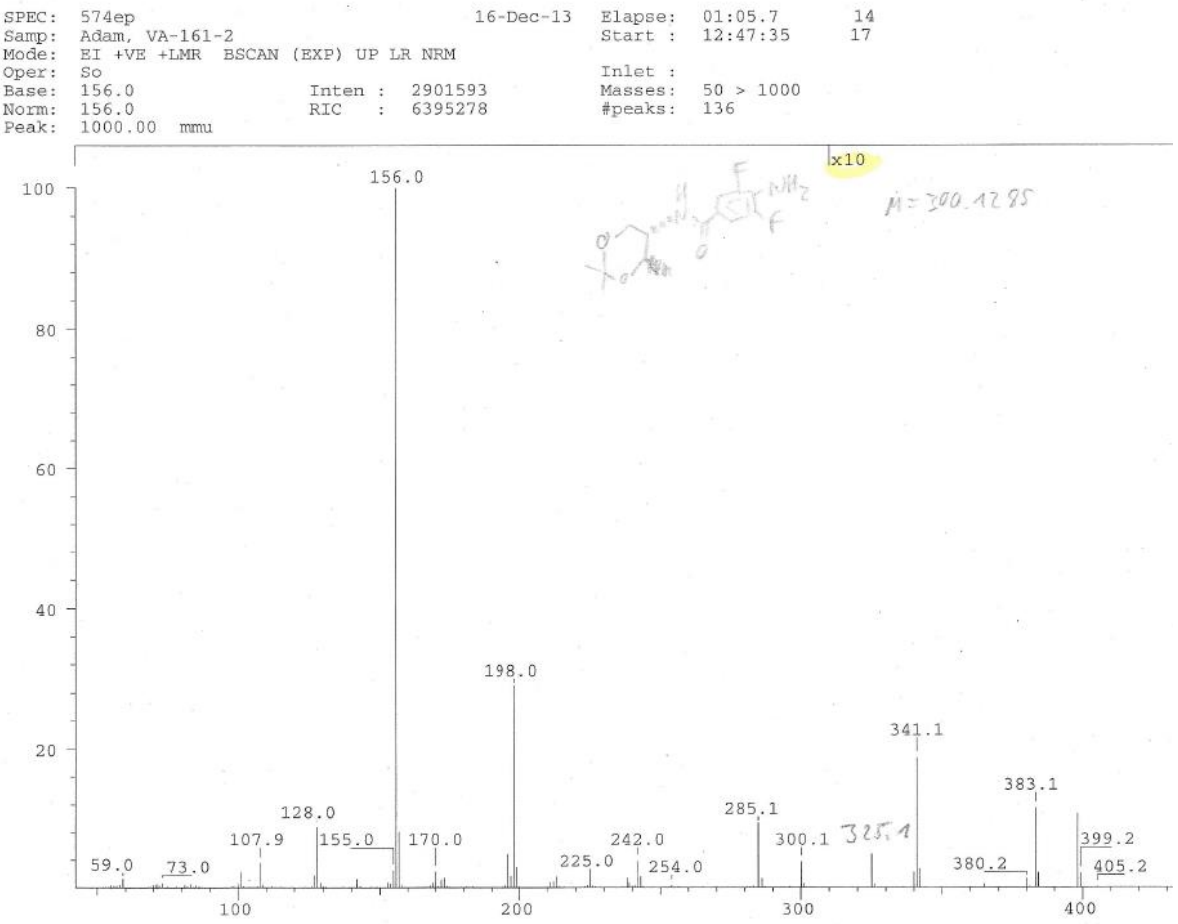
SPEC: 574ep 16-Dec-13 Elapse: 01:05.7 14
Samp: Adam, VA-161-2 Start : 12:47:35 17
Mode: EI +VE +LMR BSCAN (EXP) UP LR NRM
Oper: So Inlet :
Base: 156.0 Inten : 2901593 Masses: 50 > 1000
Norm: 156.0 RIC : 6395278 #peaks: 136
Peak: 1000.00 mmu
x10
M=300.1285
156.0
198.0
341.1
383.1
285.1
128.0
107.9
155.0
170.0
242.0
300.1
325.1
399.2
59.0
73.0
225.0
254.0
380.2
405.2
100
200
300
400

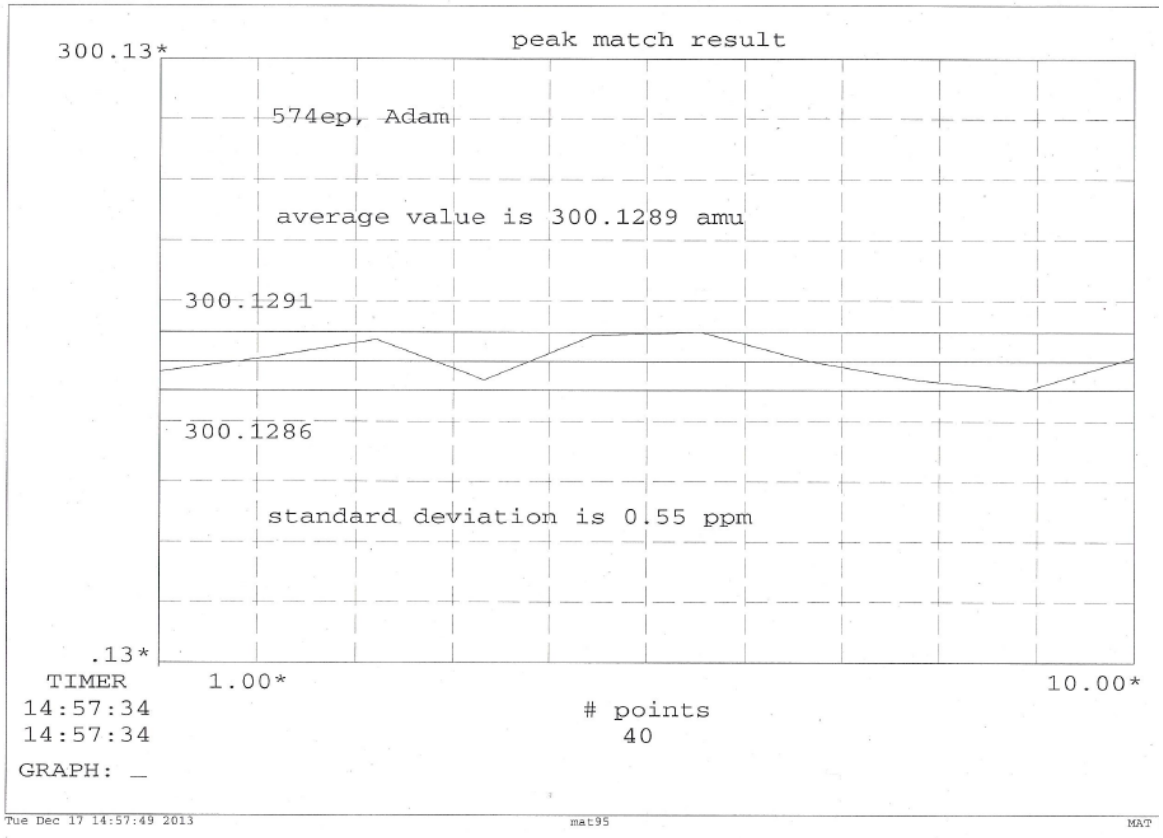
peak match result
300.13*
574ep, Adam
average value is 300.1289 amu
300.1291
300.1286
standard deviation is 0.55 ppm
.13*
TIMER
1.00*
10.00*
14:57:34
14:57:34
points
40
GRAPH: _
Tue Dec 17 14:57:49 2013
mat95
MAT

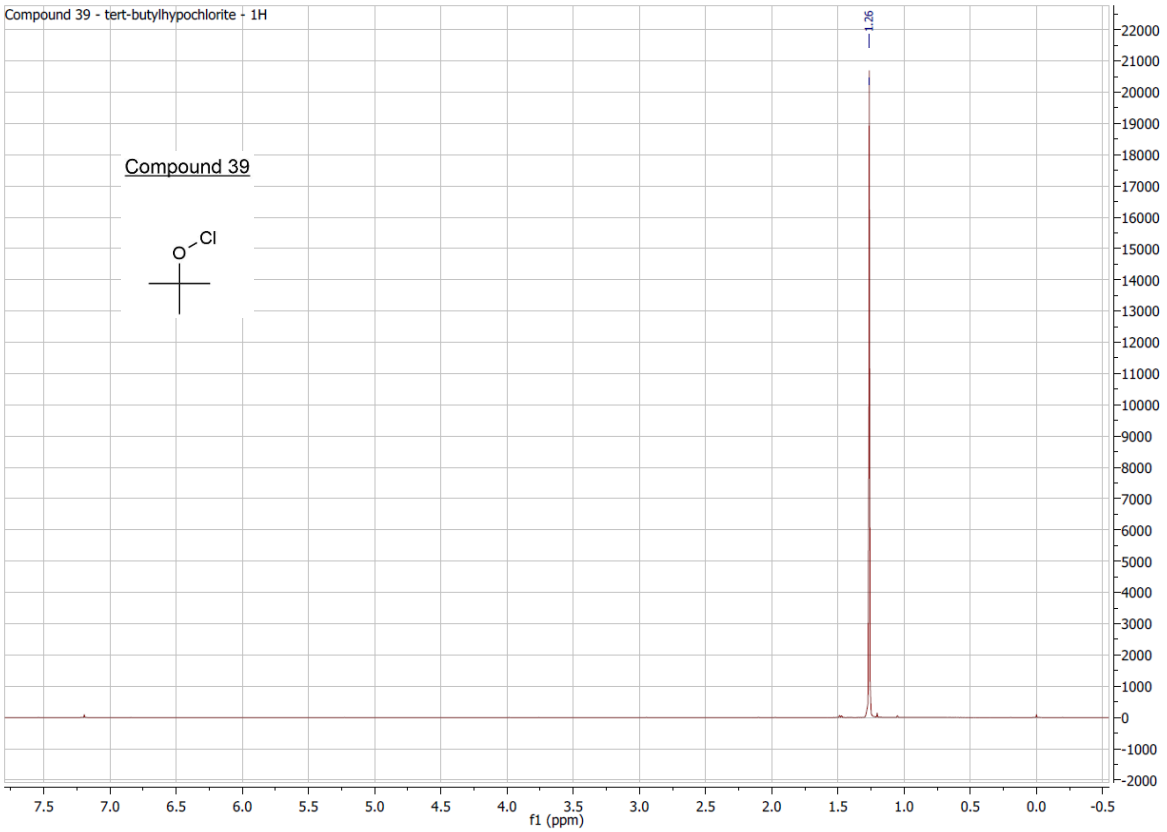
Compound 39 - tert-butylhypochlorite - 1H
Compound 39
O
Cl
1.26
f1 (ppm)

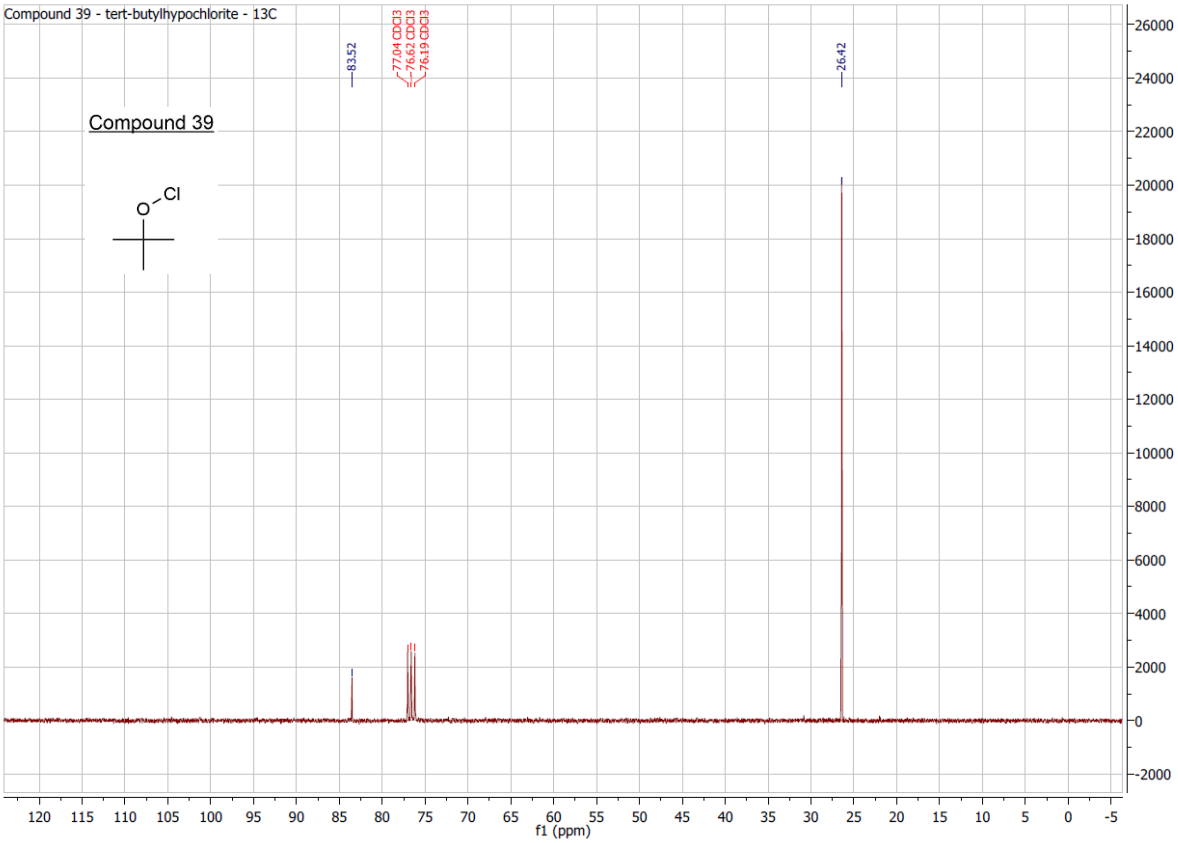
Compound 39 - tert-butylhypochlorite - 13C
Compound 39
O
Cl
83.52
77.04 CDCl3
76.62 CDCl3
76.19 CDCl3
26.42
f1 (ppm)

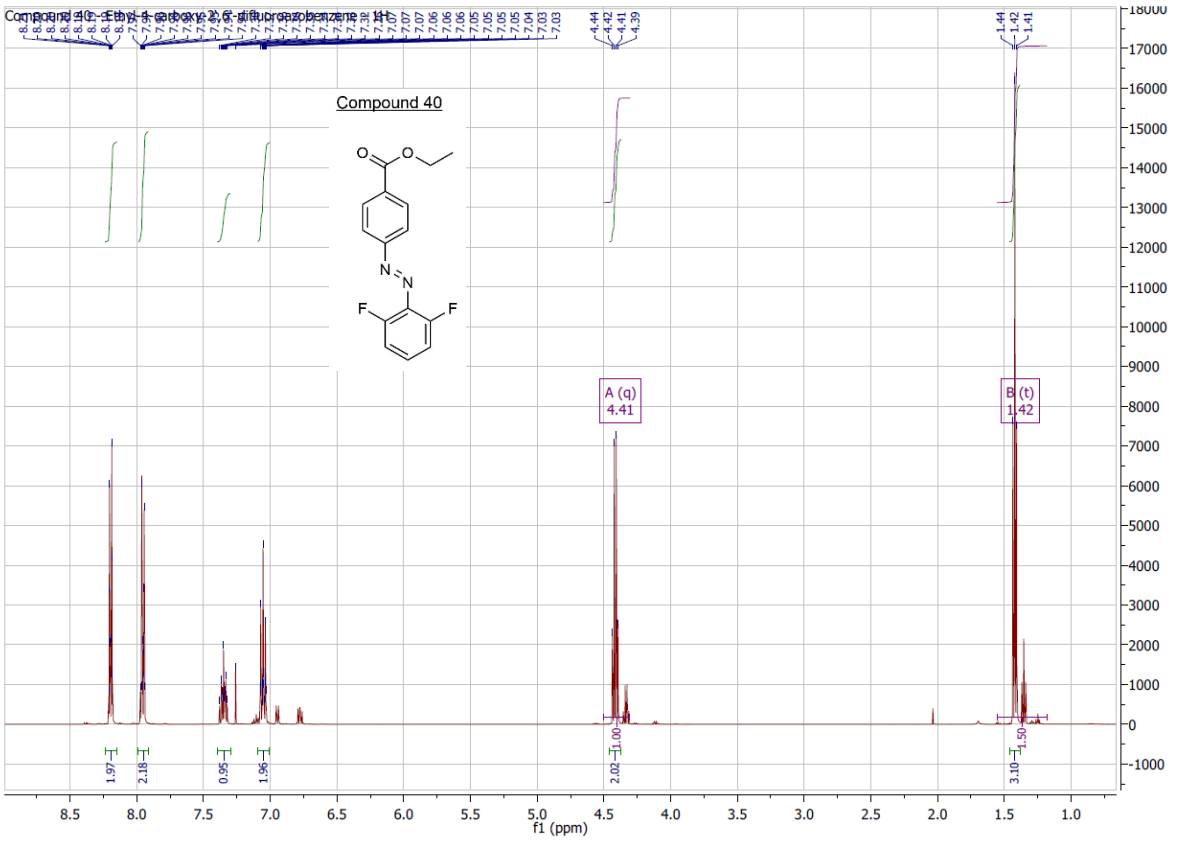
Compound 40
A (q)
4.41
B (t)
1.42
f1 (ppm)

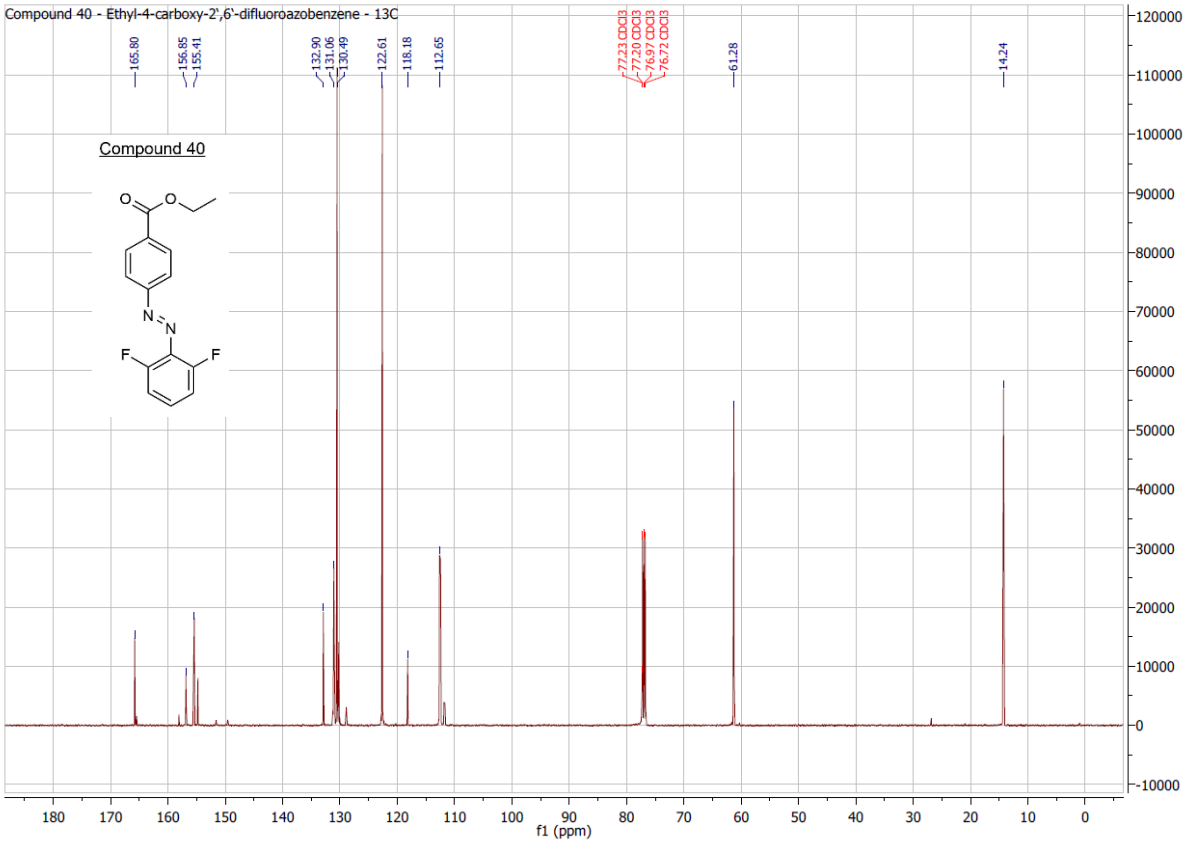
Compound 40 - Ethyl-4-carboxy-2',6'-difluoroazobenzene - 13C
Compound 40
f1 (ppm)

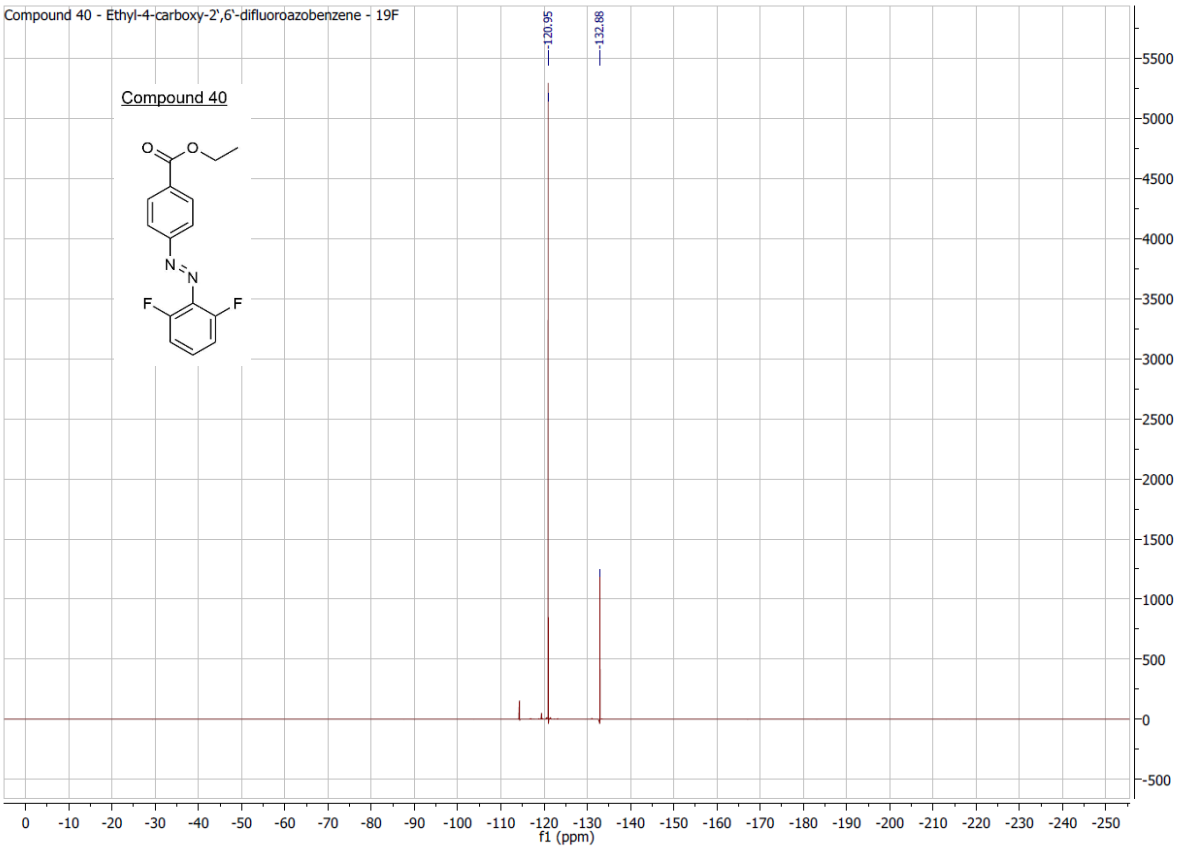
Compound 40 - Ethyl-4-carboxy-2',6'-difluoroazobenzene - 19F
120.95
132.88
Compound 40
O
O
N
N
F
F
5500
5000
4500
4000
3500
3000
2500
2000
1500
1000
500
0
-500
0 -10 -20 -30 -40 -50 -60 -70 -80 -90 -100 -110 -120 -130 -140 -150 -160 -170 -180 -190 -200 -210 -220 -230 -240 -250
f1 (ppm)

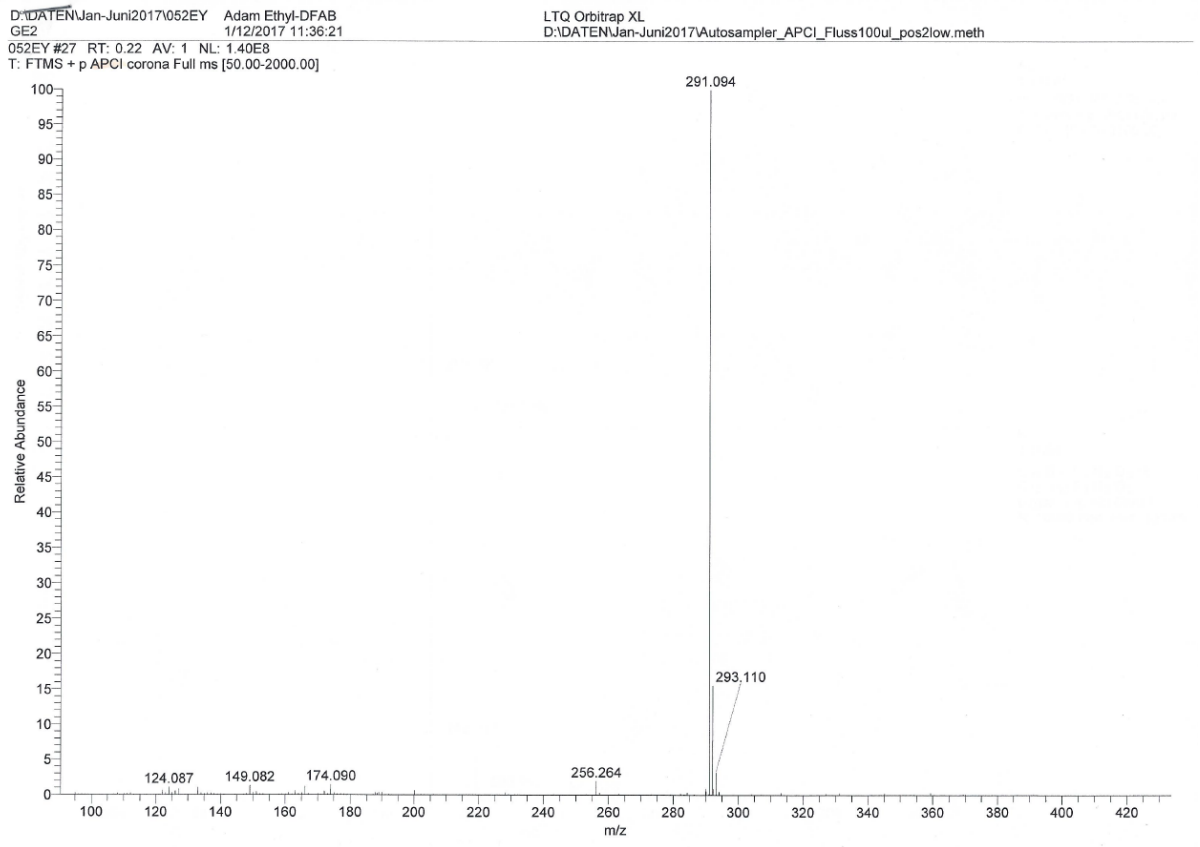
D:\DATEN\Jan-Juni2017\052EY Adam Ethyl-DFAB
GE2 1/12/2017 11:36:21
LTQ Orbitrap XL
D:\DATEN\Jan-Juni2017\Autosampler_APCI_Fluss100ul_pos2low.meth
052EY #27 RT: 0.22 AV: 1 NL: 1.40E8
T: FTMS + p APCI corona Full ms [50.00-2000.00]
291.094
293.110
124.087
149.082
174.090
256.264
Relative Abundance
m/z

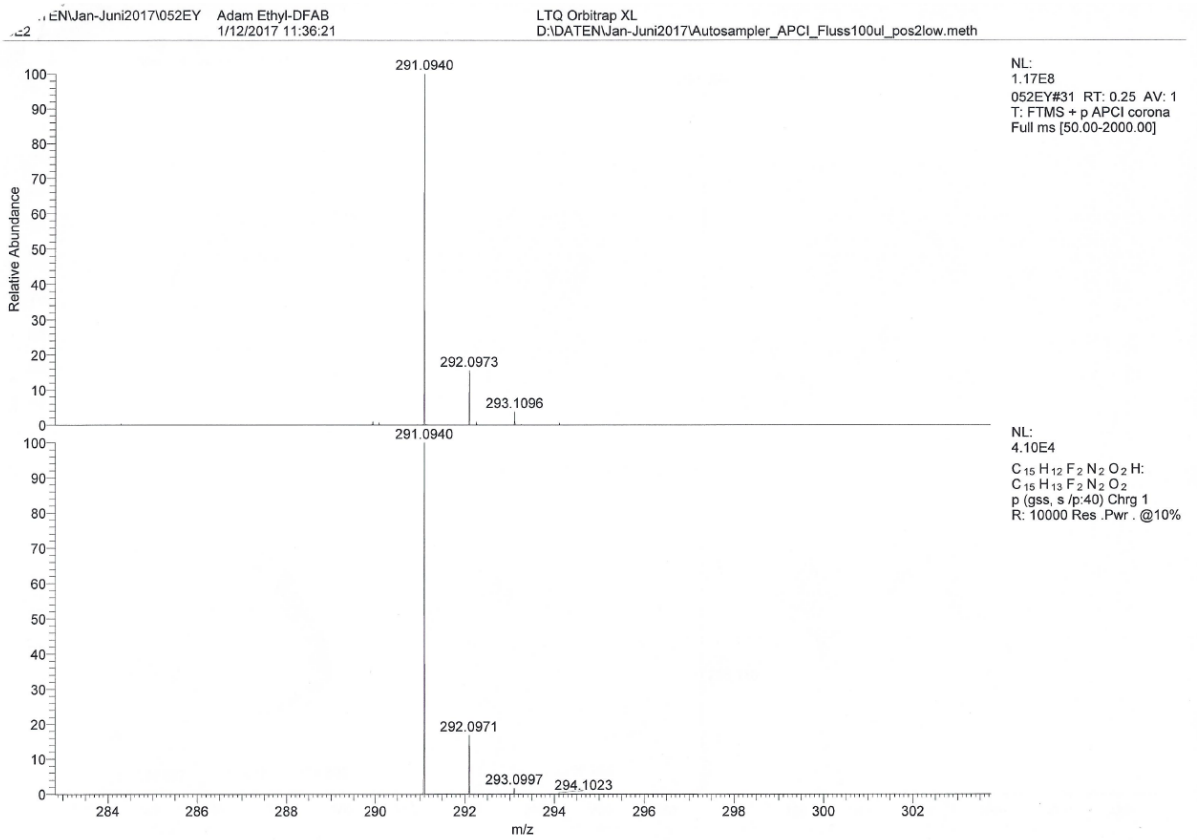
...EN\Jan-Juni2017\052EY Adam Ethyl-DFAB
...c2 1/12/2017 11:36:21
LTQ Orbitrap XL
D:\DATEN\Jan-Juni2017\Autosampler_APCI_Fluss100ul_pos2low.meth
291.0940
292.0973
293.1096
NL:
1.17E8
052EY#31 RT: 0.25 AV: 1
T: FTMS + p APCI corona
Full ms [50.00-2000.00]
Relative Abundance
291.0940
292.0971
293.0997
294.1023
NL:
4.10E4
C15 H12 F2 N2 O2 H:
C15 H13 F2 N2 O2
p (gss, s /p:40) Chrg 1
R: 10000 Res .Pwr . @10%
m/z

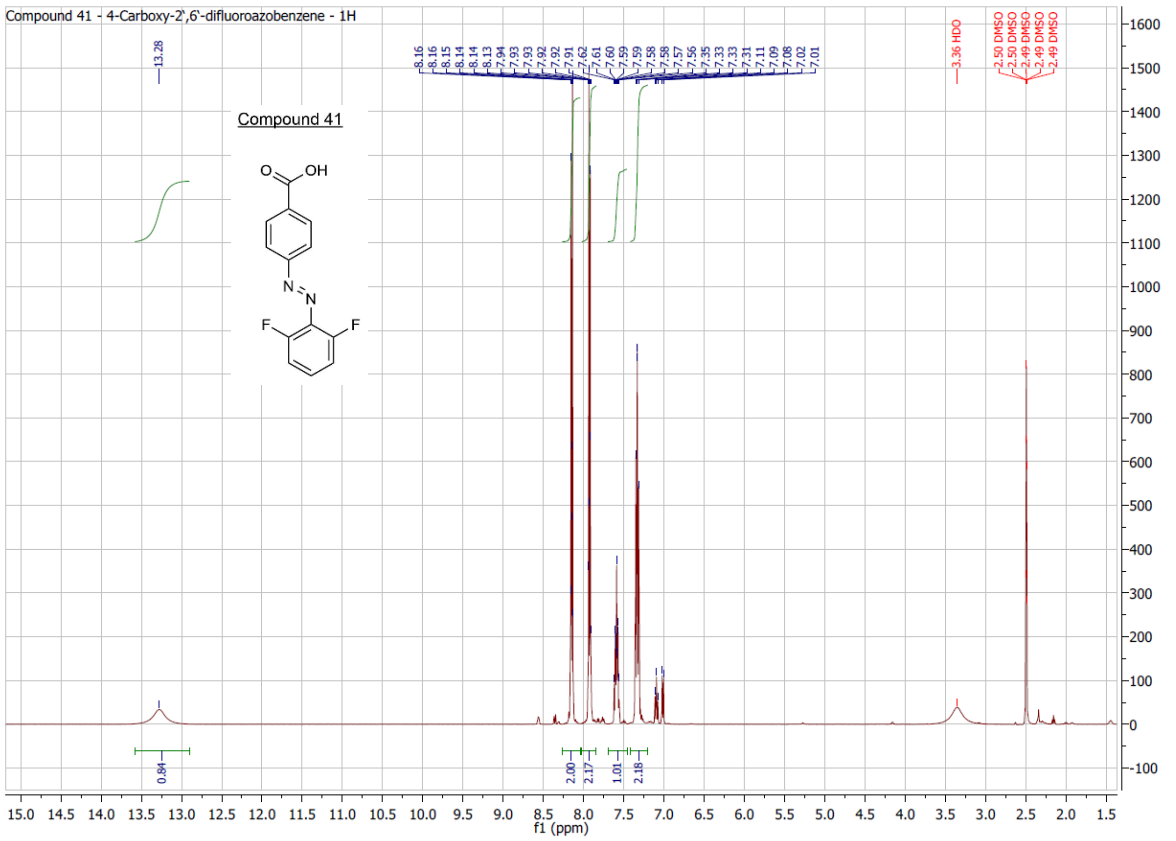
Compound 41 - 4-Carboxy-2',6'-difluoroazobenzene - 1H
Compound 41
f1 (ppm)

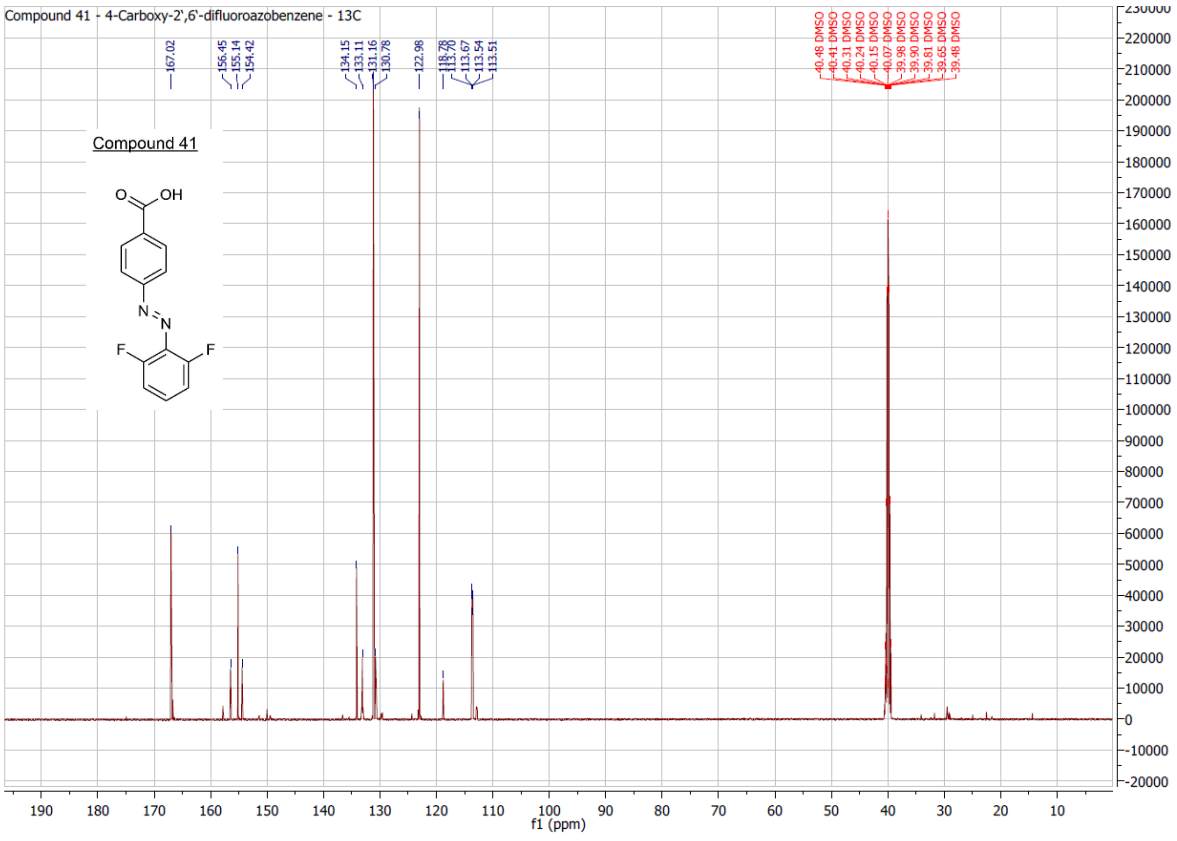
Compound 41 - 4-Carboxy-2',6'-difluoroazobenzene - 13C
Compound 41
f1 (ppm)

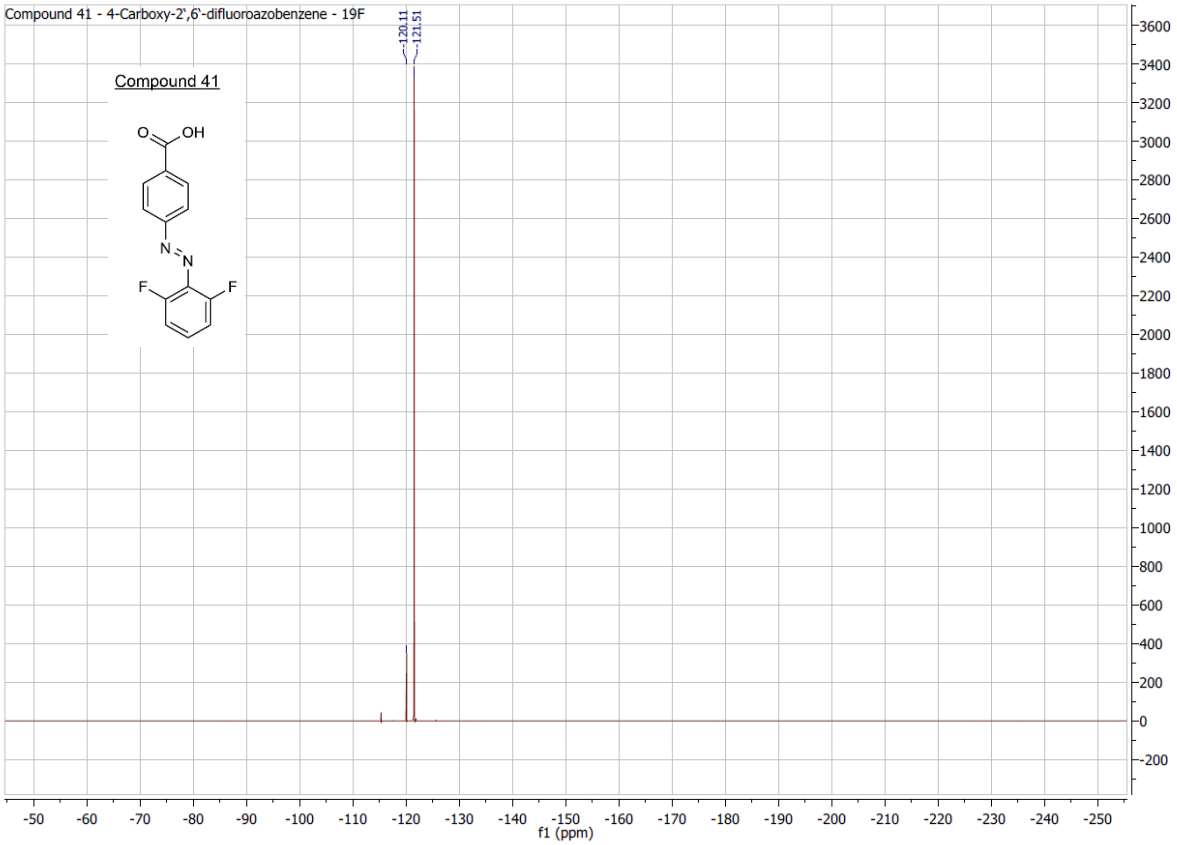
Compound 41 - 4-Carboxy-2',6'-difluoroazobenzene - 19F
120.11
121.51
Compound 41
O
OH
N
N
F
F
f1 (ppm)

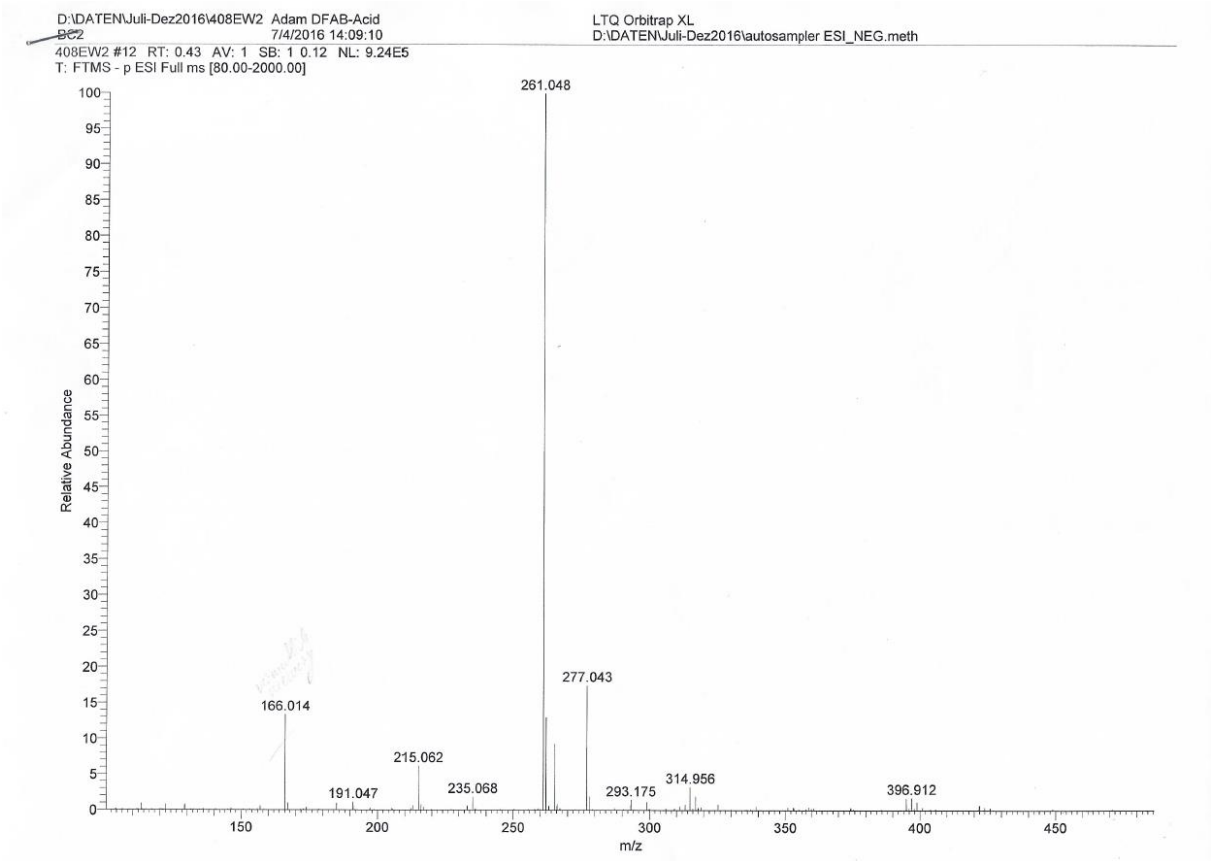
D:\DATEN\Juli-Dez2016\408EW2 Adam DFAB-Acid
DC2
7/4/2016 14:09:10
LTQ Orbitrap XL
D:\DATEN\Juli-Dez2016\autosampler ESI_NEG.meth
408EW2 #12 RT: 0.43 AV: 1 SB: 1 0.12 NL: 9.24E5
T: FTMS - p ESI Full ms [80.00-2000.00]
261.048
277.043
166.014
215.062
191.047
235.068
293.175
314.956
396.912
Relative Abundance
m/z

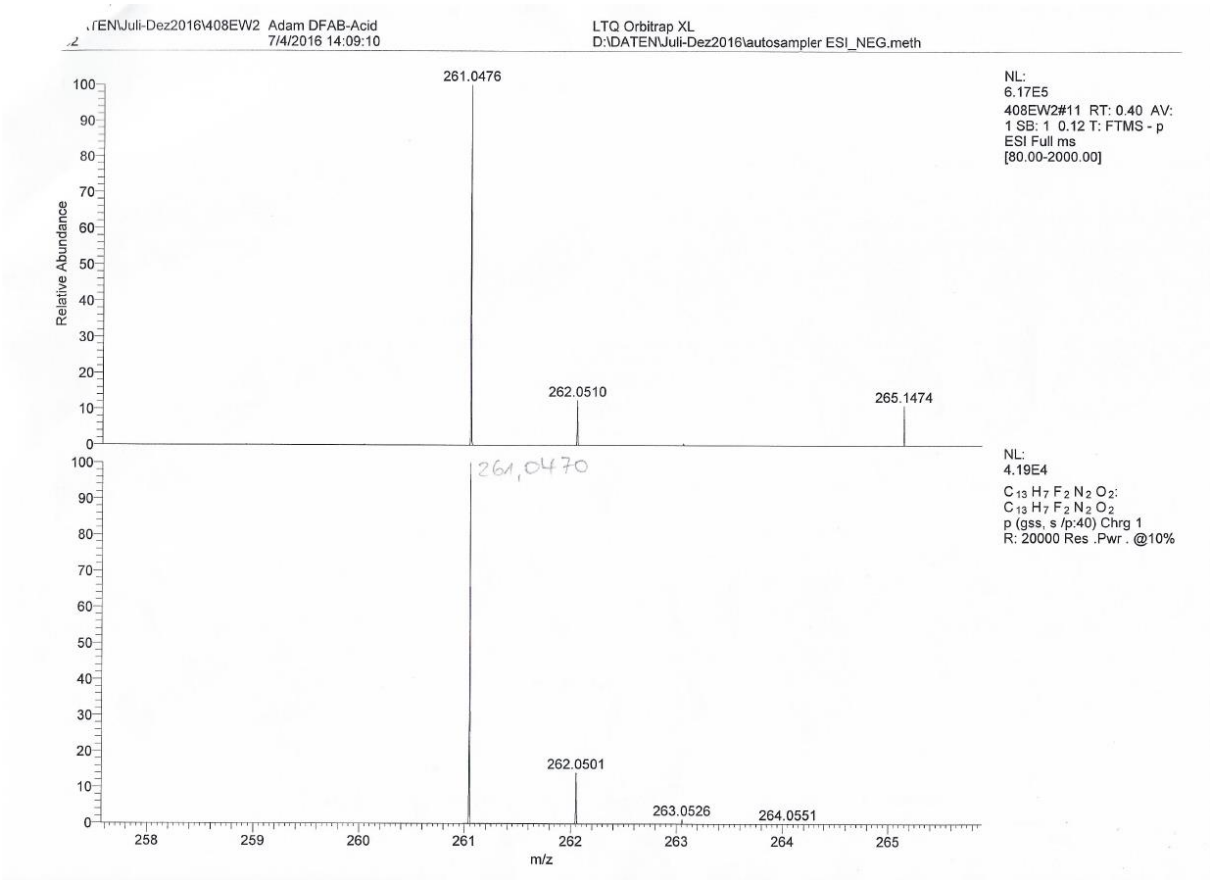
...TEN\Juli-Dez2016\408EW2 Adam DFAB-Acid
7/4/2016 14:09:10
LTQ Orbitrap XL
D:\DATEN\Juli-Dez2016\autosampler ESI_NEG.meth
261.0476
262.0510
265.1474
NL:
6.17E5
408EW2#11 RT: 0.40 AV:
1 SB: 1 0.12 T: FTMS - p
ESI Full ms
[80.00-2000.00]
Relative Abundance
261,0470
262.0501
263.0526
264.0551
NL:
4.19E4
C13 H7 F2 N2 O2:
C13 H7 F2 N2 O2
p (gss, s /p:40) Chrg 1
R: 20000 Res .Pwr . @10%
m/z

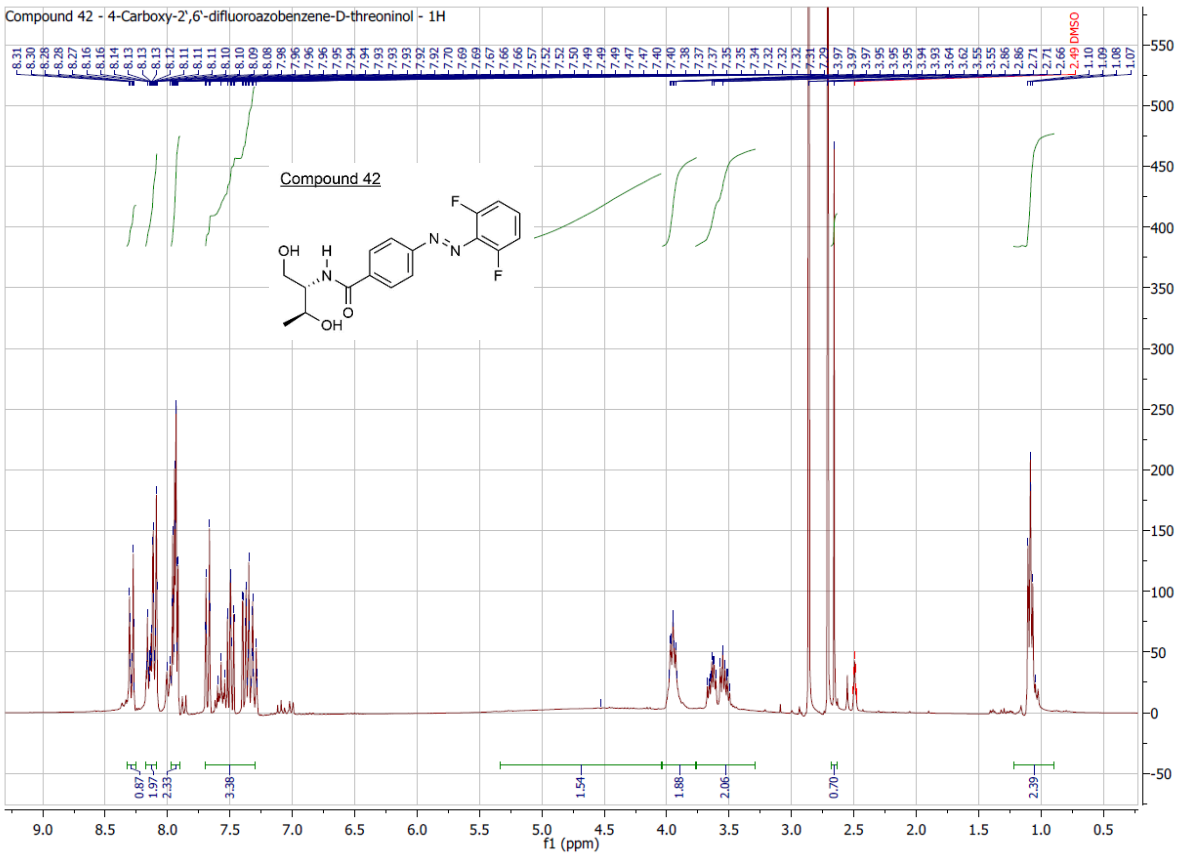
Compound 42 - 4-Carboxy-2',6'-difluoroazobenzene-D-threoninol - 1H
Compound 42
f1 (ppm)

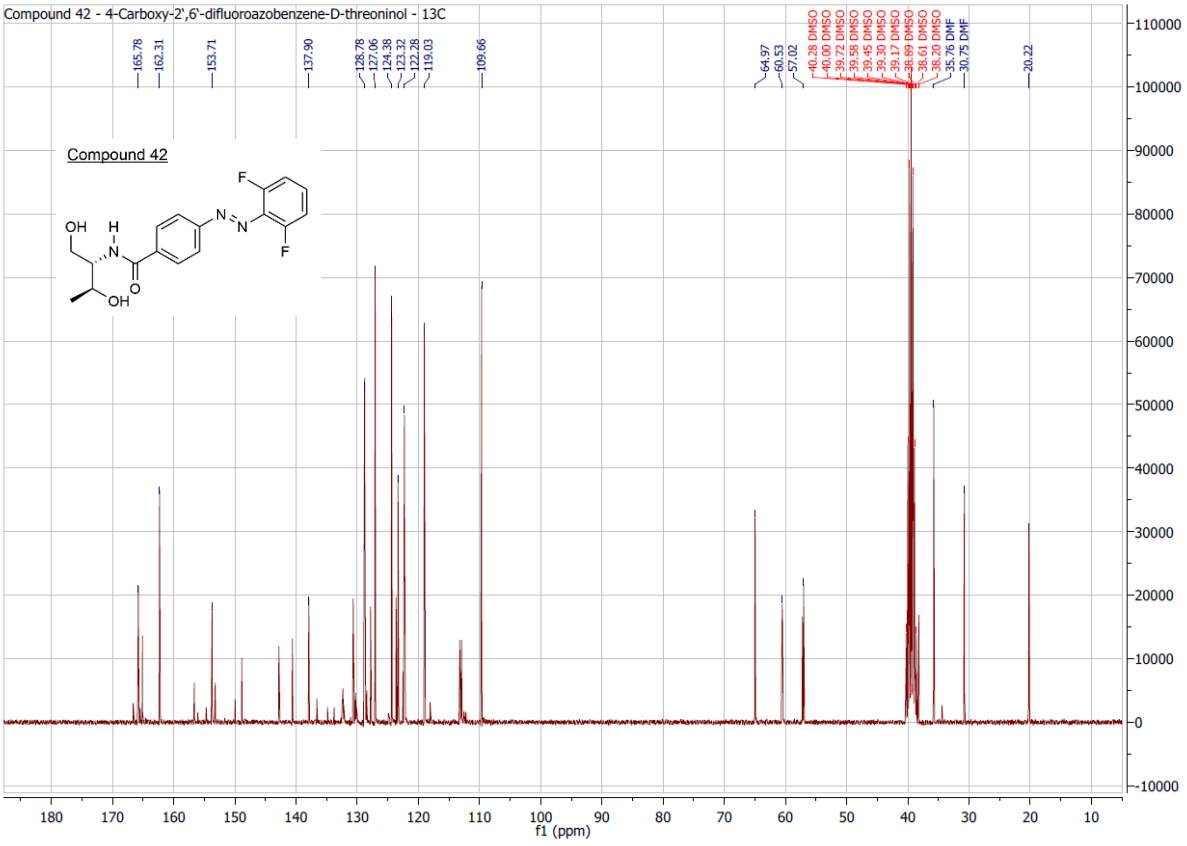
Compound 42 - 4-Carboxy-2',6'-difluoroazobenzene-D-threoninol - 13C
Compound 42
f1 (ppm)

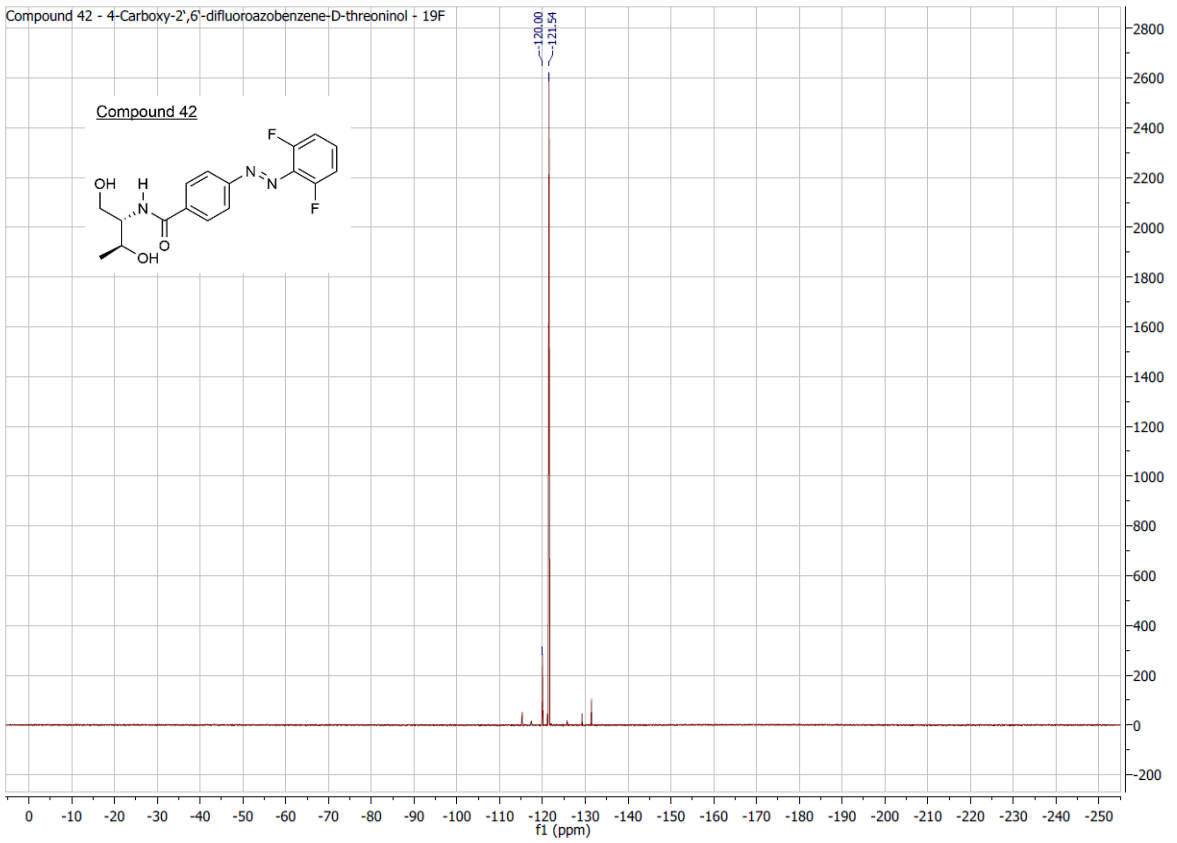
Compound 42 - 4-Carboxy-2',6'-difluoroazobenzene-D-threoninol - 19F
Compound 42
120.00
121.54
f1 (ppm)

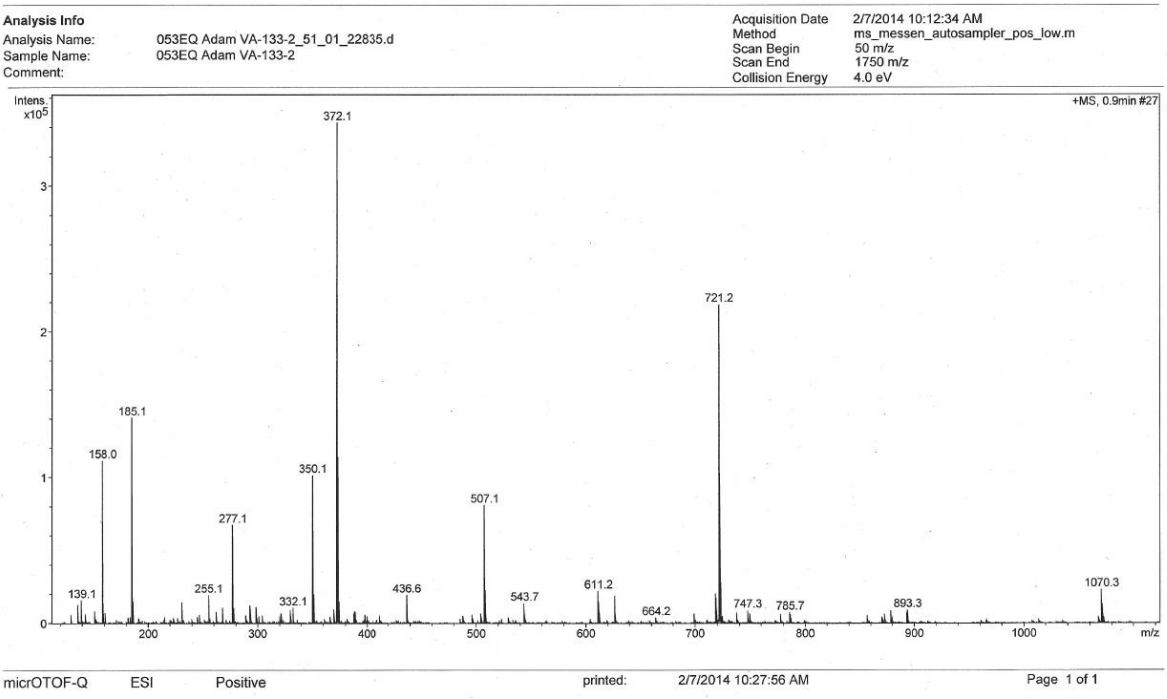
Analysis Info
Analysis Name: 053EQ Adam VA-133-2_51_01_22835.d
Sample Name: 053EQ Adam VA-133-2
Comment:
Acquisition Date 2/7/2014 10:12:34 AM
Method ms_messen_autosampler_pos_low.m
Scan Begin 50 m/z
Scan End 1750 m/z
Collision Energy 4.0 eV
Intens. x10^5
+MS, 0.9min #27
372.1
721.2
185.1
158.0
350.1
507.1
277.1
139.1
255.1
332.1
436.6
543.7
611.2
664.2
747.3
785.7
893.3
1070.3
m/z
micrOTOF-Q ESI Positive
printed: 2/7/2014 10:27:56 AM
Page 1 of 1

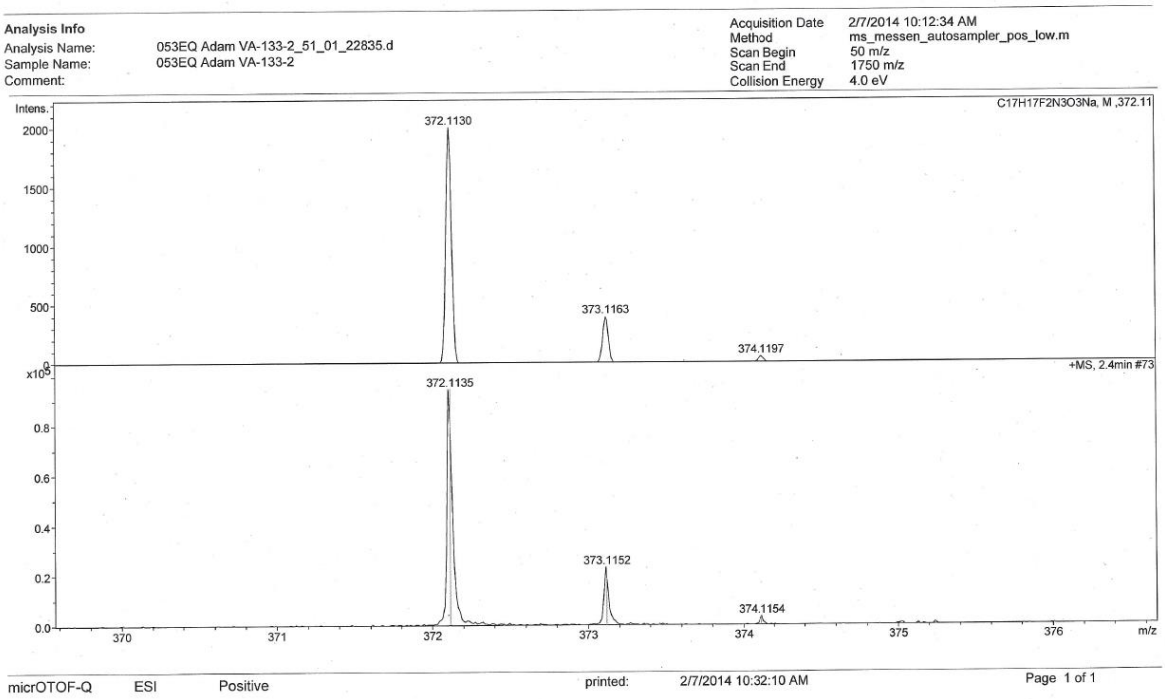
Analysis Info
Analysis Name: 053EQ Adam VA-133-2_51_01_22835.d
Sample Name: 053EQ Adam VA-133-2
Comment:
Acquisition Date 2/7/2014 10:12:34 AM
Method ms_messen_autosampler_pos_low.m
Scan Begin 50 m/z
Scan End 1750 m/z
Collision Energy 4.0 eV
C17H17F2N3O3Na, M ,372.11
Intens.
372.1130
373.1163
374.1197
+MS, 2.4min #73
x10
372.1135
373.1152
374.1154
m/z
micrOTOF-Q ESI Positive
printed: 2/7/2014 10:32:10 AM
Page 1 of 1

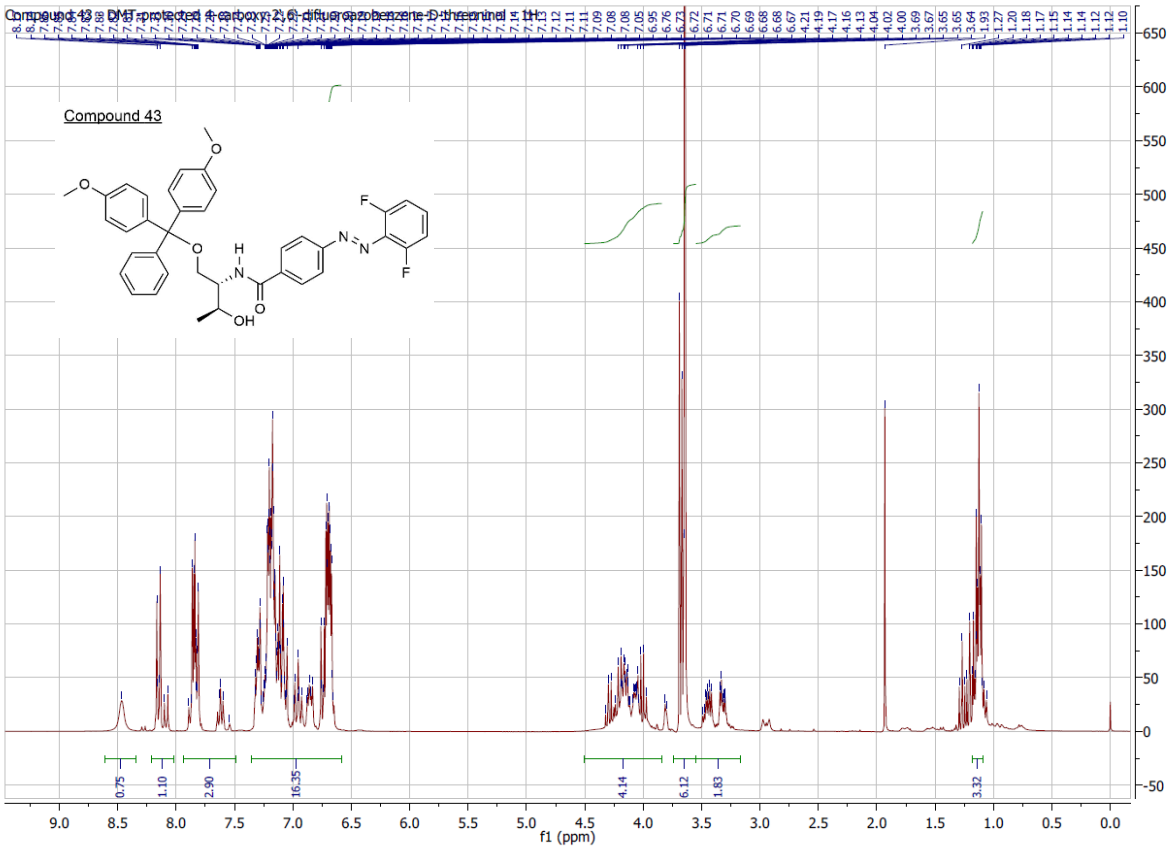
Compound 43
f1 (ppm)

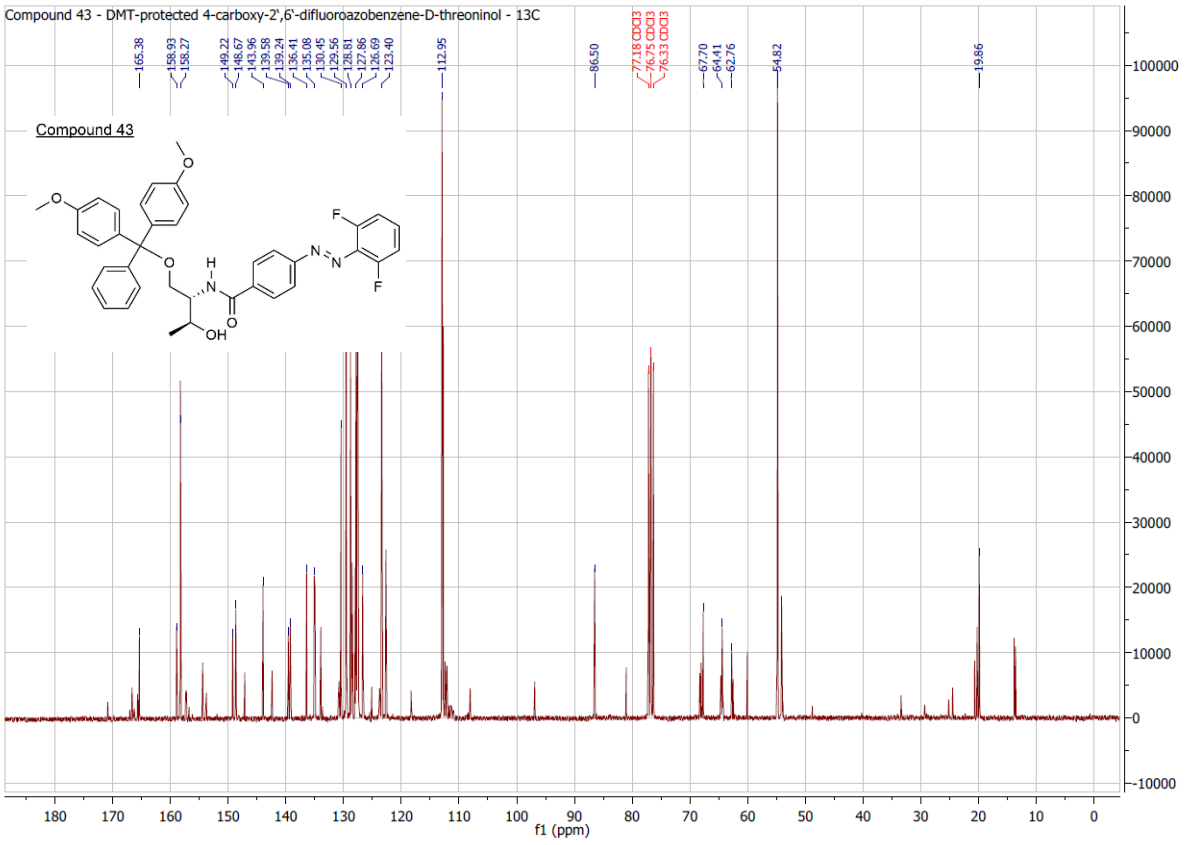
Compound 43 - DMT-protected 4-carboxy-2',6'-difluoroazobenzene-D-threoninol - 13C
Compound 43
f1 (ppm)

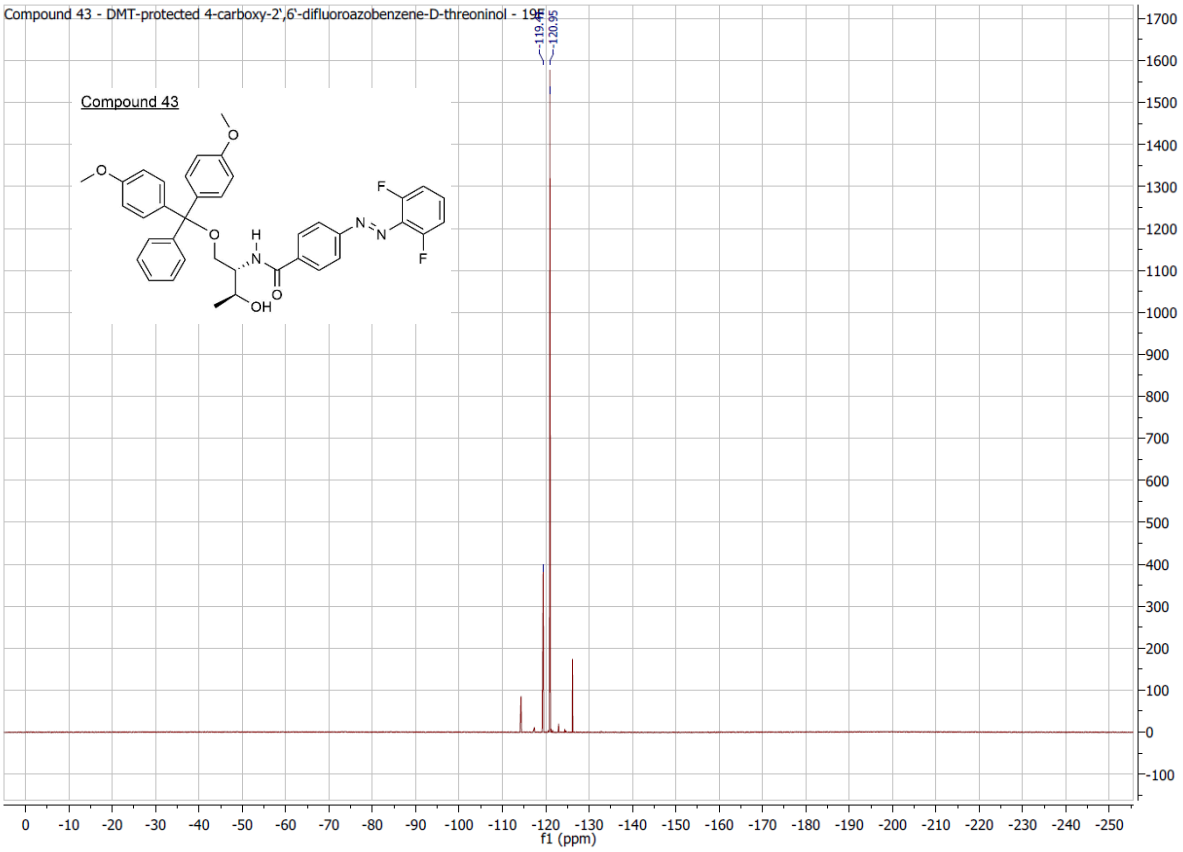
Compound 43 - DMT-protected 4-carboxy-2',6'-difluoroazobenzene-D-threoninol - 19F
Compound 43
119.47
120.95
f1 (ppm)

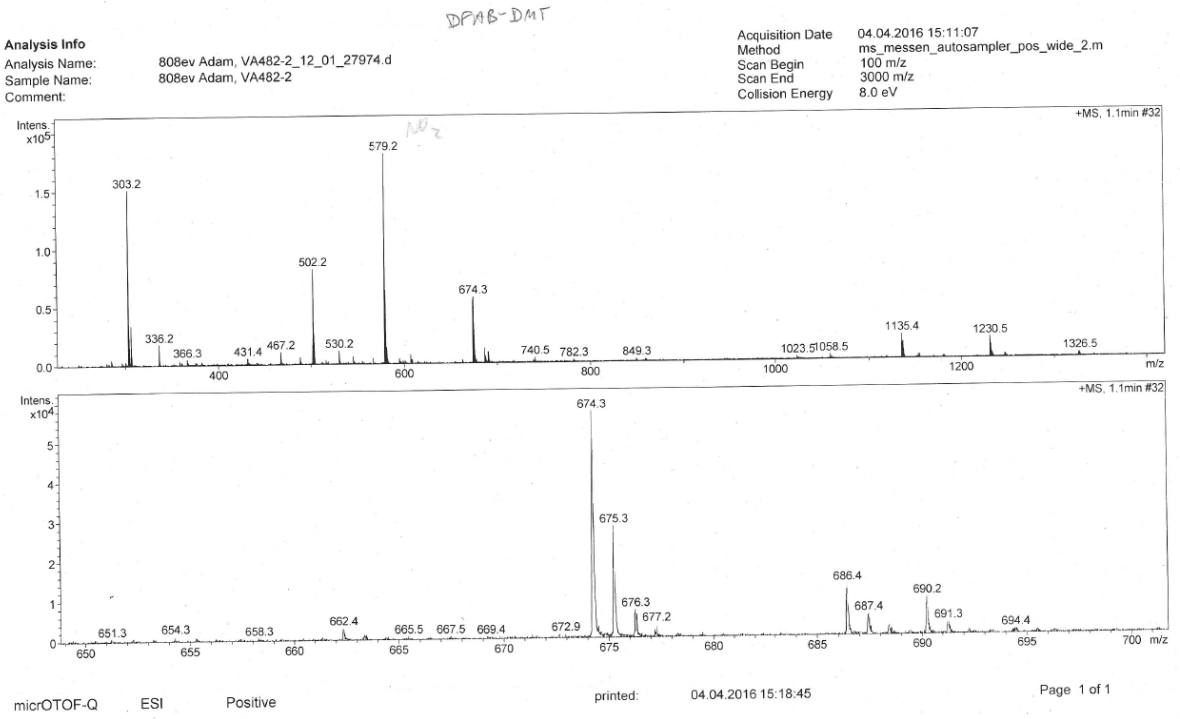
DFAB-DMT
Analysis Info
Analysis Name: 808ev Adam, VA482-2_12_01_27974.d
Sample Name: 808ev Adam, VA482-2
Comment:
Acquisition Date 04.04.2016 15:11:07
Method ms_messen_autosampler_pos_wide_2.m
Scan Begin 100 m/z
Scan End 3000 m/z
Collision Energy 8.0 eV
+MS, 1.1min #32
579.2
303.2
502.2
674.3
675.3
686.4
690.2
m/z
micrOTOF-Q ESI Positive
printed: 04.04.2016 15:18:45
Page 1 of 1

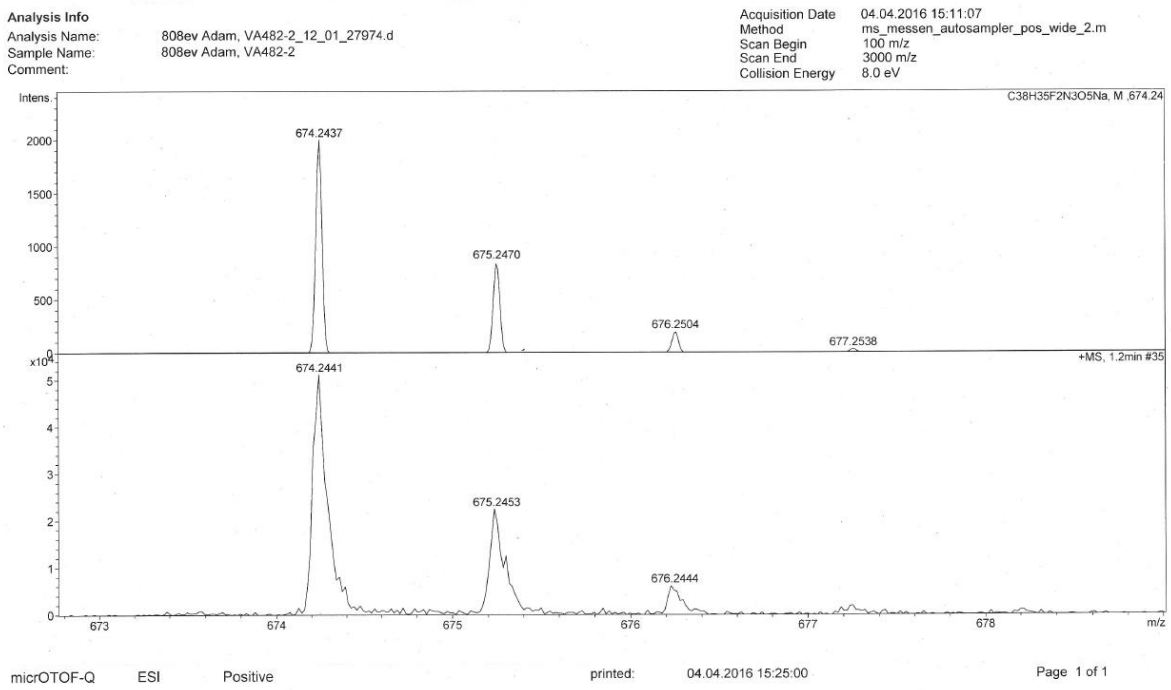
Analysis Info
Analysis Name: 808ev Adam, VA482-2_12_01_27974.d
Sample Name: 808ev Adam, VA482-2
Comment:
Acquisition Date 04.04.2016 15:11:07
Method ms_messen_autosampler_pos_wide_2.m
Scan Begin 100 m/z
Scan End 3000 m/z
Collision Energy 8.0 eV
Intens.
C38H35F2N3O5Na, M ,674.24
674.2437
675.2470
676.2504
677.2538
+MS, 1.2min #35
x10
674.2441
675.2453
676.2444
673
674
675
676
677
678
m/z
micrOTOF-Q ESI Positive
printed: 04.04.2016 15:25:00
Page 1 of 1

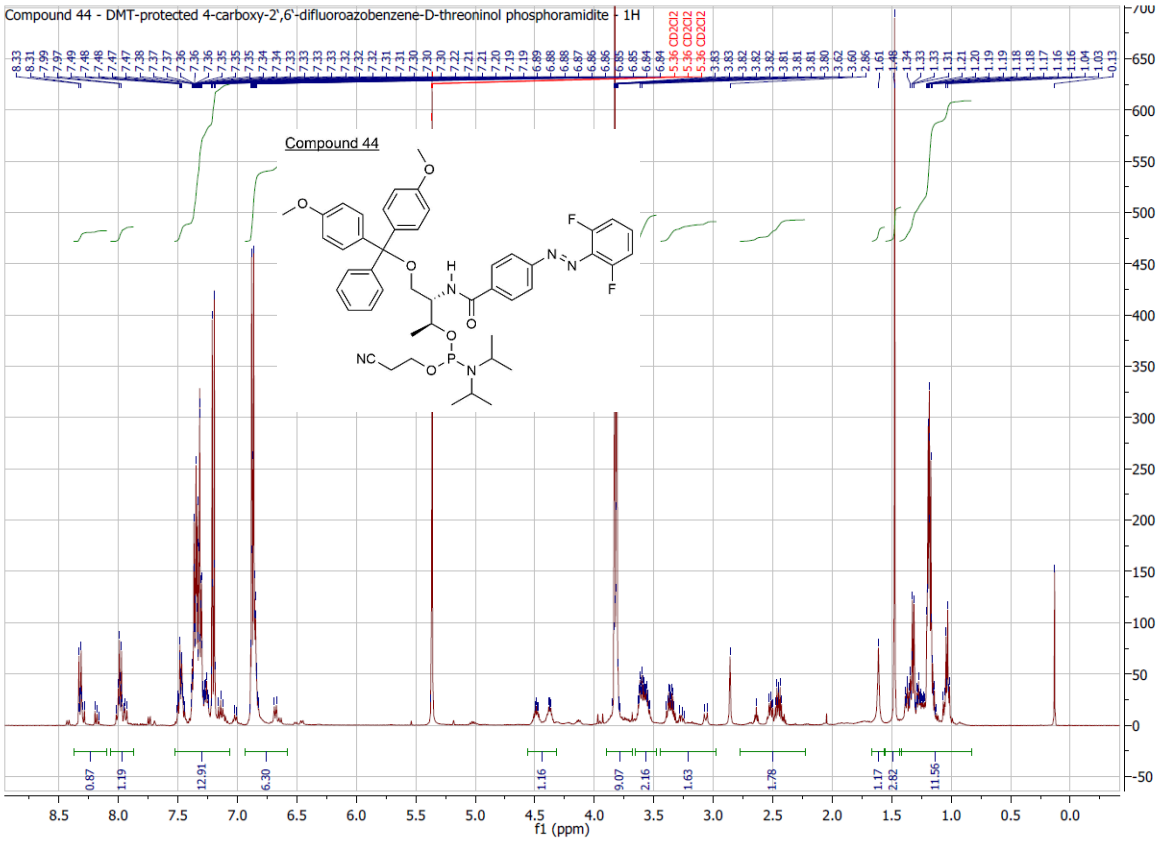
Compound 44 - DMT-protected 4-carboxy-2',6'-difluoroazobenzene-D-threoninol phosphoramidite - 1H
Compound 44
f1 (ppm)

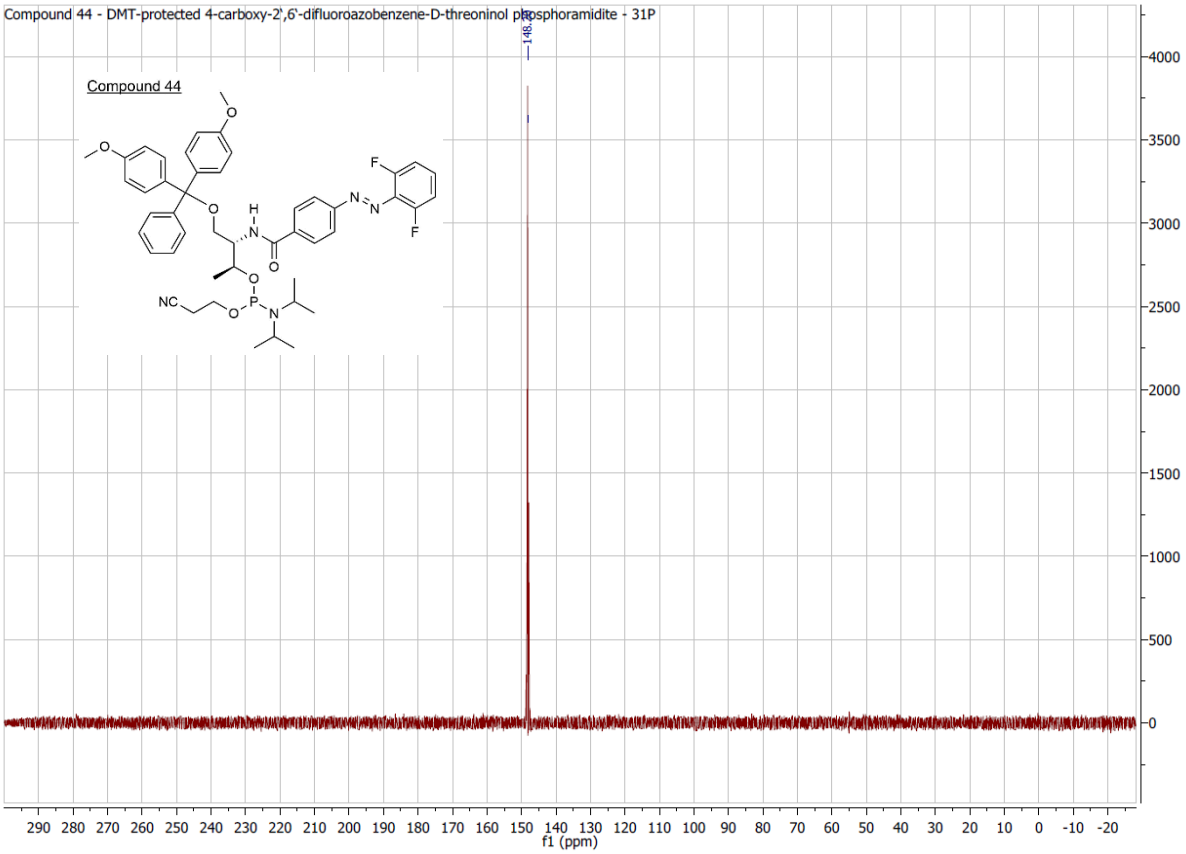
Compound 44 - DMT-protected 4-carboxy-2',6'-difluoroazobenzene-D-threoninol phosphoramidite - 31P
Compound 44
f1 (ppm)

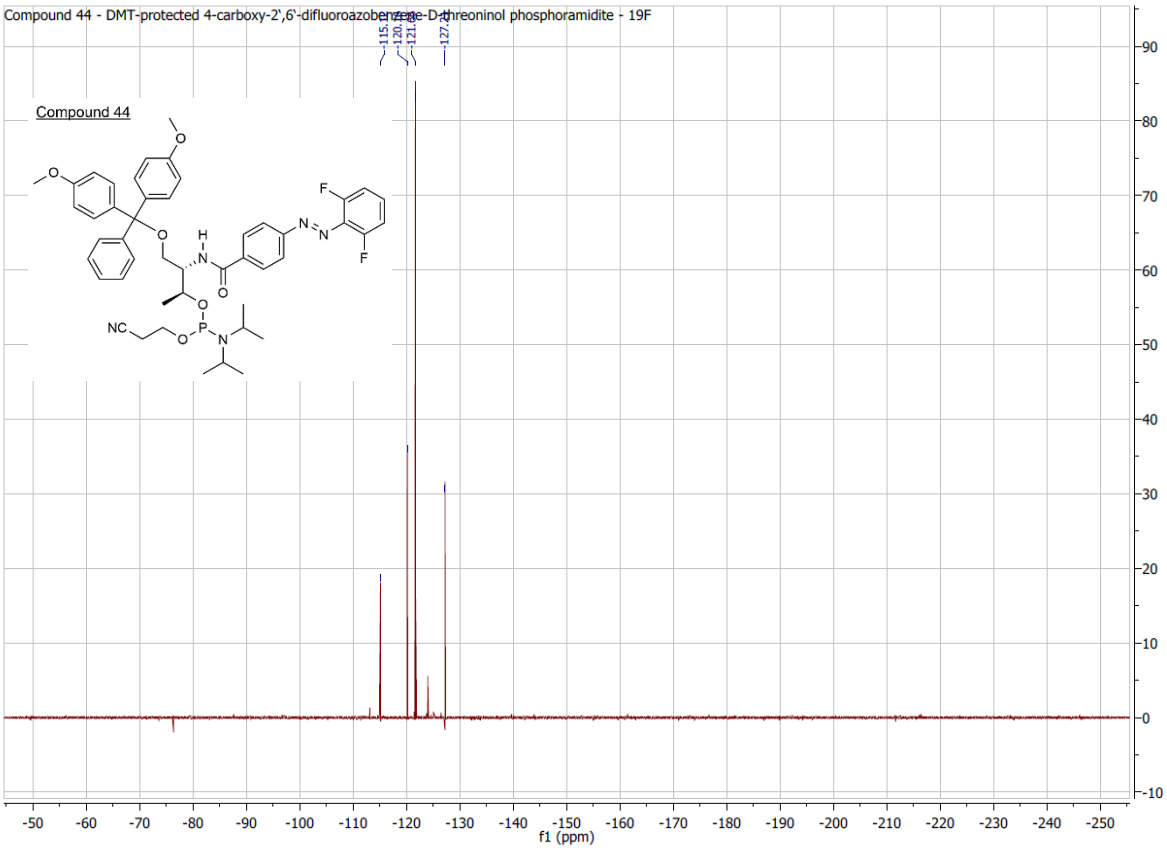
Compound 44 - DMT-protected 4-carboxy-2',6'-difluoroazobenzene-D-threoninol phosphoramidite - 19F
Compound 44
f1 (ppm)

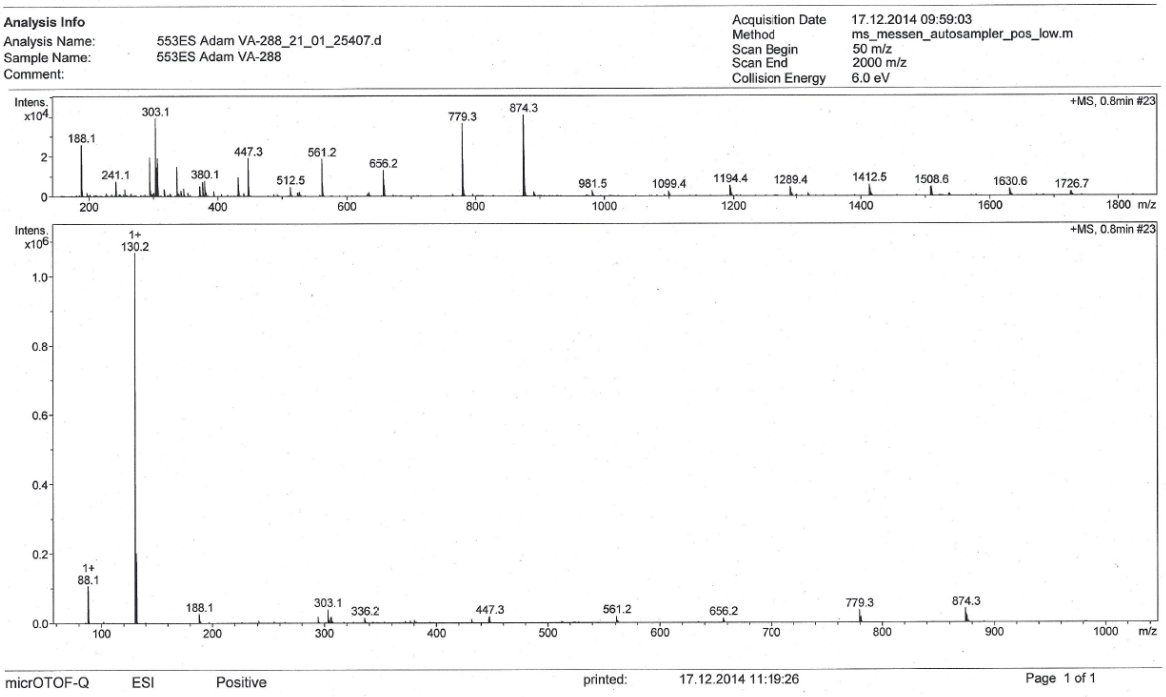
Analysis Info
Analysis Name: 553ES Adam VA-288_21_01_25407.d
Sample Name: 553ES Adam VA-288
Comment:
Acquisition Date 17.12.2014 09:59:03
Method ms_messen_autosampler_pos_low.m
Scan Begin 50 m/z
Scan End 2000 m/z
Collision Energy 6.0 eV
+MS, 0.8min #23
m/z
micrOTOF-Q ESI Positive
printed: 17.12.2014 11:19:26
Page 1 of 1

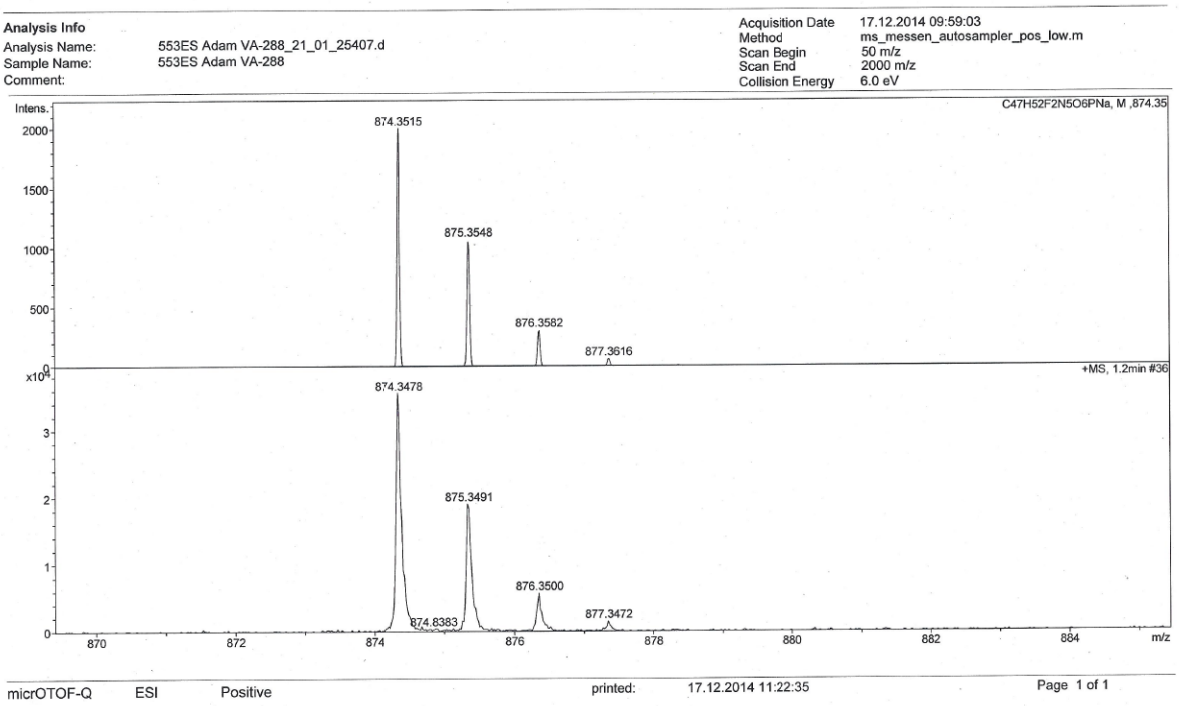
Analysis Info
Analysis Name: 553ES Adam VA-288_21_01_25407.d
Sample Name: 553ES Adam VA-288
Comment:
Acquisition Date 17.12.2014 09:59:03
Method ms_messen_autosampler_pos_low.m
Scan Begin 50 m/z
Scan End 2000 m/z
Collision Energy 6.0 eV
Intens.
C47H52F2N5O6PNa, M ,874.35
874.3515
875.3548
876.3582
877.3616
+MS, 1.2min #36
x10^4
874.3478
875.3491
876.3500
874.8383
877.3472
m/z
micrOTOF-Q ESI Positive
printed: 17.12.2014 11:22:35
Page 1 of 1

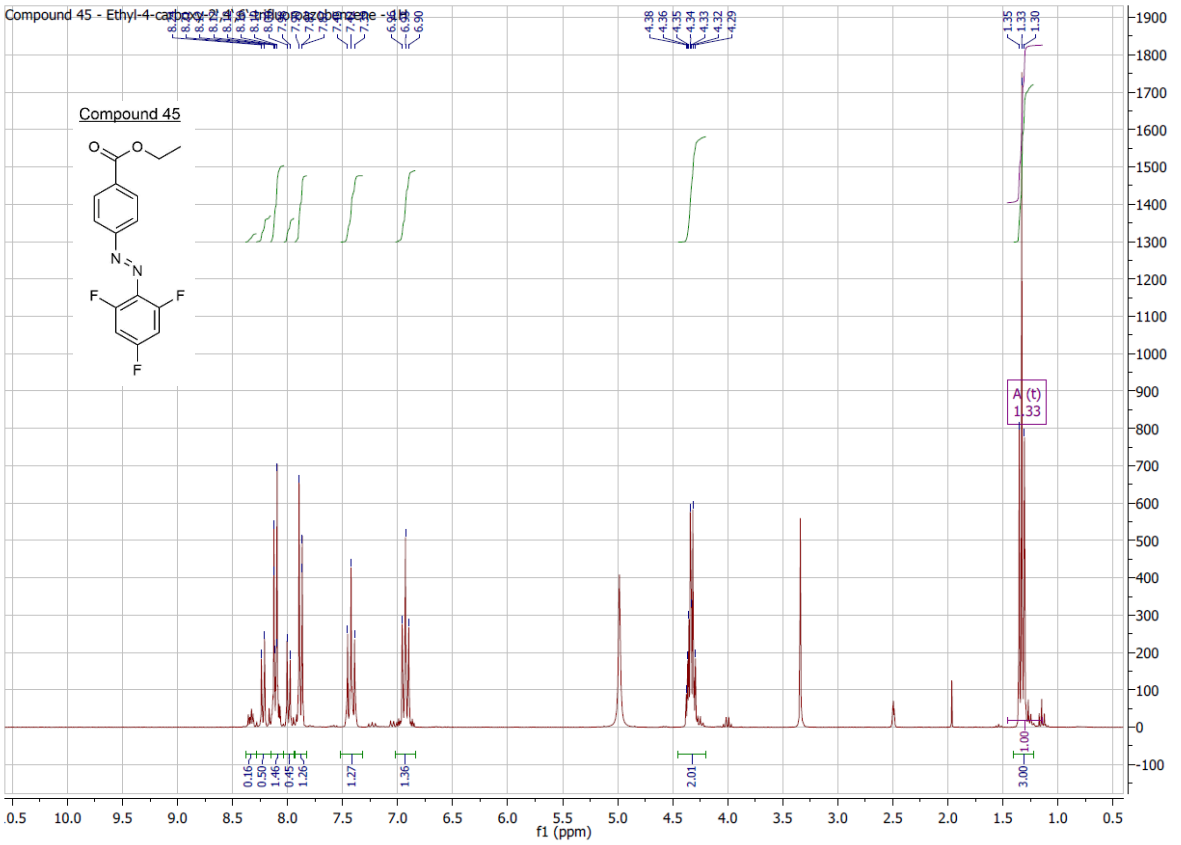
Compound 45 - Ethyl-4-carboxy-2',4',6'-trifluoroazobenzene - 1H
Compound 45
A (t)
1.33
f1 (ppm)

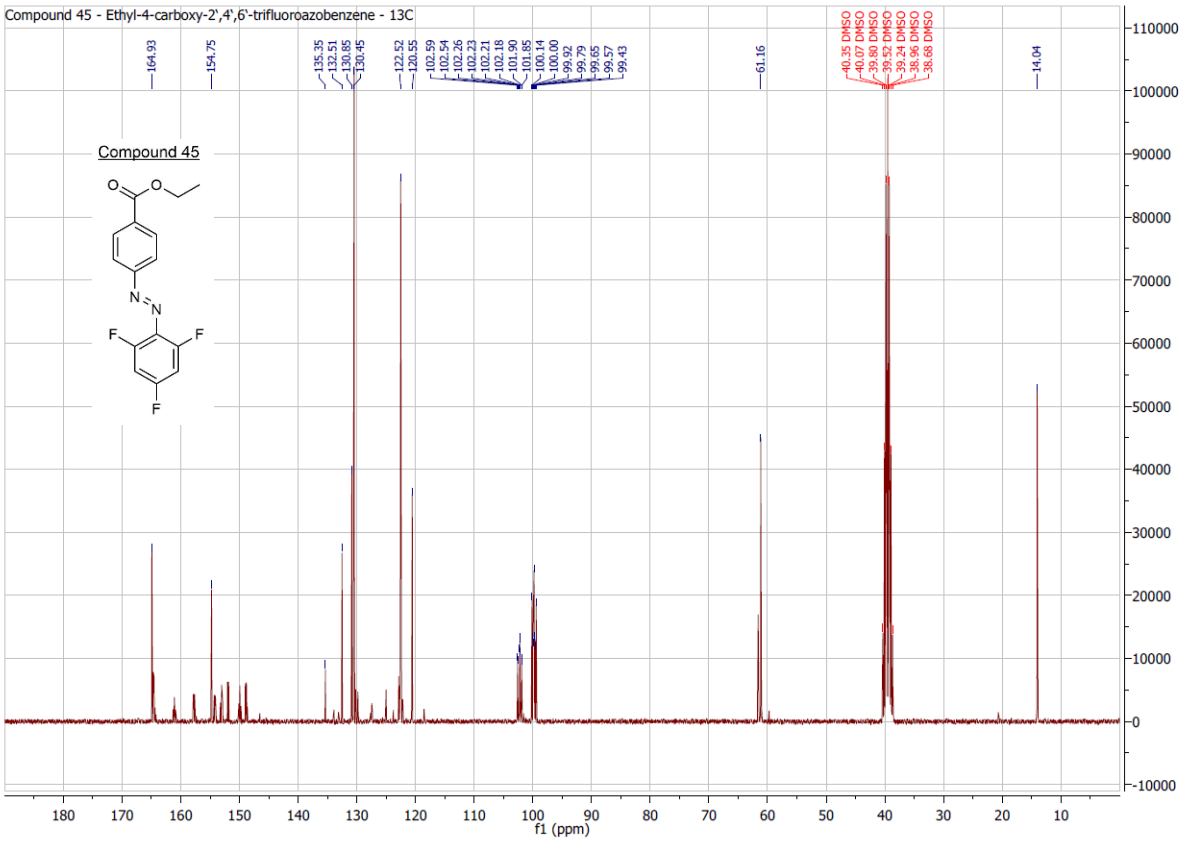
Compound 45 - Ethyl-4-carboxy-2',4',6'-trifluoroazobenzene - 13C
Compound 45
f1 (ppm)

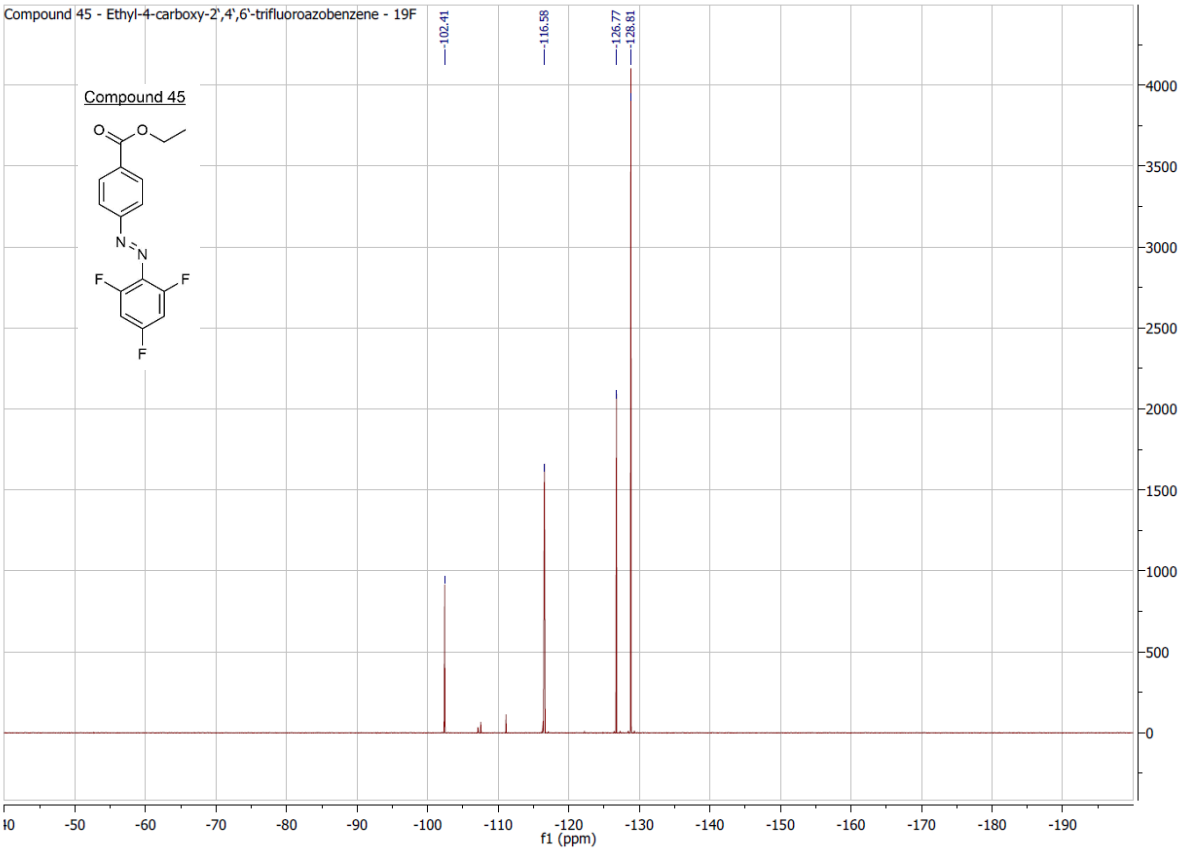
Compound 45 - Ethyl-4-carboxy-2',4',6'-trifluoroazobenzene - 19F
-102.41
-116.58
-126.77
-128.81
Compound 45
f1 (ppm)

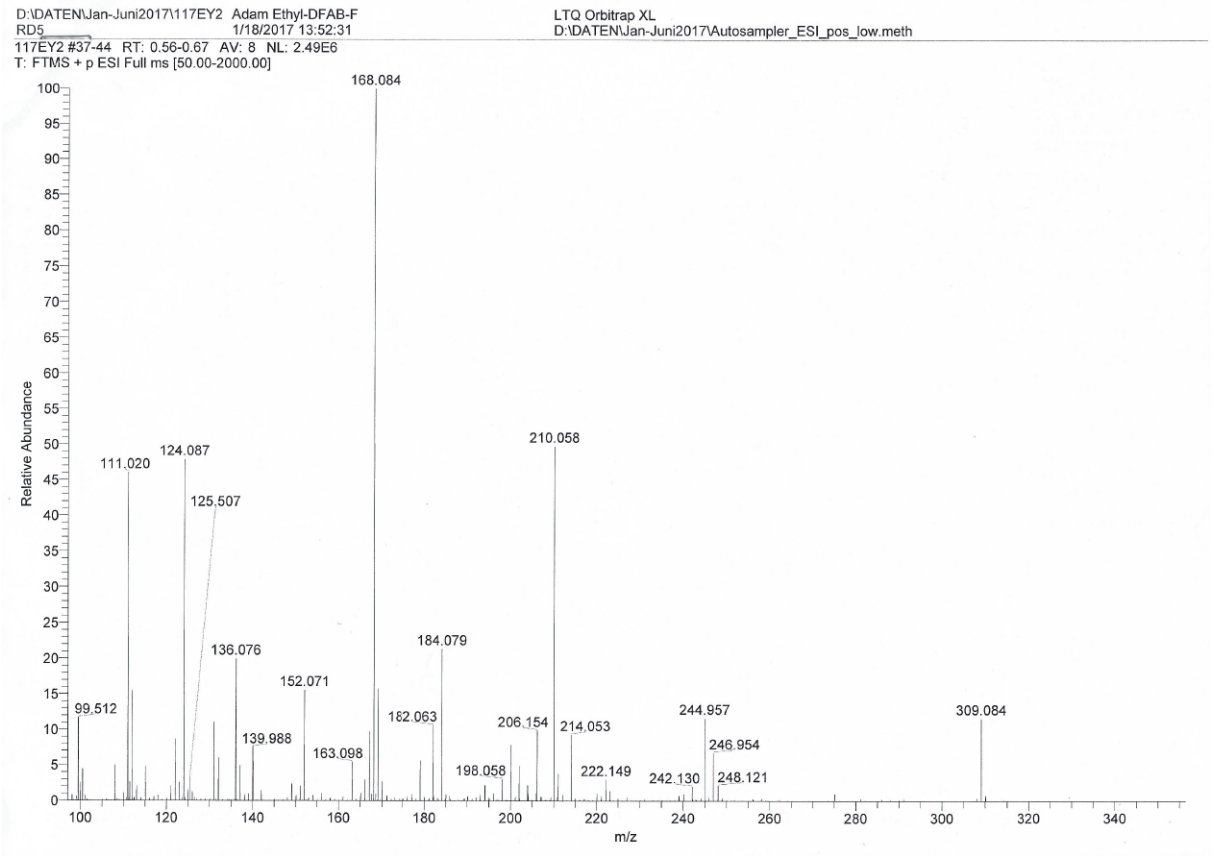
D:\DATEN\Jan-Juni2017\117EY2 Adam Ethyl-DFAB-F
RD5 1/18/2017 13:52:31
LTQ Orbitrap XL
D:\DATEN\Jan-Juni2017\Autosampler_ESI_pos_low.meth
117EY2 #37-44 RT: 0.56-0.67 AV: 8 NL: 2.49E6
T: FTMS + p ESI Full ms [50.00-2000.00]
Relative Abundance
m/z
168.084
210.058
111.020
124.087
125.507
136.076
184.079
152.071
99.512
162.063
206.154
214.053
139.988
163.098
198.058
222.149
244.957
246.954
242.130
248.121
309.084

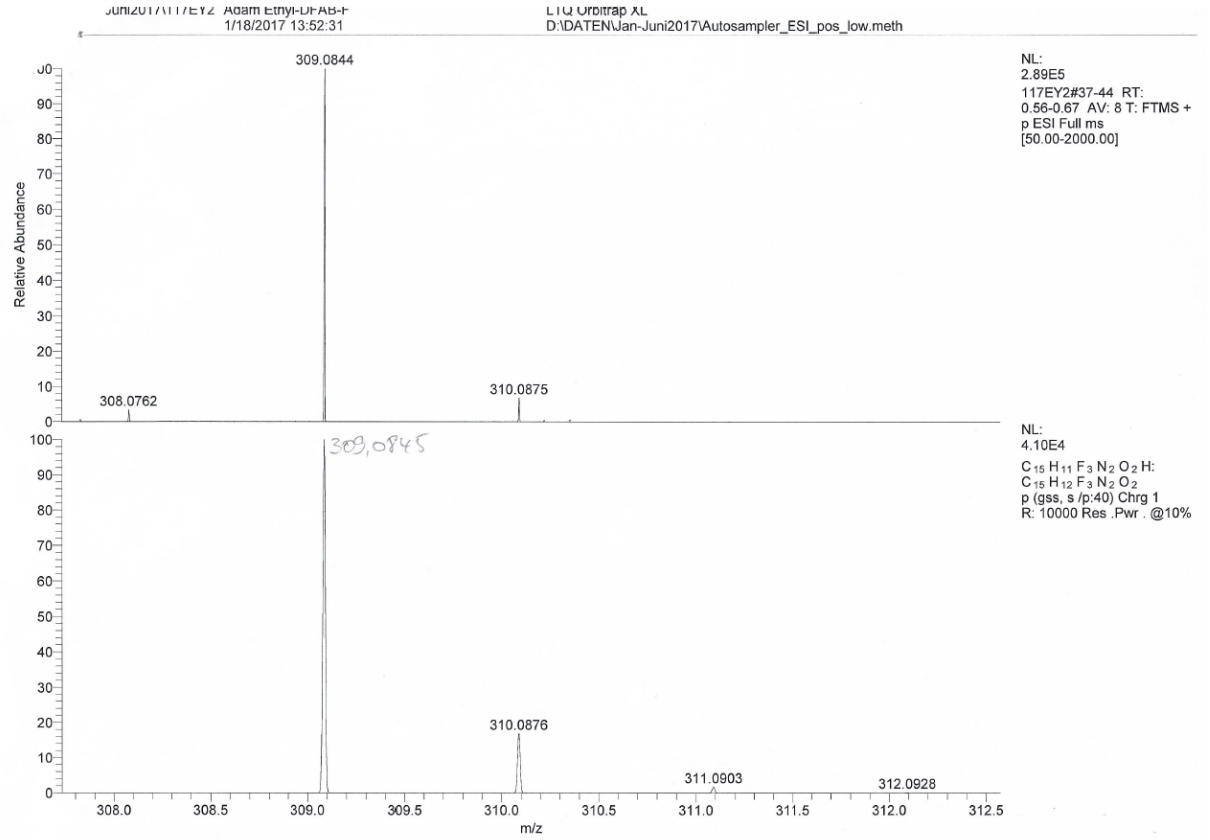
Juni2017\117EY2 Adam Ethyl-DFAB-F
1/18/2017 13:52:31
LTQ Orbitrap XL
D:\DATEN\Jan-Juni2017\Autosampler_ESI_pos_low.meth
309.0844
308.0762
310.0875
Relative Abundance
NL:
2.89E5
117EY2#37-44 RT:
0.56-0.67 AV: 8 T: FTMS +
p ESI Full ms
[50.00-2000.00]
309,0845
310.0876
311.0903
312.0928
NL:
4.10E4
C15 H11 F3 N2 O2 H:
C15 H12 F3 N2 O2
p (gss, s /p:40) Chrg 1
R: 10000 Res .Pwr . @10%
m/z

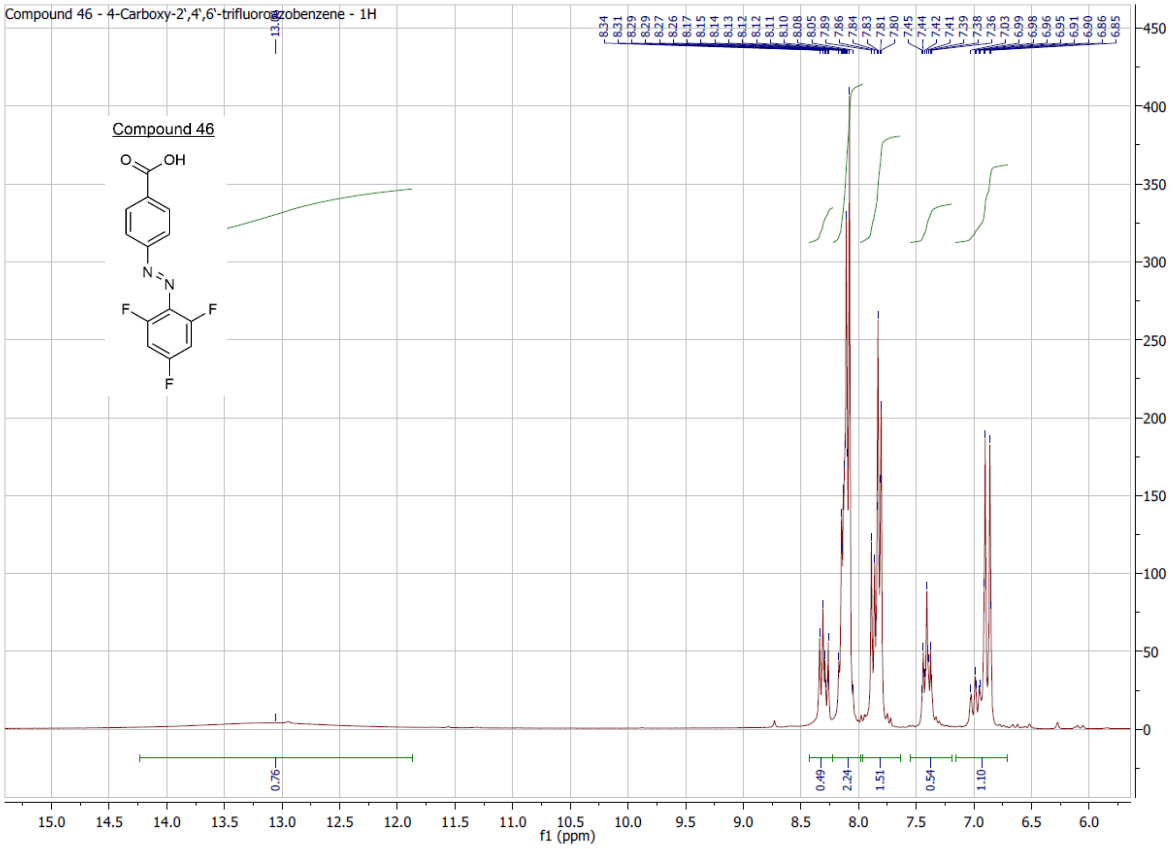
Compound 46 - 4-Carboxy-2',4',6'-trifluoroazobenzene - 1H
Compound 46
f1 (ppm)

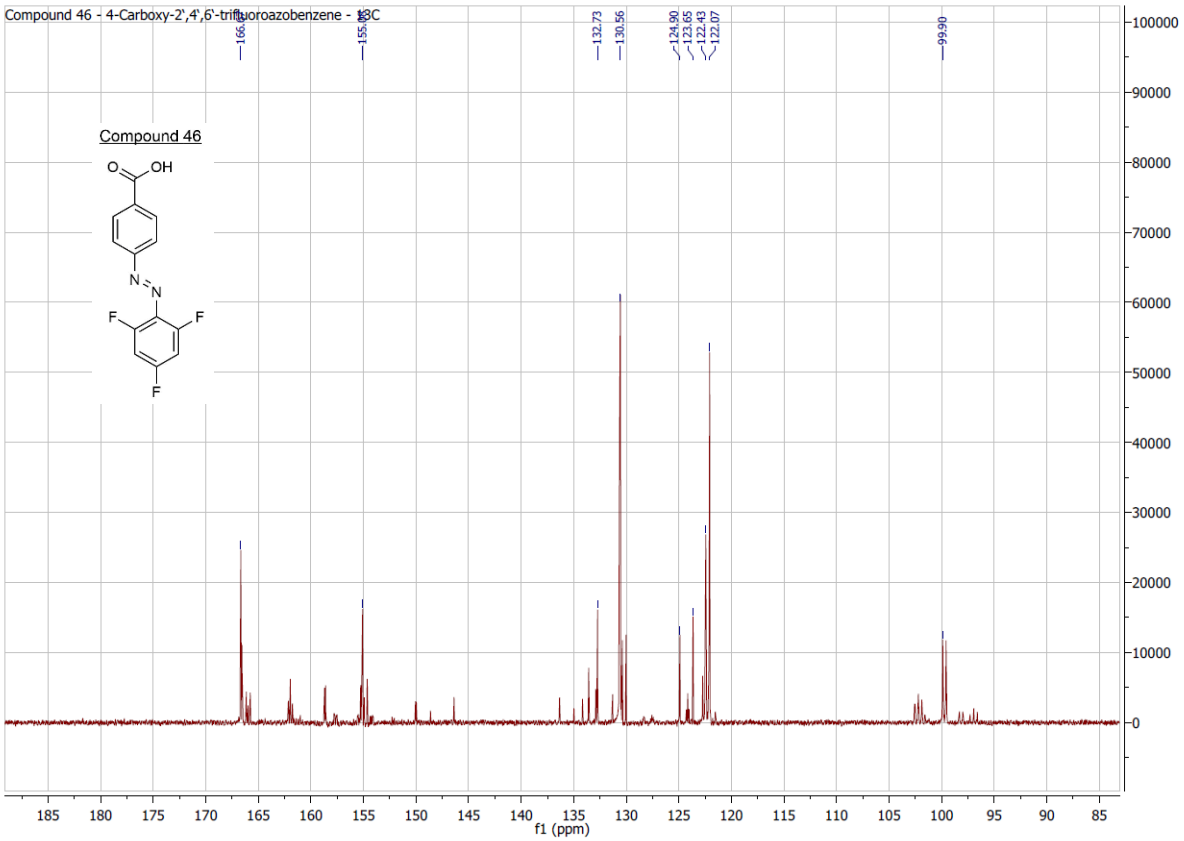
Compound 46 - 4-Carboxy-2',4',6'-trifluoroazobenzene - 13C
Compound 46
f1 (ppm)

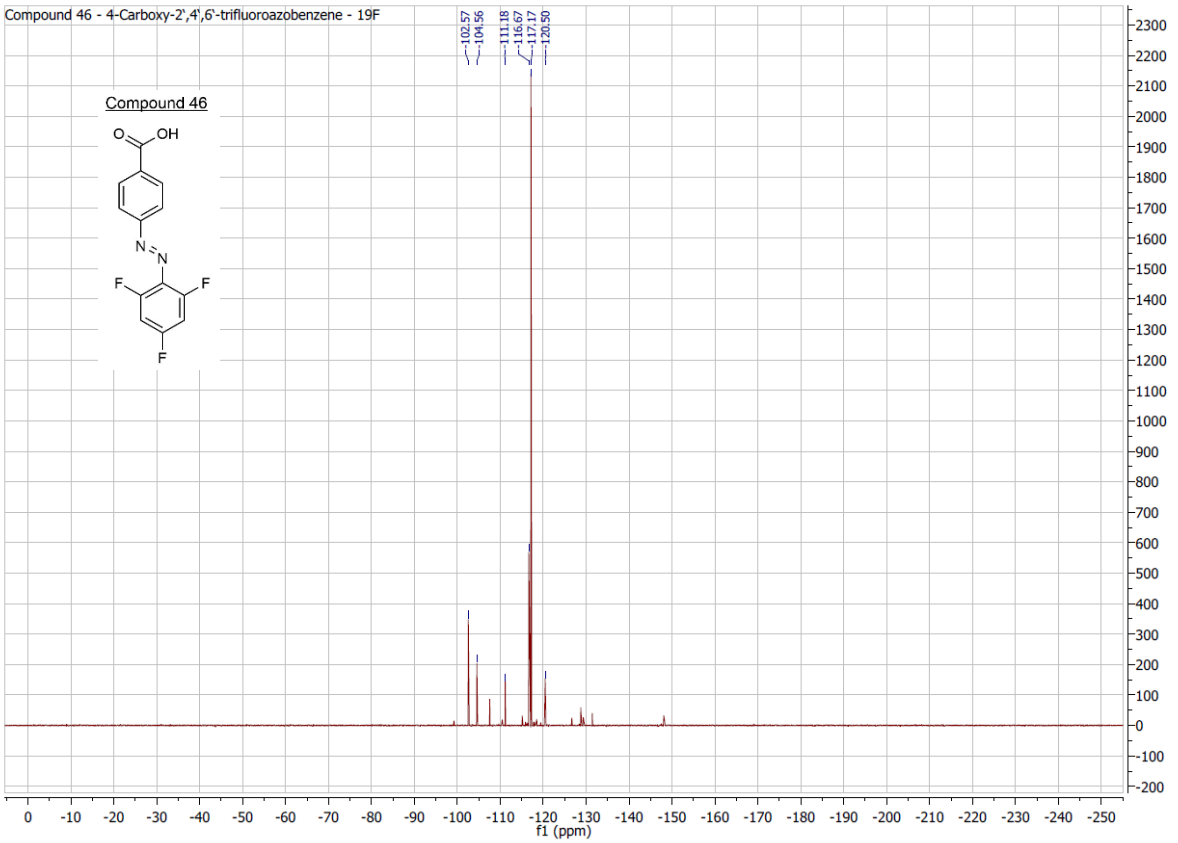

Im ESI Neu Signal.

SPEC: 231ez 14-Jun-17 Elapse: 01:34.5 21
Samp: Adam, TriFab-Acid Start : 14:14:58 23
Mode: EI +VE +LMR BSCAN (EXP) UP LR NRM
Oper: So Inlet :
Base: 121.1 Inten : 16751291 Masses: 50 > 1000
Norm: 121.1 RIC : 224406682 #peaks: 1121
Peak: 5.00 mmu

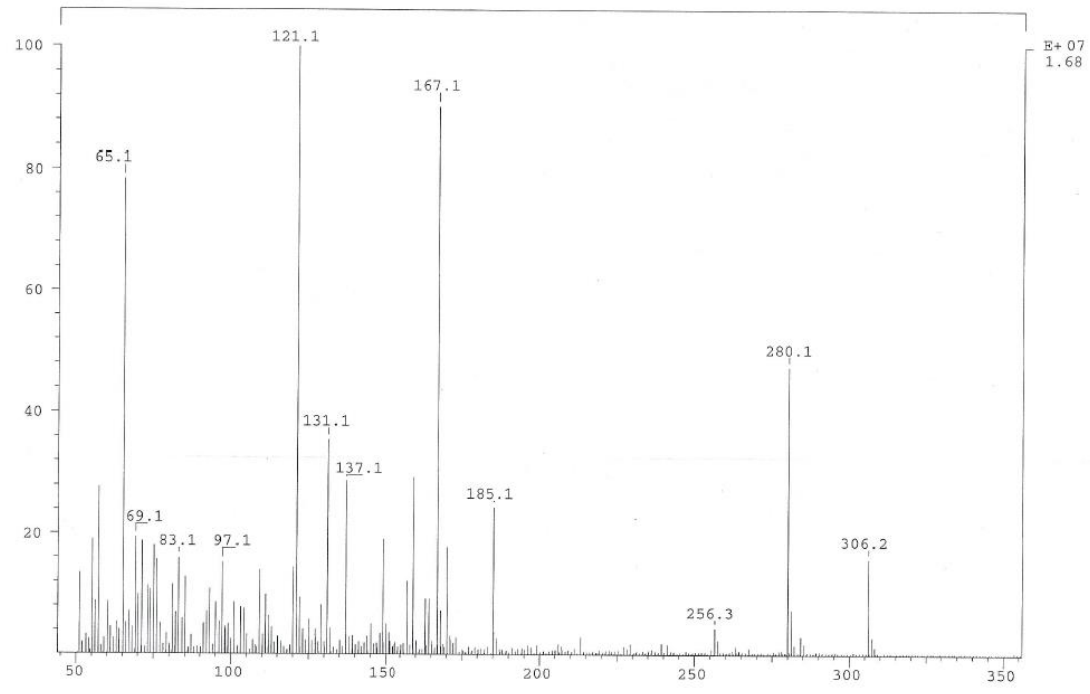

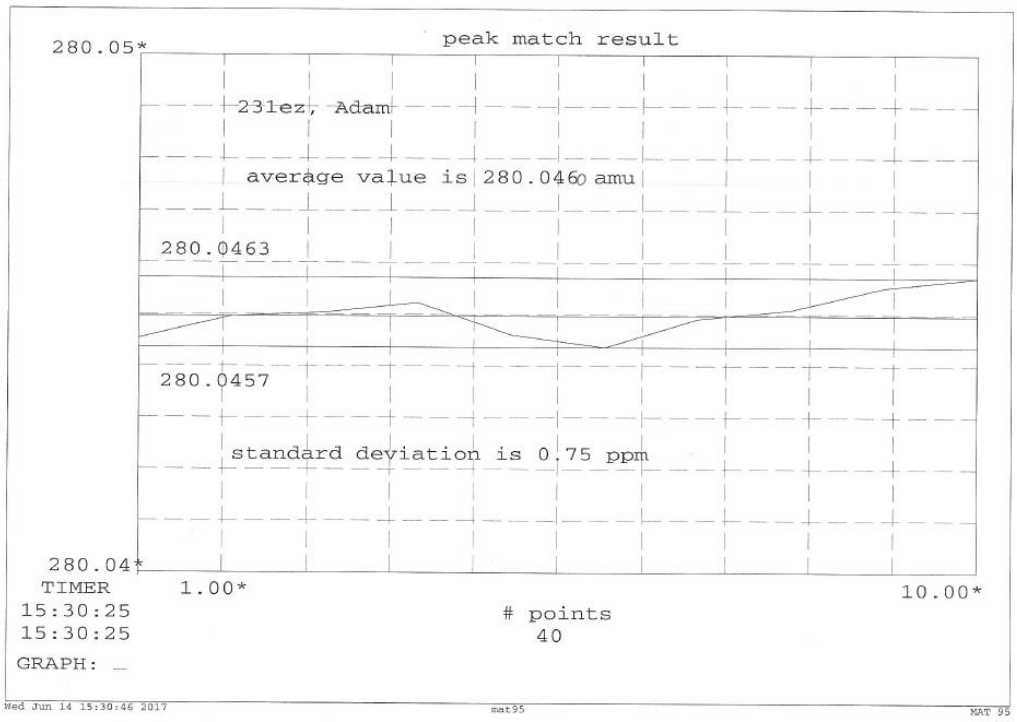
peak match result
280.05*
231ez, Adam
average value is 280.0460 amu
280.0463
280.0457
standard deviation is 0.75 ppm
280.04*
TIMER
1.00*
10.00*
15:30:25
15:30:25
points
40
GRAPH: _
Wed Jun 14 15:30:46 2017
mat95
MAT 95

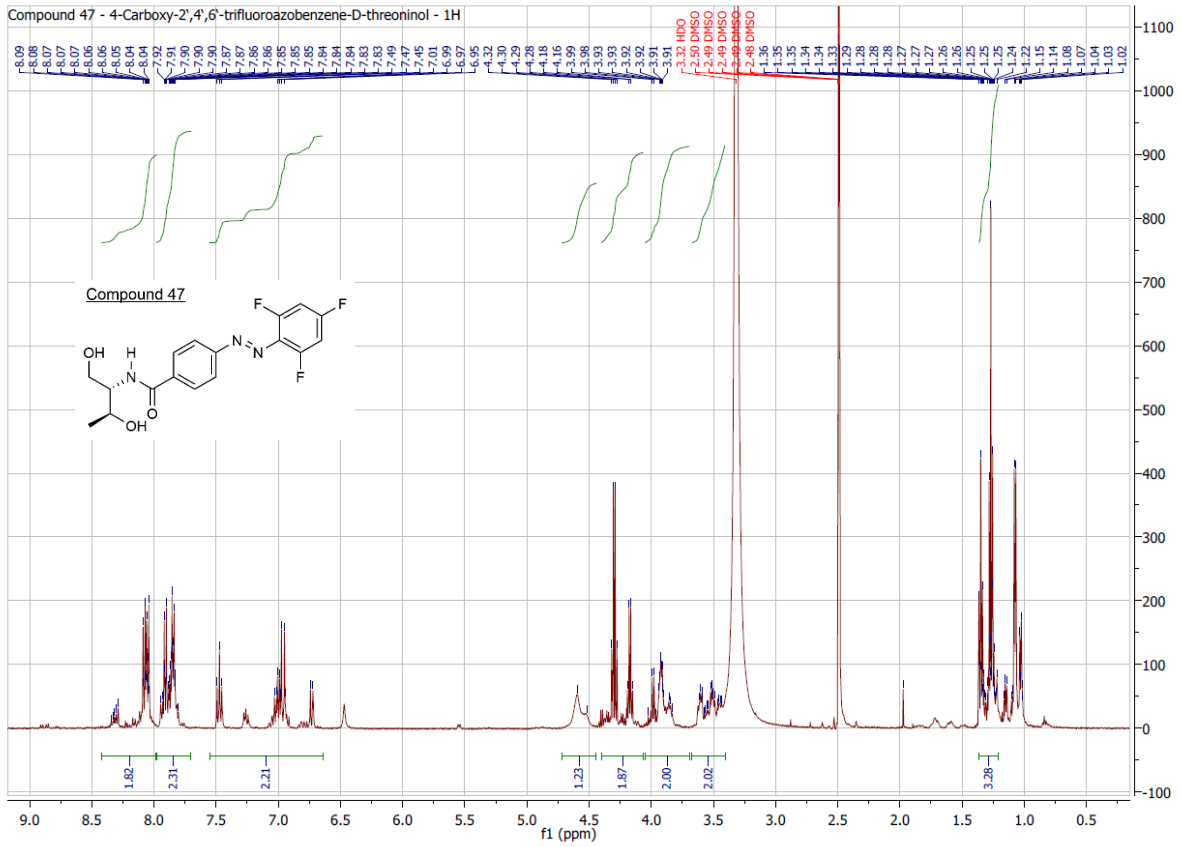
Compound 47 - 4-Carboxy-2',4',6'-trifluoroazobenzene-D-threoninol - 1H
Compound 47
f1 (ppm)

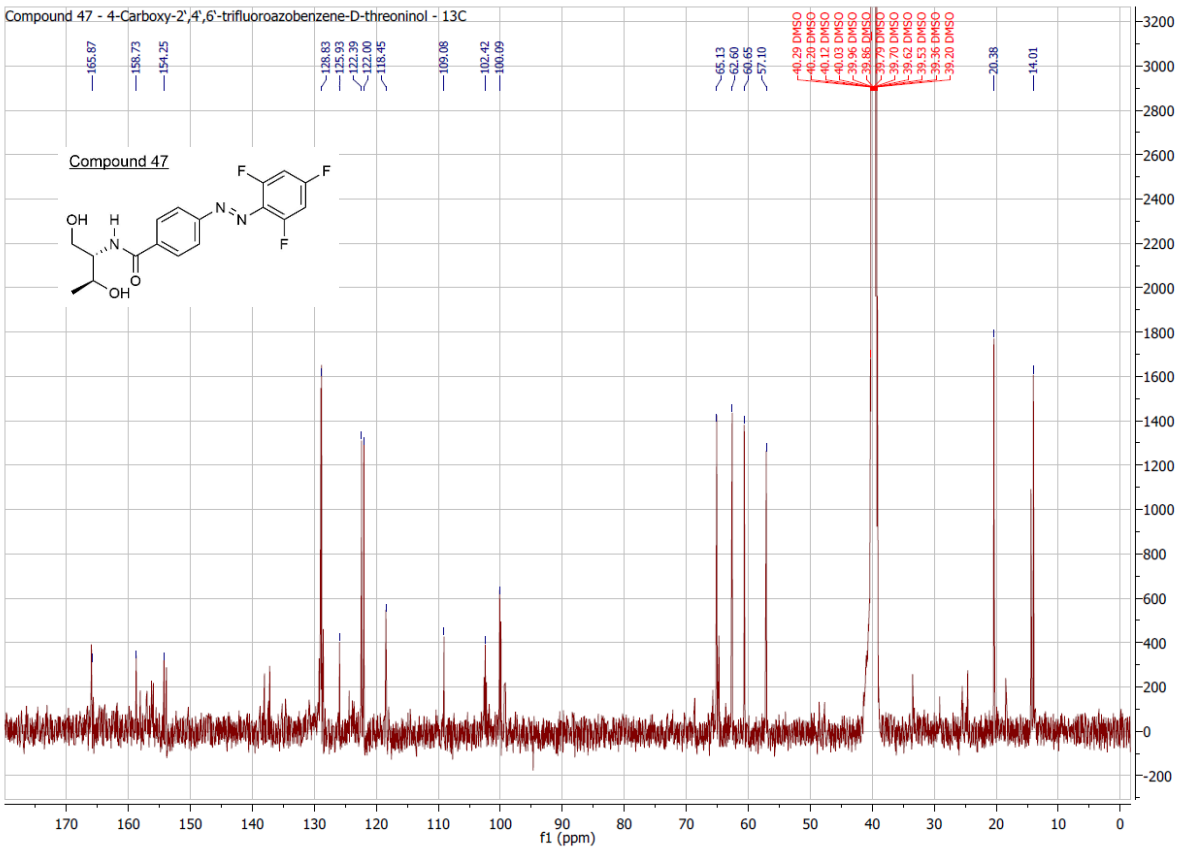
Compound 47 - 4-Carboxy-2',4',6'-trifluoroazobenzene-D-threoninol - 13C
Compound 47
f1 (ppm)

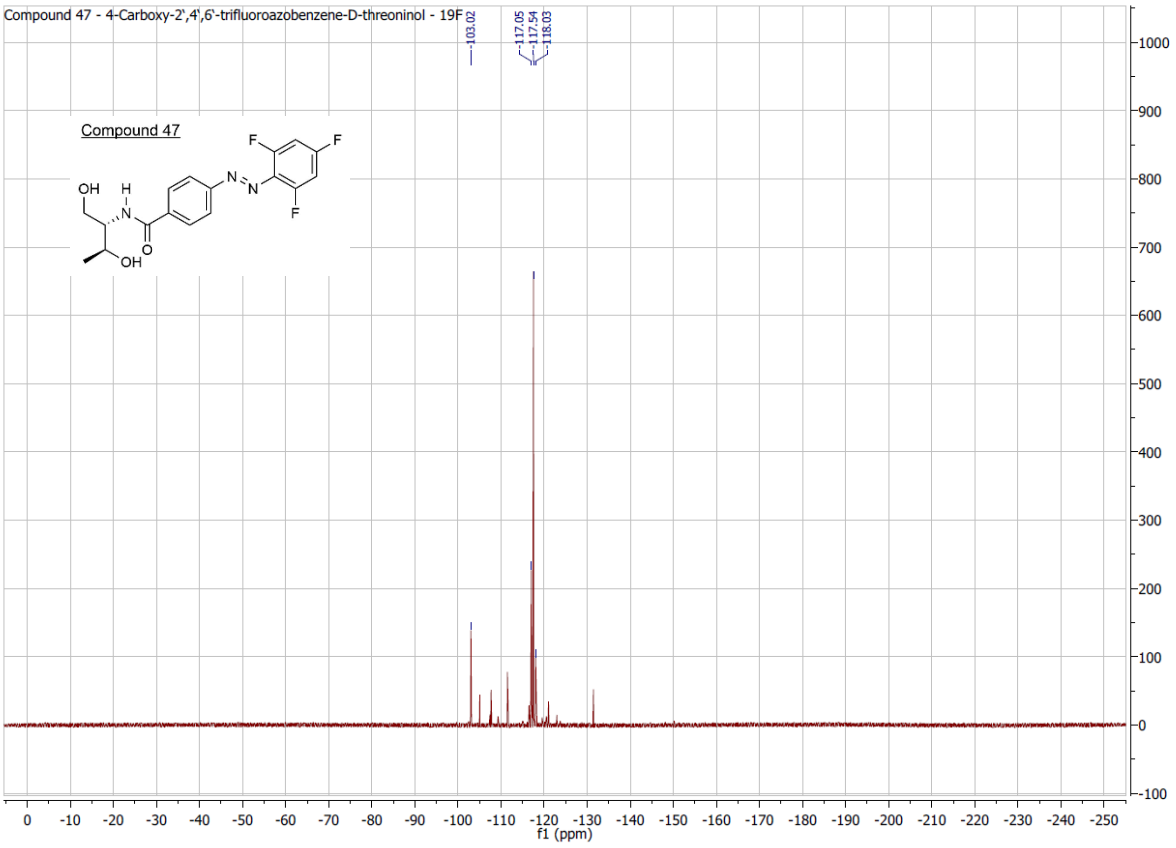
Compound 47 - 4-Carboxy-2',4',6'-trifluoroazobenzene-D-threoninol - 19F
103.02
117.05
117.54
118.03
Compound 47
f1 (ppm)

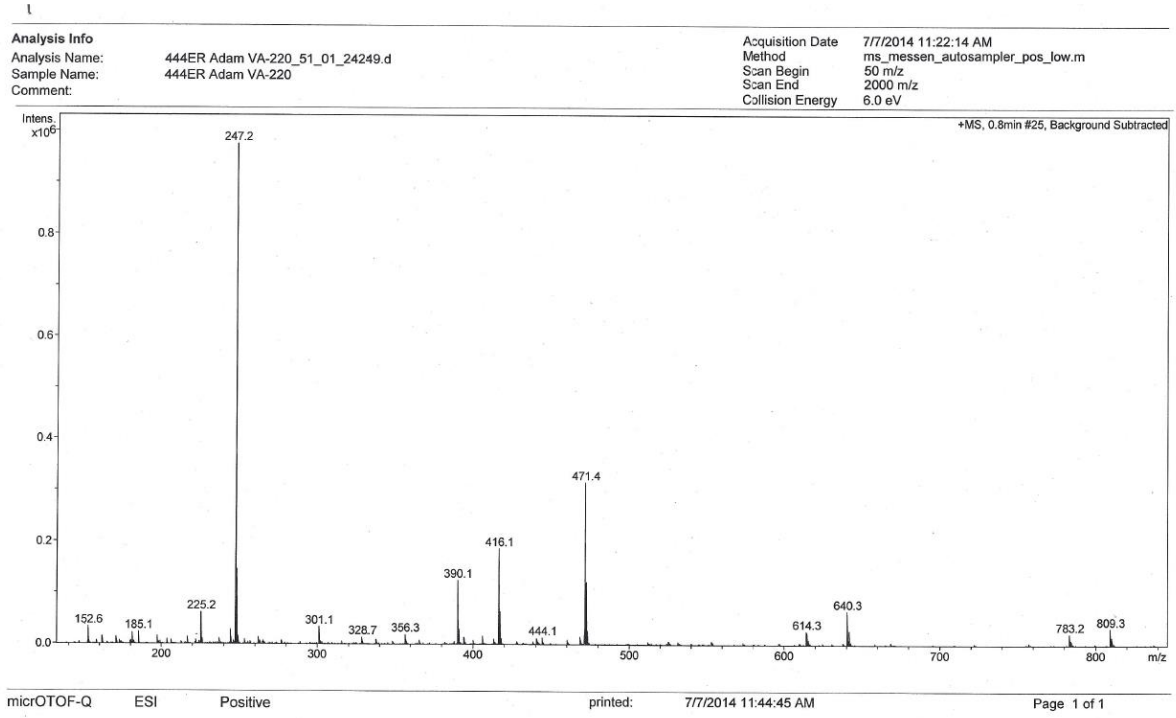
Analysis Info
Analysis Name: 444ER Adam VA-220_51_01_24249.d
Sample Name: 444ER Adam VA-220
Comment:
Acquisition Date 7/7/2014 11:22:14 AM
Method ms_messen_autosampler_pos_low.m
Scan Begin 50 m/z
Scan End 2000 m/z
Collision Energy 6.0 eV
+MS, 0.8min #25, Background Subtracted
Intens. x10^6
247.2
471.4
416.1
390.1
640.3
225.2
152.6
185.1
301.1
328.7
356.3
444.1
614.3
783.2
809.3
m/z
micrOTOF-Q ESI Positive
printed: 7/7/2014 11:44:45 AM
Page 1 of 1

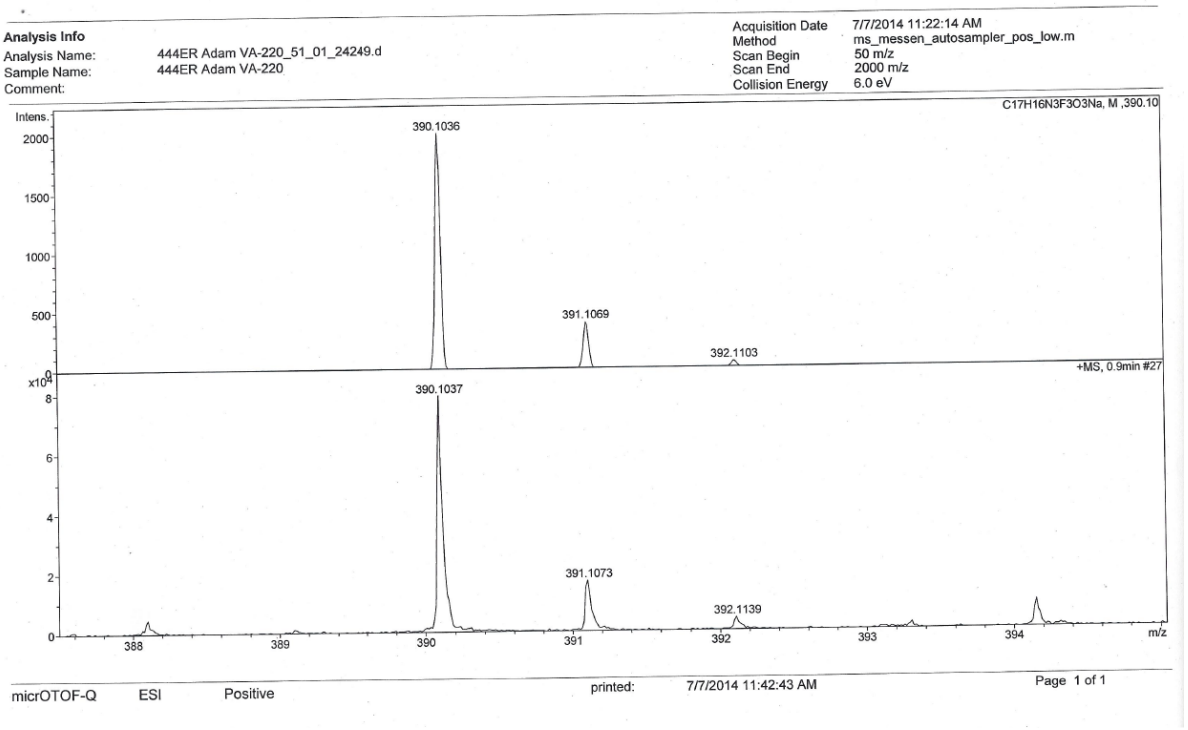
Analysis Info
Analysis Name: 444ER Adam VA-220_51_01_24249.d
Sample Name: 444ER Adam VA-220
Comment:
Acquisition Date 7/7/2014 11:22:14 AM
Method ms_messen_autosampler_pos_low.m
Scan Begin 50 m/z
Scan End 2000 m/z
Collision Energy 6.0 eV
C17H16N3F3O3Na, M ,390.10
Intens.
390.1036
391.1069
392.1103
+MS, 0.9min #27
x10^4
390.1037
391.1073
392.1139
m/z
micrOTOF-Q ESI Positive
printed: 7/7/2014 11:42:43 AM
Page 1 of 1

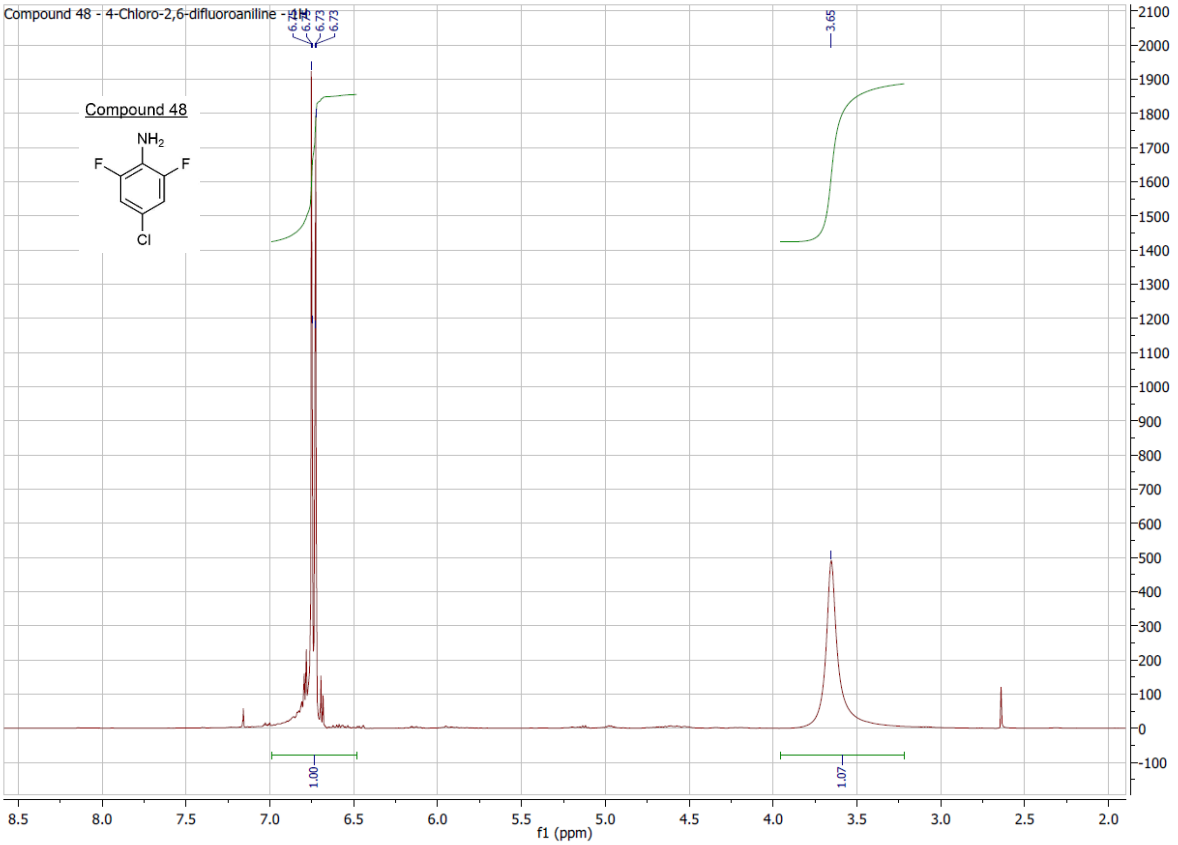
Compound 48 - 4-Chloro-2,6-difluoroaniline - 1H
Compound 48
NH2
F
F
Cl
6.73
6.73
6.73
3.65
1.00
1.07
f1 (ppm)

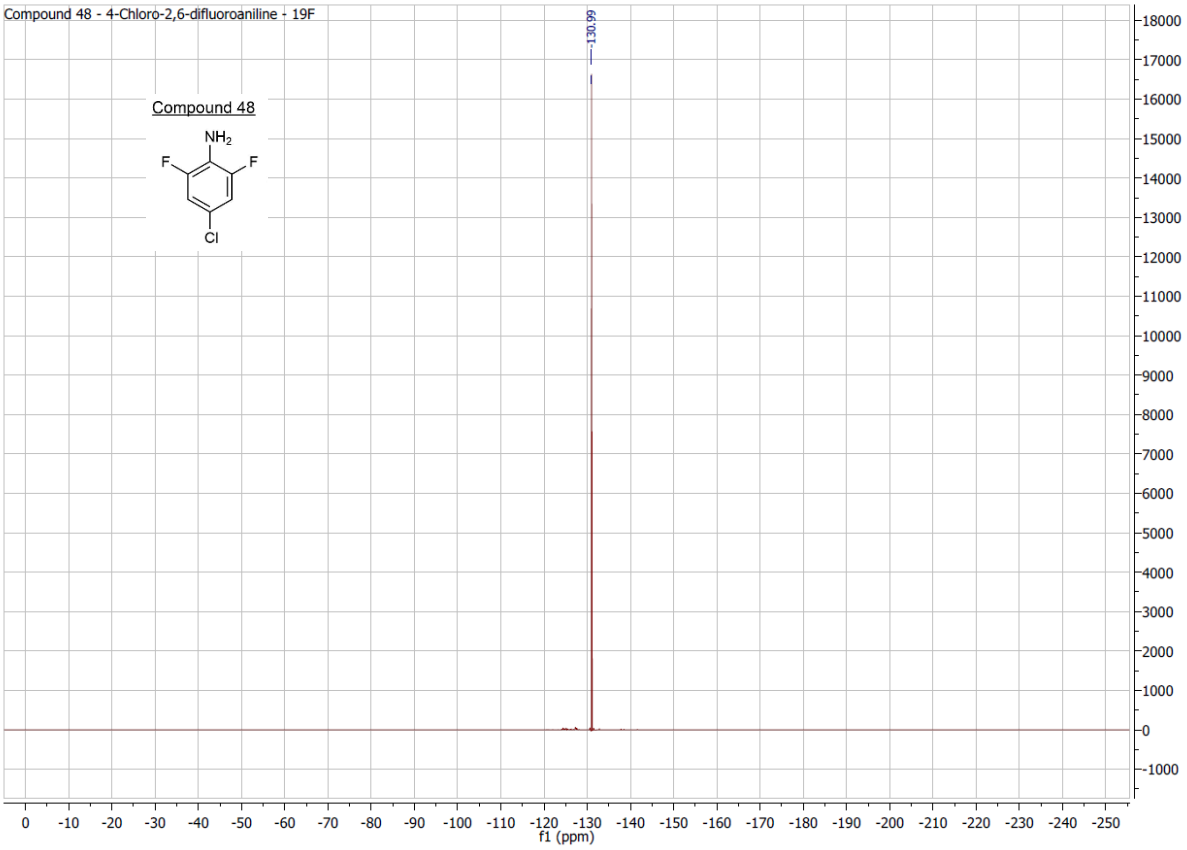
Compound 48 - 4-Chloro-2,6-difluoroaniline - 19F
Compound 48
NH2
F
F
Cl
-130.99
f1 (ppm)

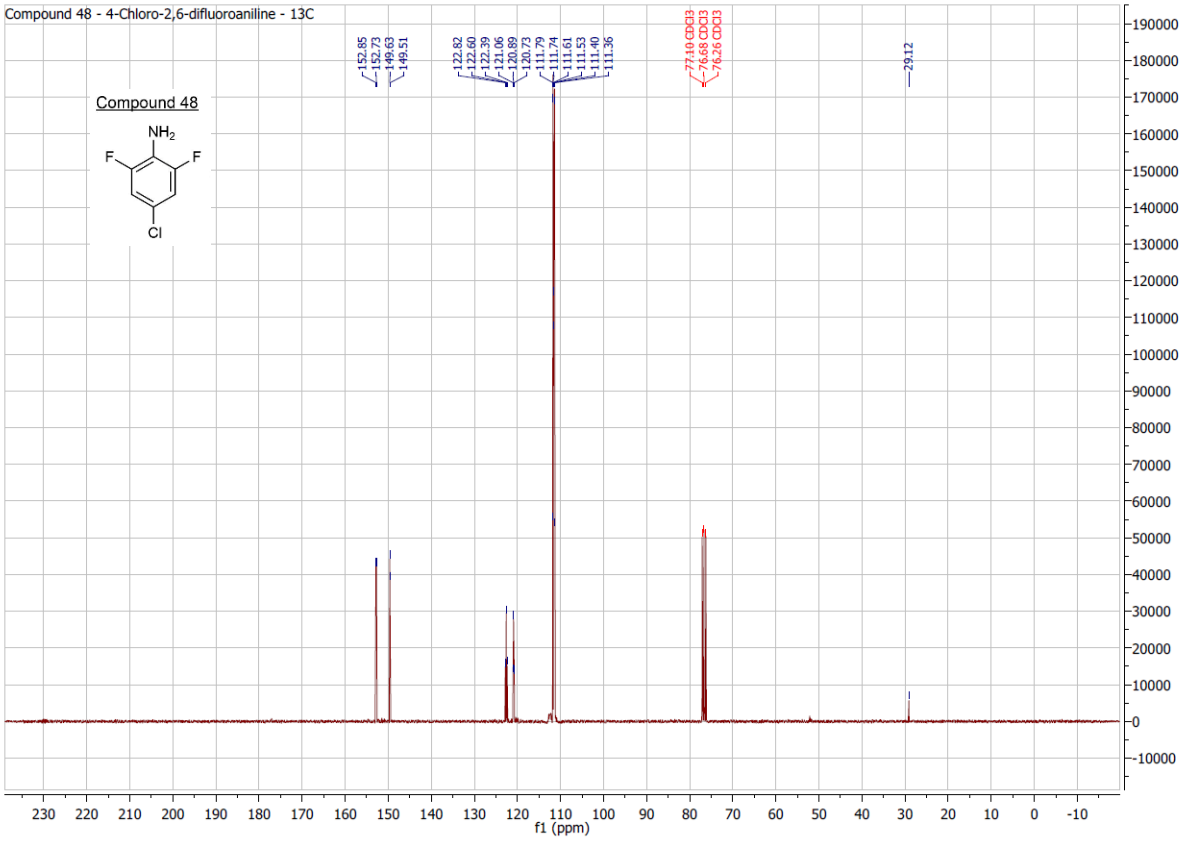
Compound 48 - 4-Chloro-2,6-difluoroaniline - 13C
Compound 48
NH2
F
F
Cl
152.85
152.73
149.63
149.51
122.82
122.60
122.39
121.06
120.89
120.73
111.79
111.74
111.61
111.53
111.40
111.36
77.10 CDCl3
76.68 CDCl3
76.26 CDCl3
29.12
f1 (ppm)

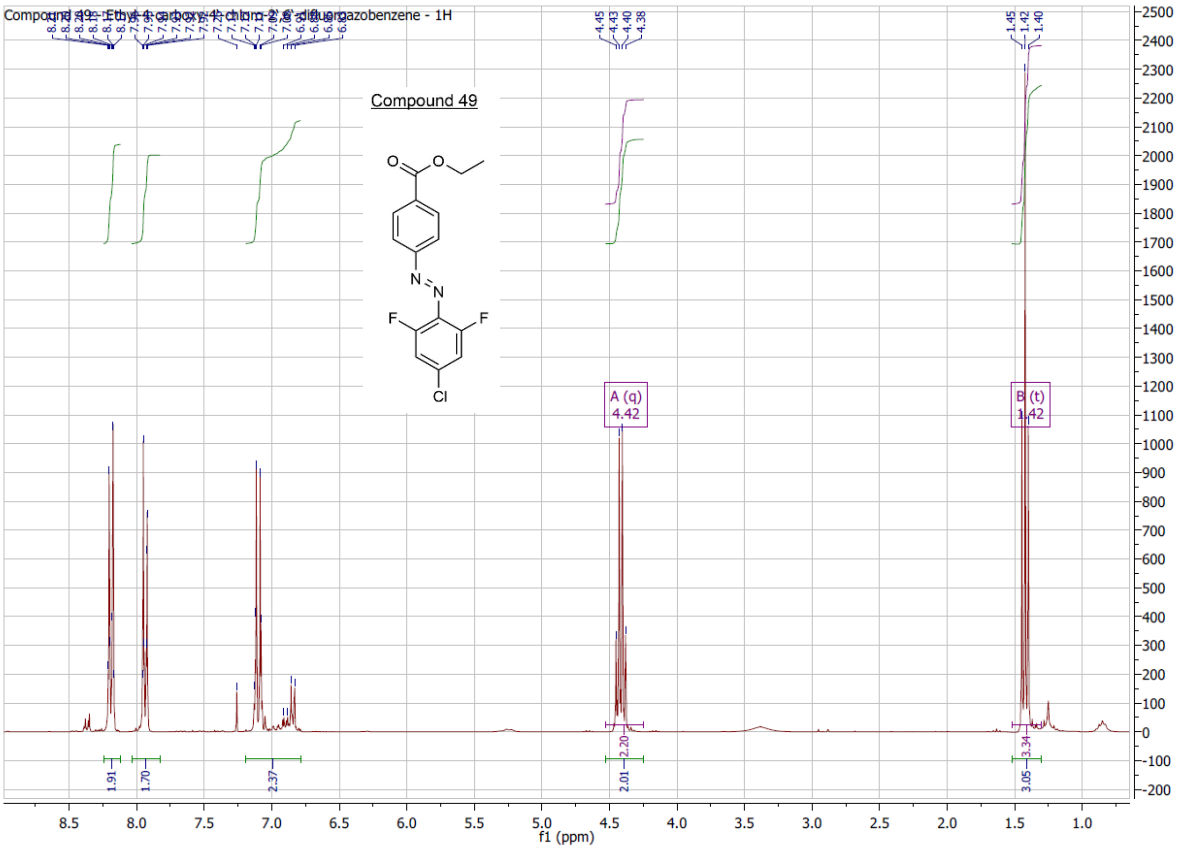
Compound 49 - Ethyl-4-carboxy-4`-chloro-2`,6`-difluoroazobenzene - 1H
Compound 49
A (q)
4.42
B (t)
1.42
f1 (ppm)

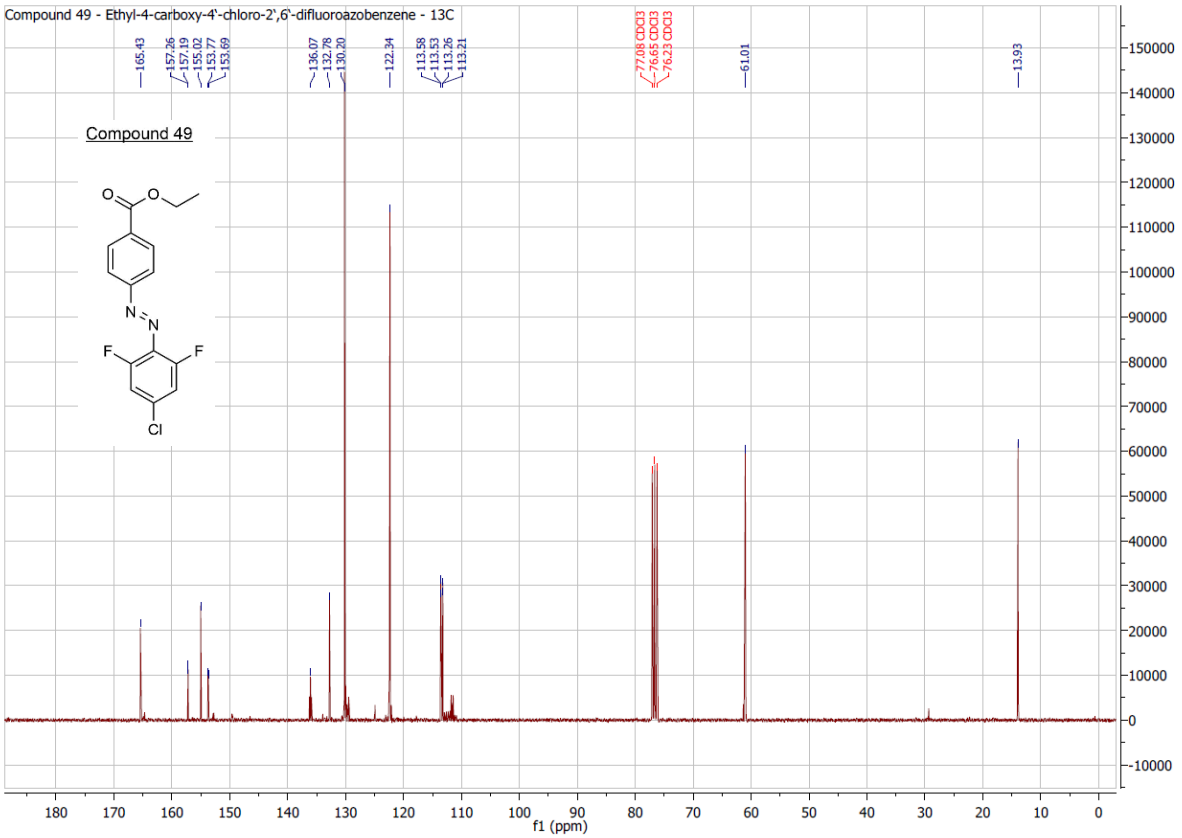
Compound 49 - Ethyl-4-carboxy-4`-chloro-2`,6`-difluoroazobenzene - 13C
Compound 49
f1 (ppm)

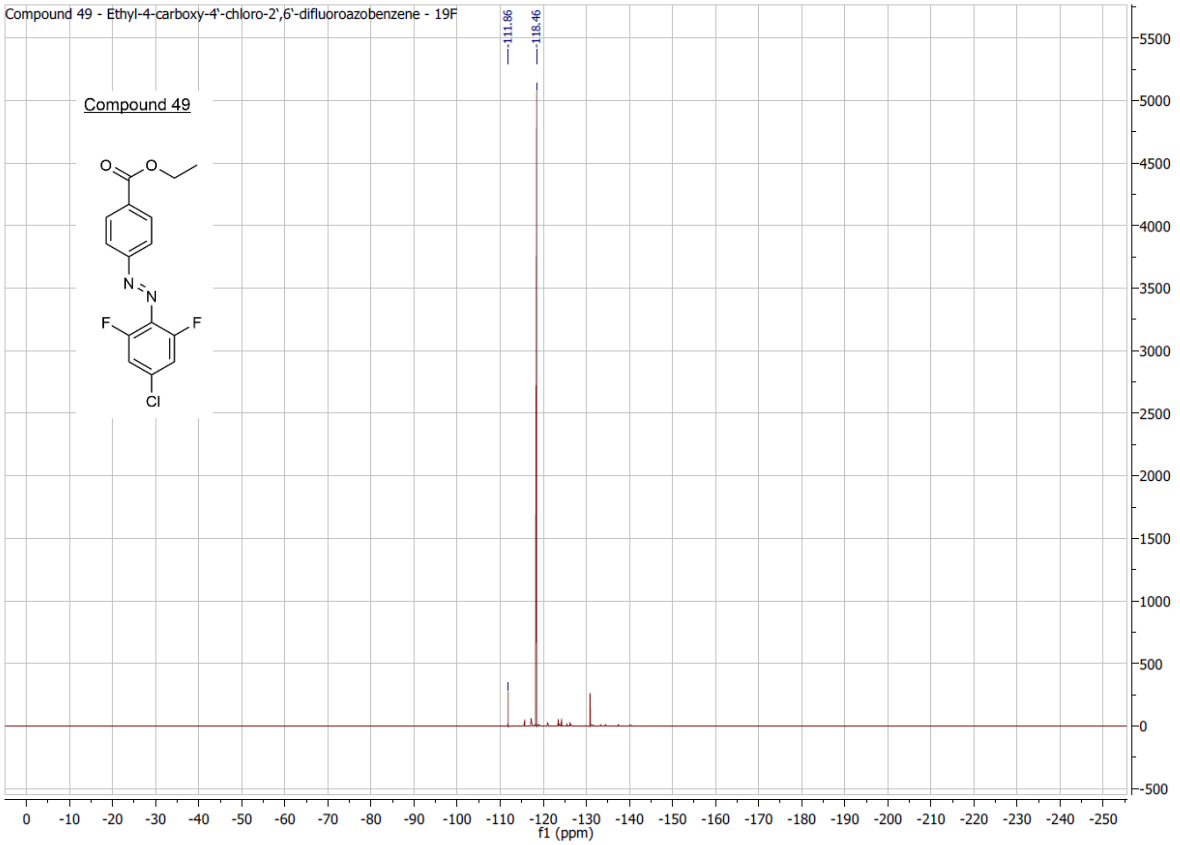
Compound 49 - Ethyl-4-carboxy-4'-chloro-2',6'-difluoroazobenzene - 19F
111.86
118.46
Compound 49
O
O
N
N
F
F
Cl
5500
5000
4500
4000
3500
3000
2500
2000
1500
1000
500
0
-500
0 -10 -20 -30 -40 -50 -60 -70 -80 -90 -100 -110 -120 -130 -140 -150 -160 -170 -180 -190 -200 -210 -220 -230 -240 -250
f1 (ppm)

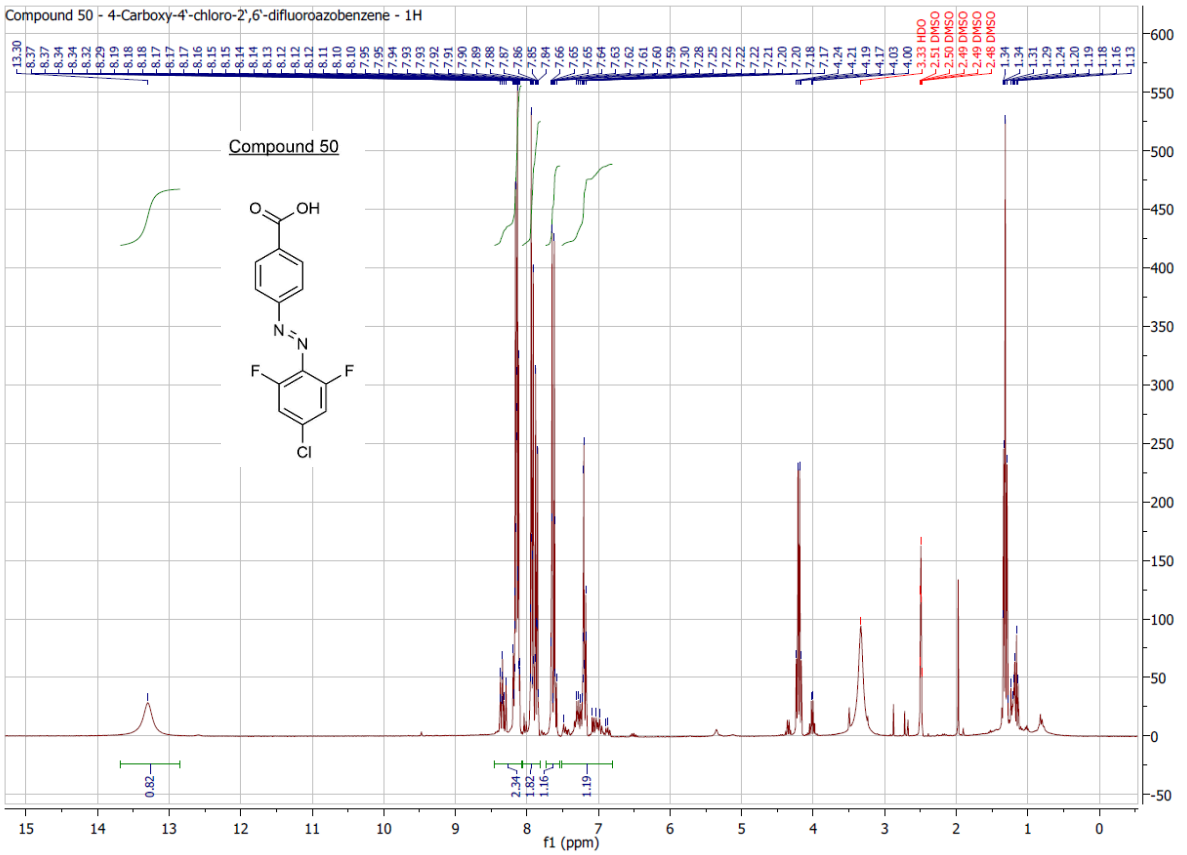
Compound 50 - 4-Carboxy-4'-chloro-2',6'-difluoroazobenzene - 1H
Compound 50
f1 (ppm)

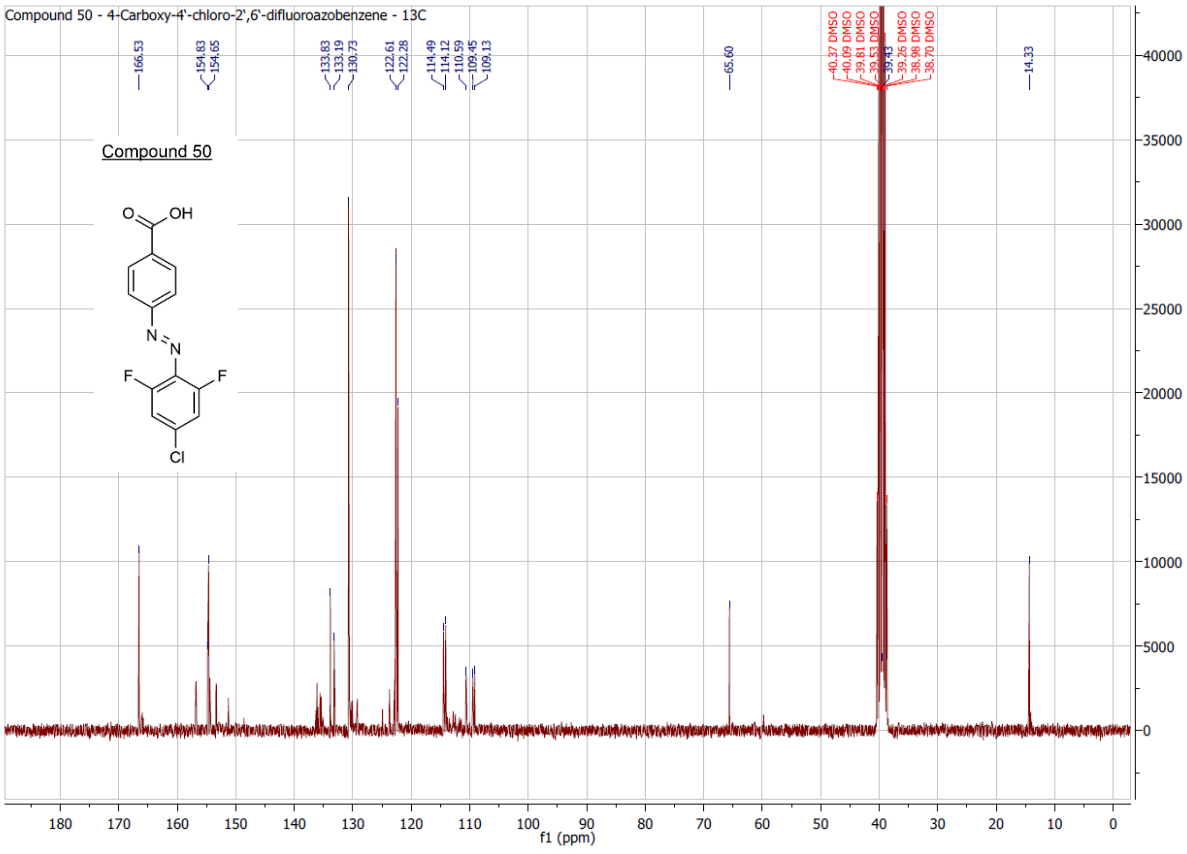
Compound 50 - 4-Carboxy-4'-chloro-2',6'-difluoroazobenzene - 13C
Compound 50
f1 (ppm)

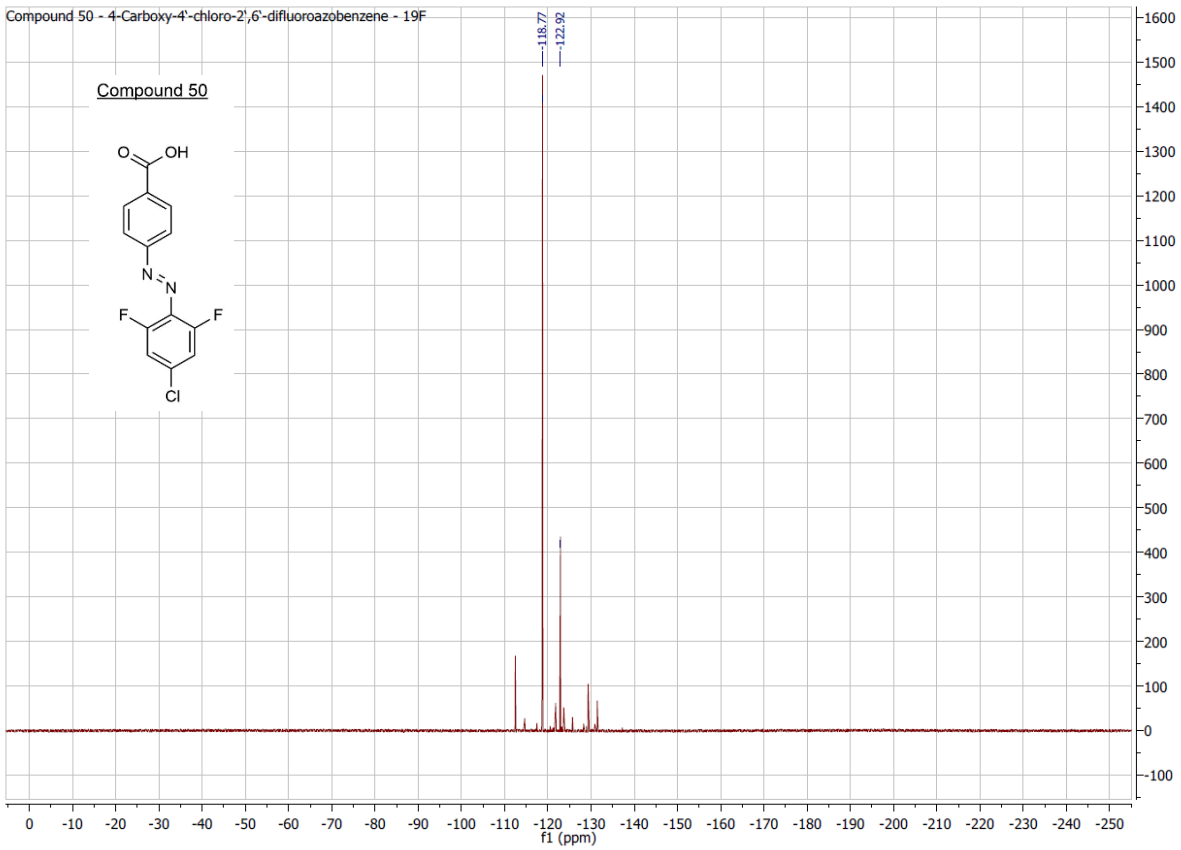
Compound 50 - 4-Carboxy-4'-chloro-2',6'-difluoroazobenzene - 19F
Compound 50
118.77
122.92
f1 (ppm)

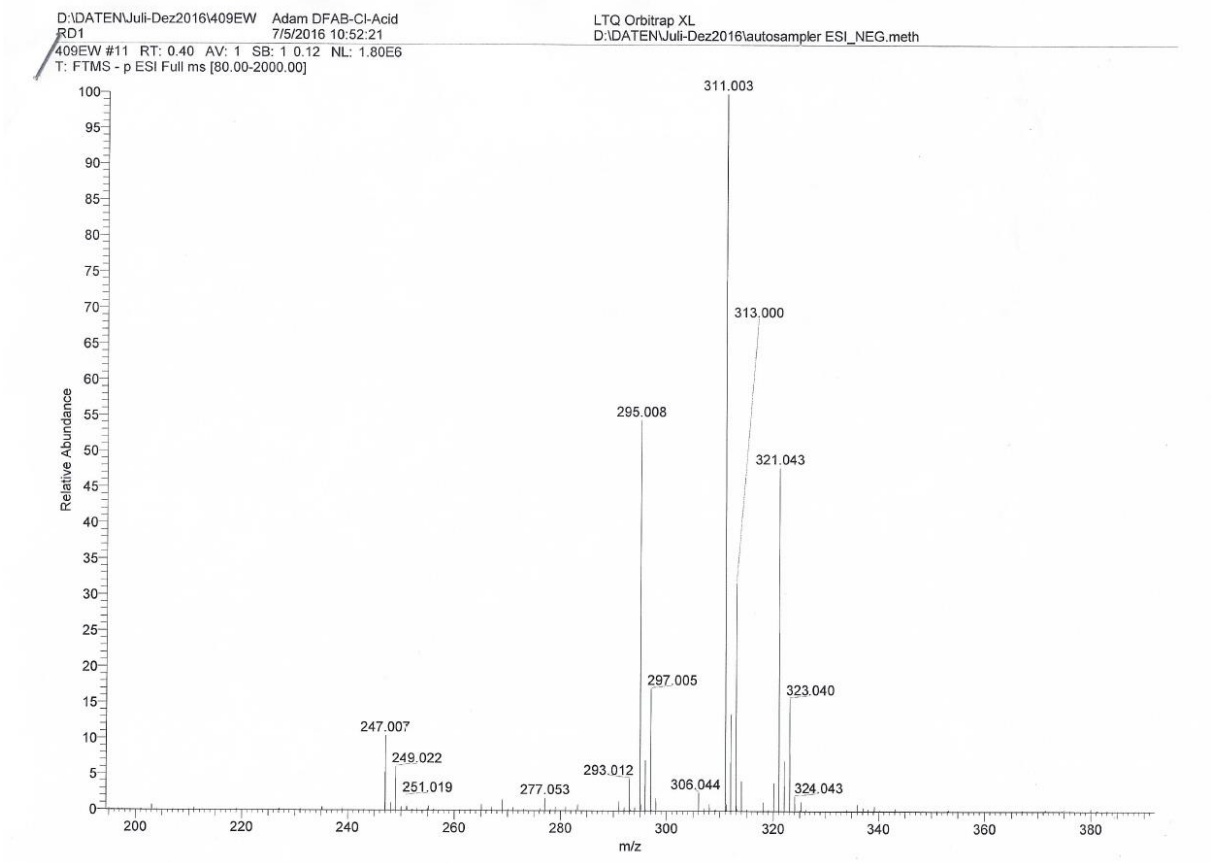
D:\DATEN\Juli-Dez2016\409EW Adam DFAB-Cl-Acid
RD1 7/5/2016 10:52:21
409EW #11 RT: 0.40 AV: 1 SB: 1 0.12 NL: 1.80E6
T: FTMS - p ESI Full ms [80.00-2000.00]
LTQ Orbitrap XL
D:\DATEN\Juli-Dez2016\autosampler ESI_NEG.meth
311.003
313.000
295.008
321.043
297.005
323.040
247.007
249.022
251.019
277.053
293.012
306.044
324.043
Relative Abundance
m/z

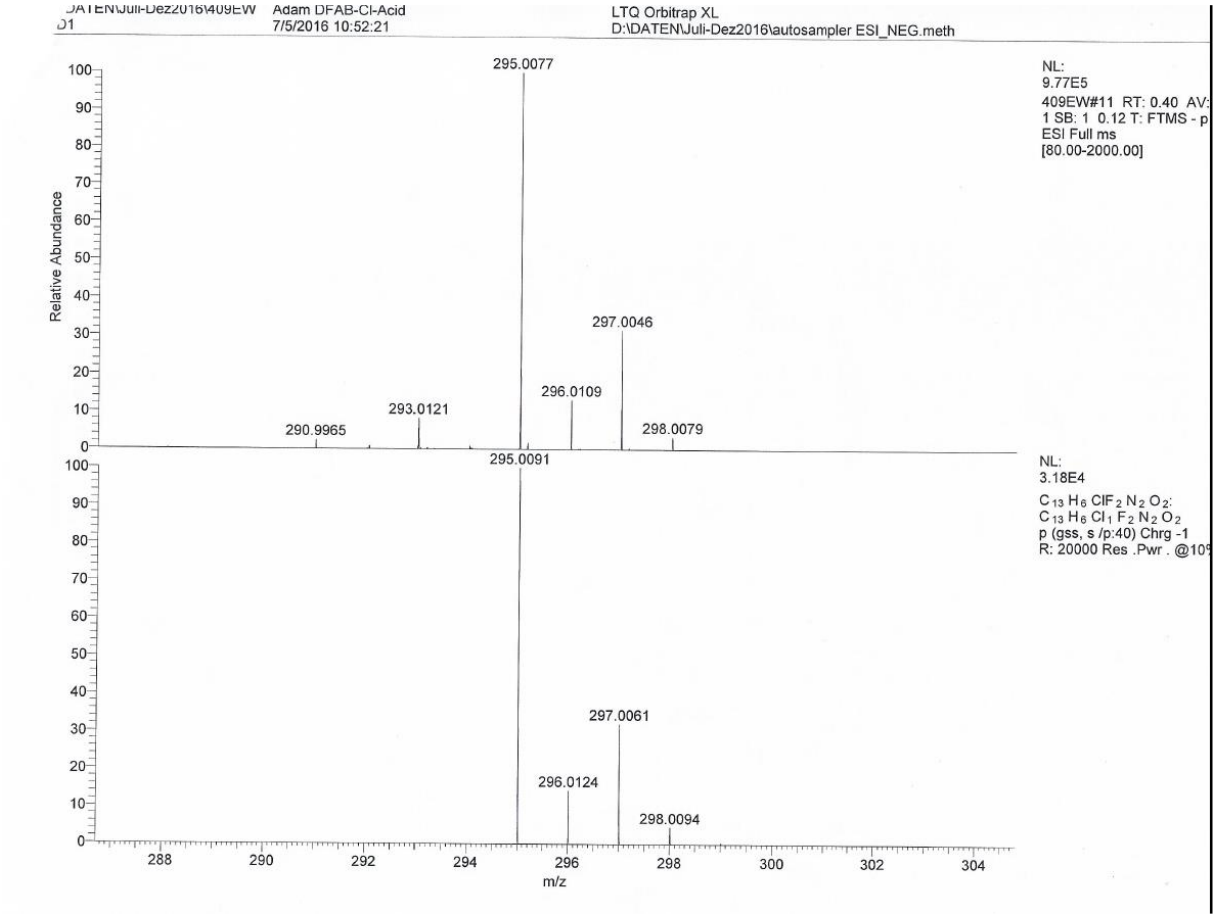
DATEN\Juli-Dez2016\409EW Adam DFAB-Cl-Acid
D1 7/5/2016 10:52:21
LTQ Orbitrap XL
D:\DATEN\Juli-Dez2016\autosampler ESI_NEG.meth
NL:
9.77E5
409EW#11 RT: 0.40 AV:
1 SB: 1 0.12 T: FTMS - p
ESI Full ms
[80.00-2000.00]
295.0077
297.0046
296.0109
293.0121
290.9965
298.0079
Relative Abundance
NL:
3.18E4
C13 H6 ClF2 N2 O2:
C13 H6 Cl1 F2 N2 O2
p (gss, s /p:40) Chrg -1
R: 20000 Res .Pwr . @10
295.0091
297.0061
296.0124
298.0094
m/z

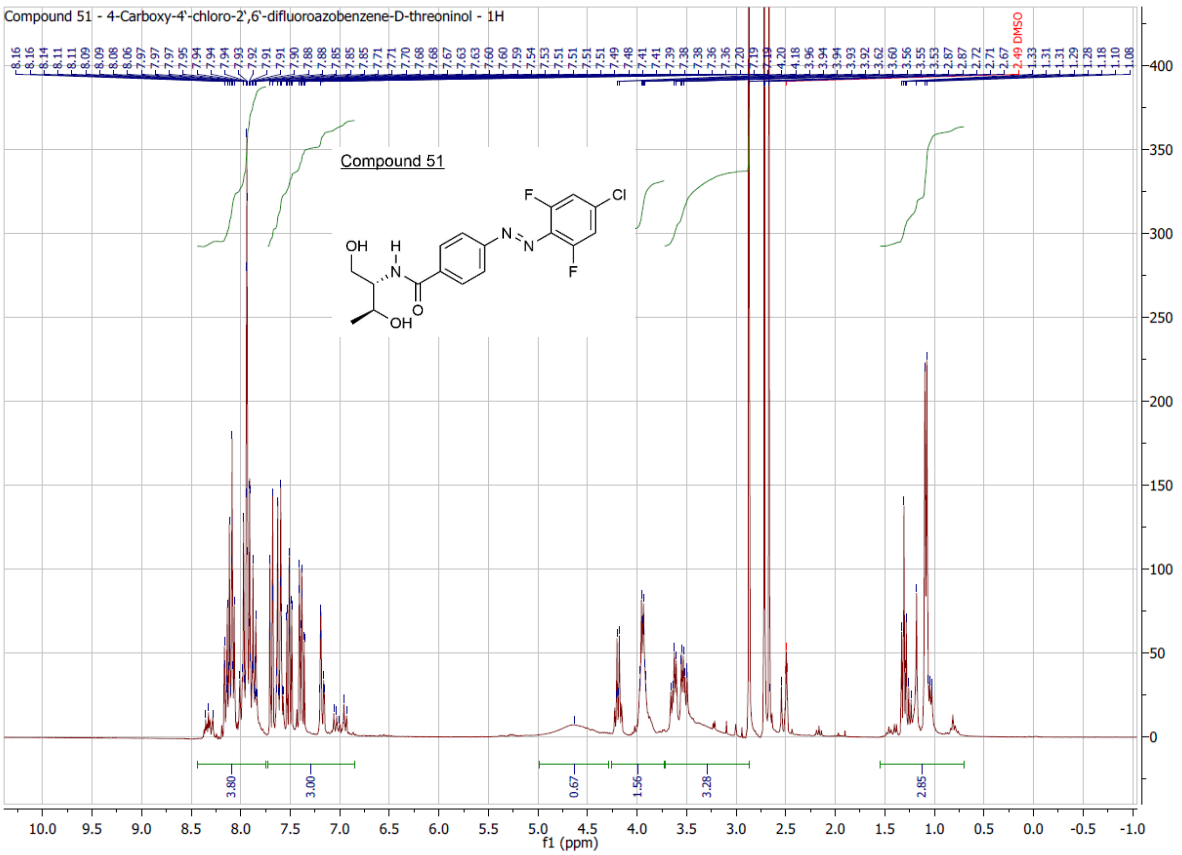
Compound 51 - 4-Carboxy-4'-chloro-2',6'-difluoroazobenzene-D-threoninol - 1H
Compound 51
f1 (ppm)

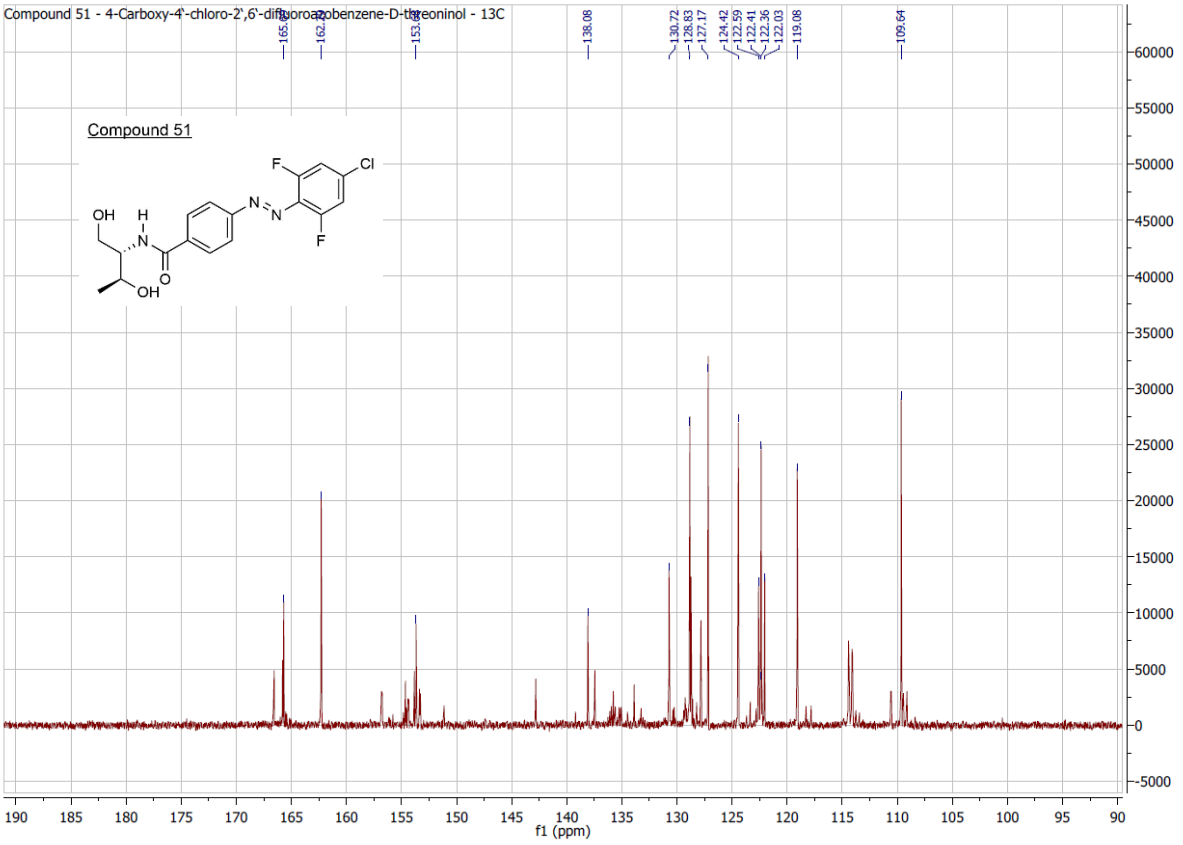
Compound 51 - 4-Carboxy-4'-chloro-2',6'-difluoroazobenzene-D-threoninol - 13C
Compound 51
f1 (ppm)

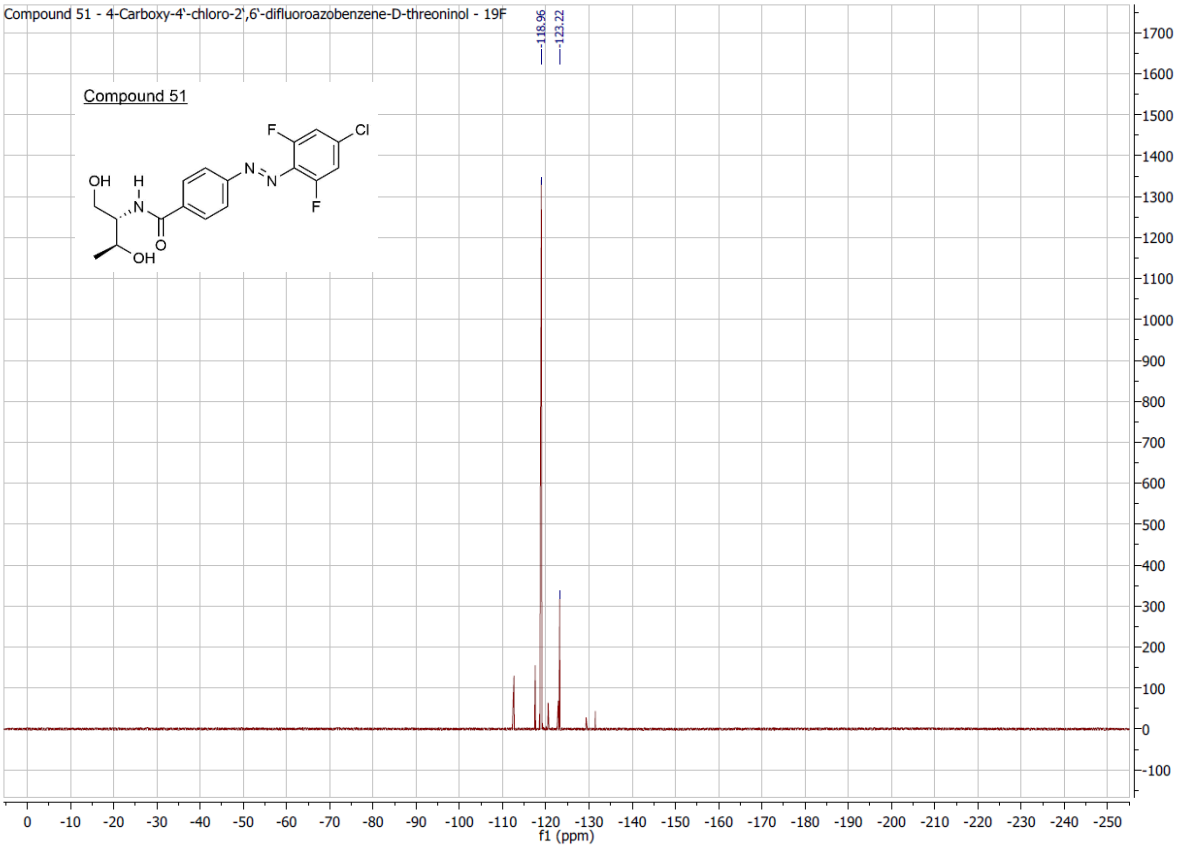
Compound 51 - 4-Carboxy-4'-chloro-2',6'-difluoroazobenzene-D-threoninol - 19F
-118.96
-123.22
Compound 51
F
Cl
OH
H
N
N
N
F
O
OH
f1 (ppm)

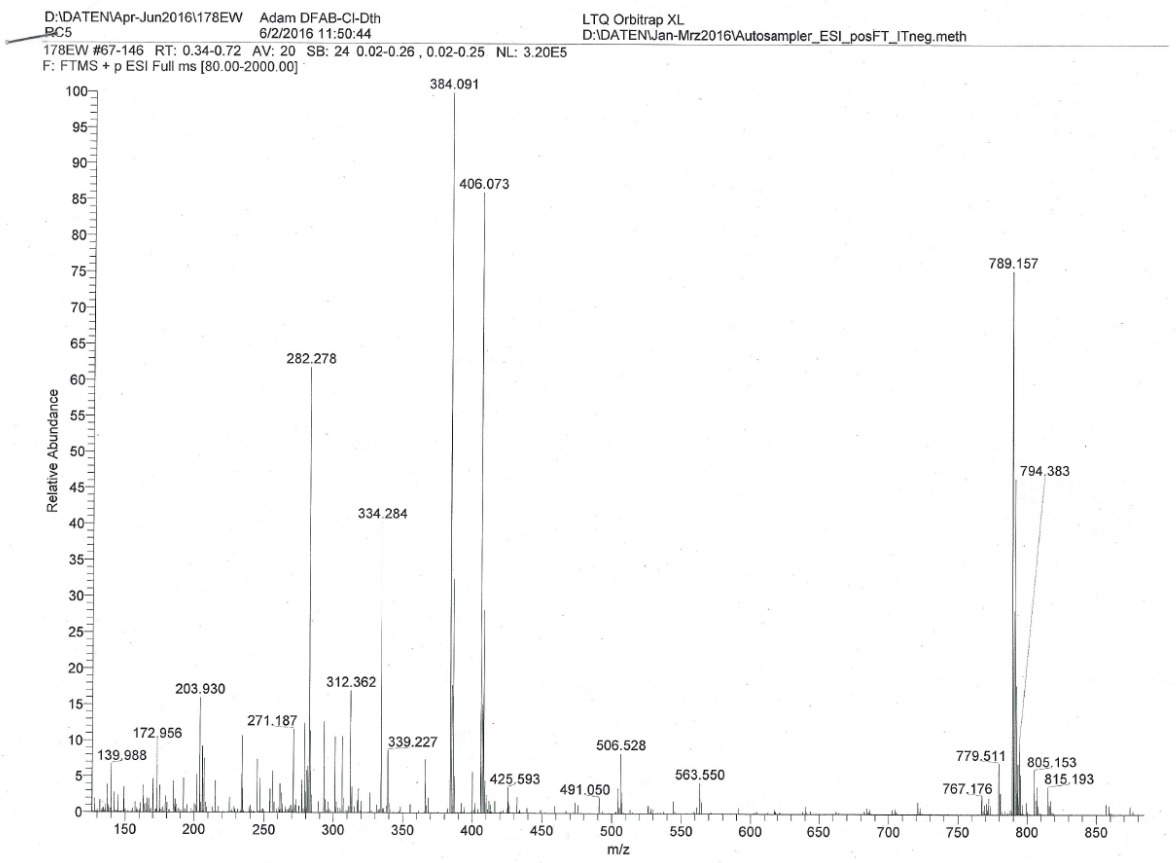
D:\DATEN\Apr-Jun2016\178EW Adam DFAB-Cl-Dth
RC5 6/2/2016 11:50:44
LTQ Orbitrap XL
D:\DATEN\Jan-Mrz2016\Autosampler_ESI_posFT_ITneg.meth
178EW #67-146 RT: 0.34-0.72 AV: 20 SB: 24 0.02-0.26 , 0.02-0.25 NL: 3.20E5
F: FTMS + p ESI Full ms [80.00-2000.00]
384.091
406.073
789.157
282.278
794.383
334.284
203.930
312.362
271.187
172.956
339.227
139.988
506.528
425.593
491.050
563.550
779.511
805.153
767.176
815.193
Relative Abundance
m/z

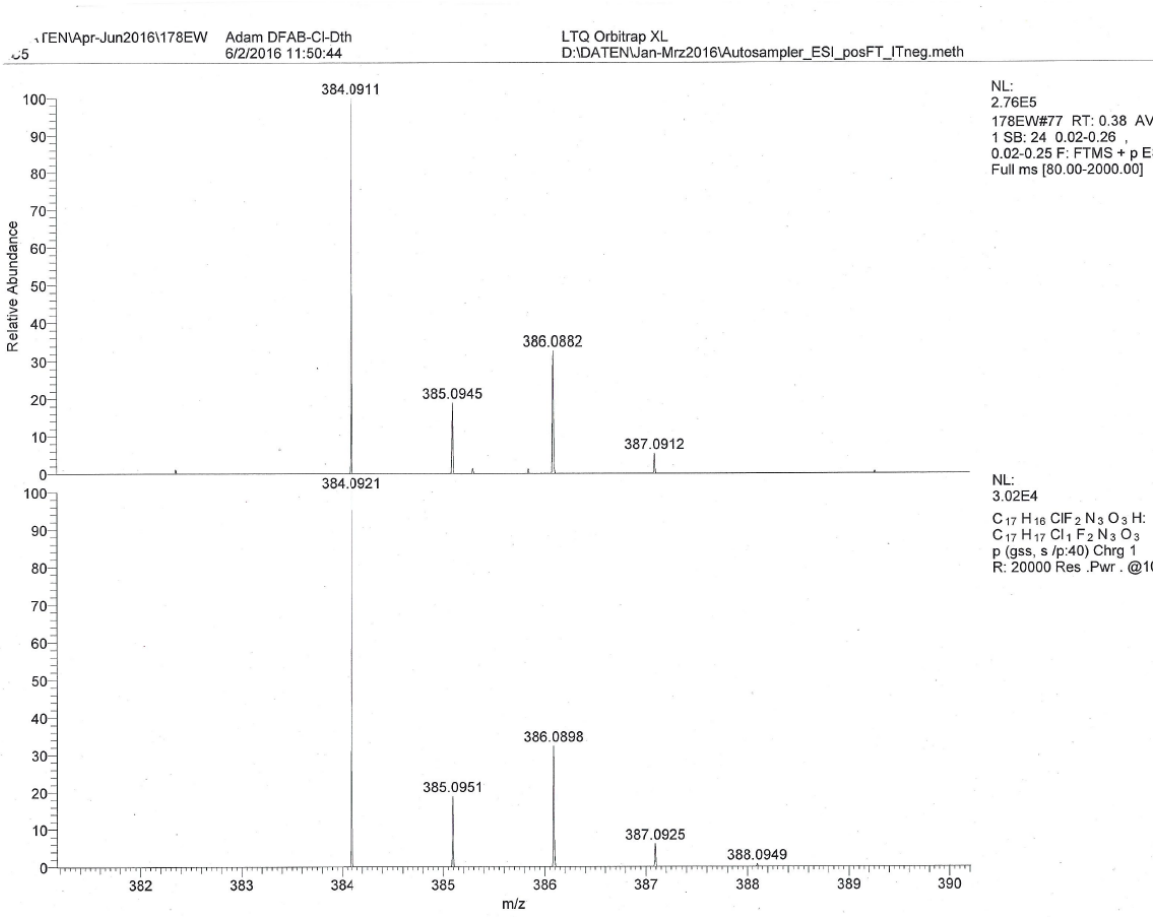
ATEN\Apr-Jun2016\178EW
Adam DFAB-Cl-Dth
6/2/2016 11:50:44
LTQ Orbitrap XL
D:\DATEN\Jan-Mrz2016\Autosampler_ESI_posFT_ITneg.meth
NL:
2.76E5
178EW#77 RT: 0.38 AV
1 SB: 24 0.02-0.26 ,
0.02-0.25 F: FTMS + p E
Full ms [80.00-2000.00]
384.0911
386.0882
385.0945
387.0912
Relative Abundance
NL:
3.02E4
C17 H16 ClF2 N3 O3 H:
C17 H17 Cl1 F2 N3 O3
p (gss, s /p:40) Chrg 1
R: 20000 Res .Pwr . @1
384.0921
386.0898
385.0951
387.0925
388.0949
m/z

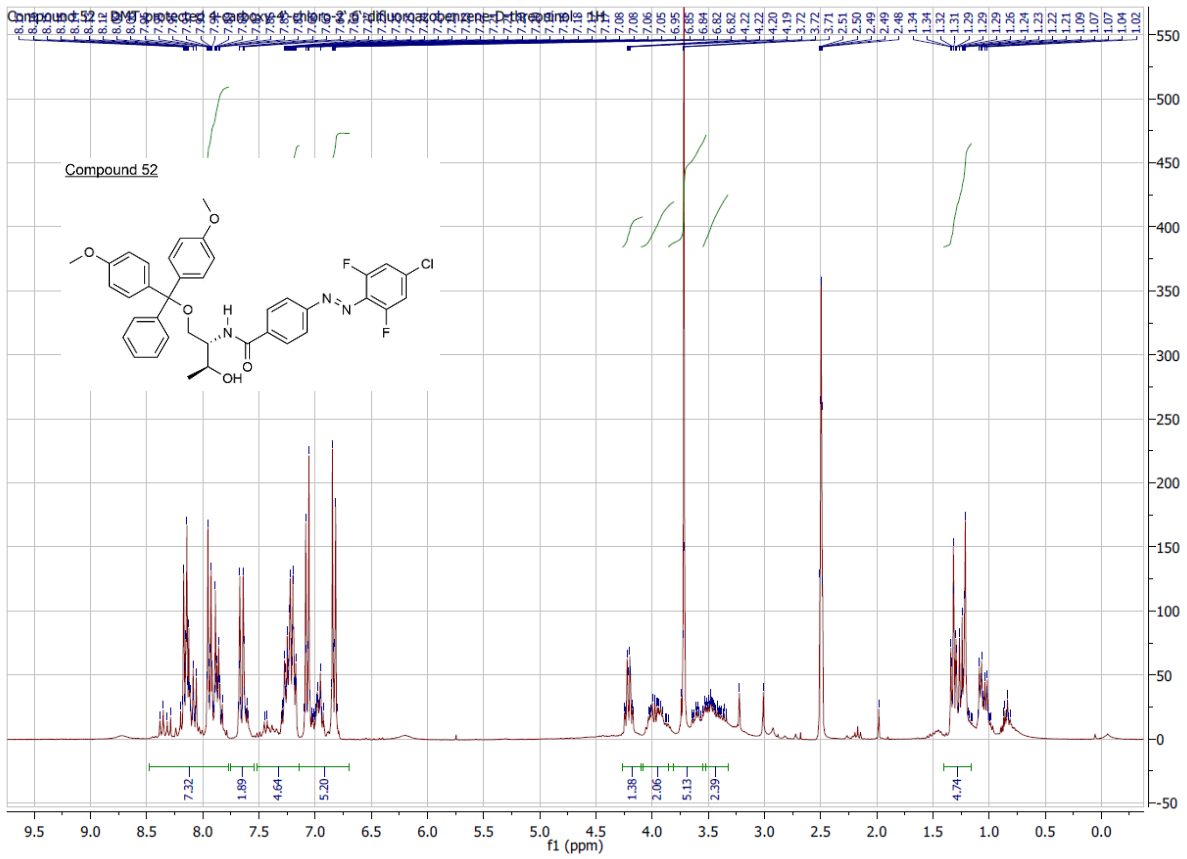
Compound 52
f1 (ppm)

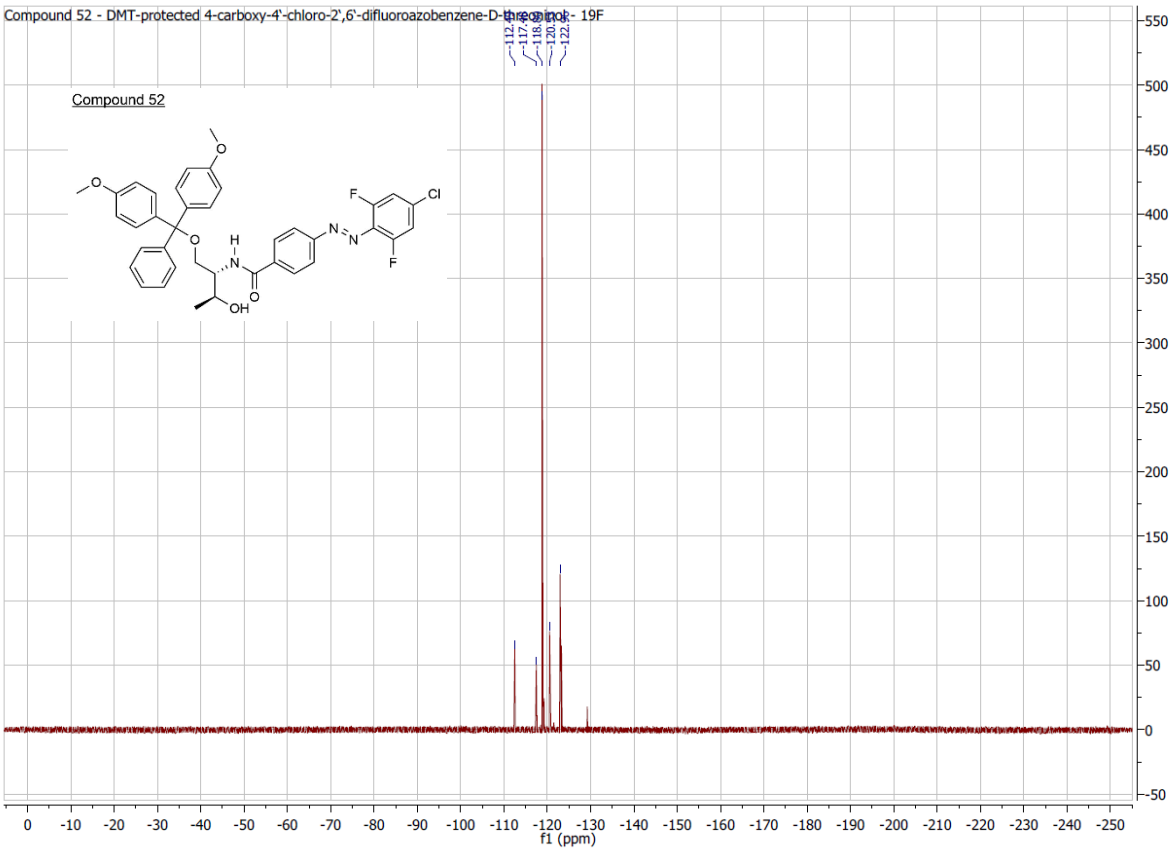
Compound 52 - DMT-protected 4-carboxy-4'-chloro-2',6'-difluoroazobenzene-D-threoninol - 19F
Compound 52
f1 (ppm)

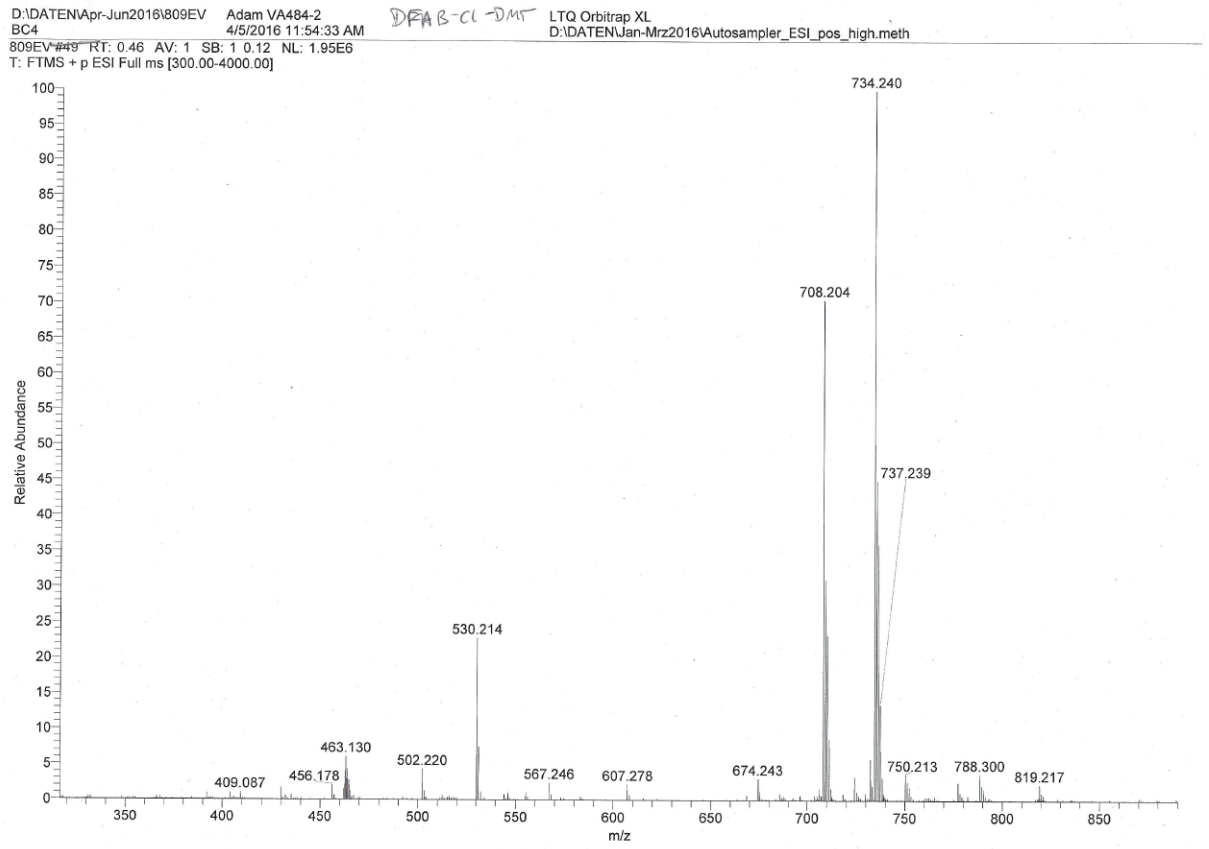
D:\DATEN\Apr-Jun2016\809EV Adam VA484-2
BC4 4/5/2016 11:54:33 AM
DFAB-Cl-DMT
LTQ Orbitrap XL
D:\DATEN\Jan-Mrz2016\Autosampler_ESI_pos_high.meth
809EV #49 RT: 0.46 AV: 1 SB: 1 0.12 NL: 1.95E6
T: FTMS + p ESI Full ms [300.00-4000.00]
Relative Abundance
m/z
734.240
708.204
737.239
530.214
463.130
502.220
409.087
456.178
567.246
607.278
674.243
750.213
788.300
819.217

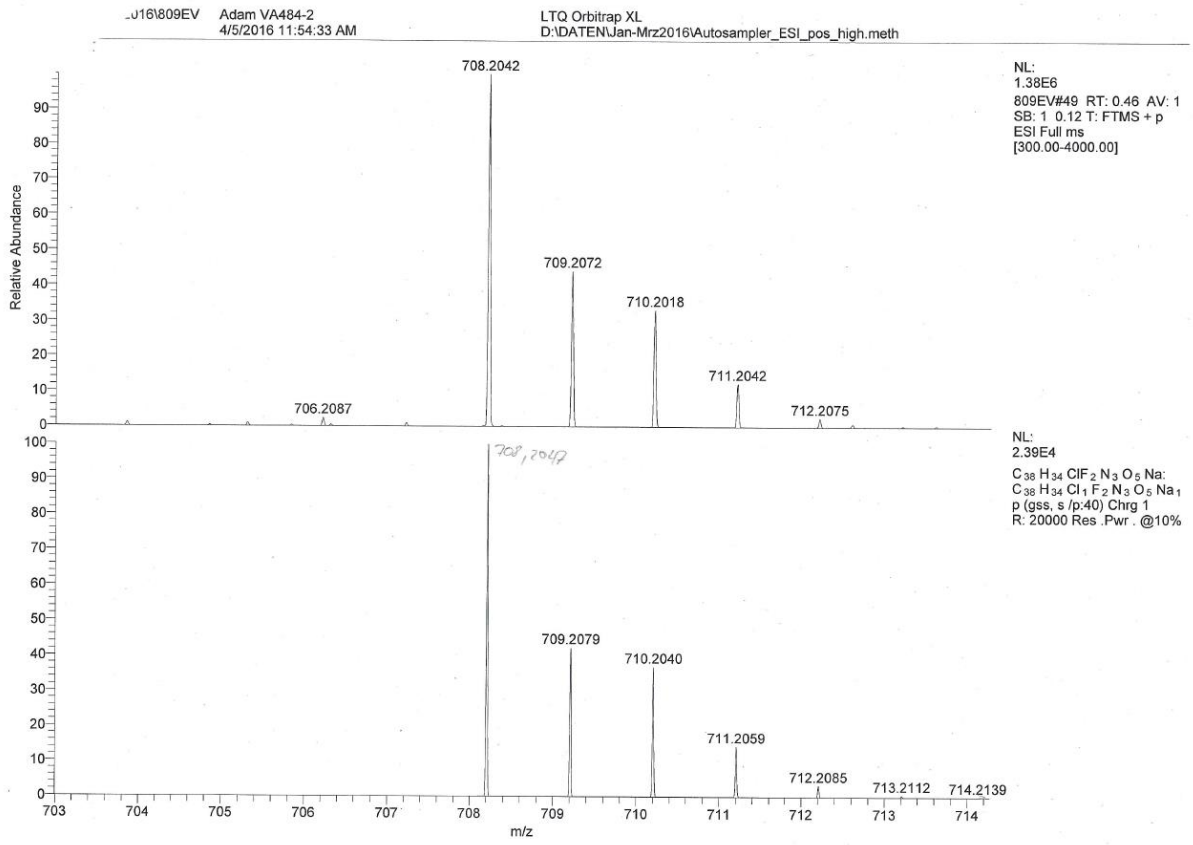
Adam VA484-2
4/5/2016 11:54:33 AM
LTQ Orbitrap XL
D:\DATEN\Jan-Mrz2016\Autosampler_ESI_pos_high.meth
NL:
1.38E6
809EV#49 RT: 0.46 AV: 1
SB: 1 0.12 T: FTMS + p
ESI Full ms
[300.00-4000.00]
708.2042
709.2072
710.2018
711.2042
706.2087
712.2075
NL:
2.39E4
C38 H34 ClF2 N3 O5 Na:
C38 H34 Cl1 F2 N3 O5 Na1
p (gss, s /p:40) Chrg 1
R: 20000 Res .Pwr . @10%
708.2042
709.2079
710.2040
711.2059
712.2085
713.2112
714.2139
Relative Abundance
m/z

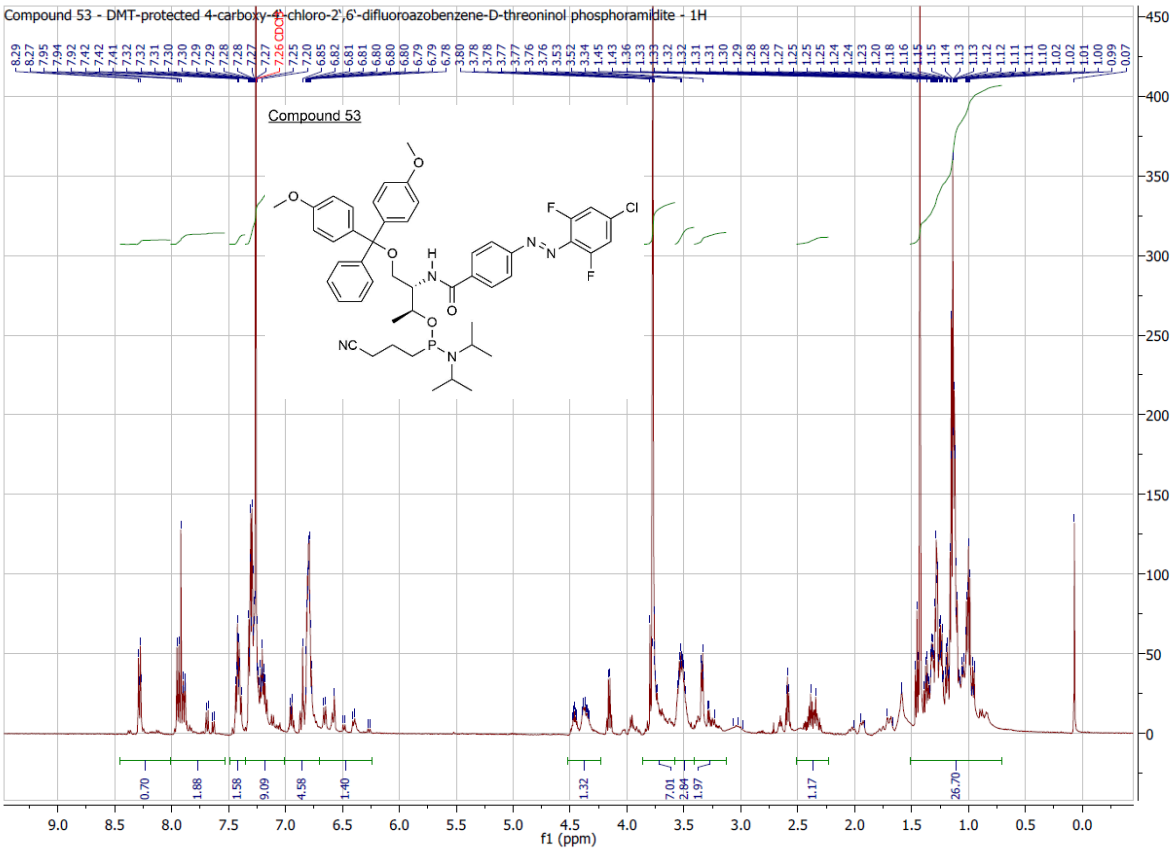
Compound 53 - DMT-protected 4-carboxy-4'-chloro-2',6'-difluoroazobenzene-D-threoninol phosphoramidite - 1H
Compound 53
f1 (ppm)

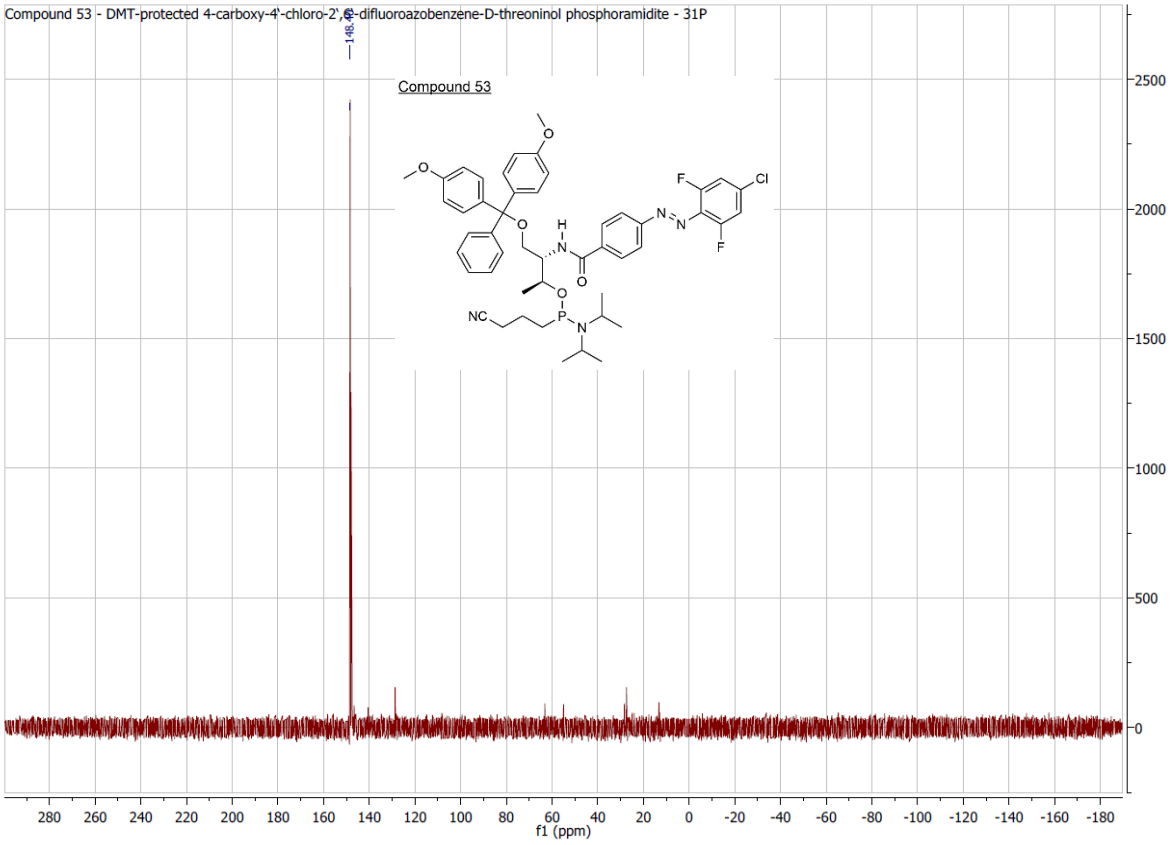
Compound 53 - DMT-protected 4-carboxy-4'-chloro-2',6'-difluoroazobenzene-D-threoninol phosphoramidite - 31P
Compound 53
f1 (ppm)

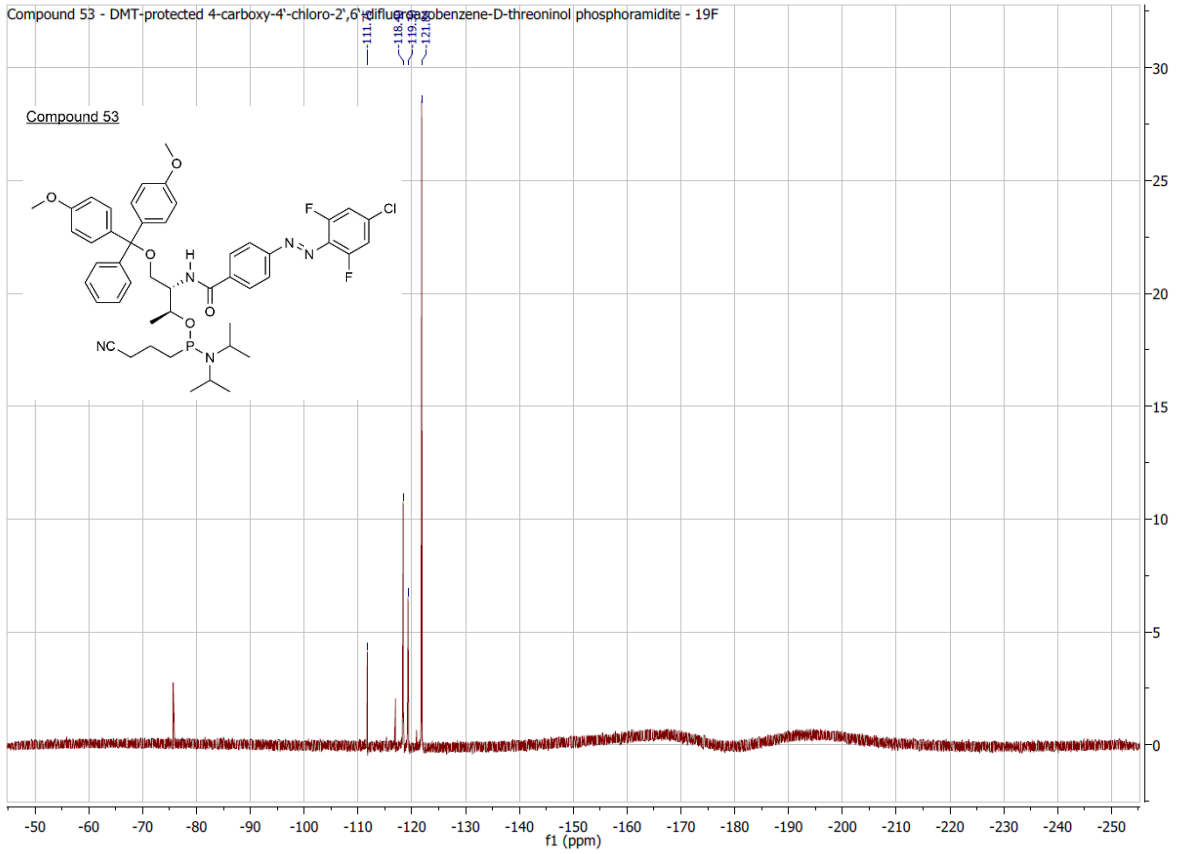
Compound 53 - DMT-protected 4-carboxy-4'-chloro-2',6'-difluoroazobenzene-D-threoninol phosphoramidite - 19F
Compound 53
f1 (ppm)

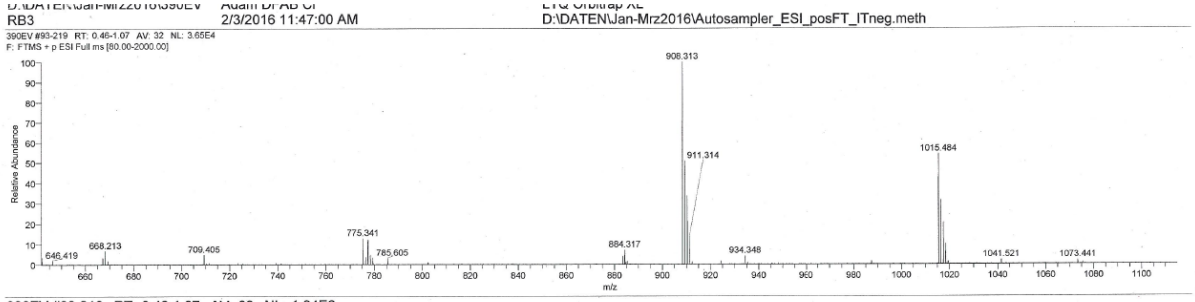
RB3
2/3/2016 11:47:00 AM
D:\DATEN\Jan-Mrz2016\Autosampler_ESI_posFT_ITneg.meth
Relative Abundance
m/z

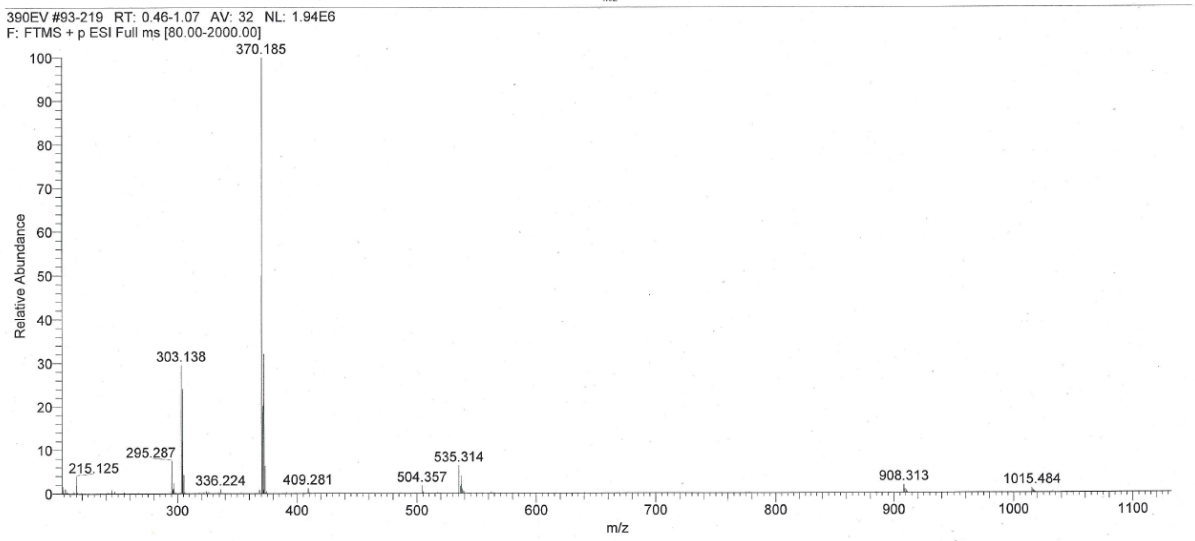
390EV #93-219 RT: 0.46-1.07 AV: 32 NL: 1.94E6
F: FTMS + p ESI Full ms [80.00-2000.00]
Relative Abundance
m/z

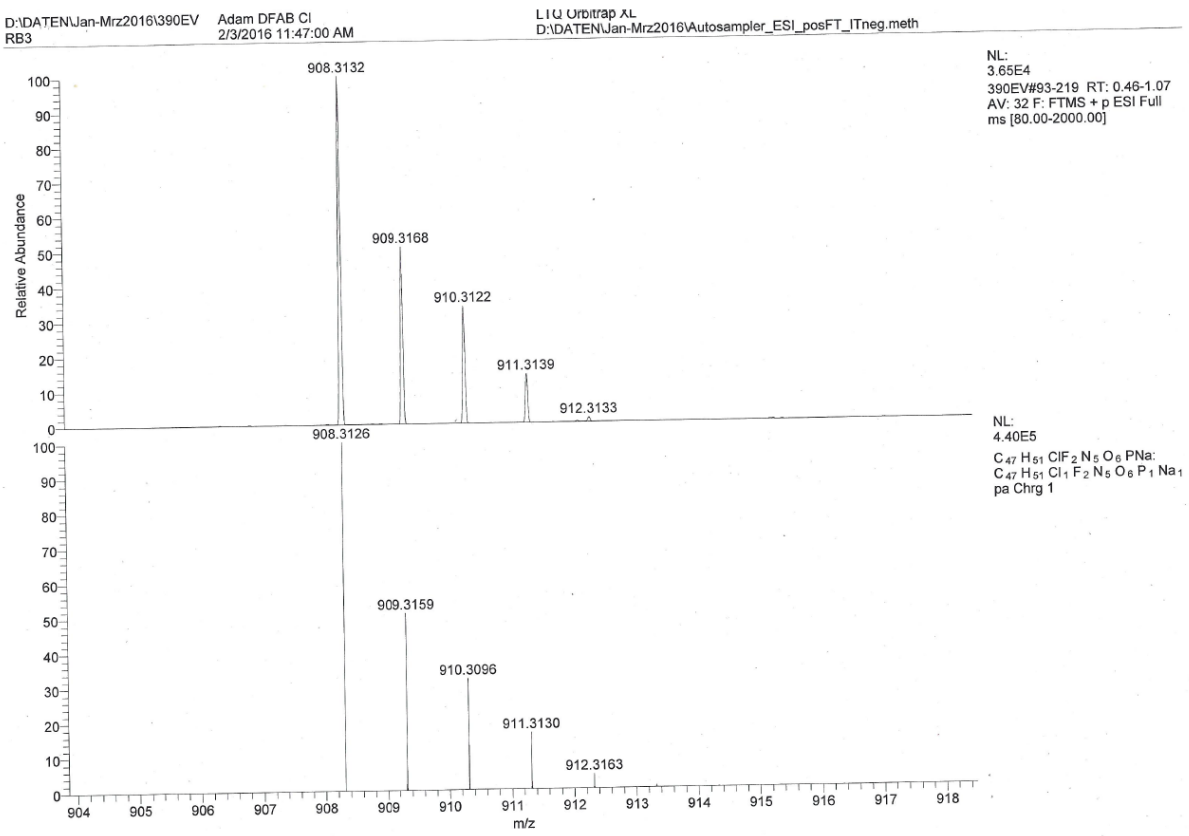
D:\DATEN\Jan-Mrz2016\390EV RB3
Adam DFAB Cl
2/3/2016 11:47:00 AM
LTQ Orbitrap XL
D:\DATEN\Jan-Mrz2016\Autosampler_ESI_posFT_ITneg.meth
NL:
3.65E4
390EV#93-219 RT: 0.46-1.07
AV: 32 F: FTMS + p ESI Full
ms [80.00-2000.00]
908.3132
909.3168
910.3122
911.3139
912.3133
Relative Abundance
NL:
4.40E5
C47 H51 ClF2 N5 O6 PNa:
C47 H51 Cl1 F2 N5 O6 P1 Na1
pa Chrg 1
908.3126
909.3159
910.3096
911.3130
912.3163
m/z

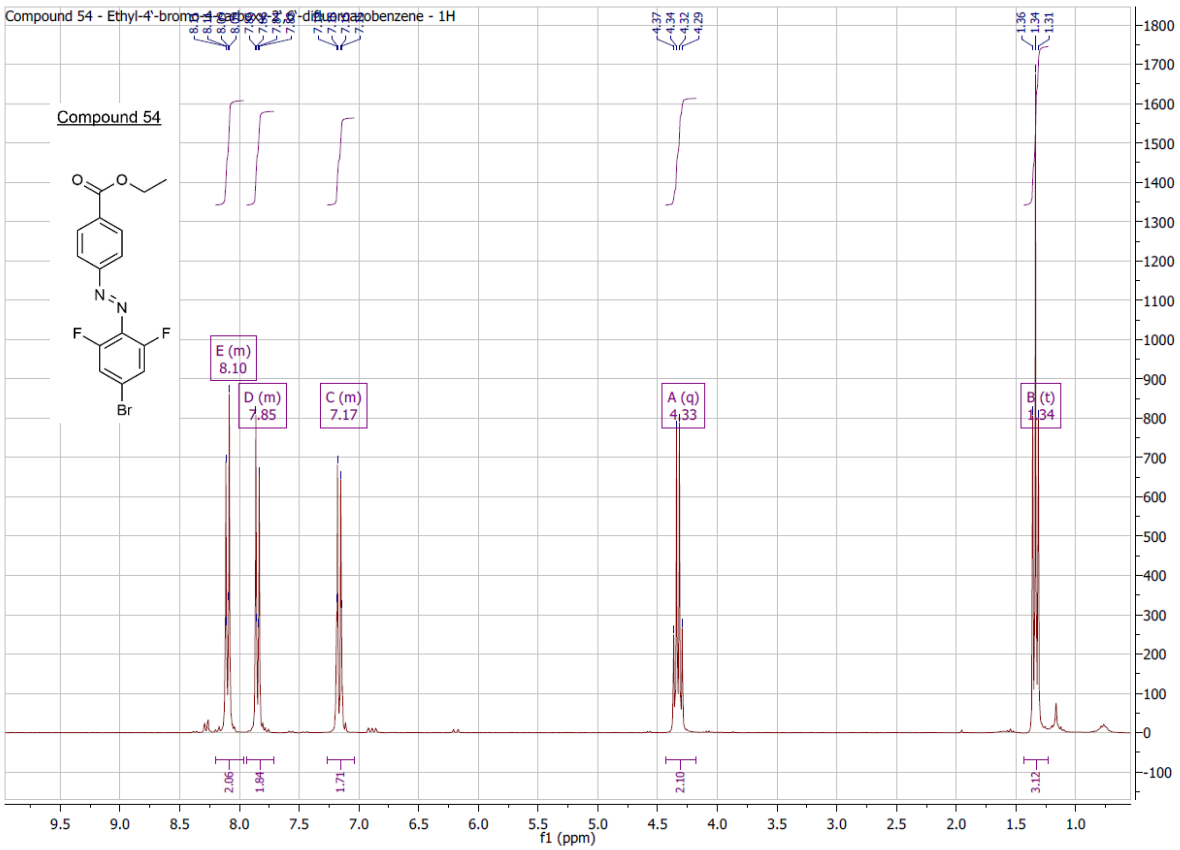
Compound 54 - Ethyl-4'-bromo-4-carboxy-2',6'-difluoroazobenzene - 1H
Compound 54
E (m)
8.10
D (m)
7.85
C (m)
7.17
A (q)
4.33
B (t)
1.34
f1 (ppm)

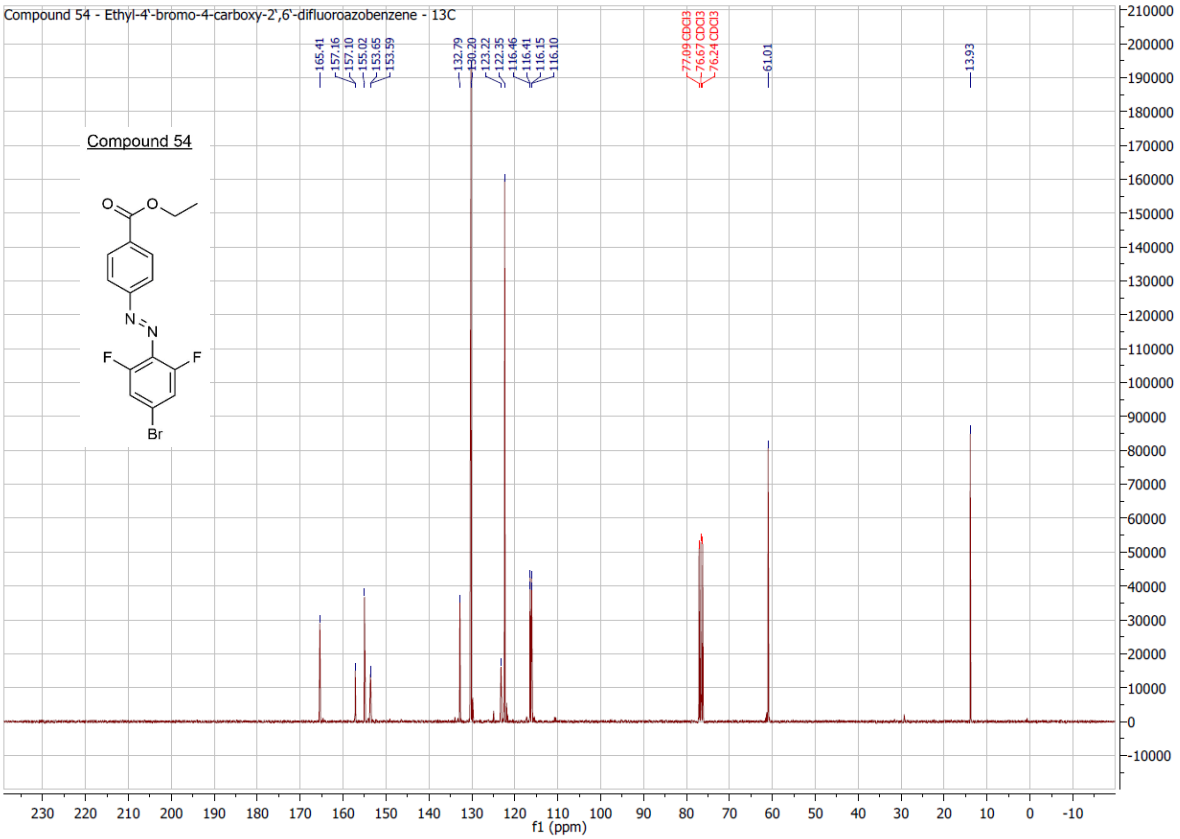
Compound 54 - Ethyl-4'-bromo-4-carboxy-2',6'-difluoroazobenzene - 13C
Compound 54
f1 (ppm)

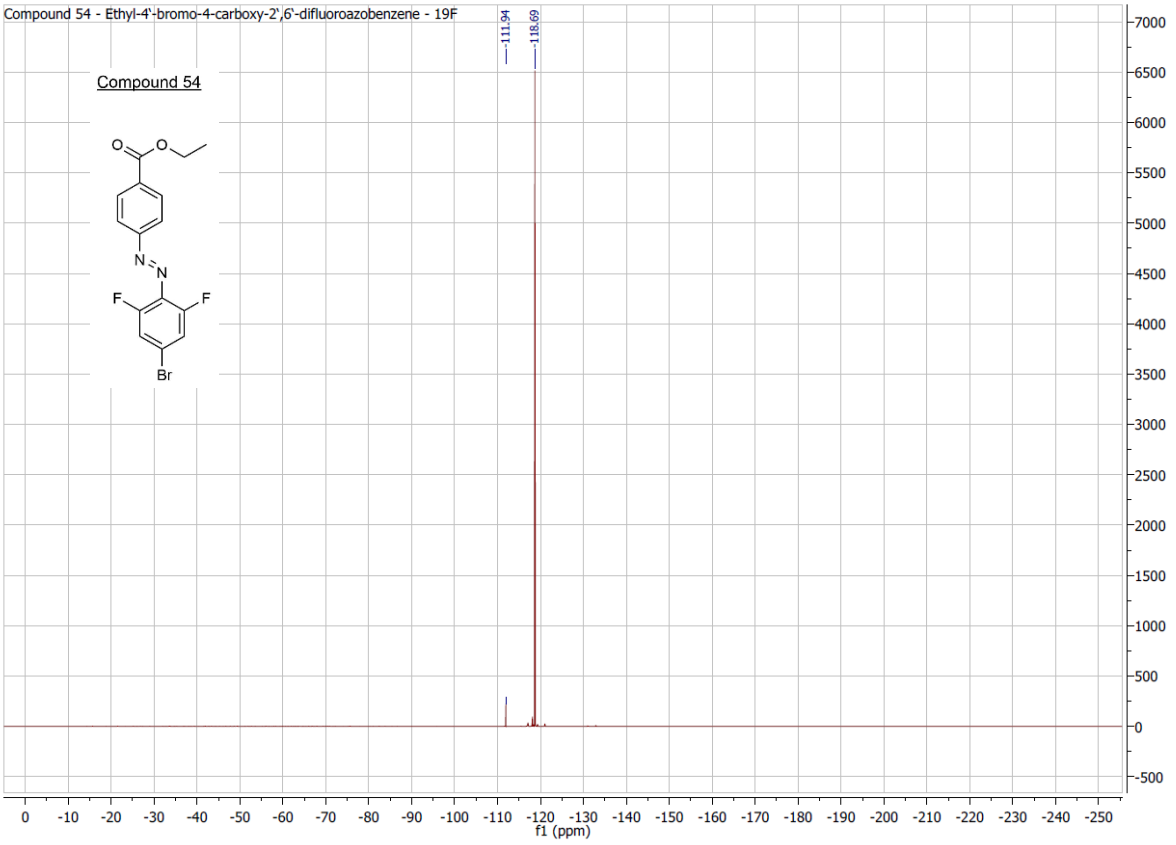
Compound 54 - Ethyl-4'-bromo-4-carboxy-2',6'-difluoroazobenzene - 19F
111.94
118.69
Compound 54
O
O
N
N
F
F
Br
7000
6500
6000
5500
5000
4500
4000
3500
3000
2500
2000
1500
1000
500
0
-500
0 -10 -20 -30 -40 -50 -60 -70 -80 -90 -100 -110 -120 -130 -140 -150 -160 -170 -180 -190 -200 -210 -220 -230 -240 -250
f1 (ppm)

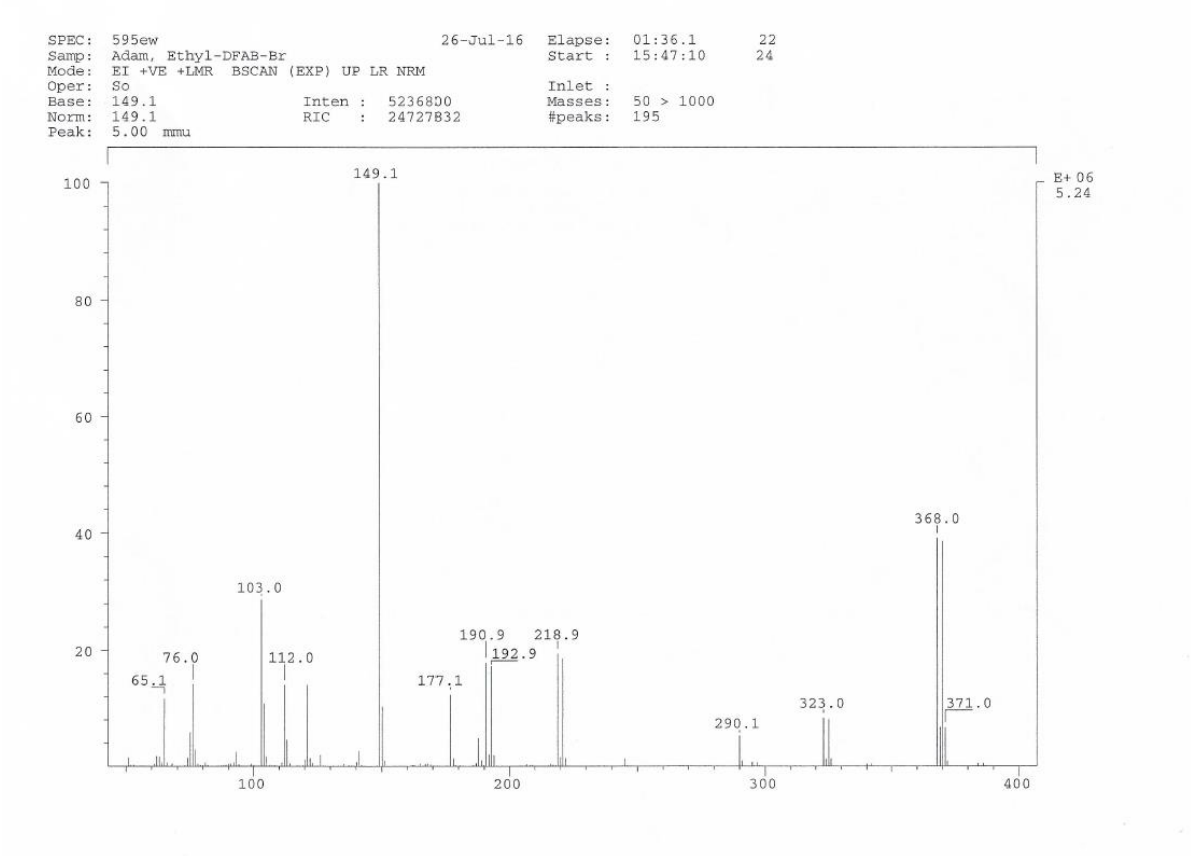
SPEC: 595ew 26-Jul-16 Elapse: 01:36.1 22
Samp: Adam, Ethyl-DFAB-Br Start : 15:47:10 24
Mode: EI +VE +LMR BSCAN (EXP) UP LR NRM
Oper: So Inlet :
Base: 149.1 Inten : 52368D0 Masses: 50 > 1000
Norm: 149.1 RIC : 24727832 #peaks: 195
Peak: 5.00 mmu
E+06
5.24
100
80
60
40
20
149.1
368.0
103.0
190.9
218.9
192.9
76.0
112.0
65.1
177.1
323.0
371.0
290.1
100
200
300
400

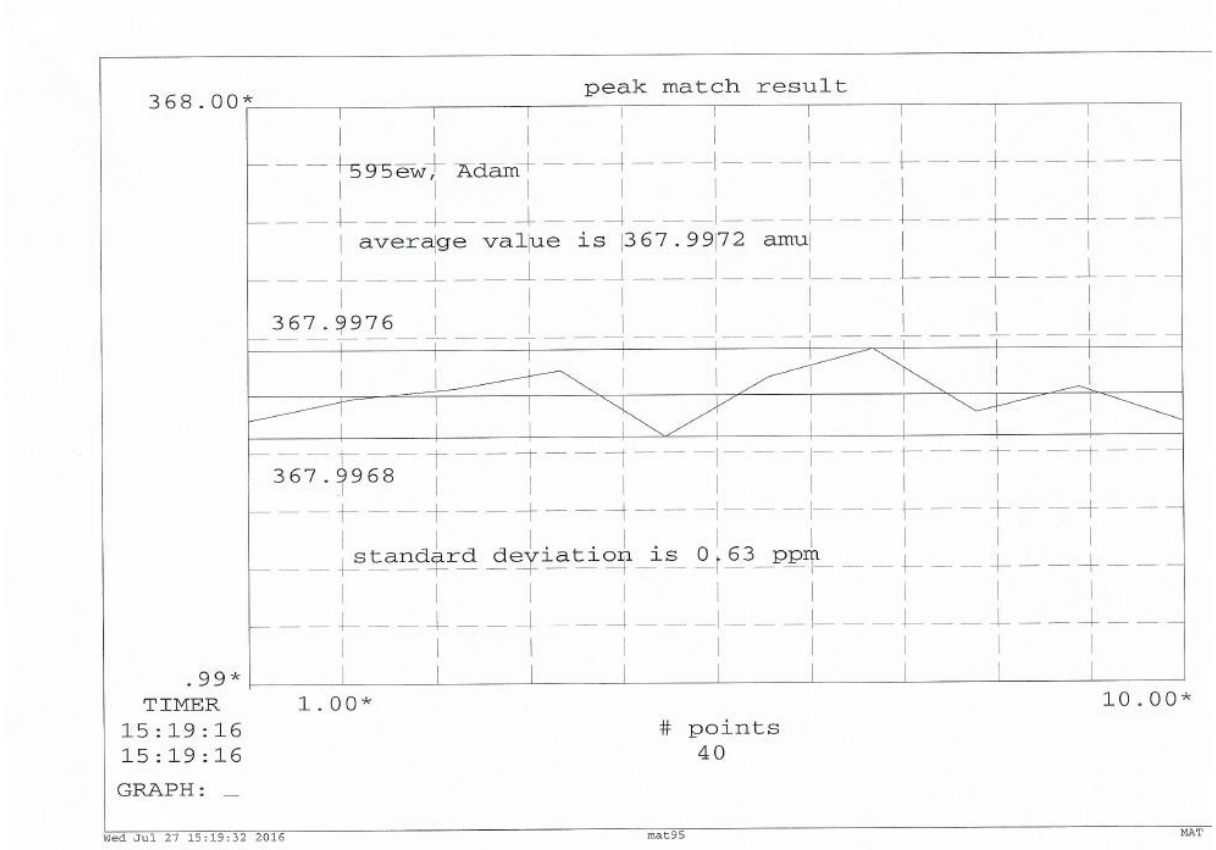
peak match result
368.00*
595ew, Adam
average value is 367.9972 amu
367.9976
367.9968
standard deviation is 0.63 ppm
.99*
TIMER
15:19:16
15:19:16
1.00*
10.00*
points
40
GRAPH: _
Wed Jul 27 15:19:32 2016
mat95
MAT

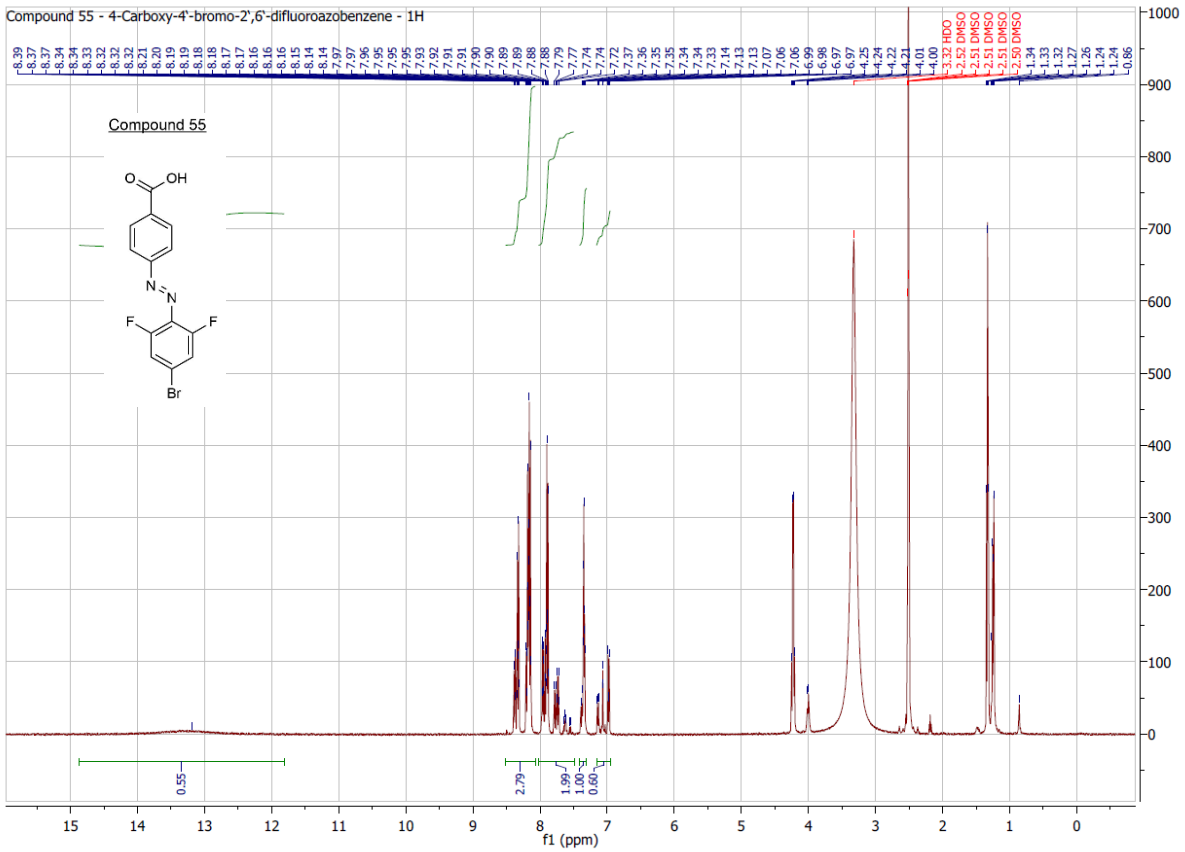
Compound 55 - 4-Carboxy-4'-bromo-2',6'-difluoroazobenzene - 1H
Compound 55
f1 (ppm)

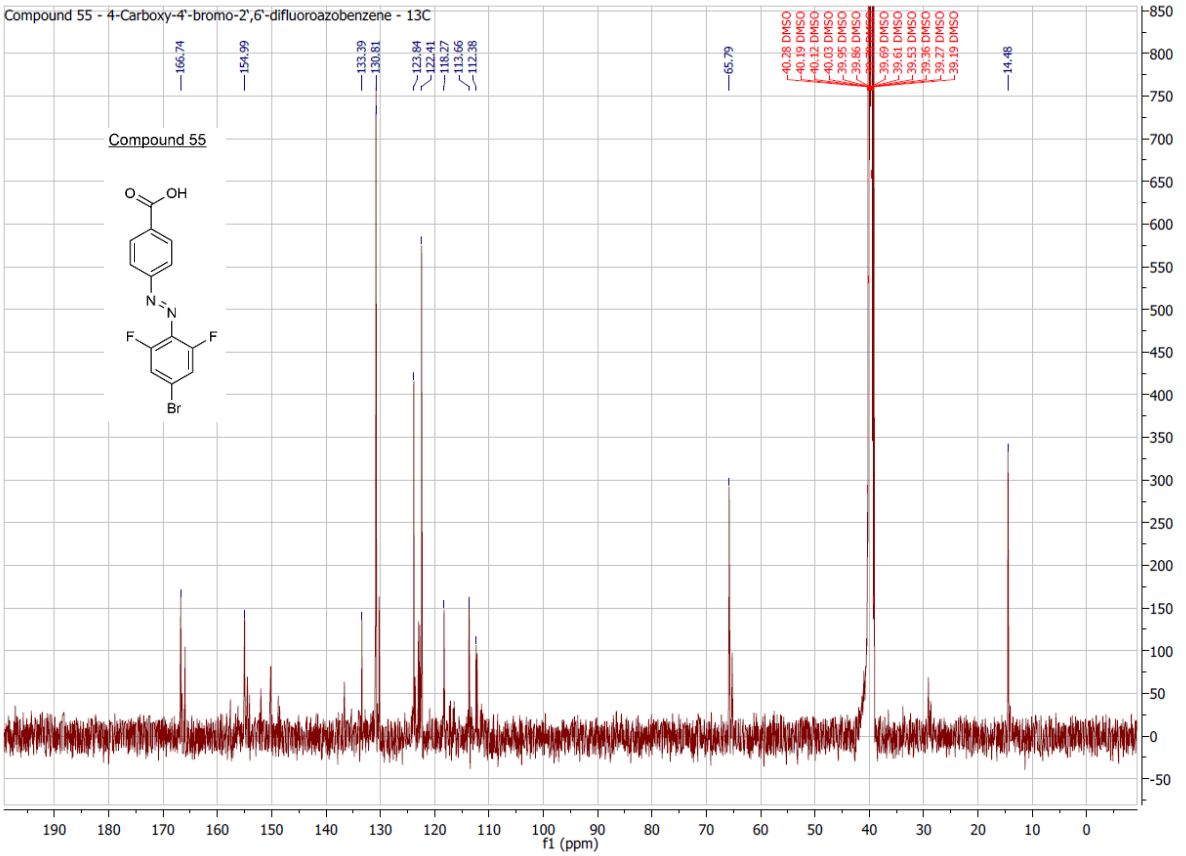
Compound 55 - 4-Carboxy-4'-bromo-2',6'-difluoroazobenzene - 13C
Compound 55
f1 (ppm)

150°C

SPEC: 008ex 22-Aug-16 Elapse: 03:13.4 45
Samp: Adam, DFAB-Br-Acid Start : 13:27:07 56
Mode: EI +VE +LMR BSCAN (EXP) UP LR NRM
Oper: So Inlet :
Base: 121.0 Inten : 309788 Masses: 50 > 1000
Norm: 121.0 RIC : 9969024 #peaks: 832
Peak: 5.00 mmu

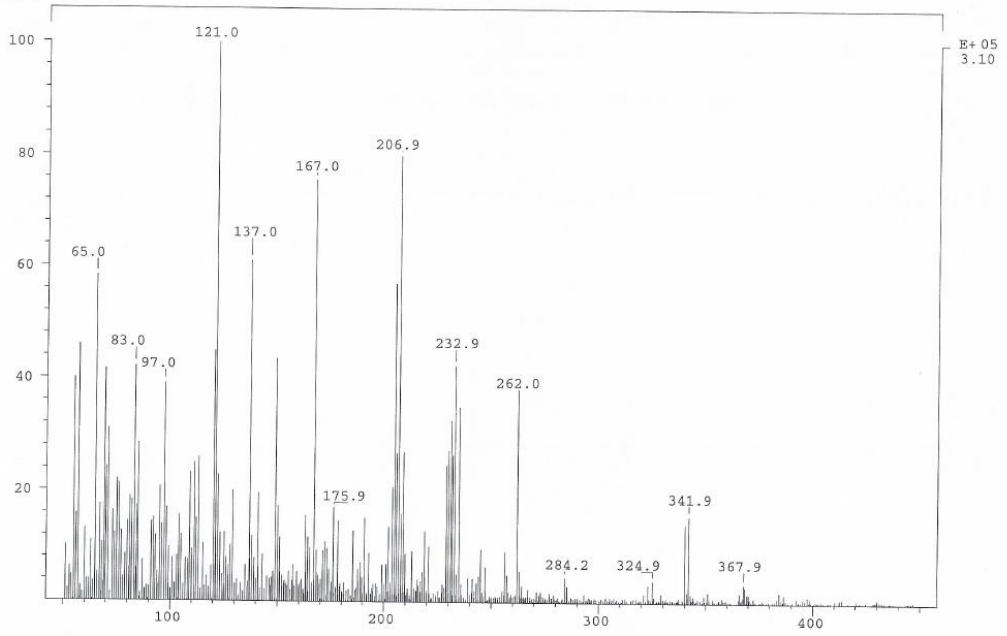

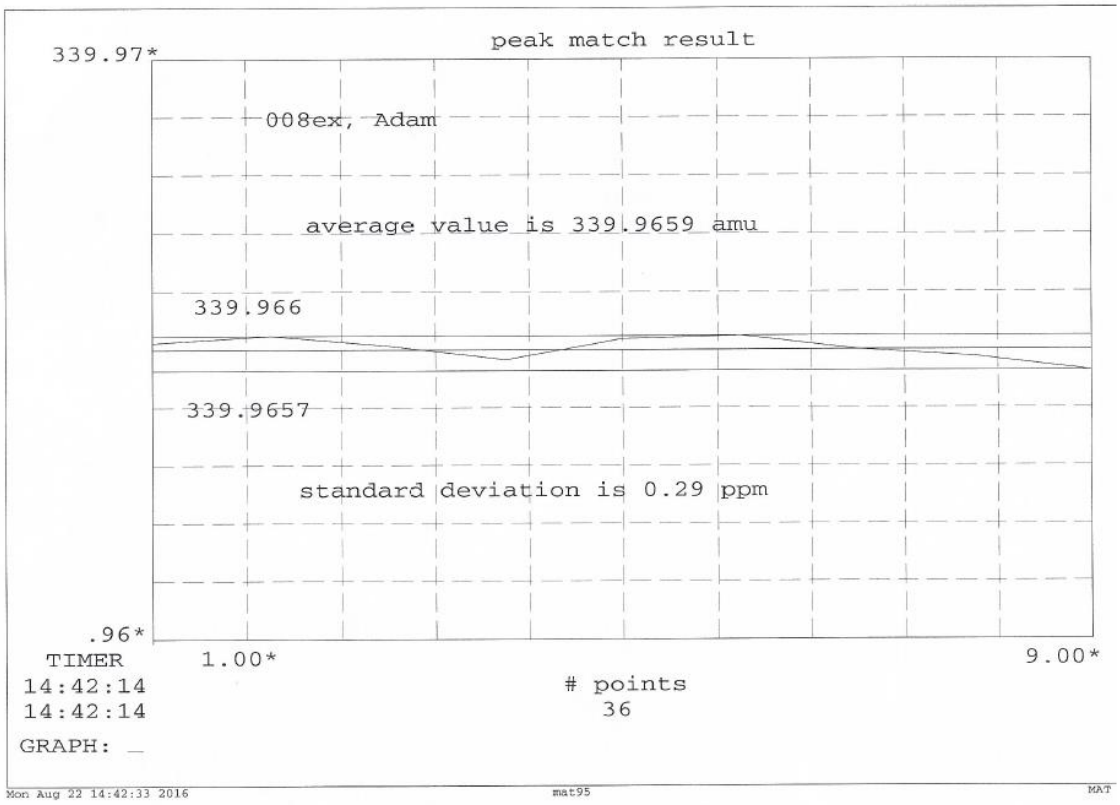

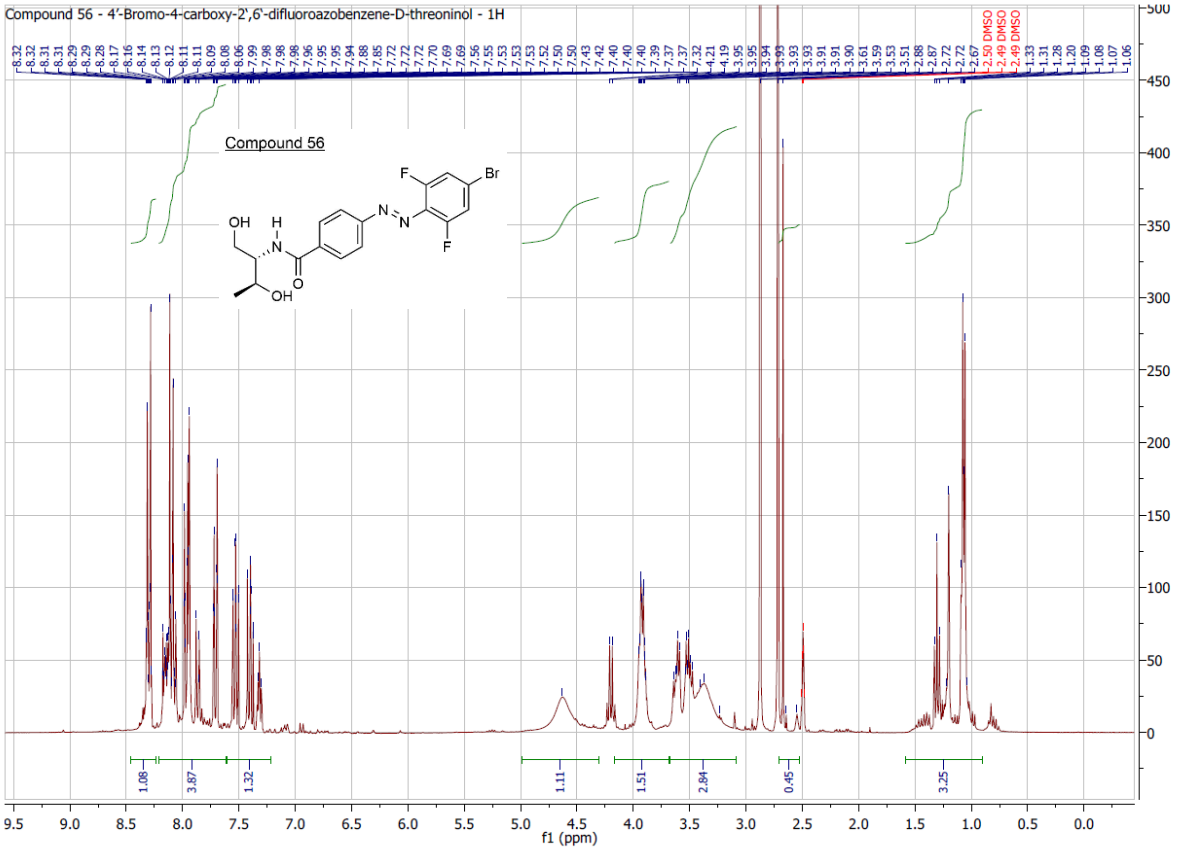
Compound 56 - 4'-Bromo-4-carboxy-2',6'-difluoroazobenzene-D-threoninol - 1H
Compound 56
f1 (ppm)

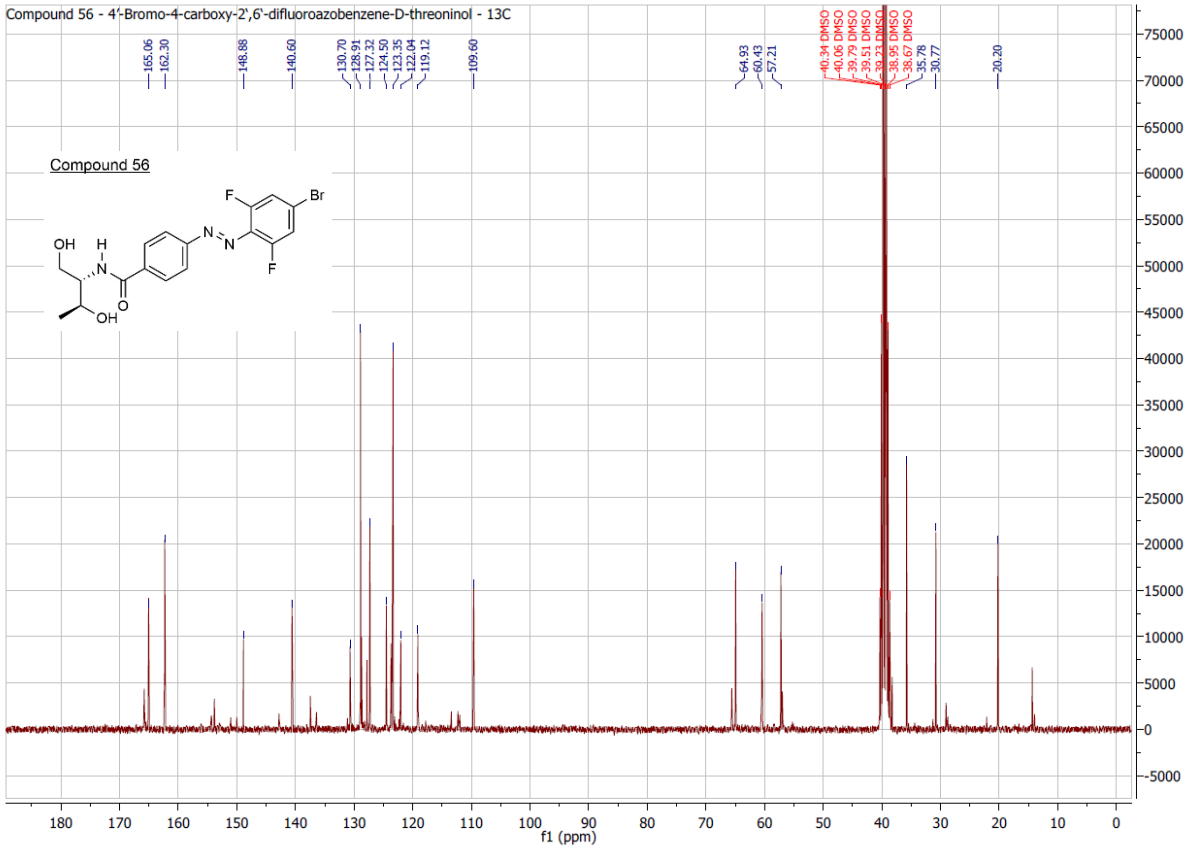
Compound 56 - 4'-Bromo-4-carboxy-2',6'-difluoroazobenzene-D-threoninol - 13C
Compound 56
f1 (ppm)

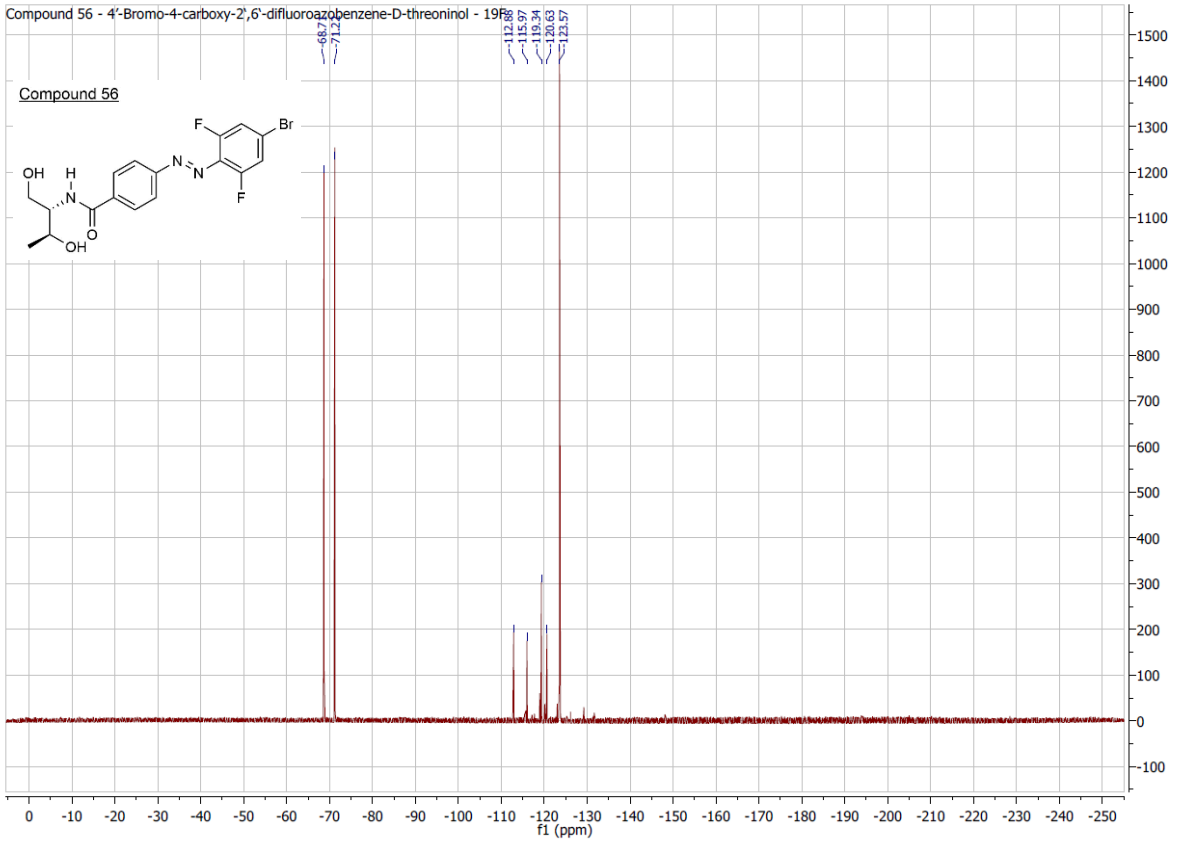
Compound 56 - 4'-Bromo-4-carboxy-2',6'-difluoroazobenzene-D-threoninol - 19F
Compound 56
68.7
71.22
112.88
115.97
119.34
120.63
123.57
f1 (ppm)

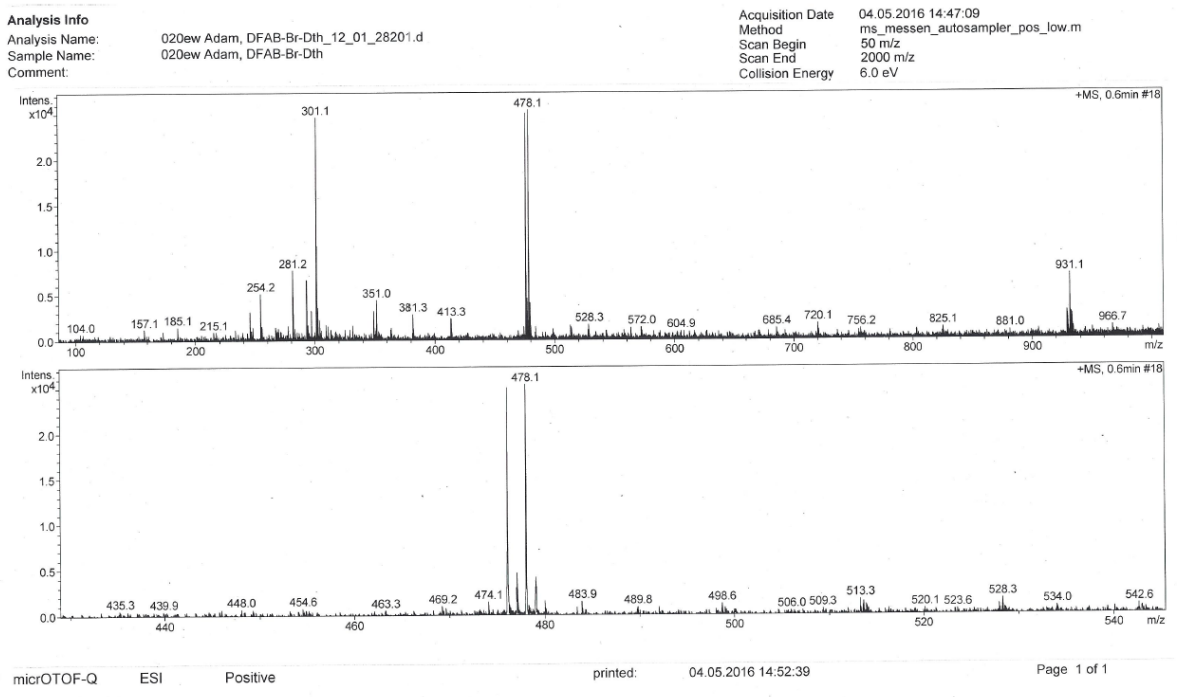
Analysis Info
Analysis Name: 020ew Adam, DFAB-Br-Dth_12_01_28201.d
Sample Name: 020ew Adam, DFAB-Br-Dth
Comment:
Acquisition Date 04.05.2016 14:47:09
Method ms_messen_autosampler_pos_low.m
Scan Begin 50 m/z
Scan End 2000 m/z
Collision Energy 6.0 eV
+MS, 0.6min #18
478.1
301.1
281.2
254.2
351.0
931.1
m/z
micrOTOF-Q ESI Positive
printed: 04.05.2016 14:52:39
Page 1 of 1

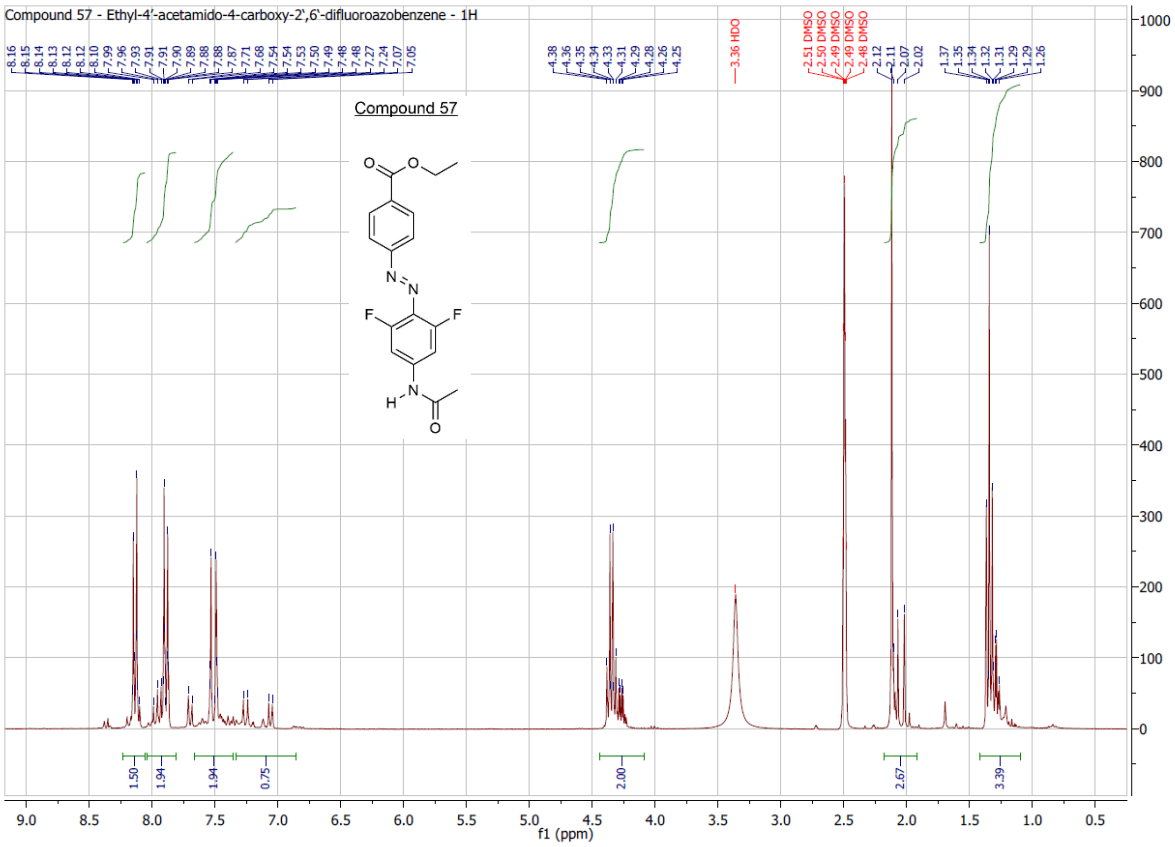
Compound 57 - Ethyl-4'-acetamido-4-carboxy-2',6'-difluoroazobenzene - 1H
Compound 57
3.36 HDO
2.51 DMSO
2.50 DMSO
2.49 DMSO
2.48 DMSO
f1 (ppm)

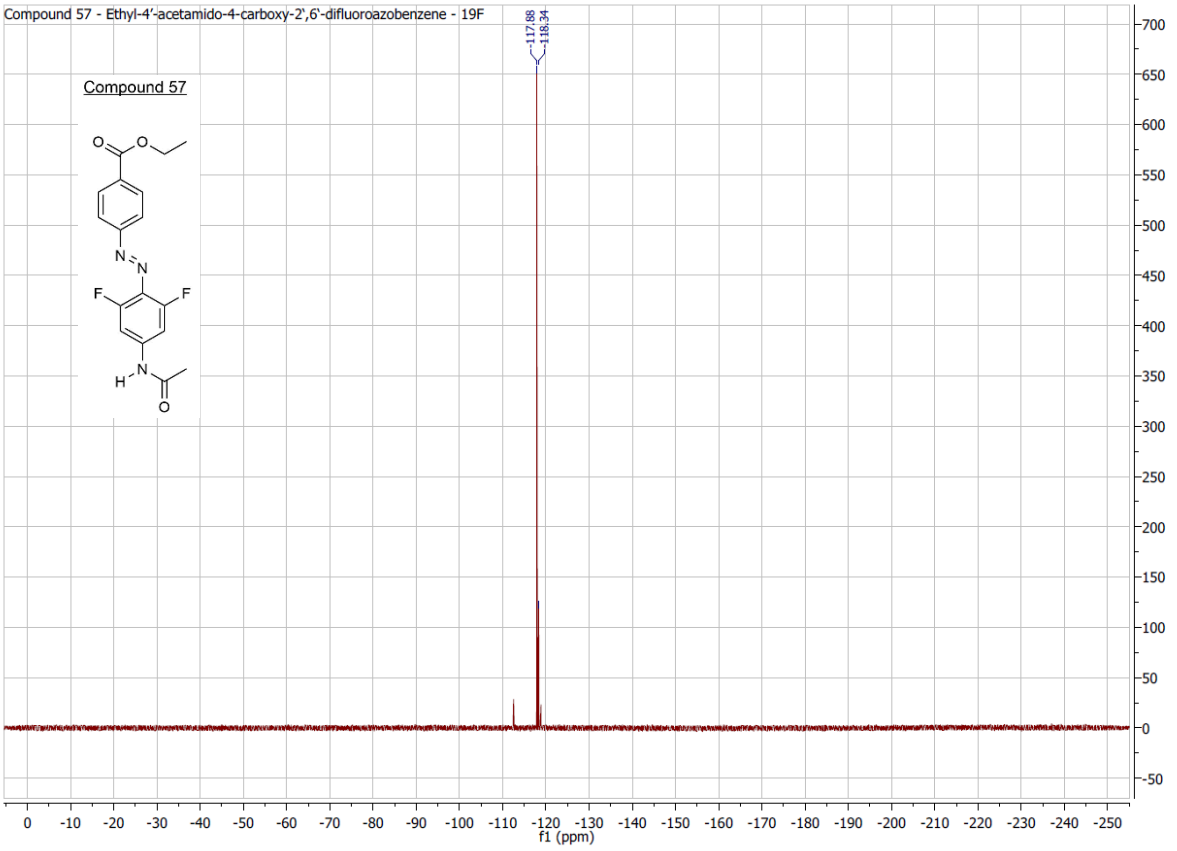
Compound 57 - Ethyl-4'-acetamido-4-carboxy-2',6'-difluoroazobenzene - 19F
Compound 57
-117.88
-118.34
f1 (ppm)

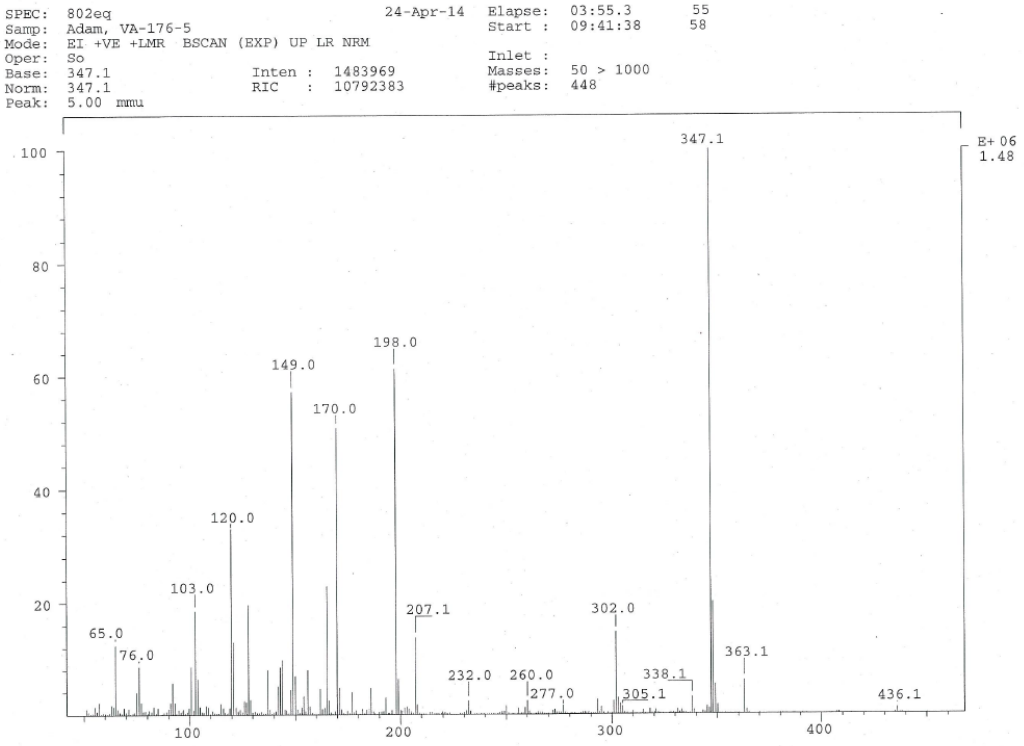
SPEC: 802eq 24-Apr-14 Elapse: 03:55.3 55
Samp: Adam, VA-176-5 Start : 09:41:38 58
Mode: EI +VE +LMR BSCAN (EXP) UP LR NRM
Oper: So Inlet :
Base: 347.1 Inten : 1483969 Masses: 50 > 1000
Norm: 347.1 RIC : 10792383 #peaks: 448
Peak: 5.00 mmu
E+ 06
1.48
347.1
198.0
149.0
170.0
120.0
103.0
207.1
302.0
65.0
76.0
363.1
232.0
260.0
338.1
277.0
305.1
436.1
100
80
60
40
20
100
200
300
400

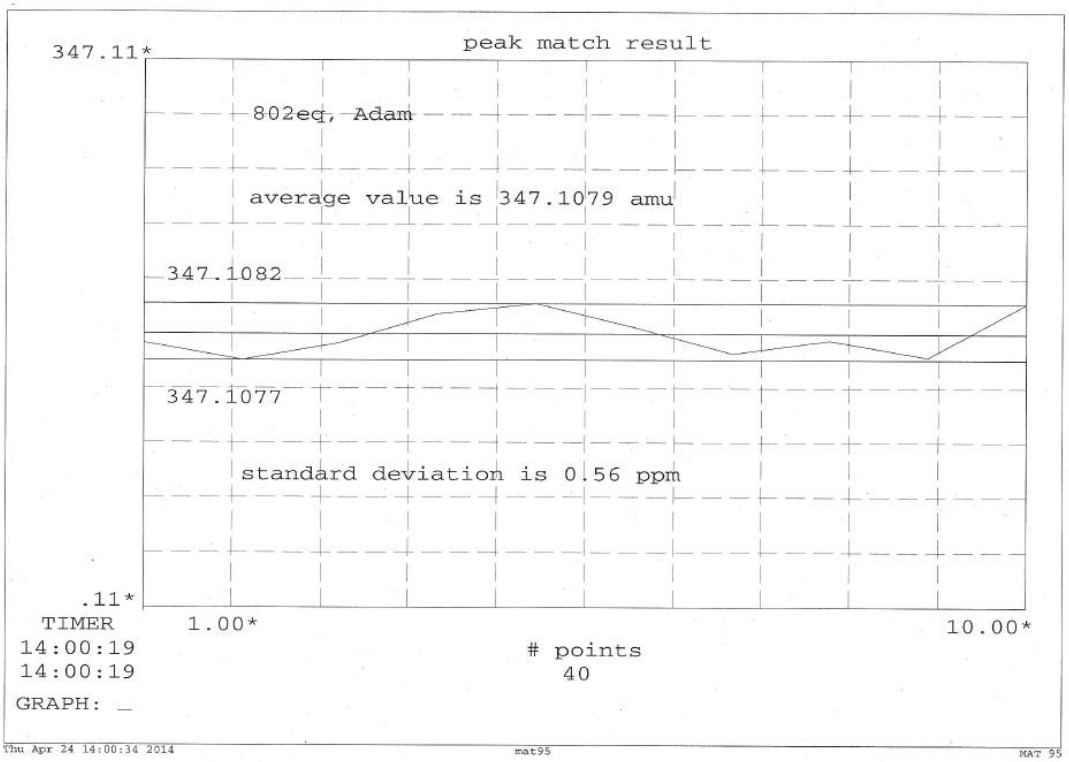
peak match result
347.11*
802eq, Adam
average value is 347.1079 amu
347.1082
347.1077
standard deviation is 0.56 ppm
.11*
TIMER
14:00:19
14:00:19
GRAPH: _
1.00*
10.00*
points
40
Thu Apr 24 14:00:34 2014
mat95
MAT 95

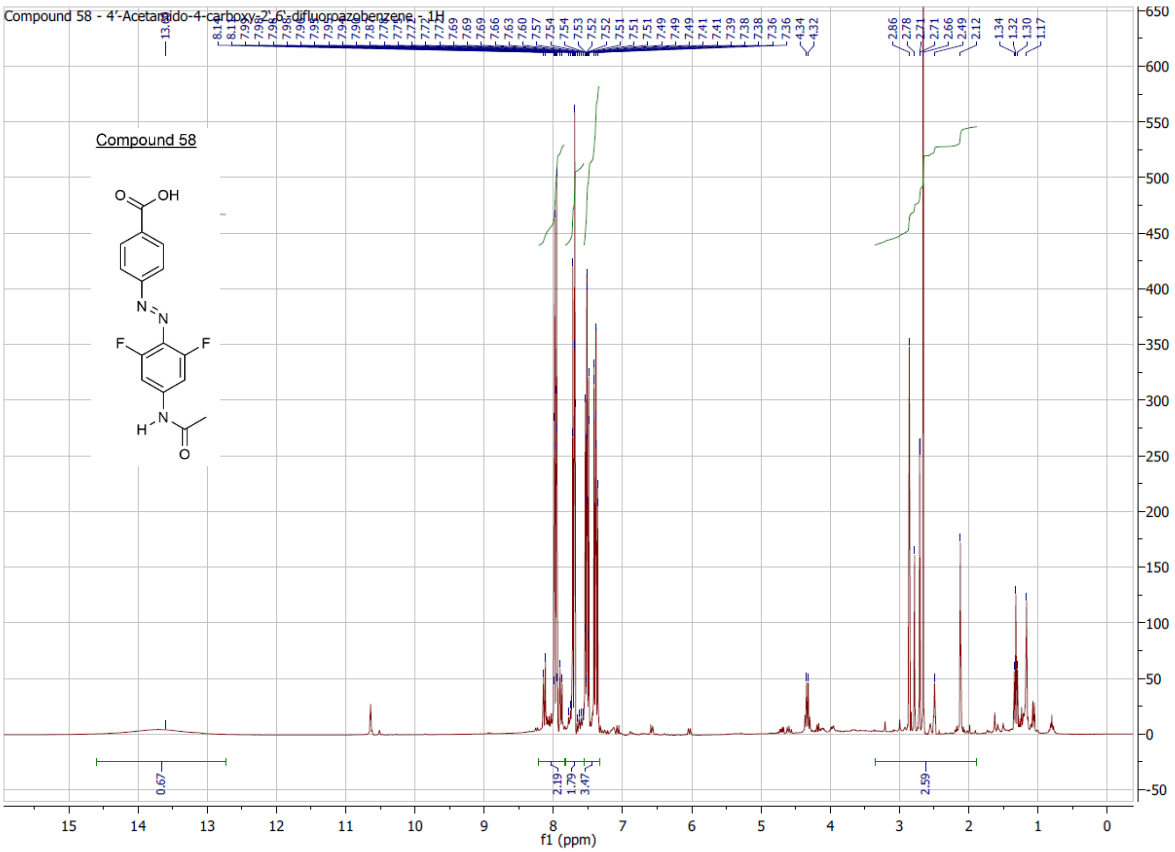
Compound 58 - 4'-Acetamido-4-carboxy-2',6'-difluoroazobenzene - 1H
Compound 58
f1 (ppm)

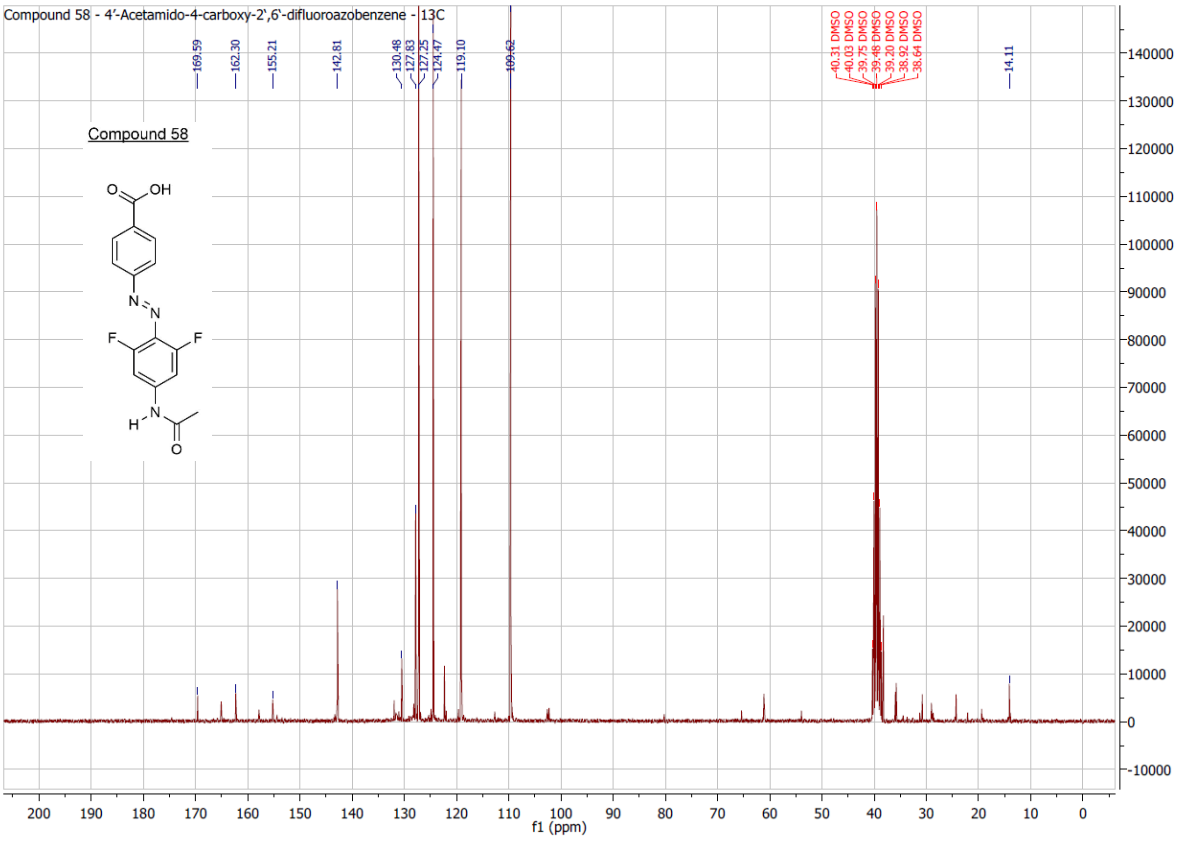
Compound 58 - 4'-Acetamido-4-carboxy-2',6'-difluoroazobenzene - 13C
Compound 58
f1 (ppm)

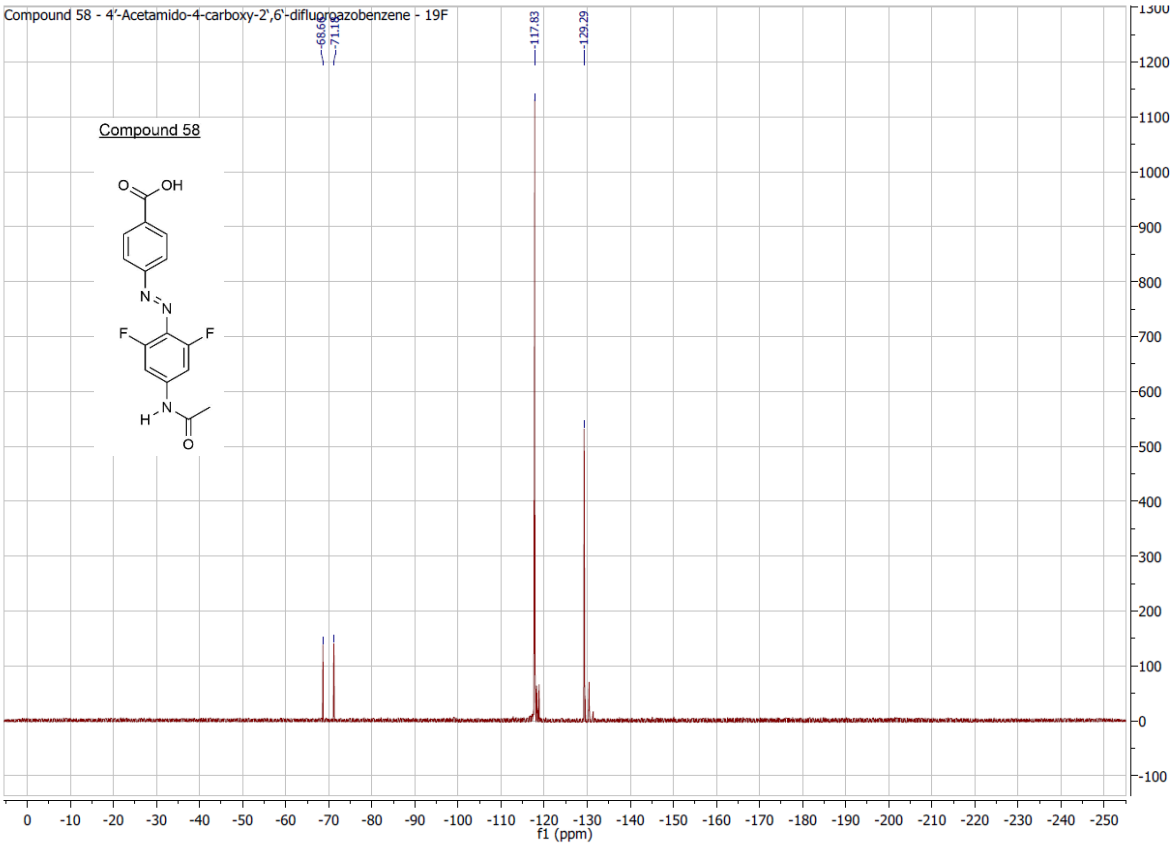
Compound 58 - 4′-Acetamido-4-carboxy-2′,6′-difluoroazobenzene - 19F
-66.66
-71.16
-117.83
-129.29
Compound 58
O
OH
N
N
F
F
H
N
O
f1 (ppm)

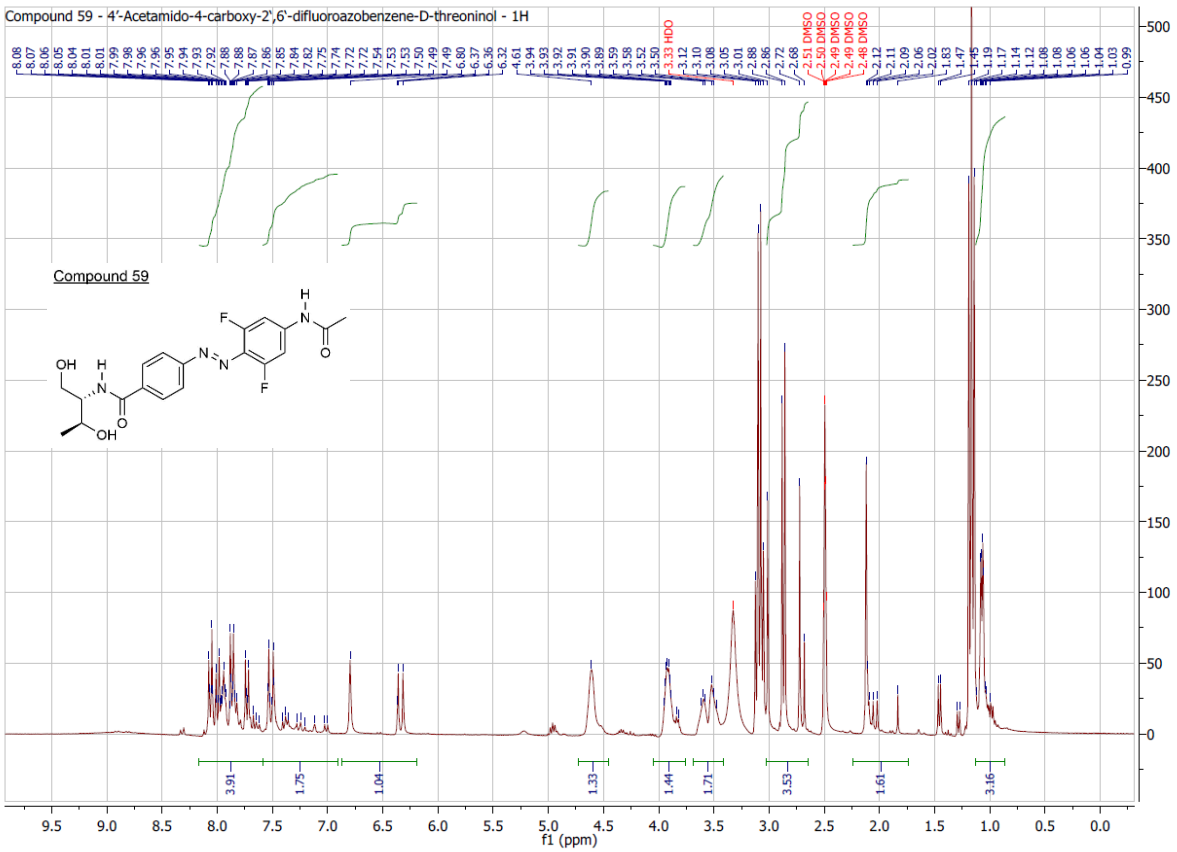
Compound 59 - 4'-Acetamido-4-carboxy-2',6'-difluoroazobenzene-D-threoninol - 1H
Compound 59
f1 (ppm)

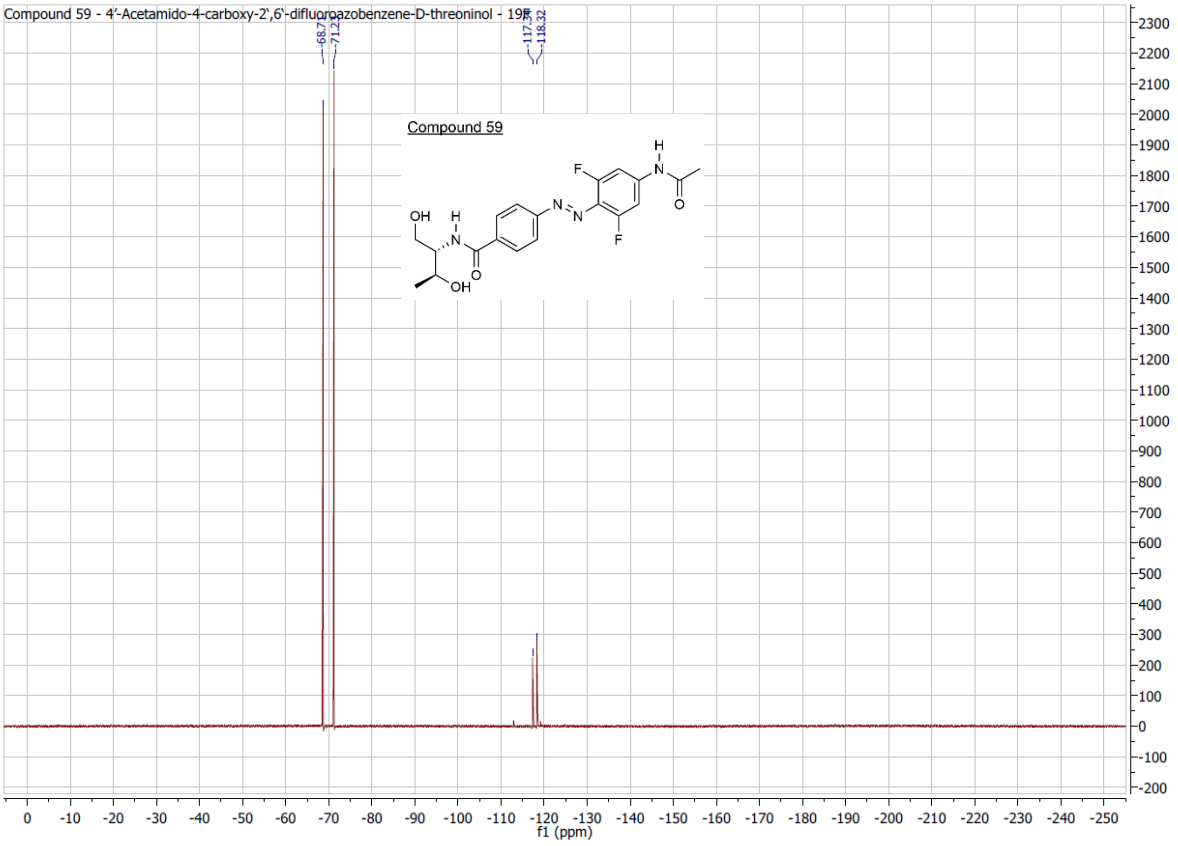
Compound 59 - 4'-Acetamido-4-carboxy-2',6'-difluoroazobenzene-D-threoninol - 19F
Compound 59
f1 (ppm)

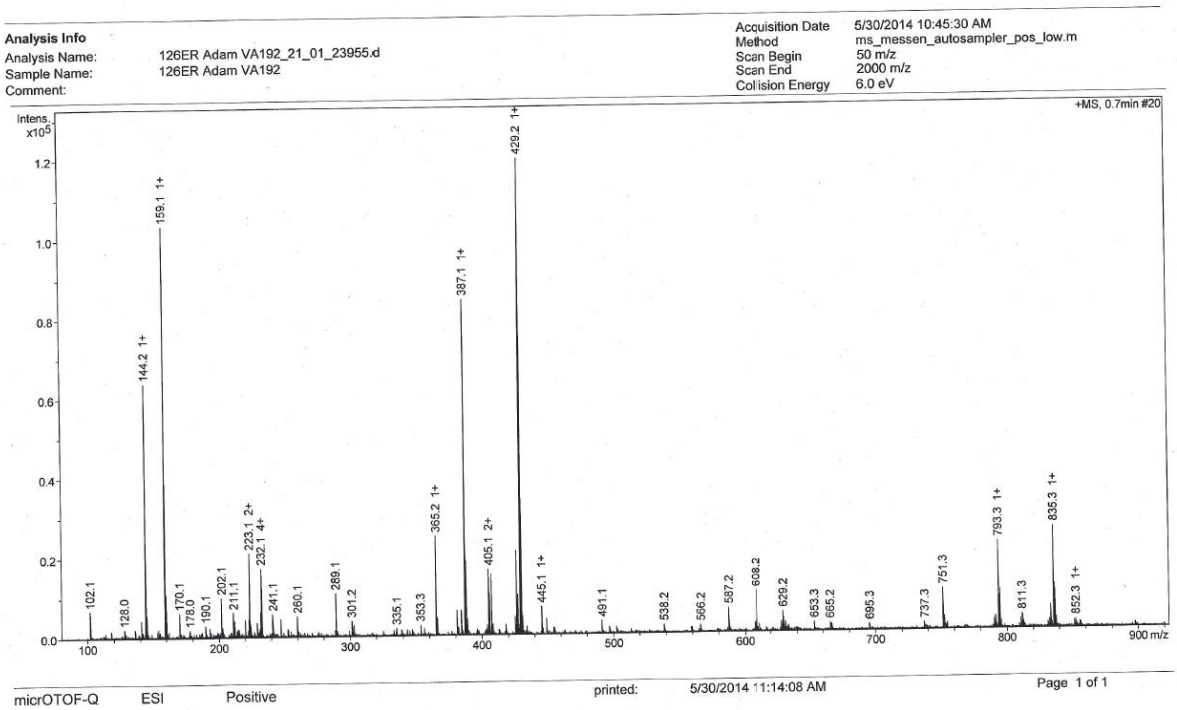
Analysis Info
Analysis Name: 126ER Adam VA192_21_01_23955.d
Sample Name: 126ER Adam VA192
Comment:
Acquisition Date 5/30/2014 10:45:30 AM
Method ms_messen_autosampler_pos_low.m
Scan Begin 50 m/z
Scan End 2000 m/z
Collision Energy 6.0 eV
+MS, 0.7min #20
Intens. x10^5
429.2 1+
159.1 1+
387.1 1+
144.2 1+
365.2 1+
223.1 2+
232.1 4+
405.1 2+
445.1 1+
793.3 1+
835.3 1+
751.3
608.2
629.2
289.1
102.1
128.0
170.1
178.0
190.1
202.1
211.1
241.1
260.1
301.2
335.1
353.3
491.1
538.2
566.2
587.2
653.3
665.2
695.3
737.3
811.3
852.3 1+
m/z
micrOTOF-Q ESI Positive
printed: 5/30/2014 11:14:08 AM
Page 1 of 1

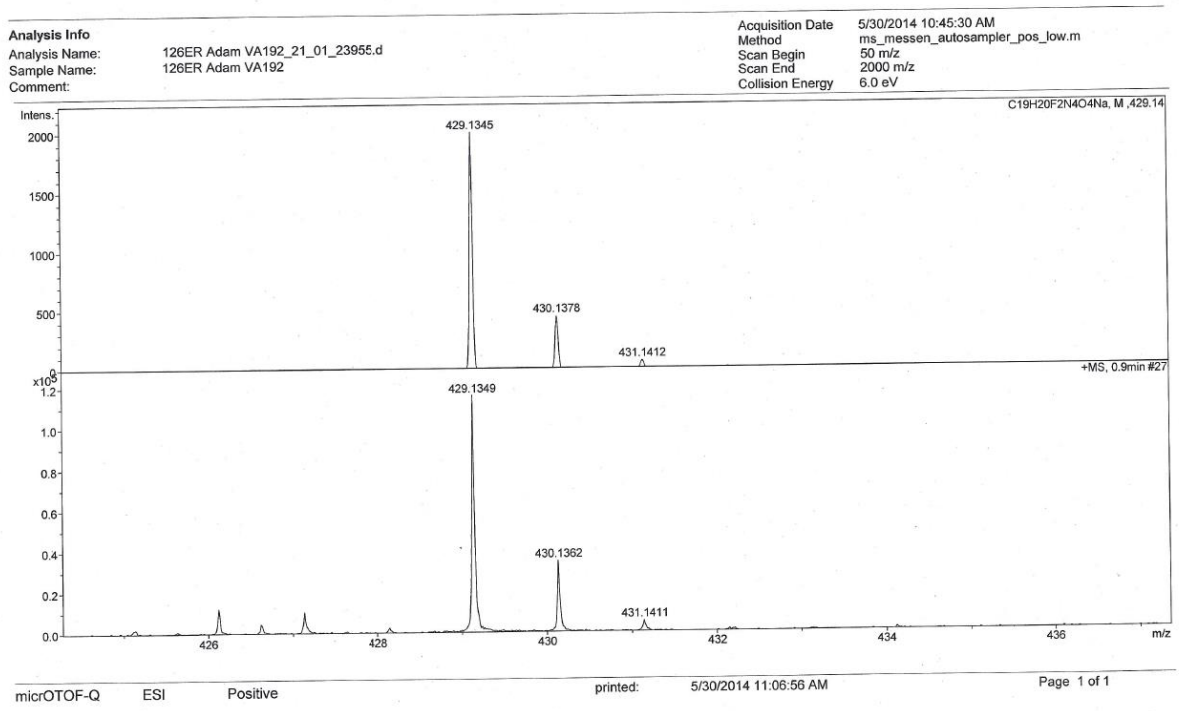
Analysis Info
Analysis Name: 126ER Adam VA192_21_01_23955.d
Sample Name: 126ER Adam VA192
Comment:
Acquisition Date 5/30/2014 10:45:30 AM
Method ms_messen_autosampler_pos_low.m
Scan Begin 50 m/z
Scan End 2000 m/z
Collision Energy 6.0 eV
C19H20F2N4O4Na, M ,429.14
Intens.
429.1345
430.1378
431.1412
+MS, 0.9min #27
x10^5
429.1349
430.1362
431.1411
m/z
micrOTOF-Q ESI Positive
printed: 5/30/2014 11:06:56 AM
Page 1 of 1

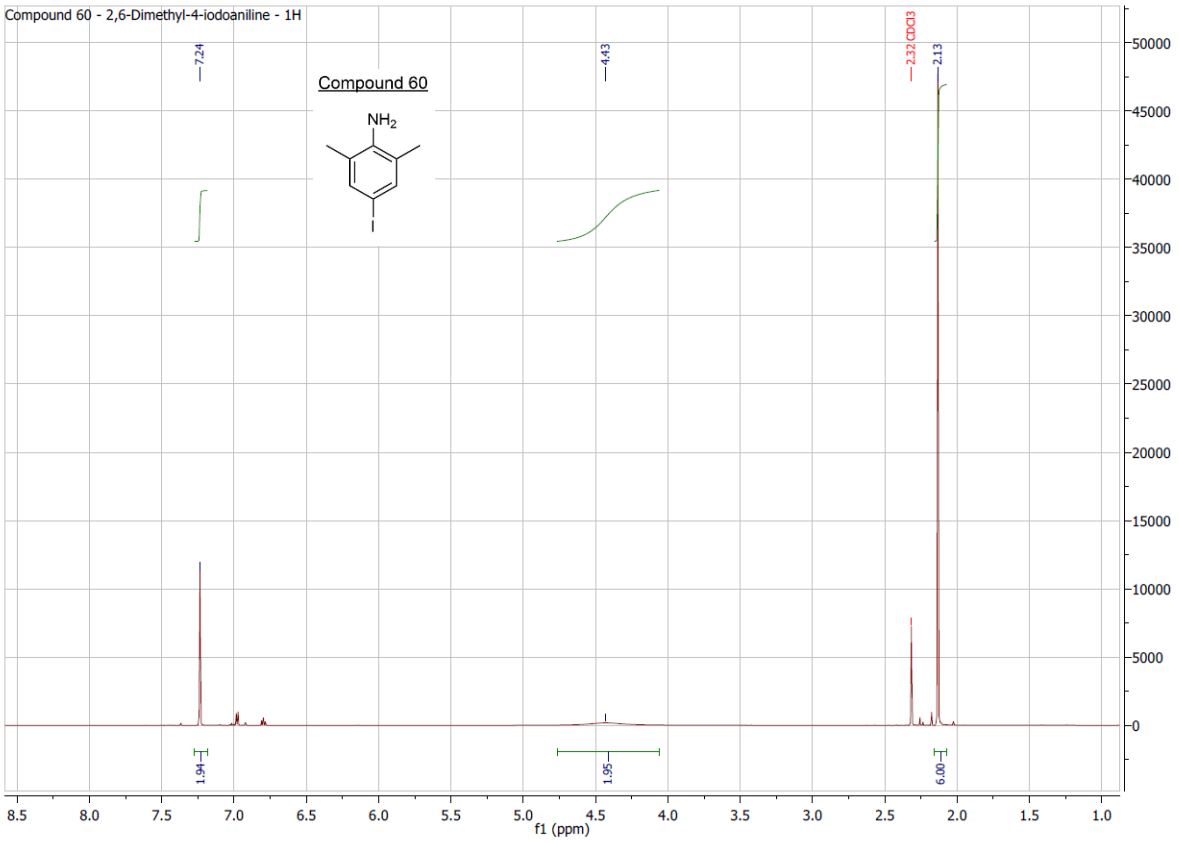
Compound 60 - 2,6-Dimethyl-4-iodoaniline - 1H
Compound 60
NH2
I
7.24
4.43
2.32 CDCl3
2.13
1.94
1.95
6.00
f1 (ppm)

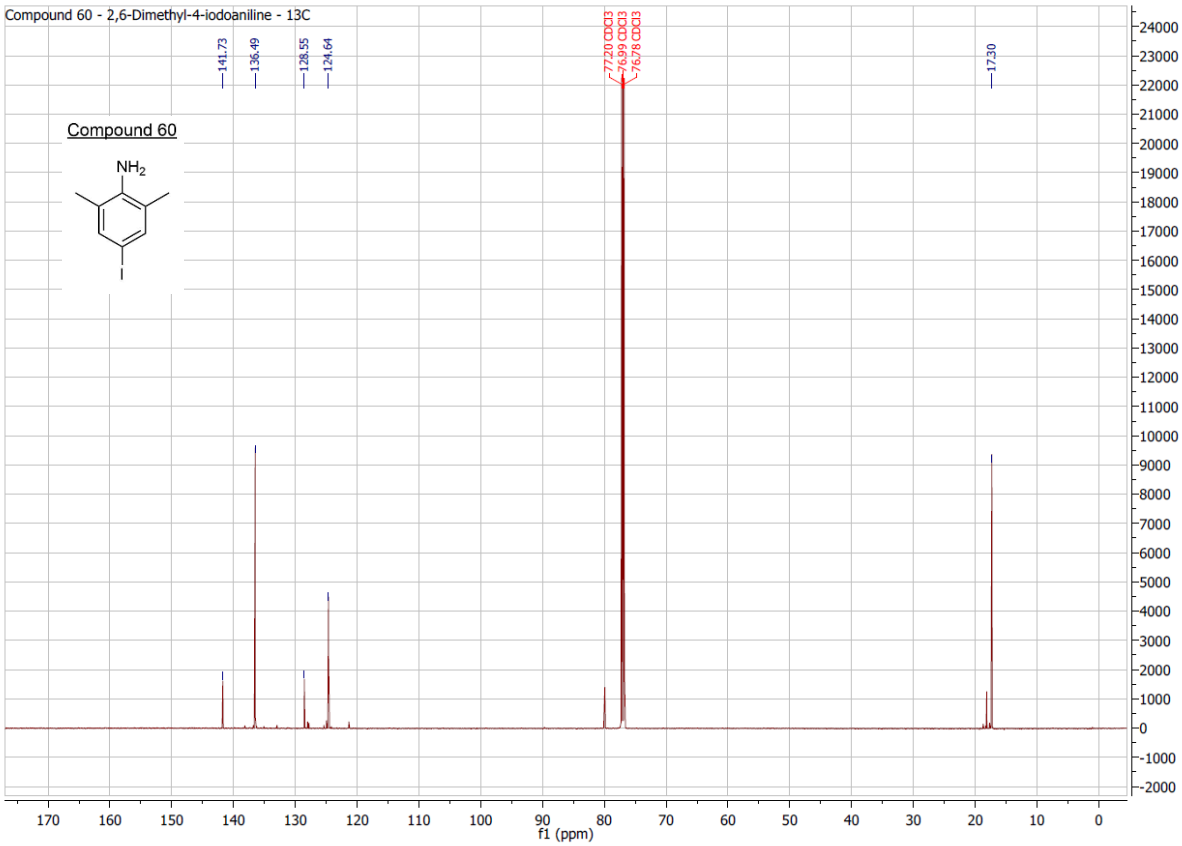
Compound 60 - 2,6-Dimethyl-4-iodoaniline - 13C
Compound 60
NH2
I
141.73
136.49
128.55
124.64
77.20 CDCl3
76.99 CDCl3
76.78 CDCl3
17.30
f1 (ppm)

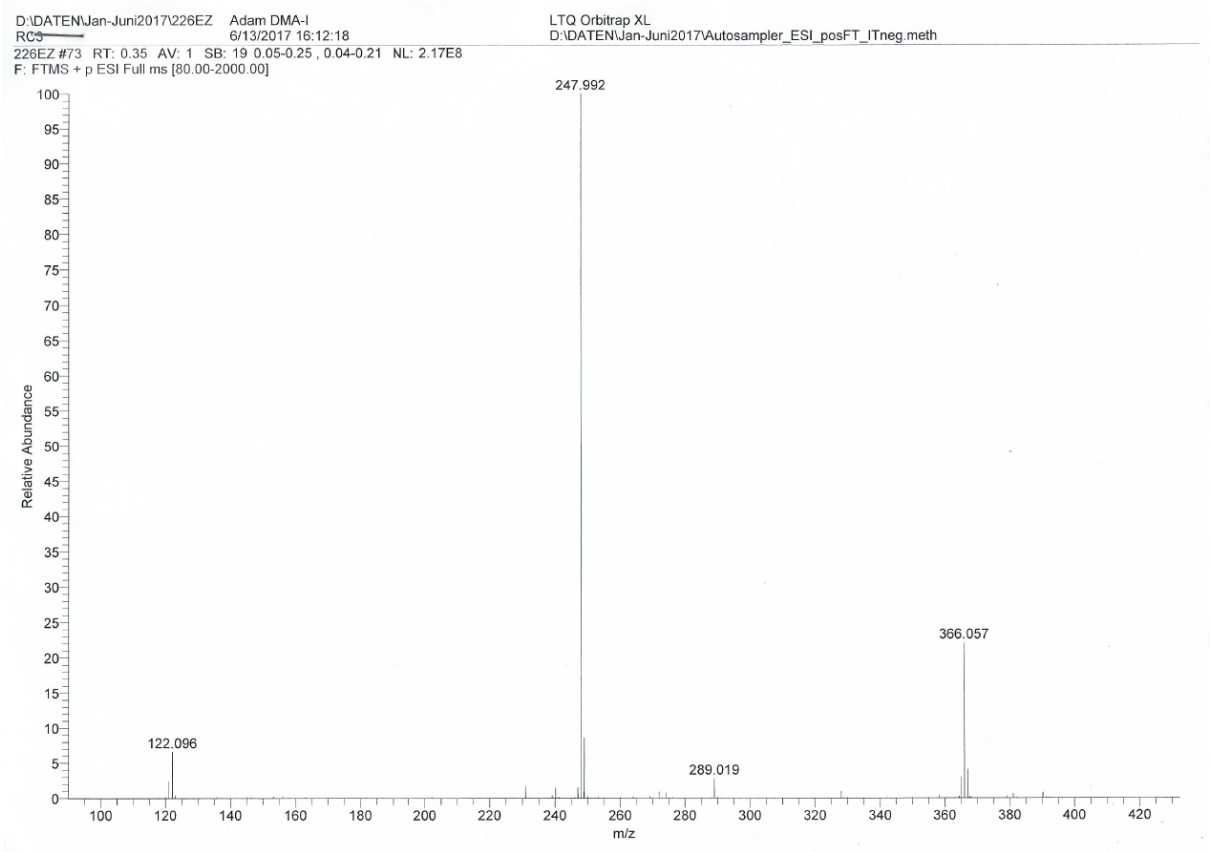
D:\DATEN\Jan-Juni2017\226EZ Adam DMA-I
RC3
6/13/2017 16:12:18
LTQ Orbitrap XL
D:\DATEN\Jan-Juni2017\Autosampler_ESI_posFT_ITneg.meth
226EZ #73 RT: 0.35 AV: 1 SB: 19 0.05-0.25 , 0.04-0.21 NL: 2.17E8
F: FTMS + p ESI Full ms [80.00-2000.00]
247.992
366.057
122.096
289.019
Relative Abundance
m/z

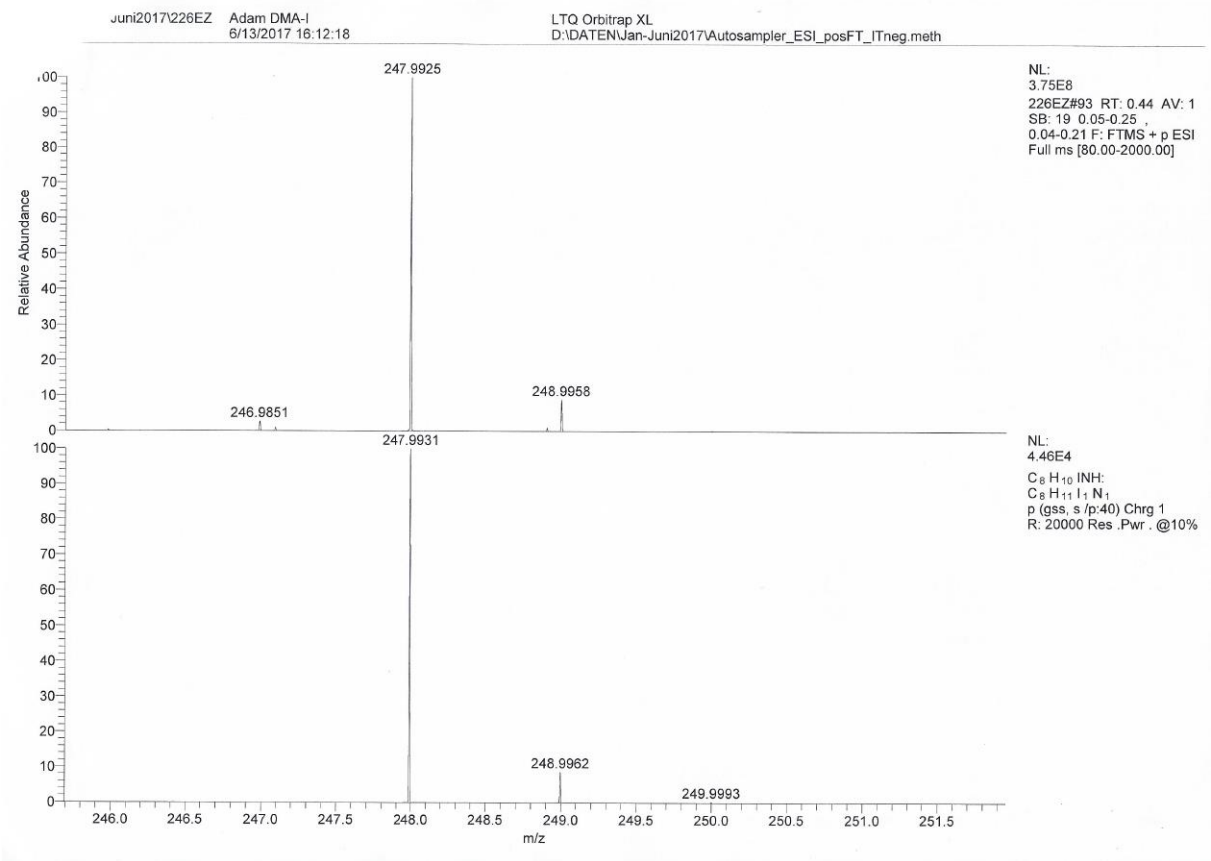
Juni2017\226EZ Adam DMA-I
6/13/2017 16:12:18
LTQ Orbitrap XL
D:\DATEN\Jan-Juni2017\Autosampler_ESI_posFT_ITneg.meth
247.9925
248.9958
246.9851
NL:
3.75E8
226EZ#93 RT: 0.44 AV: 1
SB: 19 0.05-0.25 ,
0.04-0.21 F: FTMS + p ESI
Full ms [80.00-2000.00]
247.9931
248.9962
249.9993
NL:
4.46E4
C8 H10 INH:
C8 H11 I1 N1
p (gss, s /p:40) Chrg 1
R: 20000 Res .Pwr . @10%
Relative Abundance
m/z

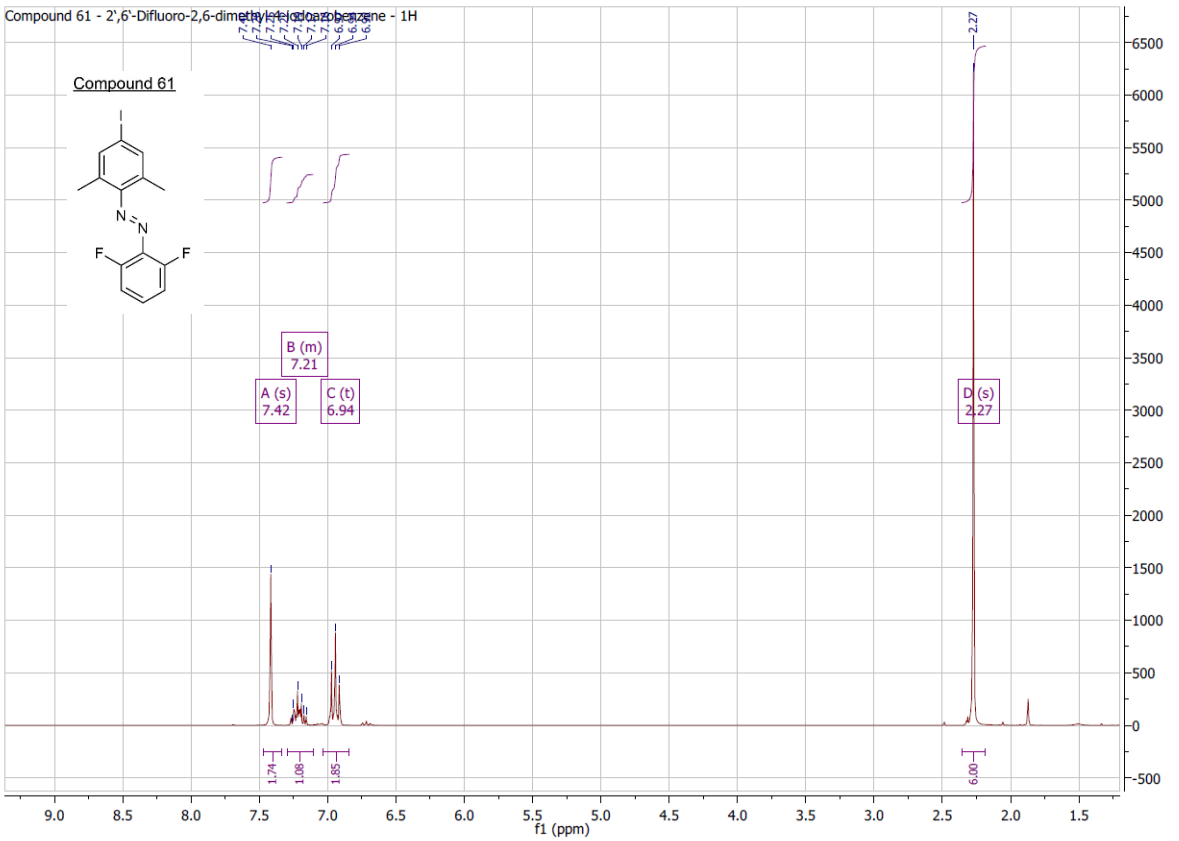
Compound 61 - 2',6'-Difluoro-2,6-dimethyl-4-iodoazobenzene - 1H
Compound 61
B (m)
7.21
A (s)
7.42
C (t)
6.94
D (s)
2.27
f1 (ppm)

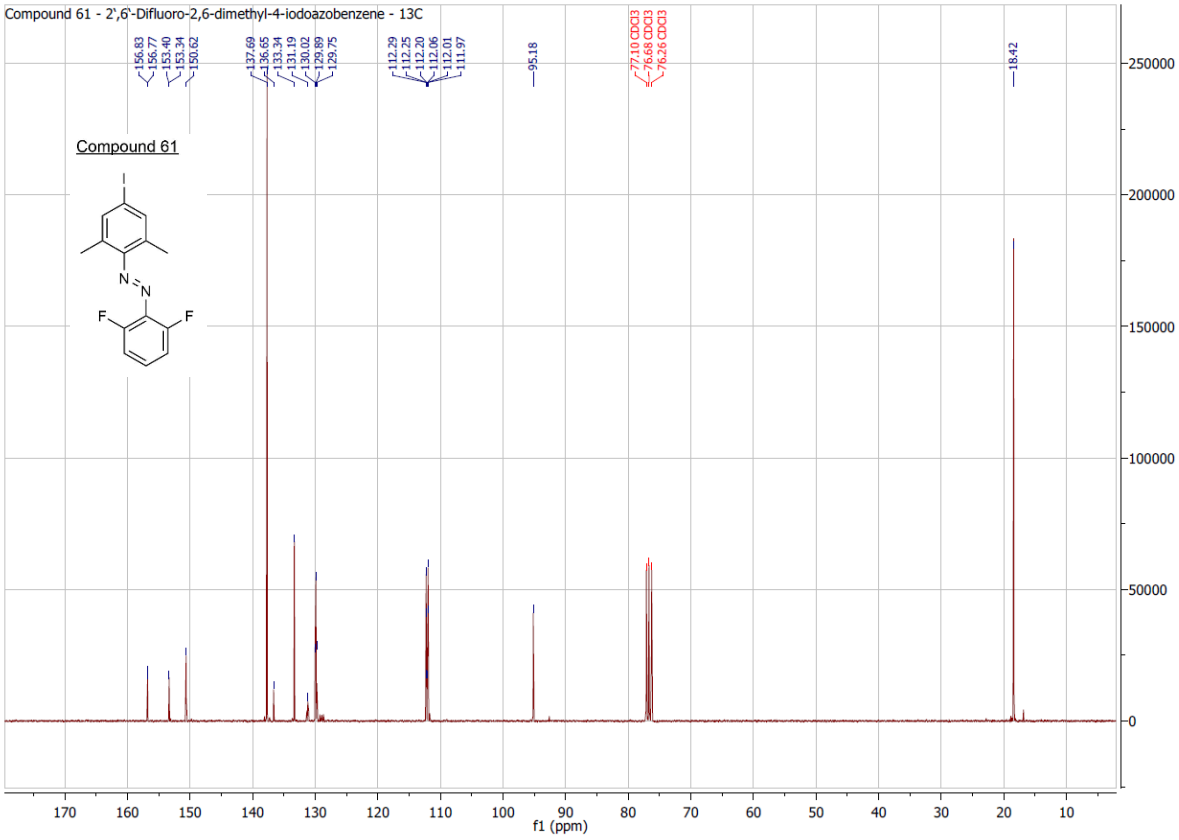
Compound 61 - 2',6'-Difluoro-2,6-dimethyl-4-iodoazobenzene - 13C
Compound 61
f1 (ppm)

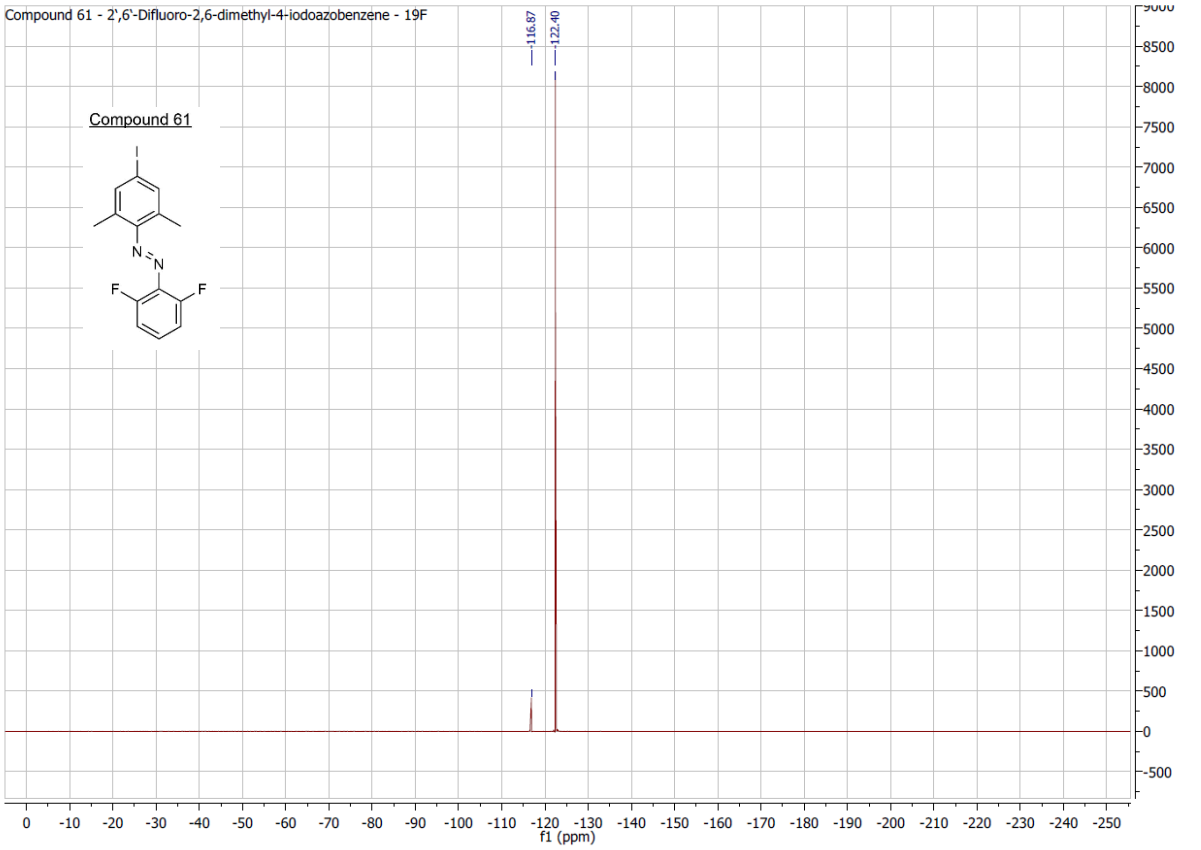
Compound 61 - 2',6'-Difluoro-2,6-dimethyl-4-iodoazobenzene - 19F
116.87
122.40
Compound 61
f1 (ppm)

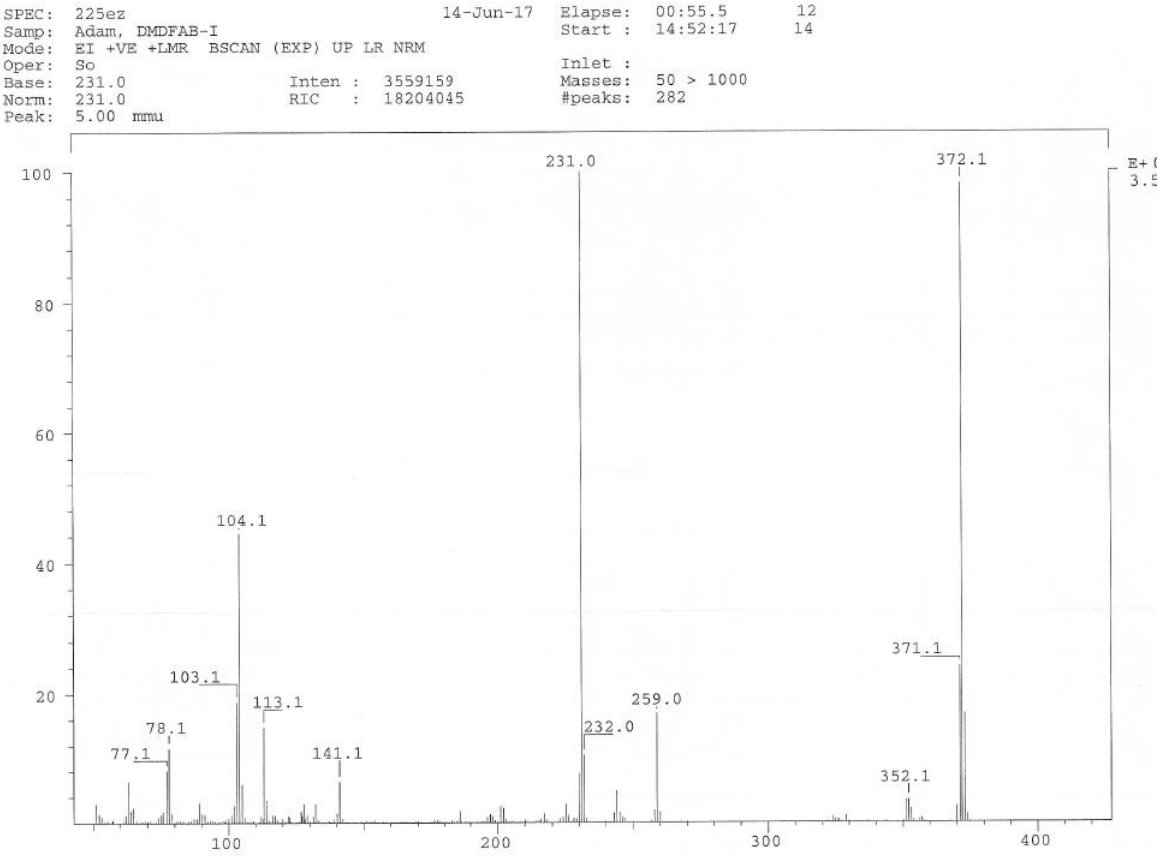
SPEC: 225ez
14-Jun-17
Elapse: 00:55.5
12
Samp: Adam, DMDFAB-I
Start : 14:52:17
14
Mode: EI +VE +LMR BSCAN (EXP) UP LR NRM
Oper: So
Inlet :
Base: 231.0
Inten : 3559159
Masses: 50 > 1000
Norm: 231.0
RIC : 18204045
#peaks: 282
Peak: 5.00 mmu
231.0
372.1
104.1
103.1
113.1
78.1
77.1
141.1
259.0
232.0
371.1
352.1

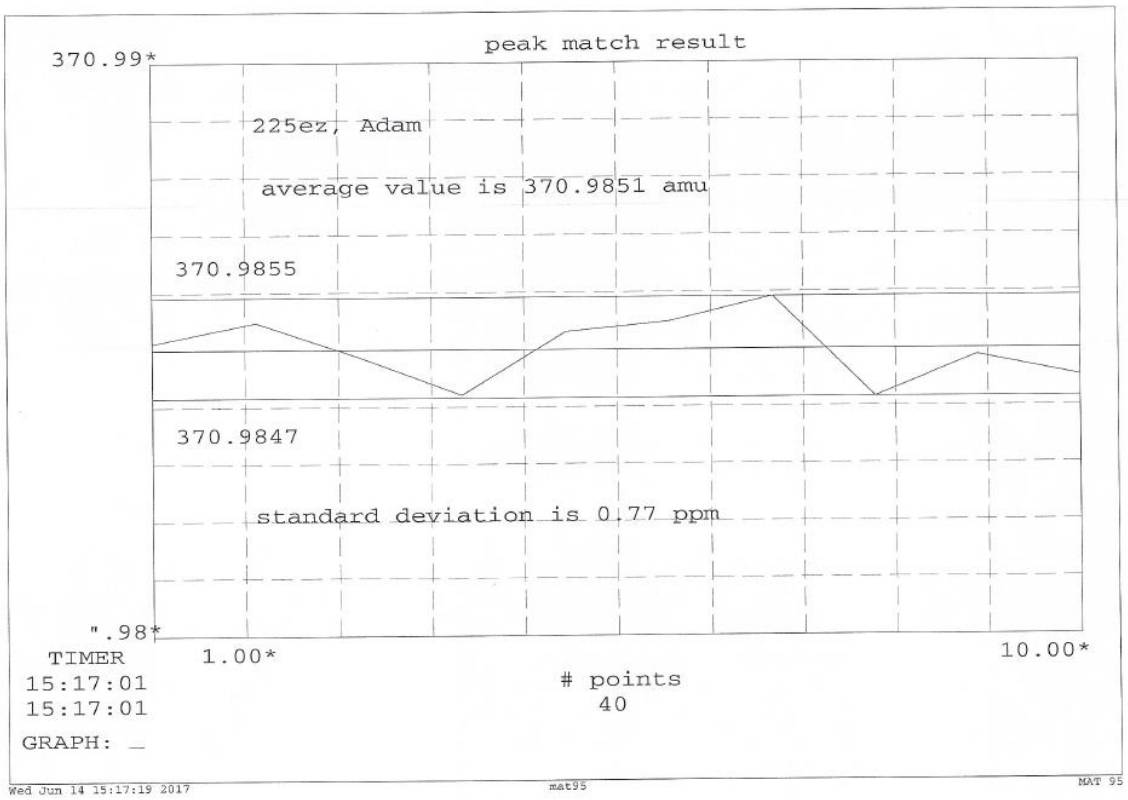
peak match result
370.99*
225ez, Adam
average value is 370.9851 amu
370.9855
370.9847
standard deviation is 0.77 ppm
".98*
TIMER
15:17:01
15:17:01
GRAPH: _
1.00*
10.00*
points
40
Wed Jun 14 15:17:19 2017
mat95
MAT 95

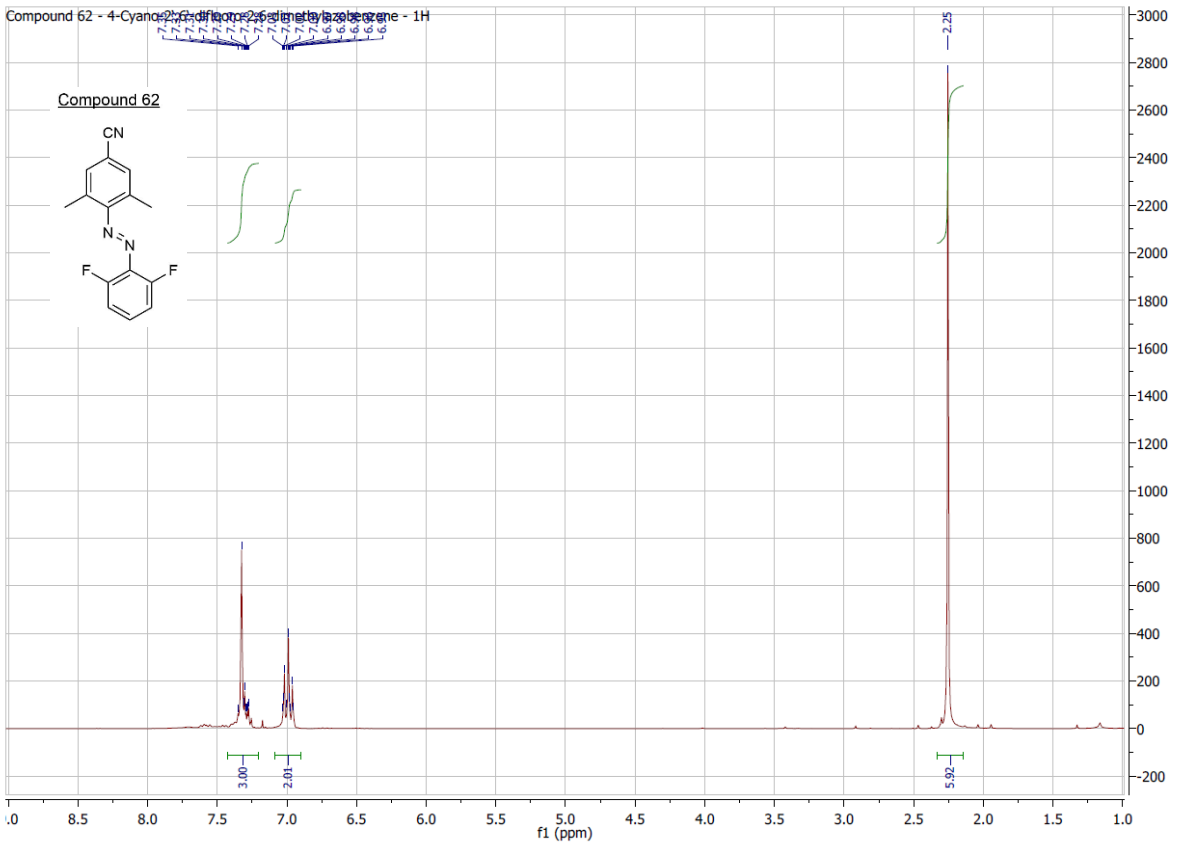
Compound 62 - 4-Cyano-2',6'-difluoro-2,6-dimethylazobenzene - 1H
Compound 62
CN
N
N
F
F
2.25
3.00
2.01
5.92
f1 (ppm)

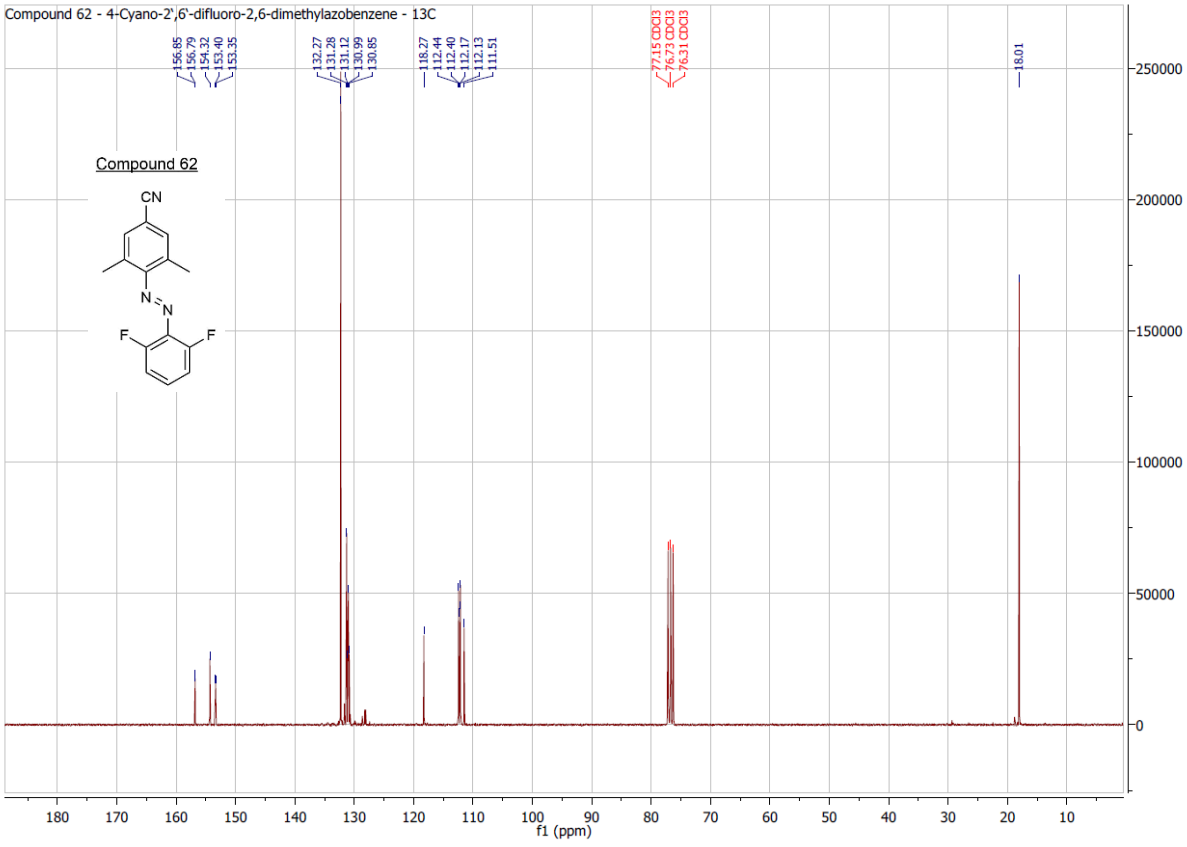
Compound 62 - 4-Cyano-2',6'-difluoro-2,6-dimethylazobenzene - 13C
Compound 62
CN
N
N
F
F
156.85
156.79
154.32
153.40
153.35
132.27
131.28
131.12
130.99
130.85
118.27
112.44
112.40
112.17
112.13
111.51
77.15 CDCl3
76.73 CDCl3
76.31 CDCl3
18.01
f1 (ppm)

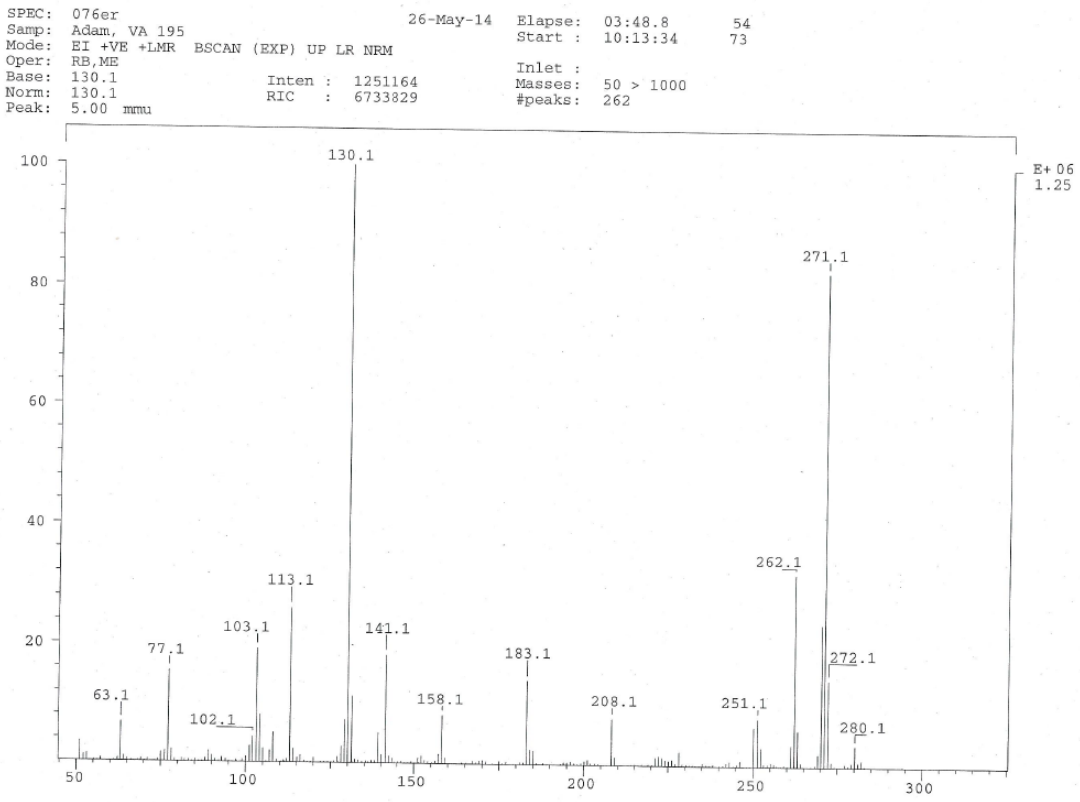
SPEC: 076er
Samp: Adam, VA 195
Mode: EI +VE +LMR BSCAN (EXP) UP LR NRM
Oper: RB,ME
Base: 130.1
Norm: 130.1
Peak: 5.00 mmu
Inten : 1251164
RIC : 6733829
26-May-14
Elapse: 03:48.8 54
Start : 10:13:34 73
Inlet :
Masses: 50 > 1000
#peaks: 262
E+06
1.25
130.1
271.1
262.1
113.1
103.1
141.1
77.1
183.1
272.1
63.1
158.1
208.1
251.1
102.1
280.1

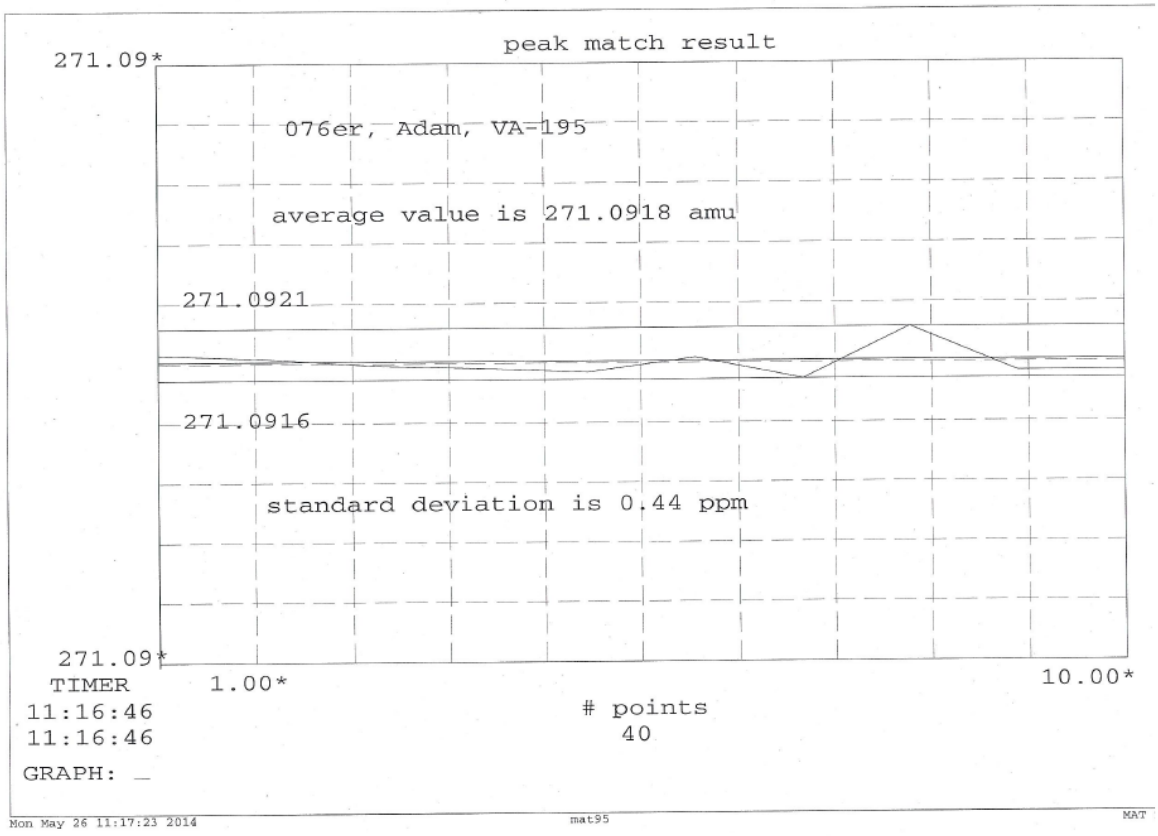
peak match result
271.09*
076er, Adam, VA-195
average value is 271.0918 amu
271.0921
271.0916
standard deviation is 0.44 ppm
271.09*
TIMER
1.00*
10.00*
11:16:46
11:16:46
points
40
GRAPH:
Mon May 26 11:17:23 2014
mat95
MAT

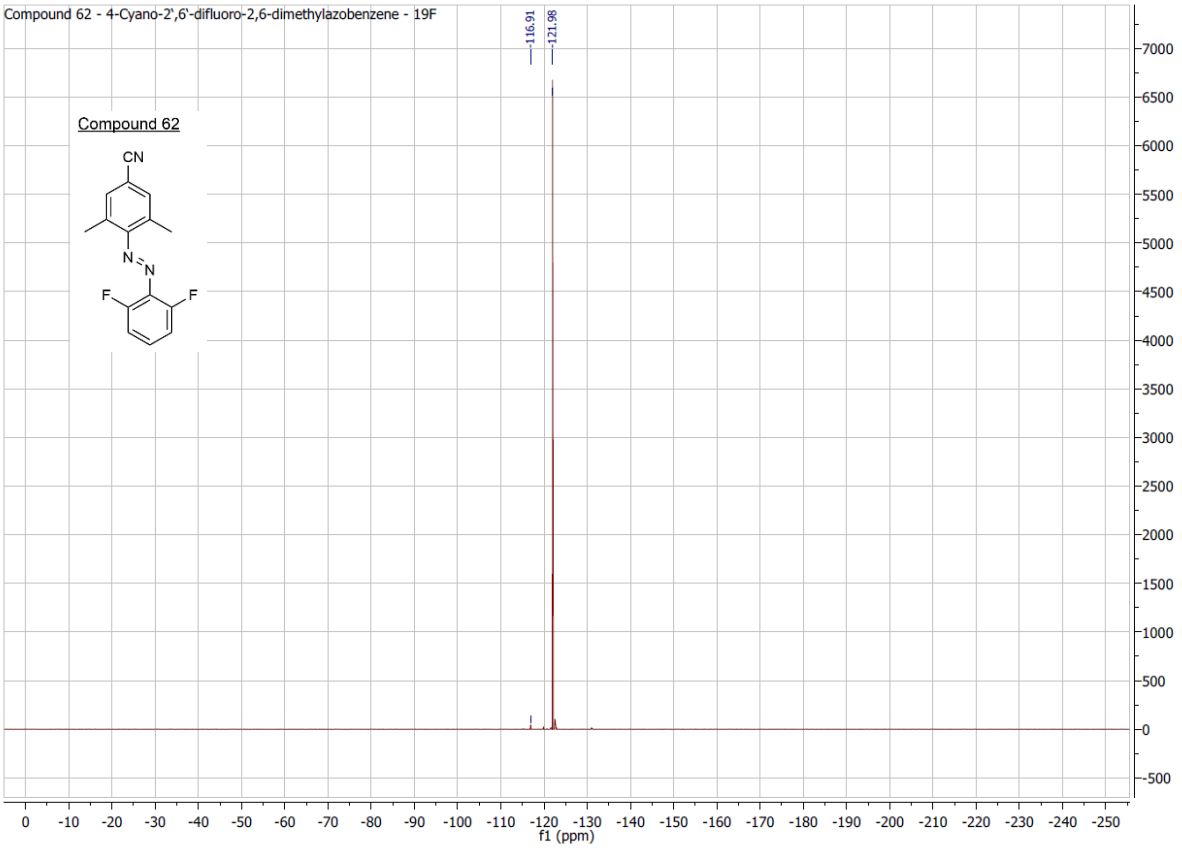
Compound 62 - 4-Cyano-2',6'-difluoro-2,6-dimethylazobenzene - 19F
116.91
121.98
Compound 62
CN
N
N
F
F
f1 (ppm)

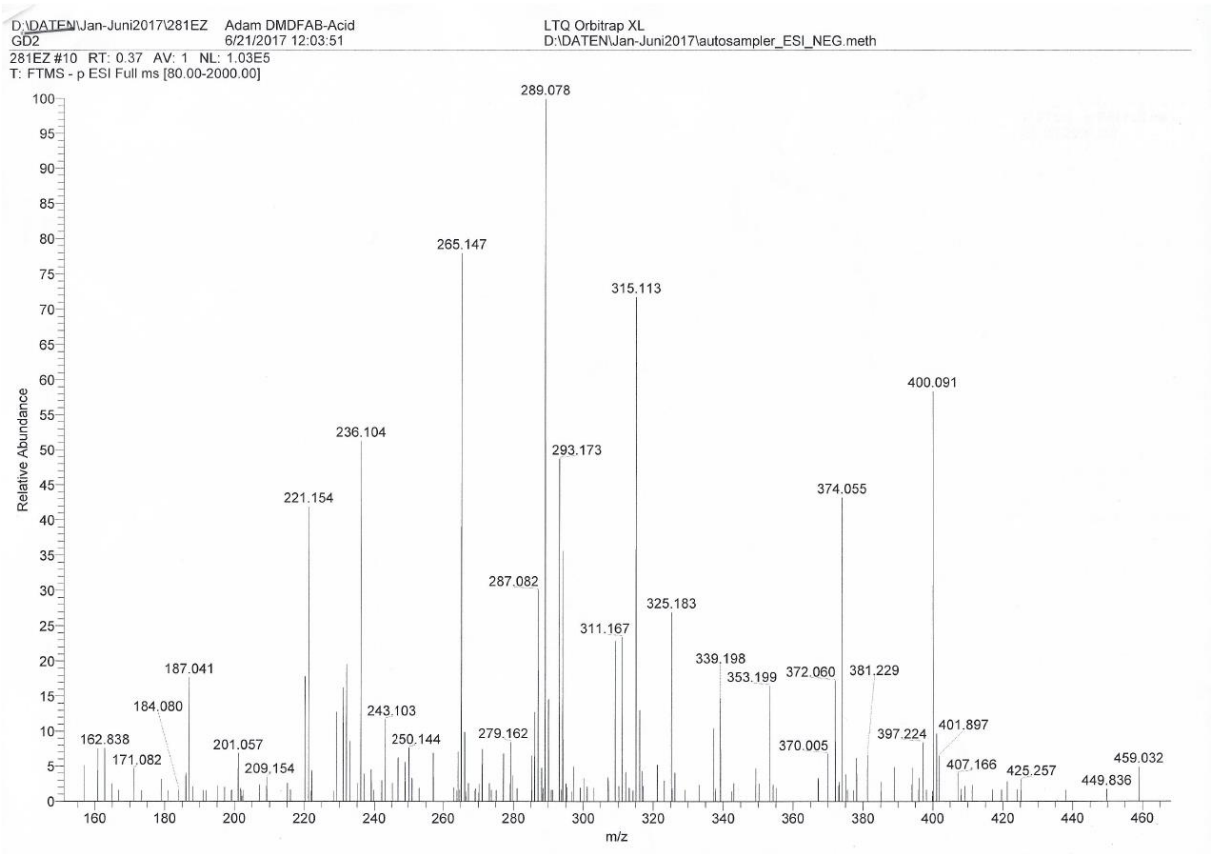
D:\DATEN\Jan-Juni2017\281EZ Adam DMDFAB-Acid
GD2 6/21/2017 12:03:51
LTQ Orbitrap XL
D:\DATEN\Jan-Juni2017\autosampler_ESI_NEG.meth
281EZ #10 RT: 0.37 AV: 1 NL: 1.03E5
T: FTMS - p ESI Full ms [80.00-2000.00]
Relative Abundance
m/z
289.078
265.147
315.113
400.091
236.104
293.173
374.055
221.154
287.082
325.183
311.167
339.198
353.199
372.060
381.229
187.041
184.080
243.103
162.838
171.082
201.057
250.144
279.162
209.154
370.005
397.224
401.897
407.166
425.257
449.836
459.032

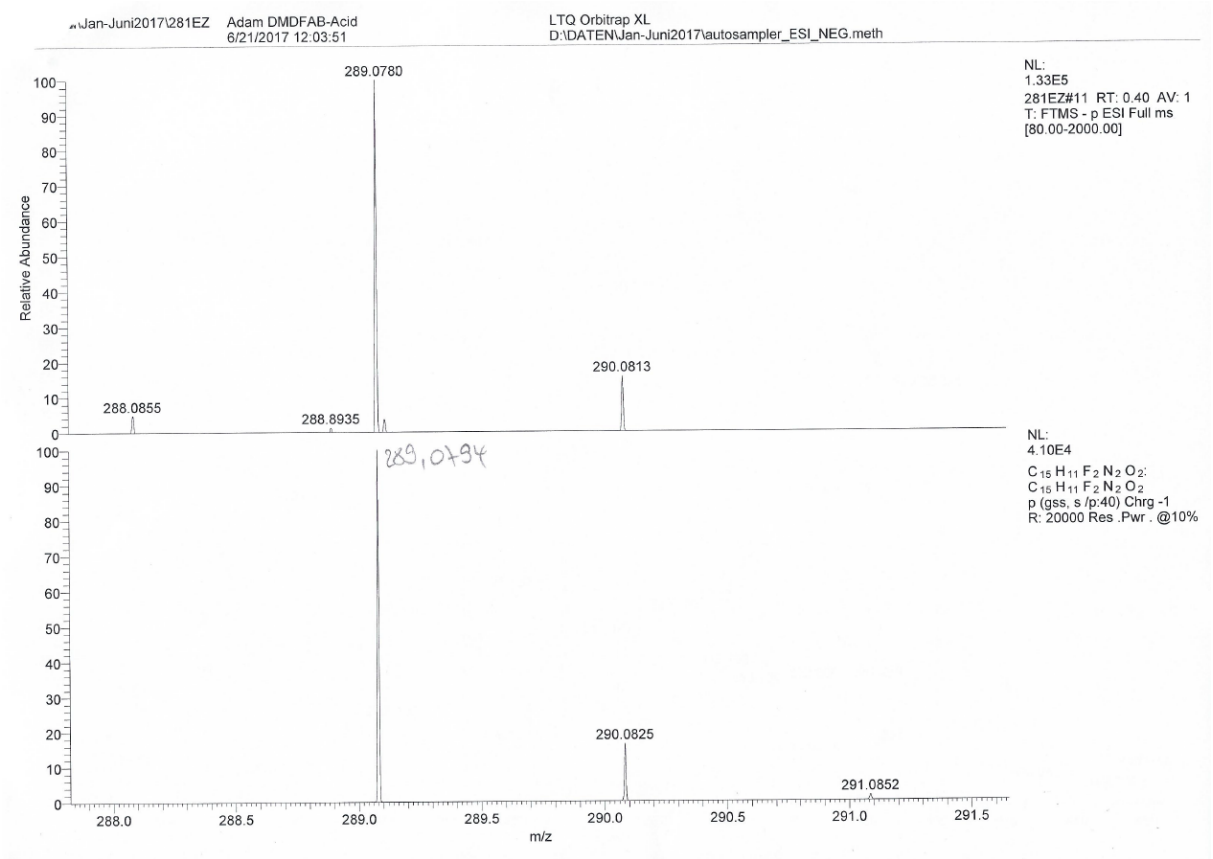
Jan-Juni2017\281EZ Adam DMDFAB-Acid
6/21/2017 12:03:51
LTQ Orbitrap XL
D:\DATEN\Jan-Juni2017\autosampler_ESI_NEG.meth
NL:
1.33E5
281EZ#11 RT: 0.40 AV: 1
T: FTMS - p ESI Full ms
[80.00-2000.00]
289.0780
290.0813
288.0855
288.8935
Relative Abundance
NL:
4.10E4
C15 H11 F2 N2 O2:
C15 H11 F2 N2 O2
p (gss, s /p:40) Chrg -1
R: 20000 Res .Pwr . @10%
289,0794
290.0825
291.0852
m/z

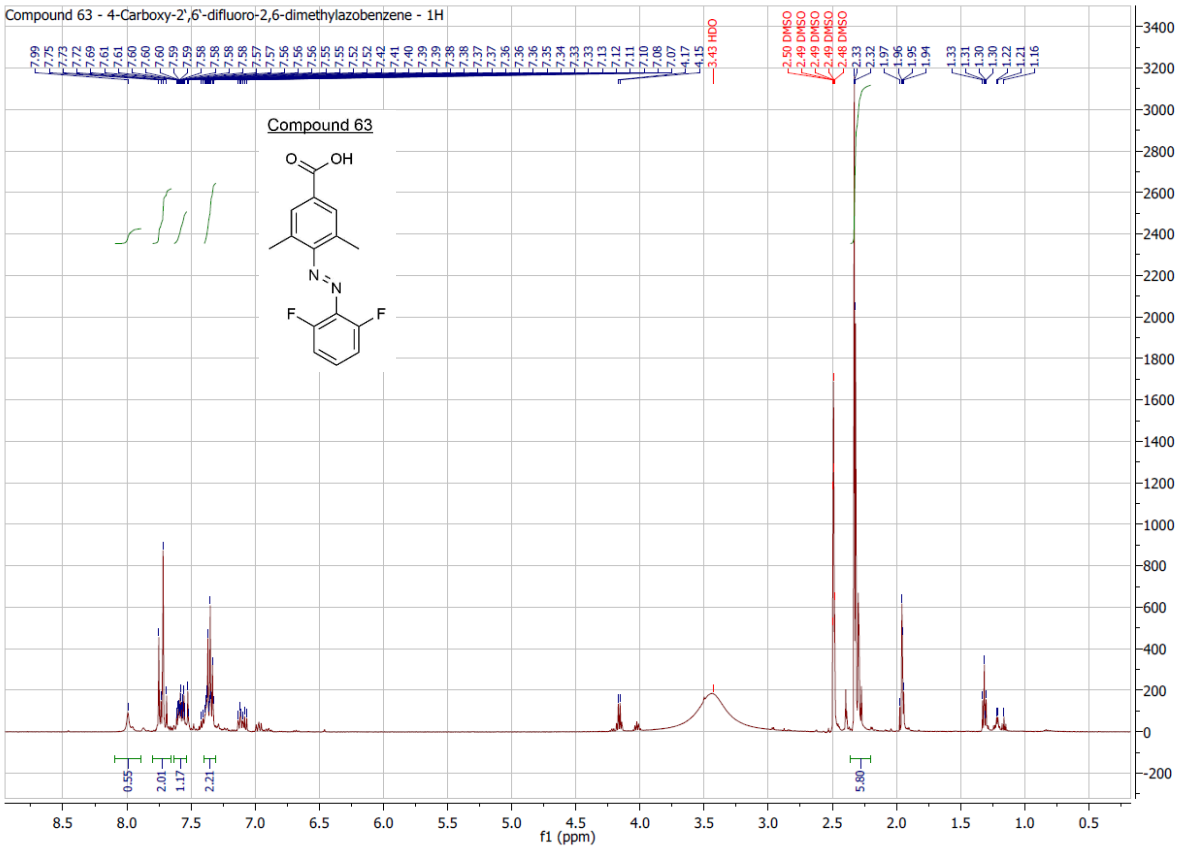
Compound 63 - 4-Carboxy-2',6'-difluoro-2,6-dimethylazobenzene - 1H
Compound 63
f1 (ppm)

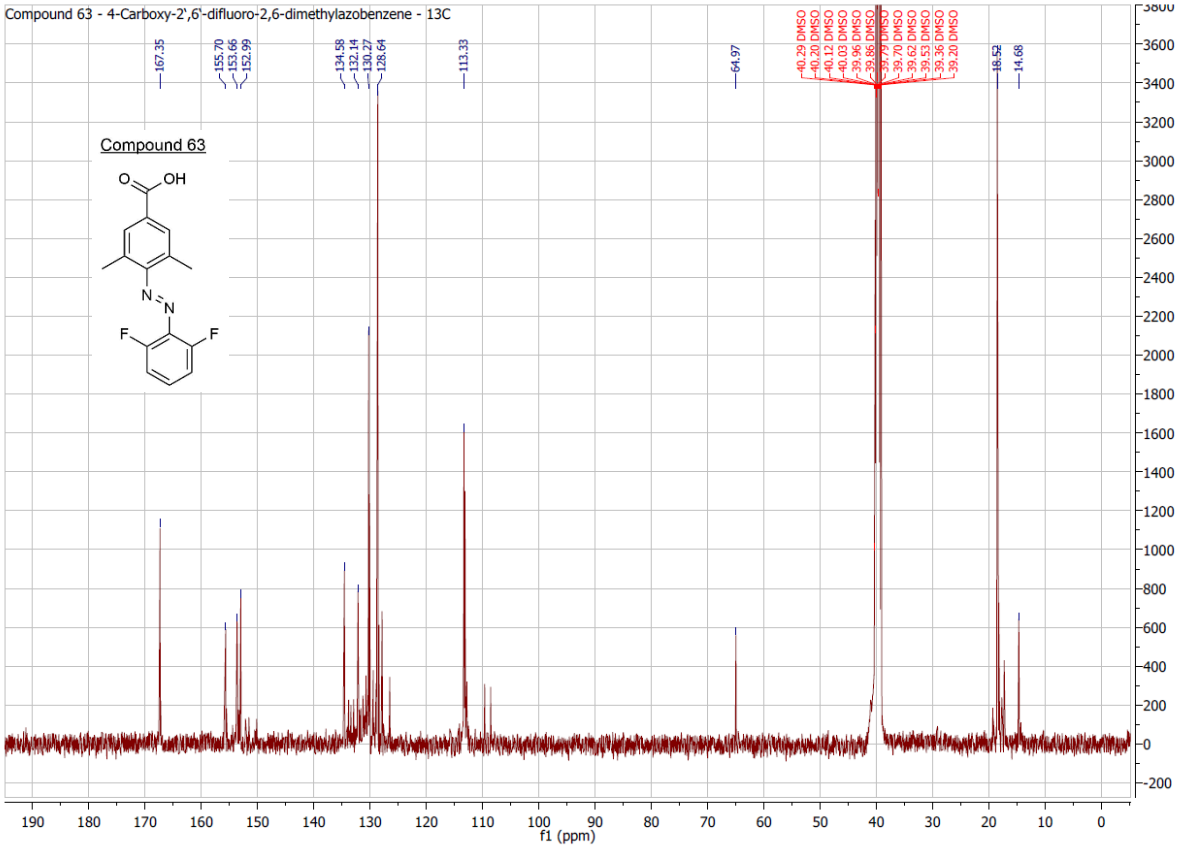
Compound 63 - 4-Carboxy-2',6'-difluoro-2,6-dimethylazobenzene - 13C
Compound 63
f1 (ppm)

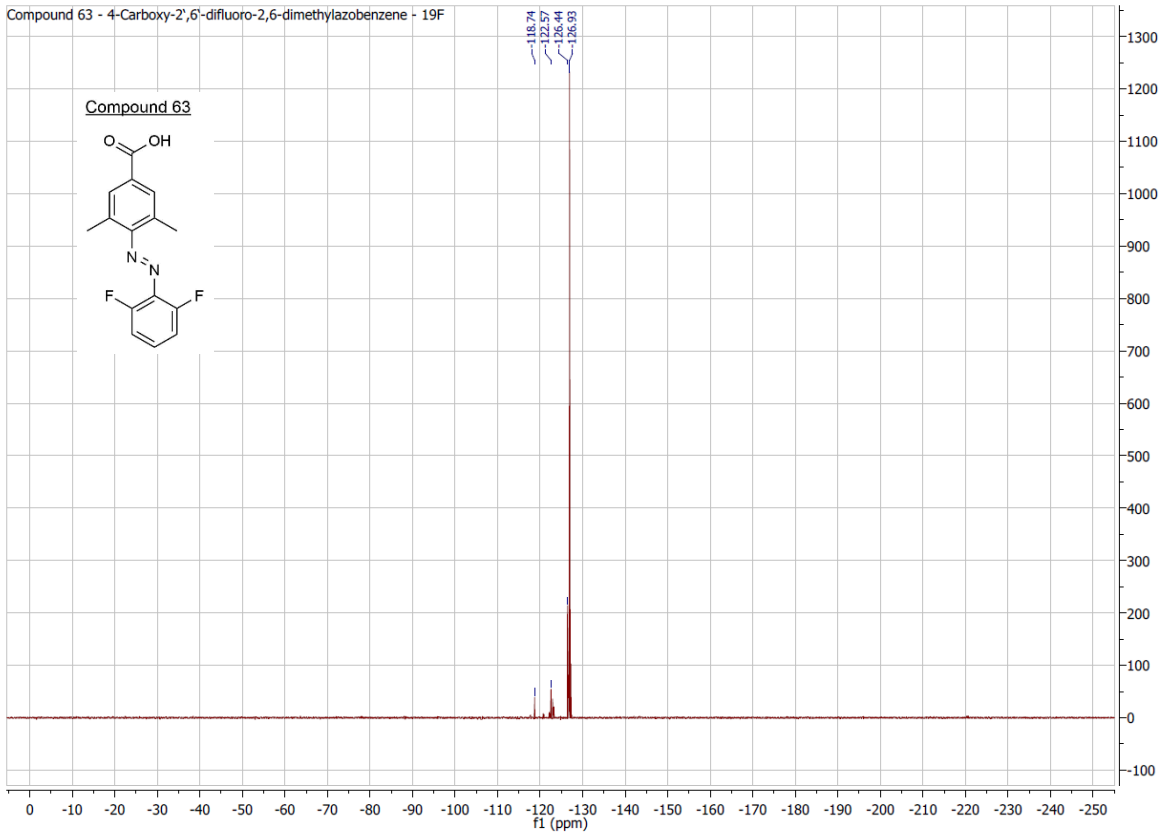
Compound 63 - 4-Carboxy-2',6'-difluoro-2,6-dimethylazobenzene - 19F
118.74
122.57
126.44
126.93
Compound 63
O
OH
N
N
F
F
f1 (ppm)

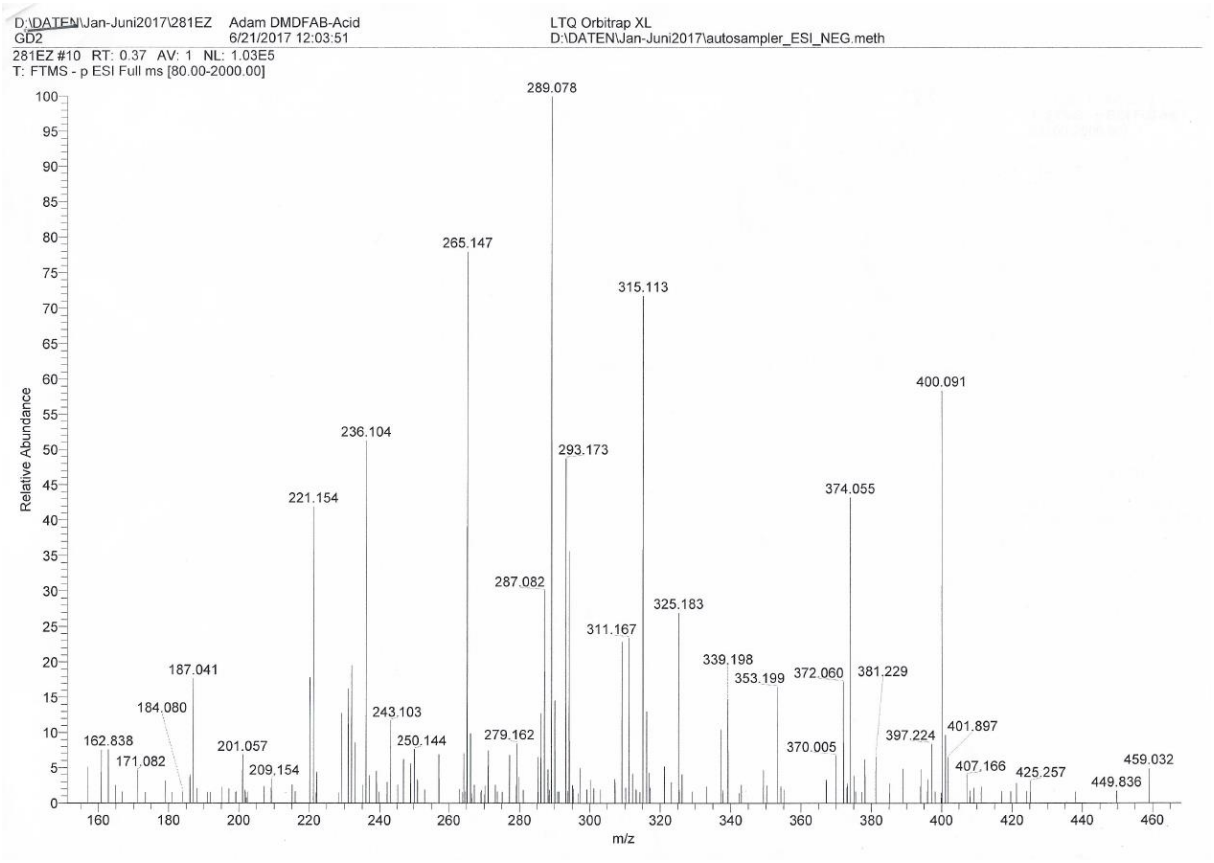
D:\DATEN\Jan-Juni2017\281EZ Adam DMDFAB-Acid
GD2 6/21/2017 12:03:51
LTQ Orbitrap XL
D:\DATEN\Jan-Juni2017\autosampler_ESI_NEG.meth
281EZ #10 RT: 0.37 AV: 1 NL: 1.03E5
T: FTMS - p ESI Full ms [80.00-2000.00]
Relative Abundance
m/z
289.078
265.147
315.113
400.091
236.104
293.173
374.055
221.154
287.082
325.183
311.167
339.198
353.199
372.060
381.229
187.041
184.080
243.103
279.162
250.144
397.224
401.897
162.838
171.082
201.057
209.154
370.005
407.166
425.257
459.032
449.836

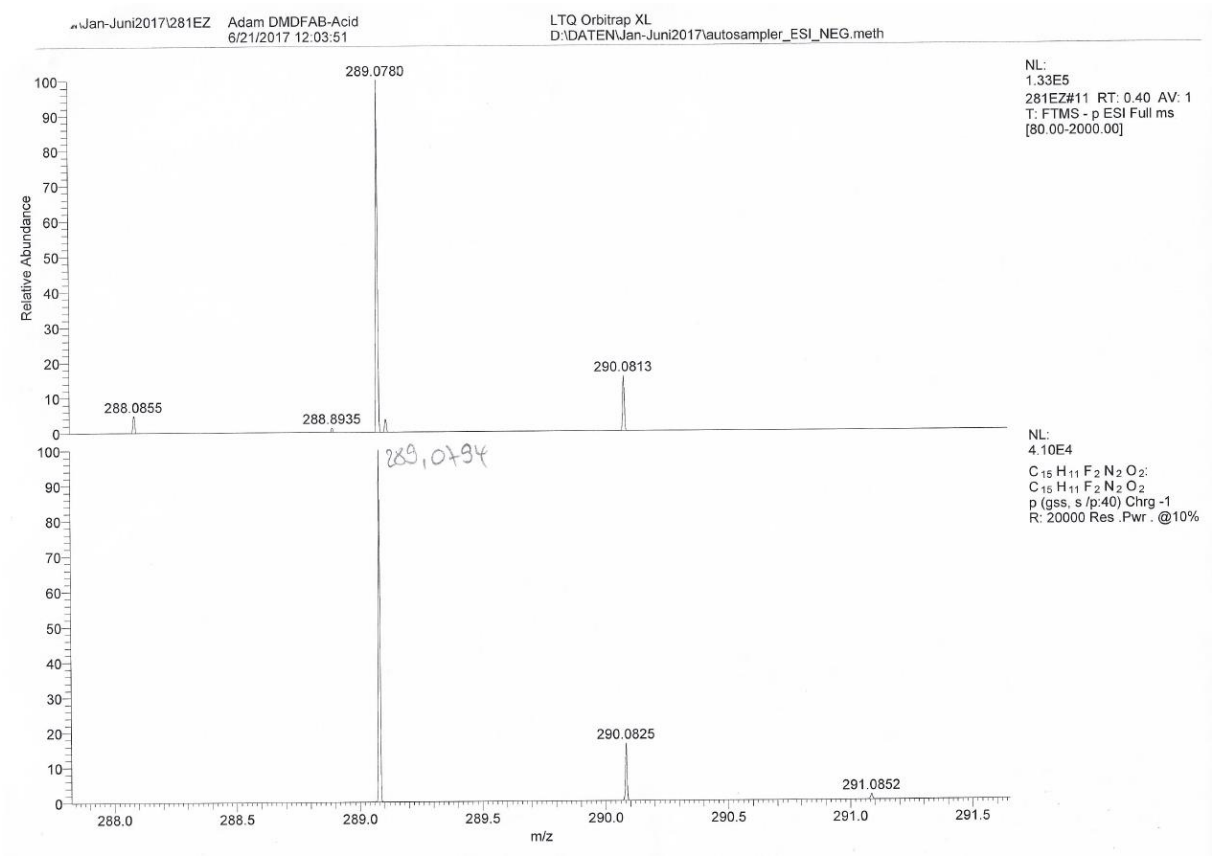
\Jan-Juni2017\281EZ Adam DMDFAB-Acid
6/21/2017 12:03:51
LTQ Orbitrap XL
D:\DATEN\Jan-Juni2017\autosampler_ESI_NEG.meth
NL:
1.33E5
281EZ#11 RT: 0.40 AV: 1
T: FTMS - p ESI Full ms
[80.00-2000.00]
289.0780
290.0813
288.0855
288.8935
NL:
4.10E4
C15 H11 F2 N2 O2:
C15 H11 F2 N2 O2
p (gss, s /p:40) Chrg -1
R: 20000 Res .Pwr . @10%
289,0794
290.0825
291.0852
Relative Abundance
m/z

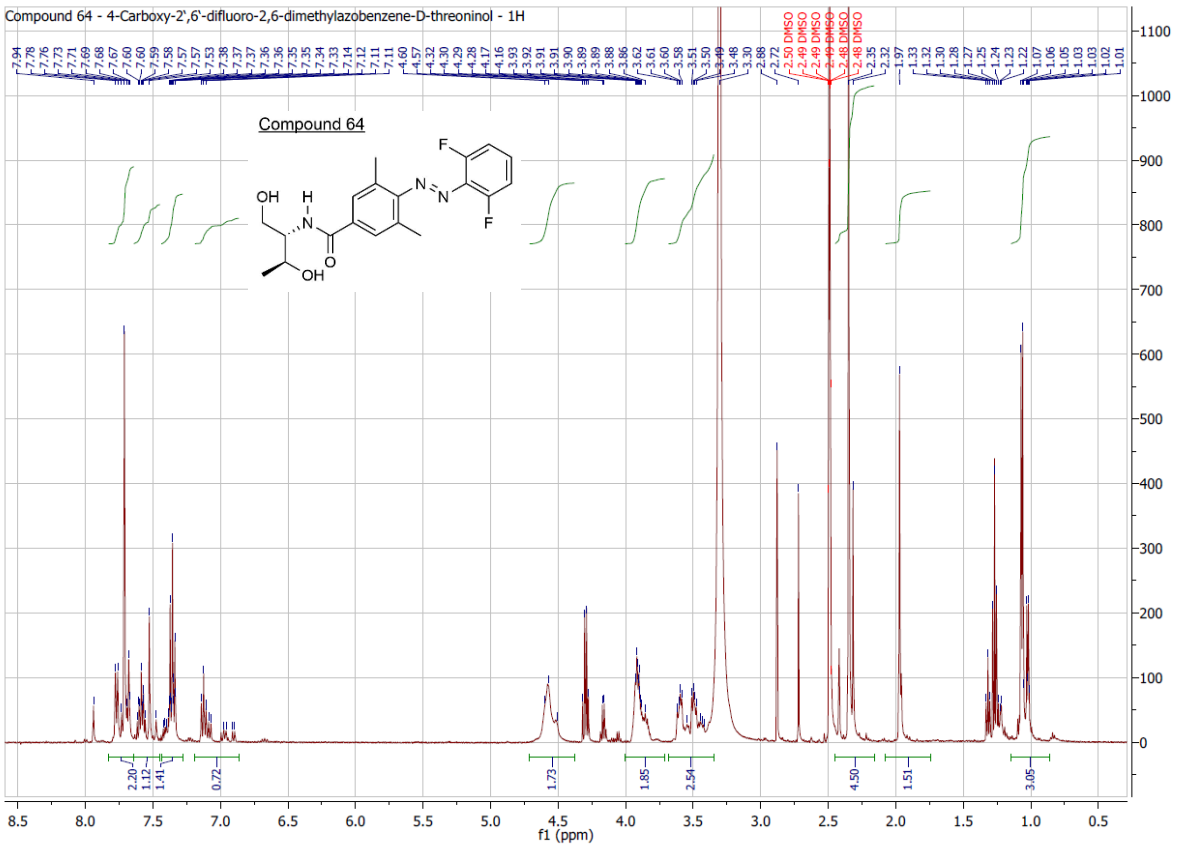
Compound 64 - 4-Carboxy-2',6'-difluoro-2,6-dimethylazobenzene-D-threoninol - 1H
Compound 64
f1 (ppm)

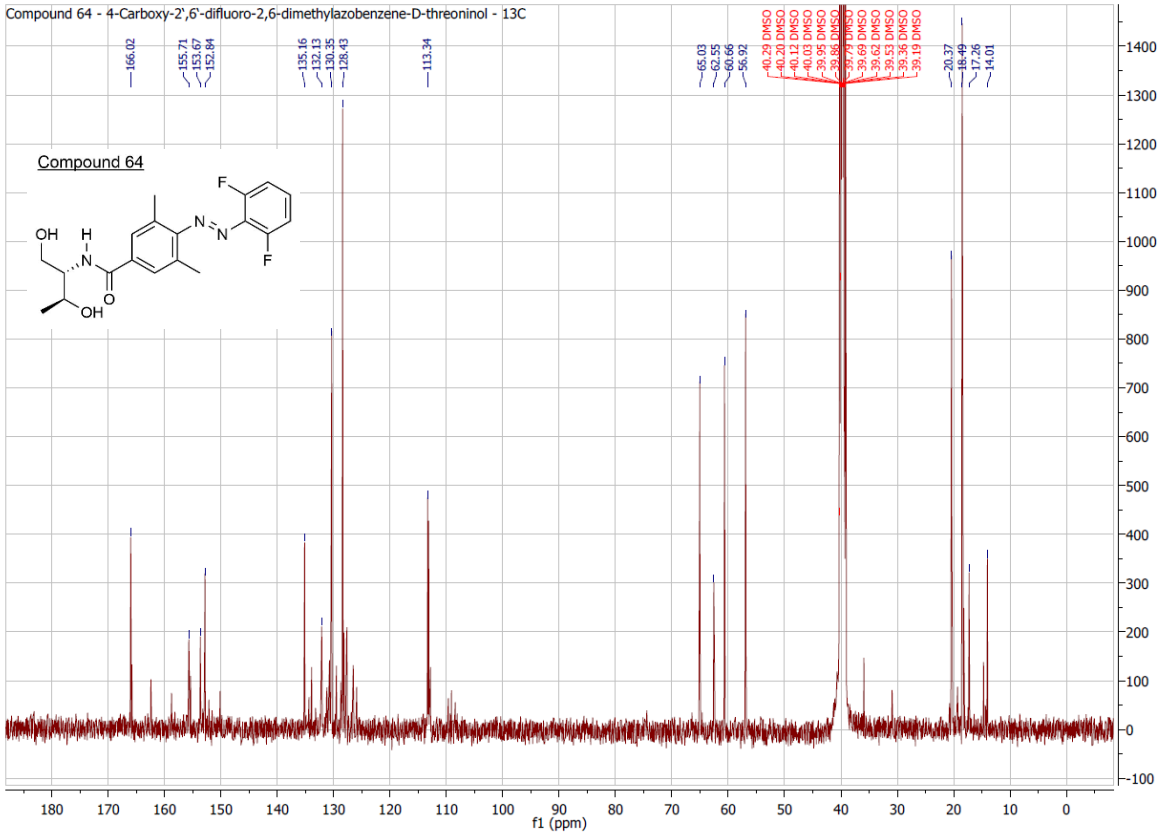
Compound 64 - 4-Carboxy-2',6'-difluoro-2,6-dimethylazobenzene-D-threoninol - 13C
Compound 64
f1 (ppm)

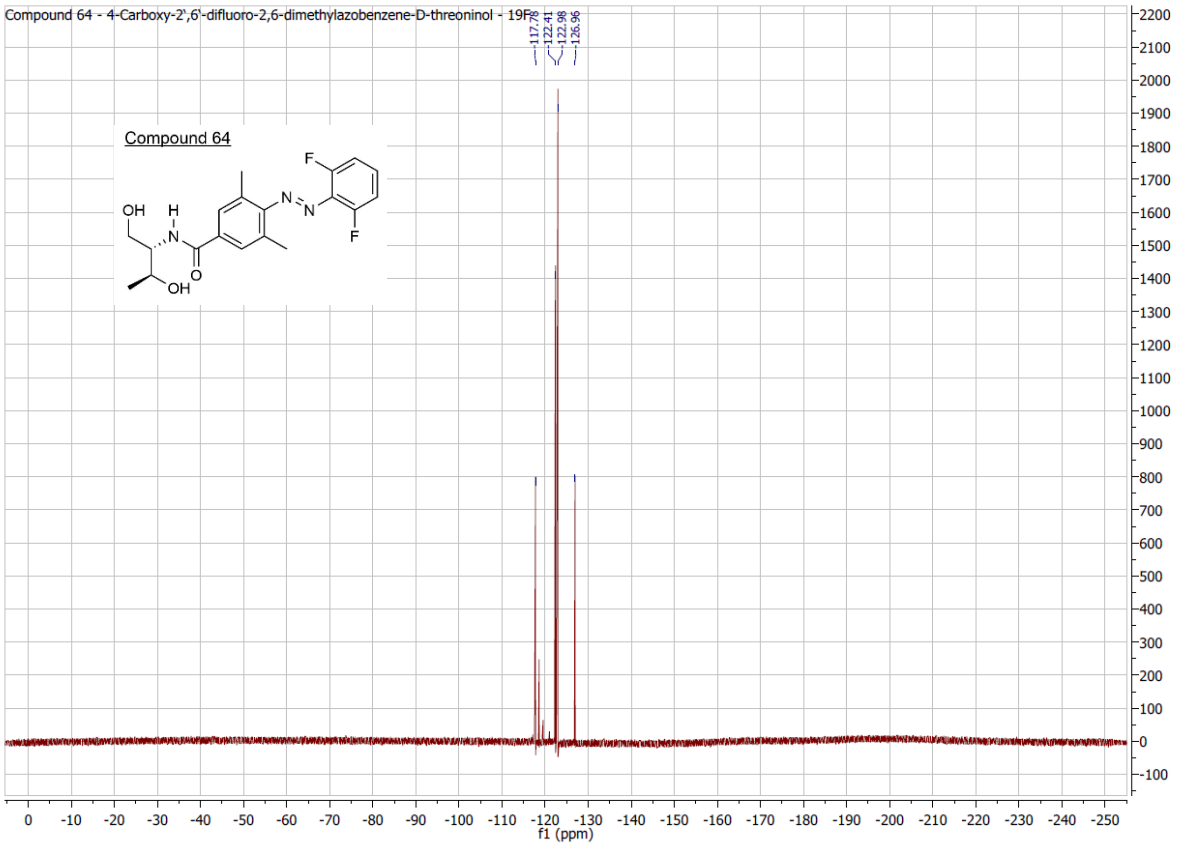
Compound 64 - 4-Carboxy-2',6'-difluoro-2,6-dimethylazobenzene-D-threoninol - 19F
117.78
122.41
122.98
126.96
Compound 64
F
OH
H
N
N
N
F
O
OH
f1 (ppm)

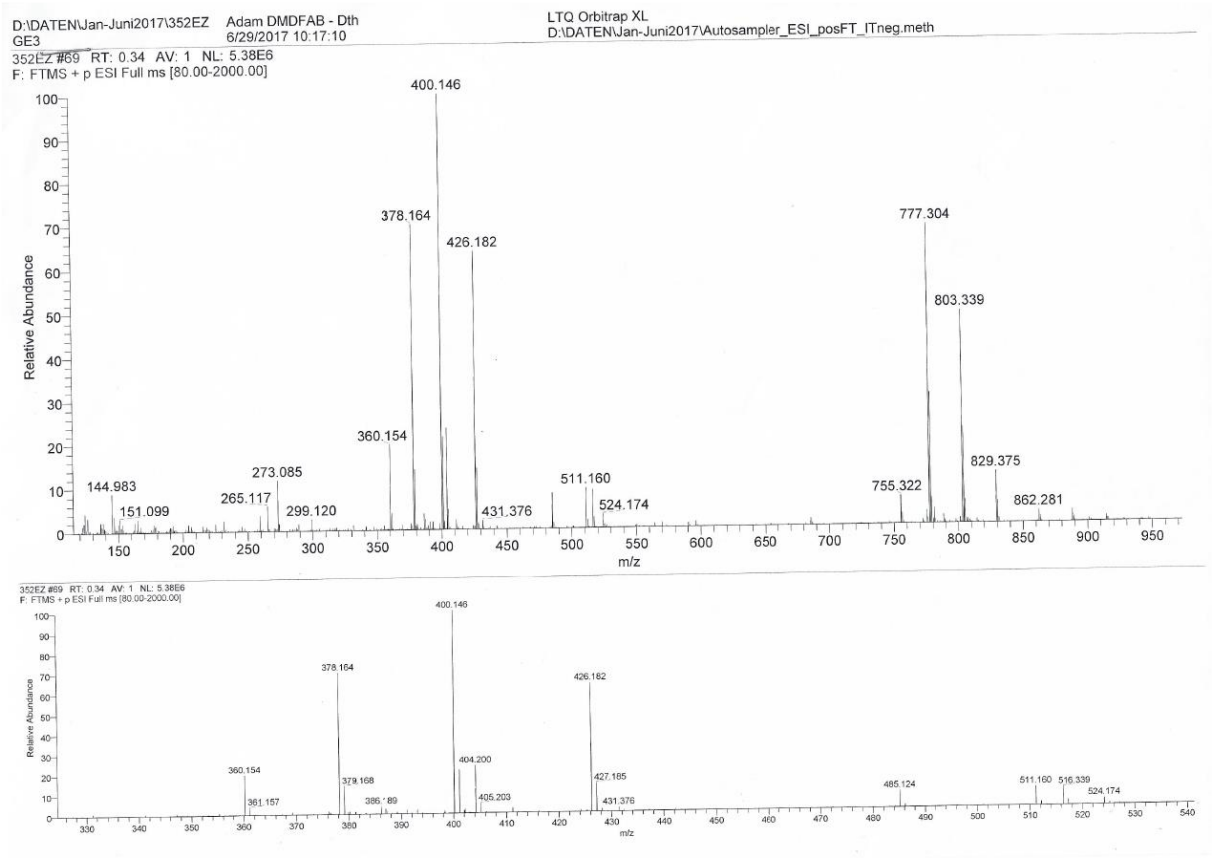
D:\DATEN\Jan-Juni2017\352EZ GE3
Adam DMDFAB - Dth
6/29/2017 10:17:10
LTQ Orbitrap XL
D:\DATEN\Jan-Juni2017\Autosampler_ESI_posFT_ITneg.meth
352EZ #69 RT: 0.34 AV: 1 NL: 5.38E6
F: FTMS + p ESI Full ms [80.00-2000.00]
Relative Abundance
m/z
400.146
378.164
426.182
777.304
803.339
360.154
829.375
273.085
511.160
144.983
265.117
755.322
862.281
151.099
299.120
524.174
431.376

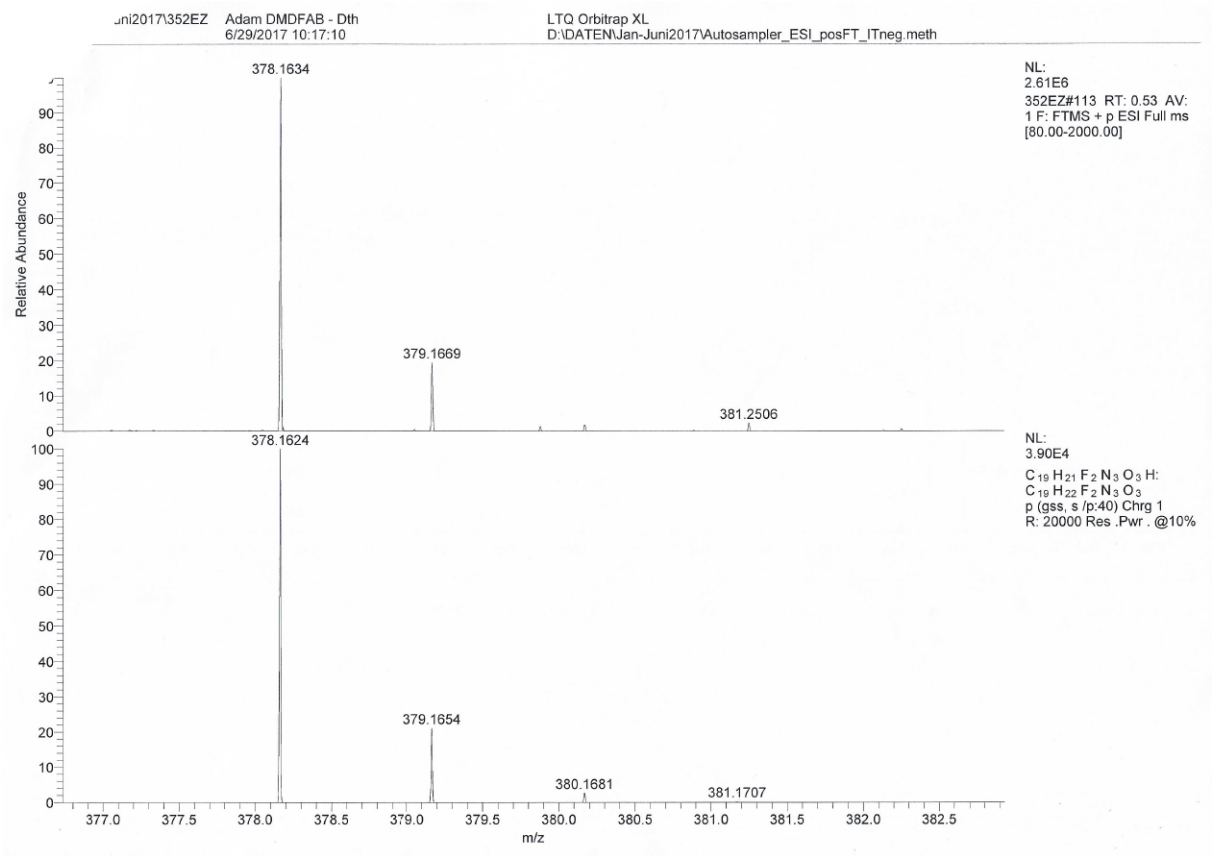
Juni2017\352EZ Adam DMDFAB - Dth
6/29/2017 10:17:10
LTQ Orbitrap XL
D:\DATEN\Jan-Juni2017\Autosampler_ESI_posFT_ITneg.meth
NL:
2.61E6
352EZ#113 RT: 0.53 AV: 1 F: FTMS + p ESI Full ms [80.00-2000.00]
378.1634
379.1669
381.2506
Relative Abundance
NL:
3.90E4
C19 H21 F2 N3 O3 H:
C19 H22 F2 N3 O3
p (gss, s /p:40) Chrg 1
R: 20000 Res .Pwr . @10%
378.1624
379.1654
380.1681
381.1707
m/z

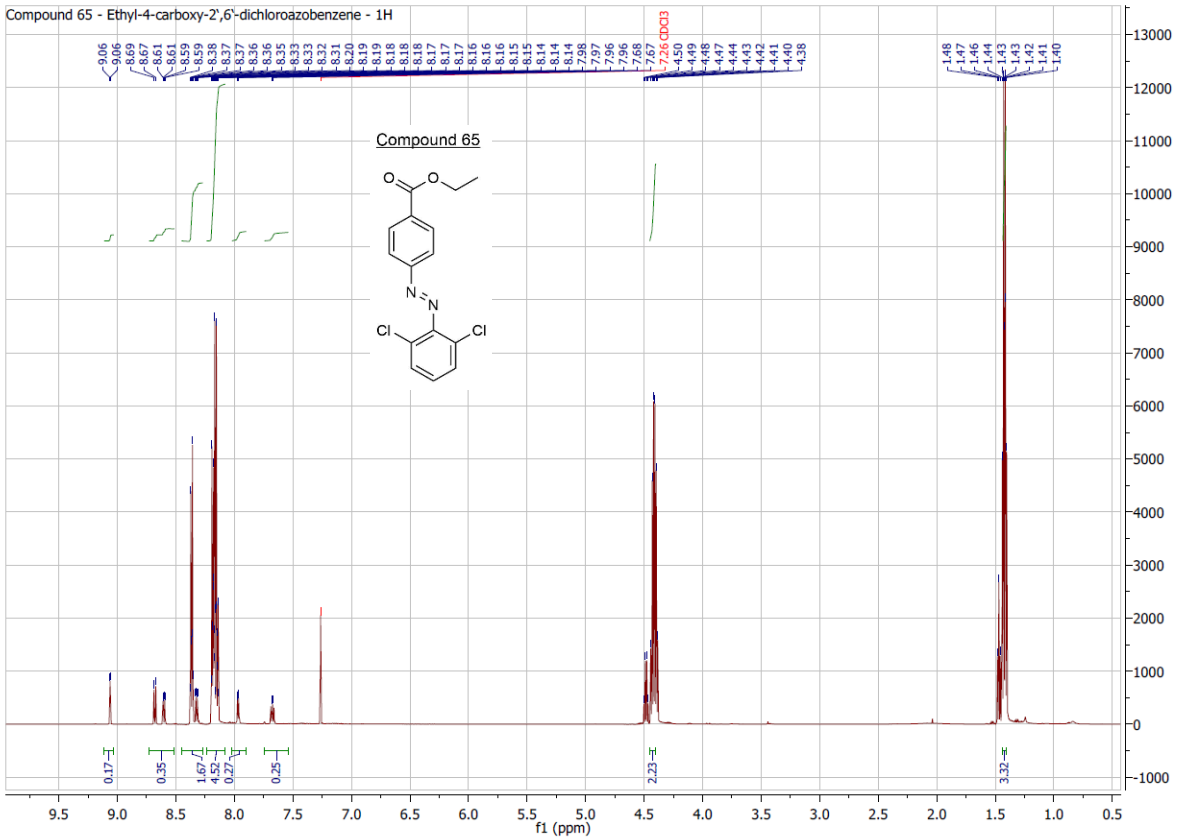
Compound 65 - Ethyl-4-carboxy-2',6'-dichloroazobenzene - 1H
Compound 65
f1 (ppm)

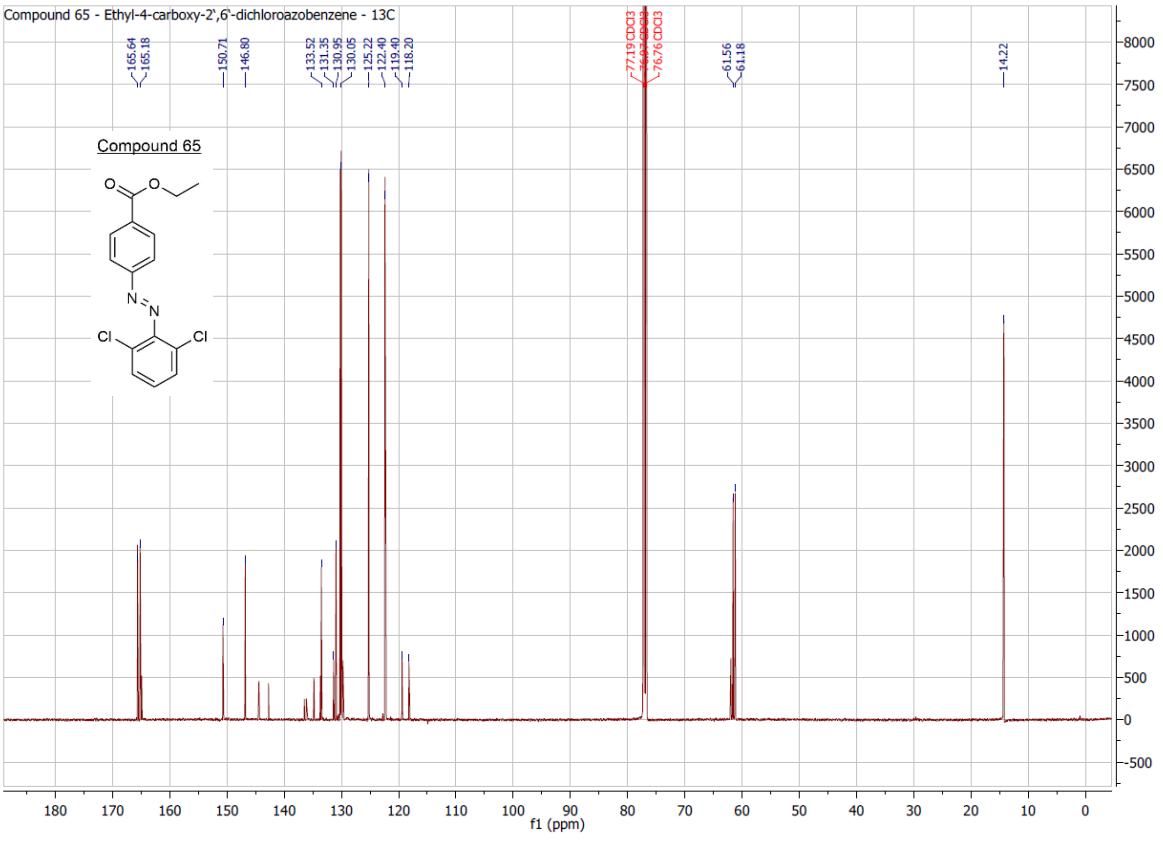
Compound 65 - Ethyl-4-carboxy-2',6'-dichloroazobenzene - 13C
Compound 65
f1 (ppm)

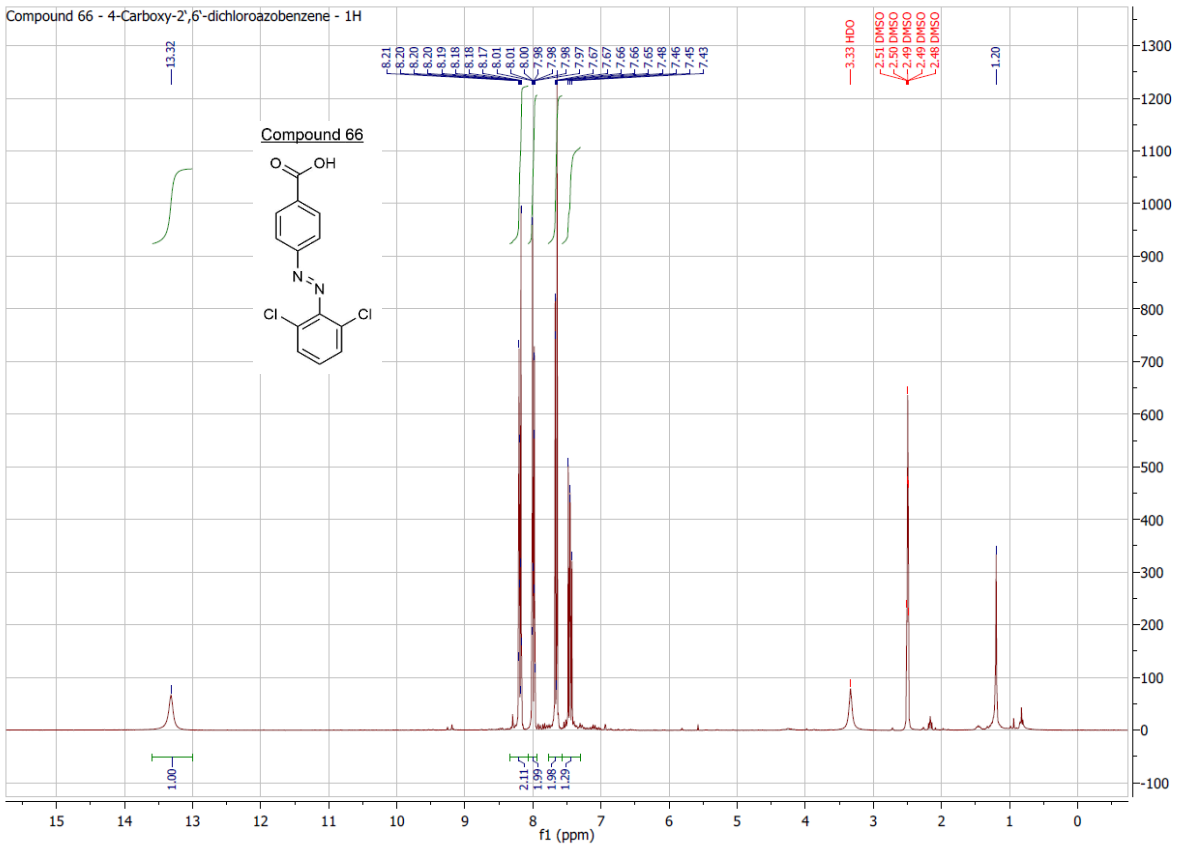
Compound 66 - 4-Carboxy-2',6'-dichloroazobenzene - 1H
Compound 66
f1 (ppm)

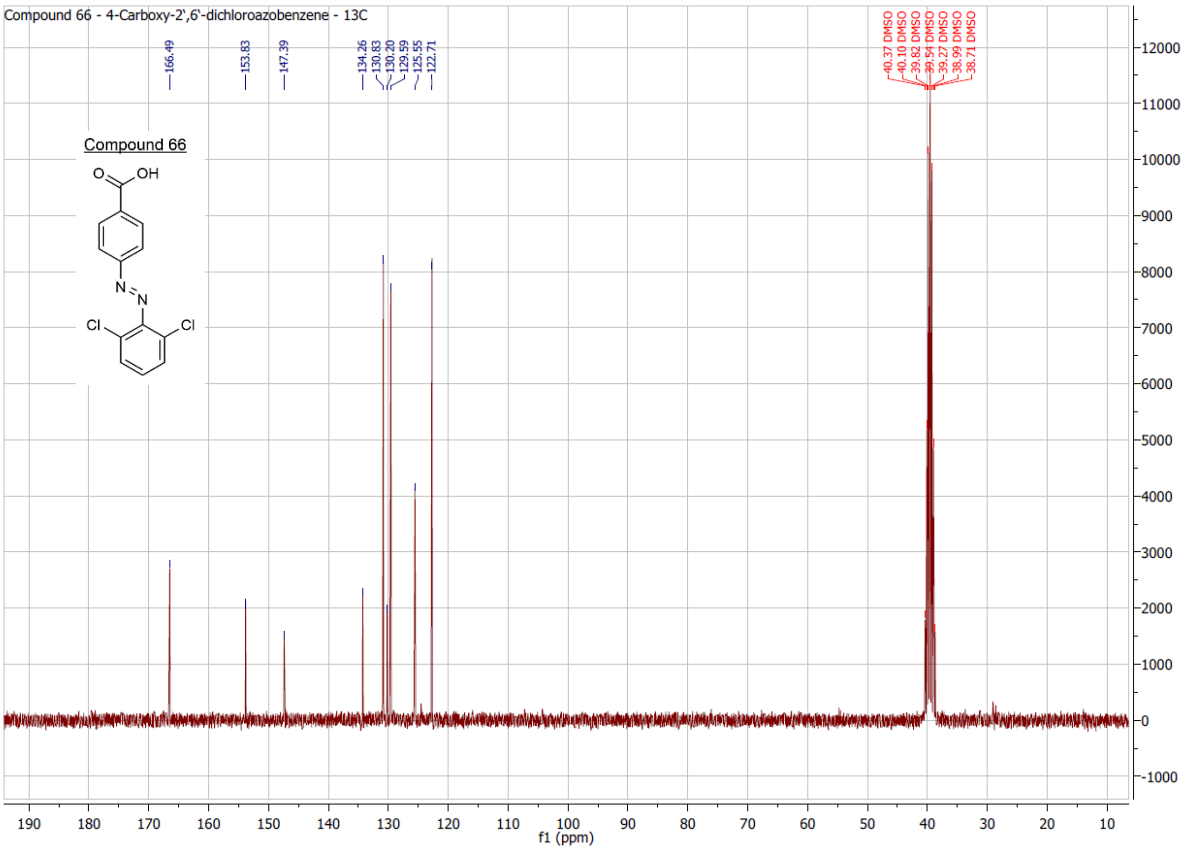
Compound 66 - 4-Carboxy-2',6'-dichloroazobenzene - 13C
Compound 66
f1 (ppm)

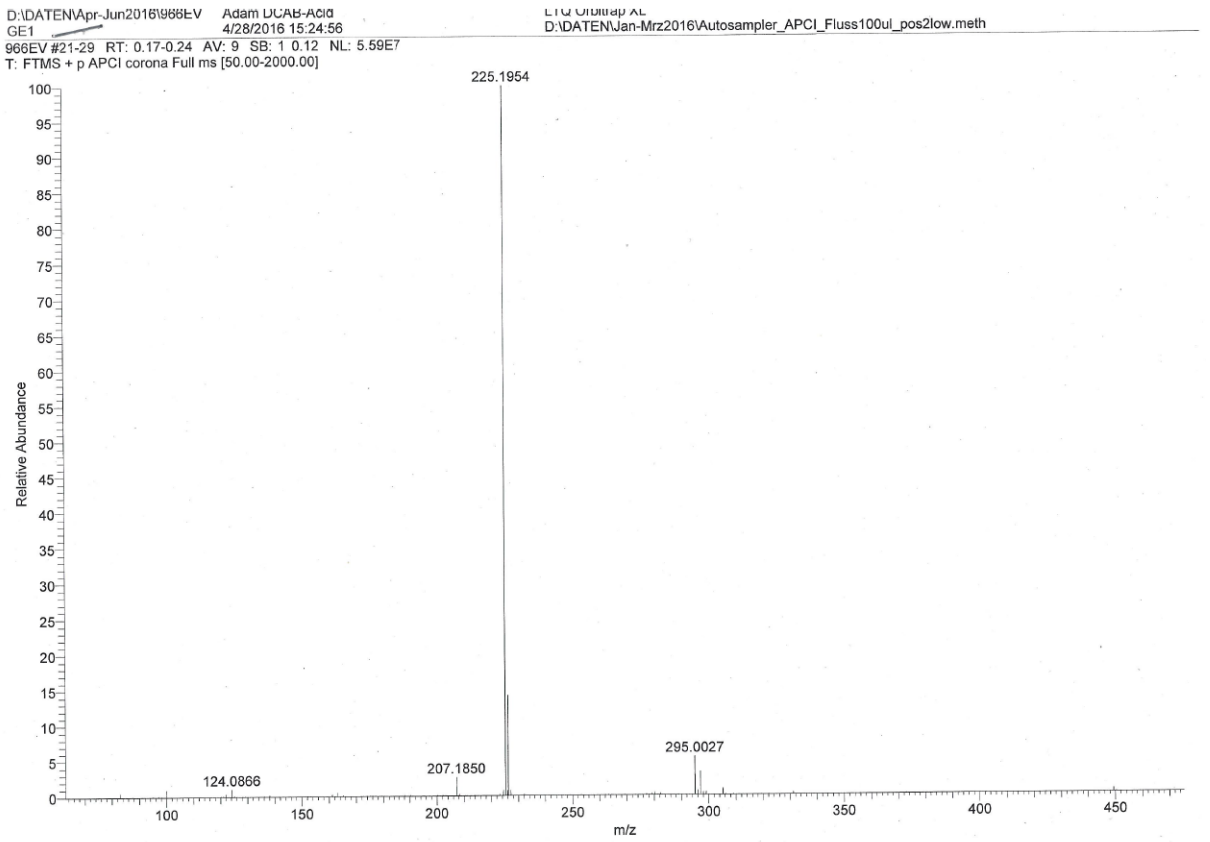
D:\DATEN\Apr-Jun2016\966EV Adam DCAB-Acid
GE1 4/28/2016 15:24:56
LTQ Orbitrap XL
D:\DATEN\Jan-Mrz2016\Autosampler_APCI_Fluss100ul_pos2low.meth
966EV #21-29 RT: 0.17-0.24 AV: 9 SB: 1 0.12 NL: 5.59E7
T: FTMS + p APCI corona Full ms [50.00-2000.00]
225.1954
295.0027
207.1850
124.0866
Relative Abundance
m/z

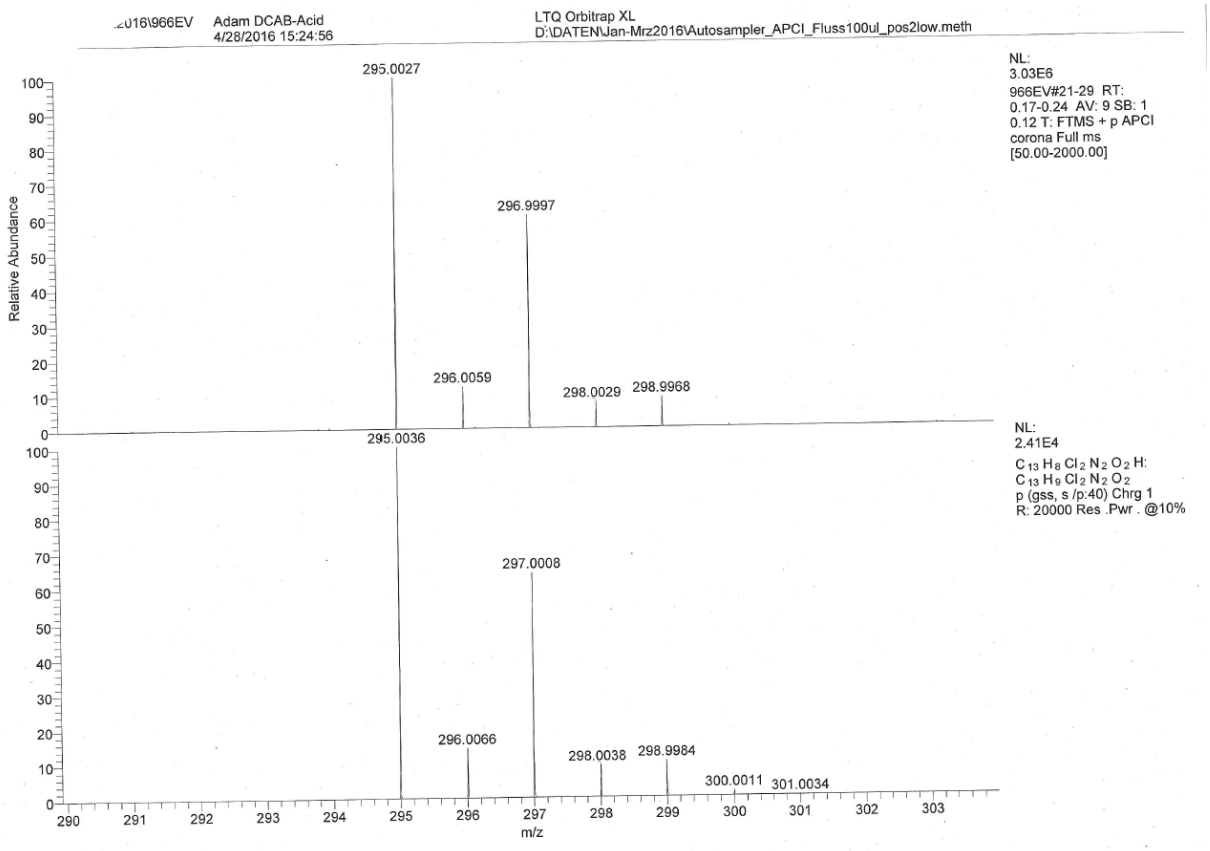
2016\966EV Adam DCAB-Acid
4/28/2016 15:24:56
LTQ Orbitrap XL
D:\DATEN\Jan-Mrz2016\Autosampler_APCI_Fluss100ul_pos2low.meth
NL:
3.03E6
966EV#21-29 RT:
0.17-0.24 AV: 9 SB: 1
0.12 T: FTMS + p APCI
corona Full ms
[50.00-2000.00]
295.0027
296.9997
296.0059
298.0029
298.9968
295.0036
NL:
2.41E4
C13 H8 Cl2 N2 O2 H:
C13 H9 Cl2 N2 O2
p (gss, s /p:40) Chrg 1
R: 20000 Res .Pwr . @10%
297.0008
296.0066
298.0038
298.9984
300.0011
301.0034
Relative Abundance
m/z

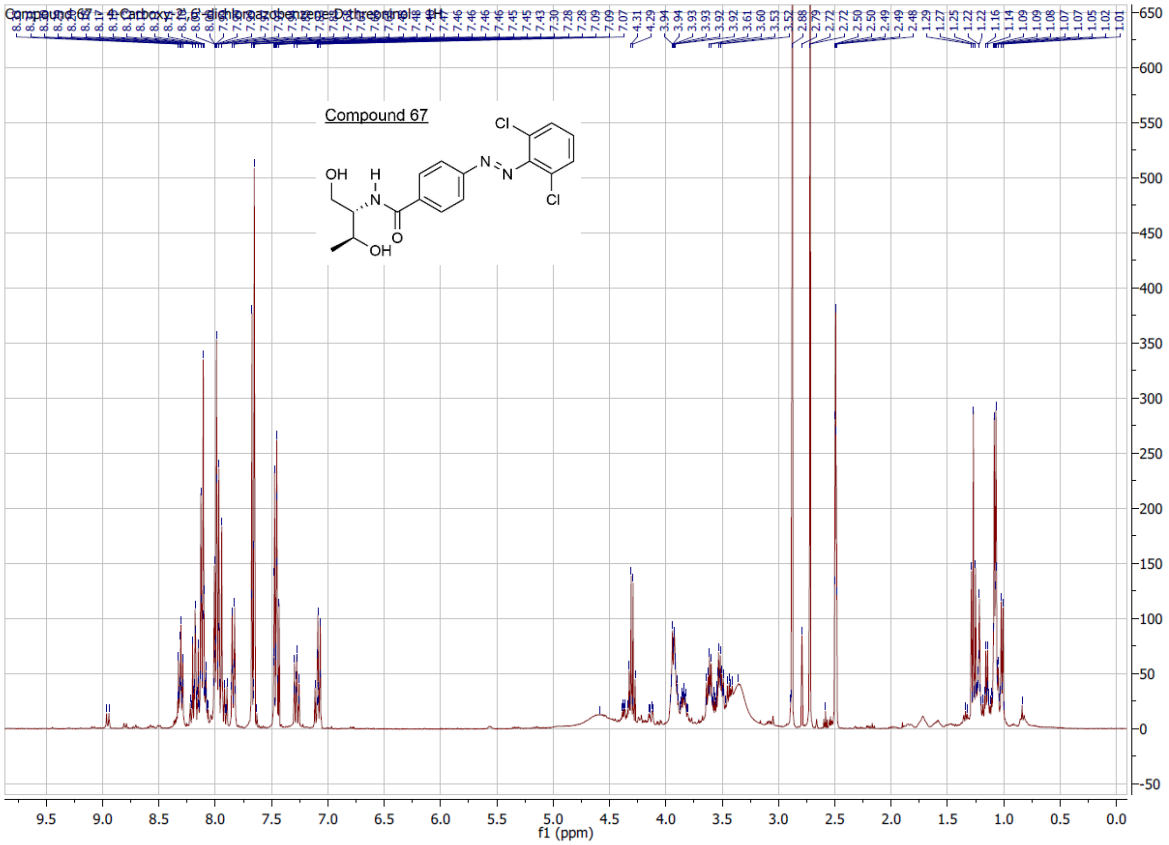
Compound 67
Cl
N
N
Cl
OH
H
N
O
OH
f1 (ppm)

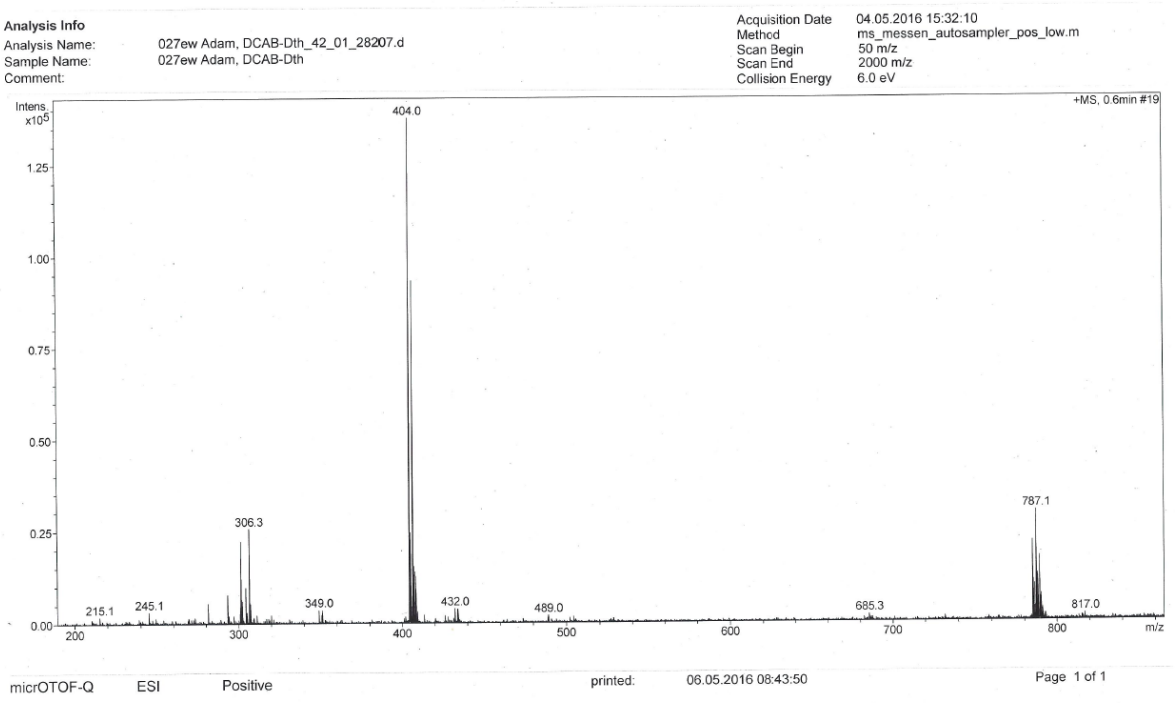
Analysis Info
Analysis Name: 027ew Adam, DCAB-Dth_42_01_28207.d
Sample Name: 027ew Adam, DCAB-Dth
Comment:
Acquisition Date 04.05.2016 15:32:10
Method ms_messen_autosampler_pos_low.m
Scan Begin 50 m/z
Scan End 2000 m/z
Collision Energy 6.0 eV
+MS, 0.6min #19
Intens.
x10^5
404.0
306.3
787.1
215.1
245.1
349.0
432.0
489.0
685.3
817.0
m/z
micrOTOF-Q ESI Positive
printed: 06.05.2016 08:43:50
Page 1 of 1

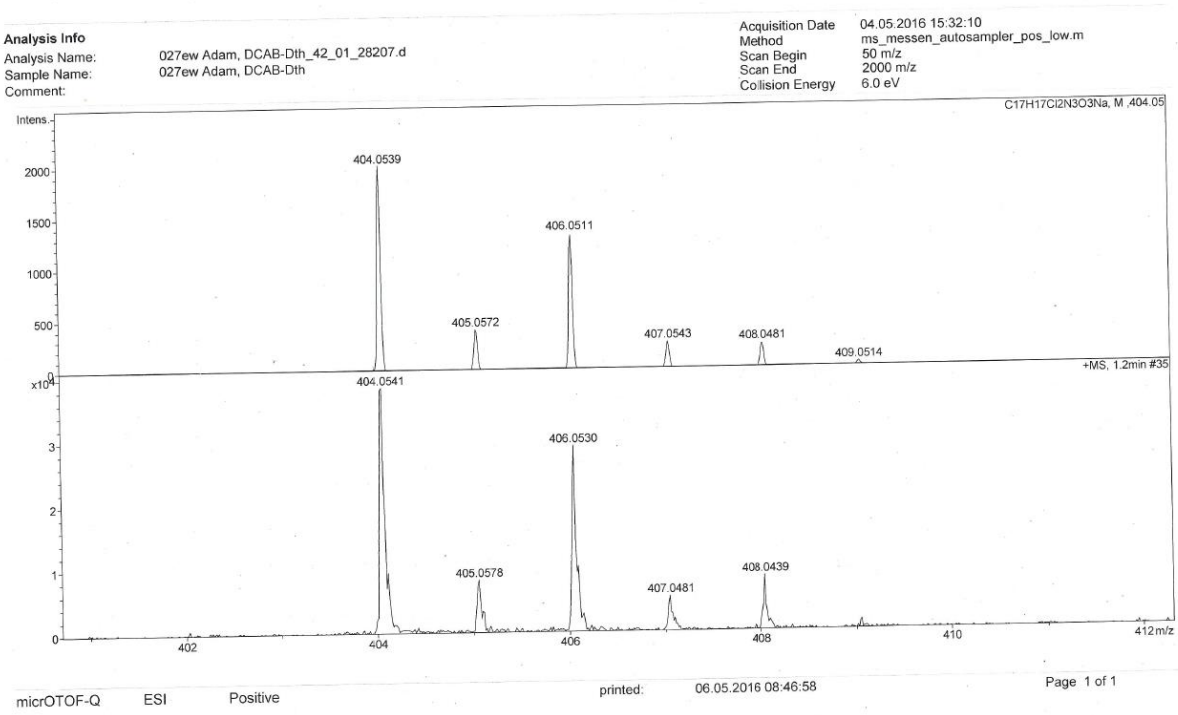
Analysis Info
Analysis Name: 027ew Adam, DCAB-Dth_42_01_28207.d
Sample Name: 027ew Adam, DCAB-Dth
Comment:
Acquisition Date 04.05.2016 15:32:10
Method ms_messen_autosampler_pos_low.m
Scan Begin 50 m/z
Scan End 2000 m/z
Collision Energy 6.0 eV
C17H17Cl2N3O3Na, M ,404.05
Intens.
404.0539
406.0511
405.0572
407.0543
408.0481
409.0514
+MS, 1.2min #35
x10^4
404.0541
406.0530
405.0578
407.0481
408.0439
m/z
micrOTOF-Q ESI Positive
printed: 06.05.2016 08:46:58
Page 1 of 1

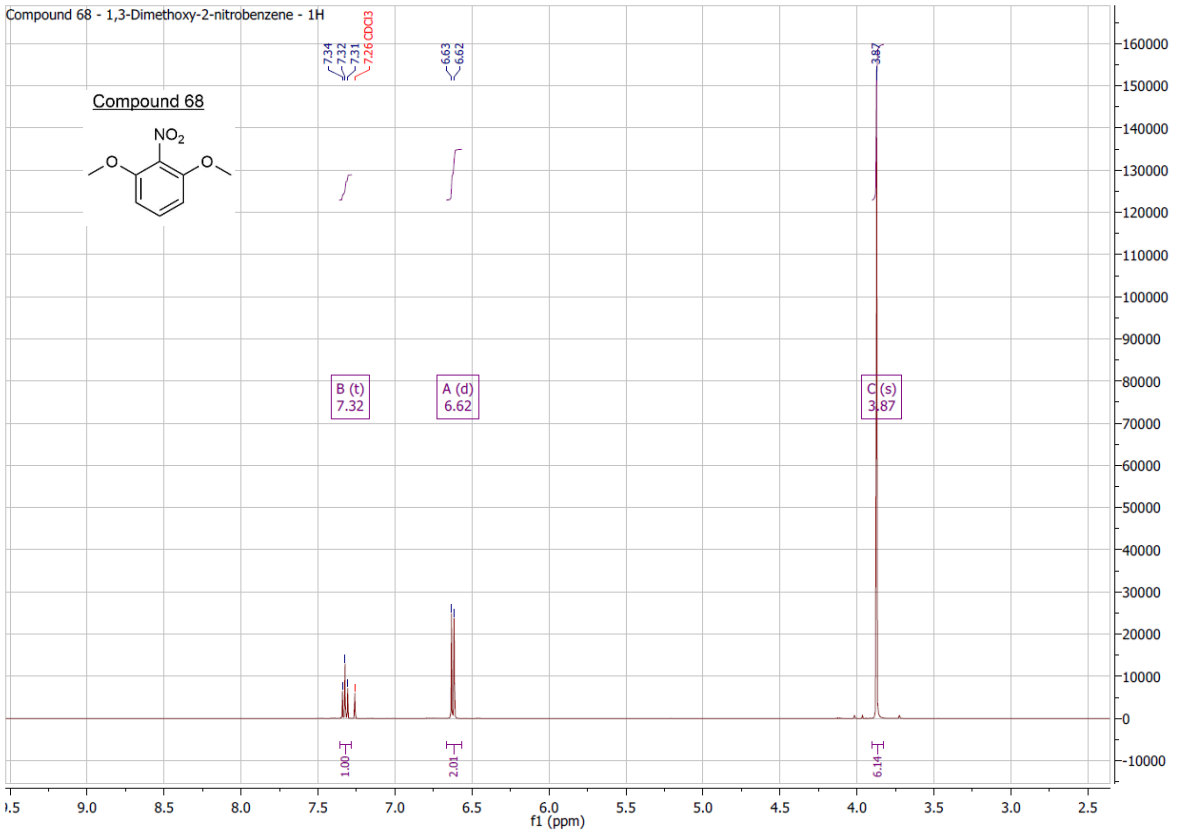
Compound 68 - 1,3-Dimethoxy-2-nitrobenzene - 1H
Compound 68
NO2
O
O
7.34
7.32
7.31
7.26 CDCl3
6.63
6.62
3.87
B (t)
7.32
A (d)
6.62
C (s)
3.87
1.00
2.01
6.14
f1 (ppm)

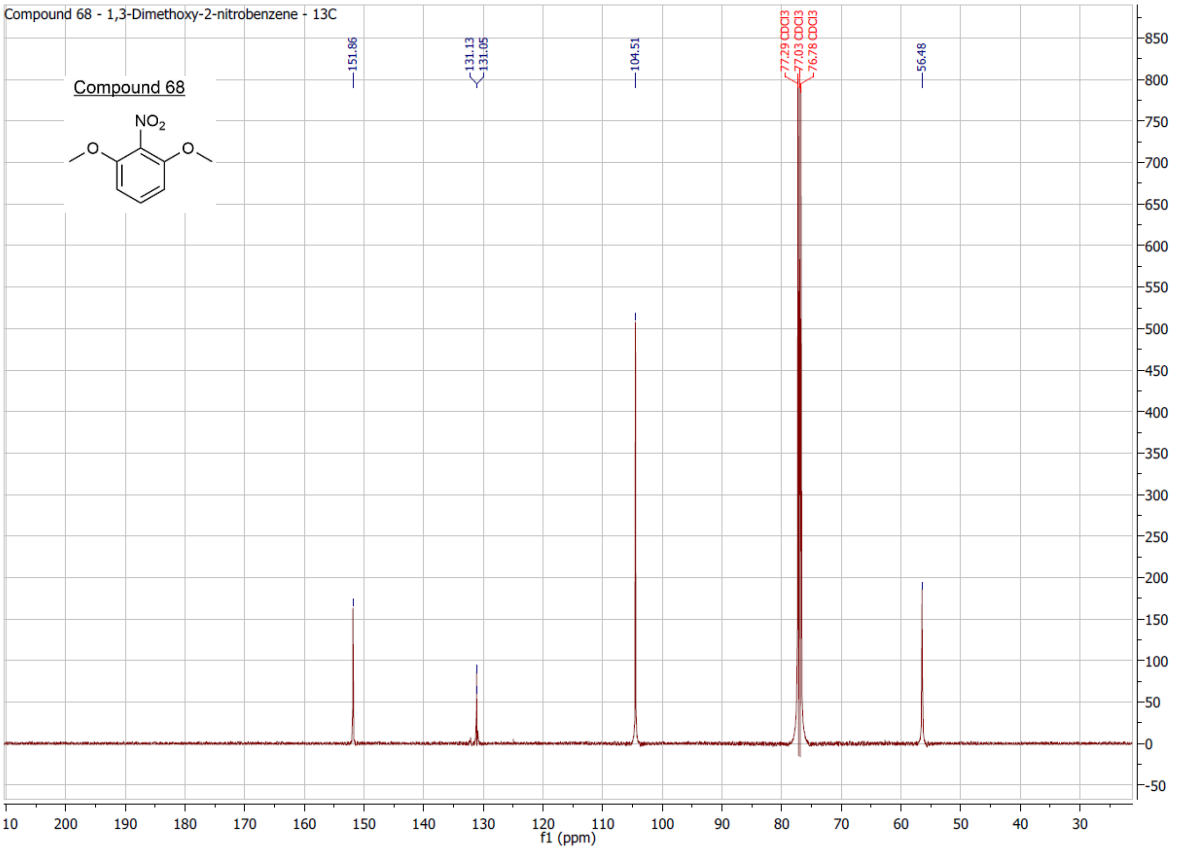
Compound 68 - 1,3-Dimethoxy-2-nitrobenzene - 13C
Compound 68
NO2
O
O
151.86
131.13
131.05
104.51
77.29 CDCl3
77.03 CDCl3
76.78 CDCl3
56.48
f1 (ppm)

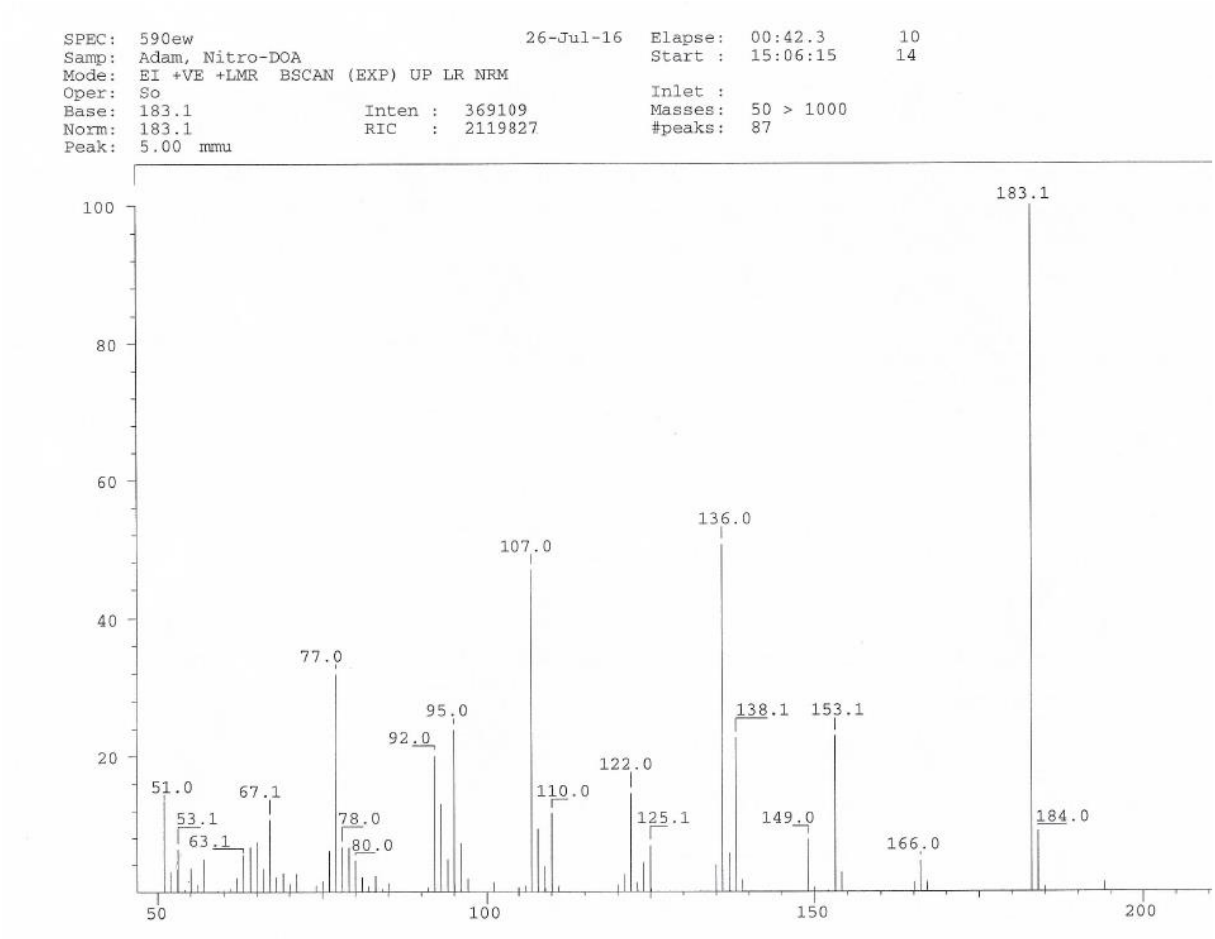
SPEC: 590ew 26-Jul-16 Elapse: 00:42.3 10
Samp: Adam, Nitro-DOA Start : 15:06:15 14
Mode: EI +VE +LMR BSCAN (EXP) UP LR NRM
Oper: So Inlet :
Base: 183.1 Inten : 369109 Masses: 50 > 1000
Norm: 183.1 RIC : 2119827 #peaks: 87
Peak: 5.00 mmu
183.1
136.0
107.0
77.0
95.0
92.0
138.1
153.1
122.0
51.0
67.1
110.0
53.1
78.0
125.1
149.0
184.0
63.1
80.0
166.0
100
80
60
40
20
50
100
150
200

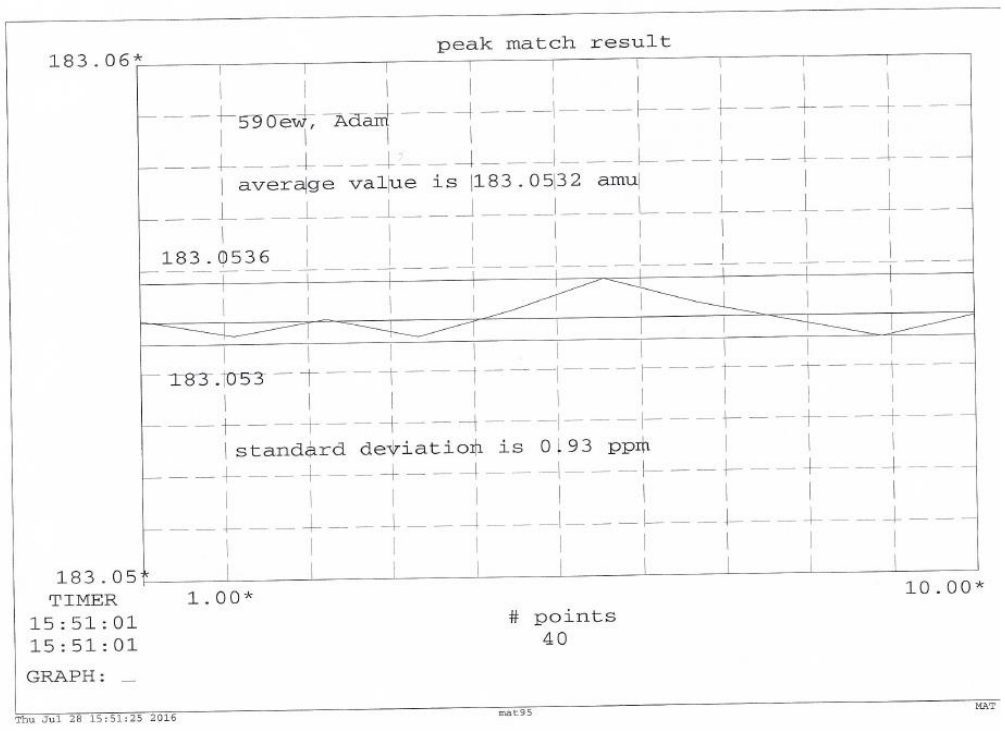
peak match result
183.06*
590ew, Adam
average value is 183.0532 amu
183.0536
183.053
standard deviation is 0.93 ppm
183.05*
1.00*
10.00*
TIMER
15:51:01
15:51:01
points
40
GRAPH:
Thu Jul 28 15:51:25 2016
mat95
MAT

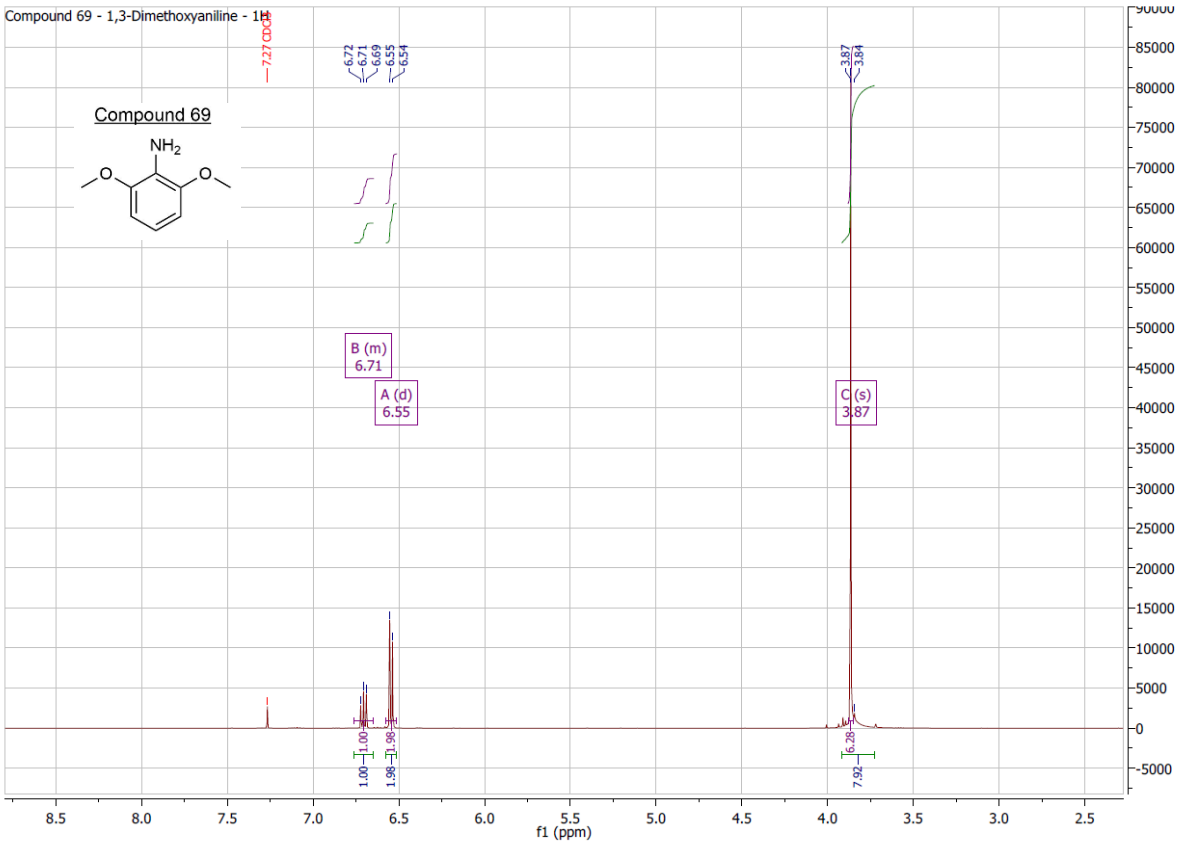
Compound 69 - 1,3-Dimethoxyaniline - 1H
Compound 69
NH2
B (m)
6.71
A (d)
6.55
C (s)
3.87
f1 (ppm)

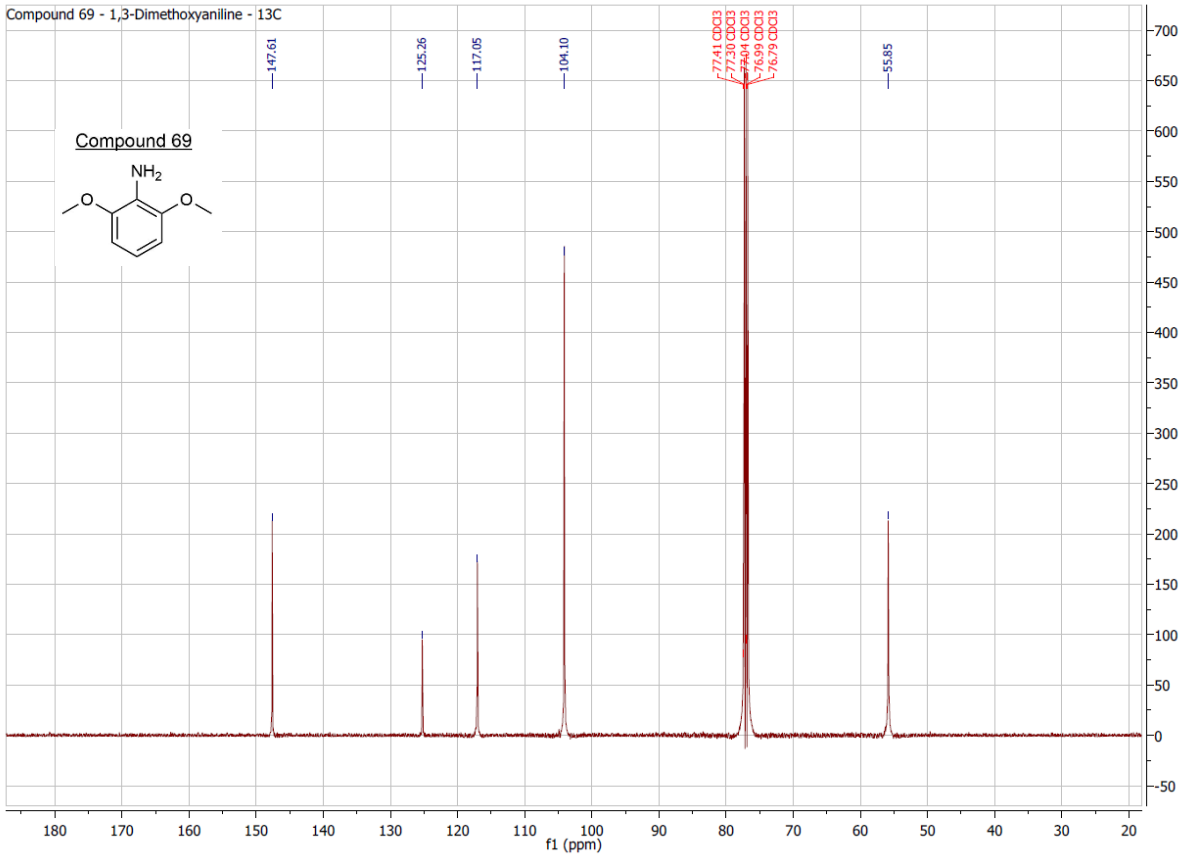
Compound 69 - 1,3-Dimethoxyaniline - 13C
Compound 69
NH2
147.61
125.26
117.05
104.10
55.85
f1 (ppm)

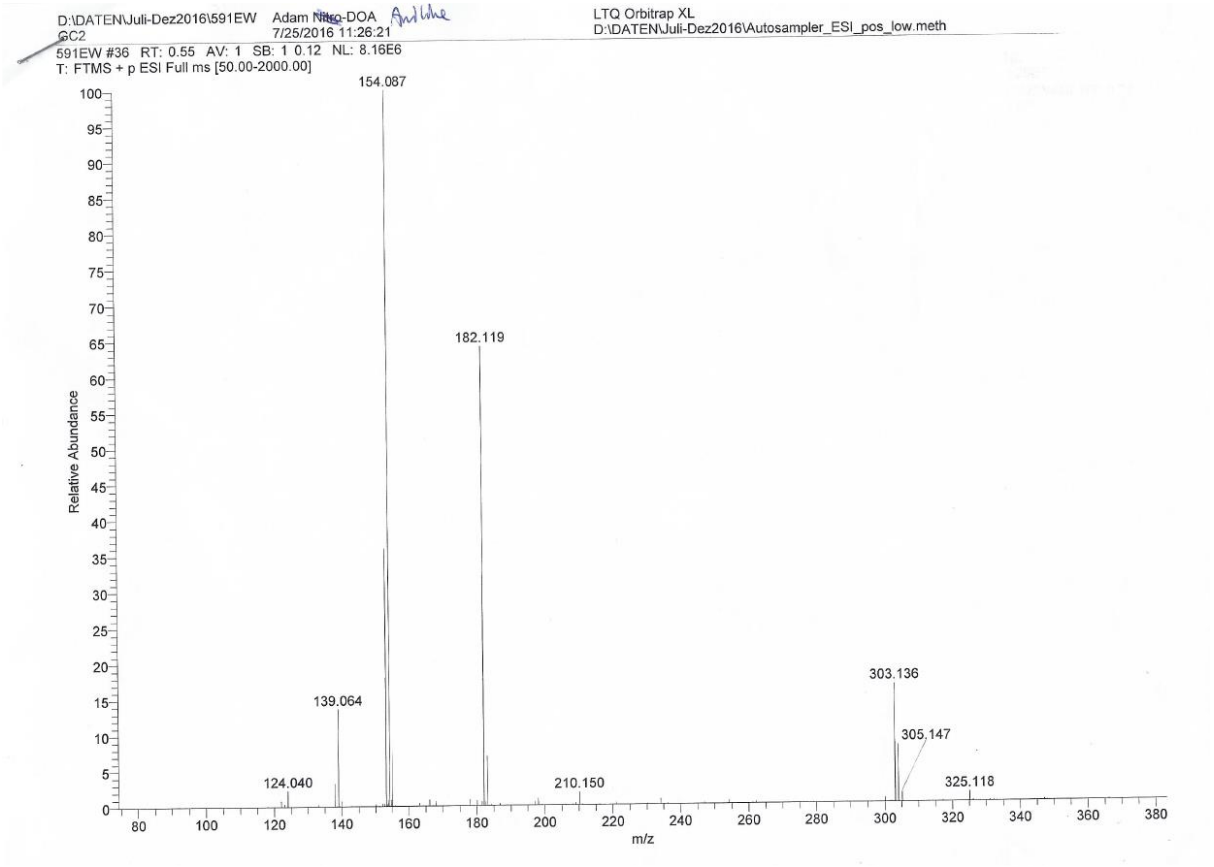
D:\DATEN\Juli-Dez2016\591EW Adam Nitro-DOA
GC2 7/25/2016 11:26:21
LTQ Orbitrap XL
D:\DATEN\Juli-Dez2016\Autosampler_ESI_pos_low.meth
591EW #36 RT: 0.55 AV: 1 SB: 1 0.12 NL: 8.16E6
T: FTMS + p ESI Full ms [50.00-2000.00]
154.087
182.119
303.136
139.064
305.147
124.040
210.150
325.118
Relative Abundance
m/z

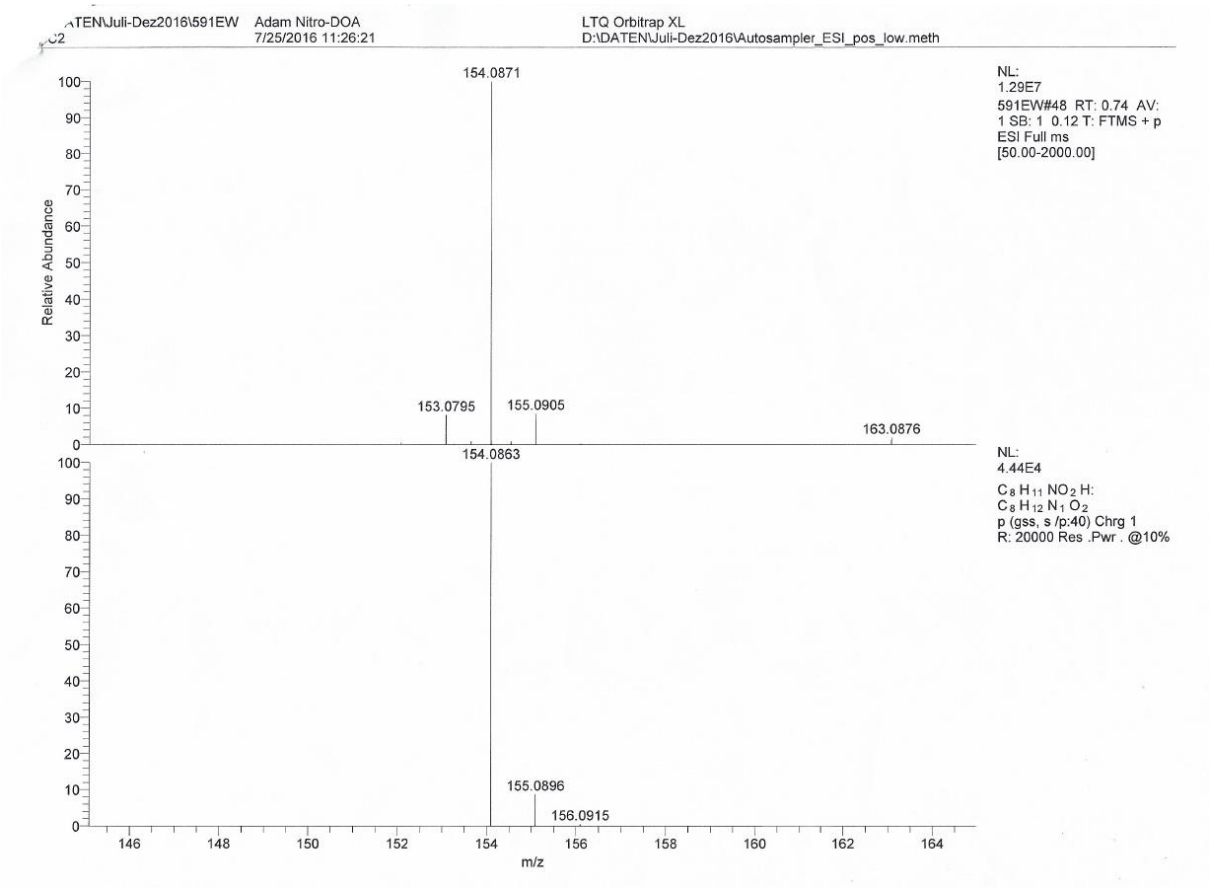
ATEN\Juli-Dez2016\591EW Adam Nitro-DOA
C2 7/25/2016 11:26:21
LTQ Orbitrap XL
D:\DATEN\Juli-Dez2016\Autosampler_ESI_pos_low.meth
154.0871
NL:
1.29E7
591EW#48 RT: 0.74 AV:
1 SB: 1 0.12 T: FTMS + p
ESI Full ms
[50.00-2000.00]
153.0795
155.0905
163.0876
154.0863
NL:
4.44E4
C8 H11 NO2 H:
C8 H12 N1 O2
p (gss, s /p:40) Chrg 1
R: 20000 Res .Pwr . @10%
155.0896
156.0915
Relative Abundance
m/z

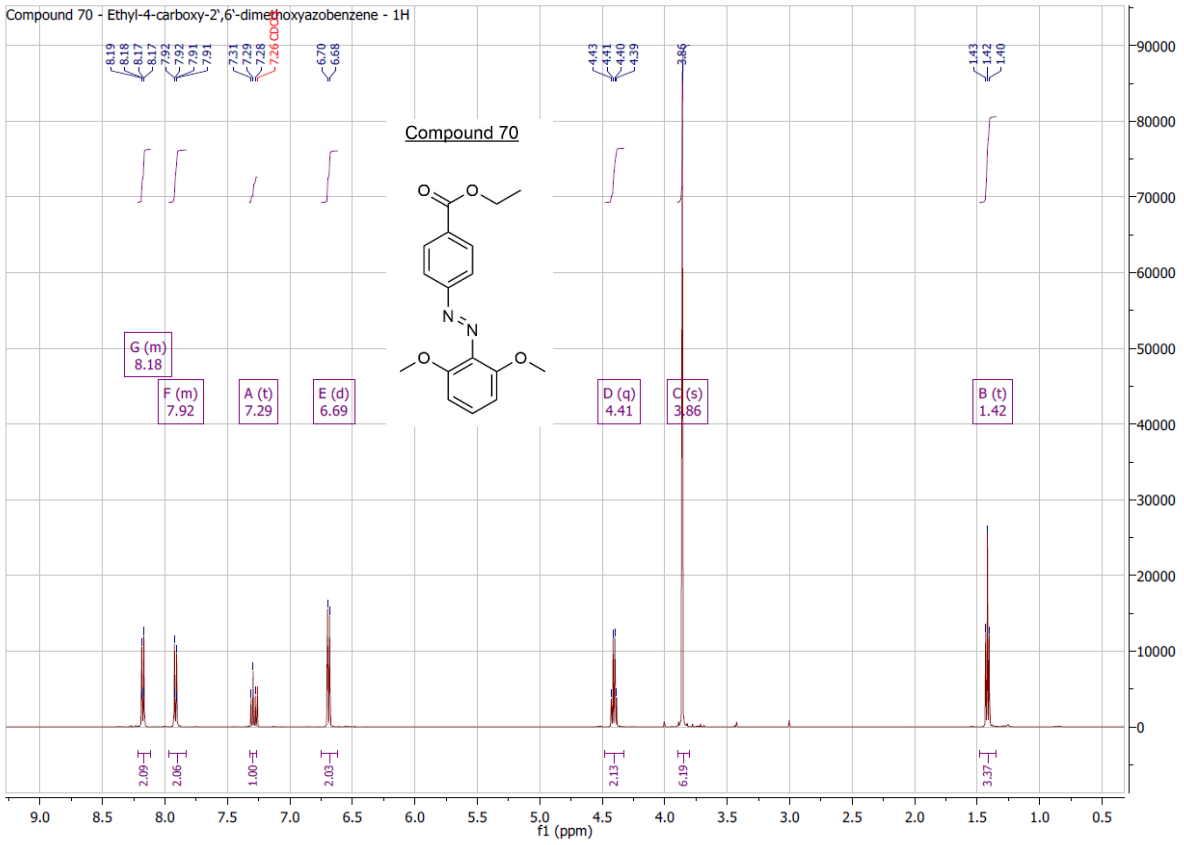
Compound 70 - Ethyl-4-carboxy-2',6'-dimethoxyazobenzene - 1H
Compound 70
G (m) 8.18
F (m) 7.92
A (t) 7.29
E (d) 6.69
D (q) 4.41
C (s) 3.86
B (t) 1.42
f1 (ppm)

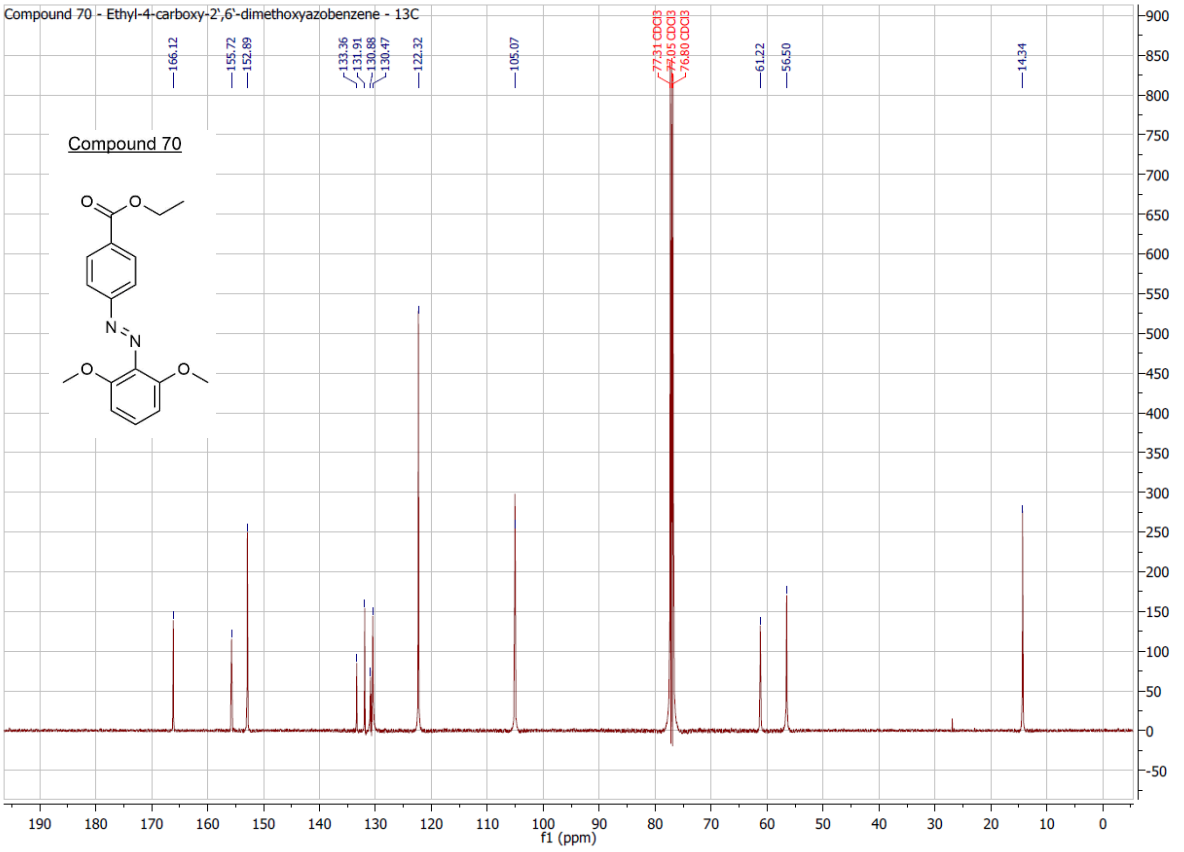
Compound 70 - Ethyl-4-carboxy-2',6'-dimethoxyazobenzene - 13C
Compound 70
166.12
155.72
152.89
133.36
131.91
130.88
130.47
122.32
105.07
77.31 CDCl3
77.05 CDCl3
76.80 CDCl3
61.22
56.50
14.34
f1 (ppm)

Analysis Info

Analysis Name:	592EW Adam Ethyl DOAB_19_01_28538.d
Sample Name:	592EW Adam Ethyl DOAB
Comment:	
Acquisition Date	20.07.2016 13:59:25
Method	ms_messen_autosampler_pos_low.m
Scan Begin	50 m/z
Scan End	2000 m/z
Collision Energy	8.0 eV

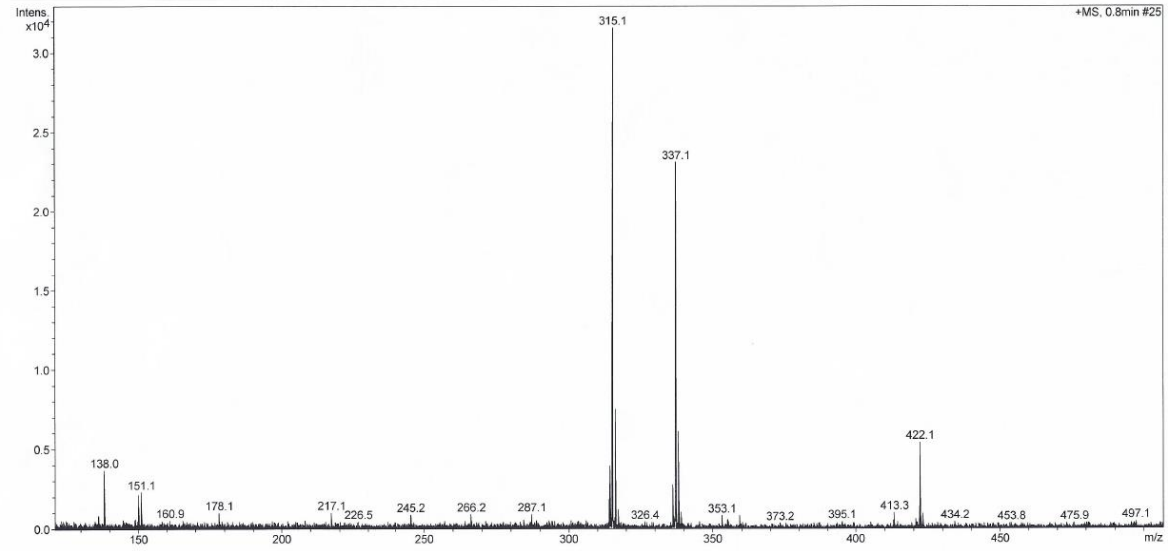

micrOTOF-Q ESI Positive printed: 20.07.2016 14:59:04 Page 1 of 1

Analysis Info

Analysis Name:	592EW Adam Ethyl DOAB_19_01_28538.d
Sample Name:	592EW Adam Ethyl DOAB
Comment:	
Acquisition Date	20.07.2016 13:59:25
Method	ms_messen_autosampler_pos_low.m
Scan Begin	50 m/z
Scan End	2000 m/z
Collision Energy	8.0 eV

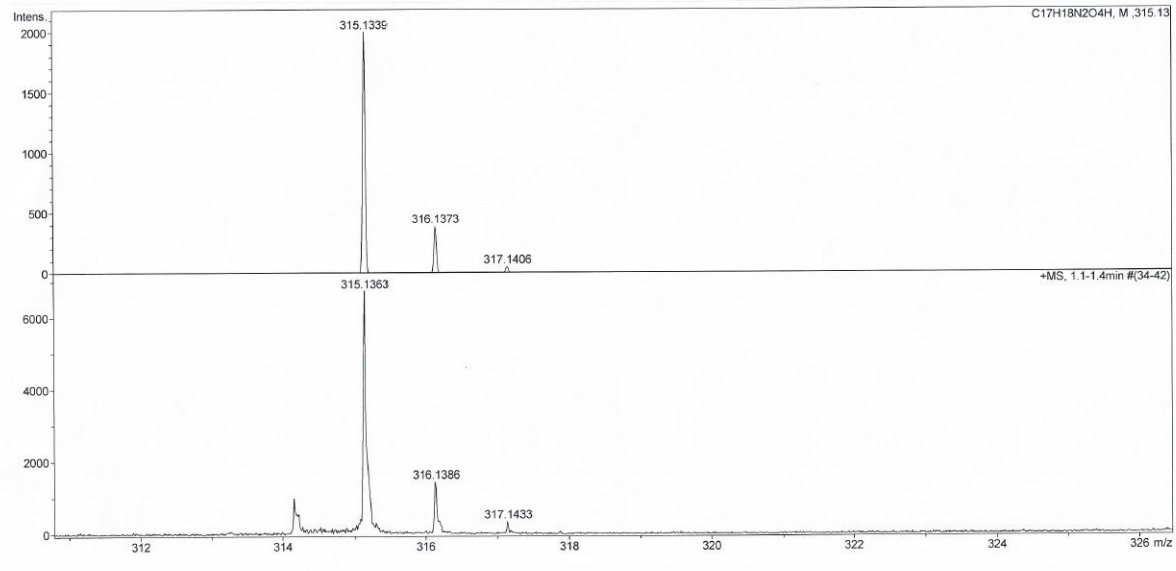

micrOTOF-Q ESI Positive printed: 20.07.2016 14:57:15 Page 1 of 1

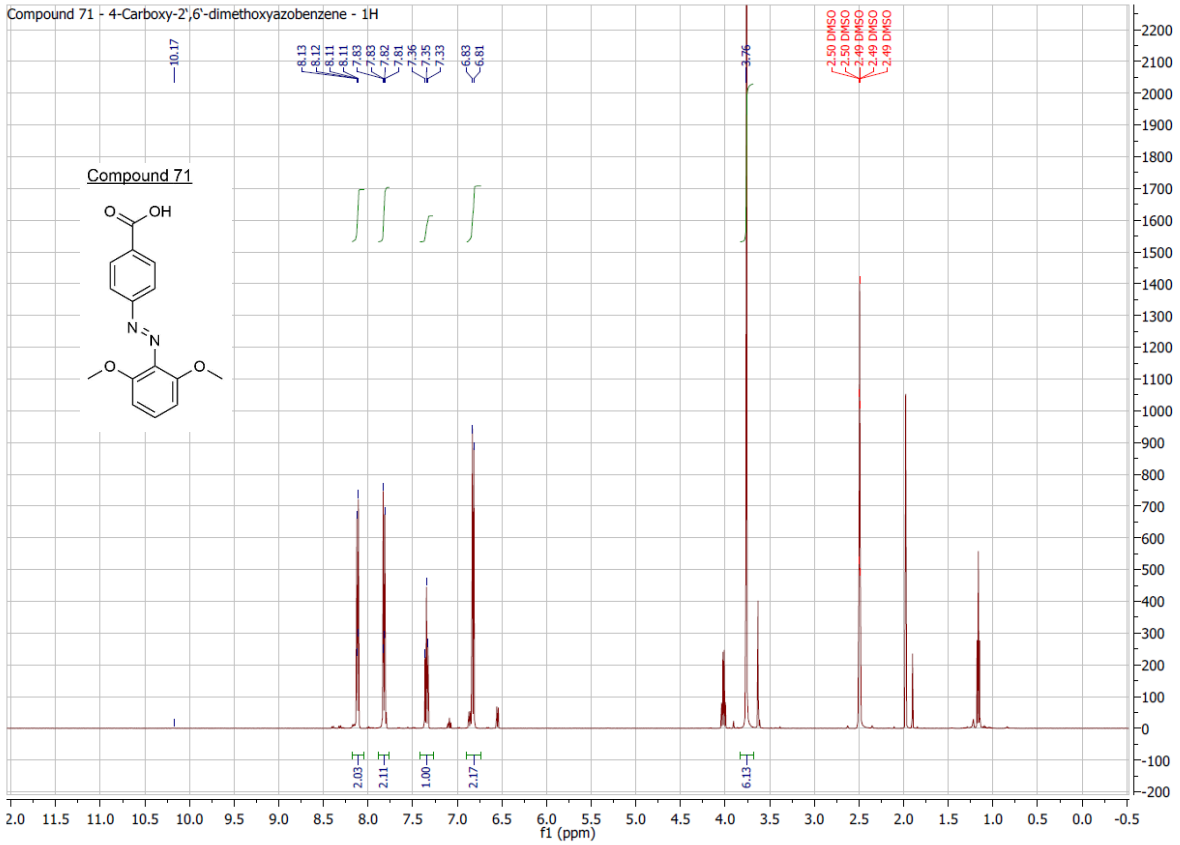
Compound 71 - 4-Carboxy-2',6'-dimethoxyazobenzene - 1H
Compound 71
f1 (ppm)

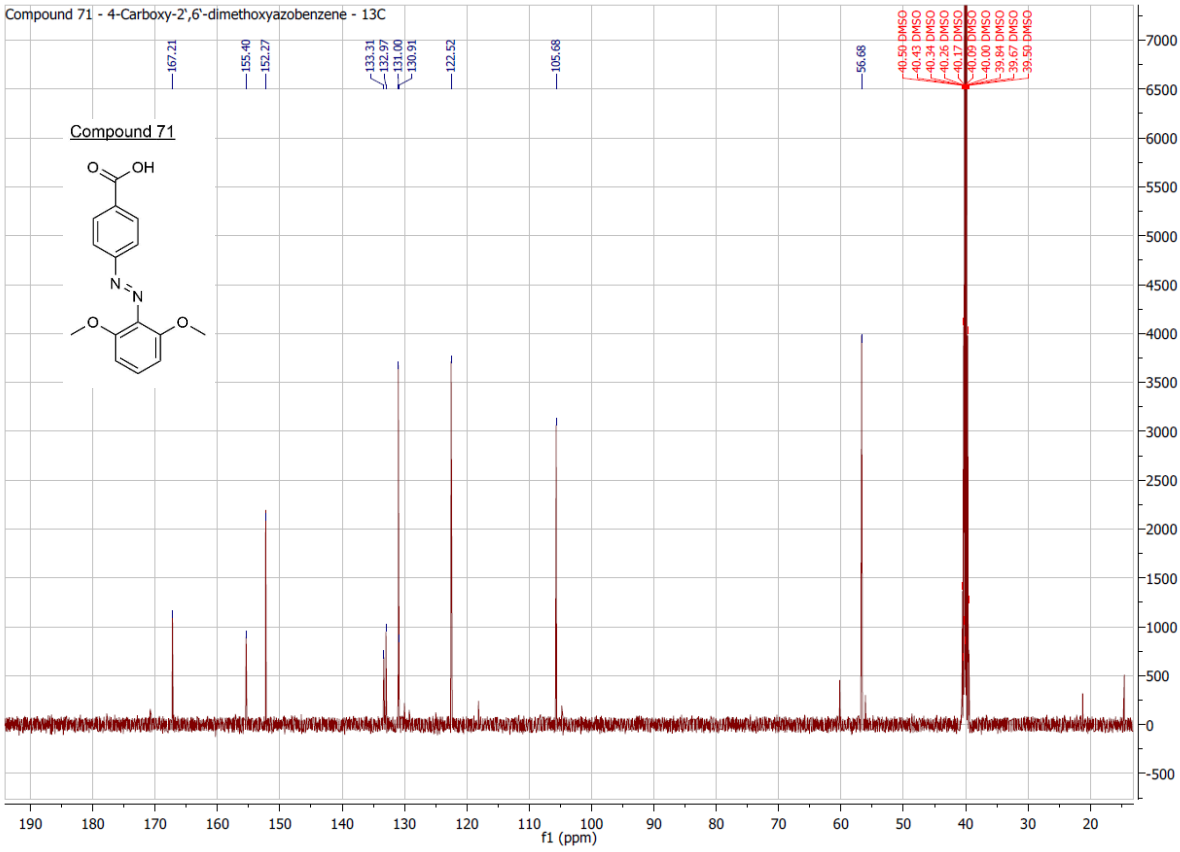
Compound 71 - 4-Carboxy-2',6'-dimethoxyazobenzene - 13C
Compound 71
f1 (ppm)

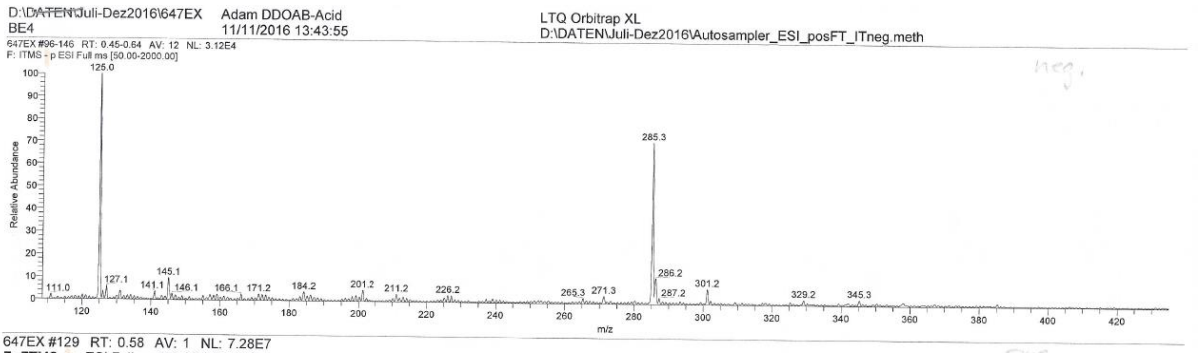
D:\DATEN\Juli-Dez2016\647EX
BE4
Adam DDOAB-Acid
11/11/2016 13:43:55
LTQ Orbitrap XL
D:\DATEN\Juli-Dez2016\Autosampler_ESI_posFT_ITneg.meth
647EX #96-146 RT: 0.45-0.64 AV: 12 NL: 3.12E4
F: ITMS - p ESI Full ms [50.00-2000.00]
Relative Abundance
m/z
125.0
285.3
111.0
127.1
145.1
141.1
146.1
166.1
171.2
184.2
201.2
211.2
226.2
265.3
271.3
286.2
287.2
301.2
329.2
345.3

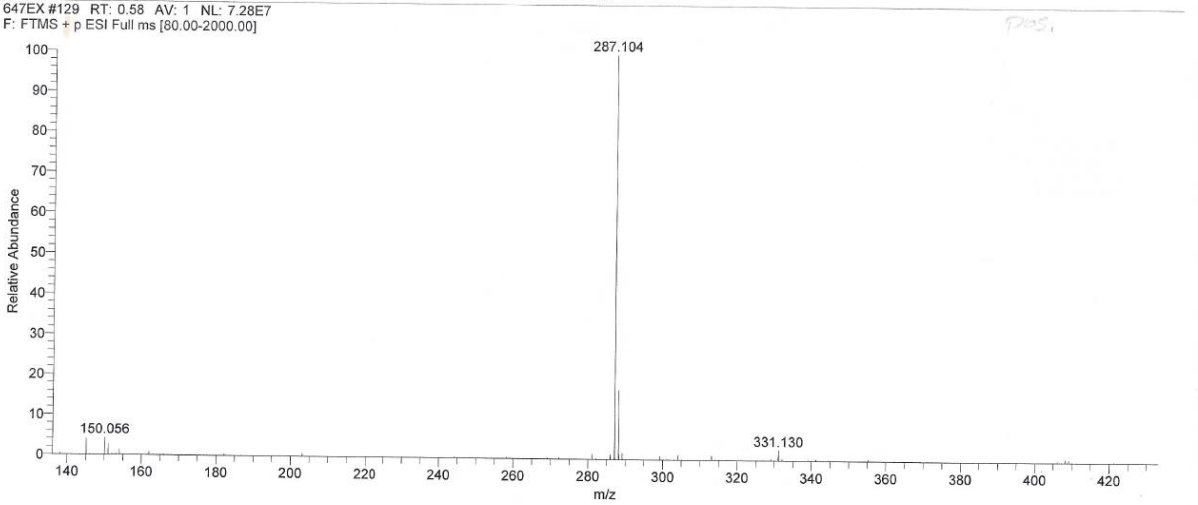
647EX #129 RT: 0.58 AV: 1 NL: 7.28E7
F: FTMS + p ESI Full ms [80.00-2000.00]
Relative Abundance
m/z
287.104
150.056
331.130

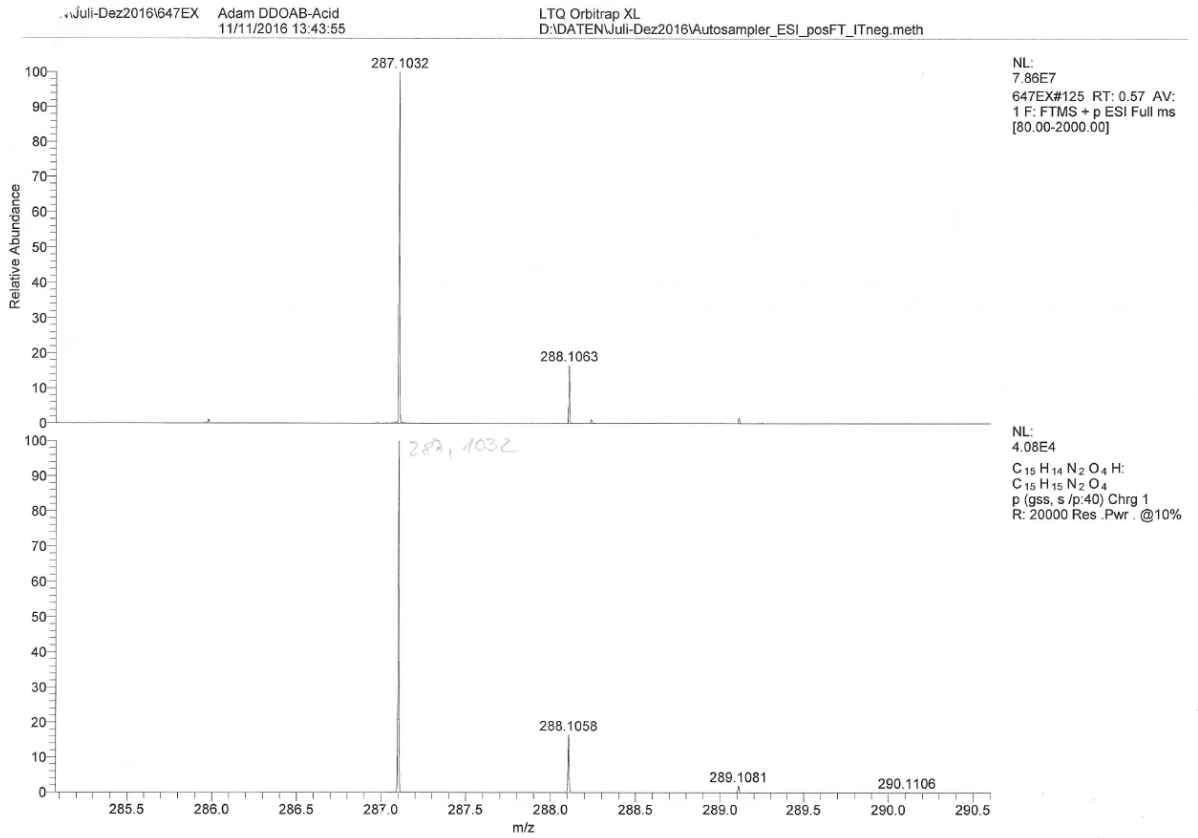
Juli-Dez2016\647EX
Adam DDOAB-Acid
11/11/2016 13:43:55
LTQ Orbitrap XL
D:\DATEN\Juli-Dez2016\Autosampler_ESI_posFT_ITneg.meth
Relative Abundance
m/z
287.1032
288.1063
NL:
7.86E7
647EX#125 RT: 0.57 AV: 1 F: FTMS + p ESI Full ms [80.00-2000.00]
NL:
4.08E4
C15 H14 N2 O4 H:
C15 H15 N2 O4
p (gss, s /p:40) Chrg 1
R: 20000 Res .Pwr . @10%
288.1058
289.1081
290.1106

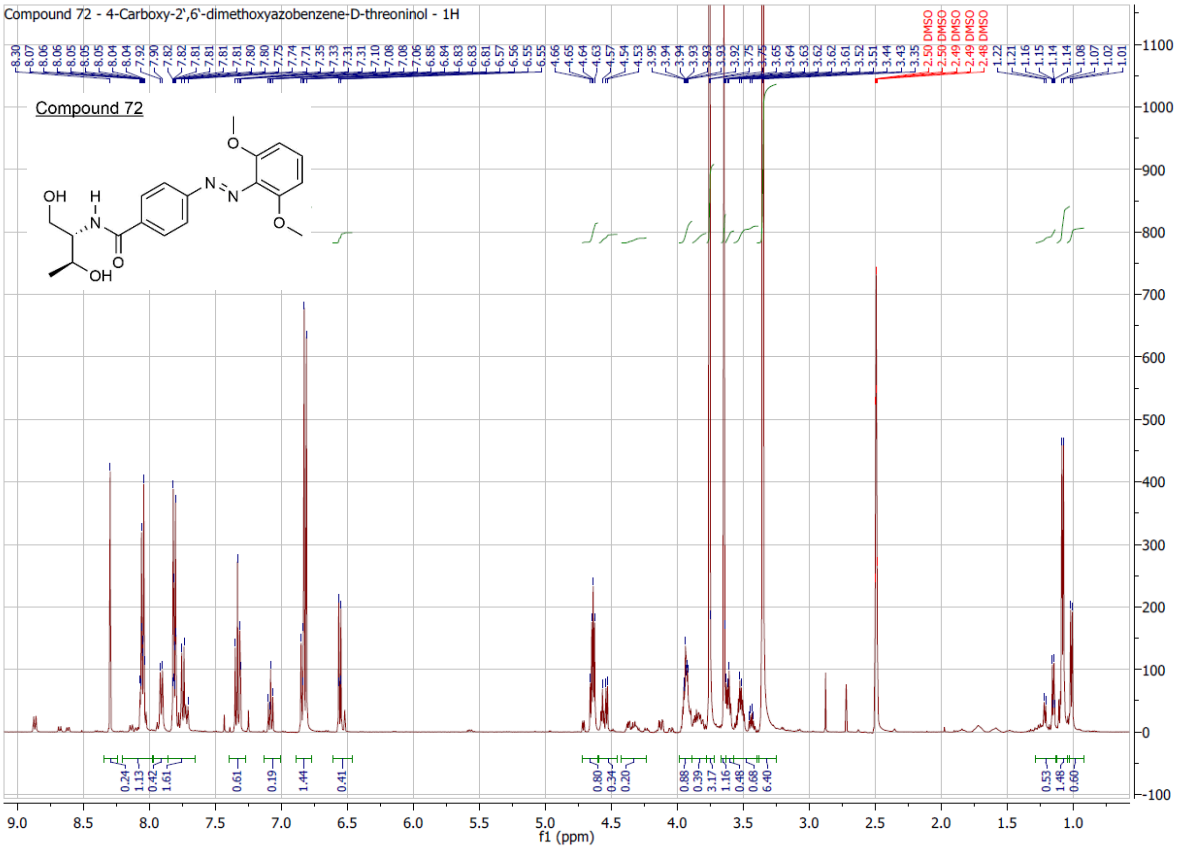
Compound 72 - 4-Carboxy-2',6'-dimethoxyazobenzene-D-threoninol - 1H
Compound 72
f1 (ppm)

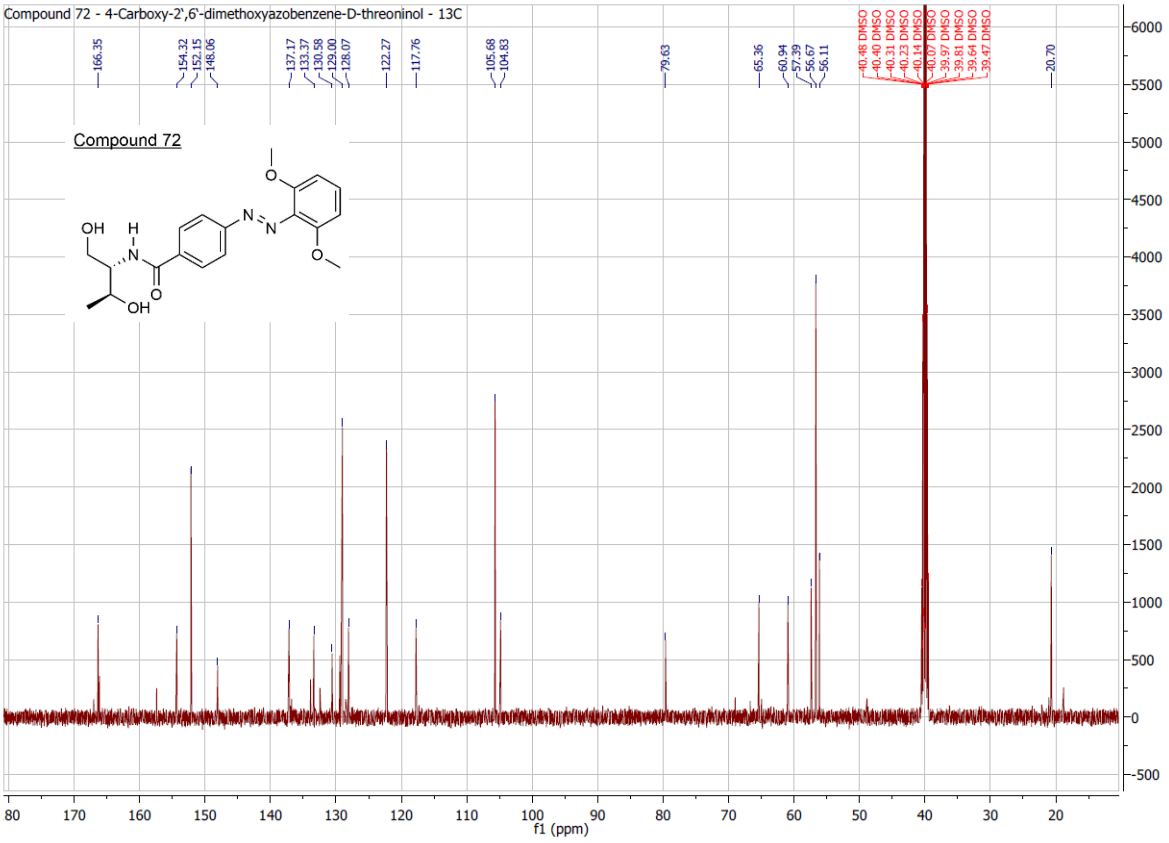
Compound 72 - 4-Carboxy-2',6'-dimethoxyazobenzene-D-threoninol - 13C
Compound 72
f1 (ppm)

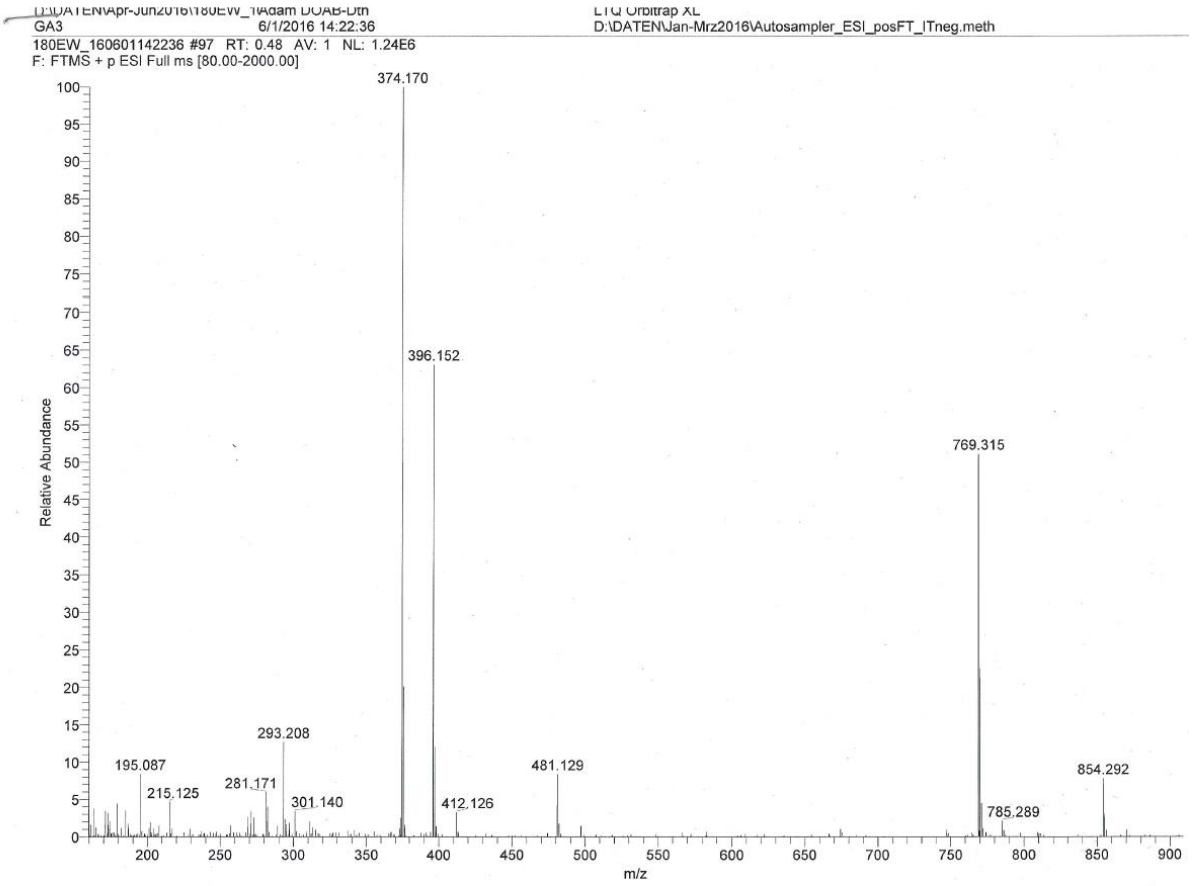
GA3
6/1/2016 14:22:36
LTQ Orbitrap XL
D:\DATEN\Jan-Mrz2016\Autosampler_ESI_posFT_ITneg.meth
180EW_160601142236 #97 RT: 0.48 AV: 1 NL: 1.24E6
F: FTMS + p ESI Full ms [80.00-2000.00]
374.170
396.152
769.315
293.208
195.087
215.125
281.171
301.140
412.126
481.129
785.289
854.292
Relative Abundance
m/z

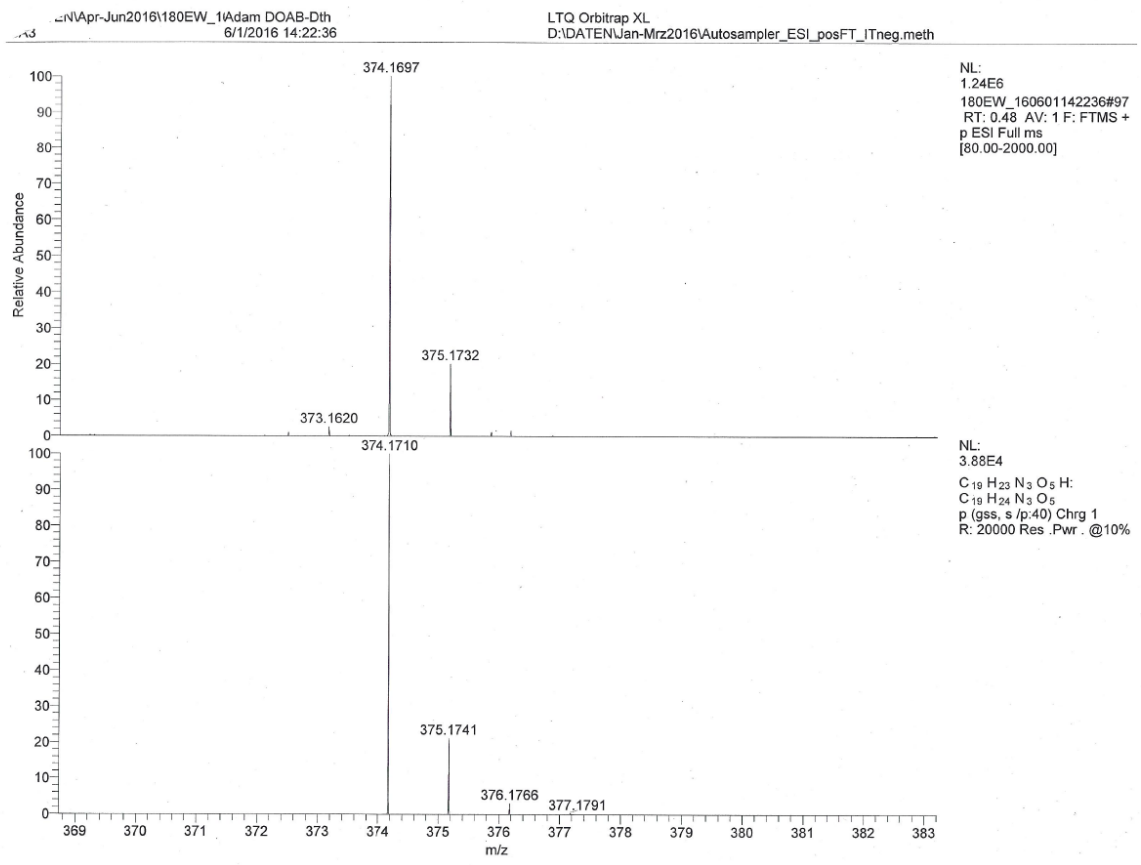
6/1/2016 14:22:36
LTQ Orbitrap XL
D:\DATEN\Jan-Mrz2016\Autosampler_ESI_posFT_ITneg.meth
374.1697
375.1732
373.1620
NL:
1.24E6
180EW_160601142236#97
RT: 0.48 AV: 1 F: FTMS +
p ESI Full ms
[80.00-2000.00]
374.1710
375.1741
376.1766
377.1791
NL:
3.88E4
C19 H23 N3 O5 H:
C19 H24 N3 O5
p (gss, s /p:40) Chrg 1
R: 20000 Res .Pwr . @10%
Relative Abundance
m/z

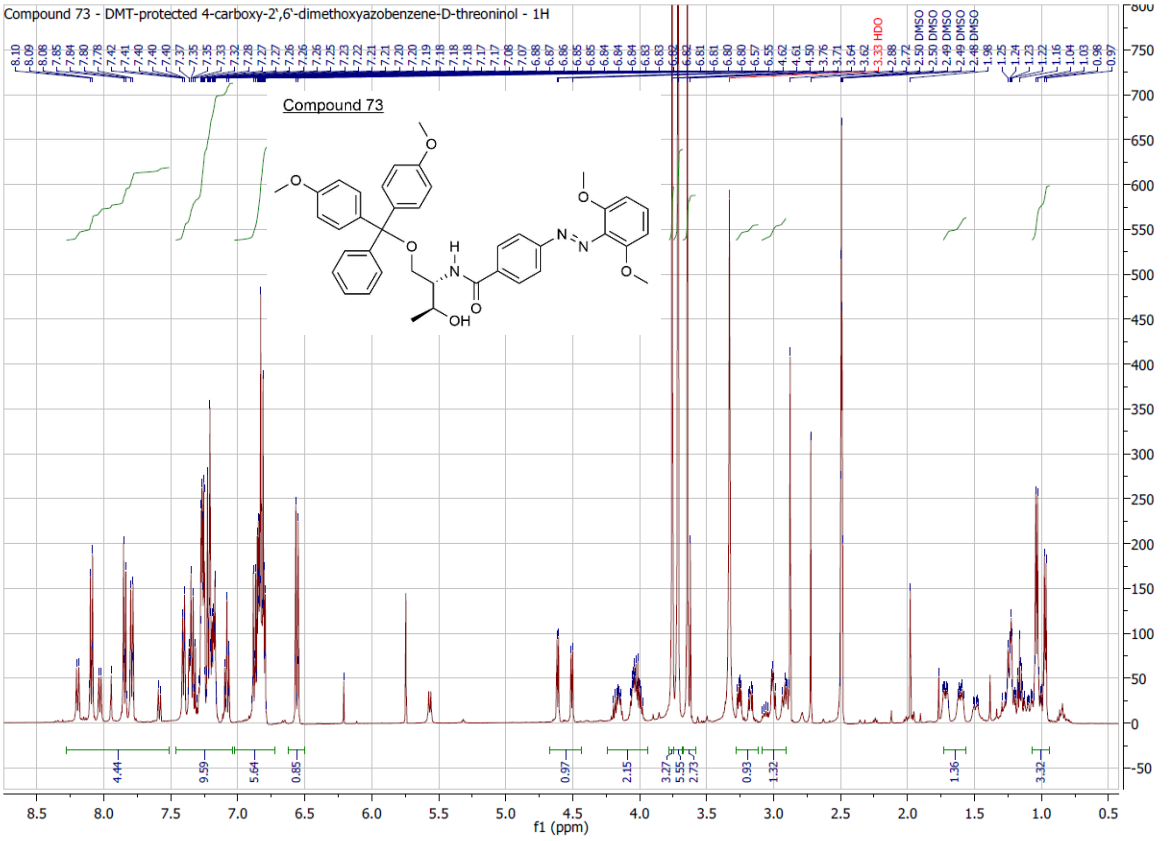
Compound 73 - DMT-protected 4-carboxy-2',6'-dimethoxyazobenzene-D-threoninol - 1H
Compound 73
f1 (ppm)

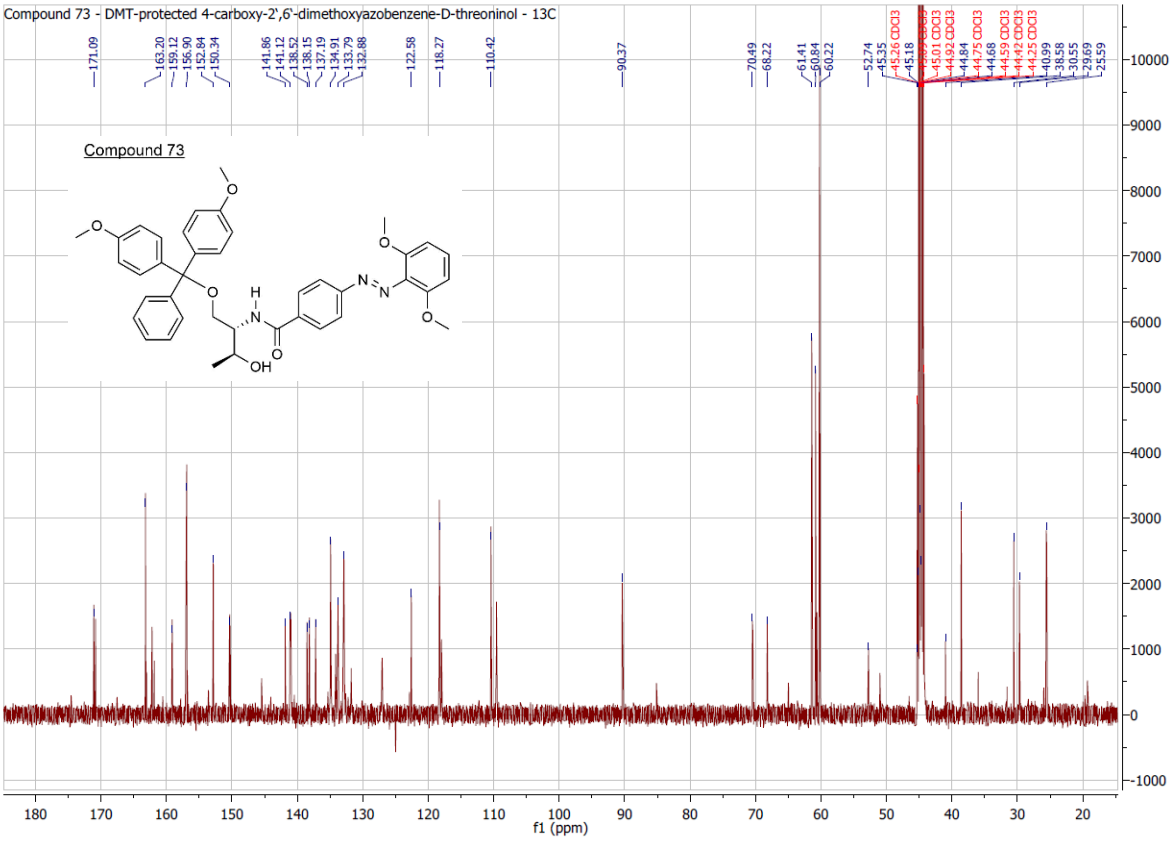
Compound 73 - DMT-protected 4-carboxy-2',6'-dimethoxyazobenzene-D-threoninol - 13C
Compound 73
f1 (ppm)

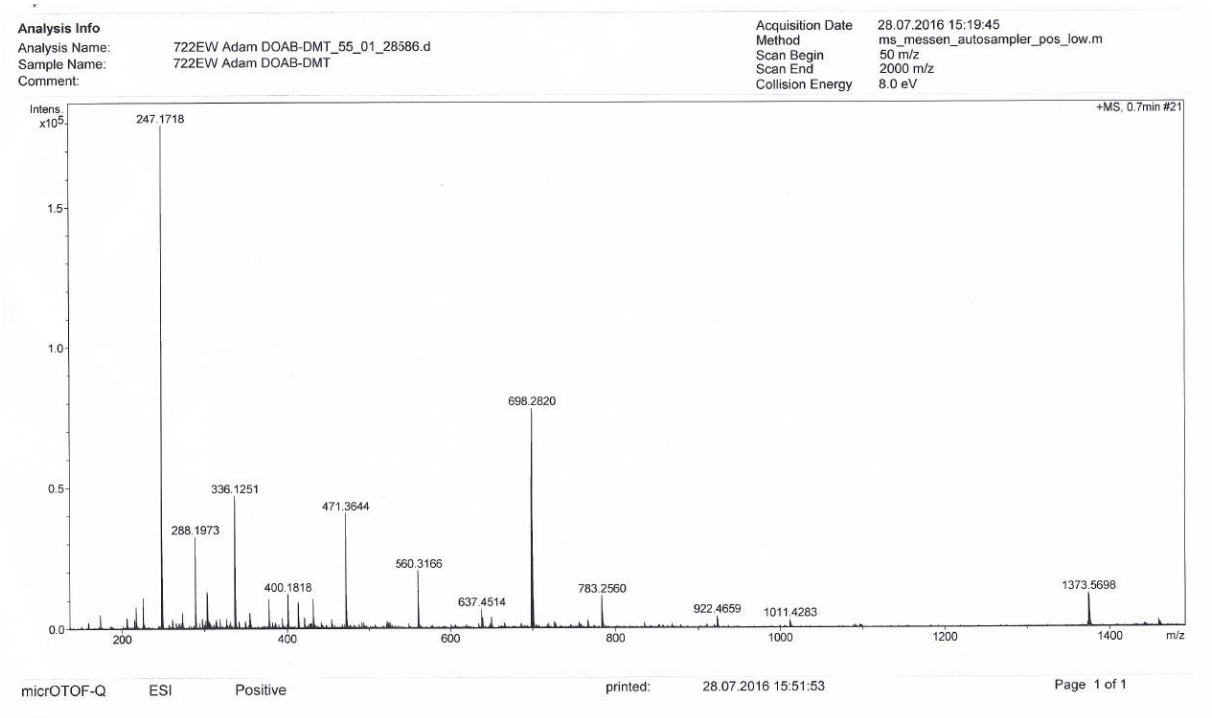
Analysis Info
Analysis Name: 722EW Adam DOAB-DMT_55_01_28586.d
Sample Name: 722EW Adam DOAB-DMT
Comment:
Acquisition Date 28.07.2016 15:19:45
Method ms_messen_autosampler_pos_low.m
Scan Begin 50 m/z
Scan End 2000 m/z
Collision Energy 8.0 eV
Intens.
x10^5
+MS, 0.7min #21
247.1718
698.2820
336.1251
471.3644
288.1973
560.3166
400.1818
637.4514
783.2560
922.4659
1011.4283
1373.5698
m/z
micrOTOF-Q ESI Positive
printed: 28.07.2016 15:51:53
Page 1 of 1

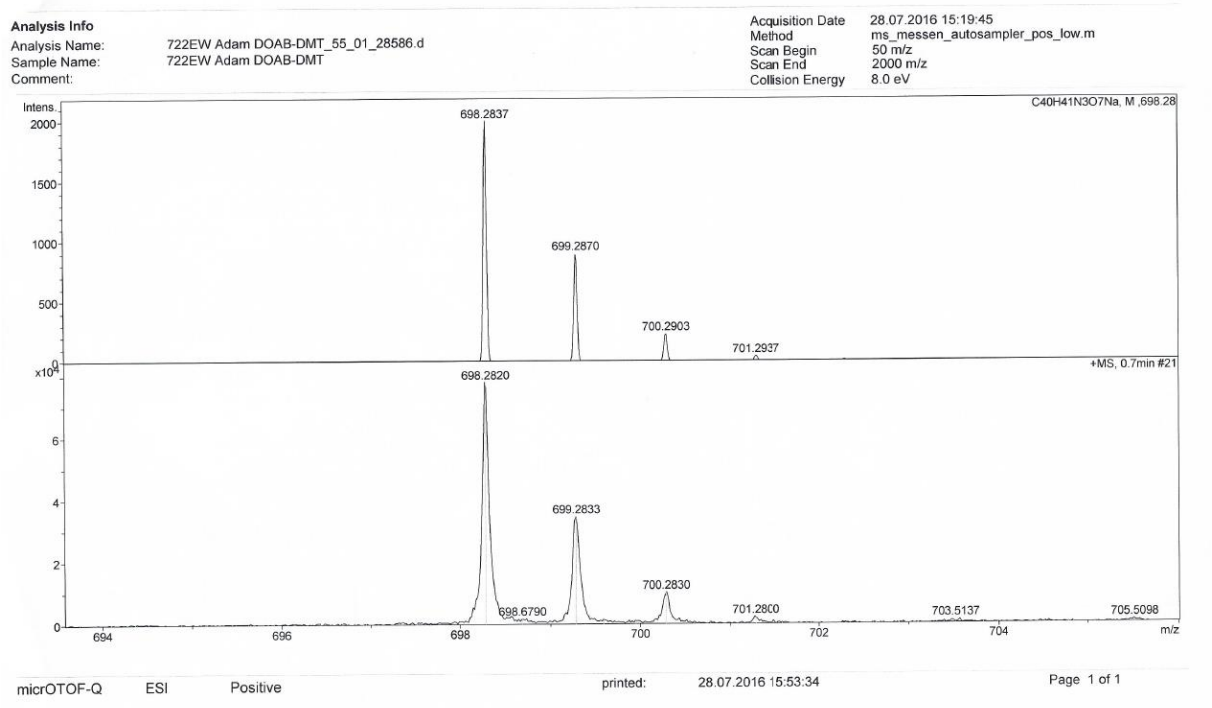
Analysis Info
Analysis Name: 722EW Adam DOAB-DMT_55_01_28586.d
Sample Name: 722EW Adam DOAB-DMT
Comment:
Acquisition Date 28.07.2016 15:19:45
Method ms_messen_autosampler_pos_low.m
Scan Begin 50 m/z
Scan End 2000 m/z
Collision Energy 8.0 eV
Intens.
C40H41N3O7Na, M ,698.28
698.2837
699.2870
700.2903
701.2937
x10^4
+MS, 0.7min #21
698.2820
699.2833
700.2830
698.6790
701.2800
703.5137
705.5098
m/z
micrOTOF-Q ESI Positive
printed: 28.07.2016 15:53:34
Page 1 of 1

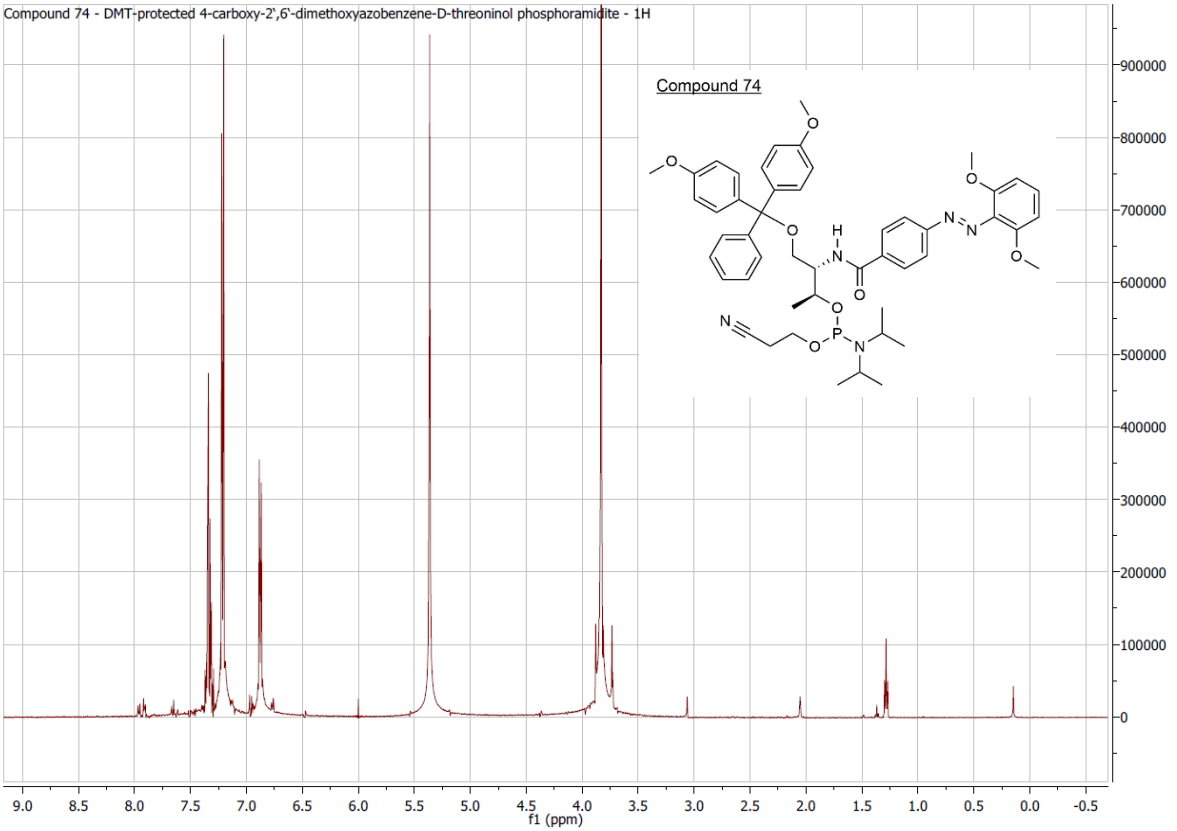
Compound 74 - DMT-protected 4-carboxy-2',6'-dimethoxyazobenzene-D-threoninol phosphoramidite - 1H
Compound 74
f1 (ppm)

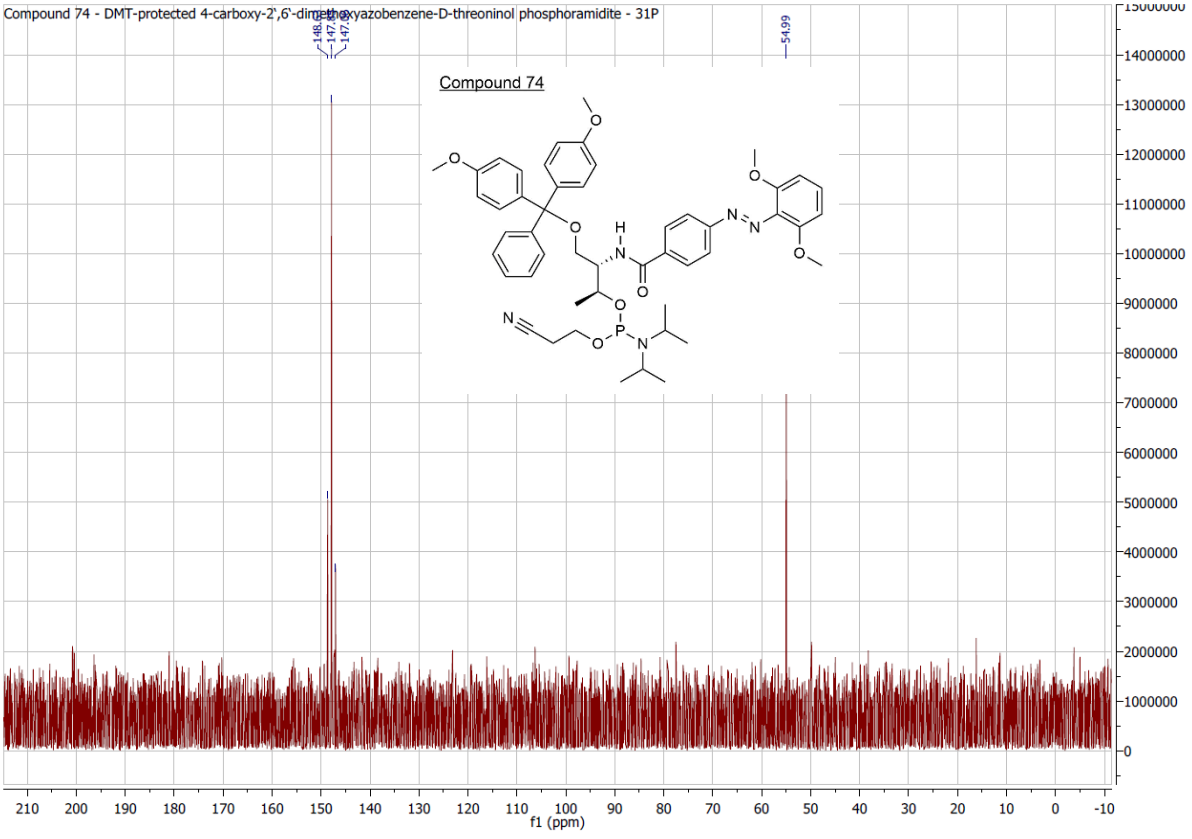
Compound 74 - DMT-protected 4-carboxy-2',6'-dimethoxyazobenzene-D-threoninol phosphoramidite - 31P
Compound 74
f1 (ppm)

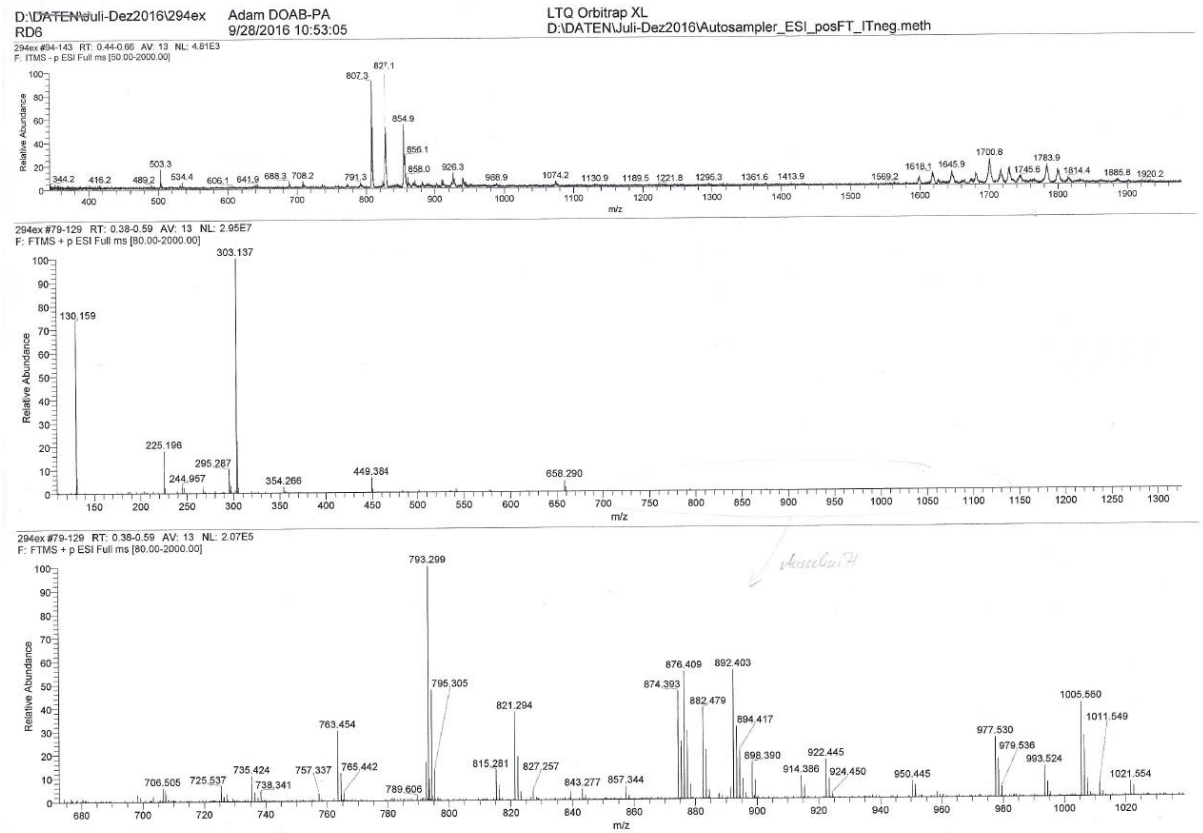
D:\DATEN\Juli-Dez2016\294ex RD6
Adam DOAB-PA
9/28/2016 10:53:05
LTQ Orbitrap XL
D:\DATEN\Juli-Dez2016\Autosampler_ESI_posFT_ITneg.meth
294ex #94-143 RT: 0.44-0.66 AV: 13 NL: 4.81E3
F: ITMS - p ESI Full ms [50.00-2000.00]
294ex #79-129 RT: 0.38-0.59 AV: 13 NL: 2.95E7
F: FTMS + p ESI Full ms [80.00-2000.00]
294ex #79-129 RT: 0.38-0.59 AV: 13 NL: 2.07E5
F: FTMS + p ESI Full ms [80.00-2000.00]
Relative Abundance
m/z

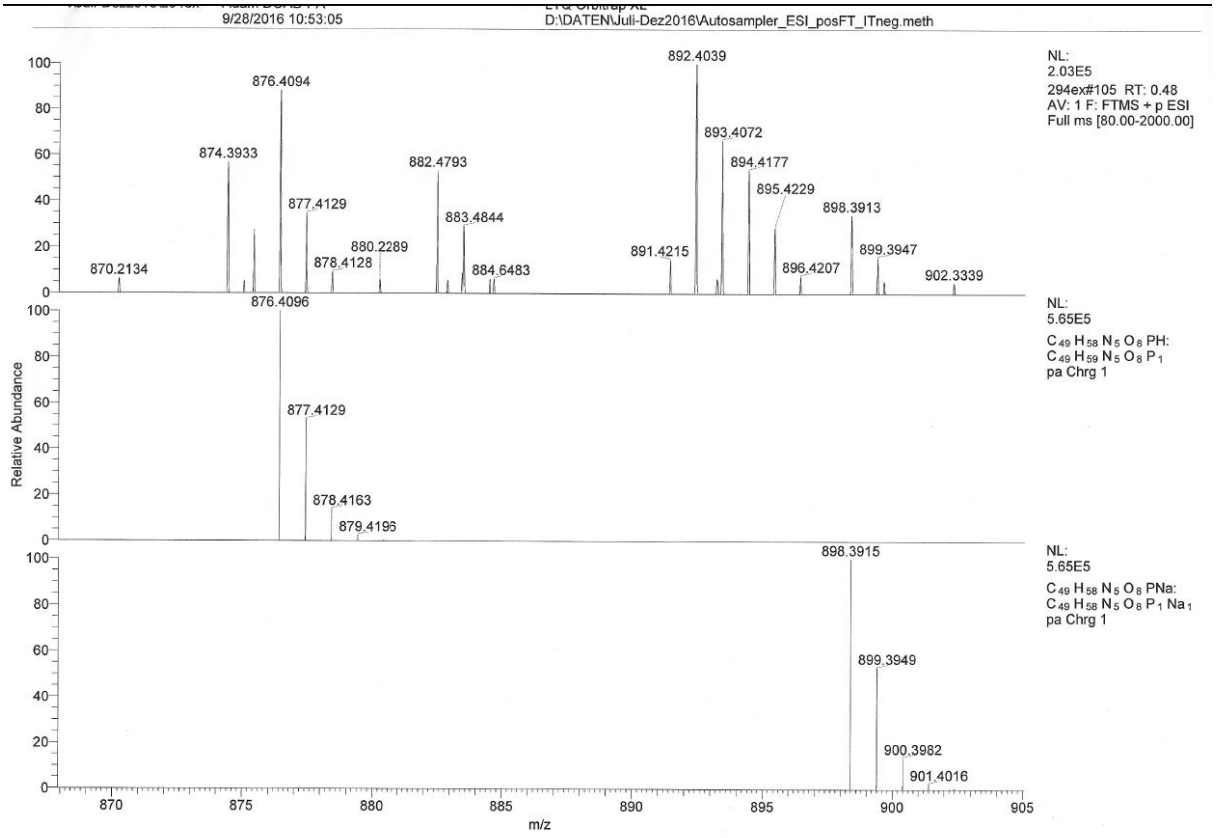
9/28/2016 10:53:05
D:\DATEN\Juli-Dez2016\Autosampler_ESI_posFT_ITneg.meth
NL:
2.03E5
294ex#105 RT: 0.48
AV: 1 F: FTMS + p ESI
Full ms [80.00-2000.00]
NL:
5.65E5
C49 H58 N5 O8 PH:
C49 H59 N5 O8 P1
pa Chrg 1
NL:
5.65E5
C49 H58 N5 O8 PNa:
C49 H58 N5 O8 P1 Na1
pa Chrg 1
Relative Abundance
m/z

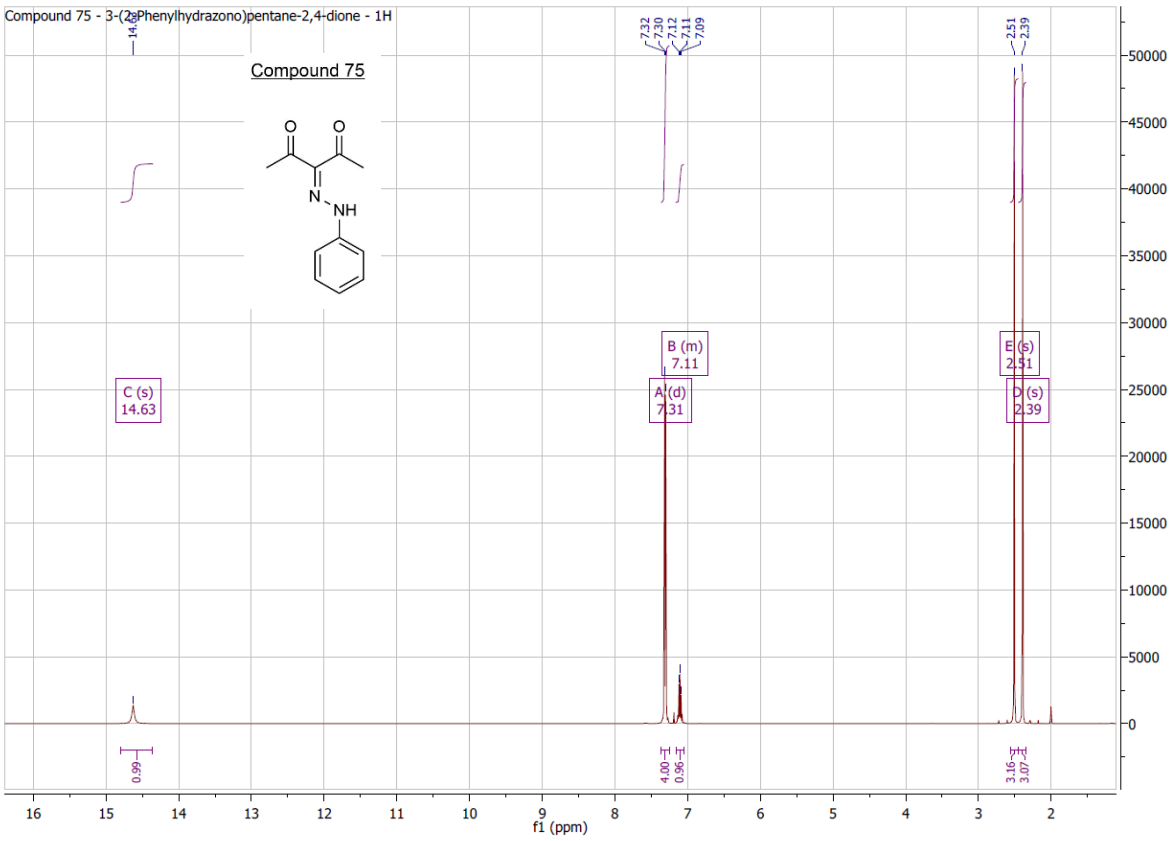
Compound 75 - 3-(2-Phenylhydrazono)pentane-2,4-dione - 1H
Compound 75
C (s)
14.63
B (m)
7.11
A (d)
7.31
E (s)
2.51
D (s)
2.39
f1 (ppm)

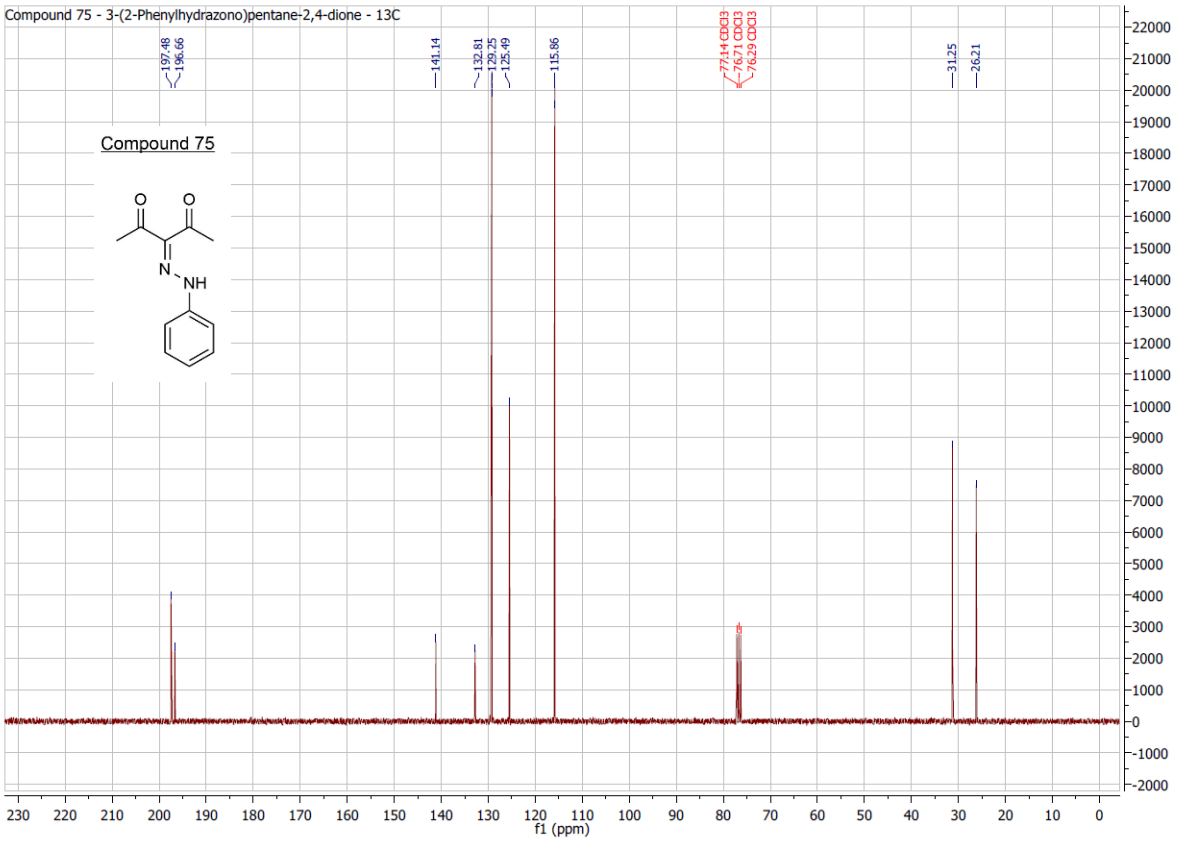
Compound 75 - 3-(2-Phenylhydrazono)pentane-2,4-dione - 13C
Compound 75
f1 (ppm)

D:\DATEN\Apr-Jun2016\191EW Adam VA_324
GB2 6/2/2016 15:42:46
LTQ Orbitrap XL
D:\DATEN\Jan-Mrz2016\Autosampler_ESI_posFT_ITneg.meth

EI 7.21. nicht möglich

191EW #65-105 RT: 0.32-0.52 AV: 11 SB: 27 0.01-0.28 , 0.02-0.27 NL: 9.57E4
F: FTMS + p ESI Full ms [80.00-2000.00]

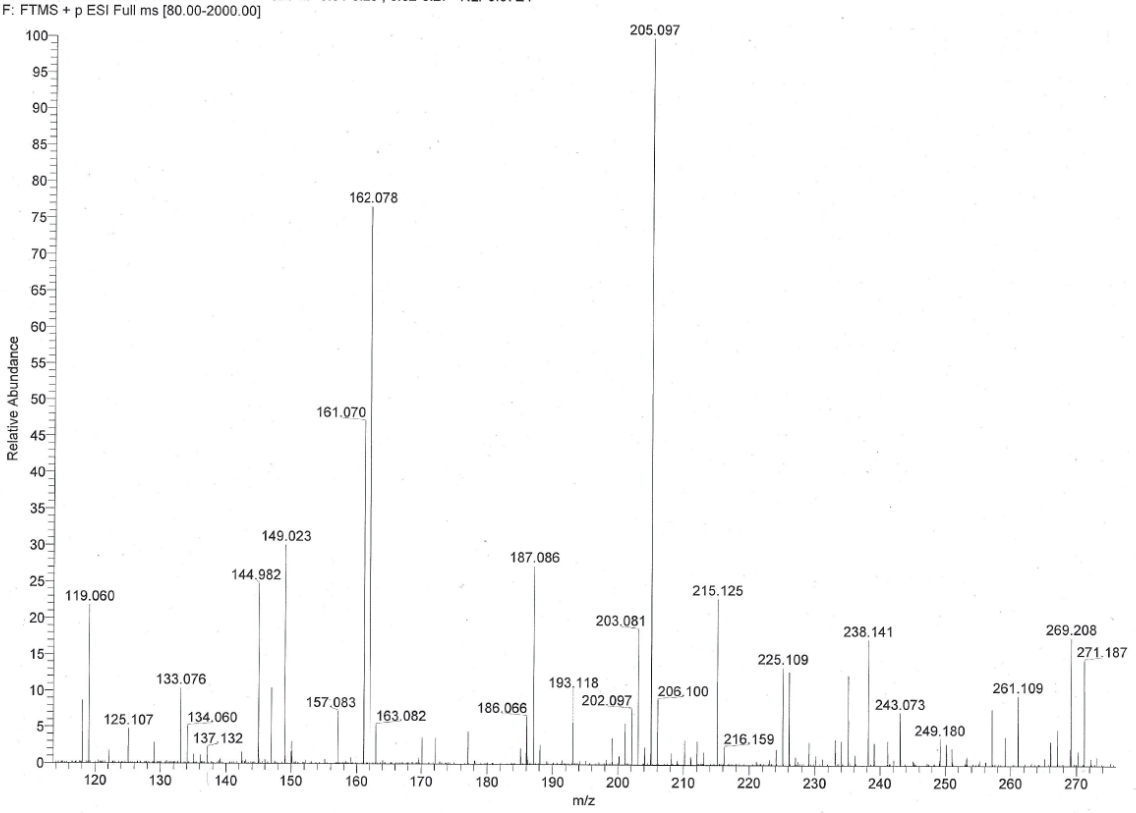

D:\DATEN\Apr-Jun2016\191EW Adam VA_324
GB2 6/2/2016 15:42:46
LTQ Orbitrap XL
D:\DATEN\Jan-Mrz2016\Autosampler_ESI_posFT_ITneg.meth

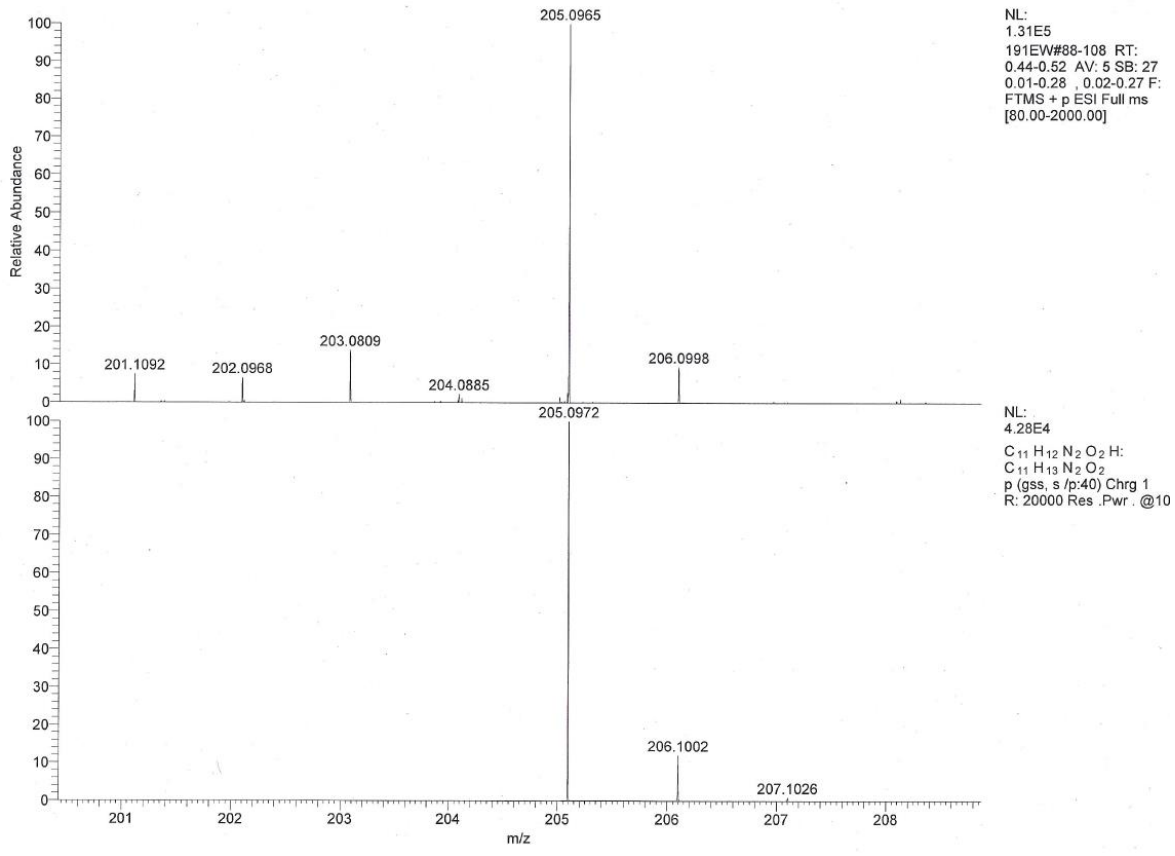

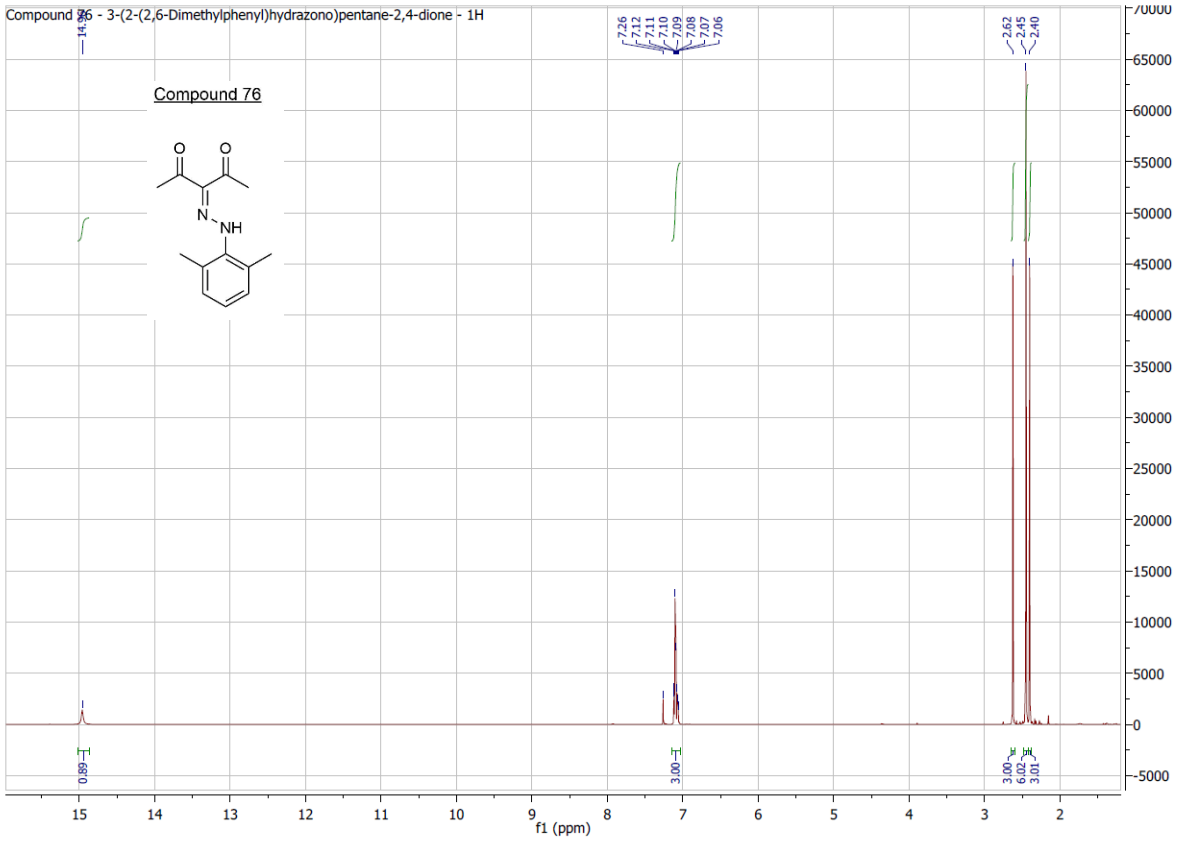
Compound 76 - 3-(2-(2,6-Dimethylphenyl)hydrazono)pentane-2,4-dione - 1H
Compound 76
f1 (ppm)

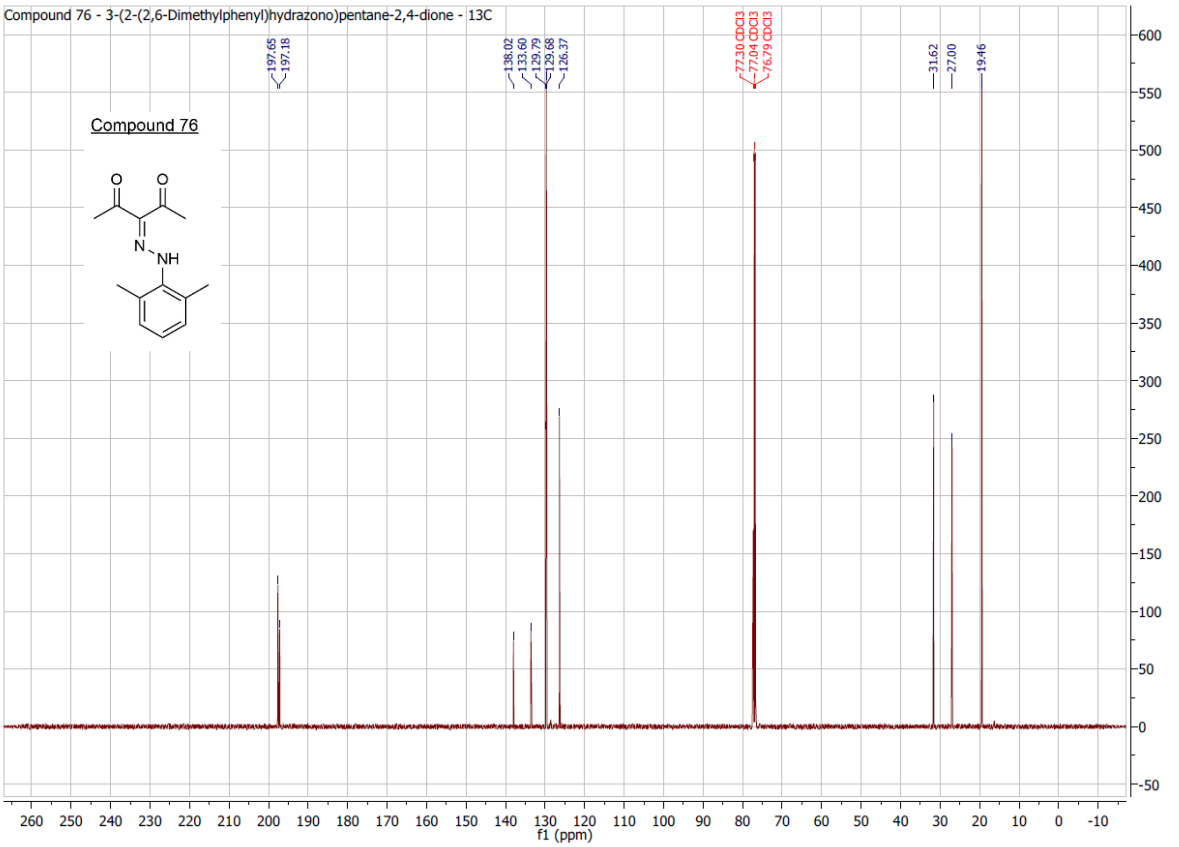
Compound 76 - 3-(2-(2,6-Dimethylphenyl)hydrazono)pentane-2,4-dione - 13C
Compound 76
f1 (ppm)

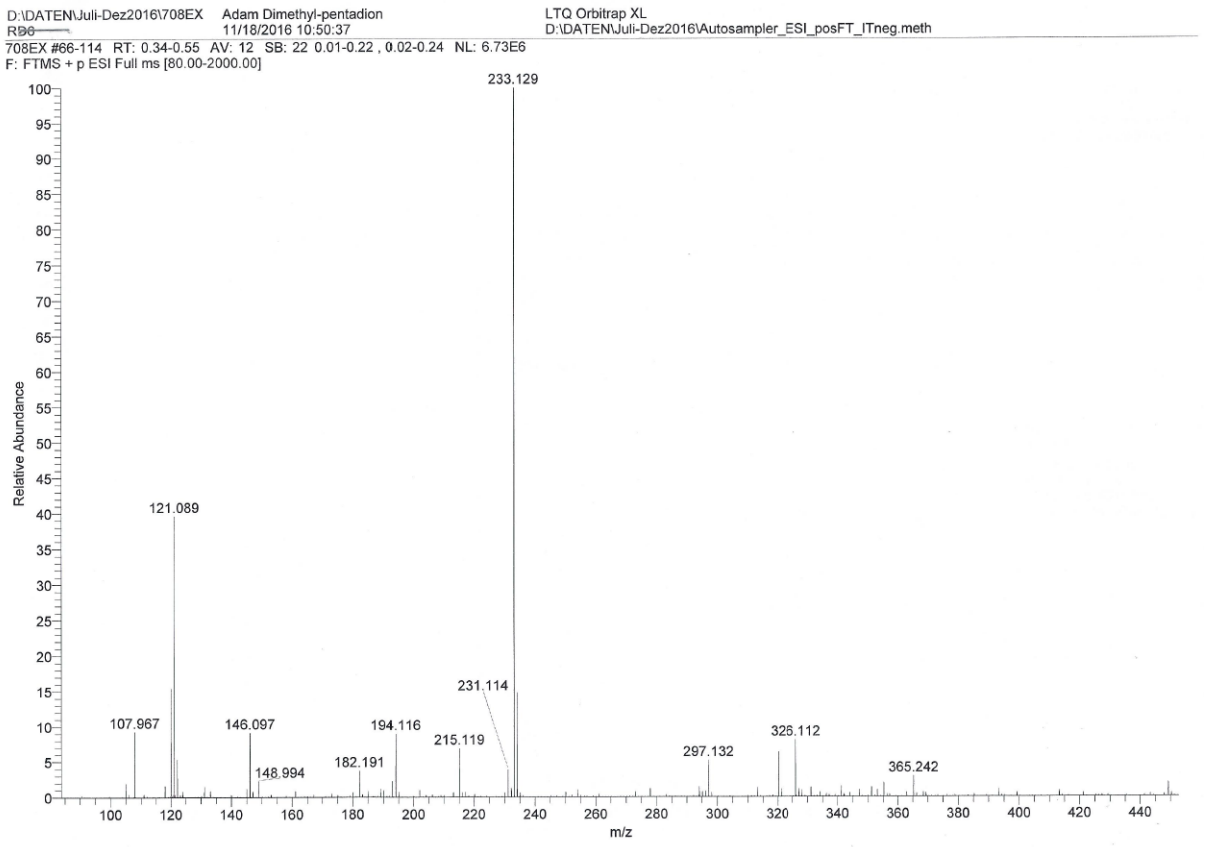
D:\DATEN\Juli-Dez2016\708EX Adam Dimethyl-pentadion
11/18/2016 10:50:37
LTQ Orbitrap XL
D:\DATEN\Juli-Dez2016\Autosampler_ESI_posFT_ITneg.meth
708EX #66-114 RT: 0.34-0.55 AV: 12 SB: 22 0.01-0.22 , 0.02-0.24 NL: 6.73E6
F: FTMS + p ESI Full ms [80.00-2000.00]
Relative Abundance
m/z
233.129
121.089
107.967
146.097
148.994
182.191
194.116
215.119
231.114
297.132
326.112
365.242

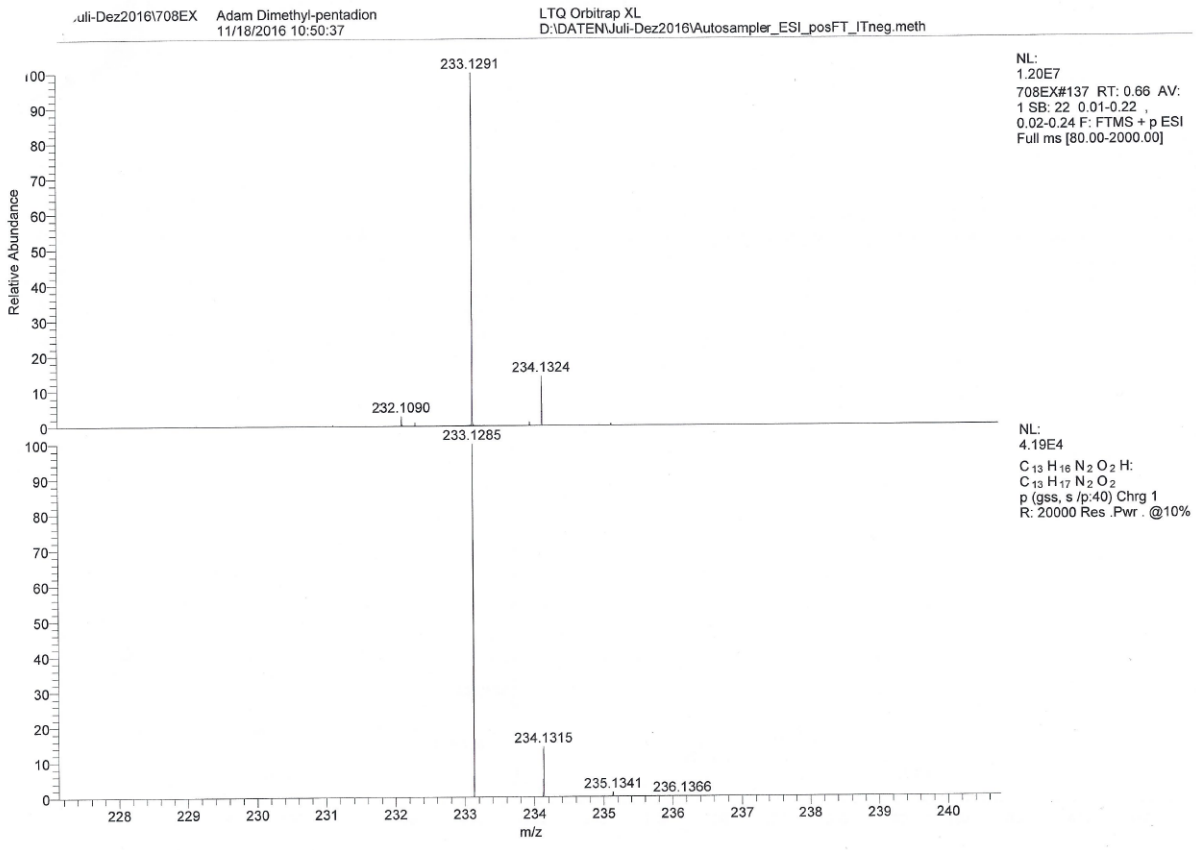
uli-Dez2016\708EX Adam Dimethyl-pentadion
11/18/2016 10:50:37
LTQ Orbitrap XL
D:\DATEN\Juli-Dez2016\Autosampler_ESI_posFT_ITneg.meth
NL:
1.20E7
708EX#137 RT: 0.66 AV: 1 SB: 22 0.01-0.22 , 0.02-0.24 F: FTMS + p ESI Full ms [80.00-2000.00]
233.1291
234.1324
232.1090
NL:
4.19E4
C13 H16 N2 O2 H:
C13 H17 N2 O2
p (gss, s /p:40) Chrg 1
R: 20000 Res .Pwr . @10%
233.1285
234.1315
235.1341
236.1366
Relative Abundance
m/z

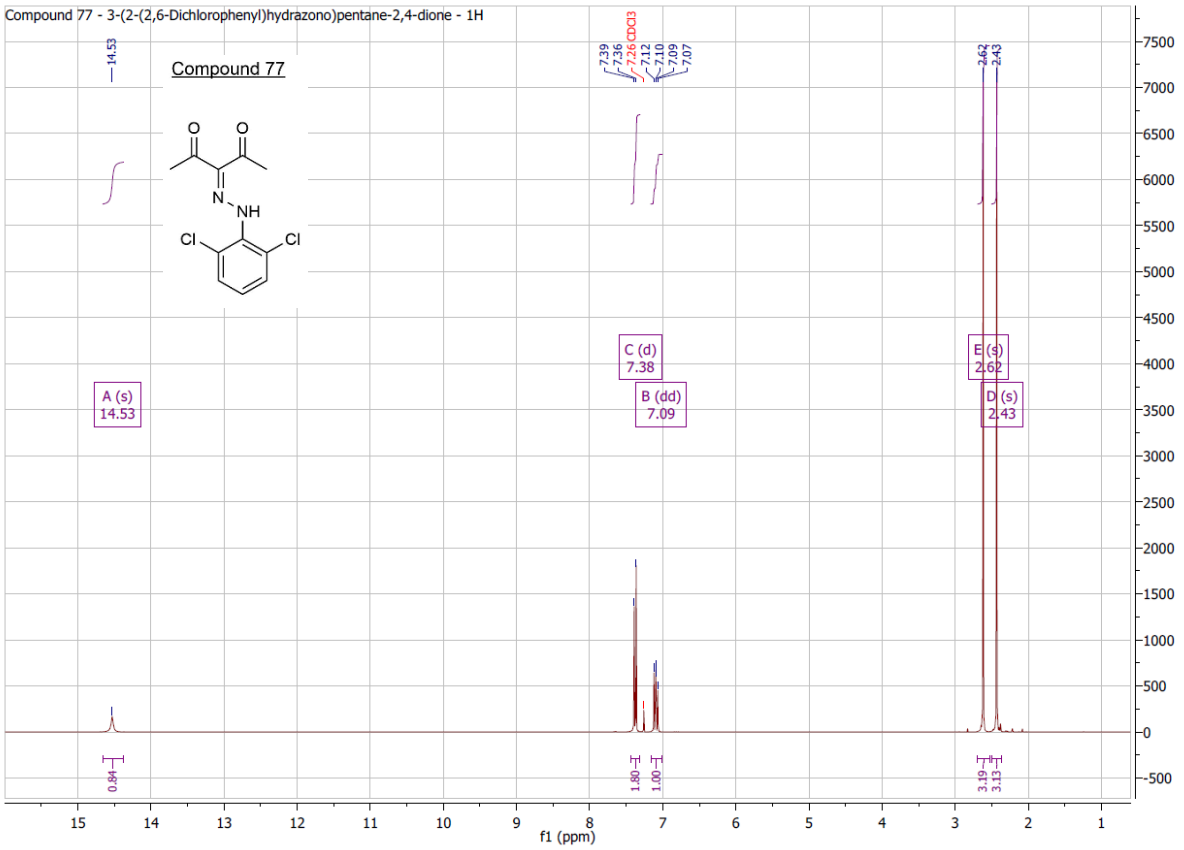
Compound 77 - 3-(2-(2,6-Dichlorophenyl)hydrazono)pentane-2,4-dione - 1H
Compound 77
A (s)
14.53
C (d)
7.38
B (dd)
7.09
E (s)
2.62
D (s)
2.43
f1 (ppm)

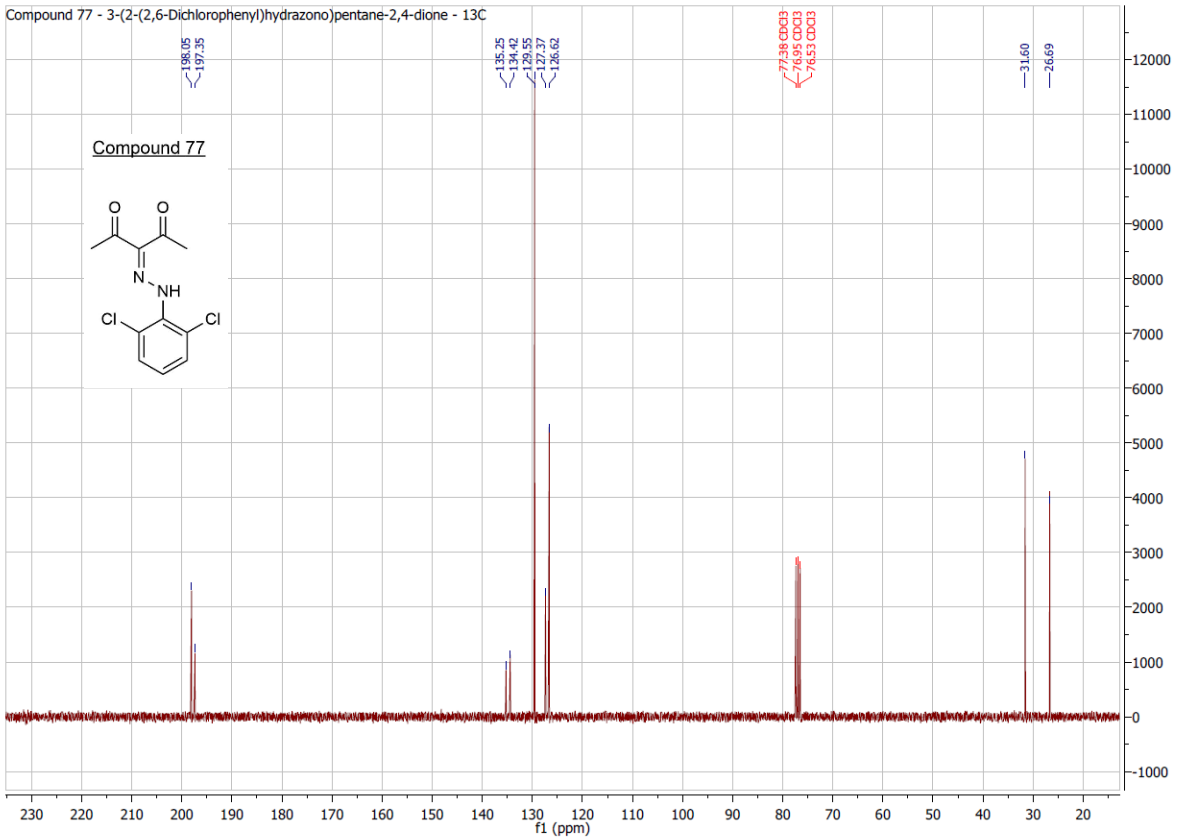
Compound 77 - 3-(2-(2,6-Dichlorophenyl)hydrazono)pentane-2,4-dione - 13C
Compound 77
f1 (ppm)

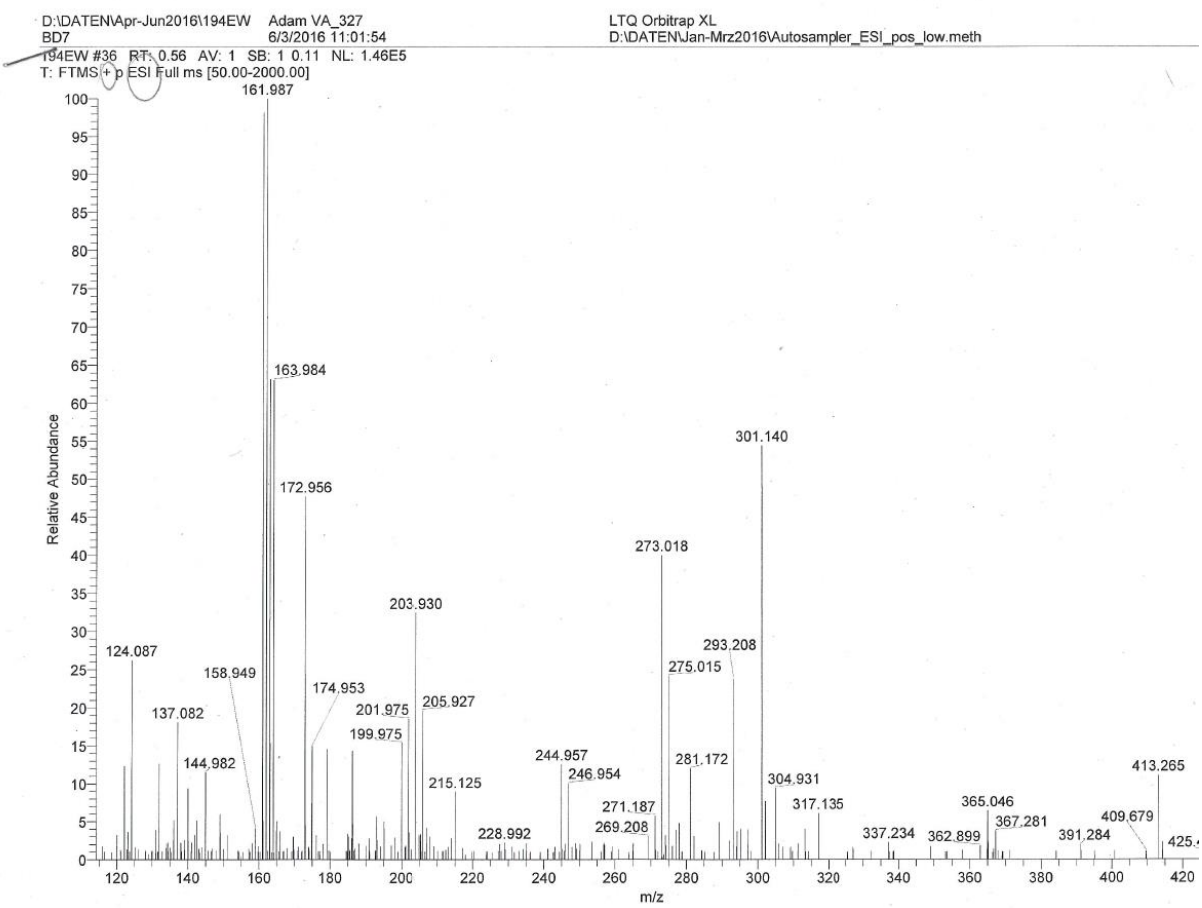
D:\DATEN\Apr-Jun2016\194EW Adam VA_327
BD7 6/3/2016 11:01:54
LTQ Orbitrap XL
D:\DATEN\Jan-Mrz2016\Autosampler_ESI_pos_low.meth
194EW #36 RT: 0.56 AV: 1 SB: 1 0.11 NL: 1.46E5
T: FTMS + p ESI Full ms [50.00-2000.00]
Relative Abundance
m/z
161.987
163.984
172.956
301.140
273.018
203.930
293.208
124.087
275.015
158.949
174.953
205.927
137.082
201.975
199.975
144.982
244.957
281.172
246.954
304.931
215.125
317.135
271.187
269.208
228.992
365.046
367.281
409.679
413.265
337.234
362.899
391.284

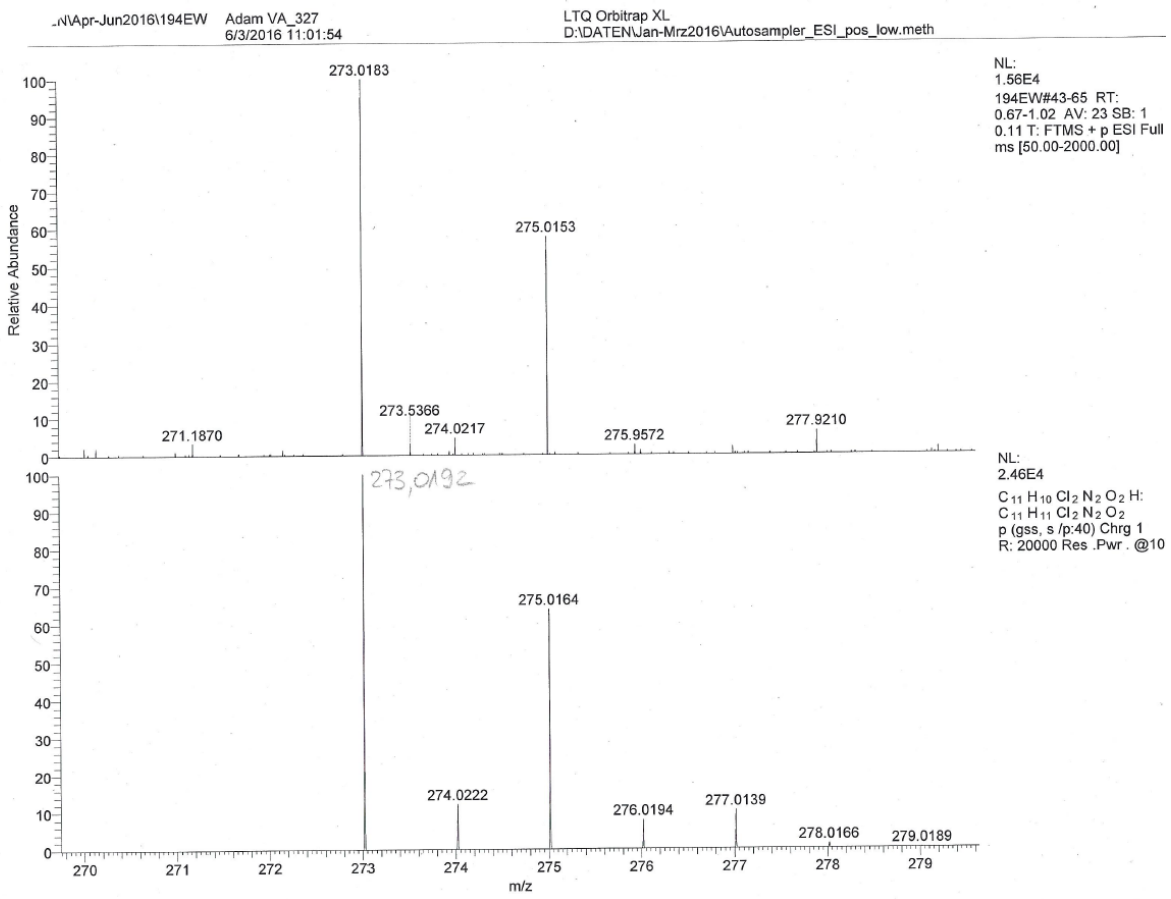
Adam VA_327
6/3/2016 11:01:54
LTQ Orbitrap XL
D:\DATEN\Jan-Mrz2016\Autosampler_ESI_pos_low.meth
NL:
1.56E4
194EW#43-65 RT:
0.67-1.02 AV: 23 SB: 1
0.11 T: FTMS + p ESI Full
ms [50.00-2000.00]
Relative Abundance
m/z
273.0183
275.0153
271.1870
273.5366
274.0217
275.9572
277.9210
NL:
2.46E4
C11 H10 Cl2 N2 O2 H:
C11 H11 Cl2 N2 O2
p (gss, s /p:40) Chrg 1
R: 20000 Res .Pwr . @10
273,0192
275.0164
274.0222
276.0194
277.0139
278.0166
279.0189

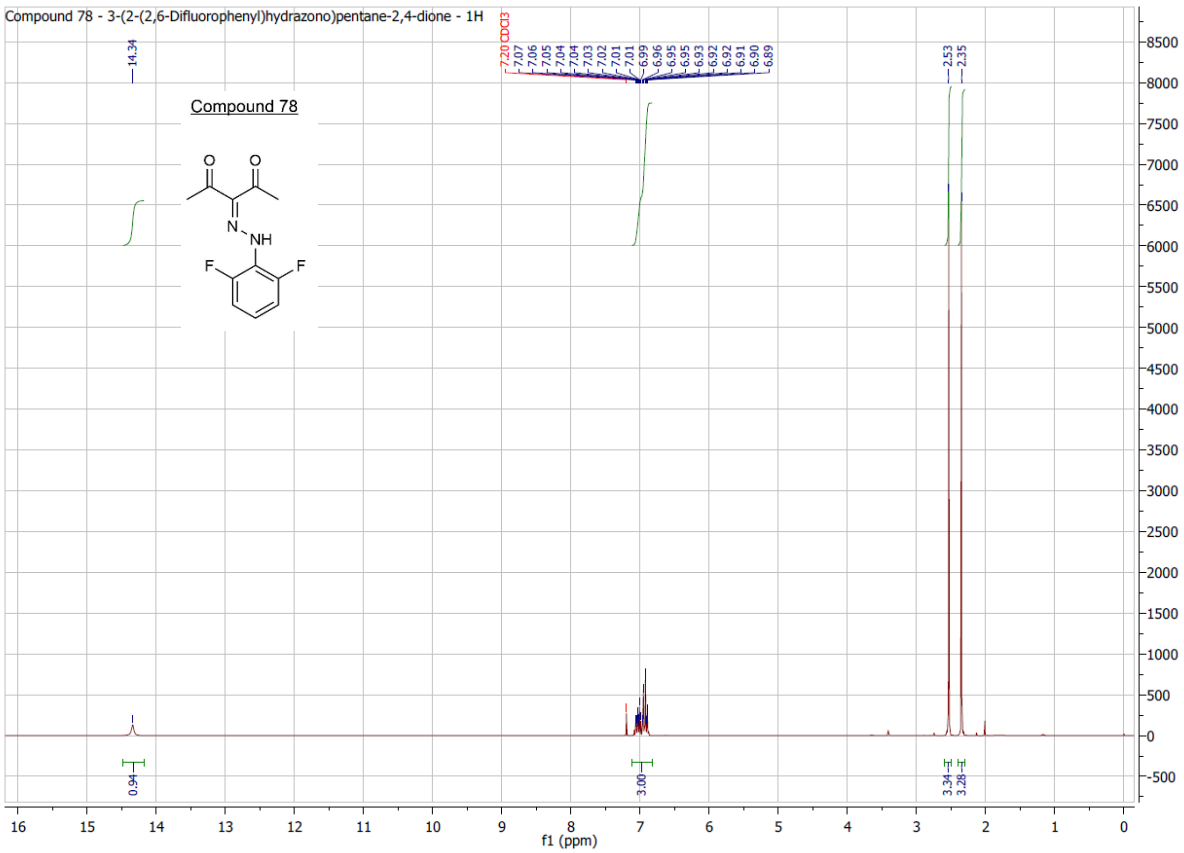
Compound 78 - 3-(2-(2,6-Difluorophenyl)hydrazono)pentane-2,4-dione - 1H
Compound 78
f1 (ppm)

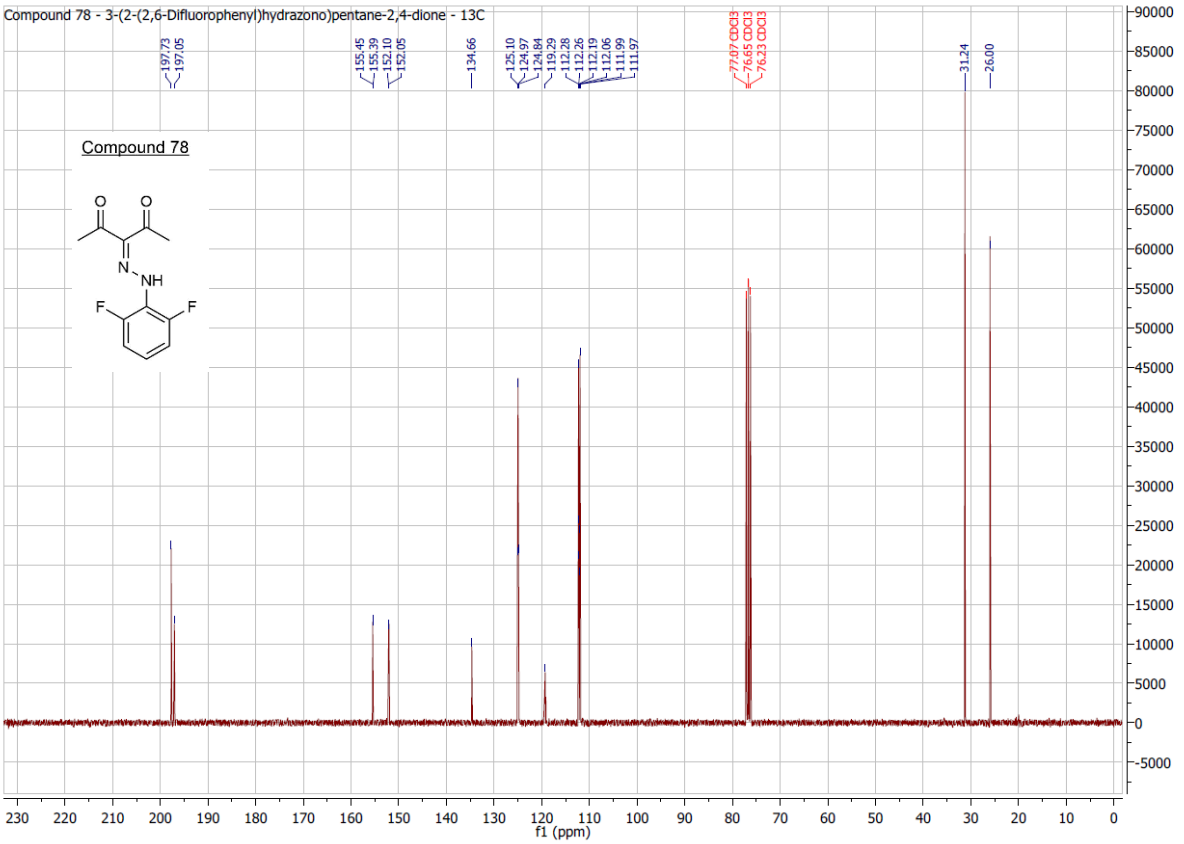
Compound 78 - 3-(2-(2,6-Difluorophenyl)hydrazono)pentane-2,4-dione - 13C
Compound 78
f1 (ppm)

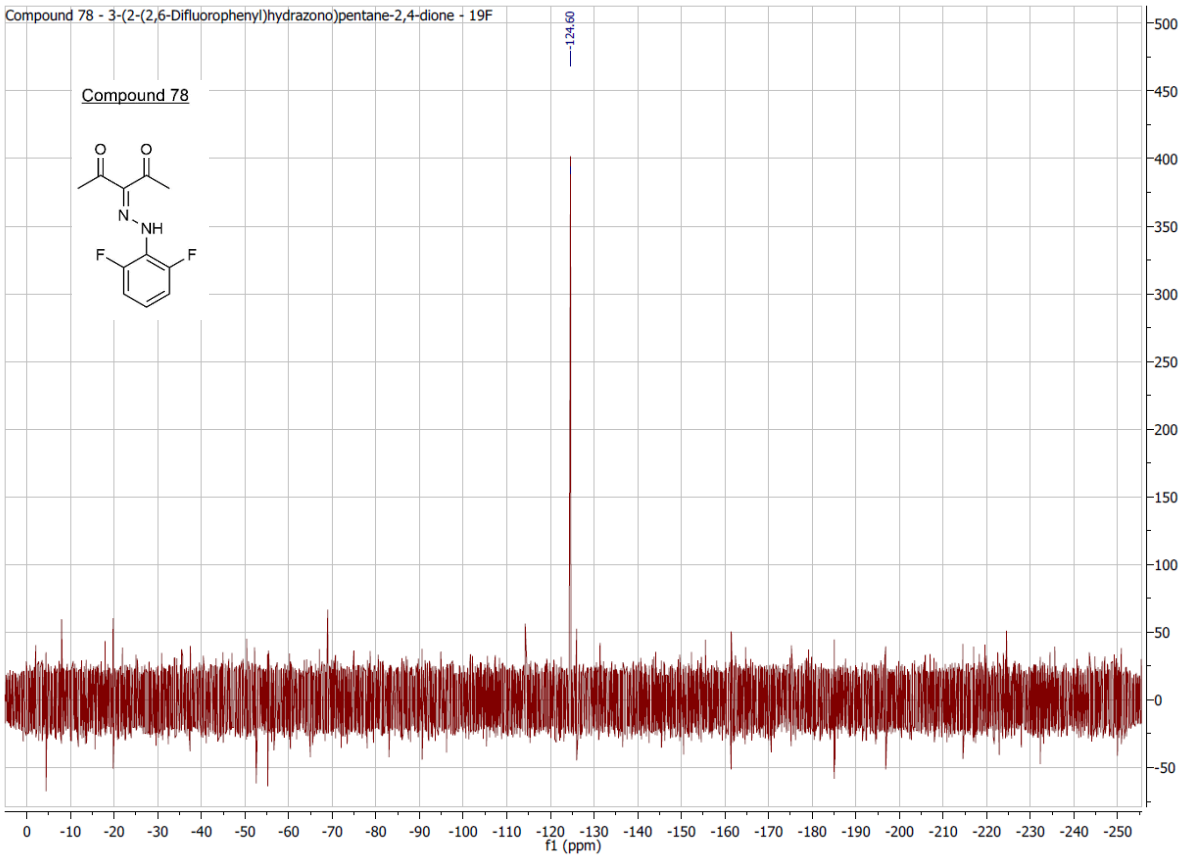
Compound 78 - 3-(2-(2,6-Difluorophenyl)hydrazono)pentane-2,4-dione - 19F
Compound 78
124.60
f1 (ppm)

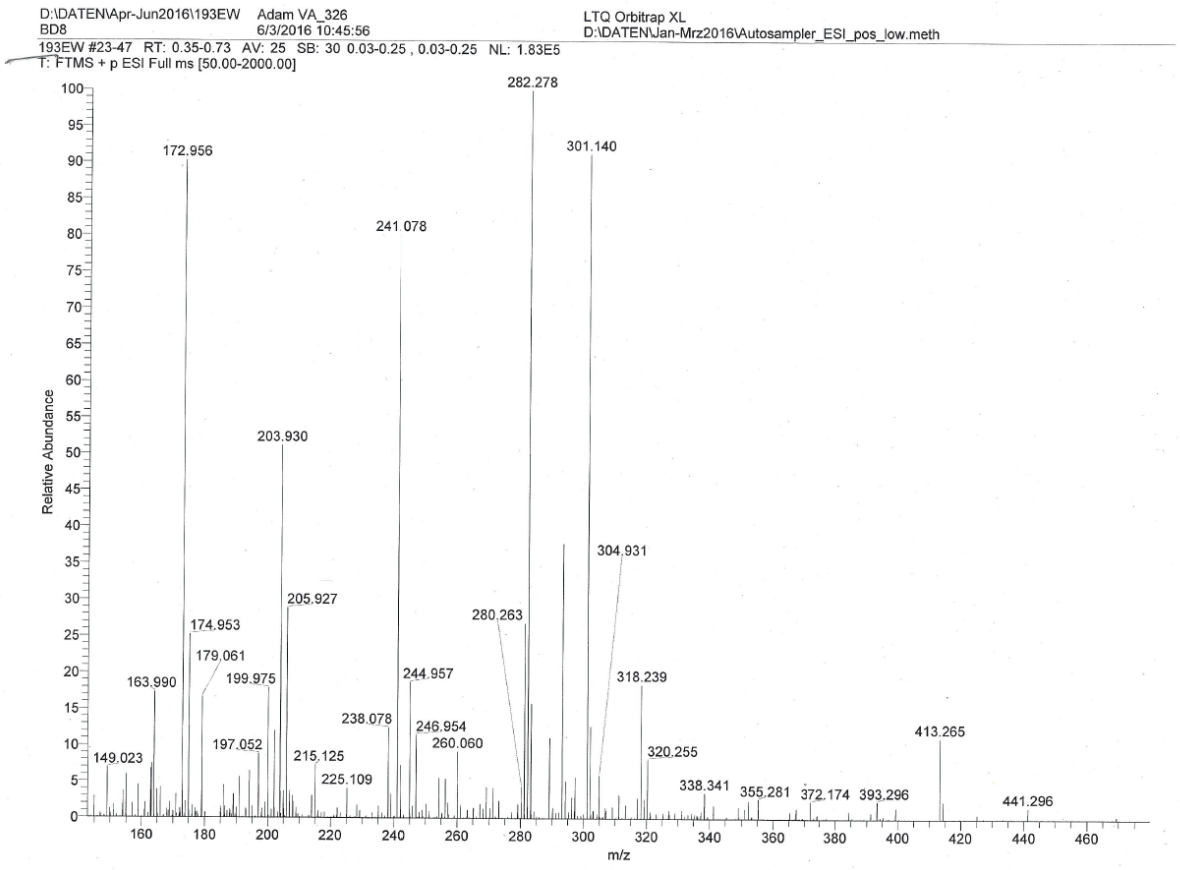
D:\DATEN\Apr-Jun2016\193EW Adam VA_326
BD8 6/3/2016 10:45:56
LTQ Orbitrap XL
D:\DATEN\Jan-Mrz2016\Autosampler_ESI_pos_low.meth
193EW #23-47 RT: 0.35-0.73 AV: 25 SB: 30 0.03-0.25 , 0.03-0.25 NL: 1.83E5
T: FTMS + p ESI Full ms [50.00-2000.00]
Relative Abundance
m/z

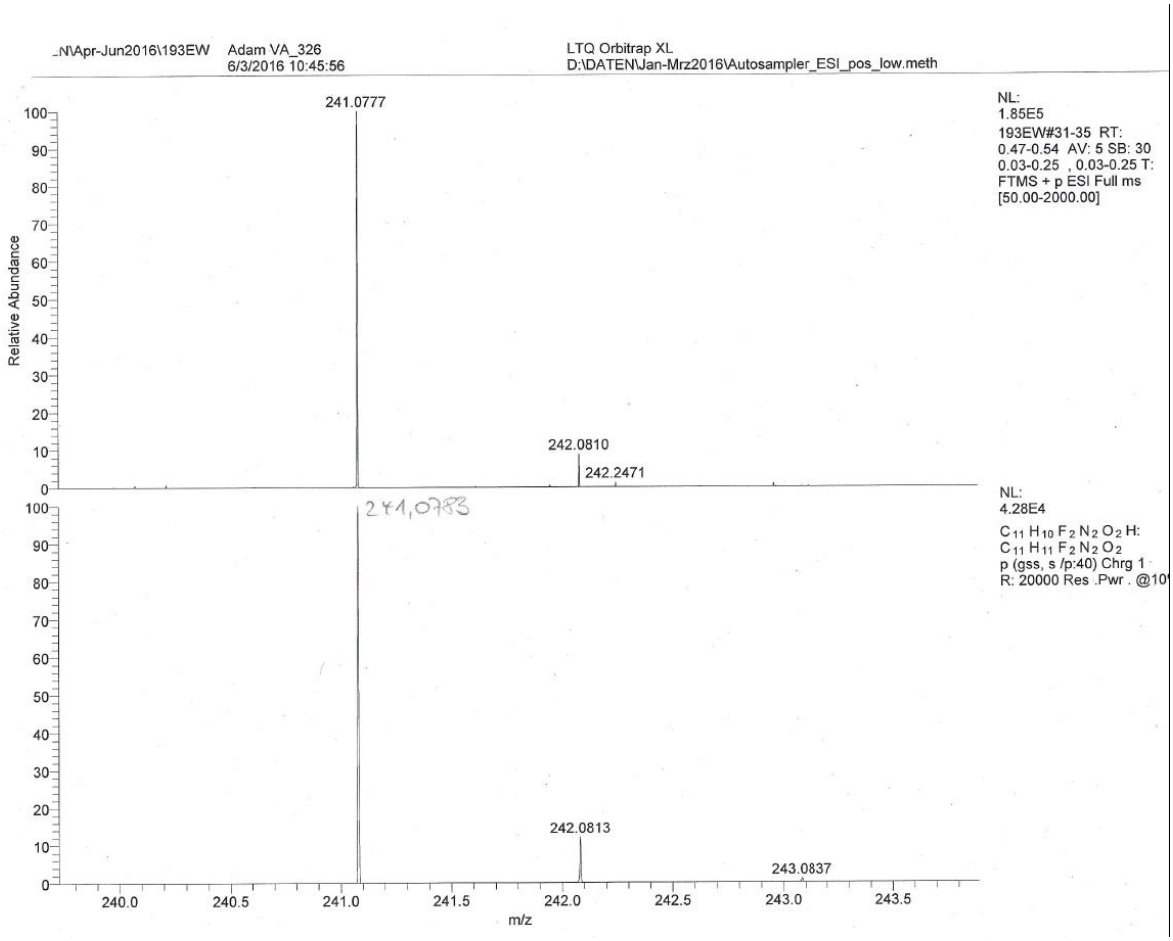
_N\Apr-Jun2016\193EW Adam VA_326
6/3/2016 10:45:56
LTQ Orbitrap XL
D:\DATEN\Jan-Mrz2016\Autosampler_ESI_pos_low.meth
241.0777
242.0810
242.2471
NL:
1.85E5
193EW#31-35 RT:
0.47-0.54 AV: 5 SB: 30
0.03-0.25 , 0.03-0.25 T:
FTMS + p ESI Full ms
[50.00-2000.00]
Relative Abundance
241,0783
242.0813
243.0837
NL:
4.28E4
C11 H10 F2 N2 O2 H:
C11 H11 F2 N2 O2
p (gss, s /p:40) Chrg 1
R: 20000 Res .Pwr . @10
m/z

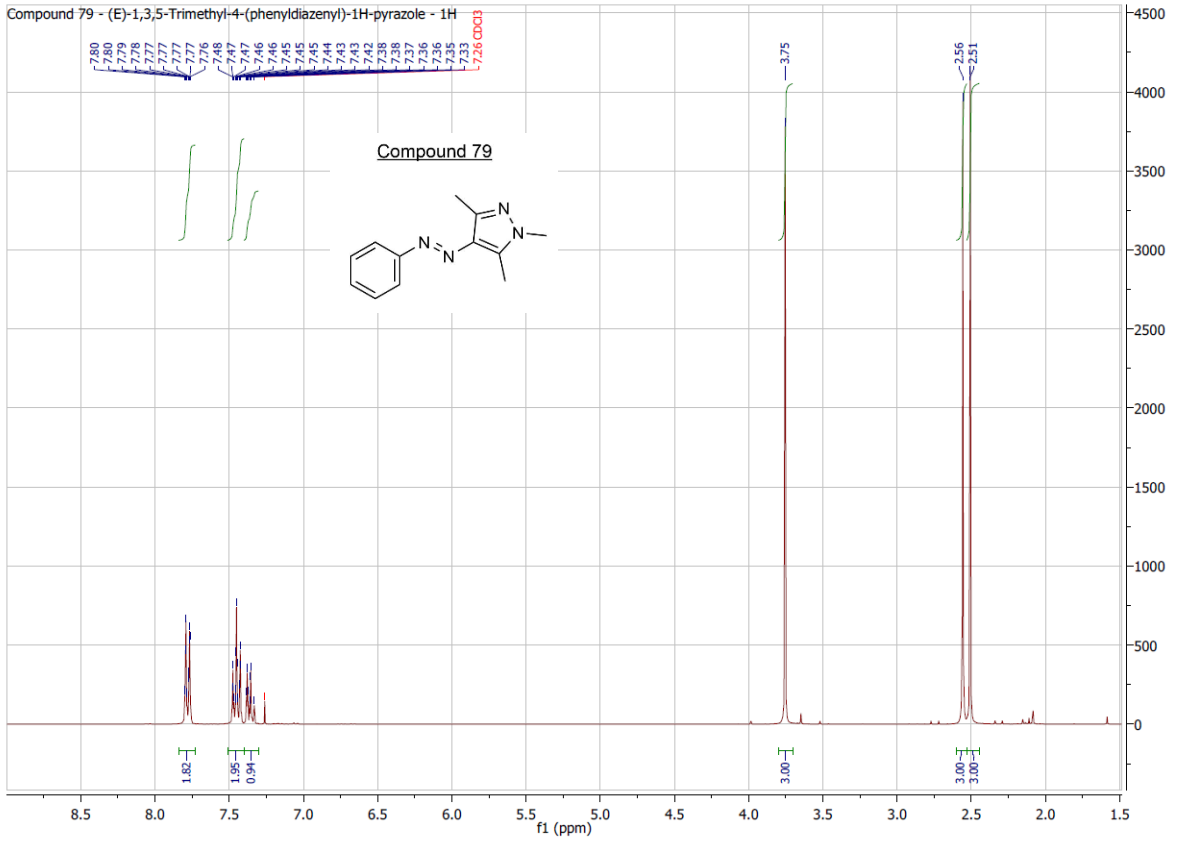
Compound 79 - (E)-1,3,5-Trimethyl-4-(phenyldiazenyl)-1H-pyrazole - 1H
Compound 79
f1 (ppm)

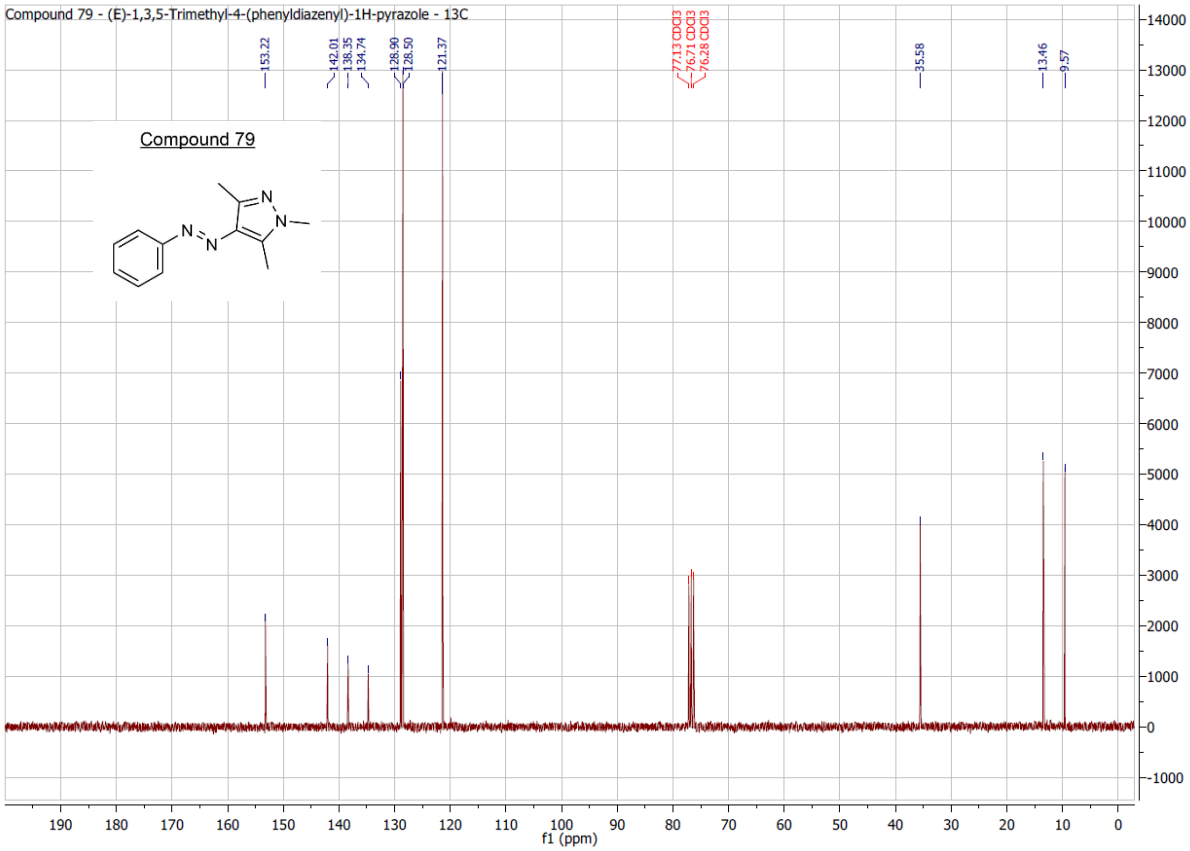
Compound 79 - (E)-1,3,5-Trimethyl-4-(phenyldiazenyl)-1H-pyrazole - 13C
Compound 79
f1 (ppm)

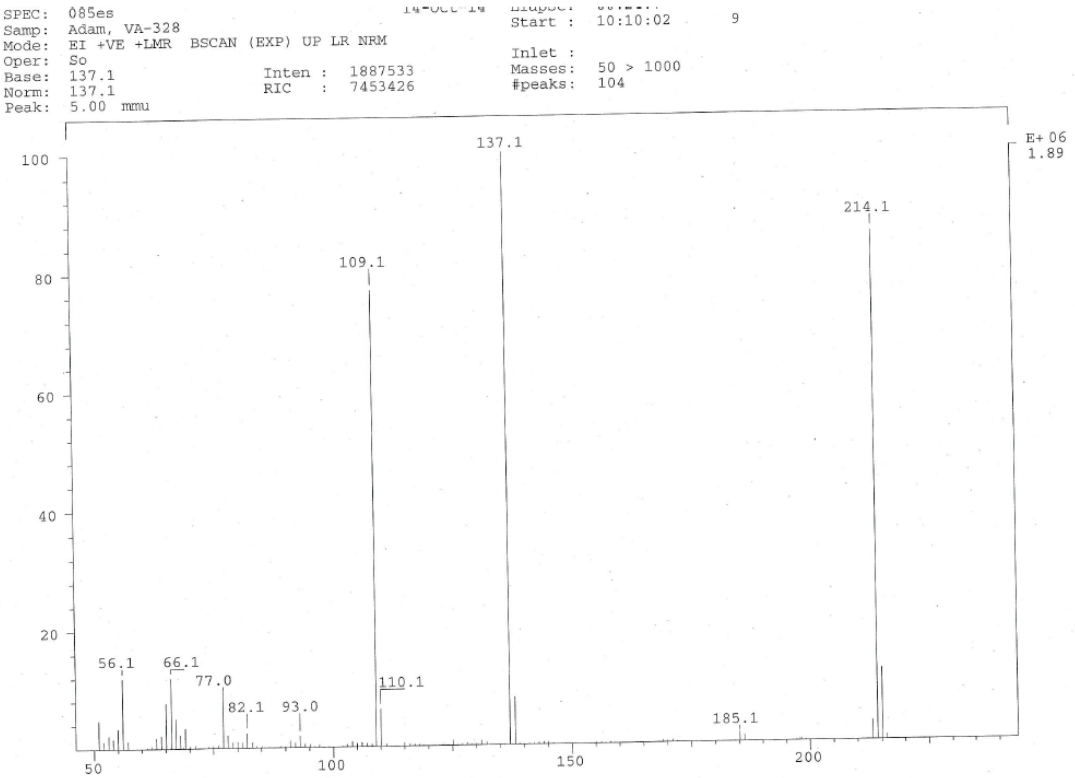
SPEC: 085es
Samp: Adam, VA-328
Mode: EI +VE +LMR BSCAN (EXP) UP LR NRM
Oper: So
Base: 137.1
Norm: 137.1
Peak: 5.00 mmu
Inten : 1887533
RIC : 7453426
Start : 10:10:02
9
Inlet :
Masses: 50 > 1000
#peaks: 104
E+ 06
1.89
137.1
214.1
109.1
56.1
66.1
77.0
82.1
93.0
110.1
185.1
100
80
60
40
20
50
100
150
200

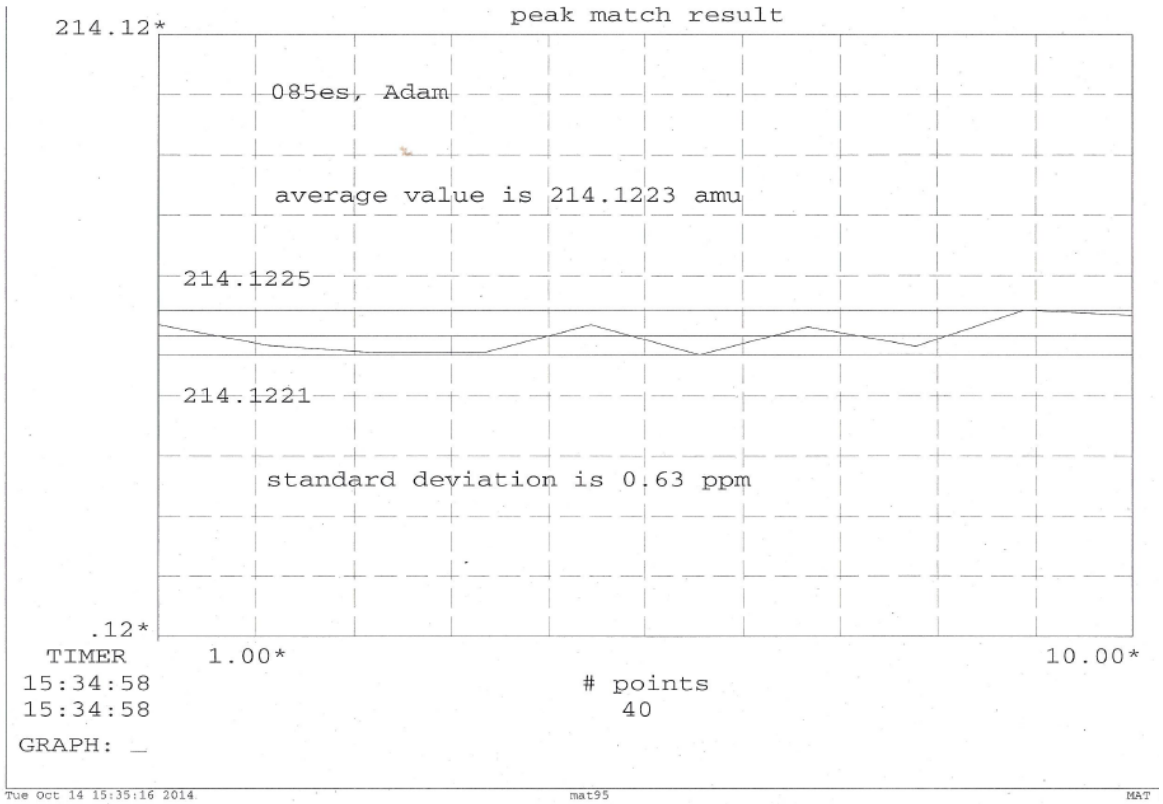
peak match result
214.12*
085es, Adam
average value is 214.1223 amu
214.1225
214.1221
standard deviation is 0.63 ppm
.12*
TIMER
1.00*
10.00*
15:34:58
15:34:58
points
40
GRAPH: _
Tue Oct 14 15:35:16 2014
mat95
MAT

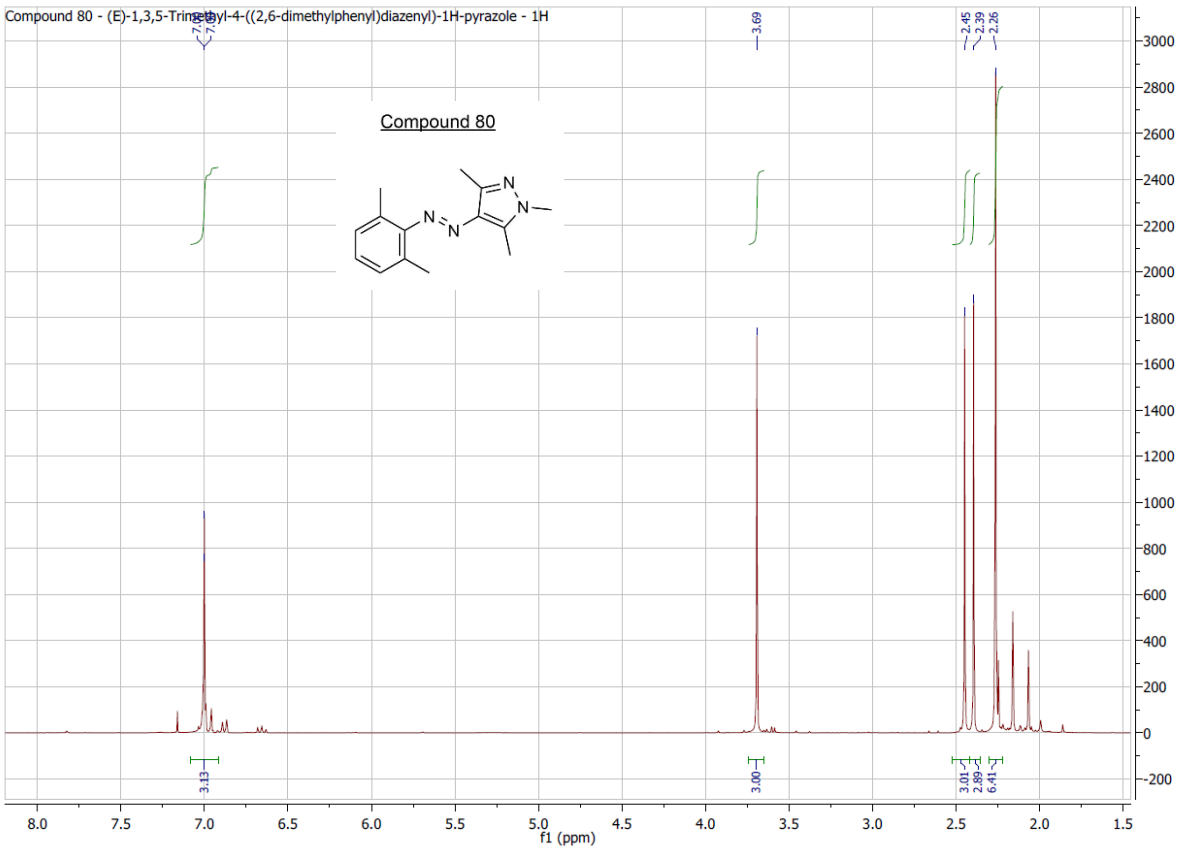
Compound 80 - (E)-1,3,5-Trimethyl-4-((2,6-dimethylphenyl)diazenyl)-1H-pyrazole - 1H
Compound 80
7.69
7.68
3.69
2.45
2.39
2.26
3.13
3.00
3.01
2.89
6.41
f1 (ppm)

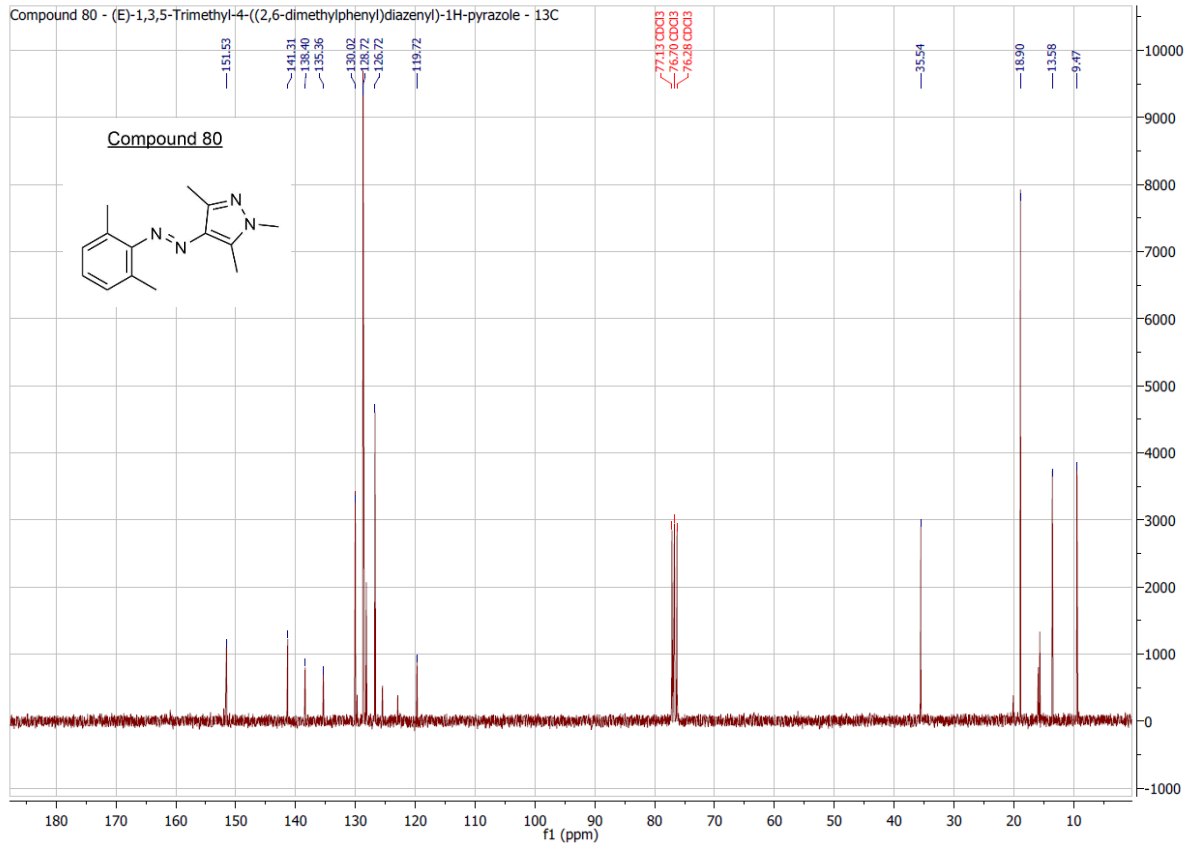
Compound 80 - (E)-1,3,5-Trimethyl-4-((2,6-dimethylphenyl)diazenyl)-1H-pyrazole - 13C
Compound 80
151.53
141.31
138.40
135.36
130.02
128.72
126.72
119.72
77.13 CDCl3
76.70 CDCl3
76.28 CDCl3
35.54
18.90
13.58
9.47
f1 (ppm)

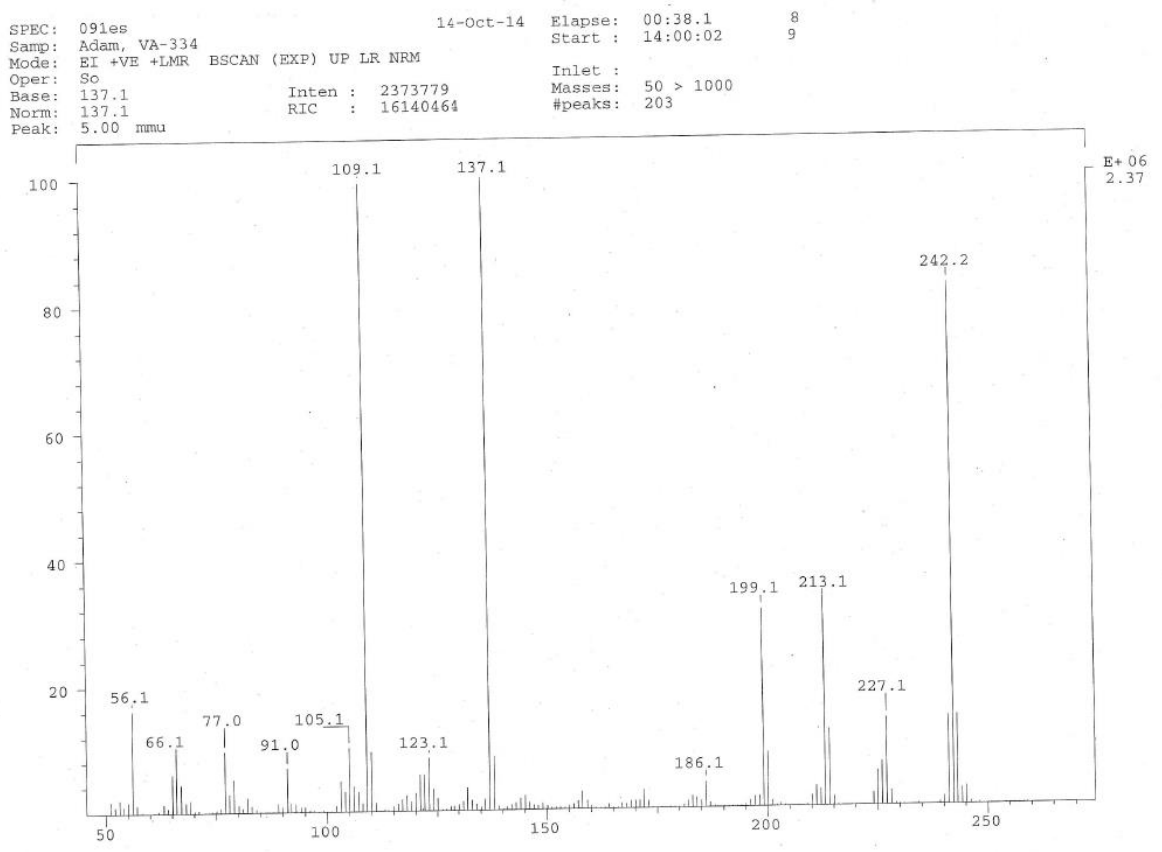
SPEC: 091es
Samp: Adam, VA-334
Mode: EI +VE +LMR BSCAN (EXP) UP LR NRM
Oper: So
Base: 137.1
Norm: 137.1
Peak: 5.00 mmu
14-Oct-14
Inten : 2373779
RIC : 16140464
Elapse: 00:38.1
Start : 14:00:02
Inlet :
Masses: 50 > 1000
#peaks: 203
E+06
2.37
109.1
137.1
242.2
199.1
213.1
227.1
56.1
66.1
77.0
91.0
105.1
123.1
186.1

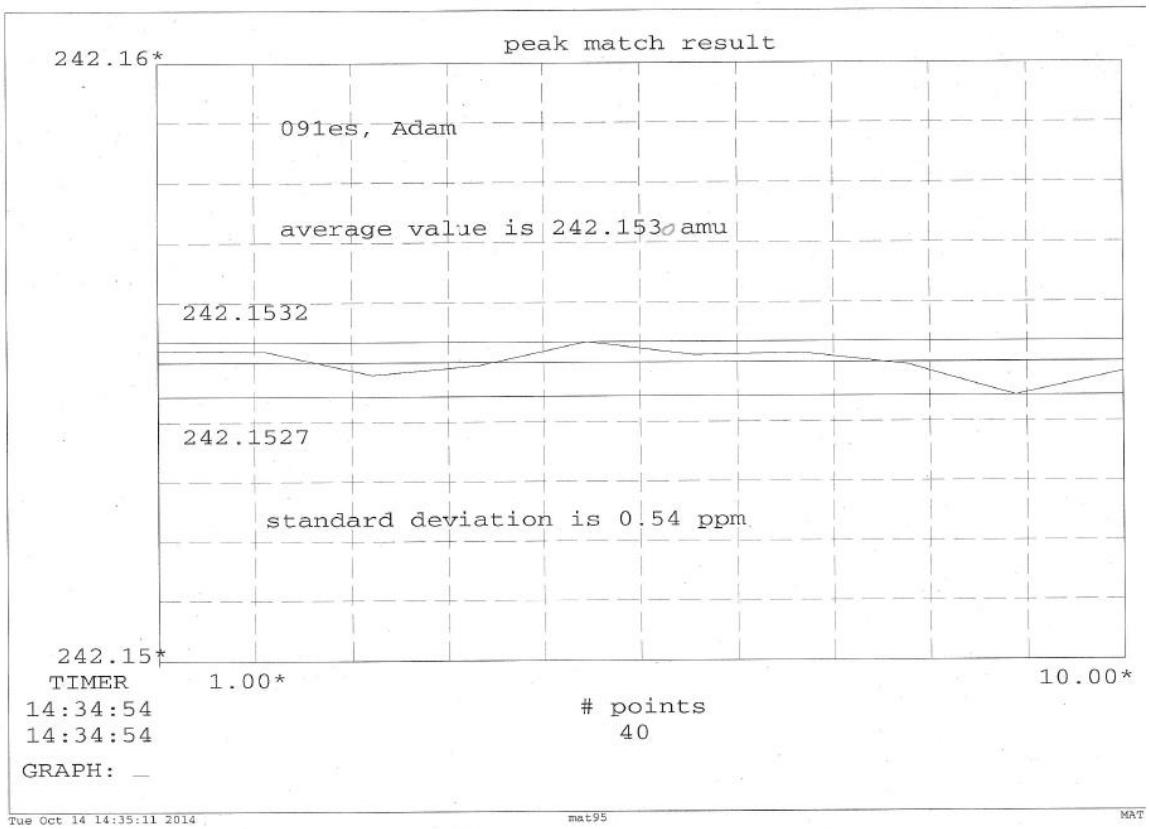
peak match result
242.16*
091es, Adam
average value is 242.153 amu
242.1532
242.1527
standard deviation is 0.54 ppm
242.15*
TIMER
1.00*
10.00*
14:34:54
14:34:54
points
40
GRAPH:
Tue Oct 14 14:35:11 2014
mat95
MAT

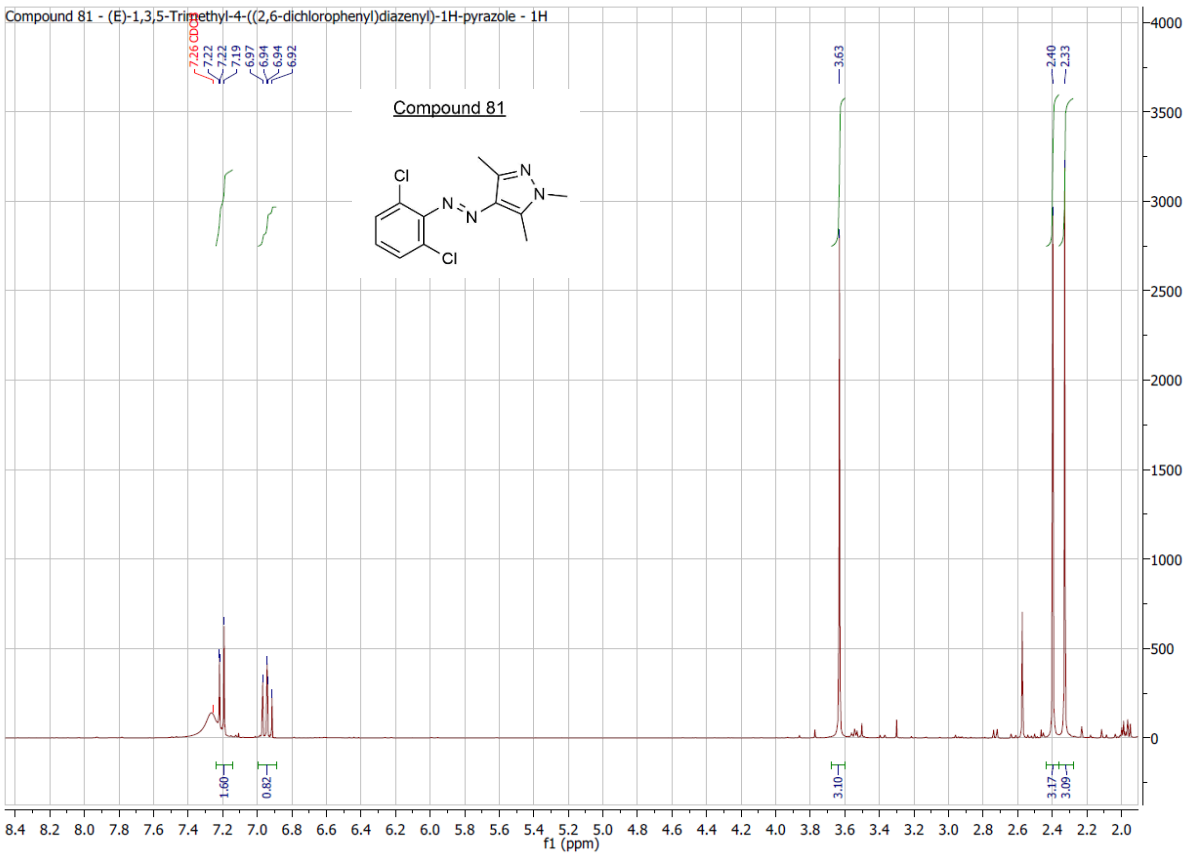
Compound 81 - (E)-1,3,5-Trimethyl-4-((2,6-dichlorophenyl)diazenyl)-1H-pyrazole - 1H
Compound 81
f1 (ppm)

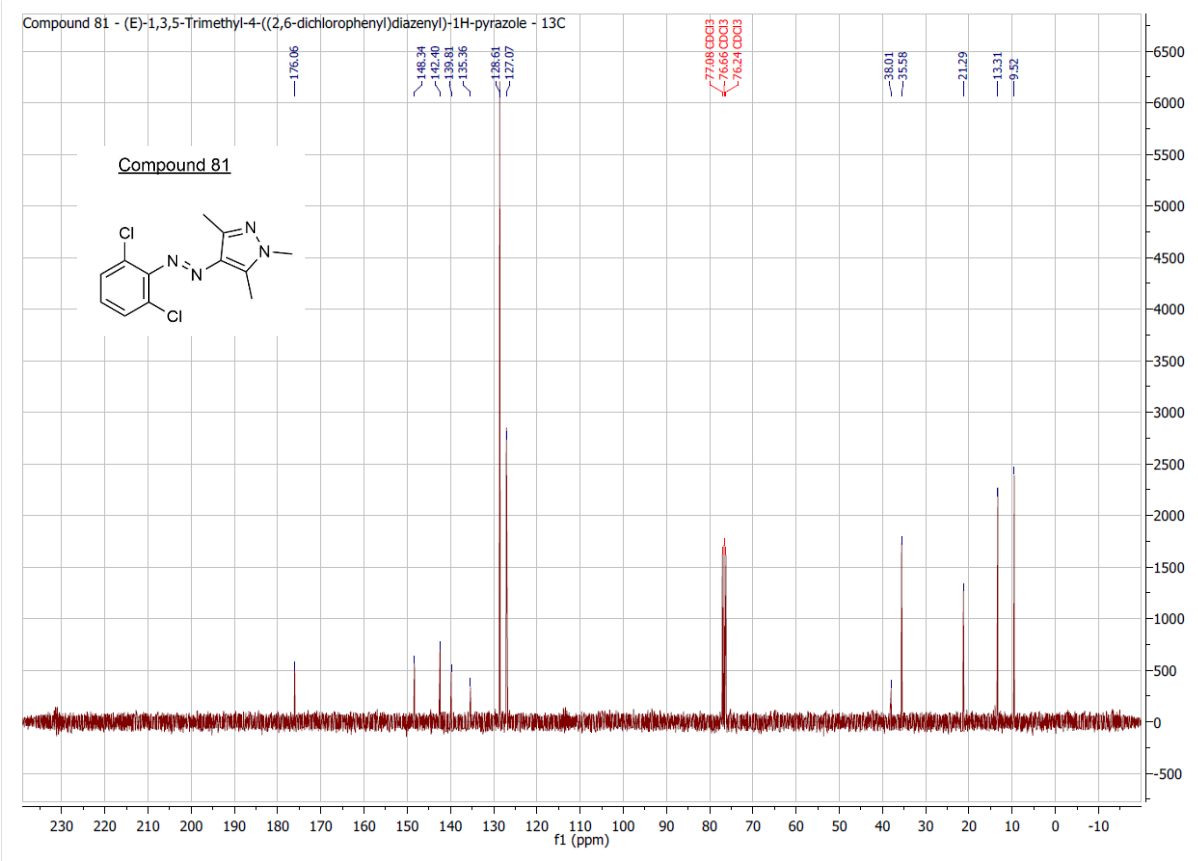
Compound 81 - (E)-1,3,5-Trimethyl-4-((2,6-dichlorophenyl)diazenyl)-1H-pyrazole - 13C
Compound 81
f1 (ppm)

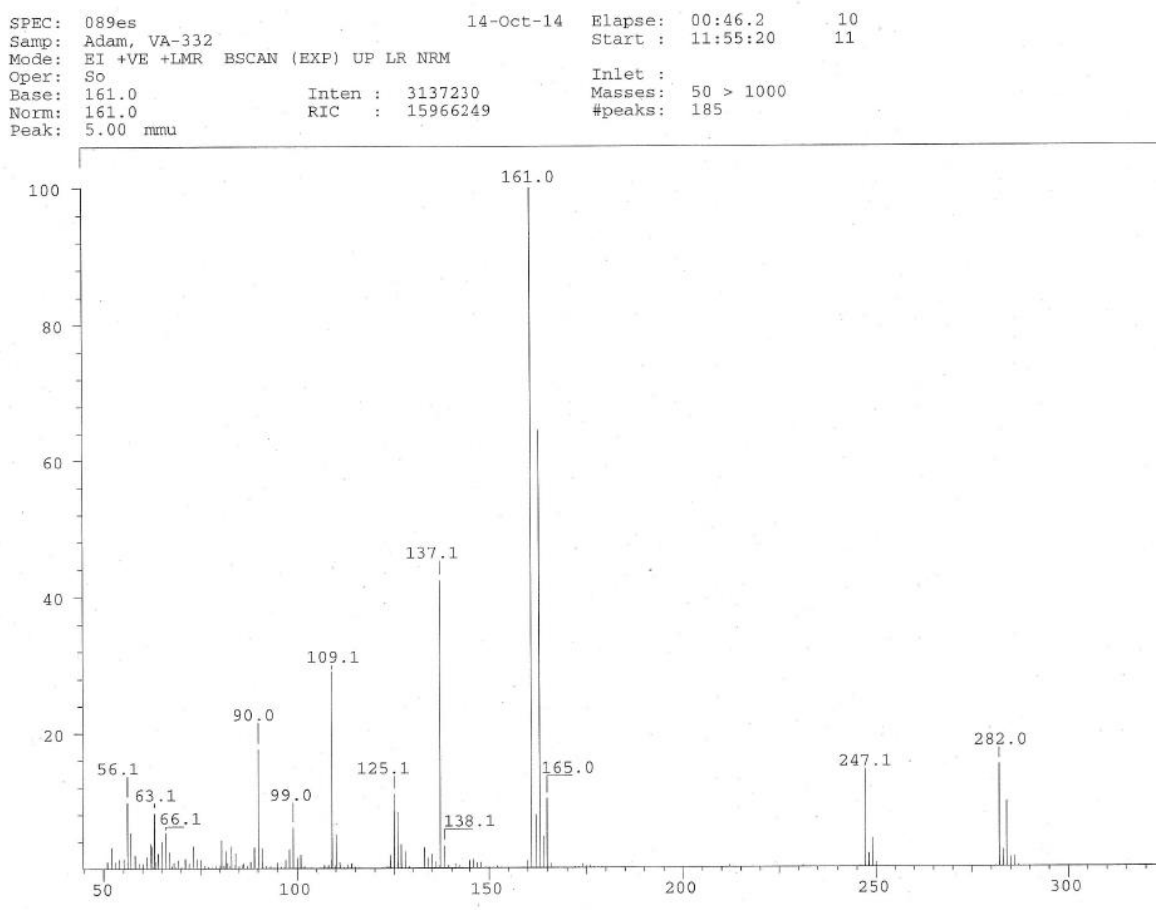
SPEC: 089es 14-Oct-14 Elapse: 00:46.2 10
Samp: Adam, VA-332 Start : 11:55:20 11
Mode: EI +VE +LMR BSCAN (EXP) UP LR NRM
Oper: So Inlet :
Base: 161.0 Inten : 3137230 Masses: 50 > 1000
Norm: 161.0 RIC : 15966249 #peaks: 185
Peak: 5.00 mmu
161.0
137.1
109.1
90.0
56.1
63.1
66.1
99.0
125.1
138.1
165.0
247.1
282.0
100
80
60
40
20
50
100
150
200
250
300

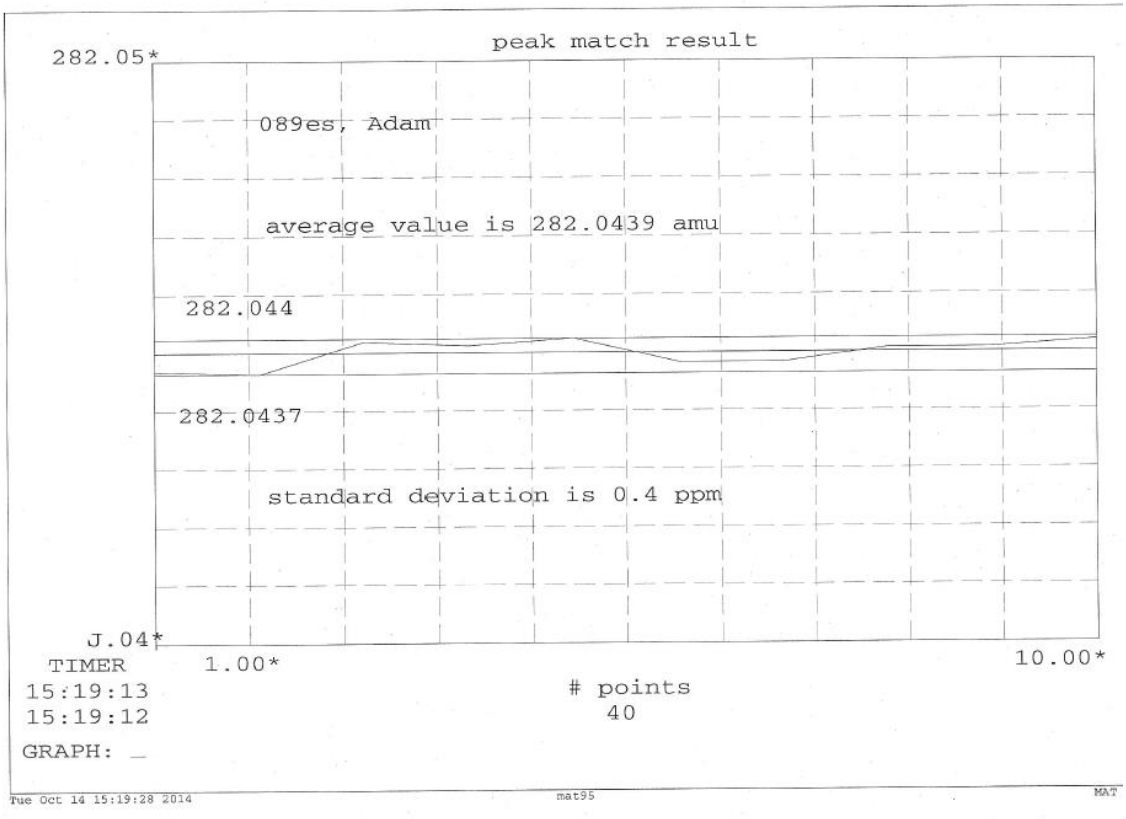
peak match result
282.05*
089es, Adam
average value is 282.0439 amu
282.044
282.0437
standard deviation is 0.4 ppm
J.04*
TIMER
1.00*
10.00*
15:19:13
15:19:12
points
40
GRAPH:
Tue Oct 14 15:19:28 2014
mat95
MAT

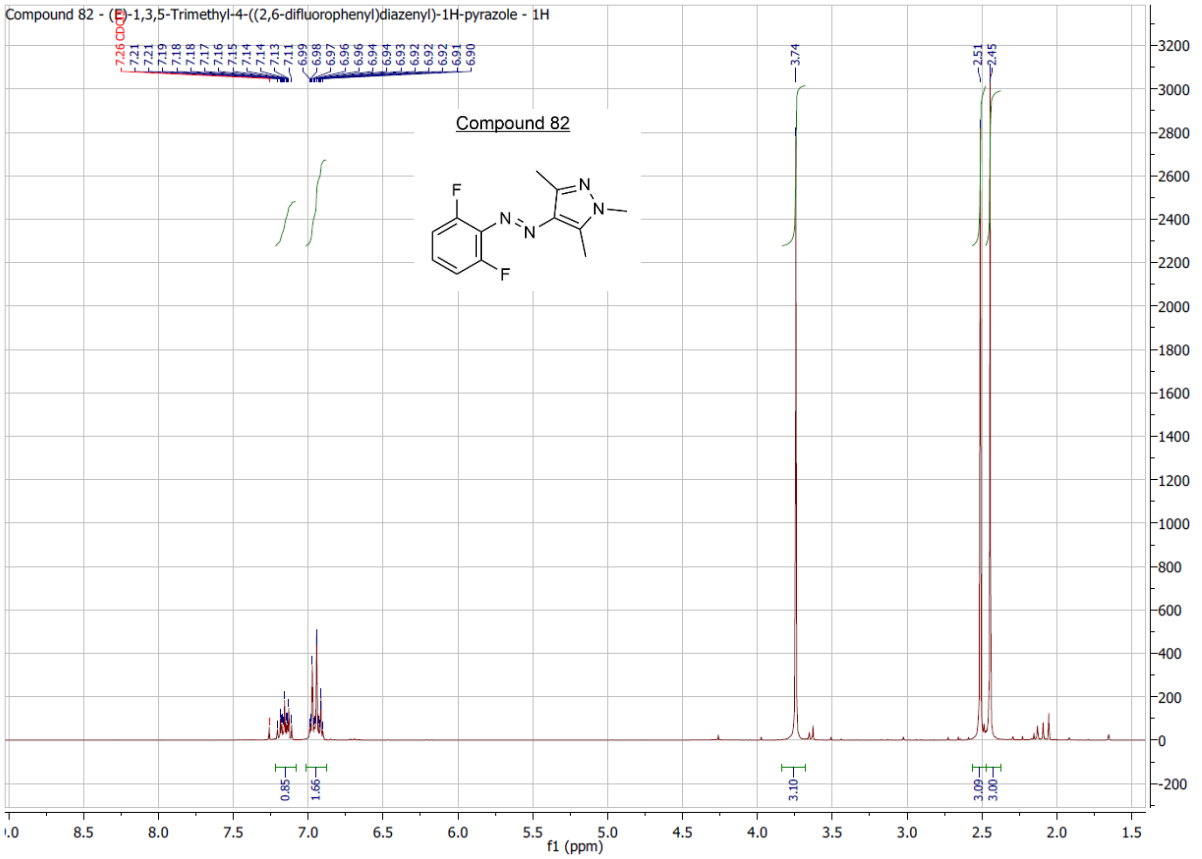
Compound 82 - (E)-1,3,5-Trimethyl-4-((2,6-difluorophenyl)diazenyl)-1H-pyrazole - 1H
Compound 82
f1 (ppm)

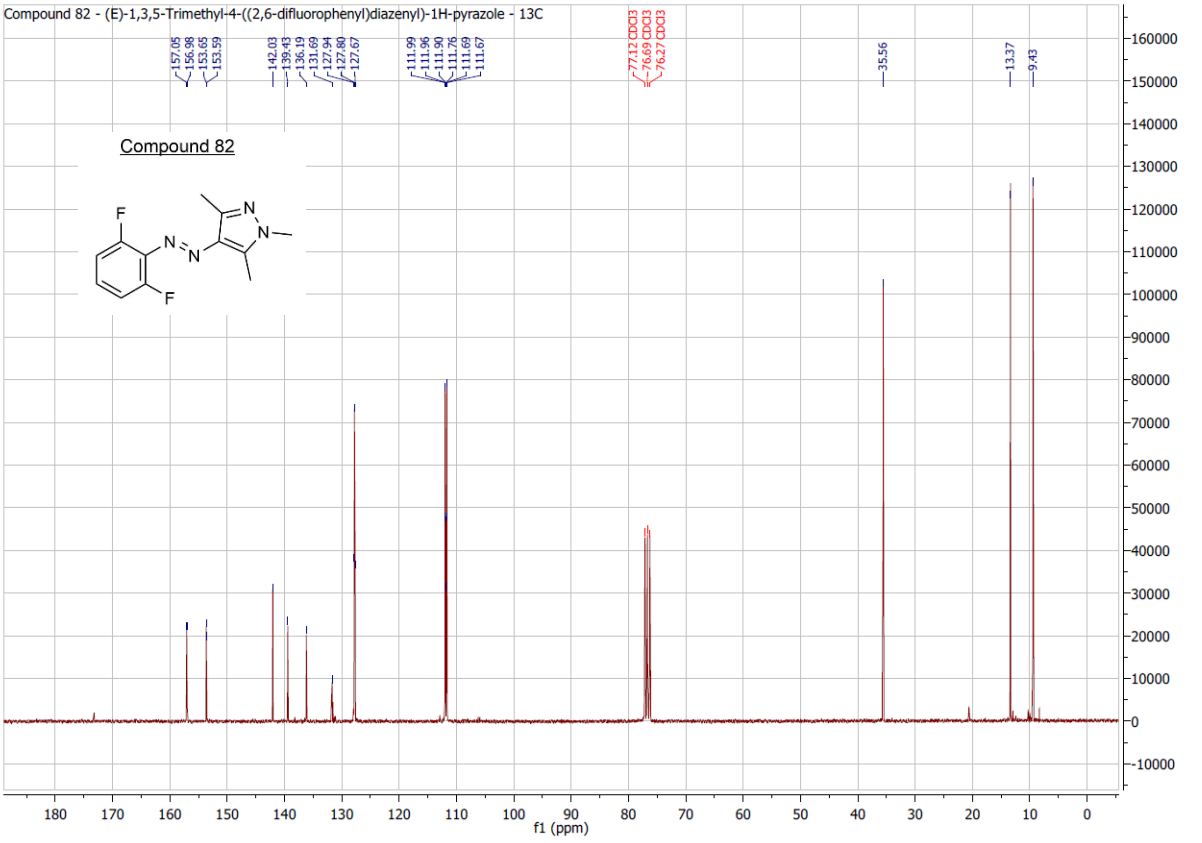
Compound 82 - (E)-1,3,5-Trimethyl-4-((2,6-difluorophenyl)diazenyl)-1H-pyrazole - 13C
Compound 82
f1 (ppm)

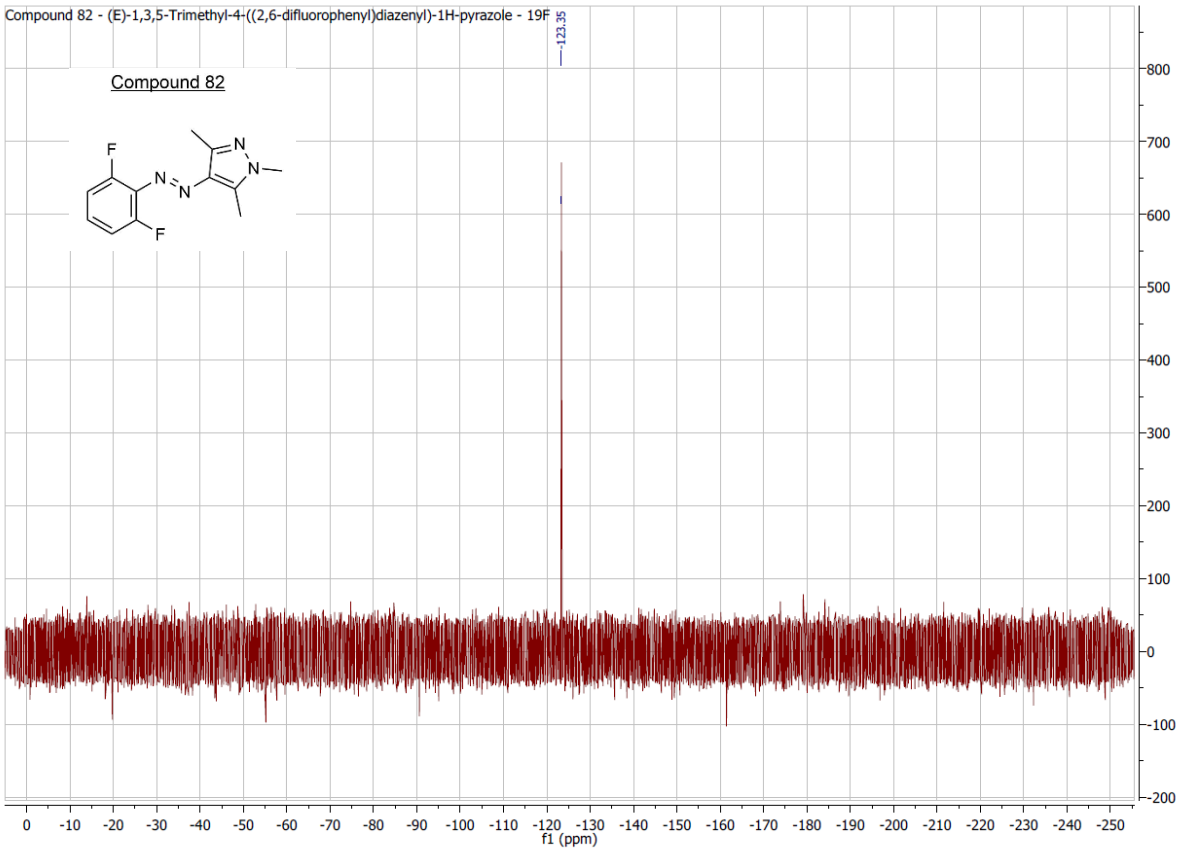
Compound 82 - (E)-1,3,5-Trimethyl-4-((2,6-difluorophenyl)diazenyl)-1H-pyrazole - 19F
Compound 82
F
N
N
N
F
-123.35
800
700
600
500
400
300
200
100
0
-100
-200
0 -10 -20 -30 -40 -50 -60 -70 -80 -90 -100 -110 -120 -130 -140 -150 -160 -170 -180 -190 -200 -210 -220 -230 -240 -250
f1 (ppm)

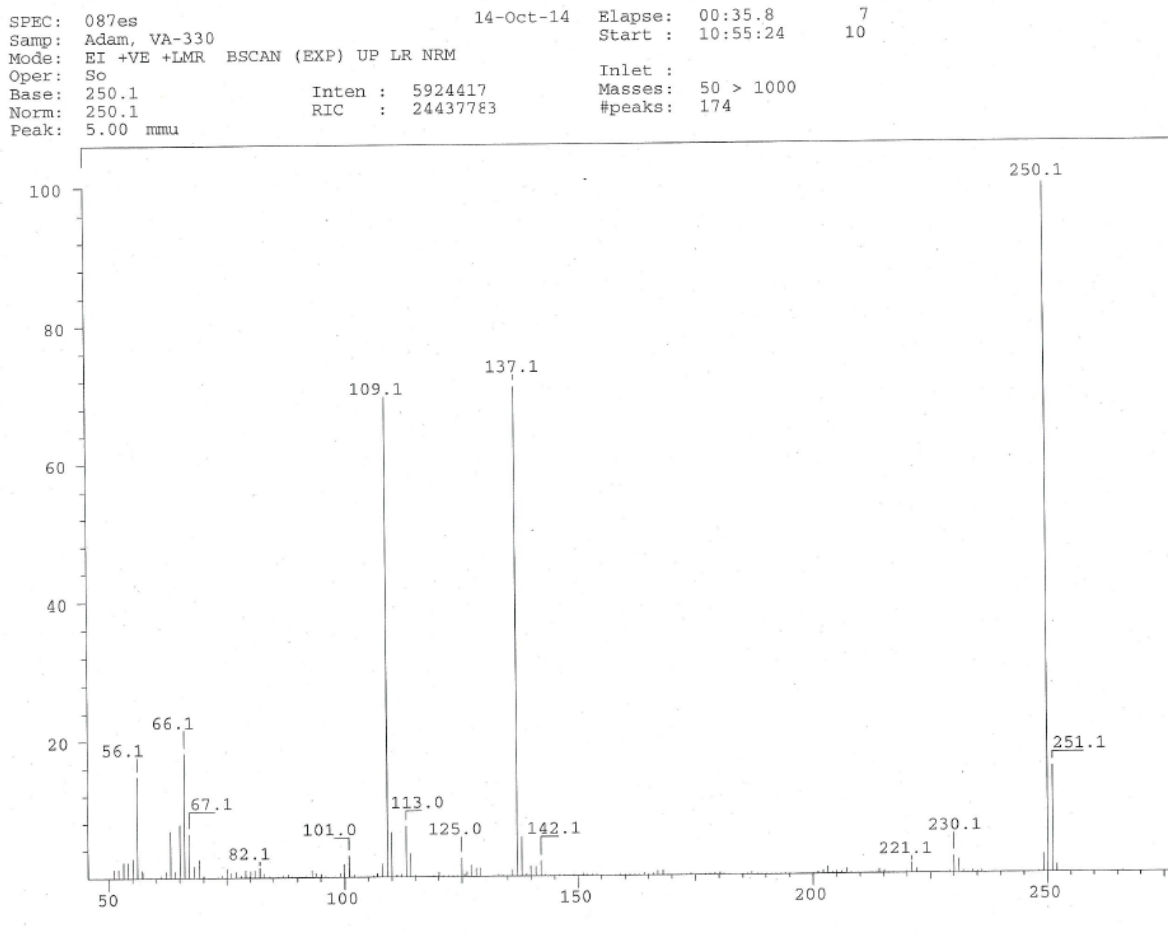
SPEC: 087es
Samp: Adam, VA-330
Mode: EI +VE +LMR BSCAN (EXP) UP LR NRM
Oper: So
Base: 250.1
Norm: 250.1
Peak: 5.00 mmu
Inten : 5924417
RIC : 24437783
14-Oct-14
Elapse: 00:35.8 7
Start : 10:55:24 10
Inlet :
Masses: 50 > 1000
#peaks: 174
100
80
60
40
20
250.1
137.1
109.1
66.1
56.1
67.1
82.1
101.0
113.0
125.0
142.1
221.1
230.1
251.1
50
100
150
200
250

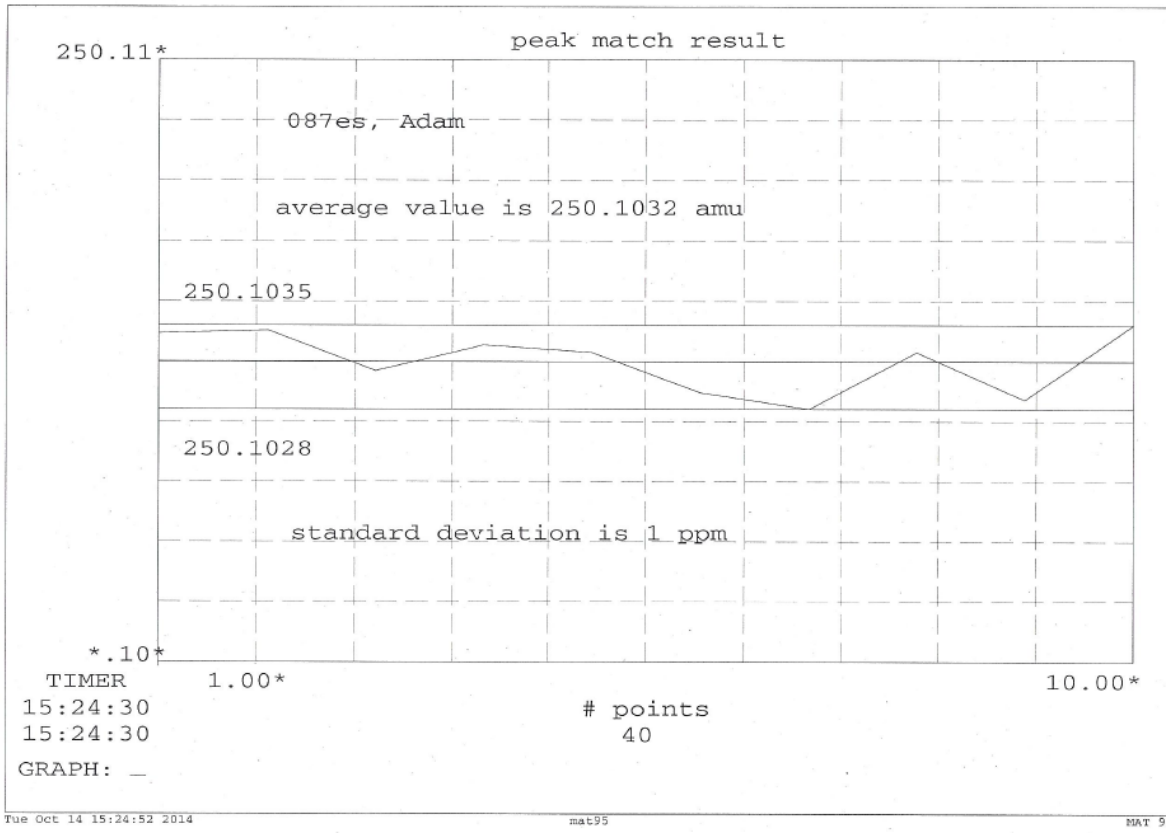
peak match result
250.11*
087es, Adam
average value is 250.1032 amu
250.1035
250.1028
standard deviation is 1 ppm
.10
TIMER
1.00*
10.00*
15:24:30
15:24:30
points
40
GRAPH: _
Tue Oct 14 15:24:52 2014
mat95
MAT 9

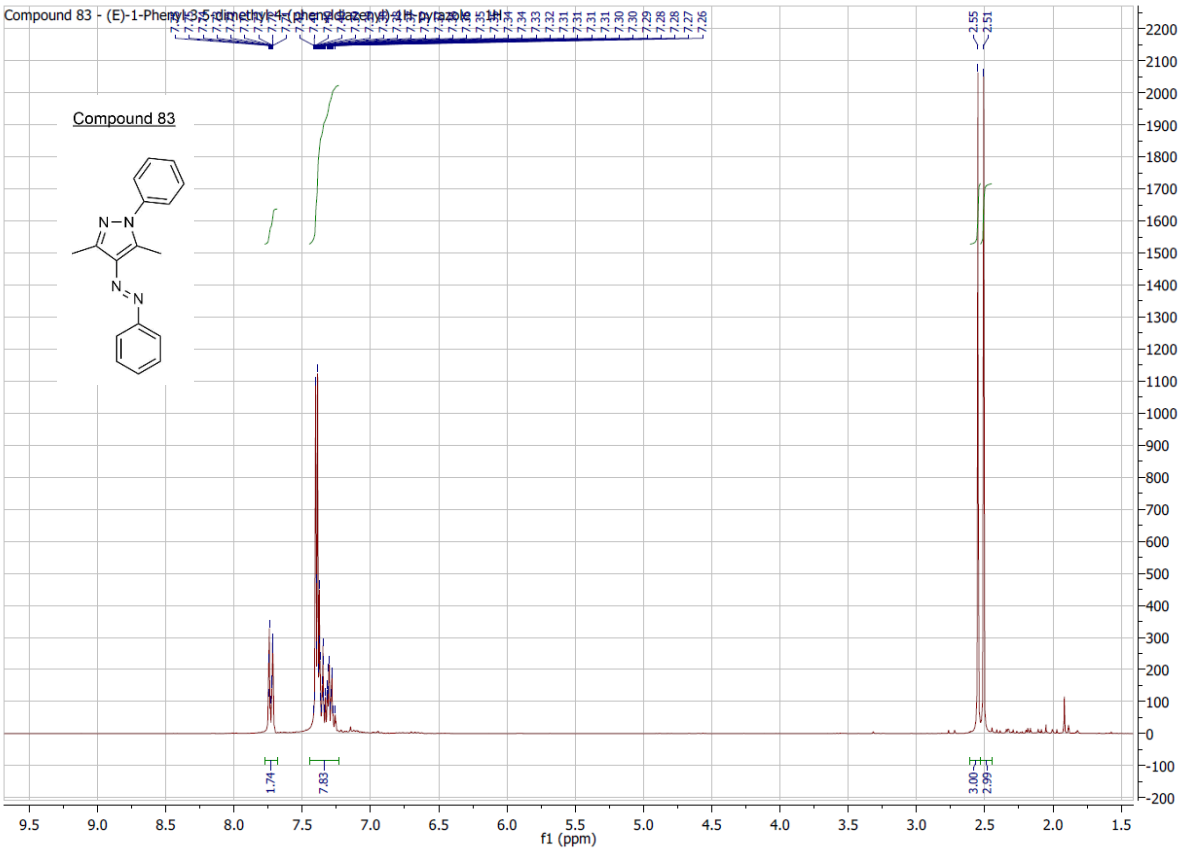
Compound 83 - (E)-1-Phenyl-3,5-dimethyl-4-(phenyldiazenyl)-1H-pyrazole - 1H
Compound 83
2.55
2.51
1.74
7.83
3.00
2.99
f1 (ppm)

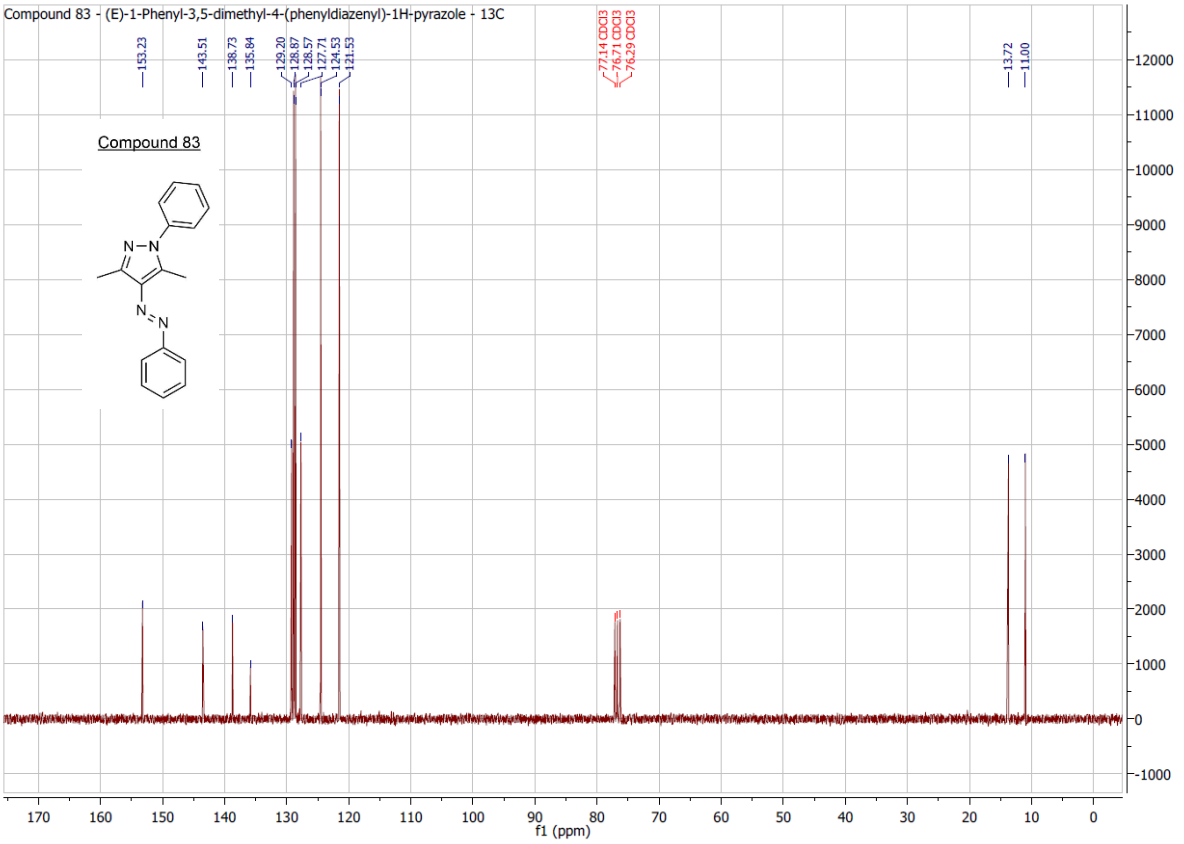
Compound 83 - (E)-1-Phenyl-3,5-dimethyl-4-(phenyldiazenyl)-1H-pyrazole - 13C
153.23
143.51
138.73
135.84
129.20
128.87
128.57
127.71
124.53
121.53
77.14 CDCl3
76.71 CDCl3
76.29 CDCl3
13.72
11.00
Compound 83
f1 (ppm)

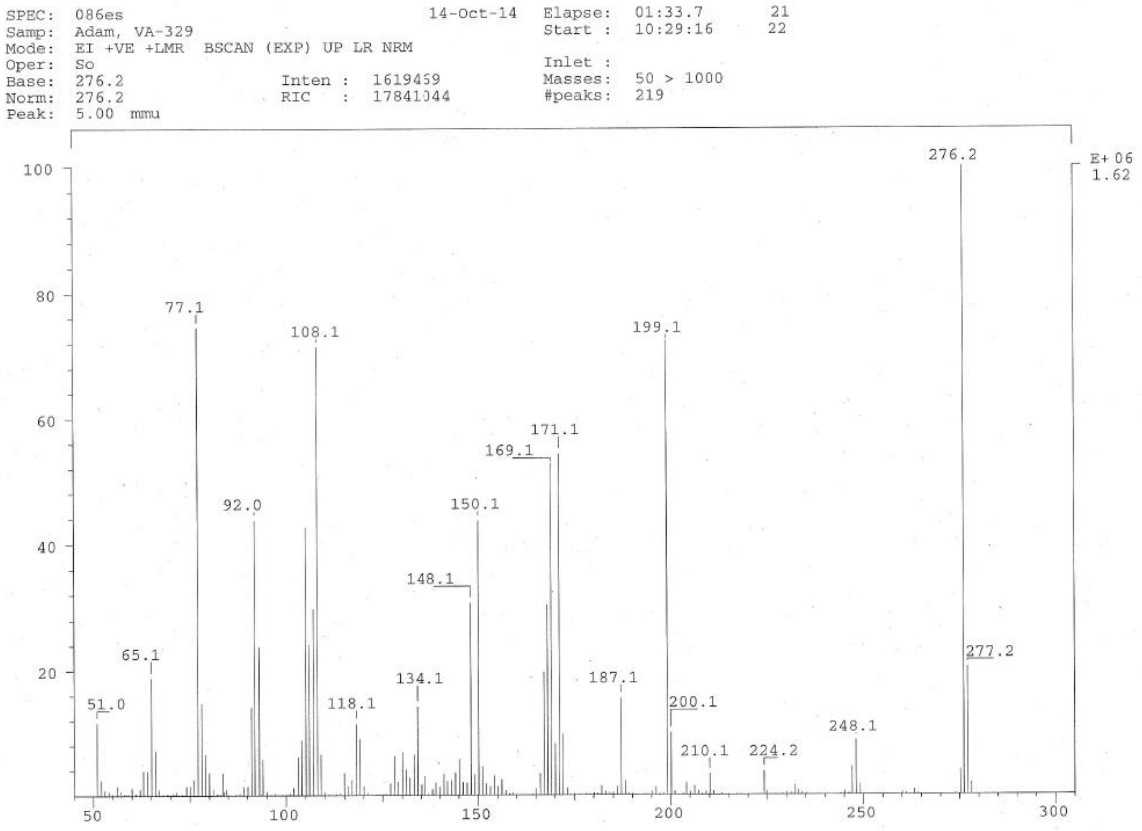
SPEC: 086es
Samp: Adam, VA-329
Mode: EI +VE +LMR BSCAN (EXP) UP LR NRM
Oper: So
Base: 276.2
Norm: 276.2
Peak: 5.00 mmu
14-Oct-14
Inten : 1619459
RIC : 17841044
Elapse: 01:33.7
Start : 10:29:16
Inlet :
Masses: 50 > 1000
#peaks: 219
21
22
E+ 06
1.62
276.2
199.1
77.1
108.1
171.1
169.1
92.0
150.1
148.1
65.1
134.1
187.1
277.2
51.0
118.1
200.1
248.1
210.1
224.2
100
80
60
40
20
50
100
150
200
250
300

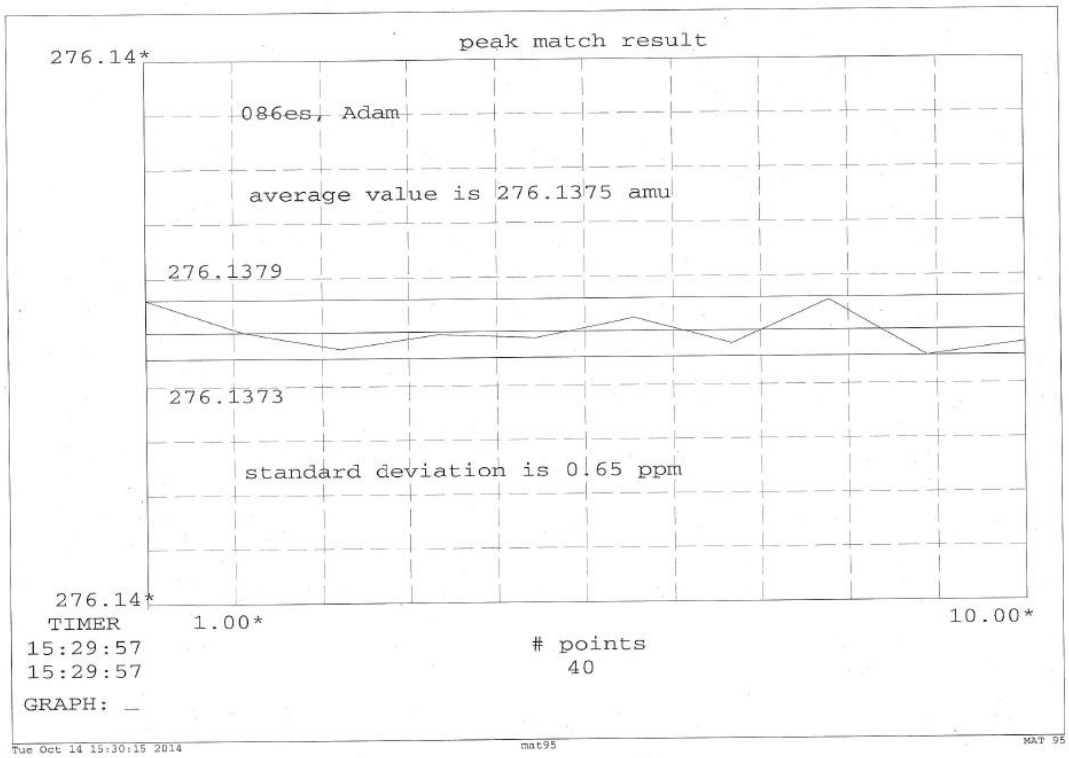
peak match result
276.14*
086es, Adam
average value is 276.1375 amu
276.1379
276.1373
standard deviation is 0.65 ppm
276.14*
TIMER
15:29:57
15:29:57
GRAPH: _
1.00*
10.00*
points
40
Tue Oct 14 15:30:15 2014
mat95
MAT 95

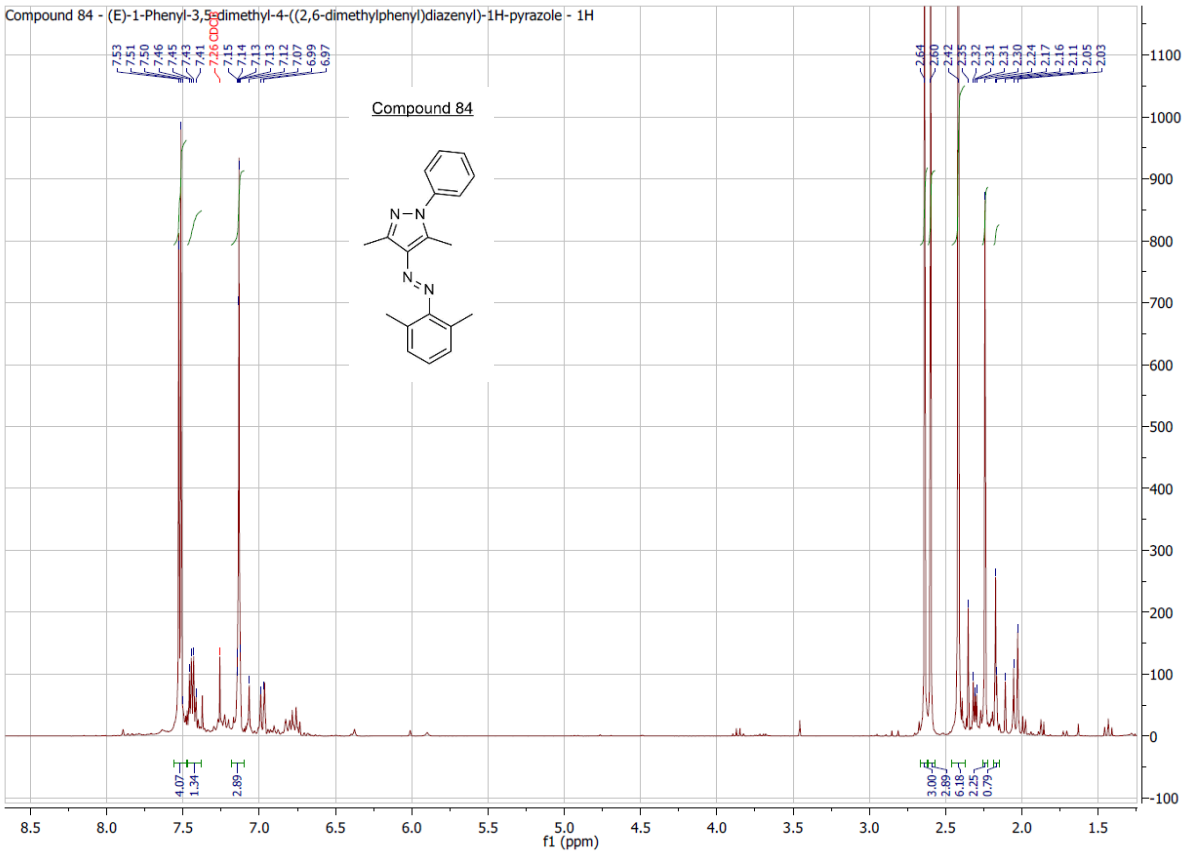
Compound 84 - (E)-1-Phenyl-3,5-dimethyl-4-((2,6-dimethylphenyl)diazenyl)-1H-pyrazole - 1H
Compound 84
f1 (ppm)

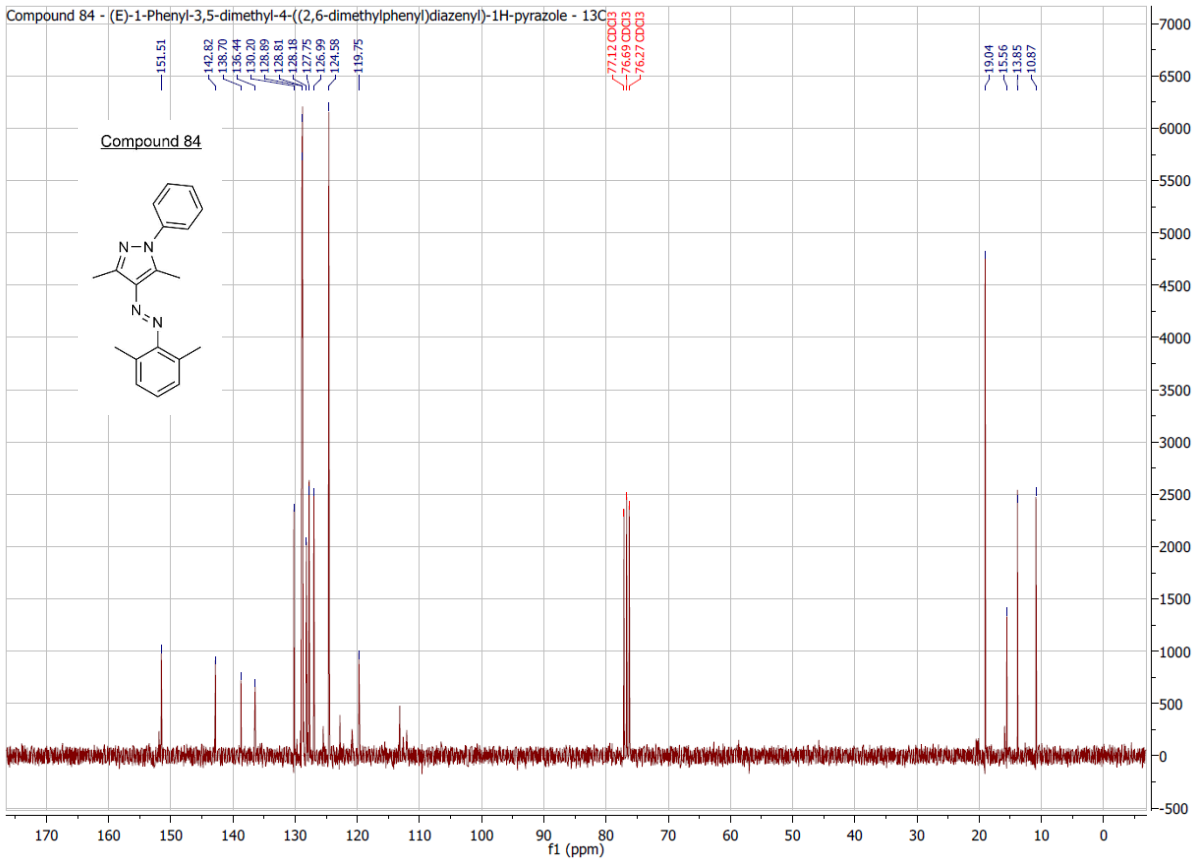
Compound 84 - (E)-1-Phenyl-3,5-dimethyl-4-((2,6-dimethylphenyl)diazenyl)-1H-pyrazole - 13C
Compound 84
f1 (ppm)

SPEC: 092es 15-Oct-14 Elapse: 00:51.2 12
Samp: Adam, VA-335 Start : 13:40:32 15
Mode: EI +VE +LMR BSCAN (EXP) UP LR NRM
Oper: So Inlet :
Base: 108.1 Inten : 2135950 Masses: 50 > 1000
Norm: 108.1 RIC : 29643963 #peaks: 274
Peak: 5.00 mmu

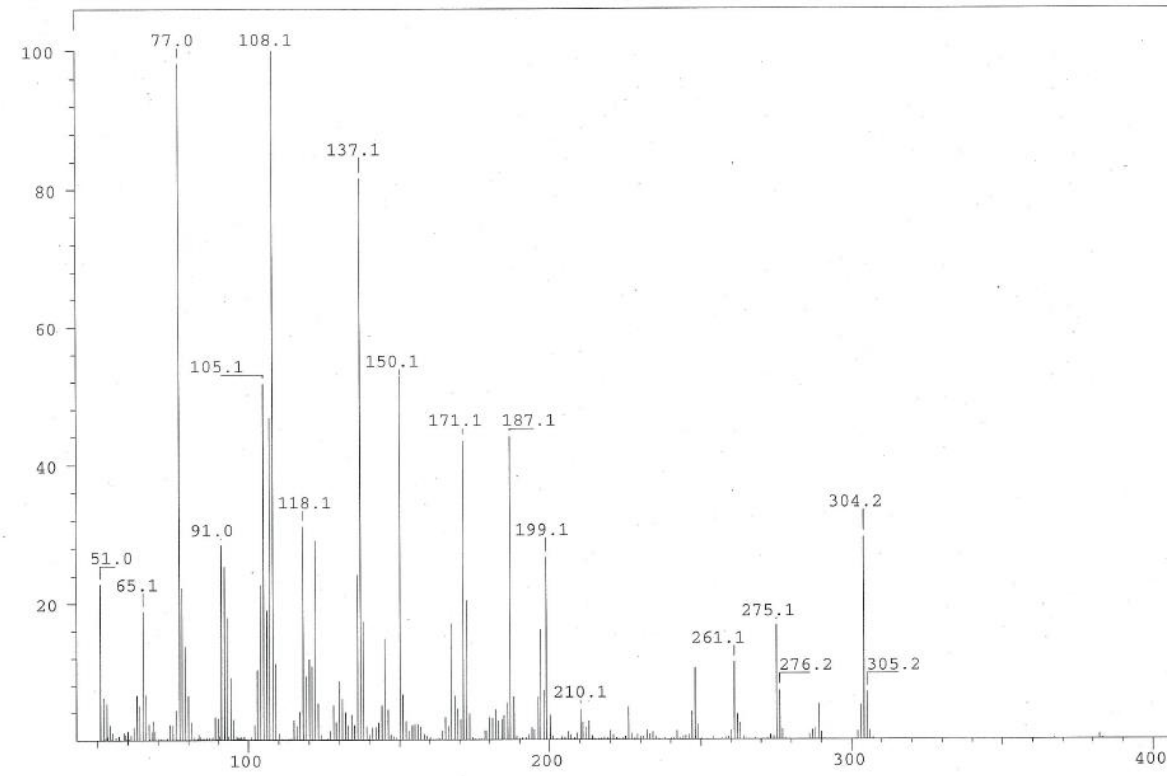

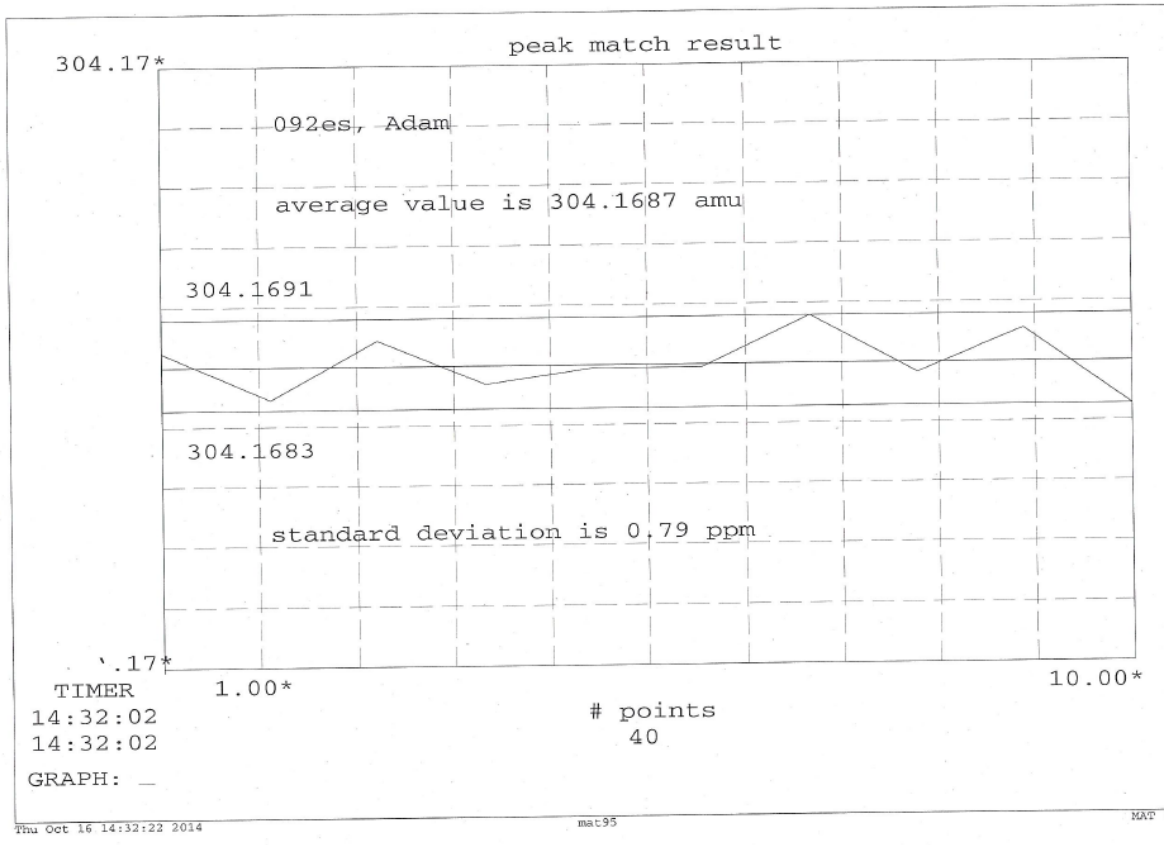

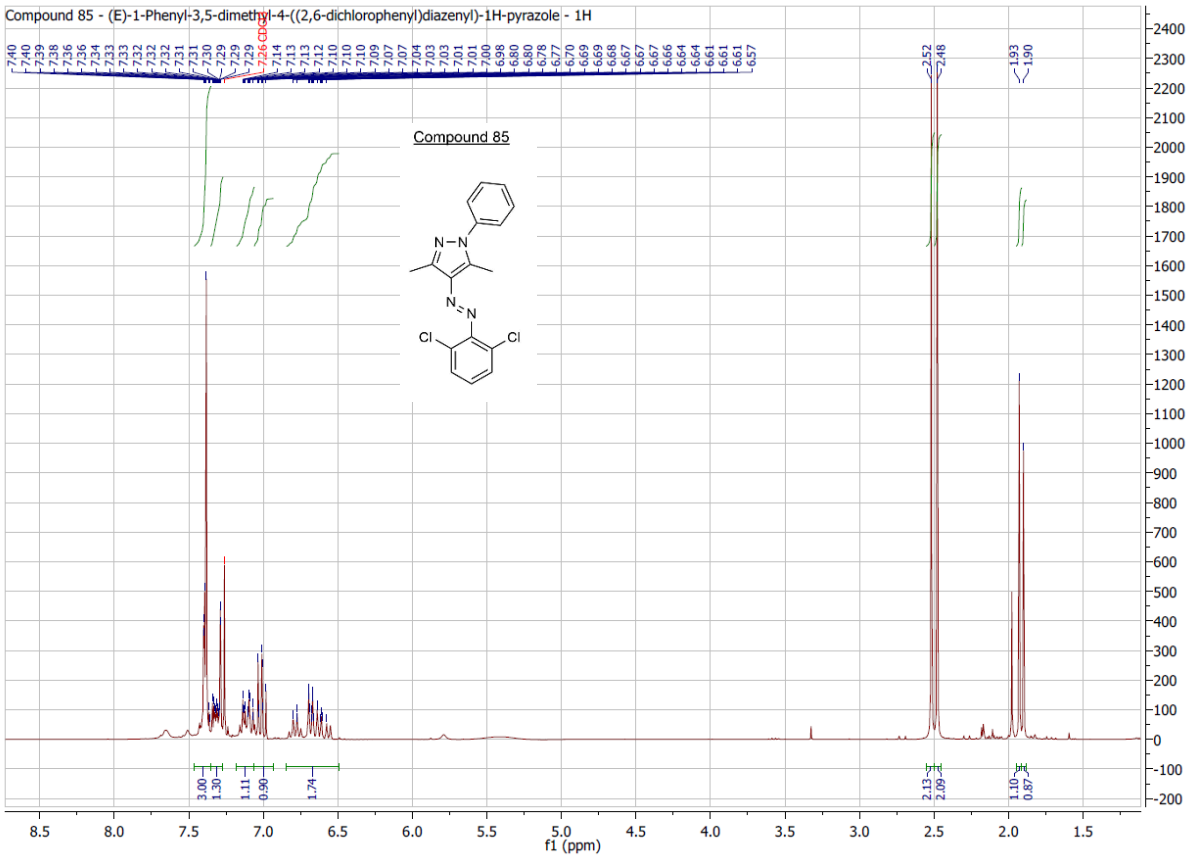
Compound 85 - (E)-1-Phenyl-3,5-dimethyl-4-((2,6-dichlorophenyl)diazenyl)-1H-pyrazole - 1H
Compound 85
f1 (ppm)

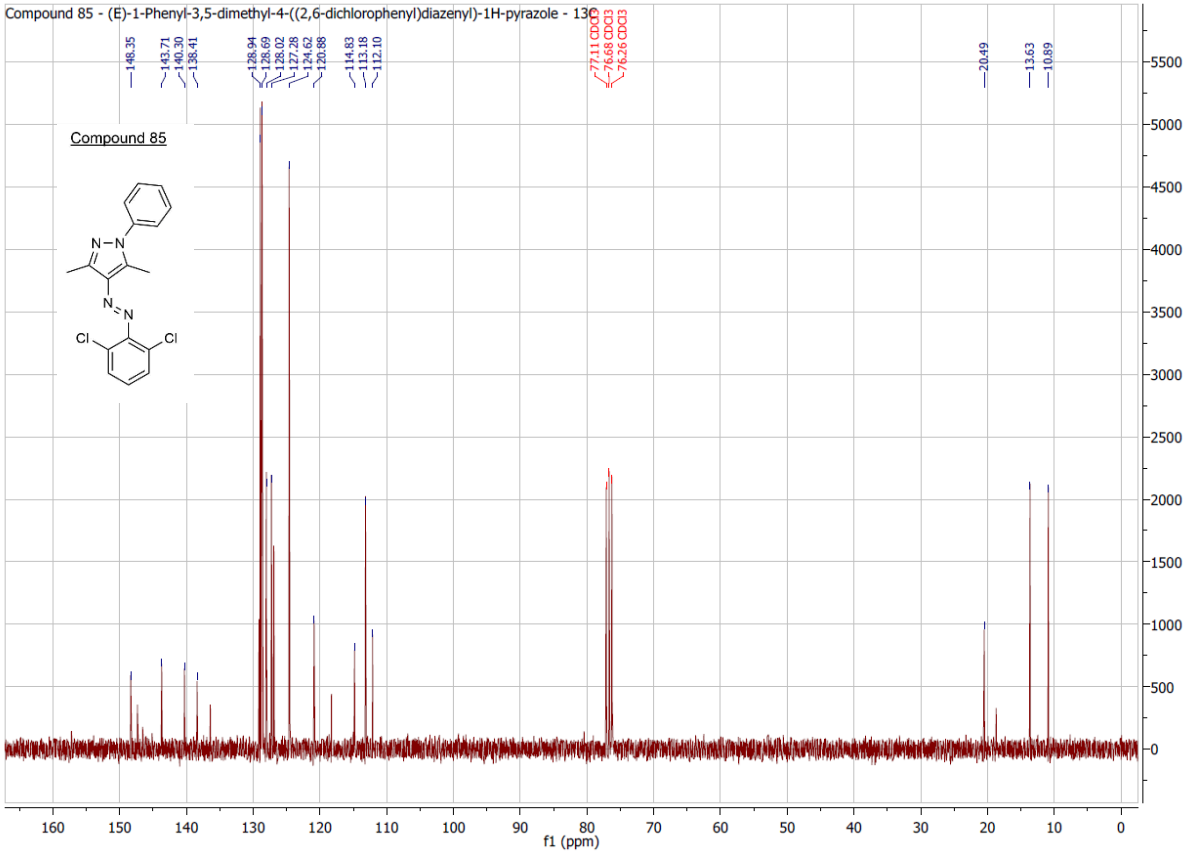
Compound 85 - (E)-1-Phenyl-3,5-dimethyl-4-((2,6-dichlorophenyl)diazenyl)-1H-pyrazole - 13C
Compound 85
f1 (ppm)

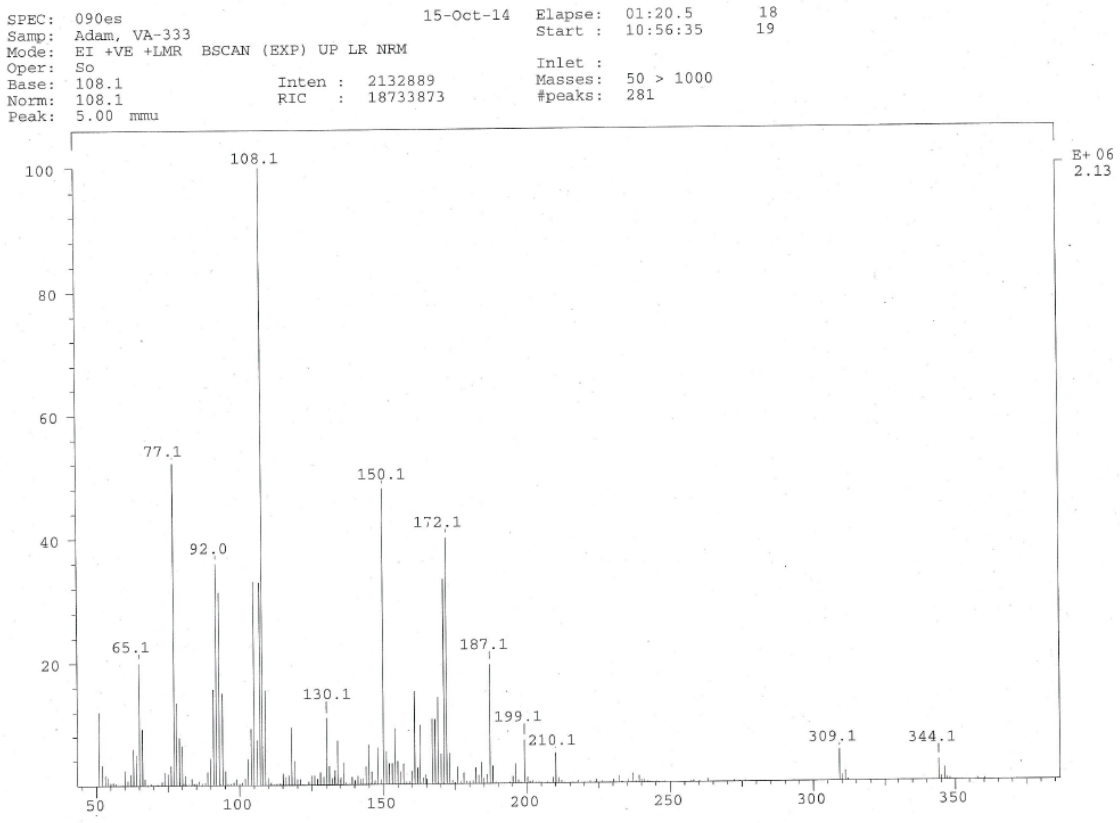
SPEC: 090es
Samp: Adam, VA-333
Mode: EI +VE +LMR BSCAN (EXP) UP LR NRM
Oper: So
Base: 108.1
Norm: 108.1
Peak: 5.00 mmu
15-Oct-14
Inten : 2132889
RIC : 18733873
Elapse: 01:20.5 18
Start : 10:56:35 19
Inlet :
Masses: 50 > 1000
#peaks: 281
E+06
2.13
108.1
77.1
150.1
172.1
92.0
65.1
187.1
130.1
199.1
210.1
309.1
344.1

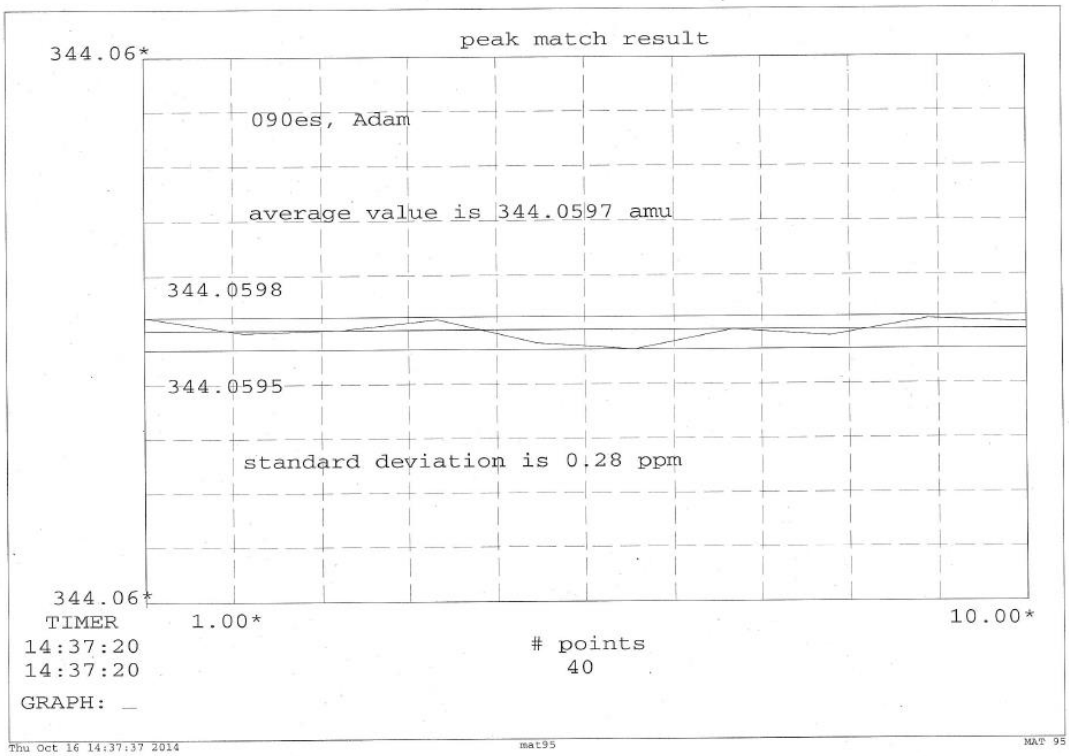
peak match result
344.06*
090es, Adam
average value is 344.0597 amu
344.0598
344.0595
standard deviation is 0.28 ppm
344.06*
TIMER
1.00*
10.00*
14:37:20
14:37:20
points
40
GRAPH:
Thu Oct 16 14:37:37 2014
mat95
MAT 95

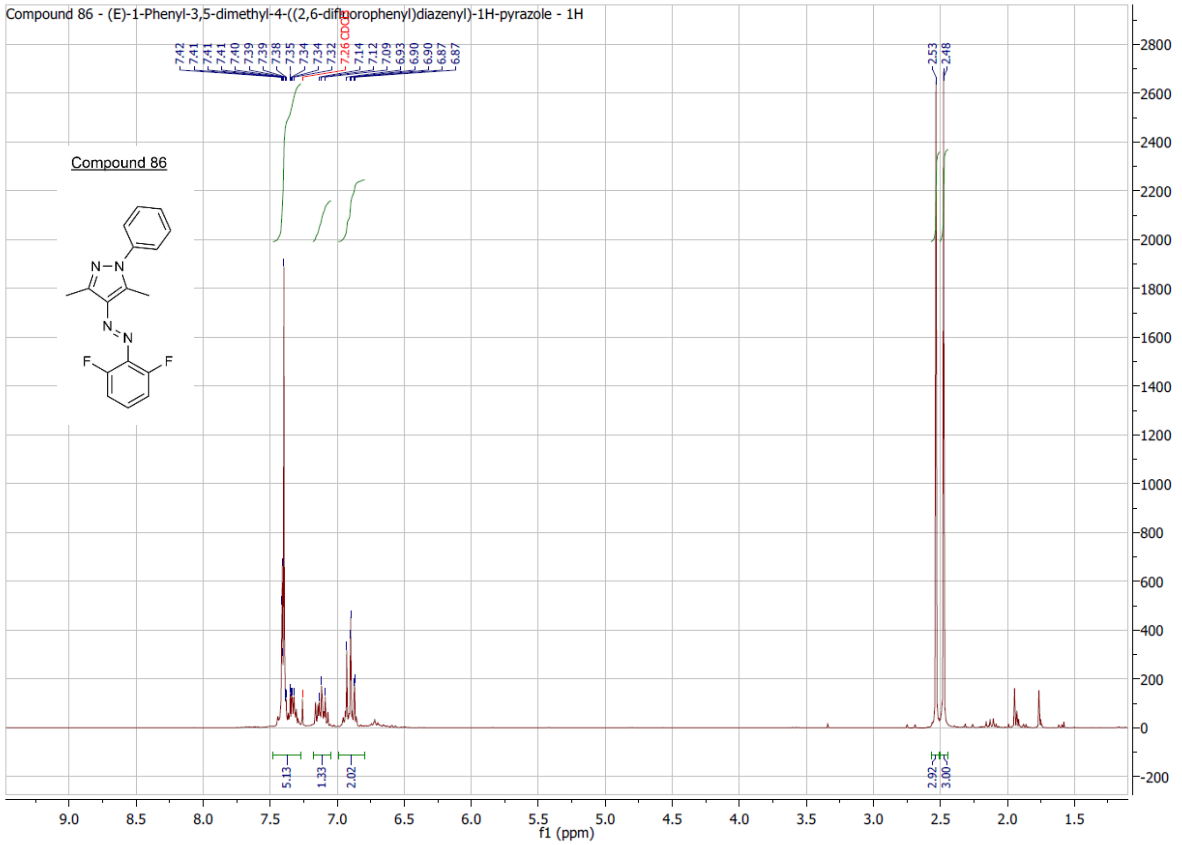
Compound 86 - (E)-1-Phenyl-3,5-dimethyl-4-((2,6-difluorophenyl)diazenyl)-1H-pyrazole - 1H
Compound 86
f1 (ppm)

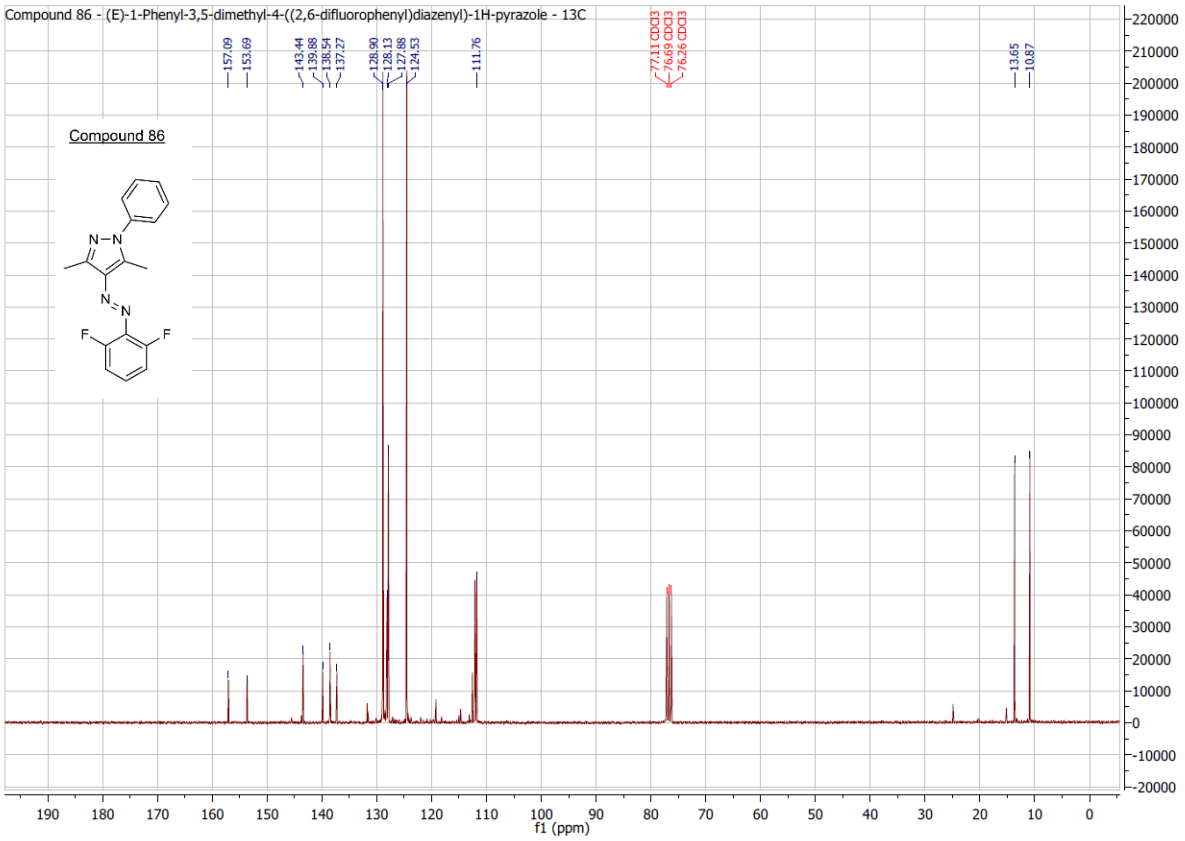
Compound 86 - (E)-1-Phenyl-3,5-dimethyl-4-((2,6-difluorophenyl)diazenyl)-1H-pyrazole - 13C
Compound 86
f1 (ppm)

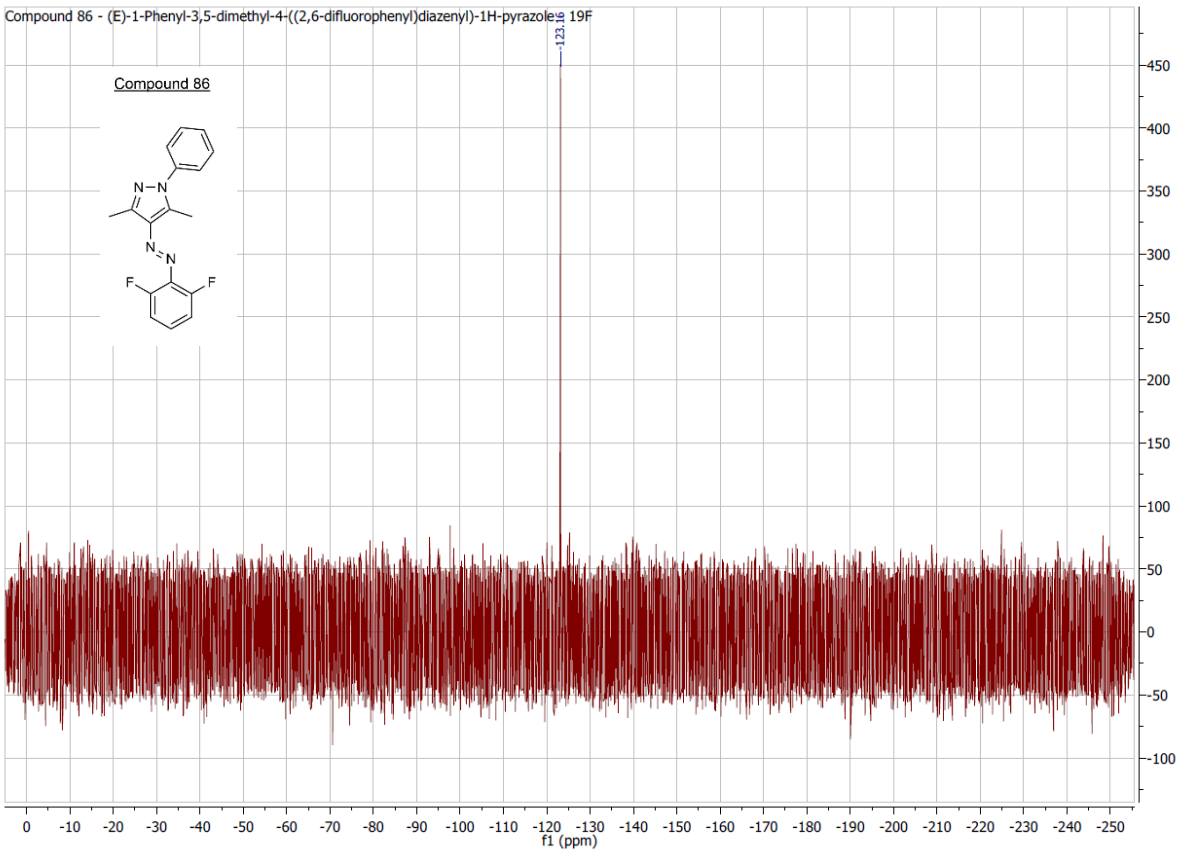

SPEC: 088es 14-Oct-14 Elapse: 01:39.2 22
Samp: Adam, VA-331 Start : 13:41:34 24
Mode: EI +VE +LMR BSCAN (EXP) UP LR NRM
Oper: So Inlet :
Base: 148.1 Inten : 1168752 Masses: 50 > 1000
Norm: 148.1 RIC : 16830411 #peaks: 276
Peak: 5.00 mmu

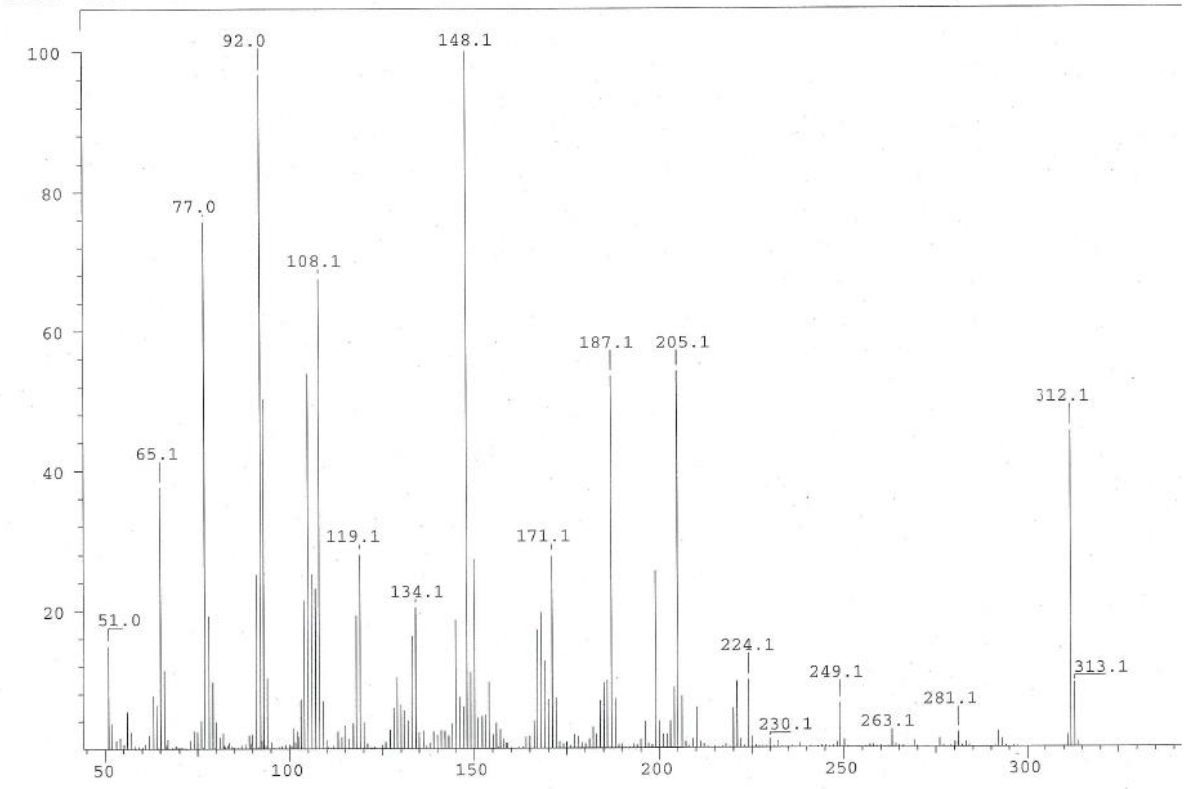

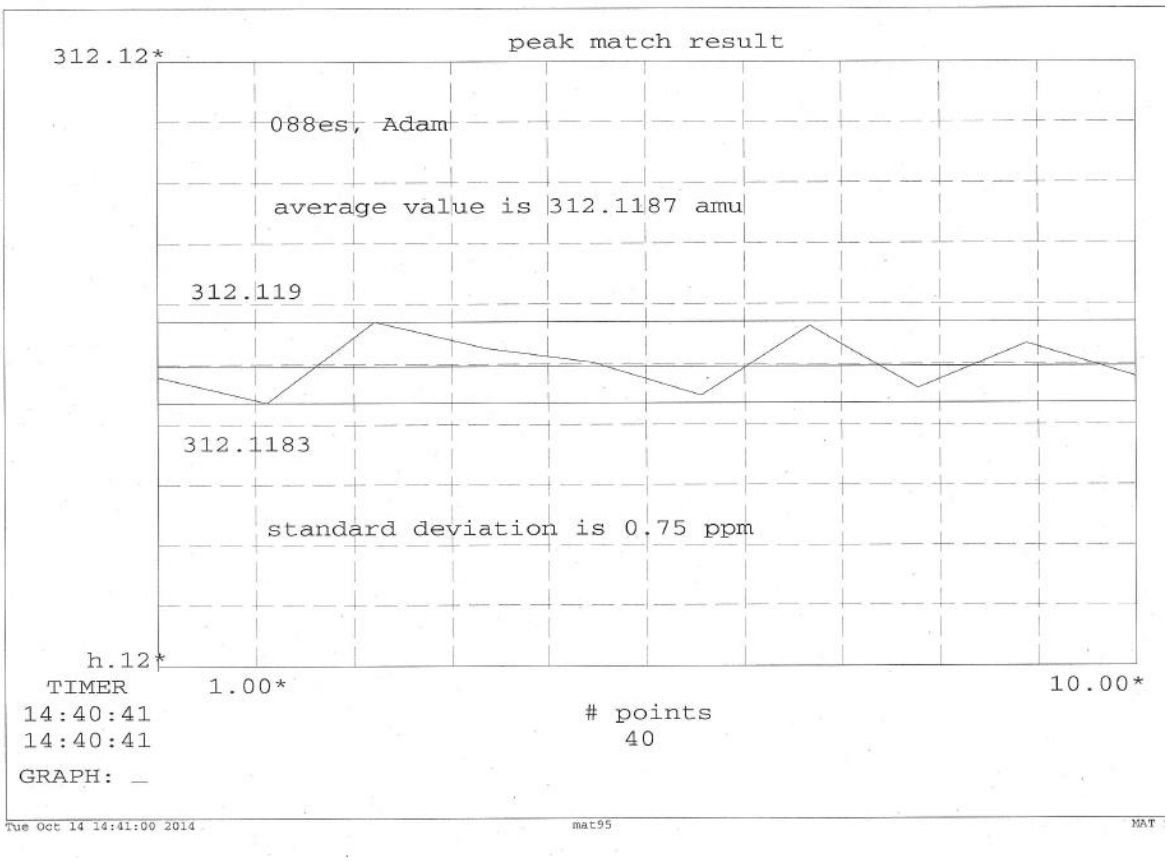
peak match result
312.12*
088es, Adam
average value is 312.1187 amu
312.119
312.1183
standard deviation is 0.75 ppm
h.12*
TIMER
1.00*
10.00*
14:40:41
14:40:41
points
40
GRAPH: _
Tue Oct 14 14:41:00 2014
mat95
MAT

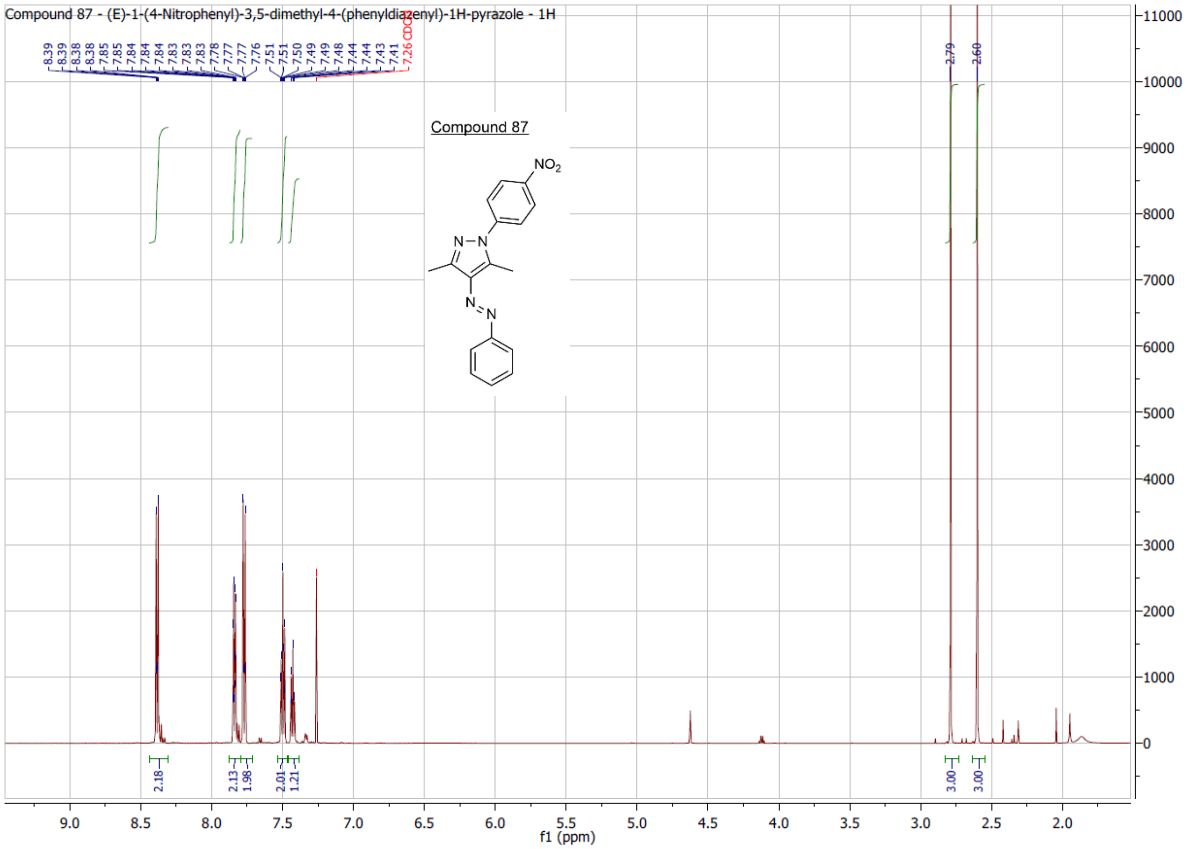
Compound 87 - (E)-1-(4-Nitrophenyl)-3,5-dimethyl-4-(phenyldiazenyl)-1H-pyrazole - 1H
Compound 87
f1 (ppm)

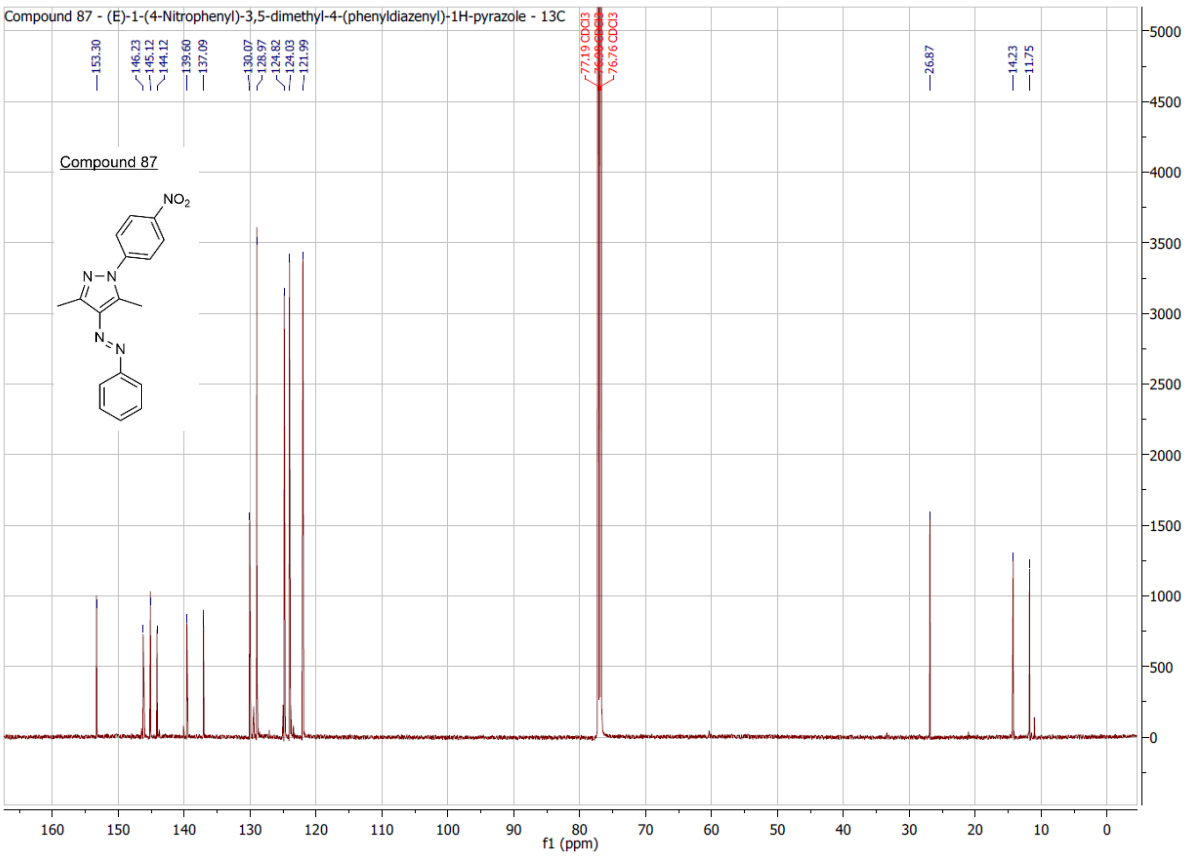
Compound 87 - (E)-1-(4-Nitrophenyl)-3,5-dimethyl-4-(phenyldiazenyl)-1H-pyrazole - 13C
Compound 87
f1 (ppm)

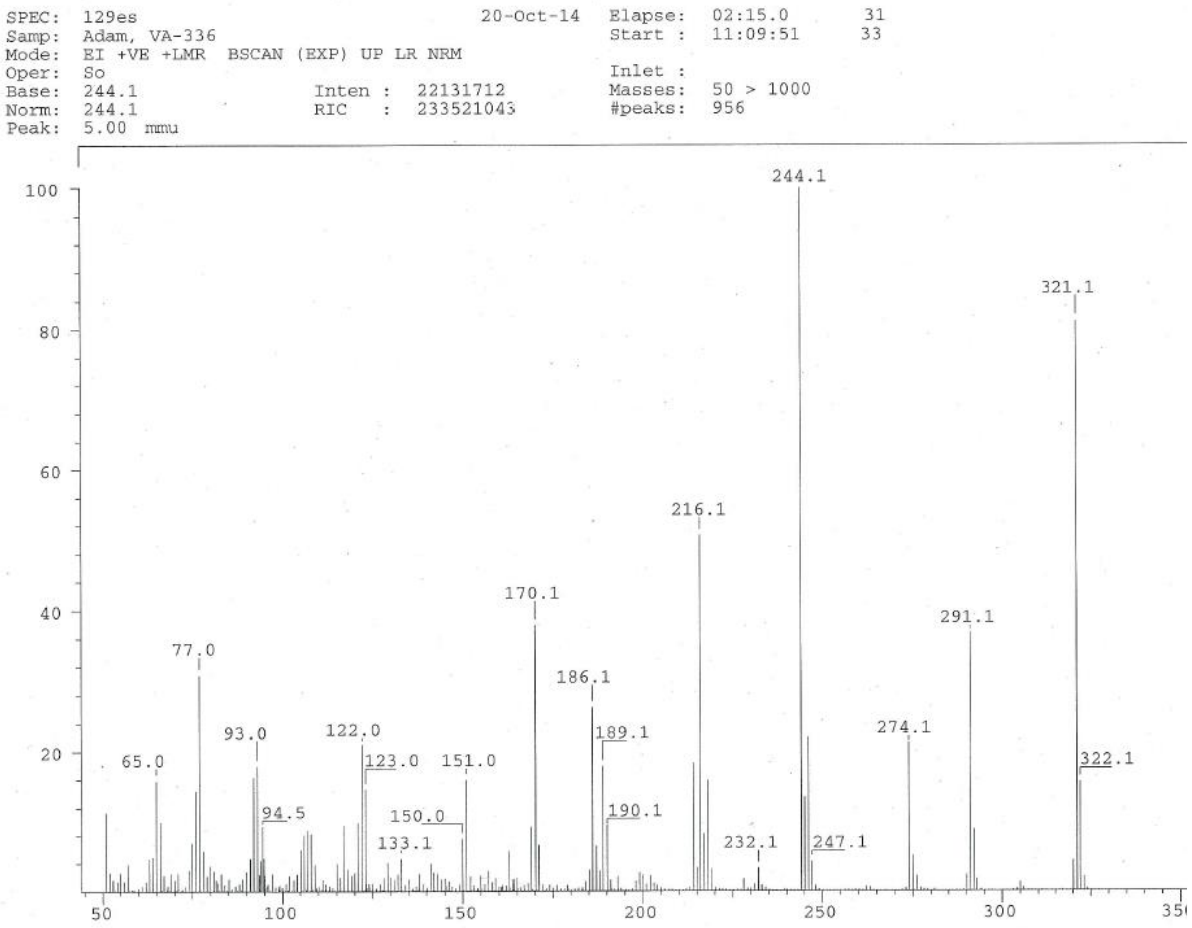
SPEC: 129es 20-Oct-14 Elapse: 02:15.0 31
Samp: Adam, VA-336 Start : 11:09:51 33
Mode: EI +VE +LMR BSCAN (EXP) UP LR NRM
Oper: So Inlet :
Base: 244.1 Inten : 22131712 Masses: 50 > 1000
Norm: 244.1 RIC : 233521043 #peaks: 956
Peak: 5.00 mmu
244.1
321.1
216.1
170.1
291.1
77.0
186.1
93.0
122.0
189.1
274.1
65.0
123.0
151.0
322.1
94.5
150.0
190.1
133.1
232.1
247.1

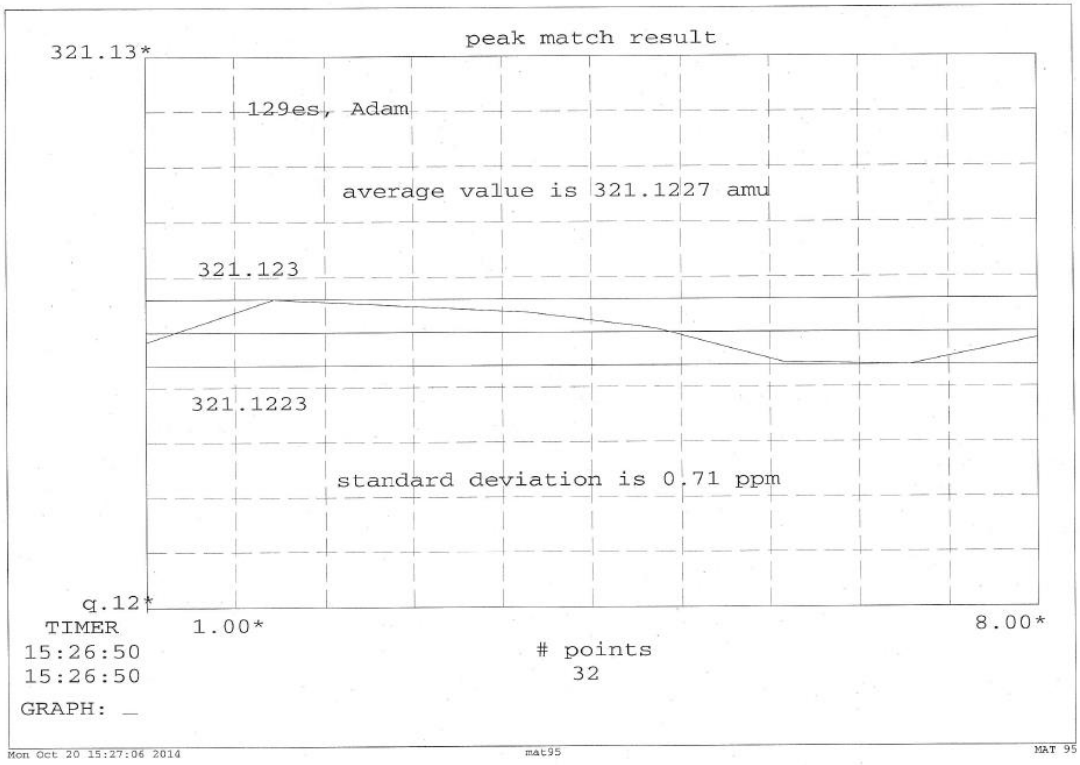
peak match result
321.13*
129es, Adam
average value is 321.1227 amu
321.123
321.1223
standard deviation is 0.71 ppm
q.12*
TIMER
1.00*
8.00*
15:26:50
15:26:50
points
32
GRAPH:
Mon Oct 20 15:27:06 2014
mat95
MAT 95

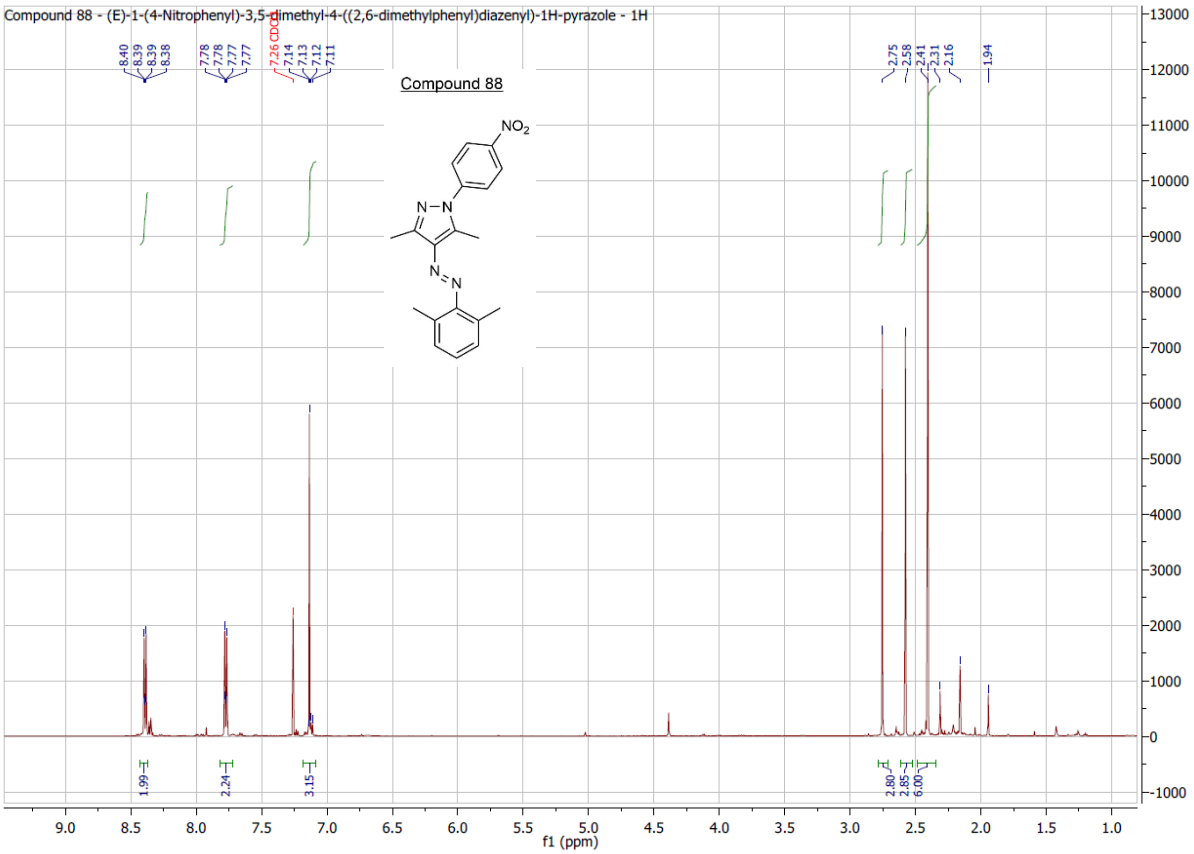
Compound 88 - (E)-1-(4-Nitrophenyl)-3,5-dimethyl-4-((2,6-dimethylphenyl)diazenyl)-1H-pyrazole - 1H
Compound 88
f1 (ppm)

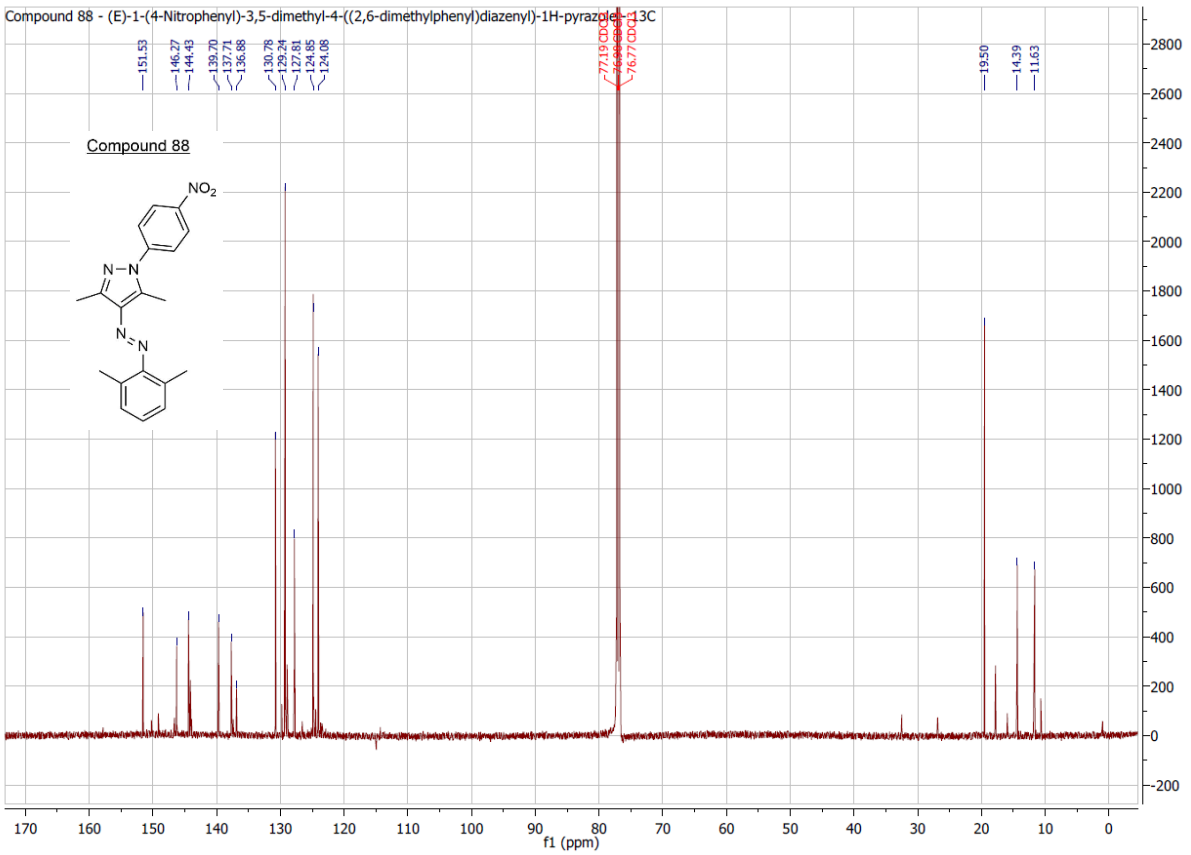
Compound 88 - (E)-1-(4-Nitrophenyl)-3,5-dimethyl-4-((2,6-dimethylphenyl)diazenyl)-1H-pyrazole - 13C
Compound 88
f1 (ppm)

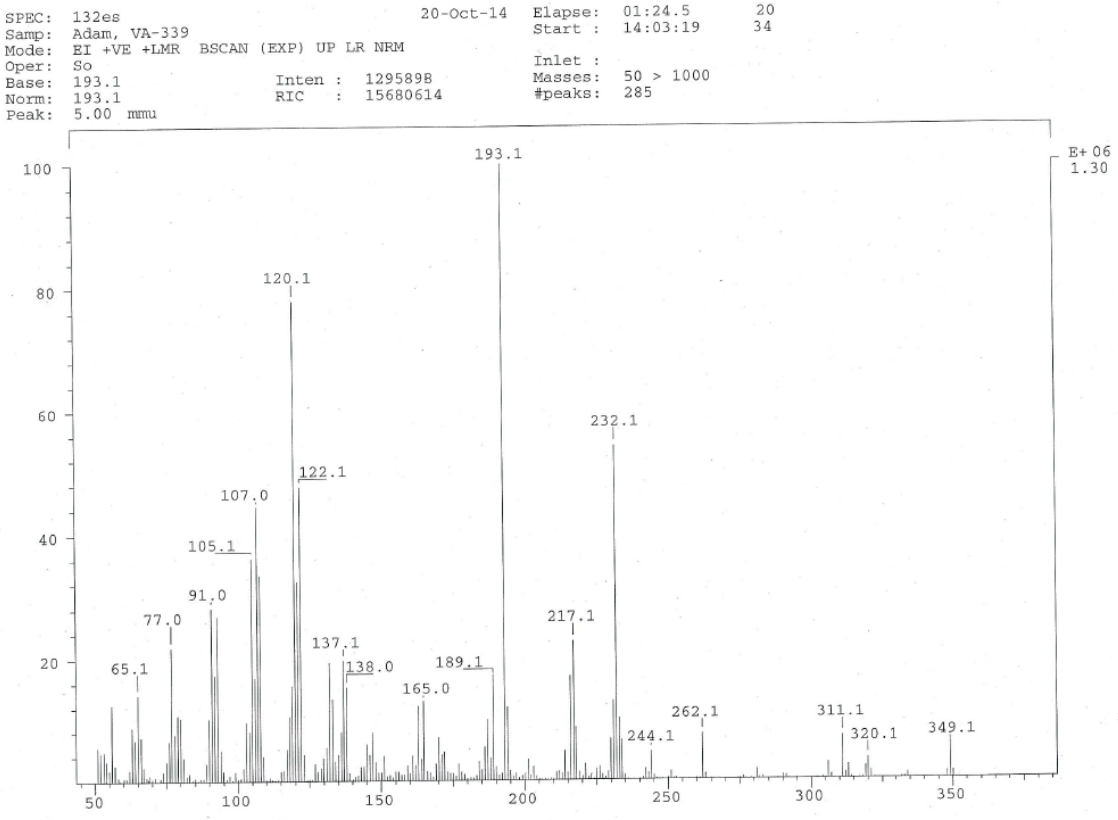
SPEC: 132es
Samp: Adam, VA-339
Mode: EI +VE +LMR BSCAN (EXP) UP LR NRM
Oper: So
Base: 193.1
Norm: 193.1
Peak: 5.00 mmu
20-Oct-14
Inten : 1295898
RIC : 15680614
Elapse: 01:24.5 20
Start : 14:03:19 34
Inlet :
Masses: 50 > 1000
#peaks: 285
E+06
1.30
193.1
120.1
232.1
122.1
107.0
105.1
91.0
77.0
65.1
137.1
138.0
189.1
165.0
217.1
262.1
244.1
311.1
320.1
349.1
100
80
60
40
20
50
100
150
200
250
300
350

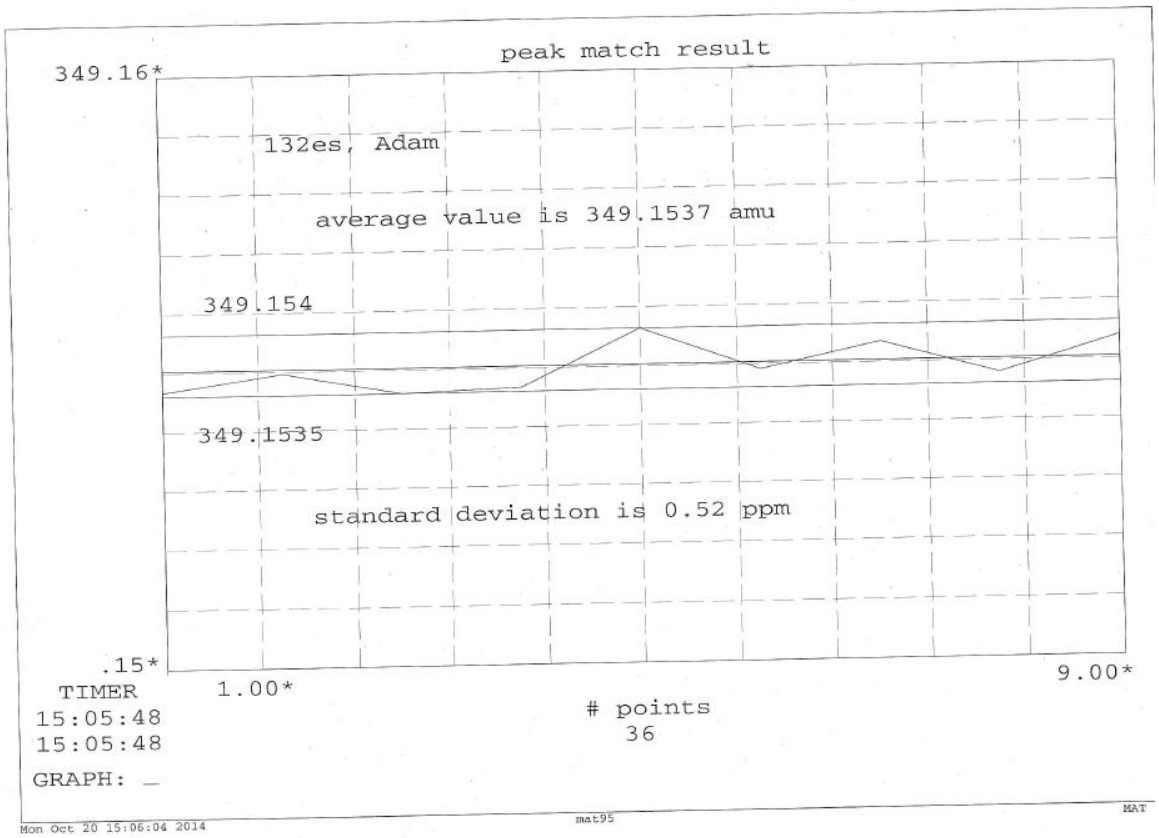
peak match result
349.16*
132es, Adam
average value is 349.1537 amu
349.154
349.1535
standard deviation is 0.52 ppm
.15*
1.00*
9.00*
TIMER
15:05:48
15:05:48
GRAPH:
points
36
Mon Oct 20 15:06:04 2014
mat95
MAT

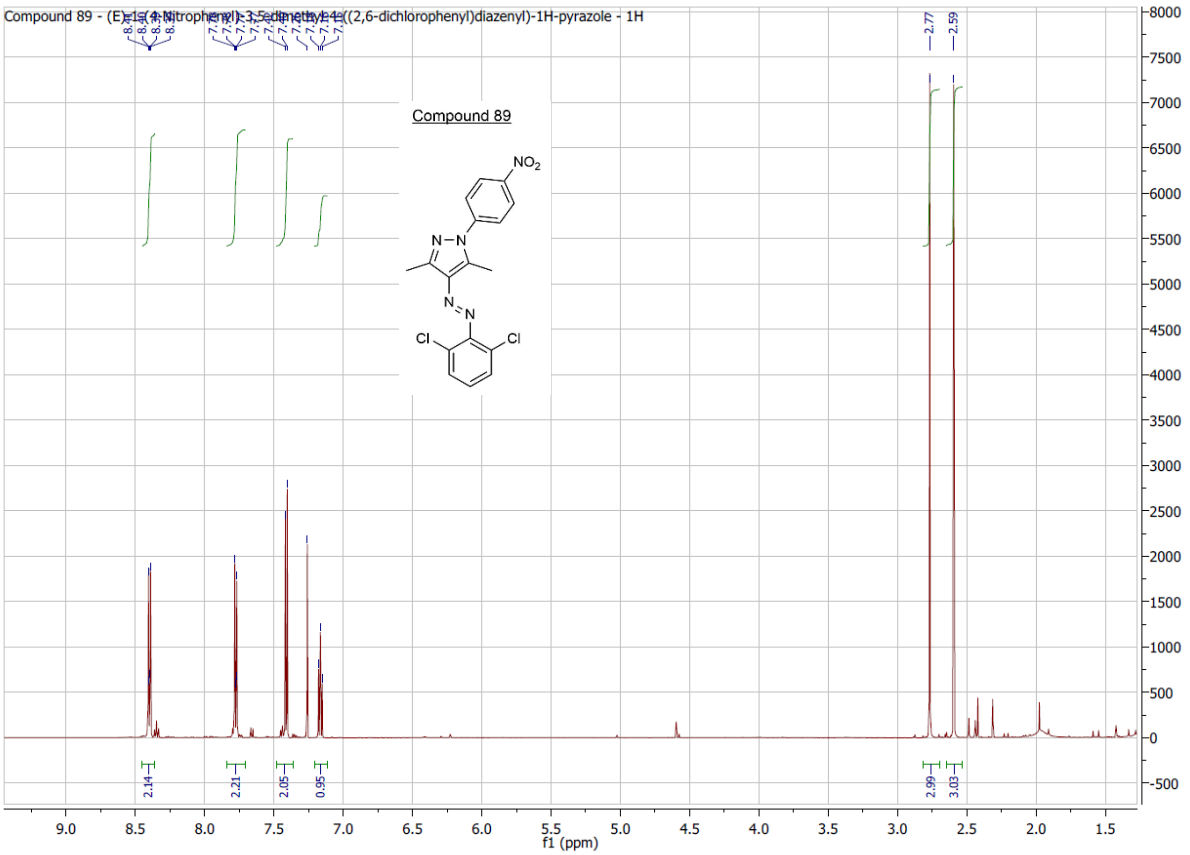
Compound 89 - (E)-1-(4-Nitrophenyl)-3,5-dimethyl-4-((2,6-dichlorophenyl)diazenyl)-1H-pyrazole - 1H
Compound 89
NO2
N–N
N=N
Cl
Cl
2.77
2.59
2.14
2.21
2.05
0.95
2.99
3.03
f1 (ppm)

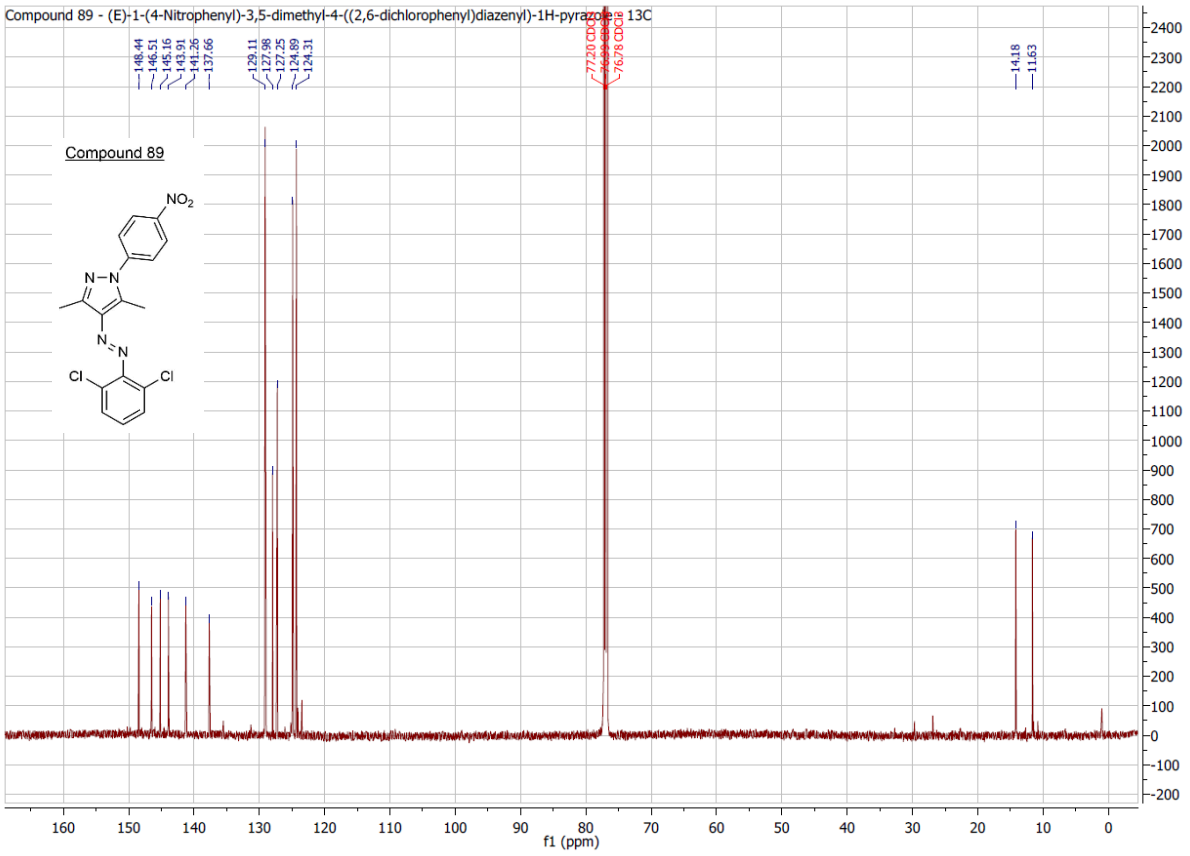
Compound 89 - (E)-1-(4-Nitrophenyl)-3,5-dimethyl-4-((2,6-dichlorophenyl)diazenyl)-1H-pyrazole - 13C
148.44
146.51
145.16
143.91
141.26
137.66
129.11
127.98
127.25
124.89
124.31
77.20 CDCl3
76.78 CDCl3
14.18
11.63
Compound 89
NO2
N–N
N=N
Cl
Cl
f1 (ppm)

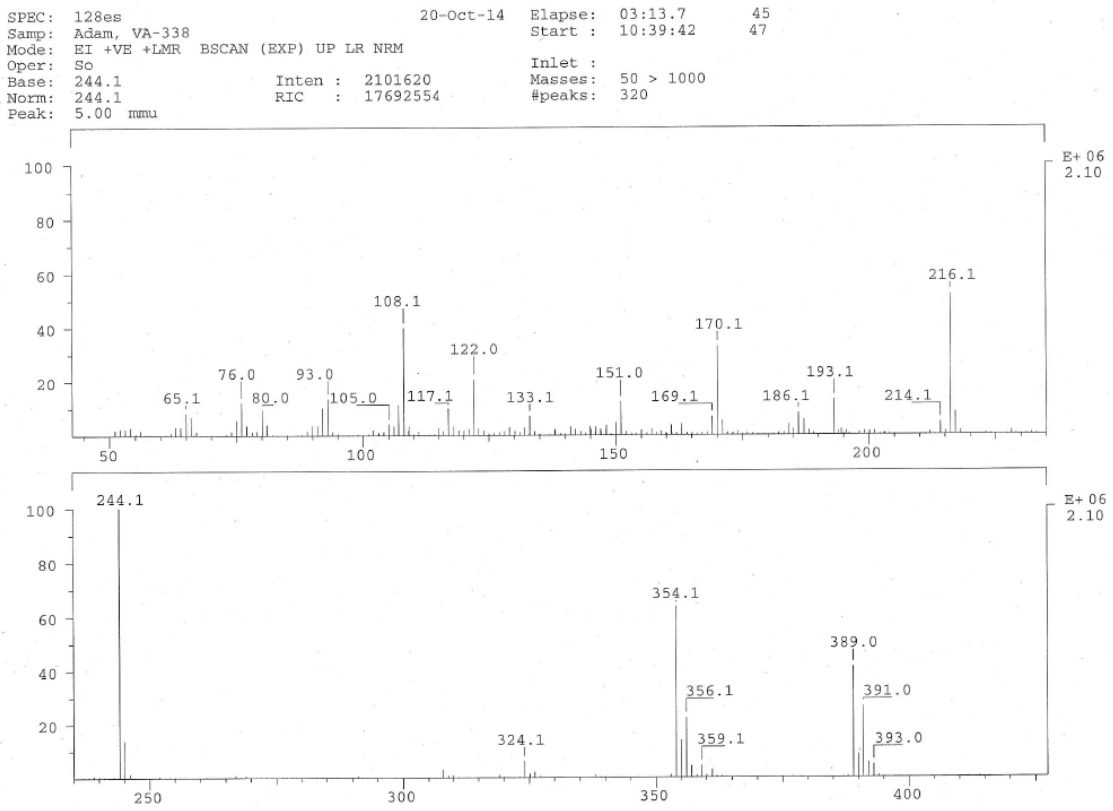
SPEC: 128es
Samp: Adam, VA-338
Mode: EI +VE +LMR BSCAN (EXP) UP LR NRM
Oper: So
Base: 244.1
Norm: 244.1
Peak: 5.00 mmu
Inten : 2101620
RIC : 17692554
20-Oct-14
Elapse: 03:13.7 45
Start : 10:39:42 47
Inlet :
Masses: 50 > 1000
#peaks: 320
E+06
2.10
216.1
108.1
170.1
122.0
76.0
93.0
151.0
193.1
65.1
80.0
105.0
117.1
133.1
169.1
186.1
214.1
244.1
354.1
389.0
356.1
391.0
324.1
359.1
393.0

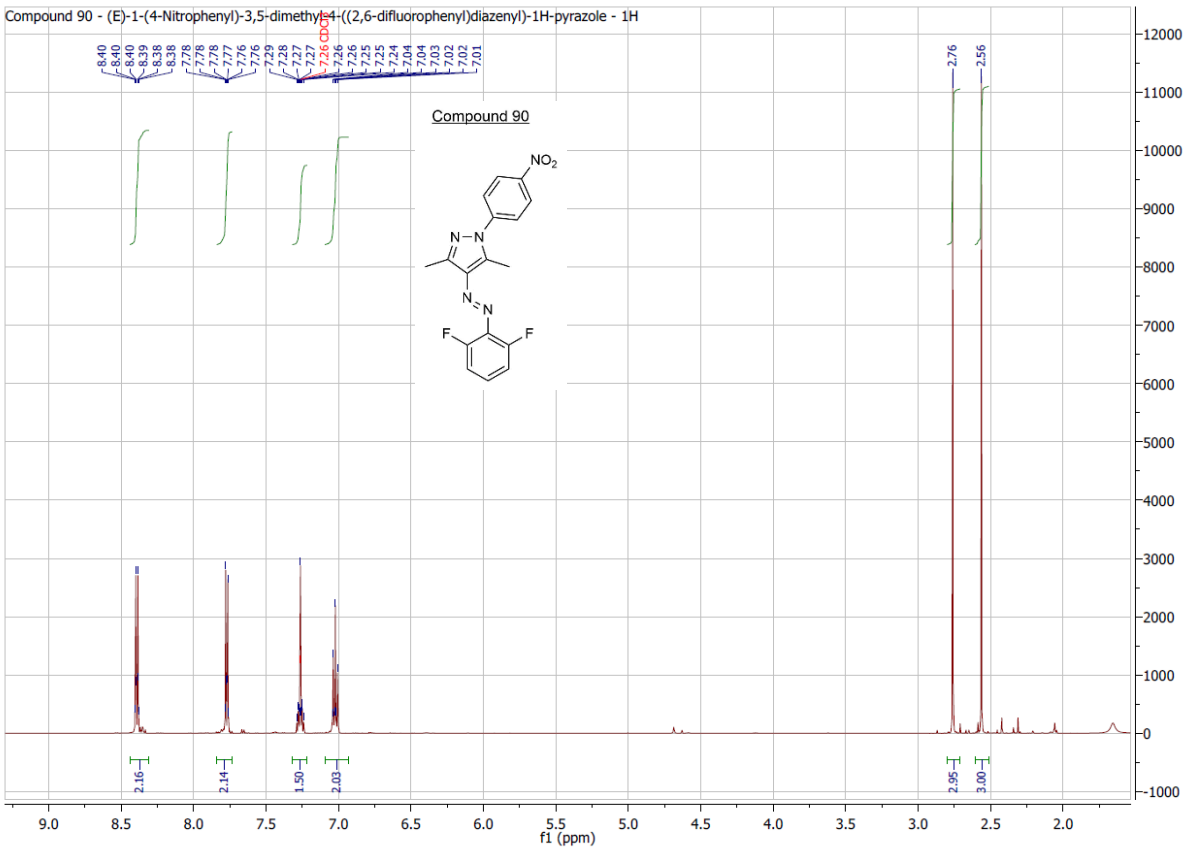
Compound 90 - (E)-1-(4-Nitrophenyl)-3,5-dimethyl-4-((2,6-difluorophenyl)diazenyl)-1H-pyrazole - 1H
Compound 90
f1 (ppm)

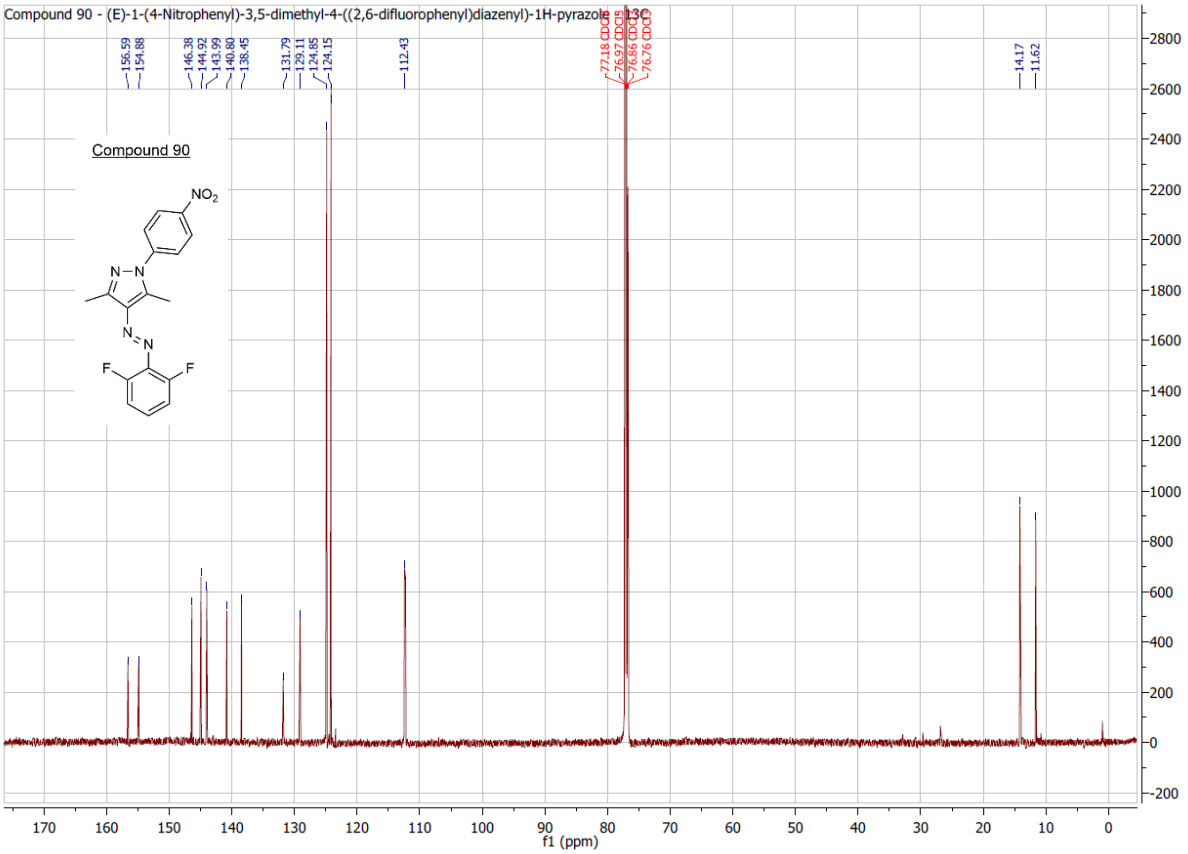
Compound 90 - (E)-1-(4-Nitrophenyl)-3,5-dimethyl-4-((2,6-difluorophenyl)diazenyl)-1H-pyrazole - 13C
Compound 90
f1 (ppm)

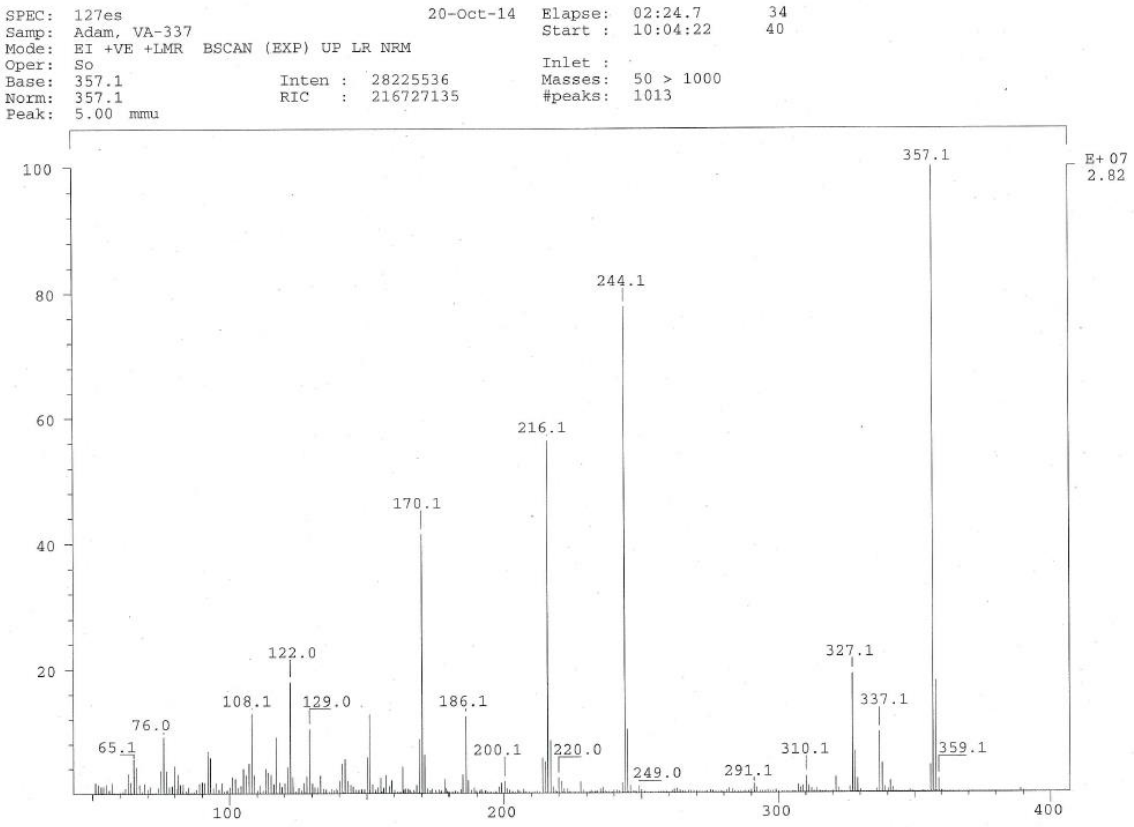
SPEC: 127es
Samp: Adam, VA-337
Mode: EI +VE +LMR BSCAN (EXP) UP LR NRM
Oper: So
Base: 357.1
Norm: 357.1
Peak: 5.00 mmu
20-Oct-14
Inten : 28225536
RIC : 216727135
Elapse: 02:24.7
Start : 10:04:22
Inlet :
Masses: 50 > 1000
#peaks: 1013
34
40
E+07
2.82
357.1
244.1
216.1
170.1
122.0
108.1
129.0
186.1
76.0
65.1
200.1
220.0
249.0
291.1
310.1
327.1
337.1
359.1
100
80
60
40
20
100
200
300
400

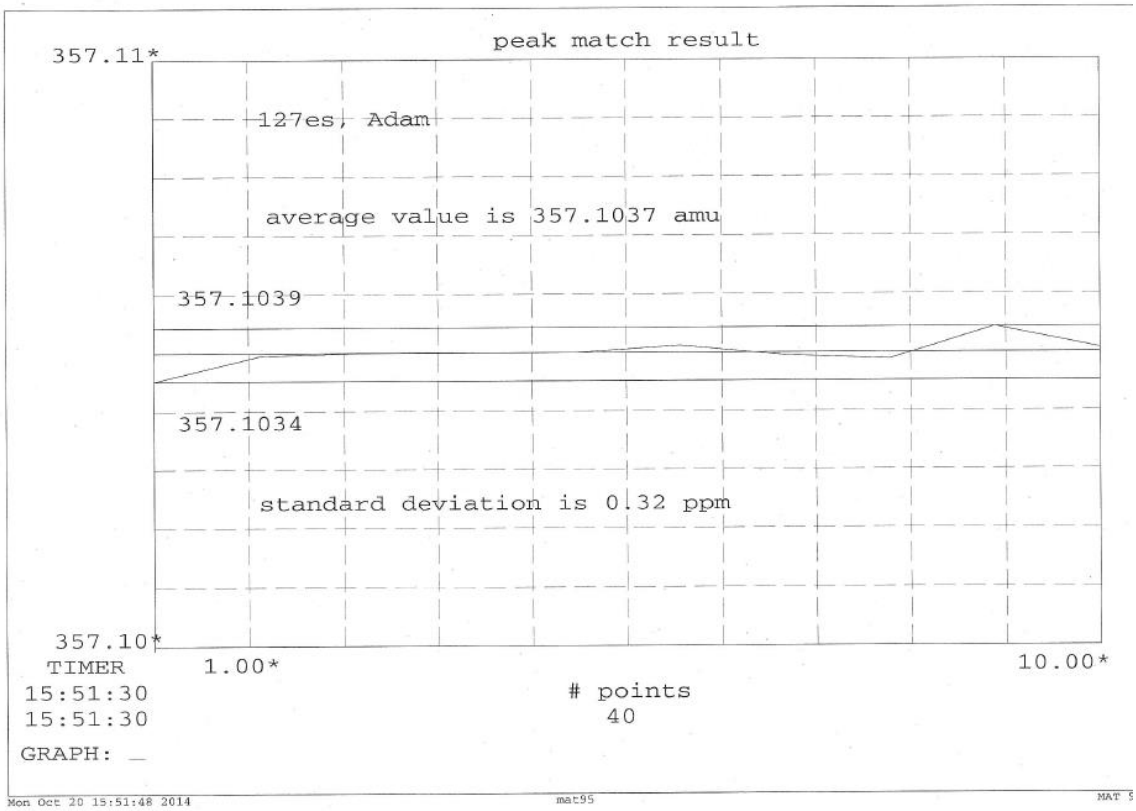
peak match result
357.11*
127es, Adam
average value is 357.1037 amu
357.1039
357.1034
standard deviation is 0.32 ppm
357.10*
TIMER
1.00*
10.00*
15:51:30
15:51:30
points
40
GRAPH: _
Mon Oct 20 15:51:48 2014
mat95
MAT

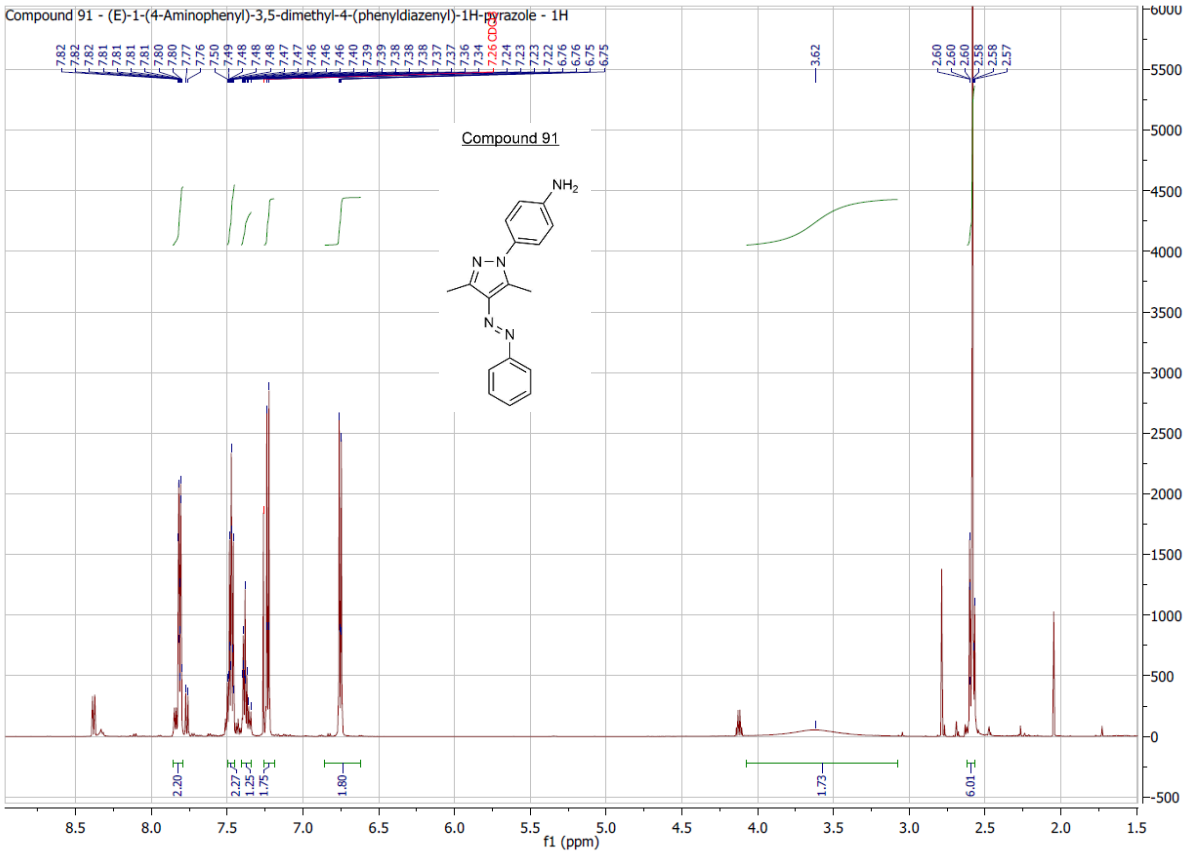
Compound 91 - (E)-1-(4-Aminophenyl)-3,5-dimethyl-4-(phenyldiazenyl)-1H-pyrazole - 1H
Compound 91
f1 (ppm)

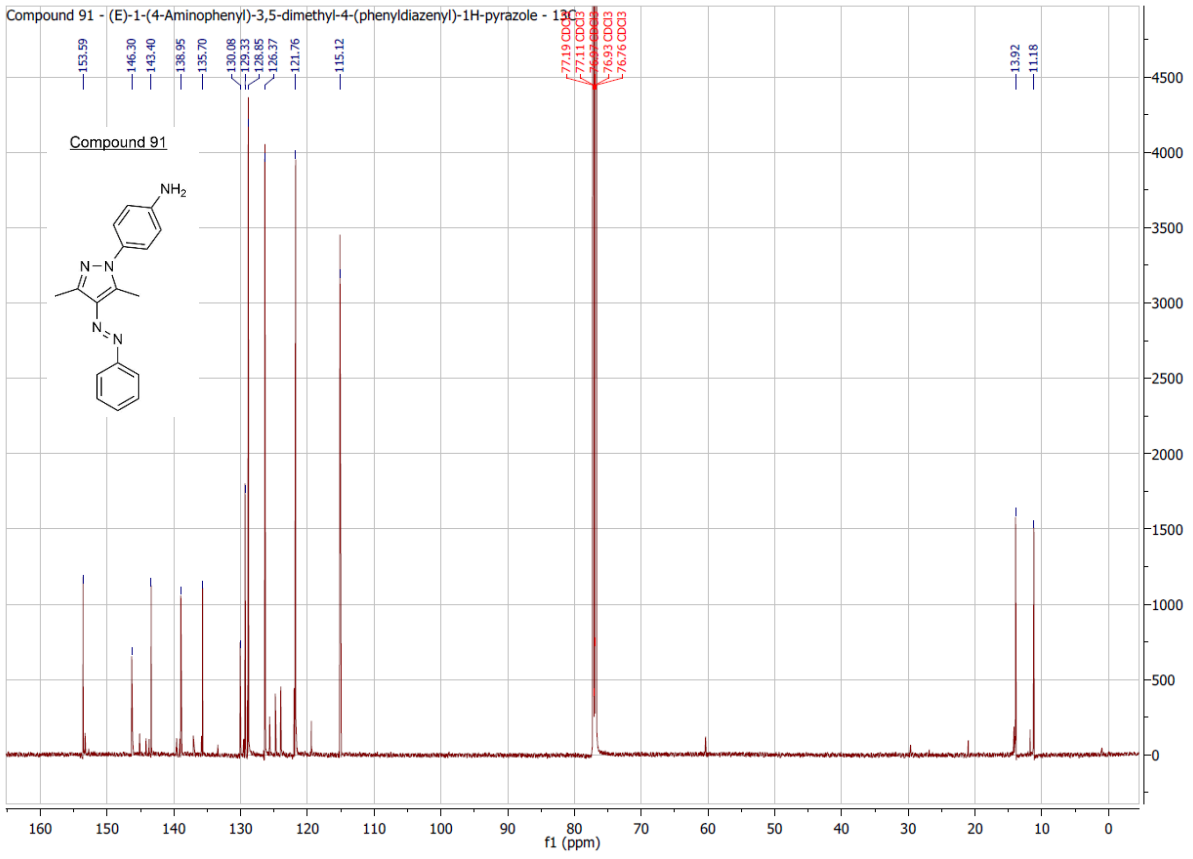
Compound 91 - (E)-1-(4-Aminophenyl)-3,5-dimethyl-4-(phenyldiazenyl)-1H-pyrazole - 13C
Compound 91
f1 (ppm)

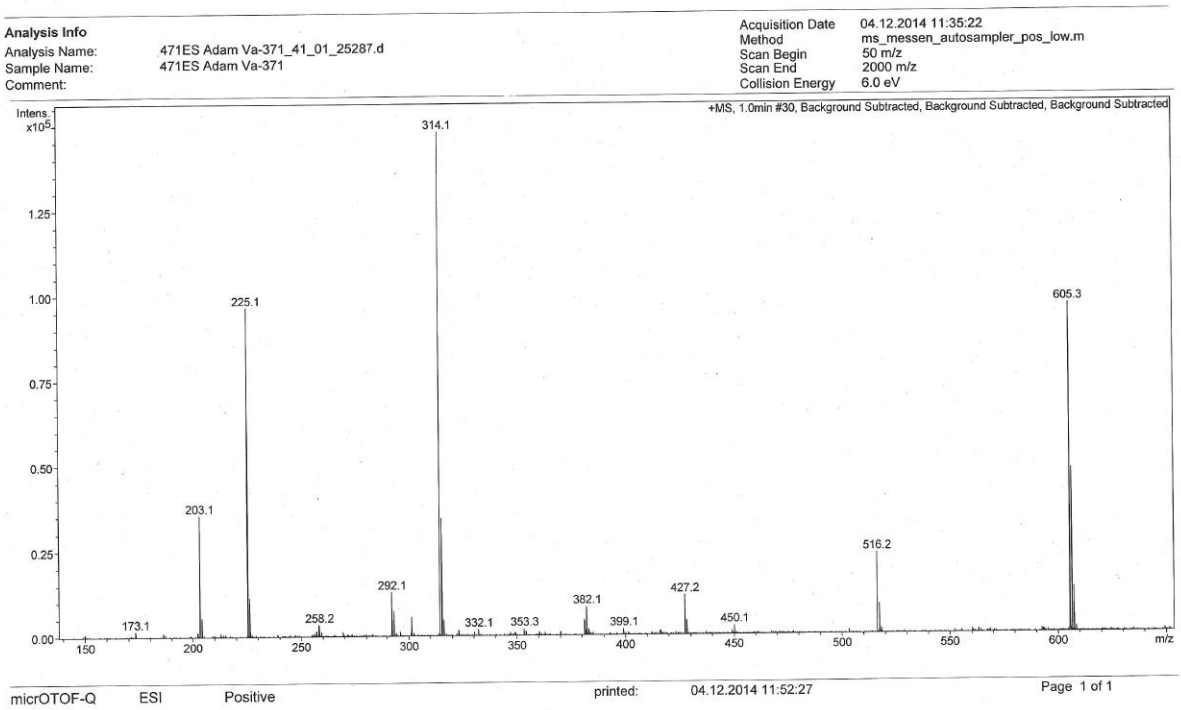
Analysis Info
Analysis Name: 471ES Adam Va-371_41_01_25287.d
Sample Name: 471ES Adam Va-371
Comment:
Acquisition Date 04.12.2014 11:35:22
Method ms_messen_autosampler_pos_low.m
Scan Begin 50 m/z
Scan End 2000 m/z
Collision Energy 6.0 eV
+MS, 1.0min #30, Background Subtracted, Background Subtracted, Background Subtracted
Intens.
x10^5
314.1
225.1
605.3
203.1
516.2
292.1
382.1
427.2
173.1
258.2
332.1
353.3
399.1
450.1
m/z
micrOTOF-Q ESI Positive
printed: 04.12.2014 11:52:27
Page 1 of 1

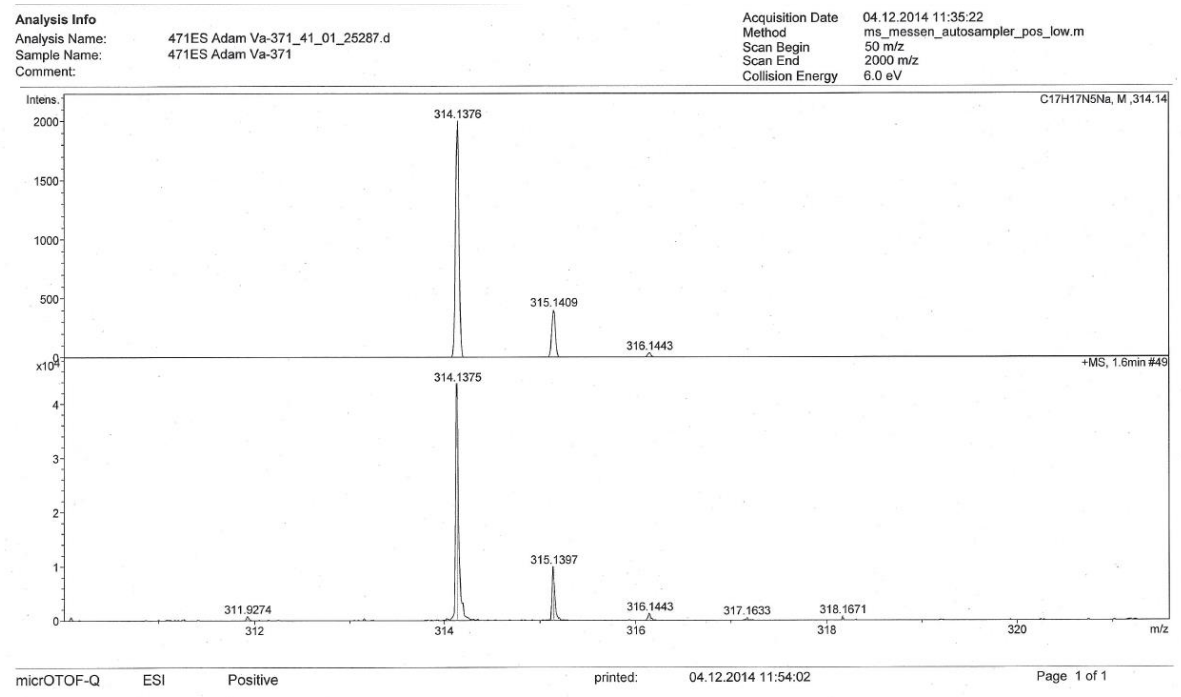
Analysis Info
Analysis Name: 471ES Adam Va-371_41_01_25287.d
Sample Name: 471ES Adam Va-371
Comment:
Acquisition Date 04.12.2014 11:35:22
Method ms_messen_autosampler_pos_low.m
Scan Begin 50 m/z
Scan End 2000 m/z
Collision Energy 6.0 eV
Intens.
C17H17N5Na, M ,314.14
314.1376
315.1409
316.1443
x10^4
+MS, 1.6min #49
314.1375
315.1397
311.9274
316.1443
317.1633
318.1671
m/z
micrOTOF-Q ESI Positive
printed: 04.12.2014 11:54:02
Page 1 of 1

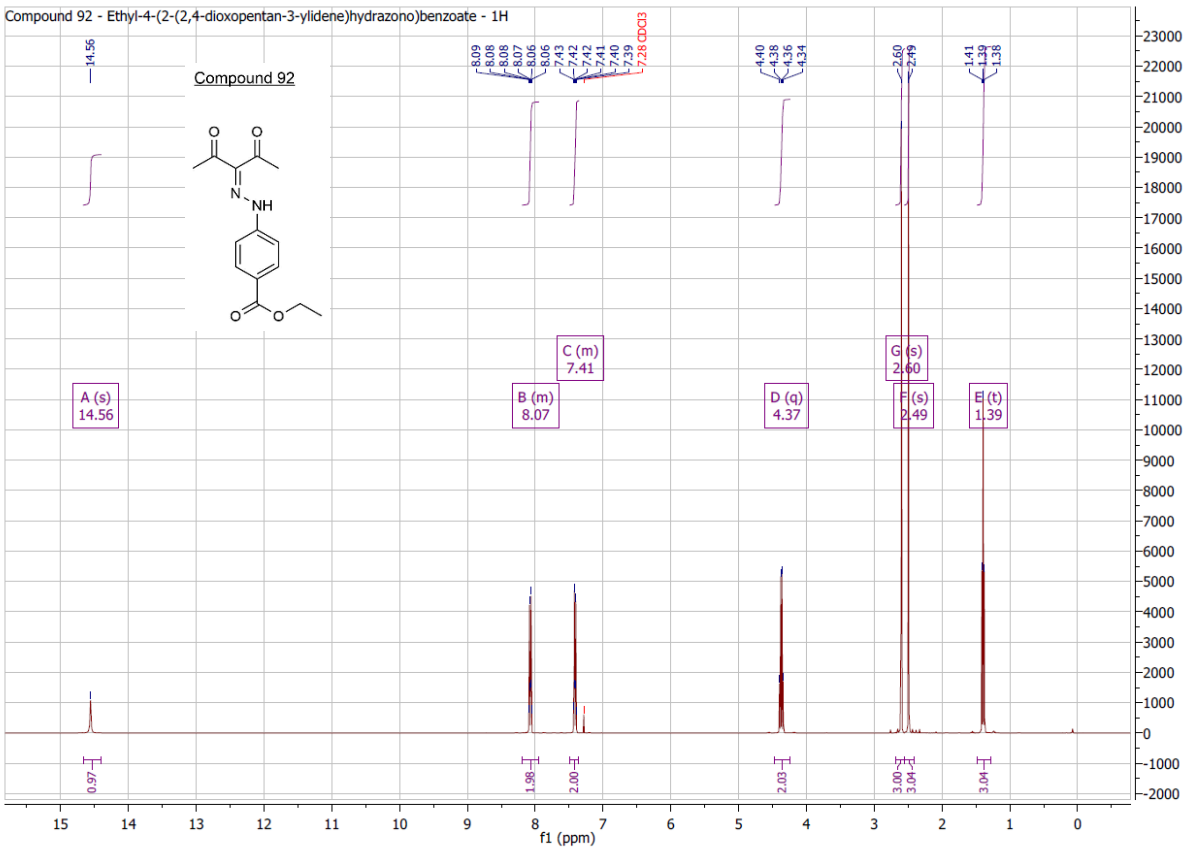
Compound 92 - Ethyl-4-(2-(2,4-dioxopentan-3-ylidene)hydrazono)benzoate - 1H
Compound 92
A (s)
14.56
B (m)
8.07
C (m)
7.41
D (q)
4.37
E (t)
1.39
F (s)
2.49
G (s)
2.60
f1 (ppm)

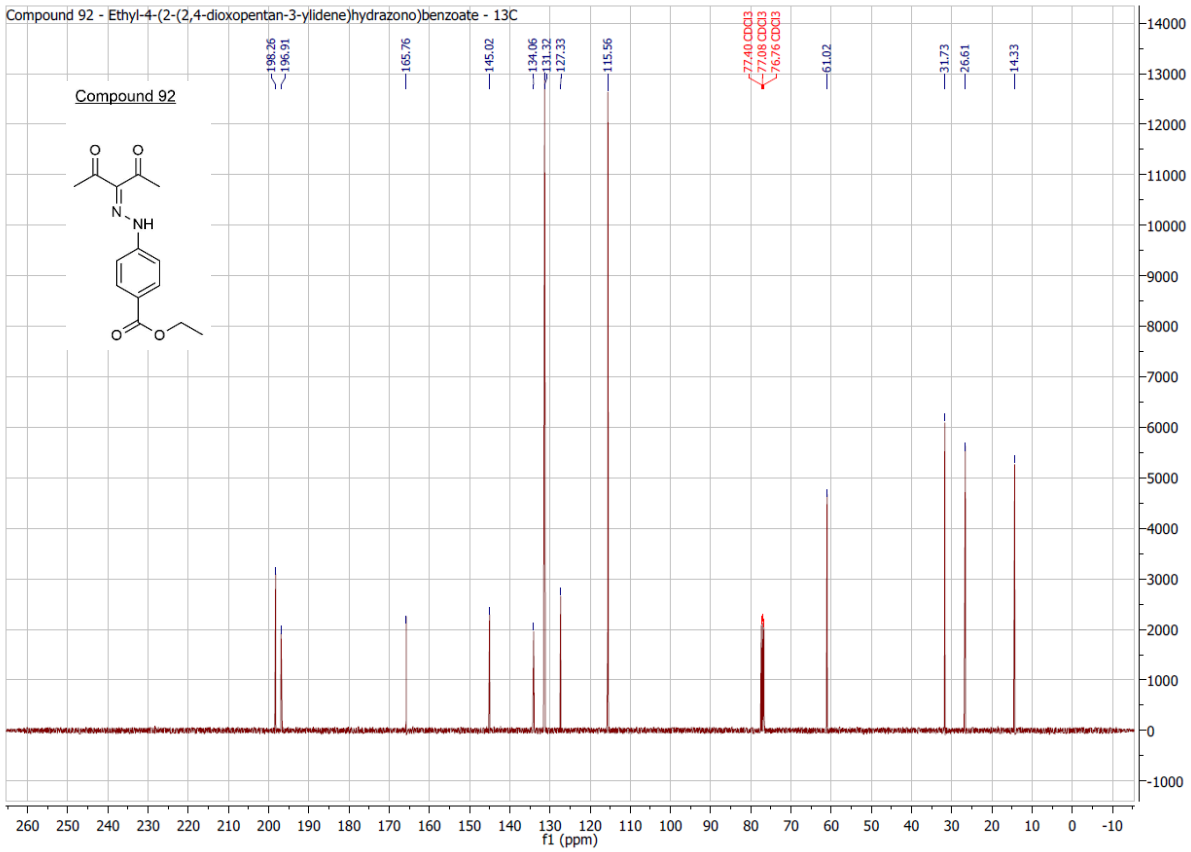
Compound 92 - Ethyl-4-(2-(2,4-dioxopentan-3-ylidene)hydrazono)benzoate - 13C
Compound 92
198.26
196.91
165.76
145.02
134.06
131.32
127.33
115.56
77.40 CDCl3
77.08 CDCl3
76.76 CDCl3
61.02
31.73
26.61
14.33
f1 (ppm)

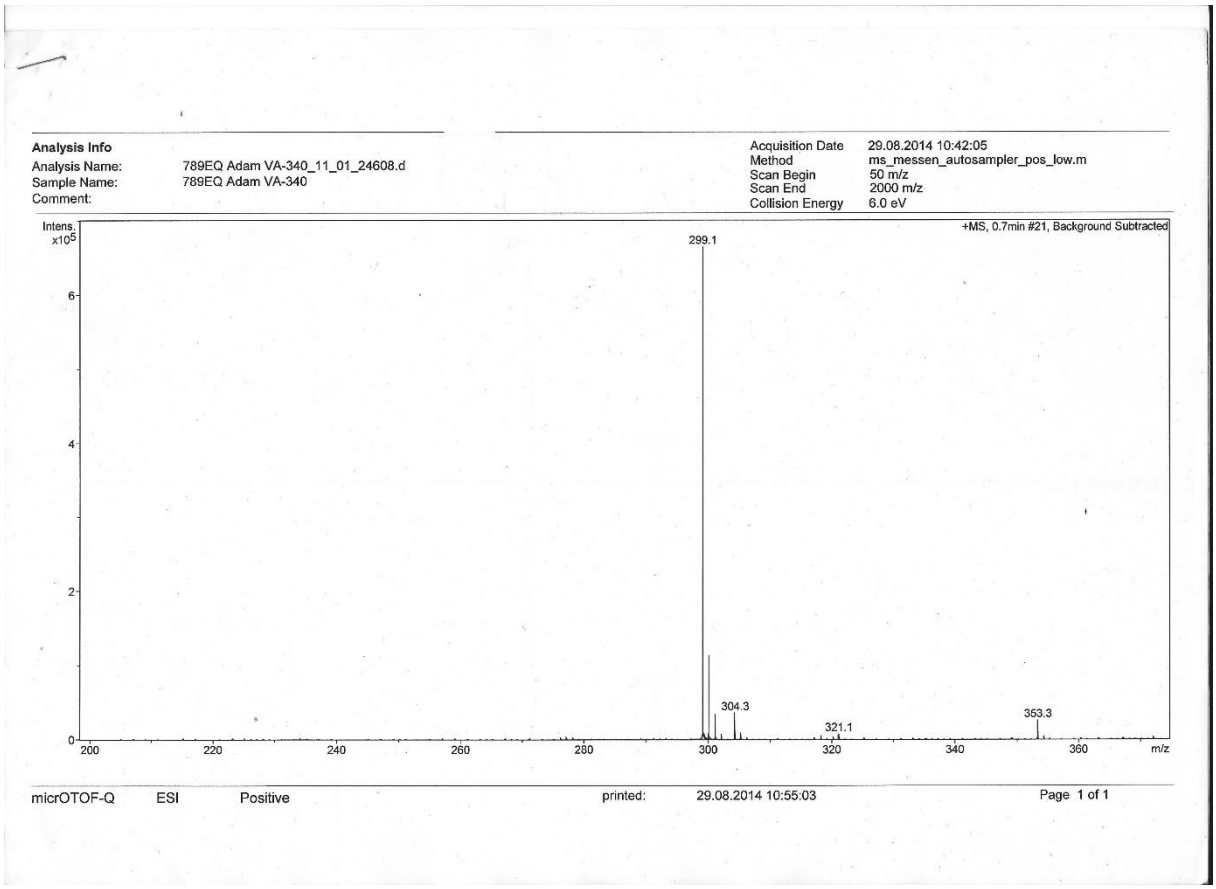
Analysis Info
Analysis Name: 789EQ Adam VA-340_11_01_24608.d
Sample Name: 789EQ Adam VA-340
Comment:
Acquisition Date 29.08.2014 10:42:05
Method ms_messen_autosampler_pos_low.m
Scan Begin 50 m/z
Scan End 2000 m/z
Collision Energy 6.0 eV
Intens.
x10^5
+MS, 0.7min #21, Background Subtracted
299.1
304.3
321.1
353.3
m/z
micrOTOF-Q ESI Positive
printed: 29.08.2014 10:55:03
Page 1 of 1

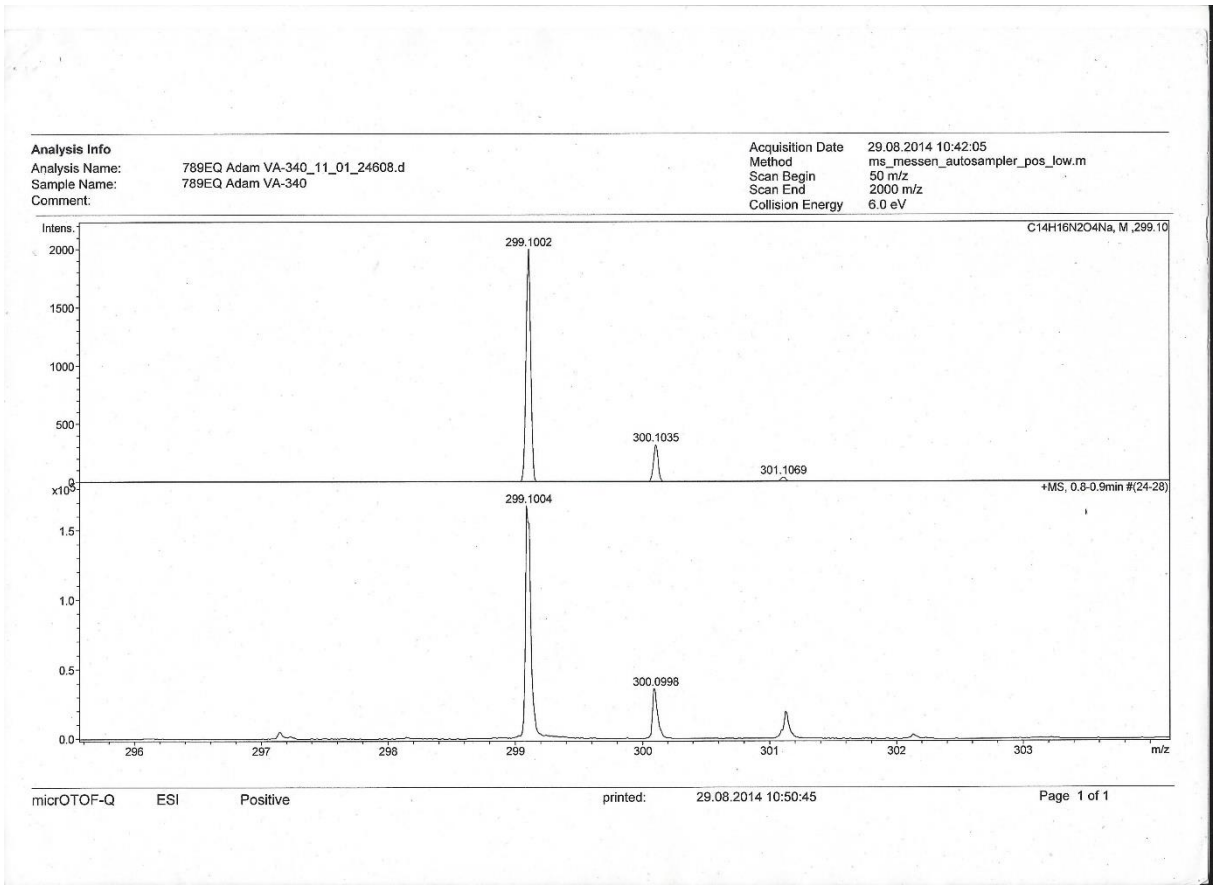
Analysis Info
Analysis Name: 789EQ Adam VA-340_11_01_24608.d
Sample Name: 789EQ Adam VA-340
Comment:
Acquisition Date 29.08.2014 10:42:05
Method ms_messen_autosampler_pos_low.m
Scan Begin 50 m/z
Scan End 2000 m/z
Collision Energy 6.0 eV
Intens.
C14H16N2O4Na, M ,299.10
299.1002
300.1035
301.1069
x10^5
+MS, 0.8-0.9min #(24-28)
299.1004
300.0998
m/z
micrOTOF-Q ESI Positive
printed: 29.08.2014 10:50:45
Page 1 of 1

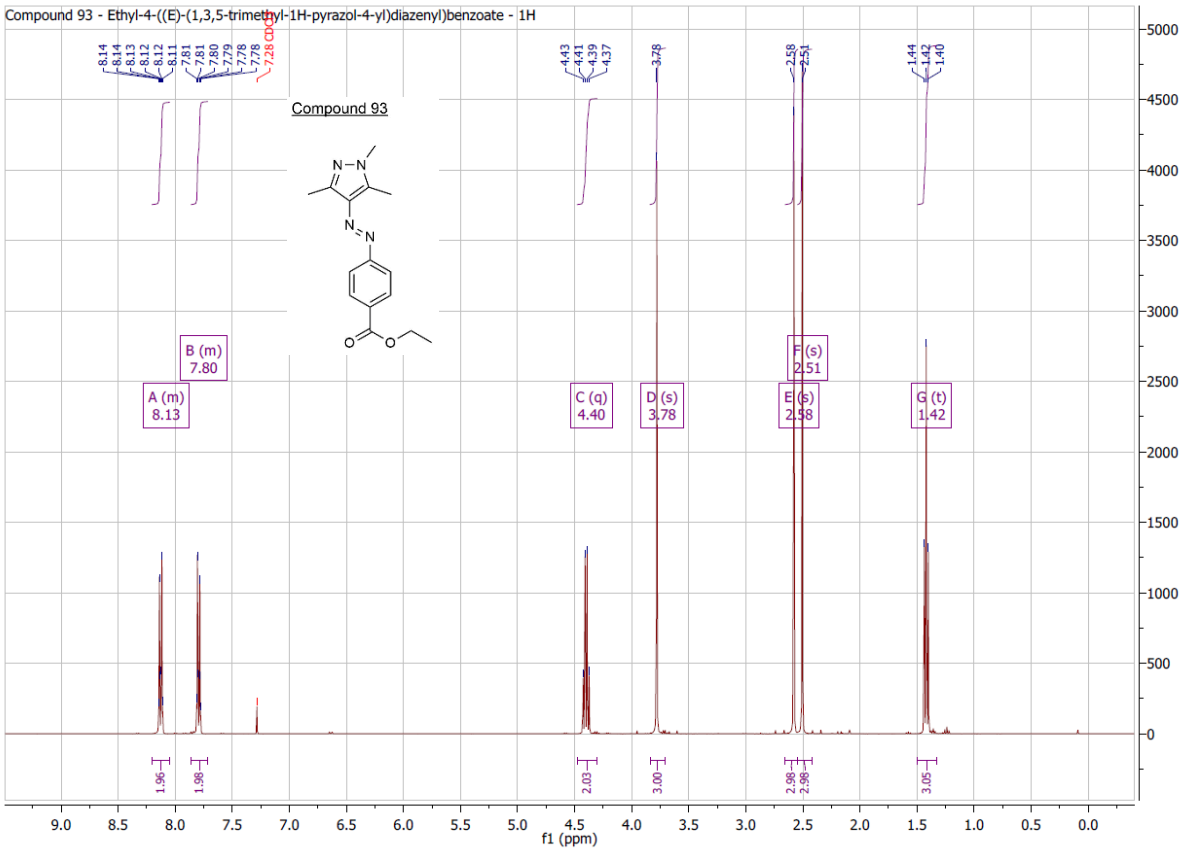
Compound 93 - Ethyl-4-((E)-(1,3,5-trimethyl-1H-pyrazol-4-yl)diazenyl)benzoate - 1H
Compound 93
A (m) 8.13
B (m) 7.80
C (q) 4.40
D (s) 3.78
E (s) 2.58
F (s) 2.51
G (t) 1.42
f1 (ppm)

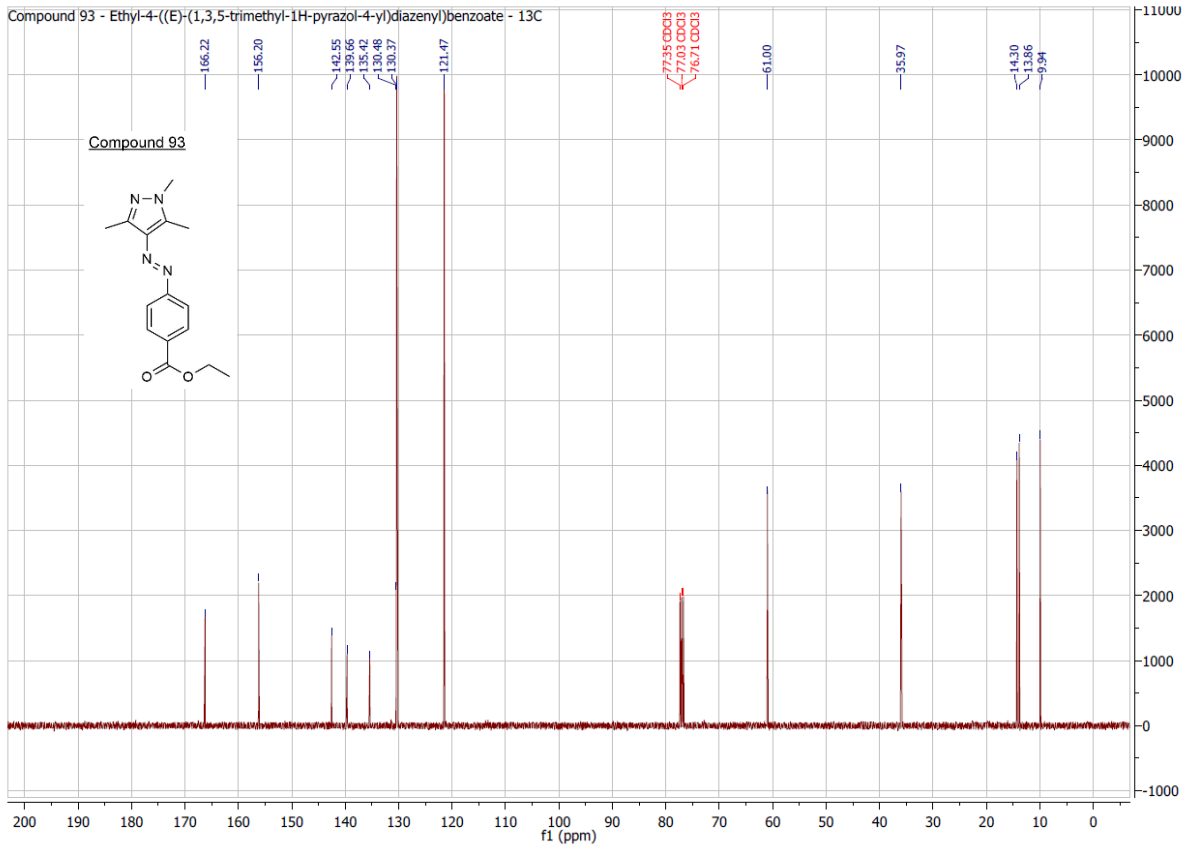
Compound 93 - Ethyl-4-((E)-(1,3,5-trimethyl-1H-pyrazol-4-yl)diazenyl)benzoate - 13C
Compound 93
f1 (ppm)

EI - ex. Masse & Zl nicht möglich, deshalb ESI

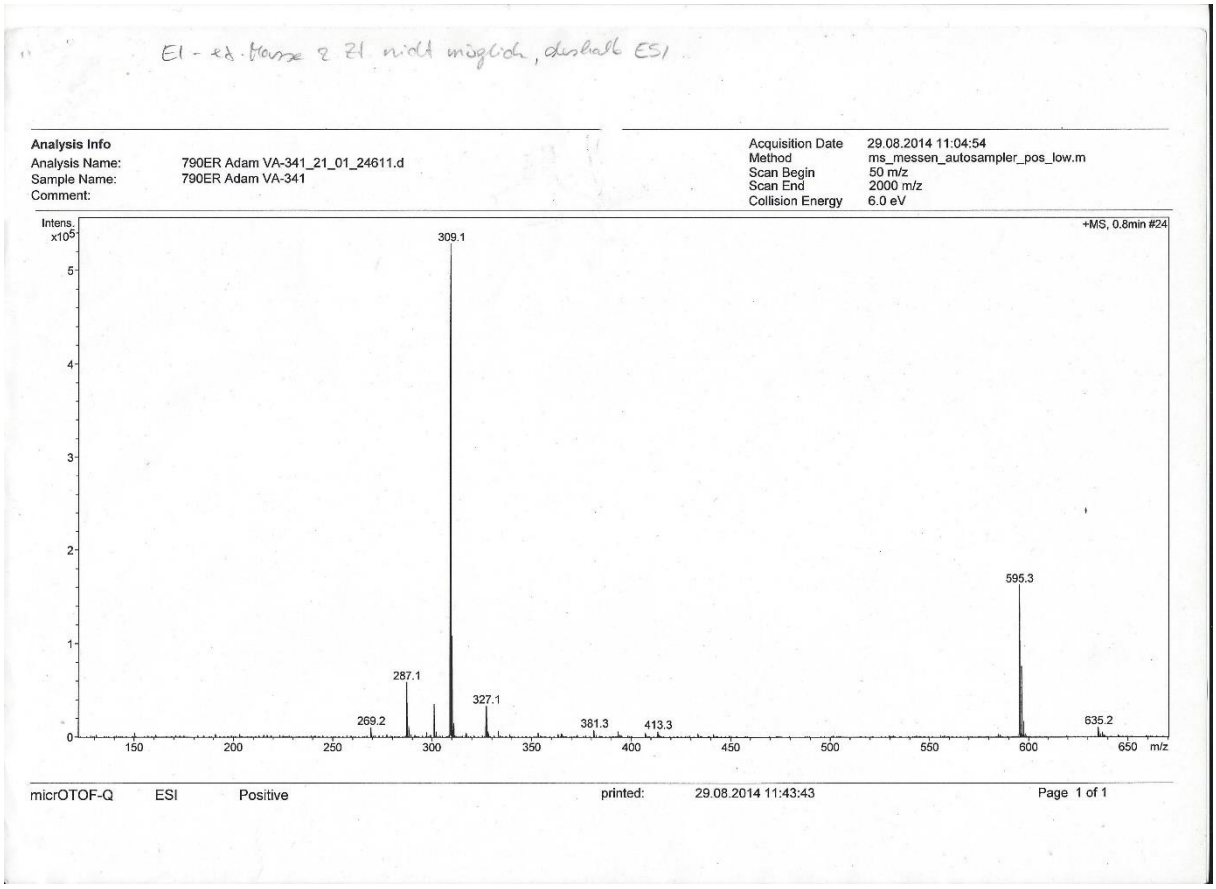

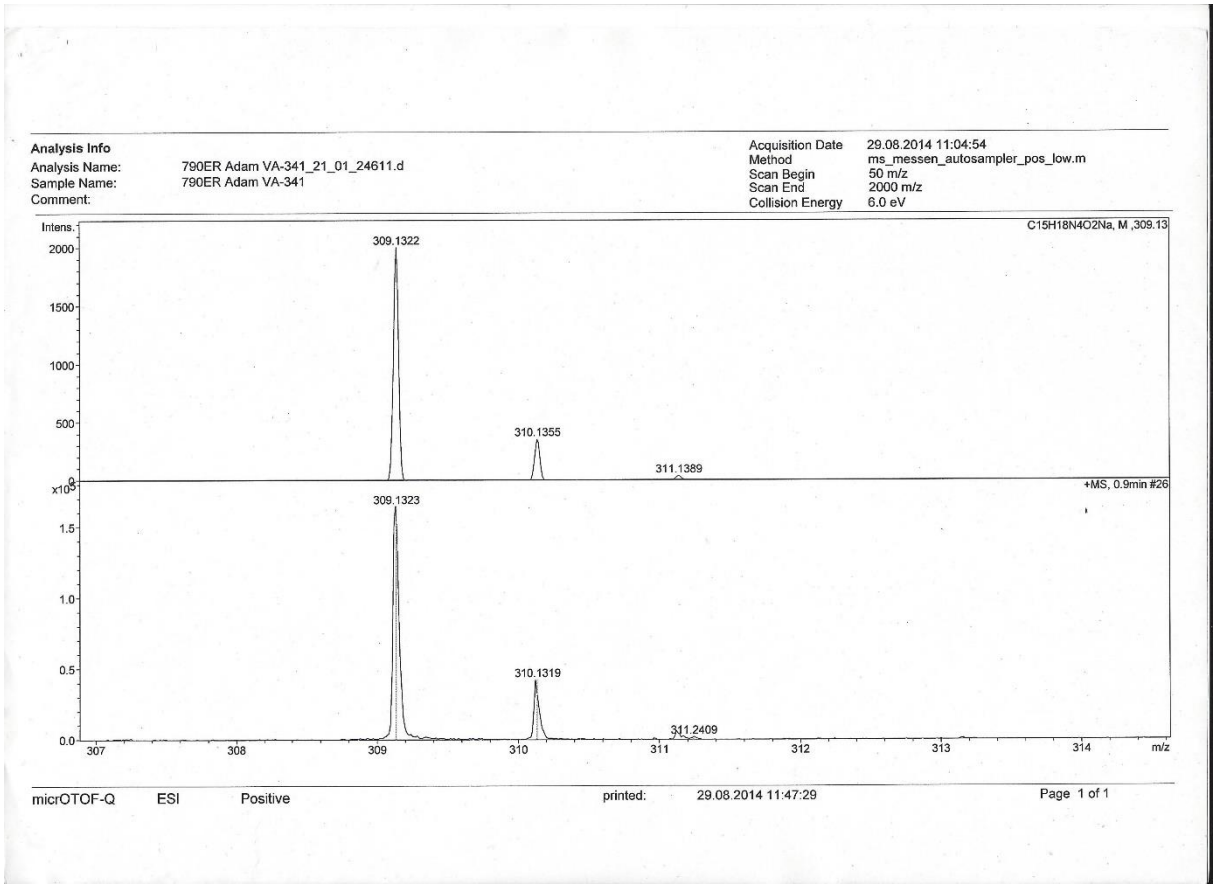

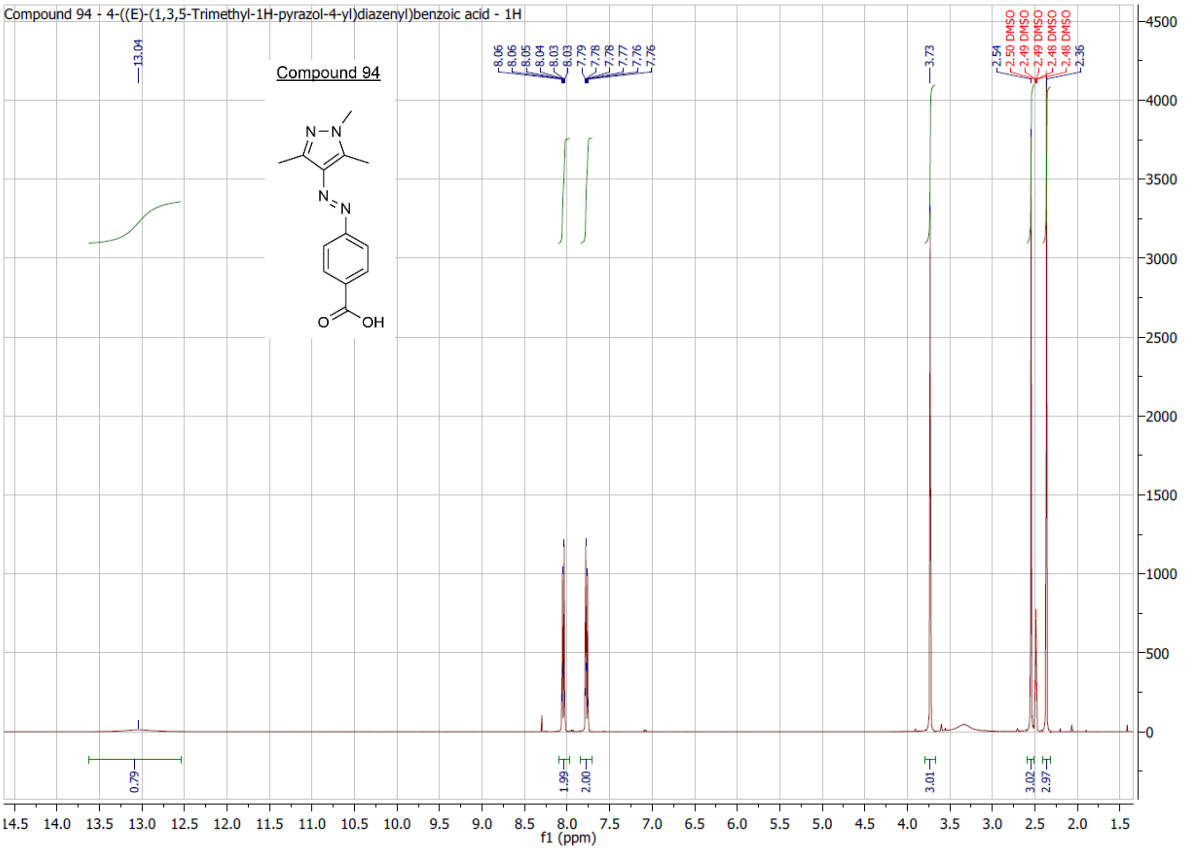
Compound 94 - 4-((E)-(1,3,5-Trimethyl-1H-pyrazol-4-yl)diazenyl)benzoic acid - 1H
Compound 94
13.04
8.06
8.06
8.05
8.04
8.03
8.03
7.79
7.78
7.78
7.77
7.76
7.76
3.73
2.54
2.50 DMSO
2.49 DMSO
2.49 DMSO
2.48 DMSO
2.48 DMSO
2.36
0.79
1.99
2.00
3.01
3.02
2.97
f1 (ppm)

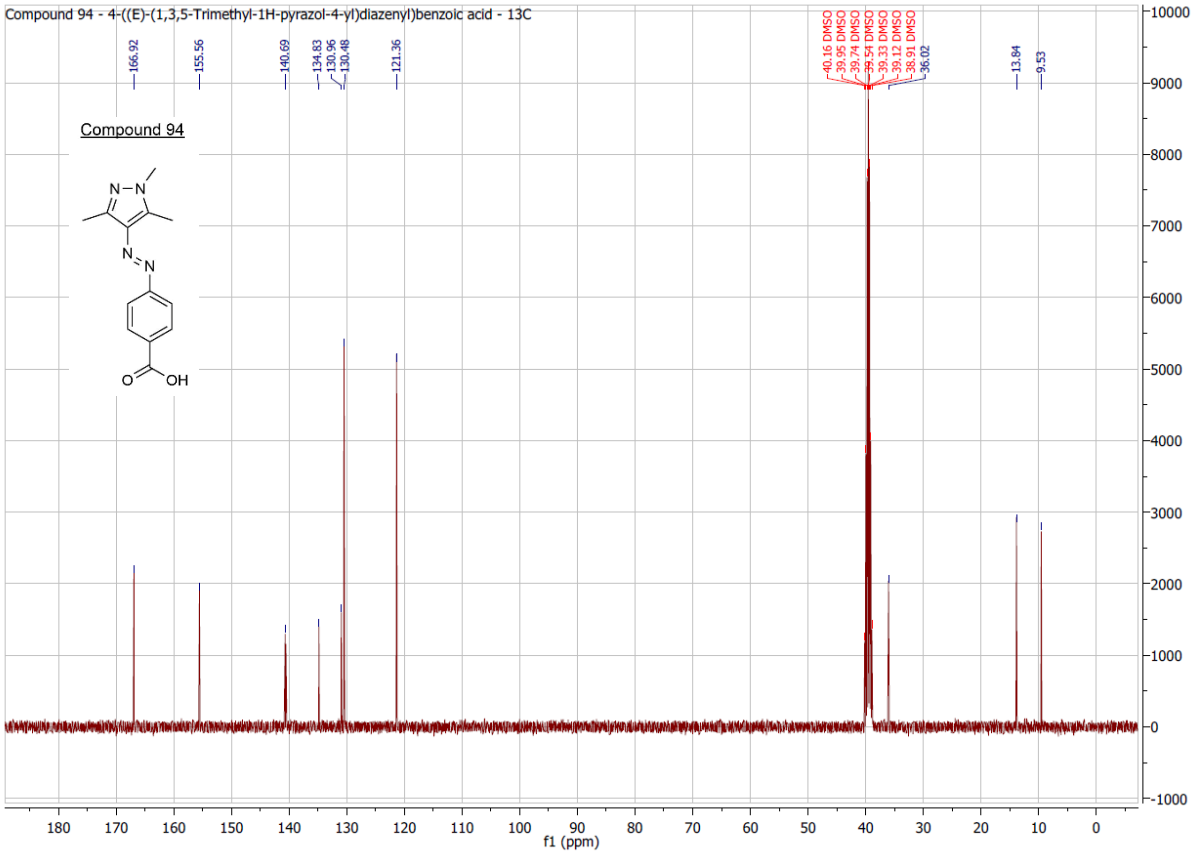
Compound 94 - 4-((E)-(1,3,5-Trimethyl-1H-pyrazol-4-yl)diazenyl)benzoic acid - 13C
Compound 94
166.92
155.56
140.69
134.83
130.96
130.48
121.36
40.16 DMSO
39.95 DMSO
39.74 DMSO
39.54 DMSO
39.33 DMSO
39.12 DMSO
38.91 DMSO
36.02
13.84
9.53
f1 (ppm)

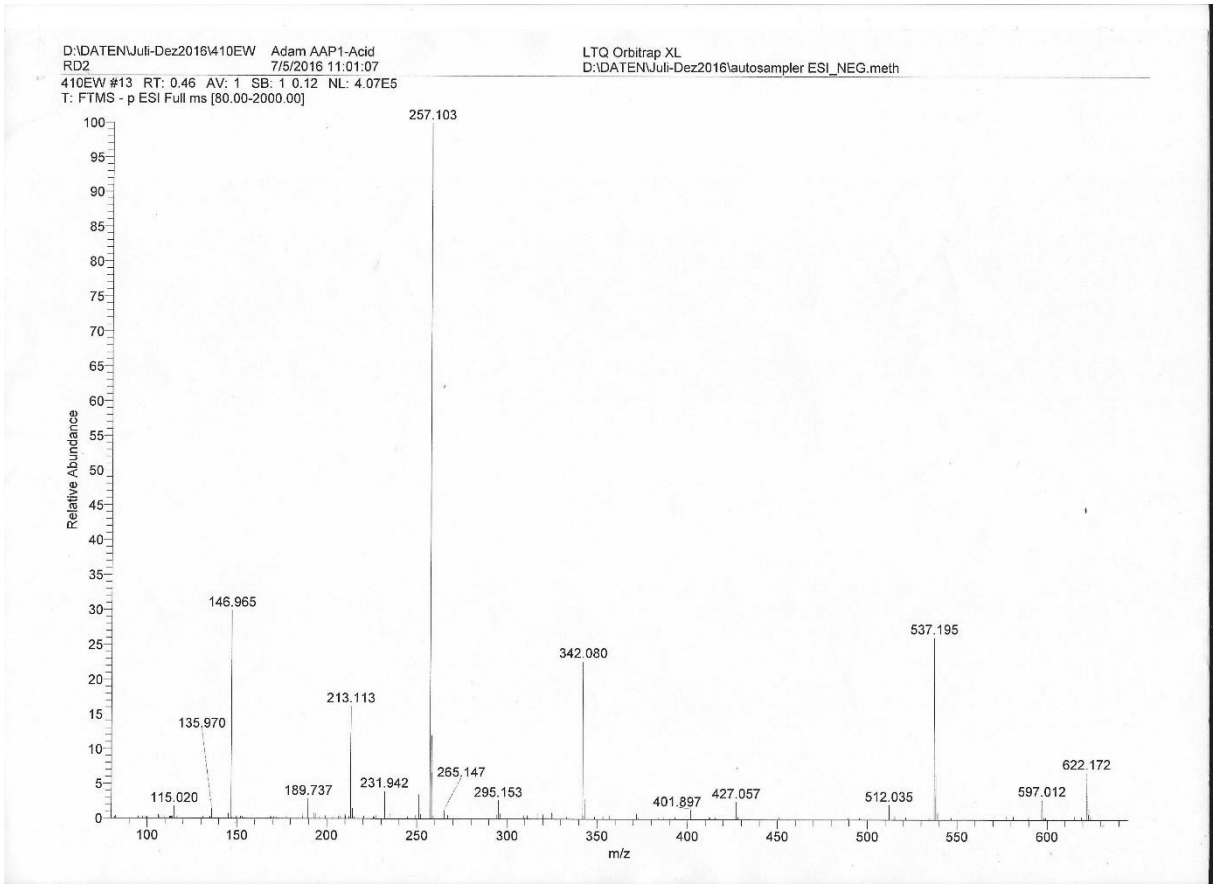
D:\DATEN\Juli-Dez2016\410EW Adam AAP1-Acid
RD2 7/5/2016 11:01:07
LTQ Orbitrap XL
D:\DATEN\Juli-Dez2016\autosampler ESI_NEG.meth
410EW #13 RT: 0.46 AV: 1 SB: 1 0.12 NL: 4.07E5
T: FTMS - p ESI Full ms [80.00-2000.00]
Relative Abundance
m/z
257.103
146.965
342.080
537.195
213.113
135.970
622.172
265.147
231.942
189.737
295.153
115.020
401.897
427.057
512.035
597.012

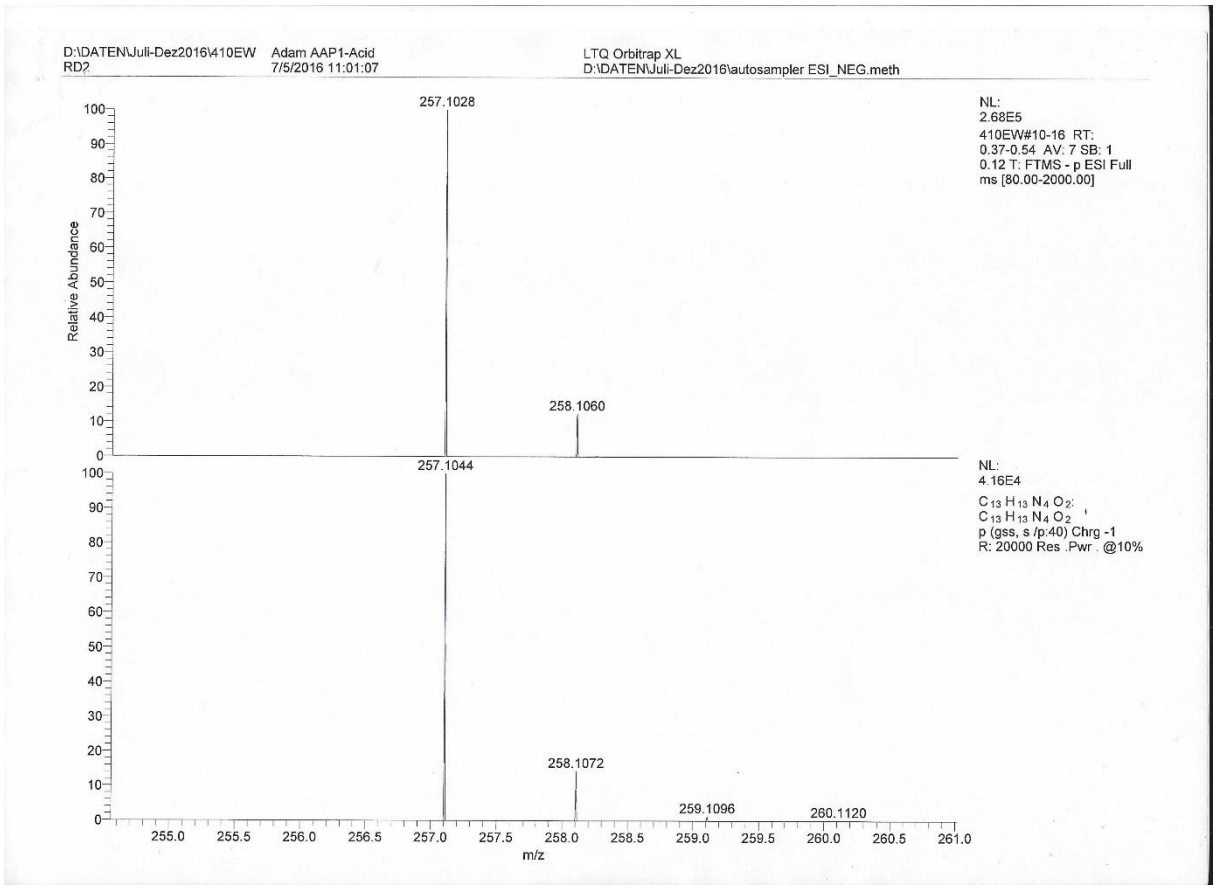
D:\DATEN\Juli-Dez2016\410EW Adam AAP1-Acid
RD2 7/5/2016 11:01:07
LTQ Orbitrap XL
D:\DATEN\Juli-Dez2016\autosampler ESI_NEG.meth
Relative Abundance
m/z
257.1028
258.1060
NL:
2.68E5
410EW#10-16 RT:
0.37-0.54 AV: 7 SB: 1
0.12 T: FTMS - p ESI Full
ms [80.00-2000.00]
257.1044
258.1072
259.1096
260.1120
NL:
4.16E4
C13 H13 N4 O2:
C13 H13 N4 O2
p (gss, s /p:40) Chrg -1
R: 20000 Res .Pwr . @10%

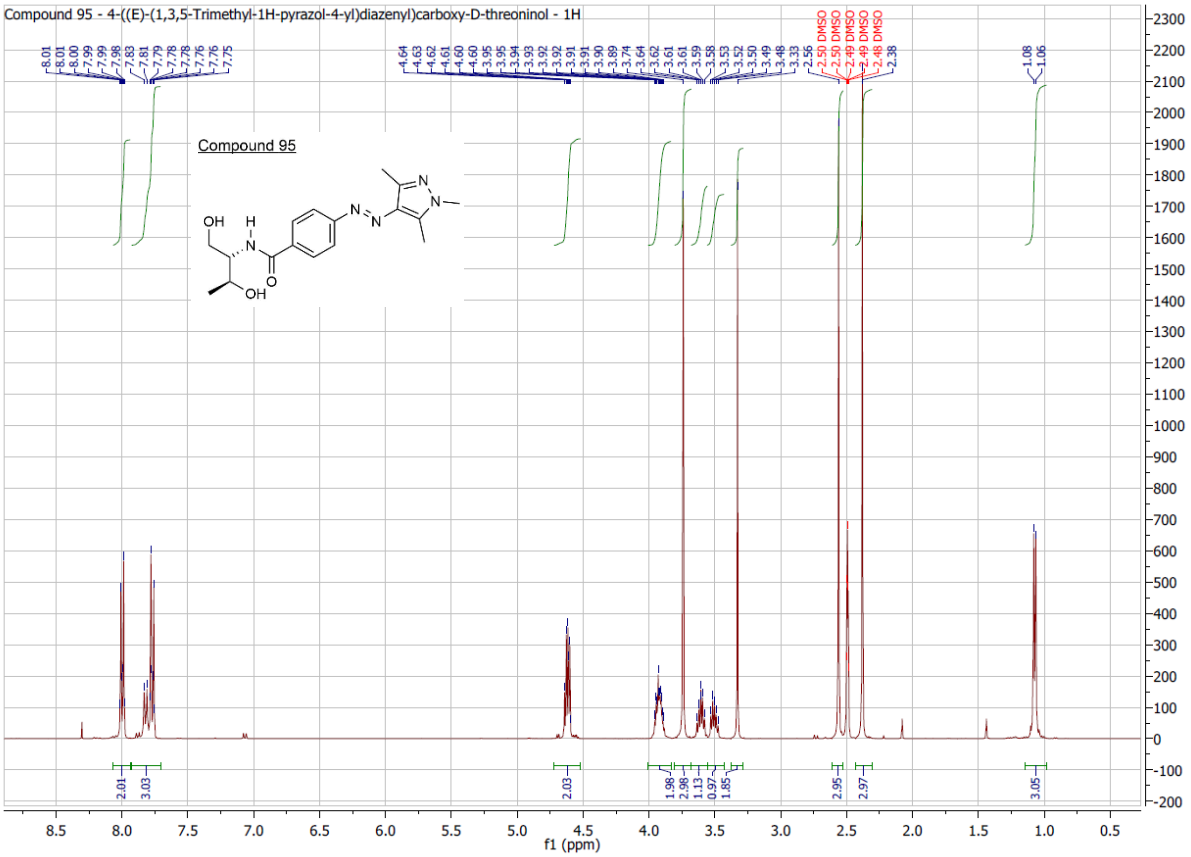
Compound 95 - 4-((E)-(1,3,5-Trimethyl-1H-pyrazol-4-yl)diazenyl)carboxy-D-threoninol - 1H
Compound 95
f1 (ppm)

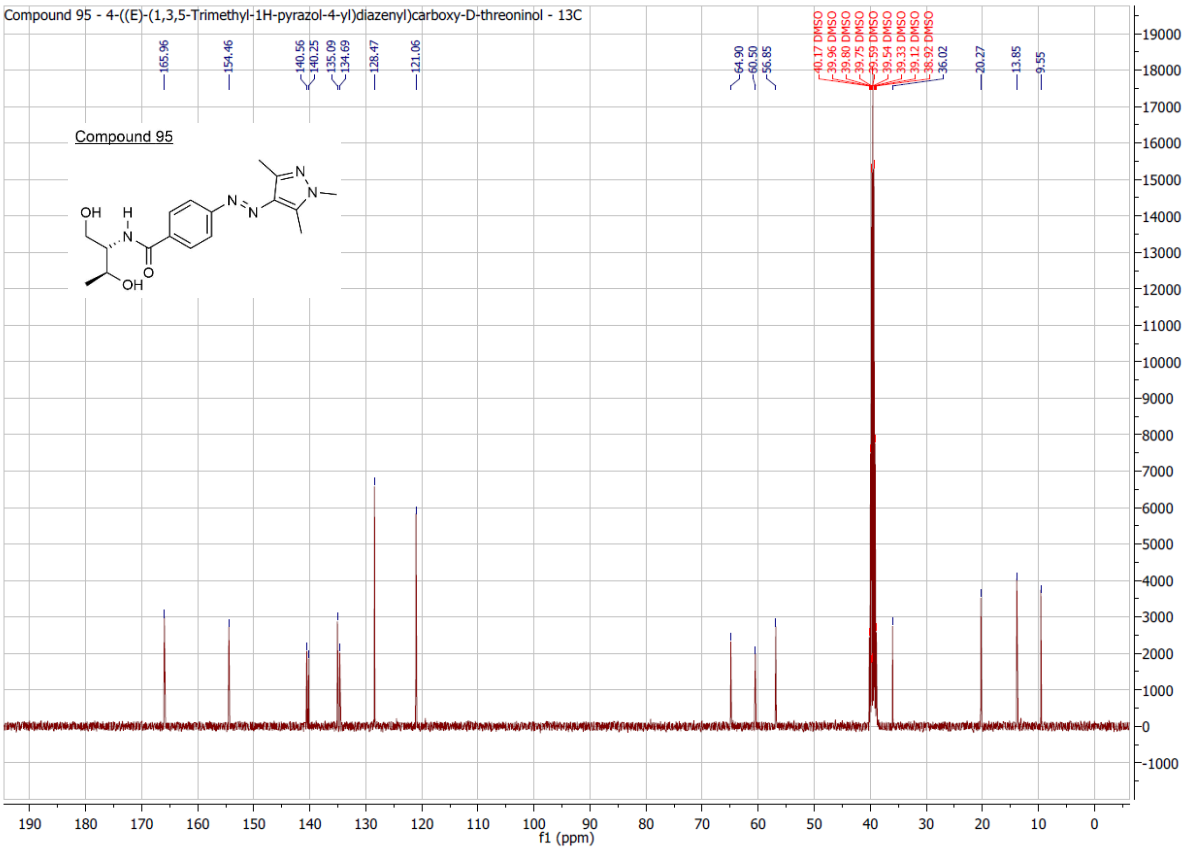
Compound 95 - 4-((E)-(1,3,5-Trimethyl-1H-pyrazol-4-yl)diazenyl)carboxy-D-threoninol - 13C
Compound 95
f1 (ppm)

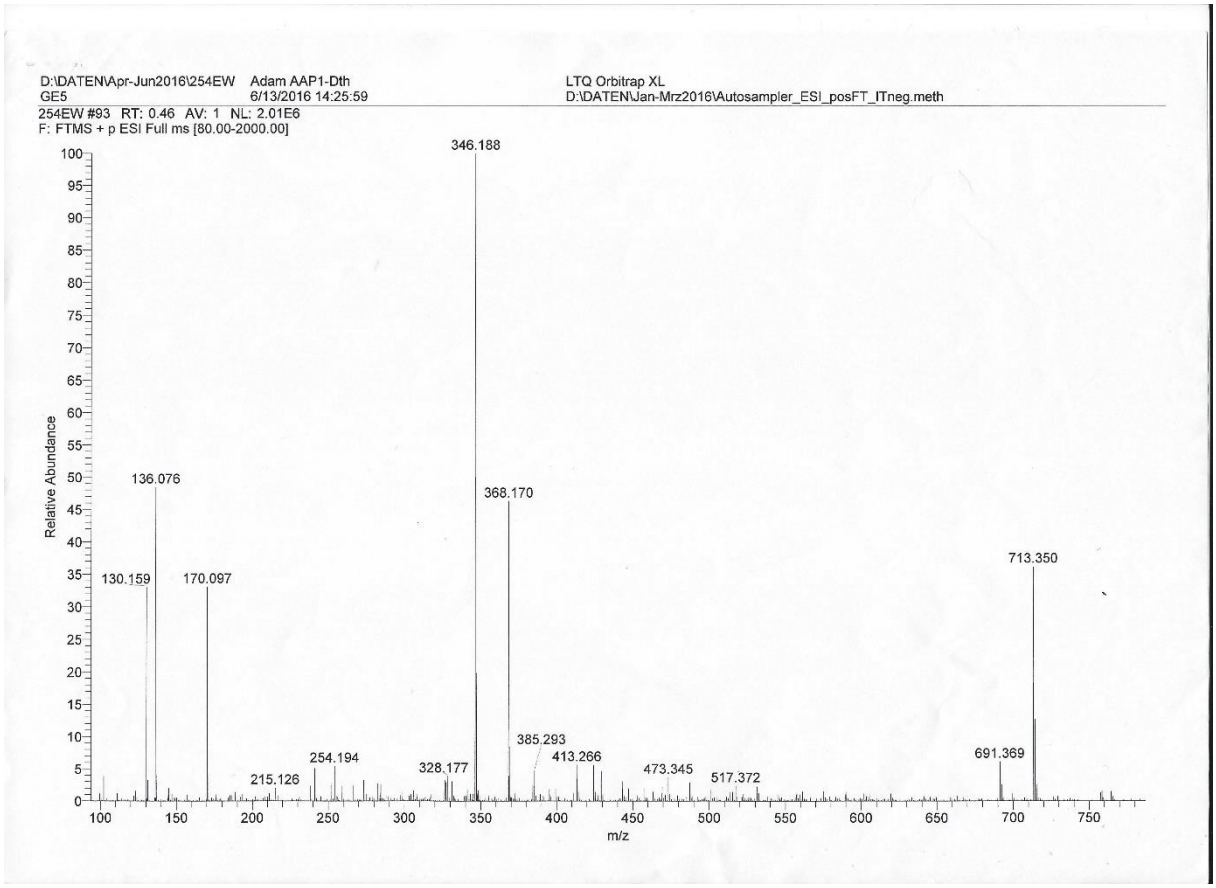
D:\DATEN\Apr-Jun2016\254EW Adam AAP1-Dth
GE5 6/13/2016 14:25:59
LTQ Orbitrap XL
D:\DATEN\Jan-Mrz2016\Autosampler_ESI_posFT_ITneg.meth
254EW #93 RT: 0.46 AV: 1 NL: 2.01E6
F: FTMS + p ESI Full ms [80.00-2000.00]
346.188
136.076
368.170
130.159
170.097
713.350
385.293
413.266
254.194
328.177
691.369
215.126
473.345
517.372
Relative Abundance
m/z

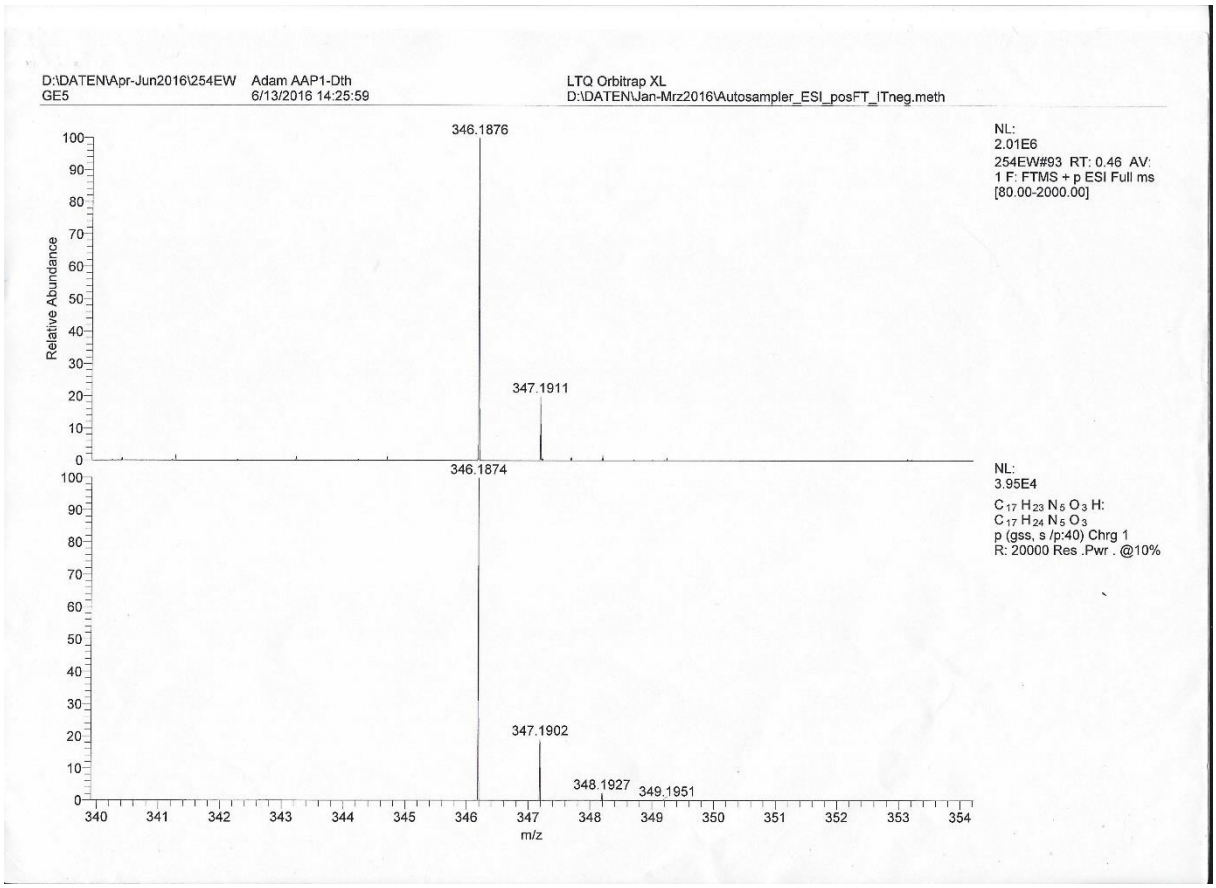
D:\DATEN\Apr-Jun2016\254EW Adam AAP1-Dth
GE5 6/13/2016 14:25:59
LTQ Orbitrap XL
D:\DATEN\Jan-Mrz2016\Autosampler_ESI_posFT_ITneg.meth
346.1876
347.1911
NL:
2.01E6
254EW#93 RT: 0.46 AV:
1 F: FTMS + p ESI Full ms
[80.00-2000.00]
346.1874
347.1902
348.1927
349.1951
NL:
3.95E4
C17 H23 N5 O3 H:
C17 H24 N5 O3
p (gss, s /p:40) Chrg 1
R: 20000 Res .Pwr . @10%
Relative Abundance
m/z

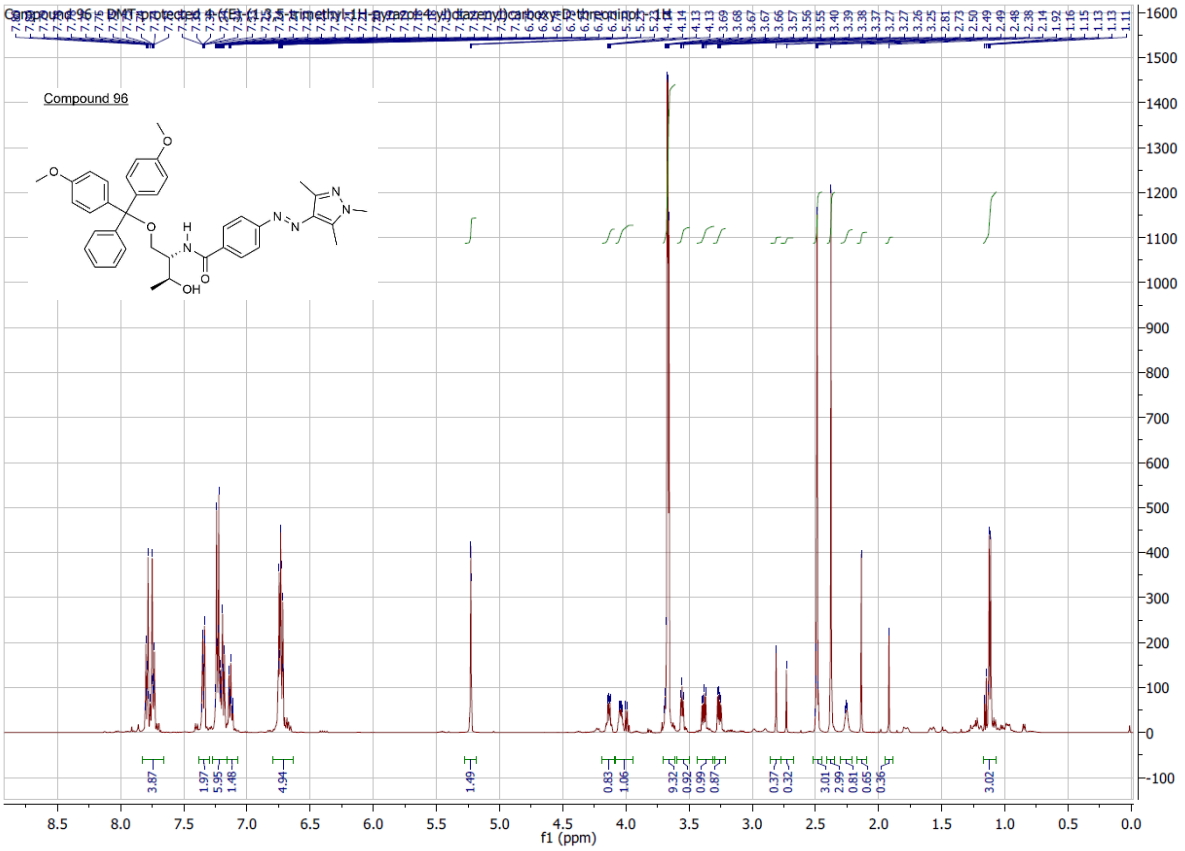
Compound 96
f1 (ppm)

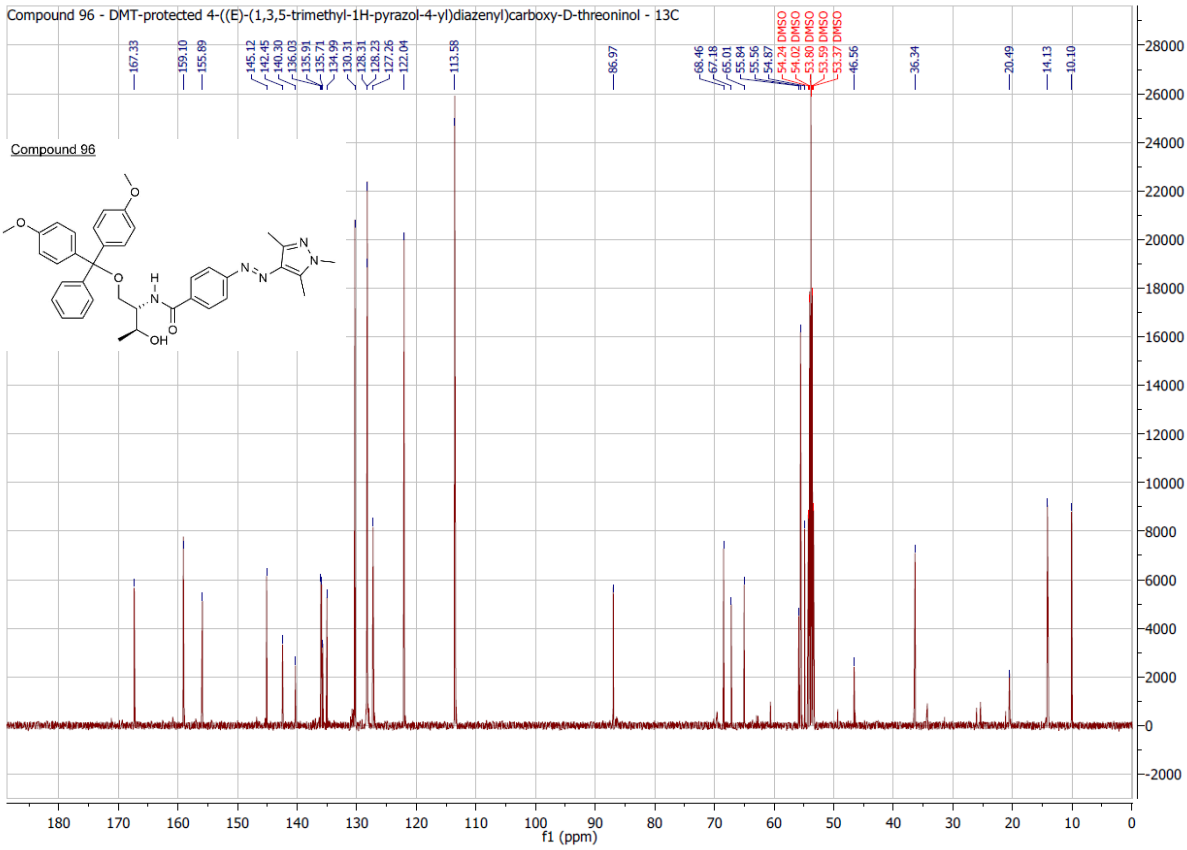
Compound 96 - DMT-protected 4-((E)-(1,3,5-trimethyl-1H-pyrazol-4-yl)diazenyl)carboxy-D-threoninol - 13C
Compound 96
f1 (ppm)

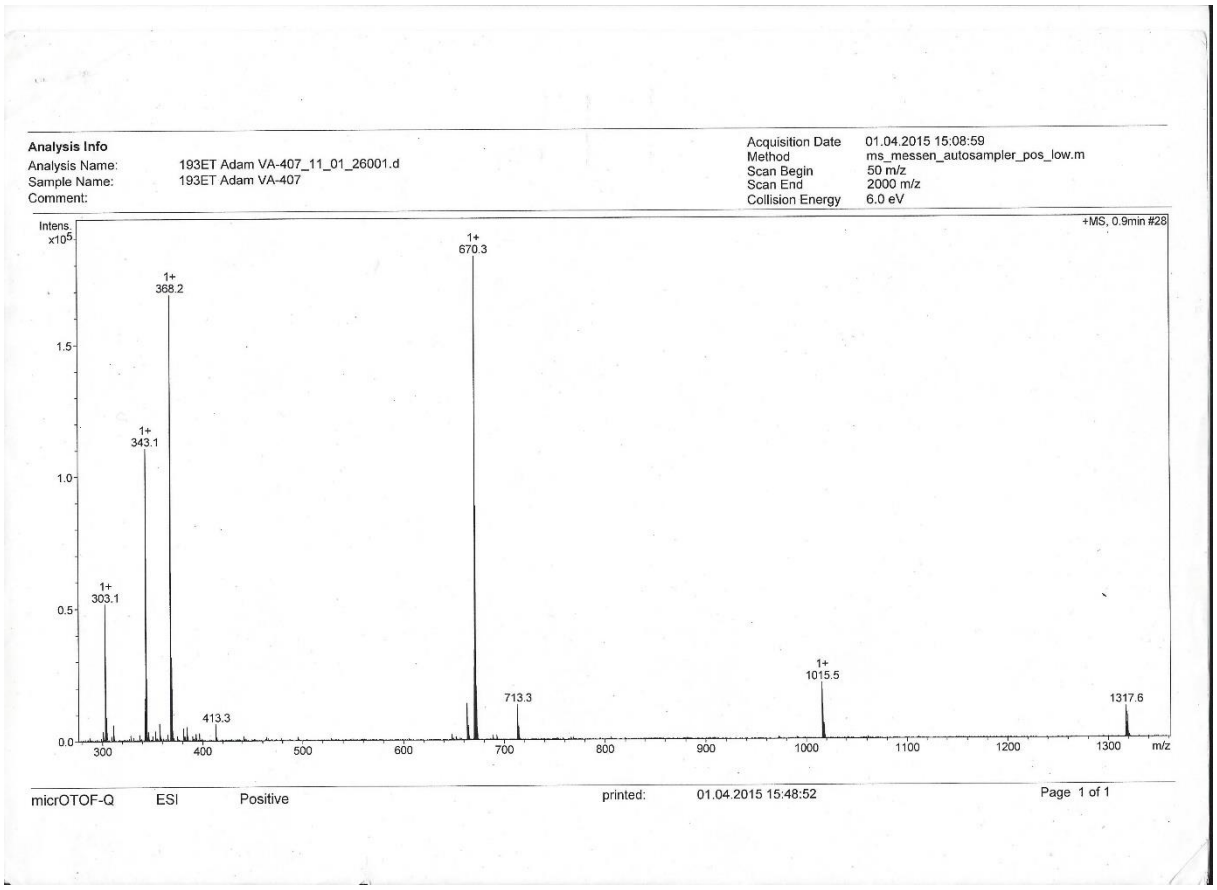
Analysis Info
Analysis Name: 193ET Adam VA-407_11_01_26001.d
Sample Name: 193ET Adam VA-407
Comment:
Acquisition Date 01.04.2015 15:08:59
Method ms_messen_autosampler_pos_low.m
Scan Begin 50 m/z
Scan End 2000 m/z
Collision Energy 6.0 eV
Intens.
x10^5
+MS, 0.9min #28
1+ 670.3
1+ 368.2
1+ 343.1
1+ 303.1
1+ 1015.5
713.3
413.3
1317.6
m/z
micrOTOF-Q ESI Positive
printed: 01.04.2015 15:48:52
Page 1 of 1

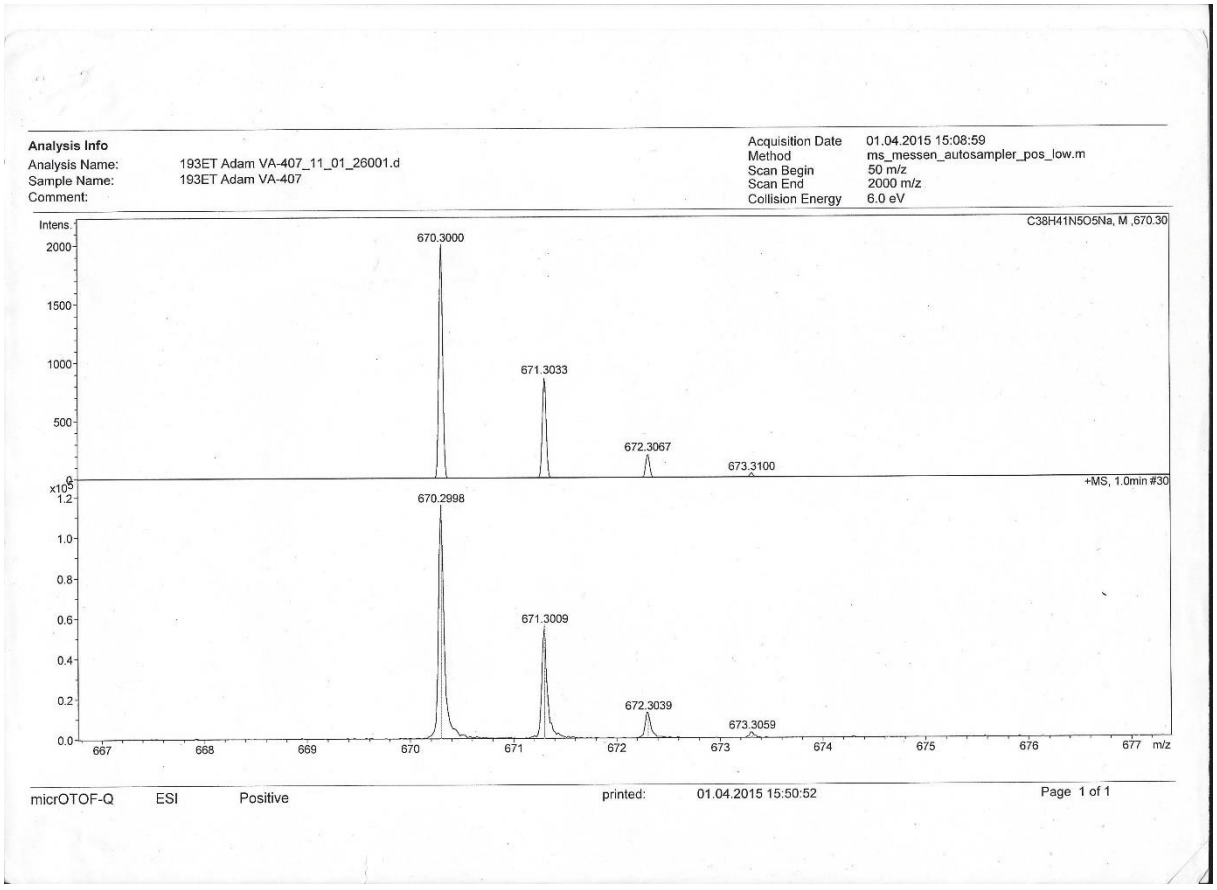
Analysis Info
Analysis Name: 193ET Adam VA-407_11_01_26001.d
Sample Name: 193ET Adam VA-407
Comment:
Acquisition Date 01.04.2015 15:08:59
Method ms_messen_autosampler_pos_low.m
Scan Begin 50 m/z
Scan End 2000 m/z
Collision Energy 6.0 eV
Intens.
C38H41N5O5Na, M ,670.30
670.3000
671.3033
672.3067
673.3100
x10^5
+MS, 1.0min #30
670.2998
671.3009
672.3039
673.3059
m/z
micrOTOF-Q ESI Positive
printed: 01.04.2015 15:50:52
Page 1 of 1

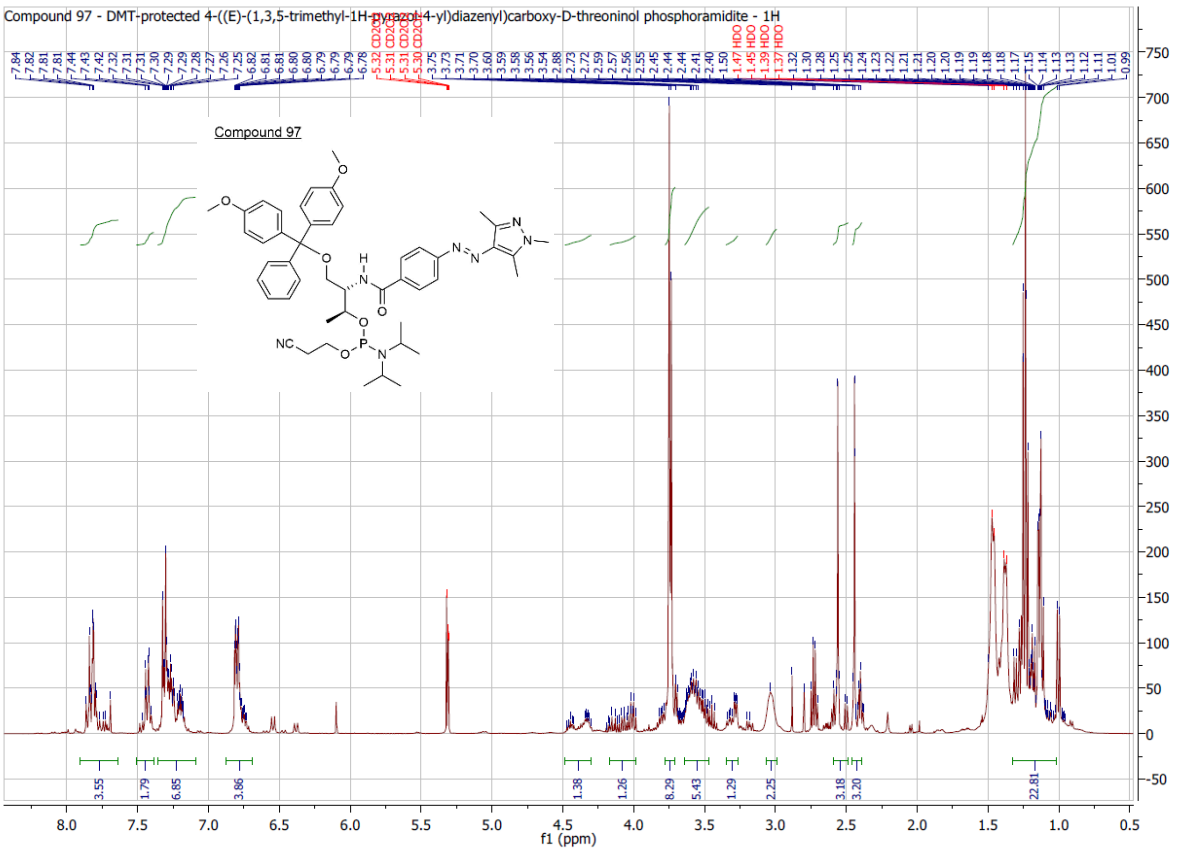
Compound 97 - DMT-protected 4-((E)-(1,3,5-trimethyl-1H-pyrazol-4-yl)diazenyl)carboxy-D-threoninol phosphoramidite - 1H
Compound 97
f1 (ppm)

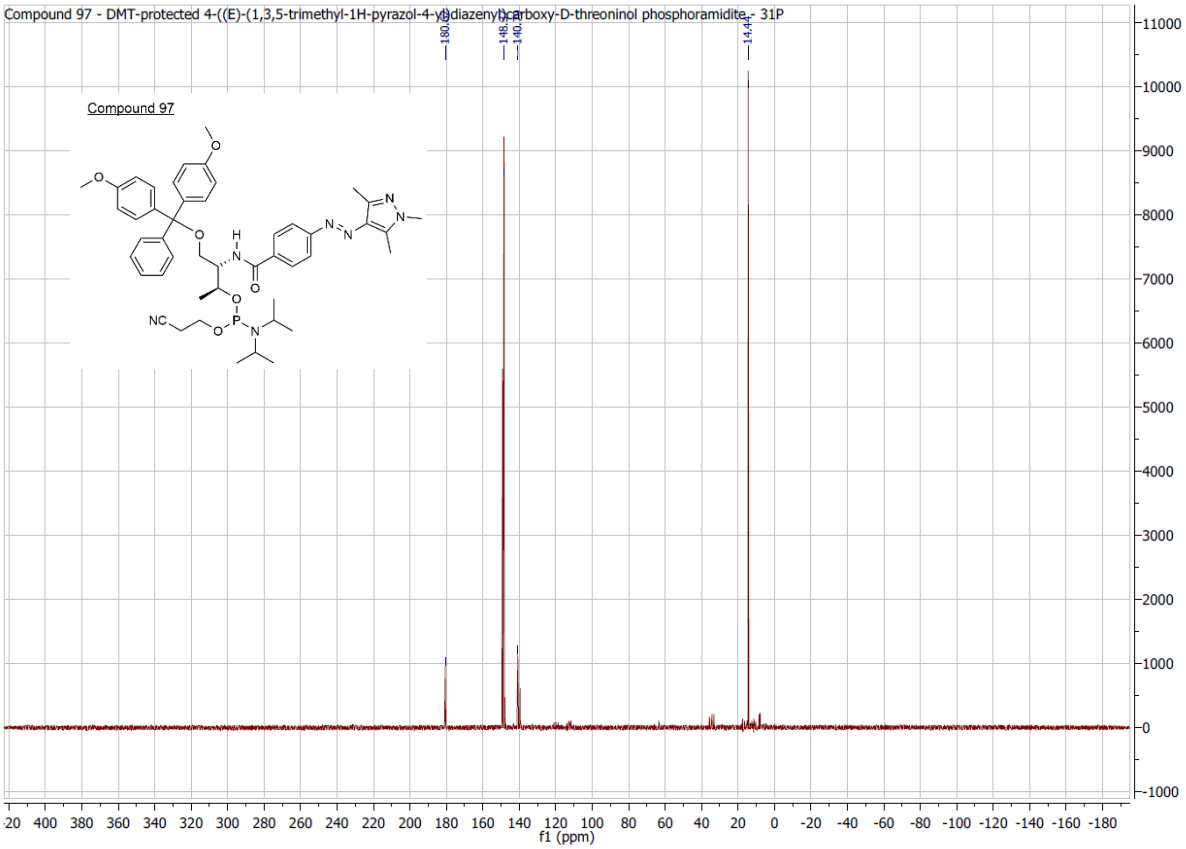
Compound 97 - DMT-protected 4-((E)-(1,3,5-trimethyl-1H-pyrazol-4-yl)diazenyl)carboxy-D-threoninol phosphoramidite - 31P
Compound 97
f1 (ppm)

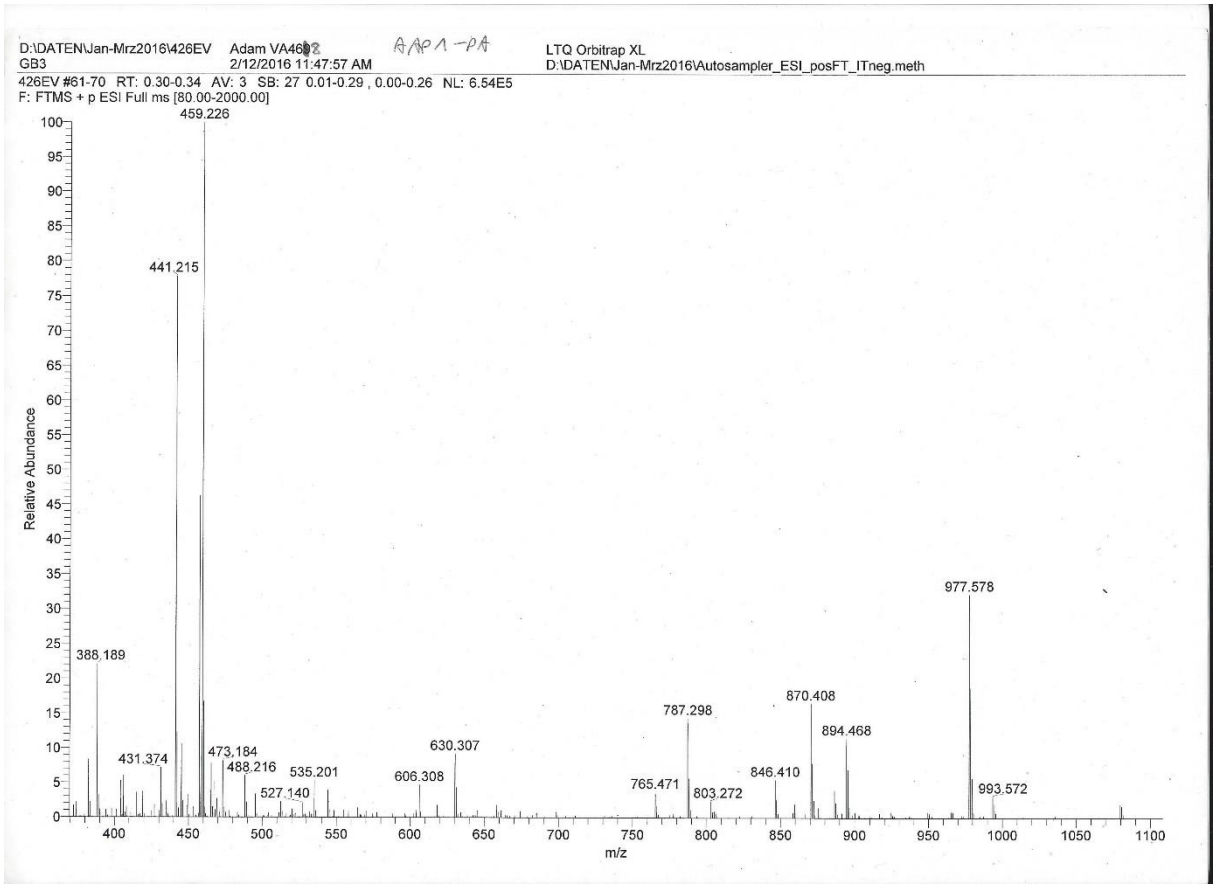
D:\DATEN\Jan-Mrz2016\426EV
GB3
Adam VA46
2/12/2016 11:47:57 AM
AAP1-PA
LTQ Orbitrap XL
D:\DATEN\Jan-Mrz2016\Autosampler_ESI_posFT_ITneg.meth
426EV #61-70 RT: 0.30-0.34 AV: 3 SB: 27 0.01-0.29 , 0.00-0.26 NL: 6.54E5
F: FTMS + p ESI Full ms [80.00-2000.00]
459.226
441.215
977.578
388.189
870.408
787.298
894.468
630.307
431.374
473.184
488.216
535.201
606.308
846.410
765.471
803.272
527.140
993.572
Relative Abundance
m/z

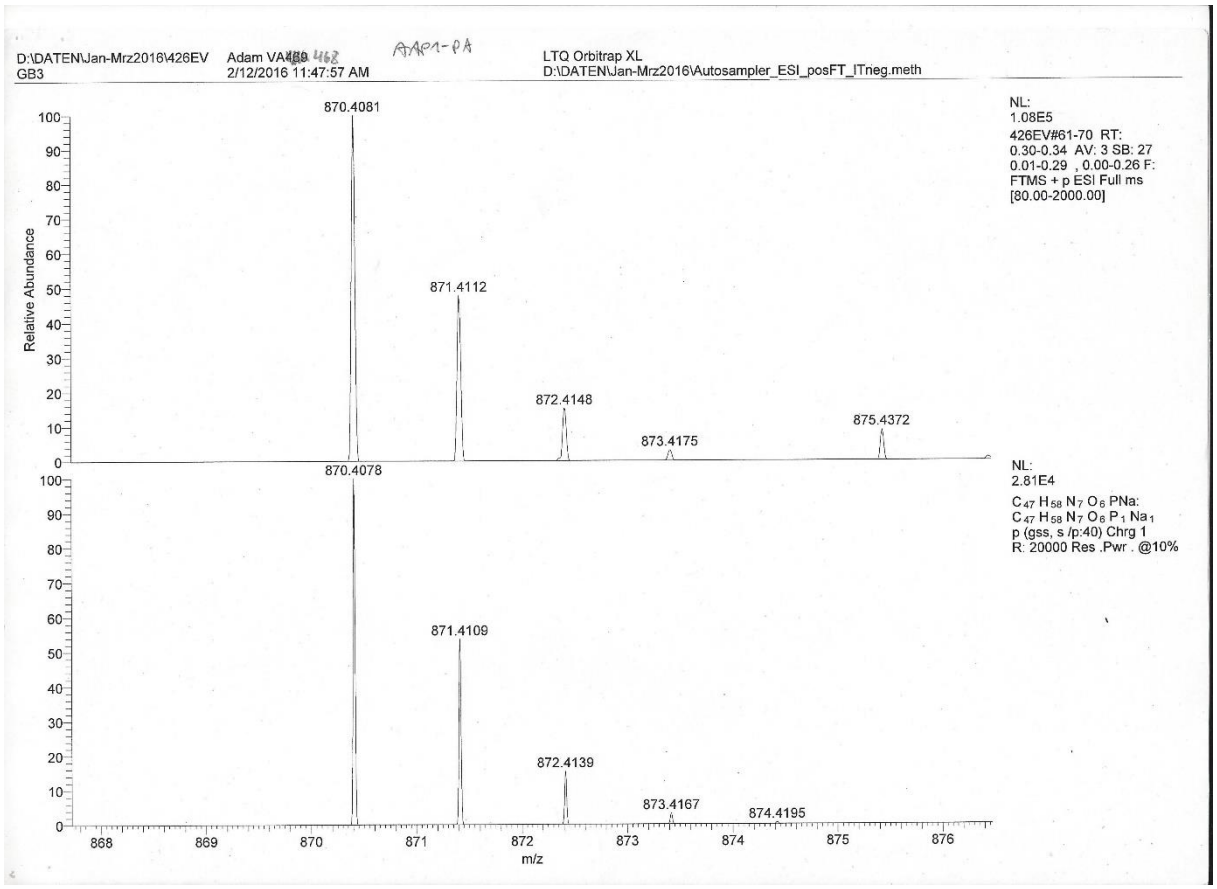
D:\DATEN\Jan-Mrz2016\426EV
GB3
Adam VA
2/12/2016 11:47:57 AM
AAP1-PA
LTQ Orbitrap XL
D:\DATEN\Jan-Mrz2016\Autosampler_ESI_posFT_ITneg.meth
870.4081
871.4112
872.4148
875.4372
873.4175
NL:
1.08E5
426EV#61-70 RT:
0.30-0.34 AV: 3 SB: 27
0.01-0.29 , 0.00-0.26 F:
FTMS + p ESI Full ms
[80.00-2000.00]
870.4078
871.4109
872.4139
873.4167
874.4195
NL:
2.81E4
C47 H58 N7 O6 PNa:
C47 H58 N7 O6 P1 Na1
p (gss, s /p:40) Chrg 1
R: 20000 Res .Pwr . @10%
Relative Abundance
m/z

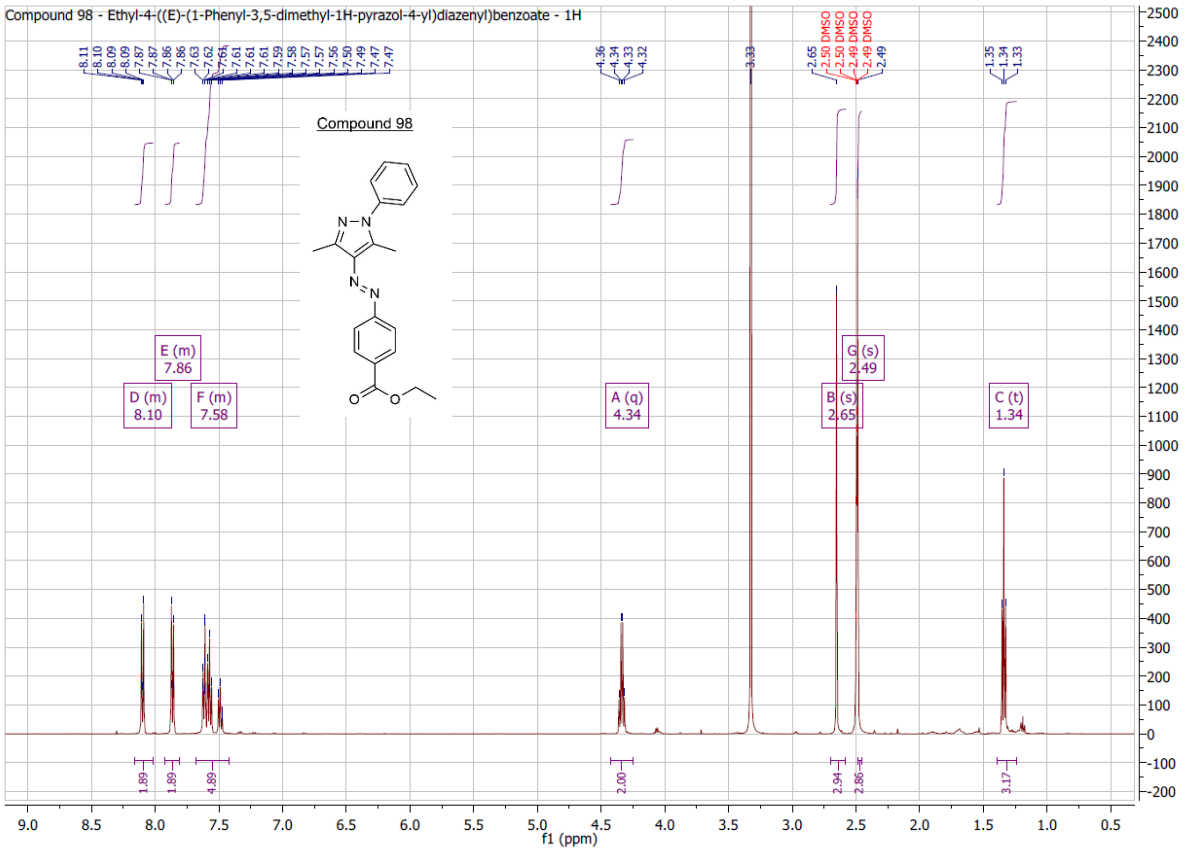
Compound 98 - Ethyl-4-((E)-(1-Phenyl-3,5-dimethyl-1H-pyrazol-4-yl)diazenyl)benzoate - 1H
Compound 98
E (m) 7.86
D (m) 8.10
F (m) 7.58
A (q) 4.34
G (s) 2.49
B (s) 2.65
C (t) 1.34
f1 (ppm)

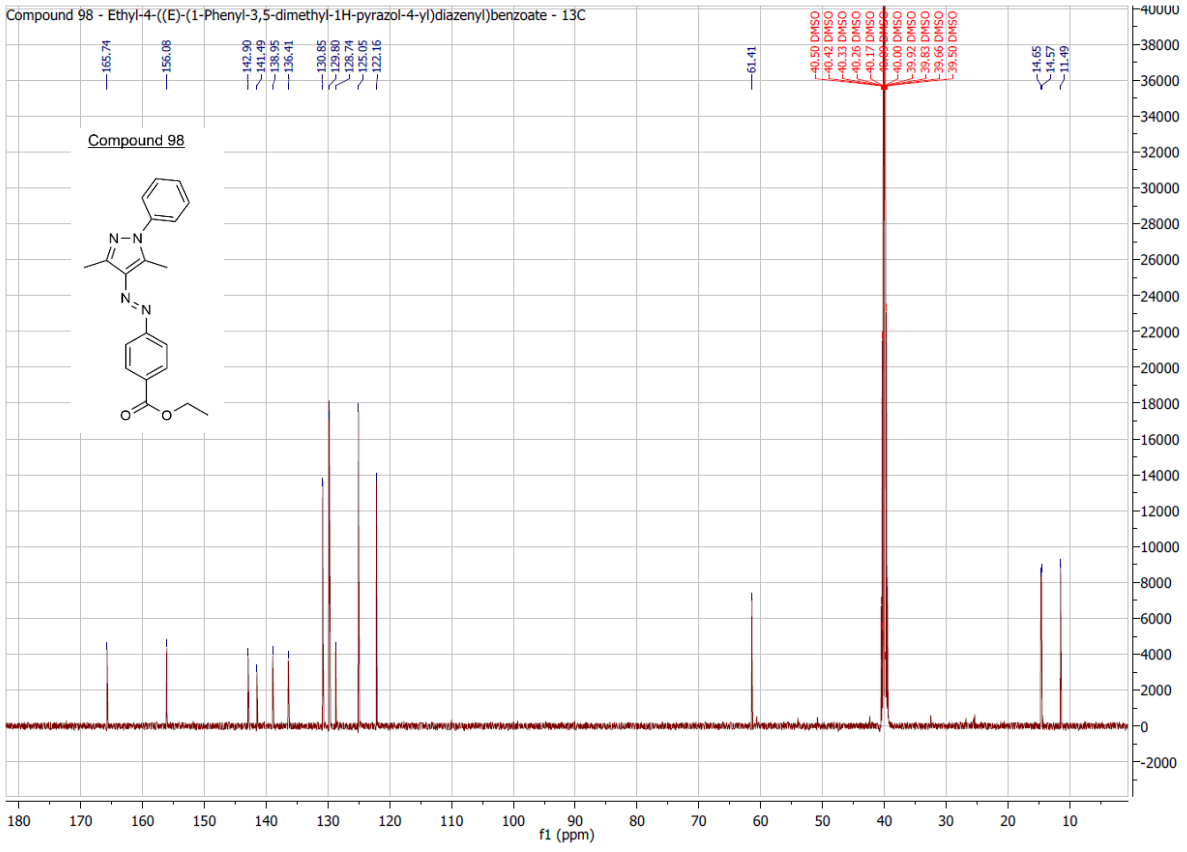
Compound 98 - Ethyl-4-((E)-(1-Phenyl-3,5-dimethyl-1H-pyrazol-4-yl)diazenyl)benzoate - 13C
Compound 98
f1 (ppm)

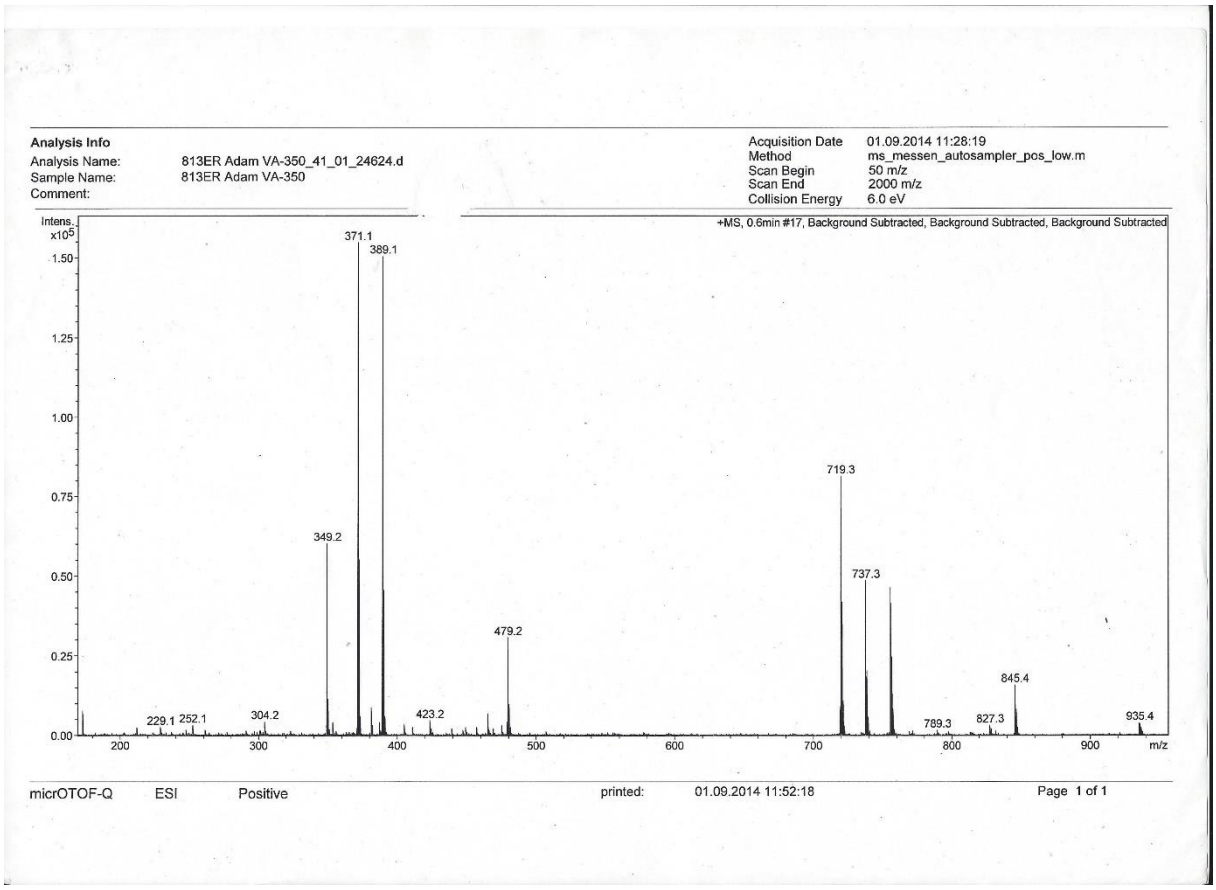
Analysis Info
Analysis Name: 813ER Adam VA-350_41_01_24624.d
Sample Name: 813ER Adam VA-350
Comment:
Acquisition Date 01.09.2014 11:28:19
Method ms_messen_autosampler_pos_low.m
Scan Begin 50 m/z
Scan End 2000 m/z
Collision Energy 6.0 eV
Intens.
x10^5
+MS, 0.6min #17, Background Subtracted, Background Subtracted, Background Subtracted
371.1
389.1
719.3
349.2
737.3
479.2
845.4
229.1
252.1
304.2
423.2
789.3
827.3
935.4
m/z
micrOTOF-Q ESI Positive
printed: 01.09.2014 11:52:18
Page 1 of 1

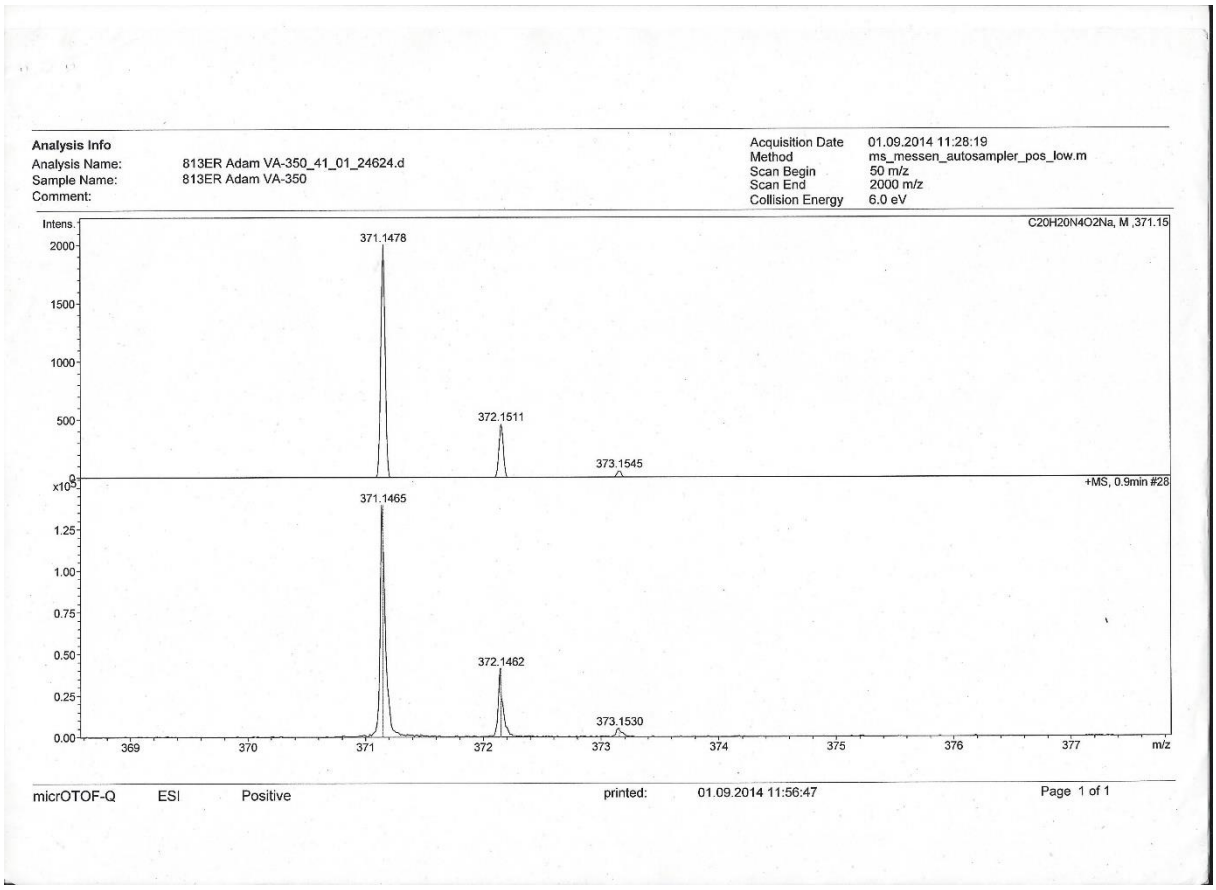
Analysis Info
Analysis Name: 813ER Adam VA-350_41_01_24624.d
Sample Name: 813ER Adam VA-350
Comment:
Acquisition Date 01.09.2014 11:28:19
Method ms_messen_autosampler_pos_low.m
Scan Begin 50 m/z
Scan End 2000 m/z
Collision Energy 6.0 eV
Intens.
C20H20N4O2Na, M ,371.15
371.1478
372.1511
373.1545
x10^5
+MS, 0.9min #28
371.1465
372.1462
373.1530
m/z
micrOTOF-Q ESI Positive
printed: 01.09.2014 11:56:47
Page 1 of 1

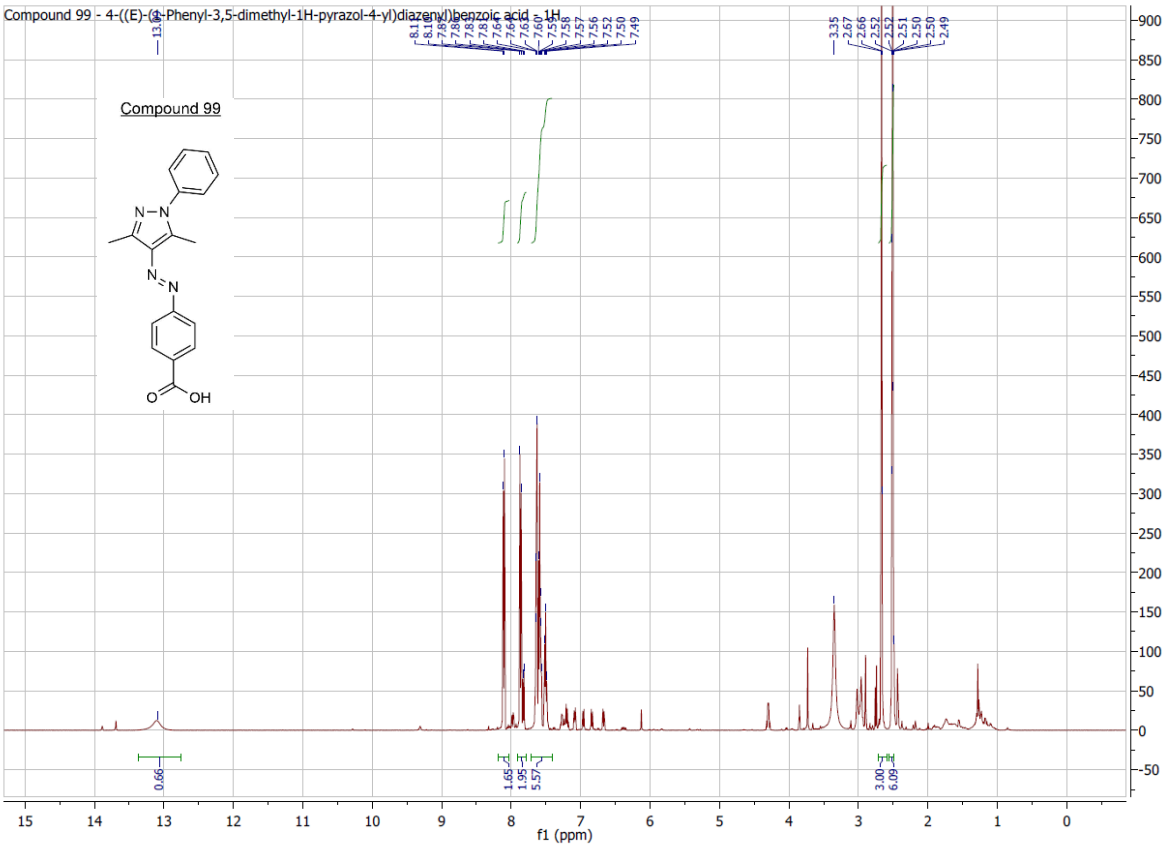
Compound 99 - 4-((E)-(1-Phenyl-3,5-dimethyl-1H-pyrazol-4-yl)diazenyl)benzoic acid - 1H
Compound 99
f1 (ppm)

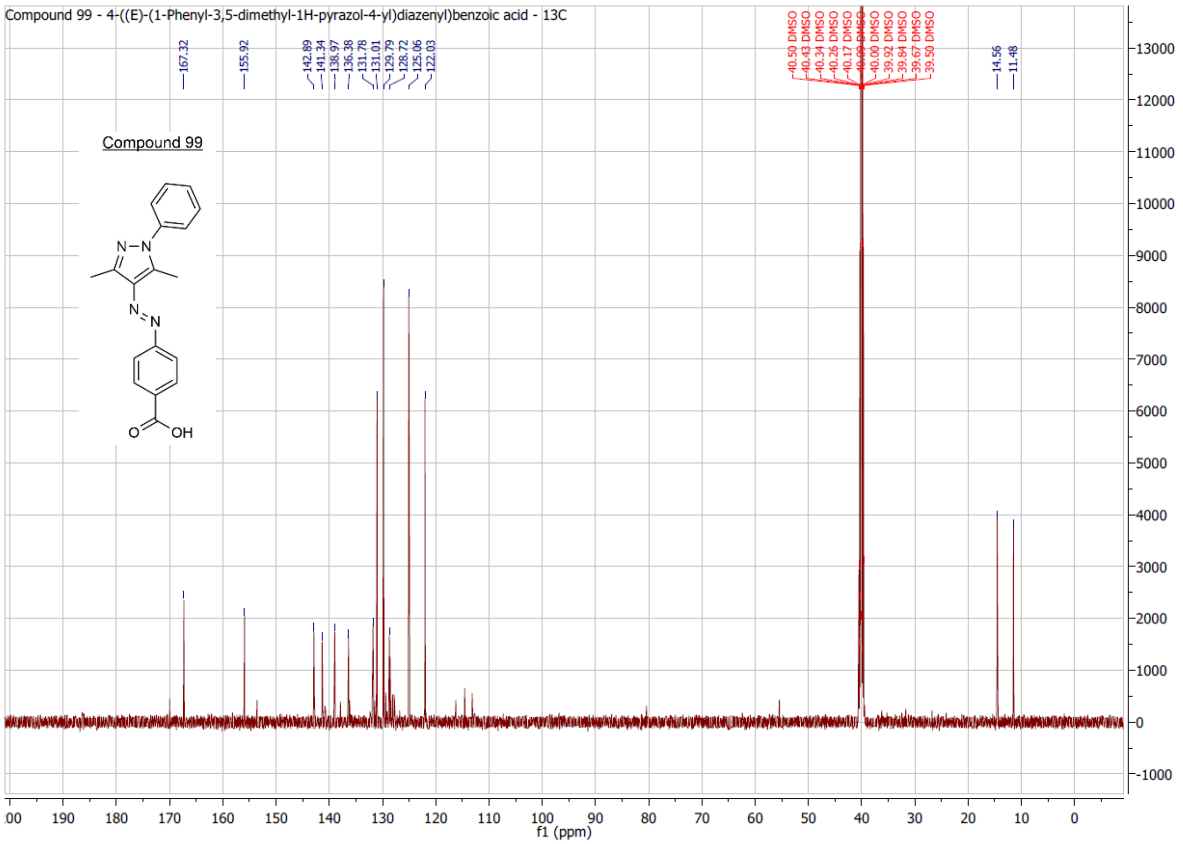
Compound 99 - 4-((E)-(1-Phenyl-3,5-dimethyl-1H-pyrazol-4-yl)diazenyl)benzoic acid - 13C
Compound 99
f1 (ppm)

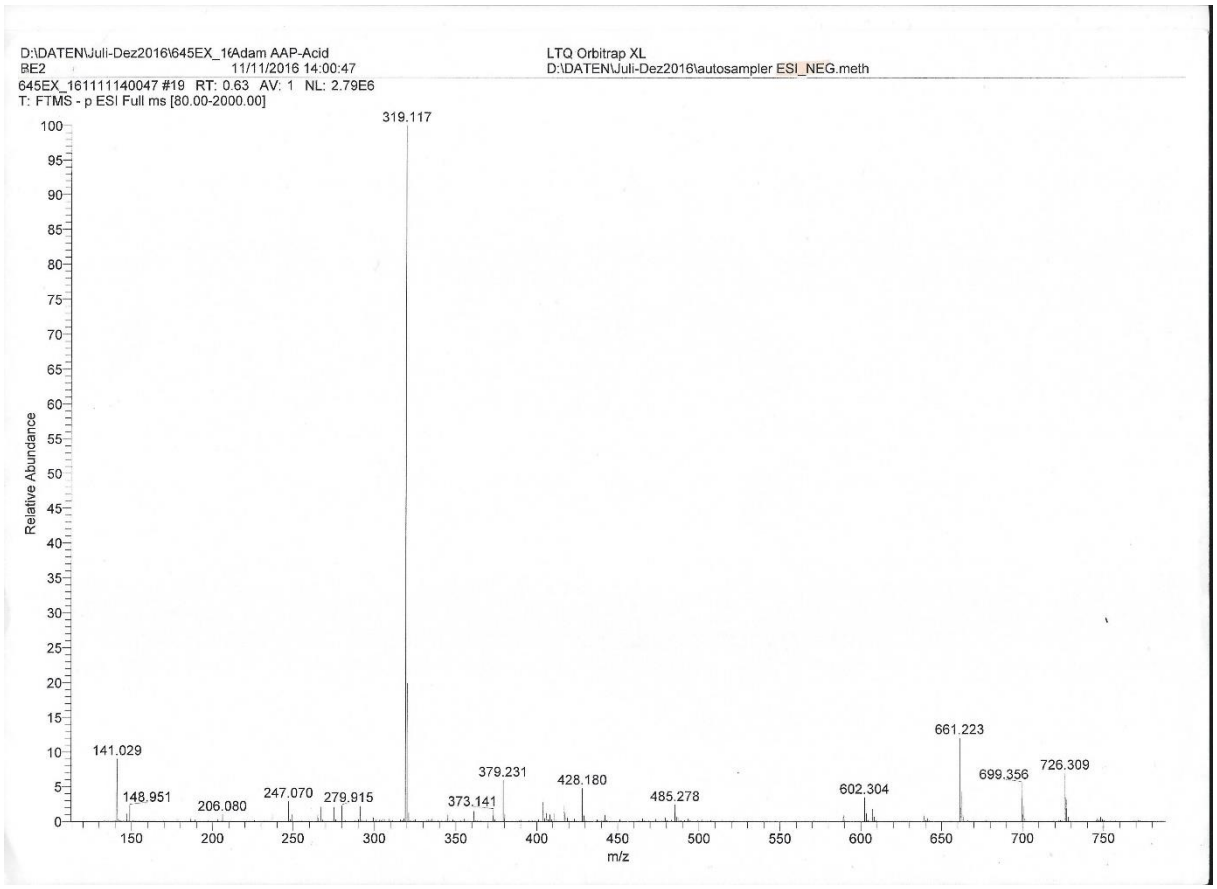
D:\DATEN\Juli-Dez2016\645EX_16\Adam AAP-Acid
BE2 11/11/2016 14:00:47
645EX_161111140047 #19 RT: 0.63 AV: 1 NL: 2.79E6
T: FTMS - p ESI Full ms [80.00-2000.00]
LTQ Orbitrap XL
D:\DATEN\Juli-Dez2016\autosampler ESI_NEG.meth
Relative Abundance
m/z
319.117
141.029
148.951
206.080
247.070
279.915
373.141
379.231
428.180
485.278
602.304
661.223
699.356
726.309

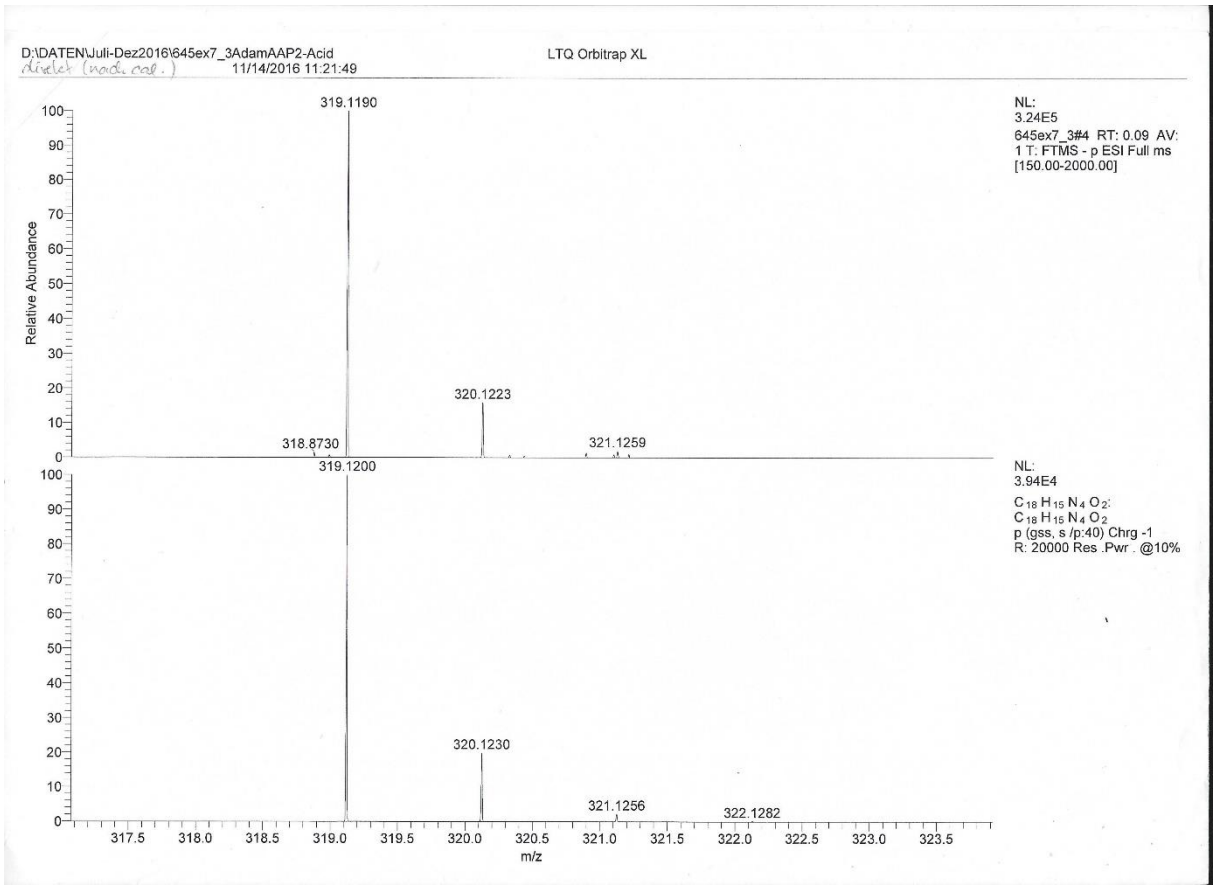
D:\DATEN\Juli-Dez2016\645ex7_3AdamAAP2-Acid
direkt (nach cal.) 11/14/2016 11:21:49
LTQ Orbitrap XL
Relative Abundance
m/z
319.1190
320.1223
318.8730
321.1259
NL:
3.24E5
645ex7_3#4 RT: 0.09 AV: 1 T: FTMS - p ESI Full ms [150.00-2000.00]
319.1200
320.1230
321.1256
322.1282
NL:
3.94E4
C18 H15 N4 O2:
C18 H15 N4 O2
p (gss, s /p:40) Chrg -1
R: 20000 Res .Pwr . @10%

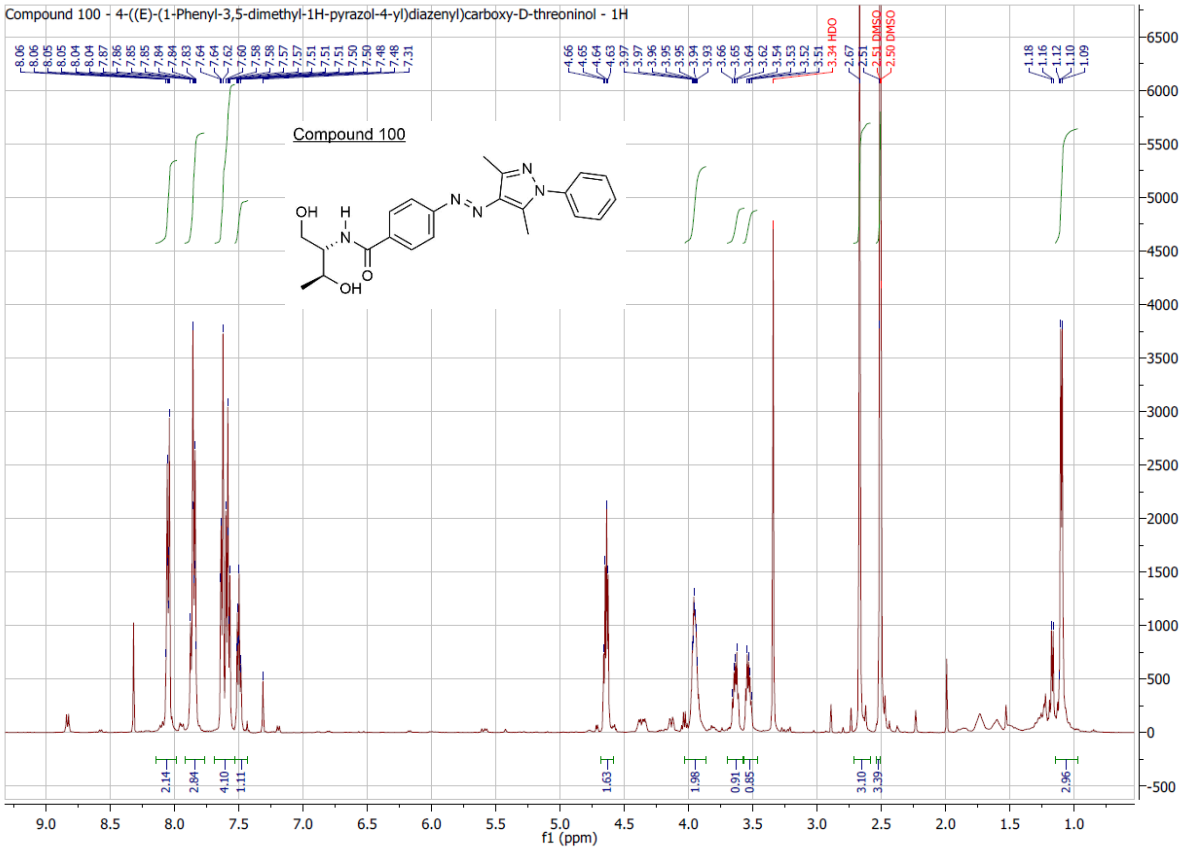
Compound 100 - 4-((E)-(1-Phenyl-3,5-dimethyl-1H-pyrazol-4-yl)diazenyl)carboxy-D-threoninol - 1H
Compound 100
f1 (ppm)

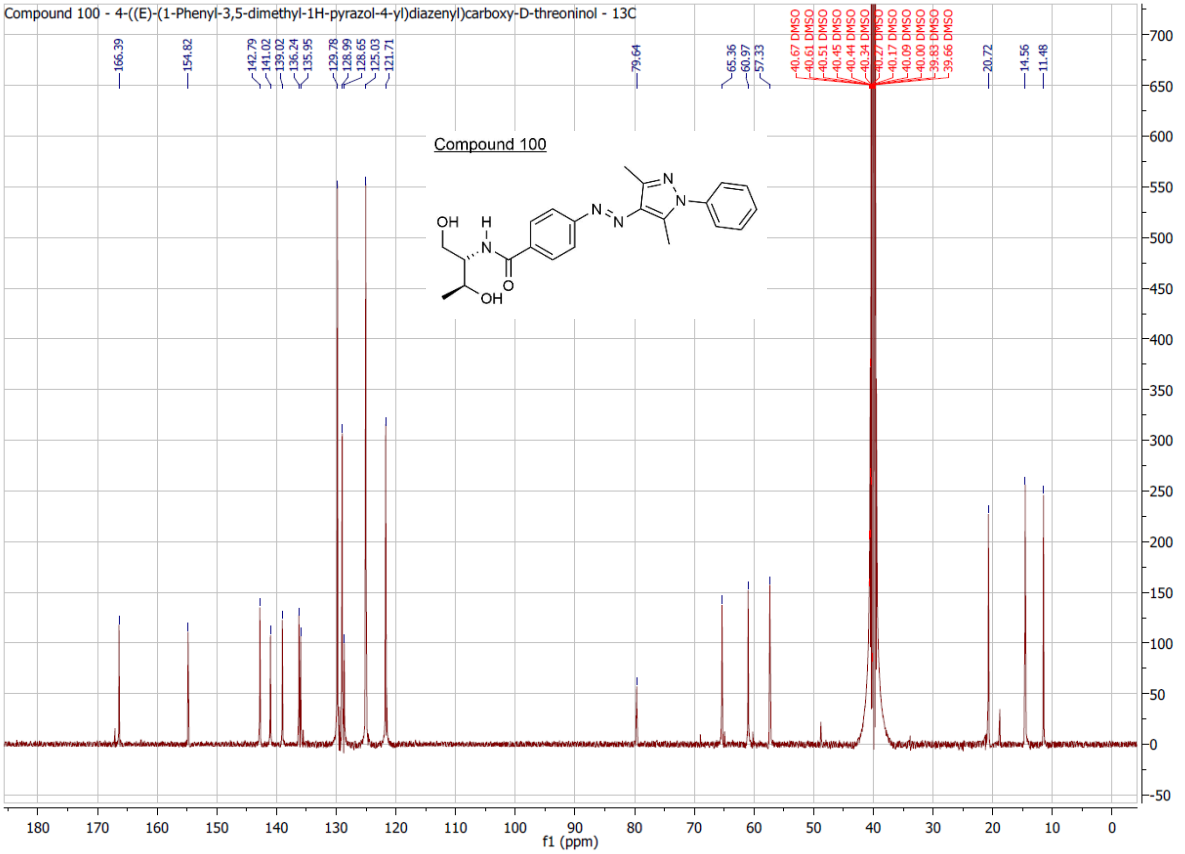
Compound 100 - 4-((E)-(1-Phenyl-3,5-dimethyl-1H-pyrazol-4-yl)diazenyl)carboxy-D-threoninol - 13C
Compound 100
f1 (ppm)

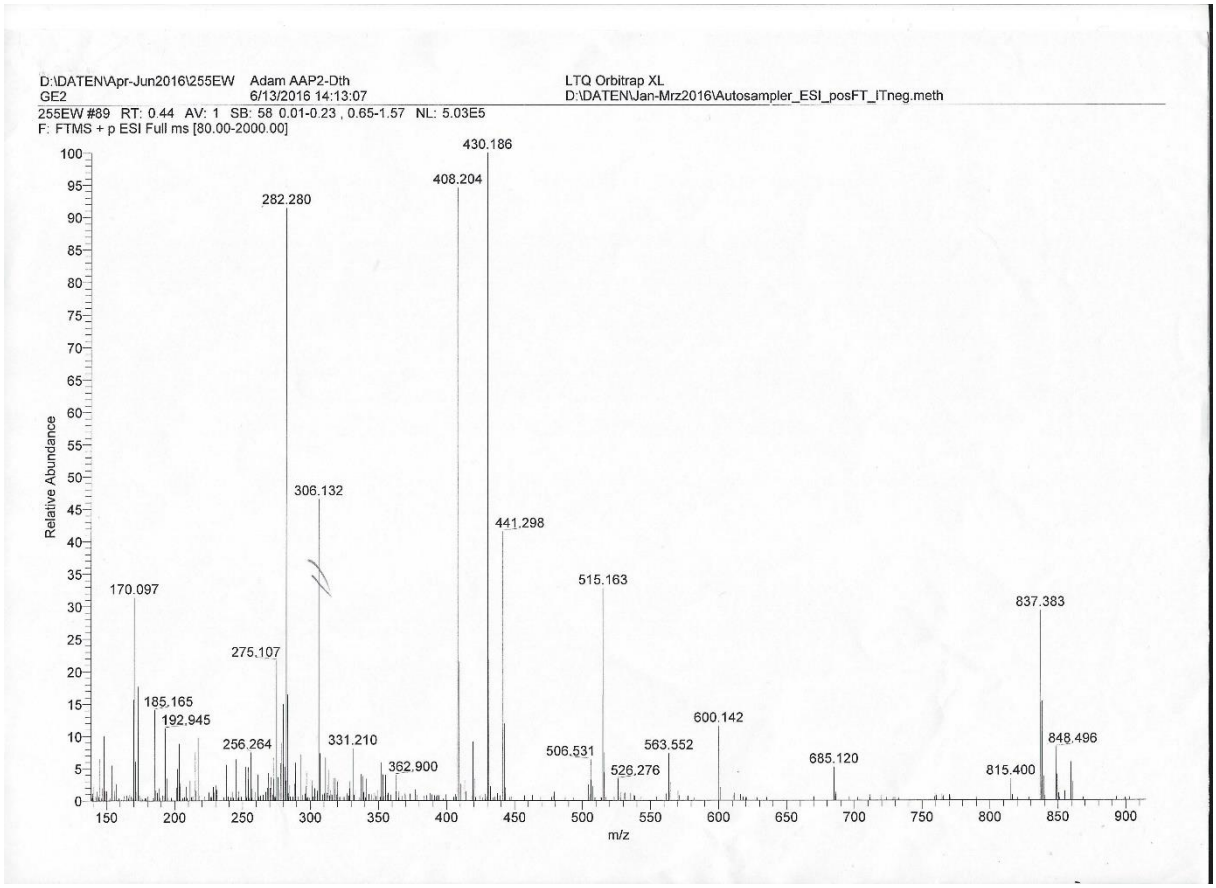
D:\DATEN\Apr-Jun2016\255EW Adam AAP2-Dth
GE2 6/13/2016 14:13:07
LTQ Orbitrap XL
D:\DATEN\Jan-Mrz2016\Autosampler_ESI_posFT_ITneg.meth
255EW #89 RT: 0.44 AV: 1 SB: 58 0.01-0.23 , 0.65-1.57 NL: 5.03E5
F: FTMS + p ESI Full ms [80.00-2000.00]
Relative Abundance
m/z
430.186
408.204
282.280
306.132
441.298
515.163
170.097
837.383
275.107
185.165
192.945
600.142
256.264
331.210
506.531
563.552
848.496
362.900
526.276
685.120
815.400

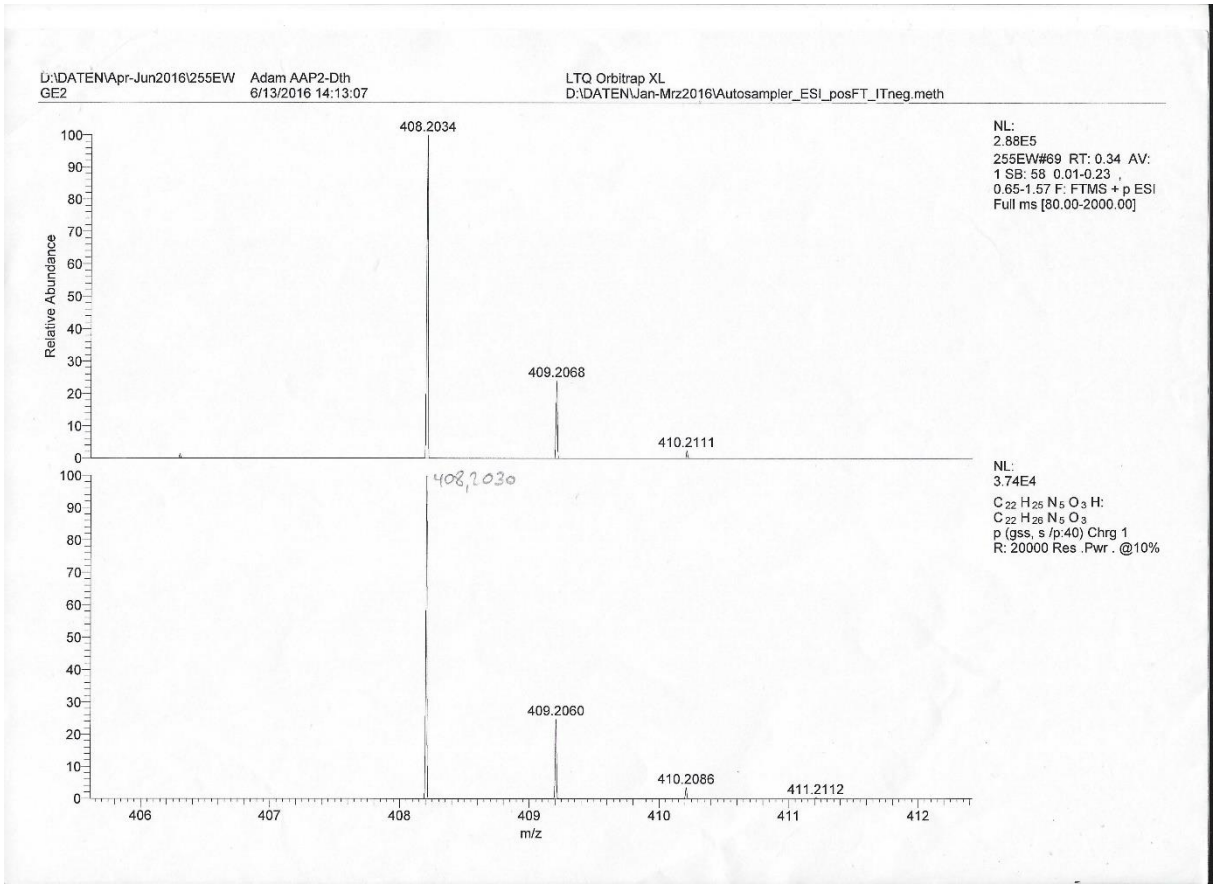
D:\DATEN\Apr-Jun2016\255EW Adam AAP2-Dth
GE2 6/13/2016 14:13:07
LTQ Orbitrap XL
D:\DATEN\Jan-Mrz2016\Autosampler_ESI_posFT_ITneg.meth
Relative Abundance
m/z
408.2034
409.2068
410.2111
NL:
2.88E5
255EW#69 RT: 0.34 AV:
1 SB: 58 0.01-0.23 ,
0.65-1.57 F: FTMS + p ESI
Full ms [80.00-2000.00]
408.2030
409.2060
410.2086
411.2112
NL:
3.74E4
C22 H25 N5 O3 H:
C22 H26 N5 O3
p (gss, s /p:40) Chrg 1
R: 20000 Res .Pwr . @10%

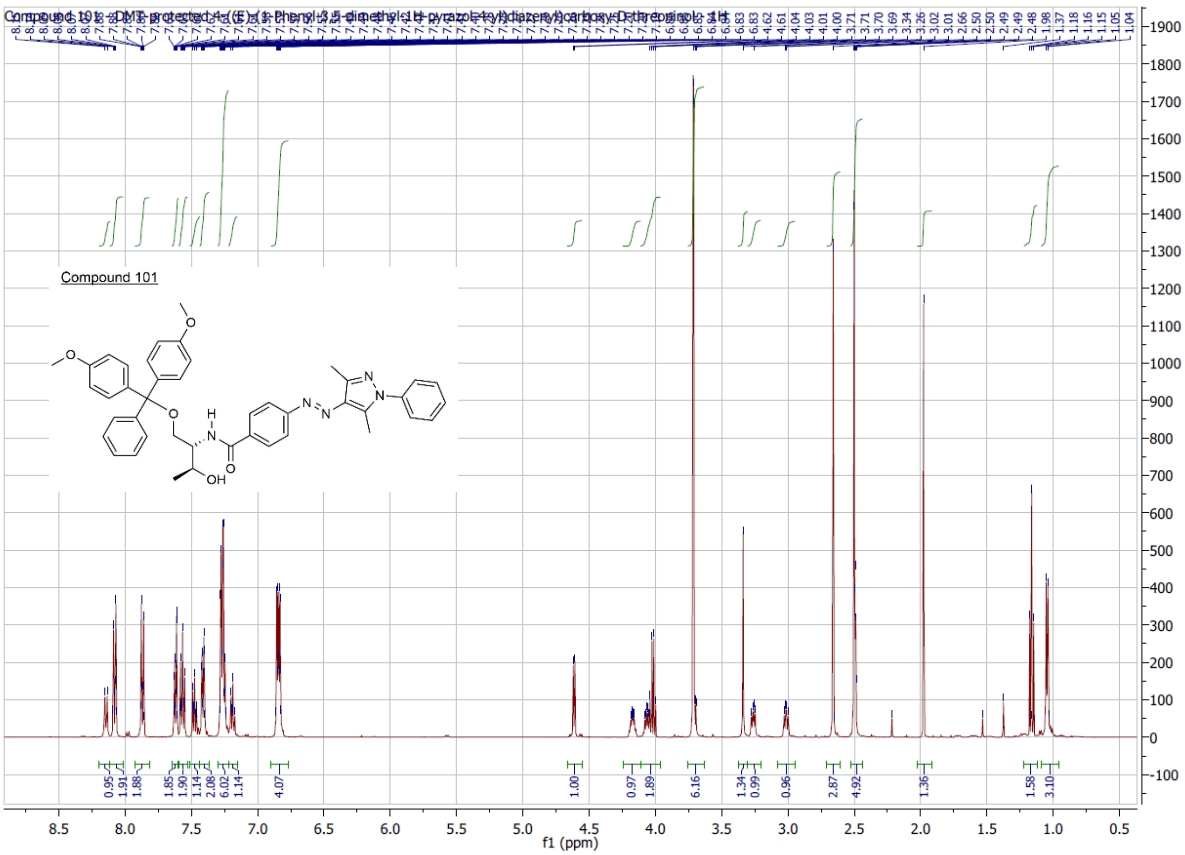
Compound 101 - DMT-protected 4-((E)-(1-Phenyl-3,5-dimethyl-1H-pyrazol-4-yl)diazenyl)carboxy-D-threoninol - 1H
Compound 101
f1 (ppm)

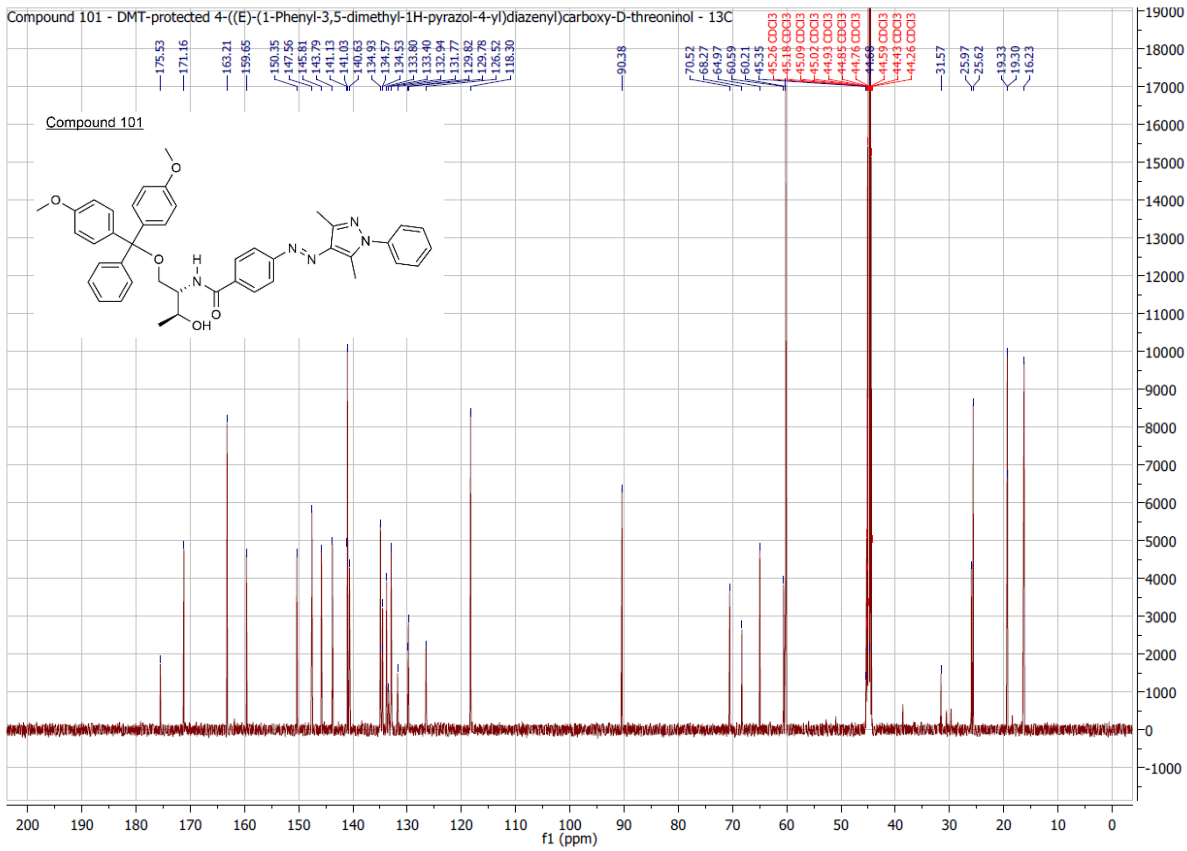
Compound 101 - DMT-protected 4-((E)-(1-Phenyl-3,5-dimethyl-1H-pyrazol-4-yl)diazenyl)carboxy-D-threoninol - 13C
Compound 101
f1 (ppm)

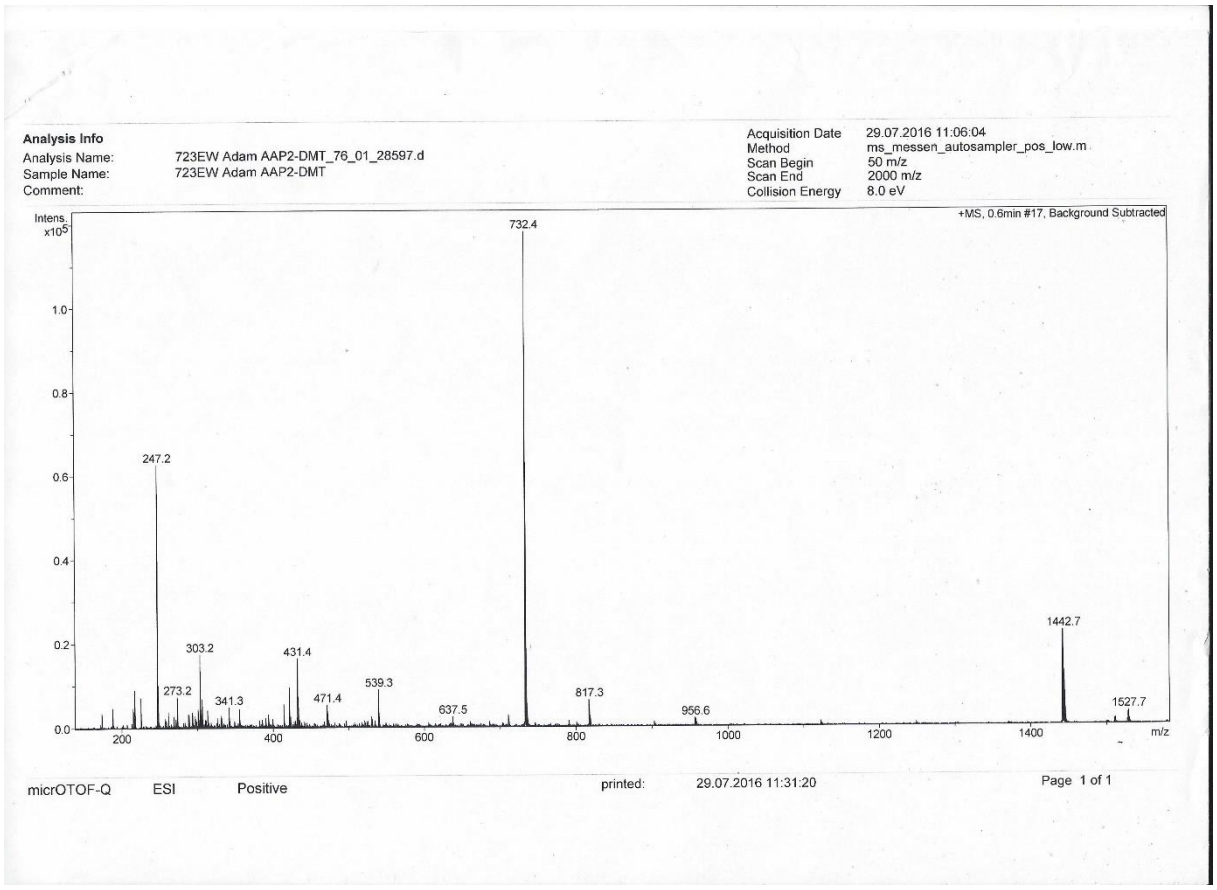
Analysis Info
Analysis Name: 723EW Adam AAP2-DMT_76_01_28597.d
Sample Name: 723EW Adam AAP2-DMT
Comment:
Acquisition Date 29.07.2016 11:06:04
Method ms_messen_autosampler_pos_low.m
Scan Begin 50 m/z
Scan End 2000 m/z
Collision Energy 8.0 eV
+MS, 0.6min #17, Background Subtracted
Intens.
x10^5
732.4
247.2
303.2
431.4
273.2
341.3
471.4
539.3
637.5
817.3
956.6
1442.7
1527.7
m/z
micrOTOF-Q ESI Positive
printed: 29.07.2016 11:31:20
Page 1 of 1

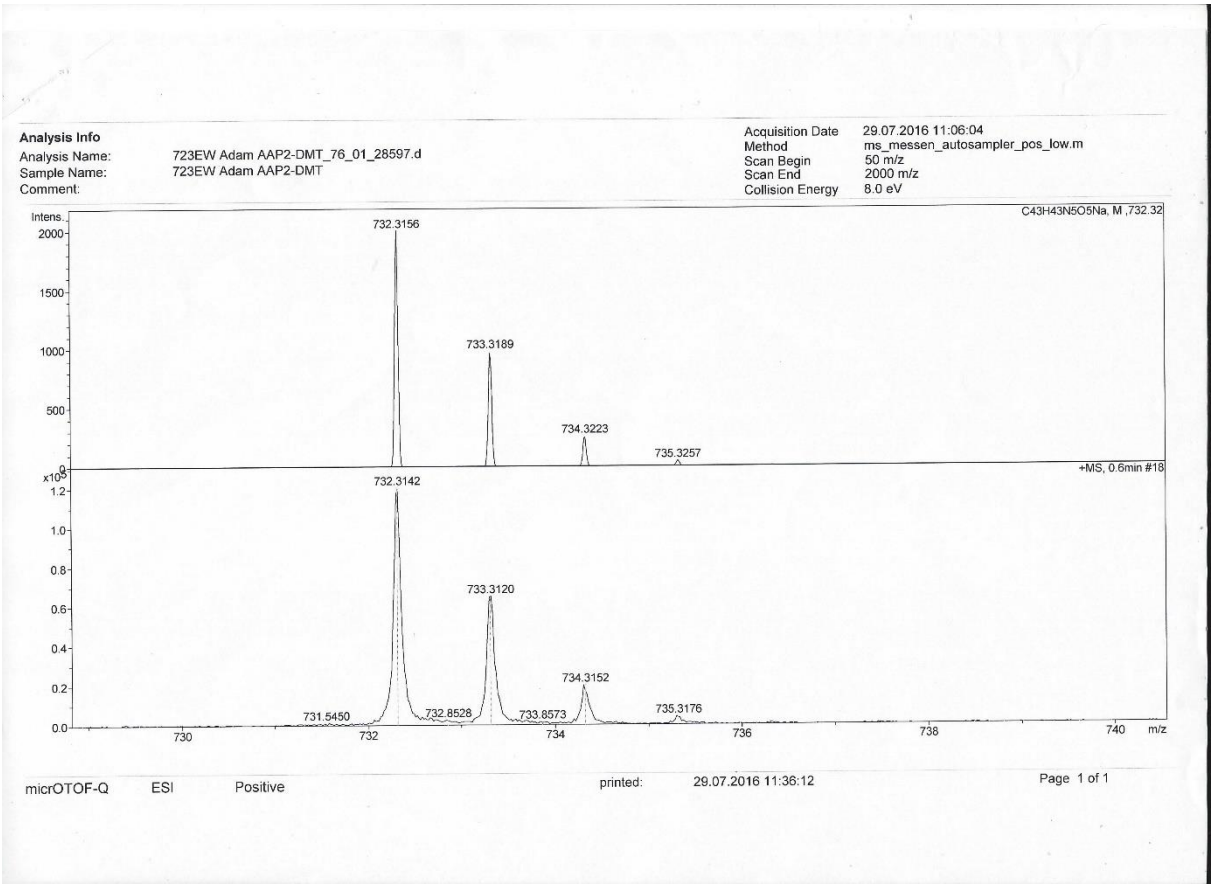
Analysis Info
Analysis Name: 723EW Adam AAP2-DMT_76_01_28597.d
Sample Name: 723EW Adam AAP2-DMT
Comment:
Acquisition Date 29.07.2016 11:06:04
Method ms_messen_autosampler_pos_low.m
Scan Begin 50 m/z
Scan End 2000 m/z
Collision Energy 8.0 eV
C43H43N5O5Na, M+, 732.32
Intens.
732.3156
733.3189
734.3223
735.3257
+MS, 0.6min #18
x10^5
732.3142
733.3120
734.3152
731.5450
732.8528
733.8573
735.3176
m/z
micrOTOF-Q ESI Positive
printed: 29.07.2016 11:36:12
Page 1 of 1

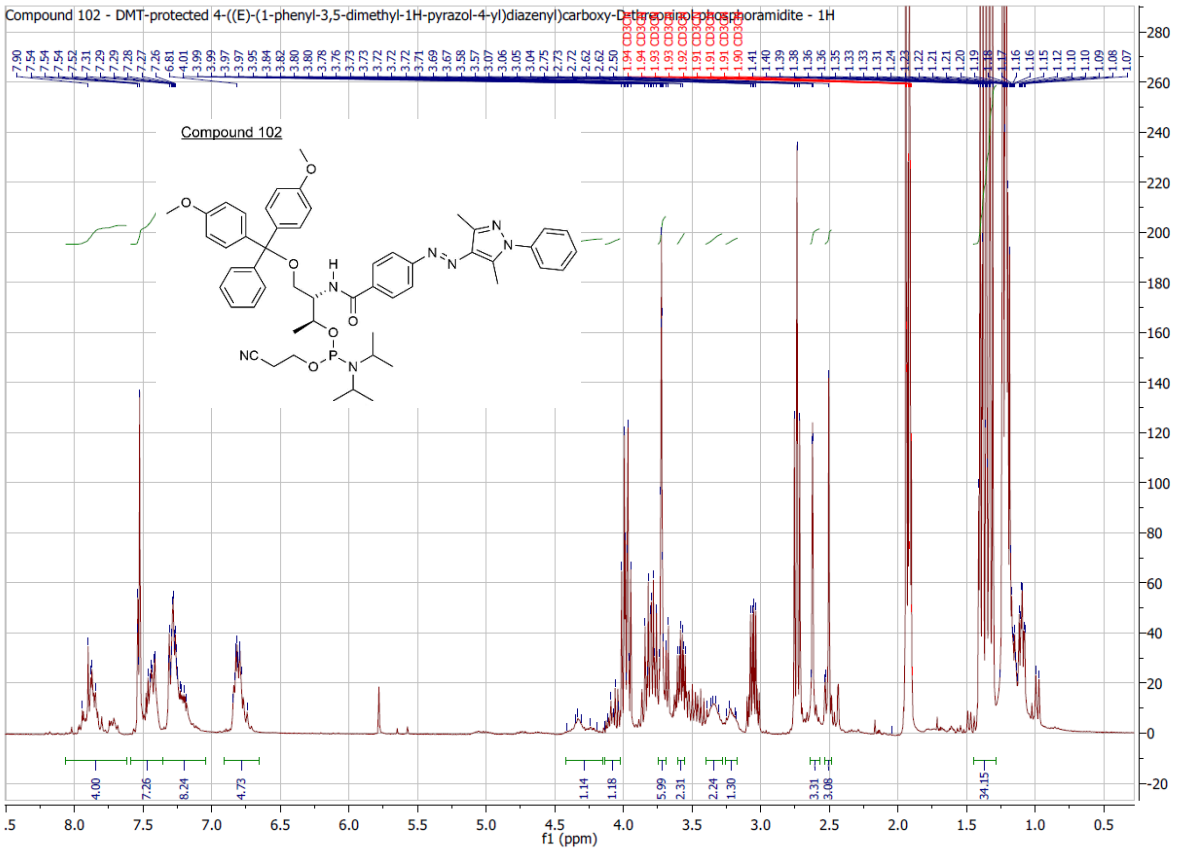
Compound 102 - DMT-protected 4-((E)-(1-phenyl-3,5-dimethyl-1H-pyrazol-4-yl)diazenyl)carboxy-D-threoninol-phosphoramidite - 1H
Compound 102
f1 (ppm)

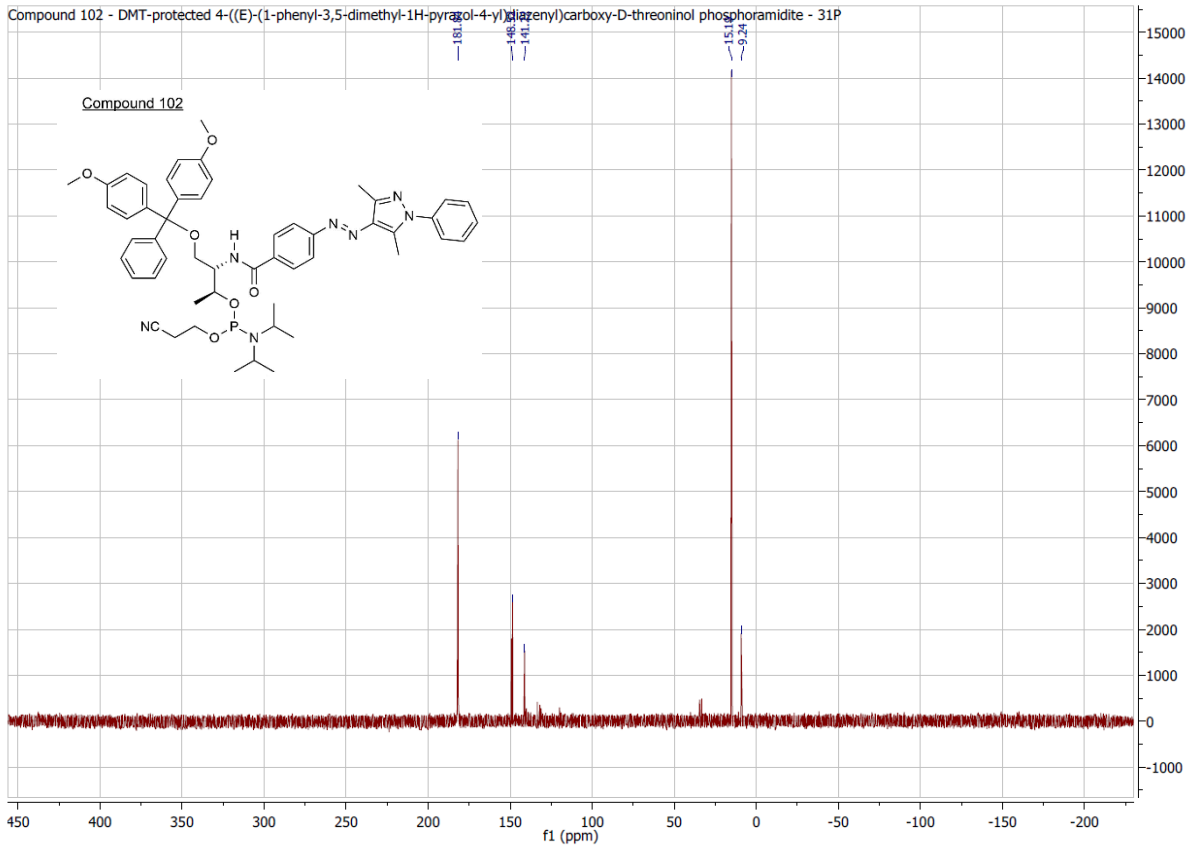
Compound 102 - DMT-protected 4-((E)-(1-phenyl-3,5-dimethyl-1H-pyrazol-4-yl)diazenyl)carboxy-D-threoninol phosphoramidite - 31P
Compound 102
f1 (ppm)

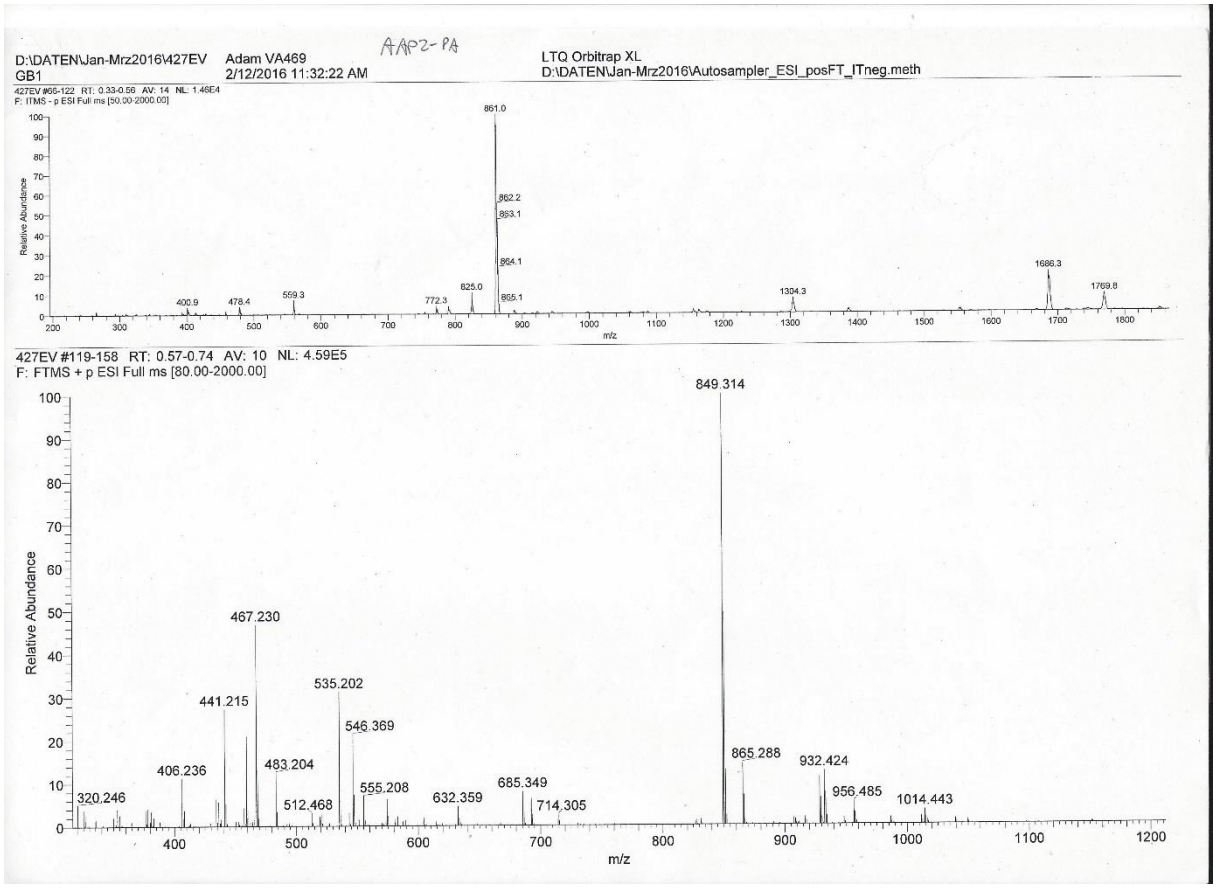
D:\DATEN\Jan-Mrz2016\427EV
GB1
Adam VA469
2/12/2016 11:32:22 AM
AAP2-PA
LTQ Orbitrap XL
D:\DATEN\Jan-Mrz2016\Autosampler_ESI_posFT_ITneg.meth
427EV #66-122 RT: 0.33-0.56 AV: 14 NL: 1.48E4
F: ITMS - p ESI Full ms [50.00-2000.00]
Relative Abundance
m/z
861.0
862.2
863.1
864.1
865.1
825.0
772.3
559.3
478.4
400.9
1304.3
1686.3
1769.8
427EV #119-158 RT: 0.57-0.74 AV: 10 NL: 4.59E5
F: FTMS + p ESI Full ms [80.00-2000.00]
849.314
467.230
535.202
441.215
546.369
483.204
406.236
320.246
512.468
555.208
632.359
685.349
714.305
865.288
932.424
956.485
1014.443

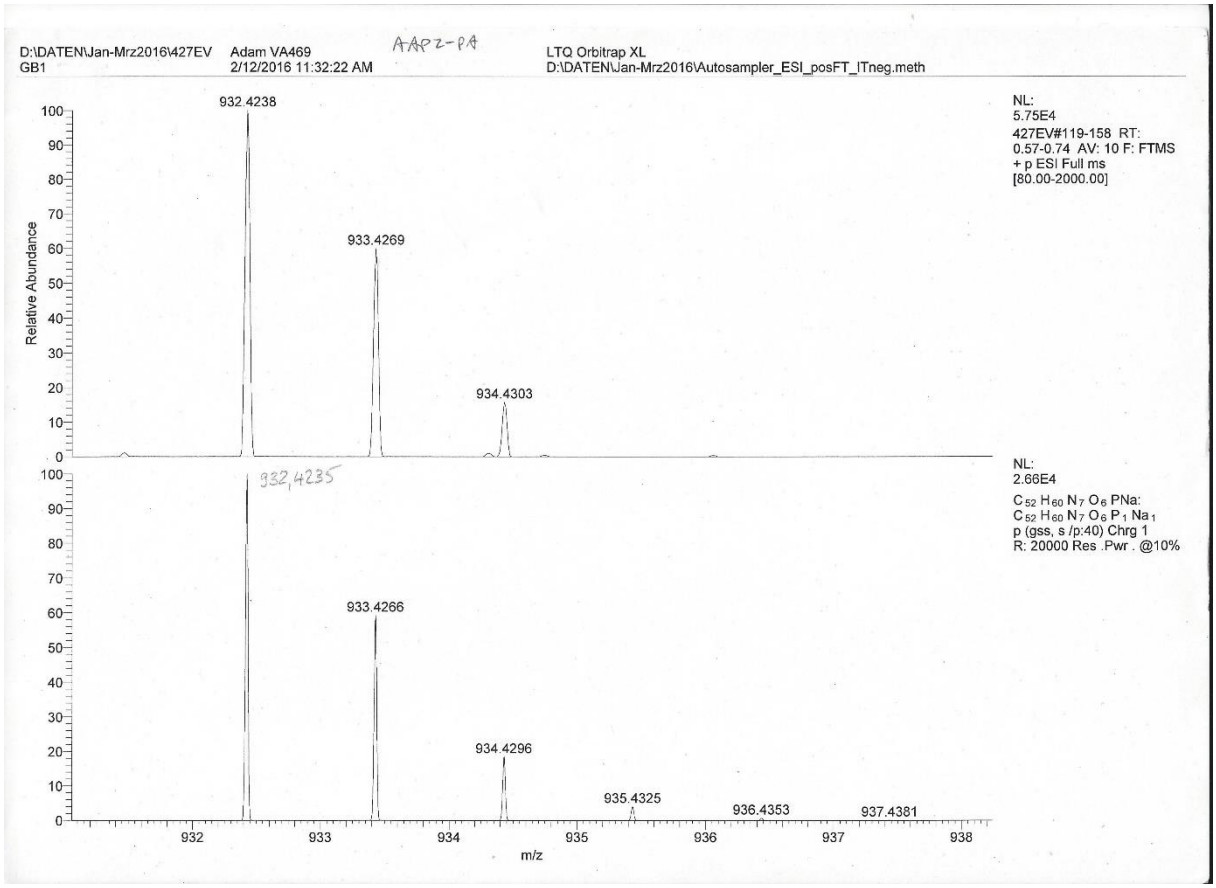
D:\DATEN\Jan-Mrz2016\427EV
GB1
Adam VA469
2/12/2016 11:32:22 AM
AAP2-PA
LTQ Orbitrap XL
D:\DATEN\Jan-Mrz2016\Autosampler_ESI_posFT_ITneg.meth
Relative Abundance
m/z
932.4238
933.4269
934.4303
NL:
5.75E4
427EV#119-158 RT:
0.57-0.74 AV: 10 F: FTMS
+ p ESI Full ms
[80.00-2000.00]
932.4235
933.4266
934.4296
935.4325
936.4353
937.4381
NL:
2.66E4
C52 H60 N7 O6 PNa:
C52 H60 N7 O6 P1 Na1
p (gss, s /p:40) Chrg 1
R: 20000 Res .Pwr . @10%

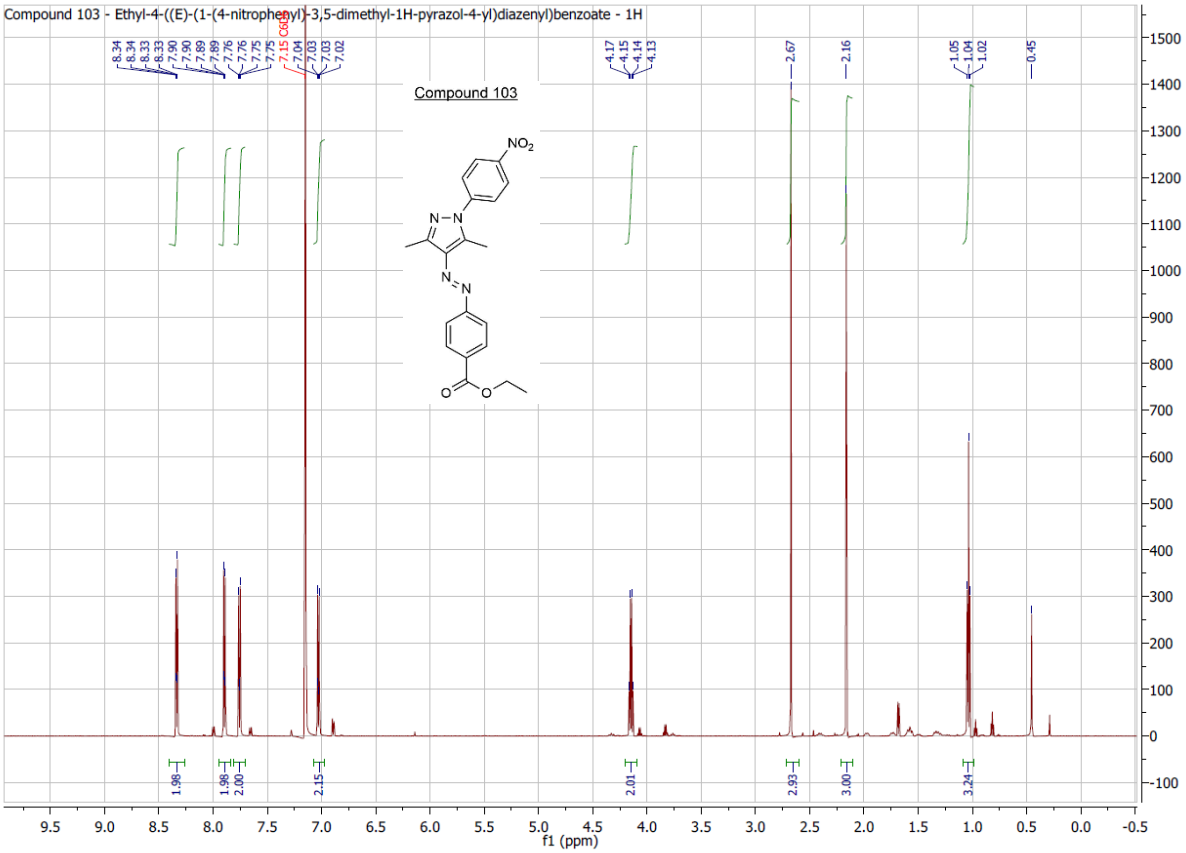
Compound 103 - Ethyl-4-((E)-(1-(4-nitrophenyl)-3,5-dimethyl-1H-pyrazol-4-yl)diazenyl)benzoate - 1H
Compound 103
f1 (ppm)

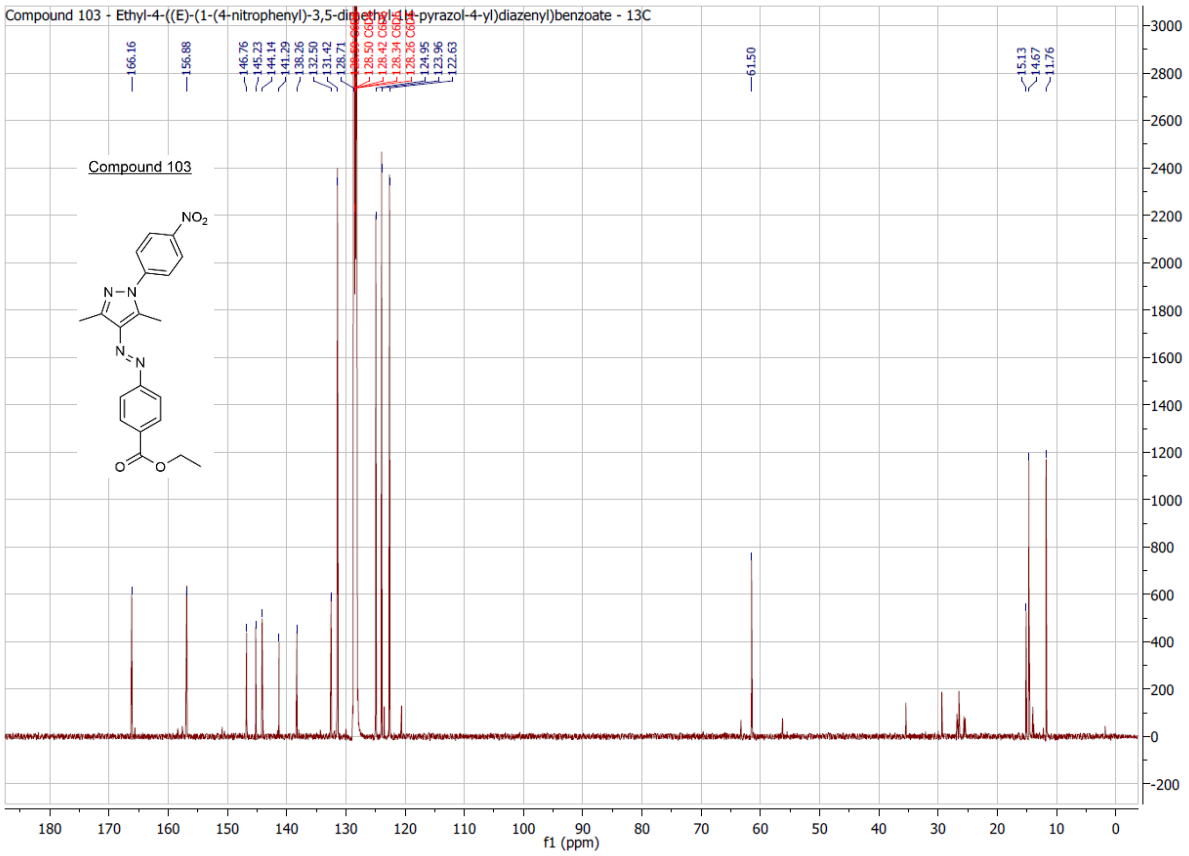
Compound 103 - Ethyl-4-((E)-(1-(4-nitrophenyl)-3,5-dimethyl-1H-pyrazol-4-yl)diazenyl)benzoate - 13C
Compound 103
f1 (ppm)

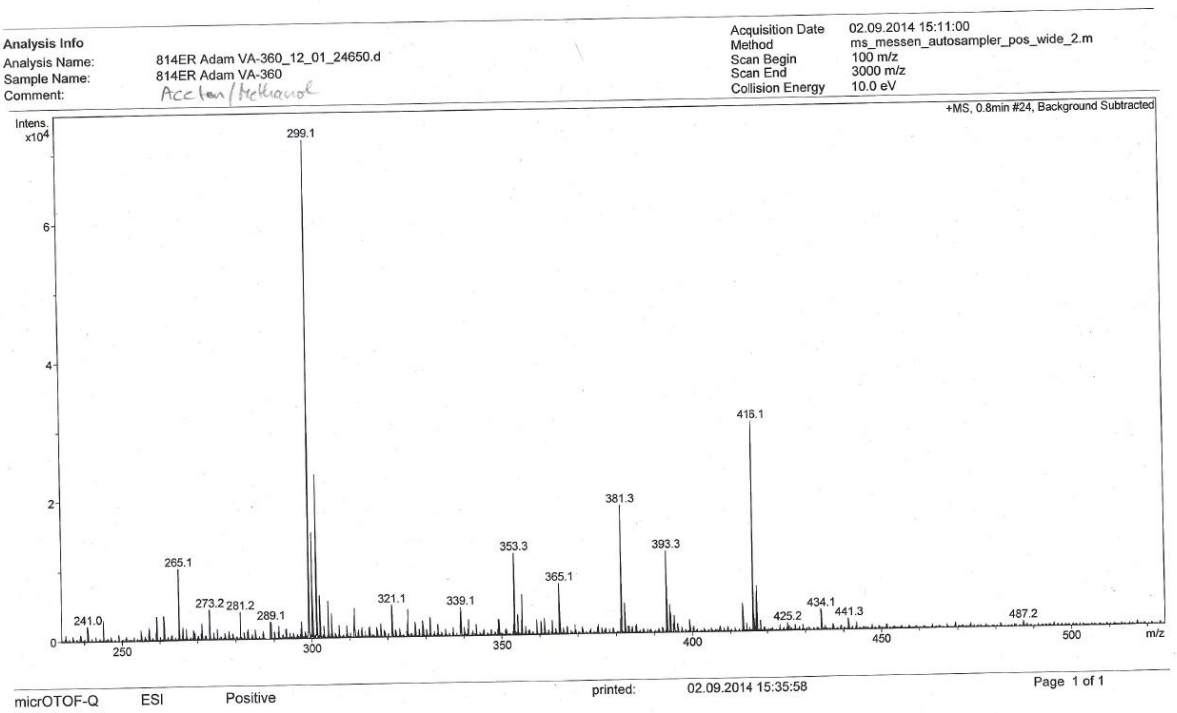
Analysis Info
Analysis Name: 814ER Adam VA-360_12_01_24650.d
Sample Name: 814ER Adam VA-360
Comment: Acetone/Methanol
Acquisition Date 02.09.2014 15:11:00
Method ms_messen_autosampler_pos_wide_2.m
Scan Begin 100 m/z
Scan End 3000 m/z
Collision Energy 10.0 eV
+MS, 0.8min #24, Background Subtracted
Intens. x10^4
299.1
416.1
381.3
353.3
393.3
265.1
365.1
273.2
281.2
289.1
321.1
339.1
241.0
425.2
434.1
441.3
487.2
m/z
micrOTOF-Q ESI Positive
printed: 02.09.2014 15:35:58
Page 1 of 1

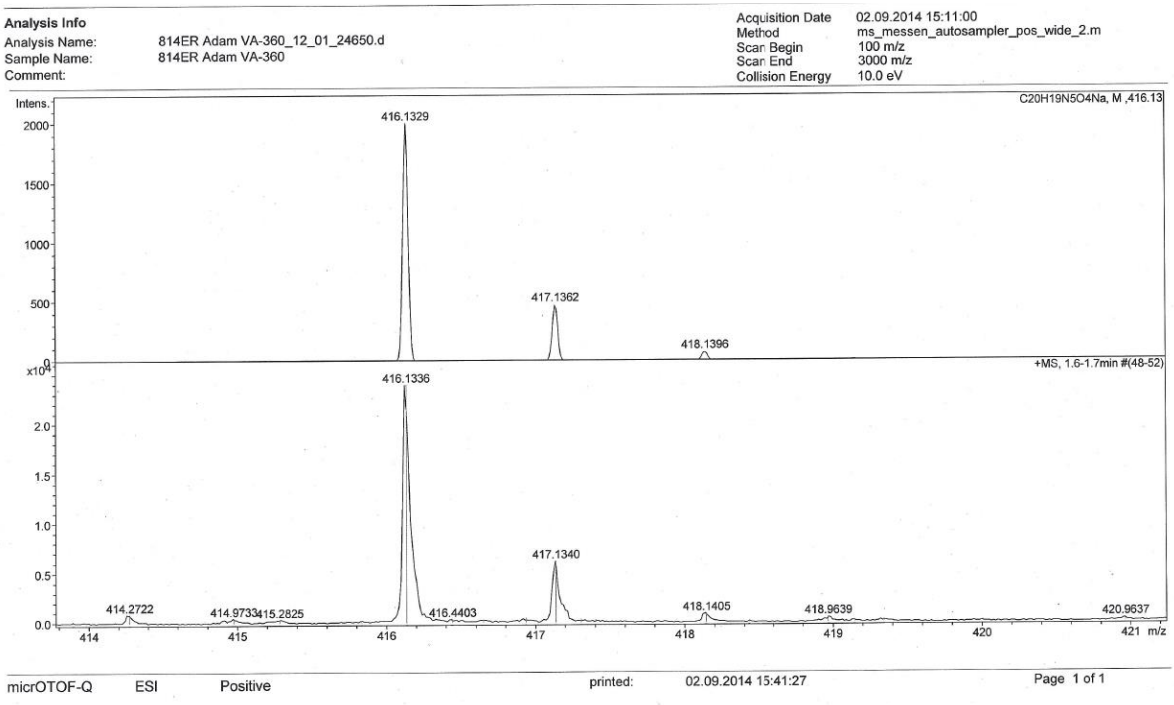
Analysis Info
Analysis Name: 814ER Adam VA-360_12_01_24650.d
Sample Name: 814ER Adam VA-360
Comment:
Acquisition Date 02.09.2014 15:11:00
Method ms_messen_autosampler_pos_wide_2.m
Scan Begin 100 m/z
Scan End 3000 m/z
Collision Energy 10.0 eV
C20H19N5O4Na, M ,416.13
Intens.
416.1329
417.1362
418.1396
+MS, 1.6-1.7min #(48-52)
x10^4
416.1336
417.1340
414.2722
414.9733
415.2825
416.4403
418.1405
418.9639
420.9637
m/z
micrOTOF-Q ESI Positive
printed: 02.09.2014 15:41:27
Page 1 of 1

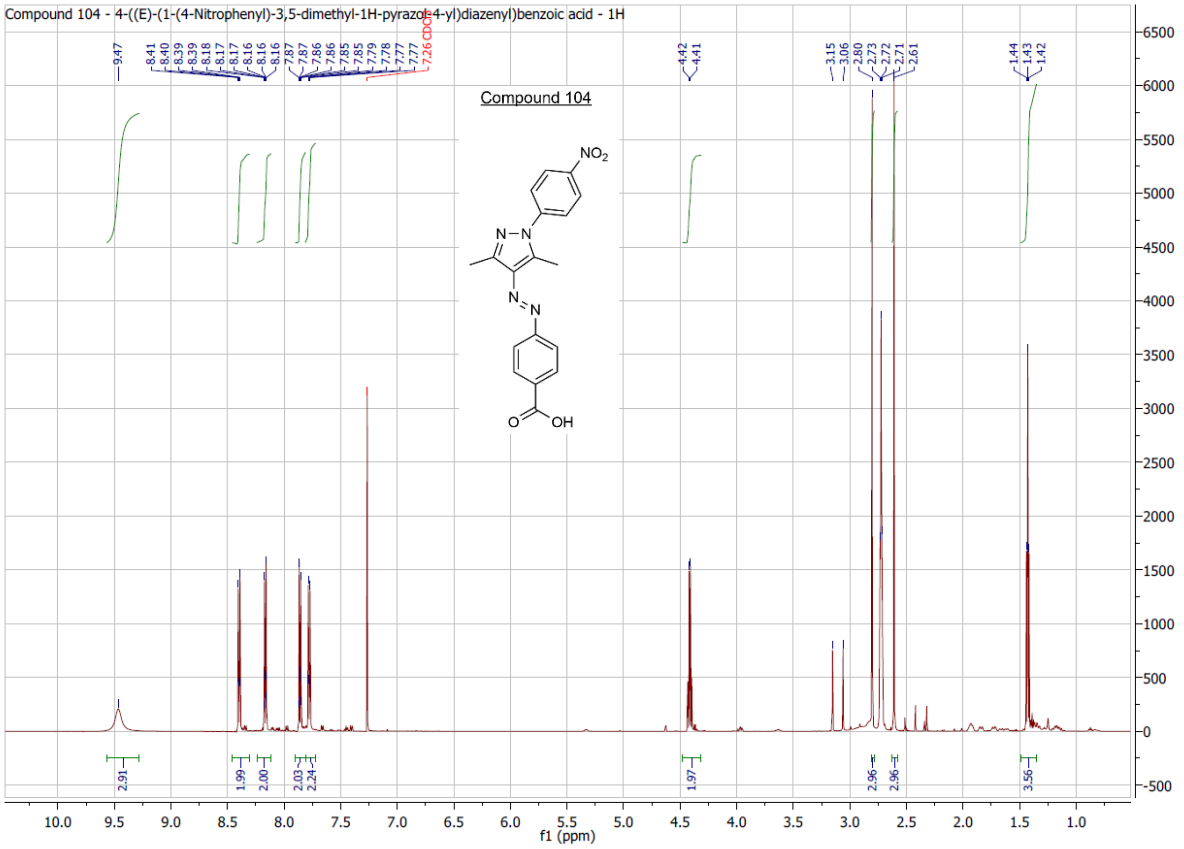
Compound 104 - 4-((E)-(1-(4-Nitrophenyl)-3,5-dimethyl-1H-pyrazol-4-yl)diazenyl)benzoic acid - 1H
Compound 104
f1 (ppm)

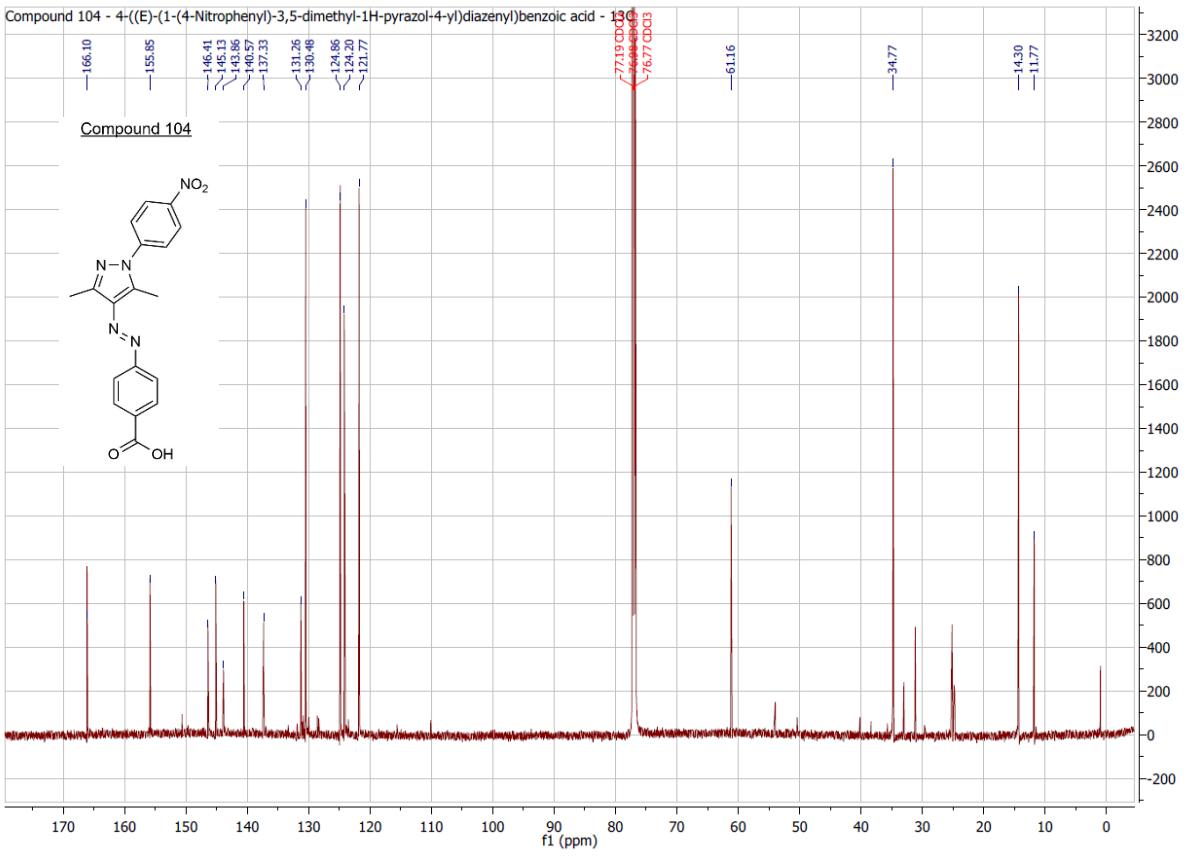
Compound 104 - 4-((E)-(1-(4-Nitrophenyl)-3,5-dimethyl-1H-pyrazol-4-yl)diazenyl)benzoic acid - 13C
Compound 104
f1 (ppm)

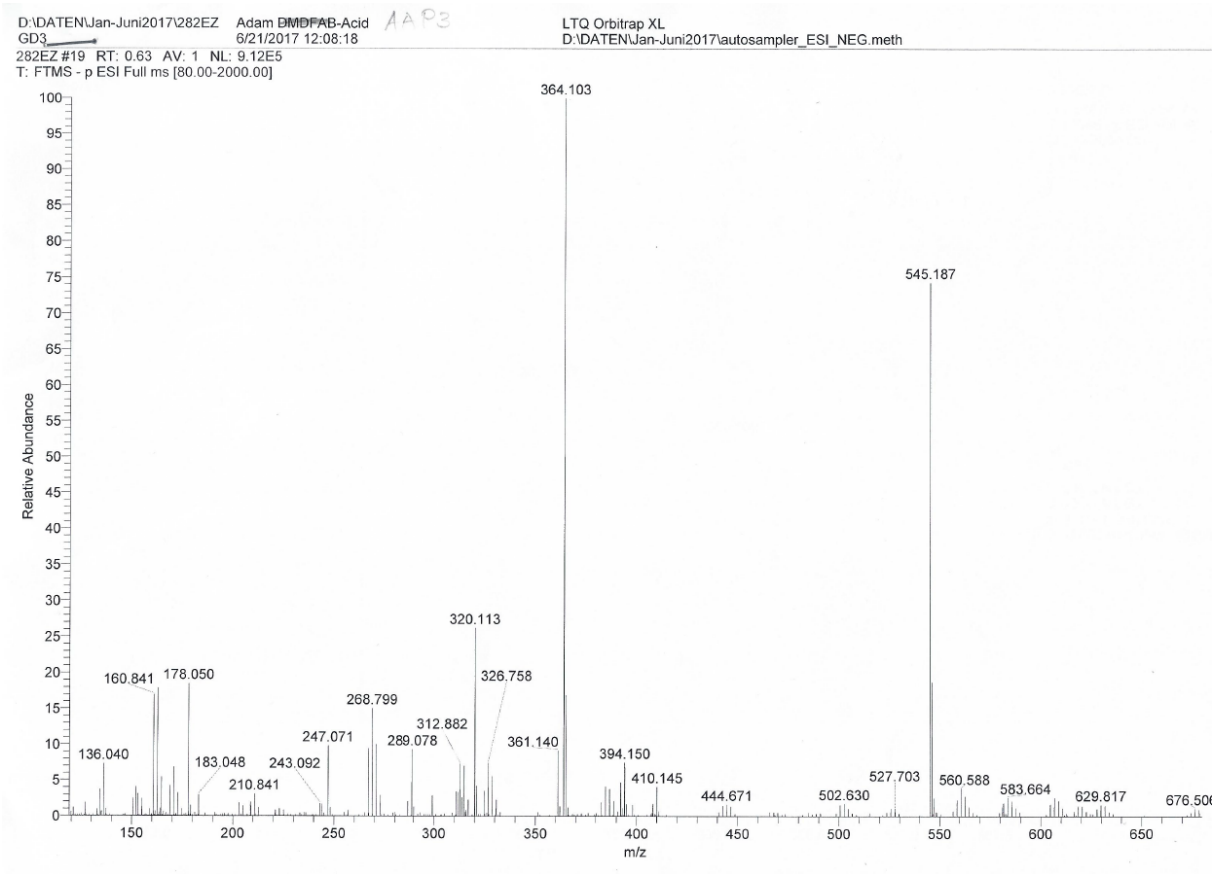
D:\DATEN\Jan-Juni2017\282EZ
GD3
Adam BMDFAB-Acid
6/21/2017 12:08:18
LTQ Orbitrap XL
D:\DATEN\Jan-Juni2017\autosampler_ESI_NEG.meth
282EZ #19 RT: 0.63 AV: 1 NL: 9.12E5
T: FTMS - p ESI Full ms [80.00-2000.00]
Relative Abundance
m/z
364.103
545.187
320.113
160.841
178.050
326.758
268.799
312.882
247.071
289.078
361.140
136.040
183.048
243.092
394.150
410.145
210.841
444.671
502.630
527.703
560.588
583.664
629.817

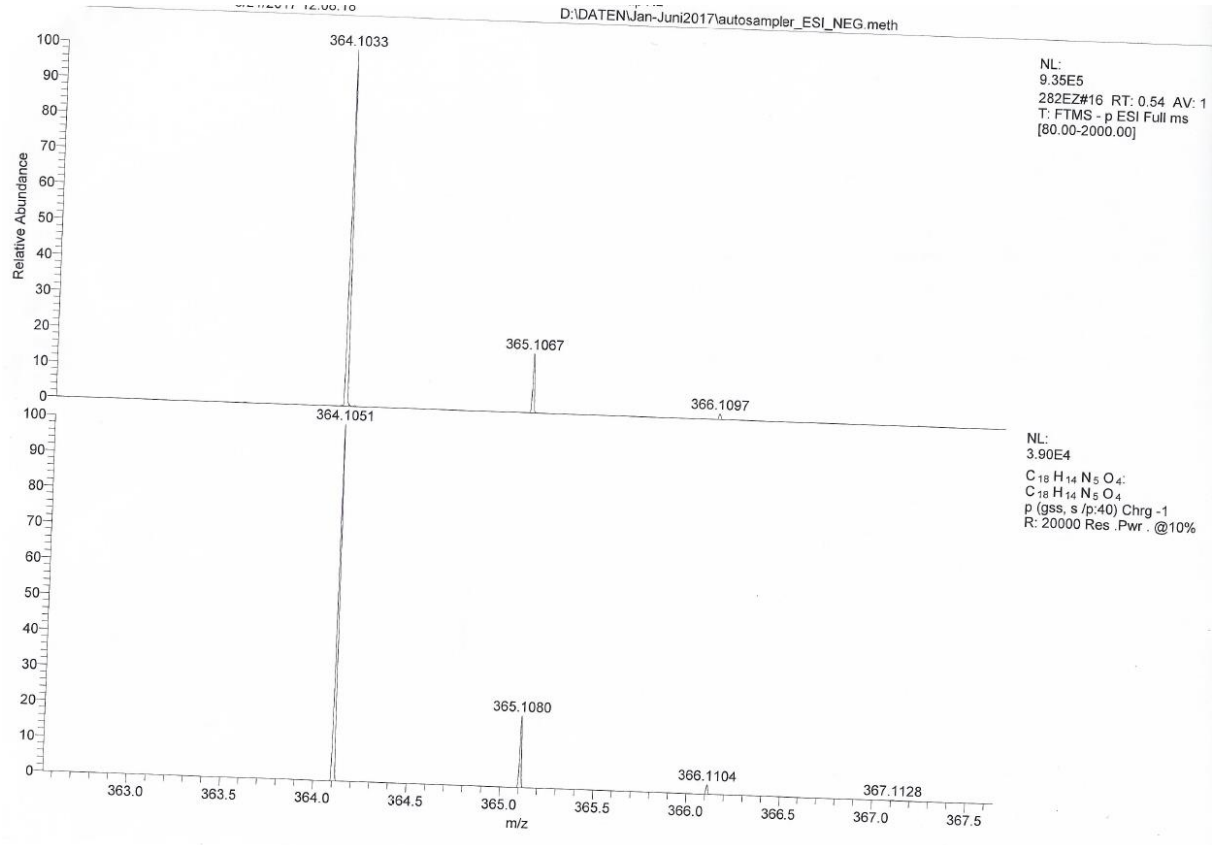
D:\DATEN\Jan-Juni2017\autosampler_ESI_NEG.meth
Relative Abundance
m/z
364.1033
365.1067
366.1097
NL:
9.35E5
282EZ#16 RT: 0.54 AV: 1
T: FTMS - p ESI Full ms
[80.00-2000.00]
364.1051
365.1080
366.1104
367.1128
NL:
3.90E4
C18 H14 N5 O4:
C18 H14 N5 O4
p (gss, s /p:40) Chrg -1
R: 20000 Res .Pwr . @10%

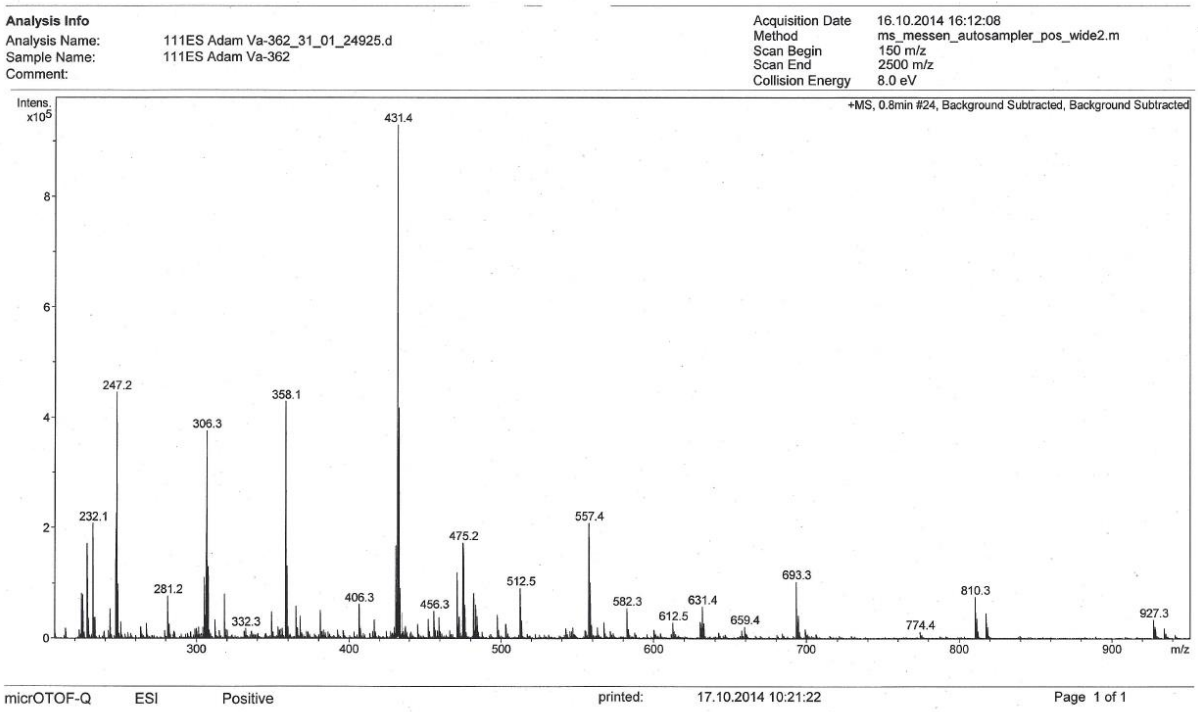
Analysis Info
Analysis Name: 111ES Adam Va-362_31_01_24925.d
Sample Name: 111ES Adam Va-362
Comment:
Acquisition Date 16.10.2014 16:12:08
Method ms_messen_autosampler_pos_wide2.m
Scan Begin 150 m/z
Scan End 2500 m/z
Collision Energy 8.0 eV
Intens.
x10^5
+MS, 0.8min #24, Background Subtracted, Background Subtracted
431.4
247.2
358.1
306.3
232.1
557.4
475.2
693.3
512.5
281.2
406.3
582.3
631.4
810.3
456.3
612.5
659.4
927.3
332.3
774.4
m/z
micrOTOF-Q ESI Positive
printed: 17.10.2014 10:21:22
Page 1 of 1

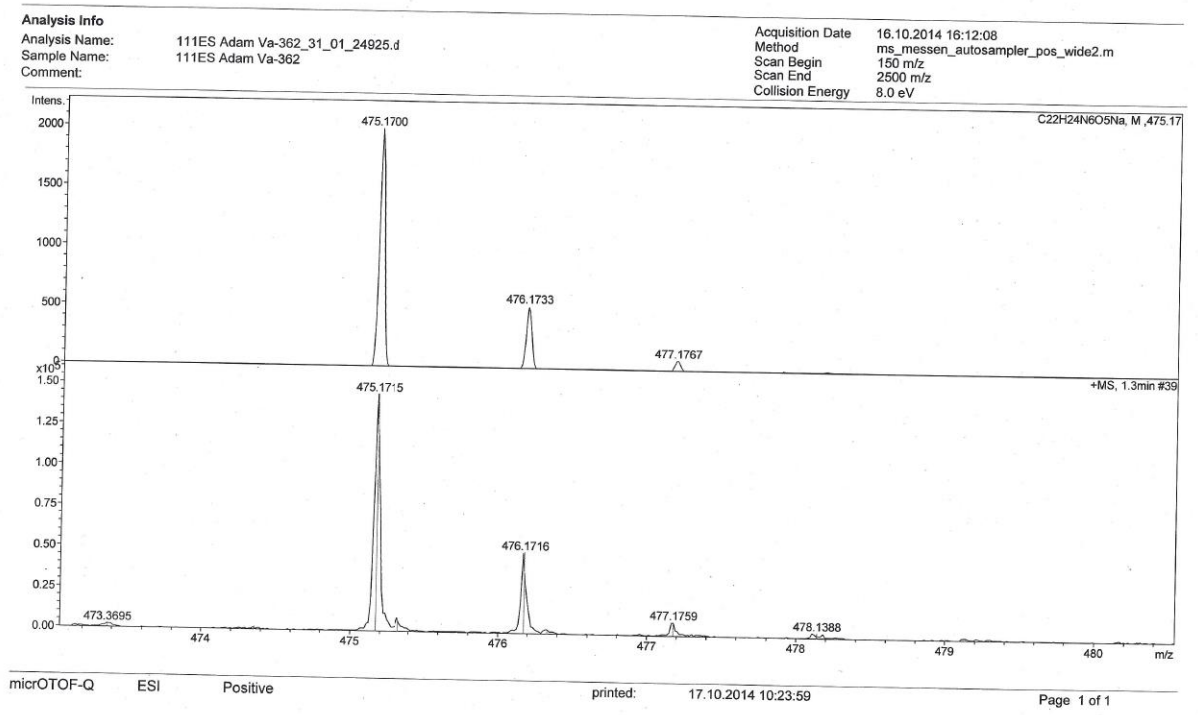
Analysis Info
Analysis Name: 111ES Adam Va-362_31_01_24925.d
Sample Name: 111ES Adam Va-362
Comment:
Acquisition Date 16.10.2014 16:12:08
Method ms_messen_autosampler_pos_wide2.m
Scan Begin 150 m/z
Scan End 2500 m/z
Collision Energy 8.0 eV
Intens.
C22H24N6O5Na, M ,475.17
475.1700
476.1733
477.1767
x10^5
+MS, 1.3min #39
475.1715
476.1716
473.3695
477.1759
478.1388
m/z
micrOTOF-Q ESI Positive
printed: 17.10.2014 10:23:59
Page 1 of 1

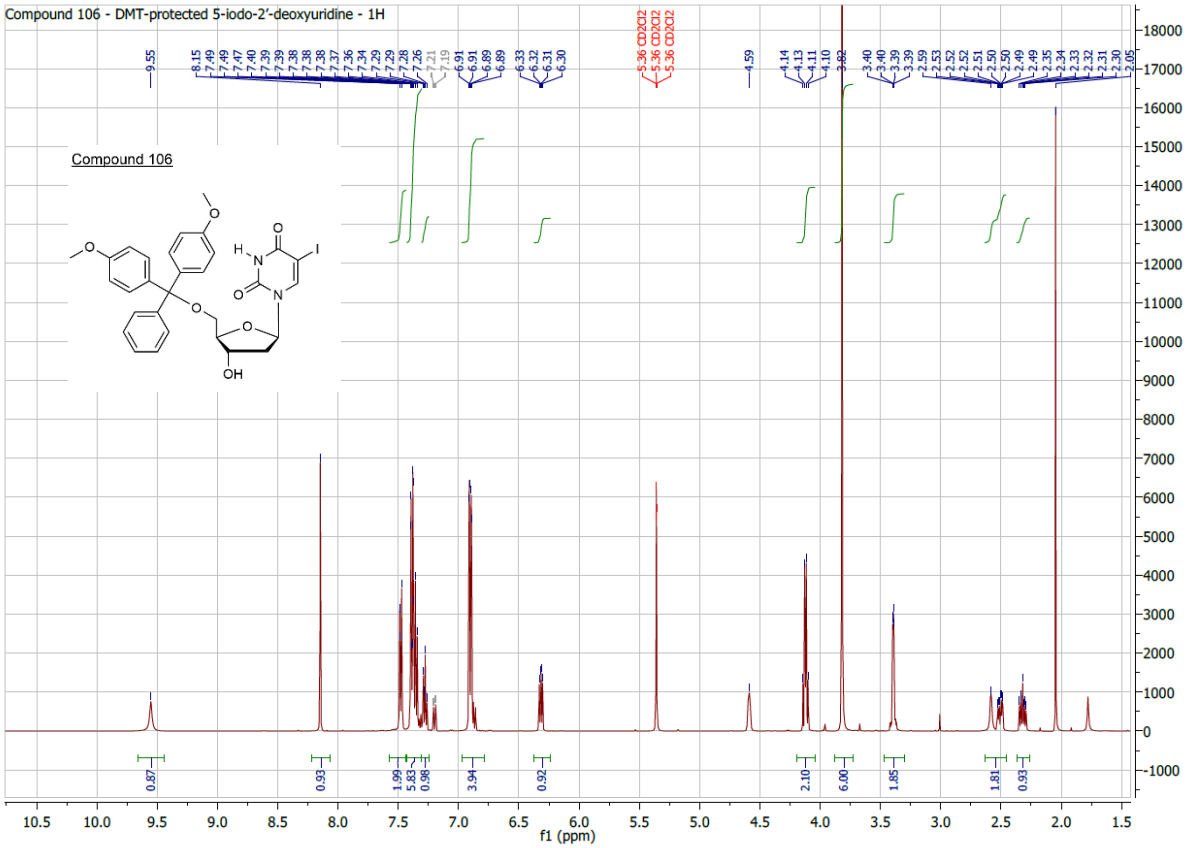
Compound 106 - DMT-protected 5-iodo-2'-deoxyuridine - 1H
Compound 106
f1 (ppm)

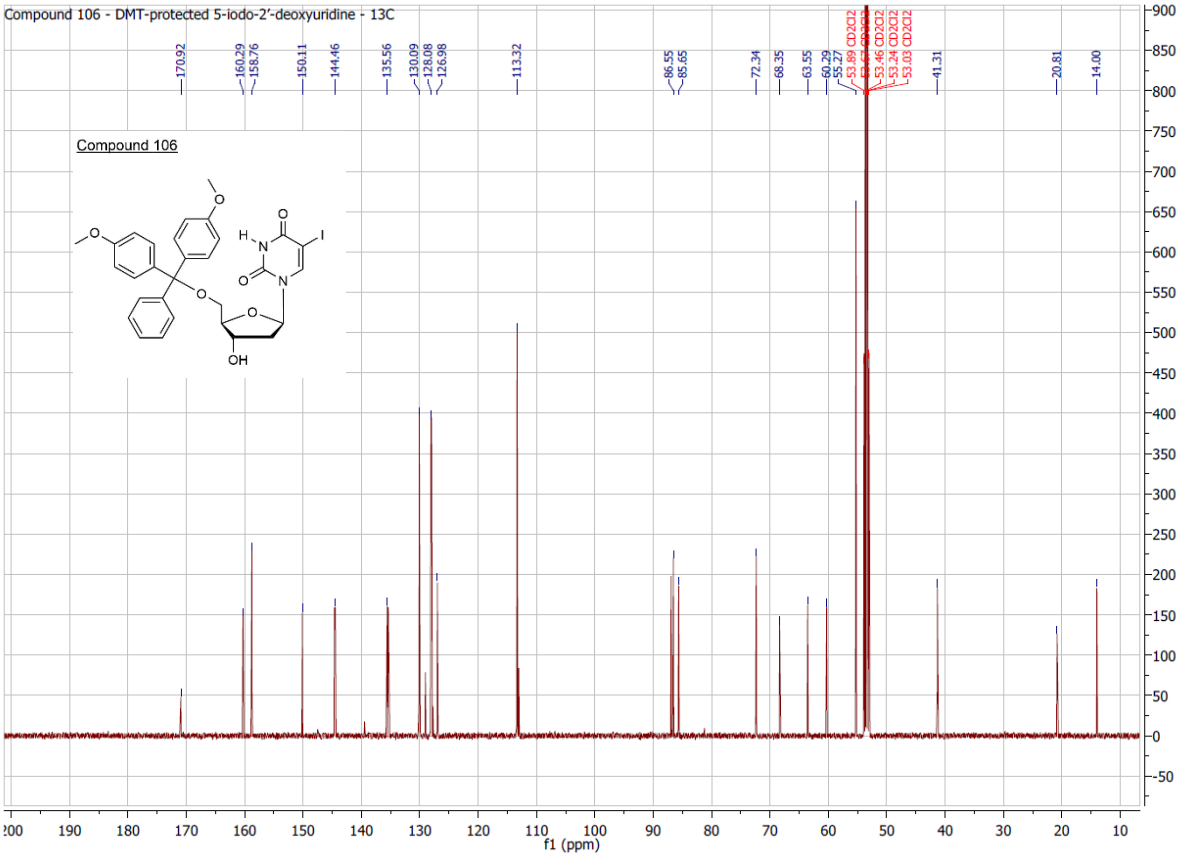
Compound 106 - DMT-protected 5-iodo-2'-deoxyuridine - 13C
Compound 106
f1 (ppm)

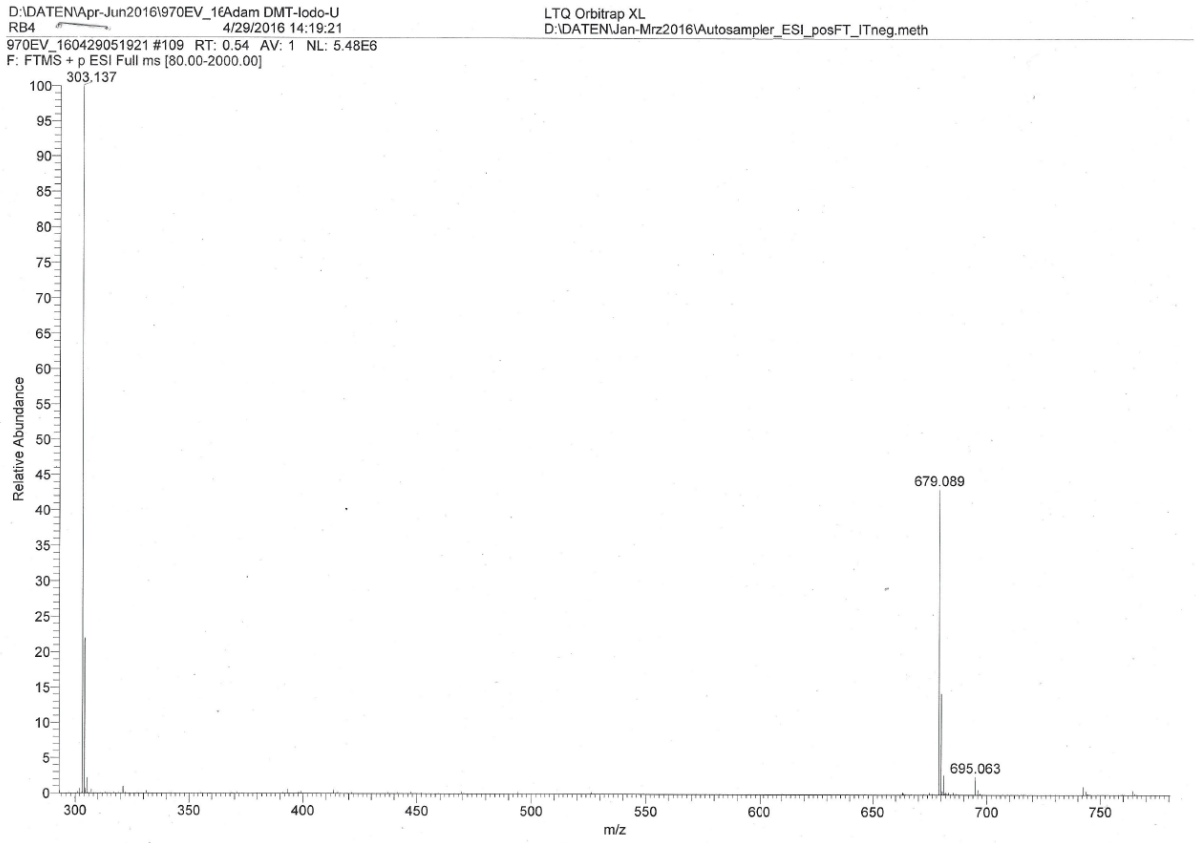
D:\DATEN\Apr-Jun2016\970EV_16Adam DMT-Iodo-U
RB4 4/29/2016 14:19:21
LTQ Orbitrap XL
D:\DATEN\Jan-Mrz2016\Autosampler_ESI_posFT_ITneg.meth
970EV_160429051921 #109 RT: 0.54 AV: 1 NL: 5.48E6
F: FTMS + p ESI Full ms [80.00-2000.00]
303.137
679.089
695.063
Relative Abundance
m/z

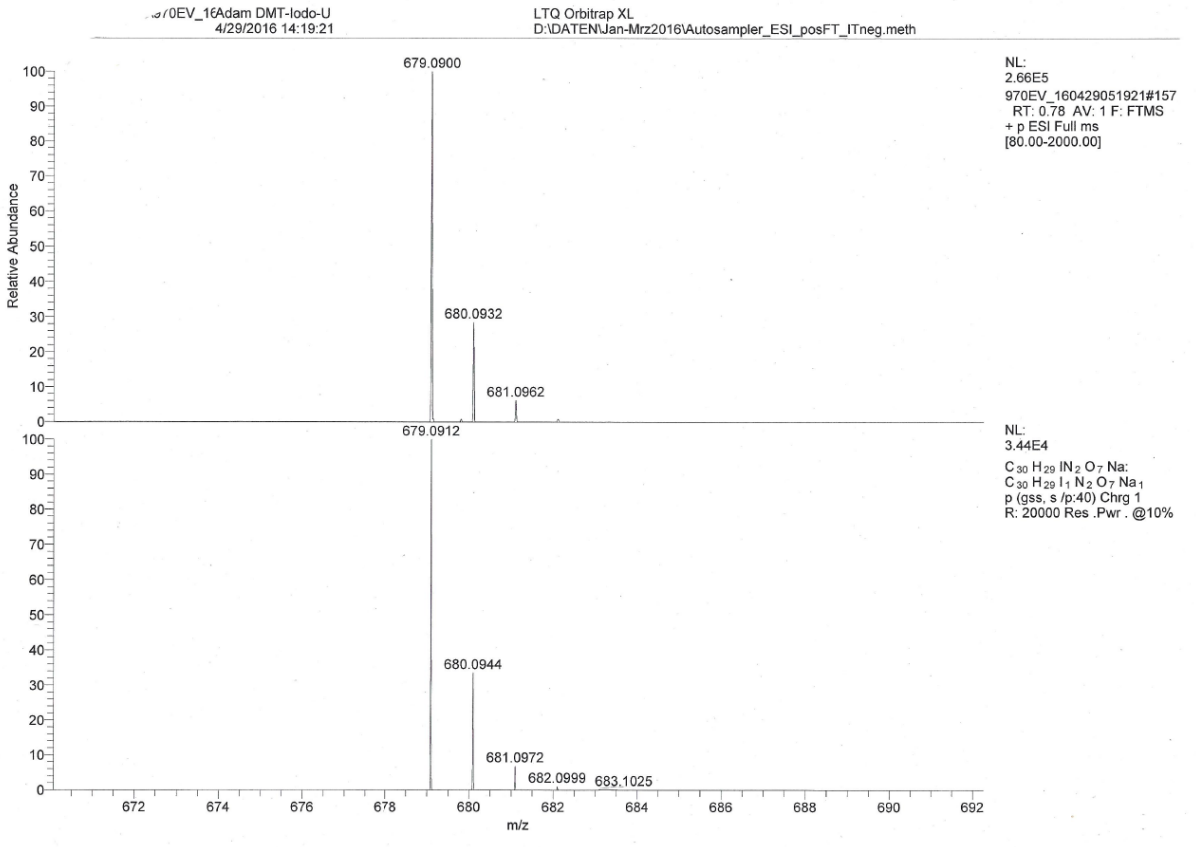
970EV_16Adam DMT-Iodo-U
4/29/2016 14:19:21
LTQ Orbitrap XL
D:\DATEN\Jan-Mrz2016\Autosampler_ESI_posFT_ITneg.meth
679.0900
680.0932
681.0962
679.0912
680.0944
681.0972
682.0999
683.1025
NL:
2.66E5
970EV_160429051921#157
RT: 0.78 AV: 1 F: FTMS
+ p ESI Full ms
[80.00-2000.00]
NL:
3.44E4
C30 H29 IN2 O7 Na;
C30 H29 I1 N2 O7 Na1
p (gss, s /p:40) Chrg 1
R: 20000 Res .Pwr . @10%
Relative Abundance
m/z

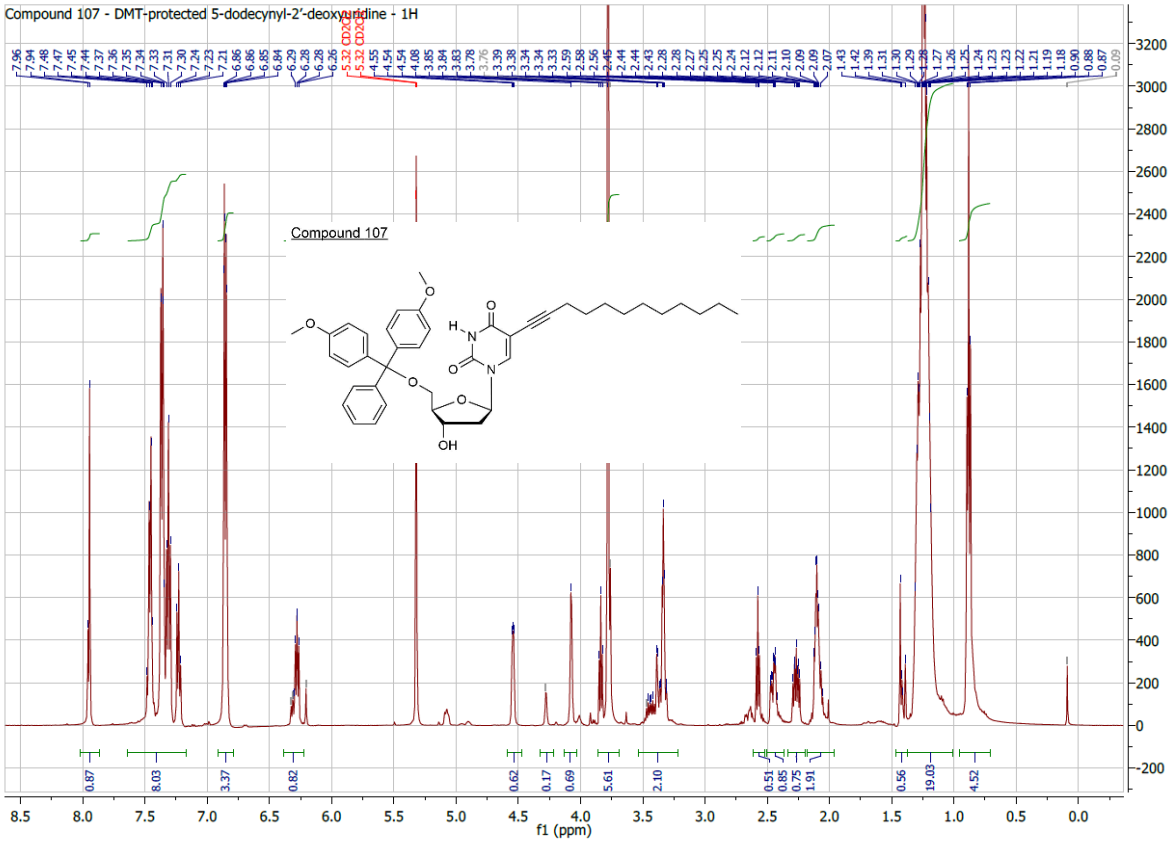
Compound 107 - DMT-protected 5-dodecynyl-2'-deoxyuridine - 1H
Compound 107
f1 (ppm)

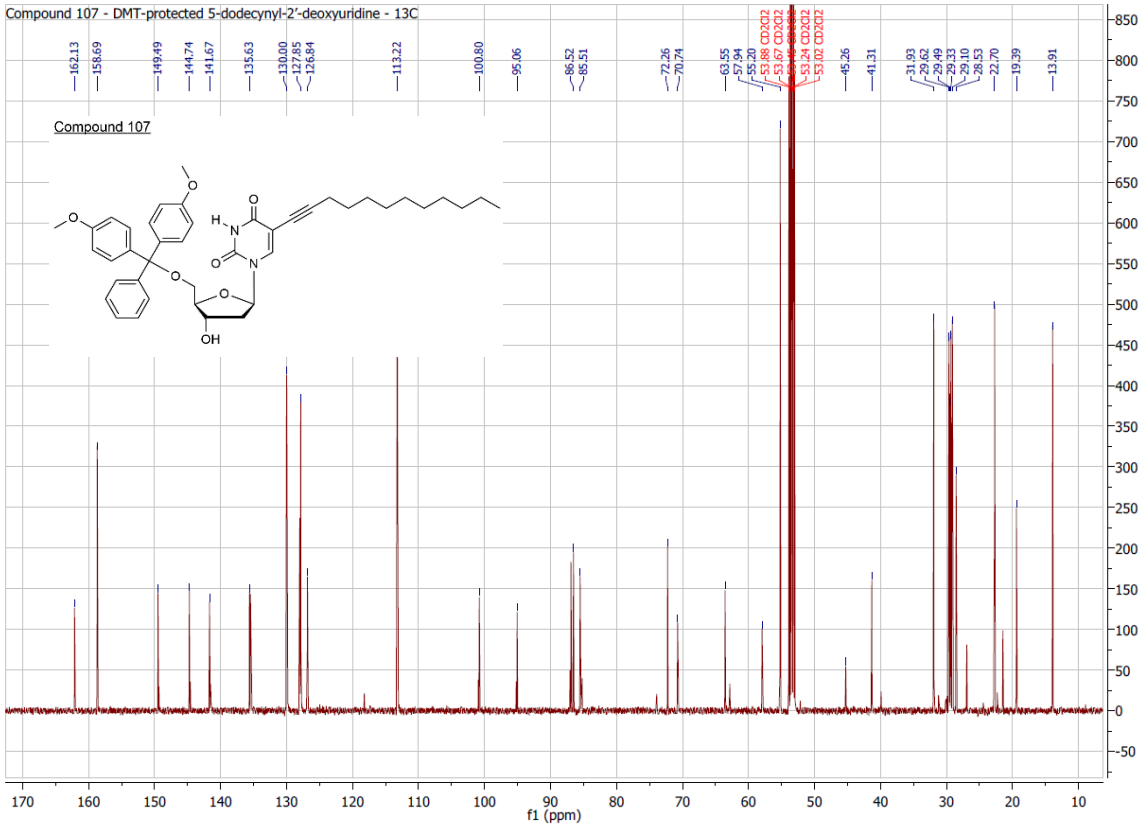
Compound 107 - DMT-protected 5-dodecynyl-2'-deoxyuridine - 13C
Compound 107
f1 (ppm)

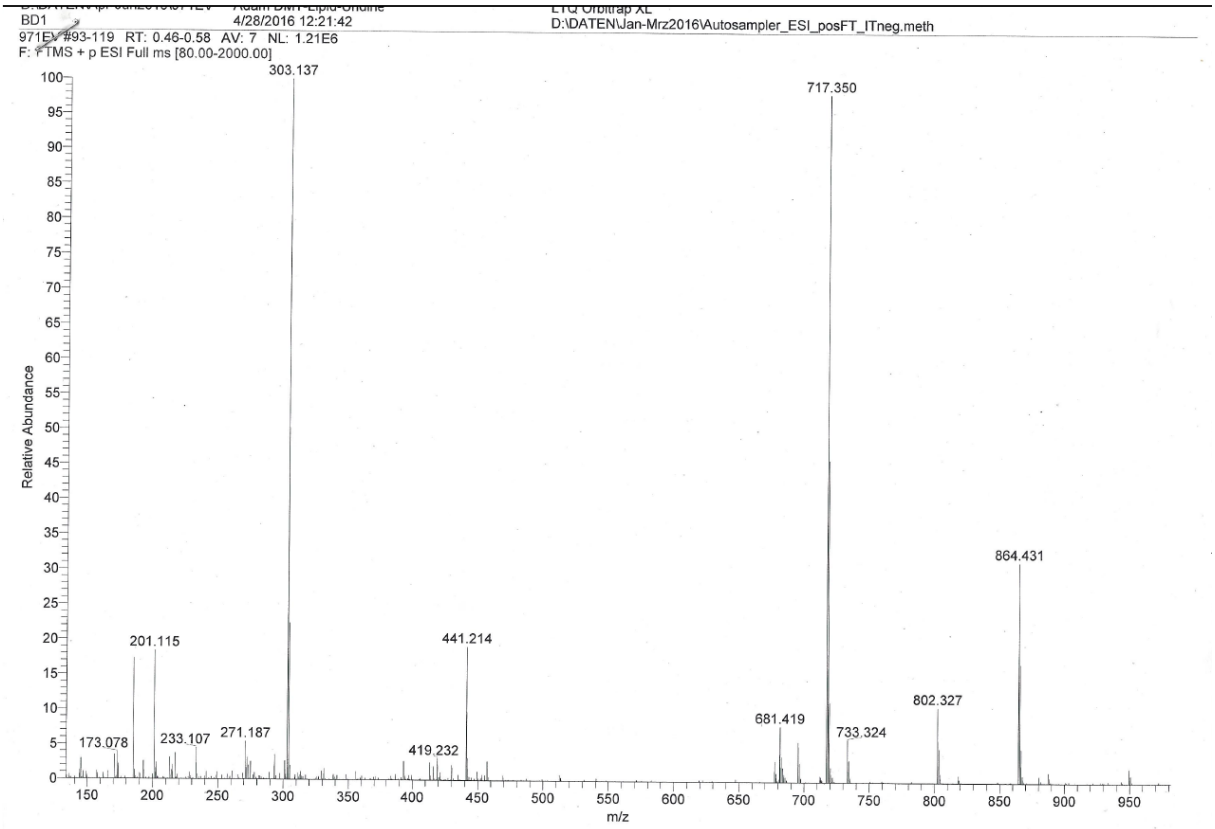
BD1
4/28/2016 12:21:42
LTQ Orbitrap XL
D:\DATEN\Jan-Mrz2016\Autosampler_ESI_posFT_ITneg.meth
971EV #93-119 RT: 0.46-0.58 AV: 7 NL: 1.21E6
F: FTMS + p ESI Full ms [80.00-2000.00]
303.137
717.350
864.431
201.115
441.214
802.327
681.419
733.324
173.078
233.107
271.187
419.232
Relative Abundance
m/z

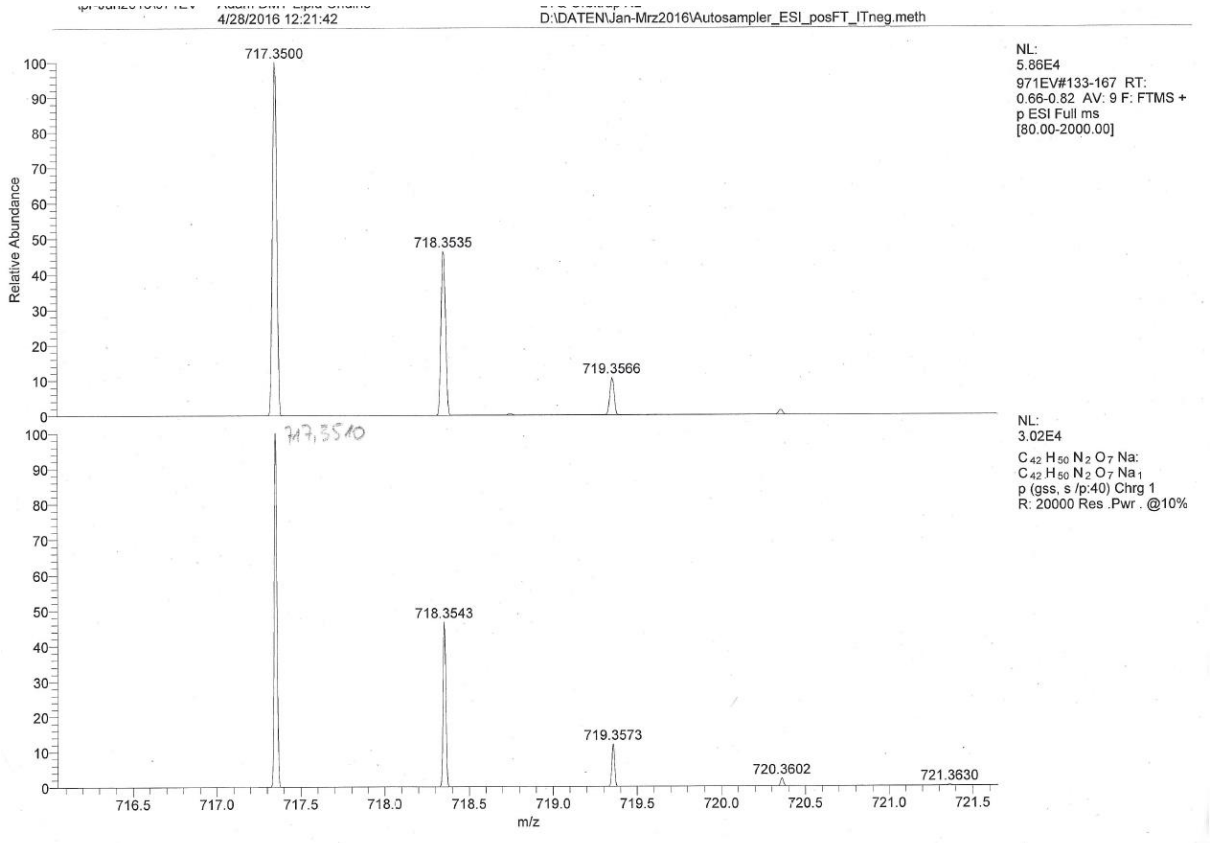
4/28/2016 12:21:42
D:\DATEN\Jan-Mrz2016\Autosampler_ESI_posFT_ITneg.meth
717.3500
718.3535
719.3566
NL:
5.86E4
971EV#133-167 RT:
0.66-0.82 AV: 9 F: FTMS +
p ESI Full ms
[80.00-2000.00]
717.3540
718.3543
719.3573
720.3602
721.3630
NL:
3.02E4
C42 H50 N2 O7 Na:
C42 H50 N2 O7 Na1
p (gss, s /p:40) Chrg 1
R: 20000 Res .Pwr . @10%
Relative Abundance
m/z

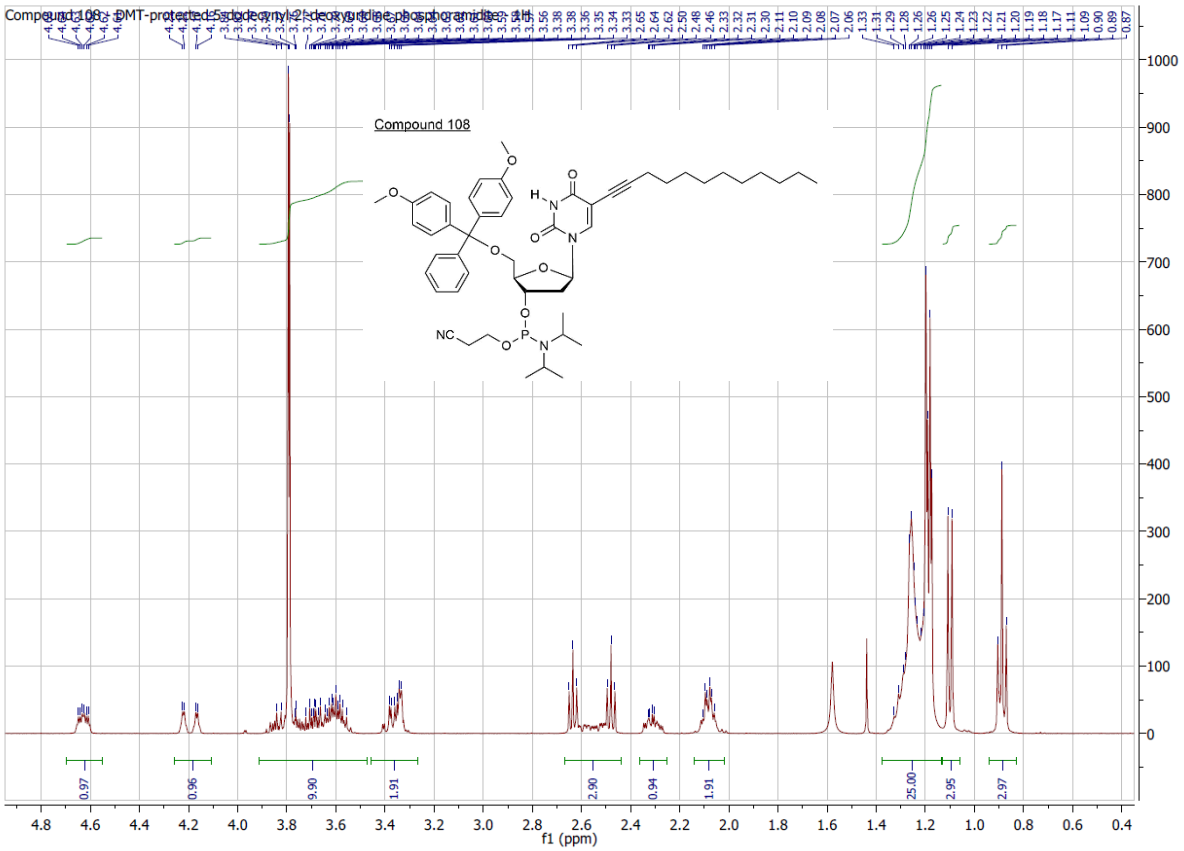
Compound 108 - DMT-protected 5-dodecynyl-2'-deoxyuridine phosphoramidite - 1H
Compound 108
f1 (ppm)

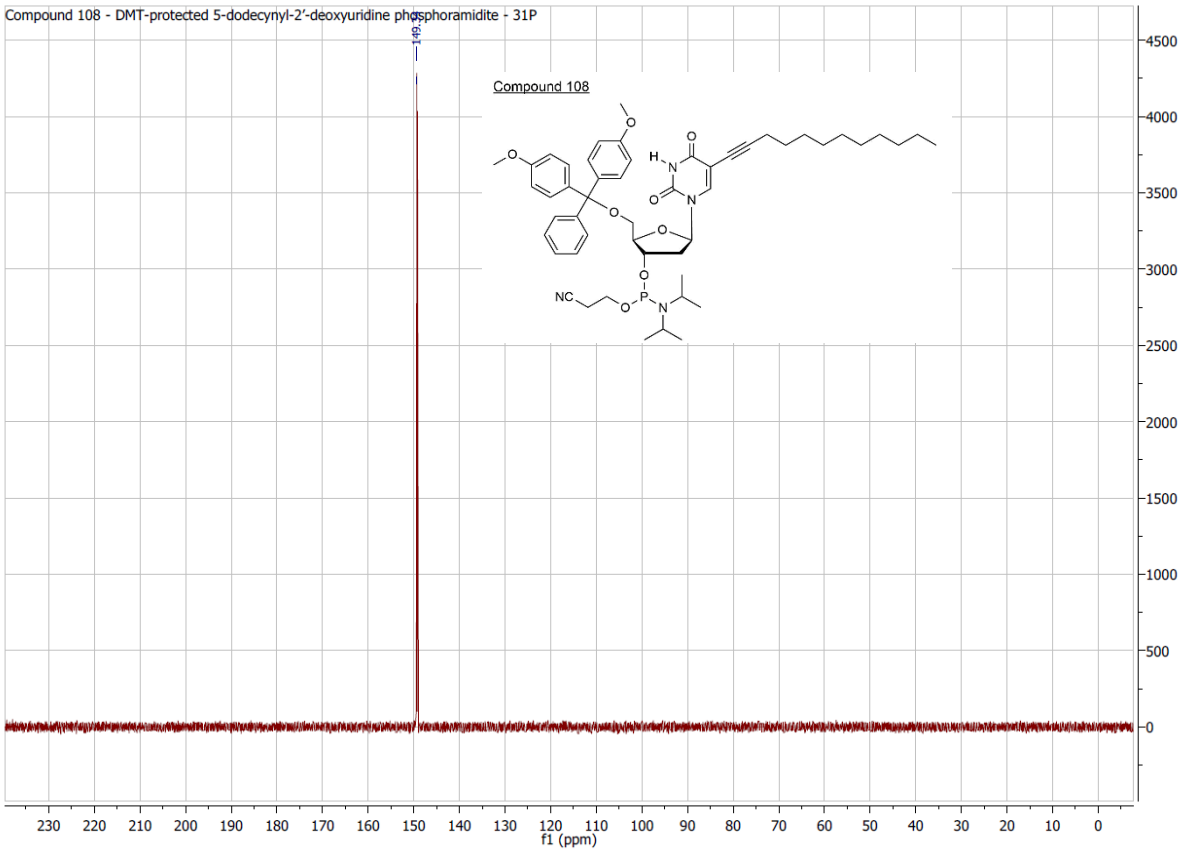
Compound 108 - DMT-protected 5-dodecynyl-2'-deoxyuridine phosphoramidite - 31P
Compound 108
f1 (ppm)

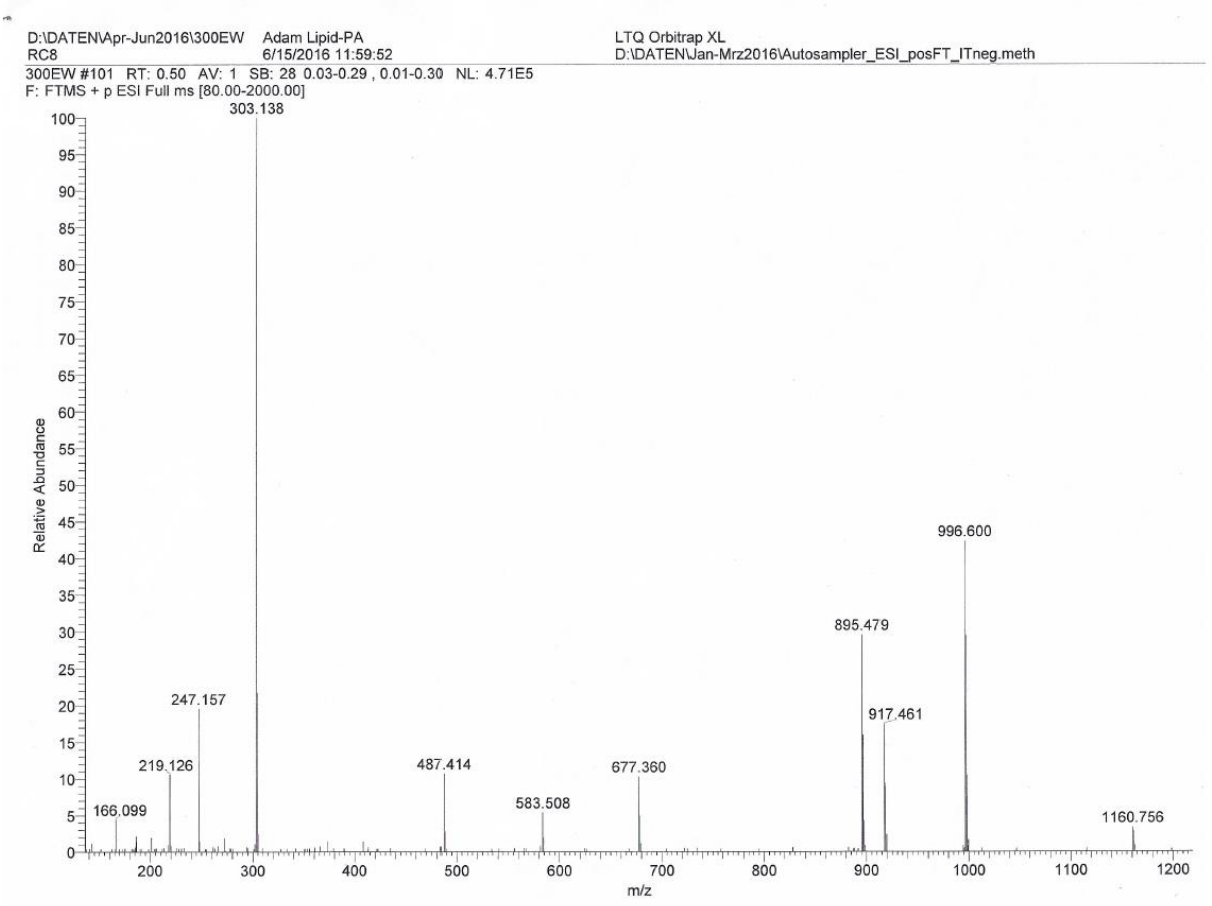
D:\DATEN\Apr-Jun2016\300EW Adam Lipid-PA
RC8 6/15/2016 11:59:52
LTQ Orbitrap XL
D:\DATEN\Jan-Mrz2016\Autosampler_ESI_posFT_ITneg.meth
300EW #101 RT: 0.50 AV: 1 SB: 28 0.03-0.29 , 0.01-0.30 NL: 4.71E5
F: FTMS + p ESI Full ms [80.00-2000.00]
303.138
996.600
895.479
247.157
917.461
219.126
487.414
677.360
583.508
166.099
1160.756
Relative Abundance
m/z

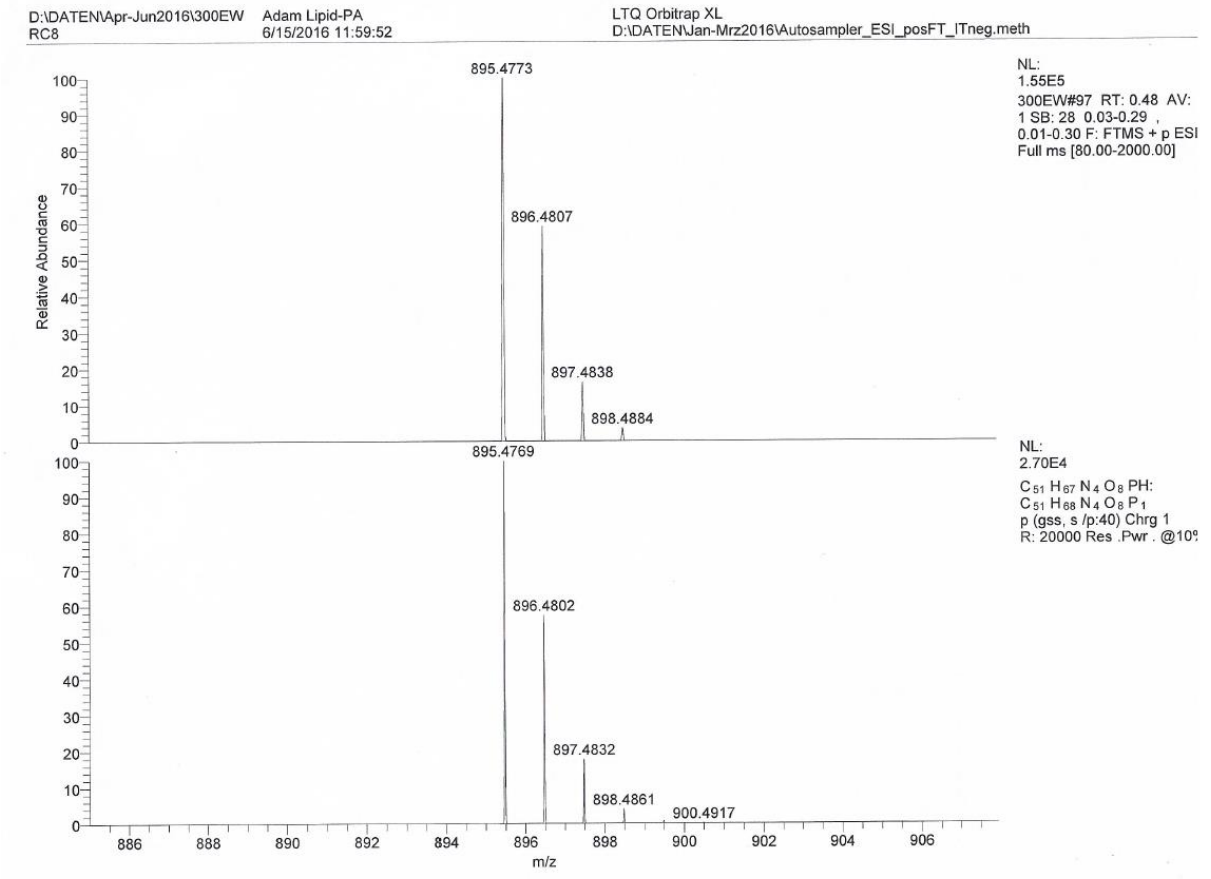
D:\DATEN\Apr-Jun2016\300EW Adam Lipid-PA
RC8 6/15/2016 11:59:52
LTQ Orbitrap XL
D:\DATEN\Jan-Mrz2016\Autosampler_ESI_posFT_ITneg.meth
895.4773
NL:
1.55E5
300EW#97 RT: 0.48 AV:
1 SB: 28 0.03-0.29 ,
0.01-0.30 F: FTMS + p ESI
Full ms [80.00-2000.00]
896.4807
897.4838
898.4884
895.4769
NL:
2.70E4
C51 H67 N4 O8 PH:
C51 H68 N4 O8 P1
p (gss, s /p:40) Chrg 1
R: 20000 Res .Pwr . @10
896.4802
897.4832
898.4861
900.4917
Relative Abundance
m/z

10.2 LCMS results for all synthesized

Sequence: 5’-GAATXGGTG-3’ (A)

Modification: X = Azobenzene (AB)

Calculated mass: 2864.79

Data file: 2016_06_01_1AB8_71_01_1381

UV-chromatogram (260 nm):

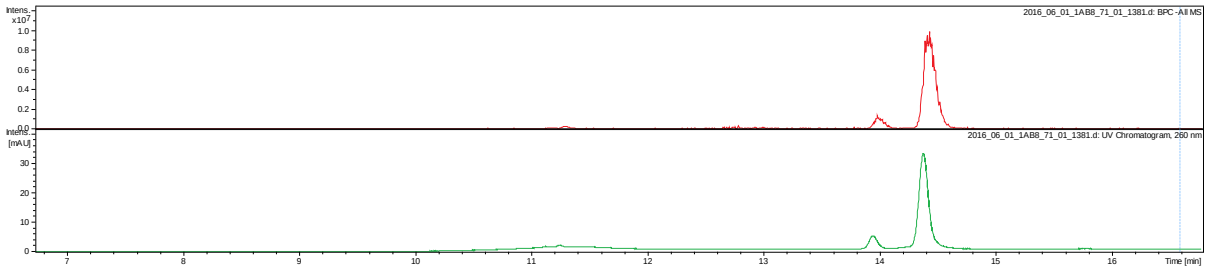

Extracted mass spectrum 1 (13.8 – 14.0 min.):

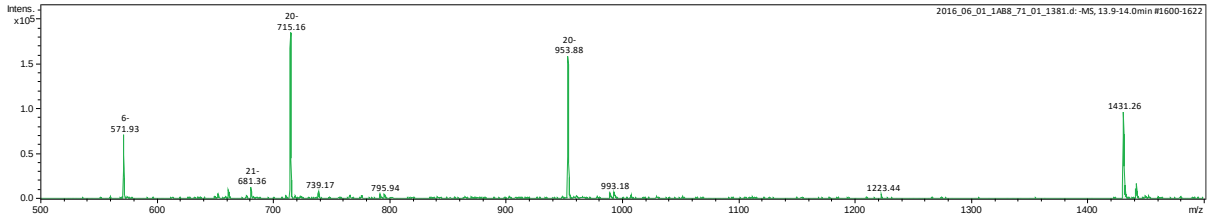

Deconvoluted mass 1: 2864.65

Extracted mass spectrum 2 (14.3 – 14.5 min.):

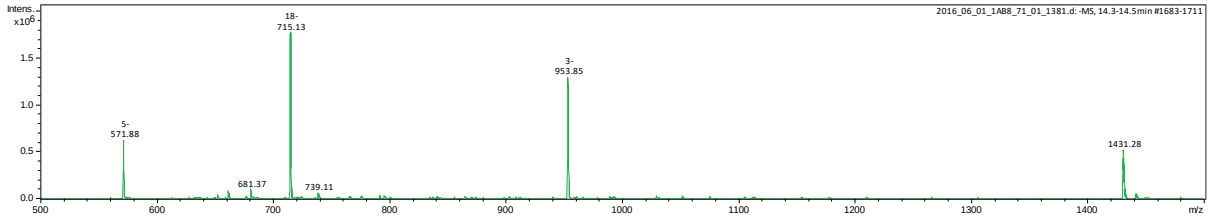

Deconvoluted mass 2: 2864.55

Sequence: 5’-GAXATGGXTG-3’ (B)

Modification: X = Azobenzene (AB)

Calculated mass: 3239.89

Data file: 2016_06_01_2AB8_72_01_1382

UV-chromatogram (260 nm):

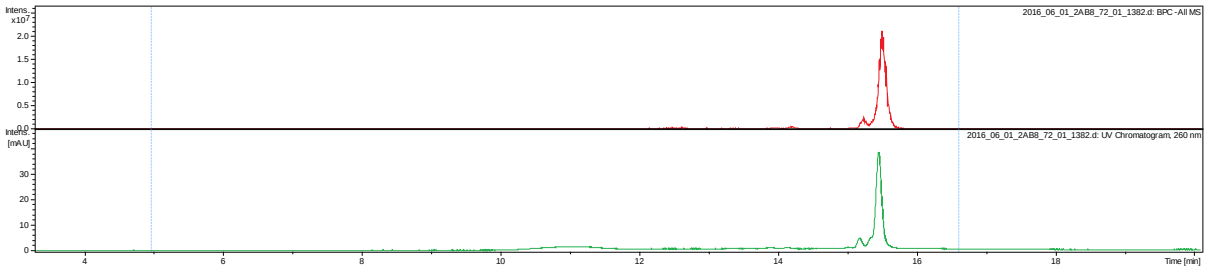

Extracted mass spectrum 1 (15.1 – 15.2 min.):

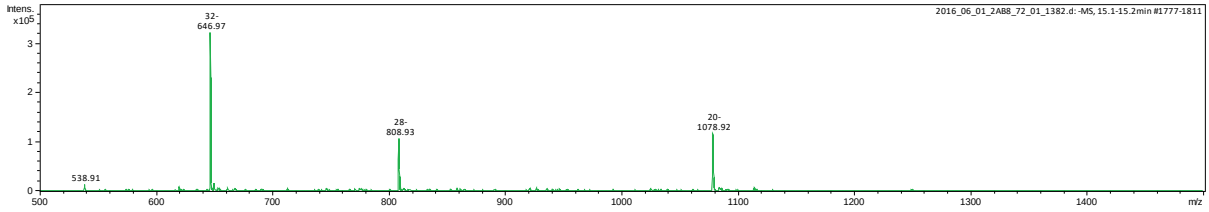

Deconvoluted mass 1: 3239.77

Extracted mass spectrum 2 (15.3 – 15.6 min.):

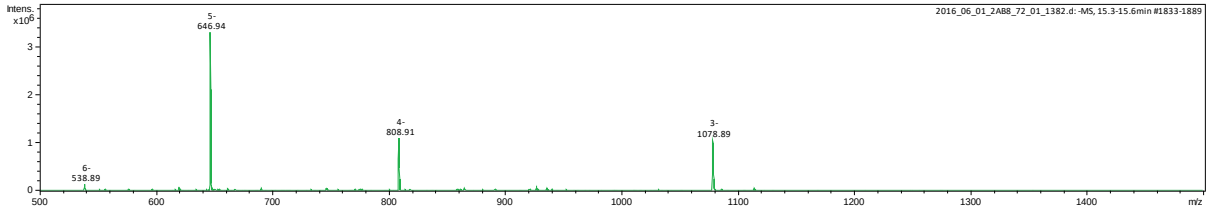

Deconvoluted mass 2: 3239.71

Sequence: 5’-GAXATXGGXTG-3’ (C)

Modification: X = Azobenzene (AB)

Calculated mass: 3614.98

Data file: 2016_10_17_3AB8_41_01_2458

UV-chromatogram (260 nm):

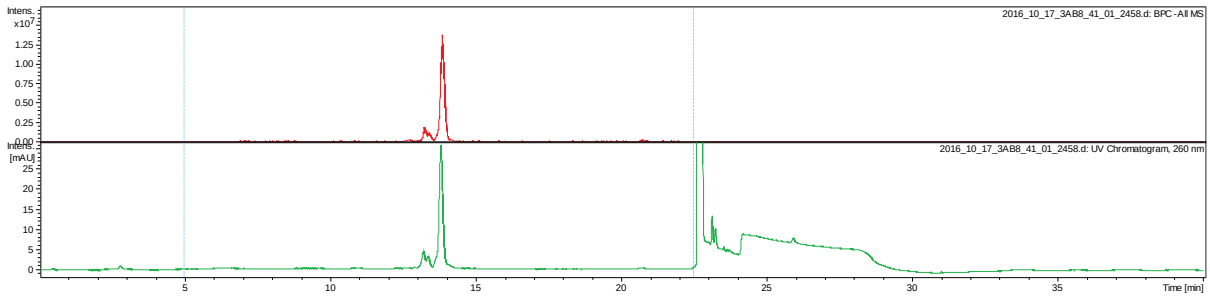

Extracted mass spectrum 1 (13.0 – 13.5 min.):

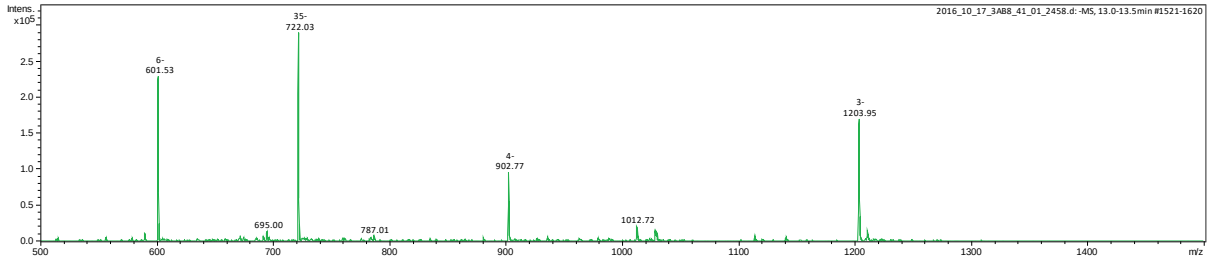

Deconvoluted mass 1: 3614.87

Extracted mass spectrum 2 (13.5 – 14.2 min.):

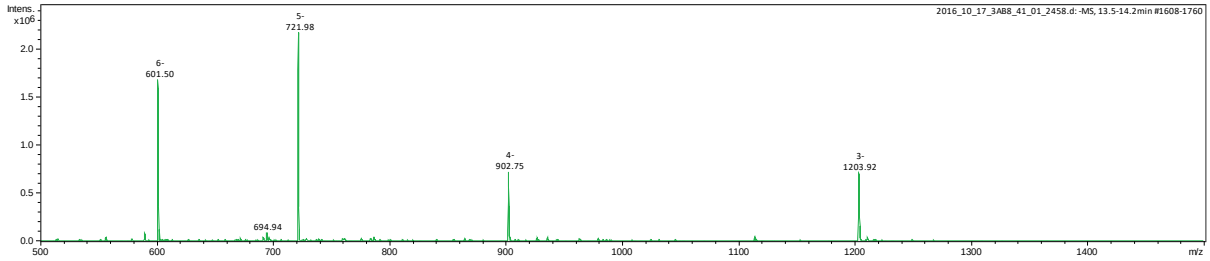

Deconvoluted mass 2: 3614.78

Sequence: 5’-CACCATXTCCGGT-3’ (D)

Modification: X = Azobenzene (AB)

Calculated mass: 3956.49

Data file: 2016_10_17_3AB8_41_01_2458

UV-chromatogram (260 nm):

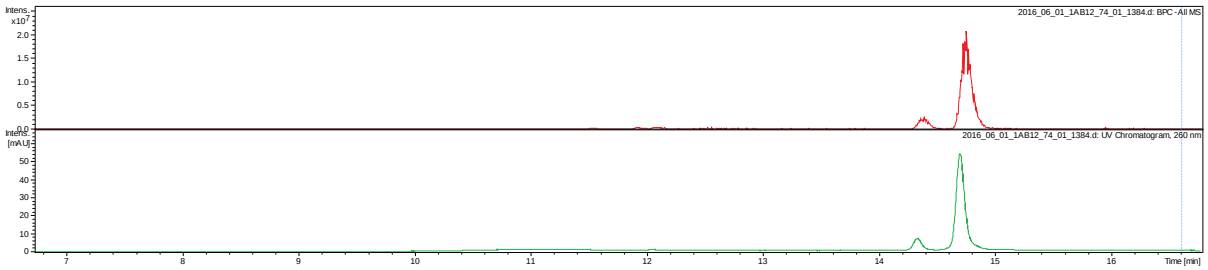

Extracted mass spectrum 1 (14.3 –14.4 min.):

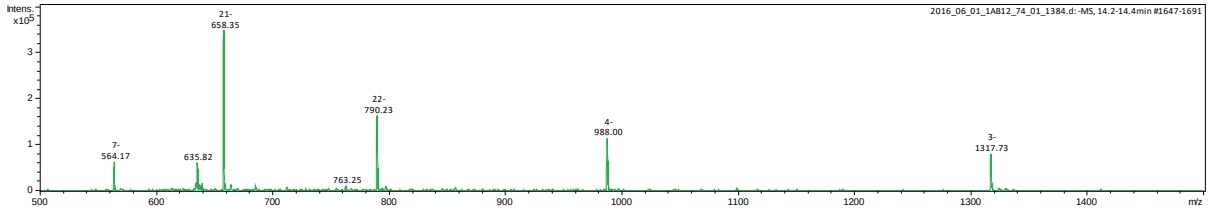

Deconvoluted mass: 3956.20

Extracted mass spectrum 1 (14.6 – 14.8 min.):

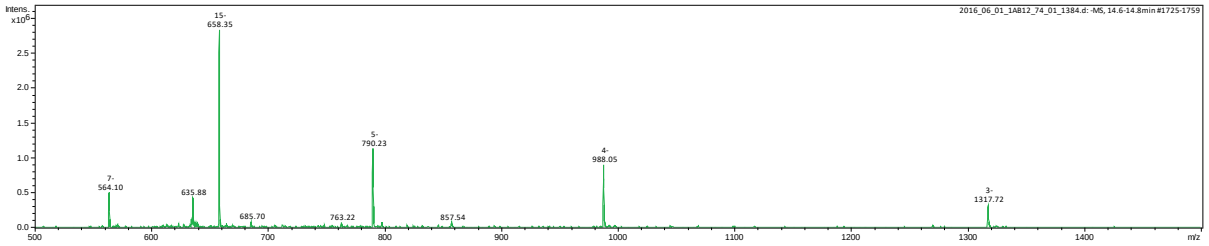

Deconvoluted mass: 3956.15

Sequence: 5’-CACXCATTCCXGGT-3’ (E)

Modification: X = Azobenzene (AB)

Calculated mass: 4331.59

Data file: 2016_06_01_2AB12_75_01_1385

UV-chromatogram (260 nm):

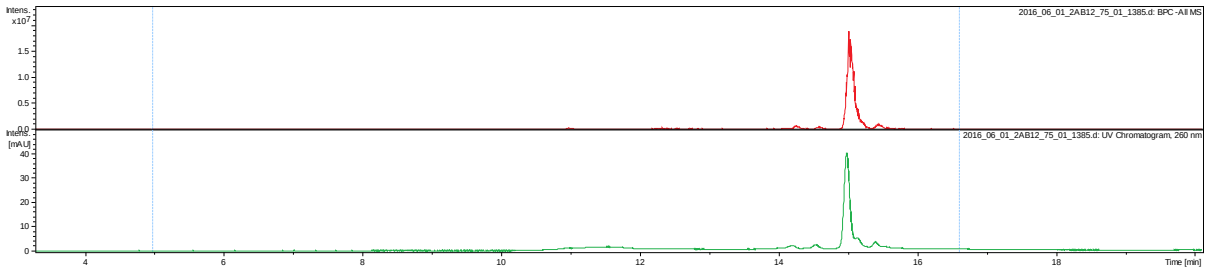

Extracted mass spectrum 1 (14.9 – 15.2 min.):

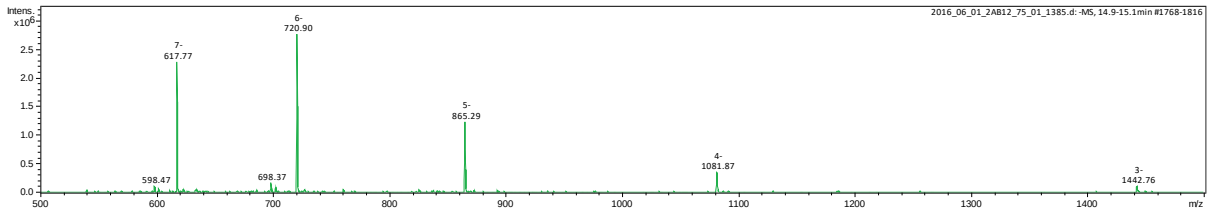

Deconvoluted mass: 4331.48

Sequence: 5’-CACXCATXTCCXGGT-3’ (F)

Modification: X = Azobenzene (AB)

Calculated mass: 4706.69

Data file: 2016_10_17_3AB12_42_01_2461

UV-chromatogram (260 nm):

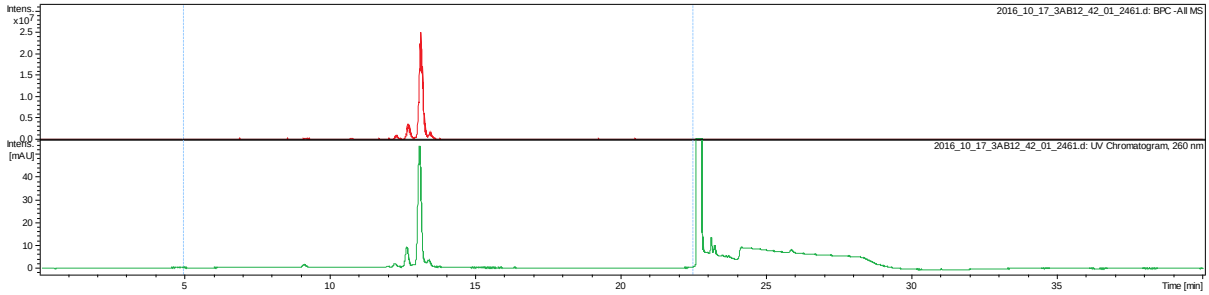

Extracted mass spectrum 1 (12.3 – 12.9 min.):

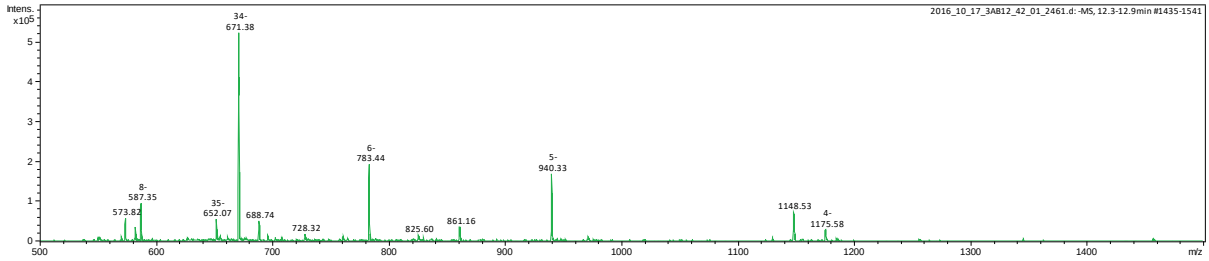

Deconvoluted mass 1: 4706.36

Extracted mass spectrum 2 (12.9 – 13.2 min.):

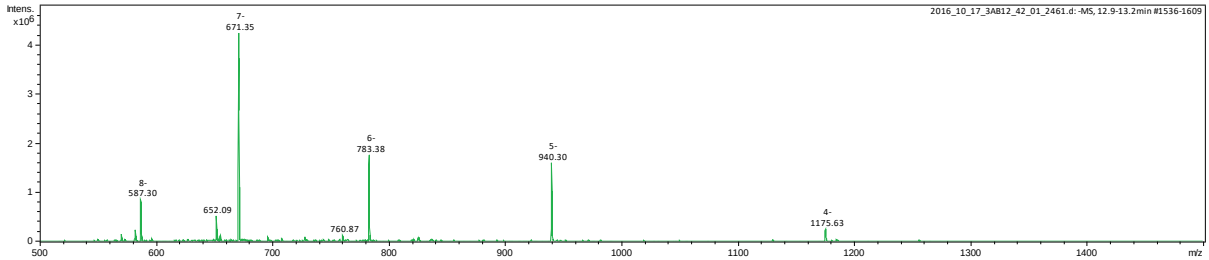

Deconvoluted mass 2: 4706.35

Sequence: 5‘-TCCXCCAXGCAXTCG-3‘ (I)

Modification: X = Azobenzene (AB)

Calculated mass: 4691.67

Data file: 2016_09_26_AB168ROo_63_01_2321

UV-chromatogram (260 nm):

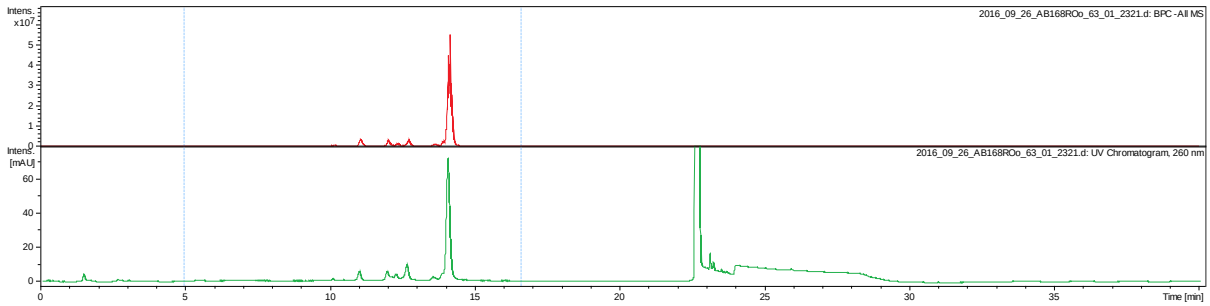

Extracted mass spectrum 1 (12.5 – 12.7 min.):

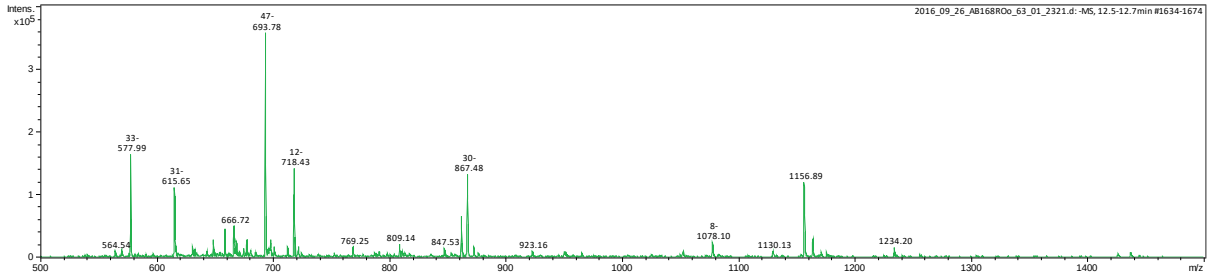

Deconvoluted mass 1: 3473.71

Extracted mass spectrum 2 (13.9 – 14.1 min.):

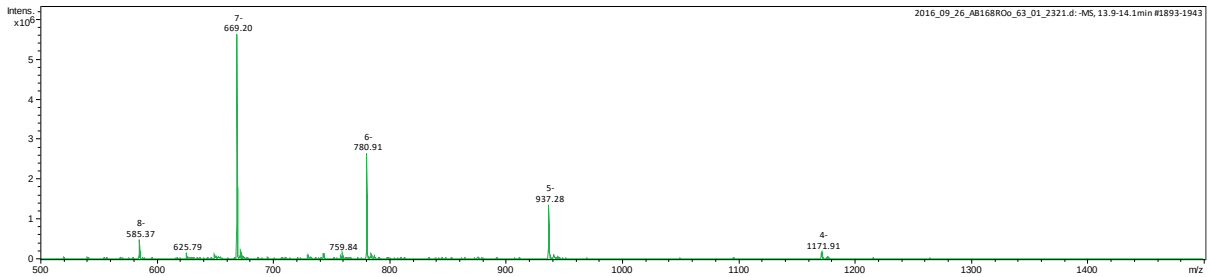

Deconvoluted mass 2: 4691.45

Sequence: 5‘-CCXGATXGCTXGT-3‘ (J)

Modification: X = Azobenzene (AB)

Calculated mass: 4144.32

Data file: 2016_09_26_AB126ROo_61_01_2319

UV-chromatogram (260 nm):

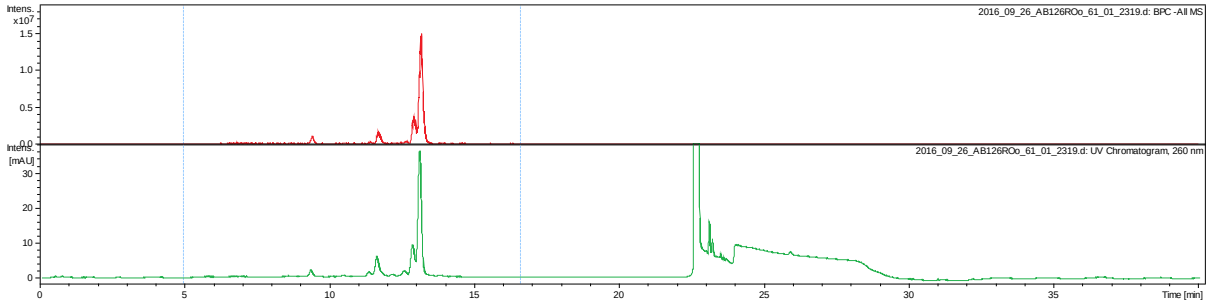

Extracted mass spectrum 1 (11.5 – 11.9 min.):

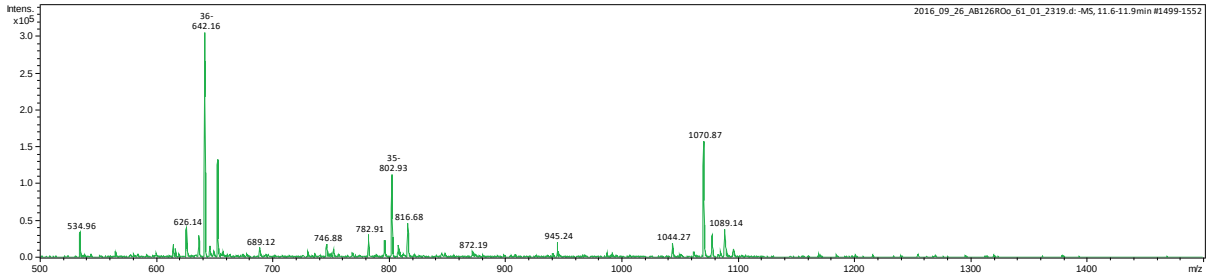

Deconvoluted mass 1: 3215.63

Extracted mass spectrum 2 (12.8 – 13.3 min.):

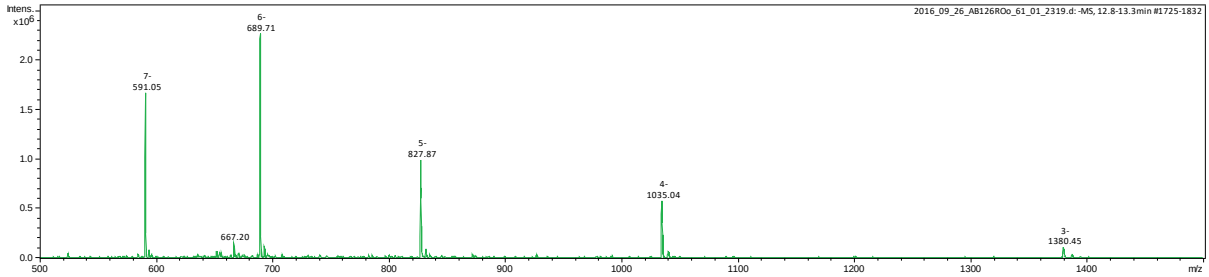

Deconvoluted mass 2: 4144.20

Sequence: 5‘-GGXAATXGGTXGA-3‘ (K)

Modification: X = Azobenzene (AB)

Calculated mass: 4257.40

Data file: 2016_09_26_AB126ROp_62_01_2320

UV-chromatogram (260 nm):

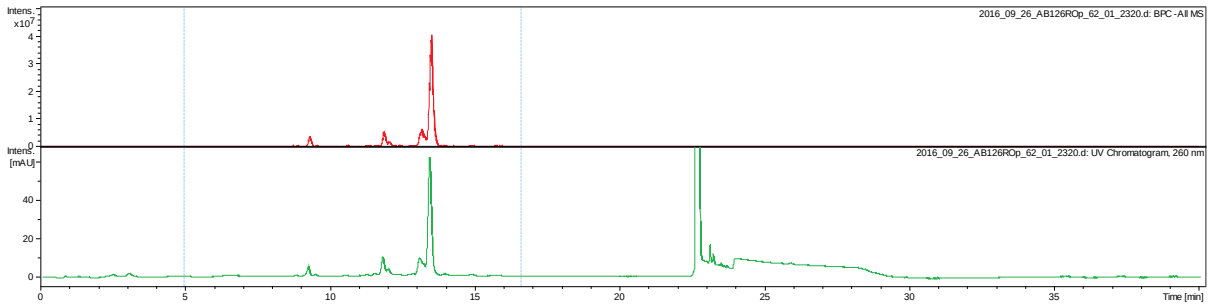

Extracted mass spectrum 1 (11.8 – 12.0 min.):

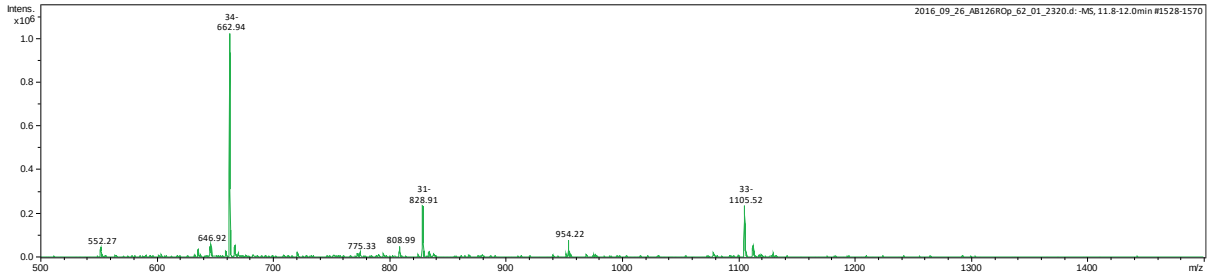

Deconvoluted mass 1: 3319.59

Extracted mass spectrum 2 (13.0 – 13.7 min.):

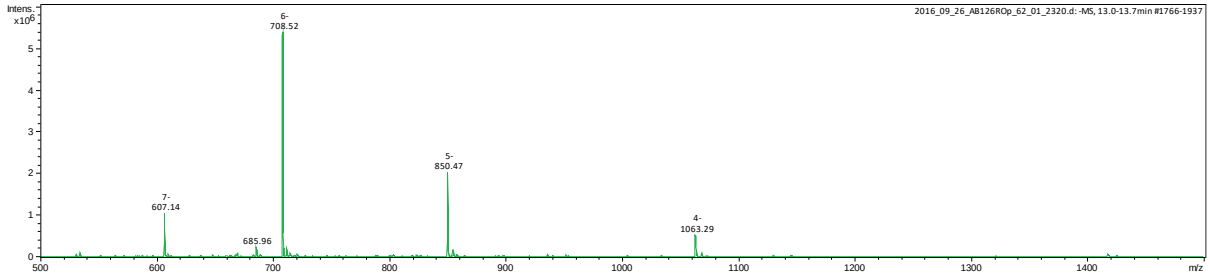

Deconvoluted mass 2: 4257.20

Sequence: 5’-GAATXGGTG-3’ (A)

Modification: X = 2’,6’-Dimethylazobenzene (DMAB)

Calculated mass: 2892.82

Data file: 2016_06_01_1DMAB8_77_01_1387

UV-chromatogram (260 nm):

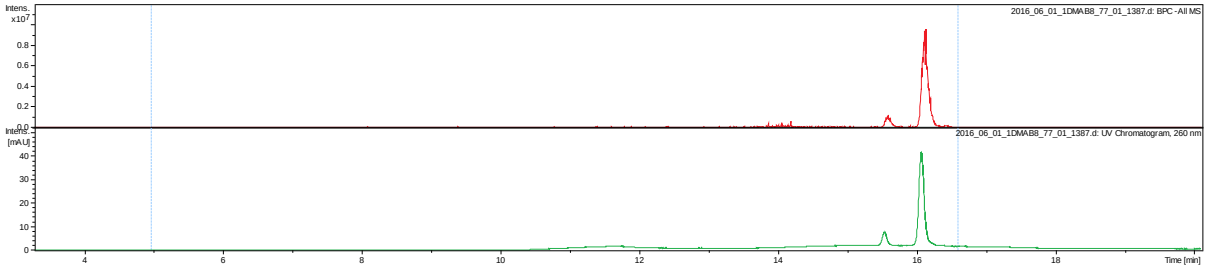

Extracted mass spectrum 1 (15.5 – 15.6 min.):

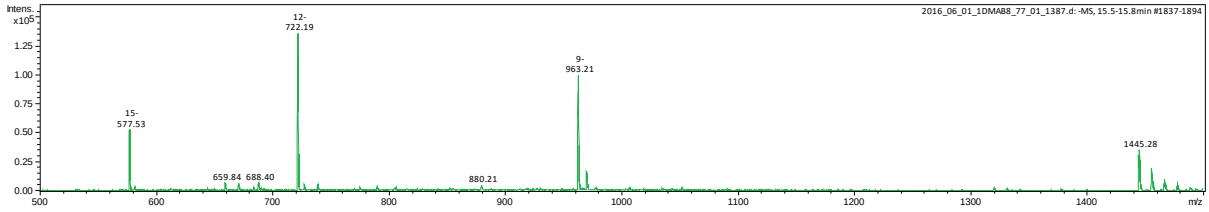

Deconvoluted mass 1: 2892.67

Extracted mass spectrum 2 (16.0 – 16.2 min.):

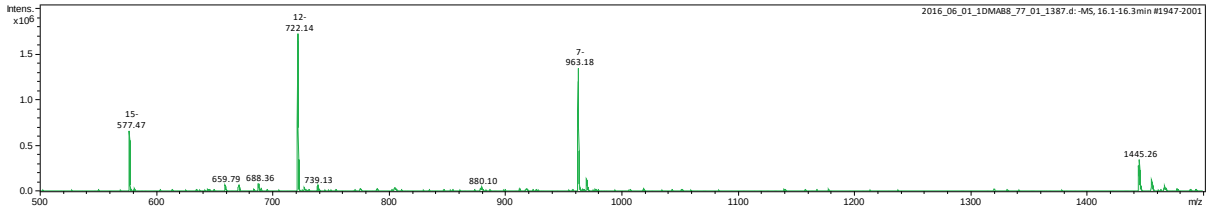

Deconvoluted mass 2: 2892.41

Sequence: 5’-GAXATGGXTG-3’ (B)

Modification: X = 2’,6’-Dimethylazobenzene (DMAB)

Calculated mass: 3295.94

Data file: 2016_10_17_2DA8_43_01_2462

UV-chromatogram (260 nm):

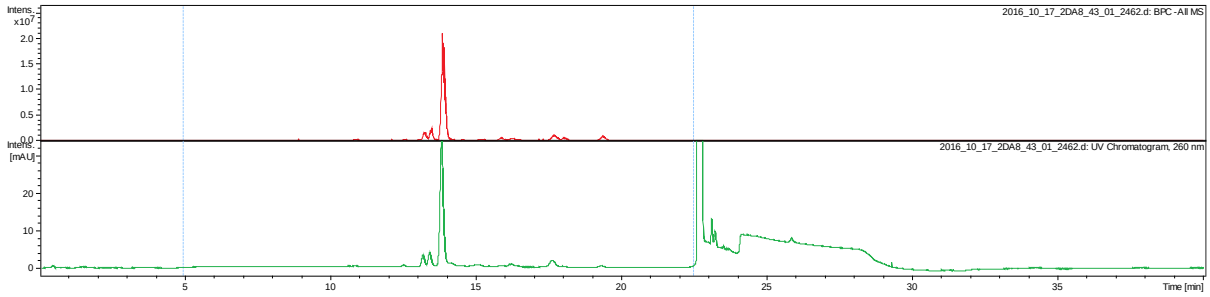

Extracted mass spectrum 1 (13.0 – 13.6 min.):

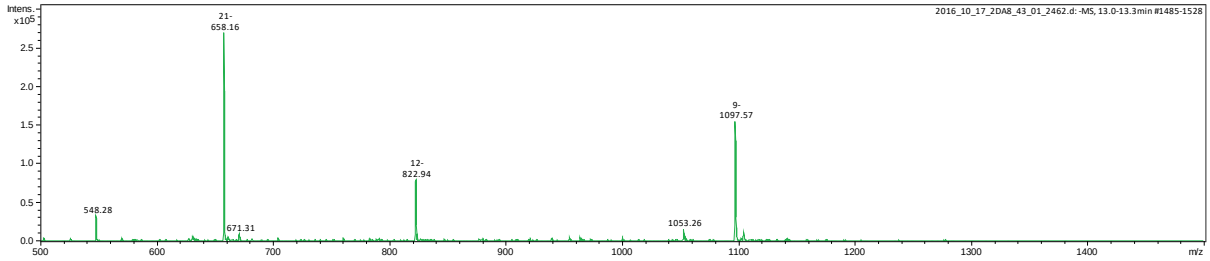

Deconvoluted mass 1: 3295.75

Extracted mass spectrum 2 (13.6 – 14.2 min.):

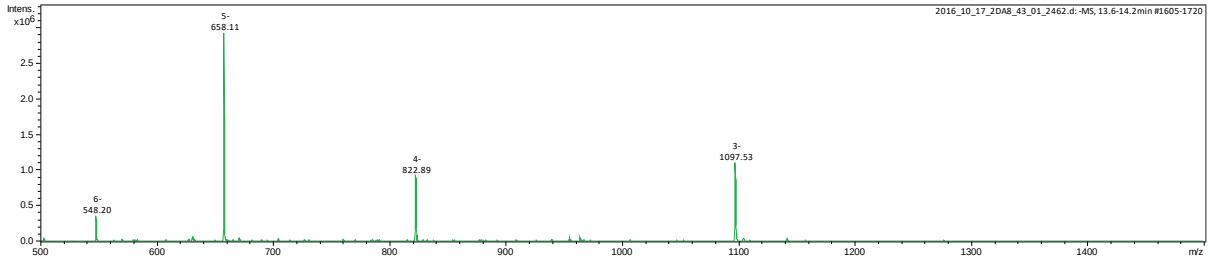

Deconvoluted mass 2: 3295.61

Sequence: 5’-GAXATXGGXTG-3’ (C)

Modification: X = 2’,6’-Dimethylazobenzene (DMAB)

Calculated mass: 3699.07

Data file: 2016_10_17_3DA8_44_01_2463

UV-chromatogram (260 nm):

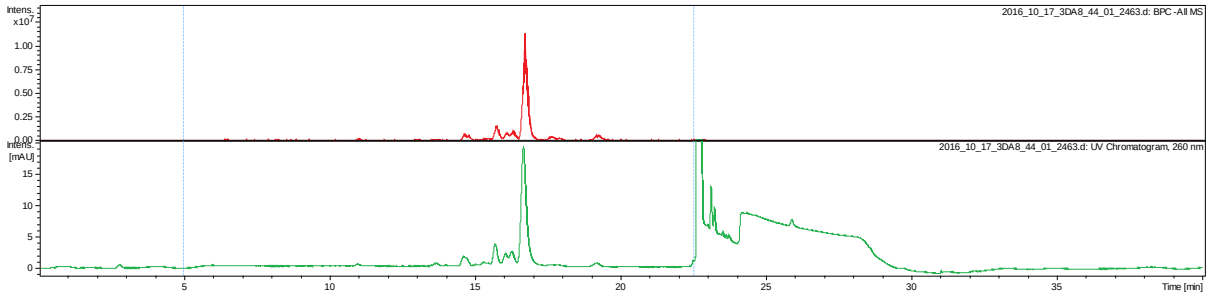

Extracted mass spectrum 1 (15.5 – 16.3 min.):

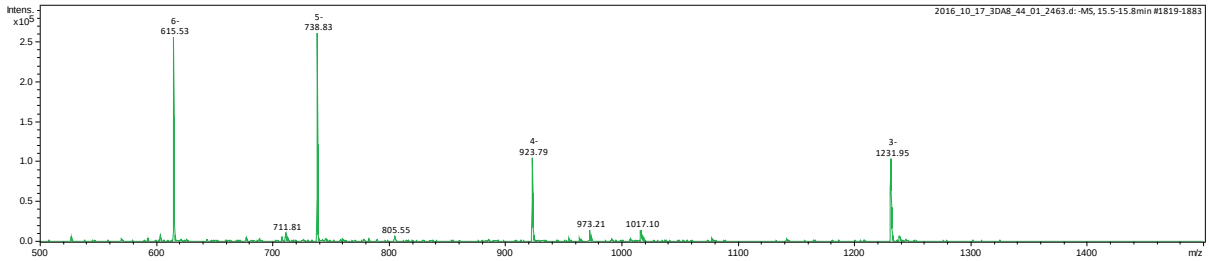

Deconvoluted mass 1: 3698.87

Extracted mass spectrum 2 (16.6 – 17.1 min.):

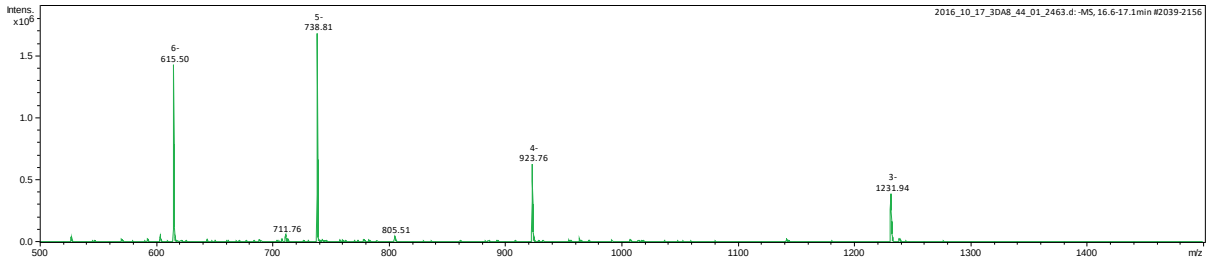

Deconvoluted mass 2: 3699.09

Sequence: 5’-CACCATXTCCGGT-3’ (D)

Modification: X = 2’,6’-Dimethylazobenzene (DMAB)

Calculated mass: 3984.52

Data file: 2016_06_01_1DMAB12_80_01_1390

UV-chromatogram (260 nm):

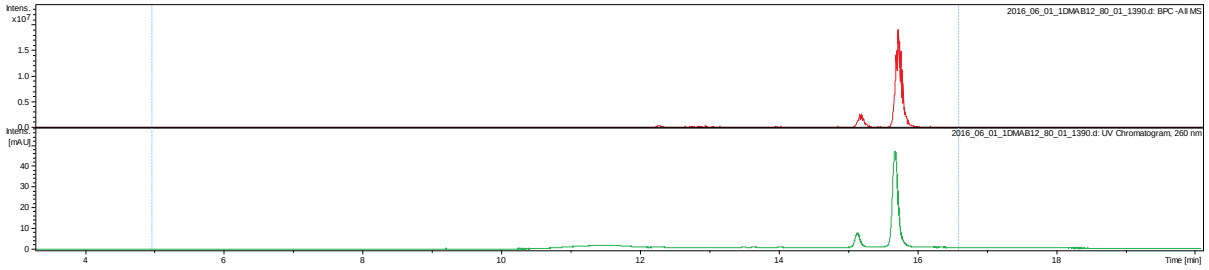

Extracted mass spectrum 1 (15.1 – 15.3 min.):

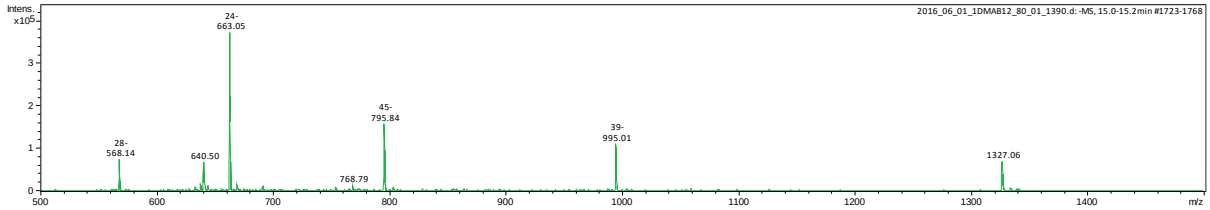

Deconvoluted mass 1: 3984.25

Extracted mass spectrum 2 (15.6 – 15.8 min.):

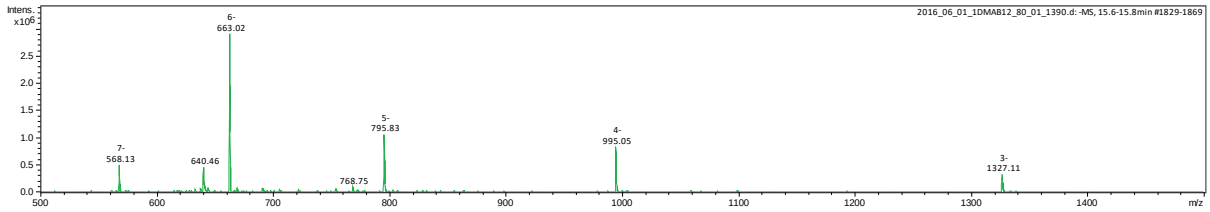

Deconvoluted mass 2: 3984.19

Sequence: 5’-CACXCATTCCXGGT-3’ (E)

Modification: X = 2’,6’-Dimethylazobenzene (DMAB)

Calculated mass: 4387.65

Data file: 2016_06_01_2DMAB12_81_01_1391

UV-chromatogram (260 nm):

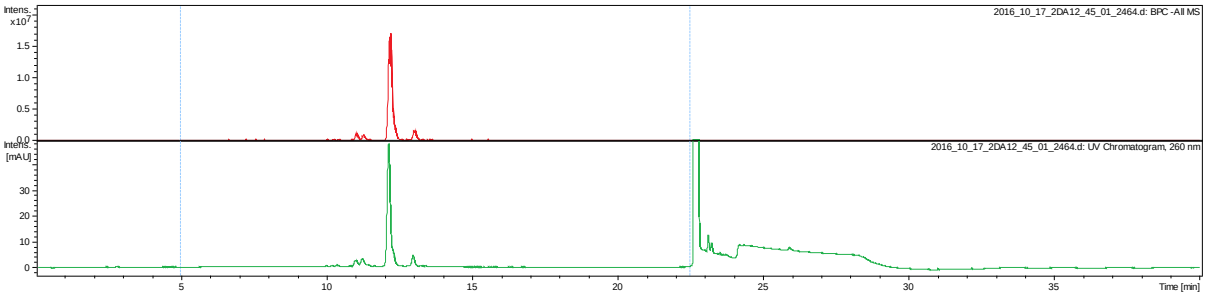

Extracted mass spectrum 1 (11.9 – 12.5 min.):

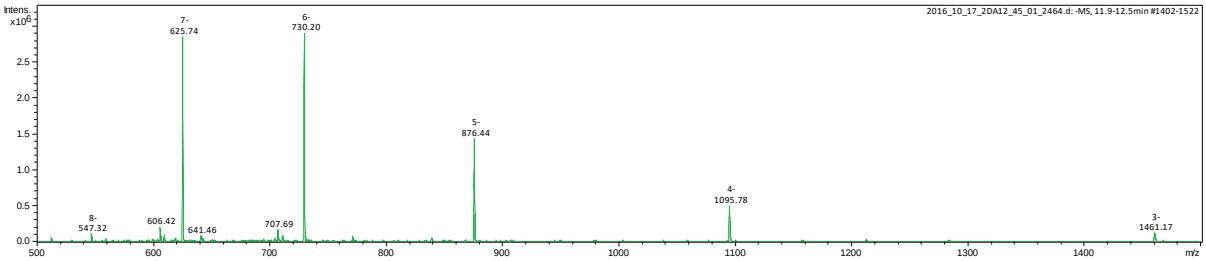

Deconvoluted mass 1: 4387.14

Sequence: 5’-CACXCATXTCCXGGT-3’ (F)

Modification: X = 2’,6’-Dimethylazobenzene (DMAB)

Calculated mass: 4790.77

Data file: 2016_10_17_3DA12_46_01_2465

UV-chromatogram (260 nm):

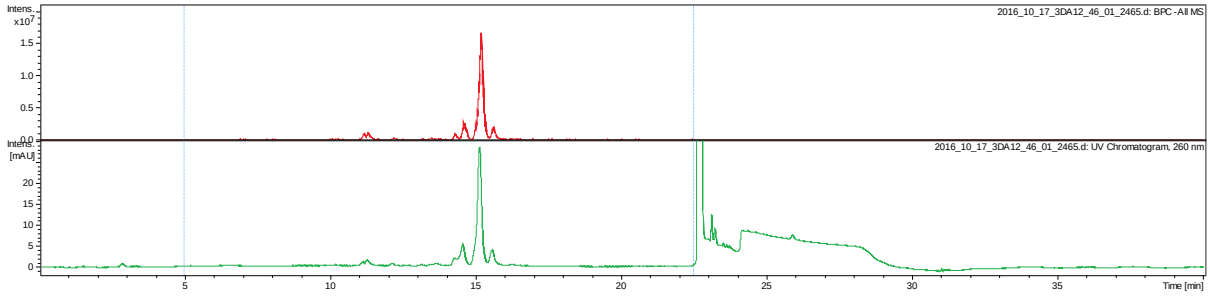

Extracted mass spectrum 1 (14.2 – 14.7 min.):

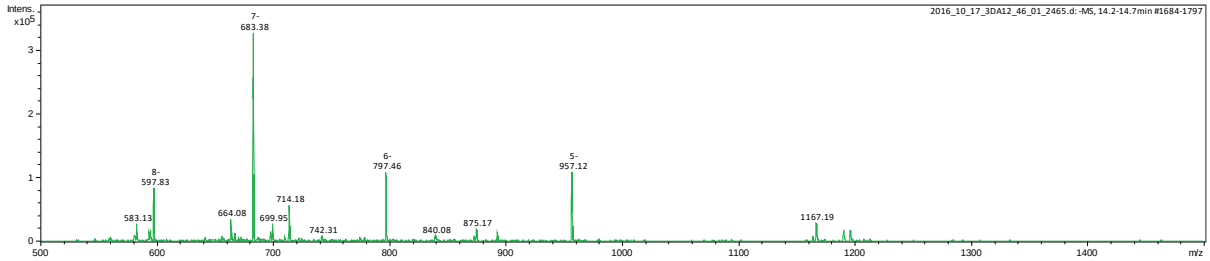

Deconvoluted mass 1: 4790.65

Extracted mass spectrum 2 (14.9 – 15.3 min.):

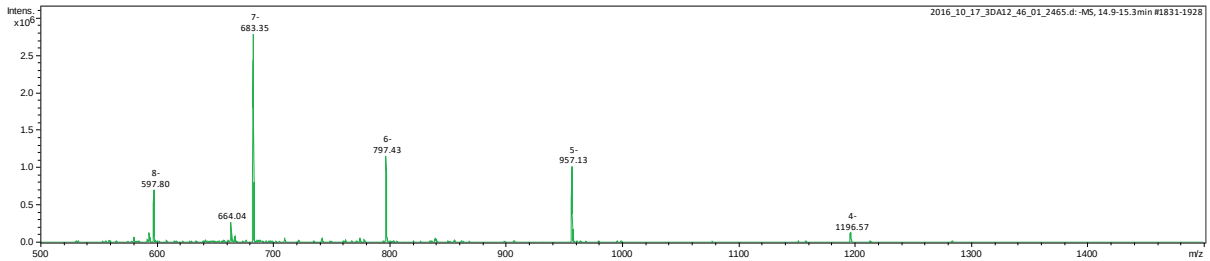

Deconvoluted mass 2: 4790.70

Sequence: 5‘-TCCXCCAXGCAXTCG-3‘ (I)

Modification: X = 2’,6’-Dimethylazobenzene (DMAB)

Calculated mass: 4775.76

Data file: 2016_09_26_DMAB168ROo_66_01_2324

UV-chromatogram (260 nm):

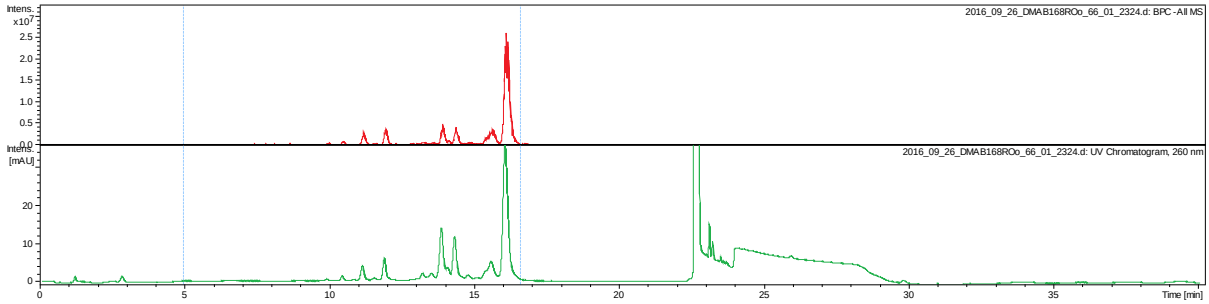

Extracted mass spectrum 1 (13.7 – 14.4 min.):

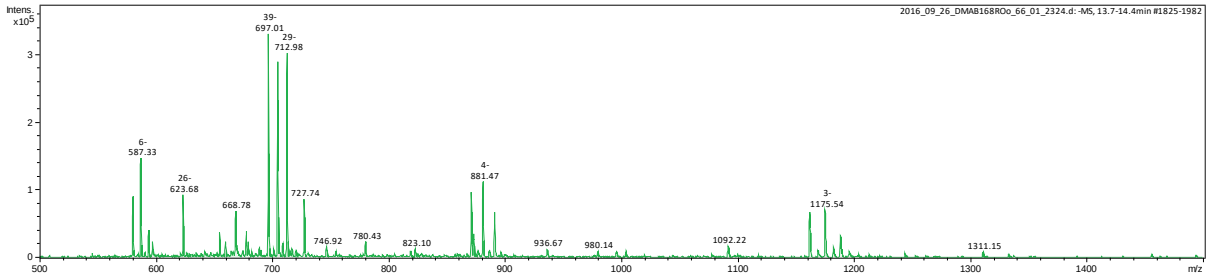

Deconvoluted mass 1: 3569.65 + 3529.65 + 3489.86

Extracted mass spectrum 2 (15.2 – 16.4 min.):

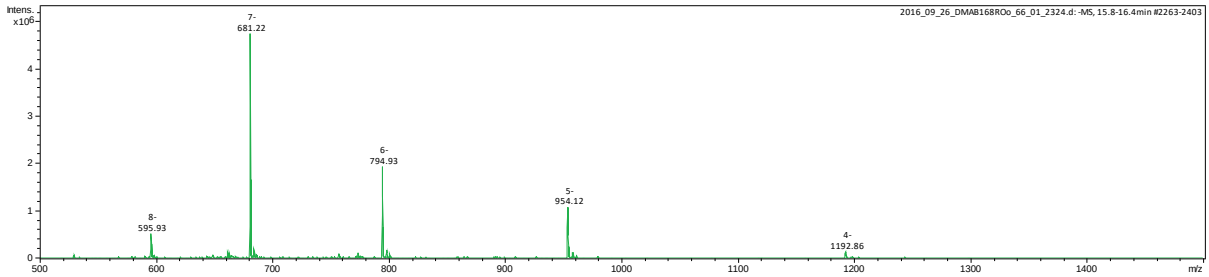

Deconvoluted mass 2: 4775.44

Sequence: 5‘-CCXGATXGCTXGT-3‘ (J)

Modification: X = 2’,6’-Dimethylazobenzene (DMAB)

Calculated mass: 4228.40

Data file: 2016_09_26_DMAB126ROo_64_01_2322

UV-chromatogram (260 nm):

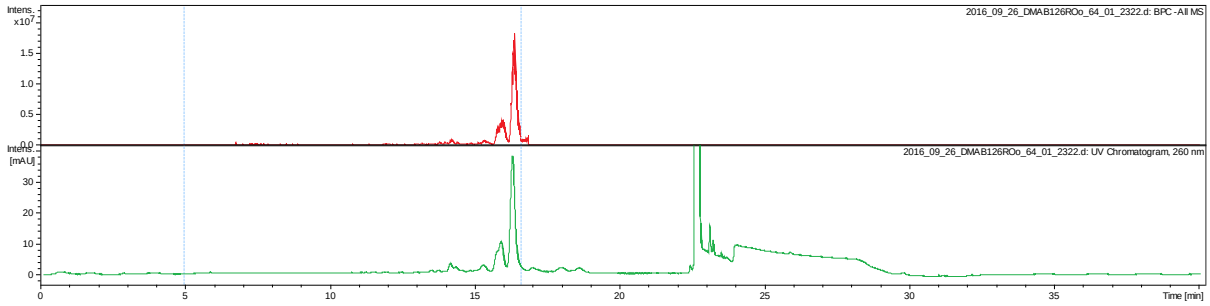

Extracted mass spectrum 1 (15.5 – 16.0 min.):

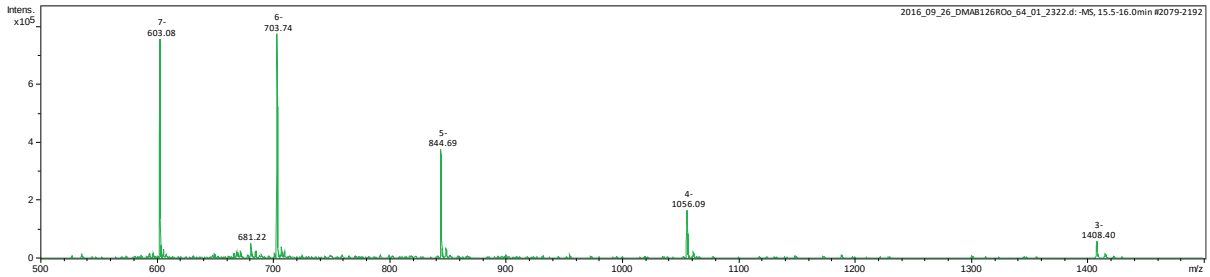

Deconvoluted mass 1: 4228.41

Extracted mass spectrum 2 (16.3 – 16.5 min.):

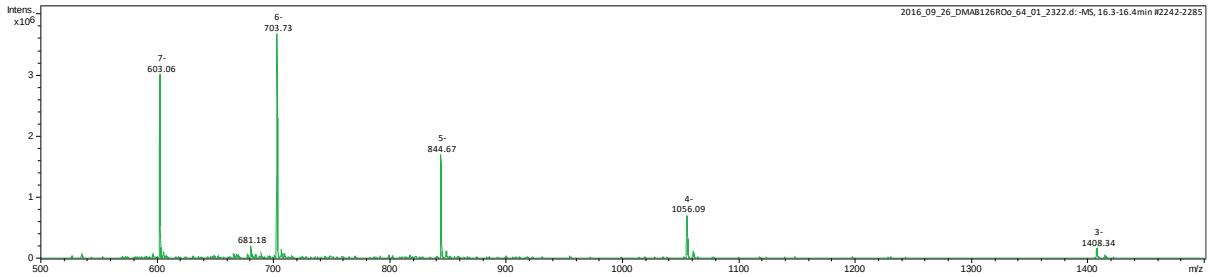

Deconvoluted mass 2: 4228.40

Sequence: 5‘-GGXAATXGGTXGA-3‘ (K)

Modification: X = 2’,6’-Dimethylazobenzene (DMAB)

Calculated mass: 4341.49

Data file: 2016_09_26_DMAB126ROp_65_01_2323

UV-chromatogram (260 nm):

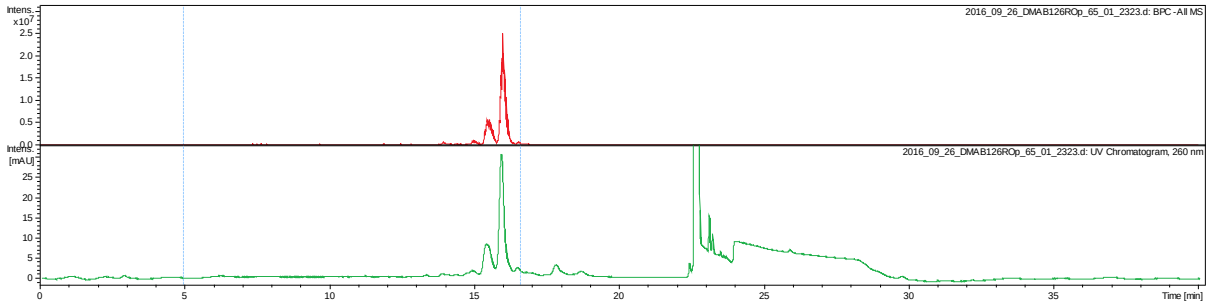

Extracted mass spectrum 1 (15.2 – 15.7 min.):

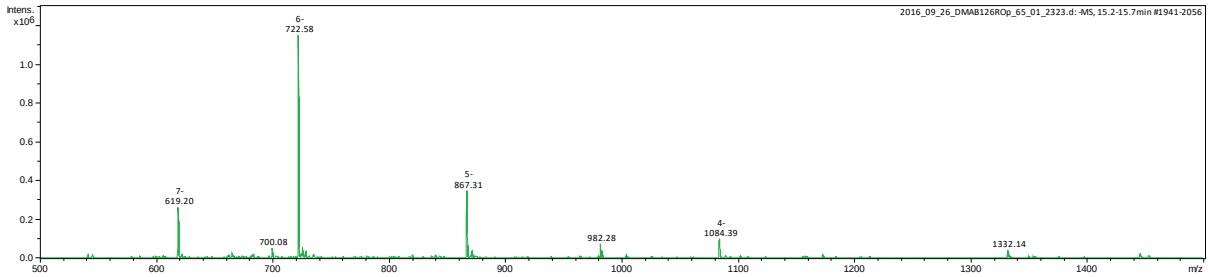

Deconvoluted mass 1: 4341.58

Extracted mass spectrum 2 (15.7 – 16.2 min.):

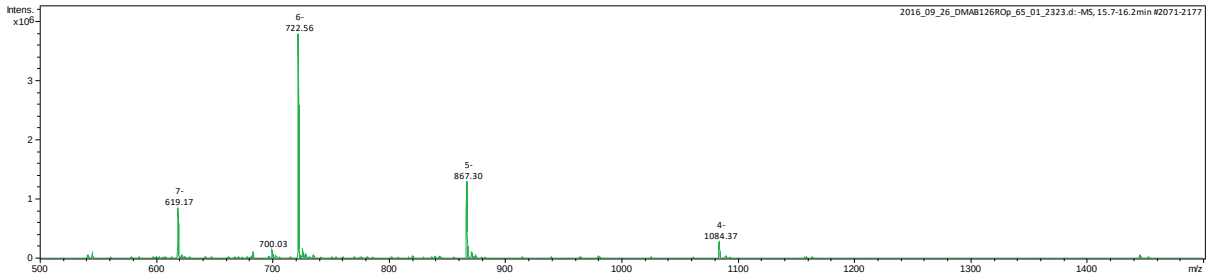

Deconvoluted mass 2: 4341.51

Sequence: 5’-GAATXGGTG-3’ (A)

Modification: X = 2’,6’-Dimethyl-4’-methylthioazobenzene (S-DMAB)

Calculated mass: 2938.81

Data file: 2016_10_17_1SD8_47_01_2466

UV-chromatogram (260 nm):

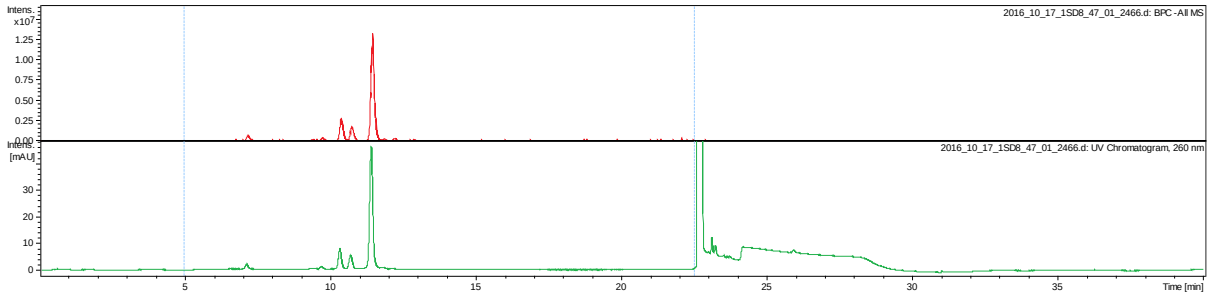

Extracted mass spectrum 1 (10.2 – 10.5 min.):

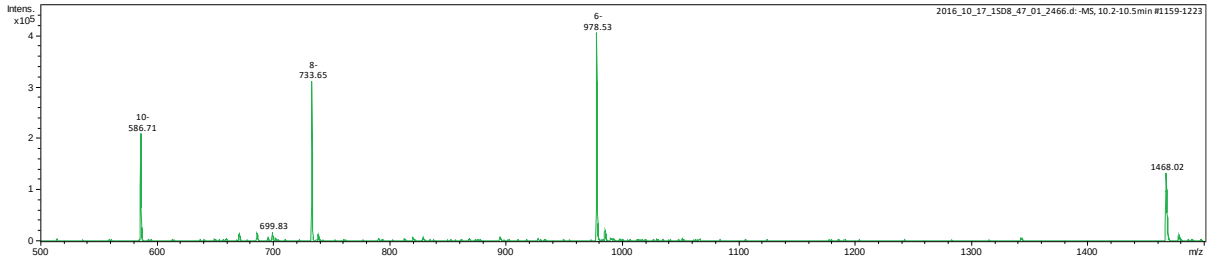

Deconvoluted mass 1: 2938.58

Extracted mass spectrum 2 (10.5 – 10.8 min.):

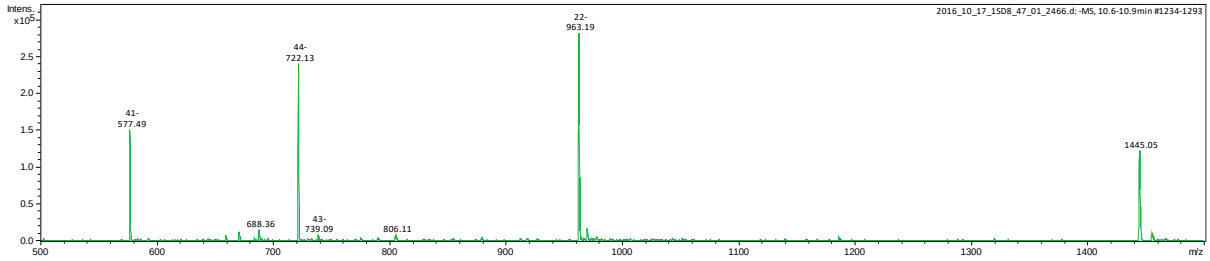

Deconvoluted mass 2: 2892.49

Extracted mass spectrum 3 (11.2 – 11.7 min.):

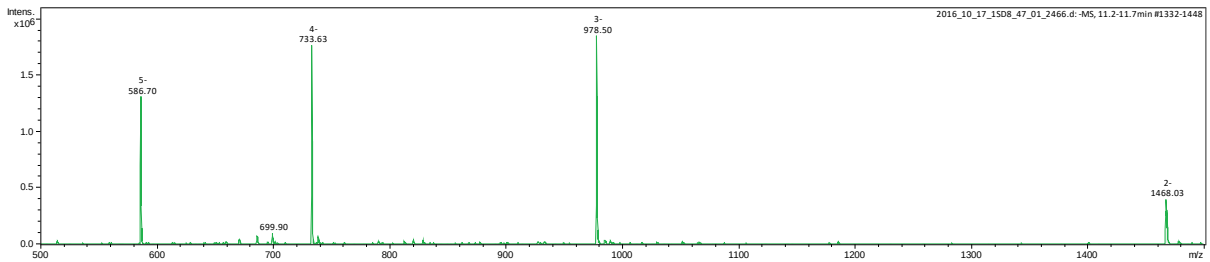

Deconvoluted mass 3: 2938.53

Sequence: 5’-GAXATGGXTG-3’ (B)

Modification: X = 2’,6’-Dimethyl-4’-methylthioazobenzene (S-DMAB)

Calculated mass: 3387.92

Data file: 2016_10_17_2SD8_48_01_2467

UV-chromatogram (260 nm):

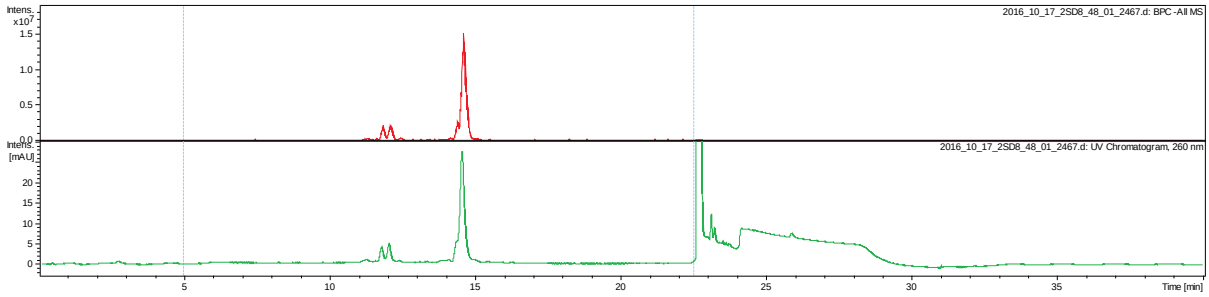

Extracted mass spectrum 1 (11.5 – 12.3 min.):

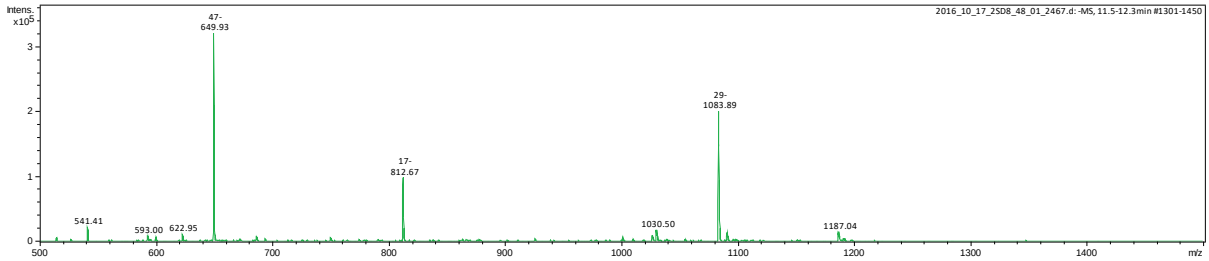

Deconvoluted mass 1: 3254.68

Extracted mass spectrum 2 (14.2 – 14.8 min.):

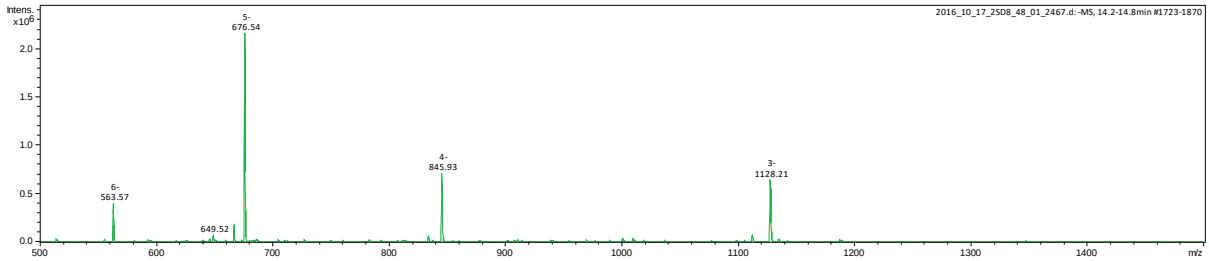

Deconvoluted mass 2: 3387.66

Sequence: 5’-GAXATXGGXTG-3’ (C)

Modification: X = 2’,6’-Dimethyl-4’-methylthioazobenzene (S-DMAB)

Calculated mass: 3837.04

Data file: 2016_10_17_3SD8_49_01_2468

UV-chromatogram (260 nm):

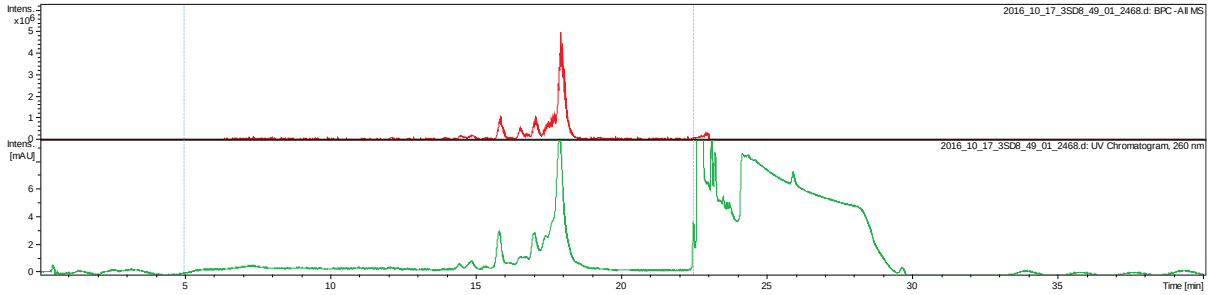

Extracted mass spectrum 1 (15.6 – 16.0 min.):

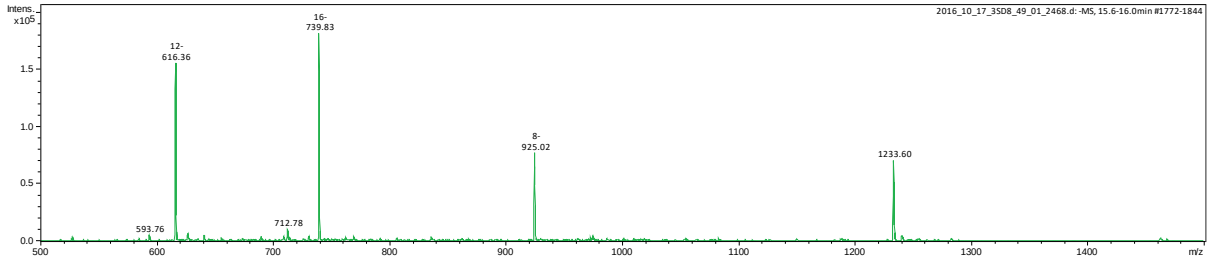

Deconvoluted mass 1: 3703.83

Extracted mass spectrum 2 (16.9 – 17.1 min.):

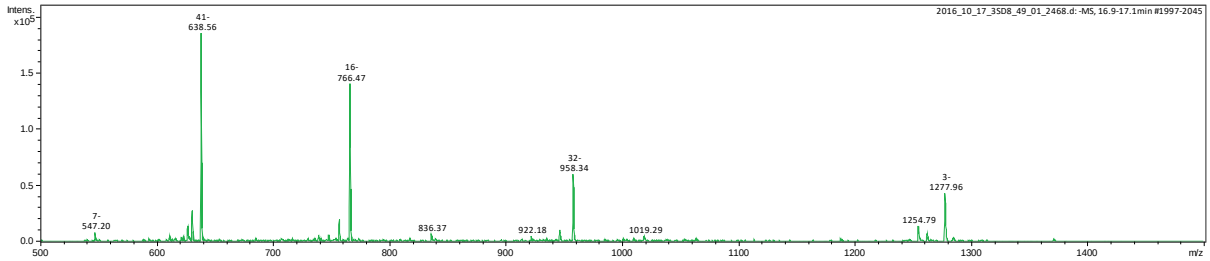

Deconvoluted mass 2: 3836.90

Extracted mass spectrum 3 (17.2 – 18.2 min.):

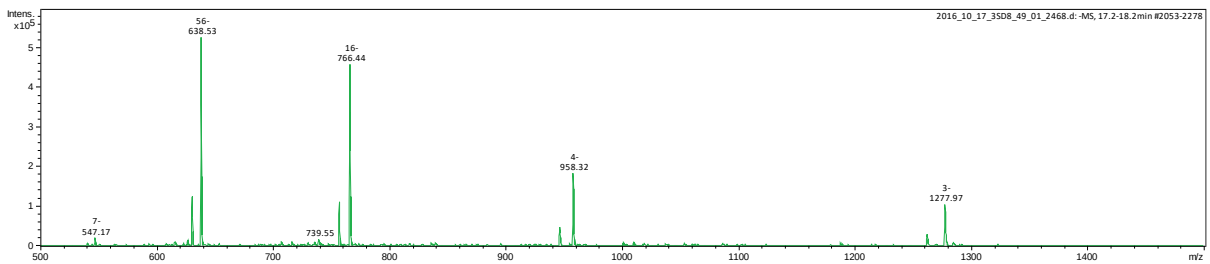

Deconvoluted mass 3: 3873.22

Sequence: 5’-CACCATXTCCGGT-3’ (D)

Modification: X = 2’,6’-Dimethyl-4’-methylthioazobenzene (S-DMAB)

Calculated mass: 4030.51

Data file: 2016_10_17_1SD12_50_01_2469

UV-chromatogram (260 nm):

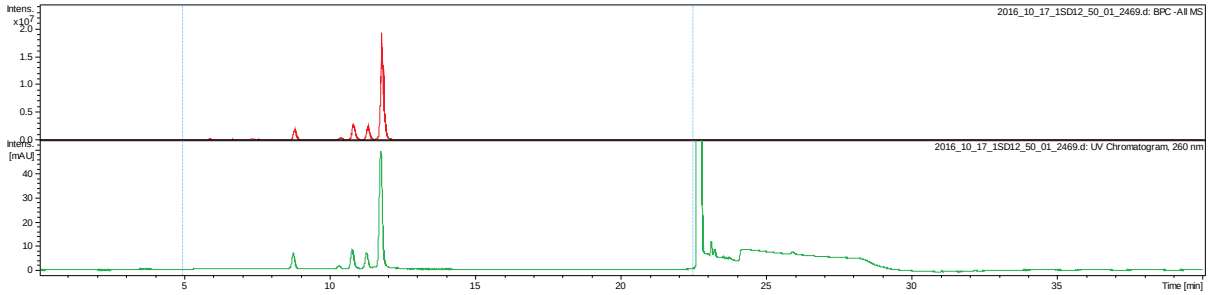

Extracted mass spectrum 1 (8.6 – 8.9 min.):

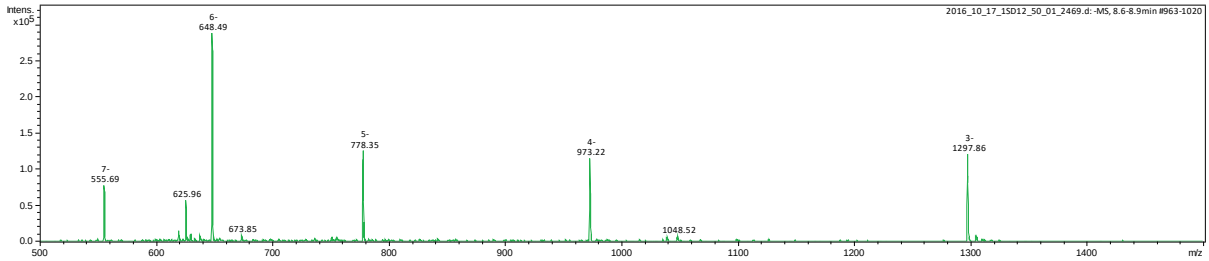

Deconvoluted mass 1: 3896.59

Extracted mass spectrum 2 (10.6 – 11.0 min.):

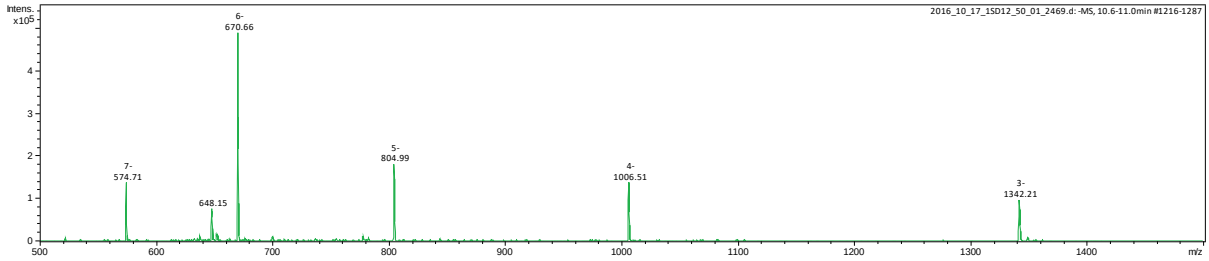

Deconvoluted mass 2: 4029.64

Extracted mass spectrum 3 (11.1 – 11.5 min.):

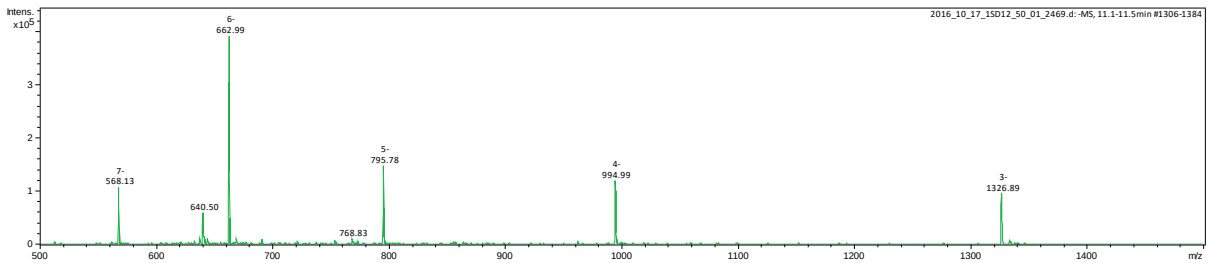

Deconvoluted mass 3: 3983.70

Extracted mass spectrum 3 (11.6 – 12.0 min.):

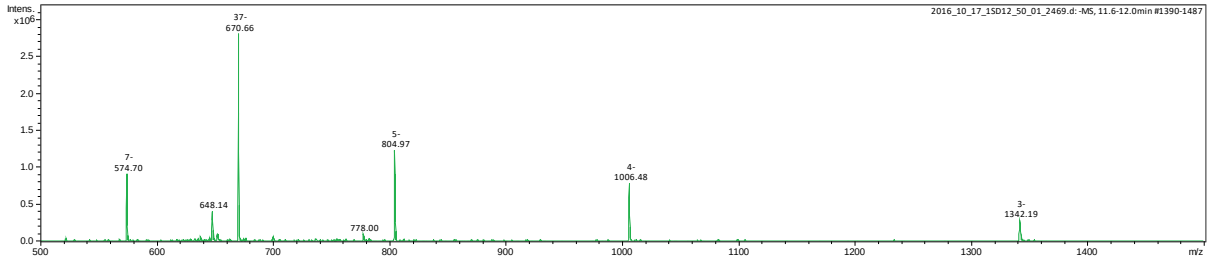

Deconvoluted mass 3: 4029.61

Sequence: 5’-CACXCATTCCXGGT-3’ (E)

Modification: X = 2’,6’-Dimethyl-4’-methylthioazobenzene (S-DMAB)

Calculated mass: 4479.63

Data file: 2016_10_17_2SD12_51_01_2470

UV-chromatogram (260 nm):

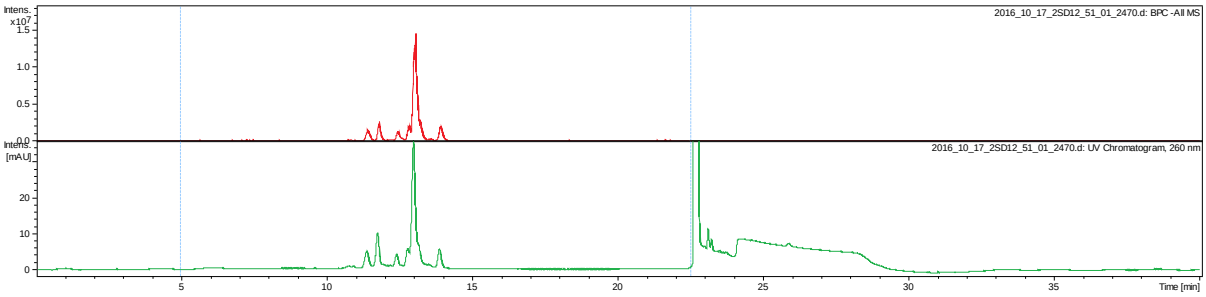

Extracted mass spectrum 1 (11.2 – 11.6 min.):

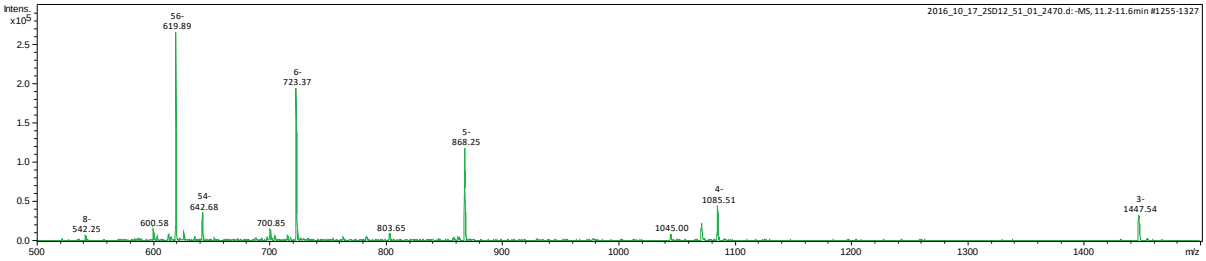

Deconvoluted mass 1: 4346.06

Extracted mass spectrum 2 (11.6 – 11.9 min.):

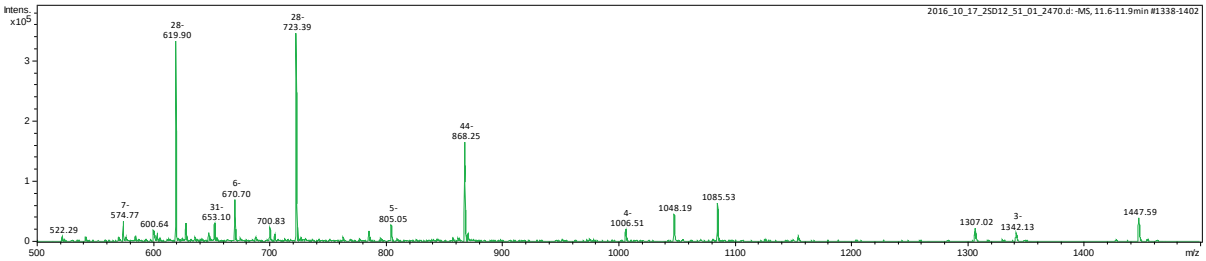

Deconvoluted mass 2: 4346.30

Extracted mass spectrum 3 (12.2 – 12.6 min.):

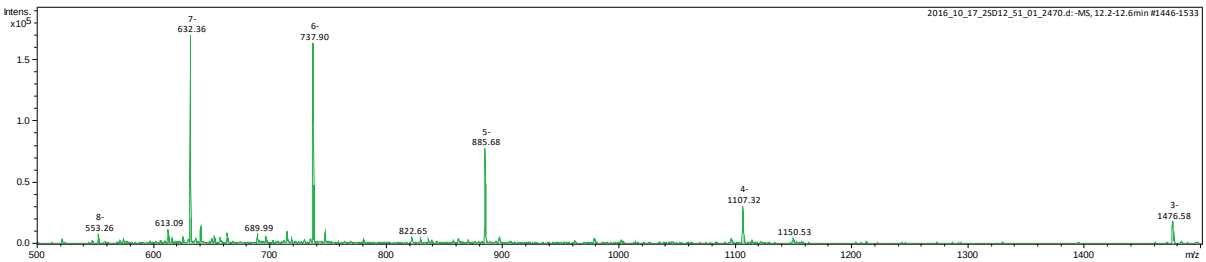

Deconvoluted mass 3: 4433.33

Extracted mass spectrum 4 (12.6 – 13.3 min.):

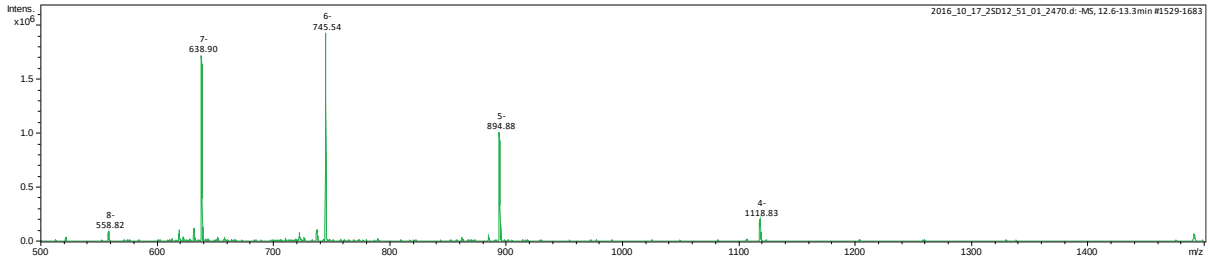

Deconvoluted mass 4: 4479.34

Extracted mass spectrum 5 (13.6 – 14.0 min.):

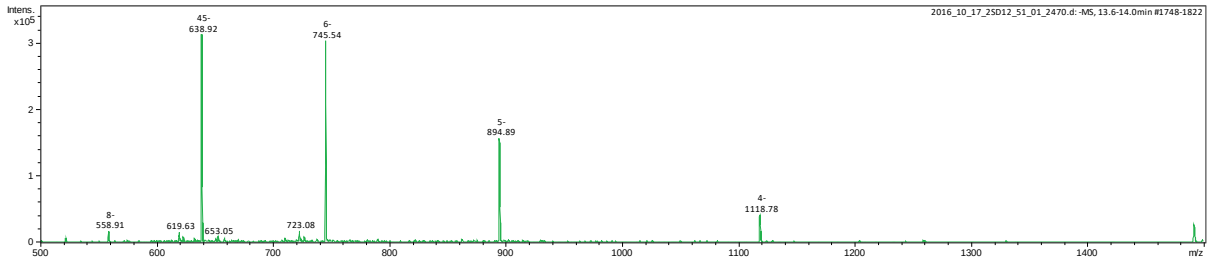

Deconvoluted mass 5: 4479.47

Sequence: 5’-CACXCATXTCCXGGT-3’ (F)

Modification: X = 2’,6’-Dimethyl-4’-methylthioazobenzene (S-DMAB)

Calculated mass: 4928.74

Data file: 2016_10_17_3SD12_52_01_2471

UV-chromatogram (260 nm):

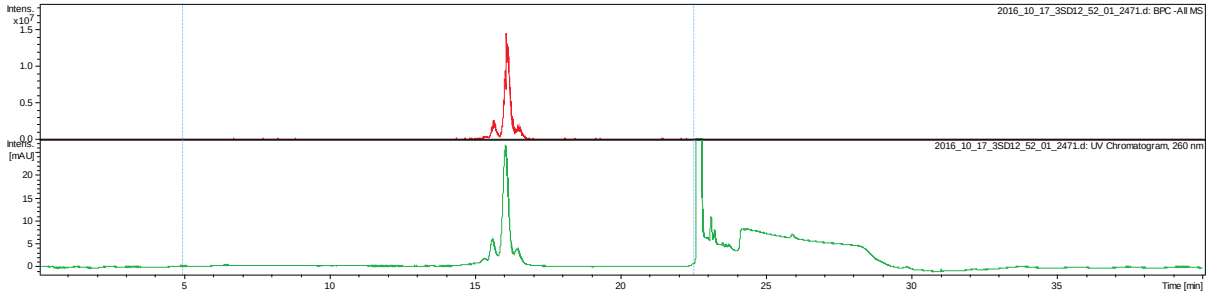

Extracted mass spectrum 1 (15.4 – 15.8 min.):

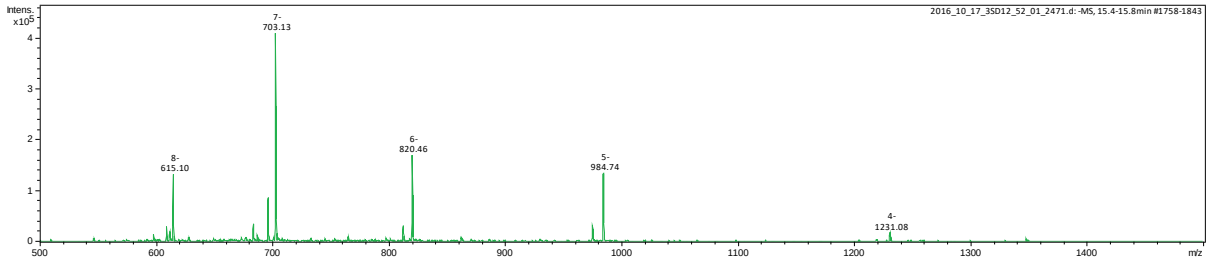

Deconvoluted mass 1: 4928.74

Extracted mass spectrum 2 (15.9 – 16.6 min.):

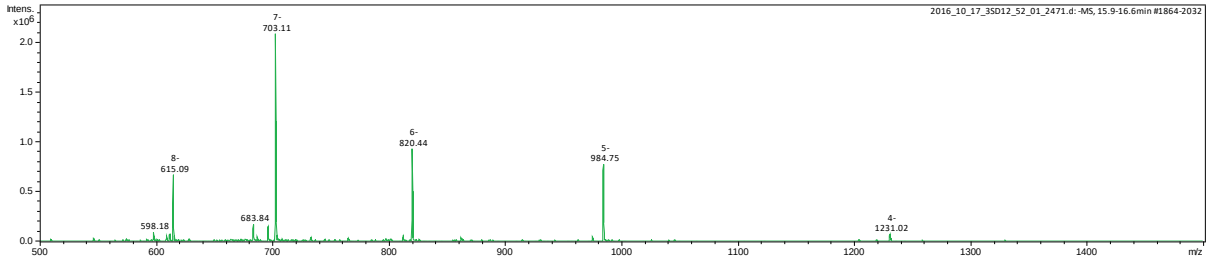

Deconvoluted mass 2: 4928.70

Sequence: 5‘-TCCXCCAXGCAXTCG-3‘ (I)

Modification: X = 2’,6’-Dimethyl-4’-methylthioazobenzene (S-DMAB)

Calculated mass: 4913.73

Data file: 2016_10_17_SDA-168ROo_55_01_2474

UV-chromatogram (260 nm):

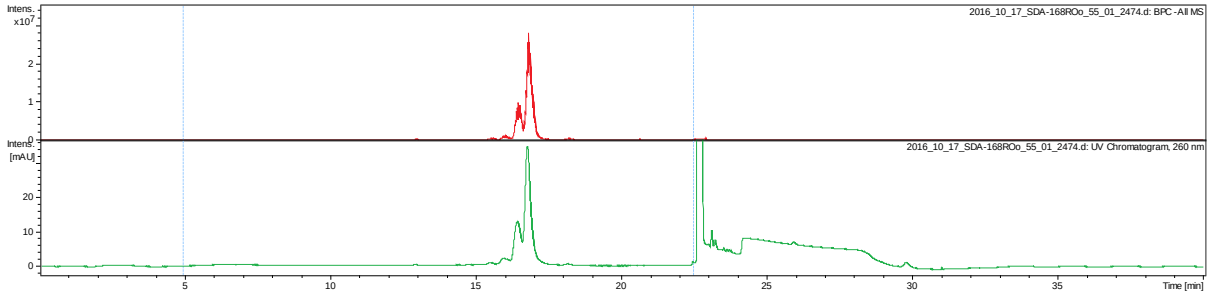

Extracted mass spectrum 1 (16.2 – 16.7 min.):

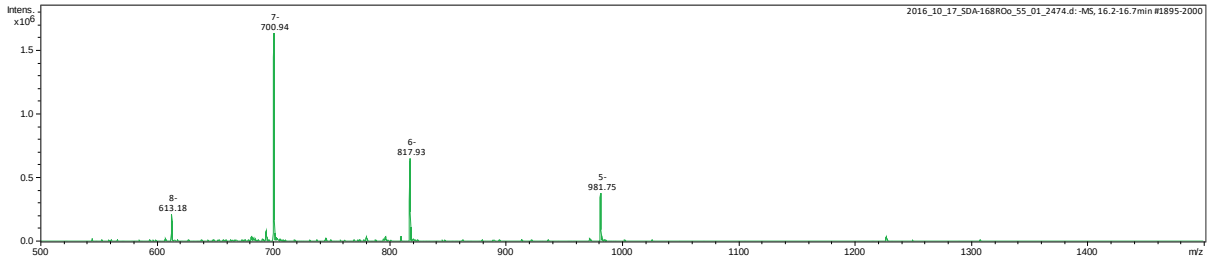

Deconvoluted mass 1: 4913.63

Extracted mass spectrum 2 (16.7 – 17.3 min.):

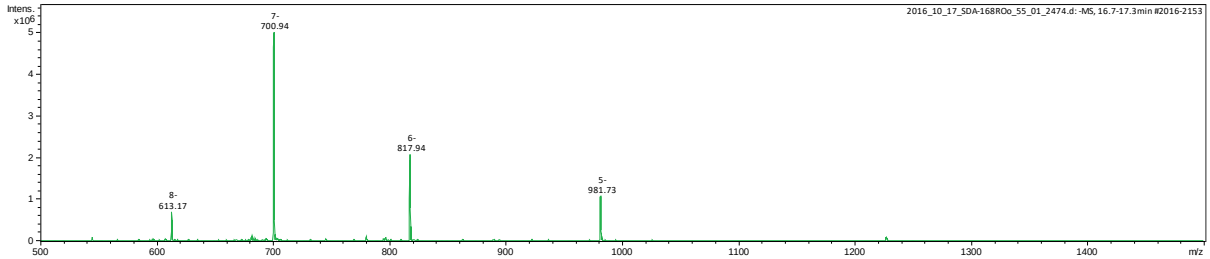

Deconvoluted mass 2: 4913.70

Sequence: 5‘-CCXGATXGCTXGT-3‘ (J)

Modification: X = 2’,6’-Dimethyl-4’-methylthioazobenzene (S-DMAB)

Calculated mass: 4366.37

Data file: 2016_10_17_SDA-126ROo_53_01_2472

UV-chromatogram (260 nm):

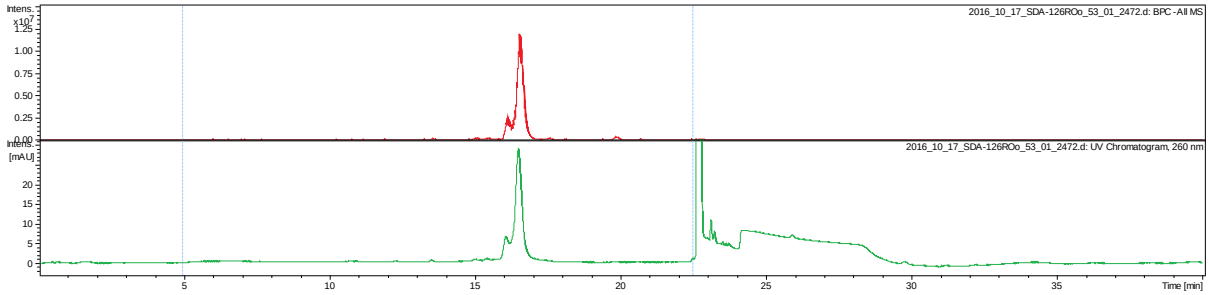

Extracted mass spectrum (15.8 – 16.2 min.):

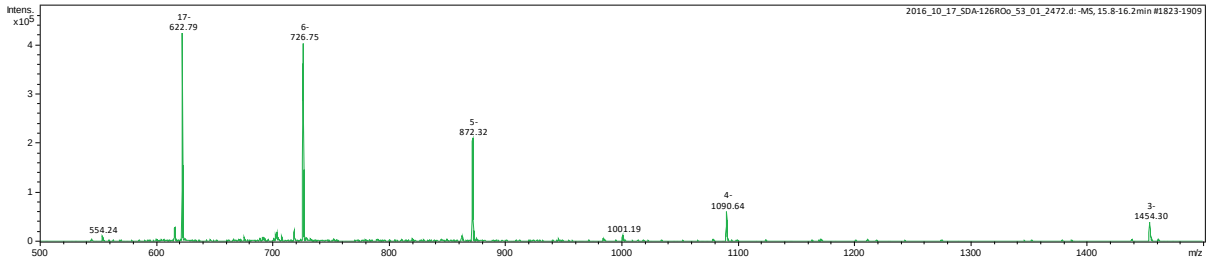

Deconvoluted mass:4366.55

Sequence: 5‘-GGXAATXGGTXGA-3‘ (K)

Modification: X = 2’,6’-Dimethyl-4’-methylthioazobenzene (S-DMAB)

Calculated mass: 4479.46

Data file: 2016_10_17_SDA-126ROp_54_01_2473

UV-chromatogram (260 nm):

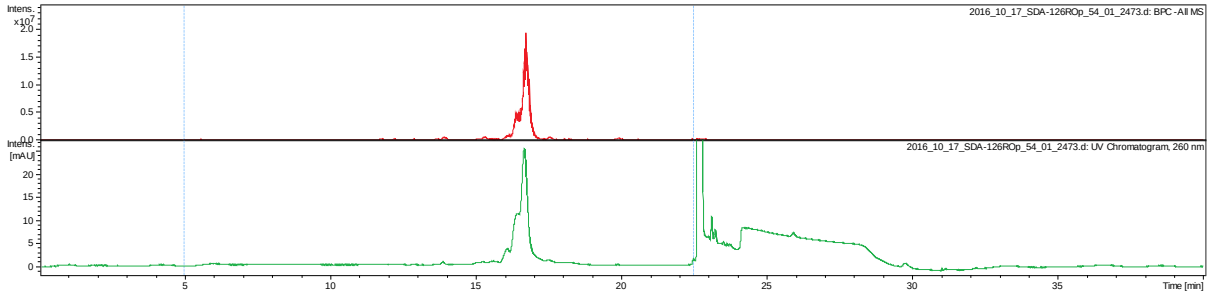

Extracted mass spectrum 1 (15.8 – 16.2 min.):

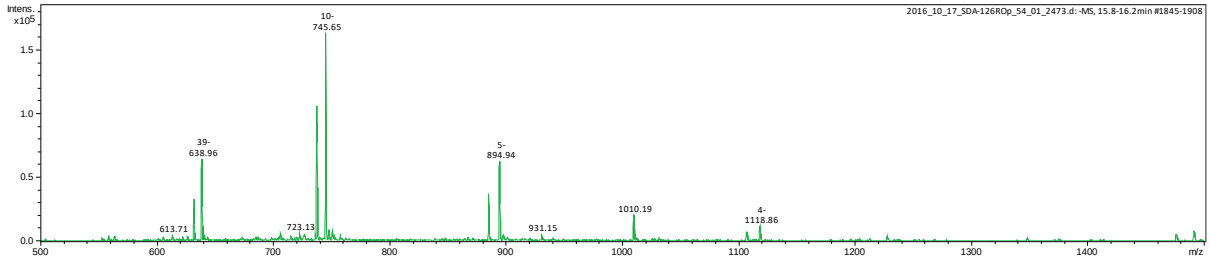

Deconvoluted mass 1: 4479.92 + 4433.75

Extracted mass spectrum 2 (16.2 – 17.2 min.):

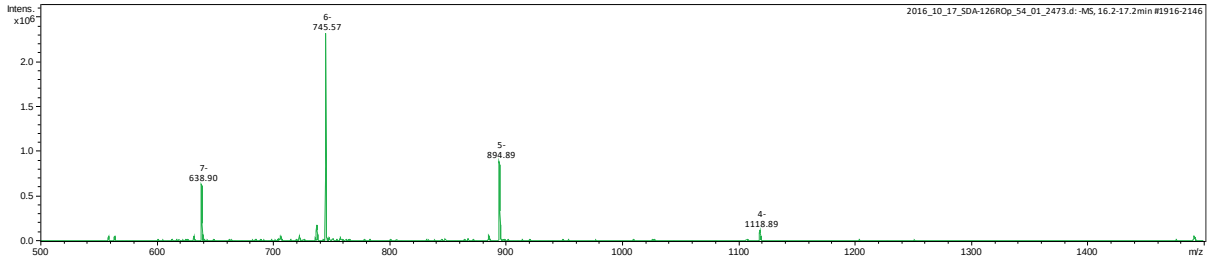

Deconvoluted mass 2: 4479.46

Sequence: 5’-GAATXGGTG-3’ (A)

Modification: X =2’,6’-Difluoroazobenzene (DFAB)

Calculated mass: 2900.77

Data file: 2016_06_01_1DF8_21_01_1358

UV-chromatogram (260 nm):

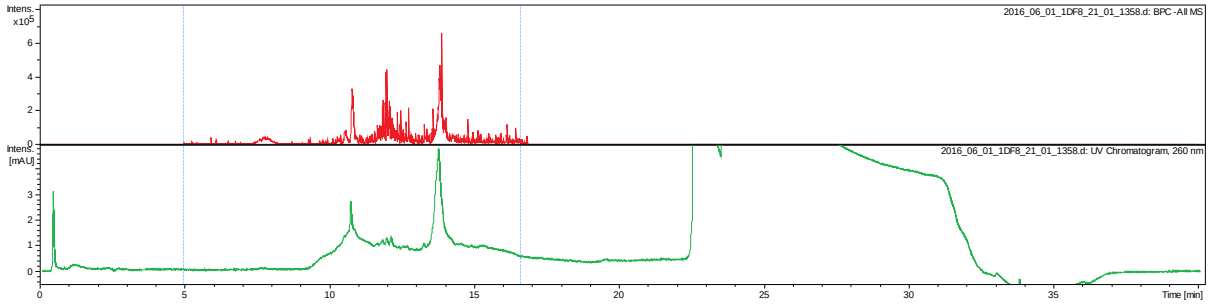

Extracted mass spectrum (13.7 – 14.0 min.):

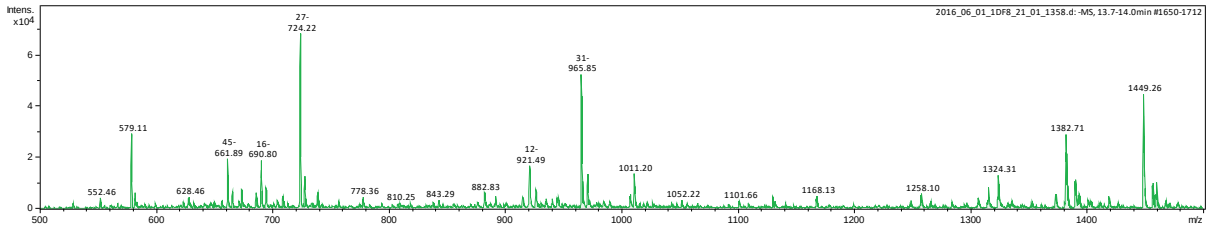

Deconvoluted mass: 2900.92

Sequence: 5’-CACCATXTCCGGT-3’ (D)

Modification: X = 2’,6’-Difluoroazobenzene (DFAB)

Calculated mass: 3992.47

Data file: 2016_06_01_1DF12_28_01_1365

UV-chromatogram (260 nm):

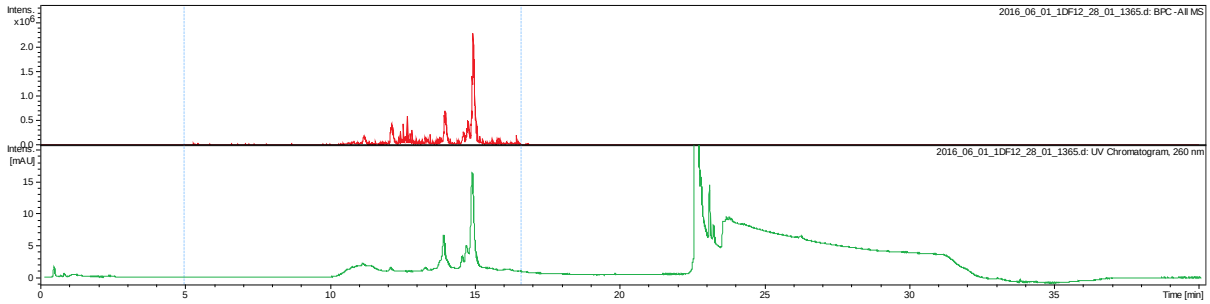

Extracted mass spectrum 1 (13.8 – 14.2 min.):

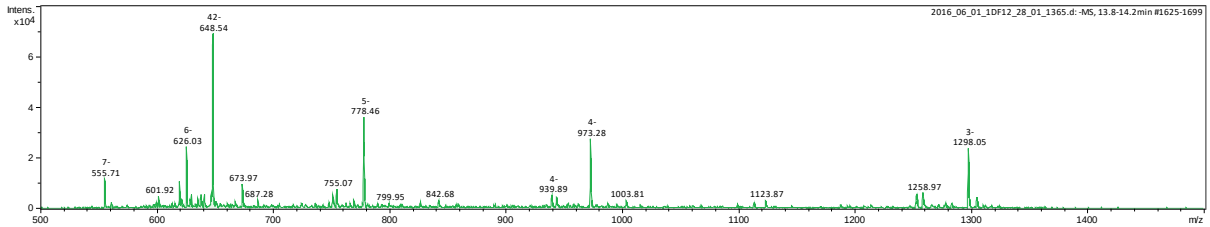

Deconvoluted mass 1: 3897.18

Extracted mass spectrum 2 (14.4 – 15.0 min.):

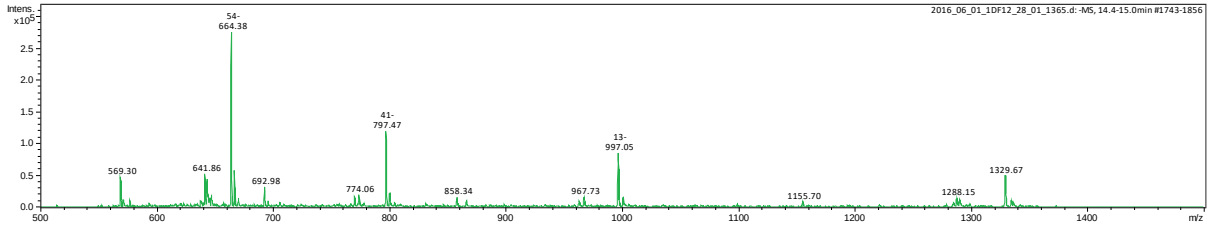

Deconvoluted mass 2: 3992.39

Sequence: 5’-GAATXGGTG-3’ (A)

Modification: X =2’,6’-Dimethoxyazobenzene (DOAB)

Calculated mass: 2924.81

Data file: 2016_09_26_1xDOAB-8_70_01_2328

UV-chromatogram (260 nm):

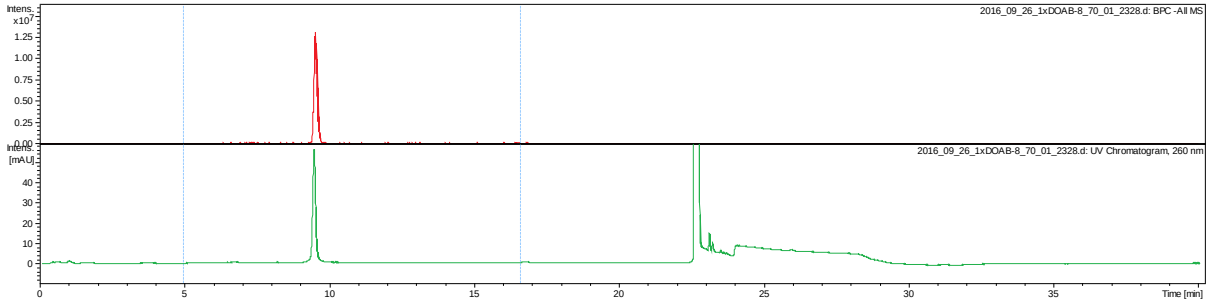

Extracted mass spectrum 1 (9.2 – 9.8 min.):

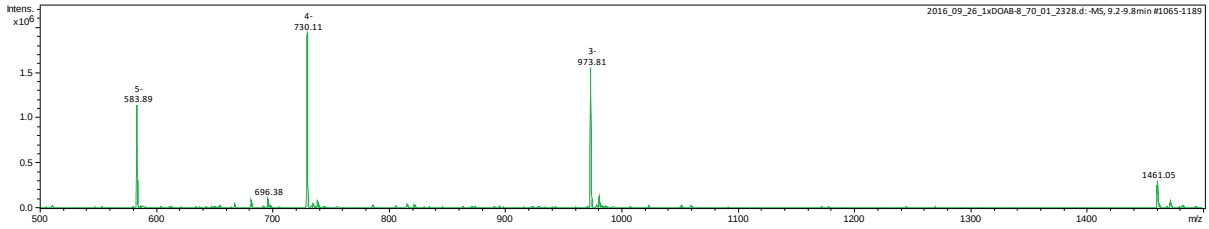

Deconvoluted mass: 2924.47

Sequence: 5’-CACCATXTCCGGT-3’ (D)

Modification: X = 2’,6’-Dimethoxyazobenzene (DOAB)

Calculated mass: 4016.52

Data file: 2016_09_26_1xDOAB-12_71_01_2329

UV-chromatogram (260 nm):

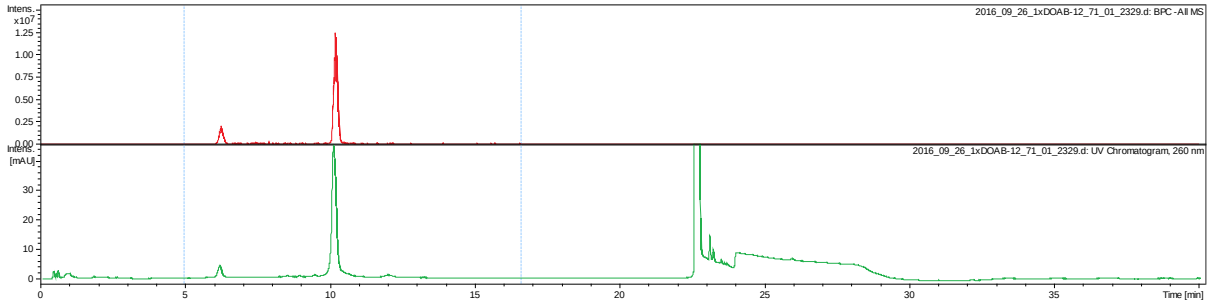

Extracted mass spectrum 1 (6.0 – 6.5 min.):

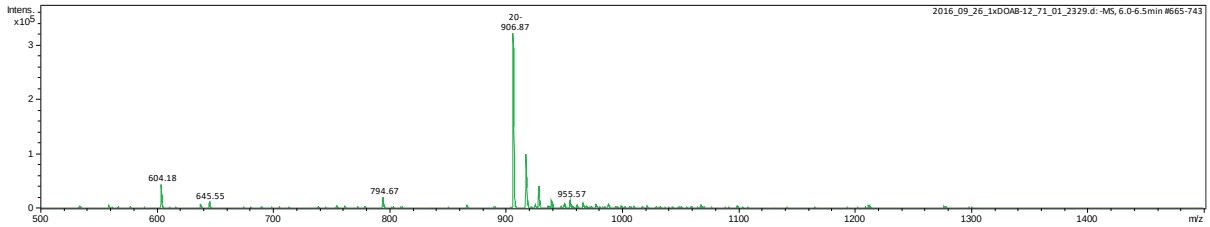

Deconvoluted mass 1: 1815.57

Extracted mass spectrum 1 (xx – xx min.):

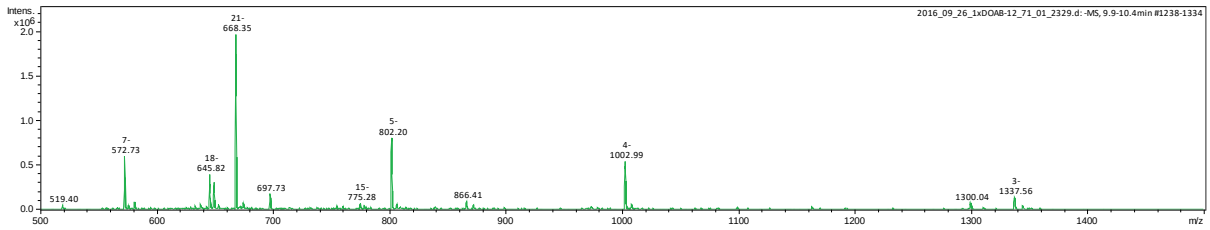

Deconvoluted mass 2: 4015.99

Sequence: 5’-GAATXGGTG-3’ (A)

Modification: X = *N*-Methyl-arylazopyrazole (AAP1)

Calculated mass: 2896.82

Data file: 2016_06_01_1AP1-8_11_01_1348

UV-chromatogram (260 nm):

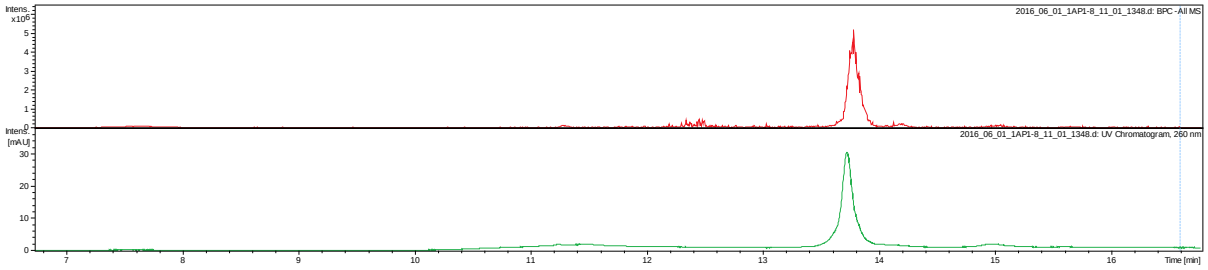

Extracted mass spectrum (13.6 – 13.8 min.):

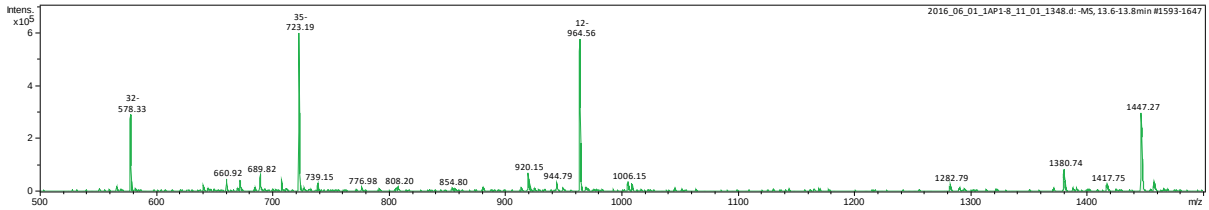

Deconvoluted mass: 2896.79

Sequence: 5’-GAXATGGXTG-3’ (B)

Modification: X = *N*-Methyl-arylazopyrazole (AAP1)

Calculated mass: 3303.96

Data file: 2016_06_01_2AP1-8.1_13_01_1350

UV-chromatogram (260 nm):

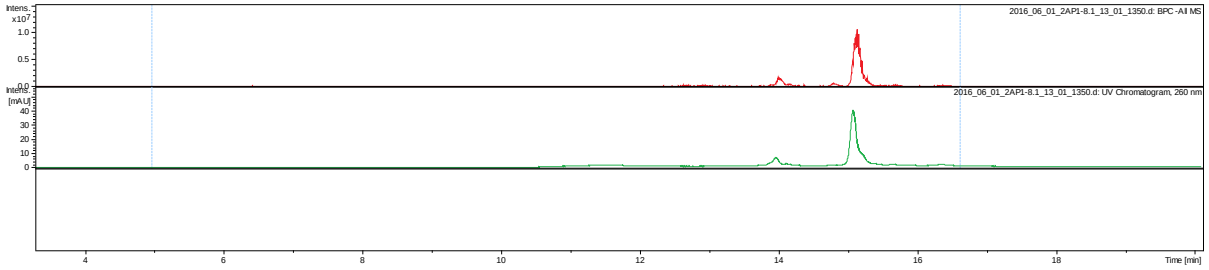

Extracted mass spectrum 1 (13.8 – 14.0 min.):

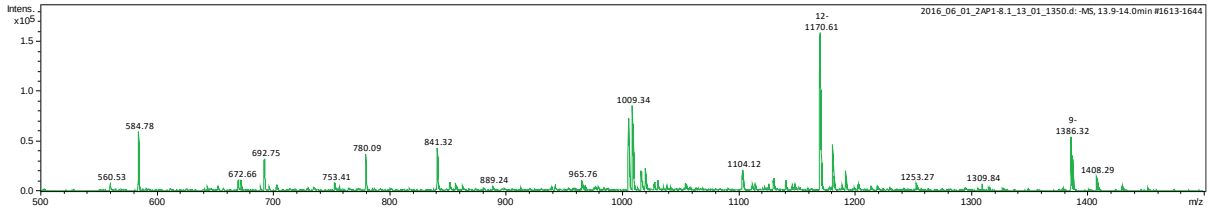

Deconvoluted mass 1: 2770.60

Extracted mass spectrum 2 (14.9 – 15.3 min.):

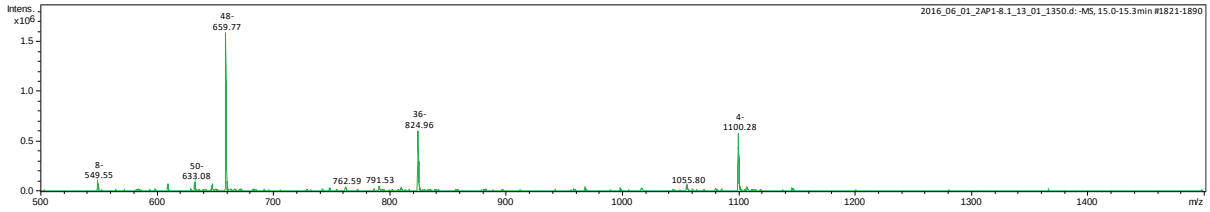

Deconvoluted mass 2: 3303.87

Sequence: 5’-GAXATXGGXTG-3’ (C)

Modification: X = *N*-Methyl-arylazopyrazole (AAP1)

Calculated mass: 3711.10

Data file: 2016_06_01_3AP1-8.1_15_01_1352

UV-chromatogram (260 nm):

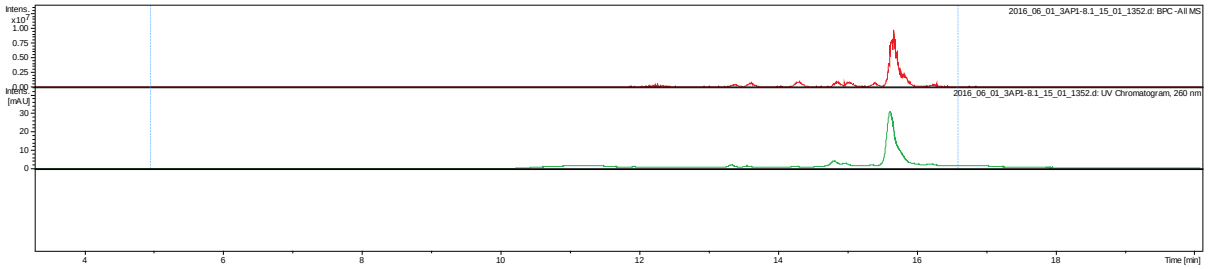

Extracted mass spectrum 1 (14.7 – 15.0 min.):

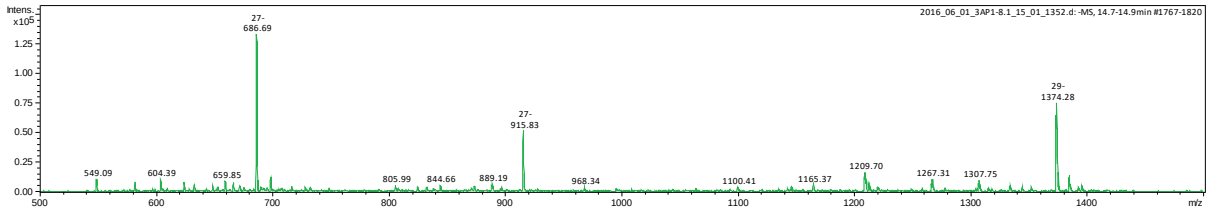

Deconvoluted mass 1: 2750.52

Extracted mass spectrum 2 (15.5 – 15.8 min.):

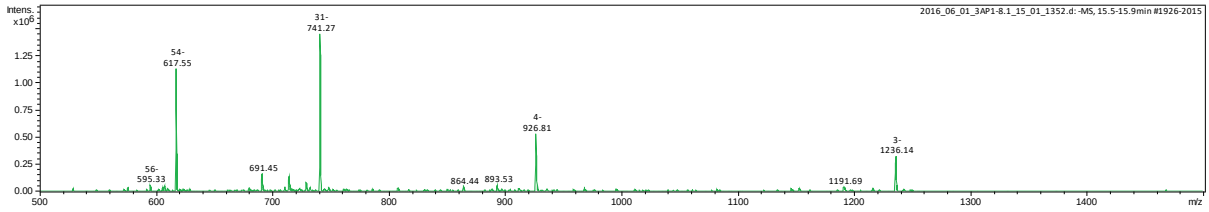

Deconvoluted mass 2: 3711.25

Sequence: 5’-CACCATXTCCGGT-3’ (D)

Modification: X = *N*-Methyl-arylazopyrazole (AAP1)

Calculated mass: 3988.53

Data file: 2016_06_01_1AP1-12_16_01_1353

UV-chromatogram (260 nm):

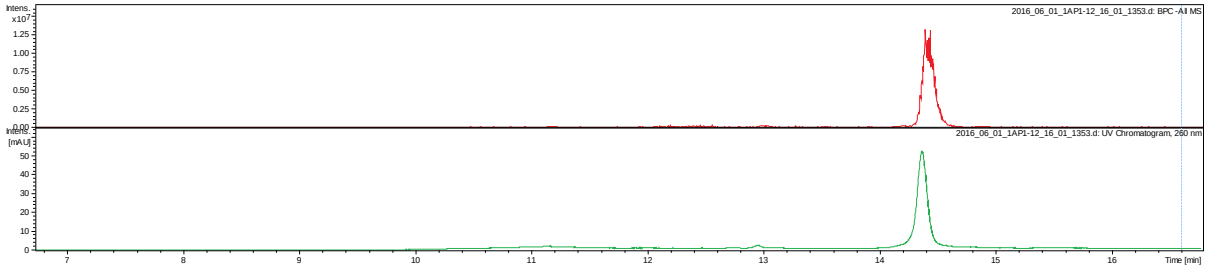

Extracted mass spectrum (14.3 – 14.5 min.):

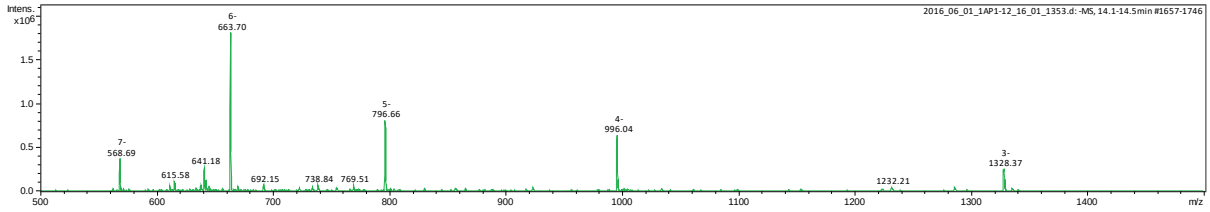

Deconvoluted mass: 3988.19

Sequence: 5’-CACXCATTCCXGGT-3’ (E)

Modification: X = *N*-Methyl-arylazopyrazole (AAP1)

Calculated mass: 4395.66

Data file: 2016_06_01_2AP1-12_18_01_1355

UV-chromatogram (260 nm):

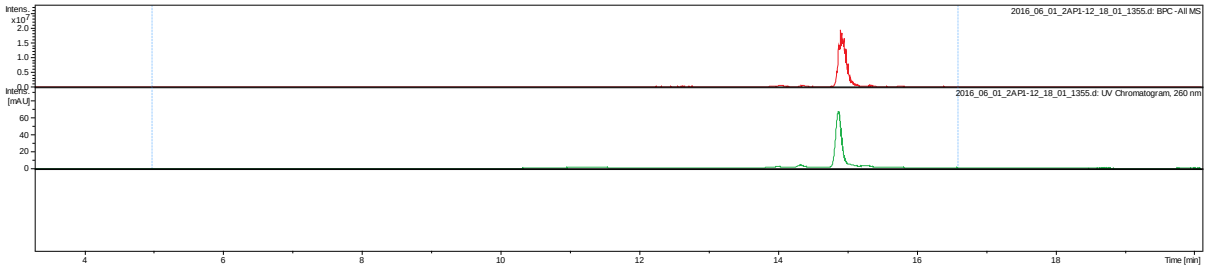

Extracted mass spectrum (14.8 – 15.0 min.):

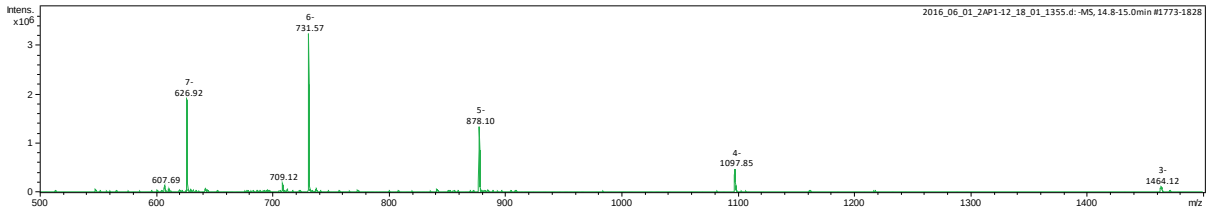

Deconvoluted mass: 4395.48

Sequence: 5’-CACXCATXTCCXGGT-3’ (F)

Modification: X = *N*-Methyl-arylazopyrazole (AAP1)

Calculated mass: 4802.80

Data file: 2016_06_01_3AP1-12_19_01_1356

UV-chromatogram (260 nm):

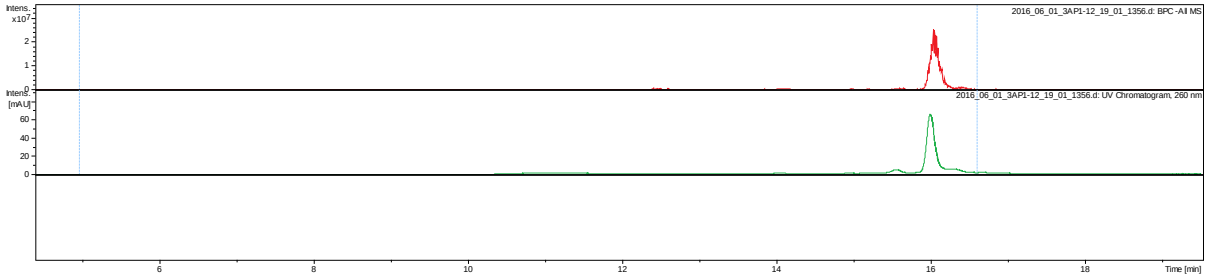

Extracted mass spectrum 1 (15.4 – 15.6 min.):

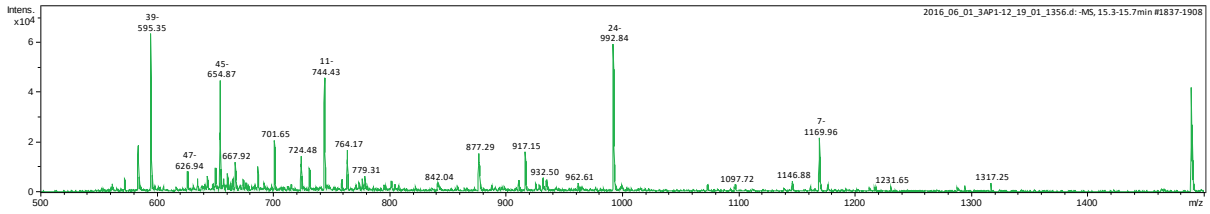

Deconvoluted mass 1: 2981.76

Extracted mass spectrum 2 (15.9 – 16.2 min.):

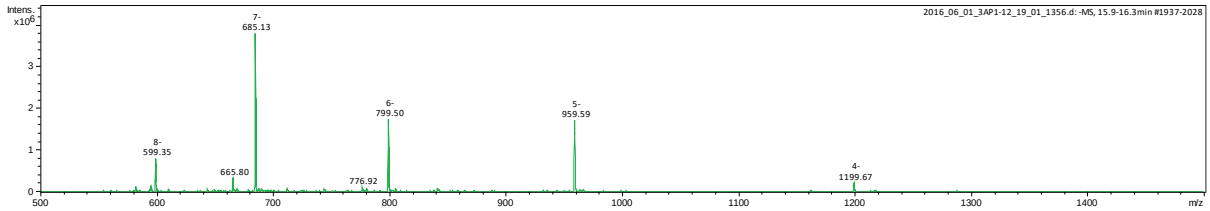

Deconvoluted mass 2: 4803.00

Sequence: 5’-CACCXATTCXCAGT-3’ (G)

Modification: X = *N*-Methyl-arylazopyrazole (AAP1)

Calculated mass: 4379.68

Data file: 2017_03_02_2xAAP1_12-mer_71_01_3851

UV-chromatogram (260 nm):

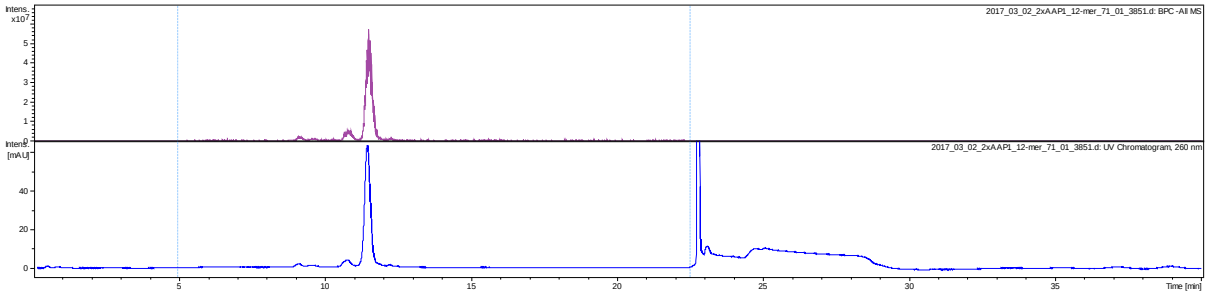

Extracted mass spectrum 1 (10.5 – 11.0 min.):

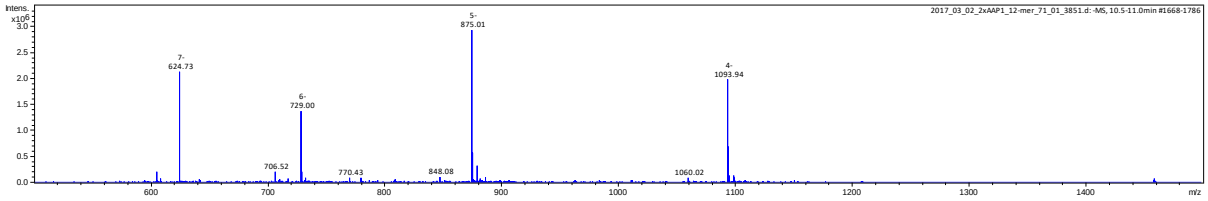

Deconvoluted mass 1: 4379.78

Extracted mass spectrum 2 (11.2 – 11.8 min.):

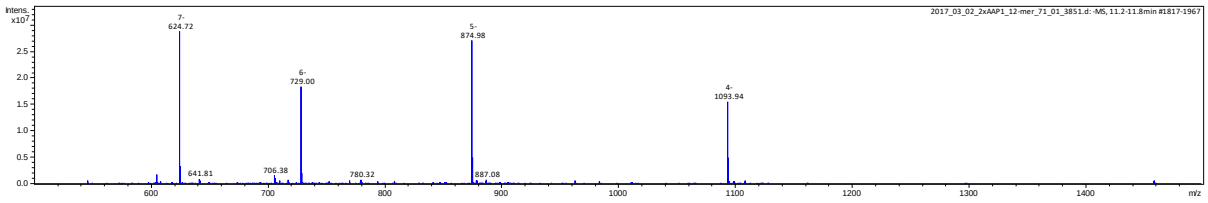

Deconvoluted mass 2: 4379.78

Sequence: 5’-CACXCATXTCCXAGT-3’ (H)

Modification: X = *N*-Methyl-arylazopyrazole (AAP1)

Calculated mass: 4786.82

Data file: 2017_03_02_3xAAP1_12-mer-50_72_01_3852

UV-chromatogram (260 nm):

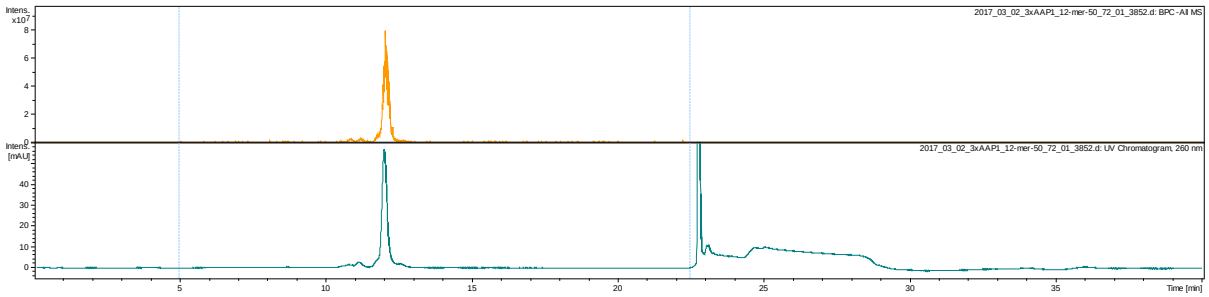

Extracted mass spectrum (11.8 – 12.4 min.):

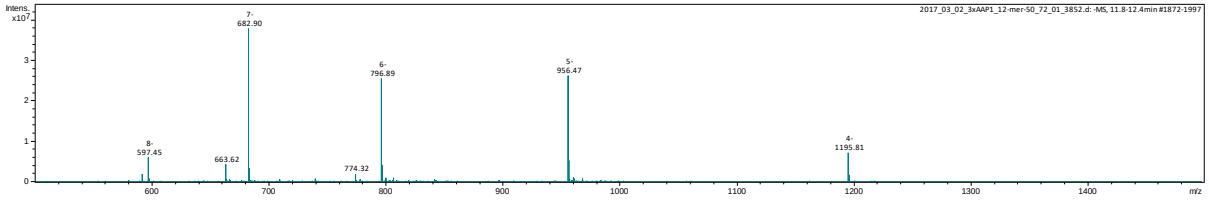

Deconvoluted mass: 4787.29

Sequence: 5‘-TCCXCCAXGCAXTCG-3‘ (I)

Modification: X = *N*-Methyl-arylazopyrazole (AAP1)

Calculated mass: 4787.89

Data file: 2016_10_17_AAP1-168ROo-1_59_01_2478

UV-chromatogram (260 nm):

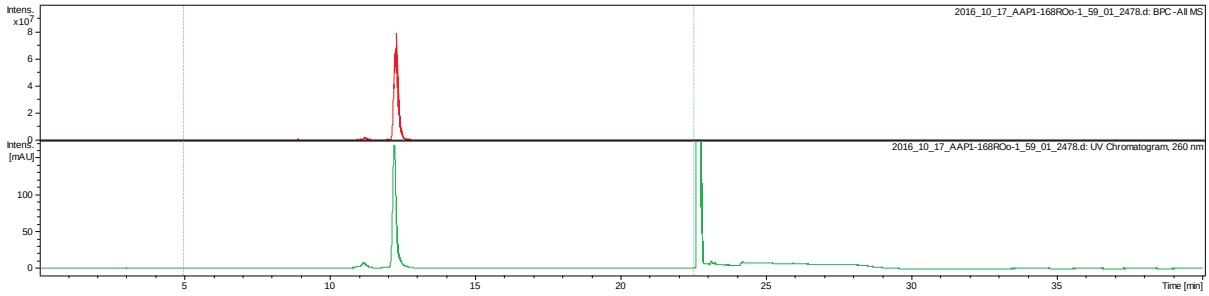

Extracted mass spectrum (12.1 – 12.5 min.):

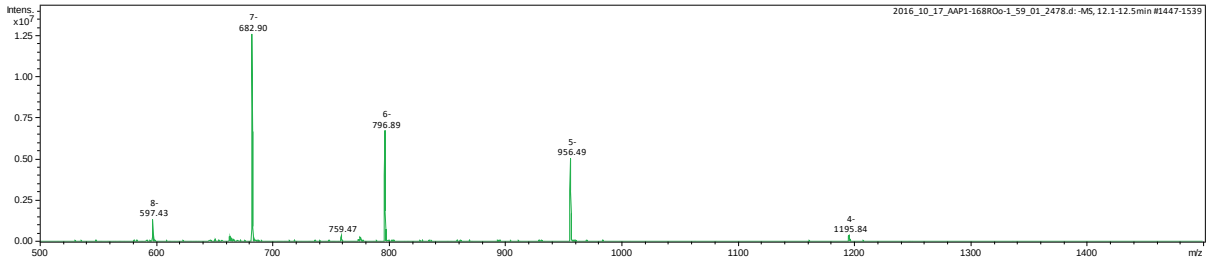

Deconvoluted mass: 4787.41

Sequence: 5‘-CCXGATXGCTXGT-3‘ (J)

Modification: X = *N*-Methyl-arylazopyrazole (AAP1)

Calculated mass: 4240.43

Data file: 2016_10_17_AAP1-126ROo_57_01_2476

UV-chromatogram (260 nm):

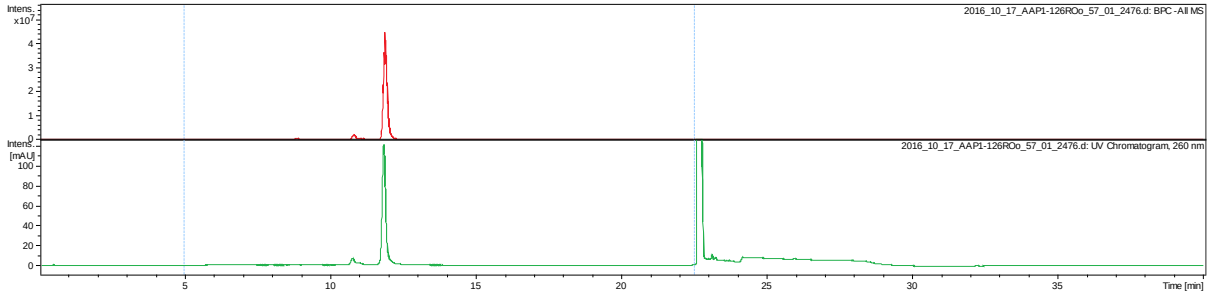

Extracted mass spectrum (11.7 – 12.2 min.):

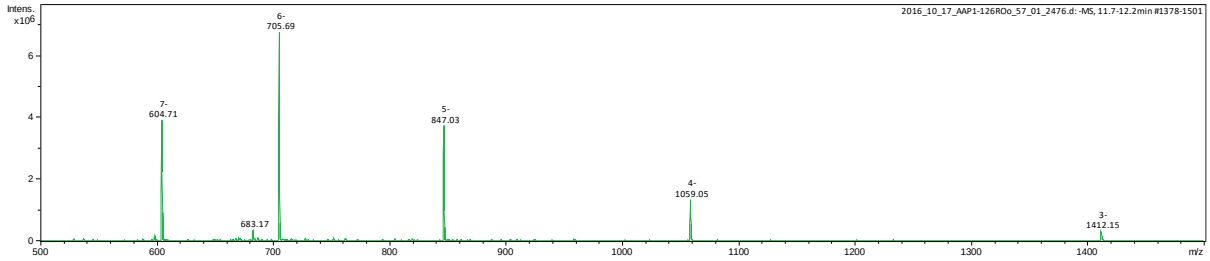

Deconvoluted mass: 4240.19

Sequence: 5‘-GGXAATXGGTXGA-3‘ (K)

Modification: X = *N*-Methyl-arylazopyrazole (AAP1)

Calculated mass: 4353.52

Data file: 2016_10_17_AAP1-126ROp_58_01_2477

UV-chromatogram (260 nm):

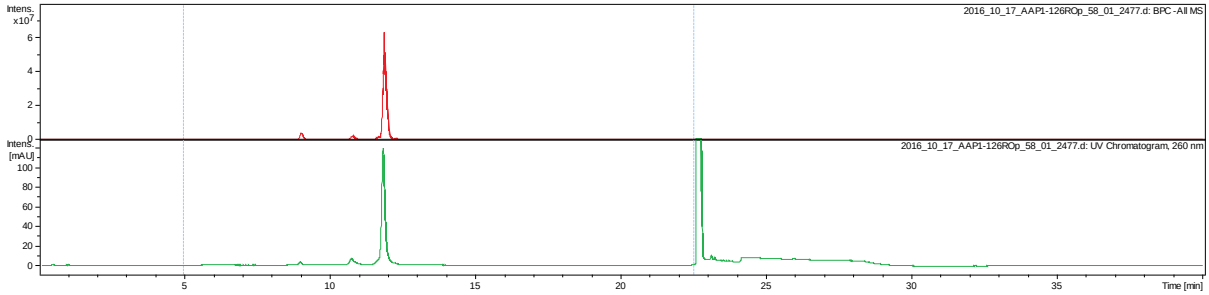

Extracted mass spectrum (11.6 – 12.2 min.):

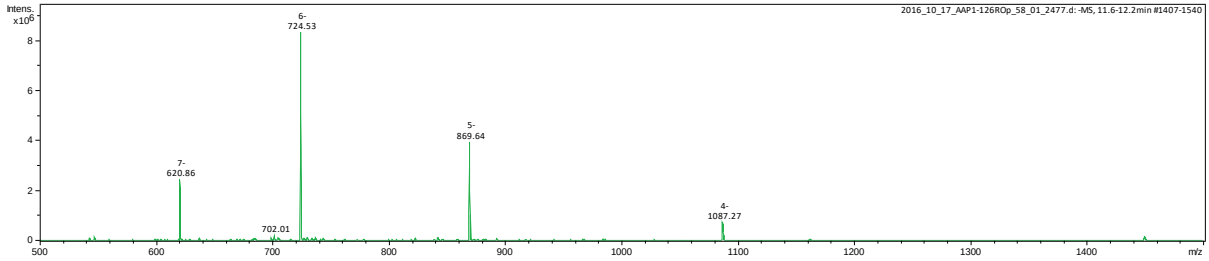

Deconvoluted mass: 4353.23

Sequence: 5‘-TCCCXCAGCXATCG-3‘ (L)

Modification: X = *N*-Methyl-arylazopyrazole (AAP1)

Calculated mass: 4380.68

Data file: 2016_11_23_AAP1-168ROo-sh_82_01_2827

UV-chromatogram (260 nm):

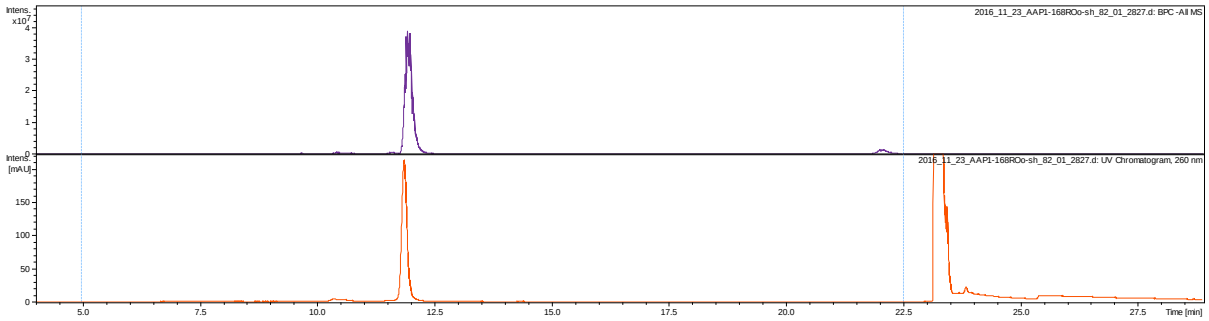

Extracted mass spectrum (11.7 – 12.1 min.):

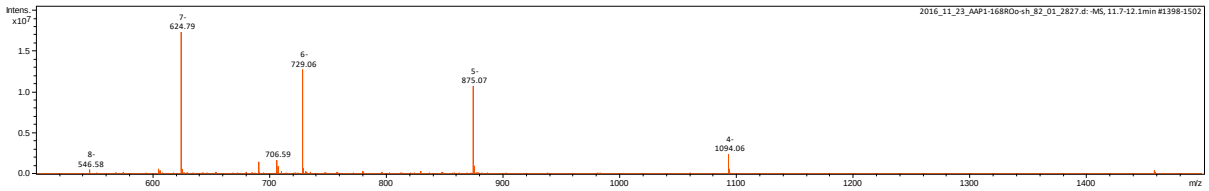

Deconvoluted mass: 4380.39

Sequence: 5’-CACCXATTCXCGGT-3’ (M)

Modification: X = *N*-Methyl-arylazopyrazole (AAP1)

Calculated mass: 4395.68

Data file: 2016_11_23_2xAAP1-12mer-sh_81_01_2826

UV-chromatogram (260 nm):

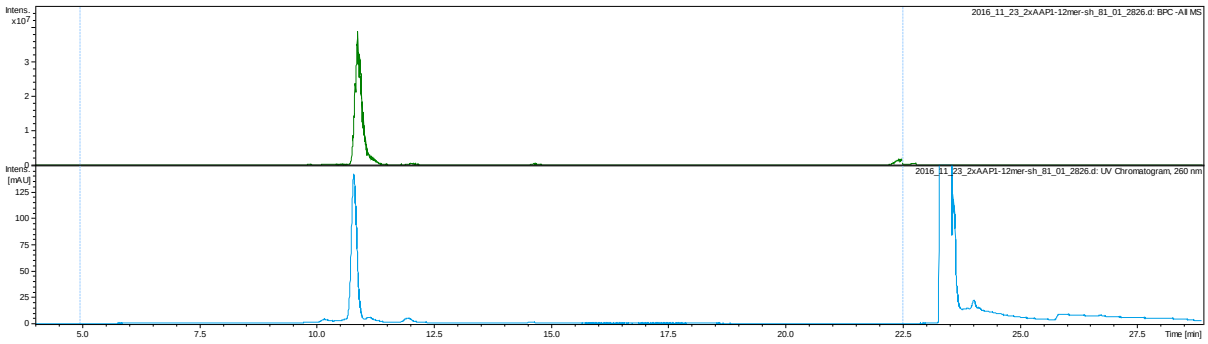

Extracted mass spectrum (10.7 – 11.0 min.):

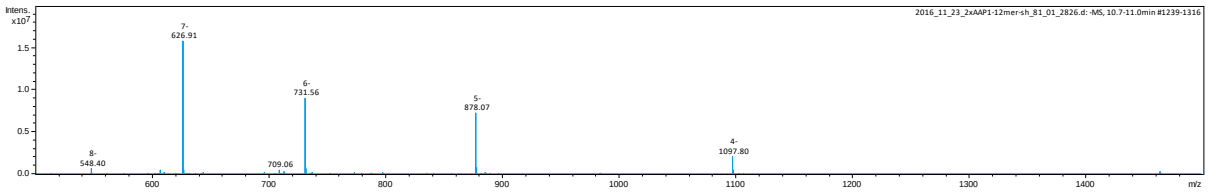

Deconvoluted mass: 4395.39

Sequence: 5’-GAATXGGTG-3’ (A)

Modification: X = *N*-Phenyl-arylazopyrazole (AAP2)

Calculated mass: 2958.84

Data file: 2016_10_23_AAP2-1_old_97_01_2565

UV-chromatogram (260 nm):

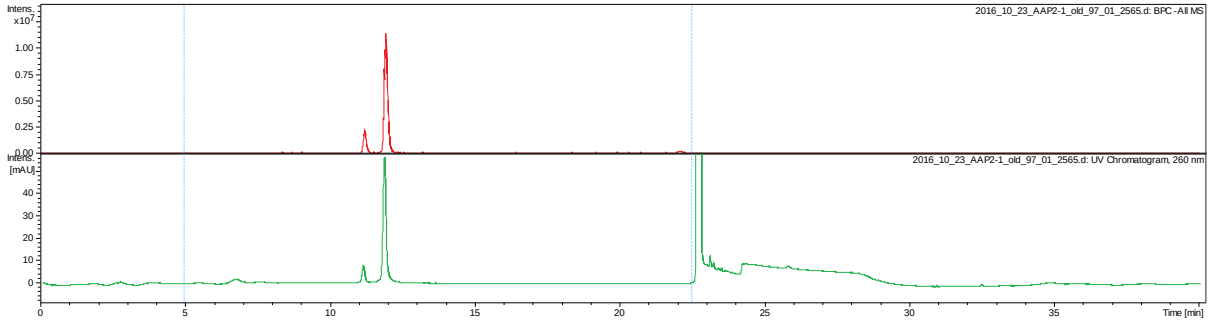

Extracted mass spectrum 1 (11.1 – 11.4 min.):

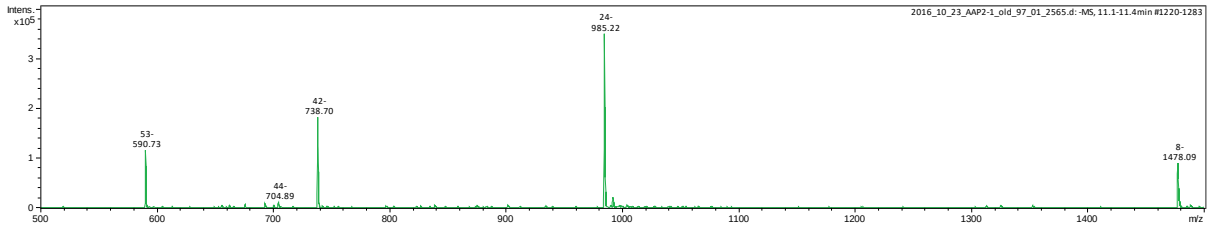

Deconvoluted mass 1: 2958.83

Extracted mass spectrum 2 (11.8 – 12.1 min.):

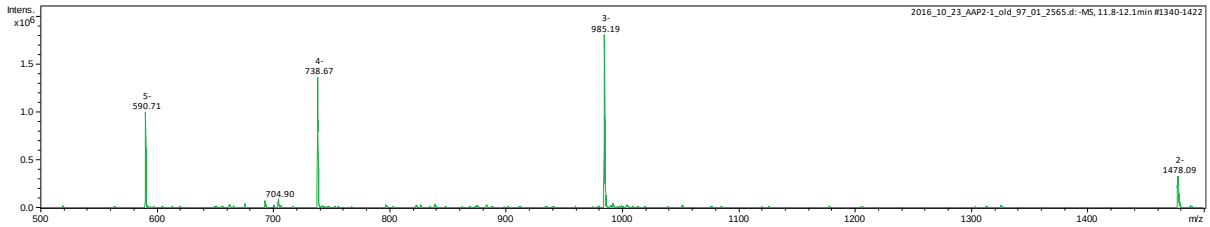

Deconvoluted mass 2: 2958.59

Sequence: 5’-GAXATGGXTG-3’ (B)

Modification: X = *N*-Phenyl-arylazopyrazole (AAP2)

Calculated mass: 3427.99

Data file: 2016_11_23_2xAAP2-in-8mer-2_73_01_2818

UV-chromatogram (260 nm):

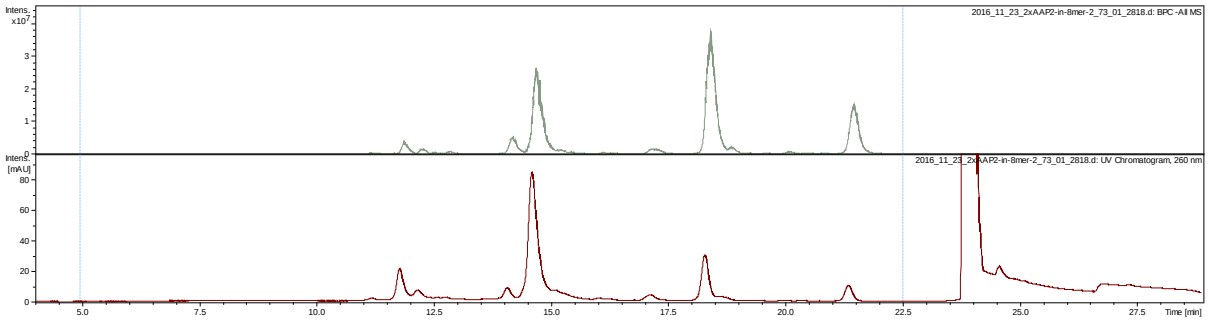

Extracted mass spectrum 1 (11.6 – 12.3 min.):

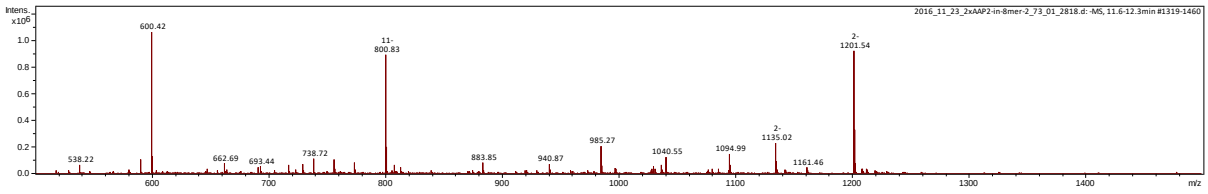

Deconvoluted mass 1: 2405.71

Extracted mass spectrum 2 (13.9 – 14.2 min.):

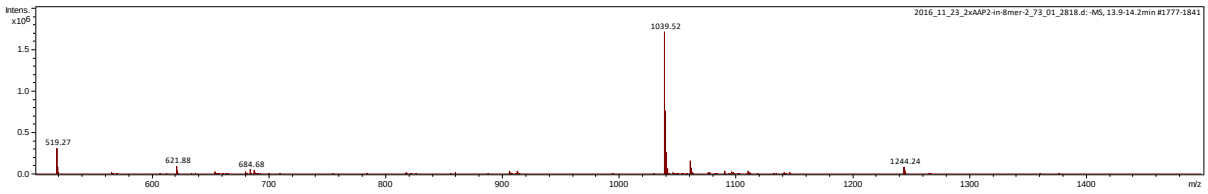

Deconvoluted mass 2: 2081.03

Extracted mass spectrum 3 (14.4 – 15.0 min.):

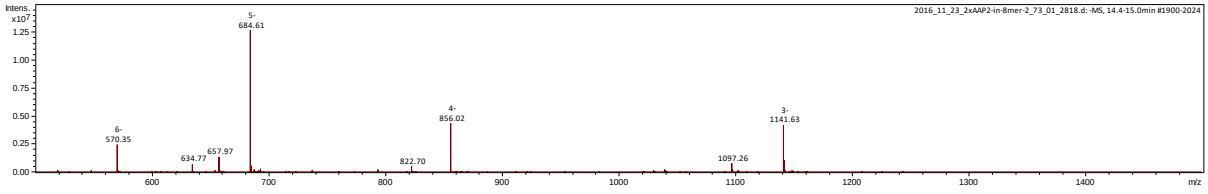

Deconvoluted mass 3: 3427.90

Extracted mass spectrum 4 (18.1 – 18.4 min.):

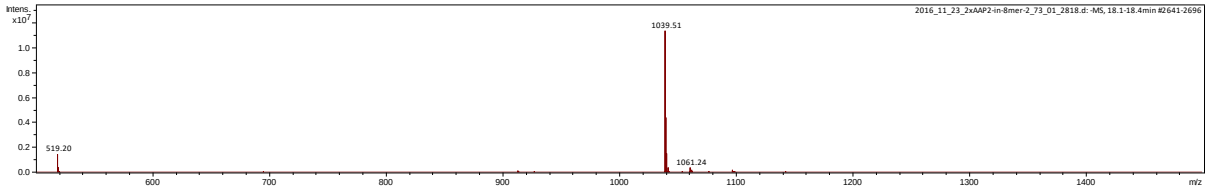

Deconvoluted mass 4: 2080.90

Extracted mass spectrum 5 (21.1 – 21.4 min.):

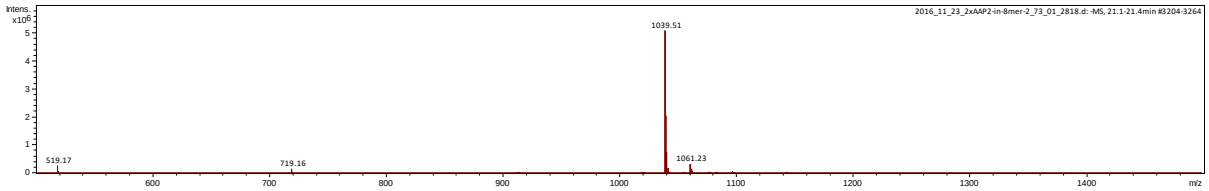

Deconvoluted mass 5: 2080.90

Sequence: 5’-GAXATXGGXTG-3’ (C)

Modification: X = *N*-Phenyl-arylazopyrazole (AAP2)

Calculated mass: 3897.14

Data file: 2016_10_23_3xAAP2_8mer-2_87_01_2555

UV-chromatogram (260 nm):

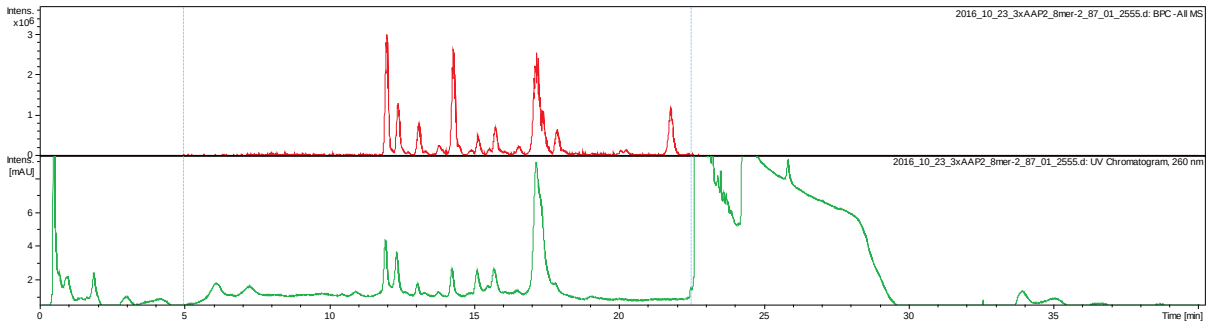

Extracted mass spectrum 1 (11.8 – 12.6 min.):

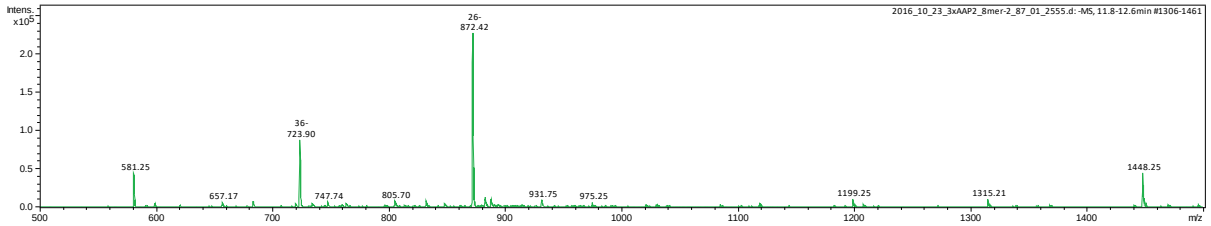

Deconvoluted mass 1: 1746.77

Extracted mass spectrum 2 (14.0 – 14.6 min.):

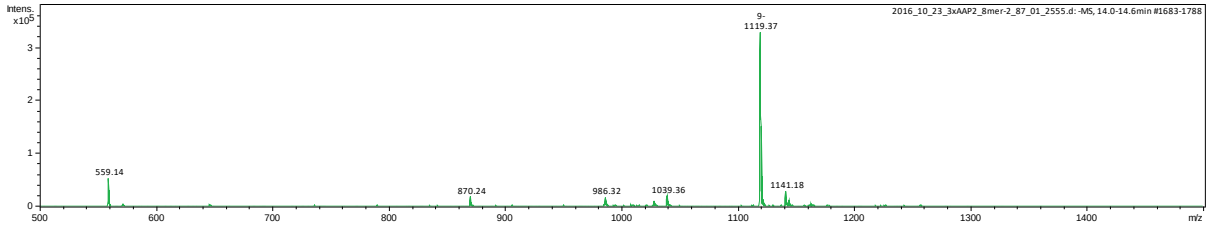

Deconvoluted mass 2: 2240.76

Extracted mass spectrum 3 (15.0 – 15.3 min.):

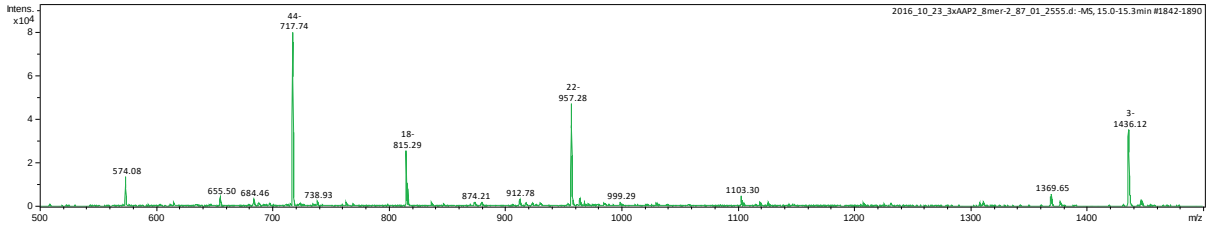

Deconvoluted mass 3: 2874.26

Extracted mass spectrum 4 (15.3 – 15.9 min.):

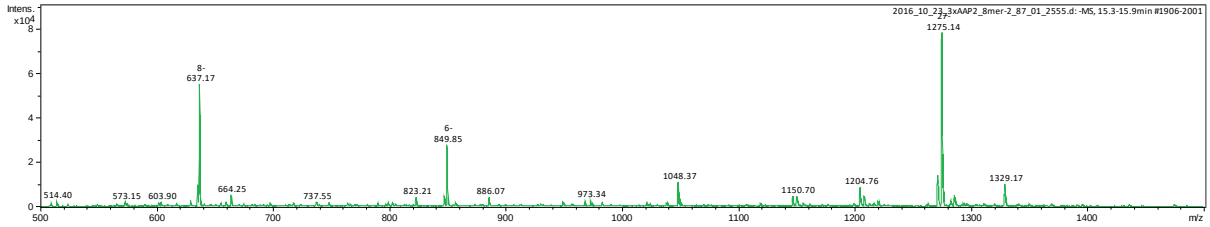

Deconvoluted mass 4: 5320.72 + 5105.13 or 2552.57

Extracted mass spectrum 5 (16.8 – 17.6 min.):

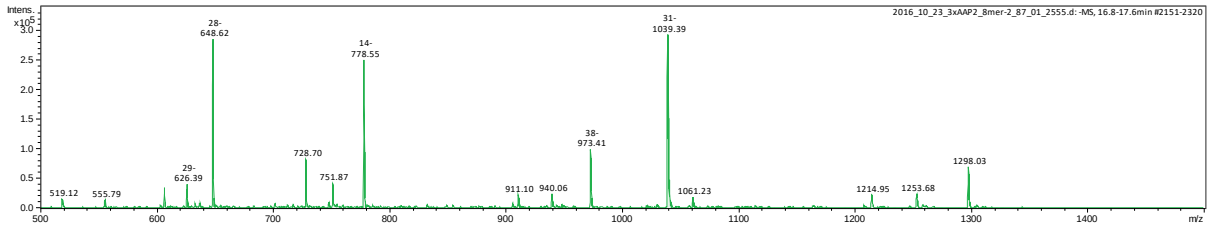

Deconvoluted mass 5: 3897.11 + 3764.06 + 3647.87

Sequence: 5’-CACCATXTCCGGT-3’ (D)

Modification: X = *N*-Phenyl-arylazopyrazole (AAP2)

Calculated mass: 4050.54

Data file: 2017_01_20_1AP2-12mer-MS_81_01_3310

UV-chromatogram (260 nm):

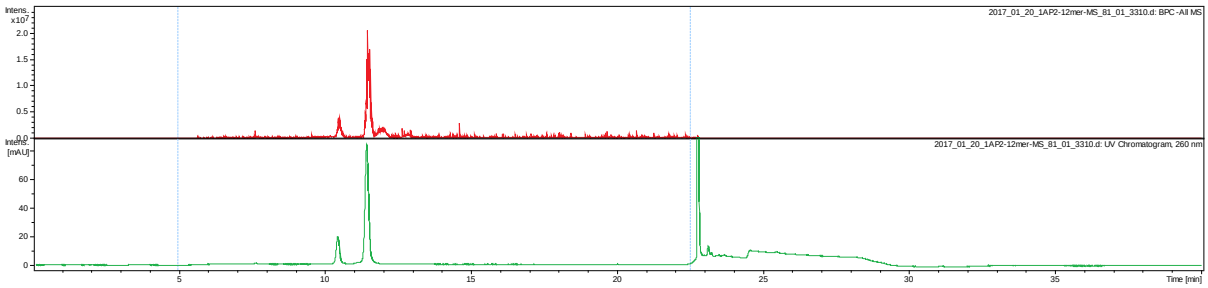

Extracted mass spectrum 1 (10.3 – 10.6 min.):

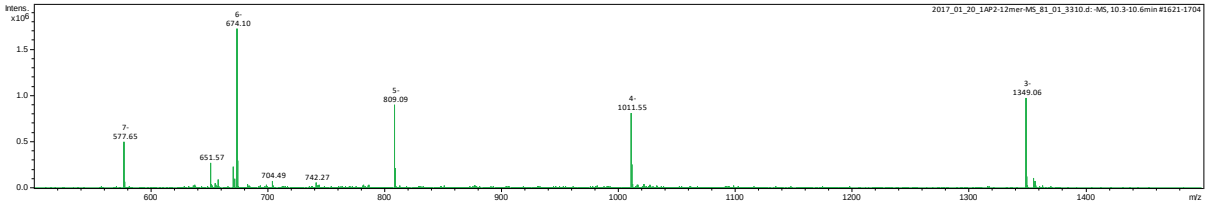

Deconvoluted mass 1: 4050.19

Extracted mass spectrum 2 (11.1 – 11.8 min.):

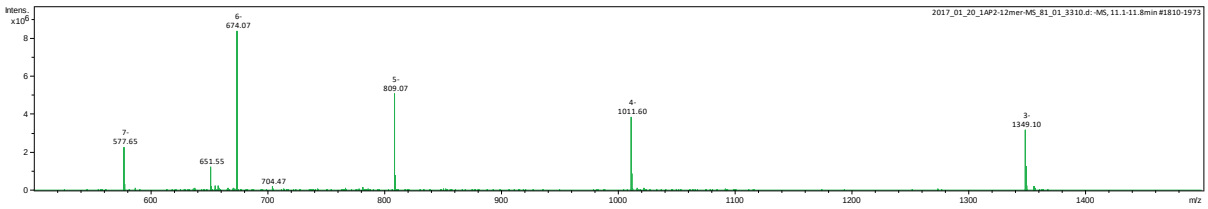

Deconvoluted mass 2: 4050.33

Sequence: 5’-CACXCATTCCXGGT-3’ (E)

Modification: X = *N*-Phenyl-arylazopyrazole (AAP2)

Calculated mass: 4519.69

Data file: 2016_09_26_2xAAP2-12_83_01_2341

UV-chromatogram (260 nm):

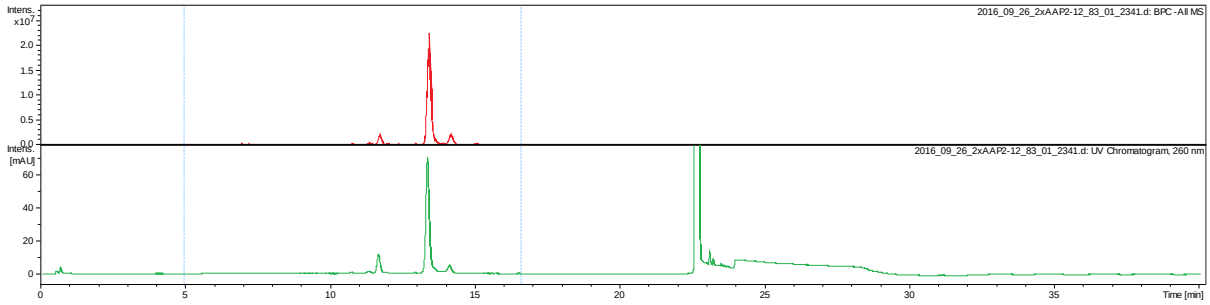

Extracted mass spectrum 1 (11.7 – 11.8 min.):

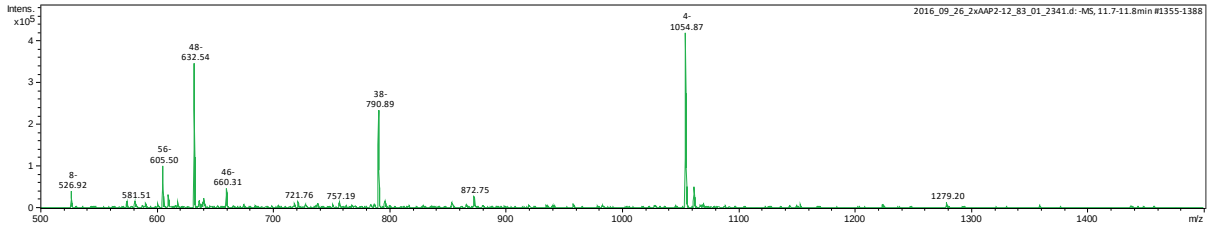

Deconvoluted mass 1: 3167.62

Extracted mass spectrum 2 (13.2 – 13.6 min.):

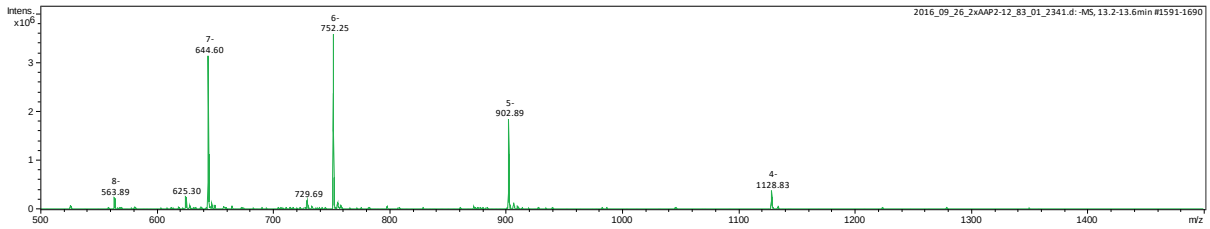

Deconvoluted mass 2: 4519.46

Extracted mass spectrum 3 (14.0 – 14.2 min.):

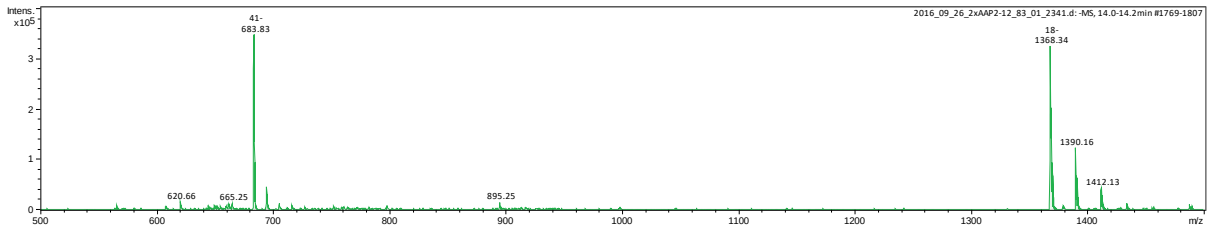

Deconvoluted mass 3: 2738.70

Sequence: 5’-CACXCATXTCCXGGT-3’ (F)

Modification: X = *N*-Phenyl-arylazopyrazole (AAP2)

Calculated mass: 4988.85

Data file: 2016_09_26_3xAAP2-12_85_01_2343

UV-chromatogram (260 nm):

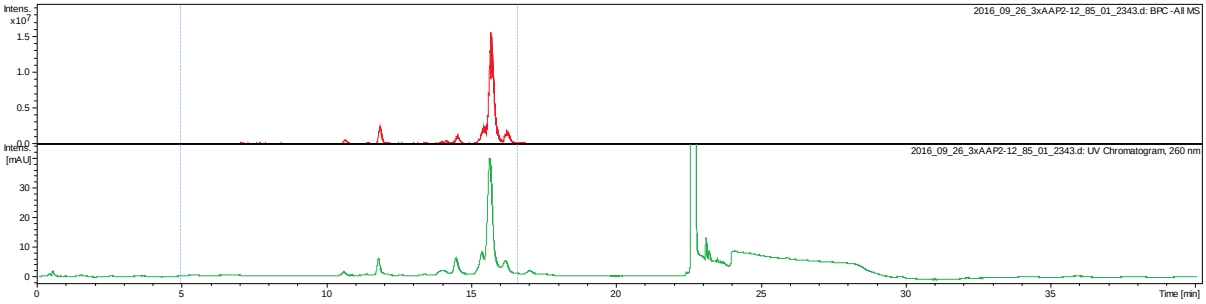

Extracted mass spectrum 1 (14.4 – 14.7 min.):

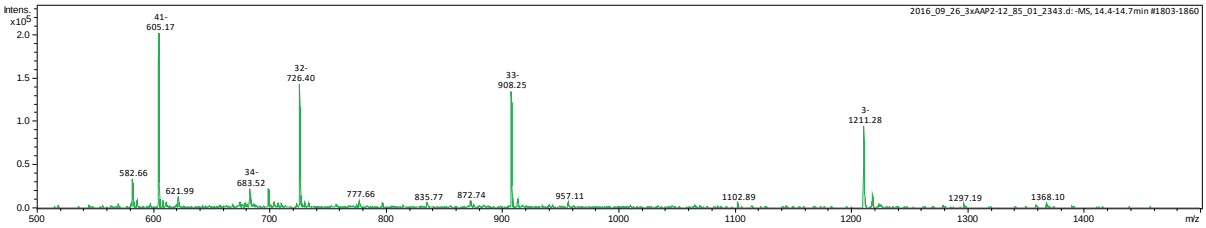

Deconvoluted mass 1: 3636.86

Extracted mass spectrum 2 (15.0 – 15.9 min.):

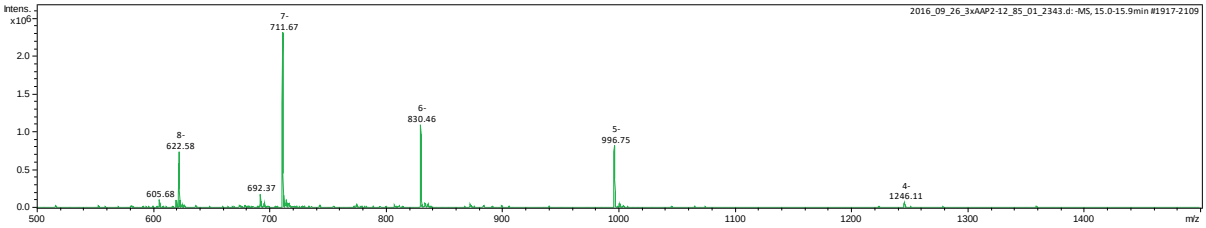

Deconvoluted mass 2: 4988.77

Sequence: 5’-CACCXATTCXCAGT-3’ (G)

Modification: X = *N*-Phenyl-arylazopyrazole (AAP2)

Calculated mass: 4503.70

Data file: 2017_03_03_2xAAP2_12-mer-50_75_01_3855

UV-chromatogram (260 nm):

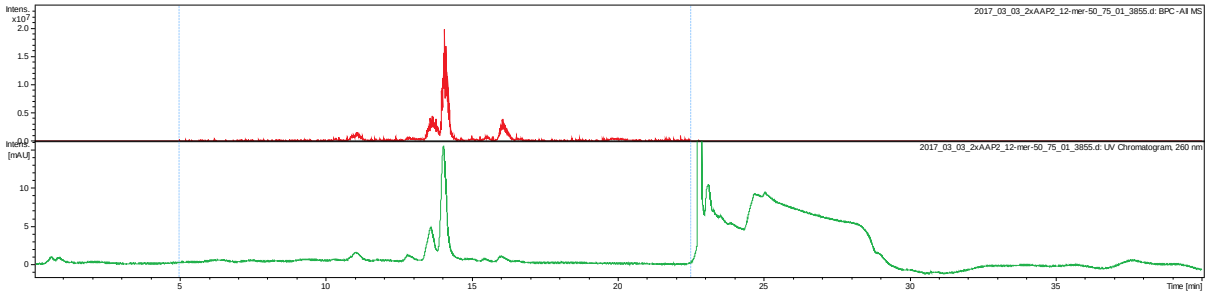

Extracted mass spectrum 1 (13.3 – 13.8 min.):

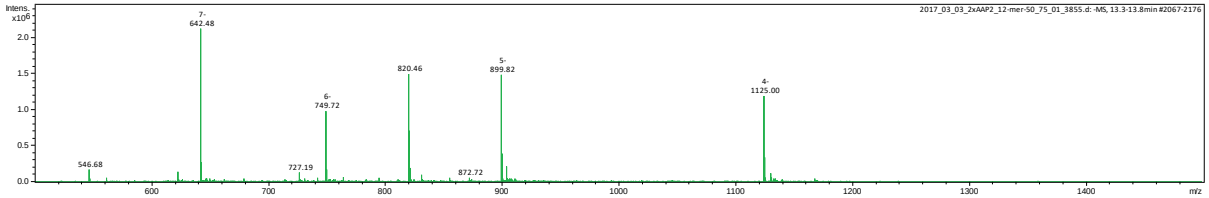

Deconvoluted mass 1: 4504.15

Extracted mass spectrum 2 (13.8 – 14.6 min.):

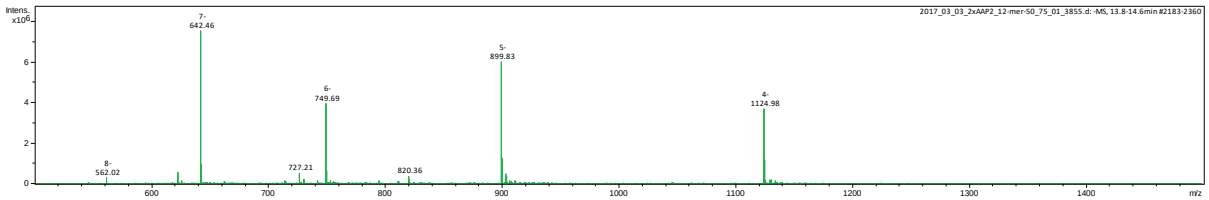

Deconvoluted mass 2: 4503.94

Sequence: 5’-CACXCATXTCCXAGT-3’ (H)

Modification: X = *N*-Phenyl-arylazopyrazole (AAP2)

Calculated mass: 4972.85

Data file: 2017_03_02_3xAAP2_12-mer-50 1_76_01_3856

UV-chromatogram (260 nm):

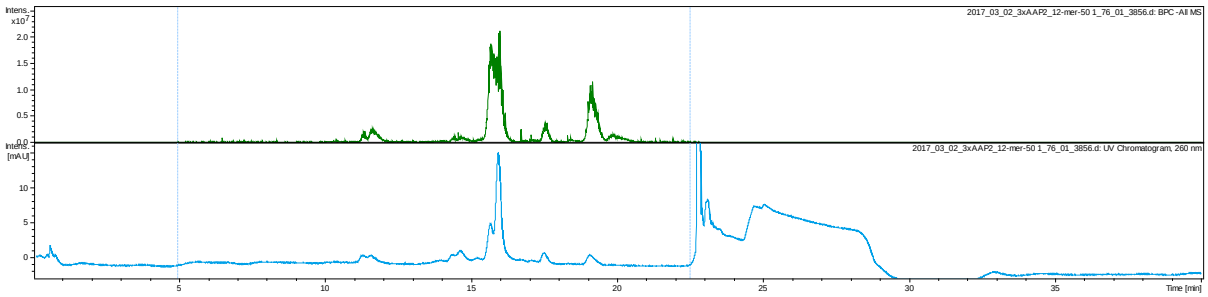

Extracted mass spectrum (15.5 – 16.2 min.):

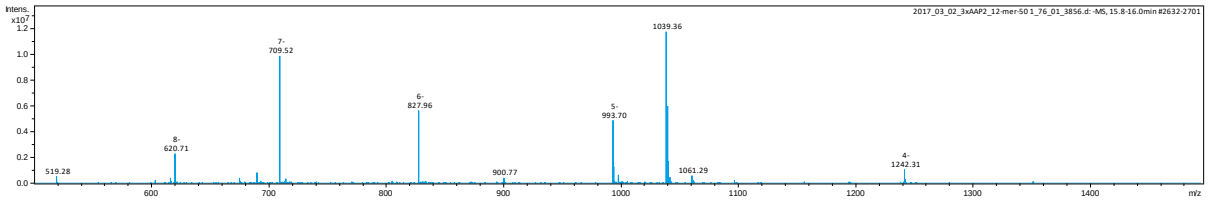

Deconvoluted mass: 4973.26

Sequence: 5‘-TCCXCCAXGCAXTCG-3‘ (I)

Modification: X = *N*-Phenyl-arylazopyrazole (AAP2)

Calculated mass: 4973.83

Data file: 2016_10_23_AAP2_168ROo-2_85_01_2553

UV-chromatogram (260 nm):

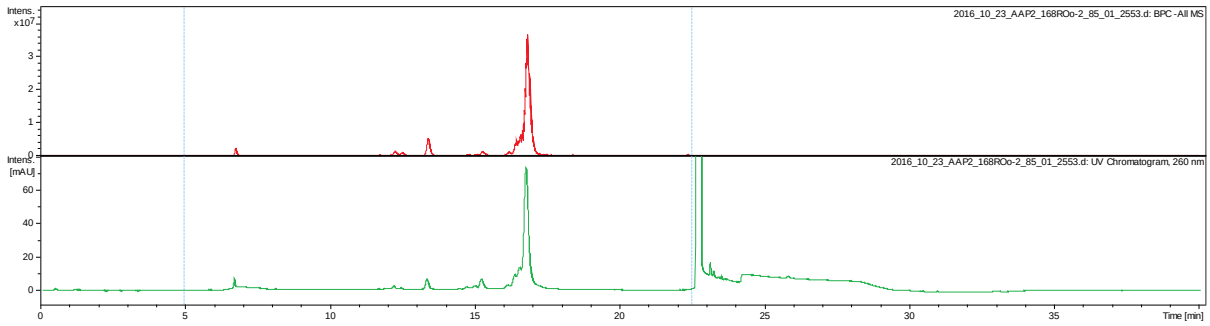

Extracted mass spectrum (16.2 – 17.2 min.):

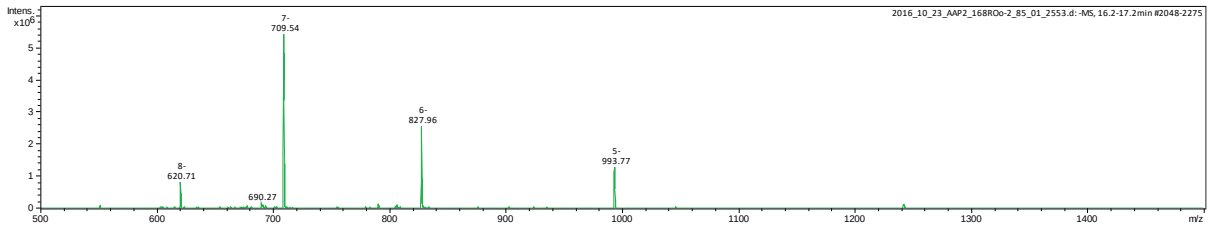

Deconvoluted mass: 4973.90

Sequence: 5‘-CCXGATXGCTXGT-3‘ (J)

Modification: X = *N*-Phenyl-arylazopyrazole (AAP2)

Calculated mass: 4426.48

Data file: 2016_10_23_AAP2_126ROo-2_83_01_2551

UV-chromatogram (260 nm):

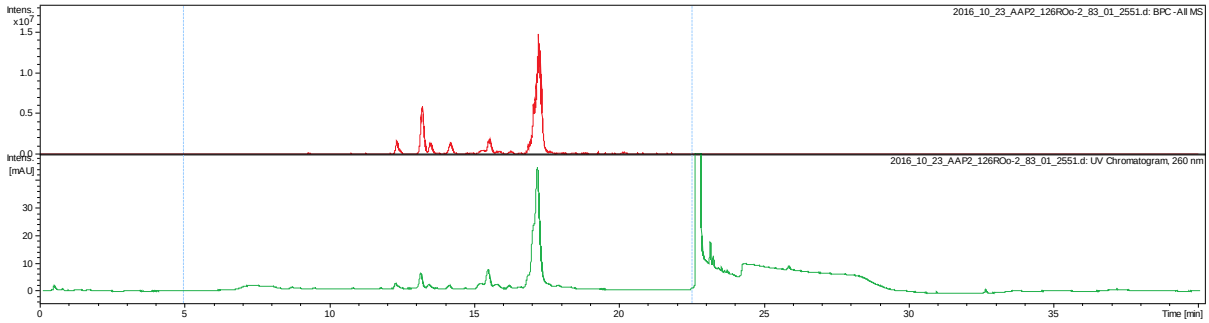

Extracted mass spectrum 1 (13.1 – 13.3 min.):

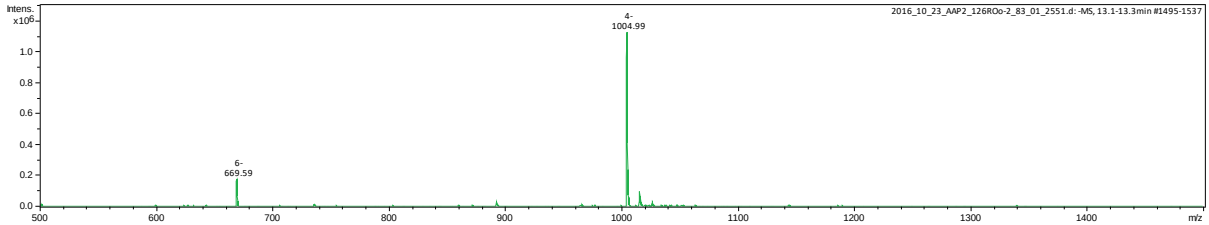

Deconvoluted mass 1: 2011.80

Extracted mass spectrum 2 (15.3 – 15.6 min.):

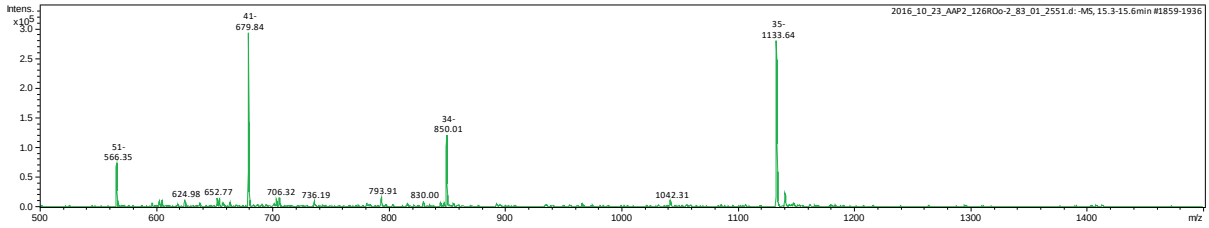

Deconvoluted mass 2: 3404.06

Extracted mass spectrum 3 (16.9 – 17.3 min.):

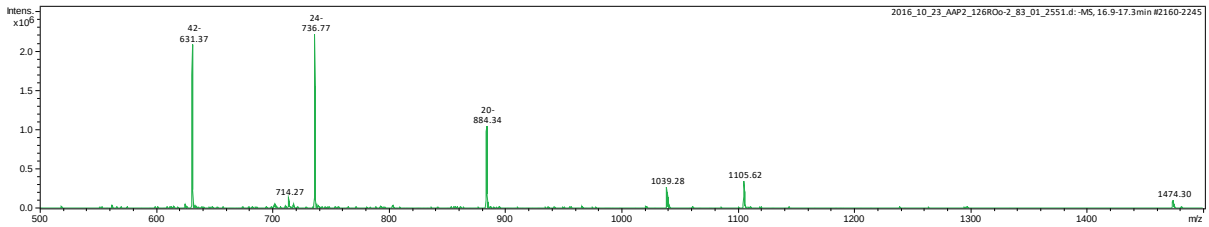

Deconvoluted mass 3: 4426.49

Sequence: 5‘-GGXAATXGGTXGA-3‘ (K)

Modification: X = *N*-Phenyl-arylazopyrazole (AAP2)

Calculated mass: 4539.56

Data file: 2016_10_23_AAP2_126ROp_88_01_2556

UV-chromatogram (260 nm):

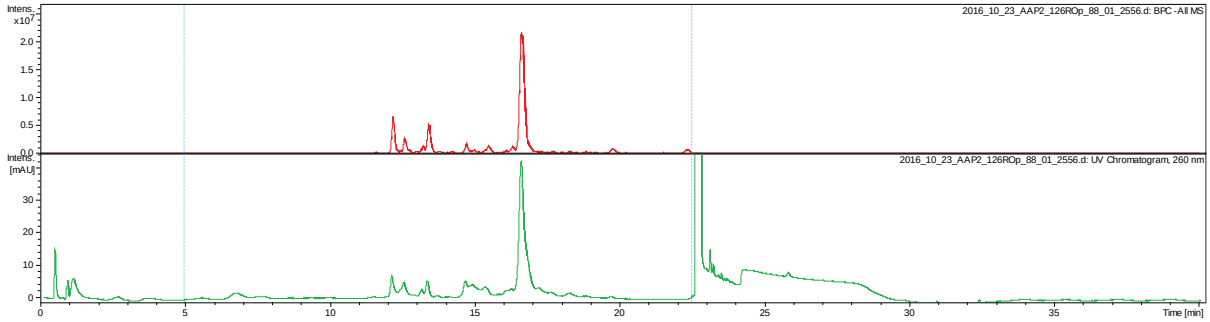

Extracted mass spectrum 1 (11.9 – 12.8 min.):

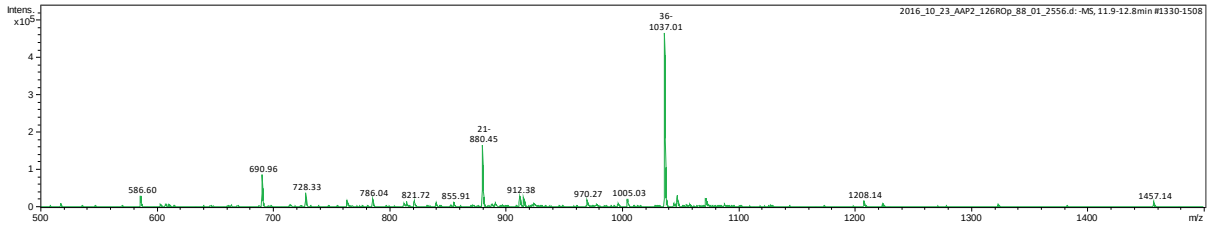

Deconvoluted mass 1: 2917.36 + 2075.90

Extracted mass spectrum 2 (13.1 – 13.6 min.):

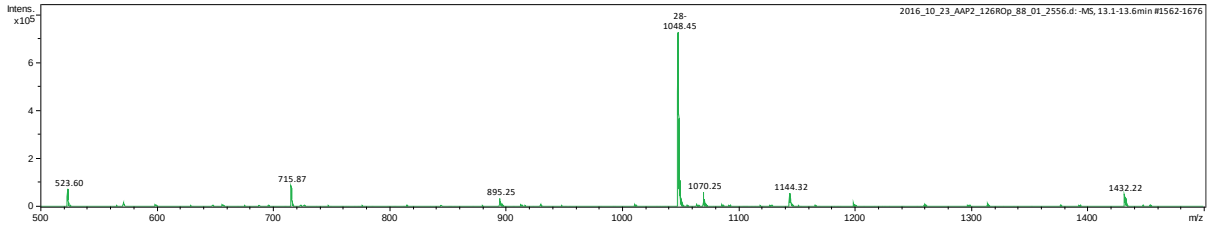

Deconvoluted mass 2: 4301.25 + 4197.82

Extracted mass spectrum 3 (14.6 – 15.6 min.):

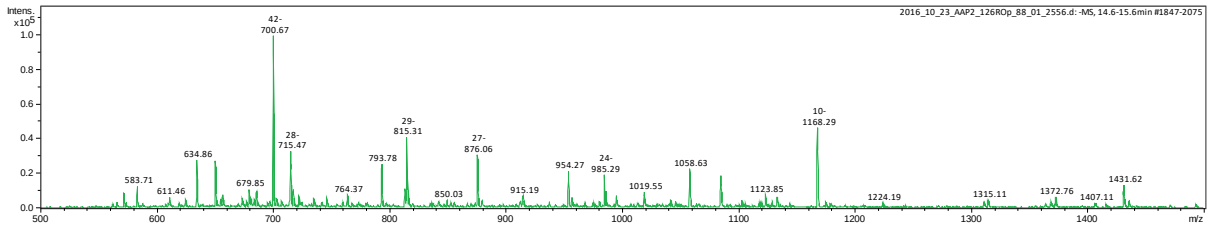

Deconvoluted mass 3: 3508.26 + 3178.92 + 3061.68 + 2865.83

Extracted mass spectrum 4 (14.6 – 15.6 min.):

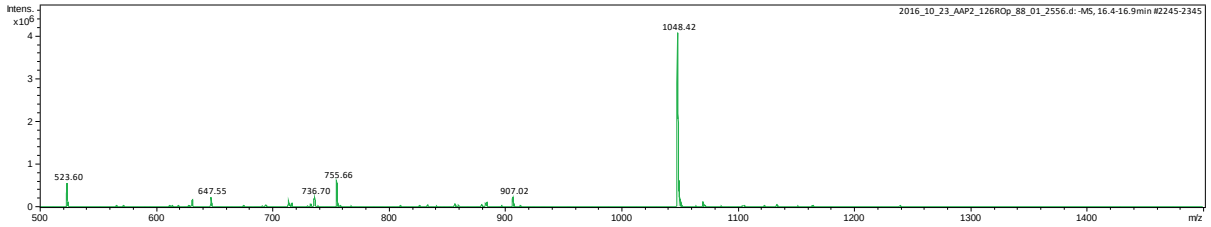

Deconvoluted mass 4: 4540.02

Sequence: 5‘-TCCCXCAGCXATCG-3‘ (L)

Modification: X = *N*-Phenyl-arylazopyrazole (AAP2)

Calculated mass: 4504.70

Data file: 2016_11_23_AAP2-168ROo-sh2_80_01_2825

UV-chromatogram (260 nm):

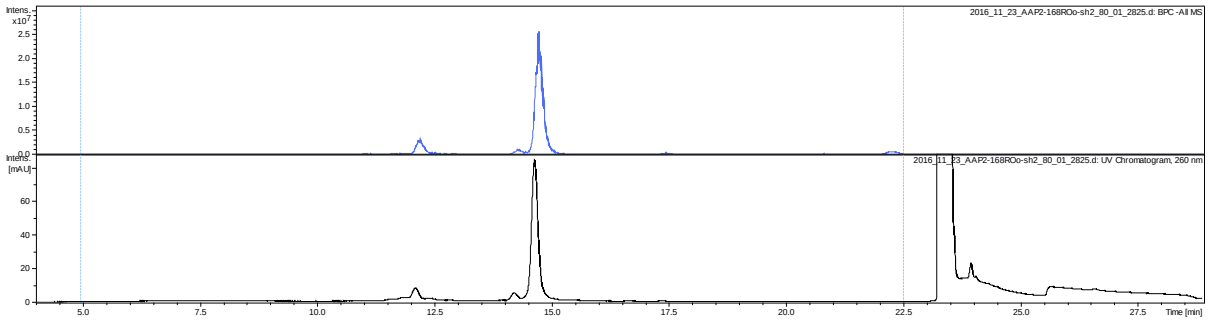

Extracted mass spectrum 1 (12.0 – 12.2 min.):

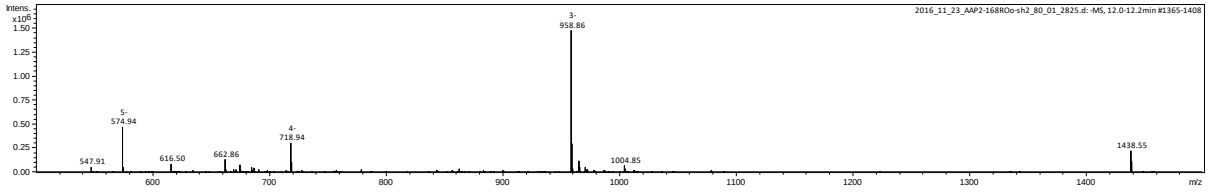

Deconvoluted mass 1: 2879.78

Extracted mass spectrum 2 (14.4 – 15.0 min.):

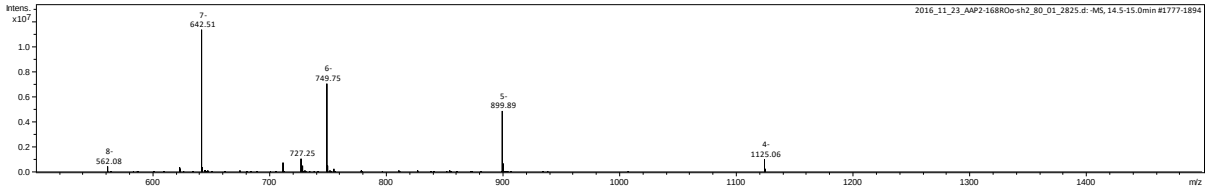

Deconvoluted mass 2: 4504.26

Sequence: 5’-CACCXATTCXCGGT-3’ (M)

Modification: X = *N*-Phenyl-arylazopyrazole (AAP2)

Calculated mass: 4519.70

Data file: 2016_11_23_2xAAP2-in-12mer-sh1_77_01_2822

UV-chromatogram (260 nm):

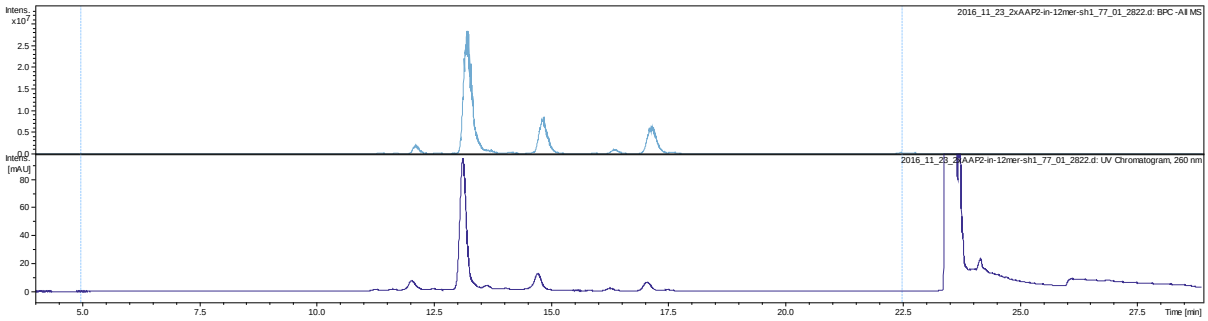

Extracted mass spectrum 1 (11.9 – 12.3 min.):

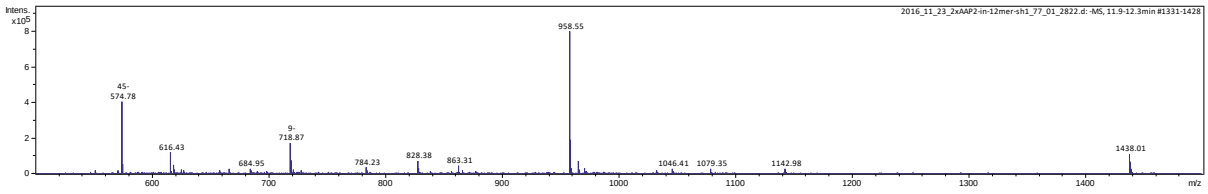

Deconvoluted mass 1: 2897.50

Extracted mass spectrum 2 (13.0 – 13.3 min.):

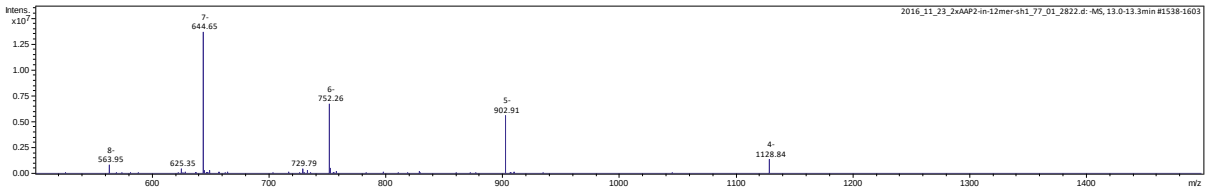

Deconvoluted mass 2: 4519.59

Extracted mass spectrum 3 (14.6 – 14.9 min.):

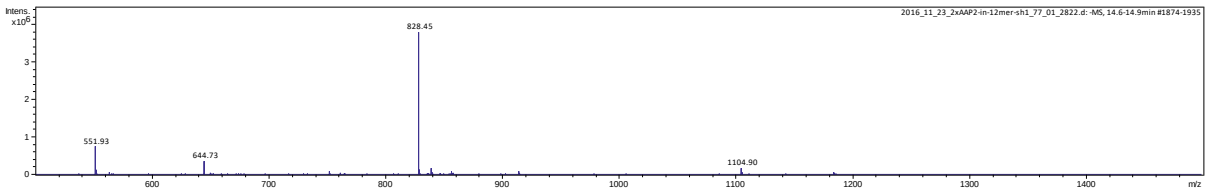

Deconvoluted mass 3: 2211.81 + 1658.92